

AD-A163 497

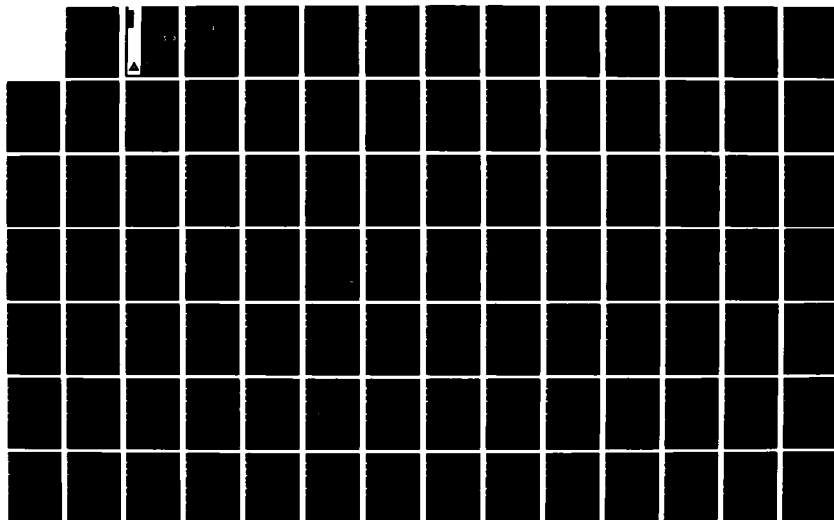
ELECTRONIC AND ATOMIC COLLISIONS ABSTRACTS OF
CONTRIBUTED PAPERS INTERNAT. (U) SRI INTERNATIONAL
MENLO PARK CA MOLECULAR PHYSICS CENTER
M J COGGIOLA ET AL 1985

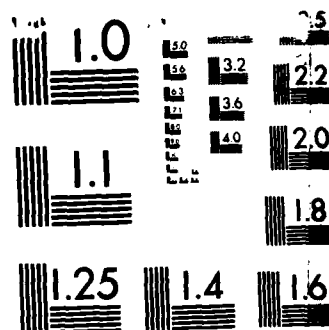
1/8

UNCLASSIFIED

F/G 7/4

NL





MICROCOPY RESOLUTION TEST CHART
NATIONAL BUREAU OF STANDARDS 1963-A

AD-A163 497

ELECTRONIC AND ATOMIC COLLISIONS

Abstracts
of
Contributed Papers

DTIC
ELECTE
JAN 29 1986
S D

Fourteenth International
Conference on the
Physics of Electronic
and Atomic Collisions

Palo Alto 1985

DTIC FILE COPY

DISTRIBUTION STATEMENT A

Approved for public release;
Distribution Unlimited

Edited by
M. J. Coggiola, D. L. Huestis, R. P. Saxon

85 11 04 128



ELECTRONIC AND ATOMIC COLLISIONS



Abstracts of Contributed Papers

Fourteenth International
Conference on the
Physics of Electronic
and Atomic Collisions

Palo Alto 1985

Edited by
M. J. Coggiola, D. L. Huestis, R. P. Saxon

The Fourteenth International Conference on the Physics of Electronic
and Atomic Collisions acknowledges support from the following organizations:

International Union of Pure and Applied Physics (IUPAP)

National Science Foundation

Department of Energy

Office of Naval Research

Air Force Office of Scientific Research

National Aeronautics and Space Administration Goddard Space Flight Center

EG&G Princeton Applied Research

International ICPEAC Organization 1983-1985

Executive Committee

Chairman

B. Bederson— USA

Vice Chairman

W.O. Mehlhorn— Germany

Secretary

J.S. Risley— USA

Treasurer

G.C. Watel— France

Treasurer-Elect

R. Morgenstern - Netherlands

Administrative Secretary

L. Roos - Netherlands

Members

J. Eichler - Germany

F. A. Gianturco - Italy

H. B. Gilbody - United Kingdom

Y. S. Gordeev - USSR

F. Gounand - France

I. V. Hertel - Germany

Y. Kaneko - Japan

D. C. Lorents - USA

T. Lucatorto - USA

M. Lubell - USA

W. E. Meyerhof - USA

F. H. Read - United Kingdom

L. Spruch - USA

N. Stolterfoht - Germany

N. Tolk - USA

General Committee

ARGENTINA

C.R. Garibotti

AUSTRALIA

I.E. McCarthy

AUSTRIA

T.D. Märk

BELGIUM

J. Momigny

CANADA

D. Roy

DENMARK

P. Hvelplund

FRANCE

J.F. Chemin

J.F. Delpech

F. Gounand

V. Sidis

G.C. Watel

GERMANY

J. Eichler

H. Haberland

I. V. Hertel

W.O. Mehlhorn

W. Raith

H.W. Schmidt-Böcking

N. Stolterfoht

INDIA

S.C. Mukherjee

ITALY

F.A. Gianturco

A. Giardini-Guidoni

JAPAN

T. Arikawa

Y. Kaneko

M. Matsuzawa

NETHERLANDS

R. Morgenstern

M.J. van der Wiel

SPAIN

A. Riera

SWITZERLAND

W. Wölfl

UNITED KINGDOM

J. Comer

H.B. Gilbody

C.L. Latimer

M.R.C. McDowell

F.H. Read

UNITED STATES

B. Bederson

R.L. Champion

A. Dalgarno

D.C. Lorents

M. Lubell

T. Lucatorto

K.B. MacAdam

W.E. Meyerhof

T.M. Miller

R.A. Phaneuf

J.S. Risley

I.A. Sellin

L. Spruch

N. Tolk

S. Trajmar

USSR

R.J. Damburg

Y.S. Gordeev

N.P. Penkin

A.M. Urnov

YUGOSLAVIA

S.V. Cvejanović

Local Committee

Chairmen

Donald C. Lorents

Molecular Physics Department

SR1 International

333 Ravenswood Avenue

Menlo Park, California 94025, USA

Telephone (415) 859-3167

Walter E. Meyerhof

Department of Physics

Stanford University

Stanford, California 94305, USA

Telephone (415) 497-4640

Members

Robert E. Anholt

Christopher H. Becker

William K. Bischel

Michael J. Coggiola

Richard A. Copeland

Philip C. Cosby

Keith T. Gillen

Hanspeter Helm

A. Peet Hickman

Robert M. Hill

David L. Huestis

Jay B. Jeffries

Ravinder Kachru

James R. Peterson

Roberta P. Saxon

Christian Stoller

Program Committee

Executive Committee

and

R. Anholt

M. Coggiola

K. Gillen

R. Hill

J. Peterson

R. Saxon

Accession For	
NTIS	<input checked="" type="checkbox"/>
CRA&I	<input type="checkbox"/>
DTIC	<input type="checkbox"/>
TAB	<input type="checkbox"/>
Unannounced	<input type="checkbox"/>
Justification	
By <i>lth. on file</i>	
Distribution	
Availability Codes	
Dist	Available for special
A-1	

Summary

→ Photon Impact:	
→ Atomic Photoionization — Experiment	1
→ Atomic Photoionization — Theory	17
→ Molecular Photoionization — Experiment	29
→ Molecular Photoionization — Theory	39
→ Photodetachment	48
→ Single Photon Dissociation	54
→ Multiphoton Processes in Atoms and Molecules	64
→ Multiphoton Processes in Molecules	81
→ Electron-Atom Collisions:	
→ Elastic Processes	91
→ Alignment and Orientation	109
→ Inelastic — I	122
→ Resonances	141
→ General Threshold and Autoionization	150
→ (e,2e) and Post Collision Interactions	170
→ Spin-Dependent Processes	178
→ Inelastic — II	197
→ Electron-Molecule Collisions:	
→ Electronically Elastic Processes — I	210
→ Electronically Elastic Processes — II	229
→ Electronic Excitation and Ionization — I	241
→ Electronic Excitation and Ionization — II	260
→ Dissociation	272
→ Electron-Ion Collisions:	
→ Elastic, Inelastic, Ionizing	285
→ Recombination	306
→ Positron-Atom, Positron-Molecule Collisions	317
→ Exotic Collisions	334
→ Atom-Atom Collisions:	
→ General	348
→ Ionization — General	362
→ Associative and Chemi-Ionization	373

next page

→ Ion-Atom Collisions	
General	380
→ Resonant Transfer and Excitation	391
Direct Excitation and Ionization	398
Ionization	403
→ Autoionization	413
Electron Detachment	419
→ Quasimolecular Collisions	424
→ Alignment and Orientation	434
→ Production and Ionization of Multiply Charged Ions	446
→ Collisions Involving Multiply Charged Ions	459
→ Charge Transfer of Multiply Charged Ions	468
Charge Transfer at eV Energies	479
Charge Transfer at keV Energies — Experiment	486
Charge Transfer at keV Energies — Theory	494
Charge Transfer at MeV Energies — Experiment	505
Charge Transfer at MeV Energies — Theory	511
→ Capture into Continuum and Convoy Electrons	524
→ Radiative and Non-Radiative Capture at High Energies	531
→ Inner Shell Vacancy Decay	543
→ Ion(Atom)-Molecule Collisions	
Rotational-Vibrational Excitation	551
Energy Transfer	565
General	572
→ Molecular Charge Transfer	579
→ Ionization and Detachment	589
→ Reactive Scattering	596
→ Three-Body Processes	606
→ Ion-Ion Collisions	610
→ Rydberg States and Reactions	621
→ Field Assisted Collisions	635
→ Clusters	647
→ Experimental Techniques	657
Post-Deadline Papers	677
Post-Post-Deadline Papers	688
Author Index	711

Contents

Photon Impact: Atomic Photoionization — Experiment

Atoms in Strong Electric and Magnetic Fields: The H-Atom <i>H. Rottke, A. Holle, Karl H. Welge</i>	1
Determination of the Transition Matrix Elements and Their Relative Phases from Experimental Photoelectron Spin Polarization Data for 5p-Autoionization of Xenon <i>Ch. Heckenkamp, F. Schäfers, U. Heinzmann</i>	2
The Photoelectron Spin-Polarization Parameters in the 5p-Autoionization Range of Xenon <i>Ch. Heckenkamp, F. Schäfers, G. Schönhense, U. Heinzmann</i>	3
Energy Dependence of the Spin-Polarization Parameters for Hg 5d Photoionization with Circularly Polarized Light <i>F. Schäfers, Ch. Heckenkamp, G. Schönhense, U. Heinzmann</i>	4
Photoelectron Spin-Polarization in the Cooper Minimum of Hg 6s <i>F. Schäfers, Ch. Heckenkamp, U. Heinzmann</i>	5
Photoionization of Atomic and Molecular Chlorine <i>J. A. R. Samson, Y. Shafer, G. C. Angel</i>	6
Measurement of the 5d Photoionization Cross Section in Laser Excited Barium Atoms Between 15 eV and 150 eV Photon Energy <i>J. M. Bizau, D. Cubaynes, P. Gérard, F. Wuilleumier, J. C. Keller, J. L. LeGouët, J.L. Picqué, B. Carré, D. Ederer, G. Wendin</i>	7
Experimental and Theoretical Determinations of Oscillator Strengths for Photoexcitation of a Core Electron in Atomic Lithium <i>P. Gérard, D. Cubaynes, J. M. Bizau, F. Wuilleumier, C. J. Zeippen</i>	8
3p Photoionization in Atomic Manganese <i>R. Malutzki, V. Schmidt</i>	9
Threshold Photoionization of Kr 3d Subshell <i>P. A. Heimann, D. W. Lindle, T. A. Ferrett, M. N. Piancastelli, D. A. Shirley</i>	10
Si 2p and 2s Resonant Excitation and Photoionization in SiF ₄ <i>T. A. Ferrett, M. N. Piancastelli, D. W. Lindle, P. A. Heimann, D. A. Shirley</i>	11
Evidence for Shape Resonance Dependent Satellite Behavior in Atomic Barium <i>U. Becker, R. Hölzel, H. G. Kerkhoff, B. Langer, D. Szostak, R. Wehlitz</i>	12
Resonance and Threshold Effects on the Neon 2p-Satellites <i>U. Becker, R. Hölzel, H. G. Kerkhoff, B. Langer, D. Szostak, R. Wehlitz</i>	13
Single and Double Photoionization of Alkaline-Earth Atoms <i>Y. Itikawa, T. Hayaishi, Y. Itoh, T. Koizumi, J. Murakami, T. Nagata, T. Sasaki, Y. Sato, H. Shibata, B. Sonntag, J. B. West, A. Yagishita, M. Yoshino</i>	14
Electron Angular Distributions from Autoionizing Barium Rydberg States <i>U. Eichmann, V. Lange, M. Völkel, W. Sandner</i>	15
Channel Interaction of the Three J=3 6p _{nd} Autoionizing Series in Barium <i>Oliver C. Mullins, Yifu Zhu, Emily Y. Xu, T. F. Gallagher</i>	16

Photon Impact: Atomic Photoionization — Theory

The Resonant Photoionization of H Atom in Intense Magnetic Fields <i>S. K. Bhattacharya, Shih-I Chu</i>	17
Photoionization of Excited Cs I States <i>Constantine E. Theodosiou</i>	18
Theoretical Study of the Configuration Interaction in the Photoionization of Mg Atom <i>T. N. Chang, Young Soon Kim</i>	19
Threshold Effects in Inner-Shell Photoionization of Open-Shell Atoms: Hartree-Fock Calculations of Boron <i>Samir K. Bhattacharya, Steven T. Manson</i>	20
Photoionization of the Excited Na 4d State <i>Alfred Z. Msezane, Steven T. Manson</i>	21
Relativistic Calculations of the Photoionization of 6s Subshells in High-Z Atoms <i>B. R. Tambe, Steven T. Manson</i>	22
Photoionization of Mercury <i>K. Bartschat, N. S. Scott</i>	23
Radiative Transitions in Calcium Ions <i>K. L. Baluja, K. T. Taylor</i>	24
Field-Induced Autoionization of Quasi-Stable Rydberg-Stark Levels <i>David A. Harmin</i>	25
Half-Scattering Processes in the Presence of Long-Range Barriers <i>David A. Harmin</i>	26
Stark Effect and Field Ionization <i>Alexander Alijah, John T. Broad, Juergen Hinze</i>	27
Application of the Analytic Perturbation Theory to the Description of the Angular Distribution of Inner Shell Photoelectrons <i>A. Bechler, R. H. Pratt</i>	28

Photon Impact: Molecular Photoionization — Experiment

Autoionizing Rydberg States of Triplet H ₂ <i>R. Kachru, N. Bjerre, H. Helm</i>	29
Dissociative Double Photoionization of Some Simple Molecules <i>Gérald Dujardin, Lucette Hellner, Sydney Leach, Dominique Winkoun</i>	30
Single Photon Double Ionization in Some Triatomic Molecules <i>P. Lablanquie, I. Nenner, P. Millie, P. Morin, J. H. Eland, J. Delwiche, M. J. Hubin-Franskin</i>	31
Selective Resonant Photoionization Processes Near the Si 2p Edge in Tetramethylsilane <i>P. Morin, G. G. B. de Souza, P. Lablanquie, I. Nenner</i>	32
Angle Resolved Photoelectron Study of the Configuration Interaction States of CO ₂ <i>P. Roy, I. Nenner, P. Morin, P. Millie, D. Roy, M. J. Hubin-Franskin, J. Delwiche</i>	33
Kinetic Energy of Fragmentation Produced by Dissociative Photoionization of NO <i>J. A. R. Samson, G. C. Angel, O. P. Rustgi</i>	34

Analysis of Photoion Branching Ratios of HF and HCl <i>Toshio Masuoka, Shichiro Mitani</i>	35
Dissociation Mechanism of Singly and Doubly Ionized CO <i>Toshio Masuoka</i>	36
Absolute Dipole Oscillator Strengths for the Valence Shell Photoabsorption and Photoionization of H ₂ S and HI <i>C. E. Brion, Y. Iida, G. K. James</i>	37
Experimental Photoionization Cross Sections and Angular Distributions for the Molecular Orbitals of H ₂ O in the 30-130 eV Photon Energy Range <i>M. S. Banna, R. Malutzki, V. Schmidt</i>	38
<i>Photon Impact: Molecular Photoionization — Theory</i>	
R-Matrix Method for Molecular Photoionization <i>C. J. Noble, J. Tennyson, P. G. Burke</i>	39
Generalized Multichannel Quantum Defect Treatment of ² Π- ² Π Rydberg-Valence State Interactions in NO <i>M. Raoult</i>	40
Spin-Orbit Autoionization and Cooper Minimum in the Hydrogen Halides <i>H. Lefebvre-Brion, A. Giusti-Suzor, G. Raseev</i>	41
Theoretical Vibrational Resolved Partial Photoionization Cross Sections of CO. The Autoionization Region between 16.9 and 19.0 eV <i>B. Leyh, G. Raseev</i>	42
Photoionization of C ₂ <i>N. T. Padial, B. I. Schneider, L. A. Collins</i>	43
Molecular Photoionization Cross Sections by the Complex Basis Function Method <i>C. W. McCurdy, C-H Yu, R. M. Pitzer</i>	44
Theoretical Study of Angular Distribution of Photoelectrons in H ₂ Molecule <i>G. Raseev, M. Raoult</i>	45
The Rotationally and Vibrationally Resolved Photoionization of H ₂ by 736Å Line <i>S. Hara</i>	46
Photoionization of H ₂ : A First Principle Study <i>N. Chandra</i>	47
<i>Photon Impact: Photodetachment</i>	
Modified Photodetachment Threshold Behavior Near Resonances <i>Y. K. Bae, J. R. Peterson</i>	48
Details of the He ⁻ 4P ^c Shape Resonance and the He (2 ³ S) Electron Affinity <i>J. R. Peterson, Y. K. Bae, M. J. Coggiola, D. L. Huestis</i>	49
The Response of the ¹ P ^o Dip in the H ⁻ Continuum Near n=3 to Large Electric Fields <i>Stanley Cohen, G. Comtet, C. J. Harvey, K. B. Butterfield, D. A. Clark, J. B. Donahue, P. A. M. Gram, D. W. MacArthur, J. E. Stewart, W. W. Smith, H. C. Bryant</i>	50
Photodetachment Spectroscopy of FeO ⁻ <i>T. Andersen, K. R. Lykke, D. M. Neumark, W. C. Lineberger</i>	51
The Photoelectron Spectrum of NaBr ⁻ <i>Thomas M. Miller, Kermit K. Murray, W. Carl Lineberger</i>	52

Field and Photodetachment of Water Clusters <i>H. Haberland, C. Ludewigt, H.-G. Schindler, D. R. Worsnop</i>	53
<i>Photon Impact: Single Photon Dissociation</i>	
One- and Two-Photon Dissociation of Na ₂ Investigated by Doppler Spectroscopy of Photofragments <i>G. Gerber, R. Möller</i>	54
Lyman- α Excitation Spectra in the Photodissociation of H ₂ <i>S. Arai, Y. Yoshimi, H. Koizumi, K. Hironaka, K. Shinsaka, M. Morita, T. Yoshida, A. Yagishita, K. Ito, Y. Hatano</i>	55
High-Resolution Photodissociation Spectroscopy in Fast Neutral H ₂ Beam <i>N. Bjerre, H. Helm</i>	56
Radiative Dissociation of Selectively Excited Rotational-Vibrational States of H ₂ (B,C) Molecules <i>H. Schmoranzer, T. Noll, J. Imschweiler, K. Molter</i>	57
Photodissociation Processes of Hydrogen Halides Studied with Synchrotron Radiation <i>J. B. Nee, M. Suto, L. C. Lee</i>	58
Photodissociation Dynamics of ICN <i>M. A. O'Halloran, H. Joswig, R. N. Zare</i>	59
Theoretical Investigation of the Photodissociation of OH ⁺ <i>Roberta P. Saxon, B. Liu</i>	60
Adiabatic Approach to Polyatomic Photodissociation: Application to C ₂ N ₂ <i>C. E. Dateo, M. Dupuis, V. Z. Kresin, W. A. Lester, Jr.</i>	61
Time Dependent Wavepacket Calculation of the Photodissociation of Cd(CH ₃) ₂ <i>Kenneth C. Kulander, Ann E. Orel</i>	62
Molecular Photodissociation Near Ionization Threshold <i>G. K. Ivanov, G. V. Golubkov</i>	63
<i>Photon Impact: Multiphoton Processes in Atoms</i>	
Multiphoton Ionization of Hydrogen Atoms <i>H. G. Muller, M. J. van der Wiel</i>	64
A New Method for the Study of Two Photon Process in Atomic Hydrogen <i>Viorica Florescu, Tudor Marian</i>	65
Absolute Two-Photon Absorption and Three-Photon Ionization Cross Sections for Atomic Oxygen <i>D. J. Barnford, W. K. Bischel, L. E. Jusinski, R. P. Saxon, J. Eichler</i>	66
Resonant MPI of Sodium Atoms by Two Intense Laser Fields <i>D. Feldmann, G. Otto, D. Petring, K. H. Welge</i>	67
Two Photon Ionization of Metastable Helium <i>H. Haberland, J. Höhne, M. Oswald</i>	68
Stepwise Multiphoton Excitation Studies of Autoionizing Rydberg Series in Mg <i>R. E. Bonanno, J. D. Fassett, T. B. Lucatorto, J. J. Snyder, C. W. Clark</i>	69
Multiphoton Studies of Highly Excited States of Atomic Iodine <i>S. T. Pratt, P. M. Dehmer, J. L. Dehmer</i>	70
Electron Correlation in Excited Valence States of Barium Studied by Resonant MPI <i>John E. Hunter, III, James S. Keller, R. Stephen Berry</i>	71

Microwave Ionization of Na Rydberg Atoms <i>H. B. van Linden van den Heuvell, J. L. Dexter, T. F. Gallagher</i>	72
Quantum Regularity in the Chaotic Classical Stadium System: Implications for Ionization, Spectroscopy, Multiphoton Processes and Reactions <i>Y. Y. Bai, K. Stefanski, H. S. Taylor</i>	73
Ionization of High Rydberg States of Hydrogen by Combined AC and DC Electric Fields <i>J. N. Bardsley, M. Comella, B. Sundaram</i>	74
Many-Mode Floquet Theory and SU(3) Dynamical Evolution of Three-Level Systems in Intense Bichromatic Fields <i>Shih-I Chu, T. S. Ho</i>	75
Transition Matrix Method for Multiphoton Ionization Processes <i>Anthony F. Starace, Peter Zoller</i>	76
Excited State Photoionization Cross Section of Ne(ns') Autoionizing Resonances <i>K. T. Lu</i>	77
Theory of Multiphoton Ionization and Autoionization of Xe <i>Pradip Gangopadhyay, Xian Tang, P. Lambropoulos, R. Shakeshaft</i>	78
An L^2 Quantum-Defect Treatment of Multiphoton Ionization <i>John T. Broad</i>	79
Scattering Amplitudes by Means of the Complex Coordinate Method. Compton Scattering and Two-Photon Ionization <i>Piotr Froelich</i>	80
<i>Photon Impact: Multiphoton Processes in Molecules</i>	
Theory of Frequency Conversion by Multiwave Raman Propagation <i>A. P. Hickman, J. A. Paisner, W. K. Bischel</i>	81
Bistable and Chaotic Behavior of Driven Molecular Systems <i>Jian-Min Yuan, Mingwei Tung, George C. Lie</i>	82
Photoabsorption of Excited Molecules: Manifestations of Cooper Minima in the Spectroscopy of Rydberg States <i>F. Masnou-Seeuws, Ch. Jungen</i>	83
Rotationally Resolved Three-Photon Ionization of Bi ₂ Studied in the Gas Phase and in a Molecular Beam <i>B. Bühler, C. Cremer, G. Gerber, J. Janes</i>	84
Resonantly Enhanced Multiphoton Ionization and Photoelectron Spectroscopy of NeXe, ArXe, KrXe, and Xe ₂ <i>P. M. Dehmer, J. L. Dehmer, S. T. Pratt</i>	85
Multiphoton Ionization of Benzene, Vinylchloride and Trifluoroethylene at 193 nm <i>Michel J. Rossi, Hanspeter Helm, Donald C. Lorents</i>	86
I. R. Multiple-Photon Excitation and Dissociation of Silicon Compounds <i>E. Borsella, L. Caneve, R. Fantoni, R. Larciprete, A. Giardini-Guidoni</i>	87
Atomic Iron Recoil in Multiphoton Dissociation of Ferrocene <i>H. T. Liou, Y. Ono, P. C. Engelking, J. T. Moseley</i>	88
Resonant Two-Photon Autoionization of H ₂ : Photoelectron Angular Distribution and the Autoionization Lineshape <i>K. Rai Dastidar, S. Ganguly, T. K. Rai Dastidar</i>	89
Two-Photon Dissociation of HD ⁺ by the $1s\sigma_g \rightarrow 1s\sigma_g$ Vibrational Transition <i>M. K. Chakrabarti, S. S. Bhattacharyya, K. K. Datta, Samir Saha</i>	90

Electron-Atom: Elastic Processes

Application of Projection Methods to Scattering Calculations <i>B. I. Schneider</i>	91
Modified Eikonal Approximations for Electron- and Positron-Atom Scattering at Intermediate Energies <i>T. T. Gien</i>	92
Relationship between Fredholm Integral Equation and Schwinger Variational Principle and Its Application to Atomic Scattering <i>S. P. Khare, Satya Prakash</i>	93
Evaluation of Damped Oscillatory Integrals in Electron-Atom Scattering <i>V. B. Sheorey, A. Basu</i>	94
A Third Order Distorted Wave Formula for Scattering by Two Potentials <i>D. P. Dewangan</i>	95
On the On-Shell Approximation in the Faddeev Equations for e-H Scattering <i>P. A. Massaro</i>	96
Faddeev Equations for Elastic and Inelastic e-H Scattering <i>P. A. Massaro</i>	97
Higher Order Born Exchange Amplitudes for Elastic Scattering of Electrons by Helium Atoms <i>N. S. Rao, H. S. Desai</i>	98
Semiempirical Model Description of the Low Energy Electron Scattering from Helium <i>R. I. Câmpeanu</i>	99
Elastic Small-Angle Electron Scattering by He, Ne and Ar at 35 keV <i>Dan Coffman, M. Fink, H. Wellenstein</i>	100
Electron-Atom Wave Functions Using Extended Numerov Algorithm <i>Joseph M. Paikeday</i>	101
Elastic e ⁻ -Kr Scattering Using Model Potential <i>D. Basu, S. Dutta, P. Khan, A. S. Ghosh</i>	102
Scattering of Electrons from Argon Atoms <i>Arati Dasgupta, A. K. Bhatia</i>	103
Elastic Scattering of Intermediate Energy Electrons from Argon <i>B. B. Srivastava, B. Singh</i>	104
Elastic Cross Sections for Electron-Argon Scattering in the Intermediate Energy (300-1000 eV) Range <i>Ione Iga, Lee Mu-Tao, J. C. Nogueira, R. S. Barbieri</i>	105
Total Cross Section Measurements for Electron Scattering from He, Ar and CH ₄ : 0.1-20 eV <i>Stephen J. Buckman, Birgit Lohmann</i>	106
Measurement of Absolute Differential Cross Sections for Elastic Electron Scattering from Mercury <i>G. Holtkamp, K. Jost, J. Kessler, F. J. Peitzmann</i>	107
Differential Scattering Cross Sections of Electrons from Xe <i>H. Nishimura, A. Danjo, T. Matsuda</i>	108

Electron-Atom: Alignment and Orientation

An 11-State Calculation of the Orientation, λ and Alignment χ Parameters for the Electron Excitation 1^1S-2^1P in Helium Below the 3^1P Threshold <i>L. C. G. Freitas, K. A. Berrington, P. G. Burke, A. E. Kingston</i>	109
Cross Sections and Coincidence Parameters for Excitation of the n^1L ($n = 2, 3, 4$) States of Helium <i>G. Csanak, D. C. Cartwright</i>	110
Polarization Correlation Measurements of $He(2^1P)$ Excitation by Electrons <i>M. A. Khakoo, J. L. Forand, K. Becker, J. W. McConkey</i>	111
Electron Impact Excitation of the 3^3P State of Helium <i>J. F. Williams, I. Humphrey</i>	112
Angular Correlations in the Electron Impact Excitation of Sodium <i>J. L. Riley, P. J. O. Teubner, J. E. Furst, M. J. Brunger</i>	113
The Differential Cross Section for Electron Excitation of the 3^1P ($m_l = 0$) State of Helium <i>D. J. Burns, N. W. P. H. Perera, B. N. De, C. R. Hummer</i>	114
Electron-Visible Photon Angular Correlations for the 3^1P State of Helium Excited by Low Energy Electrons <i>P. A. Neill, A. Crowe</i>	115
Electron Impact Excitation of the $4p^5(^2P_{3/2}) 5s^3P_1$ and $4p^5(^2P_{1/2}) 5s^1P_1$ States of Krypton <i>S. J. King, P. A. Neill, A. Crowe</i>	116
Measurement of Spin Exchange Amplitudes in Electron Impact Excitation of the 3^3P State of Helium <i>H. A. Silim, H.-J. Beyer, A. El-Sheikh, H. Kleinpoppen</i>	117
Polarization Correlation Measurements on the 3^1P State of Helium <i>K. S. Ibraheim, H.-J. Beyer, H. Kleinpoppen</i>	118
Electron Impact Excitation of the 3^2P State of Sodium <i>R. P. Fiegel, S. R. Lorentz, T. M. Miller, D. E. Golden, J. E. Furst</i>	119
Superelastic Scattering by a Heavy Atomic Target <i>T. T. Gien</i>	120
Analysis of Orientation and Alignment in Electron Impact Excitation of Heavy Rare Gases: The Ar $4s^1P$ and 3^3P Case <i>N. O. Andersen, J. W. Gallagher, I. V. Hertel, F. J. da Paixão</i>	121
<i>Electron-Atom: Inelastic — I</i>	
A Relationship Between the Direct and the Exchange Amplitudes of $e^- - H$ Collisions <i>Ik-Ju Kang, Ung-In Cho, Gye Tai Park</i>	122
Electron Impact Excitations of $3s$ and $4s$ States of Hydrogen <i>S. Saxena, G. P. Gupta, K. C. Mathur</i>	123
Electron Hydrogen Scattering at Intermediate Energies <i>Joseph Callaway</i>	124
Glauber Amplitude for $1s \rightarrow 2s, 2p$ Excitation of Hydrogen Atom by Electron Impact <i>B. Padhy, D. K. Rai</i>	125
Accurate Electron-Hydrogen Atom Cross Sections Using Hyperspherical Coordinates <i>Diane M. Hood, Aron Kuppermann</i>	126
A Completeness Test for Pseudostate Expansions <i>D. H. Madison</i>	127

Calculation of Inelastic Electron-Atom Scattering Amplitudes by the Method of Locally Complex Distortions of the Energy Spectrum <i>C. W. McCurdy, T. N. Rescigno</i>	128
Role of Excitation Energy in Second Born Approximation <i>N. S. Rao, H. S. Desai</i>	129
Distorted Wave Calculations with Different Distorting Potentials <i>C. S. Singh, D. K. Rai</i>	130
The Coupled-Channels-Optical Method for Electron-Atom Scattering <i>I. E. McCarthy, J. D. Mitroy, A. T. Stelbovics</i>	131
A Dirac R-Matrix Calculation of Electron Scattering from Fe XXIII <i>P. H. Norrington, I. P. Grant</i>	132
Schrodinger-Like Equation for Relativistic Particles <i>I. B. Goldberg</i>	133
Single Channel Relativistic Quantum Defect Relation <i>I. B. Goldberg</i>	134
Relativistic WKB Approximation to Phase-Shifts and Continuum Normalizations <i>I. B. Goldberg, J. Stein, Akiva Ron, R. H. Pratt</i>	135
Generalized Nonrelativistic WKB Approximation with Coulomb Comparison Functions <i>J. Stein, Akiva Ron, I. B. Goldberg, R. H. Pratt</i>	136
New Method for the Interpolation of Dipole Oscillator-Strength Sum Rules <i>James M. Peek</i>	137
Classical Calculation of Electron-Atom Bremsstrahlung <i>Longhuan Kim, R. H. Pratt</i>	138
Double Atomic-Field Bremsstrahlung <i>J. C. Altman, Carroll Quarles</i>	139
Molecular Bremsstrahlung <i>Lee Estep, Carroll Quarles</i>	140
<i>Electron-Atom: Resonances</i>	
The Feshbach Project Operator Method: A study of the $\text{He}^- [1s(2s^2): ^2S]$ Resonance <i>A. Berk, A. K. Bhatia, B. R. Junker, A. Temkin</i>	141
Measurements of the Elastic and Inelastic ($n=2,3$) Differential Cross Sections of Atomic Hydrogen by High Resolution Electron Impact <i>C. D. Warner, G. C. King, P. Hammond, J. Slevin</i>	142
Resonance Widths of the Lithium-Like Ions <i>Brian F. Davis, Kwong T. Chung</i>	143
Scattering of Electrons by Sodium and Potassium Atoms at Low Energies <i>S. M. Kazakov, O. V. Khristoforov</i>	144
Resonances in Metastable Excitation <i>N. J. Mason, W. R. Newell</i>	145
Theoretical Study of Partial Widths and Resonance Normalization <i>D. K. Watson</i>	146
Two-Center Coulomb Wavefunction Description of Two-Electron Atoms <i>James M. Feagin, John S. Briggs, Thomas P. Weissert</i>	147
Correlation Effects in Negative Alkali-Ions <i>Birte Christensen-Dalsgaard</i>	148

Simple Method to Calculate Resonance Widths <i>A. Macías, A. Riera</i>	149
<i>Electron-Atom: General Threshold and Autoionization</i>	
Towards Numerical Solution of the Threshold Ionization Problem <i>Christopher Bottcher</i>	150
Electron Impact Ionization of Hydrogen and Helium Atom <i>K. Roy, P. Mandal, N. C. Sil</i>	151
Electron-Impact Ionization of Hydrogen Atom from 2s-State <i>P. S. Majumdar, Madhumita Basu, A. S. Ghosh</i>	152
Absolute Triple Differential Cross Sections for the Electron Impact Ionization of He and H at 250 eV and 150 eV <i>P. Schlemmer, G. Knoth, H. Ehrhardt, K. Jung</i>	153
Quantal e^- -He Threshold Ionization <i>Derrick S. F. Crothers</i>	154
Study of Helium Doubly Excited States with a Correlated Wave Function Method <i>O. Dulieu, C. Le Sech</i>	155
An Optical Potential Model for Post-Collision Interaction in Ejected Electron Spectra <i>P. J. M van der Burgt, J. van Eck, H. G. M. Heideman, G. Nienhuis</i>	156
Absolute Double Differential Ionization Cross-Section for Electron Impact: He <i>L. Avaldi, R. Camilloni, E. Fainelli, G. Stefani</i>	157
Energy Partitioning in Near-Threshold Excitation and Ionization of Helium by Electron Impact <i>P. Hammond, F. H. Read, S. Cvejanović, G. C. King</i>	158
Ejected Electron Spectra from Autoionizing States of Helium Excited by Electron Impact <i>P. S. K. Moorhead, A. Crowe</i>	159
Excitation of Autoionizing States of Helium in Specific Momentum Transfer Electron Collisions <i>P. S. K. Moorhead, A. Crowe</i>	160
Electron Impact Ionization Cross Section Measurements of the Chlorine, Bromine, and Iodine Atoms <i>Todd R. Hayes, Robert C. Wetzel, Robert S. Freund</i>	161
The d-Shell Autoionization Ejected Electron Spectrum of the Group IB Atoms Cu, Ag and Au, Excited by Electron Impact <i>L. F. Forrest, G. K. James, M. Kurepa, V. Pejcev, K. J. Ross, M. Wilson</i>	162
Formation and Decay of Autoionization States of Sr, Ca and Ba Atoms in Slow Electron-Atom Collisions <i>S. M. Kazakov, O. V. Khristoforov</i>	163
Electron Impact Ionization of Laser Excited Barium Atoms <i>S. Trajmar, J. C. Nickel</i>	164
Production of Excited Ar II- and Ar III-Ions by Proton- and Electron-Impact <i>K.-H. Scharfner, B. Kraus, H.-J. Flaig, K. Reymann</i>	165
Electron Spectroscopy of Multiply Ionizing Electron-Rare Gas Collisions <i>M. A. Chaudhry, A. J. Duncan, R. Hippler, H. Kleinpoppen</i>	166
Partial Cross Sections for Single and Multiple Ionization of Xe Using Crossed Electron-Neutral Beams <i>D. Mathur, C. Badrinathan</i>	167

Single Electron Impact Ionization Cross Sections for Ground State and Metastable Ar^{2+} Ions <i>B. A. Huber, J. Puerta, K. Wiesemann</i>	168
Calculation of Hydrogenic Formfactors <i>Siegfried Jetzke, John T. Broad</i>	169
<i>Electron-Atom: (e,2e) and Post Collision Interactions</i>	
Importance of Higher-Order Effects in Large-Angle Coplanar Symmetric (e,2e) Processes <i>K. S. Baliyan, M. K. Srivastava</i>	170
Triply Differential Cross Sections for the $\text{H}(e,2e)\text{H}^+$ Process <i>A. C. Roy</i>	171
Near-Threshold (e,2e) Measurements in the Equatorial Plane Using a New Apparatus <i>T. J. Jones, S. Cvejanović, G. C. King, F. H. Read</i>	172
The Noncoplanar Symmetric (e,2e) Reaction on the Valence Orbitals of Xenon <i>J. P. D. Cook, I. E. McCarthy, J. D. Mitroy, E. Weigold</i>	173
Post Collision Interaction and the Auger Lineshape <i>A. Russek, W. Mehlhorn</i>	174
Post-Collision Interaction (PCI) in Inner-Shell Ionization of Argon K and Argon L Auger Spectra <i>D. Gräf, W. Hink</i>	175
PCI Effects in (e,e' Auger) and (e,2e) Cross Sections: Ar 2p <i>G. Stefani, L. Avaldi, A. Lahmam-Bennani, A. Duguet</i>	176
The Semiclassical Approximation for (e,2e) Impulsive Reactions: Mathematical Background <i>Yu. V. Popov, L. Avaldi, R. Camilloni, J. Stefani</i>	177
<i>Electron-Atom: Spin-Dependent Processes</i>	
Studies on Asymmetry for Elastic Scattering of Spin-Polarized Electrons by Spin-Polarized Hydrogen Atoms <i>N. S. Rao</i>	178
Asymmetry in Inelastic Scattering of Spin Polarized Electron with Spin Polarized Hydrogen Atom <i>Mini Kapoor, S. Saxena, K. C. Mathur</i>	179
The Three-Body Interaction with Long-Range Forces: Spin-Dependent Electron Hydrogen Collisions <i>A. Vasilakis, M. S. Lubell, K. Rubin, F. C. Tang, J. Slevin, M. Eminyan</i>	180
Spin-Dependent Electron Scattering Phase Shifts in Atomic Hydrogen <i>J. F. Williams</i>	181
Measurement of Spin-Polarized Elastic and Inelastic Differential Scattering of Electrons from Lithium Atoms <i>G. Baum, M. Moede, W. Raith, W. Schröder, U. Sillmen</i>	182
Spin Dependence in Electron Collisions with Sodium <i>P. J. O. Teubner, J. L. Riley, M. J. Brunger</i>	183
Scattering Parameters from Electron-Polarized Photon Coincidence Experiments in Sodium <i>J. L. Riley, P. J. O. Teubner</i>	184
Electron-Atom Collision Studies Using Optically State Selected Beams: Superelastic Scattering <i>J. J. McClelland, M. H. Kelley, R. J. Celotta</i>	185

Spin Polarization and Angular Distribution of MNN Auger Electrons from Krypton and Xenon	186
<i>U. Hahn, J. Semke, J. Kessler, H. Merz</i>	
Impact Excitation of Potassium and Cesium by Polarized Electrons	187
<i>P. Naß, N. Ludwig, E. Reichert</i>	
Polarization of Atomic Line Radiation After Impact Excitation by Polarized Electrons	188
<i>J. Goeke, G. F. Hanne, J. Kessler, M. Tüshaus, A. Wolcke</i>	
Spin Effects by Orientation and Exchange in Elastic Electron Collisions with Heavy Atoms	189
<i>H. Geesmann, G. F. Hanne, F. Kaussen, J. Kessler</i>	
Asymmetry of Polarized Electrons Scattered Inelastically from Mercury Atoms	190
<i>H. Borgmann, J. Goeke, G. F. Hanne, C. Hölscher, J. Kessler, A. Wolcke</i>	
Elastic Scattering of Polarized Electrons from Mercury and Xenon for Complete Evaluation of the Scattering Amplitudes	191
<i>O. Berger, J. Kessler</i>	
Semi-Relativistic Calculations of Elastic Scattering of Electrons from Xe and Hg	192
<i>R. P. McEachran, A. D. Stauffer</i>	
Electron Scattering on Heavy Atoms	193
<i>K. Bartschat, P. G. Burke, N. S. Scott</i>	
Relativistic Effects in Elastic Scattering of Electrons from Heavy Atoms	194
<i>K. Hasenburger, D. Madison, K. Bartschat, K. Blum</i>	
Polarization Phenomena in Electron-Atom Collision Processes	195
<i>Keh-Ning Huang</i>	
On Spin-Polarization of Auger Electrons	196
<i>K. Blum, B. Lohmann, E. Taute</i>	
Electron-Atom: Inelastic — II	
Multichannel Eikonal Theory of Excitation in Electron-Metastable Atom Collisions	197
<i>E. J. Mansky, M. R. Flannery</i>	
A New Approach to Scattering by Multi-Central Interactions	198
<i>D. P. Dewangan, S. B. Khadkikar</i>	
Electron-Impact Excitation from the 2^3S Metastable State of Helium to Higher Electronic States	199
<i>David C. Cartwright, G. Csanak</i>	
Small Angle "Superelastic" $3^2P \rightarrow 3^2S$ (e^- , Na) Scattering in the 10-25 eV Range	200
<i>G. F. Shen, J.-L. Cai, B. Jaduszliwer, B. Bederson</i>	
Electron Impact Excitation of Alkali Atoms	201
<i>C. E. Bielschowsky, H. G. P. Lins de Barros</i>	
Inelastic Electron Scattering from Sodium and Magnesium	202
<i>M. J. Brunger, S. J. Buckman, J. L. Riley, R. Scholten, P. J. O. Teubner</i>	
Excitation of Core in Li	203
<i>S. N. Tiwary</i>	
A Least-Squares Approach to Electron Scattering	204
<i>A. L. Merts, L. A. Collins</i>	
The Excitation of the $3^{1,3}P$ States of Magnesium by Electron Impact	205
<i>G. D. Menezes, C. B. Pagan, L. E. Machado</i>	

Angular Momentum Transfer in Electron-Helium Collisions <i>J. P. M. Beijers, J. van Eck, P. A. Zeijlman van Emmichoven, H. G. M. Heideman</i>	206
Angular Dependence of the Energy Loss Spectra for Argon by Intermediate Energy Electron Impact <i>G. Gerson B. de Souza, Heloisa M. B. Roberty, C. A. Lucas, C. E. Bielschowsky</i>	207
A Stepwise Electron and Laser Excitation Study of the 6^3P_2 Metastable State of Hg <i>C. J. Webb, W. R. MacGillivray, M. C. Standage</i>	208
Study of Electron Impact Excitation of Metastable Mercury States Using Stepwise Electron-Photon Excitation <i>G. F. Hanne, V. Nickich, M. Sohn</i>	209
<i>Electron-Molecule: Electronically Elastic Processes — I</i>	
A Density Functional Approach to Electron-Molecule Resonant Scattering <i>L. Malegat, M. Le Dourneuf, M. Tronc</i>	210
Transitions of Molecules Between High-Angular-Momentum States <i>Isao Shimamura, Amulya C. Roy</i>	211
Electron Scattering from Polyatomic and Diatomic Targets via a Fully <i>Ab Initio</i> Treatment of Interaction <i>F. A. Gianturco, U. T. Lamanna, A. Palma, L. Pantano</i>	212
Effects of Combined Manifestation of Direct and Resonant Interaction in Slow Electron-Molecule Collisions <i>G. K. Ivanov, G. V. Golubkov</i>	213
Scattering of Low Energy Electrons by HCN and CO <i>A. Jain, D. W. Norcross</i>	214
The Interaction of Low Energy Electrons with HCl-Elastic Scattering, Vibrational Excitation, and Anion States <i>A. Jain, D. W. Norcross, S. V. O'Neil, N. T. Padial, P. Rosmus</i>	215
Absolute Elastic Differential Electron Scattering Cross Sections for Carbon Monoxide <i>C. Mott, J. Nickel</i>	216
R-Matrix Method for Vibrational Excitation and Dissociative Attachment <i>P. G. Burke, L. A. Morgan, C. J. Noble</i>	217
The Application of Coherent Renormalized Multicenter Potential Model (CRMPPM) with Intramolecular Multiple Scattering (IMS) to Vibrationally Elastic and Inelastic Electron- H_2 Scattering <i>Lee Mu-Tao, L. F. C. Botelho, L. C. G. Freitas</i>	218
Theoretical Cross Sections for Low-Energy $e-H_2$ Scattering <i>A. N. Feldt, T. L. Gibson, M. A. Morrison, B. C. Saha</i>	219
Scattering of Electrons by Hydrogen Molecule in Independent United Atom Model <i>N. S. Rao, H. S. Desai</i>	220
Vibrational and Ro-Vibrational Differential Cross Sections for Electron Scattering from H_2 <i>J. E. Furst, M. Mahgerefteh, D. E. Golden</i>	221
<i>Ab Initio</i> Polarization Potentials for e^- -Molecule Scattering <i>E. Ficocelli Varracchio, U. T. Lamanna</i>	222
Low-Energy Scattering of Electrons from Li_2 <i>N. T. Padial</i>	223

Electron Elastic Cross Sections Measurements for O ₂ at Intermediate Energy (300-1000 eV) Range	224
<i>Ione Iga, Lee Mu-Tao, J. C. Nogueira, R. S. Barbieri, Maria Cristina A. Lopes</i>	
Inclusion of Exchange in the Non-Iterative PDE Method: Application to e-N ₂ Scattering	225
<i>C. A. Weatherford, K. Onda, A. Temkin</i>	
Experimental Measurements of Shape Resonances Using a Position Sensitive Detector	226
<i>Fred Currell, Tim Reddish, John Comer</i>	
Vibrational Excitation of N ₂ by Electron Impact	227
<i>S. Yagi, T. Takayanagi, K. Wakiya, H. Suzuki, Y. Fujita, K. Hoshiba, S. S. Kano, H. Takuma</i>	
Observation of Vibrational Excitation of F ₂ by Electron Impact	228
<i>Y. Fujita, K. Hoshiba, S. S. Kano, H. Takuma, S. Yagi, T. Takayanagi, K. Wakiya, H. Suzuki</i>	
Electron-Molecule: Electronically Elastic Processes — II	
Electron Attachment to H ₂ O, SO ₂ and C ₃ F ₈ in Ar, N ₂ , and CH ₄	229
<i>W. C. Wang, M. A. Fineman, L. C. Lee</i>	
Total Cross Section Measurements for Electron Scattering by OCS and SO ₂	230
<i>M. S. Dababneh, Y.-F. Hsieh, W. E. Kauppila, C. K. Kwan, T. S. Stein</i>	
Scattering of High Energy Electrons from Molecules	231
<i>Mukesh Kumar, A. N. Tripathi, V. H. Smith, Jr.</i>	
Vibrational Effects on Electron-Molecule Scattering for Polyatomics: H ₂ O	232
<i>Martin Breitenstein, Richard J. Mawhorter, Hermann Meyer, Armin Schweig</i>	
Low-Energy Electron Scattering on Methane	233
<i>J. Ferch, B. Granitza, W. Raith</i>	
Rotational and Rovibrational Excitation of CH ₄ by Electron Impact between 0.5 eV and 10 eV	234
<i>R. Müller, K. Jung, H. Ehrhardt</i>	
Multichannel Schwinger Variational Calculations of Low-Energy Electron-Molecule Collisions	235
<i>Marco A. P. Lima, Thomas L. Gibson, Winifred Huo, Vincent McKoy</i>	
Ramsauer-Townsend Effect in Electron-SiH ₄ Elastic Scattering	236
<i>A. Jain, D. G. Thompson</i>	
Elastic Differential Scattering and Vibrational Excitation of C ₂ H ₆ by Low Energy Electrons	237
<i>H. Tanaka, L. Boesten</i>	
Temporary Negative Ions in Complex Molecules: Dibenzene Chromium	238
<i>P. D. Burrow, A. Modelli, M. Guerra, K. D. Jordan</i>	
Shape Resonances Associated with the Bonding of the Hydrogen Atom with First Row Atoms in Simple Molecules	239
<i>M. Tronc, L. Malegat, M. Ben Arfo</i>	
e ⁻ -O ₃ Collisions at Low Energies	240
<i>K. N. Joshipura, H. S. Desai</i>	
Electron-Molecule: Electronic Excitation and Ionization — I	
A Linear Algebraic Approach to Electronic Excitation of Atoms and Molecules by Electron Impact	241
<i>B. I. Schneider, L. A. Collins</i>	

Electronic Excitation of Diatomic Molecules by Electron Impact <i>K. L. Baluja, P. G. Burke, C. J. Noble, J. Tennyson</i>	242
Inelastic Scattering of Electrons by Hydrogen Molecule <i>N. S. Rao</i>	243
The Lowest $^1\Sigma_u^+$ Autoionizing State of H_2 <i>S. Hara, H. Sato</i>	244
The Electron Momentum Spectroscopy of H_2 <i>M. A. Coplan, A. D. Smith, D. J. Chornay, J. H. Moore, J. A. Tossell, V. H. Smith, Jr., J. W. Liu</i>	245
Rotationally Resolved Electron-Photon Coincidence Study of the H_2 ($d^3\Pi_u$) Excitation <i>J. W. McConkey, S. Trajmar, J. C. Nickel, G. Csanak</i>	246
Elastic and Inelastic Electron Scattering Cross Sections for H_2 <i>M. Khakoo, S. Trajmar</i>	247
Recent Advances in Electron Impact Emission Experiments of H_2 , He, N_2 and Ar <i>J. M. Ajello, D. E. Shemansky</i>	248
Electron Impact Excitation of N_2 In the Near Threshold Region <i>T. Antoni, S. Trajmar, D. C. Cartwright</i>	249
Rotationally-Resolved Ionization of N_2 by Electron Impact <i>P. W. Zetner, W. B. Westerveld, J. W. McConkey</i>	250
Partial Generalized Oscillator Strength for Ionization of the Nitrogen Molecule by 1-keV Electron Impact <i>K. Kuroki, F. Nishimura, N. Oda, T. Ichimori</i>	251
Generalized Oscillator Strength for the $X^1\Sigma_g^+ \rightarrow a^1\Pi_g$ Transition in Molecular Nitrogen at 1 keV Incident Electron Energy <i>G. G. B. de Souza, C. A. Lucas</i>	252
Low-Lying Resonances in Electron-Lithium Molecule Scattering <i>H. H. Michels, R. H. Hobbs, L. A. Wright</i>	253
Observation of $f^3\Pi_g$ of F_2 Molecule by Electron Energy Loss Spectroscopy <i>K. Hoshiba, Y. Fujita, S. S. Kano, H. Takuma, T. Takayanagi, S. Yagi, K. Wakiya, H. Suzuki</i>	254
Low Energy Electron-CH Molecule Collisions <i>V. M. Chhaya</i>	255
Electron Momentum Spectroscopy of Chlorine <i>C. E. Brion, L. Frost, E. Weigold</i>	256
Low Energy Electron-Impact Excitation of HF <i>S. Cvejanović, J. Jureta</i>	257
Electron Energy-Loss Studies Using a Multidetector Spectrometer: The Spectrum of Cl_2 <i>Richard J. Stubbs, Trevor A. York, John Comer</i>	258
An Electron Energy-Loss Investigation of Free Radicals <i>Richard J. Stubbs, Trevor A. York, John Comer</i>	259
Electron-Molecule: Electronic Excitation and Ionization — II	
Threshold Excitation of N_2O <i>D. Cubrić, J. Jureta, S. Cvejanović, D. Cvejanović, P. Hammond, G. C. King, F. H. Read</i>	260

Momentum Distributions and Binding Energies of H ₂ O and NH ₃ by High Momentum Resolution Binary (e,2e) Spectroscopy <i>A. O. Bawagan, R. Müller-Fiedler, K. T. Leung, C. E. Brion</i>	261
Inner-Shell Electron Energy Loss Spectroscopy of PCl ₃ and SO ₂ <i>C. E. Brion, R. N. S. Sodhi, K. H. Sze</i>	262
Electron Energy Loss Spectroscopy of NH ₃ in the 5.5-11 eV Energy Range <i>D. Roy, M. Furlan, M.-J. Hubin-Franskin, J. Delwiche, J. E. Collin</i>	263
Small-Angle, Intermediate Energy (1.0 keV) Electron Energy Loss Spectra of Ethylene <i>Ana C. A. e Souza, G. Gerson B. de Souza</i>	264
Electron Momentum Spectroscopy of Chloromethanes <i>A. M. Grisogono, W. von Niessen, E. Weigold</i>	265
Partial and Total Electron Impact Ionization Cross Sections from Threshold up to 180 eV <i>K. Leiter, T. D. Märk</i>	266
Electron Impact Spectroscopy of Silane and Germane <i>David Spence, R.-G. Wang, M. A. Dillon</i>	267
(e,2e) Spectroscopy of Silicon Compounds: Ionization Potentials and Electron Momentum Distributions for Valence Shell Orbitals of SiF ₄ <i>R. Fantoni, A. Giardini-Guidoni, R. Tiribelli, R. Cambi, M. Rosi, F. Tarantelli</i>	268
Inner-Shell Spectra of Benzene, Pyridine and Cyclohexane Studied by keV Electron Impact <i>A. P. Hitchcock, D. C. Newbury, A. L. Johnson, J. A. Horsley, J. Stöhr</i>	269
Molecular Geometry from K-Shell Resonances in Inelastic Electron Scattering Spectra <i>A. P. Hitchcock, J. Stöhr</i>	270
The Study of Electric Dipole Forbidden Inner Shell Transitions by Electron Impact Excitation <i>I. Harrison, G. C. King</i>	271
<i>Electron-Molecule: Dissociation</i>	
Cross Sections for H ⁻ and Cl ⁻ Production from HCl by Dissociative Electron Attachment <i>O. J. Orient, S. K. Srivastava</i>	272
Ionization and Dissociative Ionization of CO, CO ₂ and CH ₄ by Electron Impact <i>O. J. Orient, S. K. Srivastava</i>	273
Electron Impact Ionization and Dissociative Ionization of Ammonia <i>O. J. Orient, S. K. Srivastava</i>	274
Dissociative Attachment of Electrons by Excited Intermediates of Resonant Multiphoton Ionization Processes <i>Y. Ono, H. T. Liou, J. T. Moseley</i>	275
Absolute Measurement of the Photoemission Cross Section for Lyman- α Radiation Produced in e ⁻ + H ₂ Collisions <i>R. C. G. Lichtenberg, Armon McPherson, N. Rouze, W. B. Westerveld, J. S. Risley</i>	276
Angular Intensity Distribution of Balmer- α and Lyman- α Emission Excited by Electron Impact on H ₂ <i>S. Arai, M. Morita, K. Hironaka, N. Kouchi, N. Oda, Y. Hatano</i>	277
Angular Distribution of Fragments from Dissociative Electron Attachment <i>Andrew U. Hazi</i>	278
Angular Difference Doppler Profiles: Dynamics of Formation of H [*] in Electron-H ₂ Collisions <i>Teiichi Ogawa, Keiji Nakajima, Hirofumi Kawazumi</i>	279

An <i>Ab-Initio</i> Study of the Dissociative Attachment to H ₂ of Electrons at Energies 6 eV to 12 eV	280
<i>S. Bhattacharyya, L. Chatterjee, K. Basuchoudhury</i>	
Dissociative Electron Attachment to Molecular Lithium	281
<i>J. M. Wadehra, H. H. Michels</i>	
VUV Fluorescence Produced by Dissociative Electron-Impact Excitation of SF ₆	282
<i>J. L. Forand, K. Becker, J. W. McConkey</i>	
Observations and Cross Sections for Electron Attachment in Molecules at Ultralow Electron Energies	283
<i>A. Chutjian, S. H. Alajajian</i>	
Photoenhanced Electron Attachment in C ₂ H ₃ Cl and C ₃ F ₃ H at 193 nm	284
<i>M. J. Rossi, H. Helm, D. C. Lorents</i>	
<i>Electron-Ion: Elastic, Inelastic, Ionizing</i>	
Electron Scattering by Excited Hydrogenic Ions Using an Optical Potential Approach	285
<i>D. H. Oza, J. Callaway</i>	
P-Wave Phase Shifts and Resonances for Electron Scattering by He ⁺	286
<i>D. H. Oza</i>	
Electron Impact Excitation of Optically Allowed Transitions in C-Like Ions	287
<i>K. M. Aggarwal</i>	
Collision Strengths for the Forbidden Transitions Among the Ground-State Configuration of S III	288
<i>Y. K. Ho, Ronald J. W. Henry</i>	
Differential Electron Scattering Cross Sections for the 3s ² S _{1,2} → 3p ² P _{1,2,3,2} Transitions in Mg II: Comparison of Experiment and Theory	289
<i>I. D. Williams, A. Chutjian, A. Z. Msezane, R. J. W. Henry</i>	
Electron Impact Excitation of the 5p ² P and 5s ² ² D States in Cd II	290
<i>Alfred Z. Msezane, Ronald J. W. Henry</i>	
Innershell Excitation of Ti ³⁺ by Electron Impact: Effects of Target Wave Functions and Coupling	291
<i>A. Z. Msezane, Ronald J. W. Henry</i>	
Distorted-Wave-Method Calculation of Electron-Impact Excitation of Atomic Ions	292
<i>Yukikazu Itikawa, Kazuhiro Sakimoto</i>	
Excitation of Doubly Excited Autoionization States in Ions	293
<i>Rajesh Srivastava, A. K. Katiyar</i>	
Collision Strengths for C II	294
<i>K. A. Jerjian, R. J. W. Henry</i>	
Electron Impact Collision Strengths for the Fine Structure Transitions in Fe XII	295
<i>S. S. Tayal, Ronald J. W. Henry</i>	
Collision Strengths for Fine Structure Transitions in Ne II and Mg IV	296
<i>A. E. Kingston, C. T. Johnson</i>	
Electron Impact Excitation of O ⁺	297
<i>B. M. McLaughlin, A. E. Kingston</i>	
Electron Impact Excitation-Autoionization of Lithium-Like Ions	298
<i>P. Defrance, S. Rachafi, S. Chantrenne</i>	
Electron Impact Ionization of Ne ⁷⁺	299
<i>S. Chantrenne, P. Defrance, S. Rachafi, D. Belić, F. Brouillard</i>	

Ionization of Ti^+ , Ti^{2+} , and Ar^{2+} by Electron Impact <i>M. J. Diserens, M. F. A. Harrison, A. C. H. Smith</i>	300
Single and Multiple Ionization of Multiply Charged Ions by Electron Impact <i>A. Müller, K. Tinschert, Ch. Achenbach, E. Salzborn, R. Becker, M. S. Pindzola</i>	301
Electron Impact Excitation of Kr^{+28} <i>A. Z. Msezane, J. Lee, R. J. W. Henry, K. J. Reed</i>	302
Measurements of Cross Section for Single and Double Ionization for Na^+ , K^+ and Ba^+ <i>T. Hirayama, K. Oda, Y. Morikawa, T. Ono, Y. Ikezaki, S. Kobayashi, T. Takayanagi, K. Wakiya, H. Suzuki</i>	303
Distorted Wave Cross Sections for Electron-Impact Ionization of the Lithium-Like Ions <i>R. I. Câmpeanu, L. Nagy</i>	304
The Atomic Databank at Belfast and Daresbury <i>K. M. Aggarwal, K. A. Berrington</i>	305
<i>Electron-Ion: Recombination</i>	
Dielectronic Recombination Measurements of P^{4+} , S^{5+} , and Cl^{6+} <i>P. F. Dittner, S. Datz, P. D. Miller, P. L. Pepmiller</i>	306
Final Rydberg State Distribution from Dielectronic Recombination <i>D. Mueller, A. Müller, C. Timmer, D. S. Belić, B. D. DePaola, N. Djurić, G. H. Dunn</i>	307
Theoretical Calculations of Electric Field Effects on Dielectronic Recombination by Matrix Diagonalization <i>D. C. Griffin, M. S. Pindzola, C. Bottcher</i>	308
Dielectronic Recombination of Mg^+ <i>A. P. Hickman</i>	309
Angular Dependence of Dielectronic Recombination Cross Sections <i>K. J. LaGattuta</i>	310
Dielectronic Recombination Satellite Structure of Lithium-Like Ions <i>L. J. Roszman, A. W. Weiss</i>	311
Diabatic States of the H_2 Molecule for the Description of $H_2^+ + e$, $H^- + H^+$, and $H(1s) + H(nl)$ Collisions <i>P. Quadrelli, K. Dressler</i>	312
The Determination of Internal Energies of Molecular Ions from Electron Impact Dissociation Measurements <i>J. B. A. Mitchell, H. Hus, R. Janssen</i>	313
The Population Distributions Among the Excited Levels of Hydrogen-Like Ions in Thermal Plasmas <i>R. J. Hutcheon, N. N. Ljepojevic, S. Volonté, R. W. P. McWhirter</i>	314
Electron-Ion Recombination Studies of Cadmium <i>R. K. Thareja, A. Khare</i>	315
Dissociative Recombination of H_2^+ by Collisions with Slow Electrons <i>Hidekazu Takagi, Hiroki Nakamura</i>	316
<i>Positron-Atom, Positron-Molecule Collisions</i>	
Application of Schwinger-Type Variational Methods to the Collisions of Positrons with Atoms and Molecules: An L^2 -Formalism <i>M. A. Abdel-Raouf</i>	317
The Theory of the Collisions of Positrons with Alkali-Atoms and Alkali-Like Ions <i>M. A. Abdel-Raouf</i>	318

New Theory of the Annihilation Parameter for e^+ -Atom(Molecule) Systems <i>E. Ficocelli Varracchio</i>	319
Positronium Formation in d-Wave Positron-Hydrogen Scattering <i>C. J. Brown, J. W. Humberston</i>	320
Electron Capture by Intermediate Energy Positrons from Alkali Atoms <i>J. M. Wadehra, Sultana N. Nahar</i>	321
Positron- and Electron-Alkali (Sodium and Potassium) Total Cross Section Measurements <i>T. S. Stein, C. K. Kwan, R. D. Gomez, Y.-F. Hsieh, W. E. Kauppila, Y. J. Wan</i>	322
Positronium Formation in Low-Energy Positron- H^- Collisions <i>Richard J. Drachman</i>	323
Partial Cross Sections for Positron Scattering from Helium <i>L. M. Diana, D. L. Brooks, S. C. Sharma, P. G. Coleman, P. K. Pendleton, B. E. Seay, L. S. Fornari</i>	324
Ionization of Helium by Positron Impact <i>D. Fromme, W. Raith, G. Sinapius</i>	325
Positron Excitation of the 2^1P State of Helium <i>R. P. McEachran, L. A. Parcell, A. D. Stauffer</i>	326
A Reliable Calculation for 2^1S Excitation of Helium Atom by Positron Impact <i>Rajesh Srivastava, Mukesh Kumar, A. N. Tripathi</i>	327
Intermediate Energy Positron (Electron)-Argon Differential Elastic Scattering Cross Section Measurements <i>W. E. Kauppila, G. M. A. Hyder, M. S. Dababneh, Y.-F. Hsieh, C. K. Kwan, T. S. Stein</i>	328
Computation of Momentum Transfer and Annihilation Cross-Section of Positrons in Noble Gases <i>A. S. Ghosh, P. S. Grover, K. V. Sinha</i>	329
A Calculation of the Lowest Partial Wave in Low Energy Positron Hydrogen Molecule Scattering <i>E. A. G. Armour</i>	330
A Calculation of the Lowest Σ_u^+ Partial Wave in Low Energy Positron Hydrogen Molecule Scattering <i>E. A. G. Armour, D. J. Baker</i>	331
Positron and Electron Total Cross-Section Measurements for Molecular Oxygen <i>C. K. Kwan, Y.-F. Hsieh, W. E. Kauppila, Steven J. Smith, T. S. Stein</i>	332
Positron Scattering by Nitrogen Molecule <i>N. Bhattacharya, D. N. Tripathi</i>	333
Exotic Collisions	
A Hyperspherical Study of the Positronium Negative Ion <i>J. Botero, C. H. Greene</i>	334
Collisions of e^+ with Ps^+ <i>M. A. Abdel-Raouf</i>	335
Accurate Calculations of the Bound-States of the Positronium Ions and Molecules <i>M. A. Abdel-Raouf</i>	336
Autoionization States of the Positronium Molecules <i>M. A. Abdel-Raouf</i>	337

Orthopositronium Localization in Gases by Density Fluctuation Scattering <i>C. V. Heer</i>	338
Interactions of Positronium with CH ₄ and C ₂ H ₆ Molecules <i>Suresh C. Sharma, Michael H. Ward, Charles A. Dark, Eric M. Juengerman</i>	339
Classical Trajectory Monte Carlo Calculation for $\mu^+ + (\mu^-p) \rightarrow (\mu^+\mu^-) + p$ and $e^+ + (e^-p) \rightarrow (e^+e^-) + p$ <i>K. Nakanishi, T. Watanabe, A. Ohsaki, K. Iguchi</i>	340
Quantum Mechanical Study for the Process of $\mu^+ + (\mu^-p) \rightarrow (\mu^+\mu^-) + p$ <i>Q. Ma, X. Cheng, Z. Liu, Y. Liu, T. Watanabe</i>	341
Ratio of the Cross-Section for Lepton and Anti-Lepton Scattering from Hydrogen Atom A Field Theoretic Approach <i>Sujata Bhattacharyya, Lali Chatterjee, Keka Basuchoudhury</i>	342
Auger Formation of (P μ d) ⁺ Muo-Molecular Ion <i>L. Chatterjee, S. Bhattacharyya</i>	343
Reactions of Positive Muon Molecular Ions in the Gas Phase <i>I. D. Reid, M. Senba, D. J. Arseneau, D. M. Garner, D. G. Fleming</i>	344
Dynamics of Muon Spin Polarization During Cyclic Charge Exchange in Noble Gases <i>M. Senba, R. E. Turner, I. D. Reid, D. M. Garner, D. J. Arseneau, D. G. Fleming</i>	345
Temperature Dependence of Muonium Spin Exchange with O ₂ <i>M. Senba, I. D. Reid, D. M. Garner, D. J. Arseneau, D. G. Fleming</i>	346
Pionium in Quantum Electrodynamics <i>A. Karimkhodzhaev, Z. Marich, R. N. Faustov</i>	347
Atom-Atom: General	
Total Scattering Cross-Sections and Interatomic Potentials for Neutral Hydrogen and Helium on Some Noble Gases <i>David N. Ruzic, Samuel A. Cohen</i>	348
Bound States of Composite Particles Using Quantum Field Theory <i>D. N. Tripathi</i>	349
Atomic Beam Scattering with Magnetic Analysis, and the Structure of Rare Gas Oxides and Fluorides <i>F. Aquilanti, E. Luzzatti, F. Pirani, G. G. Volpi</i>	350
Radiative Recombination of Kr, I ₂ (³ P ₁) Excimers <i>H. Schmoranz, P. Wollenweber, K. Barzen</i>	351
The Collisional Relaxation of Excited-State Zeeman Coherences in Atomic Ytterbium Vapor <i>A. G. Yodh, J. Golub, I. W. Mossberg</i>	352
Scattering of Oriented Ne ⁺ Atoms in One (J=2, M _J =2) State <i>Ch. Bender, W. Bever, H. Haberland, D. Hausmann, H. P. Ludescher</i>	353
The Influence of the Collisions of Metastable Atoms on the Optogalvanic Effect <i>He Maoqi, Wang Guoyi, Wang Zhaoyong</i>	354
Na ⁺ -Noble Gas Differential Cross Sections <i>M. O'Callaghan, A. Gallagher</i>	355
Final State Distribution for Na(3P ₁) + Na(3P ₁) → Na(nl ₁) + Na(3S _{1/2}) <i>S. A. Davidson, J. F. Kelly, A. Gallagher</i>	356
Collisional Transitions Between Atomic States. Interaction via Rydberg Continuum <i>G. K. Ivanov, G. V. Golubkov</i>	357

Two Electron Model Calculations of Li(2s-2p) and Na(3s-3p) Excitation in Li-Na High Energy Collisions	358
<i>Svend Erik Nielsen, Martin Larsen, John S. Dahler</i>	
Excitation and Deexcitation of Oriented Atoms in Energetic Collisions: The Role of the Massey Parameter	359
<i>Nils Andersen, Svend Erik Nielsen</i>	
H(2s) Formation in Non-Adiabatic Ground State Hydrogen Atom Collisions	360
<i>B. M. McLaughlin, K. L. Bell</i>	
Lyman-Alpha Emission from Low-Energy H Collisions with Rare-Gas Atoms	361
<i>B. Van Zyl, M. W. Gealy, H. Neumann</i>	
Atom-Atom: Ionization — General	
Electron-Spin Spectroscopy in Penning Ionization with He(2 ³ S) Metastable Atoms	362
<i>L. G. Gray, R. S. Keiffer, J. M. Ratliff, F. B. Dunning, G. K. Walters</i>	
Rare Gas Metastable-Metastable Model Potentials and Associated Penning Ionization Cross Sections	363
<i>David Hudson</i>	
The Angular Distribution of Penning Electrons: Strong Dependence on the Electron Energy For He(2 ¹ S) + Ar, Kr, Xe	364
<i>Alfred Hertzner, Harald Morgner, Klaus Roth, Günther Zimmermann</i>	
Penning Ionization Cross Sections for Collisions of He(2 ^{1,3} S) with Alkali Atoms: Comparison of Theory and Experiment	365
<i>K. F. Scheibner, J. S. Cohen, R. L. Martin, N. F. Lane</i>	
Ionization of Neon in Collisions with He [*] (2 ³ S)	366
<i>Toshio Tsuboi, Keith T. Gillen</i>	
Laser-Assisted Ionization on He(2 ¹ S, 2 ³ S) + He(1 ¹ S) Collision System	367
<i>P. Pradel, P. Monchicourt, D. Dubreuil, J. Heuzé, J. J. Laucagne, G. Spiess</i>	
Electron Spectrometric Study of Ionizing Thermal Energy Collisions of Ne(4s, 4p, 4d) Atoms with Ar Atoms	368
<i>T. Bregel, W. Bußert, J. Ganz, K. Harth, M. Raab, M.-W. Ruf, H. Hotop</i>	
Ion-Pair Production in Collisions of Na with Cl and Br	369
<i>R. H. Nevnaber, S. Y. Tang, D. P. Wang</i>	
Ion-Pair Production and the Effect of Laser Excitation in Na-Na Collisions	370
<i>S. Y. Tang, D. P. Wang, R. H. Nevnaber</i>	
Ion Pair Formation by the Collisional Reaction Rb(nl) + Rb(5s) → Rb ⁺ + Rb	371
<i>M. Cheret, L. Barbier, M. Djerad</i>	
A Correlated Orbital Method for Model Potential Calculations of the Excited States of Na ₂ Up to the Na(3p) + Na(3p) Dissociation Limit	372
<i>A. Henriot, F. Masnou-Sceux, C. Le Sech</i>	
Atom-Atom: Associative and Chemi-Ionization	
Homonuclear Associative Ionization in Collisions Between He(5 ³ P) and He(1 ¹ S) Atoms	373
<i>S. Rung, A. Pesnelle, M. Perdrix, G. Watel, J. S. Cohen</i>	
Velocity Dependence of Associative and Dissociative Ionization of Rare Gas Atoms and Simple Molecules by He 2 ³ S Atoms	374
<i>P. A. Jerram, A. C. H. Smith</i>	
Velocity Dependence of Chemi-Ionization of Rare Gas Atoms and Simple Molecules	375
<i>P. A. Jerram, A. C. H. Smith</i>	

Associative Ionization in Thermal Energy Collisions of He(2 ³ S) Atoms with Hydrogen Atoms	376
<i>H. Waibel, W. Bußert, M.-W. Ruf, H. Hotop</i>	
A New Look at Associative Ionization between Two Excited Alkali Atoms: Na(3P) + Na(3P) and Na(4D) + Na(4D) → Na ₂ ⁺ + e ⁻	377
<i>E. Meyer, H. Schmidt, R. Witte, I. V. Hertel</i>	
Polarization Dependence of Associative Ionization in Na(3p) + Na(3p) Collisions	378
<i>Harro A. J. Meijer, Herko P. v. d. Meulen, Henk G. M. Heideman, Gerard Nienhuis, Reinhard Morgenstern</i>	
Polarization Dependence of Associative Ionization and of Laser-Induced Chemi-Ionization and Excitation Transfer	379
<i>Dumont M. Jones, John S. Dahler</i>	
<i>Ion-Atom: General</i>	
Excitation of Helium by H ⁺ and H Impact: A Distorted Wave Approach	380
<i>Indira Khurana, Rajesh Srivastava, A. N. Tripathi</i>	
Proton-Hydrogen Excitation at High and Intermediate Energies	381
<i>Carlos O. Reinhold, Jorge E. Miraglia</i>	
Differential Cross Sections for the Excitation of Atomic Hydrogen by Lithium Ions at Intermediate Energy	382
<i>J. L. Peacher, G. Bhattacharya</i>	
The Search for the 2p ² 3P ^e State of the H ⁻ Ion	383
<i>A. van Wijngaarden, J. Patel, K. Becker, G. W. F. Drake</i>	
The Excitation of Sodium Atoms by Proton Impact	384
<i>O. Schöller, J. S. Briggs</i>	
Excitation of the Na(3d) Level by H ⁻ , H ⁺ , H ₂ ⁺ , or H ₃ ⁺ Ions	385
<i>L. W. Anderson, James S. Allen, Chun C. Lin, R. E. Miers</i>	
Inelastic Differential Scattering Cross Sections for Exciting 30, 66.7, and 150 keV Mg ⁺ in Collisions with He: Mg ⁺ (3s) + He → Mg ⁺ (3p) + He and Mg ⁺ (3d or 4s) + He	386
<i>E. Redd, D. M. Blankenship, D. G. Seely, T. J. Gay, J. L. Peacher, J. T. Park</i>	
Orbital and Spin Angular Momentum Analysis of the Products of He ⁺ + Ne Inelastic Collisions	387
<i>J. Grosser, R. Hasse, H.-P. Neitzke, H. Pfeiffer</i>	
Optical Model Theory of Elastic H ⁺ -H and H ⁺ -He Scattering at Intermediate Velocities	388
<i>R. M. Potvliege, C. J. Joachain, F. Furtado</i>	
Ab Initio Calculation of Potential Curves for the Ground and Excited States of C ₂ and C ₂ ⁺	389
<i>Cui Zuolin, Pan Shoufu</i>	
Semiclassical Calculation of Wave-Functions in n Dimensions	390
<i>J. B. Delos, S. K. Knudson, D. W. Noid</i>	
<i>Ion-Atom: Resonant Transfer and Excitation</i>	
Simultaneous Transfer-Excitation in High Energy Ion-Atom Collisions	391
<i>D. McLaughlin, Y. Hahn</i>	
Transfer and Excitation to the L-Shell: Theoretical State Selected Cross Sections	392
<i>Tricia M. Reeves, James M. Feagin, Eugen Merzbacher</i>	
L-Shell Resonant-Transfer-and-Excitation for La ⁴⁰⁺ + H ₂ Collisions	393
<i>M. W. Clark, E. M. Bernstein, J. A. Tanis, K. H. Berkner, P. Gohil, W. G. Graham, R. H. McFarland, T. J. Morgan, A. Müller, A. S. Schlachter, J. W. Stearns, M. P. Stockli</i>	

Correlated and Uncorrelated Electron Capture and K-Shell Excitation in $S^{13+} + He$ Collisions	394
<i>J. A. Tanis, E. M. Bernstein, M. W. Clark, W. G. Graham, R. H. McFarland, T. J. Morgan, B. M. Johnson, K. W. Jones, M. Meron</i>	
Correlations Between Charge Changing Events and K X-Ray Emission in $Ca^{4+} + H_2$ Collisions	395
<i>E. M. Bernstein, J. A. Tanis, K. H. Berkner, M. W. Clark, W. G. Graham, R. H. McFarland, T. J. Morgan, A. Müller, A. S. Schlachter, J. W. Stearns</i>	
Structure in High Energy, Multiply-Charged Ion-Atom Electron-Capture Cross Sections	396
<i>W. G. Graham, J. A. Tanis, E. M. Bernstein, M. Clark, R. H. McFarland, T. J. Morgan, K. H. Berkner, A. S. Schlachter, J. W. Stearns, A. Müller</i>	
Capture, RTE- and NTE-Processes into Highly-Charged 3.6 MeV/u Sm^{4+} Projectiles	397
<i>W. A. Schönfeldt, P. H. Mokler, D. H. H. Hoffmann, A. Warczak</i>	
<i>Ion-Atom: Direct Excitation and Ionization</i>	
Excitation and Ionization in $Si^{11+} + He$ Collisions	398
<i>M. Clark, J. Anthony, J. K. Swenson, S. M. Shafroth</i>	
Target-Thickness Dependence of the Au L X-Ray Yields Produced by 2.5 MeV/amu Sulphur Ions	399
<i>A. Berinde, C. Ciortea, Al. Enulescu, Daniela Flueraşu, I. Piticu, V. Zoran</i>	
L-Subshell Vacancy Production and Multiple Ionization Effects in $S + Au$ Collisions	400
<i>A. Berinde, C. Ciortea, Al. Enulescu, Daniela Flueraşu, I. Piticu, V. Zoran</i>	
Projectile Dependence of Au Ionization at 0.5 and 1 MeV/amu	401
<i>A. Berinde, C. Ciortea, Al. Enulescu, Daniela Flueraşu, I. Piticu, V. Zoran</i>	
Compilation and Analysis of K-Shell X-Ray Production by Hydrogen and Helium Ions in Elements from Beryllium to Uranium	402
<i>G. Lapicki</i>	
<i>Ion-Atom: Ionization</i>	
Characteristic Features of Ejected Electron Spectra for 5-25 keV He^+ Impact on Neon	403
<i>N. Tokoro, N. Oda, T. Ichimori</i>	
Electron Emission in Collisions of C^+ Ions with Atomic and Molecular Targets	404
<i>L. H. Toburen</i>	
Ionization and Charge Transfer in Collisions of H^+ and He^{2+} Ions with Li Atoms	405
<i>M. B. Shah, D. S. Elliott, H. B. Gilbody</i>	
Cross Sections for Ionization and Electron Transfer for 5-300 keV/u He^{2+} Ions in Gases	406
<i>Akio Itoh, M. E. Rudd, T. V. Goffe</i>	
Ionization of Rare Gas Atoms in 1.05 MeV/amu Fully Stripped Ion Impact	407
<i>H. Shibata, S. H. Be, T. Tonuma, H. Kumagai, M. Kase, T. Kambara, I. Kohno, H. Tawara</i>	
Electron Ejection in $He^+ - He$ Collisions: Experiment and Theory	408
<i>R. D. DuBois, S. T. Manson</i>	
Impact Parameter Dependent Emission of Electrons in Ion-Atom Collisions	409
<i>G. Schiwietz, T. J. M. Zouros, U. Stettner, N. Stolterfoht</i>	
Electron Ejection in Ion-Atom Collisions: Bethe-Born Theory for Structured Incident Ions	410
<i>Steven T. Manson, John H. Miller</i>	
Calculations of Electron Energy Distribution Ejected in Ion-Atom Collisions by Pseudostate Method	411
<i>Takeshi Mukoyama, Chii-Dong Lin, Wolfgang Fritsch</i>	

Molecular-State Close-Coupling Theory Including Continuum States: III. Detailed Continuum Scattering Amplitudes <i>W. R. Thorson, G. Bandarage</i>	412
<i>Ion-Atom: Autoionization</i>	
Autoionization Resonance Profiles in Electron Emission Spectra of Helium Produced by Fast Ions <i>A. L. Godunov, V. S. Senashenko</i>	413
He ⁺⁺ Excitation by Li ⁺ Impact: A Coincidence Investigation <i>P. van der Straten, P. M. Koenraad, R. Morgenstern</i>	414
An Experimental Investigation of the Metastable States of Beryllium Anions <i>T. J. Kvale, G. D. Alton, R. N. Compton, D. J. Pegg, J. S. Thompson</i>	415
Calculation of Probability of Autoionization in Doubly Excited He and Li ⁺ <i>J. P. Mohanty, C. S. Singh, D. K. Rai</i>	416
Cross Sections for Electron Autoionization in Low Energy Li ⁺ -Ne Collisions <i>Y. Ikezaki, M. Katano, H. Ono, T. Takayanagi, K. Wakiya, H. Suzuki</i>	417
Special Features Occurring in Double Differential Cross Sections for Transfer Ionization Collisions <i>A. Niehaus, A. G. Kuiper</i>	418
<i>Ion-Atom: Electron Detachment</i>	
Further Development of the Dynamical Complex Potential Theory of Electron Detachment <i>M. L. Du, S. E. Haywood, J. B. Delos</i>	419
Collisional Electron Detachment of Alkali Anions <i>D. Scott, M. S. Huq, R. L. Champion, L. D. Doverspike</i>	420
Theory of Electron Detachment in Slow Negative Ions Impact on Atoms, Application to H ⁻ + He → H + He + e <i>Fumihiko Koike</i>	421
Electron Detachment of H ⁻ in the Laboratory Forward Direction <i>M. G. Menendez, C. R. Mauldin, M. M. Duncan, J. L. Hopkins</i>	422
Process Selective Experiments: The Double Electron Loss of H ⁻ in Collisions with He <i>M. M. Duncan, M. G. Menendez, J. L. Hopkins, C. R. Mauldin</i>	423
<i>Ion-Atom: Quasimolecular Collisions</i>	
United Atom Rotational Coupling in H ⁺ + He Collisions <i>Chiiling Wang, Joseph Macek</i>	424
Production and Decay of 2p Vacancies in Low-Energy Ar Ions Stopping in Mg <i>Sam J. Cipolla, Larry Hicks</i>	425
L-Shell Excitation in Fast Collisions of Ne ⁺ -Ne <i>H. J. Hoffmann, U. Lais, R. Brenn</i>	426
Velocity Dependence of Quasimolecular Auger Emission in Kr-Kr Collisions <i>A. P. Shergin, R. Bilau, R. Stötzl, H. O. Lutz</i>	427
Continuum Electron Emission from Collisions of 0.1-3.2 MeV Kr Ions with Xe Targets <i>P. Clapis, R. Roser, K. J. Reed, Q. C. Kessel</i>	428
Large Angle Measurements of K-Shell Vacancy Production in Collisions of Ne and Ar Ions with Ar Targets <i>A. A. Antar, Q. C. Kessel</i>	429

K-Shell Excitation and KK Electron Capture in Symmetric Heavy Ion Collisions <i>E. Morenzoni, R. Anholt, W. E. Meyerhof</i>	430
Spectroscopy of Quasimolecular Orbitals from Interferences in $1s\sigma$ - $2p\pi$, $2p\sigma$ X-Ray Transitions <i>R. Schuch, R. Hoffmann, E. Justiniano, J. Konrad, P. H. Mokler, A. Oppenländer, W. Schadt, H. Schmidt-Böcking</i>	431
K-Vacancy Production in High Energy U + U and U + Pb Collisions at Small Impact Parameters <i>J. D. Molitoris, R. Anholt, W. E. Meyerhof, O. K. Baker, S. Andriamonje, E. Morenzoni</i>	432
Z-Dependence of Positron Peak Structure in Superheavy Collision Systems <i>H. Bokemeyer, H. Folger, H. Grein, T. Cowan, J. S. Greenberg, J. Schweppe, A. Balanda, K. Bethge, A. Gruppe, K. Sakaguchi, K. E. Stiebing, D. Schwalm, P. Vincent, H. Backe, M. Begemann, M. Klüver, N. Trautmann</i>	433
<i>Ion-Atom: Alignment and Orientation</i>	
Accuracy of Measured $H(n=3)$ Density Matrices for H^+ -He and H^+ , H_2^+ , and H_3^+ -Carbon Foil Collisions <i>W. B. Westerveld, N. Rouze, J. S. Risley</i>	434
The Na $2p^5 3s^2 \ ^2P_{1/2,3/2}$ States Excited by Proton Impact: Absolute Cross Sections and Alignment <i>R. Hintermayer, G. Keßler, T. Passarge, W. Mehlhorn</i>	435
Application of the Quasi-Coincidence Technique to Excited State Capture between Alkali Ions and Inert Gas Atoms <i>K. Neher, B. Staudenmayer, V. Kempter</i>	436
Polarization Studies of Resonant Electron Exchange in Na^+ - $Na^*(3p)$ Collisions <i>A. Bähring, R. Witte, H. Schmidt, I. V. Hertel</i>	437
Spin-Dependent Interaction in keV $Ne^+ + Na$ Collisions <i>W. Jitschin, S. Osimitsch, H. Reihl, D. Mueller, H. Kleinpoppen, H. O. Lutz</i>	438
Proton-Induced L X-Radiation: Strong Dependence of Polarization on Target Nuclear Charge <i>U. Werner, W. Jitschin, H. O. Lutz</i>	439
Alignment and Orientation of $H(2p)$ Excitation in H^+ - and H - Rare Gas Collisions <i>R. Hippler, W. Harbich, M. Faust, H. Kleinpoppen, H. O. Lutz</i>	440
The Coupling of Electronic Angular Momentum to the Molecular Axis in an Atom-Atom Collision <i>J. Grosser</i>	441
Diagonal and Nondiagonal Elements of the Integral Cross Section Matrix for $H(1s) + Ne, Ar \rightarrow H(nl)$ Collisions at Low Energy <i>S. Debus, J. Grosser, W. Krüger</i>	442
Excitation of Low-Energy H to ns States in Collisions with Rare-Gas Atoms <i>B. Van Zyl, M. W. Gealy, P. S. Ormsby</i>	443
Branching Ratios for the Decay of $n=3$ Hydrogen Atoms in Axial and Transverse Electric Fields <i>N. Rouze, C. C. Havener, W. B. Westerveld, J. S. Risley</i>	444
Correlations and Statistical Distributions in the Simultaneous Excitation of Both Atoms in He-He, H-H ₂ and Ne-Ne Collisions <i>L. Moorman, J. van Eck, H. G. M. Heideman, G. Nienhuis</i>	445

Ion-Atom: Production and Ionization of Multiply Charged Ions

Multiple Ionization of Ne, Ar, Kr, and I by Relativistic Uranium Ions <i>J. Ullrich, S. Kelbch, H. Schmidt-Böcking, S. Hagmann, R. Anholt, W. Rauch, A. S. Schlachter, A. Müller, P. Richard, Ch. Stoller, C. L. Cocke, R. Mann</i>	446
Picoampere Currents of Highly Ionized Slow Recoil Ions Produced by 70 MeV Br ¹⁸⁺ Impact <i>C. Stoller, L. Lembo, K. Danzmann, W. E. Meyerhof</i>	447
Production of Multiply Charged Ions from Molecular Targets in Heavy Ion Impact <i>H. Tawara, T. Tonuma, S. H. Be, H. Shibata, H. Kumagai, M. Kase, T. Kambara, I. Kohno</i>	448
Storage of Heavy-Ion Generated Multiply-Charged Recoil Ions in a Radio-Frequency Quadrupole Ion Trap <i>C. S. O, R. T. Short, S. D. Berry, S. B. Elston, M. Breinig, R. DeSerio, I. A. Sellin, B. Thomas, D. A. Church, H. M. Holzschneider, R. A. Kenefick</i>	449
Electron Stripping Cross Section from Multi-Charged Ions by H and He <i>S. Karashima, T. Watanabe, Y. Liu</i>	450
High Resolution Measurement of K β and K α X Rays from 33 MeV Ar Ions in Solid Targets <i>T. Kambara, Y. Awaya, M. Kase, H. Shibata, H. Kumagai</i>	451
High Resolution Measurement of Cu K X-Rays from Collision Systems of Cu Ions on C Target and C Ions on Cu Target <i>Y. Awaya, T. Kambara, M. Kase, H. Kumagai, H. Shibata, T. Mizogawa, K. Shima</i>	452
Impact Parameter Dependence of Multiple Ionization in 15 MeV F ⁶⁺ on Ne Collisions <i>S. Kelbch, C. L. Cocke, S. Hagmann, H. Schmidt-Böcking, R. Schuch</i>	453
Multiple-Electron Processes in H ⁺ + (He,Ne) Collisions at 300 keV <i>Richard L. Becker</i>	454
Generation of Continuum Pseudostates for Coupled-States Calculations of Ion-Atom Collisions <i>A. L. Ford, J. F. Reading</i>	455
Theory of Equilibrium Charge-State Distributions <i>T. Åberg, A. Blomberg, O. Goscinski</i>	456
Anomalies in the Final-Charge-State Dependence of Foil-Excited, Fast Heavy Rydberg Atoms <i>W. Koenig, A. Faibis, E. P. Kanter, D. Maor, I. Plessner, J. Sokolov, B. J. Zabransky, Z. Vager</i>	457
X-Ray Production with Atomic and Molecular Beams in Thin Foils <i>E. Morenzoni, P. Fumagalli, G. Bonani, W. Wölfl</i>	458

Ion-Atom: Collisions Involving Multiply Charged Ions

A New Variational Treatment of Direct Excitation of Atoms by Bare Nuclei at Intermediate Velocities <i>B. Brendlé, R. Gayet</i>	459
Direct Excitation of 400 MeV- Fe ²⁴⁺ by Bare Nuclei of Charge Z _p : Evidence for Finite Limits of Cross Sections when Z _p → ∞ <i>B. Brendlé, R. Gayet</i>	460
Theory of the Excitation of Highly-Stripped Projectile Ions <i>U. Thumm, J. S. Briggs, O. Schöller</i>	461
Hydrogen Excitation in Energetic Stripped-Ion Hydrogen Atom Collisions <i>A. Salop, J. Eichler</i>	462

Experimental Z_T Dependence of $1s^2 \rightarrow 2p3p$ Excitation Cross Sections of Two Electron Iron Ions Colliding with Target Atoms <i>K. Wohrer, J. P. Rozet, A. Chetoui, C. Stephan</i>	463
Autoionization of $N^{3+}(1s^2 3ln'l')$ Formed by Two-Electron Capture in $N^{5+}(1s^2)+H_2$ Collision, at 3.4 keV/amu <i>A. Gleizes, P. Benoit-Cattin, A. Bordenave-Montesquieu, S. Dousson, D. Hitz</i>	464
Electron Angular Distributions and Total Cross Sections for Two-Electron Capture Processes Observed in $N^{6,7+} + He$ Collisions by Electron Spectroscopy at 10.2 qkeV <i>A. Bordenave-Montesquieu, P. Benoit-Cattin, A. Gleizes, S. Dousson, D. Hitz</i>	465
Triple Coincidence Studies of Slow Collisions of Highly Charged Ions with Atoms: Electron Spectra <i>M. Mack, A. G. Drentje, A. Niehaus</i>	466
Analysis of High Resolution L-Auger Spectra from Multiply Ionized Ar Projectiles <i>N. Stolterfoht, Th. Schneider, D. Schneider, A. Itoh</i>	467
<i>Ion-Atom: Charge Transfer of Multiply Charged Ions</i>	
Stueckelberg Oscillations in C^{4+} -He Double-Capture Cross Section at Low Energy <i>A. Bárány, H. Danared</i>	468
An Extended Classical Barrier Model for Multi-Electron Transfer Reactions <i>A. Bárány, P. Hvelplund</i>	469
Multi-Electron Processes in Slow Collisions of Ar^{q+} with Ne, Ar, Kr <i>L. Liljeby, G. Astner, A. Bárány, H. Cederquist, H. Danared, S. Huldt, P. Hvelplund, A. Johnson, H. Knudsen, K.-G. Rensfelt</i>	470
Electron Capture by State Selected Ions in the Ar^{2+}/Ar Collision System <i>J. Puerta, B. A. Huber, K. Wiesemann</i>	471
Differential Cross Sections for Electron Transfer in $Ne^{4+} + He$ Collisions <i>L. N. Tunnell, C. L. Cocke, W. T. Waggoner, J. P. Giese</i>	472
Energy Gain Spectroscopy of Low Energy Ar^+ and Ne^+ on Atomic and Molecular Hydrogen <i>J. P. Giese, C. L. Cocke, S. L. Varghese, L. Tunnell</i>	473
Translational Energy Gain Spectroscopy Studies of Multiply Charged Ion Atom Collisions <i>P. Hvelplund, L. H. Andersen, A. Bárány, H. Cederquist, H. Knudsen, J. O. K. Pedersen</i>	474
Electron Capture Cross Sections and n,l - Level Populations for Highly Charged Slow Recoil Ions <i>R. Mann, C. L. Cocke</i>	475
State-Selective Electron Capture by Slow Multiply Charged Ions in Atomic Hydrogen <i>R. W. McCullough, F. G. Wilkie, H. B. Gilbody</i>	476
On Neutralization of Highly Charged Ions Near Metal Surfaces <i>M. Delaunay, S. Dousson, R. Geller, P. Varga, M. Fehringer, H. Winter</i>	477
A Practical Criterion to Determine Translation Factors. Application to $He^{2+} + H$ Collisions <i>J. M. Gómez Llorente, L. F. Errea, L. Méndez, A. Riera</i>	478
<i>Ion-Atom: Charge Transfer at eV Energies</i>	
Influence of Rotational Coupling on Charge Transfer Between Multiply Charged Ions and Neutral Atoms at Low Energies <i>M. Gargaud, R. McCarroll, P. Valiron, G. Zannoli</i>	479
Low Energy Charge Transfer in One Electron Systems <i>G. J. Bottrell, T. G. Heil</i>	480

Potential Curves and Coupling Elements for Charge Transfer in $\text{Al}^{+3} + \text{H}$ Collisions <i>K. Kirby, T. G. Heil</i>	481
A Crossed-Beam Study of the Single-Charge Transfer Process $\text{Hg}^{++}({}^1\text{S}) + \text{Kr}({}^1\text{S}) \rightarrow \text{Hg}^+({}^2\text{S}) + \text{Kr}^+({}^2\text{P}_{3/2}, {}^2\text{P}_{1/2})$ at eV Collision Energies <i>B. Friedrich, J. Vancura, M. Sadilek, Z. Herman</i>	482
Resonance States of Multiply-Charged Molecular Ions <i>S. Preston, A. Dalgarno</i>	483
Charge Transfer of Helium Ions in Neon <i>B. Zygelman, A. Dalgarno</i>	484
The Charge Transfer Cross Section for $\text{Xe}^+({}^2\text{P}_{3/2})$ Ions in Xe Over the Energy Range 0.4 to 4.5 eV (LAB) <i>P. Larsen, M. T. Elford</i>	485
<i>Ion-Atom: Charge Transfer at keV Energies — Experiment</i>	
Differential Charge-Transfer Cross Section for $\text{O}^+({}^4\text{S})$ and $\text{O}^+({}^2\text{D})$ Ions with Atmospheric Gases <i>D. A. Schafer, J. H. Newman, K. A. Smith, R. F. Stebbings</i>	486
Electron Capture from $\text{Li}(2\text{s})$ by 2-20 keV C^+ , N^+ and O^+ <i>F. Aumayr, G. Lakits, H. Winter</i>	487
State Selective and Total Electron Capture in $\text{H}^+ - \text{Li}(2\text{s})$ Collisions (2-20 keV) <i>Friedrich Aumayr, Hannspeter Winter</i>	488
Differential Cross Sections for 30, 66.7, and 150 keV Mg^+ Electron Capture from He <i>E. Redd, D. M. Blankenship, D. G. Seely, T. J. Gay, J. L. Peacher, J. T. Park</i>	489
Double Target Ionization Resulting from Single Charge Transfer in H^+ , He^{++} - Neon, Sodium and Magnesium Collisions <i>R. D. DuBois</i>	490
Low Energy Electron Capture by Fully Stripped Light Ions from H and H_2 <i>F. W. Meyer, A. M. Howald, C. C. Havener, R. A. Phaneuf</i>	491
10 keV/q Al^{12+} Collisions with H_2 and He: Most Populated n State and Mean ℓ Value from Lyman Spectroscopy <i>D. Vernhet, A. Touati, P. Bouisset, A. Chetoui, J. P. Rozet, K. Wohrer, C. Stephan</i>	492
Measurement of Charge Exchange Cross Sections for $\text{H}^+ + \text{He} \rightarrow \text{He}^+ + \text{H}(n=3, \ell, m_\ell)$ <i>M. C. Brower, F. M. Pipkin</i>	493
<i>Ion-Atom: Charge Transfer at keV Energies — Theory</i>	
Charge Transfer in $\text{H}^+ + \text{Na}$ Collisions <i>R. Shingal, C. W. Newby, C. J. Noble, D. R. Flower, B. H. Bransden</i>	494
"Heisenberg Core" in Classical Trajectory Monte-Carlo Calculations of Ionization and Charge Exchange <i>D. Zajfman, D. Maor</i>	495
Single Electron Capture in $\text{Li}^{3+} - \text{He}$ Collisions <i>L. Opradolce, C. Falcón, I. Casaubon</i>	496
Eikonal Cross Section in Proton-Helium Electron Capture Processes <i>K. Kobayashi, N. Toshima, T. Ishihara</i>	497
2p-2s Vacancy Transfer in $\text{Ne}^+ + \text{Ne}$ Collisions in the Energy Range of 5-500 keV <i>A. Toepfer, H. J. Lüdde, B. Jacob, R. M. Dreizler</i>	498
Comment on $\text{H}^+ + \text{He} \rightarrow \text{H}^0 + \text{He}^{i*}$ <i>J. H. McGuire</i>	499
Charge Transfer in Two Electron Systems in the Time Dependent Hartree Fock Picture <i>W. Stich, H. J. Lüdde, R. M. Dreizler</i>	500

A Unified AOMO Expansion Treatment of $p\text{-H}$, $\text{C}^{6+} + \text{H}$ and $p\text{-He}$ Collisions <i>M. Kimura, C. D. Lin</i>	501
Atomic-Orbital Expansion Representation of Electron Transfer in Two-Electron Systems <i>Wolfgang Fritsch, Chii-Dong Lin</i>	502
Continuous Energy State Model for Charge Transfer in Collisions of Fully Stripped Ions with Hydrogen Atoms <i>Fumihiko Koike</i>	503
Angular Distributions of Ions After Fast Ion-Atom Collisions <i>A. K. Kaminsky, M. I. Popova</i>	504
<i>Ion-Atom: Charge Transfer at MeV Energies — Experiment</i>	
Double and Single Electron Capture in 1-2 MeV/u O^{8+} -He Collisions <i>R. Hippler, S. Datz, P. D. Miller, P. L. Pepmiller</i>	505
Atomic Charge Exchanges in Close Collisions Between Ar^{+q} Ions and Targets in the MeV Energy Region <i>I. Ben Itzhak, D. W. Mingay, B. Rosner</i>	506
Double K- to K-Shell Vacancy Transfer in Slow Collisions of Bare Ions and Atoms <i>E. Justiniano, M. Schulz, R. Schuch, A. Oppenländer, H. Schmidt-Böcking, W. Schadt, P. Mokler</i>	507
Electron Capture Cross Sections in Fast Ion-Atom Collisions <i>H.-D. Betz, R. Höppler</i>	508
The Energy Dependence of Electron-Capture and -Loss Cross Sections in MeV/amu, Highly-Stripped, Heavy Ion Collisions <i>W. G. Graham, J. A. Tanis, E. M. Bernstein, M. Clark, R. H. McFarland, T. J. Morgan, M. P. Stockli, K. H. Berkner, R. V. Pyle, A. S. Schlachter, J. W. Stearns, B. M. Johnson, K. W. Jones, M. Meron</i>	509
Comparison of Electron Capture Process in Gas and Solid Targets for 35 MeV/u Kr^{36+} Ions <i>J. P. Rozet, A. Chetoui, P. Bouisset, C. Stephan</i>	510
<i>Ion-Atom: Charge Transfer at MeV Energies — Theory</i>	
Continuum Distorted Waves <i>Derrick S. F. Crothers</i>	511
Single and Double Electron Capture from Lithium by Fast Alpha Particle <i>S. C. Mukherjee, Mita Ghosh, C. R. Mandal</i>	512
Calculation of Cross Sections for Electron Capture from Multi-Electron Atoms by Fast Ions <i>S. C. Mukherjee, G. C. Saha, Shyamal Datta</i>	513
Potential Screening in Inner-Shell Electron Capture <i>J. E. Miraglia, R. O. Barrachina, C. R. Garibotti</i>	514
Calculation of Differential Charge-Transfer Cross Section in the Intermediate and High Energy Range Based on the Faddeev-Merkuriev Equations <i>A. L. Godunov, Sh. D. Kuniyeev, V. S. Senashenko</i>	515
Theory of Electron Capture at High Energies <i>Steven Alston</i>	516
Understanding the Exact Second-Born Capture Cross Section <i>Steven Alston</i>	517
The Normalization of Approximate Scattering States <i>S. Alston, J. S. Briggs, K. Taulbjerg</i>	518
Numerically Generated Off-Shell Radial Wavefunctions <i>Hermann Marxer, Steven Alston</i>	519
Boundary Conditions and the Strong Potential Born Approximation for Electron Capture <i>D. P. Dewangan, J. Eichler</i>	520

Comparison of Eikonal and Strong Potential Born Cross Sections for High Velocity Capture at Forward Angles <i>J. H. McGuire, J. Eichler</i>	521
Charge Transfer Cross Sections in the Eikonal Approximation <i>N. C. Sil, C. Sinha</i>	522
Analytic Evaluation of SPB Amplitude for Arbitrary Angular Momentum States <i>N. C. Sil, N. C. Deb</i>	523
<i>Ion-Atom: Capture into Continuum and Convoy Electrons</i>	
Convoy Electrons from 100 keV H on Carbon Foils Measured in Coincidence with Emerging Protons and H Atoms <i>P. Focke, W. Meckbach, I. Nemirovsky, S. D. Berry, I. A. Sellin, M. G. Menendez, M. M. Duncan</i>	524
Charge Changing Processes in Highly Charged ($V \geq V_0$) Ion-Atom Collisions Studied by 0° -Electron Spectroscopy <i>L. H. Andersen, P. Hvelplund, H. Knudsen, J. O. Pedersen</i>	525
Threshold Law for Simultaneous Rydberg Electron and Convoy Electron Production <i>H.-P. Hülskötter, M. Breinig, J. Burgdörfer, S. B. Elston, P. Engar, I. A. Sellin</i>	526
Statistical Multipoles for Cusp Electrons and Rydberg Electrons <i>Joachim Burgdörfer</i>	527
The $v=v_p$ Peak in H^0+H_2O Collisions <i>M. E. Rudd, M. A. Bolorizadeh</i>	528
On the Production of Convoy-Electrons in Ion-Foil Interaction <i>R. Schramm, H.-D. Betz, P. Koschar, M. Burkhardt, J. Kemmler, O. Heil, K. O. Groeneveld</i>	529
Dependence of the ECC "Cusp" Yield on the Projectile Z from the Study of the Simplest Collision Systems <i>D. Berényi, Á. Kövér, Gy. Szabó, L. Gulyás, K. O. Groeneveld, D. Hoffmann, M. Burkhard</i>	530
<i>Ion-Atom: Radiative and Non-Radiative Capture at High Energies</i>	
Radiative Electron Capture in Proton-Hydrogen Collision <i>Jorge E. Miraglia</i>	531
X-Ray Differential Cross Section for Radiative Electron Capture <i>J. E. Miraglia, C. R. Garibotti, A. Gonzalez</i>	532
Relativistic Treatment of Radiative Electron Capture <i>K. Hino, I. Shimamura, T. Watanabe</i>	533
Inner Shell Vacancy Production and Radiative Electron Capture in Atomic Collisions with High Energy Heavy Ions <i>D. H. H. Hoffmann, R. Anholt, P. H. Mokler, W. A. Schönfeldt, E. Morenzoni</i>	534
Eikonal Calculations of Electron Capture by Relativistic Projectiles <i>J. Eichler, R. Anholt</i>	535
Total Cross Sections for K-K Shell Electron Capture at Relativistic Energies <i>W. J. Humphries, B. L. Moiseiwitsch</i>	536
Analysis of Charge Distributions of Relativistic Heavy Ions Penetrating Through Solid Targets <i>W. E. Meyerhof, R. Anholt, P. Thieberger, H. E. Wegner, H. Gould, J. Alonso, Ch. Munger</i>	537
Charge Distribution of 85-200 MeV/amu Xe^{54+} , Xe^{53+} , and Xe^{52+} Ions Penetrating Through Solid Targets <i>H. Gould, J. Alonso, Ch. Munger, R. Anholt, W. E. Meyerhof, P. Thieberger, H. E. Wegner</i>	538

Ultrarelativistic Electron Capture in Ion-Atom Collisions <i>G. R. Deco, R. D. Rivarola</i>	539
Galerkin Methods for Solving the Schrödinger and Dirac Equations <i>C. Bottcher, M. R. Strayer</i>	540
K-Shell Ionization by Relativistic Heavy Ions <i>Ulrich Becker, Norbert Grün, Werner Scheid</i>	541
Direct Electron-Positron Pair Creation in Relativistic Heavy Ion Collisions <i>Ulrich Becker, Norbert Grün, Werner Scheid</i>	542
<i>Ion-Atom: Inner Shell Vacancy Decay</i>	
Precision X-Ray Measurements in One- and Two-Electron Argon Recoil Ions <i>H. F. Beyer, R. D. Deslattes, F. Folkmann, R. E. LaVilla</i>	543
Accuracy of Transfer Calibrations in High Resolution High Precision X-Ray Spectroscopy <i>Martin P. Stöckli, J. L. Shinpaugh, J. M. Sanders, Patrick Richard</i>	544
Projectile Dependence of L-MM Auger Electrons Ejected from Ar Target by Heavy-Ion Impact <i>H. Shibata, T. Matsuo, Y. Awaya, T. Kambara, M. Kase, H. Kumagai, N. Tokoro</i>	545
K Fluorescence Yields, Auger and X-Ray Decay Rates for Multiply Ionized Atoms <i>F. Combet Farnoux</i>	546
$K_{\beta\beta^-}$ and $K_{\alpha\beta^-}$ Decay Rates in Doubly Ionized Atoms <i>G. B. Baptista, E. C. Montenegro</i>	547
Ionization by Nuclear Resonance Scattering within the Blair Model <i>James M. Feagin, David W. Joyce, Ladislav Kochach</i>	548
Large-Angle Scattering and Nuclear-Resonance Effect in Electron Capture in $H^+ + C$ and $H^+ + N$ Collisions <i>J. N. Scheurer, O. K. Baker, D. Spooner, W. E. Meyerhof</i>	549
Nuclear-Reaction Time Delay Studies of $U + U$ Deep Inelastic Collisions at 7.5 MeV/amu <i>J. D. Molitoris, Ch. Stoller, R. Anholt, D. W. Spooner, W. E. Meyerhof, R. J. McDonald, L. G. Sobotka, G. J. Wozniak, L. G. Moretto, E. Morenzoni, M. Nessi, W. Wölfl</i>	550
<i>Ion(Atom)-Molecule Collisions: Rotational-Vibrational Excitation</i>	
Intermolecular Energy Transfer Involving Electronically Excited Molecules: $He(^1S) + H_2(B^1\Sigma_u^+)$ <i>Randall M. Grimes, William A. Lester, Jr., Michel Dupuis</i>	551
Efficiency of (R,T) Energy Transfers in He, Ar Collisions with N_2 and O_2 <i>F. A. Gianturco, A. Palma, M. Venanzi</i>	552
Theoretical Studies of the Bound States and Scattering of $H_2^+ - H_2$ and $HD - H_2$ <i>Joachim Schaefer</i>	553
Vibrational-Rotational De-Excitation of SiO in Collision with Rigid-Rotor H_2 <i>Ronald J. Bieniek</i>	554
Rotational and Vibrational Energy Transfer in Low-Velocity Molecular Collisions <i>Kazuo Takayanagi, Takashi Wada, Atsushi Ichimura</i>	555
Anisotropic Potentials for $NO(^2\Pi)$ -Rare Gases from High-Resolution Total Differential Scattering Cross Sections <i>L. Beneventi, P. Casavecchia, G. G. Volpi</i>	556
Energy Transfer in Collisions of NH_3 and $(NH_3)_2$ with Helium <i>U. Buck, H. Meyer, R. Schinke</i>	557

Rotational and Vibrational Excitation in Collisions of Na^+ Ions with N_2 , CO , O_2 , and CO_2 Molecules	558
<i>S. Kita, T. Hasegawa, A. Kohlase, H. Inouye</i>	
KeV-Energy Differential Scattering: Cross Sections, Interaction Potentials and Diffraction	559
<i>J. H. Newman, D. A. Schafer, K. A. Smith, R. F. Stebbings</i>	
Breakdown of Energy-Loss Scaling in $\text{Ne} + \text{D}_2$ Collisions	560
<i>Ralph Snyder, Arnold Russek</i>	
Energy Loss Scaling for Small Angle Rotationally Inelastic Scattering	561
<i>F. E. Budenholzer, M. H. Chang, S. C. Hu</i>	
A Study of Low keV Energy $\text{Li}^+ + \text{D}_2$ Collisions	562
<i>V. Heckman, S. J. Martin, J. Jakacky, Jr., E. Pollack</i>	
Ion Energy-Loss Spectroscopy in the Collisions of $\text{Ar}^+(\text{}^2\text{P}_j)$ with H_2	563
<i>Tomohisa Nakamura, Nobuo Kobayashi, Yozaburo Kaneko</i>	
Ion Energy-Loss Spectroscopy for Vibrational Transitions of N_2^{2+} in the Collisions with Ne, Ar and Kr	564
<i>Tomohisa Nakamura, Nobuo Kobayashi, Yozaburo Kaneko</i>	
Ion(Atom)-Molecule Collisions: Energy Transfer	
Collisional Quenching and Energy Transfer of $\text{NS B}^2\text{II}$	565
<i>Jay B. Jeffries, David R. Crosley, Gregory P. Smith</i>	
Quenching of $\text{NH}(\text{A}^3\text{II}_1)$ at 1400K	566
<i>Nancy L. Garland, Jay B. Jeffries, Richard A. Copeland, Gregory P. Smith, David R. Crosley</i>	
Collisional Quenching of $\text{A}^2\Sigma^+ \text{OH}$ between 230 and 300 K	567
<i>Richard A. Copeland, David R. Crosley</i>	
Quasi-Resonant Collisional Electronic to Rotational Energy Transfer at Thermal Energies	568
<i>J. Cuvellier, L. Petitjean, J. M. Mestdagh, D. Paillard, P. de Pujo</i>	
Pseudopotential Molecular-Structure Calculations of Alkali- H_2 Systems	569
<i>F. Rossi, J. Pascale</i>	
Energy Dependence of Rotational Rainbows in Vibrationally Inelastic Scattering	570
<i>Warren Moskowitz, Brian Stewart, James L. Kinsey, David E. Pritchard</i>	
Inducing Resonant V-R Transfer with High Rotation and Low Velocity	571
<i>Tom Scott, Peter Magill, Niel Smith, Brian Stewart, David E. Pritchard</i>	
Ion(Atom)-Molecule Collisions: General	
Dissociative Electron Capture of H_2^+	572
<i>I. Alvarez, C. Cisneros, J. de Urquijo, A. Morales, H. Martinez</i>	
Negative Ion Formation in Polar Dissociation of H_3^+ , HD_2^+ and D_3^+	573
<i>C. Cisneros, I. Alvarez, J. de Urquijo, H. Martinez, T. J. Morgan</i>	
Excitation and Dissociation Mechanisms in 3.22 keV H_2^+ -Ne Collisions	574
<i>O. Yenen, D. H. Jaacks</i>	
Formation of He_2^0 and He_2^{2+} Molecules by Charge Exchange Collisions of He_2^+ Ions in the Sub-MeV Region	575
<i>O. Haber, I. Ben Itzhak, I. Gertner, A. Mann, B. Rosner</i>	
Collision-Induced Luminescence Studies on CF_4 by He^+ , Ne^+ and Ar^+ Impact	576
<i>J. Sasaki, I. Kuen, F. Howorka</i>	
Dissociative Ionization of Hydrogen by Fast Protons	577
<i>B. G. Lindsay, F. R. Simpson, C. J. Latimer</i>	

Electronic Excitation Transfer, Collisional Dissociation and Photodissociation in Sodium Vapor <i>H. Hulsman, P. Willems</i>	578
<i>Ion(Atom)-Molecule Collisions: Molecular Charge Transfer</i>	
Total and Partial Differential Cross Sections for the Processes: $K, Cs + O_2(v=0) \rightarrow K^+, Cs^+ + O_2^-(v')$ <i>M. R. Spalburg, M. G. M. Vervaat, A. W. Kleyn, J. Los</i>	579
Balmer α Emission in Collisions of H, H^+, H_2^+ and H_3^+ with N_2, O_2 and H_2O <i>F. Yousif, J. Geddes, H. B. Gilbody</i>	580
Double Electron Capture in $Ar^{2+} + D_2$ <i>S. J. Martin, V. Heckman, J. Stevens, E. Pollack</i>	581
Electron Capture in $Li^+ + H_2$ and $Ar^+ + H_2$ Collisions in the keV Energy Region and Study of Orientation Effect of the Target Molecule <i>M. Kimura, S. Chapman, N. F. Lane</i>	582
Charge Transfer in Ion-Molecule Collisions at the keV Energy Region: Study of $H^+ + H_2$ Collisions <i>M. Kimura</i>	583
Absolute Charge Transfer Cross Sections of 50 eV - 4 keV H^+, H_2^+, H_3^+, N^+ , and N_2^+ in Cs <i>M. J. Coggiola, Y. K. Bae, J. R. Peterson</i>	584
Metastable Excited OH^- and NH_2^- Ions from H_2O^+ and NH_3^+ Beams in Rb <i>Y. K. Bae, J. R. Peterson</i>	585
Energy and Charge Transfer in O_2^+ on O_2 Collisions - Effects of a "Vibrational Rainbow" <i>K. B. McAfee, Jr., R. S. Hozack</i>	586
Observation of Collision-Energy, Product-State, and Angular Scattering Specificity in the Charge-Transfer Reaction of $Ar^+(^2P_{3/2})$ with $N_2(X^1\Sigma_g^-, v=0)$ <i>Alan L. Rockwood, Stephen L. Howard, Du Wen-Hu, Paolo Tosi, Werner Lindinger, Jean H. Futrell</i>	587
Studies of Charge Transfer Processes in a Flow Tube <i>R. G. Keese, B. L. Upschulte, R. J. Shul, R. Passarella, R. E. Leuchner, A. W. Castleman, Jr.</i>	588
<i>Ion(Atom)-Molecule Collisions: Ionization and Detachment</i>	
The Electronic Structure of Free Liquid Surfaces. Electron Spectroscopy under $He(2^3S)$ Versus HeI-Photon Impact <i>Wolfgang Keller, Harald Morgner, Werner Müller</i>	589
Excitation Transfer into Bound and Continuum Electronic States. $He(2^3S, 2^1S) +$ Halogen Containing Molecules <i>Kai Beckmann, Oskar Leisin, Harald Morgner</i>	590
Transition State Spectroscopy with Electrons: The Reaction of $He(2^3S, 2^1S)$ with Halogen Molecules <i>Arnulf Benz, Harald Morgner</i>	591
Penning Ionization Optical Spectroscopy of HCl <i>Andrew J. Yench, Abul K. Khan, Sam Brown</i>	592
Role of Helium and Neon in Glow Discharges with Nitrogen as a Trace Component: The First Negative $N_2^-(B \rightarrow X)$ and Second Positive $N_2(C \rightarrow B)$ Emission Systems of Nitrogen <i>M. J. Weiss, H. Mooney</i>	593
Ionization of CH_n^+ Ions by Electron-Loss Collision Spectroscopy <i>D. Mathur, C. Badrinathan, U. T. Raheja, F. A. Rajgara</i>	594
Single and Double Electron Detachment from Cl^- by Molecular Oxygen and Nitrogen <i>B. Hird, F. Rahman</i>	595

Ion(Atom)-Molecule Collisions: Reactive Scattering

- Formation and Decay of Rare Gas Hydride Excimers Produced in Collisions of Excited H_2 Molecules with Rare Gas Atoms 596
T. Möller, M. Beland, J. Stapelfeldt, G. Zimmerer
- The State Specific Reaction of Electronically Excited Sodium Atoms with Oxygen Molecules 597
H. Schmidt, P. S. Weiss, J. M. Mestdagh, M. H. Covinsky, Y. T. Lee
- A State Selected Study of Ion-Molecule Reactions in the $(D_2-N_2)^+$ System 598
Kenichiro Tanaka, Tatsuhisa Kato, Inosuke Koyano
- Ion-Molecule Reactions in Collision Systems of H^+ , H_2^+ , H_3^+ and their Isotopic Ions with Hydrogen and Deuterium Molecules from 0.1 to 1000 eV 599
Kazuhiko Okuno, Yozaburo Kaneko
- The Production of H_3^+ Ions with Low Internal Energy 600
A. Sen, J. B. A. Mitchell
- The Self-Consistent Time-Dependent, Hartree-Fock Method of Molecule-Ion Collisions: Theory and Application 601
Detlev H. Tiszauer
- Analysis of Distorted-Wave and Coupled-Channel-Wave Transition Amplitudes 602
S. H. Suck Salk
- A Semiclassical Theory in Phase Space for Molecular Processes: Scattering Matrix as a Special Case of Dynamical Characteristic Function 603
Kazuo Takatsuka, Hiroki Nakamura
- Comparison Between Approximate (Perturbation) and Exact (Close-Coupling) Three-Dimensional Quantal Calculations, Orientation of Transferred Angular Momentum Projection 604
C. K. Lutrus, C. R. Klein, S. H. Suck Salk
- Coupling Schemes and Decoupling Approximations for Inelastic and Reactive Collisions 605
V. Aquilanti, S. Cavalli, G. Grossi

Ion(Atom)-Molecule Collisions: Three-Body Processes

- Association/Dissociation in Dense Gases 606
M. R. Flannery
- Threshold Fragmentation of the Three-Body Systems: The Classical Theory 607
N. Simonović, P. Grujić
- Symmetry Properties of 3-Fermion Systems with Two Identical Particles 608
Shen Hengyi, Birte Christensen-Dalsgaard, John Avery
- Three Particle Bound States 609
Joseph Macek

Ion-Ion: General

- "Pseudo-Model" for Ba^+ Ion: Application to Ba^+X^+ Molecular Potentials with $X = \{H, Li, Na, K, Rb, Ba\}$ 610
A. Valance, A. Bernier, H. Bergeron
- Fine-Structure Excitation in Ion-Ion Collisions 611
R. S. Walling, J. C. Weisheit
- Ab Initio* Studies of Slow $Li^+ - Li^+$ and $Na^+ - Na^+$ Collisions 612
I. L. Cooper, A. S. Dickinson, S. K. Sur
- Charge Transfer and Ionization in Collisions of Protons with Al^+ , Ga^+ , In^+ and Tl^+ Ions 613
K. F. Dunn, M. F. Watts, G. C. Angel, H. B. Gilbody

Ionization and Charge Transfer Total Cross Sections for $H^+ + Li^+$ Collisions <i>C. O. Reinhold, C. A. Falcón</i>	614
Electron Transfer in Collisions between Protons and Li^{++} Ions <i>Thomas G. Winter</i>	615
Cross Sections for Electron Capture and Ionization in $H^+ + He^+$ Collisions <i>K. Rinn, F. Melchert, K. Rink, E. Salzborn</i>	616
Theoretical Studies of Mutual Neutralization in $p + H^-$ Collisions Using Model Potentials <i>A. M. Ermolaev</i>	617
Mutual Neutralization in $H^+ + H^-$ Collisions <i>R. Shingal, B. H. Bransden</i>	618
Charge Exchange between He^{++} and H^- at Low Energies <i>M. Terao, C. Harel, A. Salin</i>	619
One Electron Transfer in $He^{++} - H^-$ Collisions into Excited States of He^+ <i>M. Terao, M. Cherkani, S. Szűcs, F. Brouillard</i>	620
<i>Rydberg States and Reactions</i>	
Orientation Effects in Thermal Collisions Between Rydberg Atoms in Circular States and Ground State Helium <i>E. de Prunele</i>	621
Impact Ionization of State-Selected Na Rydberg Atoms by Ion Bombardment <i>K. MacAdam, N. L. S. Martin, D. B. Smith, R. G. Rolfes</i>	622
Information-Theoretical Analysis of Charge Transfer from Rydberg Atoms <i>A. Blomberg, T. Åberg</i>	623
Simple Analytical Formulas for Collisional <i>l</i> -Mixing, <i>n</i> -Changing and Ionization of Rydberg Atoms with Neutral Particles at Thermal Energy <i>L. Petitjean, F. Gounand</i>	624
The Possible Influence of Core Effects in Rydberg Atom-Neutral Collisions at Thermal Energies <i>F. Gounand, L. Petitjean</i>	625
Collisions of Rubidium Rydberg Atoms with Ammonia <i>L. Petitjean, F. Gounand, F. R. Fournier</i>	626
Theoretical Semiclassical Study of State-Changing Collisions Between Rydberg Atoms and Rotating Molecules <i>M. Kimura, N. F. Lane</i>	627
Angular Momentum Shifts of High Rydberg States by Time-Dependent External Fields <i>Y. Hahn, K. LaGattuta, I. Nasser</i>	628
Effects of Ultra-Low-Energy Resonances in Elastic Scattering of Electrons by Alkali Metal Atoms on Collision of High-Rydberg Atoms with Alkali Metal Atoms <i>Michio Matsuzawa, Naoto Koyama</i>	629
Collisions of $Rb(ns,nd)$ Atoms with SF_6 <i>B. G. Zollars, F. Lu, C. W. Walter, L. N. Goeller, L. G. Gray, K. A. Smith, F. B. Dunning, R. F. Stebbings</i>	630
State-Changing in $Rb(ns,nd)-Xe$ Collisions: Product State Distributions <i>G. B. McMillian, L. N. Goeller, K. A. Smith, F. B. Dunning, R. F. Stebbings</i>	631
State Selective Laser Detection of Rydberg Atoms <i>V. Lange, U. Eichmann, G. A. Ruff, W. Sandner</i>	632

Delayed Emission of 2p-1s and 3p-1s X-Rays from 40 MeV Ne Ions Ionized in a Thin Carbon Foil	633
<i>J. Pálinskás, R. J. Maurer, R. L. Watson</i>	
Observation of "Stark Beats" in Gas Excited 100 MeV Ne ⁶⁺ Ion Beams	634
<i>D. Schneider, W. Zeitz, G. Schiwietz, N. Stolterfoht, U. Wille</i>	
Field Assisted Collisions	
Optical Collision Spectra for Na-Ar by the Quantum Coupled-Channels Method	635
<i>F. Rebertus</i>	
Far Infrared Absorption in H ₂ , and in Mixtures of H ₂ , with He, N ₂ , CH ₄ , Ar, Induced by Binary Collisions	636
<i>Lothar Frommhold, Aleksandra Borysow, Massimo Moraldi, Wilfried Meyer, George Birnbaum</i>	
Transition Process Under Intense Laser Field: Sr(5s5p ¹ P ₁ ⁰) + Ca(4s ² ¹ S ₀) → Sr(5s ² ¹ S ₀) + Ca(3d4p ¹ F ₃)	637
<i>Hideki Yagisawa</i>	
Laser Assisted Charge Transfer Reactions in Slow Ion-Atom Collisions: Coupled Dressed Quasimolecular-States Approaches	638
<i>T. S. Ho, C. Laughlin, Shih-I Chu</i>	
Satellite Spectra in Laser Assisted Charge Transfer Collisions	639
<i>Y. P. Hsu, R. E. Olson</i>	
Non-Linearity and Photon Correlation in Laser-Assisted Charge Transfer in Helium	640
<i>S. Ganguly, K. Rai Dastidar, T. K. Rai Dastidar</i>	
Comparison of Na ⁺ Ion Production in 100-2000 eV [He ⁺ /Ar ⁺] + Na(3s,3p) Collisions Using Crossed Laser, Ion and Atom Beams	641
<i>C. R. Hummer, A. Berlin, W. W. Smith</i>	
Charged Particle Scattering in Strong Stochastic Radiation Fields	642
<i>R. Daniele, G. Ferrante, F. Morales, F. Trombetta</i>	
Electron Atom Scattering in the Field of a Symmetric Mode Locked Laser	643
<i>Marvin H. Mittleman</i>	
Direct Radiative Recombination in a Hydrogenic Non-Maxwellian Laser-Plasma	644
<i>M. Lamoureux, C. Möller, R. Yin, J. P. Matte, J. Delettrez</i>	
Radiative Electron-Atom Collisions in a Strong Laser Field	645
<i>F. H. M. Faisal</i>	
Simultaneous Electron Photon Excitation of Hydrogen Atom	646
<i>R. S. Pundir, K. C. Mathur</i>	
Clusters	
The Infrared Spectroscopy of Weakly Bound Hydrogen Cluster Ions	647
<i>L. I. Yeh, Mitchio Okumura, Y. T. Lee</i>	
Photofragmentation of Mass Resolved Clusters of Si _n ⁺	648
<i>L. A. Bloomfield, R. R. Freeman, W. L. Brown</i>	
Photofragmentation of Cluster Ions of Cesium	649
<i>Rolf Möller, Hanspeter Helm</i>	
Fragmentation of Microclusters by Electron Impact Ionization	650
<i>U. Buck, H. Meyer, M. Tolle</i>	
Photoionization of van der Waals-Clusters Investigated by a Photoion-Photoelectron-Coincidence Technique	651
<i>A. Ding, L. Cordis, K. Kretzschmar, J. Hesslich</i>	

Unimolecular and Collision Induced Fragmentations of Small $(\text{N}_2\text{O})_n^+$ - Cluster Ions <i>W. Kamke, B. Kamke, H. U. Kiefl, I. V. Hertel</i>	652
Metastable and Spontaneous Fragmentation of Benzonitrile Ions (and Cluster Ions) <i>W. Kamke, B. Kamke, H. U. Kiefl, I. V. Hertel</i>	653
Photoionization and Photodissociation of Hydrogen Bonded Alkylamine Clusters <i>P. G. F. Bisling, E. Rühl, B. Brutschy, H. Baumgärtel</i>	654
One- and Two-Color Resonance Enhanced Multiphoton Ionization of van der Waals Molecules: Studies of Spectroscopic Shifts as a Function of Degree of Aggregation <i>A. W. Castleman, Jr., P. D. Dao, S. Morgan, R. G. Keesee</i>	655
Negative Ion Formation by Impact of Rydberg Atoms on van der Waals Clusters <i>Koichiro Mitsuke, Tamotsu Kondow, Kozo Kuchitsu</i>	656
Experimental Techniques	
Photoelectron Spectroscopy Using a CCD Multichannel Detector <i>Andrea Haworth, David G. Wilden, John Comer</i>	657
High Current, Monochromatic Electron Source for Polarized Electron-Atom Scattering <i>C. S. Feigerle, D. T. Pierce, A. Seiler, R. J. Celotta</i>	658
Charge Exchange Detection of Laser-Induced Transitions in Molecular Ions <i>C. H. Kuo, I. W. Milkman, T. C. Steimle, J. T. Moseley</i>	659
A Detection System to Study the Stereochemistry of Molecular-Ions <i>A. Faibis, W. Koenig, E. P. Kanter, Z. Vager, B. J. Zabransky</i>	660
X-Ray Photoelectron Spectroscopy of Atoms and Molecules: A Windowless X-Ray Tube for High Temperature Measurements <i>M. S. Banna, B. H. McQuaide</i>	661
Multicharged Ion-Atom Merged-Beams Apparatus <i>C. C. Havener, H. F. Krause, R. A. Phaneuf</i>	662
Realization of a Truncated Spherical Analyzer for Parallel Measurement of Angular Distributions <i>D. Tremblay, D. Roy, D. Dubé</i>	663
Simple, Low Cost, Data Acquisition System for EELS <i>G. G. B. de Souza, F. C. Pontes, H. Gamal</i>	664
Detection of Low-Lying Metastable Molecules by Phosphorescence or Fluorescence <i>Hiroshi Kume, Tamotsu Kondow, Kozo Kuchitsu</i>	665
Measurements of Laser Excited Atom Population in Na Vapor and Fast Na Beams <i>D. P. Wang, S. Y. Tang, R. H. Neynaber</i>	666
Production of H_2^+ Ions in Low Vibrational States Using a Radio Frequency Storage Ion Source <i>A. Sen, J. Wm. McGowan, J. B. A. Mitchell</i>	667
Characteristics of a Laser-Generated Plasma as Source of Soft X-Rays (200 eV-1 keV) <i>H. C. Gerritsen, H. van Brug, F. Bijkerk, M. J. van der Wiel</i>	668
Diagnosis of Spin Polarization in an Optically Pumped Sodium Beam <i>J. J. McClelland, M. H. Kelley</i>	669
Electron Lenses with Controlled Magnification <i>D. W. O. Heddle, N. Papadovassilakis, Carol Trager</i>	670
Second Order Reduction of Doppler Broadening of Projectile Electron Spectra in a Position Sensitive 30° Parallel Plate Analyser <i>Joseph K. Swenson</i>	671

Characteristics of a GaAs Polarized Electron Source <i>F. C. Tang, M. Eminyan, M. S. Lubell, J. Slevin, A. Vasilakis</i>	672
Anti-Compton X-Ray Spectrometer <i>J. F. Chemin, J. N. Scheurer, S. Andriamonje</i>	673
A New Technique of Measuring Anisotropy Factors by Means of Perfectron <i>T. Arikawa, A. Fukuroda, K. Kikuchi</i>	674
Production of a Fast Beam of Hydrogen Atoms in the 3s State <i>W. Claeys, A. Cornet, V. Lorent, D. Fussen</i>	675
Electronic, Ionic, and Atomic Densities and Temperatures in H^- Multipole Sources <i>M. P. S. Nightingale, A. J. T. Holmes, T. S. Green</i>	676
Post-Deadline Papers	
Differential Cross-Section for Single and Double Capture in Ne^{7+} -He Collisions <i>P. Roncin, H. Laurent, J. Pommier, D. Hitz, S. Dousson, M. Barat</i>	677
Formation of Low Lying Autoionization States in Li^- , C and C^- Projectile Ions Studied by Zero-Degree Electron Spectroscopy <i>R. Bruch, D. Schneider, N. Stolterfoht</i>	678
Ionization-Excitation and Double Excitation of Helium by H^+ , C^{4+} , C^{3+} and C^+ at High Velocities <i>R. Bruch, E. Träbert, S. Fülling, P. H. Heckmann, B. Raith</i>	679
An Effective Operator for Dielectronic Recombination <i>Peter Winkler</i>	680
Na^+ Ion Production in a Microwave Discharge <i>M. J. Hogan, P. P. Ong</i>	681
Velocity Distribution of Ne^+ and Ar^+ in Their Parent Gases <i>P. P. Ong, M. J. Hogan</i>	682
Lattice Solution of the Two- and Three-Particle Schrödinger Equation <i>Michael V. Ivanov</i>	683
Direct Measurement of the Velocity Dependence of Associative Ionization Cross Section in $Na(3p) + Na(3p)$ Collisions <i>M-X Wang, M. S. DeVries, J. Keller, J. Weiner</i>	684
Two-Photon Ionization of Ca Atom with Taking into Account the Electron Correlations <i>M. I. Haysak, V. I. Lengyel, D. M. Petrina, I. M. Shuba, O. I. Zatsarinny</i>	685
Application of Independent United Atom Model to Inelastic Scattering of Electrons by Hydrogen Molecule <i>N. S. Rao</i>	686
Electron-Ion (He^+) Scattering at Intermediate and High Incident Electron Energy Regions ($E \geq 100$ eV) <i>N. S. Rao</i>	687
Post-Post-Deadline Papers	
GAPHYOR: An Atomic and Molecular Data Center at Orsay <i>Konstantinos Katsonis, Jean-Loup Delcroix, William Assal, Claudette Leprince</i>	688
Database on Electron Impact Ionization <i>M. A. Lennon, K. L. Bell, H. B. Gilbody, J. G. Hughes, A. E. Kingston, F. J. Smith</i>	689
X-Ray Incoherent Scattering Factors for N_2 as Determined by High Energy Electron Impact Spectroscopy <i>S. N. Ketkar, R. A. Bonham</i>	690

Energy and Angular Distributions of Secondary Electrons Produced by the Electron Impact Ionization of Helium and Molecular Nitrogen <i>R. R. Goruganthu, W. G. Wilson, R. A. Bonham</i>	691
Resonances in the Interaction of Electrons with Sodium Atoms <i>I. I. Cherlenyak, V. I. Lengyel, F. F. Papp, N. I. Romanjuk, E. P. Sabad, O. B. Shpenik, O. I. Zatsarinny</i>	692
Resonances in the Differential Cross Sections for $e + \text{Li}$ —Scattering <i>I. I. Cherlenyak, S. M. Kazakov, O. V. Kristoforov, V. I. Lengyel, E. A. Masalovich, E. P. Sabad</i>	693
The Resonance States of He on the Metal Surface <i>O. S. Erkovich, V. V. Komarov, A. M. Popova, A. E. Romanovsky, S. G. Serebrjakov</i>	694
Charge Transfer in Ion-Atom Collisions as the Three-Body Problem <i>A. R. Ashurov, G. V. Avakov, L. D. Blokhintsev, A. M. Mukhamedzhanov</i>	695
Electron Impact Excitation of Copper Atoms from Metastable States <i>I. S. Aleksakhin, I. P. Zapesochny, T. A. Snegurskaya, I. I. Shafranyosh</i>	696
Observation of Radiative Transitions Between Autoionizing States of Lithium Atoms Excited by Electron Beam <i>I. S. Aleksakhin, G. G. Bogachev, I. P. Zapesochny, E. N. Postoi, S. Yu. Ugrin</i>	697
Influence of Collision Reduction of Natural Lifetimes of Resonance Levels on Count Rate Effects of Proportional Counters <i>T. Z. Kowalski, K. W. Ostrowski, J. Zajac</i>	698
One Electron Capture into Excited States and Excitation of Targets between He^+ or Ar^+ Ions and He or Ar Atoms Collisions in the Energy Range of 70-150 keV <i>Pan Guang Yan, Lei Ziming, Liu Jia Rui</i>	699
Electron Beam Attenuation and Absorption Through Matter Using Monte Carlo Calculations <i>A. Antolak, W. Williamson, Jr.</i>	700
The Dissociation of Ions and Ion Clusters by Multiple Collisions with a Neutral Buffer Gas <i>F. L. Eisele</i>	701
Large Order Perturbation Theory for Z_1eZ_2 <i>R. J. Damburg, R. Kh. Propin, V. V. Martyschchenko</i>	702
On the Proton Impact Excitation of Zinc, Cadmium and Mercury Atoms <i>M. Ju. Ciple, V. L. Ovchinnikov, O. B. Shpenik</i>	703
On Oscillations of Total Cross Section for Exciting the 2312Å Line in $\text{Ar}^+ + \text{Cd}$ System <i>Yu. A. Ksavery</i>	704
Impact-Parameter Dependence of δ -Electron Emission in Fast Ion-Atom Collisions <i>C. Kelbch, J. Ullrich, V. Dangendorf, S. Kelbch, W. Schadt, K. Bethge, H. Schmidt-Böcking</i>	705
Evidence for Independent Particle Behavior in Fast Rydberg Hydrogen Atom Collisions with Neutral Atoms and Molecules <i>M. King, L. Wang, T. J. Morgan</i>	706
Ionization Cross Section of Ytterbium Atoms by Electron Impact <i>M. M. Ali, P. N. Volovich, V. L. Ovchinnikov, L. L. Shimon</i>	707
K-Emission Investigation by Electron Bombardment of Free Potassium Atoms <i>I. P. Zapesochny, V. S. Vukstich, A. M. Solomon</i>	708
Electron-Electron Coincidence Spectrometer for the Study of Relative Triple Differential Cross Sections for Autoionizing Transitions in Metals <i>A. A. Borovik, V. V. Vakula</i>	709

**Abstracts
of
Contributed Papers**

ATOMS IN STRONG ELECTRIC AND MAGNETIC FIELDS: THE H-ATOM

H. Rottke, A. Holle, Karl H. Welge

Fakultät f. Physik, Universität Bielefeld, D-4800 Bielefeld 1, FRG

The physics of highly excited atoms in strong external electric and magnetic fields is of inherent and general interest for two reasons: Firstly, the external forces are on a par with, or larger than the internal atomic binding forces, and, secondly, they profoundly determine the symmetry of the atomic system. Such systems with strong mixing of internal and external interactions are thus no more amenable to conventional perturbation treatments. Aside from the interest as such, the strong external force mixing is closely related for instance to Rydberg-state physics, collisional processes in external fields (plasmaphysics), and atomic species in superstrong fields (astrophysics).

The H atom, with its purely Coulombic potential, has naturally served as basis and prototype in extensive theoretical work in this field. On the other hand, almost all experimental work has been done with non-hydrogenic atoms, due to experimental obstacles encountered with the H atom. In fact, few experiments have been done until recently with H in electric fields, and none are known in magnetic fields.

In this paper we first review briefly systematic experimental studies with H in electric fields, which we have carried out recently at excitation energies around the zero-field ionization limit, $E \sim 0$.⁽¹⁾ We have employed a two-step excitation technique in crossed laser-atom beams, $H(1) + \text{vuv} \rightarrow H(2) + \text{uv} \rightarrow H^*$, with tunable vuv and uv laser light, each of parallel (Π) or perpendicular (σ) polarization. In the $n = 2$ state individual Stark sublevels of practically pure parabolic character are prepared, a special feature of the H atom, not encountered with atoms in previous studies. A sample of an ionization spectrum is shown in Fig. 1, exhibiting typical quasi-stable states at $E < 0$ and field induced oscillatory resonances in the ionization cross section at $E \geq 0$. Further results will be given and discussed in relation to existing theory.

In the second, main part of the paper we report first experiments with H in strong magnetic fields ($B \lesssim 6T$) around the ionization threshold, where the diamagnetic interaction ($H_{\text{diam}} = 1/8 \alpha^2 B^2 r^2 \sin^2 \theta$) is the dominating external force, of comparable strength with, or larger than the Coulomb interaction ($H_{\text{coul}} = -1/r$). Employing again the two-step (vuv + uv) excitation, single Paschen-Back levels are prepared in the first step. Employing field-ionization after the excitation laser pulse, ionization spectra have been taken at excitation energies

from the l-mixing regime (zero-field Rydberg states $n \geq 25$) through the n-mixing and the threshold ($H_{\text{diam}} = H_{\text{coul}}$) region up into the continuum ($E > 0$) at $B = 0$ to 6 Tesla. Depending on the initial Paschen-Back state in $n = 2$ and the uv polarization final states with $m_l = 0, \pm 1, \pm 2$ are excited, all of even parity. Fig. 2 shows a sample spectrum around the ionization threshold. We observe, for the first time, quasi-Landau resonances with the H atom. Further results will be presented and discussed in relation to theory.

1) H. Rottke, K. H. Welge; submitted for publication; Phys. Rev. A (1985).

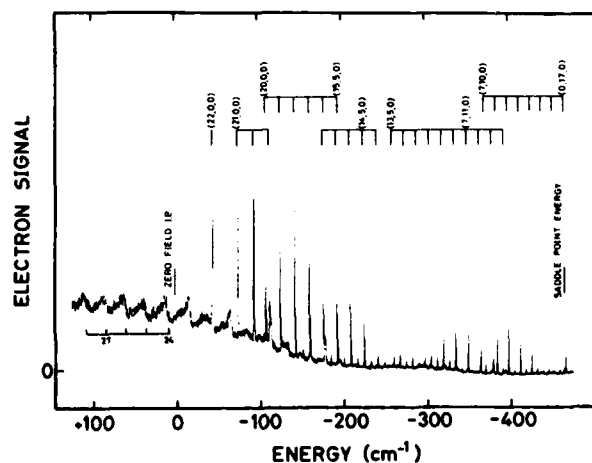


FIGURE 1 Ionization spectrum of the H atom in an electric field $F=5714$ V/cm. Excitation with Π polarized radiation from the $11,0,0 >$ parabolic state of the Stark manifold in $n=2$. Quasi-stable states labeled by parabolic quantum number notation, $|n_1, n_2, |m||$.

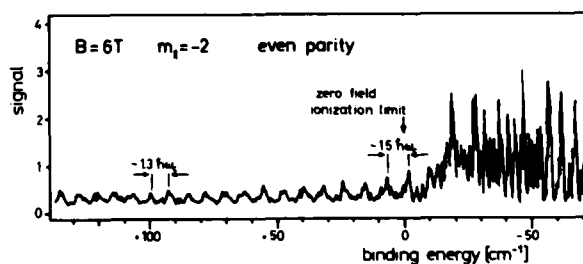


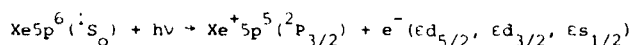
FIGURE 2 Ionization spectrum of the H atom around the ionization threshold in a magnetic field $B=6$ Tesla. Excitation with σ polarized radiation from the Paschen-Back sublevel $|m_l = -1\rangle$, $|m_s = \pm 1/2\rangle$ to final states $m_l^f = -2$, even parity.

DETERMINATION OF THE TRANSITION MATRIX ELEMENTS AND THEIR RELATIVE PHASES FROM EXPERIMENTAL PHOTOELECTRON SPIN POLARIZATION DATA FOR 5p-AUTOIONIZATION OF XENON

Ch. Heckenkamp, F. Schäfers⁺ and U. Heinzmann

Fritz-Haber-Institut der MPG, D-1000 Berlin 33, W. Germany
Fakultät für Physik der Universität Bielefeld, D-4800 Bielefeld 1, W. Germany
⁺BESSY, D-1000 Berlin 33, W. Germany

The dynamical spin-polarization parameters A , α and ξ , which have been determined from angle-resolved measurements of the photoelectron spin-polarization vector using circularly polarized VUV-radiation^{1,2} are needed to completely characterize the dipole transition matrix elements and their phase shift differences individually. For the 5p-autoionization range of xenon there are three open continuum channels according to



which are described by the three dipole transition matrix elements D_1 , D_2 , D_3 and their relative phases, respectively. Combination of the 5 dynamical parameters A , α , ξ , the photoionization cross section Q^3 and the asymmetry parameter B^4 as reported in Ref. 1 make the complete determination of D_1 , D_2 , D_3 and their relative phases possible⁵.

Fig. 1 shows the results for the three matrix elements D_1 , D_2 and D_3 corresponding to the $\epsilon d_{5/2}$, $\epsilon d_{3/2}$ and $\epsilon s_{1/2}$ channel, respectively, as well as the relative phases in units of π (the coulomb phases, which are analytically known, are eliminated).

D_1 mainly follows the energy dependence of the photoionization cross section (because D_1^2 is much stronger than D_2^2 or D_3^2) showing the pronounced d-resonance structure of the autoionization. The enhancement of the d-matrix element D_2 at about 98.5 nm corresponding to the here not completely resolved narrow s-autoionization resonance seen in the cross section and in D_3 indicates the importance of interchannel interactions in the autoionization region of xenon. This is also demonstrated by the behaviour of the d-s-phase shift difference $\pi \cdot (\mu_1 - \mu_3)$, which is close to $-\pi$ at the cross section minimum, whereas the phase shifts of both d-channels μ_1 and μ_2 are identical within the experimental uncertainties except where D_1 rises at 99.8 and 96.8 nm. This indicates that the spin-orbit interaction influences the amplitudes more than the phases in the autoionization range.

References

1. Ch. Heckenkamp, F. Schäfers, G. Schönhense and U. Heinzmann, book of abstracts 14. ICPEAC 1985

2. Ch. Heckenkamp, F. Schäfers, G. Schönhense and U. Heinzmann, Phys. Rev. Lett. **52**, 421 (1984)
3. R. E. Huffman, Y. Tanaka, J. C. Larrabee, J. Chem. Phys. **39**, 902 (1963)
4. J. A. R. Samson and J. L. Gardner, Phys. Rev. Lett. **22**, 1327 (1983)
5. Ch. Heckenkamp, Ph. D. thesis unpubl., Berlin 1984

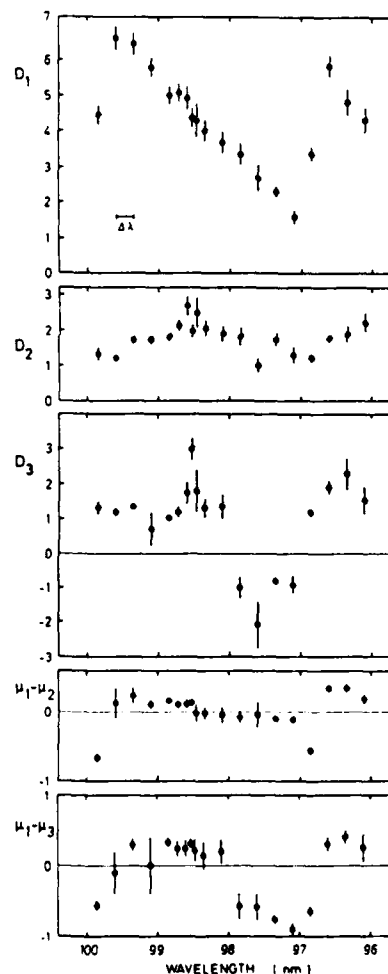


Fig. 1: "Experimental" dipole transition matrix elements D_1 , D_2 , D_3 and their relative phases in units of π in the 5p-autoionization range of xenon.

THE PHOTOELECTRON SPIN-POLARIZATION PARAMETERS IN THE
5p-AUTOIONIZATION RANGE OF XENON

Ch. Heckenkamp, F. Schäfers⁺, G. Schönhense and U. Heinzmann

Fritz-Haber-Institut der MPG, D-1000 Berlin 33, West Germany
Fakultät für Physik der Universität Bielefeld, D-4800 Bielefeld 1, West Germany
⁺BESSY, D-1000 Berlin 33, West Germany

The spin-polarization parameters for photoelectrons from free Xenon atoms have been measured in the wavelength range from 96 nm to 100 nm in an angle-resolving experiment using circularly polarized synchrotron radiation emitted out of plane by the storage ring BESSY. The experimental arrangement¹ basically consists of an especially designed rotatable electron spectrometer and a high energy Mott-detector and allows the measurement of the photoelectron spin-polarization components $A(\theta)$ parallel to the photon momentum and $P_{\perp}(\theta)$ perpendicular to the reaction plane. Knowledge of these two components for several emission angles θ allows the determination of the three parameters¹ A , α and ξ . The measurements have been performed in the 5p-autoionization range between the $2P_{3/2}$ - and $2P_{1/2}$ -thresholds of Xenon with a radiation bandwidth of $\Delta\lambda = 0.25$ nm. Fig. 1 shows data for the total photoionization cross section Q^2 and the asymmetry parameter β^3 together with the values of the spin-parameters measured. Earlier results for the spin-parameter A^4 (dotted curve), employing a completely different method, which yields the spin-polarization of the angle-integrated photoelectron flux, are also given and show good agreement with the present data. For comparison, the results of an RRPA-calculation⁵ and a semiempirical MQDT-calculation⁶, convoluted with the experimental bandwidth, are shown as full and dashed curves, respectively. The wavelength-dependences of the spin-parameters measured are in reasonable agreement with both theories.

References

1. Ch. Heckenkamp, F. Schäfers, G. Schönhense and U. Heinzmann, Phys. Rev. Lett. **52**, 421 (1984)
2. R. E. Huffmann, Y. Tanaka and J. C. Larrabee, J. Chem. Phys. **39**, 902 (1963)
3. J. A. R. Samson and J. L. Gardner, Phys. Rev. Lett. **31**, 1327 (1973)
4. U. Heinzmann, F. Schäfers, K. Thimm, A. Wolcke and J. Keßler, J. Phys. B **12**, L679 (1979) and U. Heinzmann, J. Phys. B **13**, 4353 (1980)
5. W. R. Johnson, K. T. Cheng, K. N. Huang and M. LeDourneuf, Phys. Rev. A **22**, 989 (1980)
6. C. M. Lee, Phys. Rev. A **10**, 1598 (1974)

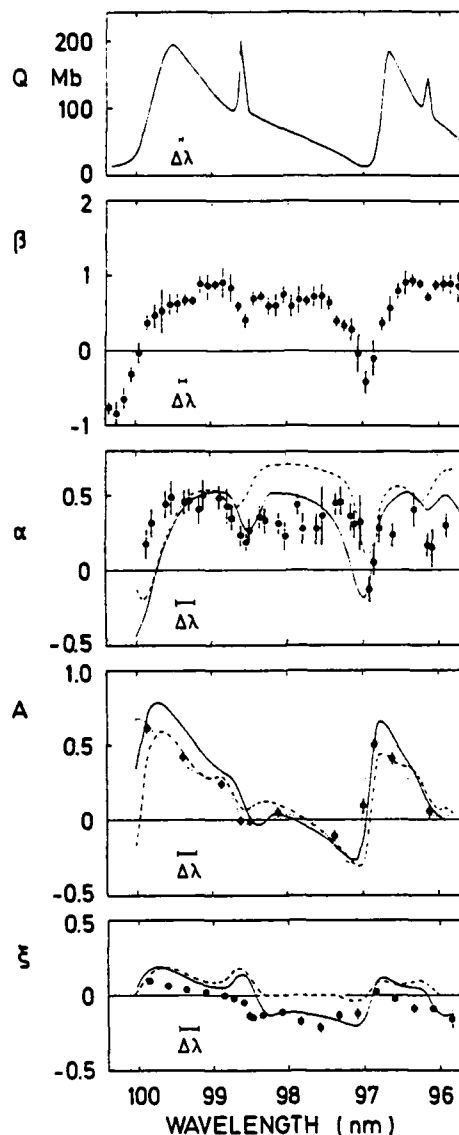


Fig. 1: Photoionization cross section Q^2 , asymmetry parameter β^3 and spin-polarization parameters in the autoionization range of Xenon. Theoretical values for α , A and ξ , are represented by the full (RRPA⁵) and dashed (semiempirical⁶) curves.

ENERGY DEPENDENCE OF THE SPIN-POLARIZATION PARAMETERS FOR Hg 5d PHOTOIONIZATION
WITH CIRCULARLY POLARIZED LIGHT

F. Schäfers⁺, Ch. Heckenkamp, G. Schönhense and U. Heinzmann

Fritz-Haber-Institut der MPG, D-1000 Berlin 33, W. Germany
Fakultät für Physik der Universität Bielefeld, D-4800 Bielefeld
BESSY, D-1000 Berlin 33, West Germany

Circularly polarized VUV-radiation from the storage ring BESSY was used to measure all three spin-polarization parameters of photoelectrons from the Hg 5d-shell in the photon energy range from threshold to 32 eV. The spin-polarization vector can be characterized by the three dynamical parameters A , α and ξ which are functions of the photon energy. Up to now only data of the spin-polarization of the total photoelectron flux, where the fine structure was not resolved, and of the polarization component perpendicular to the reaction plane P_{\perp} , described by the parameter ξ , existed¹. The new measurements were stimulated by a recent experimental analysis of the 5d-photoionization process in the approximate LS-coupling scheme².

The experimental arrangement³ is shown in Fig. 1. The circularly polarized light from the storage ring, dispersed by the 6.5 m NIM, crosses the Hg-atomic beam in a region free of electric and magnetic fields. The photoelectrons emerging under the angle θ are energy-analyzed by a rotatable analyzer system, that keeps the outgoing photoelectron beam fixed in space independent of the emission angle chosen. After acceleration to 120 keV the transverse polarization components $A(\theta)$ parallel to the photon momentum and $P_{\perp}(\theta)$, from which the three parameters A , α and ξ can be evaluated, are analyzed simultaneously in a Mott detector.

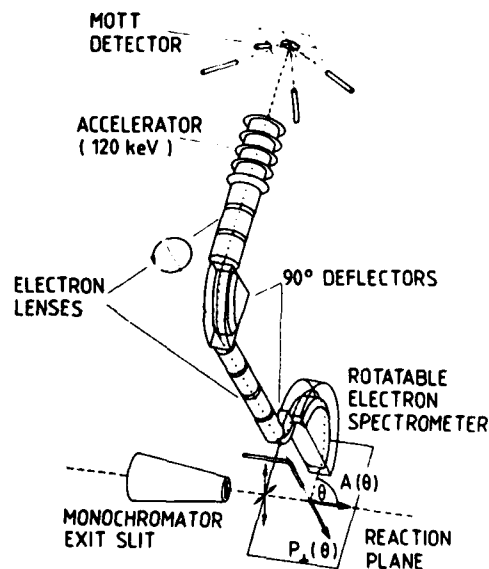


Fig. 1: Set-up of the experiment, coupled to the exit slit of the 6.5 m NIM

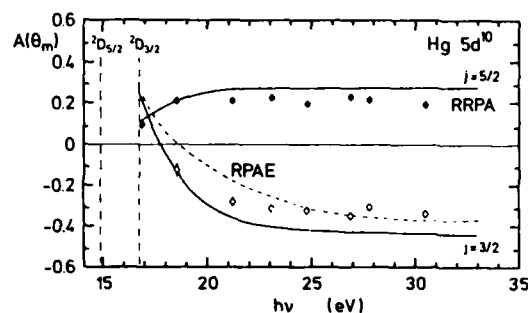


Fig. 2: Energy dependence of the spin-parameter A
solid lines: ref. 4, dashed line: ref. 5,6

As an example the energy dependence of the parameter $A(=A(\theta_m))$ is shown in Fig. 2 for both final ionic states $2D_{5/2}$ (closed circles) and $2D_{3/2}$ (open circles). The ionization thresholds are represented by the vertical dashed lines. The RRPA-calculation⁴ (solid curves) which includes correlations between 5d and 6s (8 channels) and uses experimental thresholds is in reasonable agreement with experiment. The RPAE-curve (dashed) was calculated from non-relativistic matrix elements and phase shifts^{5,6}. This curve is shifted by 2.6 eV to fit the experimental threshold.

An evaluation of transition matrix elements and their corresponding phase shifts in the exact jj-coupling scheme (6 continuum channels) on the basis of the experimental results in combination with cross section data^{7,8} is in progress.

References

1. G. Schönhense, F. Schäfers, U. Heinzmann, J. Kessler, Z. Phys. A **304**, 31 (1982)
2. G. Schönhense, U. Heinzmann, Phys. Rev. A **29**, 987 (1984)
3. Ch. Heckenkamp, F. Schäfers, G. Schönhense, U. Heinzmann, Phys. Rev. Lett **52**, 421 (1984)
4. W. R. Johnson, V. Radojević, P. Deshmukh, K. T. Cheng, Phys. Rev. A **25**, 337 (1982)
5. V. K. Ivanov, S. Yu. Medvedev, V. K. Sosnivkev, Prepr. No. 615 of A. F. Ioffe Physical Technical Institute, Leningrad (1979)
6. N. A. Cherepkov, private communication (1981)
7. S. P. Shannon, K. Codling, J. Phys. B **11**, 1193 (1978)
8. G. Schönhense, J. Phys. B **14**, L187 (1981)

PHOTOELECTRON SPIN-POLARIZATION IN THE COOPER MINIMUM OF Hg6s

F. Schäfers⁺, Ch. Heckenkamp and U. Heinzmann

Fritz-Haber-Institut der MPG, D-1000 Berlin 33, W. Germany
 Fakultät für Physik der Universität Bielefeld, D-4800 Bielefeld
 BESSY, D-1000 Berlin 33

Since Fano's prediction of the spin-polarization of photoelectrons ejected from alkali atoms near the minimum of the cross section¹, experimental and theoretical effort has been spent to the phenomenon of Cooper minima in ns- and ns²-subshells, since the relativistic effect of spin-orbit interaction in the continuous spectral range can be studied here. In theoretical calculations the position of the cross section minimum, the shape of the angular distribution and the behaviour of the spin-polarization parameters react very sensitive upon the correlations included. Recently, the Relativistic Time Dependent Local Density Approximation (RTDLDA)² was able to reproduce the experimental data of the β -parameter, describing the differential photoionization cross section, of Xe and Kr outer s-subshells^{3,4}. The rare gases are, however, not accessible for spin-polarization measurements at present due to the low cross section of 0.1 Mb and the high photon energies needed.

For ionization of the 6s-shell of mercury, however, the situation is different. Experiments indicate a Cooper minimum at about 20 eV photon energy with a cross section of 0.4 Mb⁵. At three intense rare gas resonance lines values of the β -parameter and the spin-polarization component P_{\perp} perpendicular to the reaction plane, described by the parameter ξ , have been reported^{6,7}.

The high flux of circularly polarized VUV-radiation emitted out of plane by the storage ring BESSY made angle- and spin-resolved measurements⁸ in this region possible at stored beam currents of about 500 mA.

Fig. 1 shows first results of the new measurements together with the earlier data⁷ and with the cross section⁵. In contrast to the experimental data the RRPA⁹ and the RTDLDA¹⁰ calculations yield a minimum below the $^2D_{2/3}$ -threshold (vertical dashed line) whereas a Tamm-Dankoff-calculation⁹ gives a Cooperminimum above the threshold close to the experimental data. The new data of the ξ -parameter seem to indicate a maximum close to the threshold at 17 - 18 eV photon energy which is expected to correlate with the cross section minimum. Measurements below the $^2D_{3/2}$ -threshold, where the cross section is perturbed by autoionization processes are in progress and should lead to a further clarification of this point.

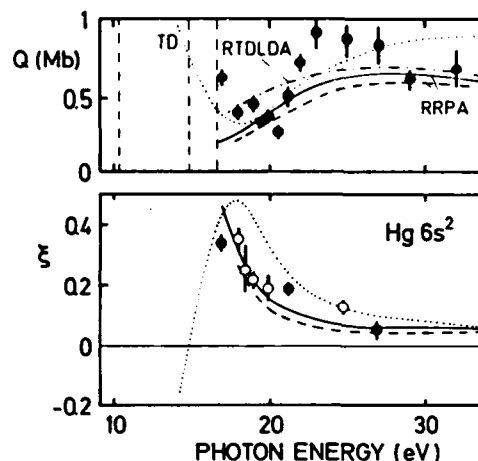


Fig. 1: Upper part: photoionization cross section Q^7 , experimental points⁵, full and dashed curve: RRPA⁸, dot-dashed: RTDLDA¹⁰, dotted: Tamm-Dankoff⁹. lower part: spin parameter ξ , full circles⁷, open circles this work, curves as above⁹.

References

1. U. Fano, Phys. Rev. A **8**, 131 (1969) and **184**, 250 (1969)
2. F. A. Parpia, W. R. Johnson, V. Radojević, Phys. Rev. A **29**, 3173 (1984)
3. A. Fahlmann, T. A. Carlson, M. O. Krause, Phys. Rev. Lett. **50**, 1114 (1983)
4. H. Derenbach, V. Schmidt, J. Phys. B **16**, L337 (1983)
5. S. P. Shannon, K. Codling, J. Phys. B **11**, 1193 (1978)
6. A. Niehaus, M. W. Ruf, Z. Phys. **252**, 84 (1972)
7. G. Schönhense, U. Heinzmann, J. Kessler, N. A. Cherepkov, Phys. Rev. Lett. **48**, 603 (1982)
8. Ch. Heckenkamp, F. Schäfers, G. Schönhense, U. Heinzmann, Phys. Rev. Lett. **52**, 421 (1984)
9. W. R. Johnson, V. Radojević, P. Deshmukh, K. T. Cheng, Phys. Rev. A **25**, 337 (1982)
10. F. A. Parpia, W. R. Johnson J. Phys. B **16**, L375 (1983)

PHOTOIONIZATION OF ATOMIC AND MOLECULAR CHLORINE

J.A.R. Samson, Y. Shafer, and G.C. Angel

Behlen Laboratory of Physics, University of Nebraska, Lincoln, NE. 68588

The relative photoionization cross sections of atomic and molecular chlorine have been measured by use of a mass spectrometer over the spectral range from 160 to 750 Å. The atomic chlorine was produced in a microwave discharge by the dissociation of Cl_2 . Approximately 20% dissociation was produced.

The absolute total absorption cross sections and ionization efficiencies of Cl_2 were measured at selected wavelengths by use of a double ionization chamber.¹ Thus, the relative ionization cross sections were placed on an absolute basis.

In Fig. 1 we have normalized the relative cross sections of atomic chlorine to the theoretical results of Shahabi and Starace², Fielder and Armstrong³, and Brown et.al.⁴. Because most of the calculated data tend to agree at higher photon energies, the region of normalization was taken around 350 Å. Good agreement is obtained for wavelengths below 500 Å. However, above 500 Å deviations of up to a factor of two occur.

Presumably, this implies that important correlation effects have been omitted near the threshold. In Fig. 2 we have normalized our results to the data of Cherepkov⁵ and also show the calculations of Combet-Farnoux⁶. The overall agreement with Cherepkov's RPA calculation is very good except at their shortest wavelength.

Acknowledgement

This material is based upon work supported by the National Science Foundation under Grant No. PHY-8214172.

References

1. J.A.R. Samson and G.N. Haddad, *J. Opt. Soc. Am.* **64**, 47 (1974).
2. S. Shahabi and A.F. Starace, *Phys. Rev. A* **30**, 1819 (1984).
3. W.R. Fielder and L. Armstrong, Jr., *Phys. Rev. A* **28**, 218 (1983).
4. E.R. Brown, S.L. Carter, and H.P. Kelly, *Phys. Rev. A* **21**, 1337 (1980).
5. N.A. Cherepkov and L.V. Charnysheva, *Izv. Akad. Nauk. SSSR, Ser. Viz.* **41**, 2518 (1977).
6. M. Lamoureux and F. Combet-Farnoux, *J. Phys. (Paris)* **40**, 545 (1979).

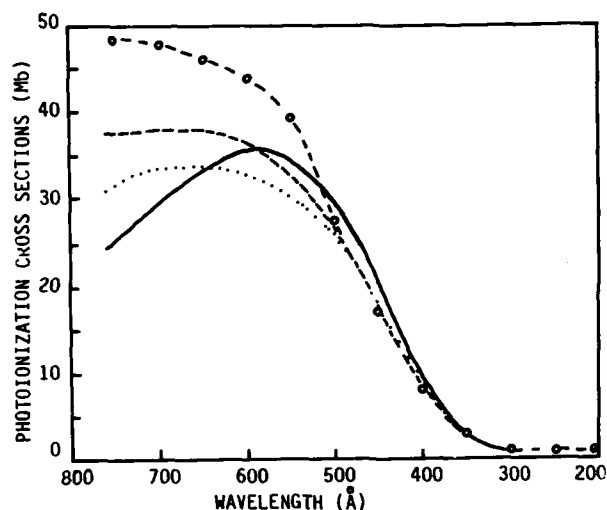


FIGURE 1. Photoionization cross sections of Cl normalized at 350 Å. Present experimental data (o): Theoretical data, ref. 2 (—), ref. 3 (····), ref. 4 (---).

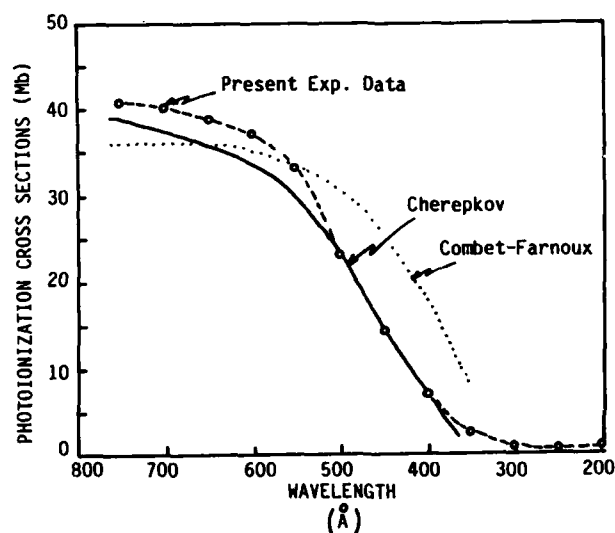


FIGURE 2. Photoionization cross sections of Cl normalized to ref. 5. Present data (o): Theoretical data, ref. 5 (—), ref. 6 (····).

MEASUREMENT OF THE 5d PHOTOIONIZATION CROSS SECTION IN LASER EXCITED
BARIUM ATOMS BETWEEN 15 eV AND 150 eV PHOTON ENERGY

J.M. Bizau, D. Cubaynes, P. Gérard, F. Willeumier

Laboratoire de Spectroscopie Atomique et Ionique and LURE, B.350,
91405-Orsay, France

J.C. Keller, J.L. LeGouët, J.L. Picqué

Laboratoire Aimé Cotton, B.505, 91405-Orsay, France

B. Carré

Service de Physique des Atomes et des Surfaces, Saclay, 91191-Gif-sur-Yvette

D. Ederer

National Bureau of Standards, Washington, D.C. 20234, USA

G. Wendin

Chalmers Institute, S. 402-20, Göteborg, Sweden.

Combining the use of laser and synchrotron radiations, we had demonstrated the feasibility of photoionization experiments in excited atoms.¹ Later on, we measured oscillator strengths for the excitation of a core electron in atoms prepared in specific excited states.² Here, we present the first experimental determination, over a broad photon energy range, of a photoionization cross section for an atom in an excited state, specifically the 5d-cross section in laser excited barium atoms. We have also calculated the variation of this cross section in the LDRPA approximation.

In our experiment, laser and synchrotron radiations irradiate an effusive beam of Ba atoms in the source volume of a cylindrical mirror analyzer used to study the energy distribution of the ejected photoelectrons.⁴ The synchrotron radiation of the ACO storage ring is monochromatized by a toroidal grating monochromator which is continuously tunable between 15 eV and 150 eV. The cw ring dye laser is locked and stabilized to the $6s\ ^1S \rightarrow 6p\ ^1P$ resonance of Ba at 5535 Å. However, as already mentioned,² all photoelectron spectra taken in the continuum as well as in the region of resonant excitation below the 5p ionization threshold,² reveal that the excited atoms are, in

our experimental conditions, in the $6s5d\ ^1,^3D$ states. The photoelectrons from the 5p and 5d subshells were simultaneously recorded at each photon energy. The relative variation of the 5d cross section was obtained from the integrated area under the 5d photoline. The absolute scale was established by normalization to the theoretical 5p cross section also calculated in this work.

The results are presented in Fig.1. The theoretical results reproduce well the general behavior of the cross section. However, if a simple HS calculation is able to describe the experimental variation at low energy, the resonant enhancement of the 5d cross section observed at the opening of the 4d ionization channels can be reproduced theoretically only by taking into account inter-shell correlations.

1. J.M. Bizau, F. Willeumier, P. Dhez, D. Ederer, J.L. LeGouët and P. Koch, "Laser Techniques for Extreme Ultraviolet Spectroscopy", AIP Proc. Ser. n°90, New York, 1982, p.331.
2. F. Willeumier, "Laser Techniques in the Extreme Ultraviolet", AIP Proc. Ser. n°119, New York, 1984, p.220 and J.M. Bizau et al., to be published.
3. C. Theodosiou, private communication.
4. J.M. Bizau, P. Gérard, F. Willeumier and G. Wendin, Phys. Rev. Lett. 53, 2083 (1984).

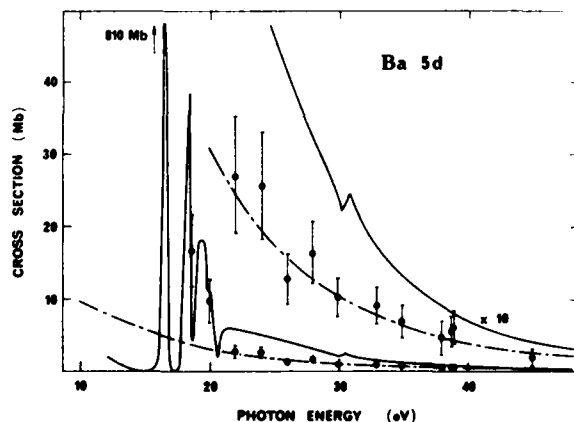


Fig.1- Variation of the 5d cross section from 10 to 40 eV. Theory is from this work (—) and from Ref.3 (---)

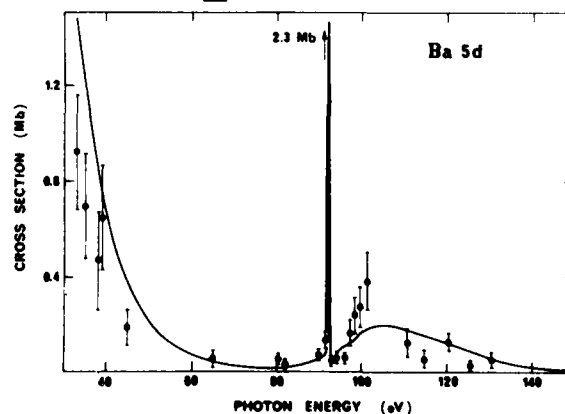


Fig.1- (continued). Variation of the 5d cross section above 40 eV photon energy. The 4d thresholds in the excited atom are around 96 and 98 eV.

EXPERIMENTAL AND THEORETICAL DETERMINATIONS OF OSCILLATOR STRENGTHS
FOR PHOTOEXCITATION OF A CORE ELECTRON IN ATOMIC LITHIUM

P. Gérard, D. Cubaynes, J.M. Bizau and F. Willeumier

Laboratoire de Spectroscopie Atomique et Ionique and LURE, B.350, 91405-Orsay, France

C.J. Zeippen

Observatoire de Paris, Section d'Astrophysique, 92190-Meudon.

In the work presented here, we have used the technique of photoelectron spectrometry to study, between 50 eV and 150 eV, the photoelectrons ejected by a monochromatic photon beam from the 2s and 1s subshells of atomic Li.¹ In this photon energy range, the 2s photoionization cross section is very weak, but in the resonance region below the 1s2s ³S ionization threshold, between 58 and 65 eV. In this energy region, we observed a huge enhancement of the 2s photoelectron line (1s²1S final state of Li⁺) due to the decay of the 1s2snp ²P autoionizing states formed by photoexcitation. We have measured the oscillator strengths of these 1s²2s ²S → 1s2snp ²P transitions. We have performed a new calculation of these oscillator strengths to study the extreme sensitivity of this parameter to the treatment of electron correlations for the first resonances.

In this experiment, we used our previously described² apparatus at the ACO synchrotron radiation facility, to measure, with a cylindrical mirror analyzer, the electrons emitted at the magic angle of 54°44' in the interaction of a monochromatic photon beam with a beam of Li vapor.

Fig.1 shows the excitation function of the 2s-photoelectron line, i.e. the integrated area under this line, when the photon energy is varied across the 1s²2s ²S → 1s(2s2p ¹P)²P resonance, around 60.40 eV. Outside of the resonance, the 2s signal is negligible in comparison with the resonant intensity. This means that the direct photoionization process is very weak, leaving no possibility for interference effects to occur. Thus, in assuming that the radiative decay of the excited states is negligible for this low-Z element, in comparison with the autoionization rate, the intensity of the 2s photoelectron peak

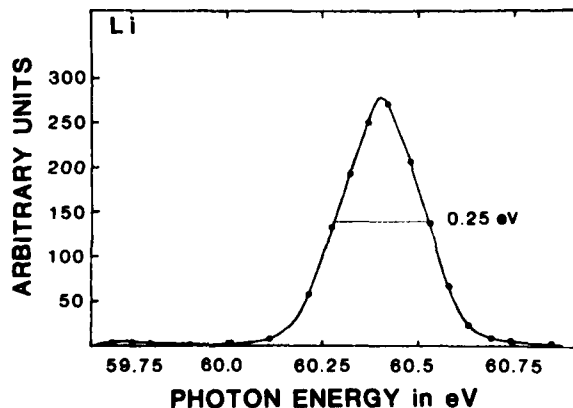


Fig.1- Excitation function of the 2s photoelectron line.

at the resonance is directly proportional to the oscillator strength of the excitation transition.¹ The relative values were put on an absolute scale by comparing the resonant 2s and the non-resonant 1s photolines, using the total photoabsorption cross section previously measured.³

Table I presents our results. The RPAE calculations⁴ are in good agreement with the experimental data but for the two first resonances. On the other hand, the values calculated by Chung,⁵ using a saddle-point technique, were in better overall agreement with the experiment. In view of this difference for the first transitions, we attempted a series of new calculations using two different programs, in order to provide a further check of the influence of electron correlations. We employed the code SUPERSTRUCTURE and the HF code CIV3. We included $\bar{3}s$, $\bar{3}p$ and $\bar{3}d$ pseudo-orbitals and we tested various optimization procedures. Our final f-values are included in Table I, from both length and velocity calculations. Our results are very close to the experimental data. The adequacy of our theoretical approach is also confirmed by the good agreement between the theoretical and experimental values of the transition energies.

Transition	Exp ($\pm 15\%$)	Theory		
		RPAE	CHUNG	This work
1s ² 2s ² S →				
1s(2s2p ³ P) ² P	0.24	0.342	0.280	0.260 L 0.235 V
1s(2s2p ¹ P) ² P	0.007		0.0075	0.0052 L 0.0045 V
(1s2s ³ S)3p ² P	0.053	0.0562	0.0466	
(1s2s ³ S)4p ² P	0.019	0.0182	0.0170	
(1s2s ³ S)5p ² P	0.008		0.0079	

Table I.- Experimental and theoretical f-values.

References

1. P. Gerard, Thesis, Univ.Orsay, 1984.
2. J.M. Bizau, P. Gérard, F. Willeumier, G. Wendin, Phys. Rev. Lett. **53**, 2083(1984).
3. G. Mehlman, J. Cooper and E. Saloman, Phys. Rev. **A25**, 2113 (1982).
4. M.Ya. Amusia, N.A. Cherepkov, D. Zivanovic and V. Radjevic, Phys. Rev. **A13**, 1466 (1976).
5. K.T. Chung, Phys. Rev. **A23**, 2957 (1981).

3p PHOTOIONISATION IN ATOMIC MANGANESE*

R. Malutzki and V. Schmidt

Fakultät für Physik, Universität Freiburg, Hermann-Herder-Str. 3, 7800 Freiburg, FRG

According to Amusia et al.¹ the manganese (Mn) atom can be described conveniently in the spin-polarised orbital approximation i.e. $3p^+$ and $3p^-$ ionisation can be distinguished: The ejection of a $3p^+$ electron produces a $5p$ that of a $3p^-$ electron a $7p$ final ionic state both with different energy. The investigation of the angular distribution of $3p^+$ -photoelectrons has been described elsewhere (Malutzki et al.²). Qualitative agreement with theoretical predictions of Amusia et al.³ has been achieved. However in this investigation no hint for the existence of the $5p$ final ionic state could be found.

With improved experimental conditions partly at the expense of reduced angular range of the electron analyser we searched again for the $3p^+$ -photoprocess. This time with success. Figure 1 gives one example at 94.5 eV photon energy (lower part). For comparison, the upper part of this figure shows an electron spectrum at 60.4 eV photon energy. The interesting region of kinetic energies is at around 30 eV because here the electrons from the radiationless decay of the $3p$ hole are expected: Coster-Kronig (CK) decay from $3p^+$ -ionisation, super Coster-Kronig (sCK) decay from $3p^-$ -ionisation. In the spectrum at lower photon energy the satellite lines (marked by arrows, see also Ref. 4-6) from $3d$ -ionisation are just in this energy region. However, at higher photon energy they move away. Instead, the $3p^7p$ photoline with a satellite (S), its subsequent CK decay as well as the $3p^5p$ photoline with its subsequent sCK decay can be seen clearly.

A first analysis of our spectra gives the following results. i) the binding energies are $E_b = 57.4$ eV for the $3p^7p$ photoline, $E_b = 60.5$ eV for the satellite S and $E_b = 75.0$ eV for the $3p^5p$ photoline. ii) Our energy separation between the $7p$ and $5p$ photolines agrees with that found in solid Mn⁷. iii) Our CK and sCK transitions give direct confirmation to the assignment of structures in the electron spectrum of Mn following electron impact⁸. iv) Because of the large level width there is a large energy shift due to post-collision interaction for photon energies just above threshold. v) Because of the large natural line width the $3p^5p$ photoline appears in the spectrum only as a small structure; however, at 80 eV photon energy the partial cross sections for ejection of a $3p^+$ or a $3p^-$ electron are nearly equal. More quantitative data will be given at the conference.

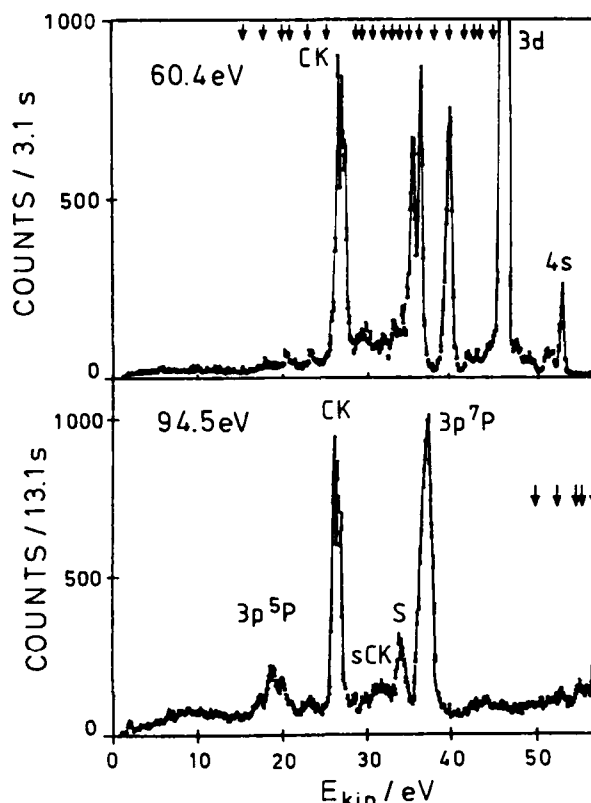


Figure 1 Electron spectra of atomic manganese.

References

1. M.Ya. Amusia, V.K. Ivanov and L.V. Cherhysheva, J.Phys. B 14, L19 (1981)
2. R. Malutzki, M.S. Banna, W. Braun and V. Schmidt, J.Phys. B 18 (1985)
3. M.Ya. Amusia, V.K. Dolmatov and V.K. Ivanov, J.Phys. B 16, L753 (1983)
4. P.H. Kobrin, U. Becker, C.M. Truesdale, D.W. Lindle, H.G. Kerkhoff and D.A. Shirley, J.Electr.Sp. 34, 129 (1984)
5. M.O. Krause, T.A. Carlson and A. Fahlman, Phys.Rev. 30, 1316 (1984)
6. E. Schmidt, H. Schröder, B. Sonntag, H. Voss and H.E. Wetzel, J.Phys. B 18, 79 (1985)
7. S.P. Kowalczyk, L. Ley, F.R. McFeely and D.A. Shirley, Phys.Rev. B 11, 1721 (1975)
8. E. Schmidt, H. Schröder, B. Sonntag, M. Voss and H.E. Wetzel, J.Phys. B 17 (1984) 707

*Work supported by the Bundesminister für Forschung und Technologie.

THRESHOLD PHOTOIONIZATION OF Kr 3d SUBSHELL*

P.A. Heimann, D.W. Lindle, T.A. Ferrett, M.N. Piancastelli, and D.A. Shirley

Materials and Molecular Research Division, Lawrence Berkeley Laboratory
Department of Chemistry, University of California, Berkeley, California 94720 USA

A threshold electron analyzer has been constructed for experiments at the Stanford Synchrotron Radiation Laboratory (SSRL). This time-of-flight analyzer has extraction, acceleration, and drift regions giving a total flight distance of 21.5 cm. It is calculated that all electrons with kinetic energies between 0 and 0.03 eV are collected, irrespective of their initial ejection angle. Figure 1 shows a scan across the Kr 3d(3/2,5/2)-np discrete resonances and 3d thresholds taken with this analyzer. The electron signal, 7 counts/s on the first resonance, has been corrected for the variation in the light intensity.

In Fig. 1, the prominent appearance of the below-threshold resonances shows the relative strength of the decay pathway to doubly ionized Kr²⁺ final states. The intensities of the

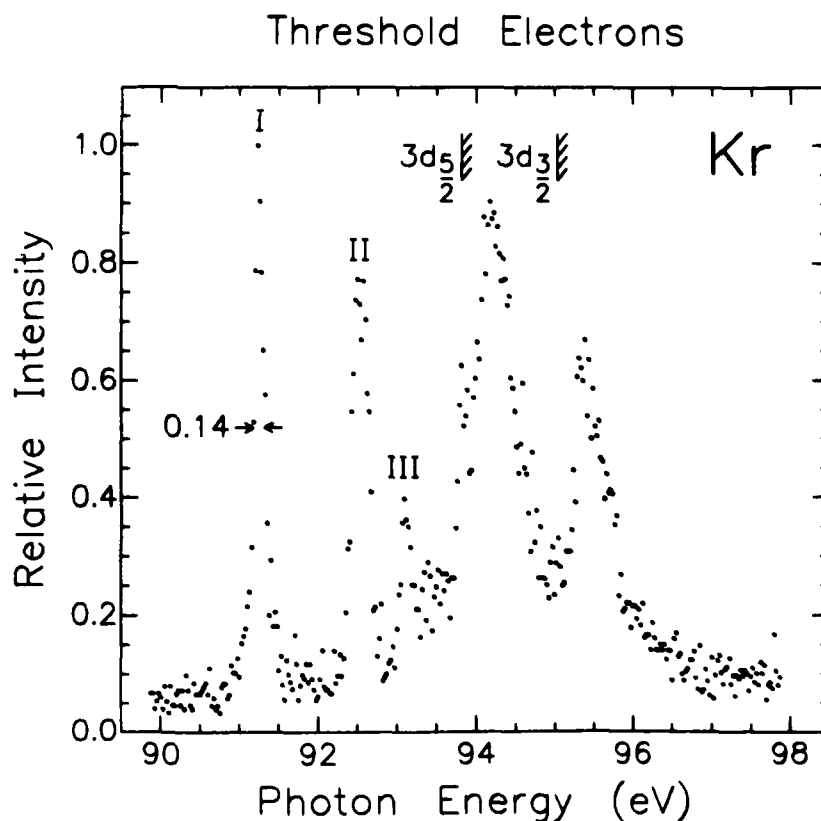
individual np resonances decrease with n less slowly in Fig. 1 than in the electron energy loss spectrum of King et al.¹ This qualitative trend shows the increasing importance of shake-off in the decay of states with a more loosely bound electron. The 3d threshold peaks are distorted by post-collisional interaction (PCI). A sharp rise occurs at about 0.17 eV above the threshold. After the maximum the intensity decreases gradually with electrons still observed at 1.4 eV above the threshold. The measured line shapes agree with the predictions of Neihaus.²

*This work was performed under Contract No. DE-AC03-76SF00098 at the Stanford Synchrotron Radiation Laboratory. Both this research and SSRL are supported by the Office of Basic Energy Sciences of the U.S. Department of Energy.

¹G.C. King, M. Tronc, F.H. Read, and R.C. Bradford, J. Phys. B **10**, 2479 (1977).

²A. Neihaus, J. Phys. B **10**, 1845 (1977).

Figure 1. The threshold spectrum of atomic krypton in the region of the 3d edges. The peaks observed at the below-threshold resonances result from their decay through shake-off: I. $3d^{-1}(^2D_{5/2})5p$ (.08 eV¹ natural linewidth), II. unresolved $3d^{-1}(^2D_{3/2})5p$, $3d^{-1}(^2D_{5/2})6p$, III. $3d^{-1}(^2D_{5/2})7p$. The 3d peaks are seen to be broadened and shifted to higher photon energies.



Si 2p AND 2s RESONANT EXCITATION AND PHOTOIONIZATION IN SiF₄*

T.A. Ferrett, M.N. Piancastelli, D.W. Lindle, P.A. Heimann, and D.A. Shirley

Materials and Molecular Research Division, Lawrence Berkeley Laboratory
Department of Chemistry, University of California, Berkeley, California 94720 USA

The discrete and continuum resonant structures in the vicinity of the Si 2p and 2s edges in SiF₄ were studied with time-of-flight photoelectron spectroscopy and synchrotron radiation in the range of 100-170 eV. Below the Si 2p threshold, the Si 2p discrete excitations to molecular and Rydberg orbitals show differing decay characteristics. On the resonances, the partial cross sections and asymmetry parameters were measured for the outer- and inner-valence states, and for the resonantly enhanced satellites. Above the Si 2p edge, the e

and t₂ shape-resonant intensity appears only in the Si 2p⁻¹ channel. Finally, the 2s excitation at 160 eV decays primarily into Si 2p satellite channels.

*This work was performed under Contract No. DE-AC03-76SF00098 at the Stanford Synchrotron Radiation Laboratory. Both this research and SSRL are supported by the Office of Basic Energy Sciences of the U.S. Department of Energy.

EVIDENCE FOR SHAPE RESONANCE DEPENDENT SATELLITE BEHAVIOR IN ATOMIC BARIUM

U. Becker, R. Hölzel, H. G. Kerkhoff, B. Langer, D. Szostak und R. Wehlitz

Institut für Strahlungs- und Kernphysik, Technische Universität Berlin,
Hardenbergstrasse 36, D-1000 Berlin 12 (Fed. Rep. of Germany)

Atomic Barium is intermediate between the rare gas structure of Xenon with its virtual hydrogenic 4f orbital and the rare earth elements where this orbital is highly contracted. This outstanding position of Ba in the periodic table has made this element a show case for phenomena related to the collapse of atomic orbitals. In transition elements such as Ba centrifugal and coulombic forces are in a delicate balance, so that the nature of the contracting orbital can depend strongly on environmental conditions such as the valence configuration for example. The strong effect of these environmental conditions on the 4d-photoabsorption of atomic Ba has been shown in the absorption spectra along the Ba isonuclear sequence¹ and theoretically explained by shape resonances in the effective potential for f-electrons². Similar effects concerning valence changes could most easily be studied by the resonance behavior of the 4d-satellite lines.

Atomic Ba shows strong configuration interaction in the initial and final ionic states³, making it a good candidate to look for pronounced satellites in the 4d-photoelectron spectrum. These electron correlation satellites correspond to different ground state configurations and should be enhanced by the shape resonance in a different way as the 4d-main line. In order to study this effect, photoelectron spectra of atomic Ba were taken in the range of the 4d - 4,f centrifugal barrier shape resonance between 100 and 140 eV. The experiment has been performed at HASYLAB with a time of flight-photoelectron spectrometer and a resistively heated atomic beam oven. Fig. 1 shows the higher binding energy part of the photoelectron spectrum at 130 eV with the 4d-main lines and their electron

correlation satellites. The sum of the satellites has a fraction of about 40 % on the total 4d-intensity showing the strength of configuration interaction in Ba

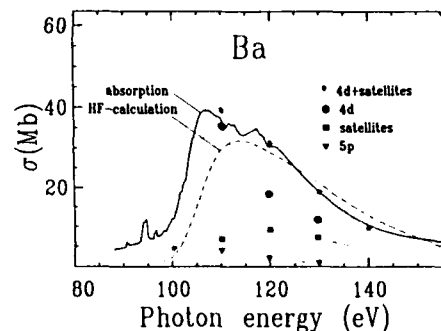


Fig. 2 Partial cross sections of atomic Ba in the range of the giant resonance

Fig. 2 shows the partial cross sections of the 4d-, 4d_{sat}- and 5p-lines in comparison with the total 4d-intensity, the absorption cross section⁴ and a HF-calculation⁵. This figure shows that main and satellite lines have completely different behavior in the resonance region. Whereas the 4d main line reaches its maximum below 110 eV, the satellites reach their maximum above 120 eV. The 6s-5d-mixing responsible for the satellite structure results in less attraction of the effective nuclear charge by admixture of electrons with 5d-character. Therefore the effect of the inner well potential may be less pronounced on the satellites than on the 4d-main lines associated with a shift of the broader maximum to higher energies. This shape resonance dependent behavior of electron correlation satellites has been demonstrated for the first time for Ba, but is expected to take place for satellite lines in the vicinity of shape resonances in general.

Reference

1. T.B. Lucatorto, T.J. McIlrath, J. Sugar and S.M. Younger, *Phys. Rev. Lett.* **47** 1124 (1981)
2. K.T. Cheng and W.R. Johnson, *Phys. Rev. A* **28** 2820 (1983)
3. W. Mehlhorn, B. Breuckmann and D. Hausmann, *Physica Scripta* **16**, 177 (1977)
4. R. Rabe, K. Radler and H.W. Wolff, *VUV Radiation Physics*, ed. by E.E. Koch et al. (Vieweg-Pergamon, Braunschweig, 1974), p. 2477
5. H.P. Kelly, S.L. Carter and B.E. Norum, *Phys. Rev. A* **25** 2052 (1982)

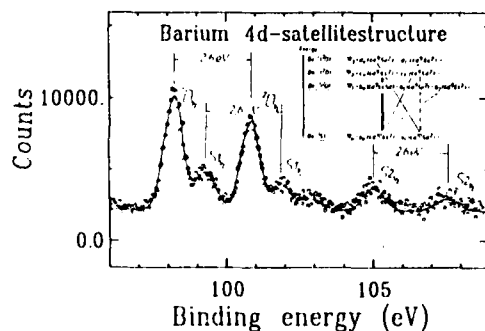


Fig. 1 4d-photoelectron spectrum of Ba at $h\nu = 130$ eV

RESONANCE AND THRESHOLD EFFECTS ON THE NEON 2p-SATELLITES

U. Becker, R. Hölzel, H. G. Kerkhoff, B. Langer, D. Szostak und R. Wehlitz

Institut für Strahlungs- und Kernphysik, Technische Universität Berlin,
Hardenbergstrasse 36, D-1000 Berlin 12 (Fed. Rep. of Germany)

The photoelectron spectrum of the valence subshells of atomic Ne is one of the systems best understood in photoionization besides He. The 2s and 2p photoelectron main lines are accompanied by satellite lines leaving the ion in an excited state: $\text{Ne}(1s^2 2s^2 2p^6) + h\nu \rightarrow e^- + \text{Ne}^+(1s^2 2s^2 2p^4 nl)$. The threshold of each satellite channel is the ionization limit of a double excitation Rydberg-series. This double excitation nature persists beyond threshold and determines the character and behavior of the corresponding satellites. There are basically three mechanisms responsible for the existence and production of photoelectron satellite lines:

- Rearrangement effects described by shake theory¹
- Configuration interaction (CI) in the initial (ISCI) and final ionic states (FISCI) described by electron correlations and spin flip processes²
- Interchannel coupling including bound and continuum states resulting in intensity sharing and resonance enhancement³.

It is generally believed that rearrangement effects and configuration interaction both play an important role on the satellite production, but there is only little evidence for the third mechanism - interchannel coupling -. The satellite intensity above the sudden limit is not very sensitive to the underlying production mechanism, because each mechanism contributes constant intensity over a wide spectral range. In contrast to this insensitivity above the sudden limit concerning the satellite nature, there is striking contrary behaviour of each mechanism in the adiabatic regime close to threshold⁴. The different satellites are characterized with decreasing kinetic energy by

- decreasing intensity for shake up processes,
- constant intensity for configuration interaction and
- by increasing intensity or/and resonance enhancement for interchannel coupling.

A study of the close to threshold behaviour of the Ne 2p-satellites was performed at the Hamburger Synchrotron Strahlungslabor HASYLAB with a time of flight (TOF)-photoelectron spectrometer in order to clear up the relative importance of the different interaction mechanism for the satellite production. For the first time interchannel coupling (IC) has been proven to be the dominant production mechanism for

several Ne 2p-satellites especially for the so called "conjugate shake up" satellites besides the already known importance of the mechanism a) and b).

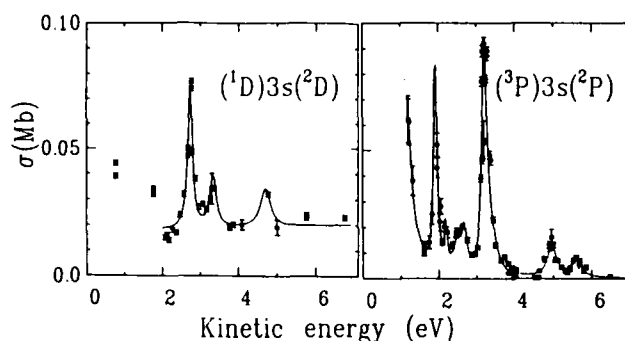


Fig. 1 Threshold behavior of the conjugate shake satellites of the Ne 2p-subshell

The effect of interchannel coupling is exhibited in the close to threshold behaviour of the corresponding satellites by pronounced resonance enhancement due to strong coupling with the double excited Rydberg-states of the neighboring satellite channels. Fig. 1a) shows the intensity of the $(^1D)3s(^2D)$ -satellite between 0 and 7 eV kinetic energy. Fig. 1b) shows the threshold behavior of a satellite which was missing up to now in the Ne valence satellite spectrum although it corresponds to the strongest double excitation Rydberg-series of the 2p-shell. This satellite $(^3P)3s(^2P)$ has been detected for the first time and shown to be produced on resonances only. This shows the relevance of interchannel coupling to the satellite structure of a simple system such as atomic Ne besides rearrangement and configuration interaction effects.

Acknowledgements

This work was performed at HASYLAB and supported by the BMFT and in part by the DFG.

References

- T.D.Thomas, Phys.Rev.Lett. **52** 417 (1984)
- R.L.Martin and D.A.Shirley, Phys.Rev. **A13** 1475 (1975)
- L.Ungier and T.D.Thomas, Phys.Rev.Lett. **53** 435 (1984)
- P.A.Heimann, C.M.Truesdale, H.G.Kerkhoff, D.W.Lindle, T.A.Ferrett, C.C.Bahr, W.D.Brewer, U.Becker and D.A.Shirley, Phys.Rev. **A** (1985)

SINGLE AND DOUBLE PHOTOIONIZATION OF ALKALINE-EARTH ATOMS

Y.Itikawa, T.Hayaishi, Y.Itoh, T.Koizumi, J.Murakami, T.Nagata, T.Sasaki, Y.Sato, H.Shibata, B.Sonntag, J.B.West, A.Yagishita and M.Yoshino

Photon Factory, National Laboratory for High Energy Physics, Ohomachi, Ibaraki 305, Japan*

Double photoionization of alkaline-earth atoms is of considerable interest in the study of electron correlation effects. Excitation of electrons in the inner-valence shell ($3p$ for Ca and $4p$ for Sr) results in a rich structure in the photoabsorption spectrum.^{1,2} The resulting excited atom ends up in various ionic stages through autoionization. We have measured the relative yields of singly and doubly charged ions of Ca and Sr as a function of photon energy with a resolution up to 0.15 nm.

The study was carried out using monochromatized synchrotron radiation as the light source, a TOF mass spectrometer as the detector and a differentially pumped effusive beam as the target. The light from the Photon Factory storage ring (2.5 GeV) was dispersed by a 1 m Seya-Namioka monochromator. The ion yields were measured for the wavelengths 35-42 nm for Ca and 40-55 nm for Sr .

Fig. 1 shows the result for Ca .³ This can be well compared with the photoabsorption spectrum.¹ Most of the peaks are identified to the excitations $3p \rightarrow nd, nf$ in Ca . The ratio of the double to single ion yields is plotted in Fig. 2. This is essentially the same as that obtained by Holland and Codling,⁴ but shows much more detailed structure. We conclude that Ca^{++} in the range of 36-40 nm is produced by the two-step process: $\text{Ca}(3p^6 4s^2 {}^1\text{S}) \rightarrow \text{Ca}(3p^5 4s^2 n\ell) \rightarrow \text{Ca}^+(3p^5 3d 4s {}^2\text{P} \text{ and } {}^4\text{P}) \rightarrow \text{Ca}^{++}(3p^6 {}^1\text{S})$. Above the $3p$ ionization limit, Ca^{++} is mainly created through the autoionization following the $3p$ ionization.

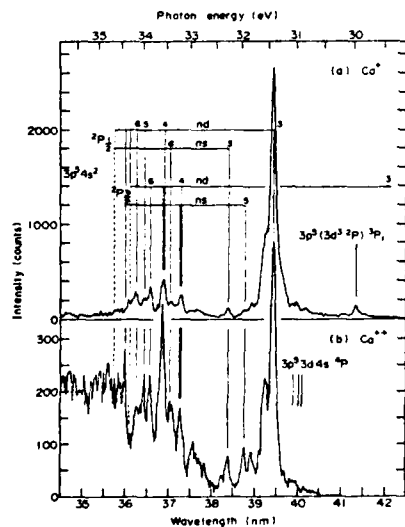


Fig. 1

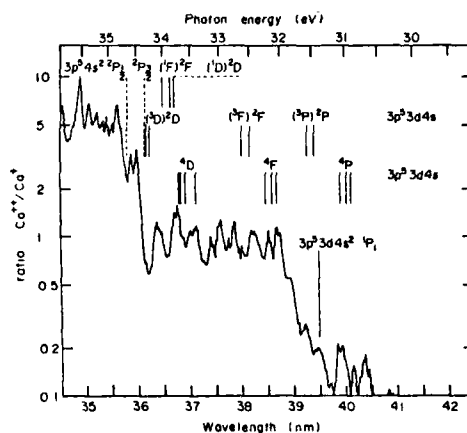


Fig. 2

Fig. 3 shows the yield of Sr^{++} . The situation is expected to be similar to the case of Ca . There is, however, a few differences. For instance, Sr^{++} cannot be produced through the two-step autoionization process at 49.2 nm, because Sr^+ has no autoionizing states below that. More detailed analysis of the experimental data for Sr is in progress.

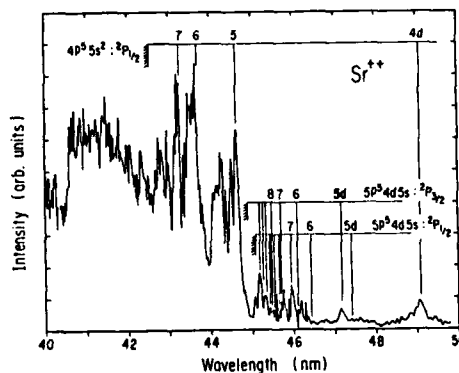


Fig. 3

References

1. M.W.D.Mansfield and G.H.Newsme, Proc. R. Soc. **A357** 77 (1977)
2. M.W.D.Mansfield and G.H.Newsme, Proc. R. Soc. **A377** 431 (1981)
3. Y.Sato et al., J. Phys. B **18** 225 (1985)
4. D.M.P.Holland and K.Codling, J. Phys. B **14** 2345 (1981)

* Collaborative research work at the Photon Factory. Correspondence should be addressed to Y.Itikawa, Institute of Space and Astronautical Science, Komaba, Meguroku, Tokyo 153, Japan.

ELECTRON ANGULAR DISTRIBUTIONS FROM AUTOIONIZING BARIUM RYDBERG STATES

U. Eichmann, V. Lange, M. Völkel and W. Sandner

Fakultät für Physik, Universität Freiburg, Hermann-Herder-Str. 3, 7800 Freiburg, West Germany

Interchannel interactions in alkaline earth atoms cause irregularities in bound state Rydberg series below the first ionization limit and autoionization above it. While both phenomena are equivalent from a theoretical point of view, their experimental investigation requires rather different techniques. In particular, a complete analysis of the autoionizing Rydberg states requires energy resolved intensity and angular distribution measurements of autoionization electrons.

We report an experiment on the angular distribution of autoionization electrons from $(6p_{3/2}ns)_{J=1}$ Rydberg states in Barium, in the energy region above the $6p_{1/2}$ threshold ($n > 12$). Autoionization can occur into four different final ionic state of Ba^+ : $6p_{1/2}$, $5d_{3/2}$, $5d_{5/2}$ and $6s_{1/2}$. In each case the angular distribution, following excitation from the bound $6sns$ (1S_0) Rydberg states with linearly polarized laser light, is given by $I(\theta) \propto 1 + \beta P_2(\cos\theta)$. The β parameters for the various final states are shown on fig. 1. We note that electrons from the two Ba^+5d final states were energetically not resolved in this experiment. In contrast to related studies^{1,2} the present work focuses on the pronounced energy (or n -) dependence of β found for each of the final ionic states, most dramatically observed in case of the Ba^+5d channels.

Examination of the process reveals a total of 13 channels being involved, leaving some 90 parameters to be determined by a complete MQDT analysis. Moreover, since no isolated perturber states are known in this energy region, any MQDT treatment could only produce weakly energy dependent β parameters, in sharp contrast to the experiment. Therefore, instead of a MQDT-parametrization we have undertaken ab initio Hartree Fock calculations of the autoionization processes under consideration. The theory produces interaction matrix elements and continuum phases for each channel; β parameters were then calculated using expressions derived from general angular correlation theory.

As shown on fig. 1, the calculations yield β -parameters which are in good agreement with the experiment for low n ($n=9$), but fail to reproduce the energy variations for high n . However, it was found that a shape resonance occurs in the $5d_{\ell f}$ channels, which causes variations in both the matrix elements and f -wave continuum phases. Even though the predicted energy position of the resonance ($\sim 120000 \text{ cm}^{-1}$) is far outside

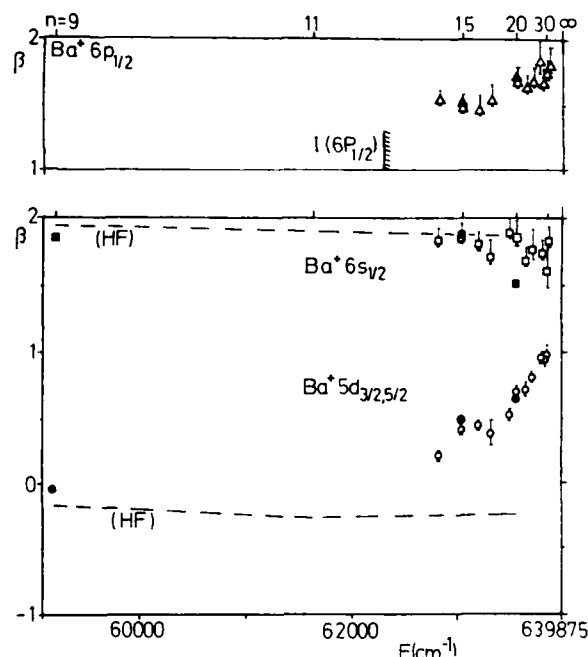


Fig. 1: β parameters for autoionization of the $Ba(6p_{3/2}ns)_{J=1}$ states into the $Ba^+6s_{1/2}$ (\square), $6p_{1/2}$ (Δ) and $5d$ (\circ) continua. Open symbols: this work, filled symbols: Ref. 1. Dashed lines: HF calculation (this work).

the region of this experiment, model calculations of the Ba^+5d β parameter in the vicinity of a shape resonance exhibit a surprising similarity with those shown on fig. 1. We note that the accuracy of the Multi Configuration Hartree Fock program in calculating the Ba^+ core may well be insufficient to reproduce the energy position of the shape resonance to a precision required for this investigation. Therefore it is conceivable that the observed energy variations in β are caused by shape resonances in the $(Ba^+5d, \ell f)_{J=1}$ channels, located about 64000 cm^{-1} above the ground state. Consequently, this work emphasizes the importance of including intrachannel resonances into the analysis of autoionization Rydberg series, in addition to the usual MQDT treatment of interchannel interactions.

References

1. W. Sandner, R. Kachru, K.A. Safinya, F. Gounand, W.E. Cooke and T.F. Gallagher Phys. Rev. A 27(1983)1717
2. R. Kachru, N.H. Tran, P. Pillet and T.F. Gallagher Phys. Rev. A 31 (1985) 218

CHANNEL INTERACTION OF THE THREE $J=3$ $6p_{3/2}$ nd AUTOIONIZING SERIES IN BARIUM

Oliver C. Mullins, Yifu Zhu, Emily Y. Xu, and T.F. Gallagher

Department of Physics, University of Virginia, Charlottesville, VA 22901

The energies and widths of a $6p_{3/2}$ nd $J=3$ autoionizing series are reported for $n=8-17$. Above the $6p_{1/2}$ ionization limit of Ba^+ ($n>10$ for the $6p_{3/2}$ nd states) the series is found to have approximately constant values for the quantum defect ($\mu \sim 2.85$) and for the scaled width ($\Gamma_n \cdot n^{*3}$ (Hartree) $\sim .07$). The values compare with those previously reported¹ for the other $6p_{3/2}$ nd series, $\mu \sim 2.74$ and $\Gamma_n \cdot n^{*3} \sim 0.11$. By reporting the scaled widths in Hartree one obtains directly the ratio of the peak widths to the peak separations. The experimental method employed was to resonantly excite $6snd^{1,3}D_2$ states using two tunable dye lasers followed by excitation of $6p_{3/2}$ nd autoionizing states using a third dye laser. The resulting barium ion signal was detected as a function of the frequency of the third laser (see Ref. 1 and references therein). The newly reported series is the dominant $6p_{3/2}$ nd series formed when photoexciting the $6snd^3D_2$ states, whereas the previously reported $6p_{3/2}$ nd series dominates when photoexciting the $6snd^1D_2$ states. Thus, the two autoionizing series are approximately represented by $6p_{3/2}(nd_{3/2}+nd_{5/2})$ and $6p_{3/2}(nd_{3/2}-nd_{5/2})$, the plus combination, hereon denoted as $6p_{3/2}nd^+$, represents the previously reported series. This coupling suggests that the effects of the Coulomb interaction of the two electrons and the spin-orbit coupling of the Rydberg electron are comparable. A detailed examination of this excitation process is currently in progress.²

Below the $6p_{1/2}$ ionization limit, the two $6p_{3/2}$ nd series interact with the $6p_{1/2}nd_{5/2}$ series, all series being $J=3$. We find that the $6p_{1/2}nd_{5/2}$, $6p_{3/2}nd^-$ interaction is somewhat smaller than that of the $6p_{1/2}nd_{5/2}$, $6p_{3/2}nd^+$ series. Evidence of channel interaction is obtained from the corresponding Lu-Fano plot, but due to the large energy width of autoionizing states, difficulties with this method can arise. Channel interaction results in the appearance of multiple peaks in the photoexcitation spectra of certain $6snd^{1,3}D_2$ states as the autoionizing state wavefunctions are mixed, thus allowing for a direct determination of channel interaction. The autoionizing state energies and widths and the photoexcitation spectra can be accounted for using multichannel quantum defect theory (MQDT). Previously, a four channel (two bound channel) MQDT analysis was successful in describing the interaction of the $6p_{1/2}nd_{5/2}$ and $6p_{3/2}nd^+$ series and the continua.¹ Here, we report the results of a six channel (three bound) MQDT analysis to treat the

interactions of the $6p_{1/2}nd_{5/2}$, $6p_{3/2}nd^+$ and the $6p_{3/2}nd^-$ series and the continua. Our MQDT treatment successfully accounts for rather extensive data over an appreciable energy range.

Finally a discrepancy is clarified concerning the energy of the $6p_{3/2}14d^+$ state and relates to the influence of the bound perturber $5d7d^3F_2$ on the $6s14d^{1,3}D_2$ states.

References

1. F. Gounand, T.F. Gallagher, W. Sandner, K.A. Safinya and R. Kachru, Phys. Rev. A **27**, 1925 (1983).
2. L. van Woerkom and W.E. Cooke, private communication.

THE RESONANT PHOTOIONIZATION OF H ATOM IN INTENSE MAGNETIC FIELDS*

S. K. Bhattacharya[†] and Shih-I Chu[‡][†]Department of Physics and Astronomy, Georgia State University, Atlanta, Georgia 30303 USA[‡]Joint Institute for Laboratory Astrophysics, University of Colorado and National Bureau of Standards, Boulder, Colorado 80309 USA

The structure of the hydrogen atom in intense magnetic fields continues to attract considerable attention in the literature. Interest in this system is partly due to the existence of intense field strengths, of the order of 10^9 to 10^{12} gauss, at certain astrophysical objects like the magnetic white dwarfs and neutron stars respectively. For magnetic fields B beyond a critical value $B_0 = m_e^2 c^3 / \hbar \approx 2.35 \times 10^9$ gauss, an adiabatic separation of the cyclotron motion of the electron from the Coulomb field dominated motion along the orthogonal direction is useful for studying some aspects of the spectrum. However, the nonseparability of these motions itself becomes responsible for certain interesting features. These include, e.g., the so-called strong field mixing pattern¹ expected around the ionization edge at somewhat lower fields, as well as the appearance of the autoionizing states above the ionization threshold. For γ in the range of 2 to 500, the energies and widths of several of the autoionizing states $\{E_{Nn_z}(m^p)\}$ below the first two excited Landau thresholds have been recently obtained via the ab initio complex-coordinate coupled-Landau-channel (CCCLC) formalism,² where N is the Landau quantum number ($N = 0, 1, 2, \dots$), n_z is the "hydrogenic" quantum number ($n_z = 0, 1, 2, \dots$, for each N), and m and p are respectively the magnetic quantum number and the "z" parity.

The presence of these autoionizing states is expected to have a pronounced effect on the excitation spectrum of the system in an appropriate radiation field. In this paper we shall present a nonperturbative complex quasi-energy formalism³ which allows accurate treatment of photoabsorption cross sections and resonant line shapes for both one-photon (in weak radiation fields) and multi-photon (in strong radiation fields) processes in the presence of intense magnetic fields on an equal footing.

Figure 1 depicts the one-photon ionization spectrum for a hydrogen atom in the presence of a strong magnetic field ($\gamma = 2$, or $B = 4.7 \times 10^9$ G). This corresponds to the photoabsorption from the tightly bound state (i.e., $N = 0$, $n_z = 0$, $m^p = 0^+$). The continuum

oscillator strength distribution $df/d\omega$ is seen to be monotonically decreasing from a finite value of about 0.5 a.u. at the ionization threshold until the kinetic energy of the photoelectron $E_k = \hbar\omega - |\text{Re}[E_{00}(0^+)]|$, approaches the first ($N = 1$) excited Landau threshold at 2 a.u., when the strong enhancements due to the presence of the $N = 1$ autoionizing resonance states ($n_z = 0, 1, 2$) can be seen. The $N = 2$ resonances are also visible for the four lowest autoionizing states. For each N , these resonances form an infinite "Rydberg" series converging to $E_k = N\gamma$ (a.u.). The asymmetric photoabsorption line shapes characterizing the bound-continuum interactions are well resolved for this system for the first time. Detailed structure of the photoionization spectra as a function of N , n_z , γ , etc., will be presented.

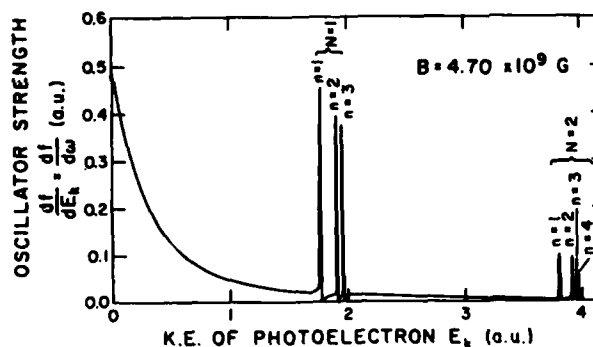


Fig. 1

*Work supported by DOE, ACS-PRF and ARO.

[‡]JILA Visiting Fellow (1985). Permanent address: Dept. of Chemistry, Univ. of Kansas, Lawrence, Kansas 66045.

References

1. A. R. P. Rau, J. Phys. B **6**, L193 (1979); J. C. Gay, Comm. At. Mol. Phys. **9**, 97 (1980); W. Fano, J. Phys. B **13**, L519 (1980).
2. S. K. Bhattacharya and S. I. Chu, J. Phys. B **16**, L471 (1983).
3. S. K. Bhattacharya and S. I. Chu, J. Phys. B (submitted).

PHOTOIONIZATION OF EXCITED Cs I STATES

Constantine E. Theodosiou

Department of Physics and Astronomy, University of Toledo, Toledo, Ohio 43606

Recent measurements and Hartree-Slater calculations disagree on the photoionization cross sections of excited cesium atom states. Of particular relevance to this work are two different measurements on Cs: (a) the $6^2D(3/2)$ photoionization by Gerwert and Kollath,¹ and (b) the $7^2S(1/2)$ photoionization by Gilbert et al.² Calculations by Manson and coworkers³ exist for both cases and they predict Cooper minima in the wavelength region of both experimental investigations. Gerwert and Kollath failed to detect any minimum between about 400 and 600 Å.¹ The one-point measurement of Gilbert et al.,² being roughly twice the theoretical value,³ is supposedly straddling a Cooper minimum; therefore, it is hardly useful in indicating the general shape of the photoionization cross section in this wavelength region.

The present work was motivated by the desire to investigate thoroughly the potential as well as the limitations of the Hartree-Slater approach. To that end we used the following improvements over the traditional application of this approximation:

1. Since we are studying photoionization of excited states, we should use the appropriate self-consistent field of this excited state rather than the ground state potential tabulated by Herman and Skilman.

2. Since cesium is a heavy element ($Z=55$), spin-orbit interaction and relativistic effects on its photoionization ought to be significant. We have included those effects by adding to the Hartree-Slater potential $V(r)$ the appropriate term from Pauli's equation:

$$V_{so}(r) = \frac{1}{2} \frac{\alpha^2}{(1+(\alpha^2/4)(E-V(r)))^2} \frac{1}{r} \frac{dV}{dr} \frac{L \cdot S}{\hbar^2}$$

where α is the fine structure constant. The full relativistic form is used here to ensure that the potential has the correct behavior near the origin.

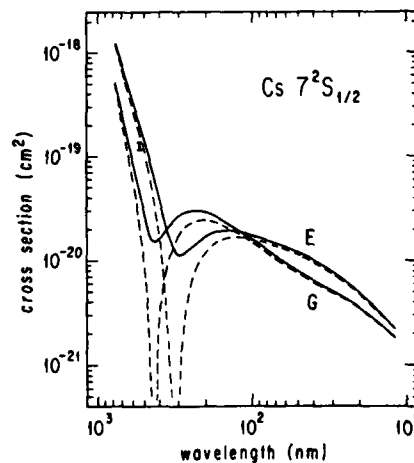
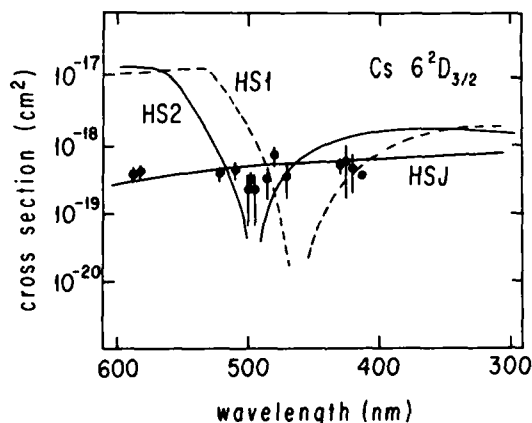
Some of our results are shown in the following Figures. In the case of $6D$ we show three curves: HS1, HS result of Refs. 3; HS2, our HS result, including spin-orbit, using the ground state configuration potential; HSJ, our HS result, including spin-orbit interaction, using the excited configuration potential; \blacklozenge , relative experimental data from Ref. 1, normalized to our curve. We notice that the HSJ curve agrees very well with experiment. Still, however, more experimental data are necessary to clarify whether the experimental Cooper minimum is actually at lower or higher wavelengths. In the case of $7S$ we show four curves: dashed lines, not including spin-orbit interaction; full lines, including

spin-orbit interaction;

C, our HS result, using the ground state configuration potential; E, our HS result, using the excited state configuration potential; I, experimental point from Ref. 2, renormalized using our⁴ accurate $7s$ lifetime. We see that the excited configuration potential yields a better agreement with experiment, although trying to fit one experimental point is not informative enough.

References

1. K. Gerwert and K.J. Kollath, J. Phys. B **16**, L217 (1983).
2. S.L. Gilbert, M.C. Noecker, and C.E. Wieman, Phys. Rev. A **29**, 3150 (1984).
3. A. Msezane and S.T. Manson, Phys. Rev. Lett. **35**, 364 (1975); *ibid* **48**, 473 (1982); J. Lahiri and S.T. Manson, Phys. Rev. Lett. **48**, 614 (1982); J. Lahiri and S.T. Manson, Abstracts of Contributed Papers, XII ICPEAC, p. 39 (1981).
4. C.E. Theodosiou, Phys. Rev. A **30**, 2881 (1984).



THEORETICAL STUDY OF THE CONFIGURATION INTERACTION IN THE PHOTOIONIZATION OF MG ATOM

T. N. Chang and Young Soon Kim

Department of Physics, University of Southern California, Los Angeles, California 90089-0484

We present the theoretical result of a comprehensive study on the effect of the configuration interaction to the photoionization of Mg Atom with particular emphasis given to the 1P autoionization structure dominated by the doubly excited states above the first ionization threshold.

The final state of the transition is represented by the superposition of the configuration wavefunctions corresponding to three configuration series, i.e., $[3pns]$, $[3pnd]$, and $[3sn(\epsilon)p]$. The basic theoretical procedure is similar to that of Fano¹ and Bates and Altick² with two important modifications.

i) Instead of using the usual HF orbit in the superposition of the wavefunctions representing different doubly excited states in the total wavefunction Ψ_E , we have employed a configuration wavefunction by diagonalizing the N-particle Hamiltonian matrix with a set of orbital wavefunctions generated in a non-local potential field which pre-diagonalizes the Hamiltonian for a given configuration series.³

ii) The principal value integral is evaluated with the exact numerical solution with the differential equation technique developed elsewhere.⁴

The 1S initial state of the transition is characterized by a superposition of wavefunctions representing configuration series $[n\ell^2, n\ell m\ell(m>n)]$ with

$\ell=0, 1, 2, \dots$. Again the wavefunction is constructed in a non-local potential which pre-diagonalizes the Hamiltonian for a configuration series of given ℓ .

In this study, we have calculated the photoionization cross section at energy above the first ionization threshold. The transition amplitude can be separated into three parts:

- 1) contribution due to the direct transition from the initial state to the final state continuum background,
- 2) contribution due to the direct transition from the initial state to the final doubly excited state embedded in the continuum, and
- 3) a second order contribution corresponding to the "two-step" transition from the initial state to the final configuration mixed state.

The result of the calculation will be presented.

This work is supported by NSF under Grant No. PHY84-08333.

References

1. U. Fano, Phys. Rev. **124**, 1866 (1961).
2. G. Bates and P. L. Altick, J. Phys. **B6**, 653 (1973).
3. T. N. Chang and Y. S. Kim, preprint (1985).
4. T. N. Chang and R. T. Poe, J. Comp. Phys. **12**, 557 (1973).

THRESHOLD EFFECTS IN INNER-SHELL PHOTOIONIZATION OF OPEN-SHELL ATOMS:
HARTREE-FOCK CALCULATIONS OF BORON*

Samir K. Bhattacharya and Steven T. Manson

Department of Physics and Astronomy, Georgia State University, Atlanta, Georgia 30303 USA

Although open-shell atoms constitute most of the periodic table, surprisingly little experimental work has been done on their photoionization. On the theoretical side, there is very little past the simple central-field level, particularly for inner shell processes.¹ We have, thus, embarked on a program of calculation, at the Hartree-Fock level, of inner-shell photoionization cross sections.

In this abstract, we report on our results for boron, an open-shell atom, whose ground state is $1s^2 2s^2 2p^2 P$. The calculations were performed using discrete wave functions for B and B^+ (fully relaxed) by the method of Clementi.² The continuum wave functions were calculated using our own code.³ Photoabsorption by a 2s electron leads to six possible channels: $(1s^2 2s 2p^1 P)_{ep}^2 S, ^2 P, ^2 D$ and $(1s^2 2s 2p^3 P)_{ep}^2 S, ^2 P, ^2 D$. The two sets of possible final states are physically distinguishable owing to the energy difference between the $^1 P$ and $^3 P$ states of the B^+ ion core. This energy difference, along with dynamical differences in the continuum wave functions for the various channels, leads to a $^3 P : ^1 P$ branching ratio which can deviate from the statistical value of 3. This is shown in Fig. 1 where it is seen that that, although there are some differences between "length" and "velocity" results, both show very significant deviations from the statistical ratio near the $^1 P$ threshold and climbs towards 3 with increasing energy. Also shown in Fig. 1 is a branching ratio determined by assuming that the $^1 P$ matrix elements were the same as the $^3 P$, only shifted by the difference in binding energy. This isolates the "kinetic energy effect". It is seen that the "kinetic energy effect" does not entirely explain the branching ratio. Thus dynamical effects on the wave function are of importance.

Results for the photoionization cross section of the 2p and 1s subshells of boron will also be presented, along with branching ratios and photoelectron angular distribution asymmetry parameters.

We are indebted to A.Z. Msezane for providing us with the discrete wave functions for B and B^+ .

*Work supported by the U.S. National Science Foundation

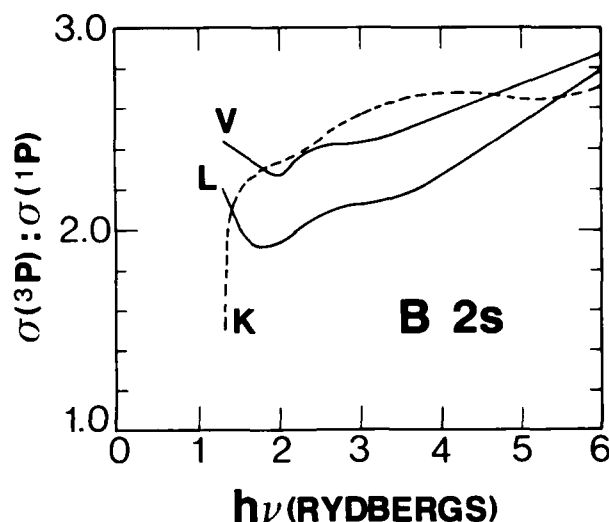


Fig. 1: $^3 P : ^1 P$ branching ratio for 2s photoionization in boron. The curves L and V are the Hartree-Fock results in "length" and "velocity" respectively, while curve K is an estimate of the "kinetic energy effect" as described in the text.

References

1. A.F. Starace in *Handbuch der Physik*, vol. 31, edited by W. Mehlhorn (Springer-Verlag, Berlin, 1982), p.1.
2. E. Clementi and C. Roetti, *At. Data Nuc. Data Tables* **14**, 177 (1974)
3. D.J. Kennedy and S.T. Manson, *Phys. Rev. A* **5**, 227 (1972).

PHOTOIONIZATION OF THE EXCITED Na 4d STATE*

Alfred Z. Msezane* and Steven T. Manson†

*Department of Physics, Atlanta University, Atlanta, Georgia 30314 USA

†Department of Physics and Astronomy, Georgia State University, Atlanta, Georgia 30303 USA

Photoionization of excited states has recently seen an upsurge of activity owing to both the availability of light sources and to the interest in some new minima which have been predicted theoretically.^{1,2} It is of importance therefore to get some feeling for the reliability of the calculations. This can be done by comparison with experiment and with more exact calculations.

In this abstract, we report on a Hartree-Fock calculation of Na 4d photoionization. The calculation was performed using discrete numerical Hartree-Fock wave functions for the initial atomic and final (fully relaxed) ionic state obtained from the code of Fischer.³ It was found that it was important to use numerical functions, rather than analytic, due to the sensitivity of the excited state orbital.⁴ The continuum wave function were calculated using our own code.⁵

The calculated cross section is shown in Fig. 1 along with an experimental point.⁶ Only a single curve is shown even though the calculation was done in both "length" and "velocity" formulations⁵ because the results are so close together. The simple Hartree-Slater central-field result (not shown) is also quite close, within 10% over the range shown. The agreement of all of the theory with the experimental point⁶ is seen to be excellent.

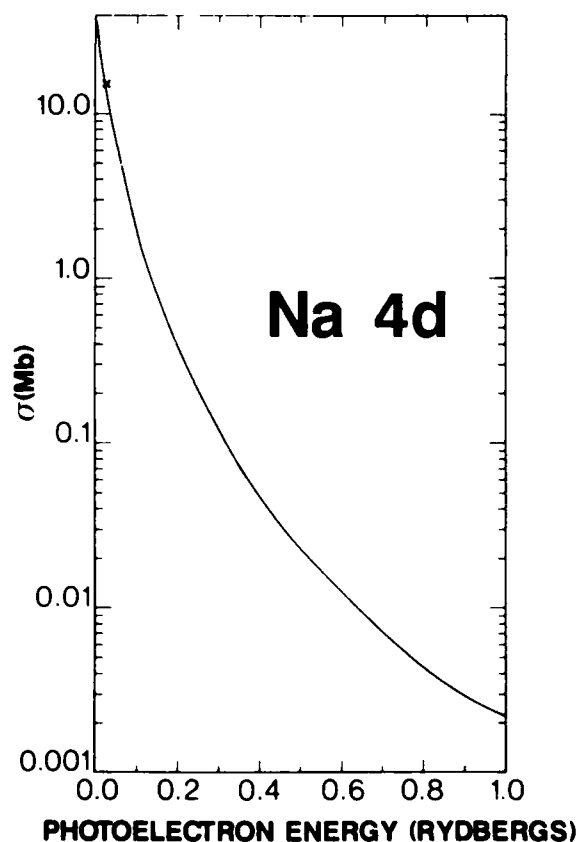
The experiment, which measured the d + f and d + p cross sections independently, found the former to be overwhelmingly dominant by at least a factor of 150. From our calculation, we find a zero in the d + p transition about 0.1eV above the measured point. This explains why the d + p transition is so small and the measurement constitutes the first, albeit indirect, evidence of the existence of an $\ell \rightarrow \ell - 1$ minimum in excited state photoionization, which has been predicted theoretically to be a widespread phenomenon.¹

*Work supported by the U.S. Department of Energy and the U.S. Army Research Office.

References

1. A.Z. Msezane and S.T. Manson, Phys. Rev. Lett. **48**, 473 (1982).
2. J. Lahiri and S.T. Manson, Phys. Rev. Lett. **48**, 614 (1982).
3. C.F. Fisher, Comput. Phys. Commun. **4**, 107 (1972).
4. A. Z. Msezane and S.T. Manson, Phys. Rev. A **30**, 1795 (1984).
5. D.J. Kennedy and S.T. Manson, Phys. Rev. A **5**, 227 (1972).
6. A.V. Smith, J.E.M. Goldsmith, D.E. Nitz, and S.J. Smith, Phys. Rev. A **22**, 577 (1980).

Fig. 1. Photoionization cross section of Na 4d. The solid curve is our Hartree-Fock result and the experimental point is from Ref. 6.



RELATIVISTIC CALCULATIONS OF THE PHOTOIONIZATION OF 6s SUBSHELLS IN HIGH-Z ATOMS*

B.R. Tambe⁺ and Steven T. Manson[#]

⁺Department of Chemistry and Physics, Southern Technical Institute, Marietta, Georgia 30060 USA
[#]Department of Physics and Astronomy, Georgia State University, Atlanta, Georgia, 30303 USA

Relativistic interactions in high-Z atoms have recently been shown to have dramatic effects on the zeros in the dipole matrix elements for photoionizing transitions^{1,2} (Cooper minima). These effects include shifts and splittings of the zeros, from their non-relativistic locations, all out of proportion to the strength of the relativistic interactions, amounting in some cases to hundreds of eV! These effects have been studied in 6p¹, 5d², and 5p³ subshells of high-Z atoms. In this abstract we report on our results for 6s subshells.

The single non-relativistic 6s \rightarrow p zero becomes two zeros, 6s \rightarrow p_{1/2} and 6s \rightarrow p_{3/2}, under the action of relativistic effects. Of primary interest is the energy splitting between these two relativistic zeros, and the relationship of their location compared to the non-relativistic case. This is a very sensitive probe of relativistic interactions.

Our study has been carried out using Dirac-Slater (DS) wave functions for initial and final states, thus incorporating relativistic interactions from the start. To make the comparison with the non-relativistic prediction, we have the Hartree-Slater (HS) results⁴ which are the non-relativistic analogue of DS.

The "trajectories" of the zeros are shown in Fig. 1 where it is seen that the zeros in the two relativistic transitions behave completely differently as a function of Z. The transition to p_{1/2} behaves rather like the non-relativistic result, but the p_{3/2} zero moves out significantly, as a function of Z. In addition, structure is seen in the p_{3/2} trajectory.

An important implication of these results is that the photoelectron angular distribution asymmetry parameter, β , will be strongly energy-dependent and rather different from the non-relativistic value of two.

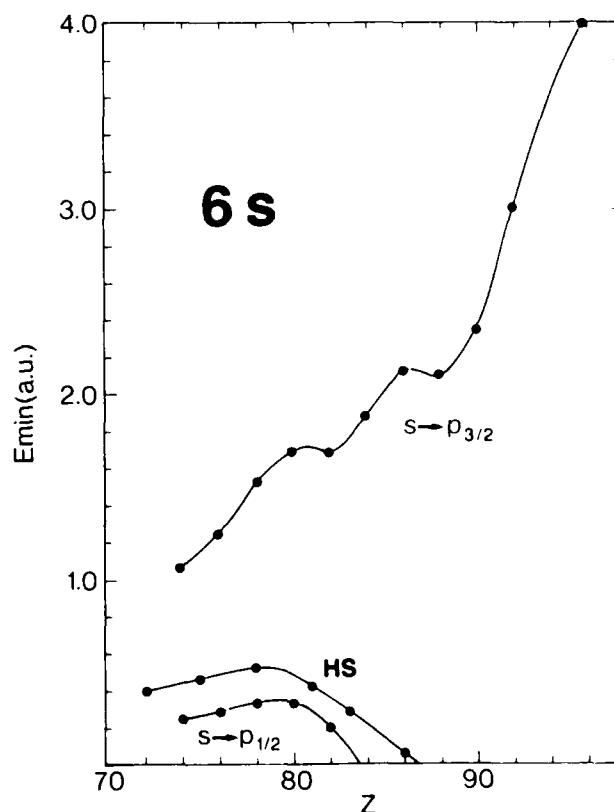
Results for cross sections and β 's for a number of Z's will be presented.

*Work supported by the U.S. National Science Foundation.

References

1. S.T. Manson, C.J. Lee, R.H. Pratt, I.B. Goldberg, B.R. Tambe, and A. Ron, Phys. Rev. A **28**, 2885 (1983).
2. B.R. Tambe and S.T. Manson, Phys. Rev. A **30**, 256 (1984).
3. B.R. Tambe and S.T. Manson, XIII ICPEAC Abstracts of Papers (ICPEAC, Berlin, 1983), p. 15.
4. S.T. Manson, Phys. Rev. A (in press).

Figure 1: Location of the zero (Cooper minimum) in the dipole matrix element for 6s photoionization in energy in atomic units (27.2eV) above threshold (E_{\min}) vs. atomic number Z. The relativistic results for transitions to p_{1/2} and p_{3/2} are shown, along with the non-relativistic HS result.



PHOTOIONIZATION OF MERCURY*

K. Bartschat and P. S. Scott

The Department of Applied Mathematics and Theoretical Physics
The Queen's University of Belfast, Belfast BT7 1NN, Northern Ireland.

The relativistic R-matrix method of Scott and Burke (1980), which allows the inclusion of all the one-body operators (spin-orbit interaction, Darwin term and mass correction term) of the Breit-Pauli Hamiltonian, has been used to calculate the photoionization of the $(6s^2)^1S_0$ ground state of mercury in the energy region between 10.43 eV (ionization potential of Hg) and 14 eV. This energy region is of particular interest as it is dominated by a wealth of structure originating from autoionizing resonances with configuration $5d^9 6s^2 ({}^2D_{3/2,5/2}) n\ell_j$.

We have performed a 5-state close-coupling calculation, where the $5d^9 6s ({}^2S_{1/2})$, $5d^9 6s^2 ({}^2D_{3/2,5/2})$ and $5d^9 6p ({}^2P_{1/2,3/2})$ ionic states have been included in the R-matrix expansion. The target wave functions used were obtained from a Thomas-Fermi model potential using the SUPERSTRUCTURE program of Eissner et al (1974). In fig. 1 we present our results for the total photoionization cross section σ and compare these results with the experimental data of Brehm (1966). Fig. 2 shows the asymmetry parameters β (experimental data from

Brehm and Höfler 1978), while in fig. 3 we give the spin polarization parameter ξ which describes the polarization of photoelectrons produced by unpolarized or linearly polarized light (experimental data from Schäfers et al (1982)).

It is intended to extend these calculations to higher energies and to use the relativistic R-matrix method to study the photoionization of other atoms such as Xe and Cd. The latest results in these areas will be presented at the conference.

References

1. B. Brehm (1966), Z. Naturforsch. **21a**, 196.
2. B. Brehm and K. Höfler (1978), Phys. Lett. **68A**, 437.
3. W. Eissner, M. Jones and H. Nussbaumer (1974), Comput. Phys. Commun. **8**, 270.
4. F. Schäfers, G. Schönhense and U. Heinzmann (1982), Z. Phys. A. **304**, 41.
5. N. S. Scott and P. G. Burke (1980), J. Phys. B. **12**, 4299.

* This work was supported by the Deutsche Forschungsgemeinschaft and the British Council.

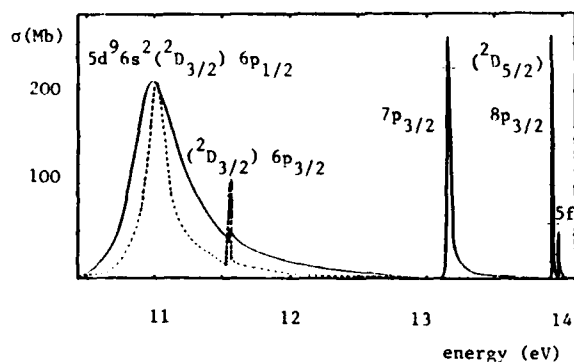


Fig.1: Total cross section σ for the photoionisation of the $(6s^2)^1S_0$ ground state of Hg; — theory, --- experiment (Brehm 1966).

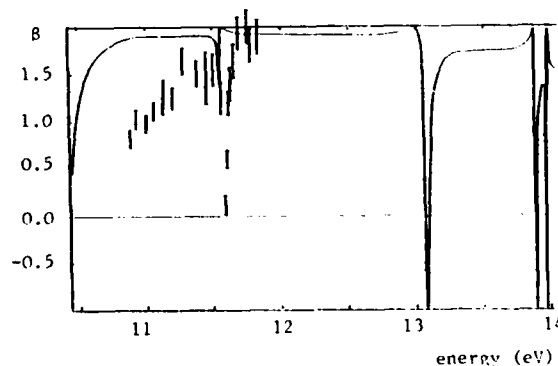


Fig.2: Angular distribution parameter β for the photoionisation of the $(6s^2)^1S_0$ ground state of Hg; — theory, \dagger experiment (Brehm and Höfler 1978).

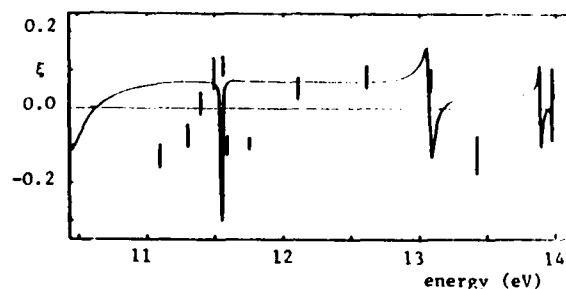


Fig.3: Spin polarisation parameter ξ for the photoionisation of the $(6s^2)^1S_0$ ground state of Hg; — theory, \dagger experiment (Schäfers et al 1982).

RADIATIVE TRANSITIONS IN CALCIUM IONS

K L Baluja¹ and K T Taylor²¹ Daresbury Laboratory, SERC, Daresbury, Warrington, WA4 4AD, England² Department of Mathematics, Royal Holloway College, Egham Hill, Egham, Surrey, TW20 OEX, England

Oscillator strengths have been obtained for transitions between low-lying states of Ca III with dominant configurations $3p^6$, $3p^5 3d$ and $3p^5 4s$ calculated using the program of Hibbert¹. These states, (all corresponding closely to a pure LS coupling scheme) were each represented by about 20 single electron configurations that allowed for internal, semi-internal and all-external correlations by means of single and double electron excitations to pseudo-orbitals $\bar{4}p$, $\bar{4}d$ and $\bar{4}f$. Of these correlations the most important was found to be that linking $3p^2$ to $3d^2$ arrangements, a fact not previously recognised for this ion. The excitation energies calculated for these states are compared with the experimental results of Borgström^{2,3} in Table 1 and the agreement is very satisfactory. Only two dipole allowed absorption transitions

State	Present Calculation	Experiment ^{2,3}
$3p^5 3d \ ^3P^o$	0.9302	0.9321
$3p^5 3d \ ^3F^o$	0.9709	0.9849
$3p^5 3d \ ^1D^o$	1.0287	1.0460
$3p^5 3d \ ^3D^o$	1.0336	1.0466
$3p^5 3d \ ^1F^o$	1.0405	1.0547
$3p^5 4s \ ^3P^o$	1.1088	1.1323
$3p^5 4s \ ^1P^o$	1.1286	1.1409
$3p^5 3d \ ^1P^o$	1.2729	1.3164

TABLE 1 Excitation energies (in au) of $3p^5 3d$ and $3p^5 4s$ levels of Ca III from the ground state.

($3p^6 \ ^1S \rightarrow 3p^5 4s \ ^1P^o$ and $3p^6 \ ^1S \rightarrow 3p^5 3d \ ^1P^o$) occur among the 9 states considered. Length and velocity values for the corresponding oscillator strengths are in excellent accord and are given in Table 2.

Transition	Length	Velocity
$3p^6 \ ^1S^e \rightarrow 3p^5 4s \ ^1P^o$	0.7093	0.7229
$3p^6 \ ^1S^e \rightarrow 3p^5 3d \ ^1P^o$	3.6883	3.6811

TABLE 2 Absorption dipole oscillator strengths in the length and velocity formulations transitions in Ca III.

A general representation of each LS π symmetry of the Ca II system was then obtained using the R-matrix method of Burke et al⁴. This involved close-coupling single-electron wavefunctions $U_{ij}(r)$ satisfying a common logarithmic boundary condition, to the multi-configurational wavefunctions of Ca III described above. This is represented by

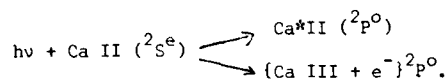
$$\psi^{LS\pi} = \sum_{ij} C_{ij} \phi_i U_{ij}(r) + \sum_j d_{jk} \phi_j \quad r \leq a \quad (1)$$

$$\left(\frac{1}{U_{ij}(r)} \cdot \frac{dU_{ij}}{dr} \right)_{r=a} = 0$$

where the boundary radius a was chosen to be 10 Bohr. The ϕ_i consist of the wavefunctions for the nine Ca III states combined with spin and angle functions for the last electron, \hat{A} is the anti-symmetrisation operator and configurations ϕ_j are composed entirely from the bound orbitals used in constructing the Ca III wavefunctions.

Matching on the spherical boundary to the strongly energy dependent single-electron multi-channel wavefunction outside, gives the coefficients C_{ij} and d_{jk} .

Radiative transitions from the ground state of Ca II are represented by



where the first arrow corresponds to photon absorption that leads to a bound-bound transition in the ion, whilst for the second, the photon has sufficient energy to ionise Ca II ($^2S^e$). We have represented both these bound and free states of Ca II by R-matrix wavefunctions of the form (1) thus allowing an equivalent representation of both sides of the dipole matrix element. These calculations are still in progress but oscillator strengths and photoionisation cross sections for Ca II will be presented at the conference.

References

1. A. Hibbert, Comput.Phys.Commun. **9**, 141 (1975).
2. A. Borgström, Ark.Fys. **38**, 243 (1968).
3. A. Borgström, Physica Scripta **3**, 157 (1971).
4. P.G. Burke, A. Hibbert and W.D. Robb, J.Phys.B **4**, 153 (1971).

FIELD-INDUCED AUTOIONIZATION OF QUASI-STABLE RYDBERG-STARK LEVELS

David A. Harmin

Joint Institute for Laboratory Astrophysics, University of Colorado and
National Bureau of Standards, Boulder, Colorado 80309 USA

The process of atomic autoionization is most familiar as a multielectron effect. In zeroth order, a doubly excited discrete state is degenerate with one or more continua from other channels. Any coupling between these channels leads to a mixed state Ψ_E , interpreted as an initially stable state that decays via the continua. Interference effects result in asymmetric Fano profiles,¹ $(\epsilon+q)^2/(\epsilon^2+1)$, $\epsilon = (E-E_0)/(\Gamma/2)$, where Γ is the width and q depends on the particular transition to Ψ_E .

One excited electron outside a closed-shell core cannot autoionize because it has a unique threshold — no discrete-continuum degeneracy is possible. However, an exception occurs when the atom is in a dc electric field $F = F\hat{z}$. Field-induced autoionization of a single electron is neither a new phenomenon² nor a theoretical perplexity,³ but it has only recently been approached⁴ in the spirit of Ref. 1. We present here a simple, useful result based on Fano's archetype.

Consider an electron photoexcited to a high Rydberg state. Outside the core one finds the potential $V(r) = -1/r + Fz$ (a.u.). The threshold is lowered from $E=0$ to $E_c = -2\sqrt{F}$, above which lie continuum states. In H, $V(r)$ applies everywhere and the Schrödinger equation is separable in parabolic coordinates.⁴ For any F , $m=|m_z|$, $E=-1/2 v^{-2}$, eigenfunctions are labeled by $n_1=0,1,\dots$ with eigenvalues⁴ $A_{n_1 m}^F(E)$ ($-1 < A < 1$). Each n_1 -channel has a potential barrier with a maximum at $E_{n_1 m}^{\max}(E) = -[2(1-A_{n_1 m}^F(E))F]^{1/2}$. Stark wave functions can always tunnel to $z \rightarrow \infty$ but when $E < E_c$ there exist quasi-stable levels $E_{n_1 m}(F)$ where the tunneling rate is negligible (n extrapolates to the principal quantum number at $F=0$). The key feature in the range $E_c < E < 0$ is that states with $A_{n_1 m}^F < A_c(E, F) \equiv 1 - 2|E/E_c|^2$ have $E > E_{n_1 m}^{\max}(E)$ and ionize, whereas those with $A_{n_1 m}^F > A_c$ are below the barrier and still stable. Thus, continua and (quasi-) discrete states are degenerate in H, though, being eigenstates, they do not mix.

A spherically symmetric core couples the n_1 -channels. To match to core boundary conditions, where $|Fz| \ll 1/r$, we appeal to Coulomb degeneracy and expand $|E n_1 m\rangle$ in spherical functions², $|E n_1 m\rangle = \sum_{\ell m} U_{n_1 \ell m} |E \ell m\rangle$. The coefficients $U_{n_1 \ell m}$ for fixed $m < v$ reduce to normalized Legendre functions,⁴ $U_{n_1 \ell m} = (2/v)^{1/2} (-1)^\ell P_{\ell m}(A_{n_1 m}^F)$. Thus we obtain from the spherical reaction matrix $\langle E \ell' m' | K | E \ell m \rangle = -\pi^{-1} \delta_{\ell' \ell} \tan \delta_\ell$

the coupling

$$\langle E n_1' m' | K | E n_1 m \rangle = -\pi^{-1} \sum_{\ell} U_{n_1' \ell m'} U_{n_1 \ell m} \tan \delta_\ell \quad (1)$$

with quantum defects $\{\mu_\ell = \delta_\ell/\pi\}$. One stable state \tilde{n}_1 ($E_{n_1 m} = \tilde{E}$) autoionizing to continua $\{n_1 \geq c\}$ has a decay rate $\Gamma = 2\pi(dA/dE)^{-1} \sum_c |K_c|^2$, where $K_c = \langle \tilde{n}_1 | K | c \rangle$ and $\pi^{-1} dA/dE$ is the \tilde{n}_1 -channel's density of states (we have ignored the shift E_0). The asymmetry parameter for photoexcitation from an initial state $|0\rangle$ is¹ $q = \tilde{d}/[\pi \sum_c K_c d_c]$, where \tilde{d} and d_c are dipoles $d_{n_1 m} = \langle E n_1 m | r_m | 0 \rangle$ (r_m depends on polarization³) or, in terms of spherical dipoles,⁴ $d_{n_1 m} = \sum_{\ell} U_{n_1 \ell m} \sec \delta_\ell d_{\ell m}^0$. The known ($F=0$) atomic parameters $\{\mu_\ell, d_{\ell m}^0\}$, transformation $U_{n_1 \ell m}$, and eigenvalues $A_{n_1 m}^F$ completely determine Γ and q .

A further simplification follows from noting that all continua satisfy $-1 < A_{n_1 m}^F(E) < A_c(E, F)$. We replace $\sum_c U_{c \ell' m'} U_{c \ell m}$ by the matrix

$$B_{\ell' \ell, m}^F(E) = (-1)^{\ell'+\ell} \int_{-1}^1 P_{\ell', m}(A) P_{\ell, m}(A) dA \quad (2)$$

which projects the total H continuum background onto ℓ -channels for fixed m [$B^F(E_c)=0$, $B^F(0)=\delta_{\ell', \ell}$]. Thus, at $E=\tilde{E}$,

$$q = -(U \sec \delta^0)/(U \tan \delta^F \sec \delta^0) \quad (3)$$

$$\Gamma = 2\pi^{-1} (dE/dA) (U \tan \delta^F \sec \delta^0)^2 \quad (4)$$

where U (d^0) is a row (column) vector, $\sec \delta$ and $\tan \delta$ diagonal matrices. Equations (3)-(4) serve to classify observed trends in autoionization lineshapes and widths in two ways: (i) with approximate eigenvalues $\tilde{A} = 2(\tilde{n}_1 + 1/2 + m/2)/\tilde{n} - 1$, the discrete states are identified through $U_{n_1 \ell m} \approx P_{\ell m}(\tilde{A})$; (ii) the range of the continua (2) scales with F through the ratio $r = |E/E_c|^2$. For example, for $p \rightarrow d$ ($m=1$) transitions in He, Li, or Na, we keep only δ_1 and d_{21}^0 and find $q = \tilde{A}/[3 \tan \delta_1 r^2(1-r)^2]$ and $\Gamma = (1-\tilde{A}^2)(1+2r)(1-r)^2$; q reverses sign and Γ is largest when $\tilde{A} = 0$, Γ increases with the continua from $r=1$ to 0, and $q \rightarrow \infty$ (symmetric profiles) at $r = 0, 1$.

References

1. U. Fano, Phys. Rev. 124, 1866 (1961).
2. M. G. Littman, M. M. Kash, and D. Kleppner, Phys. Rev. Lett. 41, 103 (1978); S. Feneuille et al., Phys. Rev. Lett. 42, 1404 (1979).
3. D. A. Harmin, Phys. Rev. A 26, 2656 (1982).
4. D. A. Harmin, in Atomic Spectra and Collisions in External Fields, eds. W. H. Navfeh and C. W. Clark, in press (1985).

HALF-SCATTERING PROCESSES IN THE PRESENCE OF LONG-RANGE BARRIERS

David A. Harmin

Joint Institute for Laboratory Astrophysics, University of Colorado and
National Bureau of Standards, Boulder, Colorado 80309 USA

The removal of a bound electron from an atom or ion by photoabsorption is a half-scattering process: the system is promoted from ψ_0 to an excited state ψ_E , and this condensed state then fragments outwards. Channels $\{i\}$ denote quantum numbers $LSJ\pi$ for the core, electron, and coupled system. The escaping electron has a channel-dependent energy $\epsilon_i = E - E_i$ for core states with nondegenerate E_i . Now the unwritten assumption is that the ionization thresholds $\epsilon_i=0$ derive from an infinite potential barrier (taken here to be Coulomb, $V = -Z/r$). This introduces a distinction — which we regard as artificial — between discrete ($\epsilon_i < 0$) and continuum ($\epsilon_i \geq 0$) states. They have tunneling integrals $\tau = \text{Im} \int_{r_1}^{r+\infty} k(r') dr' \rightarrow +\infty$ and $-\infty$, respectively, i.e., zero penetration below and zero reflection above the infinite plateau at $\epsilon_i=0$. The distinction is removed by adding to $V(r)$ a term $-Fr$ ($F>0$), which renders the barrier finite and all wave functions continuous as $r \rightarrow \infty$. This clue, borrowed from Stark theory, ultimately serves both to extend the density of states (DOS) view of the Stark effect¹ to multichannel systems² and to generalize the multichannel quantum-defect theory (MQDT) of spectra³ to arbitrary long-range barriers.

Consider a single channel wave function $\Psi(r)/r$ at excited energy ϵ . We define three regions: (A) short-range, $r \leq r_0 = \text{core}$; (B) intermediate, $r_0 \leq r \leq r_1 = \text{first turning point of } k(r) \text{ (complex at } \epsilon > -2\sqrt{Z}F)$; (C) long-range, $r_1 \leq r < \infty$. In (B) we choose energy-normalized basis functions $(f, g) = k^{-1/2}(\sin\phi, -\cos\phi)$, $\phi_\epsilon(r) = \text{Re} \int_0^r k(r') dr' + \pi/4$, $k^2(r) = 2(\epsilon - V(r))$; these WKB forms apply to highly excited states. Boundary conditions (bc) at $r = r_0$ are given by $K = \tan\delta$ ($\delta = \pi\mu$). The normalized eigenfunction in region (B) is then $\Psi = \cos\delta[f(r) - K g(r)]$. We formulate the scattering problem as follows. An "initial" state $\psi^i = f$ is scattered by the core into the state $\psi^+ = g - Hf$. $H(\epsilon)$ is chosen so that ψ^+ satisfies outgoing wave bc at $r \rightarrow \infty$. Without long-range barriers ($r_1 \rightarrow \infty$) we would have $H=1$ and $\psi^+ = e^{+i\phi}$ as usual. In the presence of barriers one finds^{1,2} $H(\epsilon) = -\cot(\phi+i\gamma) \equiv h+iH$, where $\phi(\epsilon) = \pi/2 - \phi(r_1) - \pi/4$ is the accumulated phase and $\gamma(\epsilon) = 1/4 \ln(1+e^{-2\tau})$; ϕ and $-\tau$ increase with ϵ . Note: (i) $H(\epsilon)$ has a series of poles $\phi_n(\epsilon) = n\pi - i\gamma$; (ii) the width $2\gamma(\epsilon)$ increases from $0(e^{-2\tau})$, when $\tau \gg 0$ (far below barrier), to $|\tau|$, when $\tau \ll 0$ (far above). The limits for $H(\epsilon)$, $-\cot\phi + i\pi\delta(\phi \bmod \pi)$ at $r \rightarrow +\infty$ and $0+i$ at $r \rightarrow -\infty$ (independent of

ϕ), correspond to pure discrete and continuum states. The total wave function is $\Psi(r) = \psi^i - T\psi^+ = (1+TH)f - Tg$, yielding the transition or "scattering" amplitude $T(\epsilon) = [\cot\delta - H(\epsilon)]^{-1}$. The scattering cross section for $\psi^i \rightarrow \psi^+$ is thus $D(\epsilon) = \text{Im}\{T(\epsilon)\}$, in analogy to the absorption of radiation by a system with susceptibility $T(\epsilon)$.

We normalize $D(\epsilon)$ so that it averages to unity per accumulated state [when integrated over any range $0 < \phi(\bmod \pi) < \pi$] by setting

$$D(\epsilon) = (K^{-2}+1) \text{Im}[K^{-1} - H(\epsilon)]^{-1} = \csc\delta \text{Im}[\cot\delta + \cot(\phi+i\gamma)]^{-1} \csc\delta. \quad (1)$$

This renormalizes all Ψ_ϵ per unit energy at $r \rightarrow \infty$ instead of $r < r_1$. Thus $D(\epsilon)$ is properly a DOS cross section describing the redistribution of the smooth DOS $\pi^{-1} d\phi/d\epsilon$ by the barrier (whereby the optical theorem $\text{Im}\{T\} = |T|^2$ is satisfied only on the average). The actual photoexcitation cross section $\sigma(\epsilon) = d^*D(\epsilon)d$ must include the dipoles¹ $d = \langle \Psi_\epsilon | r | \Psi_0 \rangle$. Eq. (1) reduces to $\text{Im}[\cot((\phi+\delta)+i\gamma)]$, which in the discrete region has shifted poles $\phi_n = (n-\mu)\pi - i0^+$, as expected. In the continuum ($\gamma \rightarrow \infty$) we get $T = \text{Im}(\cot\delta - i)^{-1} = \sin^2\delta$, the usual scattering result, and $D=1$ (no barrier effects).

In the Stark effect F is not an artifact. There are many degenerate channels with a range of $d\phi/d\epsilon$ and barrier sizes (the coordinates are also relabeled²). Most generally in MQDT one can parametrize a system with core bc specified by a reaction matrix $K = V \tan\delta \tilde{V}$ (diagonalized) and, for arbitrary barriers, $\{\phi_a(\epsilon), \tau_a(\epsilon)\}$ for long-range eigenchannels $\{a\}$. If K is referred to i -channels, $\{i\}$ and $\{a\}$ are related by a transformation U_{ai} (known for the Stark effect²). The multichannel matrix version of (1) is then

$$D = (K^{-2}+1)^{1/2} \text{Im}[K^{-1} - \tilde{U} H U]^{-1} (K^{-2}+1)^{1/2} = N \text{Im}[V \cot\delta \tilde{V} + \tilde{U} \cot(\phi+i\gamma) U]^{-1} N, \quad (2)$$

with $N = V \csc\delta \tilde{V}$ ($\cot\delta, H$ diagonal). The poles of (2) occur at energies where $\det[K^{-1} - \tilde{U} H U] = 0$ in both quasi-discrete and autoionizing spectra. We recover Seaton's $F=0$ "contracted" formulas³ by putting $\phi_c = \pi\nu$, $\gamma_c = 0$ ($\gamma_0 \rightarrow \infty$) for closed (open) channels.

References

1. D.A. Harmin, Phys. Rev. A **26**, 2656 (1982).
2. D.A. Harmin, Com. At. Mol. Phys., in press (1985).
3. M.J. Seaton, Rep. Prog. Phys. **46**, 167 (1983).

STARK EFFECT AND FIELD IONIZATION

Alexander Alijah, John T. Broad and Juergen Hinze

Fakultät für Chemie, Universität Bielefeld, D4800 Bielefeld, Fed. Rep. of Germany

INTRODUCTION

Perturbing an atom with a static electric field is known to alter its spectrum drastically by transforming the bound states into resonances and by introducing structure into the continuum [1]. In recent field ionization experiments [2], it has been possible to measure the broadening of high Rydberg states and peaking in the continuum for the especially simple case of atomic hydrogen in kilovolt electric fields. The combination of the two distance scales inherent in the sharply localized atomic Coulomb force and the weak, but long-range external field make quantitative theoretical interpretation difficult. Because the Schrödinger equation for the hydrogen atom in a static electric field is separable in parabolic coordinates, we were able to develop an algorithm based on the amplitude-phase approach introduced by Milne [3] for bound states and extended for scattering states by Lee and Light [4] which computes the highly oscillatory wave functions of the perturbed Rydberg and continuum spectrum accurately and efficiently.

OUTLINE OF THE THEORY

In parabolic coordinates, $\chi = \sqrt{r+z}$, $\eta = r-z$ and $\phi = \arctan(y/x)$, the Schrödinger equation for a hydrogen atom of energy E in an electric field of strength F separates to give with the usual quantization of L_z with quantum number m , a bound Schrödinger equation in χ with the effective potential,

$$V(\chi) = \frac{m^2 - 1/4}{2\chi^2} - E\chi^2 + F/4 \chi^4. \quad (1)$$

Its eigenvalues, β_1 , determine the effective charge, $\beta_2 = Z - \beta_1$, for the unbound equation in η with the effective potential

$$U(\eta) = \frac{m^2 - 1}{8\eta^2} - \frac{\beta_2}{2\eta} - \frac{F}{8} \eta, \quad (2)$$

with continuous eigenvalue $E/4$. In an analogy motivated by the perturbation theory of the field-free atom, the eigenvalues, β_1 , in the bound coordinate can be numbered by the parabolic quantum number, n_1 , while the resonances in the unbound coordinate can be characterized by the number of nodes, n_2 , inside the potential barrier, which becomes the remaining quantum number in the field-free limit.

To avoid having to follow the numerous oscillations of the wave function for Rydberg energies, we make the Milne Ansatz of deriving and numerically integrating a non-linear differential equation directly for the amplitude function,

$$w = \left(\frac{u_1^2 + u_2^2}{w_r} \right)^{1/2}, \quad (3)$$

of the desired regular solution, u_1 , and an irregular solution, u_2 . Then,

$$u_1 \sim w \sin \left[\int_0^x w^{-2} dt + \theta_0 \right], \quad (4)$$

and, if the initial conditions are chosen well, u_2 will oscillate just out of phase with u_1 to make the amplitude, w , smooth in the classically allowed region and a stable, growing exponential in the forbidden region (see Figure 1).

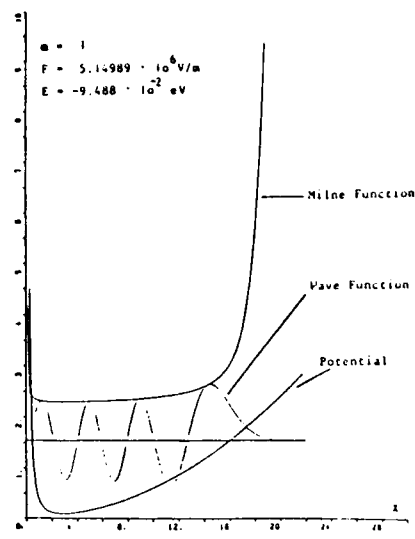


Fig. 1. Bound Coordinate

In the bound coordinate, the Milne Ansatz leads to the quantization condition,

$$\int_0^\infty w^{-2} d\chi = (n_1 + 1)\pi, \quad n_1 = 0, 1, 2, \dots \quad (5)$$

Depending both on the energy, E , and the effective charge, β_2 , the unbound coordinate exhibits a rich resonance structure caused by the barrier in the effective potential of equation (2). Lee and Light [4] approached such tunneling problems by determining separate amplitudes on each side of the barrier and matching the wave function in the middle. Before integrating numerically care must be taken with the non-analyticity caused by the Coulomb force at the origin and the explicit normalization required by the long range of the external field.

A resonance occurs at a maximum of the amplitude of the wave function inside the barrier as compared to the outside and very near to where the phase function, $\theta_B = \int_0^B w^{-2}$, at the middle of the barrier, η_B , goes through $(n_2 + 1)\pi$. A Lorentzian width, Γ_E , can be defined in terms of $d\theta_B/dE$ at the resonance energy.

RESULTS

The resonance positions, E_{res} , and widths, Γ , for some states with $n=19$, $|m|=1$, $F=10^{-6}$ a.u. are presented

n_1	n_2	$-E_{res} \cdot 10^3$	Γ	n_1	n_2	$-E_{res} \cdot 10^3$	Γ
0	17	1.9409	6.170-6	5	12	1.6469	3.772-8
1	16	1.8822	2.952-6	6	11	1.5881	8.982-9
2	15	1.8233	1.169-6	7	10	1.5293	1.852-9
3	14	1.7645	4.196-7	8	9	1.4704	3.190-10
4	13	1.7057	1.348-7	9	8	1.4114	4.548-11

REFERENCES

- [1] Landau, L.D., Lifschitz, E.M., *Theor. Phys.* **111** (1979).
- [2] Rottke, H., Welge, K.H., *J. Opt. Soc. Am. B*, **1** (1983) 485.
- [3] Milne, W.E., *Phys. Rev.* **35** (1930) 863.
- [4] Lee, S.V., Light, J.C., *Chem. Phys. Lett.*, **25** (1974) 435.

APPLICATION OF THE ANALYTIC PERTURBATION THEORY TO THE DESCRIPTION OF THE
ANGULAR DISTRIBUTION OF INNER SHELL PHOTOELECTRONS

A. Bechler* and R. H. Pratt

Department of Physics and Astronomy, University of Pittsburgh, Pittsburgh, Pennsylvania 15260 USA
*Permanent address: Institute of Theoretical Physics, University of Warsaw, Hoza 69, 00-681 Warsaw, Poland

We present results of a calculation of the inner shell photoelectron angular distribution. This calculation can be characterized by the following features:

(1) It is an analytic screened calculation with the screening effects accounted for perturbatively and with the point-Coulomb result taken as an unperturbed reference point.

(2) It is a nonrelativistic calculation, i.e. the electron wave functions used and the electron-photon interaction are nonrelativistic.

(3) It goes beyond dipole approximation, i.e. the photon plane wave is not approximated by 1.

Whereas in the total cross section the retardation contributes terms of the order $(v/c)^2$, i.e. of the same order as relativistic corrections, the retardation correction in the differential cross section is of the order v/c , and therefore it is reasonable to calculate nonrelativistic retardation corrections to the angular distribution without taking relativistic effects into account.

The calculation is based on the expansion of the screened-Coulomb potential in powers of a small parameter λ characterizing the screening, in the sense that λ^{-1} characterizes the dimensions of an atom:¹

$$V(r) = -\frac{a}{r} (1 + \lambda V_1 r + \lambda^2 V_2 r^2 + \dots). \quad (1)$$

This expansion can be used to characterize the screened atomic potential well in the interior of an atom. It can therefore be used as a starting point in the description of inner shell photoeffect when the ejected electron energy is well above threshold, since then the contribution to the matrix element comes predominantly from small distances. The photoeffect matrix element has the form

$$M_{fi} = \left(\frac{2\pi\alpha}{u} \right)^{1/2} \int d^3x \psi_f^* e^{i\vec{k} \cdot \vec{r}} \vec{\epsilon} \cdot \vec{p} \psi_i. \quad (2)$$

Both initial (bound state) and final (full continuum) wave functions have been found as expansions in powers of λ previously,^{1,2} substituting these expressions for the wave functions into (2) we find that the photoeffect matrix element for s subshells has the form

$$M_{fi} = M_{fi}^C (a + b\beta_c \cos \theta), \quad (3)$$

where θ is the angle between photon and electron momenta,

M_{fi}^C is the point-Coulomb matrix element of shifted energy² with retardation included,³ and coefficients a and b are given as expansions in powers of λ . Here β_c is the shifted velocity of the continuum electron, corresponding to the shifted momentum p_c , i.e. $\beta_c = p_c/m$.

Results of previous investigations suggest⁴ that by including the retardation factor⁵ explicitly in the expression for matrix elements one can obtain a better description for the angular distributions of photoelectrons than by using the multipole expansions⁶ in its standard form. We use results of the present analytical calculations to examine the utility of such retardation factors, and we also compare the various forms of these analytic expressions with exact numerical calculation.

References

1. J. McEnnan, L. Kissel, R. H. Pratt, Phys. Rev. A **13**, 352 (1976), Erratum A **13**, 2325 (1976), A **14**, 521 (1976).
2. A. Bechler, R. H. Pratt, preprint PITT-307, 1983 (to be published in Ann. of Phys.)
3. H. K. Tseng, R. H. Pratt, S. Yu and Akiva Ron, Phys. Rev. A **17**, 1061 (1978).
4. D. Salzmann and R. Y. Yin, preprint PITT-317, University of Pittsburgh, internal report, 1984.
5. H. A. Bethe and E. E. Salpeter, Quantum Mechanics of One and Two Electron Atoms, Springer-Verlag, Berlin, Göttingen, Heidelberg; Academic Press, Inc. New York, 1957, p. 311.
6. M. S. Wang, preprint PITT-296, University of Pittsburgh, internal report, 1982 (unpublished).

AUTOIONIZING RYDBERG STATES OF TRIPLET H_2

R. Kachru, N. Bjerre,* and H. Helm

Molecular Physics Department, SRI International, Menlo Park, CA 94025

We report the observation of autoionization spectra of the Rydberg gerade ns and nd states in triplet molecular hydrogen. A fast molecular hydrogen beam was formed by charge transfer of H_2^+ in Cs and made coaxial with a laser beam over a distance of 100 cm. The Rydberg states are excited by a frequency doubled YAG-pumped dye laser from the metastable $H_2(c^3\Pi_u)$ states present in the fast beam to high lying triplet Rydberg states which subsequently autoionize. Autoionizing states are detected by separating H_2^+ ions formed as a result of autoionization from the neutral beam and counting. Figure 1 shows the experimental spectrum obtained as the dye laser in its low

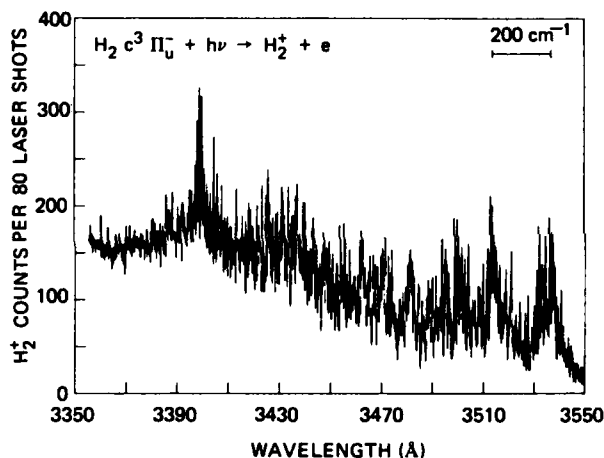


Figure 1 Low resolution autoionization spectrum of the triplet gerade Rydberg states excited from the $H_2 c^3\Pi_u$ metastable state. The resolution of the spectra is limited by the laser linewidth of 1 cm^{-1} .

resolution mode (laser linewidth 1 cm^{-1}) is scanned from 3360 to 3550 Å. The observed autoionization spectra are rich in the number of lines even in low resolution since four gerade series are accessible from the sixteen vibrational levels of the c state. The dominant peaks in Figure 1 arise from the excitation to the nd series beginning at $n=10$ near 3535 Å. The continuous background in Figure 1 is due to direct photoionization from the c state.

We have scanned smaller portions of the spectrum with a narrower laser linewidth (0.1 cm^{-1}). A portion of a high resolution spectrum obtained near 3400 Å with a 0.1 cm^{-1} resolution is shown in Figure 2. The higher resolution spectra reveal that each low resolution peak splits into several peaks, representing primarily a single value of n . Each individual peak shows a 0.2 cm^{-1} splitting indicating the fine structure splitting in the c state.

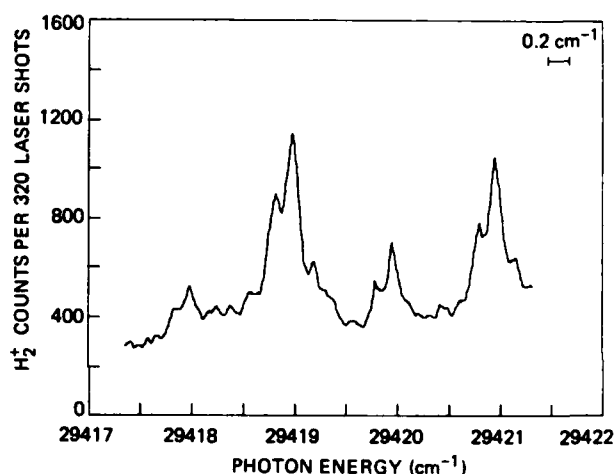


Figure 2 High resolution spectra of the autoionizing states obtained near 3400 Å. The 0.1 cm^{-1} experimental resolution is limited by the laser linewidth (0.1 cm^{-1}). The Doppler width in the fast beam is substantially smaller. The 0.2 cm^{-1} splittings observed in this spectrum corresponds to the fine structure of the c state.

Our preliminary analysis indicates that lines with n as high as 34 are discernable in the spectra. A detailed analysis of the spectra is currently being prepared.

Work supported by NSF Grant PHY84-11517.

*Permanent address: Institute of Physics, University of Aarhus, DK-8000 Aarhus C, Denmark

DISSOCIATIVE DOUBLE PHOTOIONIZATION OF SOME SIMPLE MOLECULES

Gérald Dujardin, Lucette Hellner, Sydney Leach and Dominique Winkoun

Laboratoire de Photophysique Moléculaire du C.N.R.S.
Bâtiment 213 - Université Paris-Sud - 91405 Orsay Cédex, FranceIntroduction

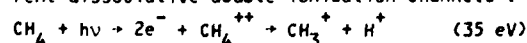
In recent years, studies of double photoionization (DPI) have mainly concerned atomic species. Double ionization of molecules has previously been studied mostly by using electron or ion impact sources. In our work, monochromatized synchrotron radiation in the 30-70 eV region is used as a source for double photoionization of molecules. The lowest electronic states of doubly charged molecular photoions produced by vertical transitions from the neutral ground state are well above the threshold energies for formation of the lowest dissociation products. The consequent instability or metastability of the doubly charged photoions can lead to their rapid dissociation. We have investigated the dissociative channels following DPI of sulfur dioxide¹, methane², carbon dioxide and ammonia, using an original photoion-photoion coincidence (PIPICO) technique. The results have enabled us to investigate the following: (i) electronic state-to-state dissociation processes in doubly charged cations, (ii) electronic state symmetries of doubly charged cations, (iii) partial and total cross sections for DPI, (iv) threshold behaviour in DPI, (v) electron correlation effects in DPI.

Experimental

The principle of our PIPICO technique is to detect, with a single detector, the two ionic fragments resulting from the dissociation of a doubly charged photoion and to measure, by delayed coincidences, the difference between their times of flight. Comparison of experimental and simulated photoion-photoion coincidence curves enable us to identify the fragment ions and to determine the kinetic energy release. By repeating the measurements at different excitation energies we can determine thresholds for various dissociation processes and measure the partial and total cross sections for dissociative double photoionization. The experimental set-up has been described in detail elsewhere².

Results

Methane will be used as an example. The measured (dissociative) DPI cross section of methane in the 34-41 eV photon energy range contains two breaks, at 35.0 and 38.5 eV, which correspond to the thresholds of two different dissociative double ionization channels:



$$\text{CH}_4 + h\nu + 2e^- + \text{CH}_4^{++} \rightarrow \text{CH}_2^+ + \text{H}^+ + \text{H} \quad (38.5 \text{ eV})$$

as determined from PIPICO curves². The two CH_4^{++} states involved at 35 and 38.5 eV are assigned as $\tilde{\text{X}}^3\text{T}_1$ and $\tilde{\text{a}}^1\text{E}$ respectively. The maximum double photoionization cross section for Methane, 0.08 Mb, is considerably less than that of the isoelectronic atomic species Neon, 0.25 Mb³; this appears to be related to the smaller extent of electron correlation effects in the more voluminous species.

State-to-state studies of the dissociation of doubly charged cations is illustrated with the case of $\text{CH}_4^{++}(\tilde{\text{a}}^1\text{E}) \rightarrow \text{CH}_2^+ + \text{H}^+ + \text{H}$. PIPICO curve simulation was carried out to first establish that the $\tilde{\text{a}}^1\text{E}$ state dissociates into three products: $\text{CH}_2^+ + \text{H}^+ + \text{H}$. Further simulations were made on the basis of three different models of the dynamics of the dissociation process: (i) simultaneous fragmentation statistical model, in which it is assumed that the internal energy of the parent CH_4^{++} is statistically distributed over the degrees of freedom of the fragments, and that rigorous energy conservation can be replaced by average energy conservation⁴; (ii) impulsive model, in which H^+ and H have equal momenta, directed along the C-H bonds; (iii) Coulomb repulsion model in which CH_2^+ and H^+ fly apart at 180° from each other, and the H atom takes off no kinetic energy. Good agreement with the experimental PIPICO curve is obtained only for the curve simulated on the basis of model (iii). This finding demonstrates the major role of Coulomb repulsion in the fragmentation process.

Results of similar studies on dissociative double photoionization of other small molecules will also be presented.

References

1. G. Dujardin, S. Leach, O. Dutuit, P.M. Guyon and M. Richard-Viard, *Chem. Phys.* **88**, 339 (1984).
2. G. Dujardin, D. Winkoun and S. Leach, *Phys. Rev.* **A31**, 000 (1985).
3. V. Schmidt, N. Sandner, H. Kuntzemüller, P. Dhez, F. Wullemier and E. Kälne, *Phys. Rev.* **A13**, 1748 (1976).
4. T. Baer, A.E. DePristo and J.J. Hermans, *J. Chem. Phys.* **76**, 5917 (1982).

SINGLE PHOTON DOUBLE IONIZATION IN SOME TRIATOMIC MOLECULES

P. LABLANQUIE, I. NENNER, P. MILLIE, P. MORIN

CEA, Département de Physico-Chimie, CEN/Saclay, 91190 Gif Sur Yvette, France

and LURE, Université Paris-Sud 91405 Orsay Cédex, France

J.H. ELAND

Physical Chemistry Laboratory, University Southparks Road, Oxford OX13Q2, U.K.

J. DELWICHE, M.J. HUBIN-FRANSKIN

Institut de Chimie, Université Sart Tilman, 4000 Liège 1, Belgium

INTRODUCTION

Double ionization of a molecule by a single VUV photon has recently become an important subject of investigation, thanks to the development of ion-ion coincidence (PIPICO) techniques /1/ which can characterize dissociative double ionization, and to the availability of suitable photon sources : HeII lamps /2/ or synchrotron radiation /1,3/. We present 1) evidence of double ionization processes in the triatomic molecules CS_2 , OCS and CO_2 which are isoelectronic in their valence shells. 2) experimental and theoretical determination the M^{++} electronic states.

EXPERIMENTAL

Synchrotron radiation from ACO, Orsay storage ring is monochromatized in the 25 to 75 eV range, and then focussed into the center of an ionization chamber, where it crosses at right angles an effusive jet of gas ; ions are then extracted into a traditional two stages time of flight spectrometer /3/. Mass spectra are obtained by use of a pulsed extraction field, and enable us to detect stable or long lived ($\tau \geq 10^{-6}$ s) doubly charged ions. D.C. extraction fields are used to measure PIPICO spectra, where we record the time-of-flight difference between temporally correlated ion pairs ; a coincidence peak appears whenever the two ions come from the same event : $\text{M}^{++} \rightarrow \text{A}^+ + \text{B}^+ + \dots$. In this way, "fast" ($\tau \leq 10^{-6}$ s) dissociative double ionization is identified and analyzed.

RESULTS

A typical PIPICO spectrum of OCS is presented in Fig. 1 : four dissociative decay channels of OCS^{++} , three of CS_2^{++} and one of CO_2^{++} have been identified corresponding either to single bond breaking (OC^+/S^+ , O^+/CS^+ ; S^+/CS^+ ; O^+/CO^+) or to complete atomization ($\text{O}^+/\text{C}^+/\text{S}$, $\text{O}/\text{C}^+/\text{S}^+$; $\text{S}/\text{C}^+/\text{S}^+$, $\text{S}^+/\text{C}/\text{S}^+$). Peak shapes in such spectra are characteristic of the kinetic energy released during the processes. Simulation of these coincidence peaks shows that in most cases, the available energy is transferred mainly into kinetic energy of the two departing ions, and not into internal excitation of the fragments.

Excitation spectra for the production of each of the dissociative channels, and of the long-lived M^{++} have

been recorded. Several deductions can be made from such measurements.

- Single photon double ionization is a surprisingly intense phenomenon (most of all in CS_2 , where it can account up to 40% of the absorption).
- The different appearance energies provide experimental determination of the position of the successive M^{++} electronic states, in the Franck Condon region.

CALCULATIONS OF M^{++} STATES

We performed a calculation of the vertical transition energies using an ab initio SCF CI method with polarized atomic orbitals. All M^{++} states have been calculated in a 10 eV range above M^{++} ground state. Comparison with experimental M^{++} appearance potentials leads to the following assignments : the M^{++} ground state (metastable) corresponds to the ejection of the two outermost electrons. The great density of states calculated above 6 eV (with respect to M^{++} ground state) makes a definite assignment of the dissociative M^{++} states, difficult. Transition moment calculations are certainly needed to clarify the situation.

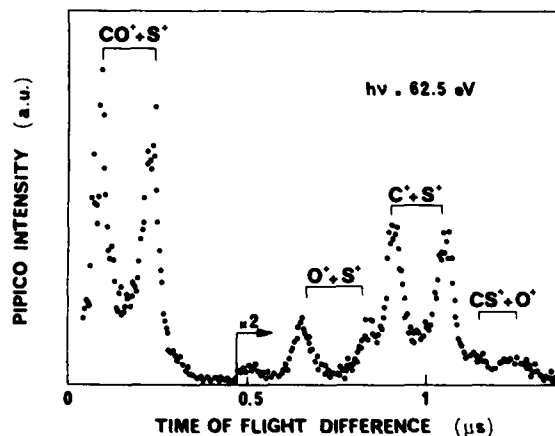


Fig. 1 : Photoion-Photoion coincidence spectrum of OCS

/1/ G. DUJARDIN, S. LEACH, O. DUTUIT, P.M. GUYON and M. RICHARD-VIARD

Chem. Phys. **88** (1984) 339

/2/ D.M. CURTIS, J.H.D. ELAND

to be published in J. Mass. Spectr. Ion. Phys.

/3/ P. LABLANQUIE, I. NENNER, P. MILLIE, P. MORIN

J.H.D. ELAND, M.J. HUBIN-FRANSKIN and J. DELWICHE

J. Chem. Phys. (in press)

SELECTIVE RESONANT PHOTOIONIZATION PROCESSES NEAR THE Si2p EDGE IN TETRAMETHYLSILANE

P. MORIN (a,c), C.G.B. DE SOUZA (b), P. LABLANQUIE (a,c) and I. NENNER (a,c)

a)CEA, IRDI, Departement de Physico Chimie, CEN Saclay, 91191 Gif sur Yvette, France

b)Istituto de Quimica, UFRJ, Cidade Universitaria, Rio de Janeiro, RJ 21910, Brazil

c)LURE, CNRS, Bâtiment 209C, Université de Paris-Sud 91405 ORSAY Cedex, France

INTRODUCTION

We report new measurements on tetramethyl silane, $\text{Si}(\text{CH}_3)_4$, photoexcited by synchrotron radiation, in the region of the Si2p edge (95-120 eV) using angular resolved photoelectron and photoion spectroscopy. Evidence of several resonances is made by measuring selective electronic decay processes (autoionization and Auger) and selective dissociation of both singly and doubly charged residual ions.

EXPERIMENT

We use synchrotron radiation from ACO storage ring in the 95-120 eV range using a toroidal grating monochromator /1/. The monochromatized photon beam is then combined with two different experimental set ups. a) photoelectrons are energy selected by a 127° cylindrical analyzer, rotatable in the vertical plane /1/. We record at magic angle, either photoelectron spectra (PES) at fixed wavelength or, keeping the binding energy constant versus incident photon wavelength, we obtain directly corresponding partial photoionization cross section. b) photoions are analyzed using a time of flight (TOF) mass spectrometer /2/ which is operated in two modes.

-Ionic fragments intensities are recorded using a pulsed voltage in the ionization chamber, which gives a time origin for TOF measurements.

-Fragments ion pairs intensities are detected by the photoion-photoion coincidence technique (PIPICO). A constant voltage is kept in the ionization chamber and a single detector provides the start and stop inputs of a time to amplitude converter.

RESULTS

Above the Si2p threshold, existence of Auger lines (from the 2p hole relaxation) has been established by photoelectron spectroscopy /3/. They show a resonant behaviour, similarly to the 2p cross section, just above the threshold. Below 106.1 eV Auger lines disappear continuously, while a high background rises in the PES. At this photon energy, one of the three main valence lines (binding energy of 21.7 eV) shows a resonant behaviour as opposed to the other valence lines. Therefore two resonances are to be distinguished: one in the discrete, is shown to autoionize into TMS^+ with an inner valence hole of a a_1 symmetry and to produce doubly excited ions (satellite) involving probably many valence excitations. The other is a shape resonance lying in the Si2p continuum which decays primarily into Auger pathways which also involves outer valence electron ejection. Singly charged

photoion fragment yield has been measured in this region and confirms the presence of two different resonances below and above threshold. Evidence of five regularly spaced features are actually seen in the first, in good accord with absorption results /4/. Photoion-photoion coincidence shows that dissociation of TMS^{++} proceeds through many different channels. Specific ion pair yield is shown to increase drastically at the resonance threshold (Fig.1). This is perfectly consistent with Auger processes since this leads primarily to doubly charged molecular ions. It also explains the "excess" of CH_3^+ and $\text{Si}(\text{CH}_3)_3^+$ ions above threshold (Fig.1).

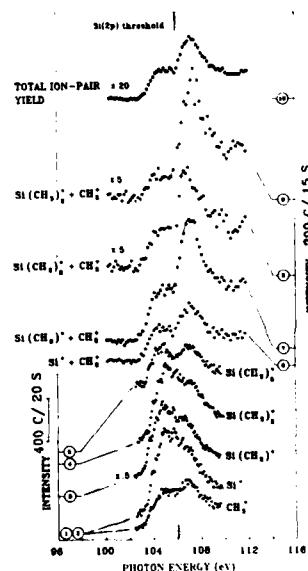


Fig.1 : Excitation spectra of ion fragments and selected ion pairs in the Si2p threshold region.

- /1/ Morin, P., Adam, M.Y., Nenner, I., Delwiche, J., Hubin-Franskin, M.J., and Lablanquie, P., Nucl. Inst. and Meth. **208** (1983) 761.
- /2/ Lablanquie, P., Nenner, I., Millié, P., Morin, P., Eland, J.H.D., Hubin-Franskin, M.J., and Delwiche, J., J. Chem. Phys. (in press).
- /3/ de Souza, G.G.B., Morin, P., Nenner, I., J. Chem. Phys. (in press).
- /4/ Sodhi, R.N.S., Daviel, S., Brion, C.E., and de Souza, G.G.B., J. Electron. Spectros. (in press).

ANGLE RESOLVED PHOTOELECTRON STUDY OF THE CONFIGURATION INTERACTION STATES OF CO_2^+ P. ROY^{*,*}, I. NENNER⁺, P. MORIN⁺, P. MILLIE⁺, D. ROY⁺, M.J. HUBIN-FRANSKIN AND J. DELWICHE⁺

LURE, Bâtiment 209C, Université de Paris-Sud, 91405 ORSAY Cedex France

⁺ Dept. de Physico-Chimie, Centre d'études Nucléaires de Saclay, 91190 GIF SUR YVETTE France^{*} CRAM et Dept. de Physique, Université Laval, QUEBEC Canada G1K-7P4⁺ Université de Liège, Sart Tilman, 4000 par LIEGE 1, Belgique

In the photoionization of molecules, the residual ion can be left in simple ionized state, associated with one hole configuration or in an excited ionized state. In a classical photoelectron spectrum (PES) they correspond respectively to the so called "main bands" or "satellite bands". Since the main line is well described in the model of "independent particle" the satellite lines requires to considerate configuration interaction (CI) (1) in initial and/or final state.

In previous CO_2 P.E.S. (2) such satellites have been evidenced but their attribution to a given symmetry was only based on calculated positions and relative intensities.

We present here angle resolved high resolution photoelectron studies of 10 satellites in CO_2 , in the 30-55 eV photon energy range. The evolution of the asymmetry parameter β and the partial cross section σ , as a function of photon energy is used for identifying symmetry of previously observed bands and of lines reported for the first time.

Synchrotron radiation emitted by the ACO storage ring crosses at a right angle an effusive jet of CO_2 . The ejected photoelectrons are detected by a 127° electrostatic analyzer. From the intensity ratio measured at two different angles in a plane perpendicular to the light direction, we extract β (3).

In figure 1, we present two typical P.E.S. : the lower one, measured at the magic angle and corrected for the transmission function of the analyzer which gives directly relative σ and the upper one taken at $\theta = 0^\circ$ which includes angular effects.

According to C.I. theories (2) two different set of satellites can be distinguished ; those associated with outer valence orbitals (mostly $2\pi_u$) are predicted to fall in the lowest part of the spectrum and those resulting from a mixing with ionization of inner valence orbitals, appear above 30 eV. On figure 2, the β values for satellites #1 to #10 in the 30-55 eV photon energy range evidenced two groups of curves : #1 to #5 have positive β values while #6 to #10 have essentially negative or zero values. We have also represented on this figure, theoretical curves for three main lines ($1\pi_u$, $3\sigma_u$ and $4\sigma_g$) (4). We consider #1, 2, 3, and 5 to have π_u symmetry because the β kinetic energy dependence is almost identical to the $A^2\pi_u$ one. On the other hand, at 1253 eV photon energy (5), the overall branching ratio relative to the total ionization associated with the lines #6 to 10 is much higher compared to #1 to 5 as

would be Σ symmetry lines as compared to Π ones. Therefore, we support the theories predicting this region to be dominated by $2\sigma_u$ and $3\sigma_g$ bands.

Moreover the same argument, applied to σ_u as opposed to σ_g orbitals of CO_2 , leads to the assignment of $2\sigma_u$ for lines #6, 7 and 8 and of $3\sigma_g$ for lines #9 and 10. New C.I. calculations including "three holes, one particle" configuration are actually in progress, and will be presented at the conference.

- (1) S.T. MANSON, J. Elect. Spectros. 9, 21 (1976)
- (2) W.DOMCKE, L.S. CEDERBAUM, J. SCHIRMER, W. VON NIESSEN, C.E. BRION and K.H. TAN, Chem. Phys. 40, 171 (1979)
- (3) P. ROY, I. NENNER, M.Y. ADAM, J. DELWICHE, M.J. HUBIN FRANSKIN, P. LABLANQUIE and D. ROY, Chem. Phys. Lett. 109, 6 (1984) 107
- (4) F.A. GRIMM, T.A. CARLSON, W.B. DRESS, P. AGRON, J.O. THOMSON and J.W. DAVENPORT, J. Chem. Phys. 72, (1980) 3041
- (5) C.J. ALLAN, U. GELIUS, D.A. ALLISON, G. JOHANSSON, H. SIEGHBACH and K. SIEGHBACH, J. Electron. Spectry. 1, (1972) 131

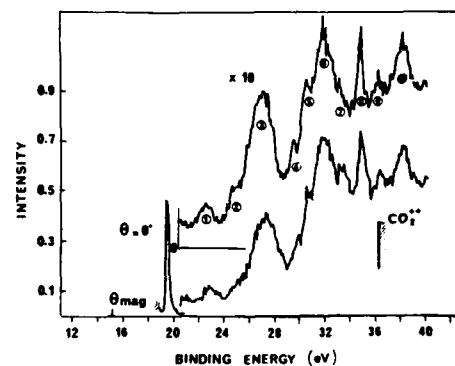


Fig.1 : Typical PES taken at $\theta = 0$ and θ mag and 45 eV photon energy. The 19.4 eV line corresponds to the C state of CO_2^+ . The X, A and B state lines are not represented.

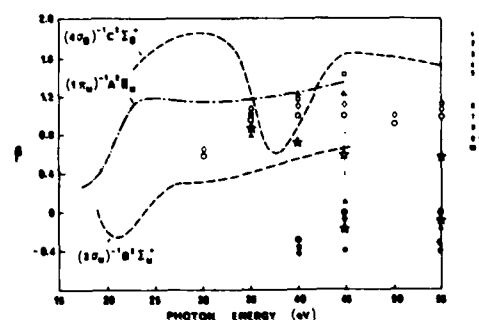


Fig.2 : Photon energy dependence of β for 10 satellite lines.

KINETIC ENERGY OF FRAGMENTATION PRODUCED BY
 DISSOCIATIVE PHOTOIONIZATION OF NO

J.A.R. Samson, G.C. Angel, and O.P. Rustgi

Behlen Laboratory of Physics, University of Nebraska, Lincoln, Nebraska 68588 USA

The kinetic energies of ions produced by dissociative photoionization of NO have been measured by use of discrete resonance lines of He (534Å), Ne (736 and 744Å), and undispersed synchrotron radiation from the Stoughton storage ring (the short wavelength limit was approximately 100Å).

A 90° cylindrical electrostatic energy analyzer was used with a resolution of about 1% to determine the energy of the ions (viz. N^+ , O^+ , NO^+). No mass analysis was used to identify the specific ions. However, the present results appear to identify the major fragments unambiguously.

Figure 1 shows a potential energy diagram of NO illustrating possible dissociative pathways. The bound electronic states $B'^1\Sigma$ (or $B^1\Sigma$) and $c^3\Pi$ ($B^1\Pi$) are known to dissociate into $N^+(^3P) + O(^3P)$ as evidenced by the large increase in the N^+ signal at these thresholds. This was observed and measured separately by mass analysis of the fragment ions.¹ No increase in the O^+ signal was observed at these thresholds. Figure 2 shows the energy spectrum of the ions produced by synchrotron radiation. A broad continuum lying between 0.9 and 1.5 eV correlates well with the predicted dissociation of the $B'^1\Sigma$ state ($v = 0$ to 13). A lower energy group peaking at 0.36 eV correlates well with dissociation of the $c^3\Pi$ state. The effect of Doppler broadening on this peak is to produce an additional energy broadening of about 250 mV at half maximum. The 0 eV peak represents, primarily, the NO^+ parent ion. However, low energy O^+ ions were observed when the 584Å line was used. By subtracting the contribution of the NO^+ peak using data obtained by the Ne 736Å line (16.85 eV), which does not dissociate NO, a weak O^+ continuum is obtained ranging from 0 to about 0.5 eV. This can be explained by perturbation of the $W^1\Delta$ and/or $w^3\Delta$ states of NO^+ by the repulsive $5\Sigma^+$ state leading to fragmentation into $O^+(^4S) + N(^4S)$.

Acknowledgment

This material is based upon work supported by the National Aeronautics and Space Administration under Grant No. NGR 28-002-01 and by the National Science Foundation under Grant No. ATM-8412820.

Reference

1. J.A.R. Samson, T. Masuoka, and P.N. Pareek, to be published.

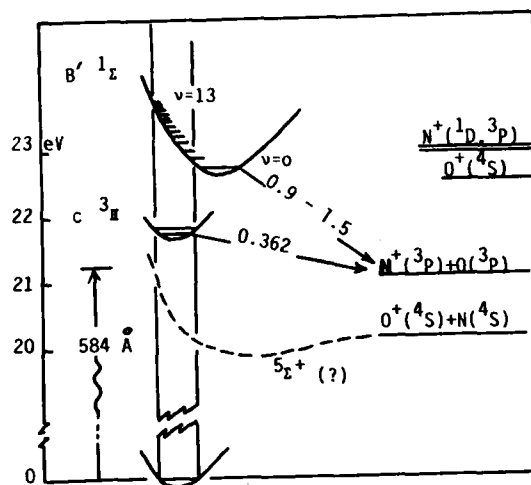


FIGURE 1. Potential energy diagram of NO. The numbers 0.362 and 0.9 - 1.5 represent the predicted energy in eV for $N^+(^3P)$.

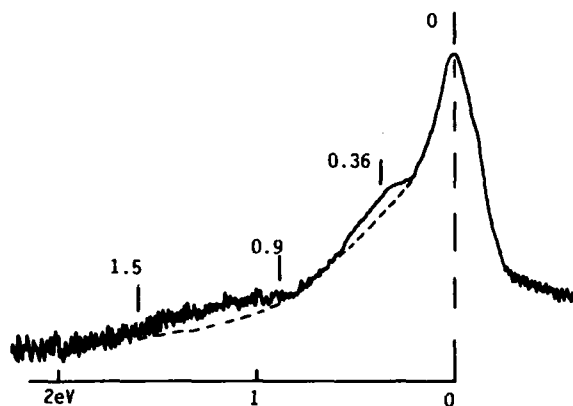


FIGURE 2. Energy spectrum of ions produced by dissociative photoionization of NO. The major peak at 0 eV is primarily NO^+ .

ANALYSIS OF PHOTOION BRANCHING RATIOS OF HF AND HCl

Toshio Masuoka and Shichiro Mitani

Research Institute for Atomic Energy, Osaka City University, Sugimoto 3-3-138, Sumiyoshi-ku, Osaka 558, Japan

A new photoion spectroscopy has been proposed to understand the dynamics of dissociative photoionization processes.^{1,2} The method depends on analyzing the photoion branching ratios measured by mass spectrometry as a function of photon energy. The photoion branching ratio $BR(A^+)$ is an integrated probability of producing the particular type of ion A^+ from the electronic states concerned with the molecular ion AB^+ and, in some cases, with AB^{2+} at higher energies. As can be expected from an analogy of integral photoelectron spectra, a differentiation of photoion branching ratio $BR(A^+)$ with respect to the energy provides a spectrum for A^+ , which clearly indicates the dissociation channels of AB^+ or AB^{2+} into A^+ .

The present work reports our analysis on HF and HCl, of which photoion branching ratios have been reported by Brion et al.^{3,4} using the electron impact experiment (e, e-ion). The photoion spectra obtained for HF and HCl are shown in the accompanying figures, in which the data points (●) represent $\Delta BR_j / \Delta E$, while the solid curves are their fittings by the third order B-spline function. Many peaks can be seen in the differential spectra and are correlated to the known electronic states of the singly and doubly ionized HF and HCl. Those electronic states include the multi-electron transitions⁴ which become dominant as a result of the strong electron correlation and the excited states of

the doubly ionized ions observed in the Auger spectra⁵ as well as the outer valence orbitals.⁶ Other possible origins for these peaks, in general, are 1) predissociation of shape resonance states with σ symmetry, 2) autoionization of highly excited neutral states (Rydberg states), and 3) ionization to very steep portions of repulsive potential curves which would give undetectable structure in photoelectron spectra because of its very flat and broad nature.

The photoion spectroscopy mentioned above has a distinct advantage over photoelectron spectroscopy in determining which electronic state predissociates into what ionic fragments. Further, it provides the sensitive method to study predissociation of highly excited states of molecular ions.

References

1. T. Masuoka, J. Chem. Phys. **8**, 2652 (1984).
2. T. Masuoka, J. Chem. Phys. in press.
3. F. Carnovale and C. E. Brion, Chem. Phys. **74**, 253 (1983).
4. S. Daviel, Y. Iida, F. Carnovale, and C. E. Brion, Chem. Phys. **83**, 319 (1984).
5. R. W. Shaw, Jr. and T. D. Thomas, Phys. Rev. A **11**, 1491 (1975).
6. F. Carnovale, R. Tseng, and C. E. Brion, J. Phys. B **14**, 4771 (1981). see also Ref. 4.
7. W. Von Niessen, L. S. Cederbaum, W. Domcke, and G. H. F. Dierksen, Chem. Phys. **56**, 43 (1981).

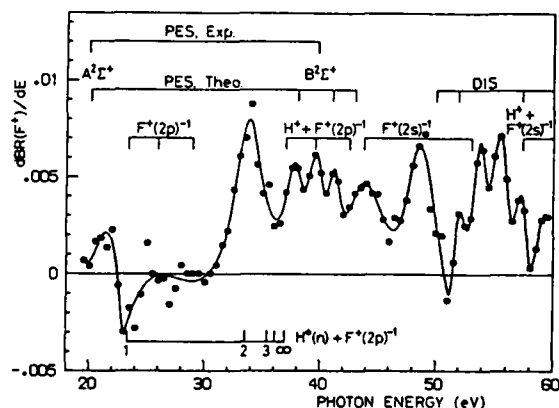


Fig. 1. The differential spectrum of the branching ratios $BR(F^+)$ from HF. The vertical dashed line indicates the first dissociation limit for $H + F^+$. Double ionization states (DIS) are from Ref. 5.

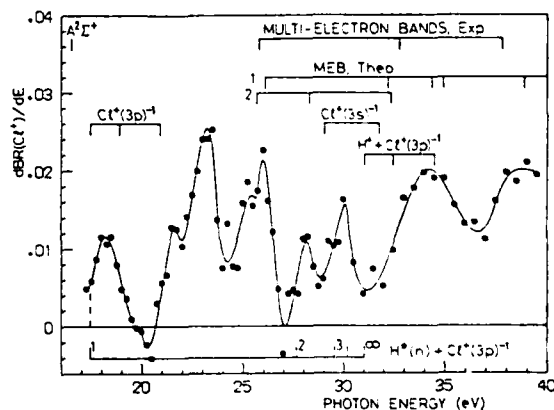


Fig. 2. The differential spectrum of the branching ratios $BR(Cl^+)$ from HCl. The vertical dashed line indicates the first dissociation limit for $H + Cl^+$. The theoretical calculations for the multi-electron transitions are also shown (Ref. 7).

DISSOCIATION MECHANISM OF SINGLY AND DOUBLY IONIZED CO

Toshio Masuoka

Research Institute for Atomic Energy, Osaka City University, Sugimoto 3-3-138, Sumiyoshi-ku, Osaka 558, Japan

Dissociative photoionization processes have been studied for CO in a wide energy region by mass spectrometry.^{1,2} The ions observed in the literature are CO^+ , O^+ , C^+ , C^{2+} , and CO^{2+} . The branching ratios (production rates) for these ions plotted on a photon energy scale may, in general, be analogous to an integral photoelectron spectrum. If the branching ratios are differentiated with respect to the photon energy, one can expect to obtain peaks corresponding to dissociation channels of singly and doubly ionized CO. In this respect, the method provides a new photoion spectroscopy.^{3,4} Obviously, it is possible to know these channels for each singly or doubly charged ion produced, while photoelectron spectroscopy does not involve this kind of information.

The differential spectra obtained for C^+ , O^+ , and C^{2+} are shown in Figs. 1-3. The mechanism producing these ions at the observed peaks in the spectra is discussed by comparing the spectra with the reported energy states of CO^+ and CO^{2+} such as the multi-electron bands⁵ ($\text{C}^2\Sigma^+$, $\text{D}^2\Pi$, $\text{F}, \text{G}^2\Sigma^+$, and $^2\Sigma^+(3\sigma)^{-1}$) and the double ionization states observed in the Auger spectra.⁶ It becomes evident that these states play a significant role in producing the observed ions. In order to infer the energy states of the dissociation products the thermochemical thresholds for the dissociative single and double ionization are also shown in the figures.

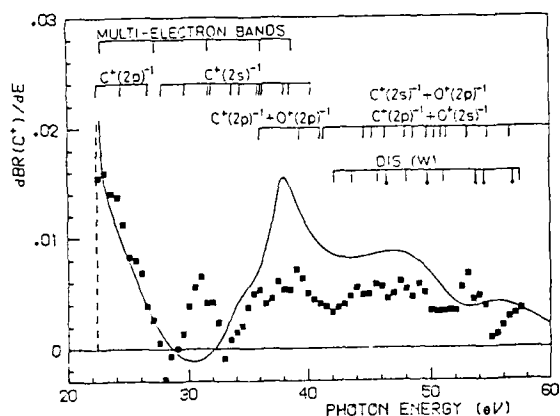


Fig. 1. The differential spectrum of the branching ratios $\text{BR}(\text{C}^+)$ (solid curve). The vertical dashed line indicates the first dissociation limit for $\text{C}^+ + \text{O}$. Multi-electron-bands are from Ref. 5. Double ionization states (DIS, W) including the shake-up states (indicated with \bullet) are from Ref. 6. \blacksquare : the results derived from Ref. 2.

References

1. T. Masuoka and J. A. R. Samson, *J. Chem. Phys.* **74**, 1093 (1981).
2. G. R. Wight et al., *J. Phys. B* **9**, 675 (1976).
3. T. Masuoka, *J. Chem. Phys.* **8**, 2652 (1984).
4. T. Masuoka, *J. Chem. Phys.* in press.
5. S. Krummacher et al., *J. Phys. B* **16**, 1733 (1983).
6. W. E. Moddeman et al., *J. Chem. Phys.* **55**, 2317 (1971).
J. A. Kelber et al., *J. Chem. Phys.* **75**, 652 (1981).

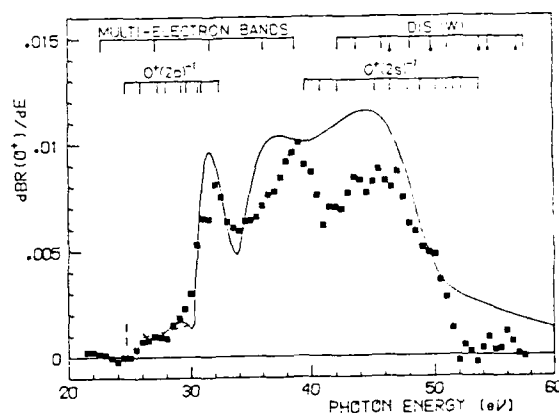


Fig. 2. The differential spectrum of the branching ratios $\text{BR}(\text{O}^+)$. The vertical dashed line indicates the first dissociation limit for $\text{O}^+ + \text{C}$.

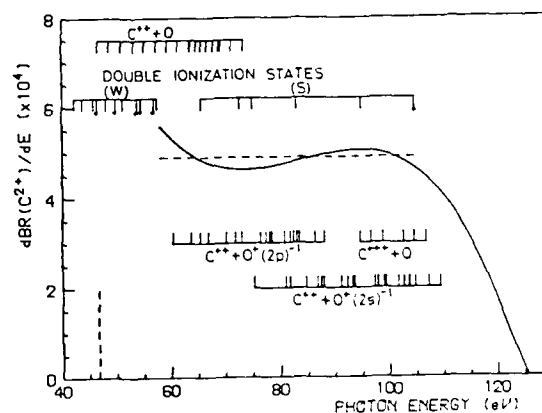


Fig. 3. The differential spectrum of the branching ratios $\text{BR}(\text{C}^{2+})$. The vertical dashed line indicates the first dissociation limit for $\text{C}^{2+} + \text{O}$. The curve oscillates below 100 eV because of the low counting statistics for differentiation and may be flat as shown with the horizontal dashed line. The thermochemical thresholds for the dissociative double ionization $\text{C}^{2+} + \text{O}$ and the series limits of the Rydberg states (shown below the curve) started from the dissociative double ionization are also indicated.

ABSOLUTE DIPOLE OSCILLATOR STRENGTHS FOR THE VALENCE SHELL
PHOTOABSORPTION AND PHOTOIONIZATION OF H_2S AND HI

C.E. Brion, Y. Iida and G.K. James

Department of Chemistry, The University of British Columbia
Vancouver, B.C. V6T 1Y6, Canada

Dipole ($e,2e$) and dipole ($e+\text{ion}$) spectroscopies¹⁻³ are used to measure the absolute dipole oscillator strengths (cross-sections) for the photoabsorption and partial photoionization (electronic states) as well as the molecular and dissociative photoionization of H_2S and HI . These studies are part of a continuing programme of systematic measurements of absolute oscillator strengths for photoionization processes in total and partial channels. The fast electron (3 or 8 keV) impact spectra are converted to absolute dipole oscillator strengths via the Bethe-Born transformation and TRK sum rule normalization¹⁻². Some typical results⁴ are shown for H_2S in the accompanying figures. The results of the two experiments may be combined to provide quantitative assessments of the dipole breakdown pattern of these molecules. The H_2S partial oscillator strengths are compared with the calculations recently reported by Langhoff et al⁵.

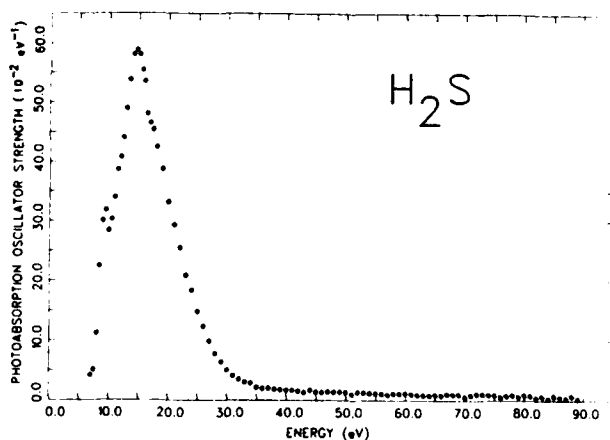


Figure 1 Photoabsorption of H_2S

This work received financial support from the Natural Sciences and Engineering Research Council of Canada and The Petroleum Research Fund administered by The American Chemical Society.

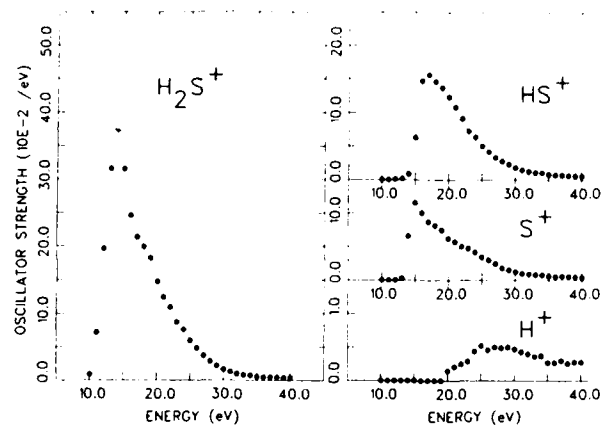


Figure 2 Oscillator Strengths for Molecular and Dissociative Photoionization of H_2S

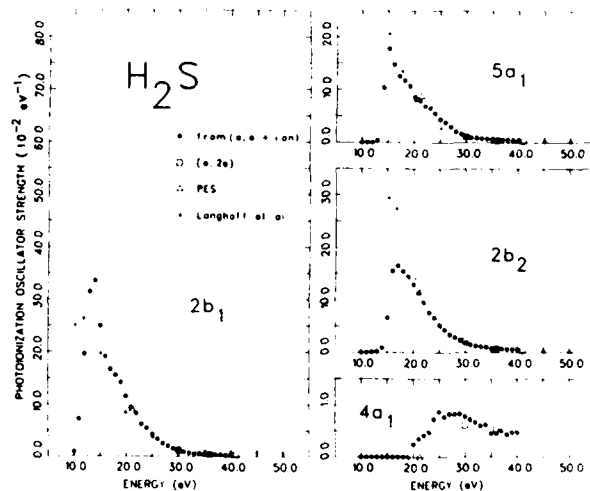


Figure 3 Electronic State Oscillator Strengths

References

1. C.E. Brion and A. Hamnett, *Adv. Chem. Phys.* **45** (1981) 1.
2. C.E. Brion in "Physics of Electronic and Atomic Collisions", Ed. S. Datz (North-Holland, 1982) pages 579-583.
3. F. Carnovale and C.E. Brion, *Chem. Phys.* **74** (1983) 253.
4. C.E. Brion, Y. Iida and J.P. Thomson, to be published.
5. P.W. Langhoff et al, to be published.

EXPERIMENTAL PHOTOIONIZATION CROSS SECTIONS AND ANGULAR DISTRIBUTIONS
FOR THE MOLECULAR ORBITALS OF H_2O IN THE 30-130 eV PHOTON ENERGY RANGE

M. S. Banna*, R. Malutzki[†] and V. Schmidt[†]

*Department of Chemistry, Vanderbilt University, Nashville, Tennessee 37235, U.S.A.

[†]Department of Physics, Freiburg University, Freiburg, West Germany

The study of photoionization in molecules using variable-energy radiation is of interest not only because the dynamical aspects of molecular photoionization can be characterized in great detail, but also because the make-up of each molecular orbital (i.e. the extent of s and p character, for example) can be correlated with the variation of the MO's partial photoelectric cross section with photon energy. Similarly, the angular distribution parameter β is also characteristic of the ionized orbital.¹

The application of these ideas has already yielded some useful information in connection with the assignment of bands in ultraviolet photoelectron spectra.² In developing this approach further it is important to determine β 's and σ 's for small molecules of well known orbital compositions since they are amenable to highly sophisticated calculations. This was the main motivation behind the present study of H_2O . It is for example of interest to compare the variation of σ 's and β 's for these molecules with that of the isoelectronic atom neon, which has been studied extensively with synchrotron radiation. Furthermore, the accurately-determined photoionization quantities (in the 30-130 eV photon energy range) should serve as crucial test cases for theory.

Light from the storage ring BESSY, monochromatized by a toroidal grating monochromator was used. A sample spectrum typical of spectra obtained with low energy photons is shown in Figure 1.

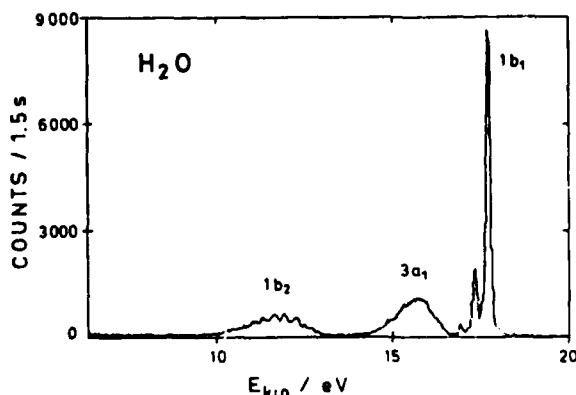


Fig. 1. The photoelectron spectrum of water with 30.3 eV photons at the quasimagic angle.

It was possible to clearly resolve vibrational bands, especially those of the first ($1b_1$) MO. At higher energies (up to ~130 eV), while the resolution was lower it was still possible to obtain an improvement over the spectrum reported a decade ago by Banna and Shirley,³ due to the absence of x-ray satellites associated with the $YM\zeta$ line in the latter spectrum. Asymmetry parameters and photoionization cross sections have been obtained for all four molecular orbitals. Thus our work is in part an extension of the work of Truesdale et al.⁴ Comparison is made with theory and with corresponding quantities for the other first-row hydrides.

The financial support of the Bundesminister für Forschung und Technologie, the Vanderbilt University Research Council and the National Science Foundation is gratefully acknowledged.

References

1. V. McKoy, T. A. Carlson and R. R. Lucchese, *J. Phys. Chem.* **88**, 3188 (1984).
2. M. N. Piancastelli, P. R. Keller, J. W. Taylor, F. A. Grimm and T. A. Carlson, *J. Am. Chem. Soc.* **105**, 4235 (1983).
3. M. S. Banna and D. A. Shirley, *J. Chem. Phys.* **63**, 4759 (1975).
4. C. M. Truesdale, S. Southworth, P. H. Kobrin, D. W. Lindle, G. Thornton and D. A. Shirley, *J. Chem. Phys.* **76**, 860 (1982).

R-MATRIX METHOD FOR MOLECULAR PHOTOIONISATION

C.J. Noble[†], J. Tennyson[†] and P.G. Burke^{*}[†]SERC Daresbury Laboratory, Warrington, England.^{*}Queen's University, Belfast, N. Ireland.

The multi-centre R-matrix method using numerically defined continuum orbitals which we have used successfully for both elastic scattering and electronic excitation for low-energy electron impact on diatomic targets^{1,2} has been extended to describe photoionisation processes. As a first application of these methods we present results for the cross sections and asymmetry parameters of the photoionisation of H_2 . We describe the $e^- + H_2^+$ system using a two-state model^{3,4}.

An important advantage of our R-matrix method is that the bound state wavefunction is calculated as a scattering problem with all channels closed. Exactly the same basis set is used for bound and scattering wavefunctions and the calculations may be matched in accuracy. We obtain a ground state energy for H_2 at its equilibrium separation of $-1.1696 E_h$ corresponding to about 90% of the correlation energy.

The most significant feature of the results we obtain is the appearance of resonances in the asymmetry parameter for photon energies around 27 eV. Examples of the results for the asymmetry parameter which we obtain at two internuclear separations are illustrated in figure 1. The structure, which we believe should be observable experimentally in vibrationally resolved spectra, is associated with the infinite series of Feshbach resonances converging towards the excited $2\Sigma_u^+$ electronic state.

We have computed vibrationally resolved observables using the adiabatic nuclei approximation and compare our results with other authors and experiment. In order to further study the autoionising region, where the adiabatic nuclei approximation is clearly invalid, given the narrow width of the Feshbach resonances, we have extended the approach of Schneider et al⁵ to describe the coupling to the nuclear motion and dissociative processes. Calculations using these extensions to the theory are now underway and those results available at the time of the Conference will be presented as will results for other systems such as CO and O_2 now under investigation.

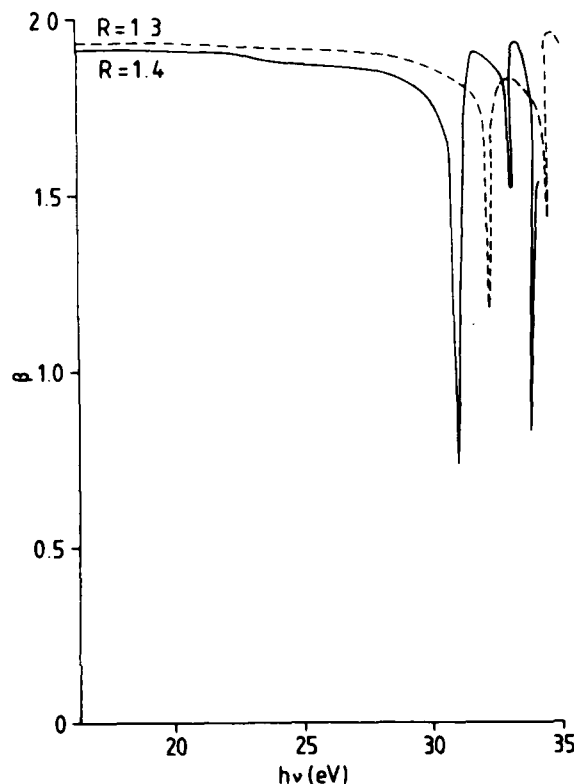


Fig.1: Asymmetry parameter β as a function of photon energy for two typical H_2 geometries.

References

1. P.G. Burke, C.J. Noble and S. Salvini, *J.Phys. B: At. Mol. Phys.* **16**, L113 (1983).
2. P.G. Burke, I. Mackey and I. Shimamura, *J.Phys. B: At. Mol. Phys.* **10**, 2497 (1977).
3. J. Tennyson, C.J. Noble and S. Salvini, *J.Phys. B: At. Mol. Phys.* **17**, 905 (1984).
4. J. Tennyson and C.J. Noble, *J.Phys. B: At. Mol. Phys.* **18**, 155 (1985).
5. B.I. Schneider, M. LeDourneuf and P.G. Burke, *J.Phys. B: At. Mol. Phys.* **12**, L365 (1979).

GENERALIZED MULTICHANNEL QUANTUM DEFECT TREATMENT OF $2\Pi-2\Pi$
RYDBERG-VALENCE STATE INTERACTIONS IN NO.

M. RAOULT

Laboratoire de Photophysique Moléculaire du CNRS*
Bâtiment 213 - Université de Paris-Sud, 91405 ORSAY CEDEX France.

The absorption spectrum of nitric oxide furnishes the classic example of Rydberg-valence state interactions in a diatomic molecule. These interactions appear as strong vibronic perturbations in the spectrum. Miescher and coworkers^{1,2,3} have described many of these perturbations and analyzed them in great detail. Based on these high-resolution spectroscopic studies Gallusser and Dressler⁴ have recently performed vibronic perturbation calculations which have yielded a quantitative representation of the experimental vibronic level positions, rotational structure and band intensities, in terms of "deperturbed" potential energy curves, dipole transition moments and Rydberg-valence state interaction energies.

The present work is an attempt to interpret the Rydberg-valence state interactions from a different point of view, namely that of scattering theory. This point of view has already been used by Giusti-Suzor and Jungen⁵ in a recent theoretical study of the competition between preionization and predissociation in the 2Π Rydberg states of NO above the ionization threshold. Their work was however limited to the continuum, i.e. to the region above the dissociation limit of the valence states. In the present work the treatment is extended into the discrete region, using the recent generalization of quantum defect theory due to Greene, Rau and Fano⁶. In addition the reactance matrix is now computed using Lippman-Schwinger equation to second order. This extension allows the study of all spectral ranges with a single unified treatment.

All of the parameters which are required to calculate the reactance matrix are determined by a least squares fitting procedure from the observed^{1,2,3,7,8} $2\Pi_{1/2}$ vibronic levels. The term values of all observed $2\Pi_{1/2}$ Rydberg and B and L valence vibronic levels lying between 45500 cm^{-1} up to the dissociation limit 71658 cm^{-1} are thus reproduced with a mean deviation of 5 cm^{-1} . Without any further adjustment of the reactance matrix the spectral range above the dissociation limit and below or above the first ionization threshold has been studied. In this range the Rydberg levels are subject to predissociation or predissociation as well as preionization. Correspondingly the spectral lines in the photoabsorption or photoionization spectra are broadened. Table I lists the observed and calculated (ref. 5 and present work) widths of some Rydberg levels. The present results are in better agreement with the recent multiphoton

ionization measurements of Anezaki et al.⁹ and the third harmonic generation measurements of Chupka et al.¹⁰ than the previous calculations⁵. The $5p\Pi$, $v=4$ level is an exception: the width calculated here is one order of magnitude larger than either that observed or that calculated in Ref. 5. This discrepancy is not yet understood.

TABLE I

Level	Energy (cm^{-1})		Width Γ (cm^{-1})	
	Obs.	Calc.	Obs.	Calc.
$6p\Pi$, $v=1$	73096.0 (c)	73100.5	~ 6 (c)	5.5 (15)
$9p\Pi$, $v=0$	73108.0 (c)	73113.0	very diffuse (c)	6.9 (5.5)
$5p\Pi$, $v=2$	73313.0 (c)	73320.5	8 (c)	2.0 (12)
$7p\Pi$, $v=1$	74268.0 (c)	74270.5	~ 2 (c)	9.0 (12)
$8p\Pi$, $v=1$	74987.9 (a)	74987.5	3.9 (a)	5.2 (7)
$6p\Pi$, $v=2$	75400.0 (c)	75406.6	very diffuse (c)	5.2 (2.9)
$9p\Pi$, $v=1$	75463.9 (a)	75460.2	3.0 (a)	2.1 (5.4)
$5p\Pi$, $v=3$	75620.0 (c)	75610.0	$10.0 < \Gamma < 30.0$ (c)	25.0 (27)
$10p\Pi$, $v=1$	75790.7 (a)	75786.5	2.7 (a)	2.4 (1.1)
$7p\Pi$, $v=2$	76600.0 (c)	76593.5	-	0.2 (2.1)
$8p\Pi$, $v=2$	77290.0 (c)	77295.0	$4.0 < \Gamma < 8.0$ (b)	3.4 (1.7)
$6p\Pi$, $v=2$	77690.0 (c)	77692.5	4.0 (b)	9.1 (12.7)
$9p\Pi$, $v=2$	77752.0 (c)	77769.4	$3.0 < \Gamma < 6.0$ (b)	5.0 (1.7)
$5p\Pi$, $v=4$	77850.0 (c)	77846.5	3.0 (b)	42.0 (1.5)
$10p\Pi$, $v=2$	78090.0 (c)	78096.6	-	2.4 (0.9)
$7p\Pi$, $v=3$	78850.0 (c)	78859.0	very diffuse (c)	4.0 (7)

(a) From Ref. 9, (b) from Ref. (10), (c) from Ref. 11. In parenthesis the theoretical values of Ref. 5.

References

1. A. Lagerqvist and E. Miescher, *Helv. Phys. Acta*, **31**, 221 (1958); *Can. J. Phys.* **44**, 1525 (1966)
2. K. Dressler and E. Miescher, *Astrophys. J.*, **141**, 1266 (1965)
3. K. Dressler and E. Miescher, *J. Chem. Phys.*, **75**, 4310 (1981)
4. R. Gallusser and K. Dressler, *J. Chem. Phys.*, **76**, 4311 (1982)
5. A. Giusti-Suzor and Ch. Jungen, *J. Chem. Phys.*, **80**, 986 (1984)
6. C.H. Greene, A.R.P. Rau and U. Fano, *Phys. Rev. A*, **26**, 2441 (1982); see also F.H. Mies, *J. Chem. Phys.*, **80**, 2514 (1984)
7. T. Ebata, N. Mikami and M. Ito, *J. Chem. Phys.*, **78**, 1132 (1982)
8. W.Y. Cheung, W.A. Chupka, S.D. Colson and D. Gauyacq (to be published).
9. Y. Anezaki, T. Ebata, N. Mikami and M. Ito, *Chem. Phys.*, **89**, 103 (1984)
10. W.A. Chupka (private communication)
11. E. Miescher and F. Alberti, *J. Chem. Phys. Ref. data*, **5**, 302 (1976).

* Laboratoire associé à l'Université de Paris-Sud.

SPIN-ORBIT AUTOIONIZATION AND COOPER MINIMUM IN THE HYDROGEN HALIDES

H. Lefebvre-Brion, A. Giusti-Suzor and G. Raseev

Laboratoire de Photophysique Moléculaire,
Bât. 213, Université de Paris-Sud, 91405 Orsay France

A theoretical study of the spin-orbit autoionization in molecules with 2Π -state ion cores has been made recently¹, using the multichannel quantum defect theory with ab-initio molecular quantities. Application to the study of the HI photoionization spectrum has stressed the importance of the ℓ -mixing, especially for the $\pi^3\sigma$ channels. A similar study is presented for the case of the HBr molecule. The vibrational interval being here nearly equal to the spin-orbit splitting, some autoionized peaks with $v^+ = 1$ can be identified in the experimental spectrum². Their appearance is explained by a vibrational type autoionization due to the variation of the spin-orbit coupling constant with the internuclear distance.

The region of the Cooper minimum is studied for the case of HI. The photoionization cross-section and the asymmetry parameter β are calculated between the first ionization threshold and 80 eV. An overall agreement is obtained with the corresponding measurements³, but no Cooper minimum is found in the total cross-section while β presents a minimum around 55 eV. Both experimental quantities go through a minimum near 45 eV. Work is in progress to include the electronic coupling with the continuum of the states corresponding to the 4d hole, probably responsible for the present disagreement with the experimental results. Theoretical predictions will be made in this energy region for the spin polarization parameters of the photoelectron.

Reference

1. H. Lefebvre-Brion, A. Giusti-Suzor and G. Raseev, J. Chem. Phys., in press.
2. P.M. Dehmer and W.A. Chupka, Argonne National Laboratory, 1978, Report ANL-78-65
3. T.A. Carlson, A. Fahlman, M.O. Krause, P.R. Keller, J.W. Taylor, T. Whitley and F.A. Grimm, J. Chem. Phys. **80**, 3521 (1984).

THEORETICAL VIBRATIONAL RESOLVED PARTIAL PHOTOIONIZATION CROSS SECTIONS OF CO.
THE AUTOIONIZATION REGION BETWEEN 16.9 AND 19.0 eV.

B. Leyh^(a,c) and G. Raseev^(a,b)

^aInstitut de Chimie, Université de Liège, Bât. 6, Sart-Tilman,
4000 Liège 1, Belgium

^bLaboratoire de Photophysique Moléculaire du CNRS, Bât. 213,
Université Paris-Sud, 91405 Orsay, France

^cAspirant du Fonds National Belge de la Recherche Scientifique.

We present a full ab-initio calculations of partial photoionization cross sections of CO including the electronic autoionization. We have focused ourselves on the region of the Rydberg states converging to $\text{CO}^+ \text{B}^2\Sigma^+$ state and perturbed by the high Rydberg converging to the $\text{A}^2\Pi$ state.

These calculations have been performed in the framework of the Two-Step Multichannel Quantum Defect Theory (MQDT) of Giusti-Suzor and Lefebvre-Brion¹. In this theory we use the concept of channel defined by a selection of quantum numbers and covering a broad energy range (negative or positive) instead of states which in the discrete region are associated with a fixed energy. The first step consists in solving the Schrödinger's equation for the electronic motion in the frozen ionic core static exchange approximation using the method of Raseev et al.². In the second step, the interchannel interactions (involving the main channels corresponding to the X, A and B ionic states) are calculated. The nuclear motion is taken into account within the Franck-Condon approximation. The resulting ab-initio quantities are introduced in a MQDT calculation. The resonance structure appears as a consequence of different asymptotic conditions enforced for open and closed channels. This treatment leads to vibrationally resolved partial and differential cross sections.

The main results can be summarized as follows :

(i) the comparison of experimental and theoretical quantum defects, intensities and widths leads to new assignments of the Rydberg series associated with the $\text{CO}^+ \text{B}^2\Sigma^+$ state : sharp ("p" π), diffuse ("p" σ), III ("s-d" / "d" π) and IV ("s+d" σ). These assignments were, in fact, a point of controversy in the literature³.

(ii) the region between 17.0 and 17.4 eV has been analyzed in greater detail. The $\text{B}^2\Sigma^+$ (3p π) and $\text{B}^2\Sigma^+$ (3p σ) structures appear as complex resonance⁴ owing to the presence of high n Rydberg states converging to $\text{CO}^+ \text{A}^2\Pi$ v=4

(iii) the vibrationally resolved partial photoionization cross sections of $\text{X}^2\Sigma^+$ v=0-3 are compared with the experimental results of Leyl et al.⁵. The vibrational selectivity is analysed and helps clarifying the different assignments.

References

1. A. Giusti-Suzor and H. Lefebvre-Brion, Chem. Phys. Lett. **76**, 132 (1980).
2. G. Raseev, H. Le Rouzo and H. Lefebvre-Brion, J. Chem. Phys. **72**, 5701 (1980).
3. E. Lindholm, Arkiv för Fysik **40**, 103 (1969).
M. Ogawa and J. Ogawa, J. Mol. Spectr. **41**, 393 (1972).
J.H. Fock, P. Gürtler and E.E. Koch, Chem. Phys. **47**, 87 (1980).
T. Betts and McKoy, J. Chem. Phys. **54**, 113 (1971).
4. A. Giusti-Suzor and H. Lefebvre-Brion, Phys. Rev. A **30**, 3057 (1984).
5. B. Leyh, M.J. Hubin-Franskin, J. Delviche, I. Nenner and P. Roy, to be published.

PHOTOIONIZATION OF C_2 N. T. Padial,* B. I. Schneider,[†] and L. A. Collins[†]

*University of New Mexico, Albuquerque, New Mexico 87131 USA

[†]Los Alamos National Laboratory, Los Alamos, New Mexico 18754 USA

The carbon molecule C_2 is found in a variety of astrophysical environments including comets and circumstellar clouds. Photoionization of C_2 is an important mechanism in determining the physical properties of these objects. We report photoionization cross sections C_2 out of the $X'^1\Sigma_g$ ground state from the $2\sigma_u$, $2\sigma_g$, and $1\pi_u$ orbitals. The calculations were performed at the frozen-core Hartree-Fock level using standard molecular structure programs to generate the bound state functions and our linear algebraic code¹ to construct the continuum orbitals. We shall also discuss photoionization of the low-lying triplet state as well as other molecules of astrophysical interest.

Reference

1. B. I. Schneider and L. A. Collins, Phys. Rev. A 24, 1264 (1981); ibid., 29, 1695 (1984).

MOLECULAR PHOTOIONIZATION CROSS SECTIONS BY THE COMPLEX BASIS FUNCTION METHOD

C. W. McCurdy, C-H Yu, and R. M. Pitzer

Department of Chemistry, Ohio State University, Columbus, Ohio 43210

The photoionization cross section can be expressed as a particular matrix element of the resolvent of the molecular electronic Hamiltonian.

$$\sigma(\omega) = -\frac{4\pi\omega}{c} \lim_{\epsilon \rightarrow 0} \text{Im} \langle \Psi_0 | \mu (E_0 + \omega - H + i\epsilon)^{-1} \mu | \Psi_0 \rangle$$

Where Ψ_0 is the ground state electronic wave function, μ is the dipole operator, ω is the frequency, c is the speed of light, and atomic units are employed. We have shown recently that by using a mixture of real and complex Gaussian basis functions to form a matrix representation of the Hamiltonian it is possible to use this expression to compute molecular photoionization cross sections from the results of a matrix diagonalization.¹ The working expression of this approach has the form

$$\lim (f, (E - H + i\epsilon)^{-1} f) = \sum_{i=1}^N \frac{(f, \phi_i)(\phi_i, f)}{E - E_i}$$

where $f = \mu \Psi_0$, and the functions, ϕ_i , and associated eigenvalues, E_i , are from a finite basis diagonalization of the Hamiltonian. This procedure is based on a variational principle for the matrix element from which the photoionization cross section is calculated, and can be applied in the presence of coupling between ionization channels. The interference between resonance features and the electron-ion scattering background is naturally incorporated by this method, and it is easily implemented for polyatomic systems. Results are reported for K-shell and valence shell ionization of N_2 at the static-exchange level. Excellent agreement with most other calculations is obtained, especially those which explicitly compute the photoionization cross section from the electron-ion scattering wavefunction. The complex basis function technique is particularly successful in reproducing resonance features in these cross sections, as shown below.

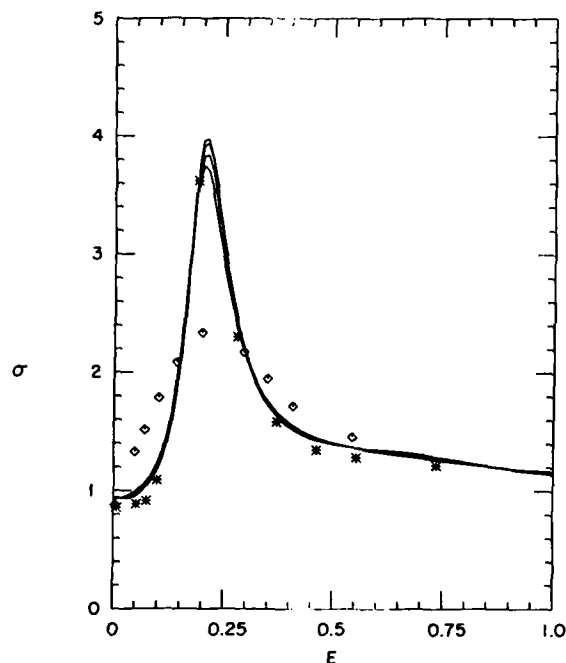


Figure 1. Total cross section for K-shell photoionization of N_2 . Solid lines are results of present calculations in several basis sets. * is Schwinger variational result and \diamond is from moment theory, both quoted from reference 2

A discussion of the variational behavior of the amplitude is given, and it is shown that the variational nature of these calculations provides a useful computational diagnostic.

Reference

1. T. N. Rescigno and C. W. McCurdy, Phys. Rev. A 31, 624 (1985).
2. D. L. Lynch and V. McKoy, Phys. Rev. A 30, 1561 (1984).

THEORETICAL STUDY OF ANGULAR DISTRIBUTION OF PHOTOELECTRONS IN H_2 MOLECULEG. Raseev^(1,2) and M. Raoult⁽¹⁾⁽¹⁾Laboratoire de Photophysique Moléculaire, Université Paris-Sud
91405 Orsay, France⁽²⁾Département de Chimie, Université de Liège, B-4000 Sart-Tilman
Liège 1, Belgique.

The photoionization of H_2 has been extensively studied experimentally and theoretically. One of the interesting regions is near 27 eV where an electronic autoionization is expected. Traces of this resonance have been seen only by Marr et al.¹ and Southworth et al.² where vibrationally unresolved angular distribution of electrons have been measured. Recent theoretical calculations by one of us Raseev^{3,4} yielded the quantum defects, photoionization cross section and angular distribution of electrons of this region. However for the $e + H_2^+$ collision the variation of the quantum defect in the autoionization region has been also obtained by Takagi and Nakamura⁵, Collins and Schneider⁶ and Tennyson and Noble⁷.

Three resonances are calculated near 27 eV corresponding, respectively, to quasi-bound states of $2p\sigma_u 2s\sigma_g$, $2p\sigma_u 3s\sigma_g$ and $2p\sigma_u 3d\pi_g$ main configuration. The first two are preionized by the $1s\sigma_g \epsilon p\sigma_u$ continuum whereas the last one autoionize in the $1s\sigma_g \epsilon p\pi_u$ continuum. Therefore enhancements have to be seen in the angular distribution of electrons or in the photoionization cross section.

Here we present the vibrationally resolved angular distribution of electrons in the spectral range of autoionizing resonances using an ab-initio method where the correlation between the motion of electrons is introduced in the initial and final states⁴. For the fixed R centroid internuclear distance $R = 1.7$ a.u. the $2p\sigma_u 2s\sigma_g$ resonance appears around 26 eV giving rise to a sharp energy variation of the angular distribution. This is in disagreement with experimental vibrationally unresolved measurements^{1,2} which present a different behaviour. As in the case of shape resonance, the vibrational motion of the nuclei averages the resonant electronic effects which in the case of H_2 depend strongly on the internuclear distance. When accounting for the nuclear motion, we obtain the angular distribution for each vibrational state of the ion. There are no experimental results to compare with these theoretical results. The vibrationally unresolved result, obtained by simple summation over the vibrational levels, presents as experiment¹ a minimum around 27 eV.

The theoretical minimum is less pronounced than the experimental one.

Reference

1. G.V. Marr, R.M. Holmes and K. Codling, J. Phys. B13, 283 (1980)
2. S. Southworth, W.D. Brewer, C.M. Truesdale, P.H. Kobrin, D.W. Lindle and D.A. Shirley, J. Electron. Spectr. 26, 43 (1982).
3. H. Le Rouzo and G. Raseev, Phys. Rev. A29, 1214 (1984).
4. G. Raseev, J. Phys. B, 18, 423 (1985)
5. H. Takagi and H. Nakamura, Phys. Rev. A27, 691 (1983).
6. L.A. Collins and B.I. Schneider, Phys. Rev. A27, 101 (1983).
7. J. Tennyson and C.J. Noble, J. Phys. B, 18, 155 (1985).

THE ROTATIONALLY AND VIBRATIONALLY RESOLVED
 PHOTOIONIZATION OF H_2 BY 736A LINE

S. Hara

Institute of Physics, University of Tsukuba, Ibaraki 305, Japan.

Intensity distribution of the photoelectron for the rotationally and vibrationally resolved molecular photoionization process is given by

$$I_{J''J'}(\theta) = \sigma_{J''J'}/4\pi [1 + \beta_{J''J'} P_2(\cos\theta)]$$

where $\sigma_{J''J'}$, and $\beta_{J''J'}$, are the cross section and the asymmetry parameter for the transition from the ($v'' = 0, J''$) state to the (v', J') state.

The vibrationally resolved cross section $\sigma_{v'}$, and the asymmetry parameter $\beta_{v'}$, are reduced to¹

$$\sigma_{v'} = \sum_j \sigma_{0j}$$

$$\beta_{v'} = [2.0 + \sum_{j \neq 0} \beta_{0j} \frac{\sigma_{0j}}{\sigma_{00}}] / [1.0 + \sum_{j \neq 0} \frac{\sigma_{0j}}{\sigma_{00}}]$$

The measurement of the ratio

$$R_j(\theta) = I_{0j}(\theta) / I_{00}(\theta) = (\sigma_{0j}/\sigma_{00}) \times$$

$$[1 + \beta_{0j} P_2(\cos\theta)] / [1 + 2.0 P_2(\cos\theta)]$$

at $\theta = 54.7^\circ$ determines σ_{0j}/σ_{00} . Therefore, an independent measurement of $R_j(\theta)$ at another angle gives β_{0j} and thus $\beta_{v'}$. The ratios σ_{0j}/σ_{00} are obtained for N_2 for $j = 2$ and 4 by the deconvolution technique².

When the cross sections for $\Delta J = J' - J'' \geq 4$ are negligible, σ_{02}/σ_{00} and β_{02} are the two essential parameters for $\beta_{v'}$. It was shown that for the photoionization of H_2 , the cross sections for $\Delta J \geq 4$ are small³, and that the measurements of the intensity ratio of the S and Q rotational branches at two angles^{3,4} determine these two parameters and $\beta_{v'}$ ¹.

We have calculated the cross sections σ_{00} , σ_{02} and β_{02} for v' from 0 to 5 for the photoionization of H_2 by 584A° line¹. Calculation for the final $H_2^+ + e$ state is carried out, in the two centre spheroidal coordinates, in the static exchange approximation with the adiabatic polarization potential added. Agreement between the calculated results with the values deduced from the experimental data^{3,4} is very satisfactory.

Here we present the results for the photoionization of H_2 by 736A° line⁵. Table 1 gives the present calculation with the p wave and with the p and f waves of the ejected photoelectron. The results derived from

experimental data^{3,4}, other theoretical^{6,7} and experimental^{8,9} results are also tabulated.

The present results and those of Raoult et al.⁷ agree with the experiments^{3,4} in σ_{02}/σ_{00} . The present results with the p and f waves give large values of β_{02} because of the interference of the p and f waves, and are in good agreement with the experimental results of Ruf et al.³. The vibrationally resolved asymmetry parameters $\beta_{v'}$, do not depend very much on β_{02} since the ratios σ_{02}/σ_{00} are rather small in the present process.

Table 1. Cross sections and asymmetry parameters.

v'		σ_{02}/σ_{00}	β_{02}	$\beta_{v'}$
0	(a)	0.0856	0.2	1.858
	(b)	0.0850	0.2	1.859
	(c)	0.0872	0.643	1.891
	(d)	0.093(2)	0.62(11)	1.882(9)
	(e)	0.091(3)	0.09(13)	1.841(12)
	(f)			1.67 (6)
	(g)	0.2118	0.348	1.711
1	(a)	0.0705	0.2	1.881
	(b)	0.0673	0.2	1.887
	(c)	0.0688	0.598	1.910
	(d)	0.076(1)	0.52(9)	1.896(3)
	(g)	0.1669	0.330	1.761
	(h)		0.83(48)	1.93 (3)

(a); ref (7), p wave. (b); present, p wave.
 (c); present, p and f waves. (d); ref (3).
 (e); ref (4). (f); ref (9).
 (g); ref (6), p and f waves. (h); ref (3) and (8).

References

1. S. Hara and S. Ogata, J. Phys. B, **18**, L59 (1985).
2. Y. Morioka et al., J. Phys. B, **18**, accepted for publication.
3. M. W. Ruf et al., J. Phys. B, **16**, 1549 (1983).
4. J. E. Pollard et al., Chem. Phys. Lett., **88**, 434 (1980).
5. S. Hara, submitted for publication.
6. Y. Itikawa, Chem. Phys., **37**, 401 (1979).
7. M. Raoult et al., J. Chim. Phys., **77**, 599 (1980).
8. A. Niehaus and M. W. Ruf, Chem. Phys., Lett., **11**, 55 (1971).
9. E. D. Poliakov et al., Chem. Phys. Lett., **96**, 52 (1983).

PHOTOIONIZATION OF H_2 : A FIRST PRINCIPLE STUDY

N Chandra*

Department of Physics, Punjabi University, Patiala 147002, India

Photoionization of H_2 has been studied¹ in detail. Angular distribution of photoelectrons for rotationally resolved states of H_2^+ has been calculated from ab-initio methods. The present calculation takes properly into account the important Coulomb phase factors which are contained¹ in the expression for molecular photoelectrons but had been neglected in an earlier report². These new results¹ which will be presented at the Conference, clearly establish the importance of including partial waves higher than $l = 1$ in the continuum orbital of even low-energy photoelectrons and thus a long standing controversy has been resolved^{3,4}. It has also been found¹ that the neglect⁴ of exchange and polarization in the final state wave function gives rise to unphysical behaviour of photoionization observables. Further, the results obtained in dipole-length length approximation are consistently better than those of velocity approximation. Also, the simple wave function of Huzinaga⁵ for the ground¹ Σ_g^+ electronic state of H_2 gives more satisfactory results than the other two more sophisticated wave functions⁵, while the final state wave function, obtained from polarized orbital method⁶, is kept the same. A sample of our new results¹ for β_Q , β_S , and the intensity ratio I_S/I_Q at 90° for 1.10 eV photoelectrons corresponding to Ne(λ 736Å) photons, convoluted, using the method of Chang³, over the experimental set up of Niehaus and Ruf³, is given in the Table I.

TABLE I

Initial State wf	Length/velocity	Final State wf	β_Q	β_S	I_S/I_Q % $\theta = 90^\circ$
Huzinaga ⁵	length	p wave	1.9678	0.2000	2.6023
		p-f coupled	1.9680	0.4954	3.2991
	velocity	p wave	1.9712	0.2000	2.3278
		p-f coupled	1.9686	0.3470	2.8551
Joy and Parr ²	length	p wave	1.9729	0.2000	2.1824
		p-f coupled	1.9716	0.4075	2.7143
	velocity	p wave	1.9726	0.2000	2.2065
		p-f coupled	1.9690	0.2746	2.6604
Hagstrom and Shull ⁵	length	p wave	1.9728	0.2000	2.1885
		p-f coupled	1.9636	-0.0338	2.4552
	velocity	p wave	1.9729	0.2000	2.1848
		p-f coupled	1.9658	0.0712	2.5016
Dill ³ , p wave			1.89(05)	0.2000	10.0
Chang ³ , p wave			1.95(01)	0.45(87)	4.1(6)
Itikawa ⁴ , p wave			1.8990	0.2047	8.2729
Itikawa ⁴ , p-f coupled			1.9045	0.3297	8.7026
Raoult et al ³ , p wave			1.954	0.2000	3.5
Niehaus and Ruf ³			1.95(01)	0.83(48) [†]	4.0(3) [†]
Ruf et al ³			1.922 [*]	0.47(14)	3.89(8)

† Reanalysed by Ruf et al³.* Theoretical value used by Ruf et al³ in their calculation of β_S .

References

- * Present address: Department of Applied Mathematics & Theoretical Physics, The Queen's University, Belfast, UK.
1. N Chandra, to be published
 2. N Chandra, Proc. 10th Int. Conf. Phys. Elect. At. Collisions. (Paris: Commissariat a l'Energie Atomique) Abs. 1210(1977)
 3. D Dill, Phys. Rev. A **6** 160(1972); E S Chang, J. Phys. B. **11** L69(1978); M Raoult et al, J. Chem. Phys. **77** 599(1980); B Ritchie, Chem. Phys. Lett. **92** 667(1982); A Niehaus and M W Ruf et al J. Phys. B. **16** 1549(1983)
 4. Y Itikawa, Chem. Phys. **37** 401(1979)
 5. S Huzinaga, Progr. Theor. Phys. **17** 162(1957); H W Joy and R G Parr, J. Chem. Phys. **28** 448(1958); S Hagstrom and H Shull, ibid **30** 1314(1959)
 6. A Temkin and K V Vasuada, Phys. Rev. **160** 109(1967); A Temkin et al, ibid **180** 57(1969)

MODIFIED PHOTODETACHMENT THRESHOLD BEHAVIOR NEAR RESONANCES

Y. K. Bae and J. R. Peterson

Molecular Physics Department, SRI International, Menlo Park, CA 94025 USA

Rapid deviations from the Wigner threshold law have been observed when resonant states are near.^{1,2} Stimulated by our observation of these effects in He⁻ and Li⁻ photodetachment^{3,4} we have now derived modified threshold laws that account for single resonances of all three types: Feshbach, shape, and virtual state.

The effects of shape and Feshbach resonances were analyzed for single opening channels. If long-range interactions in the product complex are negligible, the cross section of an opening channel near its threshold may be written as

$$\sigma_l \sim k^{2l+1} / |f_l(k)|^2 \quad (1)$$

where k , l , and $f_l(k)$ are the linear and angular momentum, and the Jost function for the outgoing electron, respectively. If no resonance is near, $f_l(k)$ is nearly constant and Eq. (1) assumes the Wigner form of the numerator. However, if a resonance is near, $f_l(k)$ depends strongly on k . Using a Taylor expansion of $f_l(k)$ near $k = 0$ we transform Eq. (1) into

$$\sigma_l \sim \frac{k^{2l+1}}{(k^2 - k_j^2)^2 + \gamma k^{4l+2}} \quad (2)$$

for $l = 0$ and l cases, where k_j and γ are related to the position and width of the resonance.

Shape resonance. Our He⁻ data near the He 2³P threshold³ deviated from the k^3 Wigner law within 4 meV. However, Eq. (2) fits not only the threshold region near the presence of the 4p^e shape resonance (Fig. 1), but it fits the entire resonance as well.

Feshbach resonance. Partial cross sections for the opening np 2P + ϵs channel in Rb⁻ photodetachment by Frey et al.,¹ and in Cs⁻ by Mead et al.,² deviated from the Wigner law within the experimental resolution ~ 30 μ eV due to Feshbach resonances below the thresholds. Fig. 2 shows that their data can be fit accurately by Eq. (2) with $l = 0$.

Virtual state. Li⁻ does not have a Feshbach resonance below the 2p 2P + ϵs threshold, but Moores and Norcross⁵ found that their *ab initio* calculations of Li⁻ photodetachment cross sections deviated from the Wigner "cusp" behavior within 30 μ eV. We found similar behavior in our measurements.⁴ Using the multichannel scattering theory of by Nesbet,⁶ we have derived the modified cusp formulae for total photodetachment cross sections to include virtual state effects:

$$\sigma \sim \sigma_0 [1 - A\kappa/(\kappa + \beta)] \quad (3a)$$

below threshold, and

$$\sigma \sim \sigma_0 [1 - B\kappa/(k^2 + \beta^2)] \quad (3b)$$

above threshold. A and B are constants, $\beta^2/2$ locates the energy of the virtual state, and $\kappa = ik$. The fit of Eqs. (3) to our Li⁻ data is shown in Fig 3.

This work was supported by AFOSR Contract F49620-82-K-0030 and NSF Grants PHY81-11912 and 84-10980.

References

1. P. Frey, M. Lawen, F. Breyer, H. Klar, and H. Hotop, Z. Phys. A **304**, 155 (1982).
2. R. D. Mead, P. A. Schultz, W. C. Lineberger, unpublished.
3. J. R. Peterson, Y. K. Bae and D. L. Huestis, submitted to Phys. Rev. Lett. (1985).
4. Y. K. Bae and J. R. Peterson, submitted to Phys. Rev. Lett. (1985).
5. D. L. Moores and D. W. Norcross, Phys. Rev. A **10**, 1646.
6. R. K. Nesbet, J. Phys. B **13**, L193 (1980).

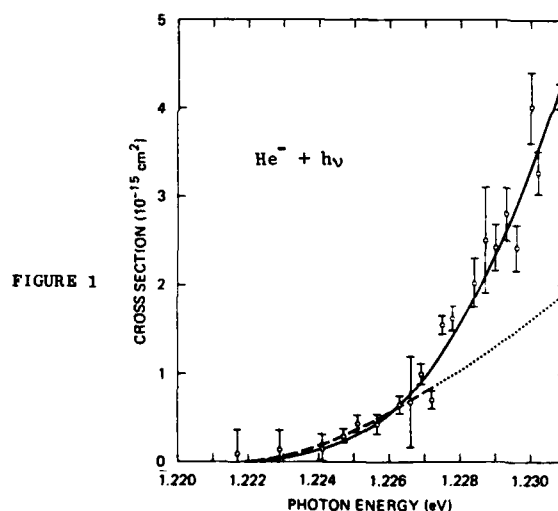


FIGURE 1

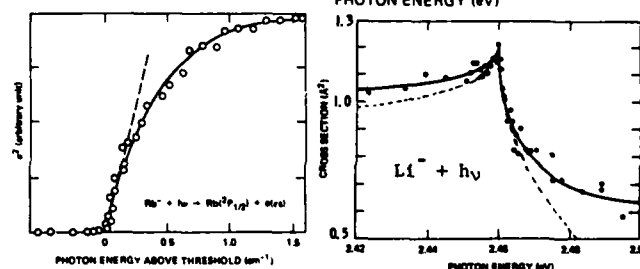


FIGURE 2

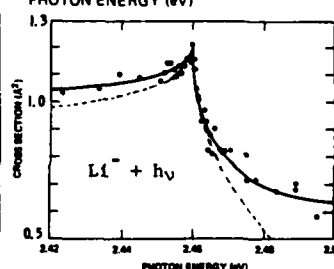


FIGURE 3

FIGURES: Dashed lines: Wigner threshold law.
Solid lines: Modified threshold form.

DETAILS OF THE $\text{He}^- 4p^e$ SHAPE RESONANCE AND THE $\text{He} 2^3\text{S}$ ELECTRON AFFINITY

J. R. Peterson, Y. K. Bae, M. J. Coggiola, and D. L. Huestis

Molecular Physics Department, SRI International, Menlo Park, CA USA

New measurements of the $(1s2p\ 2p^2\ 4p^e)\ \text{He}^-$ photo-detachment shape resonance, with a coaxial laser-ions beam arrangement and improved dye laser operation, have greatly reduced the uncertainties in the earlier data¹ and have reached the difficult long wavelengths near 1020 nm, below the $\text{He}(2^3\text{P}) + e(\epsilon p)$ channel threshold. They provide unusual detail regarding the form of an electronic shape resonance.

An analysis of the threshold region has led to a new parametric formulation of threshold behavior for opening channels that bear p-wave shape resonances. Two approximate threshold forms were actually derived and we found that they both can be used quite successfully to fit not only the threshold region but the resonance as well, yielding resonance parameters. One version, derived from resonance scattering theory is

$$\sigma \sim \frac{k^3}{(k^2 - k_1^2)^2 + \gamma k^6} \quad (1)$$

where k and l are the linear and angular momenta of the outgoing electron, and k_1 , and γ are constants. For small k , Eq. 1 can be transformed into

$$\sigma \sim \frac{k^3}{(k^2 - k_R^2)^2 + (\Gamma)^2} \quad (2)$$

where, $k_R^2/2$ and $\Gamma/2$ are give the real and imaginary parts of the resonance (S-matrix pole) in the complex energy plane. Eq. (2) is a product of the Wigner threshold law and the Breit - Wigner resonance formula.

Connerade³ has obtained successful fits to $l = 3$ photoionization shape resonances from the scattering phase shifts of a square-well potential.

Experimentally, He^- ions were formed from a 2-keV He^+ beam by two-step electron capture in Cs vapor. The +, 0, and - charge components were separated by an electrostatic quadrupole deflector Q1. The He^- ions were then merged with the laser beam over a 10 cm field-free interaction region before the He^- beam was deflected into a collector by a second quadrupole Q2. The neutrals formed along the interaction region from either auto- or photo-detachment passed Q2 undeflected and were counted. The laser optics and the dye (IR 140) was the same as before,¹ but the dye performance was improved by doubling the concentration of dimethylsulfoxide solvent.

The fitted curves from Eqs. (1) and (2) were visually the same over the threshold region and central

peak. The fit from Eq. 1 is shown in Figure 1. The resonance parameters in both equations were first established by fitting all data within 170 meV of threshold E_0 . Eq. (1) gave $E_0 + k_1^2/2 = 1234.3$ meV, and Eq. (2) gave $E_0 + k_R^2/2 = 1232.9$ meV and $\Gamma = 7.4$ meV, where E_0 is the threshold energy. These values of $E_0 + k_1^2/2$ and $E_0 + k_R^2/2$ are close to, but lie on either side of the apparent peak value 1233.6 meV. Next, these parameters were held fixed, to find E_0 using only data within 10 meV of E_0 . These threshold fits gave:

$E_0 = 1222.0 \pm 0.8$ and 1222.1 ± 1.0 meV, yielding $\text{EA}(\text{He}2^3\text{S}) 77.5 \pm 0.8$ meV from Eq. (1), and 77.6 ± 1.0 meV from Eq. (2). These results are in excellent agreement with the theoretical result of 77.51 ± 0.04 meV by Bunge and Bunge.³

This work was supported by AFOSR Contract F149620-82-K-0030 and NSF Grants PHY81-11912 and 84-10980.

References

1. J. R. Peterson, M. J. Coggiola, and Y. K. Bae, Phys. Rev. Lett. **50**, 664 (1983).
2. J. R. Peterson, Y. K. Bae, and D. L. Huestis, submitted to Phys. Rev. Lett. (1985).
3. J. P. Connerade, J. Phys. B, **17**, L165 (1984).
4. A. V. Bunge and C. F. Bunge, Phys. Rev. A **30**, 2179 (1984).

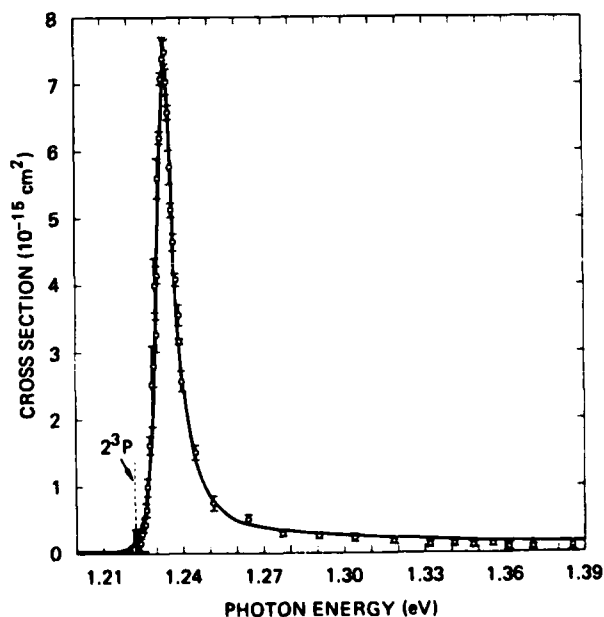


FIGURE 1: He^- photodetachment cross sections near the $\text{He}^- 4p^e$ shape resonance. Solid line is a least-squares fit to Eq. 1.

THE RESPONSE OF THE $1p^0$ DIP IN THE H^- CONTINUUM
NEAR $n=3$ TO LARGE ELECTRIC FIELDS

Stanley Cohen*, G. Comtet*, C.J. Harvey**,
K.B. Butterfield**, D.A. Clark**, J.B. Donahue**,
P.A.M. Gram**, D.W. MacArthur**, J.E. Stewart**,
W.W. Smith***, H.C. Bryant**

*Drexel University, Philadelphia, PA 19104 USA

*Universite Paris-Sud, 91400 Orsay, France

**The University of New Mexico, Albuquerque, NM 87131 USA

**Los Alamos National Laboratory, Los Alamos, NM 87545 USA

***The University of Connecticut, Storrs, CT 06268 USA

The resonances in the one-electron continuum of H^- are built on the excited states of H^0 . The $1p^0$ continuum of H^- has been studied extensively with good resolution using the method of photodetachment from a relativistic beam¹, taking advantage of the very large Doppler shifts available when the velocity of the ions approaches c . The Feshbach and shape resonances lying near $n=2$ have been studied thoroughly, not only in the field-free case but also in motional electric fields² as large as 1.3 MV/cm. Recently results on the effects on these resonances of fields up to 3 MV/cm have been acquired³. In this paper we present some preliminary results on a study of the behavior of the resonant structure near $n=3$ in large motional electric fields.

Since resonant amplitudes are coherent with the amplitude of the continuum in which they are embedded, the photodetachment cross section in the vicinity of a resonance can exhibit complicated structure due to cross terms. When the continuum amplitude is constant in the neighborhood of a Breit-Wigner resonance the cross section can be well-described by the Fano⁴ line shape, and even when these conditions may not exactly apply, the Fano form is still quite useful in parameterizing the data in a limited range. In particular, in an earlier survey of the structure near $n=3$, Fano forms were fit quite successfully to the large dip in the cross section, enabling the extraction of location and width of the dip and that of a smaller and marginally-observable recursion.

The results reported herein were taken with a set-up similar to that previously described⁵. The interaction region, of the pulsed 4th harmonic YAG beam with an 800 MeV H^- beam, was situated between two pulsed Helmholtz coils⁶. The repetition rate of the laser was 10 Hz whereas that of the pulsed magnet was 5 Hz so that on alternate laser flashes the interaction was field-free. The angle between the two beams could be varied in steps as small as 31 microradians. The products of the laser- H^- interaction, in particular the H^0 , were separated from the primary beam by a downstream magnet and directed into a scintillator.

Figures 1 and 2 show

some of our preliminary results. Fig. 1 shows the $n=3$ dip for the laser firings in which there was no applied field and Fig. 2 shows the alternate firings when a motional field of 0.78 MV/cm was present. At fields of 2.3 MV/cm the structure appears to be essentially absent. These data are currently under analysis and we hope to describe some results of fits at the time this paper is presented.

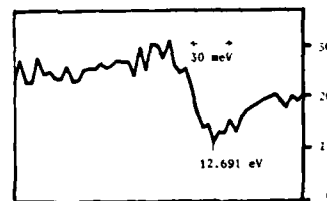


Figure 1. Region of $n = 3$ Dip under no field.

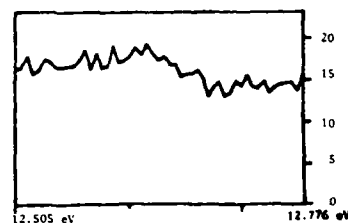


Figure 2. Same as Figure 1 with motional field of 0.78 MV/cm.

This work was done under the auspices of the U.S.D.O.E., in part under contract DE-AS0477ER03998.

References

1. H.C. Bryant, K.B. Butterfield, D.A. Clark, C.A. Frost, J.B. Donahue, P.A.M. Gram, M.E. Hamm, R.W. Hamm, W.W. Smith, *Atomic Physics 7*, D. Kleppner and F.M. Pipkin, eds. (Plenum Press, 1981) pp. 29-63.
2. H.C. Bryant, D.A. Clark, K.B. Butterfield, C.A. Frost, H. Sharifian, H. Tootoonchi, J.B. Donahue, P.A.M. Gram, M.E. Hamm, R.W. Hamm, J.C. Pratt, M.A. Yates, W.W. Smith, *Phys. Rev. A* **27**, 2889, (1983).
3. K.B. Butterfield, Ph.D. dissertation, the University of New Mexico, 1984. (Published as report LA-10149-T by Los Alamos National Laboratory.)
4. U. Fano, *Phys. Rev.* **124**, 1866 (1961).
5. W.W. Smith, C. Harvey, J.E. Stewart, H.C. Bryant, K.B. Butterfield, D.A. Clark, J.B. Donahue, P.A.M. Gram, D.W. MacArthur, G. Comtet, T. Bergeman, *Atomic Excitation and Recombination in External Fields*, eds. M.H. Nayfeh and C.W. Clark, Harwood Academic Publishers, NY, 1985.
6. G.J. Krausse and K.B. Butterfield, IEEE 16th Power Modulator Symposium, June 18-20, 1984 (Los Alamos preprint LA-UR-84-1921).

PHOTODETACHMENT SPECTROSCOPY OF FeO^-

T. Andersen, K. R. Lykke, D. M. Neumark and W. C. Lineberger

Joint Institute for Laboratory Astrophysics, University of Colorado and National Bureau of Standards,
and Department of Chemistry, University of Colorado Boulder, Colorado 80309 USA

Recent photodetachment spectroscopy studies of molecular anions as C_2^- ,¹ NH^- ,² and $\text{CH}_2\text{-CHO}^-$ ³ have shown that the rotation to electronic energy coupling plays an important role in the detachment mechanism for excited states in these systems. The autodetachment rate versus rotational energy dependence seems, however, to be markedly different for negative ion valence states^{1,2} and dipole-bound states.³ The autodetachment rate increases linearly in proportion to rotational energy for valence states, but much faster for dipole-bound states. Dipole-bound states originate from the interaction between the dipole moment of the neutral molecule and the electron and their properties are expected to be much like ordinary Rydberg states.

In order to gain more insight to the properties of dipole-bound states, diatomic systems should be studied. The system selected should have a dipole moment larger than 2 D in order to be able to support a dipole-bound state⁴ and a known electron affinity within the limits accessible for tunable lasers. The combination of these demands only leaves us with one system, the FeO^- molecule.

By means of the coaxial beam technique the excited states of FeO^- in the region 11,500–12,900 cm^{-1} above the $^4\Delta_{7/2}$ ground state have been studied. This energy region covers the five $^5\Delta_1$ spin-orbit states of the FeO ground state. Both valence and dipole-bound states are observed in this energy region.

Figure 1 illustrates the autodetachment rates versus energy for two band systems identified as a $^4\Lambda_{5/2}$ valence state (V) and a dipole-bound state (DP), respectively. The observed variations in the detachment rates are due to rotational autodetachment. The drastic increase in the detachment rate near the $^5\Delta_3$ FeO threshold indicates that this band system may be considered as a molecular complex consisting of a $\text{FeO}(^5\Delta_3)$ core and a loosely bound electron. Spectroscopy of this band system indicates that the outer electron is an s electron with a binding energy of nearly 200 cm^{-1} .

Since rotationally resolved lifetime data have been difficult to obtain for autoionization these data may also allow a better understanding of autoionization processes.

Research supported by National Science Foundation Grants CHE83-16682 and PHY82-00805 through the University of Colorado.

References

1. U. Hefter, R. D. Mead, P. A. Schulz and W. C. Lineberger, *Phys. Rev. A* **28**, 1429 (1983).
2. D. M. Neumark, K. R. Lykke, T. Andersen and W. C. Lineberger, in press.
3. K. R. Lykke, R. D. Mead and W. C. Lineberger, *Phys. Rev. Lett.* **52**, 2221 (1984).
4. W. R. Garrett, *J. Chem. Phys.* **73**, 5721 (1980) and *ibid.* **77**, 3666 (1982).

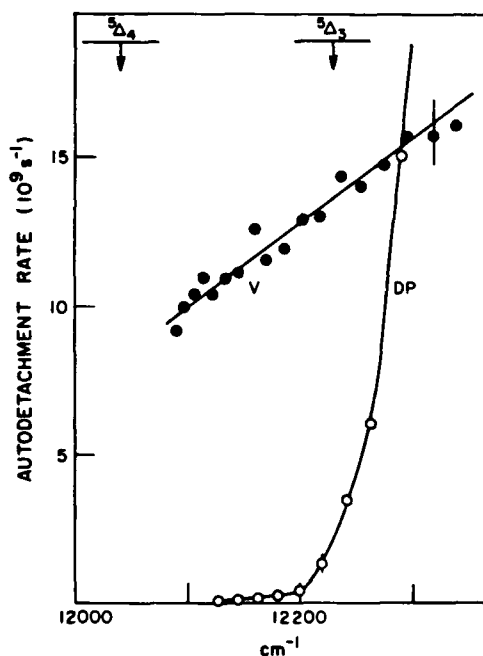


Fig. 1. Rotational dependence of the FeO^- autodetachment rates for a $^4\Lambda$ valence state (V) and a dipole-bound state (DP). The $\text{FeO}(^5\Delta_4)$ and $^5\Delta_3$ thresholds are indicated.

AD-A163 497

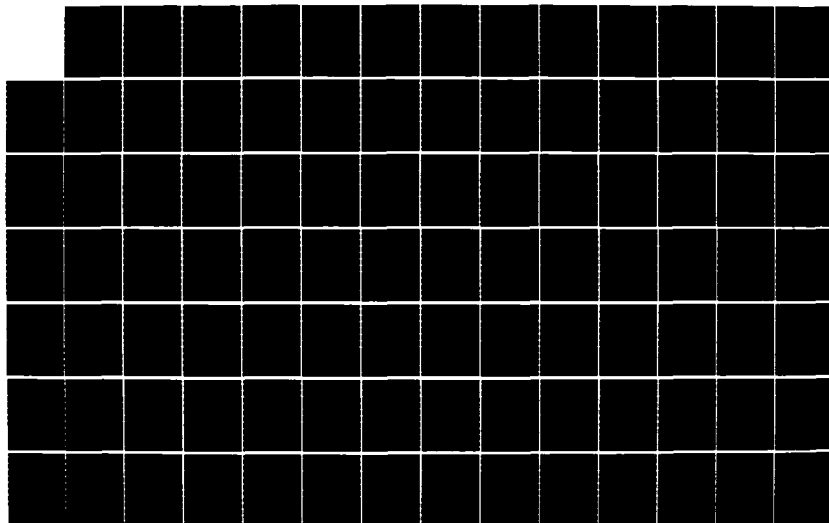
ELECTRONIC AND ATOMIC COLLISIONS ABSTRACTS OF
CONTRIBUTED PAPERS INTERNAT. (U) SRI INTERNATIONAL
MENLO PARK CA MOLECULAR PHYSICS CENTER
H J COGGIOLA ET AL. 1985

2/8

UNCLASSIFIED

FFG 7/4

NL





MICROCOPY RESOLUTION TEST CHART
NATIONAL BUREAU OF STANDARDS 1963-A

THE PHOTOELECTRON SPECTRUM OF NaBr^-

Thomas M. Miller, Kermit K. Murray, and W. Carl Lineberger

Department of Chemistry and Joint Institute for Laboratory Astrophysics
University of Colorado, Boulder, Colorado 80309 USA

There has long been interest in the interaction of an electron with a highly polar molecule. Calculations have shown that an electron can be bound in the field of a static dipole if the dipole moment is greater than the "critical" value of 1.625 D; a rotating dipole is less effective at binding an electron.¹ True dipole-bound states in negative ions have been observed recently in this laboratory² for FeO^- and $\text{H}_2\text{C-CHO}^-$. The effect of large dipole moments on electron scattering has been investigated in a number of ways.³ Narrow resonances have been observed in photodetachment experiments⁴ with the alkali-halide negative ions, including the NaBr^- ion we are dealing with here.

Among the alkali-halides, only for LiCl has the electron affinity been measured prior to this report, in an experiment utilizing an earlier incarnation of our apparatus.⁵ Calculations⁶ for NaCl^- , LiCl^- , and LiF^- show that the extra electron is placed mostly on the positive (alkali) side of the $\text{X}^1\Sigma^+$ neutral molecule in a space essentially unoccupied by other electrons. The ground state of the ion is $\text{X}^2\Sigma^+$. The non-bonding nature of the orbital leads to a negative ion in which the nuclei are more weakly bound than in the neutral molecule.

In this experiment a 2×10^{-13} A beam of NaBr^- was extracted from a flowing-afterglow ion source, mass analyzed, and crossed by the intracavity beam of an argon-ion laser operated at 488 nm (2.540 eV). An alumina crucible containing NaBr was heated in the flowing afterglow and electron attachment provided a small flow of NaBr^- while other processes produced copious amounts of Br^- . Photoelectrons were energy analyzed in a hemispherical device with a resolution of 10 meV. The energy scale was calibrated by photodetaching O^- .

The photoelectron spectrum for NaBr^- is shown in Fig. 1. The transition from $v''=0$ in the negative ion to $v'=0$ in the neutral occurs at an electron kinetic energy of 1.748 eV, which gives an electron affinity of 0.790 ± 0.015 eV for NaBr. One may compare this result to the measured⁵ $\text{EA}(\text{LiCl}) = 0.61 \pm 0.02$ eV, and the calculated⁶ $\text{EA}(\text{LiCl}) = 0.54$ eV, $\text{EA}(\text{LiF}) = 0.33$ eV, and $\text{EA}(\text{NaCl}) = 0.65$ eV, for other alkali-halide molecules.

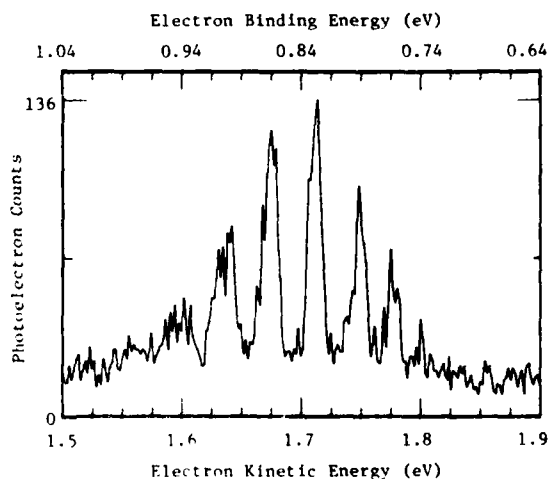
Transitions to $v'=1,2$ are at 1.711 and 1.674 eV, respectively, which gives $\omega_e^1 = 300 \text{ cm}^{-1}$ for NaBr, in agreement with infrared data.⁷ Transitions from $v''=1,2$ are at 1.776 and 1.799 eV, respectively, which gives $\omega_e'' = 250 \pm 50 \text{ cm}^{-1}$ and $\omega_e x_e''$ of approximately 10 cm^{-1} for NaBr^- . These transitions indicate a vibrational temper-

ature of 370 K. A Franck-Condon analysis of the transition strengths yields the NaBr^- equilibrium bond distance $r_e'' = 2.61 \pm 0.04 \text{ \AA}$, an increase of 0.11 \AA from NaBr. Using the bond strength⁷ $D_0(\text{Na-Br}) = 3.74$ eV, and our measured electron affinity for NaBr and the electron affinity of Br, we calculate a bond energy in the negative ion of $D_0(\text{Na-Br}^-) = 1.17$ eV. This value is far less than in the neutral molecule, consistent with the non-bonding character of the orbital of the attached electron.

We gratefully acknowledge support from the National Science Foundation under grant numbers CHE83-16628 and PHY82-00805.

References

1. W. R. Garrett, *J. Chem. Phys.* **77**, 3666 (1982).
2. K. R. Lykke, R. D. Mead, and W. C. Lineberger, *Phys. Rev. Lett.* **52**, 2221 (1984); R. D. Mead, K. R. Lykke, W. C. Lineberger, J. Marks, and J. I. Brauman, *J. Chem. Phys.* **81**, 4883 (1984); also, unpublished data for FeO^- .
3. See J. A. D. Stockdale, L. G. Christophorou, J. Turner, and V. E. Anderson, *Phys. Lett.* **25A**, 519 (1967); A. C. Allison, *J. Phys. B* **8**, 325 (1975); L. A. Collins and D. W. Norcross, *Phys. Rev. A* **18**, 467 (1978); and B. Jatusziwer, A. Tino, and B. Bederson, *Phys. Rev. A* **30**, 1269 (1984).
4. S. E. Novick, P. L. Jones, T. J. Mulloney, and W. C. Lineberger, *J. Chem. Phys.* **70**, 2210 (1979).
5. J. L. Carlsten, J. R. Peterson, and W. C. Lineberger, *Chem. Phys. Lett.* **37**, 5 (1976).
6. Y. Yoshioko and K. D. Jordan, *J. Chem. Phys.* **73**, 5899 (1980) and references therein.
7. K. P. Huber and G. Herzberg, *Constants of Diatomic Molecules* (Van Nostrand, New York, 1979).

FIGURE 1. Photoelectron Spectrum for NaBr^-

FIELD- AND PHOTODETACHMENT OF WATER CLUSTERS

H. Haberland, C. Ludewigt, H.-G. Schindler, and D.R. Worsnop

Fakultät für Physik der Univ. Freiburg, D-7800 Freiburg, Germany

Negatively charged water clusters have been produced by injecting low energy electrons into a rare gas seeded supersonic water expansion. All $(\text{H}_2\text{O})_n^-$ clusters, with the exception of $n=4$ could be produced. With heavy seeding intense beams of clusters of the type $(\text{H}_2\text{O})_n^- \text{Rg}_m$, Rg = Rare gas, could be obtained.

In a first attempt to measure the electron affinity of the clusters a field detachment experiment has been performed. The cluster ion beam traverses a high in-line electric field, before entering a quadrupole mass spectrometer. No detachment could be observed for field strengths below 55 kV/cm for $n>2$, although the intensity of the $n=3,5,8$, and 9 clusters can be orders of magnitude lower than that for $n=2$. It follows, that the often made correlation - higher intensity implies larger binding energy - cannot be made, at least not in this case.

Fig. 1 shows the measured detachment fields as a function of the number of added rare gas atoms. For $(\text{H}_2\text{O})_2^- \text{Ar}_m$, $m=0,1$, and 2 a detachment threshold of (31 ± 1) kV/cm is obtained. Adding more argon atoms this value increases and seems to saturate. Adding Kr or Xe atoms, the necessary field strengths increase so rapidly, that for large m values no field detachment could be observed.

Adding more and more rare gas atoms one obtains a negatively charged dimer in a rare gas matrix. In a polarisable medium with refractive index n the electric

field is reduced to E/n^2 . On the right of Fig. 1 the value of the electric field strength

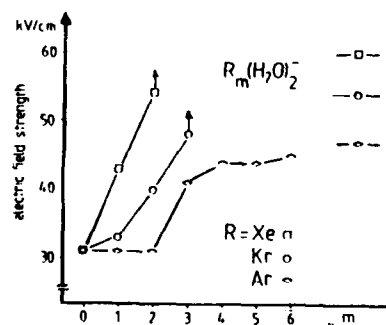


FIGURE 1 Field detachment thresholds for Ar, Kr, and Xe as a function of number of rare gas atoms per cluster.

in vacuum is sketched, which is necessary to give an electric field of 31 kV/cm in the rare gas solid. It is quite surprising that this value for argon is so close to the experimental data for $n=4$.

It is difficult to extract an accurate binding energy from the detachment field. To circumvent this problem the photodetachment apparatus shown in Fig. 2 was constructed. First results have been obtained and will be presented at the conference.

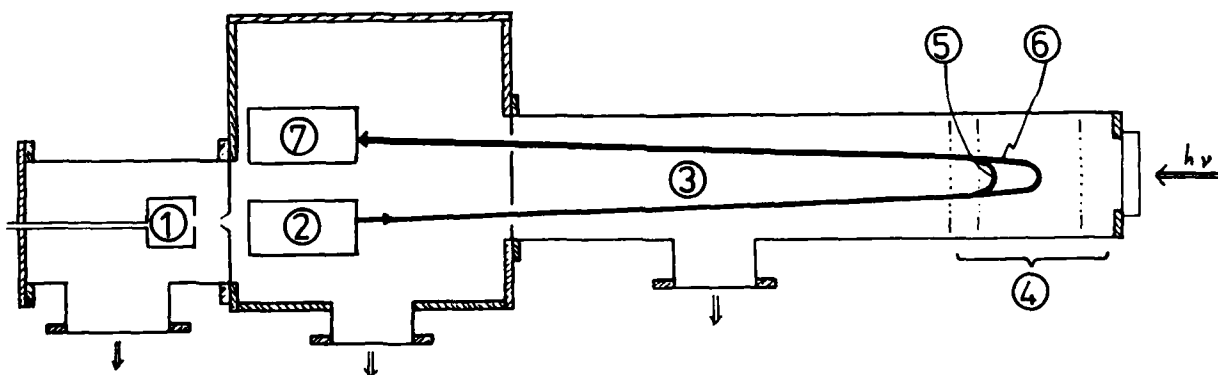


FIGURE 2 Cluster-Photo-Detachment-Apparatus. (1) Pulsed Cluster-Ion Source, (2) Ion Optics with pulse compressor, (3) reflex time of flight spectrometer, (4) time focusing reflector, (5) pass of slow ions, (6) pass of fast ions, (7) detector. The photons from a pulsed dye laser can interact on either of the two legs with the cluster ion beam.

ONE AND TWO-PHOTON DISSOCIATION OF Na_2 INVESTIGATED BY
DOPPLER SPECTROSCOPY OF PHOTOFRAGMENTS

G. Gerber, R. Möller

Fakultät für Physik, Universität Freiburg, F.R.G.

Na_2 molecules in a molecular beam are photodissociated by various Ar^+ laser lines. The state of the neutral fragments and the corresponding energy and angular distribution is determined by means of Doppler spectroscopy. Three different photodissociation processes are observed and identified: Direct photodissociation by excitation to the dissociation continuum of the $B^1\Pi_u$ state, dissociation of quasi-bound levels of the B state and two-photon induced dissociation of Na_2 leading to $\text{Na}(nl)$ fragments.

A molecular beam of Na_2 is crossed by two laser beams, all three being mutually perpendicular to each other. The first laser photodissociates Na_2 , while the second laser analyzes the fragmentation. With several Ar^+ laser lines, multi-mode and single-mode, Na_2 photodissociates into $\text{Na } 3s(J=1/2)$ and $\text{Na } 3p(J=3/2)$. By tuning a single frequency Rh6G dye laser over the $3p(J=3/2) \rightarrow 4d(J=5/2, 3/2)$ transition at 568.82 nm the velocity component of the atomic fragments relative to the analyzing laser is determined by the Doppler-shift $\Delta V = V_z \sqrt{c}$.

The excitation of the fragment is monitored by the emission of the $4p(J=1/2, 3/2) \rightarrow 3s(J=1/2)$ lines at 330 nm from the cascade $4d-4p-3s$. The polarization of the dissociating laser can be chosen arbitrarily to the direction z of the detection, e.g. parallel or perpendicular.

Trace A in Fig. 1 shows the unshifted excitation spectrum of the $3p(J=3/2) \rightarrow 4d(J=5/2, 3/2)$ transitions. Since the two fine structure components are only 1.02 GHz apart, two overlapping Doppler spectra are found. Trace B and C are Doppler spectra obtained for parallel and perpendicular polarizations. These spectra represent a fragmentation of a quasi-bound level by tunneling through the potential barrier. The quantum numbers of this quasi-bound state, excited by a single-mode laser at 457.9 nm, are determined by double-resonance spectroscopy and the width of the state is measured to $\Delta V \approx 100$ MHz. In this case we find only one value for the kinetic energy of the fragments, given by the energy W of the quasi-bound level referred to the dissociation limit. It can be shown (1) that the angular distribution can always be represented by $f(\vartheta) \sim 1 + \beta P_2(\cos \vartheta)$, where ϑ is the angle between the laser polarization and the fragment direction. The spectra represent the distribution of the z -component of the fragment velocity, which is given by

$$g(v_z) = 1 - 1/2 \beta + 3/2 \beta (v_z/v)^2 \text{ for } E_L \parallel z \quad \text{and} \\ g(v_z) = 1 + 1/4 \beta - 3/4 \beta (v_z/v)^2 \text{ for } E_L \perp z \quad \text{where}$$

v is the velocity of the fragment. The spectra in Fig. 1 are in good agreement with these distributions for the following parameters: $v = 475$ m/sec $\Rightarrow W = 430$ cm^{-1} and $\beta = -0.32$. The obtained value $W = 430$ cm^{-1} is close to $E = 398$ cm^{-1} , the energy of the quasi-bound level $v' = 31, J' = 42$ above the B-state dissociation limit.

For most Ar^+ laser lines continuous energy distributions are found due to direct dissociation by excitation to the continuum of the B-state.

Another interesting result of our molecular beam experiments is that we do not observe a population of the $\text{Na}^*(3p)$ $J=1/2$ fine structure level neither by direct dissociation via the $B^1\Pi_u$ continuum nor by tunneling through the B-state potential barrier when using the Ar^+ laser lines 489.0 nm and 476.5 nm, for instance.

These experimental results do not support the findings of Rothe et al. (2) and Janson et al. (3) who reported Na_2 photodissociation via the B-state leading to $\text{Na } D_2(3p \ J=3/2 \rightarrow 3s \ J=1/2)$ and $D_1(3p \ J=1/2 \rightarrow 3s \ J=1/2)$ line emission. However, in an additional experiment (with 489.0 nm and 476.5 nm) we are able to observe a population of the $\text{Na}^*(3p \ J=1/2)$ level, but connected with a much larger photofragment energy, as a result of a two-step excitation of a high lying Na_2 state dissociating into $\text{Na}^*(3p)$ and $\text{Na}(3p)$ atoms and populating the $\text{Na}^*(3p) \ J=3/2, J=1/2$ levels. Fig. 2 shows a Doppler spectrum of the $\text{Na}^*(3p, J=1/2)$ fragments obtained for perpendicular polarization with a kinetic energy of $W \approx 2000$ cm^{-1} .

References

- 1) R.N. Zare and D.R. Herschbach, Proc. IEEE 51, (1963) 173
- 2) R.W. Rothe, U. Krause, R. Dören, J. Chem. Phys. 72 (1980) 5145
- 3) M.L. Janson, S.M. Papernov, J. Phys. B 15 (1982) 4175

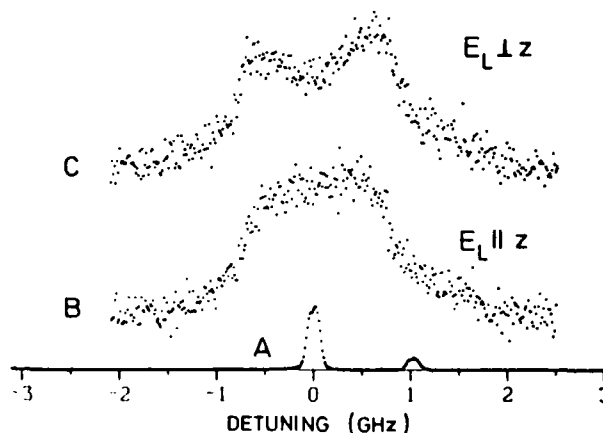


Fig. 1 Doppler Spectra of $\text{Na}^*(3p) \ J=3/2$ Fragments due to one-photon dissociation

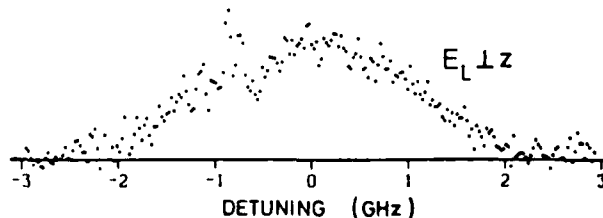


Fig. 2 Doppler Spectrum of $\text{Na}^*(3p) \ J=1/2$ Fragments due to two-photon dissociation

LYMAN- α EXCITATION SPECTRA IN THE PHOTODISSOCIATION OF H_2

S.Arai, Y.Yoshimi, H.Koizumi, K.Hironaka, K.Shinsaka, M.Morita, T.Yoshida,
A.Yagishita, K.Ito and Y.Hatano

Department of Chemistry, Tokyo Institute of Technology, Meguro-ku, Tokyo 152, Japan

*Faculty of Engineering, Hokkaido University, Kita-ku, Sapporo 060, Japan

+Photon Factory, National Laboratory of High Energy Physics, Oho-machi, Tsukuba-gun, Ibaraki 305, Japan

Dissociative and autoionizing states of molecular hydrogen have been extensively studied both theoretically and experimentally. In the case of dissociative excitation to these states, the observation of fluorescence from excited fragments is very informative to investigate these states and their dissociation processes,¹ and it has been known from the electron impact studies that the slow and fast H^* atoms are produced through the corresponding two processes.¹ The slow H^* atoms are produced by the predissociation of vibrationally excited molecular states which belong to the Rydberg series converging to the ground state of H_2^+ and the fast H^* atoms are produced by the direct dissociation (or partially involving predissociation) of the doubly excited molecular states which belong to the Rydberg series converging to the excited state of H_2^+ . In the photon impact studies, dissociative excitation of H_2 which produces the slow H^* has been already investigated by observation of atomic fluorescence in the excitation wavelength of 700-850Å.² In the shorter wavelength region where the fast H^* are produced, however, only a preliminary result, the upper limit of the cross section for photodissociation of H_2 , has been reported,³ and there has been no obvious observation of fluorescence from the fast H^* . This paper pre-

sents the first observation of Lyman- α radiation from the fast H^* (2p) produced by the photodissociation of H_2 .

Synchrotron radiation of Photon Factory was dispersed with a 1m Seya-Namioka monochromator. The monochromatic light passed through a differentially pumped gas cell (Fig.1), where H_2 pressure was maintained to 2×10^{-2} torr, and detected with a combination of sodium-salicylate and a photomultiplier. Lyman- α fluorescence was detected with a continuous dynord electron multiplier (Ceratron) through a MgF_2 window.

Fig.2 shows a Lyman- α excitation spectrum in the range of 350-550Å. In this wavelength region, the fragments are the fast H^* (2) from the doubly excited molecular states. Two thresholds are clearly found in this spectrum. The first one is at 470Å (26.4eV) and the second is at 408Å (30.4eV); the respective thresholds are indicated by arrows in Fig.2. The cross section for producing the fast H^* (2) has been estimated to be about 2 order of magnitude smaller than that of the slow H^* (2).

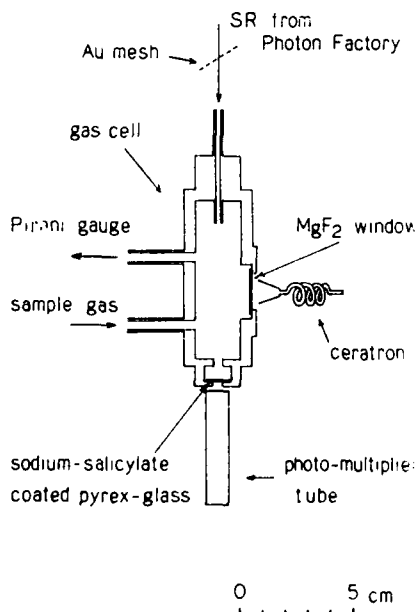


Fig.1 Interaction region

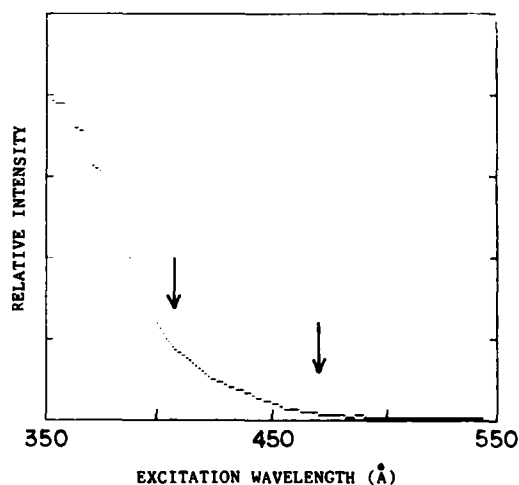


Fig.2 Lyman- α excitation spectrum of H_2

Reference

1. Y.Hatano, Comments on At.Mol.Phys., **11**, 259 (1983) and the references cited therein.
2. J.E.Mentall and E.P.Gentieu, J.Chem.Phys., **52**, 564 (1970). P.Borrell, P.M.Guyon and M.Glass-Maujean, J.Chem.Phys., **66**, 818 (1977) and the references cited therein.
3. M.Glass-Maujean, K.Kollman and K.Ito, J.Phys., **B12**, L459 (1979).

HIGH-RESOLUTION PHOTODISSOCIATION SPECTROSCOPY IN FAST NEUTRAL H_2 BEAM

N. Bjerre* and H. Helm

Molecular Physics Department, SRI International, Menlo Park, CA 94025

We have recorded high-resolution photodissociation spectra using a fast H_2 beam produced by charge exchange of H_2^+ in Cs vapor. The fast neutral beam was excited by a tunable cw dye laser, running coaxially with the molecular beam over a length of 100 cm. Photodissociation products that separate from the parent beam due to the kinetic energy released in the dissociation process were detected with an off-axis channeltron detector. The geometrical position of the detector limits the detection to fragments with a center of mass energy release $W > 200$ meV at a beam energy of 900 eV. (see Figure 1).

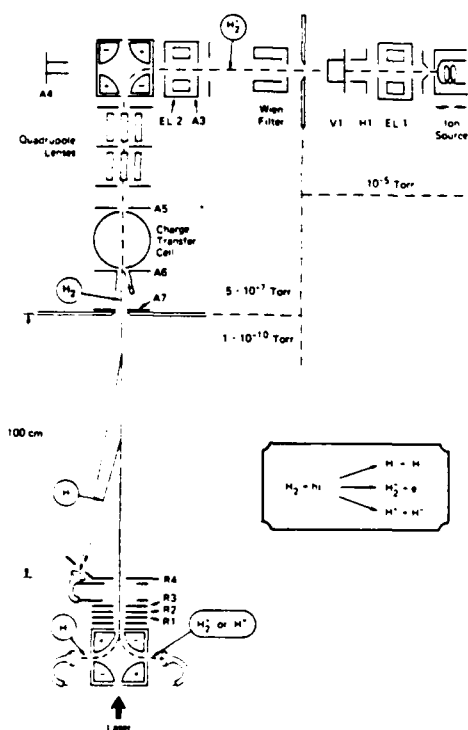


Figure 1 Fast Molecular Neutral Beam Spectrometer.

The spectrum obtained using DCM and R6G dyes consists of a large number of discrete lines superposed on a broad continuum. The discrete transitions can be assigned to bound-bound-free and bound-quasibound photodissociation¹ of H_2 $c^3\Pi_u$ through the electronic states $1^3\Pi_g$, $g^3\Pi_g^+$, $h^3\Pi_g^+$ and $j^3\Pi_g$. These states are the $3a$ and $3d$ members of the $1sn1$ Rydberg series. Among the transitions not observed previously are those

from the $(5,5)$ band of the i - c and g - c systems. The transitions to the $v=5$ level in the i state appear near 15600 cm^{-1} and show broadening due to rapid barrier tunneling with a lifetime of 10^{-13} s. Bound-free photodissociation appears as a weakly structured background between 15700 and 17300 cm^{-1} , which has not yet been assigned. The background is absent in spectra recorded with a beam energy of 2 keV , which indicates that the dominant contribution to the bound-free signal comes from low energy fragments with $W < 500\text{ meV}$.

High resolution spectra of several transitions were recorded using single-frequency laser excitation. The experimental resolution in these spectra is $\sim 100\text{ MHz}$, limited by the residual Doppler width in the fast beam. This Doppler width corresponds to a lab energy spread of 350 meV for the neutral beam. The high resolution spectra exhibit marked power broadening even at laser power levels as low as a few mW.

The narrow Doppler width in the fast beam allows partial resolution of the fine- and hyperfine-structure in both the $c^3\Pi_u$ state and in the $3d$ states. The fine-structure in the c state gives rise to a splitting of some 6 GHz .² The hyperfine structure in the $g^3\Pi_g^+$ state is at the present level of precision well represented by a Fermi contact parameter with a value very close to that of the Fermi contact parameter in the c state.² This could be expected, since the dominant contribution to the hyperfine interaction in both states comes from the $1s$ electron. The fine-structure is strongly affected by the l -uncoupling in the $3d$ system. The fine-structure in the g state of ortho hydrogen measured in the present experiment is consistent with an extrapolation of the l -uncoupling treatment of para hydrogen by Lichten et al.³

Supported by NSF grant PHY 8411517.

*Institute of Physics, Aarhus University, DK-8000 Aarhus C, Denmark

1. H. Helm, D. P. deBruijn, and J. Los, Phys. Rev. Lett. **53**, 1642 (1984).
2. W. Lichten and T. Wik, J. Chem. Phys. **69**, 5428 (1978).
3. W. Lichten, T. Wik, and T. A. Miller, J. Chem. Phys. **71**, 2441 (1979).

RADIATIVE DISSOCIATION OF SELECTIVELY EXCITED ROTATIONAL-VIBRATIONAL STATES OF $H_2(B, C)$ MOLECULES

H. Schmoranzer, T. Noll, J. Imschweiler, K. Molter

Fachbereich Physik, Universität Kaiserslautern
D-6750 Kaiserslautern, W.-Germany

Continuous vacuum-ultraviolet emission from selectively excited vibrational levels v' of the $B\ 2p\ ^1\Sigma_u^+$ state of H_2 has been observed previously^{1,2} in agreement with elaborate quantal calculations³ for rotationless transitions. The radiative transitions from B, v' levels into the dissociation continuum k'' of the bound electronic ground state $X\ 1s\ ^1\Sigma_g^+$ represents a mechanism of spontaneous radiative dissociation leading to hot $H(1s)$ atoms. Spontaneous radiative dissociation was predicted for the $C\ 2p\ ^1\Pi_u$ state, too, and more accurate calculations of transition rates for the $B-X$ continuum were made by including rotational distortion⁴.

In the present study the radiative dissociation of the C state via continuous $C-X$ vuv emission and the effect of rotational distortion on the $B-X$ emission continuum were observed for the first time.

Monochromatized synchrotron radiation from the storage ring BESSY, Berlin was utilized to selectively excite individual rovibronic B and C states of H_2 which was contained in a differentially pumped gas cell. The bandwidth of the 3 m -normal incidence monochromator used was 0.015 nm. The vuv fluorescence radiation was dispersed by a high luminosity secondary monochromator¹ of 1.4 nm bandwidth and single photons were detected by a position sensitive microchannelplate which enables to record a spectral interval of 25 nm width at a time.

The emission spectrum of the $C, v'=11, J'=1$ state, excited via the $Q(1)$ line out of $X, v''=0$, is shown in Fig. 1. The strongest $Q(1)$ emission lines of the $C, v'=11 \rightarrow X, v''$ bands occur for $v''=11, 12$ and 14 (the highest bound vibrational state). At longer wavelengths

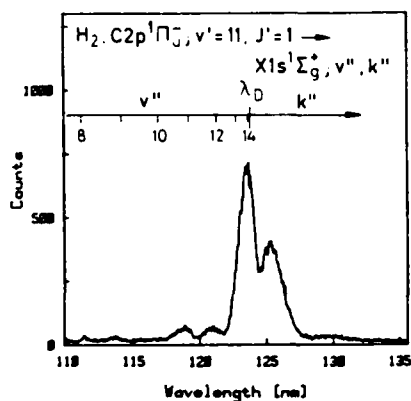


FIGURE 1 Vuv emission spectrum of $H_2\ C, v'=11, J'=1$ (v'' -progression and adjoining continuum)

than the limiting wavelength λ_D for bound-bound emission, a structured continuum is observed which is peaked at 125 nm. Similar results were obtained for other upper vibrational quantum numbers v' .

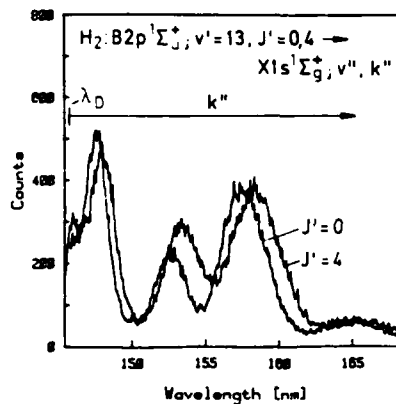


FIGURE 2 Continuous vuv emission spectra of $H_2\ B, v'=13, J'=0$ and $B, v'=13, J'=4$

As an example for the effect of rotational distortion, the emission spectra observed beyond the limiting wavelength λ_D are shown in Fig. 2 for the $B, v'=13, J'=0$ and 4 states, excited via the $P(1)$ and $R(3)$ lines. In this case the continuous spectrum exhibits at least three marked maxima. The effect of rotational distortion on the wavefunctions of the upper discrete state and the lower continuum state, besides changing relative peak intensities, results in a red shift of the intensity maxima with increasing upper rotational quantum number J' , in qualitative agreement with theory⁴.

Financial support from the Bundesministerium für Forschung und Technologie is gratefully acknowledged.

References

1. H. Schmoranzer, R. Zietz, Phys. Rev. A **18**, 1472 (1978)
2. H. Schmoranzer, R. Zietz, Abstracts XI ICPEAC (ed. K. Takayanagi, N. Oda, Kyoto, 1979), p. 56
3. A. Dalgarno, G. Herzberg, T.L. Stephens, Astrophys. J. Lett. **162**, L 49 (1970)
4. T.L. Stephens, A. Dalgarno, J.Q.S.R.T. **12**, 569 (1972)

PHOTODISSOCIATION PROCESSES OF HYDROGEN HALIDES
STUDIED WITH SYNCHROTRON RADIATION

J. B. Nee, M. Suto and L. C. Lee

Department of Electrical and Computer Engineering
San Diego State University, San Diego
California 92182

The photodissociation processes of HX (X = F, Cl, and Br) are investigated using synchrotron radiation in the 105-200 nm region as a light source. The photo-absorption and fluorescence cross sections of these molecules are measured.

For HF, only an absorption continuum in the 105-145 nm region is observed. This continuum corresponds to the $A^{1-} + X^{1}\Sigma^{+}$ transition. The absorption cross sections have a maximum of $3.5 \times 10^{-18} \text{ cm}^2$ at 118 nm and decrease to $2 \times 10^{-19} \text{ cm}^2$ at 145 nm.

For HCl, an absorption continuum corresponding to the $A^{1-} + X^{1}\Sigma^{+}$ transition appears in the 135-200 nm region. In the shorter wavelength region, discrete structures dominate the absorption spectrum. In the 120-135 nm region, the $C^{1-} (v=0,1) + X^{1}\Sigma^{+}$ transition shows very large absorption cross section, but the spin-forbidden transition, $b^{3-}_1 + X^{1}\Sigma^{+}$, also has a significant absorption cross section. Both the C^{1-} and b^{3-}_1 states do not fluoresce, indicating that these states are mainly predissociative. In the 113-120 nm region, the absorption cross sections are quite small and look like a continuum. However, the weak $V^{1}\Sigma$ state in this wavelength region shows fluorescence in the ultraviolet and visible wavelength region. This fluorescence makes this state very distinguishable from the absorption continua.

In the 105-113 nm wavelength region, the HCl absorption spectrum shows strong structures superimposing on the continua. The structures correspond to the H^{1-} , K^{1-} , M^{1-} and other unidentified states. Some states show fluorescence in the ultraviolet and visible region, but not in the vacuum ultraviolet region. These fluorescence results indicate that the lower state of the observed fluorescence is not the ground state, but some excited states, possibly $1-$ and $3-$ that are repulsive states. The investigation for the nature of the fluorescence is under-way.

For HBr, the absorption continuum for the $A^{1-} + X^{1}\Sigma^{+}$ transition is shifted to the 150-230 nm region. The absorption maximum at 175 nm has a cross section of $2.5 \times 10^{-18} \text{ cm}^2$. In the 126-150 nm region, discrete structures dominate the absorption spectrum. The oscillator strengths for both the spin-allowed transition, $C^{1-} + X^{1}\Sigma^{+}$, and the spin-forbidden transition, $b^{3-}_1 + X^{1}\Sigma^{+}$, are quite large. Similar to the case of HCl, these two states do not fluoresce, indicating

that they are mainly predissociative. In the 105-126 nm region, the absorption spectrum consists of strong structures superimposing on continua. Some of the states fluoresce in the ultraviolet and visible region. The nature of the fluorescence is under investigation.

When HBr is irradiated with excitation wavelengths shorter than 107.8 nm, a fluorescence from the excited Br^* atoms is observed. The fluorescence spectrum is dispersed and identified as the $Br^* 4p_{5/2} + 2p_{3/2}, 4p_{3/2} + 2p_{3/2}$ and $4p_{3/2} + 2p_{1/2}$ transitions at 157.7, 154.1, and 163.3 nm, respectively. From the threshold of the Br^* fluorescence, the dissociation energy for HBr is determined to be 3.65 eV.

By comparing the absorption spectra of HF, HCl and HBr, the absorption continua for the $A^{1-} + X^{1}\Sigma^{+}$ transition shift to the longer wavelengths when the halogen atoms become heavier. The ratio for the oscillator strengths of the $b^{3-}_1 + X^{1}\Sigma^{+}$ transition to the $C^{1-} + X^{1}\Sigma^{+}$ transition increases from 0.02 for HCl to 0.2 for HBr. This indicates that the spin conservation rule becomes less-vigorous as the weight of halogen atoms increased.

This work is supported by NSF under Grant No. ATM-8412618 and NASA under Grant No. NASW-319. The synchrotron radiation facility at the University of Wisconsin is supported by NSF under Grant No. DMR-44-21888.

PHOTODISSOCIATION DYNAMICS OF ICN

M. A. O'Halloran, H. Joswig, and R. N. Zare

Department of Chemistry, Stanford University, Stanford, California 94305 USA

An understanding of the detailed dynamics of the photofragmentation process is important in the elucidation of many photochemical systems. Because of the nature of the bound-free transition, the absorption spectra of many single-photon dissociation processes are broad and featureless. In order to learn about the excited state(s) and dissociative potential energy surface(s) involved in the photofragmentation processes, it is therefore necessary to examine in detail the final state distribution of photofragments.

We have been studying the photodissociation of ICN. The goal is to try and learn as much as possible about the dynamics of the photodissociation process by examining the final state distribution of the CN fragment in as much detail as possible. ICN, at pressures of 10-20 mTorr, is dissociated by 249 nm radiation from an excimer laser. The excimer laser is also used to pump a tunable dye laser which probes the CN $X^2\Sigma^+$ distribution after a delay on the order of 20 nsec. The CN fragments are produced in their ground electronic state, and the dye laser is tuned through the CN $B^2\Sigma^+ + X^2\Sigma^+$ transition to probe the final state distribution via laser induced fluorescence (LIF).

In addition to conventional measurements of vibrational and rotational populations, we are studying the alignment of angular momentum in the CN fragment. This can be determined by observing the variation in fluorescence intensity as the probe laser's polarization is rotated with respect to the direction of polarization of the photolysis laser. When such a measurement is made for a single N'' level in the final CN $X^2\Sigma^+$ distribution, the second multipole moment of the M_N distribution is exactly determined.¹

Another vector quantity that we can measure is the angular distribution of photofragments. For a linearly polarized photolysis, the normalized angular distribution of photofragments is given by

$$f(\theta) = \frac{1}{4\pi} [1 + \beta P_2(\cos\theta)]$$

where $P_2(x) = \frac{1}{2}(3x^2 - 1)$.² In this system, the atomic iodine fragment has no internal degrees of freedom, and the CN fragment's velocity is fixed once its internal energy is known. The Doppler profile of the probe transition will depend on the direction of the velocity of the CN fragment relative to the direction of observation.³

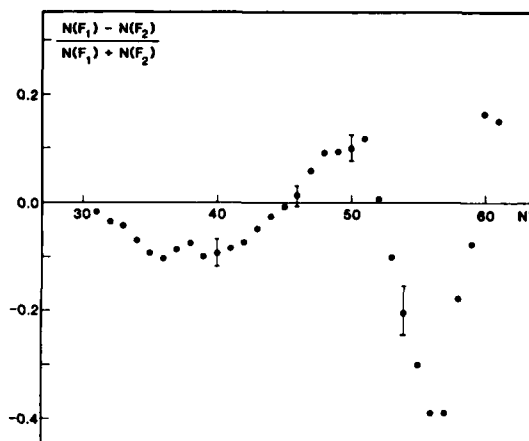


Figure 1 Population differences of the F_1 and F_2 spin-rotation doublets over total population as a function of rotational quantum number N'' for CN $X^2\Sigma^+(v''=2)$ produced in the photodissociation of ICN at 249 nm.

In the course of this study, we have also observed that the two spin-rotation components (F_1 and F_2) of the CN $X^2\Sigma^+$ fragment are unequally populated and that this difference in population changes as a function of N'' . This has previously been observed by Wittig and co-workers in the dissociation of ICN and BrCN at 266 nm.⁴ In Figure 1, the difference in population of the spin-rotation doublets divided by the total population of the two levels is plotted as a function of rotational quantum number N'' . The population differences clearly oscillate and tend to increase with N'' . This effect is attributed to interactions between the spins and angular momenta of the iodine and CN fragments. The interactions and couplings between the various angular momenta will be mediated by the dissociative potential energy surface, and so these population differences are expected to be a very sensitive function of the dynamics of the photodissociation process.

References

1. Chris H. Greene and Richard N. Zare, J. Chem. Phys. **78**, 6741 (1983).
2. Sze-cheng Yang and Richard Bersohn, J. Chem. Phys. **61**, 4400 (1974).
3. R. Vasudev, R. N. Zare, and R. N. Dixon, J. Chem. Phys. **80**, 4863 (1984).
4. F. Shokoohi, S. Hay, and C. Wittig, Chem. Phys. Lett. **63**, 110 (1984).

THEORETICAL INVESTIGATION OF THE PHOTODISSOCIATION OF OH^+

Roberta P. Saxon* and B. Liu†

*Molecular Physics Department, SKI International, Menlo Park, California 94025 USA
 †IBM Research Laboratory, San Jose, California 95193 USA

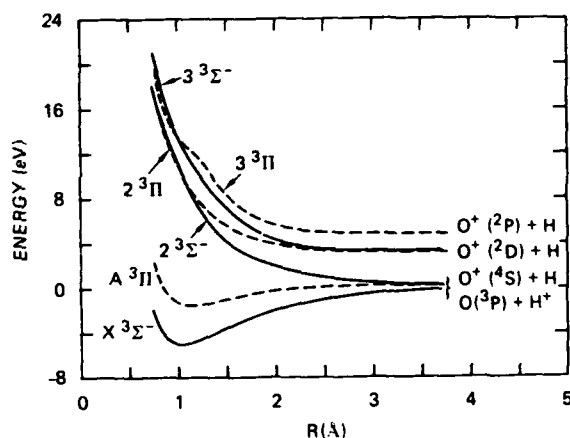
Ab initio calculations of the potential curves, transition dipole matrix elements and photodissociation cross sections of the lowest three $3\Sigma^-$ and lowest three 3Π states of the OH^+ ion have been performed to provide data of interest in the modeling of cometary atmospheres. While the potential curves of this system have previously been reported,¹ the transition moments have not been determined and the photodissociation process has not, to date, been studied experimentally.

Particular emphasis was placed in these calculations on the proper determination of the effect of Rydberg states and of Rydberg-valence interaction. While neglect of Rydberg mixing may not significantly affect the qualitative nature of the potential curves, particularly for the repulsive excited states at issue here, it can have a significant influence on the calculated transition moments. Configuration interaction calculations were carried out with a Slater-type basis set including two 3s, two 3p and one 3d Rydberg function on the O atom. Molecular orbitals determined by a complete active space MCSCF calculation on the ground state were augmented by optimized Rydberg orbitals. The resulting potential curves are shown in Figure 1. The $\text{O}(^3\text{P}) + \text{H}^+$ asymptote should lie 0.019 eV below the $\text{O}^+(^4\text{S}) + \text{H}$ limit. In this, and in previous calculations,¹ the asymptotes are obtained in the opposite order, which, however, does not affect the photodissociation cross sections reported here.

Cross sections have been obtained for photodissociation from the lowest vibrational and rotational level of the ground state to the repulsive second and third sigma and pi states. The variation of the transition moments in the Franck-Condon region is insufficient to significantly perturb the expected gaussian shape for a bound-free cross section. The peak values, positions and full widths at half maximum are listed in Table 1. Dissociation to the repulsive portion of the $\text{A } ^3\Pi$ state resulted in a peak cross section of $3.0 \times 10^{-22} \text{ cm}^2$.

Table 1. Photodissociation cross sections for transitions from $\text{OH}^+ \text{X } ^3\Sigma^-$

Final State	Peak Position (Å)	Cross Section (cm^2)	FWHM (Å)
$2 \text{ } ^3\Sigma^-$	830	2.45×10^{-18}	220
$3 \text{ } ^3\Sigma^-$	730	9.70×10^{-18}	130
$2 \text{ } ^3\Pi$	820	1.32×10^{-18}	150
$3 \text{ } ^3\Pi$	700	6.21×10^{-18}	55

FIGURE 1 OH^+ potential curves calculated in this work.

RPS supported by NSF Astronomy grant AST-8311426.

Reference

1. D. M. Hirst and M. F. Guest, *Mol. Phys.* **49**, 1461 (1983).

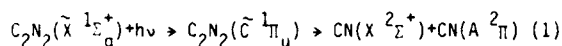
ADIABATIC APPROACH TO POLYATOMIC PHOTODISSOCIATION: APPLICATION TO $C_2N_2^*$ C. E. Dateo[†], M. Dupuis[‡], V. Z. Kresin, and W. A. Lester, Jr.[†]

Materials and Molecular Research Division, Lawrence Berkeley Laboratory, Berkeley, California 94720

[†]Also: Department of Chemistry, University of California, Berkeley, California 94720[‡]Present address: IBM Research Laboratory, Kingston, New York 14401

Polyatomic photodissociation dynamics has become an area of significant interest in recent years due to the advent of new experimental techniques for the preparation of initial states of molecules and the probing of final states of photofragments. A main goal of the present theoretical effort is the evaluation of energy distributions of the fragments.

Recent experimental studies indicate C_2N_2 undergoes indirect photodissociation at wavelengths between 164 and 158 nm.



Process (1) is an example of type II or vibrational predissociation which occurs on a single multidimensional adiabatic electronic potential energy surface (pes). Vibrational distributions have been reported for several wavelengths.^{1,2}

A golden rule formalism is used to evaluate the energy distributions of the fragments. Vibrational predissociation represents a more complicated case in this formalism because both states belong to the same pes. An approach has been developed which enables this case to be treated as a quantum transition.³ It essentially entails the use of a diabatic state representation which provides a localized description of the unimolecular process. In this diabatic representation it can be shown that relative populations can be obtained by evaluation of Franck-Condon (FC) integrals.

The main difficulty encountered in a FC formalism is obtaining an expression for the nuclear wavefunction of the dissociative state which adequately describes the relative and internal motions of the photofragments. The present adiabatic description⁴ explicitly treats the interaction between the relative and internal motion of the fragments (final-state interactions). The vibrational frequencies of the fragments as well as the equilibrium bond lengths are found to be dependent on the interfragment separation.

The theory has been applied to collinear predissociation of $C_2N_2(\tilde{C}^1\Pi_u)$ where bending vibrations and rotations are neglected. A full three-dimensional treatment will be presented separately. Ab initio multiconfiguration Hartree-Fock (MCHF) calculations

were performed to obtain diabatic electronic states. Molecular geometries, force constants, and harmonic frequencies were computed for the $\tilde{C}^1\Pi_u$ state in excellent agreement with the limited experimental data available.⁵ The nuclear wavefunction is approximated by harmonic oscillator functions that describe the three normal mode stretches. The validity of the harmonic approximation is supported by the equidistant bands of the C_2N_2 absorption spectrum.¹

For the dissociative state, the harmonic approximation is also employed, but is not essential, to describe the internal degrees of freedom. Rigorous evaluation of the FC integral entails knowledge of the frequencies and force constants of the dissociative state in the region of overlap. These are obtained from minimal basis set MCHF calculations. The translational wavefunction describing the relative motion of the fragments is determined numerically using standard methods by solving

$$\left(-\frac{\hbar^2}{2\mu} \frac{\partial^2}{\partial \rho^2} + U^{\text{eff}}(\vec{\rho}) \right) \phi^{\text{rel}}(\vec{\rho}) = E \phi^{\text{rel}}(\vec{\rho}) \quad (2)$$

where $U^{\text{eff}}(\vec{\rho})$ is the effective potential including vibrational contributions.

Vibrational distributions of the photofragments computed by the procedures discussed above will be reported and compared to experimental results. These distributions are found to be sensitive to several factors. These include the number of product vibrational levels energetically accessible which is presently uncertain due to the lack of agreement on the $C_2N_2(\tilde{X}^1\Sigma_g^+)$ dissociation energy, and the possibility of an additional electronic channel at shorter wavelengths. Comments on the validity of the various approximations and the sensitivity of results to parameters will be discussed.

References

1. G. Miller, W. Jackson, W. Halpern, J. Chem. Phys. **71**, 4625 (1979).
2. M. R. Tahrerian and T. G. Slanger, J. Chem. Phys. **81**, 3814 (1984).
3. V. Z. Kresin, W. A. Lester, Jr., M. Dupuis, and C. E. Dateo, Int. J. Quant. Chem. Symp., **18**, 691 (1984).
4. V. Z. Kresin and W. A. Lester, Jr., Chem. Phys. **90**, 335 (1984).
5. C. E. Dateo, M. Dupuis, and W. A. Lester, Jr., J. Chem. Phys., to appear.

*This work was supported by the Director, Office of Basic Energy Sciences, Chemical Sciences Division of the U.S. Department of Energy under Contract No. DE-AC03-76SF0009d

TIME DEPENDENT WAVEPACKET CALCULATION OF THE
PHOTODISSOCIATION OF $\text{Cd}(\text{CH}_3)_2$

Kenneth C. Kulander and Ann E. Ore¹*

Theoretical Atomic and Molecular Physics Group
Lawrence Livermore National Laboratory
Livermore, California 94550 USA**

Recent experiments have shown that the photodissociation of cadmium dimethyl with polarized light in the wavelength range 1900 - 3300 Å leads to an anisotropic distribution of the photofragments.¹ The experimental evidence and a consideration of the large amount of excess energy available indicate that it is likely that a substantial fraction of the photochemical events produce three fragments: Cd and 2CH_3 . In fact, classical trajectory studies^{2,3} of photodissociation in this system predict that the dominant channel is that which leads to three body dissociation. We have performed a time dependent gaussian wavepacket calculation⁴ using the excited state potential energy surface of Kellman, et al.,³ and obtain very good agreement between our product state distribution and those of refs. 2 & 3. Their model assumes the dissociation takes place with the C-Cd-C atoms remaining collinear, treating the methyls as single atoms with masses 15. We also assume the dissociating wavefunction is accurately represented by a single gaussian wavepacket. Thus, we determine the time evolution of the wavepacket by solving the time dependent Schrodinger equation assuming that the interaction potential can be represented accurately by a local Taylor's expansion truncated after the quadratic terms.^{5,6} From this single wavepacket we can extract all product state distribution for all photon energies. We also obtain the total photo-absorption cross section.⁷ By comparison, the results of Pattengill required on the order of a thousand trajectories per photon energy to obtain statistical convergence. Therefore, these calculations illustrate the computational convenience of this powerful technique which gives exact quantum mechanical results provided the local, quadratic expansion of the surface is valid over the width of the wavepacket.

References

1. C. Jonah, P. Chandra and R. Bersohn, J. Chem. Phys. 55 1903 (1971)
2. M. D. Pattengill, Chem. Phys. 75 59 (1983)
3. M. E. Kellman, P. Pechukas and R. Bersohn, Chem. Phys. Lett. 83 304 (1981)
4. K. C. Kulander and E. J. Heller, J. Chem. Phys. 69 2439 (1978)
5. E. J. Heller, J. Chem. Phys. 65 4979 (1976)
6. W. H. Miller, J. Chem. Phys. 62 1899 (1975)
7. E. J. Heller, J. Chem. Phys. 68 2066 (1978)

*Present address Aerospace Corporation, P.O. Box 92957, Los Angeles, CA 90009

**Work performed under the auspices of the U.S. Department of Energy by the Lawrence Livermore National Laboratory under Contract Number W-7405-ENG-48.

MOLECULAR PHOTODISSOCIATION NEAR IONIZATION LIMIT

G.K. Ivanov and G.V. Golubkov

Institute of Chemical Physics, Academy of Science, Moscow USSR

Molecular photodissociation (PD) at the photon energy $|h\nu - I| \sim \omega$ (I is the ionisation potential of the molecule XY , ω is the vibrational quantum of the ion XY^+) is considered by means of multichannel quantum defect (MQD) method. The proposed variant of the MQD method enables analytical description of PD spectrum defined the complete phenomenological parameters being from adiabatic picture of terms. We proceed from the fact that adiabatic terms of the system (without mixing of electron angular momentum l) are defined by equation ($\hbar = m_e = e = 1$)

$$tg\{\pi[2(U_i - \epsilon)]^{1/2}\} - K_{ee}^{(e)} - \sum_{\beta} \frac{1/V_{\beta e}}{\epsilon - U_{\beta}^e} = 0 \quad (1)$$

The ionic (U_i) and dissociative (U_{β}^e) terms, adiabatic quantum defects M_e of Rydberg levels ($K_{11}^{(e)} = -tg\pi M_e$) and configuration interaction $V_{\beta e}$ are the known functions of internuclear distances R here. The adiabatic wave function of the initial ($\psi_i = f_i G_i(R)$), Rydberg ($\psi_{\beta}^{(e)} = \phi_{\beta} X_{\beta}(R)$) and dissociative ($\psi_{\beta}^{(d)} = \psi_{\beta}^e X_{\beta}^d(R)$) molecular states are supposed to be known too (X_{β}^d is defined at the energy E got by the nuclei in accordance with the energy conservation law).

For the matrix element of the dipole transition operator \hat{D} in to the dissociative state β , we get

$$\begin{aligned} \mathcal{D}_{i\beta}^{(e)} = & \sum_{\beta'} \langle f_i | \hat{D}_{\beta'}^{(d)} | X_{\beta'}^d \rangle (\delta_{\beta\beta'} - i T_{\beta\beta'}^{(e)}) + \\ & + \sum_{\beta'} \langle f_i | \frac{\hat{D}_{\beta'}^{(e)}}{\omega_{\beta} \pi M_e} | X_{\beta'} \rangle ctg\pi \nu_{\beta} T_{\beta\beta'}^{(e)}, \end{aligned} \quad (2)$$

where all peculiarities of the energy structure of the spectrum are defined by T-matrix. Here $\nu_{\beta} = [2(E_{\beta} - E)]^{1/2}$, E_{β} is the nuclear vibrational energy in β state. The energy E measured from the ionisation threshold,

$$\mathcal{D}_{\beta}^{(d)} = \langle f_i | \hat{D} | \psi_{\beta}^e \rangle, \quad \mathcal{D}_{\beta}^{(e)} = \langle f_i | \hat{D} | \phi_{\beta} \rangle.$$

T-matrix elements are defined from the set of algebraic equations: eq. (1) of /1/ - in case of one dissociative channel or eq. (2) of /2/ - for the general multichannel case.

At the energy $E < 0$ the PD spectrum (without mixing l and with taking into account the Rydberg series $v = 0$ only) is given by expression

$$F_c(E) = \frac{(tg\pi \nu_c - \bar{K}_{cc} - \lambda_c)^2 + \delta_c^2}{(tg\pi \nu_c - \bar{K}_{cc})^2 + \gamma_c^2} \quad (3)$$

Here $\bar{K}_{\beta\beta} = \langle X_{\beta} | K_{ee}^{(e)} + \sum_{\beta'} V_{\beta\beta'} \bar{g}_{\beta'} V_{\beta'\beta} | X_{\beta} \rangle$ (\bar{g}_{β} is the real part of the Green's function describing nuclei motion in the dissociative channel β). Parameters λ_c , δ_c and γ_c depend on the number of the open channels. In the case of one dissociative channel the eq. (3) incorporates with the expression (4) of /3/ at the following parametrization of the R-matrix in /3/: $R_{11} = 0$, $R_{12} = -E_{c0}$, $R_{22} = -E_{\beta c} = -\langle X_{\beta} | V_{\beta\beta} | X_{\beta}^d \rangle$.

References

1. G.K. Ivanov, G.V. Golubkov, Chem. Phys. Lett. 117, 251, (1985)
2. G.K. Ivanov, G.V. Golubkov (in this conference)
3. A. Giusti-Suzor, U. Fano, J. Phys., 217, 747, (1984)

MULTIPHOTON IONIZATION OF HYDROGEN ATOMS

H.G. Muller and M.J. van der Wiel

FOM-Institute for Atomic and Molecular Physics, Amsterdam, The Netherlands

It is in general very difficult to compare an experiment on multiphoton ionization with theory. The high light intensity at which such an experiment has to be conducted causes the lowest order perturbation results no longer to be valid, leading to all kinds of interesting phenomena such as above-threshold ionization (ATI) and light-induced threshold shift. On the experimental side the need to reach high intensities makes focussing of the light beam imperative, causing strong inhomogeneity in the intensity, which makes it often difficult to interpret the experimental results. Detailed comparison of theory and experiment can therefore only be made for the simplest of systems, which naturally led us to the study of the hydrogen atom.

In order to avoid the difficulties associated with the intensity distribution, we employ the principle of Stark-tuning¹⁾: The state of the atom from which we want to study the ionization is prepared by means of excitation with a different color. This excitation happens only if the photons of this extra color fit exactly between the atomic ground-state and the selected excited state. Since both these states experience a (generally different) ac-Stark shift due to the presence of the ionizing light, (the light used for excitation is sufficiently weak for the corresponding shift to be negligible), the excitation can only take place at one specific intensity thereof. Therefore our photo-ionization target atoms are only produced at those times and places in our pulsed laser focus, at which exactly this intensity is reached, making it possible to perform ionization at a well defined intensity.

We use the fundamental of the YAG-laser (1.064 μm) to ionize the atomic hydrogen 3p state, which is prepared by excitation with 3 UV photons. Since comparatively little intensity is needed for this excitation the broadening of this state due to the UV caused ac-Starkshift can be kept small, leading to a sharp selection ($\sim 5\%$) of the intensity at which the 2-photon ionization from 3p takes place. In the ionizing step the 2-photon process due to the YAG-light competes with the one-photon ionization from 3p with another UV photon. The latter process ensures that 3p states, once produced, do not hang around long enough for the light intensities to have changed.

At the moment we have measured the 4-photon UV resonant MPI process, and the influence of the 1064 nm light on the line-profile (as a function of UV wavelength). Before the conference we hope to add to this the measurement of the 3 UV + 2 IR ionization rate, and possibly the 3 UV + 3 IR (ATI) rate, as a function of absolute intensity.

REFERENCES

- 1) P. Kruit, J. Kimman, H.G. Muller and M.J. van der Wiel, J.Phys.B. 16 (1983) 937.

A NEW METHOD FOR THE STUDY OF TWO PHOTON PROCESSES IN ATOMIC HYDROGEN

Viorica Florescu and Tudor Marian

Faculty of Physics, University of Bucharest, P.O.Box 5211, Bucharest-Magurele, 76900, ROMANIA

In the dipole approximation, the study of two photon processes in atomic hydrogen can be done in a systematic way, if one first calculates the functions

$$\vec{w}_{nlm}(\Omega; \vec{r}) = \int G(\vec{r}, \vec{r}'; \Omega) \hat{P} u_{nlm}(\vec{r}') d\vec{r}', \quad (1)$$

where $G(\vec{r}, \vec{r}'; \Omega)$ is the Coulomb Green's function, \hat{P} the momentum operator, u_{nlm} a bound state eigenfunction and Ω a function of the photon energy, changing with the process (emission, absorption or scattering). The functions \vec{w}_{nlm} determine also the linear response of the atom to the action of a monochromatic electromagnetic plane wave¹. The function \vec{w}_{100} , corresponding to the ground state, was studied systematically by Luban and coworkers². In a previous work³, we have considered the cases $n=2$ and $n=3$, and, recently⁴, we have given a compact formula for \vec{w}_{nlm} , valid for arbitrary (n, l, m) . For $l \neq 0$ each function \vec{w}_{nlm} is a combination of two vector spherical harmonics characterized by two radial functions, for which convenient integral representations have been found. For $l=0$, only one radial function determines \vec{w}_{n00} , which is proportional to \vec{r} .

We investigate some properties of the functions \vec{w}_{nlm} : possible series expansions, small and large r behaviour, low frequency region.

The Kramers-Heisenberg matrix elements for two photon bound-bound transitions are then directly constructed from quantities like

$$\vec{w}_{nlm, n'l'm'} = \langle u_{n'l'm'} | \vec{s}_1 \cdot \vec{P} | \vec{s}_2 \cdot \vec{w}_{nlm} \rangle, \quad (2)$$

where \vec{s}_1 and \vec{s}_2 are the polarization vectors of the photons. We obtain rather compact analytic expressions in the general case. From them, one recovers easily previous results concerning two photon bound-bound transitions for low n states and also the new formulas for $1s \rightarrow ns$, $1s \rightarrow nd$ transitions obtained by Costescu et al.⁵

Further, we make an analytic continuation in the electron energy of the expression of the functions (1) in order to construct the functions $\vec{w}_{Elm}(\Omega; \vec{r})$ corresponding to u_{nlm} replaced by the partial wave u_{Elm} in Eq. (1). By summation of the partial waves contributions

we construct also the functions

$$\vec{w}^{\pm}(\vec{p}; \vec{r}) = \int G(\vec{r}, \vec{r}'; \Omega) \hat{P} u^{\pm}(\vec{p}; \vec{r}') d\vec{r}', \quad (3)$$

where $u^{\pm}(\vec{p}, \vec{r})$ are, respectively, the scattering out and in wavefunctions for the Coulomb field, with \vec{p} the asymptotic momentum of the electron.

The functions $\vec{w}^{\pm}(\vec{p}; \vec{r})$ are expressed as combinations of the vectors \vec{r} and \vec{p} implying two scalar functions that have compact analytic representations. Their properties are studied in detail.

Using our expressions for \vec{w}^{\pm} , we establish analytic formulas for the Kramers-Heisenberg matrix elements corresponding to bound-free and free-free transitions. As a check, we reobtain the analytic results for Compton scattering by $1s$ electrons⁶.

Reference:

1. R. Podolsky, Proc. Natl. Acad. Sci., U.S. **14** 253 (1928).
2. M. Luban, B. Nudler, I. Freund, Phys. Lett. **A47**, 447 (1974); M. Luban, R. Nudler-Blum, J. Math. Phys. **18**, 1971 (1977).
3. V. Florescu and T. Marian, The linear response of the hydrogen atom to an electromagnetic monochromatic plane wave, Central Institute of Physics, Bucharest, Report No. FT-245-1984.
4. V. Florescu, T. Marian (to be published).
5. A. Costescu, I. Brandus, N. Mezincescu, J. Phys. B: At. Mol. Phys. (in press).
6. M. Gavrila, Phys. Rev. **A6**, 1360 (1972).

ABSOLUTE TWO-PHOTON ABSORPTION AND THREE-PHOTON IONIZATION CROSS SECTIONS FOR ATOMIC OXYGEN

D. J. Bamford, W. K. Bischel, L. E. Jusinski, R. P. Saxon and J. Eichler

Chemical Physics Laboratory, SRI International, Menlo Park, CA 94025

The technique of two-photon excited fluorescence has been used to measure the cross section for the $^3P_{2,1,0} + ^3P_2$ transition in atomic oxygen. The relevant energy levels, along with the excitation and detection schemes, are shown in Figure 1. Excitation was monitored by observing fluorescence at 845 nm from the $^3P_{2,1,0} + ^3S$ transition.¹ Spontaneous Raman scattering from molecular hydrogen was used to calibrate the fluorescence detection system.² The spatial and temporal profiles of the exciting dye laser pulses were carefully measured in a collimated excitation geometry, allowing the two-photon cross section (α) to be measured absolutely. A knowledge of this cross section is crucial to understanding the three-photon ionization of oxygen, with the $^3P_{2,1,0}$ level serving as the resonant intermediate state. In this case the third photon is identical to the first two. By monitoring the absolute number of ions produced by each laser pulse and using the two-photon cross section measurement described above, it was possible to determine the excited state photoionization cross section (σ_{p1}). The use of a collimated laser geometry has avoided saturation of either step in this process, thus allowing it to be well-described by a simple set of rate equations. The preliminary measured cross sections are $\alpha = 2.9 \pm 1.5 \times 10^{-28} \text{ cm}^4/\text{W}$ and $\sigma_{p1} = 6.6 \pm 3.1 \times 10^{-19} \text{ cm}^2$.

Theoretical calculations have been undertaken in parallel with the experimental measurements to provide a more complete understanding of this multiphoton process. From perturbation theory, the rate for two-photon absorption in sec^{-1} may be written¹ as:

$$W = \frac{(2\pi)^3}{h^2 c^2} I^2 P^2 g(\omega) \quad (1)$$

$$\text{where } P = \sum_k \frac{\langle f | \mathbf{e} \cdot \mathbf{r}^\lambda | k \rangle \langle k | \mathbf{e} \cdot \mathbf{r}^\lambda | g \rangle}{E_g - E_k + \hbar\omega} \quad (2)$$

and $\mathbf{r}^\lambda = \hat{\mathbf{r}} \cdot \hat{\mathbf{e}}_\lambda$, $\hat{\mathbf{e}}_\lambda$ is the laser polarization, $g(\omega)$ is the line shape function, and I is the laser intensity in Watt/cm^2 . The rate may be conveniently expressed in terms of a generalized two-photon cross section α , independent of laser flux in cm^4/W as $\alpha = \hbar\omega / I^2 = 8.746 \times 10^{-30} P^2 \text{ cm}^4/\text{W}$ for the $O(^3P_{2,1,0}) + O(^3P_2)$ transition at 225.7 nm for the laser tuned to the peak of the Doppler-broadened spectral lineshape (assuming $T=298 \text{ K}$).

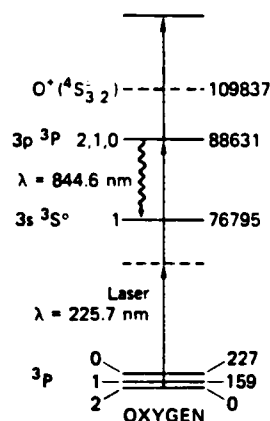


Figure 1. Relevant Energy levels for the two-photon resonant three-photon ionization of $O(^3P)$.

The matrix elements in P are being explicitly evaluated from configuration interaction calculations. Two off-diagonal sum rules employed by Huo and Jaffe³ are being used to estimate the error due to truncation of the infinite sum in Eq.(2). The calculated *ab initio* value for the two-photon cross section, α , is $2.5 \times 10^{-28} \text{ cm}^4/\text{W}$, which is in excellent agreement with the measured cross section. We estimate the error due to truncation is less than 10%. A critical analysis of the source of error in these calculations will be presented.

Work supported by the Defense Advanced Research Project Agency under contract No. N6921-84-C-0052, through the Naval Surface Weapons Center.

J. Eichler is on leave from the Hahn-Meitner Institute, D-1000 Berlin 39, W. Germany.

References

1. W. K. Bischel, B.E. Perry and D.R. Crosley, *Appl. Opt.* **21**, 1419 (1982).
2. W. K. Bischel and G. Black, "Wavelength Dependence of Raman Scattering Cross Sections from 200-600 nm", in *Excimer Lasers 1983*, edited by C. K. Rhodes, H. Egger and H. Pummer (American Institute of Physics, 1983).
3. W. H. Huo and R. L. Jaffe, *Chem. Phys. Lett.* **101**, 463 (1983).

RESONANT MPI OF SODIUM ATOMS BY TWO INTENSE LASER FIELDS

D. Feldmann, G. Otto, D. Petring and K. H. Weige

Fakultät für Physik, Universität Bielefeld, D4800 Bielefeld 1 FRG

Experimental:

The multiphoton ionization spectrum has been measured in the presence of a second laser field ($\lambda_2 = 532$ nm) in the wavelength range between 547 nm and 580 nm. Both lasers have been focused to obtain intensities up to about 10^{10} W/cm². The figure shows the Na⁺-ion yield versus the wavelength λ_1 . Both lasers are linearly polarized parallel to each other.

Discussion:

The peaks labeled A, B, C and D are observed at photon energies ω_1 for which two-photon resonant three-photon ionization is possible:

Peak "A" : $2\omega_1 = E(4^2D)$; "B" : $2\omega_1 = E(6^2D)$;

"C" : $\omega_1 + \omega_2 = E(6^2S)$; "D" : $\omega_1 + \omega_2 = E(5^2D)$.

E_i denotes the excitation energy of the state in brackets and $\omega_{1,2}$ the respective photon energy. Processes of this type have often been observed in MPI and will not be considered here in detail. We shall only discuss the additional peaks labeled "E" and "F" which cannot be explained as resonant three-photon ionization. They are observed at photon energies ω_1 which fulfill the following formal energy conserving equations: Peak "E" : $3\omega_1 = E(4^2D) + \omega_2$,

"F" : $2\omega_1 = E(3^2P_{1/2}) + \omega_2$ and

$2\omega_1 = E(3^2F_{3/2}) + \omega_2$.

Peak "E": At this photon energy the 4^2D -state is resonantly coupled into the MPI process. Two pathways can be considered: (a) The 4^2D -state can be coupled by ω_2 into the otherwise unstructured $3\omega_1$ -ionization continuum. Processes of this type have been called "autoionizing like" resonances¹. They have been described theoretically² and experimental results¹ on induced polarization anisotropy and frequency tripling have been explained by such processes. The interest in such processes arises from the possibility to selectively change the properties of an ionization continuum and they are closely related to the process of stimulated recombination. - Our experimental results³ indicate however that the 4^2D -state is reached in a different way (b): a Raman-type ($2\omega_1 - \omega_2 + \omega_1$)-excitation which proceeds in the energy region below the ionization limit.

Peaks "F": The two peaks are separated by 0.5 nm. They have the same height and show the same behavior for different polarizations and intensities of the lasers. They can be attributed to the excitation of the 3^2F -state by a Raman-type ($2\omega_1 - \omega_2$)-process with subsequent $2\omega_1$ -ionization. This conclusion is derived from the linear ω_2 -intensity dependence and preliminary measurements of electron energy spectra.

Conclusions:

At intensities of about 10^{10} W/cm² resonantly enhanced five-photon ionization can be stronger than nonresonant three-photon ionization. We find no evidence for "autoionizing like" resonances in the MPI spectrum.

References:

1. G. S. Dimov, L. I. Pavlov, E. V. Stamenov, Yu. I. Geller and A. A. Popov; Appl. Phys. **14**, 31 (1983), G. S. Dimov, L. I. Pavlov, E. V. Stamenov and J. R. Altschuller; Opt. Quant. Electr. **15**, 17 (1983)
2. see for example: Yu. I. Geller and A. A. Popov; Sov. Phys. JETP **51**, 235 (1980), P. E. Coleman and P. L. Knight; Phys. **R15**, 2455 (1982)
3. Because of restriction space details cannot be given.

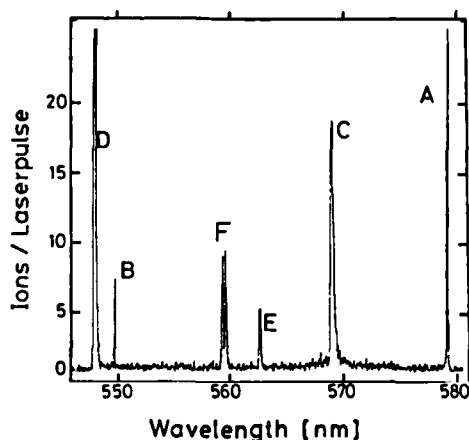


Figure: The MPI spectrum of Na-atoms.

TWO PHOTON IONISATION OF METASTABLE HELIUM

H. Haberland, J. Hühne, and M. Oschwald

Fakultät für Physik, Universität Freiburg, D 7800 Freiburg, West Germany

Two photon ionisation of metastable Helium has been studied experimentally. The total ion signal has an unexpected structure on the dipole resonance.

Metastable He-atoms (He^*) are produced in a gas discharge source. They are ionized by an excimer laser pumped dye laser with a bandwidth of 0.6 cm^{-1} . The laser is focussed on the He^* beam. At an energy of 1 mJ per pulse a power density of about 1.5 GW/cm^2 is obtained in the ionisation volume.

The He^+ ions are extracted by an electric field, accelerated, mass selected by a TOF spectrometer and detected in a secondary electron multiplier.

The He^+ -ion signal is shown as a function of the laser frequency in Fig. 1. The laser intensity was 0.8 mJ/pulse . A split resonance at 501.71 nm due to the dipole transition ($2^1\text{S}-3^1\text{P}$) and one sharp resonance at 504.35 nm due to the quadrupole transition ($2^1\text{S}-3^1\text{D}$) in the first step of the two photon ionisation process of $\text{He}(2^1\text{S})$ are observed.

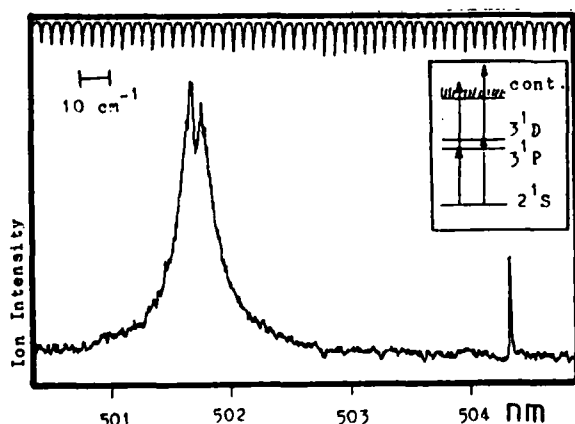


FIGURE 1 He^* two photon ionisation signal at a laser intensity of $.8 \text{ mJ/pulse}$. The sharp peak at 504.35 nm is due to the quadrupole transition.

The $2^1\text{S}-3^1\text{P}$ dipole resonance is strongly broadened due to saturation of the resonant step in the two photon process (see inset of Fig. 1). There is a rapid decrease of the signal at 501.71 nm , where the maximum of the resonance is expected. The double structure of the peak vanishes with decreasing intensities (Fig. 2). No influence of the laser polarisation could be observed, so that there is no hint of an AC-Stark shift different for

the $m=0$ and the $|m|=1$ levels of the 3^1P state. The nature of this structure is not understood presently.

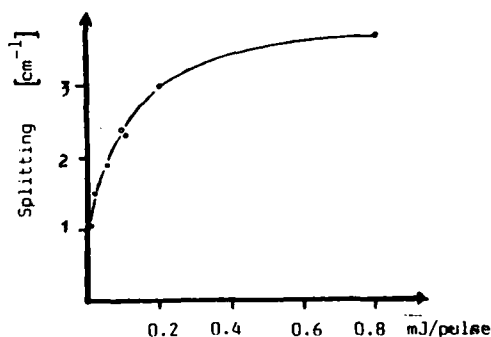


FIGURE 2 Intensity dependence of the splitting of the dipole resonance.

The quadrupole resonance appears at 504.35 nm as expected. The width of this resonance in Fig. 1 is limited by the laser bandwidth. The intensity of this resonance is remarkable high and of the same order of magnitude as the dipole resonance. Sharma, and Mathur¹, and Aymar, and Crance² calculated the generalized two photon ionisation cross section. Sharma and Marthur, who included the quadrupole contribution, predicted that the quadrupole resonance should be much smaller than the dipole resonance in contradiction to our experimental results. At high intensities the quadrupole resonance also exhibits a splitting but of much smaller width than the dipole resonance (Fig. 3).



FIGURE 3 Structure of the quadrupole resonance at a higher laser intensity.

References

1. M. Aymar, and M. Crance, J.Phys. B: Atom.Molec.Phys. 13 (1980) 2527
2. R.K. Sharma, and K.C. Marthur, Phys.Rev. A 20 (1979) 2241

STEPWISE MULTIPHOTON EXCITATION STUDIES OF AUTOIONIZING RYDBERG SERIES IN Mg

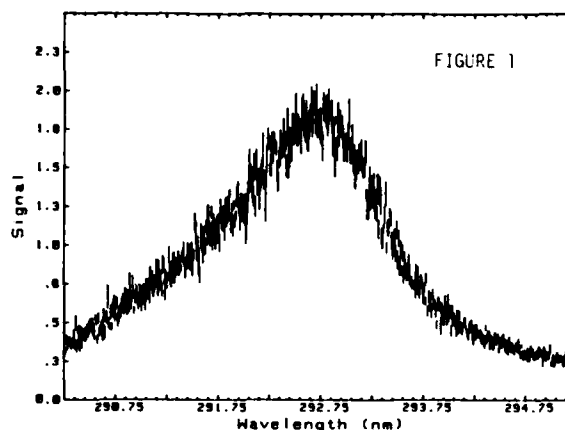
R.E. BONANNO, J.D. FASSETT, T.B. LUCATORTO, J.J. SNYDER, AND C.W. CLARK

NATIONAL BUREAU OF STANDARDS, GAITHERSBURG, MARYLAND 20899

Multiphoton excitation has been used to determine the energies and widths of autoionizing states of the type $3pn\ell$. For the lowest level of this kind, the $3p^2(^1S_0)$, a two-photon transition was utilized. For states $3pn\ell$ with $n \geq 8$ stepwise processes $3s^2 + 3sn_0\ell_0 + 3pn\ell$ were used.

Fig. 1 shows a scan of the $3p^2(^1S_0)$ level accessed by a single color two-photon process. The asymmetry of the profile is due to the fact that as the laser is scanned over the $\Gamma \sim 360 \text{ cm}^{-1}$ width of the $3p^2(^1S_0)$ resonance at $\sim 68300 \text{ cm}^{-1}$ the $3s3p(^1P_1)$ level at $35,051.3 \text{ cm}^{-1}$ provides a varying amount of near (single-photon) resonant enhancement to the $3s^2(^1S_0) + 3p^2(^1S_0)$ transition. Our initial measurements of the width and energy of this resonance agree well with the single previous measurement.¹ We believe our results represent the first observation of lineshape asymmetry due to off-resonance enhancement.

Fig. 2 shows a typical scan for transitions of the type $3s^2 + 3s25d + 3pnd$. In addition to the strong transitions at 280.3 nm and 279.5 nm associated with the $3s25d + 3p(^2P_{1/2})25d$ and $3s25d + 3p(^2P_{3/2})25d$ transitions respectively (spectator electron $\Delta n=0$ transitions), we easily observe series members between $3p18d$ and $3p34d$. This relatively wide distribution of differences between the principal quantum numbers for the "spectator" electron is a characteristic of the large difference in quantum defect² between the $3s$ and $3p$ series. By the systematic study of such spectra using several different intermediate states, we hope to provide an analytical extrapolation to the $3pns$ and $3pnd$ Rydberg series which should prove useful in calculations for dielectronic recombination of Mg^+ .

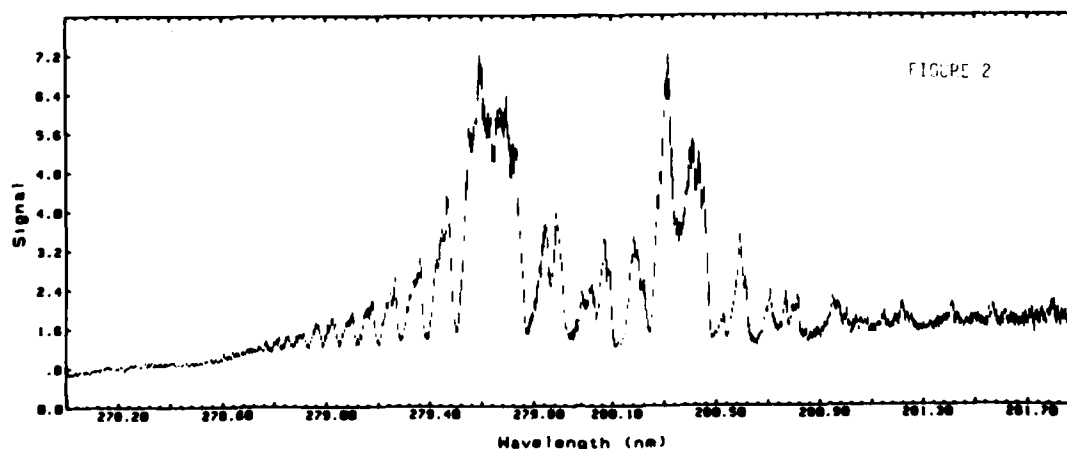


The data was taken by the technique of resonance ionization mass spectrometry (RIMS)³ in which laser-produced ions are mass analyzed and then detected with a particle multiplier/counter. The technique provides excellent sensitivity (an estimated 50% overall detection efficiency for ions produced by the laser) and a reliable measure of the total ionization efficiency of the selected species.

This work was supported by US DoE under contract DE-AI05-83, ER60185.

References

1. D.J. Bradley, C.H. Dugan, P. Ewart, and A.F. Purdie, Phys. Rev. A **13**, 1446 (1976).
2. S.A. Bhatti, C.L. Cromer, and W.E. Cooke, Phys. Rev. A **24**, 161 (1981).
3. J.D. Fasset, L.J. Moore, J.C. Travis, and F.E. Lytle, Anal. Chem. **55**, 765 (1983); C.W. Clark, J.D. Fasset, T.B. Lucatorto, L.J. Moore, and W.W. Smith, JUSA B **2** (in press 1985).



MULTIPHOTON STUDIES OF HIGHLY EXCITED STATES OF ATOMIC IODINE

S. T. Pratt, P. M. Dehmer, and J. L. Dehmer

Argonne National Laboratory, Argonne, Illinois 60439 U.S.A.

The development of high power tunable dye lasers has led to a dramatic increase in the study of high Rydberg states of atoms through the use of multiphoton and multistep excitation. Although the alkali and alkaline earth atoms have been explored in great detail using these techniques, other groups, such as the halogens, remain relatively unstudied. For this reason we have recently performed two different series of experiments using resonantly enhanced multiphoton ionization to study the high Rydberg states of atomic iodine. In the first experiments,¹ two photon excitation was used to access the odd parity, single photon forbidden, np and nf Rydberg states below the first ionization potential ($I^+ 3P_2$), while in the second experiments, two color excitation was used to access the even parity, single photon allowed manifold of autoionizing Rydberg states converging to the higher ionization potentials of iodine.

The experimental apparatus consists of a pulsed Nd:YAG pump laser, two dye lasers, a time-of-flight mass spectrometer, and an electrostatic energy analyzer; the latter was not used in the studies discussed here. Atomic iodine was produced by the photodissociation of methyl iodide, which is known to populate both the $I^+ 2P_{3/2}$ ground state and the $I^+ 2P_{1/2}$ excited state (7603.15 cm^{-1} above $2P_{3/2}$) in the wavelength region of interest (2900–2600 Å).

In the first experiment, a single laser was used both to photodissociate the methyl iodide and to probe the atomic iodine produced. The two photon resonant, three photon ionization spectrum was recorded by monitoring the I^+ ion signal as the laser wavelength was scanned. By focusing on two photon transitions from the $I^+ 2P_{1/2}$ excited state rather than those from the $2P_{3/2}$ ground state, it is possible to access the high lying Rydberg states of interest using wavelengths between 2680 Å and 2600 Å. These wavelengths are readily achieved by frequency doubling the dye laser in a KDP crystal. Using this technique, we have observed the odd parity ($3P_2$)np and nf Rydberg series to high n (> 30) for the first time. Because of the simplicity of this technique, it should be straightforward to extend this work to study the effects of external electric and magnetic fields on the high Rydberg states of atomic iodine.

In the second experiment, one laser is used to produce the atomic iodine and to pump it via two photon transitions to low lying np Rydberg states. The second laser is then used to probe transitions from these low lying states to high lying, even parity Rydberg states converging to the excited states of I^+ . These high lying Rydberg states will autoionize and the transitions are detected by monitoring the I^+ ion signal. For example, by pumping the two photon $2P_{1/2} + (1D_2) 6p[3]_{5/2}$ transition, and then probing single photon transitions from the $(1D_2) 6p[3]_{5/2}$ level to the region surrounding the $I^+ 1D_2$ threshold, we have observed $(1D_2)$ ns and nd Rydberg series up to $n > 30$. Although these Rydberg states do autoionize, the line widths are quite small and the peaks are symmetric, indicating a weak coupling to the continuum. By pumping the $(3P_2) 8p[1]_{1/2}$ transition and probing in the same region, one accesses a different set of $(1D_2)$ ns and nd states, due to the angular momentum selection rules. In this case, one of the series is quite broad and asymmetric, while others are again quite sharp. In some cases, the same final states can be accessed from two different pumped states, and in these instances, one expects to observe that the Beutler-Fano lineshape parameter, q, depends on the excitation pathway.²

This work was supported by the U.S. Department of Energy and the Office of Naval Research.

References

1. S. T. Pratt, Phys. Rev. A, submitted.
2. J. Ganz, M. Raab, H. Hotop, and J. Geiger, Phys. Rev. Lett. 53, 1547 (1984).

ELECTRON CORRELATION IN EXCITED VALENCE STATES OF BARIUM STUDIED BY RESONANT MPI

John E. Hunter III, James S. Keller, and R. Stephen Berry

Department of Chemistry and the James Franck Institute,
The University of Chicago, Chicago, Illinois 60637

Theoretical studies have shown that the low-lying, valence states of the alkaline earth atoms are likely candidates to show strong electron correlation,^{1,2} even to the extent that they may be described by molecule-like quantization (i.e. the rotation, bending, and stretching motions of a linear triatomic).^{1,3} We have used combined multiphoton ionization and photoelectron spectroscopy (MPI-PES) to investigate some of these states,^{4,5,6} with the ultimate goal of inferring as much as possible about the nature and degree of their electron correlation. Angular distributions of photoelectrons and branching ratios to different final ion core states have suggested collective motion of the valence electrons in several excited states of barium.

We collect electrons from a multiphoton ionization process resonant with the excited state of interest using several nitrogen-pumped dye lasers crossed with an atomic beam. Branching ratios to various states of the remaining ion are measured by time-of-flight resolution of the photoelectrons. Angular distributions of energy-resolved photoelectrons are obtained by synchronous rotation of the linear laser polarizations with respect to a fixed channeltron detector.

We present results on our studies of doubly-excited states of barium in which the two valence electrons have nearly equivalent principal quantum numbers. The states of the sp^2 configuration are of particular interest because of their connection to the molecular picture of electron correlation. In addition to the direct photoionization studies, we have collected angular distributions from the autoionization of the broad $sp^2^1S_0$ level. Measurements of angular distributions and branching ratios to different ion cores for the bound states are also reported.

1. J. L. Krause and R. S. Berry, *Phys. Rev. A* (in press).
2. P. F. O'Mahony and C. H. Greene, *Phys. Rev. A* **31**, 250 (1985), and references therein.
3. M. E. Kellman and D. R. Herrick, *Phys. Rev. A* **22**, 1536 (1980); D. R. Herrick and M. E. Kellman, *ibid.* **21**, 418 (1980).
4. O. C. Mullins, R.-I. Chien, J. E. Hunter III, J. S. Keller, and R. S. Berry, *Phys. Rev. A* **31**, 321 (1985).
5. O. C. Mullins, R.-I. Chien, J. E. Hunter III, D. K. Jordan, and R. S. Berry, *Phys. Rev. A* **31** (May 1985).
6. O. C. Mullins, J. E. Hunter III, J. S. Keller, and R. S. Berry, *Phys. Rev. Lett.* **54**, 410 (1985).

MICROWAVE IONIZATION OF Na RYDBERG ATOMS

H.B. van Linden van den Heuvell, J.L. Dexter and T.F. Gallagher

Department of Physics, University of Virginia, Charlottesville, VA 22901

Recently it has been observed that electric field ionization of Na by 15 GHz microwave fields exhibits a $1/3n^5$ scaling for $|m| = 0$ and 1 states,¹ and similar observations have been reported for He². This is substantially different from the $1/16n^4$ dependence observed for quasi static fields. On the other hand the $|m| = 2$ states exhibit a $1/9n^4$ dependence which is what would be expected for hydrogen in a static or microwave field. Between 15 GHz and the previous measurements done with fields of frequency ~ 1 MHz it is apparent that several changes occur in the dynamics of field ionization. In an attempt to explore this we have begun systematic measurements of the microwave ionization as a function of frequency by changing the frequency in octave steps. At 8 GHz we find that the Na $|m| = 0$ and 1 states for $16 < n < 40$ ionize at fields slightly higher than those required for 15 GHz, as would be predicted by a sideband picture recently advanced.³ Equally interesting though is the fact that a new mechanism of ionization of the $|m| = 2$ states has been observed which leads to ionization at a field of $1/21n^4$. Measurements of microwave ionization at 4 GHz are currently underway. This work has been supported by the Air Force Office of Scientific Research.

References

1. P. Pillet, W.W. Smith, R. Kachru, N.H. Tran and T.F. Gallagher, Phys. Rev. Lett. 50, 1042 (1983).
2. D.R. Marioni, W. van der Water, P.M. Kodo and T. Bergeman, Phys. Rev. Lett. 50, 1261 (1983).
3. H.B. van Linden van den Heuvell, R. Kachu, N.H. Tran, and T.F. Gallagher, Phys. Rev. Lett. 53, 1901 (1984).

QUANTUM REGULARITY IN THE CHAOTIC CLASSICAL STADIUM SYSTEM:
IMPLICATIONS FOR IONIZATION, SPECTROSCOPY, MULTIPHOTON PROCESSES AND REACTIONS

Bai, Yi Yan*, K. Stefanski** and H.S. Taylor#

*National Research Center for Science & Technology for Development, Beijing, China

**Institute of Physics, Nicholas Copernicus University, 87-100 Torun, Poland

#Department of Chemistry, University of Southern California, Los Angeles, CA 90089 USA

Classical mechanics is often used to model quantum processes such as ionization and collision phenomena. New phenomena such as chaotic diffusion ionization¹ (Ionization of highly excited hydrogen atom in strong microwave solids. Classically the electrons moves slowly, but chaotically out of the atom) have been predicted based on classical analysis² and computations¹. Surprisingly, at least at first thought, quantum mechanics showed no trace of such behavior³. Hence, the question arises as to when and why classical and quantum treatments will agree. The explanations of former years did not envision such distinction as regular (quasiperiodic) and irregular (chaotic) motion. Here, and in a paper on quantum stadium billiard problem⁴, an explanation shall be given as to why the quantum system exhibits both regular (localized) and irregular (delocalized) states while the classical system is always chaotic and delocalized. Implications for collision resonant complexes, spectroscopy and ionization will be discussed. Exactly the same mechanism of quantum localization found in the stadium is found by others⁵ to explain the spectra of hydrogen atom in very high magnetic fields. This mechanism is the Born-Oppenheimer adiabatic (BOA) approximation. What is new here that never plagued molecular problems is the problem of choosing the coordinates in which regular systems can be treated by quantum number assigning methods as BOA and self consistent field method. Assignment of quantum numbers is shown to explain the absence of chaos. For the Quantum Stadium the BOA supplies adiabatic invariants that causes the motion to be regular. In the classical case the BOA breaks down and chaos is found.

References

1. J.G. Leopold and I. Percival, Phys. Rev. Lett. 41, 944 (1978).
2. N.B. Delone, B.P. Krainov and P.L. Shepelansky, Usp. Fiz. Nauk 140, 355 (1983); Solv. Phys. Usp. 26, 551 (1983).
3. R. Blumel and U. Smilansky, Phys. Rev. A30, 1040 (1984) and references therein.
4. Y.Y. Bai, K. Stephanski and H.S. Taylor, Phys. Rev. A (1985) in press.
5. J.B. Delos, S.K. Knudson and D.W. Noid, Phys. Rev. Lett. 50, 579 (1983).

IONIZATION OF HIGH RYDBERG STATES OF HYDROGEN BY COMBINED AC AND DC ELECTRIC FIELDS

J. N. Bardsley, M. Comella and B. Sundaram

Department of Physics and Astronomy, University of Pittsburgh, Pittsburgh, PA 15260 USA

Bayfield and Pinnaduwa¹ have reported experiments in which hydrogen atoms in selected high Rydberg states at the edge of the Stark manifold interact with microwave radiation at frequencies between 6 and 9 GHz, for a period of approximately 0.4 μ s. The intensity of the radiation corresponds to a peak field strength of 8-25 V/cm. Changes in the principle quantum number n are monitored by the field-ionization technique. Separation of the states with the same value of n is achieved through laser excitation in a static electric field of strength 5-9 V/cm. Most of their data has been obtained for $n=60$ or 63. Classical theories of ionization suggest that states with $n > 70$ will be unstable for fields in the middle of this range. Ionization from states with $n \leq 60$ can thus be regarded as the consequence of a series of n -changing transitions.

We are engaged in quantum calculations to see whether this ionization results from a coherent multi-photon excitation or from the incoherent combination of several n -changing transitions in an almost random walk through phase space. Such stochastic motion has been studied in classical calculations but it has been suggested² that the onset of stochasticity occurs at higher field strengths in quantum mechanics than in classical mechanics and that the phase space diffusion may be slower.

Comparison of the Rabi flopping frequency associated with n -changing transitions and the orbital frequency of the Rydberg electron suggests the introduction of a reduced field strength $F_0 = n^5 F$, where F is measured in atomic units (51.4×10^8 V/cm.). For $F \ll 1$, transition strengths can be computed by standard multi-photon perturbation theory³ and the results are very sensitive to the frequency of the microwave radiation. Comparison between theory and experiment is possible for several resonances. The positions of the resonances are explained well by theory, but the computed values of their widths are smaller than the apparent experimental values⁴. The discrepancy could be due to the inadequacy of the perturbation theory, or could indicate that the observed peaks contain contributions from several Stark states.

Evaluation of the dipole matrix elements between states with neighboring values of n shows that extreme Stark states are coupled most strongly to other such states. Thus, as a first approximation, one can consider a single manifold of states that we call the extreme Stark ladder. When F_0 exceeds 1, perturbation theory

breaks down and alternative methods should be employed. The simplest technique involves the expansion of the time-dependent wave function in terms of the unperturbed eigenstates and the numerical integration of the coupled equations relating the expansion coefficients. The solution can best be expressed in terms of the time-development operator T that describes the propagation of the wave function through one period of the AC microwave field. Numerical integration is then required only over this relatively short time period and further propagation can be computed through matrix multiplication. The structure of this operator will be demonstrated in the poster presentation.

A third approach to a solution is through the direct numerical integration of the Schrodinger equation in parabolic coordinates. This approach provides a more complete treatment of the effects of the DC field but is most demanding of computer time. Results should be available at more moderate values of n , and the progress in developing special techniques for high n will also be reported.

This work was supported by the National Science Foundation.

References

1. J. E. Bayfield and L. Pinnaduwa, Phys. Rev. Lett. **54**, 313 (1985).
2. G. Casati, B. V. Chirikov and D. L. Shepelyansky, Phys. Rev. Lett. **53**, 2525 (1984).
3. W. J. Meath and E. A. Power, J. Phys. B **17**, 763 (1984).
4. J. N. Bardsley and B. Sundaram, submitted to Phys. Rev. Lett.

MANY-MODE FLOQUET THEORY AND SU(3) DYNAMICAL EVOLUTION OF
THREE-LEVEL SYSTEMS IN INTENSE BICHROMATIC FIELDS*

Shih-I Chu^{†§} and T. S. Ho

[†]Joint Institute for Laboratory Astrophysics, University of Colorado and
National Bureau of Standards, Boulder, Colorado 80309 USA

Department of Chemistry, University of Kansas, Lawrence, Kansas 66045 USA

The SU(3) dynamical evolution of three-level systems at two- and multiple-photon resonances induced by two strong linearly polarized monochromatic fields is studied exactly for the first time by means of the semiclassical many-mode Floquet theory (MMFT) recently developed by the authors.^{1,2} Within the rotating wave approximation (RWA), it has been recently shown by several workers³ that the eight-dimensional SU(3) coherent vector S characterizing the time-evolution of the three-level systems can be factored into three independent vectors of dimensions three, four, and one, at appropriate two-photon resonance conditions. In practice, however, if the laser-atom interactions occur away from the two-photon resonance, or if the RWA is not valid, or if damping mechanisms are included, this Gell-Mann type SU(3) dynamical symmetry will be broken. It is shown in this paper that instead of solving the time-dependent generalized Bloch equations, the SU(N) dynamical evolution of the (N^2-1) dimensional coherent vector S as well as various symmetry-breaking effects can be expediently studied by the use of the MMFT and expressed in terms of a few time-independent quasi-energy eigenvalues and eigenvectors. Furthermore, the generalized Van Vleck (GVV) nearly degenerate perturbation theory⁴ can be extended to an analytical treatment of the time-independent many-mode Floquet Hamiltonian. The general idea behind the MMFT-GVV technique is to block-diagonalize the Floquet Hamiltonian H_F so that the coupling between the model space and the remainder of the configuration space (called the external space) diminishes to a desired order. One important feature of the MMFT-GVV approach is that if the perturbed model space wave functions are exact to the n th order, the corresponding quasi-energy eigenvalues in the model space will be accurate to the $(2n+1)$ th order. In that regard, it is interesting to note that the RWA is merely the lowest order (i.e., $n = 0$) limit, namely,

model space wave functions correct only to the zeroth order and eigenvalues accurate to the first order. Furthermore, while the PWA can only deal with sequential one-photon processes, the MMFT-GVV approach is capable of treating both one-photon and multiphoton processes on an equal footing.

The MMFT-GVV method has been recently applied successfully to a unified treatment of both the SU(3) symmetries and symmetry-breaking effects of dissipationless three-level systems at two-photon resonances induced by intense bichromatic fields.⁵ The MMFT-GVV technique reduces the infinite-dimensional time-independent two-mode Floquet Hamiltonian to a three-by-three (model space) effective Hamiltonian, from which essential analytical properties and vivid geometry of the eight-dimensional coherence vector are revealed for the first time.⁵ Also to be presented are the new analysis of the SU(3) nonlinear dynamics and coherent population trapping phenomena of dissipative three-level systems using the newly developed nonHermitian MMFT-GVV formalism.⁶

*Work supported by DOE and ACS-PRF.

[§]JILA Visiting Fellow (1985). Permanent address: Dept. of Chemistry, University of Kansas, Lawrence, KS 66045.

References

1. T. S. Ho, S. I. Chu and J. V. Tietz, Chem. Phys. Lett. **96**, 464 (1983); T. S. Ho and S. I. Chu, J. Phys. B **17**, 2101 (1984); S. I. Chu and T. S. Ho, Israel J. Chem. **24**, 237 (1984).
2. S. I. Chu, Adv. At. Mol. Phys. **21**, xxxx (1985).
3. F. T. Hine and J. H. Eberly, Phys. Rev. A **25**, 2168 (1982); J. N. Fing, Phys. Lett. **80A**, 140 (1980).
4. R. Kirtman, J. Chem. Phys. **59**, 3890 (1968); P. D. Certain and J. O. Hirschfelder, J. Chem. Phys. **52**, 5977 (1970).
5. T. S. Ho and S. I. Chu, Phys. Rev. A, Feb. 1985.
6. T. S. Ho and S. I. Chu, Phys. Rev. A (accepted).

TRANSITION MATRIX METHOD FOR MULTIPHOTON IONIZATION PROCESSES

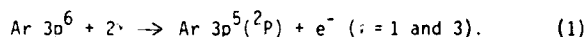
Anthony F. Starace* and Peter Zoller*

*Department of Physics and Astronomy, The University of Nebraska, Lincoln, NE 68588-0111 USA

*Institute for Theoretical Physics, University of Innsbruck, A-6020 Innsbruck, Austria

A transition matrix theory is developed to treat effects of electron correlations on two-photon ionization transitions in closed shell atoms and ions in the Random Phase Approximation (RPA). The theory extends the treatment of Chang and Fano¹ for single-photon ionization of closed shell atoms. The electromagnetic field interaction is treated in second order perturbation theory and electron correlations of the RPA type are included to infinite order. Ground and excited intermediate states are represented by a sum of configurations having a pair of virtually excited electrons in addition to the ground state or singly excited configurations. It is found that only one-particle functions, representing certain projections of excited two-particle wavefunctions, need to be calculated for the intermediate state in order to describe electron correlation in the RPA. The transition matrix equations for the unknown single particle functions in the intermediate and final states are derived using the graphical method of Starace and Shahabi². The summations over intermediate states, including the continuum, is represented by the solution of an inhomogeneous set of equations for the effective intermediate state by the well-known Dalgarno-Lewis method³. Solutions of the equations allow one to obtain non-resonant two-photon ionization cross sections, photoelectron angular distributions, etc.

Two photon ionization of argon, i.e.



will serve to illustrate the theory. We choose the following configurations for the final, intermediate, and initial states respectively:

$$|f\rangle = |3p^5 \text{ } ^f_1 L\rangle \quad (2a)$$

$$|i\rangle = |3p^5 \text{ } ^i_d 1P\rangle + |3p^5 \text{ } ^i_d \text{ } ^i_d 1P\rangle \quad (2b)$$

$$|i\rangle = |3p^6 \text{ } ^i_s\rangle + \sum_{L'S'} C(L'S') |3p^4(L'S') \text{ } ^i_d \text{ } ^i_d 1S\rangle \quad (2c)$$

The initial state correlation functions, ϕ_d^i , and coefficients, $C(L'S')$, can be calculated using the multiconfiguration Hartree-Fock code of Froese-Fischer⁴. The use of an average function, ϕ_d^i , instead of functions dependent on $L'S'$, has been found to be a good approximation⁵.

The dipole matrix element for process (1) is calculated from $\langle f|D|i\rangle$, where D is the electric dipole operator and $|i\rangle$ satisfies^{5,6}:

$$(E_i + \omega - H) |i\rangle = D|i\rangle, \quad (3)$$

where E_i is the initial state energy, ω is the photon energy, and H is the system Hamiltonian. The matrix element $\langle f|D|i\rangle$ depends on the unknown functions ϕ_d^f ($i = 1$ or 3), ϕ_d^i , and $\phi_d^i \langle \text{ } ^i_d \text{ } ^i_d \text{ } ^f \rangle$. In the simple representation of states in (2), ϕ_d^f is a HF continuum wave function and ϕ_d^i and $\phi_d^i \langle \text{ } ^i_d \text{ } ^i_d \text{ } ^f \rangle$ are obtained from a pair of uncoupled transition matrix¹ equations derived by integrating the commutator relation,

$$[H, |f\rangle \langle i|] = \omega |f\rangle \langle i| + |f\rangle \langle i| D, \quad (4)$$

over the $N-1$ coordinates of the non-interacting electrons.

References

1. T. N. Chang and U. Fano, Phys. Rev. A **13**, 263 (1976); Phys. Rev. A **13**, 282 (1976).
2. A. F. Starace and S. Shahabi, Phys. Rev. A **25**, 2135 (1982).
3. A. Dalgarno and J. T. Lewis, Proc. Roy. Soc. A **233**, 70 (1955).
4. C. Froese-Fischer, Comput. Phys. Commun. **4**, 107 (1972).
5. J. R. Swanson and L. Armstrong, Jr., Phys. Rev. A **15**, 661 (1977).
6. T. N. Chang and R. T. Poe, J. Phys. B **9**, L311 (1976).

EXCITED STATE PHOTOIONIZATION CROSS SECTION OF
Ne(ns') AUTOIONIZING RESONANCES

K.T. LU

Atomic and Plasma Radiation Division
National Bureau of Standards, Gaithersburg, MD 20899

The excited state photoionization process is a major energy transfer mechanism in laser isotope separation processes and gas laser discharge tubes. A recent investigation shows that the profiles of the Ne (ns', J=1) autoionizing resonances vary with the character of the Ne (2p⁵3p, J=1) state from which the resonance is excited whereas the resonance width is constant.¹ An analytic expression for this process is given here which accounts for all the observed features.

In contrast with the closed shell ground state of Ne, the excited p electron has alternative ways to couple with the doublet fine structure core 2p⁵(2p_{1/2,3/2}) to form two series with J=1. The channel interaction between these two series of Rydberg states has caused the two lowest 3p levels to depart from pure ¹P and ³D, LS coupled eigenstate.² The channel interaction between the two s-channels is also well known.³ Taking into account channel interactions in both lower and upper state, the photoionization cross section of the np to n's' transition can be expressed as,

$$\frac{df}{dE}(E) = 2(E-E_0) \left(\frac{d\tau}{dv_2} \right)_s \cdot$$

(1)

$$\frac{[I_1^{1/2} v_1^{3/2} \sin\pi(v_2 - \bar{v}_1) + I_2^{1/2} v_2^{3/2} \sin\pi(v_2 - \bar{v}_2) \left(\frac{d(-v_1)}{dv_2} \right)_{np}]^2}{[v_1^3 + v_2^3 \left(\frac{d(-v_1)}{dv_2} \right)_{np}]}$$

where $\left(\frac{d\tau}{dv_2} \right)_s$ and $\left(\frac{d(-v_1)}{dv_2} \right)_{np}$ represent the slope of the eigenphase shift for s' autoionizing resonances and slope of the quantum defect for p-channels respectively. The eigenphase shift π representing the electron-ion short range scattering effect is extracted from the discrete energy levels of the s-series.⁴ The slope of the eigenphase shift π at the position of the resonance measures the width Γ of the resonance profile. v_1 and v_2 are effective quantum numbers relative to the ionization limits 2p⁵(2p_{3/2}) and 2p⁵(2p_{1/2}), respectively. I_1 and I_2 are intensity factors independent of energy. The values \bar{v}_1 and \bar{v}_2 determine that effective quantum number v_2 where the oscillator strength is zero. Equation (1) has a

general feature: the effect of final state channel interaction is factored out in terms of the slope of the phase shift $\left(\frac{d\tau}{dv_2} \right)_s$ which measures the width of the resonance, and is independent of the properties of the lower state. It has the following special consequences: If the autoionizing state is excited from a pure singlet state only the singlet final state is excited, since transition to a triplet state is forbidden. This corresponds to $\left(\frac{d(-v_1)}{dv_2} \right)_p \gg 1$,

$$\text{Equation (1) simplifies to}$$

$$\frac{df}{dE}(E) \approx 2(E-E_0) \left(\frac{d\tau}{dv_2} \right)_s I_2 \sin^2\pi(v_2 - \bar{v}_2)$$

We expect an autoionizing profile with zero oscillator strength at $v_2 = 1 - \mu_{p1}$, where μ_{p1} is the quantum defect of the ¹P, and a broad wing extending to the blue. If the lower level is a triplet state, then triplet state is excited. This corresponds to $\left(\frac{d(-v_1)}{dv_2} \right)_p \approx 0$ in Equation (1). Zero oscillator strength is now expected at $v_2 = 1 - \mu_{p2}$ and a broad wing to extend to the red. If the exciting level has a mixed singlet-triplet character, both terms in Equation (1) are important. We then expect the profile to depart from the above special cases, which is in agreement with the observations.¹

The excited state dynamics of the electron-ion system described by Equation (1) is expressed in terms of quantum defect parameters, the eigen quantum defect μ_α , the mixing angle θ , and the dipole transition amplitude U_α . These parameters are known for both upper s- and lower p-channels.^{2,3} Therefore, the whole sequence of n's' autoionizing resonance with varying lower state np can be evaluated. A detailed comparison with data is subjected to further experimental measurements.

References

1. J. Ganz, M. Raab, H. Hotop, and J. Geiger, Phys. Rev. Lett. **53**, 1547 (1984).
2. A. F. Starace, J. Phys. **B6**, 76 (1973).
3. K. T. Lu and M. Mansfield, "Electron and Photon Interaction with Atoms," ed. H. Kleinpoppen and M. R. G. McDowell, Plenum, N.Y., 1975, p. 627.
4. K. T. Lu, Phys. Rev. **A4**, 579 (1971).

THEORY OF MULTIPHOTON IONIZATION AND AUTOIONIZATION OF Xe*

Pradip Gangopadhyay, Xian Tang, P. Lambropoulos and R. Shakeshaft

Department of Physics, University of Southern California, Los Angeles, CA 90089-0484

Experiments¹⁻⁵ on multiphoton ionization of rare gases, especially under large laser intensities, have generated a wealth of data on various aspects of the process. Xe in particular has received considerable attention in studies of multiphoton ionization^{1,2}, multiple-multiphoton ionization, as well as above threshold ionization.^{3,4,5} Yet the theory of these processes in rare gases other than He is virtually non-existent. In fact, except for an early calculation⁶ of 2-photon ionization of Ar, to our knowledge, there are no calculations on these processes.

In view of the experimental interest in these atoms, we have undertaken a systematic theoretical study of multiphoton processes in rare gases beginning with Xe and Kr. We have formulated at first 2- to 4-photon ionization of these atoms, including the region of autoionization that is known to exist between the two thresholds. The objective is to calculate multiphoton ionization, autoionization, photoelectron angular distributions, double ionization, as well as wave-mixing. Particular attention is to be paid to transitions involving the ns^2 subshell below the outer np^6 subshell. Experiments by Rhodes et al.⁷ have shown that such transitions play a significant role in multiple ionization as well as wave-mixing.

In this paper we present results on Xe. The calculation is based on multichannel quantum defect theory as employed by Lu⁸ in the analysis of Xe. We obtain wavefunctions by using the Lu-Fano plots. The summations over intermediate states are for the moment performed by truncating the series. As of the writing of this abstract, we have obtained 3-photon ionization cross sections through and including the autoionizing region. The total generalized cross section has been found to be in the range of 10^{-80} to 10^{-79} cm² sec². Substantial structure has been found between the $P_{3/2}$ and $P_{1/2}$ thresholds. Autoionizing peaks show certain

periodicity whose origin can be traced to the structure of the Lu-Fano plots. Many of these peaks are quite narrow, and it is doubtful that they would have been seen in single-photon ionization experiments.⁹ Our calculation includes $J=3$ states and resonances, but so far we have found that they are dominated by the $J=1$. We do not expect this to be a general feature of this process in Xe but rather a circumstantial result due to the energy and frequency range of our calculation up to this point. Angular distributions of the photoelectrons as well as 4-photon transitions, including one above threshold, will be reported.

From the results of our calculations so far, it is clear that detailed experiments are necessary as further guidance for the theory of these complex processes in such complicated systems.

References

*Work supported by NSF Grants PHY-8306263 and PHY-8119010.

1. A. L'Huillier, L-A Lompre', G. Mainfray and C. Manus, Phys. Rev. A27, 2503 (1983).
2. T. S. Luk, H. Pummer, K. Boyer, M. Shahidi, H. Egger and C. K. Rhodes, Phys. Rev. Lett. 51, 110 (1983).
3. F. Fabre, P. Agostini and G. Petite, Phys. Rev. A27, 1682 (1983).
4. P. Kruit, J. Kimman, H. G. Muller and M. J. Van der Wiel, Phys. Rev. A28, 248 (1983).
5. R. Hippler, H-J Humpert, H. Schwier, S. Jetzke and H. O. Lutz, J. Phys. B L713 (1983).
6. M. S. Pindzola and H. P. Kelly, Phys. Rev. A11, 1543 (1975).
7. K. Boyer, H. Egger, T. S. Luk, H. Pummer and C. K. Rhodes, JOSA B, 1, 3 (1984); also private communication.
8. K. T. Lu, Phys. Rev. A4, 579 (1971).
9. U. Heinzmann, J. Phys. B13, 4353 (1980); ibid 13, 4367 (1980).

AN L^2 QUANTUM-DEFECT TREATMENT OF MULTIPHOTON IONIZATION

John T. Broad

Fakultät für Chemie, Universität Bielefeld, D4800 Bielefeld, FRG

Introduction

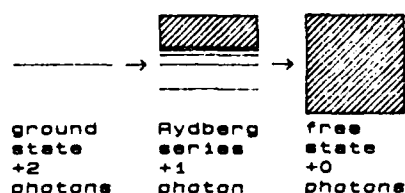
Recent experiments¹ measuring multiphoton ionization of atoms demand a theoretical interpretation more sophisticated than can be provided by simple traditional perturbation theory. While the very existence of off-resonant and free-free transitions indicate a strong perturbation of the atom at high laser intensities, a correct treatment of the field broadening and shifting of near-resonant transitions through Rydberg states already requires a non-perturbative approach even at moderate field strengths. Here we present a Floquet formulation using a special L^2 basis for the radial electronic degree of freedom to generate an efficient algorithm for computing multiphoton ionization of atoms.

Floquet Formalism²

By including the photon number operator, N , the total Hamiltonian for an atom in a field of a single frequency,

$$H = H_{\text{atom}} + N\omega + \vec{A} \cdot \vec{p} + A^2$$

becomes time-independent to allow evaluating the time evolution of an atomic bound state hit by the laser at $t = 0$ as the Laplace transform of the time-independent resolvent of H . In this dressed state picture in a Hilbert space spanned by products of atomic with photon number states, the ionization process can be pictured as:



which closely resembles the traditional description of the autoionization of a Rydberg state perturbed by a single interloper, albeit with the especially long-ranged dipole coupling. The +2, +1 and 0 in the figure designate photon number differences from the well defined and large average photon number of the coherent field. To achieve accurate results, we included photon number one higher and one lower to account for the Stark shifts of the states of interest.

 L^2 -Basis Expansion

As reported in the perturbation calculation of Ref.3 representing the Coulomb spectrum analytically in a special Laguerre-Slater L^2 basis allows efficient extrapolation to completeness of free-free transitions as well as economical expansion of the bound states. Moreover, the Pade-approximant extrapolation used defines an analytic continuation to slightly negative energies to reveal the quantum-defect perturbation of the Rydberg states caused by the $\vec{A} \cdot \vec{p}$ part of H . This means that the broadening of the Rydberg series into a quasi-continuum is caused solely by the Rabi oscillations to the ground state and not by ionization.

Results

Test results are presented for the two-photon ionization of a one-electron atom near the threshold for single-photon ionization. Extension to many-electron atoms by representing the bound states of interest of the ionic core in a Slater basis is conceptually straightforward.

References

1. P. Kruit, J. Kimman, H.G. Muller and M.J. Van der Wiel, Phys. Rev. A 28, 248 (1983).
2. A. Maquet, S-I. Chu and W.P. Reinhardt, Phys. Rev. A 27, 2946 (1983).
3. J.T. Broad, to appear in Phys. Rev. A 31, (1985).

SCATTERING AMPLITUDES BY MEANS OF THE COMPLEX COORDINATE METHOD.
COMPTON SCATTERING AND TWO-PHOTON IONIZATION

Piotr Froelich

Department of Quantum Chemistry, Uppsala University, Box 518, S-75120 Uppsala, Sweden

The serious problem of theoretical spectroscopy is that the cross sections are based on the expressions of the formal scattering theory, which are highly singular and computationally untractable. The present work explores a way to harness the singular nature of these expressions, and to give them an explicit and computationally tractable meaning.

The inelastic scattering of photons and electrons on atomic targets is conveniently characterized in terms of the so called Bethe surface /1/, which gives the dependence of the cross section on energy and momentum transfers.

We report the possibility of calculating the (first-order) Bethe surfaces and/or higher order scattering amplitudes, by a method based on the L^2 discretization of the continuum, implemented within the complex coordinate method (CCM) /2/, and without explicit calculation of the final continuum states.

The (first order) transition amplitude controlling the Bethe surface (here for Compton scattering) is calculated as /3/:

$$|T_{fc}^{(1)}(\bar{k}, E; \theta)|^2 = \frac{1}{\Gamma_m} \sum_i \frac{\langle \psi_i^0 | Q(\bar{k}, \theta) | \psi_i^0 \rangle \langle \psi_i^0 | Q(\bar{k}, \theta) | \psi_c^0 \rangle}{E_i - E_c - E}$$

with $Q(\bar{k}) = e^{i\bar{k}\bar{r}}$, $\bar{k} = \bar{k}_1 - \bar{k}_2$, $E = M\omega_1 - M\omega_2$, θ = dilation angle.

The second order transition amplitude (here for two-photon ionization) is calculated as /4/:

$$|T_{fc}^{(2)}(\omega, \theta)|^2 = \frac{1}{\Gamma_m} \sum_{i,j,k} \frac{\langle \psi_i^0 | V_A(\theta) | \psi_i^0 \rangle \langle \psi_i^0 | V_A(\theta) | \psi_j^0 \rangle \langle \psi_j^0 | V_A(\theta) | \psi_k^0 \rangle \langle \psi_k^0 | V_A(\theta) | \psi_c^0 \rangle}{(E_i - E_c - \hbar\omega)(E_j - E_c - 2\hbar\omega)(E_k - E_c - \hbar\omega)}$$

with V_A being the dipole operator. In both cases only the

ground state and square integrable functions are used. The CCM facilitates the infinite summation/integration over intermediate states, and the numerical effort is reduced to diagonalization of the matrix representing the complex dilated Hamiltonian of the target:

$$H(\theta)c_i = E_i c_i, \quad \psi_i = \hbar c_i; \quad E_i - \text{complex}$$

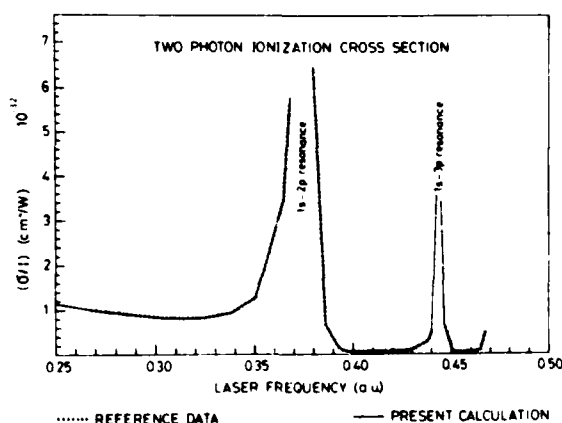
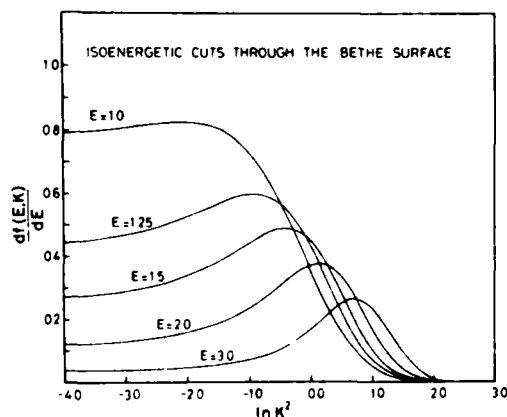
Test calculations employing the hydrogenic target are presented below. The isoenergetic cuts through the Bethe surface for Compton scattering reveal the Bethe ridge (and, consequently, the Compton profile). One can also study the Compton defect - deviations of the position and shape of this profile with respect to predictions of the sudden-impulse approximation. Such deviations are significant at low energy transfers, and close to the ionization threshold ($E=1.0$ Ry) the Compton peak ceases to exist.

The two-photon ionization spectrum shows very good agreement with the exact analytical /5/ and Floquet /6/ calculations, and is extended to the near-threshold region, where the exact results have not been reported.

The present approach is very straightforward, yet it gives the beyond sudden-impulse approximation results in a non-analytical way, by an atomic structure calculation which is applicable to many-electron atoms.

References

1. see e.g. M.Inokuti, Rev.Mod.Phys. **43**, 297 (1971)
2. see e.g. W.P.Reinhardt, Ann.Rev.Phys. **33**, 223 (1982) and the references therein.
3. P.Froelich, A.Flores-Riveros and W.Weyrich, to appear in J.Chem.Phys.
4. P.Froelich and A.Flores-Riveros, subm. for publ.
5. F.T. Chan and C.L.Tang, Phys.Rev. **185**, 42 (1969)
6. B.R.Johnson and W.P.Reinhardt, Phys.Rev. **28**, 1930 (1983)



THEORY OF FREQUENCY CONVERSION BY MULTIWAVE RAMAN PROPAGATION*

A. P. Hickman*, J. A. Paisner⁺, and W. K. Bischel*

*Chemical Physics Laboratory, SRI International, Menlo Park, California 94025 USA

⁺Lawrence Livermore Laboratory, Livermore, CA 94450 USA

The propagation through a Raman medium of a pulse with several frequency components $\omega_n = \omega_0 + n\omega_R$, where ω_0 is the initial laser frequency, and ω_R is the frequency of the Raman transition of the molecules of the medium, is a complicated process. A complete theory must simultaneously treat the pulse propagation with Maxwell's wave equation, and the two-photon induced molecular transitions with Schrodinger's equation. Recent experiments have demonstrated the practical value of the process as a means for frequency conversion. Efficient conversion has been observed in H_2 into modes as high as $k=8$. However, existing theoretical models predict a conversion efficiency several orders of magnitude too low. We have developed a theory that includes the full nonlinear response of the (two-state) molecules, and present preliminary results that exhibit very high conversion efficiencies.

We consider the one dimensional Maxwell's wave equation for an electric field of the form

$$E(z,t) = \frac{1}{2} \sum_n E_n(z,t) e^{i\omega_n(t - z/c)} + c.c. \quad (1)$$

The field amplitudes E_n satisfy^{1,2}

$$\frac{\partial E_n}{\partial z} = \frac{4\pi\alpha_{12}}{c} \omega_n [\beta E_{k+1} - \beta^* E_{n-1}] \quad (2)$$

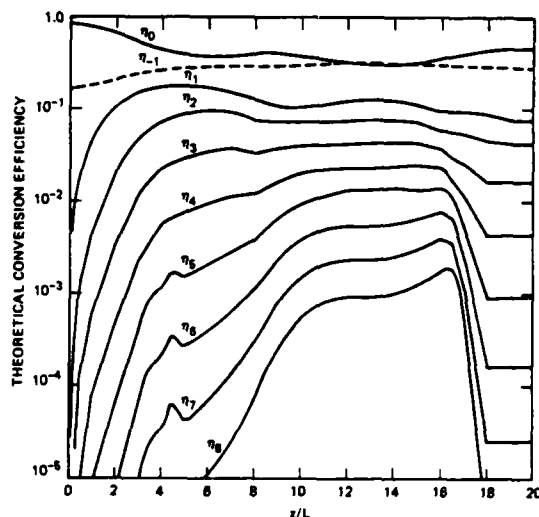
where α_{12} is the transition polarizability (assumed independent of frequency), ρ is the number density, β is related to the components (u,v,w) of the Bloch vector by $\beta = e^{-i\theta} (v-iu)/2$, where θ is defined below, and the time t is replaced by the retarded time $\tau = t - z/c$. The Bloch equations may be formulated using a two-photon Rabi frequency

$$Q(z,t) e^{i\theta(z,t)} = (\alpha_{12}/\hbar) \sum_n E_n E_{n-1}^* \quad (3)$$

that satisfies

$$\frac{\partial}{\partial z} (Q e^{i\theta}) = -\frac{1}{L} [F(\tau)^2 + Q(z,\tau)^2]^{1/2} \beta(z,\tau) \quad (4)$$

where the characteristic length $L = c/(4\pi\alpha_{12}\rho\omega_R)$, and $F(\tau)$ is determined from the initial conditions. Eimerl et al.¹ used a perturbation solution for β . We have obtained fully numerical solutions, and present in the figure the results of a preliminary calculation.

FIGURE 1 RAMAN FREQUENCY CONVERSION IN H_2

The initial conditions of the pulse are as follows: 5 mJ in the pump laser and 1 mJ in the first Stokes are focussed to a beam area of 10^{-4} cm^2 . The FWHM of the pump is 4 nsec; the FWHM of the Stokes is 2 nsec, and the Stokes pulse is displaced 2 nsec from the pump toward the leading edge of the pulse. This results in a 4.32π pulse. The Stark shift is included, and relaxation times are assumed to be long compared to the pulse length. We have calculated the fraction of the total initial energy that is converted to several higher order modes as a function of the distance of propagation of the pulse in units of the characteristic distance L , which is approximately 1.1 cm divided by the density in amagats ($1 \text{ amagat} = 2.7 \times 10^{19} \text{ cm}^{-3}$).

References

1. D. Eimerl et al., Phys. Rev. Lett. **46**, 651 (1981).
2. J. R. Ackerhalt, Phys. Rev. Lett., **46**, 922 (1981).

*Supported by NSF Engineering Grant ESC-8213373.

BISTABLE AND CHAOTIC BEHAVIOR OF DRIVEN MOLECULAR SYSTEMS

Jian-Min Yuan, Mingwei Tung and George C. Lie*

Department of Physics, Drexel University, Philadelphia, PA 19104, U.S.A.

*On leave from Chemistry Department, National Tsing Hua University, Taiwan, R.O.C.

A diatomic molecule in dense medium is shown to exhibit bistable and chaotic behavior when driven by an IR laser field. Two models have been analyzed for such behavior: A classical Morse oscillator and a quantum an-harmonic oscillator. The third model of a quantum Morse oscillator based on an $SU(2)$ algebra is being investigated. We discuss each of these models below.

For a damping constant and driven field amplitude simulating an H₂ gas irradiated by an IR laser under a high pressure condition, we show by solving the classical equation for a Morse oscillator¹, that bistability exists for a large range of driven frequency. For a larger damping constant simulating, for example, an ad-molecule on a solid surface. We have determined the bistable domain as a function of field frequency and amplitude. Periodic solutions have been found for both the upper and lower branches and their relative stabilities determined by calculating the Lyapunov exponents. Solutions of both branches go through an infinite sequence of period-doubling bifurcations leading to chaotic behavior as we vary the driven frequency gradually.

The two chaotic regions do not occur in the same frequency range.

Similar bistable behavior has been found in analyzing a quantum statistical model of an anharmonic oscillator in contact with a reservoir^{2,3}. But in this model both the upper and lower branches are stable. When an amplitude modulation of the driven field is introduced, the periodic solution of the upper branch goes through a sequence of period-doubling bifurcations leading to chaos as the modulation frequency varies. We have determined the bifurcation diagrams for this branch and calculated the Lyapunov exponents for this sequence. A strange attractor in the chaotic domain has been examined by taking Poincare surfaces of section on a series of 12 cutting planes.⁴

In order to answer the question whether a quantum Morse oscillator behaves differently from a corresponding classical one, we have carried out a study of a quantum Morse oscillator in contact with a reservoir. The hamiltonian of a Morse oscillator can be expressed in terms of generators of an $SU(2)$ algebra.⁵ The reservoir is modelled by a bath of harmonic oscillators. Its dissipative contributions to the Morse oscillator have been derived and expressed as irreversible terms in a Liouville-von Neumann equation.⁶ Dynamical behavior of such a driven damped system is under

investigation.

Reference

1. G.C. Lie and J.M. Yuan, unpublished
2. J.M. Yuan, E. Liu, and M. Tung, J. Chem. Phys. **79**, 5034 (1983).
3. E. Liu and J.M. Yuan, Phys. Rev. **A29**, 2257 (1984).
4. J.M. Yuan, E. Liu and Y. Gu, unpublished
5. R.D. Levine, Chem. Phys. Lett. **95**, 87 (1983).
6. M. Tung, E. Eschenazi, and J.M. Yuan, Chem. Phys. Lett. to appear

PHOTOABSORPTION OF EXCITED MOLECULES : MANIFESTATIONS OF COOPER MINIMA IN THE SPECTROSCOPY OF RYDBERG STATES

F. Masnou-Seeuws* and Ch. Jungen*

*Laboratoire des Collisions Atomiques et Moléculaires, Bât. 351, Université Paris-Sud, 91405 ORSAY Cedex FRANCE
+Laboratoire de Photophysique Moléculaire du CNRS, Bât. 210, Université Paris-Sud, 91405 ORSAY Cedex FRANCE

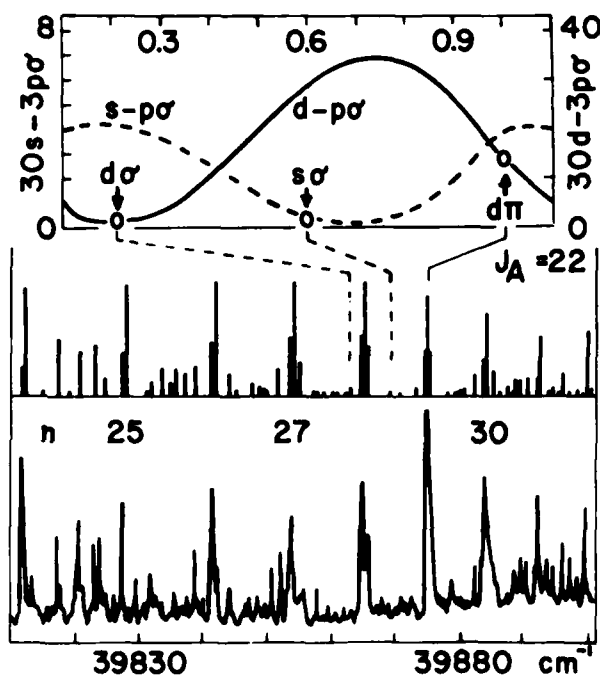
The existence of zeros of dipole matrix elements, known as Cooper minima, is well-known from photoionization of atoms.¹ The conditions for their appearance are quite restrictive for ground state atoms but much less so for atoms or molecules which have been prepared in an excited state.² In many current experiments molecular Rydberg states near threshold are excited by optical-optical double resonance, in a two-step excitation process via a low Rydberg state. Examples include the NO, Na₂, Li₂ and H₂ molecules.³⁻⁶ We have initiated a theoretical study of the Rydberg-Rydberg dipole transition moments in order to ascertain whether some of the unexpected observed features could be traced back to strong energy variations, and in particular to the occurrence of zeros in the relevant dipole amplitudes.

The manifestations of Cooper minima in molecular Rydberg spectra are not obvious because of the high number of Rydberg channels and since nuclear and electronic motion are strongly coupled. The interpretation of such spectra is best handled by multichannel quantum defect theory (MQDT)⁷, a key element of which is the description of the radial motion of the Rydberg electron outside the core in terms of phase-shifted Coulomb wavefunctions. In the spirit of Bates and Damgaard⁸ we evaluate the dipole amplitudes between Rydberg states numerically in terms of the same phase-shifted Coulomb functions which underlie the quantum defect treatment.

As an example we present the calculation of the transition moments corresponding to excitation of high Rydberg levels $ns\sigma$, $nd\sigma$, $nd\pi$, $nd\delta$ ($n > 10$) of Na₂. Labastie et al.⁴ have studied these states experimentally by pumping the $3p\sigma$ A state of Na₂. They observed the appearance of striking "fringes" which stand out from the otherwise blurred Rydberg pattern at regular intervals. While the fringe effect could be accounted for readily within the existing MQDT framework, it required the assumption of substantially reduced dipole transitions $ns\sigma-3p\sigma$ and $nd\sigma-3p\sigma$ as compared to $nd\pi-3p\sigma$.⁴

Fig. 1 demonstrates that the fringe effect is indeed related to a minimum in the $s\sigma$ and $d\sigma$ excitations. At the top are plotted the squared radial dipole integrals involving ns and nd states as functions of the quantum defects. The observed quantum defects from Ref. 4 are indicated by arrows: it can be seen that $s\sigma$ and $d\sigma$ fall near a minimum while $d\pi$ does not. At the bottom is shown a section of the observed spectrum corresponding to the

first fringe, together with rotational line intensities calculated by MQDT: the spectral concentration of intensity owing to absence of s and d lines is evident. We expect to show that Cooper minima are at the basis of a variety of phenomena observed in molecular multi-photon spectra.



References

1. U. Fano and J.W. Cooper, Rev. Mod. Phys. **40**, 441 (1968) and references therein.
2. A.Z. Msezane and S.T. Manson, Phys. Rev. Lett. **48**, 473 (1982).
3. M. Seaver, W.A. Chupka, S.D. Colson and D. Gauyacq, J. Phys. Chem. **87**, 2226 (1983).
4. P. Labastie, M.C. Bortas, B. Tribollet and M. Broyer, Phys. Rev. Lett. **52**, 1681 (1984).
5. D. Eisel, W. Demtröder, W. Müller and P. Botschwina, Chem. Phys. **80**, 329 (1983).
6. S.T. Pratt, P.M. Dehmer and J.L. Dehmer, Chem. Phys. Lett. **105**, 28 (1984).
7. M.J. Seaton, Rep. Prog. Phys. **46**, 167 (1983).
8. D.R. Bates and A. Damgaard, Phil. Trans. Roy. Soc. London **A242**, 101 (1949).

ROTATIONALLY RESOLVED THREE-PHOTON IONISATION OF Bi_2 STUDIED IN THE GASPHASE AND IN A MOLECULAR BEAM

B. Bühler, C. Cremer, G. Gerber, J. Janes

Fakultät für Physik, Universität Freiburg, F.R.G.

Multiphoton excitation and ionization is used to study atomic and molecular bismuth in the gas phase and in a molecular beam. Pulsed dye-lasers pumped by 3 ns pulses of a N_2 -laser are employed for the experiments. Survey spectra are obtained with a grazing incidence type dye-laser of $0.1\text{--}0.2\text{cm}^{-1}$ bandwidth while for high resolution studies an oscillator-amplifier dye-laser system with 0.01cm^{-1} bandwidth is used. The different processes are detected by measuring the fluorescence from excited states and the ionization signal with a thermionic diode in the gas phase experiments or by measuring the mass-selected ion signal with the Time-of-Flight method in a molecular beam.

The analysis of Rydberg series of Bi , excited by two-photon dissociation of Bi_2 followed by one-photon excitation, gives an improved value for the atomic ionization energy of $E=58761.7 \pm 0.1\text{cm}^{-1}$ (1).

A lower threshold energy for the dissociative ionization of Bi_2 is determined from wavelengths dependent three- and four-photon ionization spectra of Bi^+ and Bi_2^+ (2).

The ionization of Bi_2 is studied by various one colour and two colour multiphoton experiments. In these experiments we observed an interesting three-photon ionization process where we were able to resolve the rotational structure in the ion signal from the band head up to $J=200$ as shown in fig.1. For this specific ionization process we find a remarkable difference in the ionization probability for $P(\Delta J=-1)$ and $R(\Delta J=+1)$ transitions involving higher J values. Figs.2a and 2b show high resolution scans of parts of the ionization spectrum. The P and R lines overlapping in the region of the band head are completely resolved for higher J . Their intensities are comparable up to $J=80$. But for even

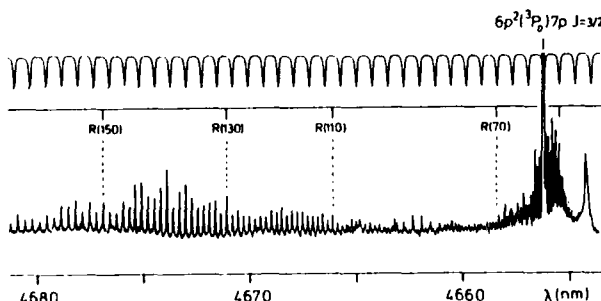


Fig.1 Three-photon ionization spectrum of Bi_2

higher J the P line intensity slowly decreases while the R line intensity increases until the R line is about ten times more intense than the P line. This is shown in fig.2b. The analysis of the energies of the resolved rotational lines show that they belong to the $v'=37-v''=4$ band of the $A(^3\Pi_0)-X(^1\Sigma_g^-)$ transition of Bi_2 and that they represent the first excitation step as shown in fig.3. The ionization process involving this excitation step proceeds via a two-photon transition from the $A(^3\Pi_0)$ state to the $4p^2(^3P_2)$ ground state of Bi_2^+ . The rotational levels of an excited electronic state $^3\Pi_0$ are energetically close to the virtual intermediate states. The relative change of P and R line intensities is therefore mainly due to the varying energy defect $\Delta\omega$ in the two-photon transition matrix element since the K -dependent splitting of rotational levels F_1 and F_2 (of $^3\Pi_0$) change in a manner that $\Delta\omega$ gets larger for P transitions while $\Delta\omega$ is reduced for R transitions. The relative intensities further depend on the different rotational line strengths for P and R transitions between a $^3\Pi_0$ -state and a $^3\Pi_0$ -state (3).

The ionization energy of Bi_2 determined from multiphoton experiments is $E=59500 \pm 200\text{cm}^{-1}$.

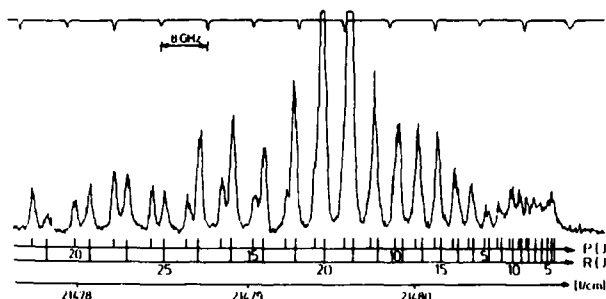


Fig.2a Rotational resolved band head of the $v'=37-v''=4$ transition of Bi_2 (A-X)

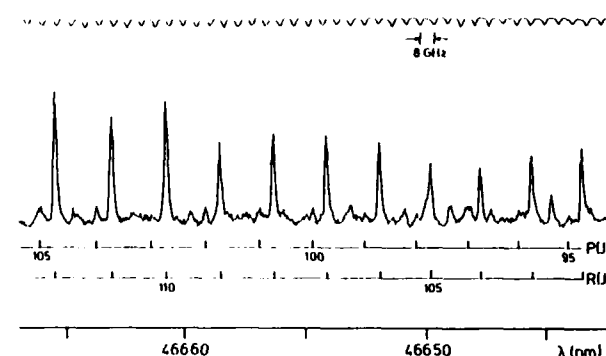


Fig.2b Part of the ionization spectrum showing strongly different P and R intensities

References

1. B. Bühler, C. Cremer, G. Gerber, Z. Phys. A320 (1985) 71
2. B. Bühler, C. Cremer, J. Janes and G. Gerber Ber. Bunsenges. Phys. Chem. 88 (1985) 00
3. I. Kovacs, Rotational Structure in the Spectra of Diatomic Molecules (Hilger, London 1969)

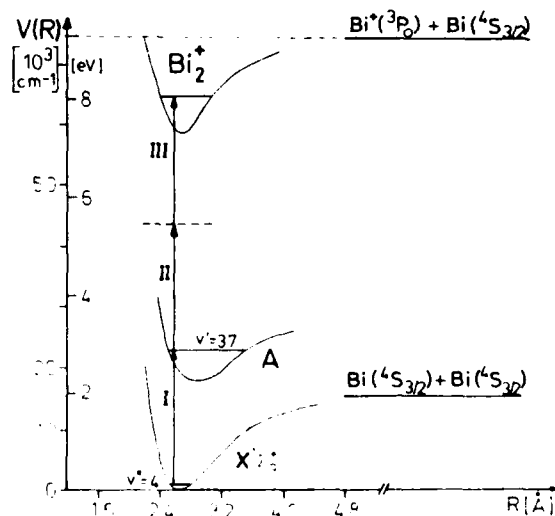


Fig.3 Schematic potential curve diagram for the three-photon ionization process in Bi_2

RESONANTLY ENHANCED MULTIPHOTON IONIZATION AND PHOTOELECTRON SPECTROSCOPY
OF NeXe, ArXe, KrXe, AND Xe₂

P. M. Dehmer, J. L. Dehmer, and S. T. Pratt

Argonne National Laboratory, Argonne, Illinois 60439 U.S.A.

Resonantly enhanced multiphoton ionization (REMPI) spectra of NeXe, ArXe, KrXe, and Xe₂ were obtained in the wavelength region corresponding to two photon transitions from the atomic Xe ground state to the Xe* 5d and 6p states. The spectra were obtained using an apparatus that combines an unskipped, cw supersonic molecular beam source with both a time-of-flight mass spectrometer and an electrostatic electron energy analyzer. Several new progressions of vibronic bands were observed for all four rare gas van der Waals molecules. These bands arise from two photon, bound-bound transitions from a ground electronic state to various resonant intermediate levels, and are detected by single photon ionization of the excited state. Because two photon transitions from the ground state of Xe₂ access states of gerade symmetry, none of the homonuclear bands have been observed in earlier single photon absorption studies, although a small number of the heteronuclear dimer bands were observed previously by Castex.¹ The KrXe bands observed to the red of the atomic Xe 6p[5/2]₂ transition are shown in Figure 1.

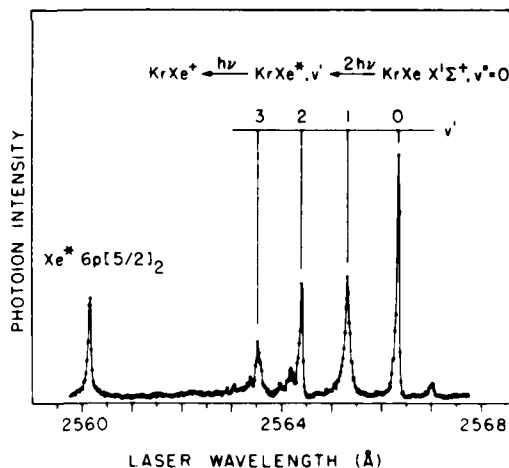


FIGURE 1. The two photon resonant, three photon ionization spectrum of KrXe.

We have also obtained the photoelectron spectra (PES) of ArXe, KrXe, and Xe₂ without interference from either atomic or (in the case of the heteronuclear dimers) homonuclear dimer photoelectron peaks by using REMPI to selectively ionize the van der Waals molecule of interest. The photoelectron spectra of ArXe and KrXe are the first such spectra of a heteronuclear rare gas dimer obtained by any technique. The REMPI-PES of KrXe obtained at the wavelength of the (0,0) band in Figure 1

is shown in Figure 2. The REMPI-PES of Xe₂ were recorded at a number of wavelengths and the relative

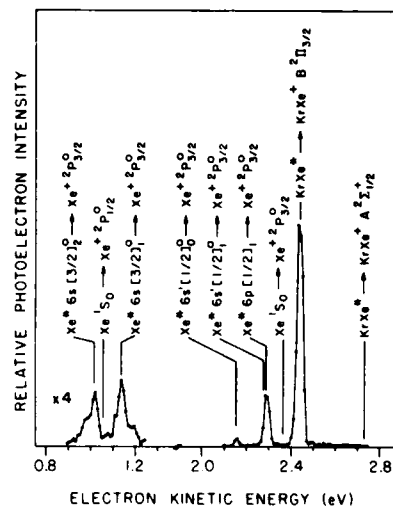


FIGURE 2. The photoelectron spectrum of KrXe following REMPI via the (0,0) band of Figure 1.

intensities of different electronic states of Xe₂⁺ are strongly dependent on the resonant intermediate level, thus providing information on the electronic character of that level. In addition, the absence of photoelectrons from atomic Xe allows the first observation of photoelectron peaks corresponding to the weakly bound C 2Π_{3/2u} and D 2Σ_{1/2g} electronic states of Xe₂⁺, thus providing lower limits for the dissociation energies of these states.

Some of the rare gas dimer bands lead primarily to the formation of the corresponding dimer ion, while others lead almost entirely to the formation of Xe⁺. The PES show that the Xe⁺ formation results from the predissociation of the intermediate level followed by photoionization of the excited atomic fragment, for example in Figure 2, KrXe* + Kr + Xe* + Kr + Xe⁺ + e. The PES allow the determination of the dissociation limits of the predissociating states, providing new information on the potential curves of the rare gas dimers.

This work was supported by the U.S. Department of Energy and the Office of Naval Research.

Reference

1. M. C. Castex, J. Chem. Phys. **66**, 3854 (1977).

MULTIPHOTON IONIZATION OF BENZENE, VINYLCHLORIDE
AND TRIFLUOROETHYLENE AT 193 NM

Michel J. Rossi, Hanspeter Helm, and Donald C. Lorents

Chemical Physics Laboratory, SRI International, Menlo Park CA 94025

Several large polyatomic molecules are known to have large multiphoton ionization (MPI) yields at excimer laser wavelengths. MPI cross sections can be extracted from experimental yield data when the photo-dynamics of the intermediate state in the case of resonant MPI is known. Such cross sections are the transferable parameters describing the multiphoton process under a variety of experimental conditions and are therefore highly desirable for a consistent description of MPI.

We report quantitative measurements of relative fractional ion yields of benzene (C_6H_6) at 248 and 193 nm, from which absolute ion yields and cross sections for the 193 nm two-photon resonant MPI process were derived using a recently completed study of the absolute ion yield at 248 nm [BE85]. The measured relative ion yields for vinylchloride (C_2H_3Cl) and trifluoroethylene (C_2F_3H) at 193 nm were then put on an absolute basis using benzene as the standard at 193 nm.

The MPI spectra were obtained in a time-of-flight (TOF) mass spectrometer which was designed to allow the interaction of a collimated laser beam with the plume of a gas expanding in a free jet. The mass spectrum was calibrated with the photofragment ions of the cited compounds in a tightly focussed beam geometry.

The salient features of the mass spectrum at around 1.0×10^6 W/cm² are the following:

For benzene at 248 nm only the molecular ion at $m/e=78$ was found. At 193 nm $m/e=78$, 64, 52 and 39 corresponding to $C_6H_6^+$, $C_5H_4^+$, $C_4H_4^+$ and $C_3H_3^+$ were detected. The power dependence for the molecular ion as well as for the fragment ions was found to be a quadratic function of the laser power.

The resonant MPI for vinylchloride at 193 nm resulted only in the presence of HCl^+ at $m/e=36$ and 38. No parent molecular ion could be detected and the HCl^+ signal had a cubic dependence on laser power.

The resonant MPI for trifluoroethylene at 193 nm resulted in the presence of $m/e=32$ corresponding to CHF^+ , which also had a cubic dependence on laser power. The parent molecular ion at $m/e=82$ could not be detected.

The ratio of the ionization yield C for benzene at 248 and 193 nm is given in equation (1), from which it is apparent, that the ion yield at 193 nm is substantially smaller than at 248 nm.

$$C_{Bz}^{248}/C_{Bz}^{193}=54.7 \quad (1)$$

This result can be understood on the basis of a significantly shorter lifetime for the one photon excited molecular system at the shorter wavelength. From relative ionization yield experiments with vinylchloride (VCl) and trifluoroethylene (TFE) at 193 nm we obtained the following fractional ionization yield ratios given in equations (2) and (3):

$$C_{VCl}^{193}/C_{Bz}^{193}=0.208 \text{ cm}^2/\text{mJ} \quad (2)$$

$$C_{TFE}^{193}/C_{Bz}^{193}=2.22 \times 10^{-3} \text{ cm}^2/\text{mJ} \quad (3)$$

Due to the different intensity dependence for the MPI fragments these ratios are not dimensionless parameters but are functions of the laser power.

Absolute cross sections for the relevant MPI transitions can be calculated and interpreted in terms of a network of competing molecular processes (e.g., dissociation, or internal conversion.)

References

- [BE85] W. K. Bischel, L. J. Jusinski, M. N. Spencer and D. J. Eckstrom, accepted for publication in J. Opt. Soc. B (1985).

I.R. MULTIPLE-PHOTON EXCITATION AND DISSOCIATION OF SILICON COMPOUNDS

E. Borsella, L. Caneve⁺, R. Fantoni, R. Larciprete⁺, A. Giardini-Guidoni
 ENEA, TIB - Divisione Fisica Applicata, C.R.E. Frascati, C.P. No. 65, 00044 Frascati (Rome), Italy

Collisionless multiple-photon excitation (MPE) of polyatomic molecules by I.R. laser radiation has become a field of major significance during the past decade. From results obtained in our as well as in other laboratories active in this field, it comes out that multiphoton resonances play a major role in MPE of the low lying vibrational states⁽¹⁾. Higher selectivity in laser isotope separation as well as enhancement of laser vapour deposition efficiency can be achieved through excitation of multiphoton rather than single photon resonances.

Recently, a detailed investigation has been performed by our group on MPE of silicon compounds i.e., SiH_4 and SiF_4 .

In order to elucidate the nature of I.R. laser photolysis of silane we have measured SiH_4 absorption in the range $930\text{--}980\text{ cm}^{-1}$ excited by a continuously tunable CO_2 laser. All the measurements were performed at room temperature under collisionless conditions. A portion of the MPA spectrum of silane is reported in Fig. 1.a at $\phi = 0.13\text{ J/cm}^2$. For comparison, in the same figure the linear absorption spectrum convoluted with the laser linewidth is reported as a continuous line.

Some structures cannot be assigned as linear absorption peaks. In order to ascertain the non linearity of the process which gives rise to the new features, absorption measurements vs laser fluence have been carried out. Slopes higher than 1 have been found at laser frequencies corresponding to multiphoton peaks (Fig. 1.b).

Decomposition of SiH_4 has been performed in parallel geometry by exciting the molecules near the ν_1 two-photon resonance (1010 cm^{-1} CO_2 laser line).

Fluorescence emitted by the fragments SiH_3 , H_2 and H has been detected and analysed through an MA apparatus in order to elucidate the gas phase reaction mechanisms in different experimental conditions.

MPE of SiH_4 has been studied in gas phase as well as under molecular beam conditions by the use of one or two line tunable pulsed CO_2 laser as radiation sources.

One and two frequency MPA of SiF_4 have been studied through opto-acoustic detection under collisionless conditions at room temperature. The one frequency spectrum shows a maximum at 1025 cm^{-1} corresponding to a two-photon resonance⁽²⁾. When the first laser was tuned at 1029.4 cm^{-1} , the two frequency MPA spectrum showed a second maximum at $\omega_2 \approx 983\text{ cm}^{-1}$. As in other polyatomic molecules, laser radiation at lower frequencies is more effectively absorbed by molecules pumped in the quasi-continuum of states by the first laser.

These results are confirmed by MPD experiments performed on SiF_4 seeded in Ar (90%) under molecular beam conditions. Two frequency MPD spectrum of SiF_4 is reported in Fig. 2 and shows a maximum at 1025 cm^{-1} followed by a series of oscillations at lower frequencies. As in case of other polyatomics⁽³⁾, simple thermal bath model for the q.c. of states cannot explain this structure, thus a more sophisticated theoretical approach is required for a full understanding of these effects.

FOOTNOTES AND REFERENCES

(⁺) ENEA student

(1) E. Borsella et al.: Chem.Phys.Lett. **101**, 86 (1983)

(2) C.W. Patterson and A.S. Pine: Cop.Comm. **44**, 170 (1983)

(3) A. Giardini-Guidoni et al.: "Collisions and Half Collisions with lasers", eds. Rahman and Guidotti, Harwood Academic Publ., New York 1984, p. 393.

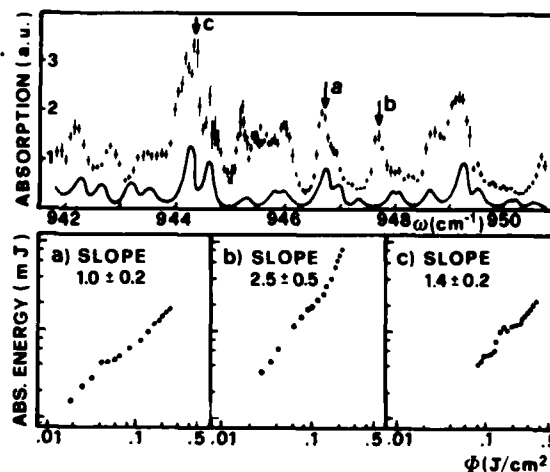


Fig. 1 - SiH_4 multiphoton absorption spectrum measured at $\phi = 0.13\text{ J/cm}^2$, $p = 0.3\text{ Torr}$. Absorbed energy vs laser fluence measured at $\omega = 946.7\text{ cm}^{-1}$ (a); $\omega = 947.7\text{ cm}^{-1}$ (b); $\omega = 948.3\text{ cm}^{-1}$ (c).

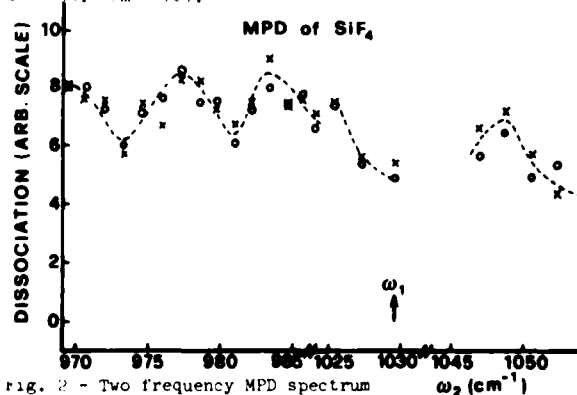


Fig. 2 - Two frequency MPD spectrum of SiF_4 .

ATOMIC IRON RECOIL IN MULTIPHOTON DISSOCIATION OF FERROCENE

H. T. Liou, Y. Ono, P. C. Engelking, J. T. Moseley

Chemical Physics Institute, University of Oregon, Eugene, Oregon 97403

We have investigated the MPI/MPD of metallocenes, and in particular, ferrocene. In this molecule, the organic ligands oppose each other to form a sandwich compound. Ferrocene has no observable fluorescence, and electronic excitation might internally convert quickly to a hot ground state. The hot ground state might then pyrolyse, following unimolecular decomposition kinetics. Another possibility is that photo-excited ferrocene would not dissociate until it had enough energy to lose two cyclopentadienyl ligands in a concerted fashion in a repulsive electronic state. Intermediate to these two scenarios is one of sequential loss of ligands through a non-concerted electronic mechanism.

Each of these choices implies definite observable effects on the resulting iron atom recoil velocity distribution. Since the ferrocene has about 25 low frequency vibrational modes, unimolecular decomposition would result in significant partitioning of the excess energy into vibrations. Pyrolysis would produce only a moderately warm distribution of iron atom velocities. In contrast, if the dissociation mechanism is totally concerted so that a center of symmetry is retained, the iron atom will be at rest in the center of mass system. Thus, a highly concerted dissociation mechanism would produce a very low velocity distribution of the iron atoms. In striking contrast to either of the above mechanisms, if the ferrocene dissociates in a non-concerted manner via electronically repulsive states, most of the available energy can end up in translational recoil. In the experiments at the laser wavelength we performed, the total available energy will be about 2 eV excess energy, either partitioned into vibrations or into atom recoil. Thus, measurement of the iron recoil velocity, even roughly, would allow a choice to be made between various dissociation mechanisms.

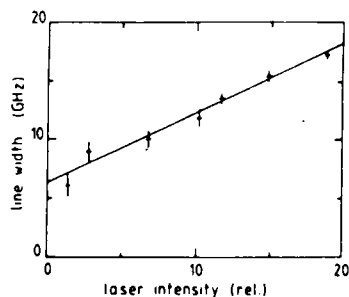


Figure 1. Dependence of Doppler linewidth on the laser intensity

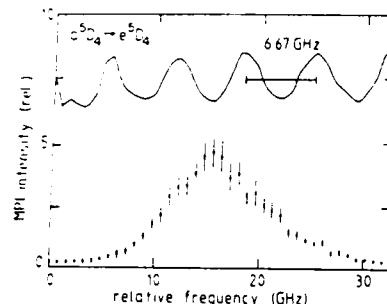


Figure 2. Line shape of Fe a $D_2 - e D_2$ two photon transition.

We investigated the iron atom recoil in the MPD of ferrocene by monitoring the Doppler line widths of the atomic iron multiphoton ionization resonances.

Figure 1 shows a plot of multiphoton ionization line width vs. laser intensity. The intercept at zero laser power is significantly wider than the line width of the probe laser. It is immediately evident that the iron atoms have a significant amount of translational energy imparted to them by the dissociation event.

Analysis of data such as that in Fig. 2 obtained as a function of laser intensity allows a separation of the velocity distribution contribution to the line shape from the contributions from lifetime broadening and saturation effects. The result is that the velocity distribution is not quite Gaussian, having less intensity in the wings of the distribution than a Gaussian distribution, and corresponds to an average iron atom recoil energy of 1.5 eV. This is consistent with equipartition of essentially all of the available energy into recoil of the Fe and cyclopentadienyl fragments.

We thus conclude that ferrocene undergoes MPD in a non-concerted manner that efficiently delivers recoil energy and momentum to the central iron atom, with very little energy going into internal excitation of the cyclopentadienyl fragments.

TWO-PHOTON DISSOCIATION OF HD^+ BY THE $1s\sigma_g \rightarrow 1s\sigma_g$
VIBRATIONAL TRANSITION

M. K. Chakrabarti[†], S. S. Bhattacharyya[†], K. K. Datta^{*} and Samir Saha^{*}

[†]Department of General Physics and X-rays, I.A.C.S., Jadavpur, Calcutta 700032, India
^{*}Indian Journal of Physics, I. A. C. S., Jadavpur, Calcutta 700032, India

Using linearly polarised light with wavelength range $\lambda = 16000 - 17000\text{\AA}$, non-resonant two-photon dissociation (TPD) cross sections of HD^+ are calculated from initial $v_1 = 6$, $J_1 = 0$ level of $1s\sigma_g$ ground state. All possible bound and free intermediate states are considered.

From perturbation theory, TPD rate from initial state $|i\rangle$ to final state $|f\rangle$ is given by

$$dw_{fi}^{(2)} = (\mu k_f / c^2 h^3) I^2 |T_{fi}^{(2)}|^2 d\Omega_{k_f}, \quad (1)$$

where k_f = wavevector of the dissociating fragments, μ = reduced mass, I = intensity of the incident photon and $T_{fi}^{(2)}$ = TPD matrix element. The generalised TPD cross section is

$$\sigma_{fi}^{(2)} = (\mu k_f \epsilon_p^2 a_0^2 / 2\pi I_0) |T_{fi}^{(2)}|^2. \quad (2)$$

Here ϵ_p = photon energy in Hartree, $I_0 = (ce^2 / 2\pi a_0^4)$ in Hartree/cm²sec, a_0 in cm, $\sigma_{fi}^{(2)}$ in cm⁴sec and all other quantities are in a.u.

With radiation gauge (\vec{A}, \vec{p}) form of interaction Hamiltonian, we have

$$T_{fi}^{(2)} = \sum_n \langle f | \hat{e} \cdot \vec{d} | n \rangle \langle n | \hat{e} \cdot \vec{d} | i \rangle / (E_n - E_i - \epsilon_p), \quad (3)$$

where \hat{e} = unit polarisation vector of incident light, \vec{d} = electric dipole operator of the molecule and $w_n = (E_f - E_n)(E_n - E_i) / \epsilon_p^2$. \sum_n in Eq. (3) is over complete set of molecular eigenstates $|n\rangle$.

For $J_1 = 0$, selection rule for two-step process demands $J_f = 2, 0$. Then, with the help of angular momentum algebra, we get

$$\sigma_{fi}^{(2)} = 8\pi\mu k_f \epsilon_p^2 a_0^2 I_0^{-1} \left(\frac{4}{45} S_{210}^2 + \frac{1}{9} S_{010}^2 \right), \quad (4)$$

where $S_{J_f 10} = S_{J_f 10}^b + S_{J_f 10}^f$ = TPD radial matrix element ('b' and 'f' stand for 'bound' and 'free' intermediate states), with

$$S_{J_f 10}^b = \sum_v \langle R_{k_f J_f}^{(\Lambda_f)}(r) | Q_{\Lambda}(r) | R_{v1}^{(\Lambda)}(r) \rangle \langle R_{v1}^{(\Lambda)}(r) | Q_{\Lambda}(r) | R_{6,0}^{(\Lambda)}(r) \rangle / (E_{v1} - E_{6,0} - \epsilon_p), \quad (5)$$

$$\text{and } S_{J_f 10}^f = \int S_{J_f 10}(k) dk,$$

$$\text{where } S_{J_f 10}(k) = (w_k k^2 / 8\pi^3) \langle R_{k_f J_f}^{(\Lambda_f)}(r) | Q_{\Lambda}(r) | R_{k1}^{(\Lambda)}(r) \rangle$$

$$\langle R_{k1}^{(\Lambda)}(r) | Q_{\Lambda}(r) | R_{6,0}^{(\Lambda)}(r) \rangle$$

$$/ (E_{k1} - E_{6,0} - \epsilon_p).$$

Here $Q_{\Lambda}(r)$ = intrinsic/electronic transition

dipole moment of the molecule.

The asymptotic part of free-free radial matrix element of $S_{J_f 10}(k)$ in Eq.(7) is evaluated analytically with a converging factor¹. An essential 2nd order singularity appears at $k=k_f$ which reduces to 1st order due to the presence of the factor w_k in Eq.(7) and the integration of Eq.(6) then becomes possible. In electric field gauge (\vec{E}, \vec{p}) , as there is no w_k , one fails to evaluate $S_{J_f 10}^f$ via Eq.(6) due to the 2nd order singularity¹ in $S_{J_f 10}(k)$.

Results and discussions :

(i) From Table 1, one notices that $\sigma_{fi}^{(2)}$ are oscillatory in the wavelength range considered. This is because of the involvement of competing bound and free channels in intermediate states.

(ii) Contribution to $\sigma_{fi}^{(2)}$ comes mostly from the $1s\sigma_g \rightarrow 2p\sigma_u \rightarrow 1s\sigma_g$ channel with some contribution from the channel $1s\sigma_g \rightarrow 1s\sigma_g(b) \rightarrow 1s\sigma_g$. Other channels like $1s\sigma_g \rightarrow 1s\sigma_g(f) \rightarrow 1s\sigma_g$, $1s\sigma_g \rightarrow 2p\pi_u \rightarrow 1s\sigma_g$ have negligible contribution.

(iii) $\sigma_{fi}^{(2)}$ for vibrational transition is found to be larger by several orders of magnitude than that for electronic transition¹.

TABLE 1. Calculated TPD radial matrix elements $S_{J_f 10}(=S_{J_f 10}^b + S_{J_f 10}^f)$ and cross sections $\sigma_{fi}^{(2)}$ of HD^+ for the $1s\sigma_g \rightarrow 1s\sigma_g$ vibrational transition from $v_1=6, J_1=0$ level of $1s\sigma_g$ state. The upper entries are for $J_f=2$ while the lower entries are for $J_f=0$.

λ (\AA)	$S_{J_f 10}^b$	$S_{J_f 10}^f$	$S_{J_f 10}$	$\sigma_{fi}^{(2)}$ (cm ⁴ sec)
16000	-8.97(-4) [†] 8.81(-4)	1.50(-1) -1.48(-1)	1.49(-1) -1.47(-1)	2.39(-54)
16300	3.02(-3) -2.72(-3)	-1.73(-1) 1.70(-1)	-1.70(-1) 1.67(-1)	2.63(-54)
16500	-1.85(-2) 1.72(-2)	1.97(-1) -1.94(-1)	1.78(-1) -1.77(-1)	2.58(-54)
16700	6.90(-3) -6.49(-3)	2.35(-1) -2.30(-1)	2.42(-1) -2.36(-1)	4.04(-54)
17000	-2.85(-3) 2.68(-3)	-2.92(-1) 2.90(-1)	-2.95(-1) 2.93(-1)	4.60(-54)

[†] -8.97(-4) = -8.97 x 10⁻⁴.

Reference :

- (7) M.K.Chakrabarti, S.S.Bhattacharyya, K.K.Datta and S. Saha, Chem.Phys.Lett. **113**, 492(1985).

APPLICATION OF PROJECTION METHODS TO SCATTERING CALCULATIONS*

B. I. Schneider⁺⁺Theoretical Division, Los Alamos National Laboratory, Los Alamos, New Mexico, 87545 USA

The results of a study on the use of L^2 basis set expansions for a number of different operators which appear in scattering problems will be presented. The object of the study was to ascertain the performance of such expansions for simple model potentials having long-range character. The results of the calculations demonstrate that the Schwinger form of the separable expansion is best for the problems studied. The standard separable expansion also works quite well, while the L^2 expansion of the Green's function is quite poor.

Work performed under the auspices of the U.S. Department of Energy.

MODIFIED EIKONAL APPROXIMATIONS FOR ELECTRON- AND POSITRON-ATOM SCATTERINGS AT INTERMEDIATE ENERGIES*

T.T. Gient†

Royal Holloway and Bedford Colleges (Univ. London), Egham Hill, Egham, Surrey TW20 0EX, England

In the modified Glauber approximation¹, scattering terms of order higher than the second one were chosen to be represented by the corresponding eikonal terms of the Glauber expansion. The contribution from higher order scattering terms to the scattering amplitude has been confirmed to be quite significant especially at large scattering angles in some calculations². It is, therefore, worthwhile to find out how this contribution varies from one model to the other. In this work, we investigate some alternative possibilities of replacing the "Glauberized" forms of these terms by those given by some other closely-related eikonal approximations. In this connection, we shall propose two new modified eikonal methods of approximation: the modified WKB and the modified straightline-corrected Glauber approximations. In particular, we apply these methods of approximation to the calculation of $e^+ - H$ elastic scattering and the results of differential cross section are compared to experimental data³.

Since the calculations of these newly proposed modified eikonal amplitudes including the unitarized eikonal-Born-series one⁴ are much more difficult than the calculation of the modified Glauber amplitude, we are also specially interested in finding out whether or not the values (without exchange) calculated with these modified eikonal methods under exactly the same conditions of approximation would differ significantly from those given by the modified Glauber method.

Detailed results of this work will be reported at the conference with discussion and useful conclusions.

*Research work supported by the Natural Sciences and Engineering Research Council of Canada.

†On sabbatical leave from the Department of Physics, Memorial University of Newfoundland, St. John's, Newfoundland, Canada A1B 3X7 (permanent address)

¹T.T. Gien, J. Phys. B 9, 3203-12 (1976)

²R.P.L. Walters, Phys. Rept. (1985, in the press)

³J.L. Williams, J. Phys. B 8, 2191-9 (1975)

⁴F.W. Byron Jr., C.J. Joachain and R.M. Potvliege
J. Phys. B 15, 3915-43 (1982)

RELATIONSHIP BETWEEN FREDHOLM INTEGRAL EQUATION AND SCHWINGER VARIATIONAL PRINCIPLE
AND ITS APPLICATION TO ATOMIC SCATTERING

S.P. Khare and Satya Prakash

Physics Department, Institute of Advanced Studies, Meerut University, Meerut-250005, INDIA

We iterate Fredholm integral equation¹ p times and obtain the scattering amplitude for the transition from i^{th} to f^{th} state as

$$f^{fi}(k_f, k_i) = f_{3p}^{fi}(k_f, k_i) + \frac{1}{2\pi^2} \sum_m \frac{f_{3p}^{fm}(k_f, q) f^{mi}(q, k_i)}{q^2 - k_m^2 - i\epsilon} dq, \quad (1)$$

where f and f_{3p} are exact and p^{th} Born scattering amplitudes, respectively. The other symbols have their usual meanings. To obtain approximate solution we take

$$f_{in} = f^{mi}(q, k_i) = \lambda_{p,n} f_{Bn}^{mi}(q, k_i) \quad (2)$$

for all values of m , where $\lambda_{p,n}$ is a complex multiplying factor and n is non-zero positive integer. Putting (2) in (1) we obtain

$$f_{out} = f_{3p} + \lambda_{p,n} (f_{3p+n} - f_{3p}). \quad (3)$$

We drop the superscripts fi to simplify the notations. Now we determine $\lambda_{p,n}$ by making $(f_{out} - f_{in})^2$ stationary with respect to $\lambda_{p,n}$. This yields

$$\lambda_{p,n} = \frac{f_{3p}}{f_{3p} + f_{Bn} - f_{3p+n}}. \quad (4)$$

It is easy to see that with the above value of $\lambda_{p,n}$ we have

$$f_{out} = f_{in} = \frac{f_{3p} f_{Bn}}{f_{3p} + f_{Bn} - f_{3p+n}} \quad (5)$$

for all values of n and p . Thus the above solution of the Fredholm integral equation is self consistent.

Now in the fractional form for the direct scattering amplitude $[f]$ as obtained from the Schwinger variational principle (Eq. (10.66) of Ref.1) we take outgoing ψ_k^+ and incoming ψ_k^- scattered waves correct to $(n-1)^{\text{th}}$ and $(p-1)^{\text{th}}$ Born-approximations respectively and easily obtain from it an equation which is identically the same as (2). Thus we establish that the self consistent solution of the Fredholm integral equation is the same as obtained from Schwinger variational principle for all the values of p and n .

In the present investigation we have taken $n=p=2$ and have obtained imaginary part of $[f_{2,2}]$ in the forward direction correct

to the order of k_1^{-3} asymptotically for e^+ -H elastic scattering and thus total collisional cross section is obtained with the help of the optical theorem. Since imaginary part of the third Born term and the real part of the fourth Born term fall as k_1^{-4} asymptotically¹ they are neglected and the imaginary part of the fourth Born term is replaced by $f_{3,4}$, the fourth term of the Glauber series. Furthermore the real part of the third Born in the forward direction for hydrogen atom is zero when evaluated through closure².

Our results for the total collisional cross sections are shown in Table 1. They exhibit satisfactory agreement with the adopted cross sections of de Heer et al.³ The present method gives different cross sections for electron and positron scattering unlike the Khare and Lata method⁴ and EBS method¹, both of which are correct only to the order of k_1^{-2} and the modified Glauber approximation⁴. All of them yield same cross sections for the two projectiles. The extension of the present method to the multielectron targets is of interest.

Table 1

Total collisional cross sections (in a_0^2) for the scattering of electrons and positrons by hydrogen atoms.

E(eV)	Present results		Ref. 3
	e^-	e^+	e^-
30	10.270	10.970	12.720
50	9.780	9.958	10.300
100	6.773	6.823	6.850
200	4.177	4.180	4.180
300	2.926	2.926	3.060
400	2.432	2.432	2.430

Financial assistance from the Indian Council of Medical Research New Delhi, India is gratefully acknowledged.

References

1. J.J. Joachain, Quantum Collision Theory, N.H. Press (1975).
2. D.P. Dewangan, J. Phys. B. 13, L595 (1980).
3. F.W. de Heer, M.R.J. McDowell and R.W. Wagenaar, J. Phys. B. 10, 1945 (1977).
4. S.P. Khare and Kusum Lata, Phys. Rev. A. 29, 3137 (1984).

EVALUATION OF DAMPED OSCILLATORY INTEGRALS IN ELECTRON-ATOM SCATTERING

V.B. Sheorey and A. Basu

Physical Research Laboratory, Navrangpura, Ahmedabad 380 009, India

The scattering of electrons by an atom or a positive ion can be described by an integral equation of the form,

$$F(kl;r) = F_0(kl;r) + \int_0^{\infty} G(kl;r,r') U(r') F(r') dr'$$

where, F_0 is the regular solution of the homogeneous equation at $r = 0$; G is the Green's function constructed from the linearly independent solutions of the homogeneous equation and incorporates the required boundary conditions on F ; the angular momentum of the partial wave considered is l and $k^2 = E$ is the impacting particle energy in rydberg units. The potential $U(r)$ describes the static field due to the target and for large r is, generally, exponentially decreasing. If allowance for electron exchange is made then $U(r)$ also contains an integral operator. Such an integral equation can be solved either iteratively or by non-iterative techniques.^{1,2}

We consider the iterative solution for such an equation. A convenient iterative procedure is to put $F = F_0$ on the RHS of the equation and then iterate the resulting equation. This procedure generates the well-known Born series. We propose a method in which the integrands arising from the above equation, which are all of the exponentially damped oscillatory type, are expanded in terms of Chebyshev polynomials. The integrals themselves, both the definite and indefinite integrals, can then be simply evaluated by appropriate summation of the expansion coefficients.

The application of our method to elastic electron-hydrogen scattering in both the static and the static-exchange approximations shows that this method requires much less computation, at least by an order of magnitude, as compared with usual quadrature methods, to give results of comparable accuracy. The problems of convergence of the iterative scheme still remain but these may be solved by an appropriate iteration-variation technique.^{1,3}

Furthermore, some problems in atomic scattering require the evaluation of damped oscillatory integrals where the damping is slower than exponential. Some of these integrals can be converted to the exponentially damped oscillatory type by a suitable deformation of the integration contour⁴. Such integrals can then be also conveniently evaluated by our technique.

References:

1. P.G. Burke and M.J. Seaton, *Methods of Comput. Phys.* **10**, 1, (1971).
2. R.J.W. Henry, *Phys. Repts.*, **68**, 1, (1981).
3. V.B. Sheorey, *Proc. Phys. Soc.*, **92**, 531, (1967).
4. N.C. Sil, M.A. Crees, M.J. Seaton, *J. Phys. B., At. Mol. Phys.*, **17**, 1 (1984).

A THIRD ORDER DISTORTED WAVE FORMULA FOR SCATTERING BY TWO POTENTIALS

D.P. Dewangan

Physical Research Laboratory, Navrangpura, Ahmedabad 380 009, India

We develop a new distorted wave formulation for scattering of a particle by a target in which the full interaction V can be divided into two parts $V = V_1 + V_2$ in such a way that the scattering problem, in which either part of the full interaction is operative at a time, can be solved exactly. We show that the exact T matrix element for excitation from the initial state ϕ_i to the final state ϕ_f can be put in the form

$$T_{fi} = T_{fi}^{\text{TODW}} + t_{fi} \quad (1)$$

where

$$T_{fi}^{\text{TODW}} = T_{fi}^{\text{DW2}} + T_{fi}^{\text{DW2}} - T_{fi}^{\text{Cor}} \quad (2)$$

$$t_{fi} = \langle \phi_f | \{ V_1 G_1 V_2 G_1 V_2 G_1 + V_2 G_2 V_1 G_2 V_1 G_2 + V_2 G_0 V_2 G_2 V_1 G_1 + V_2 G_0 V_1 G_1 V_2 G_1 + V_1 G_0 V_1 G_1 V_2 G_2 + V_1 G_0 V_2 G_2 V_1 G_1 \} | \phi_i \rangle \quad (3)$$

In (3), $G_1 = 1/(E - H_0 - V_1 + i\epsilon)$ and $G_2 = 1/(E - H_0 - V_2 + i\epsilon)$, H_0 being the unperturbed Hamiltonian and E the total energy of the system. In (2)

$$T_{fi}^{\text{DW1}} = \langle \phi_f | V_1 | \chi_i^+ \rangle + \langle \chi_f^- | V_2 | \chi_i^+ \rangle \quad (4)$$

$$T_{fi}^{\text{DW2}} = \langle \phi_f | V_2 | \xi_i^+ \rangle + \langle \xi_f^- | V_1 | \xi_i^+ \rangle \quad (5)$$

$$T_{fi}^{\text{Cor}} = \langle \phi_f | (V_1 + V_2) | \phi_i \rangle + \langle \phi_f | V_1 G_0 V_2 + V_2 G_0 V_1 | \phi_i \rangle \quad (6)$$

where $G_0 = 1/(E - H_0 + i\epsilon)$ and

$$\chi_{i,f}^+ = (1 + \frac{1}{E - H_0 - V_1 + i\epsilon} V_1) \phi_{i,f} \quad (7)$$

$$\xi_{i,f}^+ = (1 + \frac{1}{E - H_0 - V_2 + i\epsilon} V_2) \phi_{i,f} \quad (8)$$

A glance at (3) reveals that the term t_{fi} is of the fourth order in interaction, i.e. it contains contributions from the fourth and higher order perturbation theory. This implies that T_{fi}^{TODW} is exact up to the third order in the full interaction V . Indeed, we can expand T_{fi}^{TODW} in powers of V_1 and V_2 to show that it not only contains the first three Born transition amplitudes fully but also includes a part of each higher order Born term starting from the fourth Born amplitude.

Clearly, under many circumstances, those higher order terms which are not included in T_{fi}^{TODW} would be small. Then it will be a good approximation to write

$$T_{fi} \approx T_{fi}^{\text{TODW}} \quad (9)$$

We notice that T_{fi}^{DW1} in (2) is the familiar distorted wave formula of Goldberger and Watson¹ for scattering by two potentials in which the potential V_1 is treated exactly and the second potential V_2 is treated only to the first order in distorted waves. Similarly, T_{fi}^{DW2} is the Goldberger-Watson distorted wave formula in which the roles of V_1 and V_2 are now interchanged. The formula (2) gives a method of combining two distorted wave transition amplitudes for the cases in which T_{fi}^{DW1} and T_{fi}^{DW2} can be computed. The term T_{fi}^{Cor} in (2) is needed to avoid 'double counting'. We also remark that there is no difficulty in developing the formulation in the prior form. However, we omit any further discussions on this as it does not provide any additional information.

Reference

- 1 Goldberger M.L. and Watson K.M., 1964, Collision Theory, Wiley, New York.

ON THE ON-SHELL APPROXIMATION IN THE FADDEEV
 EQUATIONS FOR e-H SCATTERING

P.A. Massaro

Dipartimento di Fisica dell'Università, Sezione INFN, Bari, Italy

Treating the e-H scattering problem by the Faddeev approach or by other integral equations, the on-shell high energy approximation is usually used to reduce the dimensionality of the equations. The aim of this note is to elucidate the reliability of such approximation.

To be definite we consider the Faddeev equations for the elastic e-H channel, including only the 1s intermediate state^{1,2}

$$(\vec{k}'1s|\gamma^\pm|\vec{k}1s) = (\vec{k}'1s|\gamma(1)^\pm|\vec{k}1s) + \int d\vec{k}'' \frac{1}{E+1\epsilon-E''} (\vec{k}'1s|\gamma(1)^\pm|\vec{k}''1s) (\vec{k}''1s|\gamma^\pm|\vec{k}1s) \quad (1)$$

where γ^\pm and $\gamma(1)^\pm$ are three body and two body transition operators.

The on-shell approximation is obtained by writing the polar term as

$$\frac{1}{E+1\epsilon-E''} = -i\pi \delta(E-E'') + P \frac{1}{E-E''}$$

and by omitting the principal-value part.

The exact equations for the singlet and triplet amplitudes can be written as^{3,4}

$$f^\pm(\vec{k}', \vec{k}) = f_1^\pm(\vec{k}', \vec{k}) - \frac{i}{4\pi k} \int_0^\infty dk'' k''^2 \delta(k''-k) \int d\vec{k}'' f_1^\pm(\vec{k}', \vec{k}'') f^\pm(\vec{k}'', \vec{k}) - \frac{1}{2\pi^2} P \int_0^\infty dk'' \frac{k''^2}{k''^2-k^2} \int d\vec{k}'' f_1^\pm(\vec{k}', \vec{k}'') f^\pm(\vec{k}'', \vec{k}) \quad (2)$$

where $f_1^\pm = f^\pm + g^{\text{Ock}}$, being f^\pm the Born amplitude and g^{Ock} the Ockur exchange amplitude⁵.

For large k values the functions $f_1^\pm(\vec{k}, \vec{k}'')$ have a sharp maximum at $k'' = k$ and we can assume that the functions

$$g^\pm(k'', k; \theta) = \int d\vec{k}'' f_1^\pm(\vec{k}', \vec{k}'') f^\pm(\vec{k}'', \vec{k}) \quad (3)$$

have the same behaviour. Then a good evaluation of the principal-value part is

$$P \int_{k-\delta k}^{k+\delta k} dk'' \frac{k''^2}{k''^2-k^2} g^\pm(k'', k; \theta) \quad (4)$$

(we assume that g^\pm vanishes outside the small interval $(k-\delta k, k+\delta k)$).

Expanding around $k'' = k$

$$\frac{k''^2}{k''^2-k^2} g^\pm(k'', k; \theta) = \sum_{m=0}^{\infty} \frac{d_m^\pm(k, \theta)}{m!} (k''-k)^m$$

we have (to the first order δk)

$$P \int_{k-\delta k}^{k+\delta k} \frac{dk''}{k''-k} \frac{k''^2}{k''^2-k^2} g^\pm(k'', k; \theta) = P \int_{k-\delta k}^{k+\delta k} \frac{dk''}{k''-k} \sum_{m=0}^{\infty} \frac{d_m^\pm(k, \theta)}{m!} (k''-k)^m \approx 2d_1^\pm(k, \theta) \delta k \quad (5)$$

where

$$d_1^\pm(k, \theta) = \left. \frac{\partial}{\partial k''} \left(\frac{k''^2}{k''^2-k^2} g^\pm(k'', k; \theta) \right) \right|_{k''=k} \approx \frac{3}{4} g^\pm(k, k; \theta) \quad (6)$$

The ratio of the two integrals in equations (2) can be evaluated as

$$\frac{\text{principal-value part}}{\text{on-shell part}} \approx \frac{\delta k}{k} \quad (7)$$

Similar evaluations can be made for the inelastic channels (inclusion of more virtual states).

Even at low energies the on-shell approximation can be useful when we solve equations (2) by the method of successive approximations. Writing

$$f_{n+1}^\pm(\vec{k}', \vec{k}) = f_1^\pm(\vec{k}', \vec{k}) - \frac{i}{4\pi k} \int_0^\infty dk'' k''^2 \delta(k''-k) \int d\vec{k}'' f_1^\pm(\vec{k}', \vec{k}'') f_n^\pm(\vec{k}'', \vec{k}) - \frac{1}{2\pi^2} P \int_0^\infty dk'' \frac{k''^2}{k''^2-k^2} \int d\vec{k}'' f_1^\pm(\vec{k}', \vec{k}'') f_n^\pm(\vec{k}'', \vec{k}) \quad (8)$$

we can choose (to evaluate the second order) $f_n^\pm(\vec{k}'', \vec{k})$ as a function with a sharp maximum at $k''=k$ and vanishing outside a small interval $(k-\delta k, k+\delta k)$.

References

1. P.A. Massaro, Nuovo Cimento D **1**, 9 (1982)
2. I.H. Sloan and E.J. Moore, J. Phys. B **1**, 414 (1968)
3. P.A. Massaro, Abstracts of Contributed Papers of XIII International Conference on the Physics of Electronic and Atomic Collisions, Berlin 1983, p.98
4. P.A. Massaro, in Few Body Problems in Physics, edited by B. Zeitnitz (North Holland, Amsterdam, 1984), vol. II p.359
5. V.I. Ockur, Sov. Phys. JETP **18**, 503 (1964).

FADDEEV EQUATIONS FOR ELASTIC AND INELASTIC e-H SCATTERING

P.A. Massaro

Dipartimento di Fisica dell'Università, Sezione INFN, Bari, Italy

Previously a careful analysis has been done for the elastic e-H channel at high and intermediate energies^{1,2,3}. In such treatment only the 1s intermediate state has been retained in the Faddeev equations. In this work the method is generalized by including the 2s and 2p virtual states.

For the elastic and 1s-2s, 1s-2p inelastic e-H channels the Faddeev equations for the singlet and triplet amplitudes can be written as

$$f_{1s,1s}^{\pm}(\vec{k}, \vec{k}') = \lambda f_{1s,1s}^{(1)\pm}(\vec{k}, \vec{k}') + \lambda \frac{ik}{4\pi} \int d\vec{k}'' f_{1s,1s}^{(1)\pm}(\vec{k}'', \vec{k}') f_{1s,1s}^{\pm}(\vec{k}, \vec{k}'') + \lambda \frac{ik_1}{4\pi} \int d\vec{k}_1'' f_{1s,2s}^{(1)\pm}(\vec{k}_1'', \vec{k}') f_{1s,2s}^{\pm}(\vec{k}, \vec{k}_1'') + \lambda \frac{ik_2}{4\pi} \int_{u=-1}^1 d\vec{k}_2'' f_{1s,2pu}^{(1)\pm}(\vec{k}_2'', \vec{k}') f_{1s,2pu}^{\pm}(\vec{k}, \vec{k}_2'') \quad (1)$$

$$f_{1s,2s}^{\pm}(\vec{k}, \vec{k}') = \lambda f_{1s,2s}^{(1)\pm}(\vec{k}, \vec{k}') + \lambda \frac{ik}{4\pi} \int d\vec{k}'' f_{1s,2s}^{(1)\pm}(\vec{k}'', \vec{k}') f_{1s,1s}^{\pm}(\vec{k}, \vec{k}'') + \lambda \frac{ik_1}{4\pi} \int d\vec{k}_1'' f_{2s,2s}^{(1)\pm}(\vec{k}_1'', \vec{k}') f_{1s,2s}^{\pm}(\vec{k}, \vec{k}_1'') + \lambda \frac{ik_2}{4\pi} \int_{u=-1}^1 d\vec{k}_2'' f_{2s,2pu}^{(1)\pm}(\vec{k}_2'', \vec{k}') f_{1s,2pu}^{\pm}(\vec{k}, \vec{k}_2'') \\ f_{1s,2pm}^{\pm}(\vec{k}, \vec{k}') = \lambda f_{1s,2pm}^{(1)\pm}(\vec{k}, \vec{k}') + \lambda \frac{ik}{4\pi} \int d\vec{k}'' f_{1s,2pm}^{(1)\pm}(\vec{k}'', \vec{k}') f_{1s,1s}^{\pm}(\vec{k}, \vec{k}'') + \lambda \frac{ik_1}{4\pi} \int d\vec{k}_1'' f_{2s,2pm}^{(1)\pm}(\vec{k}_1'', \vec{k}') f_{1s,2s}^{\pm}(\vec{k}, \vec{k}_1'') + \lambda \frac{ik_2}{4\pi} \int_{u=-1}^1 d\vec{k}_2'' f_{2pu,2pm}^{(1)\pm}(\vec{k}_2'', \vec{k}') f_{1s,2pu}^{\pm}(\vec{k}, \vec{k}_2'')$$

where

$$f_{\gamma\gamma'}^{(1)\pm} = f_{\gamma\gamma'}^B \pm g_{\gamma\gamma'}^{Ock}$$

being $f_{\gamma\gamma'}^B$ the usual Born amplitudes for the $\gamma-\gamma'$ transitions and $g_{\gamma\gamma'}^{Ock}$ the Ockur exchange amplitudes⁴; λ is the coupling constant for the interacting particles ($\lambda=1$ is the physical value). The kernels for the 2s-2p transitions are singular in the forward directions but this singularity can be easily remedied by introducing a small energy difference between the 2s and 2p states.

The only important approximation made in equations (1) is the on-shell approximation which is obtained by omitting the principal-value part in the polar term of the exact equations. A discussion on the reliability of

such approximation is done in another communication.

Equations (1) cannot be easily used without a partial wave decomposition. However we can work in total wave by using single-variable integral equations.

As in the previous works^{2,3} we choose the incident vector \vec{k} in the z-axis direction and the (x-z) plane as scattering plane. Furthermore we introduce the kernels

$$\tilde{K}_{\gamma\gamma'}^{\pm}(k; u, v) = \int_0^{2\pi} d\omega f_{\gamma\gamma'}^{(1)\pm}(k; u, v, \omega)$$

where $u = \cos\theta$, $v = \cos\theta''$, $\omega = \phi''$.

The required one-dimensional equations are

$$f_{1s,1s}^{\pm}(k; u) = \lambda f_{1s,1s}^{(1)\pm}(k; u) + \lambda \frac{ik}{4\pi} \int_{-1}^1 dv \tilde{K}_{1s,1s}^{\pm}(k; u, v) f_{1s,1s}^{\pm}(k; v) + \lambda \frac{ik_1}{4\pi} \int_{-1}^1 dv \tilde{K}_{1s,2s}^{\pm}(k; u, v) f_{1s,2s}^{\pm}(k; v) + \lambda \frac{ik_2}{4\pi} \int_{u=-1}^1 \int_{-1}^1 dv \tilde{K}_{1s,2pu}^{\pm}(k; u, v) f_{1s,2pu}^{\pm}(k; v) \\ f_{1s,2s}^{\pm}(k; u) = \lambda f_{1s,2s}^{(1)\pm}(k; u) + \lambda \frac{ik}{4\pi} \int_{-1}^1 dv \tilde{K}_{1s,2s}^{\pm}(k; u, v) f_{1s,1s}^{\pm}(k; v) + \lambda \frac{ik_1}{4\pi} \int_{-1}^1 dv \tilde{K}_{2s,2s}^{\pm}(k; u, v) f_{1s,2s}^{\pm}(k; v) + \lambda \frac{ik_2}{4\pi} \int_{u=-1}^1 \int_{-1}^1 dv \tilde{K}_{2s,2pu}^{\pm}(k; u, v) f_{1s,2pu}^{\pm}(k; v) \\ f_{1s,2pm}^{\pm}(k; u) = \lambda f_{1s,2pm}^{(1)\pm}(k; u) + \lambda \frac{ik}{4\pi} \int_{-1}^1 dv \tilde{K}_{1s,2pm}^{\pm}(k; u, v) f_{1s,1s}^{\pm}(k; v) + \lambda \frac{ik_1}{4\pi} \int_{-1}^1 dv \tilde{K}_{2s,2pm}^{\pm}(k; u, v) f_{1s,2s}^{\pm}(k; v) + \lambda \frac{ik_2}{4\pi} \int_{u=-1}^1 \int_{-1}^1 dv \tilde{K}_{2pu,2pm}^{\pm}(k; u, v) f_{1s,2pu}^{\pm}(k; v) \quad (2)$$

Both elastic and inelastic amplitudes can be evaluated exactly from equations (2) without partial wave decomposition.

The method can be further generalized by including any number of intermediate virtual states.

References

1. P.A. Massaro, Nuovo Cimento D 1, 9 (1982)
2. P.A. Massaro, Abstracts of Contributed Paper of XIII ICPEAC, Berlin 1983, p.98
3. P.A. Massaro, in Few Body Problems in Physics, edited by B. Zeitnitz (North Holland, Amsterdam, 1984), vol III p.359
4. V.I. Ockur, Sov. Phys. JETP 18, 503 (1964).

HIGHER ORDER BORN EXCHANGE AMPLITUDES FOR ELASTIC SCATTERING OF ELECTRONS BY HELIUM ATOMS

N.S.Rao* and H.S.Desai**

* Physical Research Laboratory, Theoretical Physics Area, Navrangpura, Ahmedabad 380 009
 ** Physics Department, Faculty of Science, M.S.University, Baroda 390 002

In view of the recent developments for the study of spin exchange effects in electron - hydrogen collision processes^{1,2,3,4} it is proposed in this paper to extend these studies^{3,4,7} for elastic scattering of electrons by helium atom at intermediate incident energy region. Towards this proposal, we would like to derive the second Born exchange amplitude for elastic scattering of electrons by helium atom to study the asymmetry and collision cross sections. The basic approximations to obtain the exchange amplitude are discussed earlier⁷.

The second Born amplitude for exchange processes can be written as⁶

$$F_B^{(2)} = -(2\pi)^2 \langle \phi_{pb} | V_p G_d^{(+)} V_d | \phi_a \rangle \quad (1)$$

In this paper we would like to obtain the closed form of (1) for elastic scattering of electrons by helium atom. The real and imaginary parts of the exchange amplitude (1) can be obtained in closed form as

$$\text{Re } F_{EB}^{(2)} = D^n(y_m) \left[\text{Re } F_{E2} \right] \quad (2)$$

$$\text{Im } F_{EB}^{(2)} = D^n(y) \left[\text{Im } F_{E2} \right] \quad (3)$$

Where the terms in the square brackets of real (2) and imaginary (3) parts are obtained in the closed form for the hydrogen atom^{4,7}, $D^n(y_m)$ is n^{th} order differentiation with respect to the exponential parameter (y_m) of the target wavefunction⁶. Using these real (2) and imaginary (3) parts and the direct scattering amplitude⁶ the collision cross section can be calculated more accurately. And the present approach can be tested by the study of asymmetry¹.

Finally we conclude by the encouragement of our earlier studies^{3,4,5,6,7}, that the present study will give reasonably good results. Final results of the present study will be presented at the time of conference.

One of the authors (N S R) is thankful to the Physical Research Laboratory, Ahmedabad, India for the award of a Post Doctoral Fellowship.

References

1. M.R.C Mc Dowell et al., J.Phys.B 17, 3951 (1984)
2. G. D. Fletcher et al., J. Phys. B Lett 48, 1671 (1982)
3. N. S. Rao J. Phys. B (Communicated), (1985)
4. N. S. Rao and H. S. Desai Ind. J. of. Pure and Apply. Phys. (Communicated), (1984)
5. N. S. Rao and H. S. Desai Curr. Sci. 52 593 (1983)
6. N. S. Rao and H. S. Desai Pramana, 17, 309 (1981)
7. C. N. Chandra Prabha, N. S. Rao and H. S. Desai, J. M. S. University XXX 2, 39 (1981)

SEMIEMPIRICAL MODEL DESCRIPTION OF THE LOW ENERGY ELECTRON SCATTERING FROM HELIUM

R.I.Câmpeanu

Department of Physics, University of Cluj-Napoca, Romania

In a recent paper Schrader¹ has shown that the elastic scattering of positrons from rare gases can be well modelled with a simple, semiempirical potential. In the present work we propose a similar approach to the electron elastic scattering problem.

Our central model potential is

$$V = V_{st} + V_{pol} + V_{exch} \quad (1)$$

where V_{st} is the static potential of the atom and V_{pol} is the polarization potential taken of the simple form

$$V_{pol} = \begin{cases} -\alpha/2r^4 & \text{for } r \geq r_0 \\ -\alpha/2r_0^4 & \text{for } r < r_0 \end{cases} \quad (2)$$

with r_0 the single disposable parameter of the model. In order to choose the appropriate exchange potential V_{exch} , we tested several local approximations and we found that only the asymptotically adjusted free electron gas exchange model can give s and p-wave phaseshifts concomitantly within the experimental range^{2,3}; for $r_0 = 2.678 a_0$ we obtained the experimental phaseshifts at 10 eV.

Our model was then tested against experimental, total elastic and momentum transfer cross sections.

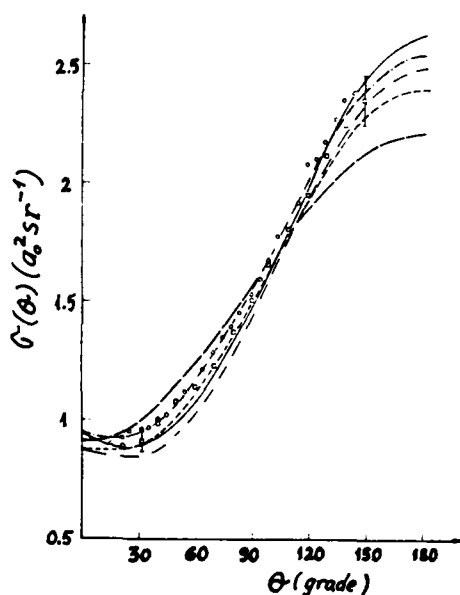


Fig.1 Differential cross sections at 5 eV: — our model; □ Register et al⁴; ○ Andrick⁵

Fig.1 presents the comparison for the differential cross sections for 5 eV electrons scattering from helium. Our fit at 10 eV agrees with the measurements of Register et al⁴ for angles smaller than 90°, while for angles larger than 130° we are in very good

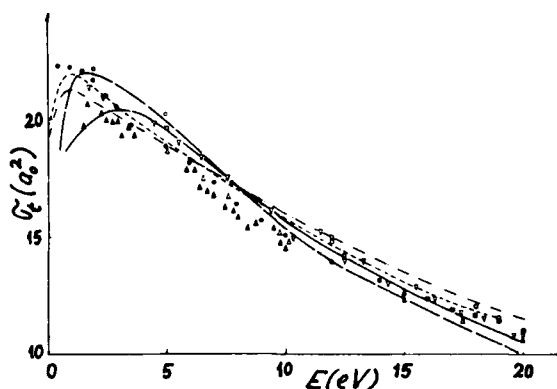


Fig.2 Total elastic cross sections for e⁻He scattering: — our model; v Stein et al⁶,

agreement with the experimental results of Andrick and Bitsch⁵.

Fig.2 shows that our model based on the fit at 10 eV yields total elastic cross sections which are in very good agreement with the measurements of Stein et al⁶. Only at impact energies lower than 3 eV our data are probably too low.

References

1. D.M.Schrader, Phys.Rev.A **20**,918(1979)
2. J.F.Williams, J.Phys.B **12**,265(1979)
3. W.R.Newell,D.F.C.Brewer,A.C.H.Smith, J. Phys.B **14**,3209(1981)
4. D.F.Register,S.Trajmar,S.K.Srivastava, Phys.Rev.A **21**,1134(1980)
5. D.Andrick,A.Bitsch, J.Phys.B **8**,393(1975)
6. T.S.Stein,W.E.Kaupilla,V.Pol,J.H.Smart, G.Jesion, Phys.Rev.A **17**,1600(1978)

ELASTIC SMALL-ANGLE ELECTRON SCATTERING BY He, Ne AND Ar AT 35keV

Dan Coffman and M. Fink

Physics Department, The University of Texas at Austin, Austin, Texas 78712

H. Wellenstein

Physics Department, Brandeis University, Waltham, Massachusetts 02154

Geiger and Morón-León have reported experimental observations of a strong forward peak in the cross section for elastic scattering of 15-25keV electrons by rare gas atoms.¹ Their data also exhibit structures similar to Fraunhofer diffraction patterns. Such interference patterns would require that each atom represent a black disk of from 30-50Å diameter in the path of the electrons (Shadow Scattering)! No recent ab initio theory can explain this effect. We repeated the experiment at the University of Texas. Many elements of our apparatus² are different from those used by the previous researcher so that a truly independent confirmation of this surprising effect could be achieved. We used a gas jet for the scattering target, the electron beam was formed by a telefocus electron gun, the electron analyser was of the Moellenstedt type³ and the scattered electrons were recorded by a scintillator photomultiplier arrangement. The primary beam was trapped in a Wood's horn. Measurements were carried out for He, Ne and Ar in the angular range of 2-20 mrad. The electron energy was set at 35keV. The scattering signal from the gas jet, the residual gas and the primary beam were recorded independently. The right-left symmetry was always maintained within the counting noise. Our cross sections for all 3 rare gases disagree in shape with Geiger and Morón-León values and agree very well with numerical results based on relativistic partial wave treatment and relativistic Hartree Fock potentials.⁴ All charge cloud polarization effects have been neglected in these calculations. No indication of shadow scattering could be found. The small forward peak predicted by Nesbeth⁵ was at too small angles to be reached by our measuring technique. At all angles the energy loss spectra were recorded to ensure that the inelastic scattering contributions are well separated from the elastic line and only elastic scattered electrons are used in the evaluations of the cross sections.

The disagreements of the previous measurements with the present ones invite comparisons between the two experiments to find some plausible causes for the absence of the shadow effect. Any long range potential produced in the scattering process can generate a strong forward peak, i.e. a small percentage of ions or metastable excited states present in the scattering volume are possible candidates.⁶ Furthermore, insufficient vacuum

conditions can cause additional scattering of electrons after they left the analyser and transverse a relative long distance to the photographic plate. A third possibility can rest with the alternation of the primary electron beam when the scattering volume was filled with gas and when it was empty. In the smallest angle the background can amount up to 50% of the final signal.

Since there are now two contradicting experimental results there is still a possibility that in spite of all the tests, care and attention which we have given to all details that the Geiger and Morón-León results are right. Therefore a third experiment is presently underway at Indiana University which will provide the final answer. We hope that these results will be available at the time of the conference.⁷

References

1. J. Geiger and D. Morón-León, Phys. Rev. Let. **42**, 1336 (1979).
2. J.J. McClelland and M. Fink, Phys. Rev. in press.
3. H.F. Wellenstein, J. Appl. Phys. **45**, 5668 (1974).
4. M. Fink, private communication.
5. R.K. Nesbeth and S. Geltman, IBM Research Report RJ 4311 (47139) 5/22/84.
6. R.A. Bonham and E.M. Peixoto, Phys. Rev. **177**, 204 (1969).
7. S. Ketkar and R.A. Bonham, private communication.

ELECTRON-ATOM WAVE FUNCTIONS USING EXTENDED NUMEROV ALGORITHM

Joseph M. Paikeday

Southeast Missouri State University, Cape Girardeau, Missouri 63701, USA.

The extended Numerov Algorithm reported earlier¹ is used to compute the scattered wave functions of electrons on selected target atoms in their ground state. The extended Numerov algorithm (ENA) used in the present study satisfies the following:

$$\sum_{i=1}^{N+1} A_i (\phi_{N+i-1} + \phi_{N-i+1}) / (1 + \delta_{i1}) = (\Delta r)^2 \sum_{i=1}^{N+1} A_i \phi_{N+i} / (1 + \delta_{i1}) \quad (1)$$

in which, ϕ is the radial part of the scattered wave function corresponding to a given angular momentum number l and δ is the Kronecker symbol and the $2N+2$ values of A_i are determined by inverting a matrix "B" satisfying certain optimization conditions based on the electron-atom interaction used to obtain the scattered wave functions. For the selected target atoms He, Ne, Ar, Kr and Xe the electron-atom interaction used is a local form of the energy-dependent effective potential² given by:

$$V_e(r, E) = \langle \phi_0 | V | \phi_0 \rangle + V_p(r, E) + V_{ex}(r, E) + iV_{ab}(r, E) \quad (2)$$

in which the first term of the interaction potential is computed from the analytic Hartree-Fock-Clementi³ wavefunctions and is approximated in the following form:

$$\langle \phi_0 | V | \phi_0 \rangle \approx \langle \phi_0 | Z/r - \frac{1}{2} (1/r^2) | \phi_0 \rangle = (2Z/r) \sum C_n (e^{-\xi r})^n \quad (3)$$

in which a single parameter ξ is used in the exponential term in Eq. (3). To determine this and the coefficients C_n the following method⁴ has been employed:

$$(r/Z) \langle \phi_0 | V | \phi_0 \rangle_{r=r_i} = V_{oi} = \sum_{n=1}^N C_n X_i^n = \sum_{n=1}^N X_{in} C_n, \quad M < N \quad (4)$$

$$\sum_{i=1}^M X_{in} V_{oi} = \sum_{i=1}^M B_{nm} C_m; \quad B_{nm} = \sum_{i=1}^M X_{in} X_{im} \quad (5)$$

$$\text{and } C_m = \sum_{n=1}^N (B^{-1})_{mn} (r/Z) \sum_{i=1}^M X_{in} \langle \phi_0 | V | \phi_0 \rangle_{r=r_i} \quad (6)$$

The second term in Eq. (2) is the energy-dependent polarization potential in which α_d of Eq. (7) is the experimental value of the dipole polarizability of the target atom and the parameter D is determined so that the total cross section at a selected incident energy of the electron agrees with the experimental value within 5%. Thus,

$$V_p(r, E) = \alpha_d / (r^4 + f(E, D)) \quad (7)$$

For the target atoms He, Ne and Argon, the exchange interaction is represented by the local energy-dependent form

$$V_{ex}(r, E) = (\frac{1}{2}) \{ E - \langle \phi_0 | V | \phi_0 \rangle + (\{ E - \langle \phi_0 | V | \phi_0 \rangle \}^2 + 8\pi\rho(r))^{1/2} \} \quad (8)$$

where $\rho(r)$ is the atomic electron density of the target atom in its ground state and E is the incident energy of the electron.⁵ The last term in the interaction in the Eq. (2) is the energy dependent absorption potential⁶ given by:

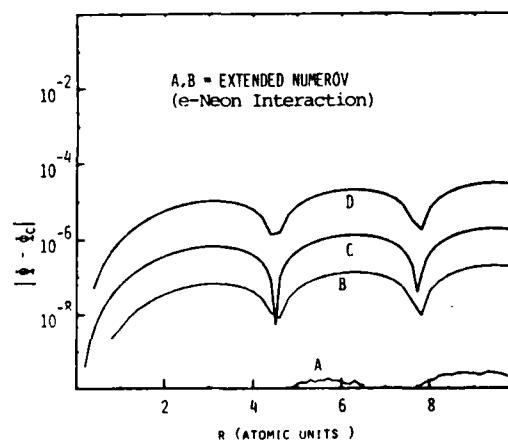
$$V_{ab}(r, E) = W(E) E^2 / \{ E - \langle \phi_0 | V | \phi_0 \rangle \}^2 R_{nl}^2(r, Z) \quad (9)$$

where $R_{nl}(r, Z)$ is the appropriate orbital function of the optical electron of the target atom and $W(E)$ is a parametric function of energy E (in Ry atomic units). For Xe atoms, the relativistic exchange potential⁷ is used in the form:

$$V_{ex}(r, E) = \alpha(E, r) 3(3/8\pi)^{1/3} \rho^{1/3}(r) \quad (10)$$

$$\text{where } \alpha(r) = (2/3) + f(r) \ln[a+b/s(r)] + \{ \ln(\beta + (1+\beta^2)^{1/2}) / \{ (1+\beta^2)^{1/2} - 1 \} \}, \quad \beta(r) = \epsilon(\rho(r))^{1/3} \quad (11)$$

The computed scattered wavefunctions of electrons by He, Ne, Ar, Kr, and Xe using the extended Numerov algorithm shows considerable improvement in the accuracy over the ordinary Numerov method for incident energies in the range $100 < E < 1000$ eV and for partial waves in the range $0 < l < 15$. A comparison of the results obtained for Neon at $E=100$ eV is shown in Fig. (1). Curves A and B represent the error in the computed ϕ_l using ENA and curves C and D for the Numerov algorithm for p-waves using $\Delta h = 0.1a_0$ and $0.2a_0$ (a_0 = Bohr radius). Extension of the ENA to multichannel matrix formulation is in progress for selected target atoms in the intermediate energy range.



References:

1. J.M. Paikeday, XIII ICPEAC, p.96. Berlin, 1983
2. J.M.P., Journal of Chem. Phys. 65, 397 (1976)
3. E. Clementi & R. Roetti, At. Data Nucl. Data 14 (1974)
4. J.M. Paikeday, Bulletin of Am. Phys. Soc., 25, 4, 584 (1980)
5. V.V. Balashov, et al., J. Phys. B: 14, 357 (1981)
J.B. Furness & I.E. McCarthy, J. Phys. B: 6, 2280 (1973)
6. J.F. Vanderpoorten, et al., J. Phys. B: 8, 1670 (1975)
7. O. Gunnarsson, et al. Phys. Rev. B, 10, 1319 (1974)
A.K. Rajagopal, J. Phys. C: 11, L943 (1978)
B. Awe, F. Kemper et al., J. Phys. B: 16, 603 (1983)

ELASTIC e^- -Kr SCATTERING USING MODEL POTENTIAL

D.Basu, S.Dutta, P.Khan and A.S.Ghosh

Department of Theoretical Physics
Indian Association for the Cultivation of Science, Jadavpur, Calcutta 700032, India.

Khan et al¹ have proposed a model potential to calculate the elastic e^- -atom scattering parameters at low incident energies. In the case of electrons, their model potential takes the form

$$V_m = V_{STAT} + V_{POL} + V_{EX}$$

where V_{STAT} , V_{POL} and V_{EX} are the static, polarization and local exchange potential respectively. The polarization potential V_{POL} behaves asymptotically as $-\alpha/2x^4$, α being dipole polarizability. The short range correlation effect is included by them via an adjustable parameter. Their polarization potential reads as

$$V_{POL}(x) = -(1-e^{-(x/x_c)^6}) \frac{\alpha}{2x^4}$$

where x_c is the cut-off parameter which is adjusted so as to reproduce the p -wave phase shift for e^- -atom scattering at a low incident energy. Following the notation of Khan et al¹, the local-exchange potential is written in the form

$$V_{EX}(r) = -\frac{1}{\pi K_0} \left[\frac{1}{2} (K_0^2 - K_{max}^2) \right. \\ \left. \times \ln \left| \frac{K_0 - K_{max}}{K_0 + K_{max}} \right| + K_0 K_{max} \right]$$

The energy of the electron, $K_0^2/2$, is given by

$$K_0^2/2 = K_1^2/2 + K_{max}^2/2 + 1/(1+K_1^2/2), \quad \ell = 0$$

and

$$K_0^2/2 = K_1^2/2 + K_{max}^2/2 + 1/(1+\lambda K_1^2), \quad \ell \gg 1$$

Khan et al¹ and Dutta et al² have obtained encouraging results for e^- -He and e^- -Ar scattering using this model.

Here, we have extended the method of Khan et al¹ to calculate e^- -Kr scattering at low energies. The elaborate R-matrix calculations have been performed by Fon et al³. The results of Fon et al³ are found to be in good agreement with the measured values⁴ above 8 eV. We have tuned our cut-off parameter x_c for the p -wave phase shift at 8 eV (p -wave phase shift of Fon et al at 8 eV = $-.640$ rad, the present results = $-.642$ rad). We have also tuned the parameter λ to reproduce the s -wave phase shifts.

With this model potential, we have solved the following differential equations

$$\left(\frac{d^2}{dr^2} - \frac{\ell(\ell+1)}{r^2} + V(r) + k_1^2 \right) u_\ell(r) = 0$$

by using Numerov's method with variable step-size. The lowest step-size near the origin is $1/2048 a_0$.

Our results for the s , p - and d -wave phase shift at three energies are shown in Table 1 and the values of the total cross section are shown in Table 2. Final results will be presented at the conference.

Table 1. s -, p - and d -wave phase shifts (rad)

Energy (eV)	s-	p-	d-
3	-0.5554	-0.2415	0.1766
8	-1.1116	-0.6428	0.7830

Table 2. Total cross section (σ_T , 10^{-16} cm^2)

Energy (eV)	σ_T (Present)	σ_T (Fon et al ³)
3	9.787	9.779
8	26.942	27.592

References

- 1 P.Khan, S.Dutta, D.Bhattacharyya and A.S.Ghosh Phys. Rev. A **29**, 3129 (1984).
- 2 S.K.Dutta, S.K.Mandal, P.Khan and A.S.Ghosh, Phys. Rev. A (in press).
- 3 W.C.Fon, K.A.Berrington and A.Hibbert, J. Phys. B: At. Mol. Phys. **17**, 3279 (1984).
- 4 M.S.Dababneh, W.E.Kaupila, J.P.Downing, F. Laperriere, V.Pol, J.H.Smart and T.S.Stein, Phys. Rev. A **22**, 1872 (1980).

SCATTERING OF ELECTRONS FROM ARGON ATOMS

Arati Dasgupta and A. K. Bhatia

Laboratory for Astronomy and Solar Physics
NASA/Goddard Space Flight Center
Greenbelt, Maryland 20771

Recently, we successfully applied the method of polarized orbitals to study scattering of electrons from neon¹ and photoionization of atomic sodium². We have carried out a similar calculation for scattering of electrons from argon. But in this calculation, only the 3p orbital is perturbed and the perturbed orbital $3p \rightarrow d$ is obtained using Sternheimer's approximation. The perturbation of the 1s, 2s, 2p and 3s orbital is taken into account by adjusting the perturbed $3p \rightarrow d$ orbital to give the experimental polarizability 11.06\AA^3 .

The total wave function for the electron-argon system is constructed using this modified $3p \rightarrow d$ orbital. Phase shifts are calculated in the exchange, exchange-adiabatic and polarized orbital approximations and compared with those obtained in other calculations. The calculated differential, total elastic and momentum transfer cross sections are compared with the theoretical and experimental results.

Reference

1. A. Dasgupta and A. K. Bhatia, Phys. Rev. A 30, 1241 (1984)
2. A. Dasgupta and A. K. Bhatia, Phys. Rev. A 31, 759 (1985)

ELASTIC SCATTERING OF INTERMEDIATE ENERGY ELECTRONS FROM ARGON

B.B. Srivastava and S. Singh

Physics Department, Meerut University, Meerut-250005, INDIA

Theoretical procedure based on a two-potential treatment¹ of the first-order static and the second-order polarization-absorption parts of the optical potential which governs the direct scattering to second order in a multiple scattering expansion has been used to calculate the differential cross sections (DCS) for the elastic scattering of electrons from argon atoms at a number of incident energies in the range 100 to 1000 eV. This treatment leads to the result that under reasonable assumptions the direct scattering amplitude can be expressed as $f_{ST} + f_E - f_{EST}$, where f_{ST} is the scattering amplitude due to the static potential, V_{00} , computed using the partial wave procedure, and f_E and f_{EST} are the eikonal scattering amplitudes due to the optical and the static potential, respectively. In these calculations f_E and f_{EST} have been calculated¹ using instead of the usual eikonal wave function the somewhat better Blankenbecler and Goldberger wave function. The exchange has been included both by the Ochkur² approximation and by the procedure of Vanderpoortan¹. For the ground state of the argon atom the wave function due to Sheorey¹ has been used.

The calculated DCS have been compared with the experimental data of Jansen³ et al., Williams and Willis⁴ and Srivastava⁵ et al. The results which will be presented in detail show that the DCS calculated by this procedure are in quite good agreement with the experimental data. The procedure of Vanderpoortan¹ for the inclusion of exchange contribution is found to work better in this case.

Financial support from Council of Scientific and Industrial Research, New Delhi for this research work is gratefully acknowledged.

References

1. B.B. Srivastava and S.S. Dhal, XIII ICPEAC Abstracts of contributed papers (ed. J. Eichler et al) p.80 and the references therein.
2. V.I. Ochkur, Sov. Phys. JETP 18, 503 (1964)
3. R.H.J. Jansen et al, J. Phys. B 9, 185 (1976)
4. J.P. Williams and B.A. Willis, J. Phys. 38, 1670 (1975)
5. B.B. Srivastava et al, Phys. Rev. A 27, 2156 (1981).

ELASTIC CROSS SECTIONS FOR ELECTRON-ARGON SCATTERING IN THE
INTERMEDIATE ENERGY (300 - 1000 eV) RANGE*.

Ione Iga, Lee Mu-Tao, J.C. Nogueira and R.S. Barbieri*

Departamento de Química, Universidade Federal de São Carlos, 13.560, São Carlos, SP, Brasil

In this communication, we report the measured absolute values of the differential, integral and momentum transfer cross sections for electron-Ar elastic scattering in the 300-1000 eV energy range. In our determination, the crossed electron-atom beam technique has been used. The beam of atoms was obtained by flowing Ar through a capillary array. The elastically scattered electrons were selected by a Möllenstedt energy analyzer⁽¹⁾ and detected by a channeltron. Scattering angles were varied by rotating the electron gun around the atomic beam and the angular range covered was between -100° to $+120^\circ$.

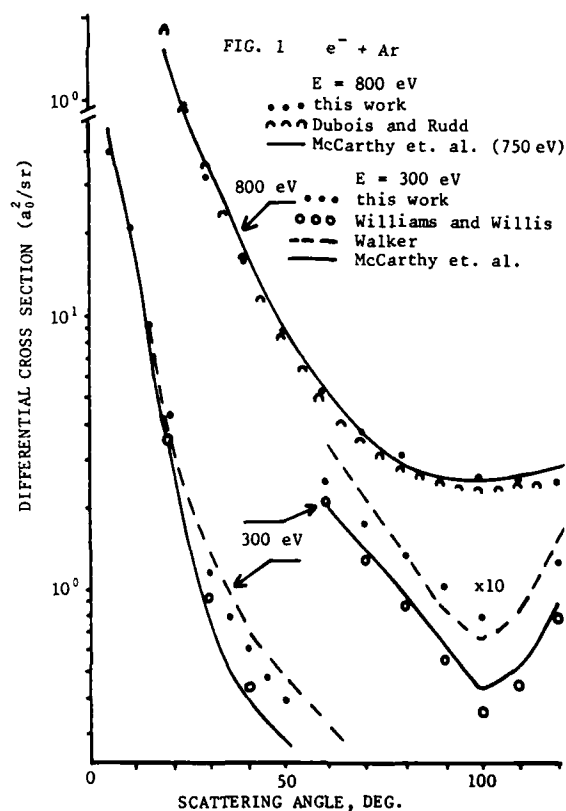
The relative flow technique developed by Srivastava et. al.⁽²⁾ was utilized to normalize the differential cross sections. For this purpose, the measured absolute cross sections of $\bar{e}-N_2^{3-4}$ scattering were used as secondary standards. The cross sections obtained in this manner are expected to be accurate within 16%. Our measured cross sections are compared with the experimental results of several authors³⁻⁶ as well as with the theoretical results of Walker⁹ and McCarthy et. al.¹⁰ showing good agreement. Some of the obtained DCS are shown in Figure 1.

* Work supported by CNPq, grant nº 40.3582/82-FA

* R.S. Barbieri thanks CNPq for the scholarship.

References

1. G. Möllenstedt, *Optik* **9** 473 (1952).
2. S.K. Srivastava, A. Chutjian and S. Trajmar, *J. Chem. Phys.* **63** 2659 (1975).
3. R.D. Dubois and M. Rudd, *J. Phys. B: At. Mol. Phys.* **9** 2657 (1976).
4. R.H.J. Jansen, F.J. de Heer, H.J. Luyken, B. Van Wingerden and H.J. Blaauw, *J. Phys. B: At. Mol. Phys.* **9** 185 (1976).
5. J.P. Bromberg, *J. Chem. Phys.* **61** 963 (1974).
6. J.F. Williams and A. Crowe, *J. Phys. B: At. Mol. Phys.* **8** 2233 (1975).
7. D.W. Walker, *Adv. Phys.* **20** 257 (1971).
8. I.E. McCarthy, C.J. Noble, B.A. Phillips and A.D. Turnbull, *Phys. Rev. A* **15**, 2173 (1977).



TOTAL CROSS SECTION MEASUREMENTS FOR ELECTRON SCATTERING FROM He, Ar AND CH₄: 0.1-20 eV

Stephen J. Buckman and Birgit Lohmann

Atomic and Molecular Physics Laboratories, Research School of Physical Sciences,
Australian National University, Canberra, Australia.

Absolute total cross sections for low energy electron scattering have been measured in helium, argon and methane using a new time-of-flight apparatus. The experimental apparatus is similar in design to that of Ferch et al.¹, but incorporates a different gating method for production of the pulsed electron beam, and a somewhat more versatile electron optical design. The spectrometer consists of a 250 mm long molybdenum flight tube and a series of electrostatic electron lenses and deflection elements. Electrons emitted from a tungsten filament are formed by the electron optical elements into a well-defined electron beam which is subsequently gated by sweeping it across a small aperture with an RF square wave pulse (100-200 kHz) applied to a pair of deflection plates. Further electron optics are then used to decelerate the electrons from the gating energy of (typically) 150 eV, to energies in the region 0.1 eV to 20 eV when they enter the flight tube. Magnetic steering of the type used by Ferch et al.¹ is not employed in this apparatus. Those electrons which are not scattered within the flight tube are re-accelerated on leaving the tube and detected by a channeltron. The solid angle subtended at the exit of the flight tube is very small ($\Omega/4\pi = 2.2 \times 10^{-5}$), ensuring that the contribution from forward scattered electrons is negligible.

The absolute electron energies are determined directly from their measured time-of-flight, obtained using conventional fast timing electronics. Absolute pressure measurements within the flight tube are obtained by using a spinning rotor viscosity gauge. The system is evacuated using a 330 l/s turbomolecular pump, resulting in base pressures of 1.0×10^{-9} mbar. During operation, with gas flowing to the flight tube, the pressure within the flight tube, as measured by the spinning rotor gauge, is greater by a factor of at least 150 than the pressure in the chamber, as measured by an ionization gauge in the vicinity of the filament. The total cross section is measured by recording energy spectra with and without gas in the flight tube and then applying the Beer-Lambert attenuation relation. When a measurement is made without gas in the flight tube, in order to ensure stable operation of the hot filament and the electron optics the gas flow is re-directed to the chamber in such a way that the pressure measured at the

ionization gauge remains constant.

We have measured the total cross section for electron scattering from helium in the range 0.1 eV to 12 eV, with an overall uncertainty (one standard deviation) of less than 3%. Our results are in excellent agreement with a recent theoretical calculation due to Nesbet², and also with recent experimental results^{1,3}. Measurements will also be presented of the total cross sections in argon and methane, and these results will be compared with other recent measurements and theoretical calculations.

References

1. J. Ferch, W. Raith and K. Schröder, J. Phys. B: Atom. Molec. Phys. 13, 1481 (1980).
2. R.K. Nesbet, Physical Review A 20, 58 (1979).
3. R.K. Jones and R.A. Bonham, Aust. J. Phys. 35, 559 (1982).

MEASUREMENT OF ABSOLUTE DIFFERENTIAL CROSS SECTIONS FOR ELASTIC ELECTRON SCATTERING FROM MERCURY

G. Holtkamp, K. Jost, J. Kessler and F.J. Peitzmann

Physikalisches Institut der Universität Münster, D-4400 Münster, W.-Germany

INTRODUCTION

Relative phases between scattering amplitudes and the ratio f/g , of their magnitudes can be determined in "triple scattering experiments" involving polarized electrons /1/,/2/. However, in order to make the determination of scattering amplitudes complete, one needs their individual magnitudes, which can be determined by measuring the differential cross section $|f|^2 + |g|^2$ additionally. Up to now, for mercury the absolute differential cross section has only been measured at 300eV, 400eV and 500eV /3/, i.e. scarcely overlapping with the energy range from 18eV to 360eV, where data of triple scattering experiments exist. Furthermore these cross section measurements /3/ concentrate on small scattering angles, whereas the spin effects in triple scattering experiments occur at large angles. Therefore it is planned to extend the measurements of absolute differential cross sections both to lower energies and to larger scattering angles. Nevertheless, small scattering angles will be measured as well, because the differential cross section itself is a sensitive tool to explore the validity of theories apart from its utility for the above purposes.

EXPERIMENTAL METHODS AND RESULTS

It is planned to perform measurements by means of two different methods; the first one employs a static gas target and the second one utilizes an atomic beam target. This redundant determination of differential cross sections should facilitate to judge their reliability.

Static gas target. The setup and the procedure for measurements of this kind are described by Bromberg /3/. Inelastically scattered electrons are removed from the scattered beam by a simulated spherical analyzer /4/ before detecting the elastically scattered electrons; appropriate tests ensure a transmission of unity. In order to obtain absolute differential cross sections, one has to measure the primary and scattered electron currents at various target densities for each scattering angle and each energy. The target densities are determined via pressure and temperature measurements. Furthermore, the relevant geometrical dimensions

which determine the solid angle of detection must be known accurately. Extrapolation of a set of data points to zero target density yields the desired quantity. Preliminary results will be shown at the conference together with other data /3/,/5/ and /6/.

Atomic beam target. In contrast to the above, this method has the advantage of having a scattering volume independent of scattering angle, provided the atomic beam diameter in the scattering plane is small enough to be "seen" completely by the detection system. Because of the difficulty of determining absolute target densities within an atomic beam, this method yields at first only relative elastic differential cross sections. However, this fault can be repaired by measuring additionally the inelastic processes as described in /7/. Integrating procedures with respect to energy loss and scattering angle yield a total cross section, which is still relative, indeed, but which can be fitted to an absolutely measured total cross section /8/. By applying this fitting factor to the relatively measured elastic and inelastic differential cross sections, each of them is brought to an absolute scale.

REFERENCES

- /1/ W.Wübker, R.Möllenkamp and J.Kessler, Phys. Rev.Letters 49 (1982) 272.
- /2/ R.Möllenkamp, W.Wübker, O.Berger, K.Jost and J.Kessler, J.Phys.B:At.Mol.Phys. 17 (1984) 1107.
- /3/ J.P.Bromberg, J.Chem.Phys. 51 (1969) 4117.
- /4/ K.Jost, J.Phys.E:Sci.Instrum. 12 (1979) 1006.
- /5/ D.W.Walker, Adv.Phys. 20 (1971) 257 and private communications.
- /6/ M.Fink and A.C.Yates, Technical report No.88, Dept. of Physics, The University of Texas at Austin (1970).
- /7/ K.Jost and R.Möllenkamp, X.ICPEAC Paris (1977), Abstracts of papers p. 394.
- /8/ K.Jost and B.Ohnmus, Phys.Rev.A 19 (1979) 641.

DIFFERENTIAL SCATTERING CROSS SECTIONS OF ELECTRONS FROM Xe

H. Nishimura, A. Danjo and T. Matsuda

Department of Physics, Niigata University, 8050 Ikarashi
Niigata 950-21 Japan

The differential cross sections (DCS) of electrons from Xe have been measured using a crossed beam method at incident energies of 5 to 200 eV and angular range between 10° to 125° . The electron spectrometer consists of a hemispherical electron monochromator and the same type of analyzer. The energy and angular resolution of the spectrometer are typically 50 m eV and $\pm 2^\circ$ respectively. Absolute values of the elastic DCS are given by normalizing the relative values to the absolute elastic DCS for He¹ with the relative flow technique². The absolute DCS for inelastic scattering is determined normalizing the relative value to the absolute elastic DCS obtained with the method above. Fig. 1 shows the present results of elastic DCS for Xe with the experimental results of Williams and Crowe³, and the theoretical results of McCarthy et al.⁴, and McEachran and Stauffer⁵. In Fig. 2, integral cross sections for elastic scattering are shown along with the experimental results of Williams and Crowe, and the calculations of McCarthy et al. Also are shown the total cross sections measured by Wagenaar and de Heer⁶, and Dababneh et al.⁷ for the comparison at low impact energies. Fig. 3 shows the energy loss spectrum at an electron energy of 30 eV and an electron scattering angle of 30° . The inelastic DCS for the $6s[1/2]_1^0$, $6s^*[1/2]_1^0$ and $7s[1/2]_1^0$ excitations will be reported.

References

- ¹D. F. Register, S. Trajmar and S. K. Srivastava: Phys. Rev. **A21**, 1134(1980).
- ²S. K. Srivastava, A. Chittjan and S. Trajmar: J. Chem. Phys. **63**, 2659(1975).
- ³J. F. Williams and A. Crowe: J. Phys. **B8**, 2233 (1975).
- ⁴L. E. McCarthy, C. J. Noble, B. A. Phillips and A. D. Turnbull: Phys. Rev. **A15**, 2173(1977).
- ⁵R. P. McEachran and A. D. Stauffer: J. Phys. **B17**, 2507(1984).
- ⁶R. W. Wagenaar and F. J. De Heer: J. Phys. **B13**, 3855(1980).
- ⁷M. S. Dababneh, W. E. Kuuppila, J. P. Downing, F. Laperriere, V. Pol, J. H. Smart and T. S. Stearn: Phys. Rev. **A22**, 1472(1980).

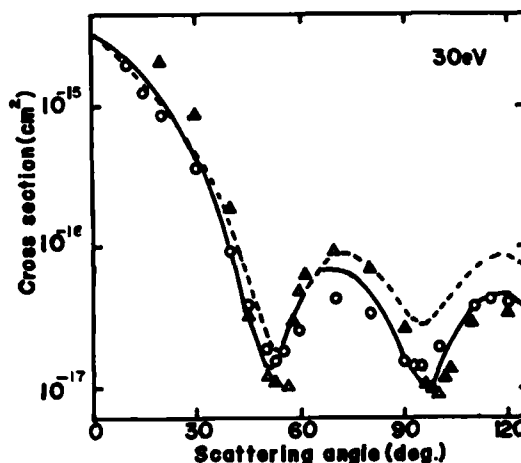


Fig. 1. Differential cross sections for elastic scattering as a function of scattering angle at 30 eV. \circ This work, Δ Williams and Crowe (1975), — McCarthy et al. (1977), --- McEachran and Stauffer (1984).

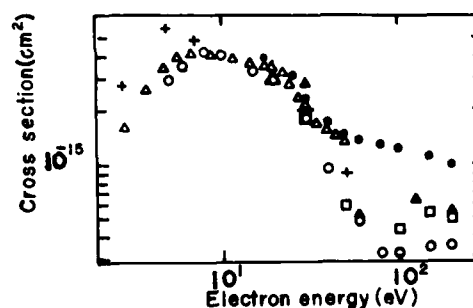


Fig. 2. Integral cross sections for elastic scattering as a function of impact energy. \circ This work, Δ Williams and Crowe (1975), \bullet Wagenaar and de Heer (total, 1980), Δ Dababneh et al. (total, 1984), \square McCarthy et al. (1977), $+$ McEachran and Stauffer (1984).

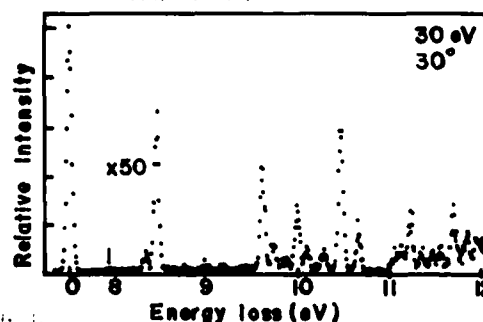


Fig. 3.

AN 11-STATE CALCULATION OF THE ORIENTATION, λ AND ALIGNMENT χ PARAMETERS
FOR THE ELECTRON EXCITATION 1^1S-2^1P IN HELIUM BELOW THE 3^1P THRESHOLD

L.C.G. Freitas[†], K.A. Berrington^{*}, P.G. Burke^{*} and A.E. Kingston^{*}

[†]Departamento de Quimica, Universidade Federal de Sao Carlos,
via Washington Luiz km234, 13560 Sao Carlos, SP Brazil.

^{*}Department of Applied Mathematics and Theoretical Physics,
The Queen's University of Belfast,
Belfast BT7 1NN, Northern Ireland.

The first results of an R-matrix electron helium scattering calculation, in which the eleven lowest target states are included, were reported by Freitas et al¹ (1984). In that paper a series of Feshbach resonances arising from the coupling to the $n=2$ and $n=3$ states were presented. In a subsequent calculation (Berrington et al¹ (1985) the authors confirm the preliminary finding that the explicitly inclusion of the $n=3$ target states can have a significant effect on the excitation cross section for transitions from the ground state to the $n=2$ levels at electron energies between the $n=2$ and $n=3$ levels.

The study of the electron-photon angular correlations is well recognised as a valuable technique in the investigation of electron excitation processes. In particular for the $1^1S + 2^1P$ electron-helium excitation there have been many theoretical and experimentally studies of electron-photon angular correlations. The aim of the present communication is to present orientation λ and alignment χ parameters for the $1^1S + 2^1P$ excitation process obtained from our 11-state R-matrix calculations.

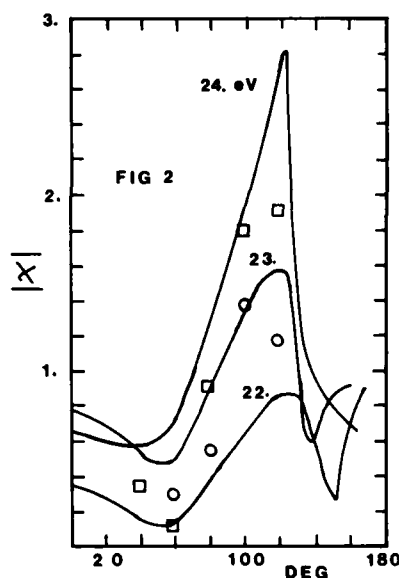
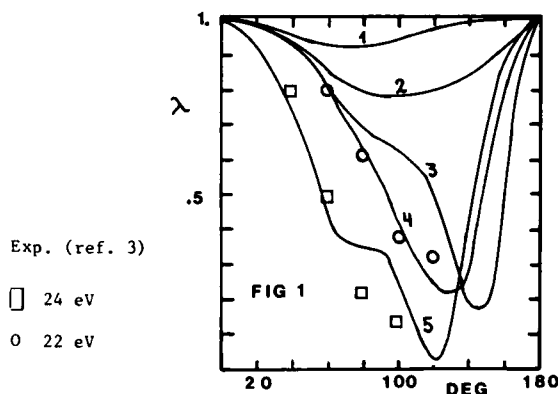
Figure 1 gives our λ parameter for a range of energies between the 2^1P threshold (21.22 eV) and the 3^1P threshold (23.09 eV). At the 2^1P threshold $\lambda=1$ at all angles of scattering, as the electron energy increases λ decreases in a regular way at all scattering angles. However in the region of the 2^1S^e threshold (22.44 eV) λ can vary significantly if the electron energy is varied by as little as 0.01 eV. Our theoretical values of χ are given in Fig. 2, χ also varies rapidly with energy in the region of the 2^1S^e resonance.

Fig. 1 and 2 also compare our present 11-state results for λ and χ with observations of Crowe et al³ (1983).

Fig. 1

ELECTRON ENERGY (eV)

1	-	21.28
2	-	21.50
3	-	22.0
4	-	23.
5	-	24.



References

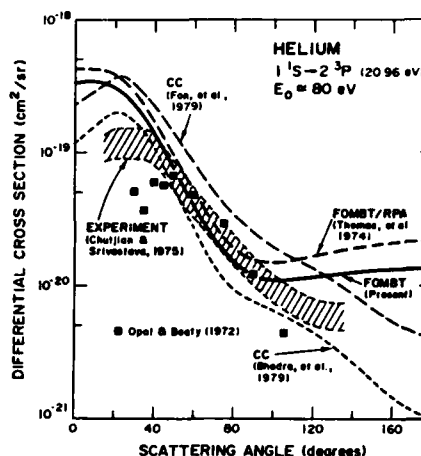
1. Berrington K.A., Burke P.G., Freitas L.C.G. and Kingston A.E., 1985, J. Phys. B.: At. Mol. Phys.
2. Berrington K.A., Burke P.G. and Sinfield H.L., 1975, J. Phys. B.: At. Mol. Phys. 8, 1459-73.
3. Crowe A., Nogueira J.C. and Liew Y.C., 1983, J. Phys. B.: At. Mol. Phys. 16, 481-489.
4. Freitas L.C.G., Berrington K.A., Burke P.G., Hibbert A., Kingston A.E. and Sinfield A.L., 1984, J. Phys. B.: At. Mol. Phys. 17, L303-309.

CROSS SECTIONS AND COINCIDENCE PARAMETERS FOR EXCITATION OF THE n^1L ($n = 2, 3, 4$) STATES OF HELIUM

G. Csanak and D. C. Cartwright
University of California, Los Alamos National Laboratory
Los Alamos, New Mexico 87545 (USA)

Although a substantial amount of theoretical research has been reported¹ on the electron-impact excitation of helium from its ground electronic state, a theory that can be used to obtain differential and integral cross sections in good agreement with experimental data, for all transitions and energies below the Born-region, has not yet been developed. The close-coupling formulation works well for treating the resonance processes near the $n = 2$ and 3 thresholds, but becomes less accurate for energies above the first ionization threshold because the number of open channels that can be included must be restricted due to practical computer limitations. Previous calculations for electron-impact excitation of the lowest electronic states of helium,² neon,³ and argon,⁴ based on the first-order many-body theory (FOMBT),⁵ produced results that agree reasonably well with experiment for incident electron energies from about 30 to 100 eV. This previous research using FOMBT is being extended to higher principal quantum numbers and a wider range of incident electron energies in order to compare with recent experimental results.

Differential and integral cross sections for excitation of the n^1L ($n = 2, 3, 4, 5$) states of helium, from the ground electronic state (1^1S) and using the FOMBT, will be reported. Differential cross sections obtained using the FOMBT for excitation of the $n = 2$ states of helium agree well with previously reported results (Fig. 1). The electron-photon coincidence parameters, λ and χ , will also be reported for the excitation of the 2^1P and 3^1P states at energies not reported before, but for which recently experimental results have been obtained⁶ and R-matrix theory calculations have been reported.⁷



REFERENCES

1. B. H. Bransden and M. R. C. McDowell, *Phys. Rep.* **30C**, 207 (1977); *ibid* **46**, 249 (1978).
2. L. D. Thomas, Gy. Csanak, H. S. Taylor, and B. S. Yarlagadda, *J. Phys. B*, **7**, 1719 (1974); A. Chutjian and L. D. Thomas, *Phys. Rev. A*, **11**, 1583 (1975).
3. G. D. Meneses, N. T. Padial, and Gy. Csanak, *J. Phys. B*, **11**, L237 (1978).
4. G. D. Meneses and Gy. Csanak, in *Coherence and Correlation in Atomic Collisions*.
5. H. Kleinpoppen and J. F. Williams, Eds. (New York, Plenum) pp. 179-186 (1980).
6. L. E. Machado, E. P. Leal, and G. Csanak, *Phys. Rev. A*, **29**, 1811 (1984).
7. N. T. Padial, G. D. Meneses, F. J. da Paixão, Gy. Csanak, and D. C. Cartwright, *Phys. Rev. A*, **23**, 2194 (1981).
8. Gy. Csanak, H. S. Taylor, and R. Yaris, *Phys. Rev. A*, **3**, 1322 (1971).
9. P. A. Neill and A. Crowe, *J. Phys. B*, **17**, L791 (1984).
10. W. C. Fon, K. A. Berrington, and A. E. Kingston, *J. Phys. B*, **12**, 819 (1980).

POLARIZATION CORRELATION MEASUREMENTS OF $\text{He}(2^1\text{P})$ EXCITATION BY ELECTRONSM. A. Khakoo, L. Forand, K. Becker⁺ and J.W. McConkeyDepartment of Physics, University of Windsor, Windsor, Ontario, N9B 3P4, Canada
⁺ Department of Physics, Lehigh University, Bethlehem, Pennsylvania 18015, USA

Although the majority of electron-photon coincidence experiments have involved $\text{He}(2^1\text{P})$ excitation, there is only one example¹ in the literature where this was studied using the polarization correlation rather than the complimentary angular correlation technique. This has been because of the more favourable signal strengths when using the latter technique. Even in the single example cited¹ a full Stokes' parameter analysis was not possible because a circular polarization analyser was not available. Recently Williams² has reported measurements of the circular polarization at an electron energy of 81.2 eV and scattering angles of $\pm 10^\circ$ and $\pm 90^\circ$.

Excitation of the 3^1P state may be studied via the $3^1\text{P} - 2^1\text{S}$ decay at 501.6 nm and recently Ibrahim et al.⁵ have extended the earlier polarization correlation analysis of Standage and Kleinpoppen⁶ to larger scattering angles. In both cases the incident electron energy was 80 eV.

The significance of the circular polarization measurements are that they establish the sign of the orbital angular momentum transfer $\langle \vec{L} \rangle$ in the collision or, equivalently, of the atomic orientation or of the relative phase parameter χ . Following the initial work of Kohmoto and Fano³ who recognized that the sign of $\langle \vec{L} \rangle$ was related to the attractive or repulsive nature of the effective interaction potential, considerable discussion on this point has occurred in the literature. A discussion with references to earlier work has been given recently by Andersen et al.⁴.

We have now added a circular polarization analyser and are in the process of carrying out a comprehensive series of linear and circular polarization measurements covering a variety of incident electron energies and scattered electron angles. Full details of these will be presented at the conference but initial measurements confirm the trends noted previously².

The polarization analyser consists of two flat gold-coated reflectors. The angle of incidence is chosen on the one hand to maximize the linear polarization sensitivity of the device when operated as a two-reflector linear polarizer as in our earlier work¹, and on the other to give the necessary $\pi/2$ retardation between the two reflected components when operated in the circular polarization analysis mode. In this latter mode the plane of incidence of the first reflector is rotated, relative to the incident electron direction, through an angle ϕ defined by

$$\tan 2\phi = -S_1/S_2$$

where S_1 and S_2 are the two linear Stokes parameters. The second reflector is capable of rotation about an axis defined by the reflected beam from the first, using a stepper motor attached to the device. Measurements taken with the plane of incidence of this second reflector at $\pm 45^\circ$ to that of the first yields the third Stokes parameter (circular polarization) directly. Full details of the performance and use of this device have been given by Westerveld et al.⁷ and will be illustrated at the conference.

This work was supported by the Natural Sciences and Engineering Research Council of Canada (NSERC).

References

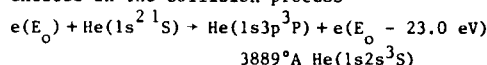
1. K.H. Tan, J. Fryar, P.S. Farago and J.W. McConkey, *J. Phys. B* **10**, 1073 (1977).
2. J.F. Williams, Abstr. 13th ICPEAC, Berlin, 132 (1983).
3. M. Kohmoto and U. Fano, *J. Phys. B* **14**, L477 (1981).
4. N. Andersen, I.V. Hertel and H. Kleinpoppen, *J. Phys. B* **17**, L901 (1984).
5. K.S. Ibrahim, H.A. Silim, H-J. Bever, H. Kleinpoppen, I. McGregor and L.C. McIntyre, Abstr. 9th I.C.A.P., Seattle, B46 (1984).
6. M.C. Standage and H. Kleinpoppen, *Phys. Rev. Letts.* **36**, 577 (1976).
7. W.B. Westerveld, K. Becker, P. Zetner, J.J. Corr and J.W. McConkey, *App. Opt.* in press (1985).

ELECTRON IMPACT EXCITATION OF THE 3^3P STATE OF HELIUM

J F Williams and I Humphrey*

Department of Physics, University of Western Australia, Nedlands, WA 6009

Electron-photon angular and polarization correlations have been measured to determine the density matrix (multipole moments) of the 3^3P state of helium excited in the collision process



The measurements require (i) the detection of the incident electrons scattered through an angle θ_e and losing the 3^3P excitation energy; (ii) the linear and circular polarization analysis of the emitted photons; (iii) the time coincidence identification of those electrons (i) and photons (ii) originating from the same atom; and then (iv) the dependence of the angular and polarization correlation of the coincidence signal.

Figures will be presented at the conference as follows.

Figure 1 will show the coordinate system and illustrate the experimental system.

Figure 2 will show energy loss spectra for (i) an incident energy E_0 of 48.0 eV and $\theta_e = 45^\circ$ and (ii) $E_0 = 23.7$ eV and $\theta_e = 70^\circ$. Curve (i) shows the dominance of the 2^1P cross section at an energy 26.8 eV above the threshold while curve (ii) shows the appreciable size of the $n=3$ triplet states at an energy about 0.7 eV above threshold and at $\theta_e = 70^\circ$.

Figure 3 will show the linear polarization of the 3889°A radiation from the $3^3P \rightarrow 2^3S$ transition.

Figure 4 will show a typical (e,hv) time coincidence spectrum for $E_0 = 40$ eV, $\theta_e = 40^\circ$.

Figure 5 will show an enlarged section of the true coincidence region but with better statistics. The exponential decay results from the lifetime of the 3^3P state which is determined from each coincidence spectrum. The spectrum of figure 3 yields a lifetime of 97.8 ± 3.2 nsec. The average lifetime from a number of such spectra is 101.8 ± 2.5 nsec. The weighted mean of the best values in the literature is 107.3 ± 2.1 nsec.

Figure 6 will show the total area under the true coincidence peak yields the total number of (e,hv) coincidence pairs for a given E_0 and θ_e for a given linear or circular polarization angle, μ , that is one data point. The measurement has been repeated for various values of μ to produce the data of figure 7.

The data have been analyzed as follows. The energy eigenstates of an atom at time t are

$$|\psi^k(t)\rangle = \sum_{JFM_F} a^k(JFM_F) |JIFM_F\rangle \exp(-\frac{i}{2}t) \exp(-iEt/\hbar)$$

and the transition probability rate to the final state $|\psi_f\rangle$ is

$$w(t) = \frac{2\pi}{\hbar} |\langle \psi_f | H | \psi(t) \rangle|^2 \rho(E_F) = \frac{c}{3} \sum_{MM'} \epsilon^* \rho_{MM'} \epsilon (-1)^{M+M'} \\ = k \epsilon^+ \begin{pmatrix} \rho_{-1-1} & \rho_{10} & \rho_{11} \\ \rho_{0-1} & \rho_{00} & \rho_{01} \\ \rho_{1-1} & \rho_{-10} & \rho_{11} \end{pmatrix} \epsilon$$

For $P \rightarrow S$ transitions and the above geometry

$$w(t) = a(\rho_{11} + \frac{1}{2}\rho_{00}) + (\rho_{11} - \frac{1}{2}\rho_{00}) \sin 2\beta - \sqrt{2} \text{Im} \rho_{10} \cos 2\beta$$

Using the parametrization $\sigma = \rho_{00} + 2\rho_{11}$ and $\lambda = \rho_{00}/\sigma$ and

$$\rho_{10} = |\rho_{10}| \exp(i\chi)$$

$$\text{then } w(t) = \frac{k\sigma}{2} \{1 + (1-2\bar{\lambda}) \sin 2\beta - 2\bar{\lambda}(1-\bar{\lambda}) \overline{\sin \chi} \cos 2\beta\}$$

= a sinusoidal function with unknowns $\bar{\lambda}$ and $\overline{\sin \chi}$.

The bars denote averages over the hyperfine structure and the excited state may contain an incoherent mixture of pure states. The measured polarization correlation and the fitted sinusoidal function are shown.

Figure 7 will show the derived parameters of $\bar{\lambda}$ and $\bar{\chi}$ as well as the Stokes parameters η_1 , η_2 and η_3 which are defined

$$\eta_2 = \frac{w(t)_{\beta=0} - w(t)_{\beta=\pi/2}}{w(t)_{\beta=0} + w(t)_{\beta=\pi/2}} = -\alpha_2 \{\bar{\lambda}(1-\bar{\lambda})\}^{1/2} \overline{\sin \chi}$$

$$\eta_3 = \frac{w(t)_{\beta=3\pi/4} - w(t)_{\beta=\pi/4}}{w(t)_{\beta=3\pi/4} + w(t)_{\beta=\pi/4}} = 2\alpha_1 (2\bar{\lambda}-1)$$

$$\eta_1 = -4\alpha_1 \{\bar{\lambda}(1-\bar{\lambda})\}^{1/2} \overline{\cos \chi} \text{ where } \alpha_1 = 15/82 \text{ and } \alpha_2 = 54/41$$

For pure states $\eta_1^2 + \eta_2^2 + \eta_3^2 = 1$ but for triplet states the most coherent observation possible yields $\eta_1^2 + \eta_2^2 + \eta_3^2 < 1$ where

$$\eta_1^2 + \eta_2^2 + \eta_3^2 = 4\alpha_1^2 + (\alpha_2^2 - 16\alpha_1^2) (\sin^2 \chi) \bar{\lambda}(1-\bar{\lambda}) \\ \approx 0.1338 + 1.1993 \sin^2 \chi [\bar{\lambda}(1-\bar{\lambda})]$$

There are no theoretical or experimental values for comparison. Further measurements are being made to improve the statistical accuracy to test the coherency condition for the 3^3P sub-states and the dynamical behaviour of the $\bar{\lambda}$ and $\bar{\chi}$ parameters.

* Now at Princeton University, NJ

ANGULAR CORRELATIONS IN THE ELECTRON IMPACT EXCITATION OF SODIUM

J.L. Riley, P.J.O. Teubner, J.E. Furst and M.J. Brunger

School of Physical Sciences, The Flinders University of South Australia,
Bedford Park, South Australia 5042, Australia

The most commonly used procedure in experiments involving electron photon coincidence techniques in atomic physics is to measure angular correlations. That is the coincidence count rate is measured as a function of the angle of emission of the photon in the scattering plane. The data derived from such experiments have proven to be a sensitive test of the theory of electron collisions with atomic hydrogen and with helium (see for example the review article by Blum and Kleinpoppen¹ and references therein).

The theory of angular correlation experiments has been developed by Macek and Jaecks² for the general case of an atom which radiates under LS coupling rules. This theory can be applied to the excitation of the 3^2P state in sodium and demonstrates that the angular correlation is essentially isotropic. Here the isotropy arises from the depolarising influence of the unresolved HFS in the excited state. Nevertheless it has been proposed³ that angular correlations can be used to derive scattering parameters for the excitation of the state.

We present the first angular correlation to be measured in the electron impact excitation of sodium. The incident electron energy was 54.4eV and the electron scattering angle was 5° . The deduced values of the parameters λ and $\cos \chi$ will be presented and compared with those derived from a coincidence experiment using a polarised photon technique.

We conclude that the polarised photon technique is superior because not only does this technique contain more information in principle but it also has demonstrable experimental advantages.

We also present an analysis of the experimental limitations in coincidence experiments in sodium. We find that apart from the well known role played by the window width⁴, the major influence of the ratio $(Q/\sigma)^{1/2}$ limits the use of coincidence experiments in the excitation of sodium to scattering angles less than 15° at energies in excess of 12eV. Here Q is the total cross section for the excitation of the state and σ the differential cross section. In addition we present an analysis of the factors affecting the timing resolution in coincidence experiments. Results which demonstrate the dominant role played by the geometry of the electron spectrometer will be presented. These

results confirm, in part, the predictions of Volkel and Sandner⁵.

References

1. K. Blum and H. Kleinpoppen, Phys.Rep 52, 203 (1979).
2. J. Macek and D.H. Jaecks, Phys.Rev.A 4, 2288 (1971).
3. G.A. Parker, T.M. Miller and D.E. Golden, Phys.Rev.A 25, 583 (1982).
4. I.E. McCarthy and E. Weigold, Phys.Rep 27, 275 (1976).
5. M. Volkel and W. Sandner, J.Phys.E 16, 456 (1983).

THE DIFFERENTIAL CROSS SECTION FOR ELECTRON EXCITATION OF
THE 3^1P ($m_l = 0$) STATE OF HELIUM*

D.J. Burns, N.W.P.H. Perera, B.N. De and C.R. Hummer[†]

Behlen Laboratory of Physics, University of Nebraska,
Lincoln, Nebraska 68588, USA

The differential cross section for excitation of the 3^1P ($m_l = 0$) state in helium by electrons has been investigated for a range of scattering angles and for incident energies up to 80 eV. This was done by detecting the inelastically scattered electrons in coincidence with 501.6 nm photons that are emitted when the state decays to the 2^1S level. The electrons are detected by an analyser consisting of a series of zoom lenses, a hemi-spherical energy selector and a multichannel plate. The detection geometry is such that the photons are detected by a non-polarizing filter and detector located in the scattering plane and at 90° to the electron beam axis. For this arrangement the coincidence rate at a given scattering angle is proportional to $\sigma_0(\theta)$, the differential cross section of $m_l = 0$.

It has been found that the coincidence rate must be normalised to the scattered electron counts, rather

than the photon counts. This necessitates measuring the relative differential cross section for the $n = 3$ manifold of states at each impact energy. This is obtained from analysis of the energy-loss spectrum at each scattering angle and is a by-product of our measurements.

Measurements over an incident energy range from 40 - 80 eV will be presented for angles from 10° to 60° . Results will be compared with a series of model calculations by Madison² and others. So far, our data agrees best with a theoretical model in which the calculation of the distorted waves uses an excited state potential in both channels, instead of the ground state potential.

*Work supported by the National Science Foundation.

[†]Present address: Department of Physics U-46,
University of Connecticut, Storrs, Connecticut 06268.

References

1. C.R. Hummer and D.J. Burns, submitted to Phys. Rev.
2. D.H. Madison, J. Phys. B 12, 3399, 1979.

ELECTRON-VISIBLE PHOTON ANGULAR CORRELATIONS FOR THE 3^1P STATE OF HELIUM
EXCITED BY LOW ENERGY ELECTRONS

P A Neill and A Crowe

Department of Pure and Applied Physics, The Queen's University of Belfast,
Belfast, United Kingdom

Most previous angular correlation studies of excitation of the 3^1P state of helium have been made by observation of the scattered electrons in coincidence with the 53.7 nm VUV radiation emitted in decay to the ground state, Eminyan et al¹, Crowe et al², Gelebart et al³ and McAdams and Williams⁴. Such measurements are only valid under conditions where the 3^1S and 3^1D differential cross sections are negligible compared with that for the 3^1P state. These three states cannot easily be resolved in the scattered electron channel. The decay of the 3^1S and 3^1D states to 2^1P is followed by emission of 58.4 nm VUV radiation as it decays to the ground state. In the photon channel this radiation cannot readily be isolated from the 53.7 nm radiation without the unacceptable loss of intensity and possible polarisation effects of a VUV monochromator and hence these states contribute to the observed coincidence signal. van Linden van den Heuvell et al⁵ have deconvoluted the 3^1P and 3^1D contributions to their observed signal, but the statistical uncertainty associated with measurements of this type hinders the accuracy of the resulting angular correlation parameters.

This problem can be avoided by observing the 501.6 nm photons due to the decay of the 3^1P state to the 2^1S state. The only previous measurement of this type was reported by Eminyan et al¹ at an incident electron energy of 80 eV and for electron scattering angles $\theta_e \leq 30^\circ$. The experiment of Standage and Kleinpoppen⁶ in which the polarisation state of this photon was determined gives equivalent information. The disadvantage of the visible photon detection is the large branching ratio (40:1) in favour of the ground state decay.

In this laboratory angular correlations between scattered electrons and 501.6 nm photons have been measured over a wide range of incident electron energies and scattering angles using the apparatus of Crowe et al⁷ with the VUV photon detector replaced by a photomultiplier.

Data will be presented for incident electron energies in the range 29.6 eV to 80.0 eV.

References

1. M Eminyan, K B MacAdam, J Slevin, M C Standage and H Kleinpoppen, *J Phys B* **8**, 2058 (1975).
2. A Crowe, T C F King and J F Williams, *J Phys B* **14**, 1219 (1981).
3. G Gelebart, H Leguesdron and J Peresse, *Phys Lett* **87A**, 345 (1982).
4. R McAdams and J F Williams, *J Phys B* **15**, L247 (1982).
5. H B van Linden van den Heuvell, E M van Gasteren, J van Eck and H G M Heideman, *J Phys B* **16**, 1619 (1983).
6. M C Standage and H Kleinpoppen, *Phys Rev Lett* **36**, 577 (1976).
7. A Crowe, J C Nogueira and Y C Liew, *J Phys B* **16**, 481 (1983).

ELECTRON IMPACT EXCITATION OF THE $4p^5(^2P_{3/2}) 5s\ ^3P_1$ AND
 $4p^5(^2P_{1/2}) 5s\ ^1P_1$ STATES OF KRYPTON

S J King, P A Neill and A Crowe

Department of Pure and Applied Physics, The Queen's University of Belfast,
 Belfast, United Kingdom

Excitation of the lowest lying excited states of krypton, viz $4p^5(^2P_{3/2}) 5s\ ^3P_1$ and $4p^5(^2P_{1/2}) 5s\ ^1P_1$, have been studied using the scattered electron-photon angular correlation technique. Compared with the situation in lighter atoms, the analysis of these angular correlations may be complicated by the presence of spin-orbit coupling effects. Blum et al¹ and da Paixao et al² have shown that the angular correlations for excitation of a $J = 1$ from a $J = 0$ state for heavy atoms in the presence of spin-orbit coupling can be characterised by four independent parameters ($\lambda, \chi, \epsilon, \Delta$) compared with only two (λ, χ) for an LS-coupled system.

Experimentally, λ, χ and ϵ , where $\cos \chi = \cos \bar{\chi} \cos \Delta$, can be determined by measuring two independent angular correlations. We have chosen to measure one angular correlation in the scattering plane and a second over a conical surface, the axis of the cone being perpendicular to the scattering plane. This allows both angular correlations to be determined simultaneously. Details of the experimental arrangement will be presented together with the analysis which enables λ, χ and ϵ to be determined.

The only other angular correlation data for these states have been presented by McGregor et al³ at 36 and 60 eV for scattering angles of 20° and 30°, and by Nishimura et al⁴, at energies in the range 40 to 80 eV and scattering angles $\leq 30^\circ$. The only common data from these two groups is that measured at an incident electron energy of 60.0 eV and electron scattering angles of 20° and 30°. There are large differences between the data.

Figure 1 shows the angular correlation measured in the scattering plane for the 1P state by McGregor et al³ and Nishimura et al⁴. It can be seen that they have nearly opposite phases. The correlation measured in this laboratory is not in agreement with either of the previous correlations. Further data from this laboratory at 60 eV and over a range of electron scattering angles will be presented, together with arguments for its preference over the previous data and a comparison with very recent calculations⁵.

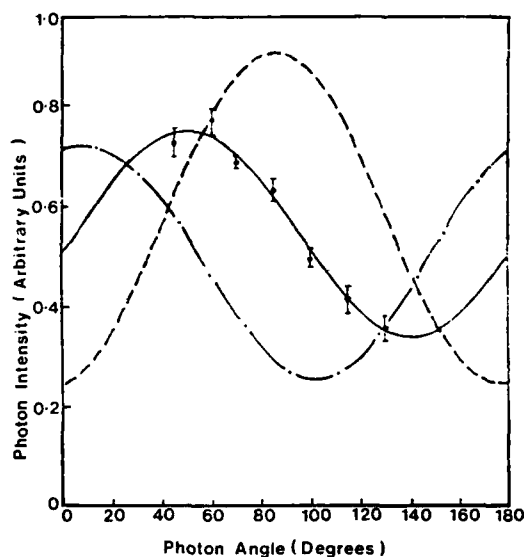


Fig 1: Angular correlations measured in the scattering plane for the $4p^5(^2P_{1/2}) 5s\ ^1P_1$ state of krypton for an incident electron energy of 60 eV and a scattering angle of 20°. The dot-dash line is from McGregor et al³. The dashed correlation is calculated from the λ, χ and ϵ values of Nishimura et al⁴. The data shown is from this laboratory and the full line is a fit of the appropriate angular correlation function to that data.

References

1. K Blum, F J da Paixao and Gy Csanak, *J Phys B : At Mol Phys* **13**, L257, (1980).
2. F J da Paixao, N T Padial and Gy Csanak, *Phys Rev Lett* **45**, 1164, (1980).
3. I McGregor, D Hils, R Hippler, N A Malik, J F Williams, A A Zaidi and H Kleinpoppen, *J Phys B : At Mol Phys* **15**, L411, (1982).
4. H Nishimura, A Danjo, T Koike, K Kani, H Sugahara and A Takahashi, Abstracts 13th Int Conf on Physics of Electronic and Atomic Collisions, Berlin, p 130 (1983).
5. G D Meneses, F J da Paixao and N T Padial (private communication).

MEASUREMENT OF SPIN EXCHANGE AMPLITUDES IN ELECTRON
IMPACT EXCITATION OF THE 3^3P STATE OF HELIUM

H A Silim, H-J Beyer, A El-Sheikh and H Kleinpoppen

Atomic Physics Laboratory, University of Stirling, Stirling FK9 4LA, Scotland

We have carried out for the first time a polarization correlation measurement on the 3^3P state of He excited by electrons. 60 eV electrons are selected by a 127° monochromator and crossed with the He beam. Scattered electrons, having lost the energy corresponding to the excitation of any of the $n=3$ states, are observed through a 127° analyser and the decay light of the 3^3P state (3889\AA) is detected at right angles to the scattering plane through an interference filter and analysed for linear and circular polarization. An example of the time correlation spectrum between the scattered electrons and the photons is shown in figure 1 (polarization analysers removed). The long lifetime of the 3^3P state of 95 μsec results in a correspondingly wide coincidence signal and, therefore, a large number of background coincidence counts below the peak. This necessitates long measuring times (typically 24h per signal).

From the polarization correlation signals the Stokes parameters of the light are determined for each electron scattering angle. These are related to the scattering parameters of the excitation process in the same way as for the 1^1P states^{1,2}. However, the fine structure of the 3^3P states causes considerable depolarization of the states between the excitation and the emission of the light. The depolarization factors G can be calculated from Blum and Kleinpoppen², and are $G = 15/41$ for the linear and $G = 27/41$ for the circular polarization Stokes parameters. Using the parameters α (corresponding to λ in the 1^1P case) and γ (corresponding to χ in the 1^1P case) we obtain:

$$\eta_1 = (I_{45} - I_{135}) / (I_{45} + I_{135}) = -(30/41) \sqrt{\alpha(1-\alpha)} \cos \gamma$$

$$\eta_2 = -(I_L - I_R) / (I_L + I_R) = (54/41) \sqrt{\alpha(1-\alpha)} \sin \gamma$$

$$\eta_3 = (I_0 - I_{90}) / (I_0 + I_{90}) = (15/41) (2\alpha - 1)$$

α and γ have been derived from the measured Stokes parameters and preliminary results are shown in figures 2 and 3. No theoretical values are available. It should be noted that in contrast to the 1^1P case where the underlying scattering amplitudes contain contributions from both direct and exchange processes, the 3^3P scattering amplitudes are pure spin-exchange amplitudes, and thus measurements on the 3^3P states allow very specific tests of the scattering theory.

REFERENCES

- 1 M C Standage and H Kleinpoppen, Phys. Rev. Lett. **36** 577-80 (1976)
- 2 K Blum and H Kleinpoppen, Phys. Reports **52** 203-261 (1979)

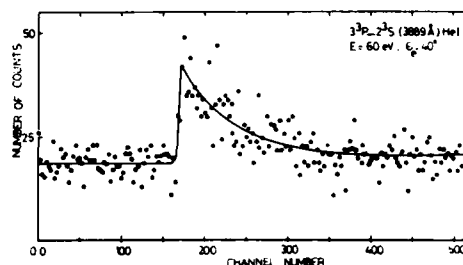


Figure 1. Time correlation spectrum between electrons scattered by 40° and $3^3P \rightarrow 2^3S$ decay light. Time per channel 1.6 nsec; accumulation time 18h.

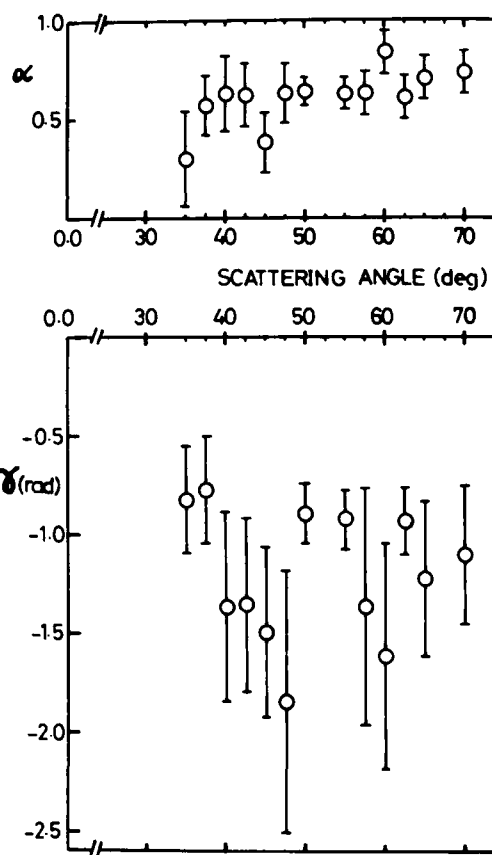


Figure 2. Parameter $\alpha = |a_0|^2 / (|a_0|^2 + 2|a_1|^2)$ and phase shift γ between the excitation amplitudes a_0 ($M_L=0$) and a_1 ($M_L=\pm 1$) as a function of the scattering angle.

POLARIZATION CORRELATION MEASUREMENTS ON THE 3^1P STATE OF HELIUM

K S Ibraheim, H-J Beyer and H Kleinpoppen
Atomic Physics Laboratory, University of Stirling, Stirling, FK9 4LA, Scotland

We have studied the polarization correlations for electron impact excitation of the 3^1P state of helium covering an extended range of electron impact energies and scattering angles. The scattered electrons, having lost the energy corresponding to the excitation of the $n=3$ states, are observed in coincidence with the light emitted in a direction perpendicular to the scattering plane. The Stokes parameters for linear and circular polarization are measured and analysed in the same way as in the previous measurement by Standage and Kleinpoppen¹ which was restricted to 80 eV and small scattering angles. From the Stokes parameters the values of the usual scattering parameters λ and χ are derived, and the present results of χ for the various energies are shown in figure 1 using the range 0 to -2π for convenience. For all energies a

change of χ through the line $-\pi$ is indicated corresponding to a sign change of the angular momentum transfer to the atom which was also borne out by the circular polarization Stokes parameter². The large angle angular correlation measurements by McAdam and Williams³ are also shown. Even though their results did not point towards a sign change of the angular momentum transfer they are nevertheless fairly consistent with the present results.

REFERENCES

- 1 M C Standage and H Kleinpoppen, Phys. Rev. Lett. **36**, 577 (1976).
- 2 K S Ibraheim, H-J Beyer and H Kleinpoppen 2nd ECAP Amsterdam 1985, Book of Abstracts.
- 3 R McAdam and J F Williams, J Phys. B **15**, L247-51 (1982).

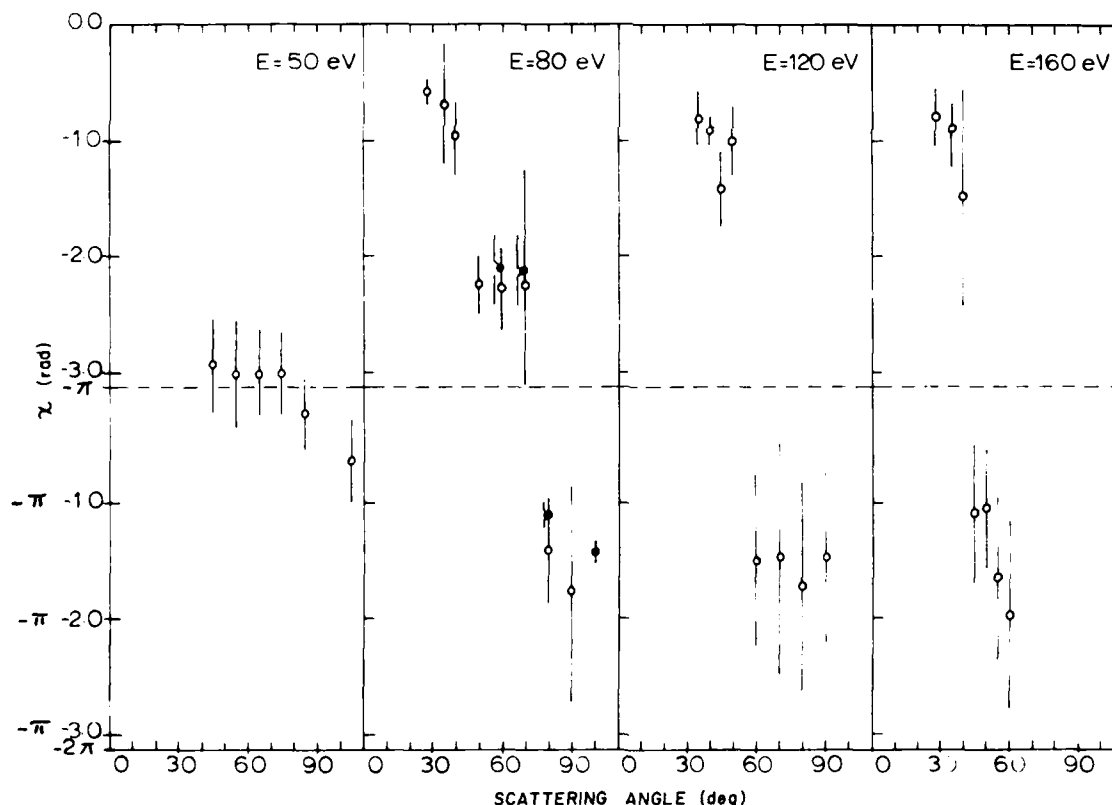


Figure 1. Phase difference χ between the excitation amplitudes a_0 ($M_L=0$) and a_1 ($M_L=\pm 1$) of the 3^1P state of He as a function of the electron scattering angle for different values of the incident electron energy. \circ present work; \bullet McAdam and Williams³.

ELECTRON IMPACT EXCITATION OF THE 3^2P STATE OF SODIUM

R. P. Fiegel, S. R. Lorentz, T. M. Miller, D. E. Golden, J. E. Furst
Department of Physics and Astronomy, Univ. of Okla., Norman, Oklahoma 73019 USA

Electron-photon coincidence experiments from electron impact excitation processes have rendered new information about atomic collision processes. Of particular importance in the current generation of experiments is the observation of effects due to electron exchange processes.¹ The coherence of the excitation may be tested and some insight gained into the role of exchange in collisions even in experiments in which no spin analysis is performed. This then provides a direct test of the Percival Seaton hypothesis.

We have measured differential cross sections for the electron impact excitation of the 3^2P state in Sodium, in the energy range 10 to 50 eV. The next step in our investigation has been to measure scattering amplitudes and phases (λ, χ), using the angular correlation technique, for the 3^2P state. This process did not include any state selection of the ground state. Comparison will be made with calculated values and other experiments.

We will further present expressions deriving the relationship between the angular correlation parameters and the scattering amplitudes where the ground state Na atoms are prepared in a single hyperfine level.²

References

1. P. J. O. Teubner, J. L. Riley, J. E. Furst and S. J. Buckman, J. Phys. B. 18 351 (1985).
2. G. A. Parker, T. M. Miller, M. Mahgerefteh and D. E. Golden, Phys. Rev. A 29 1770 (1984).

SUPERELASTIC SCATTERING BY A HEAVY ATOMIC TARGET*

T.T. Gient†

Royal Holloway College (Univ. London), Egham Hill, Egham, Surrey TW20 0EX, England

We develop the formalism of superelastic scattering by a heavy atomic target whose charged cloud in its excited state is assumed to have been somehow tipped off-balance by electron impact out of the "superelastic scattering plane".

The charged cloud of an excited heavy atomic target is, therefore, referred to three different frames: charged cloud, natural and collision frames. Since the distribution of the charged cloud is symmetric in its charged cloud frame, by a suitable choice of axes, only three independent and real density matrix elements are required to represent the "superelastic scattering system" of a heavy atomic target where the spin-orbit coupling effect is expected to be present. Formulae of the measurable alignment and orientation coefficients in the collision and natural frames are given in terms of the tip-over angles and the density matrix elements in the charged cloud frame. It is then shown that the formalism of superelastic scattering of a tipped-over charged cloud can accommodate without violation of parity a "fictive" plane asymmetry effect. This effect was previously pointed out to apparently exist in superelastic scattering experiments¹. We also show that the magnitude of this "fictive" plane asymmetry effect depends on how greatly the charged cloud has been tipped over.

A mechanism is then proposed to produce this tip-over of the charged cloud by electron impact without violating parity. We suggest that the tip-over may be caused by another electron which non-superelastically scatters on the charged cloud into directions outside the superelastic scattering plane and was simply not observed in previous superelastic scattering experiments.

We show that with linearly polarized laser, the electron signal of super-elastic scattering measured inside the superelastic scattering plane is

$$I(\vec{e}) = \frac{1}{2}(I + I_3 \cos 2\psi + I_1 \sin 2\psi) \quad (1)$$

The measured "asymmetry angle" ω is therefore given by

$$\tan 2\omega = - \frac{2(\sin^2 \theta_{V1-}^{col} - \cos^2 \theta_{V2-}^{col})}{\sin^2 \theta_{V0}^{col} - \sin^2 \theta_{V1+}^{col} + (1 + \cos^2 \theta_{V2+}^{col})} \quad (2)$$

Measuring ω at five laser directions would enable the determination of all five alignment coefficients at different scattering electron angles. The tip-over angle of the charged cloud can then be determined. Thus, one may be able to verify whether the tip-over angle will only be significantly great at small

scattering angles or not and a check of the self-consistency of our tip-over hypothesis can, therefore, be provided. To have a further check of our hypothesis, we suggest that when superelastic scattering experiments are performed, it would be worthwhile to position electron detectors outside the superelastic scattering plane, especially inside the plane of maximum tip-over angle, to watch for those non-superelastically scattered electrons which have so far been totally ignored in these experiments. We also show that within the tip-over hypothesis, there exist two relations which the alignment and orientation coefficients in the collision frame must satisfy. These relations can also be verified experimentally. It is worth noting that such a "fictive" plane asymmetry effect may have been observed in some recent superelastic scattering experiments².

* Research work supported by NSERC of Canada

† On sabbatical leave from the Department of Physics, Memorial University of Newfoundland, Canada (permanent address) during 1984-1985

¹ T.T.Gien, J. Phys. B 15, 2481-2508 (1982); *ibid*, 4617-27 (1982)

² D.R. Register et al., Phys. Rev. A 28, 151-60 (1983)

ANALYSIS OF ORIENTATION AND ALIGNMENT IN ELECTRON IMPACT EXCITATION OF HEAVY RARE GASES: THE Ar 4s 1P AND 3P CASE

N. Andersen,* J. W. Gallagher,† I. V. Hertel‡ and F. J. da Paixão†

*Physics Dept., University of Aarhus, DK-8000 Aarhus, Denmark and
Physics Laboratory II, HC Ørsted Institut, DK-2100 Copenhagen, Denmark†Joint Institute for Laboratory Astrophysics, University of Colorado and
National Bureau of Standards, Boulder, Colorado 80309 USA

‡Institut für Molekülphysik, Freie Universität Berlin, D1000 Berlin 33, Germany F.R.

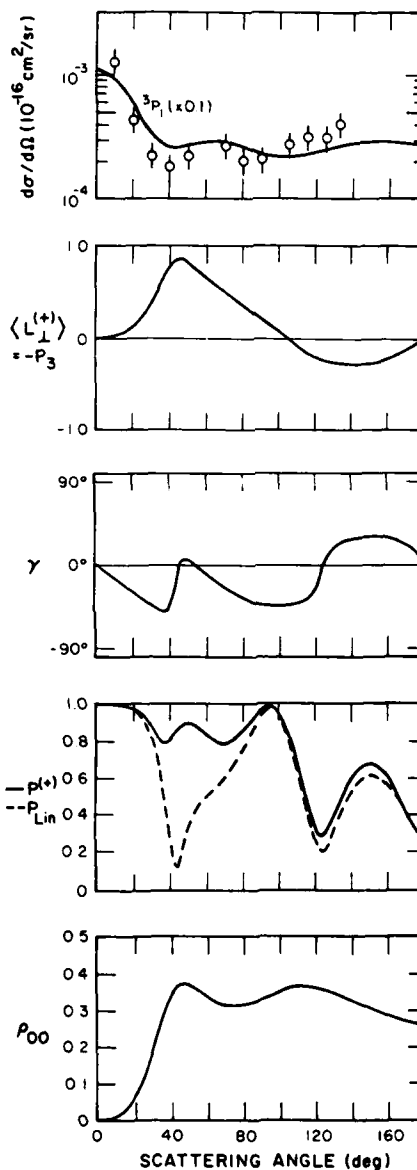
Traditionally,¹ orientation and alignment of heavy rare gases excited by electron impact have been analyzed in terms of the parameters λ , $\bar{\chi}$, $\cos \Delta$ and $\cos \epsilon$. It is, however, difficult to relate these parameters to physical pictures of the collision dynamics and shape of the atom after the excitation process. Generalizing the ideas presented earlier for the helium case,² we here suggest an illustrative way of reanalyzing the available data for the heavier rare gases which at the same time relates in a more direct way with the experimentally observable quantities. To this end we use the angular momentum $L_1^{(+)} = -P_3$, the alignment angle γ of the charge cloud, the degree of linear polarization $P_{\text{lin}} = (P_1^2 + P_2^2)^{1/2}$ perpendicular to the collision plane [or alternatively the total degree of polarization $P^{(+)} = (P_1^2 + P_2^2 + P_3^2)^{1/2}$] and finally the relative height of the charge cloud $\rho_{00} = [(1+P_1)(1-P_4)] / [(3+P_1)+P_4(1-P_1)]$, using the conventional definition of the Stokes parameters (P_1, P_2, P_3) measured perpendicular to and the linear polarization P_4 in the collision plane. The density matrix in the natural frame² can then be decomposed as

$$\begin{pmatrix} \rho_{11} & 0 & \rho_{1-1} \\ 0 & \rho_{00} & 0 \\ \rho_{-11} & 0 & \rho_{-1-1} \end{pmatrix} = \frac{1}{2} (1-\rho_{00}) \begin{pmatrix} 1-P_3 & 0 & -P_{\text{lin}} \exp(-2i\gamma) \\ 0 & 0 & 0 \\ \text{c.c.} & 0 & 1+P_3 \end{pmatrix} + \rho_{00} \begin{pmatrix} 0 & 0 & 0 \\ 0 & 1 & 0 \\ 0 & 0 & 0 \end{pmatrix}$$

and the relations of the new parameters to the old ones are:

$$\begin{aligned} \rho_{00} &= \frac{1}{2} (1-\lambda)(1-\cos \epsilon) \text{ and} \\ (1-\rho_{00})(P_1, P_2, P_3) &= \left(\lambda - \frac{1}{2} (1-\lambda)(1+\cos \epsilon), \right. \\ &\quad \left. -2\sqrt{\lambda(1-\lambda)} \cos \Delta \cos \bar{\chi}, 2\sqrt{\lambda(1-\lambda)} \cos \Delta \sin \bar{\chi} \right). \end{aligned}$$

An example of this analysis for the 4s[3/2] $_1^0$ (3P_1) state of argon at 16 eV initial electron energy is shown in the right column, using the results of da Paixão et al.³ The graphs display in a smooth way the close relation between angular momentum $L_1^{(+)}$, alignment angle γ and coherence ($P^{(+)}$) caused mainly by direct and exchange interaction, and, on the other hand, the pure effect of spin flip processes $\propto \rho_{00}$. More examples will be presented at the conference.



References

1. F. J. da Paixão, N. T. Padial, G. Csanak and K. Blum, Phys. Rev. Lett. **45**, 1164 (1980).
2. N. O. Andersen, I. V. Hertel and H. Kleinpoppen, J. Phys. B **17**, L901 (1984).
3. F. J. da Paixão, N. T. Padial and G. Csanak, Phys. Rev. A **30**, 1697 (1984).

A RELATIONSHIP BETWEEN THE DIRECT AND THE EXCHANGE AMPLITUDES OF
 $e^- - H$ COLLISIONS

by

Ik-Ju Kang,* Ung-In Cho* and Gye Tai Park*

*Southern Illinois University at Edwardsville, Edwardsville, IL 62026 USA

*Yonsei University, Seoul, Korea

It is well-known that for the ionization of H-atom by electron impact, $e^-(k_0) + H(1s) \rightarrow e^-(k_1) + e^-(k_2) + H^+$, there exists a relationship between the direct (D) and the exchange (E) amplitudes which was found first by Peterkop⁽¹⁾ as

$$E(k_1, k_2) = D(k_1 \leftrightarrow k_2) \quad (1)$$

For the excitation of He-atom by electron impact Ockur⁽²⁾ found a relationship between the direct (D) and the exchange (E) amplitudes in the high energy limit which is given as

$$E = D(q^2/k_0^2) \text{ with } q = k_1 - k_0. \quad (2)$$

In this paper, a relationship is obtained between the D and E for

$$e^-(k_0) + H(1s) \rightarrow e^-(k_1) + H(nlm)$$

which may be valid in the intermediate energy region. The S-matrix formalism is employed to describe the process with the coulomb waves representing electrons in the continuum states. The initial bound and the continuum state wave functions are parameterized respectively as

$$\psi_{1s}^t = N_{1s} e^{-\lambda r} e^{-b\kappa_0 r} e^{ia\kappa_0 \cdot \mathbf{r}} \quad (3)$$

and

$$\chi_{k_0}^t = N_{k_0} e^{-\lambda r} e^{-ia\kappa_0 r} e^{ib\kappa_0 \cdot \mathbf{r}}. \quad (4)$$

The quantity M is defined as

$$M = \langle \chi_{k_1}^t(1) \psi_{n1}(2) | v_{12} | \chi_{k_0}^t(1) \psi_{1s}^t(2) \rangle. \quad (5)$$

and evaluated with the use of the generating function of the associated Laguerre function and further approximations. Since the quantity M is related to the D and the E as

$$D = M(a=0, b=1, \kappa_0=1/\lambda_0, k_0=ik_0) \quad (6)$$

and

$$E = M(a=1, b=0, \kappa_0=ik_0, ik_0=1/\lambda_0) \quad (7)$$

a relationship between the D and the E is obtained and given as

$$E = D q^2/k_1^2 G(b=0)/G(b=1), \quad (8)$$

with

$$G(\beta) = (\delta/\delta s)^N \times (N+P)!/N! \times \beta/(1-s)^{P+1} \times \quad (9)$$

$$1/q^2 + \beta^2 \begin{cases} s=0 \\ N=n-1+1 \\ P=2l+1 \end{cases}$$

and

$$\beta = (1+s)/(1-s) + b\kappa_0 \quad (10)$$

Thus, the relation obtained as in Eq. (8) has an appearance similar to that of Ockur's in Eq. (2) and has an additional factor of $G(b=0)/G(b=1)$, which is not unity.

It is remarked that the relationship in Eq. (8) remains valid for all of the excited states (n,l) of the hydrogen, including the 1s-state. Furthermore, the expression for the M in Eq. (5) is good for any excited states of (n,l) so that no other integration is needed for the purpose of evaluating various excitation processes.

References:

1. R. K. Peterkop, Proc. Phys. Soc. (London) **77**, 1220 (1961)
2. V. I. Ockur, Zn. Eksperim. i Teor. Fiz. **45**, 734 (1963)

ELECTRON IMPACT EXCITATIONS OF 3s AND 4s STATES OF HYDROGEN

S.Saxena,G.P.Gupta and K.C.Mathur

Department of Physics, University of Roorkee, Roorkee 247667, India

A distorted wave approximation is used to compute the differential and integral cross sections for the 1s-ns ($n=3,4$) excitations of hydrogen atom by electron impact. A comparative study is made by using distorted waves (Coulomb waves) either in the initial channel or in the final channel or in both the channels.

The differential and integral cross sections for the excitation of hydrogen atom from an initial state i to a final state f are respectively given by

$$\left(\frac{d\sigma}{d\Omega}\right)_{i-f} = \frac{1}{4\pi^2} \frac{k_f}{k_i} \left[\frac{1}{4} |T_+|^2 + \frac{3}{4} |T_-|^2 \right] \quad (1)$$

$$\text{and } \sigma_{i-f} = \frac{2\pi}{k_i k_f} \frac{k_f}{k_i - k_f} \left(\frac{d\sigma}{d\Omega}\right)_{i-f} q \, dq \quad (2)$$

where $\vec{q}(\vec{k}_i - \vec{k}_f)$ is the momentum transfer vector, \vec{k}_i and \vec{k}_f are the momenta of incident and scattered electron respectively.

The T-matrices for the electron impact excitation of hydrogen atom, in the Coulomb-projected Born approximation (distortion in the final channel only), in the modified-Born approximation (distortion in the initial channel only) and in the two-potential approximation (distortion in both the channels), are respectively

given by

$$T_{i-f}^{\text{CPB}} = \langle \chi_f^{(-)} | V' | \phi_i \rangle \quad (3)$$

where $V' = \frac{1}{r_{12}}$ is the Coulomb interaction between the incident and target electron.

$$T_{i-f}^{\text{MB}} = \langle \phi_f | V | \chi_i^{(+)} \rangle \quad (4)$$

where $V = \frac{1}{r_{12}} - \frac{1}{r_2}$ is the total interaction potential of the incident electron with the target hydrogen atom.

$$T_{i-f}^{\text{TP}} = \langle \phi_f | U | \chi_i^{(+)} \rangle + \langle \chi_f^{(-)} | W | \chi_i^{(+)} \rangle \quad (5)$$

where $U = -\frac{\delta}{r_2}$ and $W = \frac{1}{r_{12}} - \frac{1-\delta}{r_2}$, δ is the screening parameter.

Figures 1 and 2 show our results for electron impact excitations (1s-3s and 1s-4s) of atomic hydrogen at 100eV. The curves IC, FC, BC1, BC2 and B are the calculations which include (i) distortion in the initial channel only (IC); (ii) distortion in the final channel only (FC); (iii) distortion in both initial and final channels (BC1, with δ_i and δ_f calculated according to the procedure of Junker¹; and BC2, with $\delta_i = \delta_f = 1$); and (iv) no distortion in either channels i.e. the first Born calculation (B). In figure 1, we compare our results with the calculation of Syms et al.² (curve DWPO).

Detailed results will be shown at the conference.

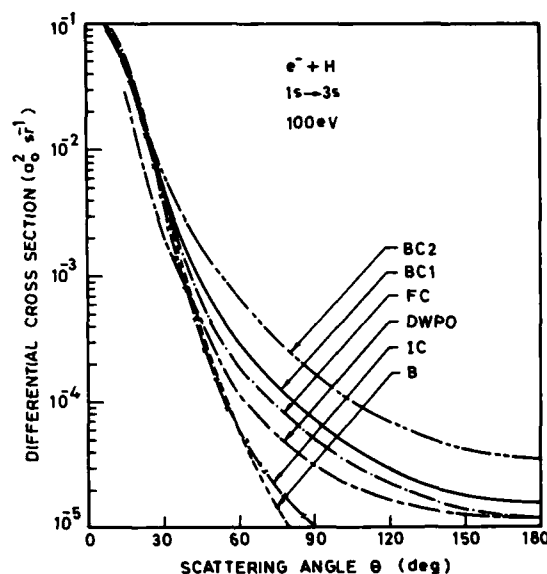


Fig 1

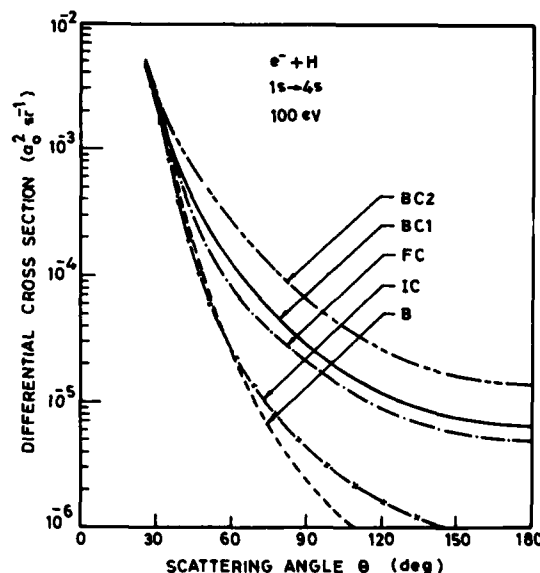


Fig 2

References

1. B.R.Junker, Phys. Rev. A11, 1552 (1975).
2. R.F.Syms, M.R.C. McDowell, L.A. Morgan and V.P. Myerscough, J.Phys. B 8, 2817 (1975).

ELECTRON HYDROGEN SCATTERING AT INTERMEDIATE ENERGIES

Joseph Callaway

Department of Physics and Astronomy, Louisiana State University, Baton Rouge, LA 70803-4001, U.S.A.

This paper reports calculations of cross sections for elastic scattering and excitation of the $n=2$ states of hydrogen atoms by electrons of incident energies from 15 to 54 eV. The calculations are of the close coupling type, and employ a basis of eleven states including the exact $1s, 2s, 2p$, and $3d$ atomic states plus seven pseudostates. The parameters of this set are listed in Table 7 of Ref. 1 ("Standard 5-4-2"). The calculations are made variationally as described previously¹.

The basis set employed has two pseudo thresholds in the energy range of interest. Structure associated with these pseudo threshold is removed using an amplitude averaging technique² in each partial wave in which noticeable structure occurs. This is accomplished by making a least squares fit to the scattering or transition amplitude with a low order polynomial in the energy. Tests on a model for which exact answers are known have shown that results accurate to within a few percent can be obtained in this way³. However, in order to apply this technique successfully, we have found it desirable to make calculations at a large number of energies, both in the region of the pseudo thresholds and outside of it. The present calculations were made at 85 different energies between $k^2=1.1$ and $k^2=4.0$ for the $L=0, 1$, and 2 partial waves and for somewhat smaller numbers for $L=3, 4$, and 5 .

Some improvements were made in the variational programs which permitted accurate calculations to be carried out through $L=5$ (although with a smaller basis for $L=4$ and 5). The elastic scattering cross section is quite well covered at this L , and the $2s$, reasonably so even at $k^2=4$. However, a large number of partial waves contribute to the $2p$ excitation, and in order to estimate their contribution, the unitarized Born approximation with exchange was employed to estimate in all cases, the contribution of partial wave with $L > 6$.

The calculated cross section for $2s$ excitation decreases rapidly between $k^2=1.1$ and $k^2=1.6$ due to a sharp decrease in the $1s$ and $1D$ contributions and

falls off more slowly thereafter. The $1D$ amplitude is quite small in the range of $k^2=1.6-1.8$. In contrast, the $2p$ excitation cross section has a broad maximum with the peak close to $k^2=3.0$.

The present results may be summarized by giving coefficients in a least squares fit to the collision strength ($Q=2k^2\sigma$) of the form

$$Q = \sum_{i=1}^n \frac{a_i}{X^{i-1}} + a_{n+1} \ln X$$

in which $X=k^2/E_x$, E_x being the excitation energy. The fits given below were constrained in that the coefficients a_1 and a_{n+1} were set equal to the first Born approximation values.

Table I

Coefficients in the least squares fit to the collision strength ($n=5$)

i	$2s$	$2p$
1	0.888	0.895
2	-2.176	-11.161
3	1.532	16.652
4	1.979	-3.206
5	-1.808	-2.838
6	0.0	4.439

References

1. J. Callaway, Phys. Repts. **45**, 89(1978).
2. P.G. Burke, K. A. Berrington, and C. V. Sukumar, J. Phys. **B14**, 2891(1981).
3. D. H. Oza and J. Callaway, Phys. Rev. **A30**, 1101(1984).

GLAUBER AMPLITUDE FOR $1s \rightarrow 2s, 2p$ EXCITATION OF HYDROGEN
ATOM BY ELECTRON IMPACT

B. Padhy* and D. K. Rai

Department of Physics, Banaras Hindu University, Varanasi-221005 India.

The Glauber approximation has been successfully used over the last decade for calculation of cross sections for the atomic and molecular collision processes. However, the exact Glauber amplitude has been obtained in closed form¹ for the case of a charged particle scattered by a hydrogen atom; but numerical computations are required for the case of other complex atoms including helium². As an alternative method Yates³ proposed the evaluation of the first few terms of the Glauber series in an exact manner and neglected the other higher order terms assuming that their contribution would be negligible for high incident energies. Yates reported closed form expressions for the first three terms of the Glauber series for the elastic scattering of an electron by a hydrogen atom in its ground state. The calculated differential cross section is found to be in good agreement with the exact Glauber cross section, thereby justifying his neglect of higher order terms.

Though Yates³ himself mentions about extending his method to the inelastic electron-hydrogen atom scattering, no such results have been reported so far. In this note we present closed form expressions for the third term of the Glauber series for the electron impact $1s \rightarrow 2s, 2p$ excitations of a hydrogen atom as well as the corresponding differential cross sections through order $(1/k_i^2)$, \vec{k}_i being the incident wave vector.

Atomic units are used throughout. The axis of quantization of the atomic wave functions is specified by $\hat{z} = \hat{k}_i$ and the momentum transfer vector $\vec{q} = (\vec{k}_f - \vec{k}_i)$ is assumed to be perpendicular to the axis of quantization.

Expanding the Glauber amplitude in the form of an infinite series

$$f_a(i \rightarrow f) = \sum_{n=1}^{\infty} i^{n-1} f_n(i \rightarrow f), \quad (1)$$

the differential cross section through order $(1/k_i^2)$ is written as

$$\left(\frac{d\sigma}{d\Omega}\right) = (k_f/k_i) [f_1^* f_1 + f_2^* f_2 - f_1^* f_2 - f_1 f_2^*]. \quad (2)$$

For the $1s \rightarrow 2s$ excitation of the hydrogen atom we get

$$f_1 = -8\sqrt{2}/(q^2 + 2.25)^3, \quad (3)$$

$$f_2 = -(13\pi k_i)^{-1} (2 + \frac{3}{2}\lambda) \frac{\partial}{\partial \lambda} \left[\frac{4\pi}{\lambda^2 (q^2 + \lambda^2)} \ln \left(\frac{q^2 + \lambda^2}{q\lambda} \right) \right]_{\lambda=1.5}, \quad (4)$$

and

$$f_3 = (3\sqrt{2}\pi^2 k_i)^{-1} (2 + \frac{3}{2}\lambda) \frac{\partial}{\partial \lambda} \left(-\frac{3\pi^2 L}{\lambda^2 (q^2 + \lambda^2)} \right)_{\lambda=1.5}, \quad (5)$$

where

$$L = 4 \left\{ \ln \left(\frac{q^2 + \lambda^2}{q\lambda} \right) \right\}^2 + \frac{1}{3} \pi^2 - 2A,$$

with

$$A = -\sum_{n=1}^{\infty} \frac{1}{n^2} \left(-\frac{\lambda^2}{q^2} \right)^n, \quad \text{if } q^2 > \lambda^2, \\ = \frac{1}{6} \pi^2 + 2 \left\{ \ln(q/\lambda) \right\}^2 + \sum_{n=1}^{\infty} \frac{1}{n^2} \left(-\frac{q^2}{\lambda^2} \right)^n, \quad \text{if } q^2 < \lambda^2. \quad (6)$$

Table I. Results of the present calculation for 100 ev incident energy. $\left(\frac{d\sigma}{d\Omega}\right)_0$ corresponds to $1s \rightarrow 2s$ excitation and $\left(\frac{d\sigma}{d\Omega}\right)_p$ to $1s \rightarrow 2p$ excitation. Results are in units of $\text{\AA}^2/\text{sr}$.

$\theta(\text{deg})$	$(d\sigma/d\Omega)_0$	$(d\sigma/d\Omega)_p$	$\theta(\text{deg})$	$(d\sigma/d\Omega)_0$	$(d\sigma/d\Omega)_p$
0	2.103	1.011(2)	40	4.568(-3)	5.046(-3)
5	1.086	2.310(4)	60	2.344(-3)	7.758(-4)
10	4.344(-1)	4.530	80	1.117(-3)	2.180(-4)
20	5.474(-2)	2.854(-1)	100	6.035(-4)	8.389(-5)
30	8.290(-3)	2.683(-2)	130	3.200(-4)	3.220(-5)

+ The number in the parentheses shows the power of 10 by which the quantity is to be multiplied.

The first three terms of the vector amplitude for the $1s \rightarrow 2p$ excitation are given by

$$\vec{f}_1 = -11\sqrt{2} i \vec{q} / [q^2 (q^2 + 2.25)^3], \quad (7)$$

$$\vec{f}_2 = (3\sqrt{2} i / \pi k_i) \frac{\partial}{\partial \lambda} \left[\frac{4\pi}{\lambda^2 (q^2 + \lambda^2)} \right]_{\lambda=1.5}, \quad (8)$$

$$\vec{f}_3 = (-13 i / \pi^2 k_i) \left\{ \frac{\partial}{\partial \lambda} \left(\frac{4\pi}{\lambda^2 (q^2 + \lambda^2)} \right)^2 - \frac{4\pi^2 \vec{q}}{q^2 (q^2 + \lambda^2)} (P - A) \right\}_{\lambda=1.5}, \quad (9)$$

where

$$P = \frac{2\pi q}{q^2 (q^2 + \lambda^2)} [\lambda^2 \ln \lambda^2 - q^2 \ln q^2 + (q^2 - \lambda^2) \ln (q^2 + \lambda^2)], \quad (10)$$

$$P = \pi^2/6 + 2 \left\{ \ln(q/\lambda) \right\}^2 + (1 - \frac{q^2}{\lambda^2}) \ln(1 + \frac{q^2}{\lambda^2}), \quad (11)$$

and the expression for A is the same as given in Eq. (6). The differential cross sections for 100 ev incident energy, are given in table I. These results agree with the exact Glauber results reported by Gien.⁴

References

- * Present address-Department of Physics, I. I. T. College, Bhubaneswar 751014 India.
1. B.K. Thomas and E. Gerjuoy, J. Math. Phys. **12**, 1567 (1971).
2. B.K. Thomas and F.F. Chan, Phys. Rev. A **8**, 252 (1973).
3. A.C. Yates, Chem. Phys. Lett. **25**, 480 (1974).
4. T.T. Gien, Phys. Rev. A **20**, 1457 (1979).

ACCURATE ELECTRON-HYDROGEN ATOM CROSS SECTIONS USING HYPERSPHERICAL COORDINATES

Diane M. Hood and Aron Kuppermann

Arthur Amos Noyes Laboratory of Chemical Physics, California Institute of Technology, Pasadena, California 91125 USA

We have obtained converged cross sections and phases for scattering electrons off hydrogen atoms using hyperspherical coordinates. Our motivation for using this new technique is that previous methods -- coupled channel expansions using target atom eigenfunctions,¹ polarization functions and pseudostates,² and variational methods³ -- have all presented difficulties. The coupled channel calculations tend to converge slowly with respect to basis set size, and the variational method with pseudostates interjects spurious resonances. Previous applications of hyperspherical coordinates^{4,5} have used methods that, while adequate for computing the energy level of the bound state of H^- and the position of scattering resonances, are not well suited for full scattering calculations.

We have obtained converged surface functions at a set of discrete values of the hyperradius, which acts as a parameter. They are calculated by expansion in a basis set of the hyperspherical angle, which is obtained by a finite difference method and includes the effect of the potential.

The scattering functions are then expanded in these surface functions, and the resulting coupled equations are solved numerically at each energy. We have so far performed calculations for $J=0$ and $J=1$ up to the $n=4$ threshold using a VAX 11/780 with an FPS 164 attached processor. Both the magnitude and the phases of the elements of the scattering matrix are converged with respect to the number of surface functions used. The method is accurate as well as efficient. These calculations are aimed at producing accurate state-to-state differential cross sections and polarization cross sections. The results obtained so far will be presented.

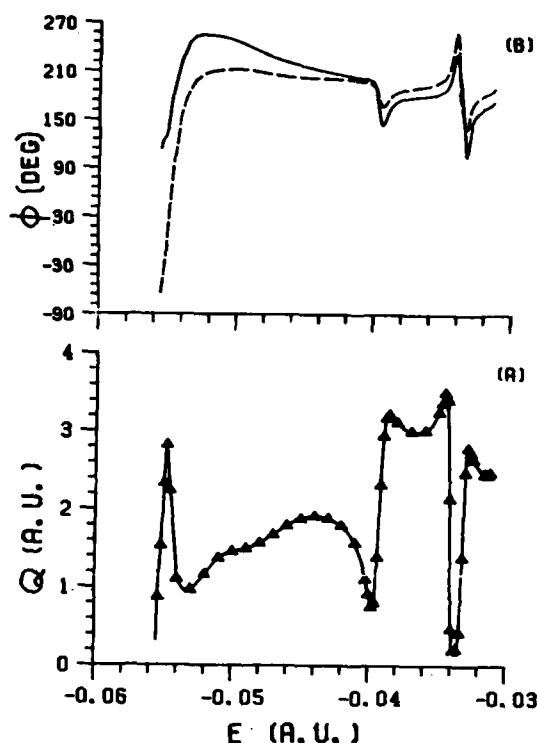


FIGURE 1 (a) Triplet, odd $J=1$ contribution to the $2s \rightarrow 3d$ cross section in the $n=3$ to $n=4$ energy range, (b) Phases of the corresponding S-matrix elements, $(2s1) \rightarrow (3d1)$ and $(2s1) \rightarrow (3d3)$.

References

1. P. B. Burke, S. Ormonde and W. Whitaker, Proc. Phys. Soc., **92**, 319 (1967).
2. S. Geltman and P. G. Burke, J. Phys. B, **3**, 1062 (1970).
3. J. Callaway, Phys. Rev. A, **26**, 199 (1982).
4. C. D. Lin, Phys. Rev. A, **23**, 1585 (1981).
5. H. Klar and M. Klar, Phys. Rev. A, **17**, 1007 (1978).

A COMPLETENESS TEST FOR PSEUDOSTATE EXPANSIONS

D.H. Madison

Physics Department, Drake U., Des Moines, IA. 50311 USA

In close coupling calculations, scattering wave functions are expanded in terms of an appropriately chosen complete set of wave functions. Such complete sets typically contain an infinite number of terms representing both bound and continuum states. In practical close coupling calculations, the series is truncated after including a limited number of terms of the bound state type. A common practice is to approximate the neglected bound and continuum terms by a small number of bound-type states called pseudostates. While various schemes for choosing these pseudostates have been employed, the key question concerns the extent to which the pseudostate basis set approximates the results which would be obtained from the full complete set. However, it has not been possible to unambiguously answer this question since exact results have not been known.

Madison¹ has recently reported a calculation of the second order distorted wave amplitude for electron excitation of hydrogen in which no approximations were made in the evaluation of the second order amplitude. As a result, an infinite sum over discrete and continuum intermediate states was performed in this calculation. Since these results represent an exact answer for a complete set, they provide the opportunity for checking the completeness of various pseudostate expansions. This is a most important check since it represents an exact answer for the scattering problem. While it has been possible to check pseudostate basis sets by using them to calculate various known atomic parameters, such a procedure does not necessarily represent a reliable check of completeness for the scattering problem since there is no guarantee that a particular atomic parameter will be sensitive to the same radial range that is important for the scattering problem.

We have calculated second order distorted wave amplitudes for electron-excitation of the 2p state of hydrogen using various pseudostate basis sets which have been used in close coupling calculations. These results will be compared with the exact answer obtained from the full complete set of bound and continuum states. The best pseudostate basis set will be given.

Acknowledgements

Helpful discussions with J. Callaway are gratefully acknowledged.

Work supported by the National Science Foundation under Grant No. Phy-8310644 and by a Northwest Area Foundation grant of the Research Corporation.

Reference

1. D.H. Madison, Phys. Rev. Lett. 53, 42 (1984).

CALCULATION OF INELASTIC ELECTRON-ATOM SCATTERING AMPLITUDES BY THE
METHOD OF LOCALLY COMPLEX DISTORTIONS OF THE ENERGY SPECTRUM

C. W. McCurdy* and T. N. Rescigno†

*Department of Chemistry, Ohio State University, Columbus, Ohio 43210

†Theoretical Atomic and Molecular Physics Group, Lawrence Livermore National Laboratory, Livermore, California 94550

Recently we have demonstrated that the array of techniques employing complex basis functions, which have been broadly applied in the calculation of resonance positions and lifetimes, can also be used in the practical calculation of scattering amplitudes and total photoionization cross sections.¹ In that work, which primarily used potential scattering examples, we showed that resolvent matrix element of the form

$$\lim_{\epsilon \rightarrow 0} (f, (E - H + i\epsilon)^{-1} g)$$

can be calculated for a wide range of types of functions f and g , by employing a finite matrix representation of the Hamiltonian, H , in a basis of square-integrable functions. That is to say that by finding the matrix eigenfunctions satisfying

$$(\phi_i, H \phi_j) = E_i \delta_{ij}$$

we can construct an apparently convergent spectral approximation to the resolvent matrix element of the form

$$\lim_{\epsilon \rightarrow 0} (f, (E - H + i\epsilon)^{-1} g) = \sum_{i=1}^N \frac{(f, \phi_i)(\phi_i, g)}{E - E_i}$$

The key to these calculations is the use of a basis of complex-valued functions together with a definition of the inner product without complex conjugation. Thus the eigenvalues, E_i , appearing in the expressions above are complex as are the associated functions ϕ_i . Although this approach is superficially similar to the complex coordinates approach,^{2,3} in which the coordinates are scaled according to $r \rightarrow re^{i\alpha}$, the two techniques differ dramatically in the present context. The eigenvalues, E_i , above do not lie on rays in the complex plane, but rather on curves which are

distorted off the real energy axis only in a local interval. Furthermore this procedure avoids well known divergences which are known to plague the complex coordinates approach when the functions f and g are not exponentially bounded.⁴ A formal many-electron expression for the T-matrix for inelastic electron-atom scattering which is amenable to this approach is

$$T = (\psi_f(H-E) \psi_i) + (\psi_f(H-E) \frac{1}{(E - H + i\epsilon)} (H-E) \psi_i)$$

where ψ_i and ψ_f are antisymmetrized unscattered states in the initial and final channels. We apply this procedure to the computation of the 1s-1s, 1s-2s, and 1s-2p amplitudes for electron-hydrogen atom scattering in the 1s, 2s, 2p approximation and compare the results with those of close coupling calculations. In addition we present results for the 2s-2p transition in electron-lithium atom scattering.

References

1. T. N. Rescigno and C. W. McCurdy, Phys. Rev. A **31**, 624 (1985).
2. J. Nuttall and H. L. Cohen, Phys. Rev. **188**, 1542 (1969).
3. B. R. Johnson and W. P. Reinhardt, Phys. Rev. A **29**, 2933 (1984).
4. R. T. Baume, M. C. Crocker, and J. Nuttall, Phys. Rev. A **12**, 486 (1975).

ROLE OF EXCITATION ENERGY IN SECOND BORN APPROXIMATION

N.S. Rao* and H.S. Desai**

* Physical Research Laboratory, Theoretical Physics Area, Navrangpura, Ahmedabad 380 009, India

** Physics Department, Faculty of Science, M.S. University, Baroda 390 002, India

The theoretical study of electron collisions with atomic systems has attracted a considerable amount of interest in recent years. Firstly, there is an increasing demand for electron collision cross sections in other fields such as astrophysics, laser physics and plasma physics. Secondly, a number of important advances have occurred on the experimental side. These experiments provide very stringent tests of the theory and have stimulated the development of new theoretical approaches. Motivated to these, we have improved our earlier work on elastic¹ and inelastic² scattering of electrons by helium and hydrogen atoms to study the role of excitation energy (DE) in the Second Born approximation and hence on DCS for elastic and inelastic processes of helium and hydrogen atoms^{1,2}.

Basically DE can be calculated by using optical theorem and target polarization property. Using these models DE's are calculated earlier³. In the present study two DE's are used to calculate DCS in the Second Born approximation for elastic and inelastic scattering of electrons by helium and hydrogen atoms at incident energy $E \leq 700$ eV. With these results an attempt is made to show explicitly the variation of DCS results corresponding to two DE's for helium and hydrogen atoms.

It is observed from our DCS calculations that the sensitivity of real and imaginary parts of the second Born approximation due to DE is as follows

$$\text{Re } b_{\text{HEA}}^{(2)} > \text{Re } b_{\text{HEA}}^{(2)} > \text{Im } b_{\text{HEA}}^{(2)} \quad (1)$$

Finally we conclude that the effect of DE is considerable in total integrated cross section than in DCS calculations. The selection of DE is more important in the intermediate angular and incident energy regions both elastic and inelastic processes. The DE obtained by means of optical theorem gives good results in the elastic process. Unfortunately, there was no specified method for DE calculation in inelastic process. Perhaps this may be one of the reasons for considerable deviations between experimental and theoretical comparisons⁴ in the inelastic process.

N.S.R. is thankful to Physical Research Laboratory, Ahmedabad, India, for the award of a Post-Doctoral Fellowship.

References

1. N.S. Rao and H.S. Desai, *Pramana* **17**, 309 (1981).
2. N.S. Rao and H.S. Desai, *Curr. Sci.* **52**, 480 (1983).
3. F.W. Byron and C.J. Joachim, *J. Phy. B.* **10** 207 (1977)
4. B.H. Bransden et al., *J. Phy. B.* **15**, 4605 (1982).

DISTORTED WAVE CALCULATIONS WITH DIFFERENT DISTORTING POTENTIALS

C. S. Singh and D. N. Rai

Department of Physics, Banaras Hindu University, Varanasi-221005, India

It has been known for sometime that if both the initial- and final- channel distorted waves are calculated with use of the final channel distorting potential V_f , the first order results are in much better agreement with the experimental data¹. In view of this we are making a detailed comparison of differential cross sections obtained for electron impact excitation of 2^1S and 2^3S states of

helium-atom. Distorted wave methods with different choices (either initial channel distorting potential or final channel distorting potential) for the distorting potential have been used. Results would be shown in the conference.

Reference

1. D.H. Madison, Phys.Rev.Lett. 53, 42 (1984).

THE COUPLED-CHANNELS-OPTICAL METHOD FOR ELECTRON-ATOM SCATTERING

I.E. McCarthy*, J.D. Mitroy* and A.T. Stelbovics†

* The Flinders University of South Australia, Bedford Park 5042, Australia
 † Murdoch University, Murdoch 6150, Australia

Electron-atom scattering may be described in terms of reaction channels defined by target states $|i\rangle$ and total spin S . The target states satisfy the Schrödinger equation

$$(\epsilon_i - H_T)|i\rangle = 0. \quad (1)$$

Where appropriate we regard $|i\rangle$ as a discrete notation for the continuum, using box normalization and the usual limiting processes.

The coupled-channels method is based on an anti-symmetric expansion of the total wave function $\Psi_S^{(+)}(E)$ in target states $|i\rangle$. For each value of S (suppressed for convenience) we have a set of coupled equations that we can express in a matrix notation in channel space (all operators act on $\Psi_S^{(+)}(E)$).

$$E^{(+)} - K - V = 0. \quad (2)$$

Here K is the kinetic energy operator of the projectile, V includes direct and exchange potentials.

Before taking the box-normalization limits channel space is discrete but of infinite dimension. After taking limits the ionization continuum renders (2) meaningless.

Before taking limits we choose a finite set of channels including the entrance channel, projected by an operator P , for which we solve the coupled equations explicitly using an appropriate representation. The complementary projection operator Q projects the remaining states including the continuum. We write a projected set of coupled equations using an optical potential operator $V^{(Q)}$.

$$P(E^{(+)} - K - V^{(Q)})P = 0, \quad (3)$$

$$V^{(Q)} = V + VQ[Q(E^{(+)} - K - V)Q]^{-1}QV. \quad (4)$$

After the limiting procedure the continuum is introduced into (4) in terms of integrals over the continuum kinematic variables. Equations (3),(4) constitute a meaningful coupled-channels theory, the Coupled-Channels-Optical theory. They do not constitute a basis for a complete solution of the electron-atom problem, since the spectral representation of (4) implies a knowledge of $\Psi^{(+)}$. However since the second term of (4) is of second order in (3) it is hoped that an approximate evaluation of (4) will yield a good description of scattering processes within P-space.

The authors' Coupled-Channels-Optical method^{1,2} involves approximating $\Psi^{(+)}$ in the spectral expansion of (4) by the Born approximation for discrete target states

and by the Born approximation with screening correlation for the continuum and performing the kinematic integrals by a multidimensional method.

The P-space equations (3) are written as coupled integral equations (solved using Gaussian quadratures) in a distorted-wave momentum representation for channels i, j, ℓ in P-space

$$\begin{aligned} \langle \chi^{(-)}(\underline{k}_i) | T_{ij} | \chi^{(+)}(\underline{k}_j) \rangle &= \langle \chi^{(-)}(\underline{k}_i) | U | \chi^{(+)}(\underline{k}_j) \rangle \delta_{ij} \\ &+ \langle \chi^{(-)}(\underline{k}_i) | W_{ij} | \chi^{(+)}(\underline{k}_j) \rangle + \int d^3q \langle \chi^{(-)}(\underline{k}_i) | W_{i\ell} | \chi^{(-)}(\underline{q}) \rangle \\ &\times \frac{1}{E^{(+)} - \epsilon_\ell - \frac{1}{2}q^2} \langle \chi^{(-)}(\underline{q}) | T_{\ell j} | \chi^{(+)}(\underline{k}_j) \rangle, \end{aligned} \quad (5)$$

$$T_{ij} \equiv \langle \phi_i | T | \phi_j \rangle, \quad (6)$$

$$W = V^{(Q)} - U, \quad (7)$$

$$[E^{(+)} - \epsilon_i - K - U] \chi^{(+)}(\underline{k}_i) = 0. \quad (8)$$

Here U is a local central potential chosen to cancel as much of $V_{ij}^{(Q)}$ as possible. A typical choice is

$$U = V_{00}^D, \quad (9)$$

where V_{00}^D is the direct part of the ground-state (static) potential.

Thus far the method has been applied with $U = 0$ (momentum representation) to hydrogen, and to lithium, sodium and potassium using a Hartree-Fock one-electron, inert-core description of target structure.

The differential cross sections for 1s, 2s and 2p states of hydrogen are essentially within experimental error. Elastic and dipole transitions for the alkalis have correct total cross sections and correct positions for angular maxima and minima, but the theory is a significant overestimate of backward scattering, indicating the sensitivity to configuration interaction.

Static-exchange calculations for helium and argon using (9) show that the distorted-wave representation accelerates the convergence of the solution of the integral equation very satisfactorily.

Progress will be reported in the use of the distorted-wave representation, in CI descriptions of target structure and in the use of (5) as an approximation for (e, 2e) reactions.

References

1. I.E. McCarthy and A.T. Stelbovics, Phys.Rev.A **28**, 2693 (1983)
2. I.E. McCarthy and A.T. Stelbovics, Phys.Rev.A **28**, 1322 (1983)

A DIRAC R-MATRIX CALCULATION OF ELECTRON SCATTERING FROM Fe XXIII

P.H. Norrington* and I.P. Grant+

*Department of Applied Mathematics and Theoretical Physics, Queen's University, Belfast, BT7 1NN, Northern Ireland
 +Department of Theoretical Chemistry, Oxford University, 1 South Parks Road, Oxford, OX1 3TG, England

The R-Matrix method¹ provides a flexible approach to the calculation of low energy electron scattering processes from atoms and molecules. For electron-atom scattering the space surrounding the target atom can be neatly divided into two regions: the inner region describes the complicated interaction (including exchange) of the incident electron with the target atom; while in the outer region, where the electron motion can be treated non-relativistically, the interaction consists of long-range potentials and is much simpler. The expansion of the wavefunction in the inner region in terms of suitable basis functions bears a close resemblance to that used in bound state problems and similar solution techniques can be applied. In light atoms, where L-S coupling dominates, Hartree-Fock techniques can be used.² As the atomic number increases, it becomes necessary to include Breit-Pauli terms and to transform to an intermediate coupling representation.³ The method has been applied recently to a number of heavy atoms such as Cs, Tl and Hg.⁴ However a more satisfactory approach for heavy atoms would use the Dirac Hamiltonian in the inner region, and this is the method we have employed.

A preliminary Dirac R-matrix calculation for electron scattering by Ne^+ has been reported⁵ and has shown good agreement with the corresponding Breit-Pauli R-matrix calculation. Here we report on a more complicated case which provides a further comparison with an earlier Breit-Pauli calculation.⁶

We have considered two representations of the target atom: a 5-state case ($1s^2 2s^2$, $1s^2 2s 2p$) and a 10-state case ($1s^2 2s^2$, $1s^2 2s 2p$, $1s^2 2p^2$). Cross-sections for the excitation from $1s^2 2s^2 \ ^1S_0^e$ to $1s^2 2s 2p \ ^3P_1^e$ have been obtained. For the 5-state calculation, the incident electron energy lies in the range from 7 to 25 Ryd and, for the 10-state calculation, it is in the range 13.1 to 25 Ryd. At these energies all channels are open. The transition is spin-forbidden in L-S coupling, but relativistic mixing of the final state with $1s^2 2s 2p \ ^1P_1^e$ enhances the cross-section by a factor of two. Our Dirac results for the 5- and 10-state cases agree well with

each other above 13.1 Ryd and lie between the earlier Breit-Pauli values. The two 10-state calculations agree to within about 2%. The better quality of the Dirac 5-state results is due to a better representation of the ground state.

The agreement with the Breit-Pauli R-matrix code here provides further evidence to validate the Dirac method and encourages its use for heavier systems. Methods to improve the efficiency of the program, which involves substantial extra computation, are under investigation. We intend soon to apply it to electron scattering from Hg using a core potential similar to that used in a recent Breit-Pauli calculation.⁴

References

1. Burke P.G. and Robb W.D. 1975 *Advances in Atomic and Molecular Physics*, Vol. 11, ed. D.R. Bates and B. Bederson (New York: Academic) pp. 143-214.
2. Berrington K.A., Burke P.G., Le Dourneuf M., Robb W.D., Taylor K.T. and Vo Ky Lan 1978 *Comput Phys Commun* 14 367-412.
3. Scott N.S. and Taylor K.T. 1982 *Comput Phys Commun* 25 347-87.
4. Bartschat K. and Scott N.S. 1984 *J Phys B: At Mol Phys* 17 3787-95.
5. Norrington P.H. and Grant I.P. 1981 *J Phys B: At Mol Phys* 14 L261-7.
6. Scott N.S. and Burke P.G. 1980 *J Phys B: At Mol Phys* 13 4299-314.

SCHRÖDINGER-LIKE EQUATION FOR RELATIVISTIC PARTICLES

I. B. Goldberg

Racah Institute of Physics, Hebrew University, Jerusalem 91904 ISRAEL
and

Department of Physics and Astronomy, University of Pittsburgh, Pittsburgh, Pennsylvania 15260 USA

We present here a method for obtaining a solution of the Dirac equation in a spherically symmetric potential, by solving a modified Coulomb equation. In subsequent papers we show how this method can be utilized.

We write the Dirac equation in the form

$$\begin{aligned} \frac{dg}{dr} &= -\frac{k}{r} g + \left(\frac{1+\epsilon}{\lambda} + \frac{\alpha Z_0}{r} s(r) \right) f \\ \frac{df}{dr} &= \frac{k}{r} f + \left(\frac{1-\epsilon}{\lambda} - \frac{\alpha Z_0}{r} s(r) \right) g \end{aligned} \quad (1)$$

where the various quantities have their usual meaning, and $s(r)$ is a smooth, monotonically decreasing, screening function such that $s(0) = 1$ and in the tail region $r \geq r_t$, $s(r) = Z_t/Z_0$.

We write the solution of the Dirac equation (1) in the form

$$\begin{aligned} g &= \cos \xi \cdot u + \sin \xi \cdot v \\ f &= Q(-\sin \xi \cdot u + \cos \xi \cdot v) \end{aligned} \quad (2)$$

where $v = (u' - \frac{\gamma}{r} u) \cdot \frac{1}{P}$, $P = \frac{1}{\lambda} \sqrt{\epsilon^2 - 1}$ and $Q = \{(\epsilon-1)/(\epsilon+1)\}^{1/2}$. For continuum states P is the momentum of the particle and Q is the ratio between the amplitude of the small component f and the large component g in the asymptotic region. For bound states P and Q are imaginary but g and f defined in eq. (2) remain real.

In the case of point Coulomb potential, where $s(r) = 1$, g and f defined by eq. (2) solve the Dirac equation (1) if $\gamma = \pm \sqrt{k^2 - \alpha^2 Z_0^2}$, $\tan \xi \equiv \theta \cdot Q = \alpha Z_0 Q / (k - \gamma)$ and u satisfies the Coulomb equation

$$\frac{d^2 u}{dr^2} + \left(p^2 + \frac{2\alpha Z_0 \epsilon}{\lambda r} - \frac{\gamma(\gamma-1)}{r^2} \right) u = 0 \quad (3)$$

When the potential is screened, we still have a solution in the form (2), if the following relations hold:

$$r \frac{d\theta}{dr} = \alpha Z_0 s(r) \cdot (\theta^2 + 1) - 2k\theta \quad (4a)$$

$$\tan \xi(r) = Q \cdot \theta(r) \quad (4b)$$

$$\gamma(r) = [k(Q^2 \theta^2 - 1) + \alpha Z_0 s(1 - Q^2) \cdot \theta] / (Q^2 \theta^2 + 1) \quad (4c)$$

$$\omega(r) = \frac{1}{2} \left(-\frac{d\gamma}{dr} + \frac{\epsilon+1}{\lambda} \cdot \frac{k+\gamma}{\theta} + \frac{\epsilon-1}{\lambda} (k-\gamma) \cdot \theta \right) \quad (4d)$$

and u satisfies the modified Coulomb equation

$$\frac{d^2 u}{dr^2} + \left(p^2 + \frac{2\omega(r)}{r} - \frac{\gamma(r)[\gamma(r)-1]}{r^2} \right) u = 0. \quad (5)$$

Equation (5) has the following properties:

(i) In the nonrelativistic limit it reduces to the Schrodinger equation with screening function $s(r)$. We choose the sign of γ such that $\gamma = -k$ in this limit, and the angular momentum of the Schrodinger equation is $\ell = k$ ($k > 0$) or $\ell = -k-1$ ($k < 0$).

(ii) As the origin is approached, $\gamma(r) \rightarrow -\text{sign}(k) \cdot \sqrt{k^2 - \alpha^2 Z_0^2}$. This assures the correct behavior of u (and consequently the behavior of g and f) near the origin.

(iii) In the asymptotic region, when r tends to infinity, the solution u of the modified Coulomb equation (5) tends to the solution u_c of the Coulomb equation (3), with $\gamma = \gamma_t$ and $Z = Z_t$. The solution of the Dirac equation is given by eq. (2) with $\xi = \xi_t = \arctan [(\alpha Z_t Q) / (k - \gamma_t)]$.

Helpful discussions with Prof. R. H. Pratt and Dr. J. Stein are gratefully acknowledged.

SINGLE CHANNEL RELATIVISTIC QUANTUM DEFECT RELATION

I. B. Goldberg

The Racah Institute of Physics, Hebrew University, Jerusalem 91904, ISRAEL
and

Department of Physics and Astronomy, University of Pittsburgh, Pittsburgh, Pennsylvania 15260 USA

In a preceeding work¹ (referred to hereafter as I) we have defined the modified Coulomb equation (I.5), the solutions of which are used to obtain the solution of the Dirac equation (I.1). The resemblance of eq. (I.5) to the Schrodinger equation suggests that the quantum defect relation for the Dirac equation can be derived in a way which is analogous to the nonrelativistic case.

the tail region ($r \geq r_t$) the solution of (I.5) can be written as

$$\begin{aligned} u &= \cos(\xi_t - \xi) \cdot u_c + \sin(\xi_t - \xi) \cdot v_c \\ v &= -\sin(\xi_t - \xi) \cdot u_c + \cos(\xi_t - \xi) \cdot v_c \end{aligned} \quad (1)$$

where u_c is a solution of the Coulomb equation (I.3), $v_c = [u_c' - (\gamma_t/r)u_c]$ and $\xi_t = \arctan[(\alpha Z_t Q)/(k - \gamma_t)]$. By eqs. (I.4a and I.4b) $\xi(r) = \xi_t$ in the tail region for $k < 0$, and $(\xi - \xi_t) \sim r^{-2\gamma}$ for $k > 0$. Therefore, the asymptotic behavior of u and v is given by the asymptotic behavior of u_c and v_c .

One can find a pair of independent solutions of the Coulomb equation (I.3), regular and irregular at the origin, with the following asymptotic behavior:

(i) Above threshold ($\epsilon > 1$)

$$\begin{pmatrix} y_1 \\ y_2 \end{pmatrix} \sim_{r \rightarrow \infty} \frac{2\eta \gamma e^{-\pi\eta/2}}{\Gamma(\gamma + i\eta)} \begin{pmatrix} \sin \omega \\ \cos \omega \end{pmatrix} \quad (2)$$

where $\eta = \alpha Z\epsilon/\sqrt{\epsilon^2 - 1}$ and

$$\omega = pr + \eta \ln 2pr + \frac{\pi}{2}(1 - \gamma) - \arg \Gamma(\gamma + i\eta)$$

(ii) Below threshold ($\epsilon < 1$)

$$\begin{pmatrix} y_1 \\ y_2 \end{pmatrix} \sim_{r \rightarrow \infty} \frac{v}{\pi} \Gamma(1 - \gamma + v) \left(\frac{2x}{v} \right)^v e^{-x/v} \begin{pmatrix} \sin \pi(\gamma - v) \\ -\cos \pi(\gamma - v) \end{pmatrix} + \text{exponentially decreasing terms} \quad (3)$$

where $x = \alpha Z\epsilon \cdot (r/\lambda)$ and $v = \alpha Z\epsilon/\sqrt{1 - \epsilon^2}$. These two functions, y_1 and y_2 , are analytic functions of the energy near threshold.

Let u be a regular solution of (I.5), and let u_c be the corresponding Coulomb function according to eq. (1). Then u_c can be expressed as a linear combination of y_1 and y_2 ($\gamma = \gamma_t$):

(i) Above threshold ($\epsilon > 1$). Here we write

$$u_c = \cos \delta \cdot y_1 + \sin \delta \cdot y_2 \sim_{r \rightarrow \infty} \frac{2\eta \gamma e^{-\pi\eta/2}}{\Gamma(\gamma + i\eta)} \sin(\omega + \delta) \quad (4)$$

Thus δ is the phase shift caused by the non-Coulomb potential in equation (I.5).

(ii) Below threshold ($\epsilon < 1$). Here we write

$$u_c = \cos \pi\mu \cdot y_1 + \sin \pi\mu \cdot y_2 \quad (5)$$

When u corresponds to a bound state, its exponentially growing component should vanish. Let $\epsilon_{n,k}$ be the energy of the bound state, then

$$\gamma - \nu(\epsilon_{n,k}) - \mu(\epsilon_{n,k}) = |k| - n = \text{integer} \quad (6)$$

Therefore $\mu(\epsilon_{n,k})$ is the quantum defect caused by the non-Coulomb part of the potential.

Since the functions u_c , y_1 and y_2 are analytic functions near the threshold, we can continue analytically the quantum defect function $\mu(\epsilon)$ to values above threshold, and we get the relation²

$$\cot \delta = (1 - \cos 2\pi\gamma e^{-2\pi\eta}) \cot \pi\mu - \sin 2\pi\gamma e^{-2\pi\eta} \quad (7)$$

and at the threshold we have

$$\delta(\epsilon = 1) = \pi\mu(\epsilon = 1). \quad (8)$$

Let g_1 and g_2 be the Dirac functions in the point Coulomb potential, corresponding to the substitution of y_1 and y_2 in (I.2). Let g be the solution of the Dirac equation (I.1) corresponding to the solution u of the modified Coulomb equation (I.5). Then, by (I.2) and (1), δ and μ are the phase shift and the quantum defect of the Dirac function g caused by the non-Coulomb potential in the Dirac equation (I.1). Equation (7) gives, therefore, the single channel relativistic quantum defect relation.

Helpful discussions with Prof. R. H. Pratt are gratefully acknowledged.

References

1. I. B. Goldberg, "Schrodinger-like Equation for Relativistic Particles", ICPEAC XIV (1985).
2. W. R. Johnson and K. T. Cheng, J. Phys. B 12, 863 (1979).

RELATIVISTIC WKB APPROXIMATION TO PHASE-SHIFTS AND CONTINUUM NORMALIZATIONS

I. B. Goldberg, J. Stein, Akiva Ron and R. H. Pratt*

Racah Institute of Physics, Hebrew University, Jerusalem 91904 ISRAEL

*Department of Physics and Astronomy, University of Pittsburgh, Pittsburgh, Pennsylvania 15260 USA

The generalized WKB method, for which Coulomb functions are used as comparison functions,¹ was employed for getting approximate solutions to the modified Coulomb equation for the relativistic case.² By using the exact relation (eq. 2 of ref. 2) between the modified Coulomb functions and the Dirac functions, we obtained approximate phase shifts and continuum normalizations of relativistic particles in a spherically symmetric potential. The calculations have been done for a wide range of energies (1 eV - 1 MeV), angular momenta ($|k| = 1, 2, \dots, 10$) and atomic numbers ($Z = 6, 50, 92$). The potentials used in the calculations were the DHFS of Liberman³ and the APT potential of Pratt.⁴

Exact phase shifts and continuum normalizations of the Dirac functions were obtained by solving numerically the Dirac equation in the same potential. The comparison between the exact and approximate results shows that the higher the energy or the angular momentum are, the higher is the accuracy of the approximation. This feature is common to the three elements studied.

We present here the results for tin ($Z = 50$), calculated in the DHFS potential with Coulombic tail of charge $Z_{\text{tail}} = 1$. Figure 1 shows the relative error of the continuum normalizations $[N(\text{WKB})/N(\text{exact}) - 1]$ as a function of the energy for various angular momenta. Figure 2 shows the phase shift error $[\delta(\text{WKB}) - \delta(\text{exact})]$ for the same energies and angular momenta.

Two special cases are worth mentioning. (i) For $k = -1$ (s wave) the modified Coulomb equation has no classical turning point and the generalized WKB method has been slightly modified in order to be applied for this case. (ii) When the modified Coulomb equation has more than one classical turning point, the generalized WKB method cannot be applied. This case may be connected with the occurrence of a shape resonance.

References

1. J. Stein, A. Ron, I. B. Goldberg and R. H. Pratt, "Generalized Nonrelativistic WKB Approximation...", ICPEAC XIV (1985).
2. I. B. Goldberg, "Schrodinger-Like Equation for Relativistic Particles", ICPEAC XIV (1985).
3. D. Liberman, J. T. Waber and D. T. Cromer, Phys. Rev. **137**, A27 (1965).
4. J. McEnnan, L. Kissel and R. H. Pratt, Phys. Rev. A **13**, 532 (1976).

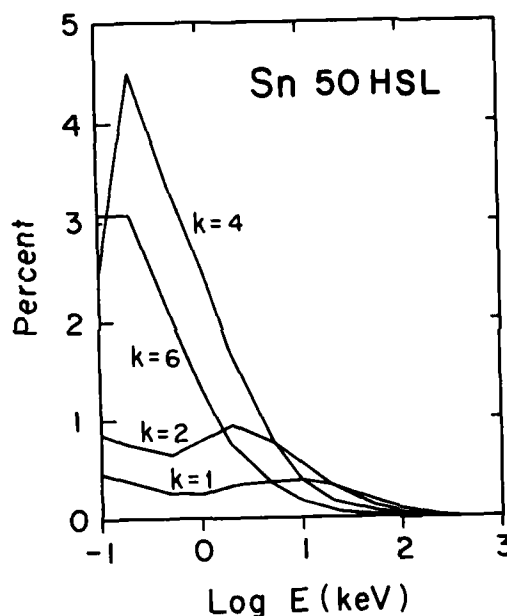


Fig. 1. Relative normalization error for tin.

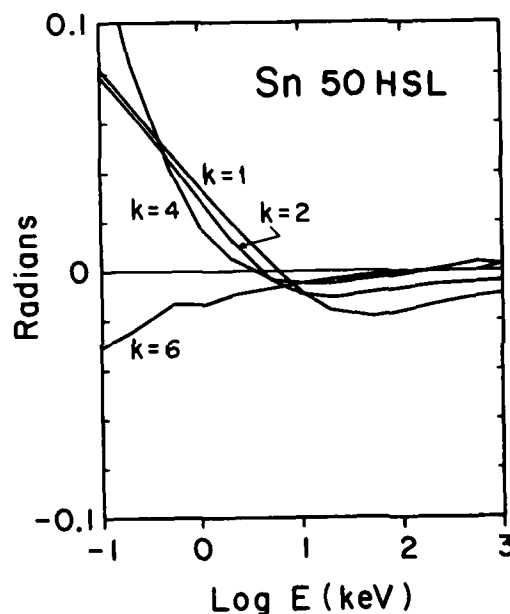


Fig. 2. Phase-shift error for tin.

GENERALIZED NONRELATIVISTIC WKB APPROXIMATION WITH COULOMB COMPARISON FUNCTIONS

J. Stein, Akiva Ron, I. B. Goldberg* and R. H. Pratt†

*Racah Institute of Physics, Hebrew University, Jerusalem 91904 ISRAEL

†Department of Physics and Astronomy, University of Pittsburgh, Pittsburgh, Pennsylvania 15260 USA

We have derived expressions for the normalizations and phase shifts of continuum wave functions in screened Coulomb potentials within the generalized WKB formalism.¹ The Schrodinger equation for the exact solution, $Y(\rho)$, and the equation for the comparison function, $U(R)$, are

$$\frac{d^2 Y}{d\rho^2} + \left(1 - \frac{2\eta s(\rho)}{\rho} - \frac{\ell(\ell+1)}{\rho^2}\right) Y = \frac{d^2 Y}{d\rho^2} + k^2(\rho) Y = 0,$$

$$\frac{d^2 U}{dR^2} + \left(1 - \frac{2H}{R} - \frac{\ell(\ell+1)}{R^2}\right) U = \frac{d^2 U}{dR^2} + K^2(R) U = 0,$$

where $s(\rho)$ is the screening function, $\eta = [(-mZe^2)/\hbar^2] \cdot \hbar / \sqrt{2mE}$ and H is a parameter. Now the generalized WKB approximation $y(\rho)$ to $Y(\rho)$ is

$$y(\rho) = A(\rho) U[R(\rho)]$$

where

$$\frac{dR}{d\rho} = \frac{k(\rho)}{K(R)} \quad \text{and} \quad A = \left(\frac{K(R(\rho))}{k(\rho)} \right)^{1/2}.$$

The formalism of Barlett, Rice and Good² is a special case of our formalism in the limit $H \rightarrow \infty$ namely, for low energies. Then one practically uses Bessel comparison functions (their $J_{2\ell+1}$ approximation) instead of Coulomb comparison functions.

We have calculated data for three elements: carbon, aluminum and iron for energies ranging from 0.1 keV up to 100 keV and $\ell = 0, 2$ and 10. We used the Herman-Skillman potentials with Latter's tail. Apart from comparing our results with exact numerical values which we computed, we also compared them with normalizations and phase shifts calculated within the framework of different approaches to the problem: a) The standard WKB approximation with Langer's³ correction. b) The Analytic Perturbation Theory (APT) approach.⁴ Langer's correction consists of the substitution $\ell(\ell+1) \rightarrow (\ell + \frac{1}{2})^2$ which improves the results dramatically, except for $\ell = 0$. We present results for aluminum. Figure 1 shows the relative errors in the normalizations and Fig. 2 shows the difference of the phase shifts from exact numerical results for both approximations: our (solid lines) and the standard (dashed lines). All quantities are shown as function of energy (drawn on a logarithmic scale) for $\ell = 0, 2$, and 10.

One sees clearly that for $\ell = 0$ the standard results are much worse than our WKB ones. Our results are also better for high energies and low ℓ values. Only for low

energies and $\ell \neq 0$ the standard results are somewhat better than ours. The same is also true for carbon and iron. We have used throughout $H = \eta$ and other choices of H can further improve the results. Our results are also better than the APT ones when energies are high and ℓ values big, and the APT results are better for small values of ℓ although the discrepancy is not too large.

References

1. S. C. Miller, Jr. and R. H. Good, Jr., Phys. Rev. **91** (1953).
2. R. H. Barlett, M. H. Rice and R. H. Good, Jr., Annals of Phys. **2**, 372 (1957).
3. R. E. Langer, Phys. Rev. **51**, 669 (1937).
4. J. McEnnan, L. Kissel and R. H. Pratt, Phys. Rev. **13**, 532 (1976).

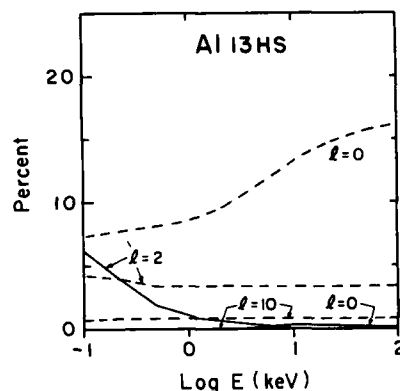


Fig. 1. Relative errors in the normalizations of aluminum continuum wave functions for our (solid lines) and the standard (dashed lines) WKB approximations.

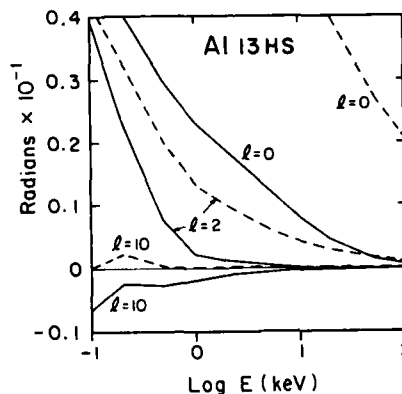


Fig. 2. Phase shift differences of aluminum continuum wave functions for our (solid lines) and the standard (dashed lines) WKB approximations.

NEW METHOD FOR THE INTERPOLATION OF DIPOLE OSCILLATOR-STRENGTH SUM RULES

James M. Peek

Sandia National Laboratories, Albuquerque, New Mexico 87185 USA

There are several sum rules for complete sums of the dipole oscillator strength weighted by the k -th power of the excitation energy, $S(k)$, that require only the occupied orbitals for evaluation. It is also well known that the interpolation of these data, available for certain integer k , with respect to k provides a number of useful scattering parameters, including the stopping and straggling mean-excitation energy and the Lamb-shift energy. A number of interpolation or other indirect calculative techniques have been motivated by the difficulties encountered in their direct evaluation. An entirely new interpolation method is reported here.

One of the more accurate interpolation methods that uses only conveniently calculated $S(k)$ data relies upon a quadratic spline fit to an auxiliary function of $S(k)$ ¹. It has been possible to improve upon these results for the case of atoms by using hydrogen values for $S(k)$ and their convenient effective-nuclear-charge scaling properties. A suitable restructuring of the hydrogenic $S(k)$ formulas and a relationship between the target atom's $S(k)$ are required. This defines the effective nuclear charge as a function of k , $Z(k)$. The $Z(k)$ curve is expected to be a rather smooth function, decreasing toward the target's ionic charge plus one as k decreases and increasing to a value approaching the nuclear charge as k becomes large. This proves to be true and the interpolation of $Z(k)$ can be done with reasonable accuracy and simplicity.

The preceding method implies an $S(k)$ curve for all k within the interpolation range, $-1 \leq k \leq 2$, for the target atom. The derivatives of this curve at $k = 0(1)$ provide an approximation to the stopping (straggling) mean-excitation energies. Data for the stopping mean-excitation energies are shown in Fig. 1 for the series of atoms studied in Ref. 2. The Ref. 2 data should be considered exact in the context of this comparison. It can be seen that the present results are more accurate than are the Ref. 1 data, with the average of

relative error magnitudes being 0.35% and 1.7%. These errors are 0.7% and 2.0% for the straggling mean-excitation energy.

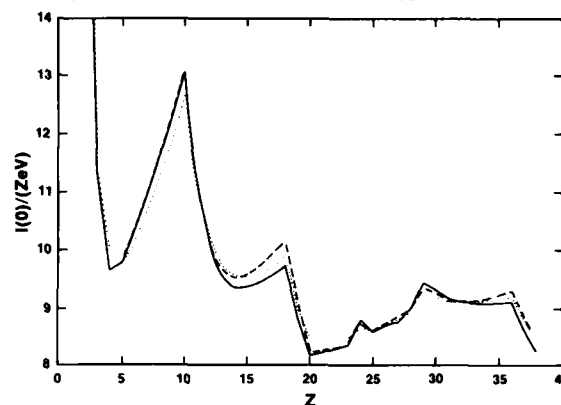


FIGURE 1. The stopping mean-excitation energy $I(0)$ divided by the target's atomic number Z is shown as a function of Z . The solid curve represents the "exact" results from Ref. 2, the short-dash curve gives the Ref. 1 data, and the long-dash curve presents the present results.

The Ref. 1 method requires only occupied orbitals to evaluate the interpolation method, while the present technique requires slightly more structure information. Either method is considerably easier to use than the direct calculation of these sums and their accuracy, especially in the case of this new method, is sufficient for many applications. For example, data from a study of the effects due to several different target wave functions on mean-excitation energies were generated with great ease. These data will be presented.

References

1. J. M. Peek, L. C. Pitchford, and E. J. Shipsey, *Phys. Rev. A* **29**, 1096 (1984).
2. M. Inokuti, J. L. Dehmer, T. Baer, and J. D. Hanson, *Phys. Rev. A* **23**, 95 (1981).

CLASSICAL CALCULATION OF ELECTRON-ATOM BREMSSTRAHLUNG

Longhuan Kim and R. H. Pratt

Department of Physics and Astronomy, University of Pittsburgh, Pittsburgh, Pennsylvania 15260 USA

Bremsstrahlung is one of the basic atomic processes. Many theories of the bremsstrahlung process have been developed and various calculations of bremsstrahlung radiation cross sections have been performed. Analytic formulas for the cross sections of electron-atom bremsstrahlung are available for both classical and quantum mechanical (either nonrelativistic or relativistic) approaches. Each has its own approximations, limitations and regions of applicability. A comprehensive study of the applicability of these analytical methods was carried out by Pratt and co-workers, comparing the results from these simple analytical formulas with the results of numerical partial wave calculations.^{1,2}

It is believed that a classical method is good for low incident electron energies. The characteristic quantity

$$n = v_1(1-k/T_1), \quad v_1 = Z\alpha/\beta_1, \quad \beta_1 = \sqrt{2T_1},$$

may be used to specify the range of validity of the classical method in electron and photon energy. For $n > 0.7$, classical results for the Coulomb potential

case agree with accurate numerical partial wave results of quantum mechanics in the same potential within 5%.^{2,3}

Analytic formulas for the classical bremsstrahlung cross section are available only for the Coulomb potential. For screened potentials a numerical method is necessary. Recently we have developed a computer code to calculate the classical bremsstrahlung doubly differential cross sections for both the Coulomb potential and screened potentials. The code calculates numerically the trajectory of an incident electron in a central potential according to classical dynamics, then calculates the dipole radiation emitted on that trajectory, and integrates over all the trajectories in the incident beam of electrons. It is assumed that electron energy loss due to the radiation is negligible and does not affect the orbit. Retardation effects are also neglected.

One test of the numerical accuracy of the code is obtained by examining the numerical results for the Coulomb potential case, for which analytic results are available. For $2 \leq Z \leq 92$ and $10 \text{ eV} \leq T_1 \leq 500 \text{ keV}$ the numerical error is generally less than 1% except when $Z = 2$ and $T_1 = 500 \text{ keV}$.

We have calculated the bremsstrahlung spectra and angular distributions of radiation from neutral He, Al, Ag, Au atoms described as Dirac-Slater potentials, for incident electron energies 10 eV - 500 keV. Comparison

with the earlier numerical quantum mechanical calculations show that for low incident electron energy the classical method is also generally good for screened potentials. As an example, in Table I we show our results for $Z = 13$ and $T_1 = 1 \text{ keV}$.

Table I: Numerical Classical Bremsstrahlung Cross Sections $d\sigma = (\beta_1^2 k/Z^2)d\sigma/dK \text{ (mb)}$, $Z=13$, $T_1=1 \text{ keV}$

k/T_1	0.1	0.4	0.6	0.8	1.0
EC	9.98	7.35	6.77	6.40	6.16
CC	10.15	7.90	7.44	7.16	6.94
ES	3.77	3.99	4.06	4.13	4.17
CS	3.82	4.23	4.46	4.65	4.79
R	1.01	1.01	1.00	0.99	0.98

EC: Exact quantum mechanical Coulomb result; CC: numerical classical Coulomb result; ES: Exact quantum mechanical screened result; CS: Numerical classical screened result; R = (CC/CS)/(EC/ES).

In analytic approaches the atomic form factor is often used to predict cross sections for screened potentials. However the form factor method is good only for relatively high electron energies and light elements. For

example, for $Z = 79$, $T_1 = 5 \text{ keV}$, the Elwert-Born form-factor method gives 30%-100% error.³ Our present numerical classical results give far less error (4% at the soft photon endpoint and about 10% in the hard photon region). For relatively low electron energy our classical approach gives better results than the form-factor method. It also takes much less computer time than a full numerical partial wave quantum mechanical calculation.

With increasing electron energy the discrepancy between classical results and partial wave results increases both in the Coulomb potential and screened potential cases. However we find that the ratio between Coulomb results and screened results, predicted classically, remains close to that of the full quantum mechanical calculation. This indicates that the screening factor (defined as the ratio of screened to Coulomb result) found classically can be used together with quantum Coulomb results to obtain useful predictions. While the atomic form factor method is good for sufficiently high energies, it does require calculation of triply differential cross sections.

References

1. H. K. Tseng and R. H. Pratt, Phys. Rev. A **3**, 100 (1971).
2. R. H. Pratt, in "Fundamental Processes in Energetic Atomic Collisions", edited by H. O. Lutz, J. S. Briggs, and H. Kleinpoppen, Plenum Press, NY, 1983, pp. 148-182.
3. I. J. Feng, Ph.D. Dissertation, University of Pittsburgh, 1982, unpublished.

DOUBLE ATOMIC-FIELD BREMSSTRAHLUNG

J. C. Altman and Carroll Quarles

Physics Department, Texas Christian University
Fort Worth, Texas 76129 USA

Double atomic-field bremsstrahlung is the simultaneous radiation of two photons by an electron in the Coulomb field of an atom. The process is fourth order in QED and has been computed in the first Born approximation by Smirnov.¹ In a coincidence experiment, we have observed two photons radiated at 90 and 270 degrees with respect to a 75 keV electron beam incident on thin film targets of Ag, Tb, Au or U. One photon energy (k_1) was fixed at 20 keV in a Si(Li) detector, and the second photon energy (k_2) was varied from 10 to 50 keV in an HpGe detector. The energy window was ± 5 keV. A modification of the conventional fast-slow coincidence technique was used.

We interpret the observed coincidences as due to double atomic-field bremsstrahlung and determine the absolute cross section by normalization to the single bremsstrahlung spectrum observed in each detector using the tabulated theoretical cross sections.² The results for Au and U are shown in Fig. 1. The curves shown are our evaluation of Smirnov's formula. The data disagrees with the theory in both magnitude and photon energy dependence. In Fig. 2, the cross section divided by the square of the atomic number is plotted versus Z for the case of $k_1=20$ keV and $k_2=40$ keV. The data agrees with a Z^2 dependence but, within the errors, is also consistent with Z^3 or a more complex Z dependence.

A variety of other processes which could lead to two-photon coincidences have been estimated to make a small contribution to the observed rate. When the photon energy window includes a target x-ray, it is possible to have simultaneous inner-shell ionization and bremsstrahlung radiation. We find some preliminary evidence for this effect as an enhancement in the coincidence rate for Au over that for U for $k_1=20$ and $k_2=10$ keV. We hope to have additional data on this radiative inner-shell ionization process by meeting time.

The results reported here have been submitted for publication.³

This research is supported by The Robert A. Welch Foundation.

References

1. Smirnov, A. I., Sov. J. Nucl. Phys. **25** (5), 548 (1977).

2. Kissel, Lynn, C. A. Quarles, and R. H. Pratt, Atomic Data and Nuclear Data Tables **28**, 381 (1983).
3. Altman, J. C. and C. A. Quarles, Phys. Rev. A (to be published).

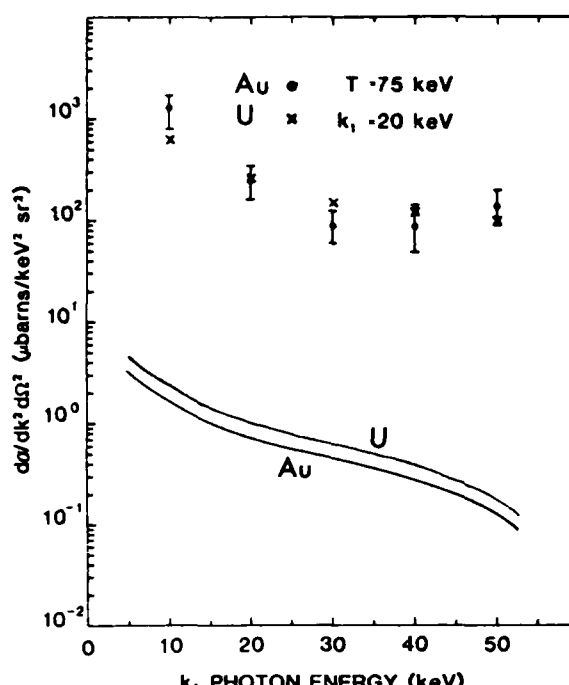


FIGURE 1 Cross section in $\mu\text{b}/\text{keV}^2 \text{sr}^2$ for Au and U versus k_2 . The errors on the U data are comparable to those shown for Au.

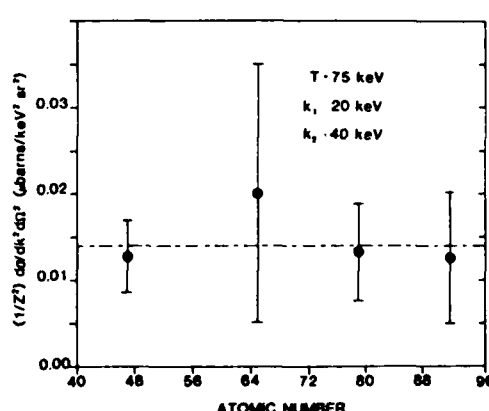


FIGURE 2 Cross section divided by Z^2 versus Z for $k_1=20$ keV and $k_2=40$ keV.

MOLECULAR BREMSSTRAHLUNG

Lee Estep and Carroll Quarles

Department of Physics, Texas Christian University
Fort Worth, Texas 76129 USA

The bremsstrahlung radiation spectrum has been observed at 90 degrees for electrons of 10 and 15 keV on a variety of molecular gas targets. The apparatus has been described previously.¹ The targets were selected to investigate first, the additivity of the bremsstrahlung cross section; and second, molecular-field effects related to different geometry or different atomic bond lengths. Additivity refers to computing the molecular cross section by adding the atomic cross sections for the constituent atoms, and it is expected to be valid for electron bombarding energy as high as 10 keV. In the first category, we have studied sulfur bearing molecules of H_2S , SO_2 , and SF_6 . Typical results are shown in Fig. 1 for 10 keV incident electrons. The solid lines are the result of adding the atomic cross sections.² The data are scaled to the theory in a one-parameter fit over the region of 5 keV to the endpoint. As can be seen, the region below about 5 keV is increasingly affected by attenuation in the vacuum chamber and detector window, and has not been included in the fit. The agreement is good for all three gases and for both 10 and 15 keV electrons.

The second category is represented by the ethane series: C_2H_2 , C_2H_4 , and C_2H_6 . Results are shown for 15 keV in Fig. 2. In this case the fit to theory is not as good as that observed for the sulfur gases. There are several possible reasons for this: (1) The hypothesis of additivity may not be correct for these gases. (2) The atomic cross sections for carbon or hydrogen may be inaccurate. (3) There may be some contribution from electron-electron bremsstrahlung which enhances the cross section below the electron-electron endpoint of 7.3 keV.

In addition, we will present data comparing normal with isobutane, nitrogen with neon, and molecular hydrogen with helium.

This research is supported by The Robert A. Welch Foundation.

References

1. Semaan, Mars and Carroll Quarles, Phys. Rev. A **24**, 2280 (1981).
2. Kissel, Lynn, C. A. Quarles, and R. H. Pratt, At. Data and Nucl. Data Tables **28**, 381 (1983).

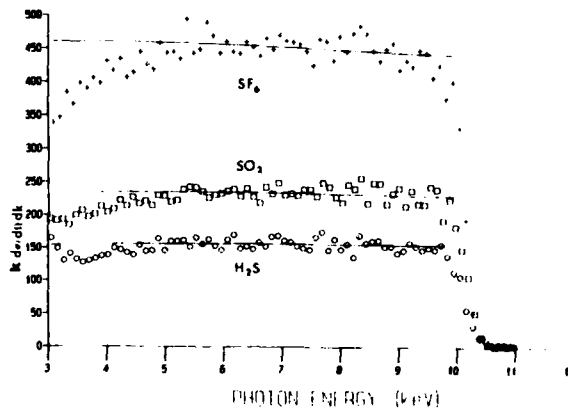


FIGURE 1 Plot of $k d\sigma/d\Omega dk$ in mb/sr for 10 keV electrons on sulfur hexafluoride, sulfur dioxide and hydrogen sulfide versus radiated photon energy.

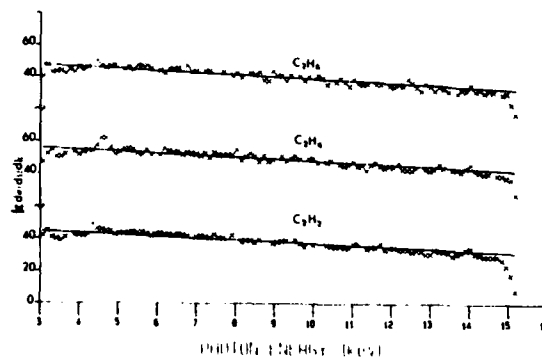


FIGURE 2 Plot of $k d\sigma/d\Omega dk$ in mb/sr for 15 keV electrons on ethyne, C_2H_2 , ethene, C_2H_4 and ethane, C_2H_6 versus radiated photon energy.

THE FESHBACH PROJECT OPERATOR METHOD: A STUDY OF THE $\text{He}^-[1s(2s^2):2s]$ RESONANCE

A. Berk*, A. K. Bhatia, B. R. Junker+, A. Temkin

Atomic Physics Office
 Laboratory for Astronomy and Solar Physics
 NASA/Goddard Space Flight Center
 Greenbelt, Maryland 20771 USA

* Permanent address: Sachs/Freeman Associates, Inc., Bowie, MD 20715

+ Permanent address: Office of Naval Research, Arlington, VA 22211

An explicit form of the Feshbach projection operators $[P \text{ and } Q (=1-P)]$ for the many-electron target has been derived.¹ We have now calculated QHQ energies for the $\text{He}^-[1s(2s^2):2s]$ resonance. In Table I, resonance energies obtained from 40 term configuration interaction wavefunctions using both the Feshbach and quasi-projection operator methods² are listed.

Table I: Projection operator and quasi-projector energies (E, \hat{E}) in eV for the lowest e-He resonance $\text{He}^-[1s(2s^2):2s]$

TARGET	TARGET ENERGY \hat{E}_0	QUASI-PROJECTOR ^a $\hat{E} - E_0$	FESHBACH PROJECTOR $E - E_0 \quad E - \hat{E}_0$
closed	77.487	19.360	19.582 18.067
open	78.249	19.378	19.655 18.902
CI	78.780	19.377	19.603 19.381
Complex rotation (ref. 3);		19.387	
Experiment (ref. 4):		19.367±0.009	

a. Ref. 2 with additional optimization.

 E_0 = exact target energy = -79.0016 eV.

The Feshbach projector energy is seen to be higher than the respective quasi-projector energy [Also, importantly, this difference does not vanish as the target approaches a closed shell.] Furthermore, $E - \hat{E}_0$ increases monotonically to a value close to experiment. Table I suggests that if one can use a set of improving ground states, it is preferable to deduce the resonant energy by subtracting \hat{E}_0 , whereas if one is confined to a comparatively simple target function, then subtraction of the exact E_0 is preferable¹. For the present 2-electron target the former is clearly the case, to the extent that calculations of the energy shift, Δ , will also be undertaken.

The width of the He^- resonance is also being calculated, using the exchange approximation for the non-resonant continuum,

$$P\Psi_0 = \mathcal{A} \left\{ \sum_i u_0(r_i) \psi_i^{(1)} \right\}.$$

Here \mathcal{A} is the antisymmetrizer and u_0 is the exchange approximate scattering function coming from $\langle \psi_0 | (H-E) P \Psi_0 \rangle = 0$ for the channel wave function ψ_0 associated with each target approximation.¹ Equations and solutions for the targets listed in Table I are being developed. It should be noted that the usual expression for the width matrix element $\langle Q \Phi | H-E | P \Psi_0 \rangle$ reduces to $\langle \Phi | H-E | P \Psi_0 \rangle$. Thus that calculation does not require any additional projectors other than what is used in the QHQ calculation for Φ . This should make the width calculation quite straightforward, and we expect to present results at the meeting.

References

1. A. Temkin and A. K. Bhatia, Phys. Rev. A 31 (to be published).
2. A. Temkin, A. K. Bhatia, and J. N. Bardsley, Phys. Rev. A 5, 1663 (1972).
3. B. R. Junker and C. L. Huang, Phys. Rev. A 18, 313 (1978).
4. S. Cvejanovic, J. Comer, and F. Read, J. Phys. B 7, 468 (1974).

MEASUREMENTS OF THE ELASTIC AND INELASTIC ($n=2,3$) DIFFERENTIAL
CROSS SECTIONS OF ATOMIC HYDROGEN BY HIGH RESOLUTION ELECTRON IMPACT

C.D. Warner, G.C. King, P. Hammond and J. Slevin[†]

Physics Department, Schuster Laboratory, Manchester University, U.K.

[†]Physics Department, University of Stirling, U.K.

Atomic hydrogen is of great interest to both theoretical and experimental physicists. The hydrogen atom neutral state wave functions have exact algebraic descriptions, a powerful starting point for determining differential cross sections for the scattering of electrons from atomic hydrogen into various exit channels. Theoretical treatments^{1,2} have predicted large numbers of temporary negative ion states of hydrogen, only some of which have been seen experimentally^{3,4}. Experimentally, atomic hydrogen has proved to be a challenging species to study because of the difficulty of dissociating naturally occurring molecules while inhibiting their recombination back into molecules. A sophisticated source⁵ has been employed using an RF discharge to dissociate hydrogen molecules. This source has been combined with a high sensitivity, high energy resolution electron spectrometer to study excitation functions of the elastic ($n=1$) and inelastic ($n=2, 3$) channels of atomic hydrogen.

High energy resolution of typically 25 meV has been achieved and the considerable improvement in sensitivity over earlier work has enabled much new resonance structure to be observed. The elastic ($n=1$) channel excitation functions (see Figure 1) show negative ion resonances with the following symmetries: $1s$, $3p$ and $1d$. The $1d$ resonance structure in the elastic channel has not been reported in the literature though Williams³ gives elastic excitation functions showing the $1s$ and $3p$ resonances. Inelastic differential cross section measurements have been carried out and results from these studies will be presented. These measurements are also of much higher sensitivity than earlier work⁴ and show an abundance of resonance structure between the threshold of the $n=2$ state and the ionization energy. Possible interpretations of the resonance structure will be suggested and comparisons will be drawn between the current data and existing theoretical predictions.

References

1. J. Callaway, *Phys. Reports*, **45**, 89 (1978) and refs. therein
2. Y.K. Ho and J. Callaway, *Phys. Rev. A*, **27**, 1887 (1983)
3. J.F. Williams, *Electron and Photon Interactions with Atoms*, Ch. 7 (Plenum, 1976)
4. J.F. Williams and B.A. Willis, *J. Phys. B*, **8**, 1641 (1975)
5. J. Slevin and W. Sterling, *Rev. Sci. Instrum.*, **52**, 1780 (1981)

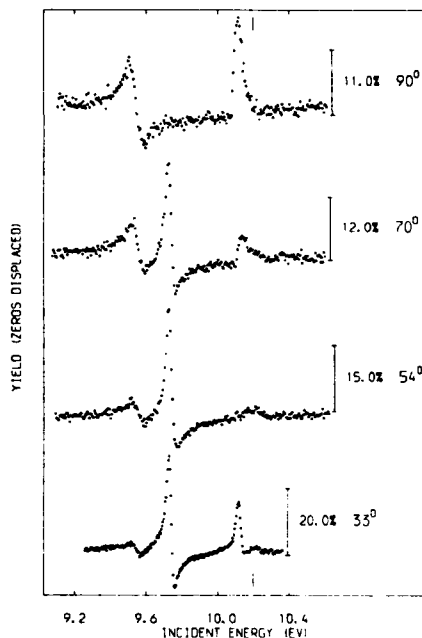


Figure 1 Elastic differential cross section in atomic hydrogen for angles 33°, 54°, 70° and 90°. The bars indicate the relative size of the observed features with respect to the background.

RESONANCE WIDTHS OF THE LITHIUM-LIKE IONS*

Brian F. Davis[†] and Kwong T. Chung⁺⁺

[†]Department of Chemical and Physical Sciences, University of North Carolina at Wilmington, Wilmington, NC 28403-3297

⁺⁺Department of Physics, North Carolina State University, Raleigh, North Carolina 27695-8202 USA

In the past, the accurate measurement of the autoionizing width of a three-electron ion has been limited to the He⁺ system for which an electron transmission scattering experiment was adopted.¹ Very recently, an optical emission spectroscopy technique has been developed to measure the $[(1s(2s2p)^3P)^2P^0$ and $(1s2p2p)^2D$ resonances in LiI² and BeII³. The widths of these states have been obtained by analyzing the broadened line profiles resulting from the optical transitions $(1s2p2p)^2P \rightarrow [(1s(2s2p)^3P)^2P^0$ and $[(1s2p)^3P3d]^2D^0 \rightarrow (1s2p2p)^2D$ which are seen in beam-foil light sources. These radiative transitions are observed because the upper state, although core-excited, is metastable against autoionization in the LS coupling scheme due to conservation of parity. These lines are broadened due to the fact that the lower state primarily decays by autoionization. The total width of these lines is the sum of the radiative and autoionization widths of the upper and lower states. In the energy region of interest, the relativistic spin-induced autoionization rates of the upper states are very small. The radiative width is also much smaller than the Auger width for these low Z systems.

In this work, we present results for the calculated widths for lithium-like ions. A total of twelve different resonances are considered for LiI, BeII and BIII. These results are obtained by using the saddle-point complex-rotation method. The total wave functions are of the configuration interaction type and are given by the sum of a closed-channel segment and an open-channel segment. The vacancy in the resonance is built into the closed-channel segment using the saddle-point method⁴. The open-channel is given by the product of a two-electron target state and an outgoing electron wave function. When the complex-rotation is carried out, the coordinates of the closed channel as well as the target state wave function are rotated with the hamiltonian. The complex energy eigenvalue is obtained by searching for the stabilized complex energy expectation value of the hamiltonian with respect to variations of the rotational angle, the non-linear parameters in the outgoing wave function and the linear parameters in the total wave function. In general, we found that the convergence is excellent for the real part of the eigenvalue, whereas for the imaginary part it depends sensitively on its magnitude. For example,

the width of BeII $(1s2p2p)^2D$, 1.0129×10^{-3} a.u., converges to all five digits but for BeII $[(1s2s)^1, 3d]^2D$, there is only one-digit convergence with a width of 0.3×10^{-5} a.u.

When the calculated results are compared with those of the optical emission measurements^{2,3}, we find that the agreement is very good for BeII and for the $(1s2p2p)^2D$ and $[(1s2s)^3S, 3d]^2D$ resonances of LiI. However, for the $[(1s(2s2p)^3P)^2P^0]$ of Li, our calculated result, 3.71 meV is larger than the experimental result of 2.6 ± 0.13 meV by about 40%. Due to this substantial difference between the theory and experiment, a detailed study was made of the convergence of this width with respect to the closed channel, open channel target state, and outgoing electron wave function to assess the stability and the reliability of the theoretical result. It appears that our result is stable within the framework of the saddle-point complex-rotation method.

It is interesting to note that in the present calculation, no orthogonality condition has been explicitly imposed in constructing the open and closed-channel segments of the wave function. Nevertheless, in the case of this Li $[(1s(2s2p)^3P)^2P^0]$ calculation, we found that the overlap integral of the open and closed channel is only 0.000007. This small overlap suggests that carrying out the saddle-point variation procedure for the closed-channel segment results in a wave function that is essentially orthogonal to the open channel. The detailed results of this calculation will be presented in the conference.

*Support by the National Science Foundation, Grant No. PHY 84-5469

Reference

1. See, for example, references quoted in B. F. Davis and K. T. Chung, Phys. Rev. A **29**, 1878 (1984)
2. S. Mannervik, H. Cederquist, and M. Kisielinski, Phys. Scripta T8, 107 (1984)
3. H. Cederquist, M. Kisielinski, S. Mannervik, and T. Andersen, J. Phys. B **17**, 1969 (1984)
4. K. T. Chung, Phys. Rev. A **20**, 1743 (1979)

SCATTERING OF ELECTRONS BY SODIUM AND POTASSIUM ATOMS AT LOW ENERGIES

S.M. Kazakov and O.V. Khristoforov

Physics department, Chuvash State University, Cheboksary 428015, USSR

We report here on measurements of elastic and inelastic electron scattering by sodium and potassium atoms, at energies between 1 and 5 eV. The energy loss spectra and the energy dependence of the intensity of some lines were studied.

The electron spectrometer with a 127° electrostatic energy analyzer for electrons scattered through 90° in vapor-filled cell was described earlier¹. The energy spread of the primary electron beam used was typically 150 meV and the energy resolution of the analyzer was 40 meV. The vapor pressure in the cell did not exceed 10^{-3} Torr as determined from the temperature of a metal-filled container. The electron beam current in the collision zone was about 10^{-7} A.

The energy dependences of the differential cross sections (DCS) for elastic scattering through 90° and excitation of resonance n^2P - levels are shown in Fig.1 and 2. There is a good agreement with a previous experiments²⁻³ in the behavior of the elastic scattering curves near the first inelastic threshold (peak 1 in Fig.1, 2), and some deviations are attributed to the different angular resolutions of the instruments. However, we found a wealth of heretofore unobserved structures in the DCS which are due to formation and decay of shortlived Na^- and K^- ions and threshold-effects. The energy position of some structures are given in table 1. The energy-determination accuracy is estimated at ± 30 meV.

Table 1

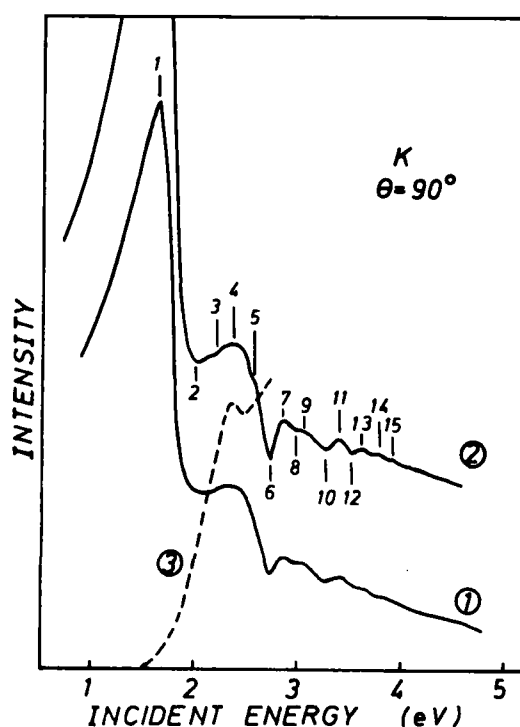
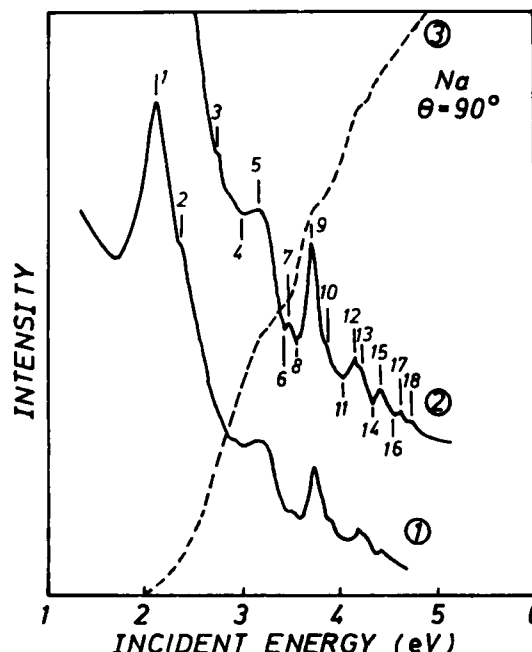
Num- ber	E(eV)		Num- ber	E(eV)		Num- ber	E(eV)	
	Na	K		Na	K		Na	K
1	2.10	1.61	7	3.47	2.87	13	4.22	3.62
2	2.35	2.01	8	3.56	2.99	14	4.33	3.79
3	2.72	2.18	9	3.72	3.08	15	4.40	3.93
4	2.99	2.37	10	3.87	3.28	16	4.53	-
5	3.15	2.56	11	4.02	3.40	17	4.62	-
6	3.41	2.74	12	4.17	3.53	18	4.73	-

Reference

1. S.M. Kazakov et al., Sov.Phys. JETP 51, 847, (1980).
2. M.Eyb, J. Phys. B 9, 101, (1976).
3. M.Eyb, H.Hofmann, J. Phys. B 8, 1095 (1975).

FIGURES 1 and 2 Energy dependence of the DCS:

1,2 - elastic scattering, 3 - excitation of n^2P - levels.



RESONANCES IN METASTABLE EXCITATION

N.J. Mason and W.R. Newell

Department of Physics and Astronomy, University College London, Gower Street, London WC1E 6BT.

Metastable states in atoms and molecules provide a convenient natural energy storage system especially for the transport of energy through plasmas. Renewed interest in such applications of atomic and molecular systems has placed a fresh demand on the need for accurate total metastable cross sections.

Cross sections for the excitation of metastable states in rare gases and some diatomic molecules (N_2 , H_2) are measured using a monochromated pulsed electron beam with time of flight analysis of the scattered products.

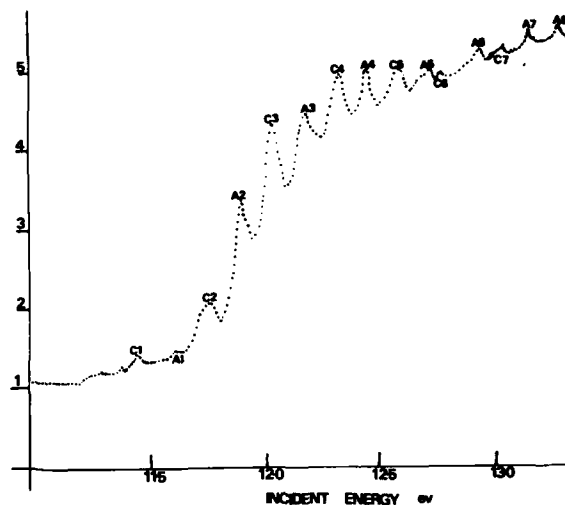
The experimental arrangement consists of a newly designed electron gun which produces a beam of $1\mu A$ at $6eV$ incident on an electro static hemispherical monochromator. Special attention has been given to the electron beam extraction system and the influence of the initial pupil associated with the harpin cathode on the performance of later stages of the gun. The pupil is subsequently focussed to infinity at the monochromator with the aid of a field lens inserted between the accelerating and decelerating regions of the staged electron gun.

By operating the three element field lens with the centre element below the cathode potential it is possible to utilize it also as a filter lens which will provide some pre-energy selection before the beam enters the monochromator. The nett effect of this, combined with the zero beam angle in the monochromator, is to give an enhanced (25%) transmission of the electron beam through the monochromator with an energy resolution of $30meV$ at $2eV$ input. Since there is a nett momentum transfer to the atomic beam direction it is necessary to place the detector at an angle which accomodates the effect of the momentum transfer to the metastable atoms and also ensure that all of the metastables are detected.

A $10V$, $100\mu s$, negative pulse applied to the filter lens is sufficient to modulate the electron beam. The time of flight spectra consist of photons which arrive as a prompt pulse, followed by scattered electrons which arrive at the detector within $30ns$ of the trailing edge of the primary electron pulse and finally metastables and ions which have flight times of $\sim 70\mu s$ depending on the particular atomic species under study. The positive ions are removed by the application of a small positive voltage at the entrance of the detector.

A typical metastable excitation cross section in H_2 is given in Figure (1). The features labelled A1 to A8 are resonance structures observed in the metastable

channel while the features C1 to C7 are ultraviolet emission structures. These were only seen when the detector was sensitized with cesium iodide. The features C1 to C7 can be removed in the time of flight mode.

Figure 1. Resonance structure in H_2

Resonance structures in the rare gases N_2 and H_2 will be presented and compared to current work ^{1,2} in this field.

REFERENCES

1. S J Buckman, P Hammond, G C King and F U Read
J. Phys. B: At. Mol. Phys. **16** (1983) 4219.
2. S A Elston, S A Lawton and F M J Pichanick
Phys. Rev. **10**, 225, (1974)

THEORETICAL STUDY OF PARTIAL WIDTHS AND RESONANCE NORMALIZATION

D. K. Watson, University of Oklahoma, Norman, OK *

The theoretical determination of partial widths in multichannel resonance problems is studied using a variety of methods including the use of the golden-rule formula with explicitly normalized resonance wavefunctions. In addition we determine the residues of the open-channel submatrix of the resonant T matrix by direct differentiation of the T matrix denominator. We compare these residues to the golden rule partial widths obtained with different normalizations of the resonance wavefunctions. A new expression for the normalization factor of resonance wavefunctions is derived. A recently introduced method of determining multichannel resonances which searches the complex plane for the poles of the T matrix is employed to investigate these methods for a model problem. Essentially exact results are obtained with small sets of basis functions. Accurate representations of the normalized resonance wavefunctions are easily constructed using the appropriate multichannel Green's function which enforces the correct asymptotic behavior in each channel. We compare our results to the exact results and to the results of other methods.

*Supported by the National Science Foundation Grant PHY-8403031 and by the Air Force Office of Scientific Research Grant AFOSR-84-0379.

TWO-CENTER COULOMB WAVEFUNCTION DESCRIPTION OF TWO-ELECTRON ATOMS

James M. Feagin,* John S. Briggs,+ and Thomas P. Weissert*

*California State University, Fullerton, CA 92634, USA

+Universität Freiburg, 7800 Freiburg, W. Germany

Considerable progress has been made in the understanding of the highly correlated motion of two electrons in H^- ions and in doubly excited states of the helium atom. Following the pioneering work of Macek,¹ attention has been focussed upon the approximate separation of the problem using hyperspherical coordinates, and examples of this approach abound in the literature. To the extent that the inter-electron axis is "stiff" when the two electrons are highly correlated, one can imagine that the relative electron vector \vec{R} (one of the Jacobi coordinates) may be a useful coordinate to describe such motion. Indeed, it has been shown that some aspects of threshold laws for three-body break-up are better derived using Jacobi coordinates.² There is the further advantage that the adiabatic problem where R is held fixed can be solved exactly. The solutions are just those of the two-center Coulomb problem, initially derived to describe states of the H_2^+ molecular ion.

At the same time, one would like to develop a method with all the numerical utility of the *adiabatic* hyperspherical methods, but one that better characterizes other symmetries of two-electron states. In hyperspherical analyses to date, symmetries for the most part are only surmised on the basis of numerical data.

In the center of mass (CM) system, the other Jacobi coordinate is the separation \vec{r} of the two-electron CM and the ionic core. Two-center Coulomb functions are eigenfunctions of

$$\left(-\frac{\nabla_{\vec{r}}^2}{2\mu_{12,3}} - \frac{Z}{|\vec{r} + \frac{1}{2}\vec{R}|} - \frac{Z}{|\vec{r} - \frac{1}{2}\vec{R}|} \right) \phi_n(\vec{r}, R) = \epsilon_n(R) \phi_n(\vec{r}, R) \quad (1)$$

which define correlation potentials $\epsilon_n(R)$ as scaled H_2^+ binding energies.

$$\epsilon_n(R) = \mu_{12,3} Z^2 E(H_2^+), \quad R = R(H_2^+)/\mu_{12,3} Z \quad (2)$$

Here $\mu_{12,3} = 2$, the reduced mass of the two-electron CM relative to the ion Z . One finds³ a remarkable qualitative similarity of the potentials $\epsilon_n(R)$ as a function of R with adiabatic hyperspherical potentials as a function of the hyperradius. This similarity is especially pronounced in doubly excited levels.

One finds, for example, that the $1s\sigma_g$ potential describes predominantly the $(1s\sigma_g)^1S^e$ series, while the $2p\sigma_u$ level the $(1s\sigma_g)^3S^e$ series. As in hyperspherical

analyses, the independent particle designation $n\bar{n}l'$ is not exact. Although we find by numerical integration of the correlation potentials the position of the lowest members of these series to be high, we do find the relative position of other members of a series to be better. (Also, we find as expected the $(1s2s)^3S^e$ ground state of $2p\sigma_u$ to lie below the first excited $(1s2s)^1S^e$ state of $1s\sigma_g$.) Thus, the method appears to represent correlation energies best, and one expects improvement in describing doubly excited states.

A difficulty with the two-center description occurs in the separated-atom limit. Physically, the system wavefunction for large R must describe one electron at rest relative to an atomic (electron-ion) center of mass. The two-center functions for large R describe, however, a long, rigid rod of mass $\mu_{12,3} = 2$ with one end bound to the ion. Thus, the correlation potentials are too low at large R by a factor two. It has been shown⁴, however, that this difficulty can be resolved by scaling the mass $\mu_{12,3}$ and including the diagonal matrix element of $\nabla_{\vec{r}}^2/2\mu_{12}$ in the determination of the correlation energies, where $\mu_{12} = 1/2$ is the two-electron reduced mass. These studies were mostly concerned with correcting the same difficulty in H_2^+ , but did calculate ground state energies in helium and in H^- .

We will present details of our classification scheme and indicate the molecular-like rotational and radial couplings that would lead in our description to autoionization in doubly excited states. We shall also compare our description with other related descriptions⁵, and indicate how our analysis might be included in an adiabatic hyperspherical treatment.

References

1. J. Macek, J. Phys. **B1**, 831 (1968).
2. J. M. Feagin, J. Phys. **B17**, 2433 (1984).
3. J. M. Feagin, Bull. Am. Phys. Soc. **29**, 801 (1984).
4. G. Hunter and H. O. Pritchard, J. Chem. Phys. **46**, 2153 (1967).
5. D. R. Herrick and O. Sinanoglu, Phys. Rev. **A11**, 97 (1975).

AD-A163 497

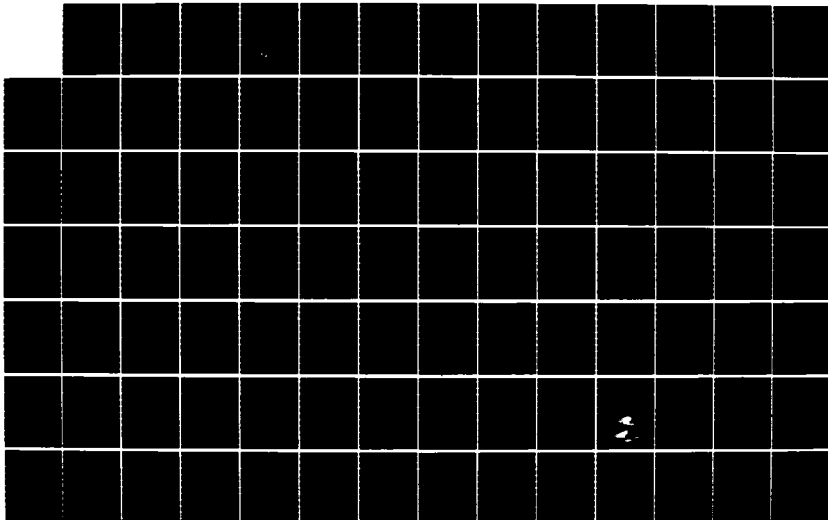
ELECTRONIC AND ATOMIC COLLISIONS ABSTRACTS OF
CONTRIBUTED PAPERS INTERNAT. (U) SRI INTERNATIONAL
MENLO PARK CA MOLECULAR PHYSICS CENTER
M J COGGIOLA ET AL. 1985

3/8

UNCLASSIFIED

FFG 7/4

ML





MICROCOPY RESOLUTION TEST CHART
NATIONAL BUREAU OF STANDARDS-1963-A

CORRELATION EFFECTS IN NEGATIVE ALKALI-IONS

Birte Christensen-Dalsgaard

Kemisk Laboratorium IV, H.C.Ørsted Institute
DK-2100 Copenhagen Ø, Denmark

It is well known that the ground state of the negative alkali ions are stable only due to a large degree of correlation, therefore these seem natural candidates in which to study strongly correlated motion.

For the description of eg the detachment process (which in general is too complex to allow the use of elaborate wavefunctions for the atoms(ions) involved), we need to construct simple functions which resembles the real ones in as many physical aspects as possible. In this connection the understanding of the role of radial and angular correlation is very important.

Except for the few lowest resonances of the negative alkali-ions, nothing is known theoretically about the resonance spectrum of these. This despite the fact they have a rich resonance spectrum, as is known from transmission spectroscopy¹.

In the present work, the negative ions are described as consisting of two valence electrons moving in a Thomas-Fermi-Dirac-Amaldi plus polarization model-potential². The motion of the two electrons are described using the hyperspherical approach, in which the radii of the two electrons are replaced with a hyperradius R and a hyperangle α , defined through:

$$R = (r_1^2 + r_2^2)^{1/2}$$

$$\alpha = \arctan(r_2 / r_1)$$

Solving the Schrödinger equation for a fixed value of R :

$$H_{\text{fixed}} \phi_{\nu}(R; \alpha, C) = \lambda_{\nu}(R) \phi_{\nu}(R; \alpha, C) \quad (1)$$

leads to a complete set of adiabatic functions on which the total wavefunction can be expanded:

$$\Psi = R^{-5/2} \sin^{-1} \alpha \cos^{-1} \alpha \sum_{\nu} F_{\nu}(R) \phi_{\nu}(R; \alpha, C)$$

This expansion leads to the radial equation

$$\left(\frac{d^2}{dR^2} - U_{\nu\nu}(R) + E \right) F_{\nu}(R) + \sum_{\mu} W_{\nu\mu}(R) F_{\mu}(R) = 0 \quad (2)$$

where the effective potential is

$$U_{\nu\nu}(R) = (\lambda_{\nu}(R) - 0.25) / R - \langle \phi_{\nu} | \frac{d^2}{d\alpha^2} | \phi_{\nu} \rangle$$

For the ground state $\nu=0,1,2$ were included in solving (1). In (2) all couplings to higher states were neglected. The resultant radial function is shown in Fig.1.

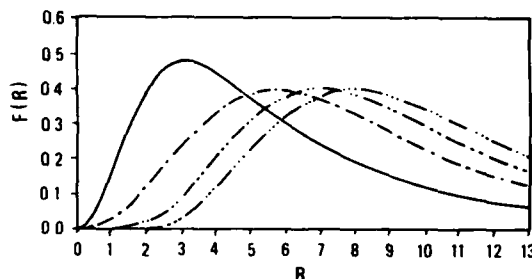


Fig 1 The radial function for H^- (—), Li^- (---), Na^- (····) and K^- (-·-·-).

Examples of the analysis of the angular functions are shown below. All the alkalis have similar correlation pattern, for simplicity we only show the results for Na^- .

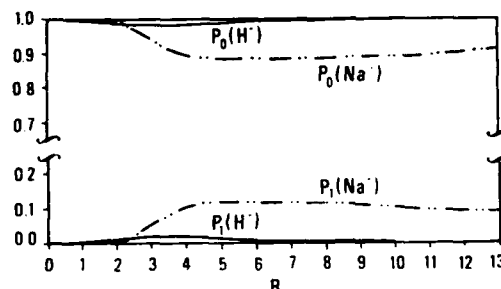


Fig 2 The probability $p_L(R)$ for the ground state to be in angular state Y_{L00} , $L=0$ and 1

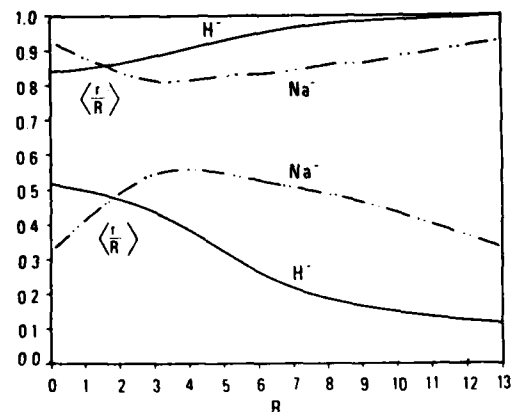


Fig 3 The expectation value of $1/R$ and R . If the expansion of the complex were due only to the outer electron, we would have $\langle 1/R \rangle = 1/R$.

1 A.R. Johnson, E.W. Murray private communication
2 W. Fissner, B. Tuschke, Z. Physik, 11, 11 (1969)

This work is supported by the Danish National Science Foundation.

SIMPLE METHOD TO CALCULATE RESONANCE WIDTHS

A. Macías and A. Riera

Departamento de Química Física y Química Cuántica and C.S.I.C.
Universidad Autónoma de Madrid. 28049 MADRID (Spain)

We propose a very simple method to calculate life-times of autoionizing states, based on the use of the "golden rule" expression

$$\Gamma = 2\pi \rho(E) |\langle \phi^r | H | \chi^c \rangle|^2$$

ϕ^r is calculated by TDM1, and χ^c by diagonalizing H in a basis set orthogonal to ϕ^r and varying an overall scaling parameter so that $E^c = E^r$. $\rho(E)$ is assumed to be inversely proportional to the energy separation and convergence of Γ with $\rho(E)$ is quickly obtained.

We compare our results for some $1,3D$ resonances of H^- and He under the $n=2$ threshold with the literature.

For $Z > 2$ we present the coefficients of Hylleraas type Z^{-1} perturbation expansions² in the form

$$E = Z^2 E(0) + Z E(1) + E(2) \dots$$

$$\gamma = \gamma(0) + Z^{-1} \gamma(1) + Z^{-2} \gamma(2) \dots$$

and Γ is given by $\Gamma(eV) = 27.21 2\pi \gamma^2$ (which is more useful than direct expansion of Γ).

		E^r au	Γ eV
H^-	$1D$	1	-0.1272
		2	-0.1237
		3	-0.1223
		4	-0.1199
	$3D$	1	-0.1243
		2	-0.1223
		3	-0.1214
		4	-0.1196
He	$1D$	1	-0.6983
		2	-0.5681
		3	-0.5554
		4	-0.5361
	$3D$	1	-0.5832
		2	-0.5598
		3	-0.5413
		4	-0.5327

Γ eV ³	Γ eV ⁴	Γ eV ⁵
	10. 10 ⁻³	78. 10 ⁻³
6.7 10 ⁻²	7.29 10 ⁻²	36.58 10 ⁻²
1.5 10 ⁻²	1.87 10 ⁻²	5.35 10 ⁻²
5.7 10 ⁻⁴	5.81 10 ⁻⁴	5.25 10 ⁻⁴
	7.1 10 ⁻³	10.3 10 ⁻³
0.6 10 ⁻⁶	2.72 10 ⁻⁶	214. 10 ⁻⁶
2.8 10 ⁻⁴	1.92 10 ⁻⁴	1.0 10 ⁻⁴
	3.31 10 ⁻⁶	100. 10 ⁻⁶
	1.36 10 ⁻⁴	0.29 10 ⁻⁴

		$E(0)$ au	$E(1)$ au	$E(2)$ au
$1D$	1	-0.2500	0.18512	-0.07023
	2	-0.18048	0.09769	-0.03915
	3	-0.18036	0.11823	-0.07574
	4	-0.15601	0.05368	-0.01491
$3D$	1	-0.18050	0.08106	-0.02323
	2	-0.18035	0.09910	-0.03350
	3	-0.15607	0.04850	-0.01092
	4	-0.15605	0.05689	-0.01960

$\gamma(0)$	$\gamma(1)$	$\gamma(2)$
3.5344 10 ⁻²	-2.8427 10 ⁻²	-6.1324 10 ⁻³
2.0351 10 ⁻²	-1.4283 10 ⁻²	-1.5292 10 ⁻²
1.4363 10 ⁻²	-3.6943 10 ⁻²	1.7472 10 ⁻²
1.3434 10 ⁻²	-1.1234 10 ⁻²	-4.7347 10 ⁻²
2.7568 10 ⁻⁴	-9.5072 10 ⁻⁴	4.9109 10 ⁻⁴
3.0189 10 ⁻³	-4.0555 10 ⁻³	-3.6738 10 ⁻⁵
4.6420 10 ⁻⁴	-2.7877 10 ⁻³	4.6329 10 ⁻³
2.0448 10 ⁻³	-2.1274 10 ⁻³	-1.4657 10 ⁻³

References.

1. P.L. Altick and E.N. Moore, Phys. Rev. Lett., **15**, 100 (1965).
2. E.A. Hylleraas, Z. Phys., **65** 209 (1930); E.A. Hylleraas and J. Midtal, J. Phys. Rev., **103** 829 (1956); **109**, 1013 (1958); J.O. Hirschfelder, N. Byers-Brown and S.J. Epstein, Adv. Q. Chem., **1**, 255 (1984); G.W.F. Drake and A. Dalgarno, Proc. Roy Soc. **320** 549 (1971); N. Moiseyev and F. Weinhold, Phys. Rev. A., **20**, 27 (1979).
3. G. Aspromalis, Y. Komninos and C.A. Nicolaides, J. Phys. B., **17**, L151 (1984).
4. A.K. Bhatia and A. Temkin, Phys. Rev. A., **11**, 2018 (1975).
5. M.J. Conneely and L. Lipsky, J. Phys. B., **11**, 4135 (1978).

TOWARDS NUMERICAL SOLUTION OF THE THRESHOLD IONIZATION PROBLEM

Christopher Bottcher

Oak Ridge National Laboratory,* Oak Ridge, TN 37831 USA

I will focus on the two-dimensional model¹ of the electron-impact ionization problem

$$e + H \rightarrow e + p + e \quad (1)$$

described by the Hamiltonian

$$H = -\frac{1}{2} \left(\frac{\partial^2}{\partial r_1^2} + \frac{\partial^2}{\partial r_2^2} \right) + \left(\frac{1}{r_1 + r_2} - \frac{1}{r_1} - \frac{1}{r_2} \right) \quad (2)$$

where r_1 and r_2 are the electron-nuclear distances. The ionization problem is solved if one can obtain a set of asymptotic solutions of the Schrödinger equation

$$H\psi = E\psi \quad (3)$$

valid at hyperspherical radii $\rho \sim 10 a_0$ ($r_1 = \rho \cos \alpha$, $r_2 = \rho \sin \alpha$). Such solutions can be matched to short-range functions to obtain a scattering amplitude.

The complex action defined by $\psi = \exp(iS)$ satisfies

$$(\nabla S)^2 = 2(E - V) + i\nabla^2 S \quad (4)$$

A starting point is provided by the Peterkop form²

$$S \sim \kappa \rho + \frac{C}{\kappa} \ln \frac{\rho}{a} + \lambda F(\alpha) \quad (5)$$

($2E = \kappa^2$, $C = -\rho V$) where a , λ , F are arbitrary. Equation (5) is valid at very large $\rho \sim 25/E$ and $\alpha > \alpha_0(\rho) \rightarrow 0$

very slowly as $\rho \rightarrow \infty$. The classical orbits defined by Eq. (5) have a condensation point depending on a , λ , and F : as a or λ is varied a complete set of outgoing wave solutions is generated. Figure 1 shows orbits for $a = 1$ and $\lambda = 0$ (labeled W). Those labeled T correspond to the dipole solution of Temkin.³

Two steps, now, have to be carried through. (a) The asymptotic formula (5) must be extended to $\alpha = 0$ by a uniform approximation. (b) The resulting solution must be integrated inwards in ρ in a stable fashion. Progress toward these objectives will be described at the conference.

* Research sponsored by the U.S. Department of Energy, Division of Basic Energy Sciences under Contract No. DE-AC05-84OR21400 with Martin Marietta Energy Systems, Inc.

1. C. Bottcher in "Electronic and Atomic Collisions," Eds. J. Eichler, I. V. Hertel, and N. Stolterfoht, (Elsevier Science Publishers B.V., 1984), p. 187.
2. R. Peterkop, Sov. Phys. JETP **16**, 442 (1963).
3. A. Temkin, Phys. Rev. **A22**, 324 (1980).

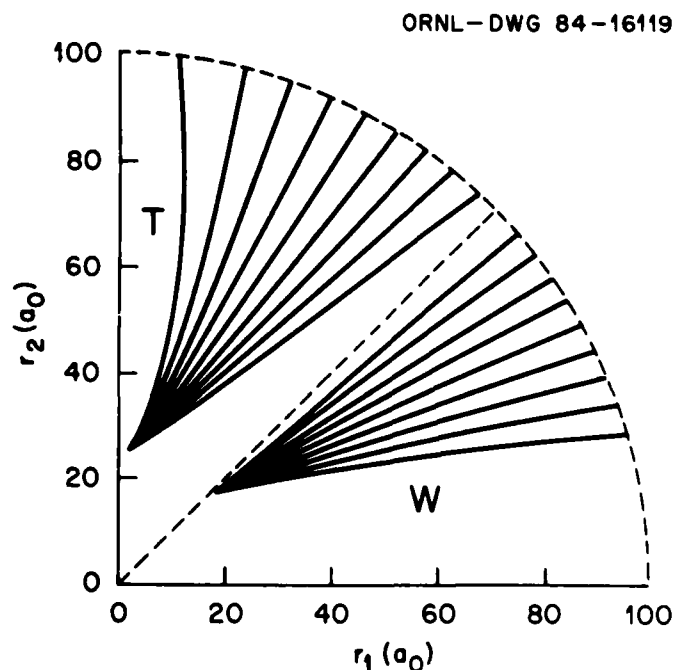


FIGURE 1. Orbits for: $a=1$, $\lambda=0$ (W); dipole solution of Temkin (T).

ELECTRON IMPACT IONISATION OF HYDROGEN AND HELIUM ATOM

K.Roy, P.Mandal and N.C.Sil

Department of Theoretical Physics
Indian Association for the Cultivation of Science, Jadavpur, Calcutta 700032, India.

In this work we study the electron impact ionisation of atomic hydrogen and helium using three body scattering formalism of L.D.Faddeev¹. We consider here an electron (particle 1) with mass m_1 is incident on a bound system of an electron (particle 2) with mass m_2 and a nucleus (particle 3) with mass m_3 and designate their respective coordinates and momenta by \vec{r}_α and \vec{k}_α ($\alpha = 1, 2, 3$). The relative coordinate of particles 1 and 2 is denoted by \vec{r}_{12} and the coordinate of their centre of mass by \vec{S}_{12} . The conjugate momenta are given by \vec{x}_{12} and \vec{q}_{12} . Similarly we define the coordinates and momenta for the other pair of particles. Following Faddeev¹, we write the final-state wave function Ψ_f^- for an ionising collision as :

$$\Psi_f^-(1,2) = \phi^{(23)} + \phi^{(31)} + \phi^{(12)} - 2\phi^{(0)} \quad (1)$$

where we have retained only the first order term in the integral equation for Ψ_f^- . Here $\phi^{(ij)}$ are solutions of the two-particle sub systems where the third particle propagates

freely. Asymptotically, $\phi^{(ij)}$ goes over to the state $\phi^{(C)}$, where all the interacting particles are free

$$\phi^{(0)} = (2\pi)^{-9/2} \exp(i \sum_{\alpha=1}^3 \vec{k}_\alpha \cdot \vec{r}_\alpha) \quad (2)$$

Taking account of the indistinguishability of the electrons, we may now write the matrix element for ionisation as

$$T_{fi}^\pm = \langle \phi_f^\pm | V_1 | \phi_i^\pm \rangle \quad (3)$$

with

$$\phi_f^\pm = \Psi_f^\pm(1,2) \pm \Psi_f^\pm(2,1)$$

$$\phi_i^\pm = \Psi_i^\pm(1,2) \pm \Psi_i^\pm(2,1)$$

where the wave function in the incident channel $\Psi_i(1,2)$ is given by

$$\Psi_i(1,2) = \exp(i\vec{k}_1 \cdot \vec{r}_1 + i\vec{q}_1 \cdot \vec{S}_{23}) \phi_0(\vec{R}_{23}) \quad (4)$$

$\phi_0(\vec{R}_{23})$ denotes the normal state of the atom and V_1 is the interaction potential in the incident channel. The cross section is obtained as a linear combination of $|T^+|^2$ and $|T^-|^2$ with appropriate weight factors.

The wave function Ψ_f^- as given by (1) has earlier been used by Macek² to explain charge transfer to continuum in ion-atom scattering

and by Mandal, Roy and Sil³ for positron impact ionisation of atoms. Though the additional effect of the rearrangement channel, such as electron capture, positronium formation is absent in the problem of electron scattering, the effect of electron-electron correlation is taken into account to first order through the wave function (1) in the present calculation. Numerical results will be presented at the conference.

References

- ¹ L.D.Faddeev, Sov. Phys. - JETP, 12, 1014 (1961).
- ² J.Macek, Phys. Rev. A1, 235 (1970).
- ³ P.Mandal, K.Roy and N.C.Sil, Proc. VII Int. Conf. on Positron Annihilation, New Delhi (1985).

ELECTRON-IMPACT IONIZATION OF HYDROGEN ATOM FROM 2s-STATE

P. S. Majumdar, Madhumita Basu and A. S. Ghosh

Theoretical Phys Dept., Indian Association for the Cultivation of Science, Calcutta 700032, India.

The absolute measurements of the ionisation cross section of hydrogen atom (σ_{2s}) have been performed by different groups¹⁻³. The first measurement of σ_{2s} was made by Koller¹ in the energy range 3.4 - 10 eV. Dixon et al² extended the energy range upto 498.5 eV. Recently, Defrance et al³ have tried to improve the results of the earlier measurements and reported the results for σ_{2s} . Theoretically, this process has been studied by Rudge and Schwartz⁴ using first Born (FBA) and Born-Exchange (BE) approximation. Independently, Prasad⁵ have also reported the σ_{2s} using the FBA, BE and Born-Ochkur approximations. All experimental data are in mutual agreement and all the theoretical cross sections are much higher than the experimental ones below 100 eV. The situation suggests that this process should further be investigated theoretically in the said energy range.

Here, we have investigated the process using three models (DCA, DW1 and DW2). In all the models, the slower electron is represented by a Coulomb wave with unit charge. The differences between the three models are given below

i) In DCA, the faster electron wavefunction is represented by a Coulomb wave of unit charge and the incoming electron wavefunction is represented by a plane wave.

ii) The faster electron wavefunction is represented by a Coulomb wave of unit charge. The wavefunction of the incident electron is obtained by static-exchange approximation. This model is denoted by DW1.

iii) In DW2, the faster electron is represented by a plane wave and the incident electron wavefunction is same as that of DW1.

We have employed these models to calculate the total ionisation cross sections in e^- -H scattering and our DW1 and DCA results are closer to the measured values than those of BE and DW2.

The scattering amplitude for ionisation is given by

$$f_{ion}^{\pm}(\vec{k}_f, \vec{k}_c) = \langle \bar{A}_{k_f}^*(z, \vec{r}_1) \bar{A}_{k_c}^*(z, \vec{r}_2) | -\frac{1}{r_1} + \frac{1}{r_{12}} | \Psi^{\pm}(\vec{r}_1, \vec{r}_2) \rangle$$

where

$$\Psi^{\pm}(\vec{r}_1, \vec{r}_2) = (1 \pm P_{12}) [\phi_{2s}(\vec{r}_2) F(\vec{r}_1)]$$

Here, $\phi_{2s}(\vec{r}_2)$ is the wavefunction of the hydrogen atom in the 2s state. $\bar{A}_{k_c}(z, \vec{r}_2)$ is the wavefunction of slower electron. $F(\vec{r}_1)$ and $\bar{A}_{k_f}(z, \vec{r}_1)$ take different forms for the different models given below.

Model DCA :

$\bar{A}_{k_f}(z, \vec{r}_1)$ is the Coulomb function of the unit charge and $F(\vec{r}_1) = e^{i\vec{k}_1 \cdot \vec{r}_1}$.

Model DW1 :

$\bar{A}_{k_f}(z, \vec{r}_1)$ is same as in DCA and $F(\vec{r}_1)$ satisfies the static-exchange equation.

Model DW2 :

$\bar{A}_{k_f}(z, \vec{r}_1) = e^{i\vec{k}_f \cdot \vec{r}_1}$ and $F(\vec{r}_1)$ is same as in DW1.

In the case of DW2 we invoke the Peterkop⁷ condition of exchange. In case of DCA and DW1, this condition is automatically satisfied.

Total cross section (σ_{2s}) is obtained after performing the partial-wave analysis.

Primary results obtained are found to be very encouraging and the final results will be reported at the conference.

References

- 1 H.H.Koller, Inaugural dissertation Universitat Zurich (1969).
- 2 A.J.Dixon, M.F.A.Harrison and A.C.H.Smith, J. Phys. B: At. Mol. Phys. **9** 2617 (1976).
- 3 P.Defrance, W.Clayes, A.Cornent and G.Poulaert J. Phys. B: At. Mol. Phys. **14** 111 (1981).
- 4 M.R.H.Rudge and S.B.Schwartz, Proc. R. Soc. London **28** 563 (1966).
- 5 S.S.Prasad, Proc. Phys. Soc. **87**, 393 (1966).
- 6 A.S.Ghosh, P.S.Mazumdar and M.Basu, Z. Phys. A: Atoms and Nuclei **319** 13 (1984).
- 7 R.K.Peterkop, Proc. Phys. Soc. **77** 1220 (1961).

ABSOLUTE TRIPLE DIFFERENTIAL CROSS SECTIONS FOR THE ELECTRON IMPACT IONIZATION OF He AND H AT 250 eV AND 150 eV

P. Schlemmer, G. Knoth, H. Ehrhardt, and K. Jung

Fachbereich Physik der Universität Kaiserslautern, D-6750 Kaiserslautern, West-Germany

The comparison between measured absolute triple differential cross sections for the processes $e + H \rightarrow p + e + e$ and $e + He \rightarrow He^+ + e + e$ and several theoretical approaches have demonstrated¹ that for impact energies between 250 eV and 600 eV second order effects are of importance even for small momentum transfers such as 0.25 a.u.. Second order terms have been introduced by using 2. Born², Eikonal³, distorted waves⁴ or 1. Born extended by post collision interactions⁵.

New experiments are presented for the electron impact ionization of atomic hydrogen and helium (ejection of a s-electron) for impact energies 250 eV and 150 eV. In this energy range higher order effects should gain importance. The figure shows an example of such measurements.

If the first Born approximation would be correct, the momentum transfer vector must be an axis of symmetry for the binary peak (right hand side lobe) and also for the recoil peak (backward scattering, left hand side lobe). The maximum of the binary peak deviates from Θ_{0A} by as much as 20°. This is a consequence of second order effects.

In first order theories the recoil intensity can never be larger than the intensity of the binary peak. But this is experimentally found as can be seen from the figure. On the other hand, if the momentum transfer $|\vec{q}|$ is reduced to zero, then the structure of the triple differential cross section must merge into a $\cos^2\Theta$ distribution with \vec{q} as the symmetry axis. But this limit cannot be reached for impact energies of 250 eV and below because of the inelasticity of the process even not for $\Theta_A = 0$. This proves the necessity of more complex calculations than first order even for such high impact energies.

Acknowledgements

This work was supported by the Deutsche Forschungsgemeinschaft (SFB 91).

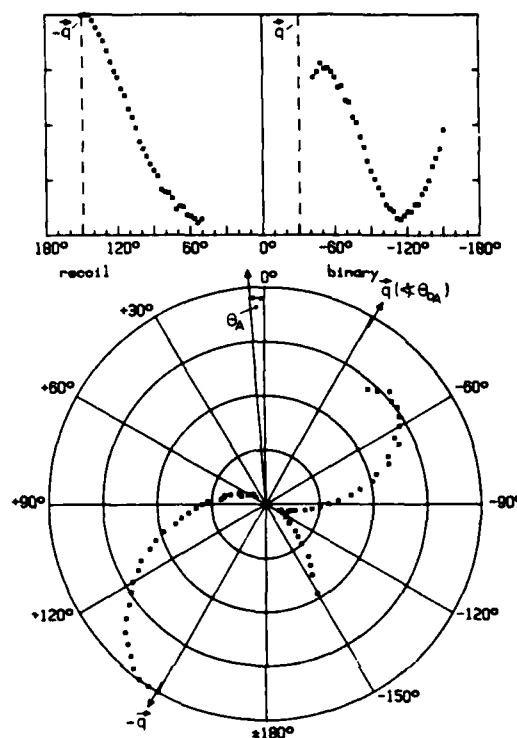


Fig. 1:

Cartesian and polar diagram of the triple differential cross section for the electron impact ionization of helium for $E_0 = 150$ eV, $E_B = 5$ eV, $\Theta_A = 4^\circ$, $|\vec{q}| = 0.4$ a.u.. The direction of the momentum transfer vector is indicated by \vec{q} , respectively $-\vec{q}$.

References

1. Müller-Fiedler R, Schlemmer P, Jung K and Ehrhardt H 1985, Z. Phys. A - Atoms and Nuclei **320**, 89
Ehrhardt H, Knoth G, Schlemmer P, Jung K 1985, to be published
2. Ehrhardt H, Fischer M, and Jung K 1982, Z. Phys. A - Atoms and Nuclei **304**, 119
3. Byron Jr. FW, Joachain CJ, and Piraux B 1983, Phys. Lett. **99A**, 427
4. Bransden BH, Smith JJ, Winters KH 1978, J. Phys. B **11**, 3095
Madison DH, Calhoun RV, Shelton WN 1977, Phys. Rev. A **16**, 552
5. H. Klar, private communication.

QUANTAL e^- - He THRESHOLD IONIZATION

Derrick S.F. Crothers

Department of Applied Mathematics and Theoretical Physics
The Queen's University of Belfast
Belfast BT7 1NN Northern Ireland

We address the semiclassical approximation and its application to the threshold law for electron-atom ionization,¹ and note that the JWKB Green-Liouville method is particularly well suited to Coulomb potentials and their singularities.² We avoid singular wave functions, classical differential cross sections and matching procedures at arbitrary finite distances. Rather, matching occurs in terms of current probability densities on the hyperspherical surface at infinity. By using the Kohn variational principle perturbatively we estimate the quantal electron-helium singlet threshold ionization cross section to be given by

$$Q = 4.72 E^{m_{12}} a_0^2$$

where E is the energy above threshold in au and $m_{12} \approx 1.127$ is the well known Wannier^{3,4} exponent. At $E=0.8$ ev the probability for either escaping electron to have energy E_r at right angles to the incident electron beam is found to be some 40% higher than experiment^{5,6} and to be given by

$$p_{0.8}(E_r, \pi/2) = 3.46 (10^{-19} \text{ cm}^2 \text{ sr}^{-1} \text{ eV}^{-1}).$$

The coincidence yield⁵ when the angle θ_{12} between the two escaping electrons in the $\pi/2$ plane is 150° is expressed as a ratio R to the yield at $\theta_{12} = 180^\circ$. It too is found to be higher than experiment, taking the values 0.42, 0.50, 0.59, 0.66 and 0.73 at $E=0.2, 0.4, 0.8, 1.6$ and 3.0 (ev) respectively. Finally we compare with the triple differential cross section experimental values⁷ and obtain good qualitative and quantitative agreement, provided we retain singlet amplitudes up to the fourth partial wave.

Acknowledgement

I am grateful to Dr. Alain Huetz for communication of results prior to publication.

1. Peterkop R., 1971, J.Phys.B.Atom.Molec.Phys., 4, 513-521.
2. Bárány A. and Crothers, D.S.F., 1983, Proc.Roy.Soc. Lond. A, 385, 129-143.
3. Wannier G., 1953, Phys.Rev. 90, 817-825.
4. Read F.H., 1984, J.Phys.B.Atom.Molec.Phys., 17, 3965-3986.
5. Cvejanović S. and Read F.H., 1974, J.Phys.B.Atom.Molec.Phys., 7, 1841-1852.
6. Pichou F., Huetz A., Joyez G. and Landau M., 1978, J.Phys.B.Atom.Molec.Phys., 11, 3683-3692.
7. Fournier-Lagarde P., Mazeau J. and Huetz A., 1984, J.Phys.B.Atom.Molec.Phys., 17, L591-596.

STUDY OF HELIUM DOUBLY EXCITED STATES WITH A CORRELATED WAVE FUNCTION METHOD

O. Dulieu, C. Le Sech

Département d'Astrophysique Fondamentale (U.A. 812)
Observatoire de Meudon, 92190 Meudon, France

It has been shown that Pluvinaige's method ¹ can be applied successfully to study ground and excited states of two electron molecules ^{2,3}. Some $1,3\sigma_g$ states of hydrogen molecule with both electrons excited have also been calculated, suggesting that this method could be a good candidate to describe autoionizing states ⁴.

In the present work, the method is applied to the study of autoionizing states of Helium. The Schrödinger equation is :

$$\left(-\frac{\hbar^2}{2m} \nabla_1^2 - \frac{\hbar^2}{2m} \nabla_2^2 - \frac{Z}{r_1} - \frac{Z}{r_2} + \frac{1}{r_{12}} \right) \psi(\vec{r}_1, \vec{r}_2) = E \psi(\vec{r}_1, \vec{r}_2)$$

The starting point of Pluvinaige's method is to rewrite the wave function $\psi(\vec{r}_1, \vec{r}_2) = \phi(\vec{r}_1, \vec{r}_2) u(\vec{r}_1, \vec{r}_2)$ and to separate then Schrödinger equation so that $\phi(\vec{r}_1, \vec{r}_2)$ and $u(\vec{r}_1, \vec{r}_2)$ are solution of :

$$\left(-\frac{\hbar^2}{2m} \nabla_1^2 - \frac{\hbar^2}{2m} \nabla_2^2 - \frac{Z}{r_1} - \frac{Z}{r_2} \right) \phi = \epsilon \phi$$

$$\left(-\frac{\hbar^2}{2m} \nabla_1^2 - \frac{\hbar^2}{2m} \nabla_2^2 + \frac{1}{r_{12}} \right) u = k^2 u$$

The solution $\psi(\vec{r}_1, \vec{r}_2) = \phi(\vec{r}_1, \vec{r}_2) u(\vec{r}_1, \vec{r}_2)$ would be exact if $\epsilon = 0$, k being a constant. Our approximation considers $\epsilon = 0$, $k^2 = H' - E$ as a perturbation, H' being a constant. More details can be found in references quoted above.

The present approach has some interesting points :

- the approximate wave function describes exactly the coulombic repulsion $1/r_{12}$.

- though $\psi(\vec{r}_1, \vec{r}_2)$ is a correlated wave function, it preserves the configuration idea.

- the wave function ψ is the product of two functions : ϕ stands for the orbital motion of the unscreened electrons, and u describes the electrons' correlation as a collision in the coulombic field $1/r_{12}$.

Calculations and results : For He ($n_1 \ell_1, n_2 \ell_2$) configurations, the hamiltonian matrix is calculated on the basis of antisymmetrized and eigen functions of L^2 and S^2 , built with the $\phi_{n\ell}(\vec{r}_1, \vec{r}_2) u(r_{12})$ correlated orbitals.

Eigenvalues are deduced after diagonalization.

Energies for $n_1 = 2, n_2 = 2$ are reported in table hereafter :

State ⁵	This work	Exp ⁶	Theory ⁷	Theory ⁸
$1S(2, 2a)$	-0,77610	-0,7767	-0,77524	-0,77363
$1S(2, 2b)$	-0,61727	-0,6198	-0,61513	-0,60351
$1D(2, 2a)$	-0,70147	-0,7028	-0,69748	-
$1P(2, 2a)$	-0,68100	-0,6938	-0,68835	-0,69337
$3P(2, 2a)$	-0,75850	-0,7604	-0,75829	-0,76364

Energy (a.u.) with $k = 0,3$.

More results and autoionizing widths will be presented at the Conference.

References

1. P. Pluvinaige, J. Phys. Radium, **12**, 789 (1951)
2. M. Aubert-Frécon and C. Le Sech, J. Chem. Phys. **74**, 2931 (1981)
3. A. Herriet, M. Aubert-Frécon, C. Le Sech and F. Masnou-Seeuws, J. Phys. B, **17**, 3417 (1984)
4. C. Le Sech and M. Aubert-Frécon, J. Phys. B **15**, L135-L137 (1982)
5. Classifications used by Lipsky and al. (ref. 7)
6. W.C. Martin, J. Phys. Chem. Ref. Data, **2**, 257 (1973)
7. L. Lipsky, R. Anania and M.J. Conneely, Atomic and nuclear Data Tables, **20**, 127 (1977)
8. J. Macek, J. Phys. B **1**, 831 (1968)

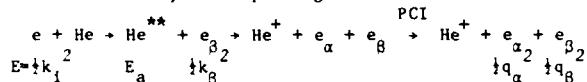
AN OPTICAL POTENTIAL MODEL FOR POST-COLLISION INTERACTION IN EJECTED ELECTRON SPECTRA

P.J.M. van der Burgt, J. van Eck, H.G.M. Heideman and G. Nienhuis

Fysisch Laboratorium, Rijksuniversiteit Utrecht, Princetonplein 5,
3584 CC Utrecht, The Netherlands.

Post collision interaction (PCI) in electron scattering experiments causes an exchange of energy and angular momentum between the scattered electron and the electron ejected by an autoionizing state. In order to study these processes van de Water et al.¹ formulated a model for PCI for the case that the scattered electron is captured into a singly excited state. Their model is based on a formal separation of PCI from the initial excitation and subsequent decay of the autoionizing state. Similar to the resonance theory of Feshbach² a standard optical potential technique is applied, which allows a separation of the transition amplitude into the parts $T = T_p + T_{opt}$, T_p describing the direct excitation of singly excited states, and T_{opt} containing the effect of autoionizing states on the excitation process.

In the same way a model for PCI may be formulated for the case that the scattered electron remains in a continuum state, corresponding to the reaction:



The transition amplitude becomes:

$$T_{opt} = \int d\vec{k}_{\beta} \langle \vec{k}_{\beta} | P | \vec{k}_{\alpha} \rangle \langle \vec{k}_{\alpha} | PHQ | \vec{k}_{\beta} \rangle \quad (1)$$

$$\frac{1}{E - E_a - \frac{1}{2}k_{\beta}^2 + \frac{1}{2}k_{\alpha}^2} \langle \vec{k}_{\beta} | QHP | \vec{k}_{\alpha} \rangle$$

where $|0\rangle$ denotes the ground state of the helium atom, $|a\rangle$ the autoionizing state, $|\vec{k}\rangle$ a free electron state of momentum \vec{k} and $|\vec{q}\rangle$ an electron state of momentum \vec{q} in the Coulomb field of the He^{+} ion. The projection operator P projects on the subspace of states with at least one electron in a 1s orbital, the complementary operator $Q = I - P$ projects on the subspace containing the doubly excited states. We now introduce the Coulomb interaction between both outgoing electrons $V_{\alpha\beta} = |\frac{1}{r_{\alpha}} - \frac{1}{r_{\beta}}|^{-1}$ and assume that the decay of the autoionizing state is not influenced by the scattered electron. The first matrix element of (1), describing decay of the autoionizing state and subsequent PCI becomes (analogous to eq. (2.14) of ref. 1):

$$\langle \vec{k}_{\beta} | P | \vec{k}_{\alpha} \rangle \langle \vec{k}_{\alpha} | PHQ | \vec{k}_{\beta} \rangle = \langle \vec{k}_{\beta} | \vec{k}_{\alpha} \rangle \langle \vec{k}_{\alpha} | PHQ | \vec{k}_{\beta} \rangle +$$

$$+ \iint \langle \vec{k}_{\alpha} | \vec{k}_{\beta} | PV_{\alpha\beta} P | \vec{k}_{\alpha} \rangle \frac{1}{E - \frac{1}{2}k_{\alpha}^2 - \frac{1}{2}k_{\beta}^2 - E_a + i\epsilon} \langle \vec{k}_{\beta} | \vec{k}_{\alpha} \rangle \langle \vec{k}_{\alpha} | PHQ | \vec{k}_{\beta} \rangle \quad (2)$$

where $|\vec{k}_{\alpha}\rangle$ and $|\vec{k}_{\beta}\rangle$ are eigenstates of $H_{\alpha\beta}$. Substituting the amplitude for decay of the autoionizing state: $\chi(\vec{k}_{\alpha} + a) = \langle \vec{k}_{\alpha} | PHQ | a \rangle$ the first term in (2) becomes: $\chi(\vec{k}_{\alpha} + a) \int \langle \vec{k}_{\beta} | \vec{r} \rangle \langle \vec{r} | \vec{k}_{\beta} \rangle d\vec{r}$. Expansion into partial waves results in a radial integral equivalent to the shake down model³. Analogous to van de Water et al.¹ an expansion in partial waves can be made of the second term of (2), resulting in an integral over the radial coördinates of both electrons.

Recently van der Burgt et al.⁴ have measured the angular distribution of ejected electrons from the $\text{He}^{**}(2s^2)^1S$ autoionizing state after its electron impact excitation via the $\text{He}^{-}(2s2p)^2D$ resonance. Figure 1 shows the measured angular distribution, which is anisotropic due to both angular momentum exchange during the PCI and interference with the direct ionization of helium. Apparently the probability for angular momentum exchange has a maximum at 50° and has minima around 0° and 90° .

Calculations for this case, based on the optical potential model sketched above are in progress and results will be presented at the conference.

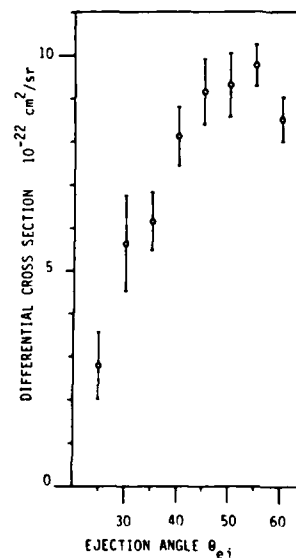


Figure 1.
Differential cross sections for resonant excitation and decay of the $\text{He}^{**}(2s^2)^1S$ autoionizing state. The cross sections are determined for ejected electrons with energy 33.5 eV.

References

1. W. van de Water, H.G.M. Heideman, and G. Nienhuis, J. Phys. B **14**, 2935 (1981).
2. H. Feshbach, An. Phys. **19**, 287 (1962).
3. F. Read, J. Phys. B **10**, L297 (1977).
4. P.J.M. van der Burgt, J. van Eck, and H.G.M. Heideman, J. Phys. B **18**, to be published (1985).

ABSOLUTE DOUBLE DIFFERENTIAL IONIZATION CROSS-SECTION FOR ELECTRON IMPACT: He

L. Avaldi, R. Camilloni, E. Fainelli and G. Stefani

Istituto di Metodologie Avanzate Inorganiche del CNR
Area della Ricerca di Roma, C.P. 10 00016 Monterotondo (Italy)

A detailed understanding of atomic and molecular ionization by electron impact is important in many fields such as astrophysics, upper atmosphere, plasma and radiation physics and, of course, it is of intrinsic interest because of its fundamental nature. Informations on the dynamics of ionization can be searched for by measuring absolute double differential cross sections (DDCS) for ejection of secondary electrons of energy E_B at an angle ϑ by primary electrons of energy E_0 .

Within the last twenty years knowledge of the ionizing process has improved very rapidly^{1,2,3}. To summarize the theoretical and experimental results Y.K. Kim⁴ has recently proposed some "recommended" cross-sections, which represent a consistent set of DDCS for He, independent from any specific theory or experiment. They satisfy known theoretical and experimental requirements on asymptotic and threshold behavior, angular symmetry and values of integrated cross-sections. Within this approach the DDCS can be represented by a truncated series of Legendre polynomials

$$\frac{d^2\sigma}{d\Omega dE_B} = \sum_{n=0}^6 a_n P_n(\cos \vartheta) \quad (1)$$

whose coefficients have been used as fitting parameter in order to reproduce and generate DDCS's for any combination of ϑ (0° - 180°), E_B (0-40) and E_0 (100-2000 eV). Recent experiments of H. Ehrhardt et al.⁵ have tested the reliability of these recommended DDCS over the full range of E_B and E_0 previously mentioned.

In this work absolute differential cross-section on He for 500 eV incident energy are presented. The ejected electron energy ranges between 40 and 237.75 eV, while the angular range is 5° - 145° . The work is meant to give a contribution in completing the mapping of DDCS for secondary electron energies approaching the limit $E_B = (E_0 - B)/2$, where B is the He's ionization energy. Although the vast majority of ionizations occur away from this kinematic region, it is anyway of interest to ascertain to which extent Kim's formula (1) can be applied, approaching the domain where binary collisions are dominant and exchange effects are important.

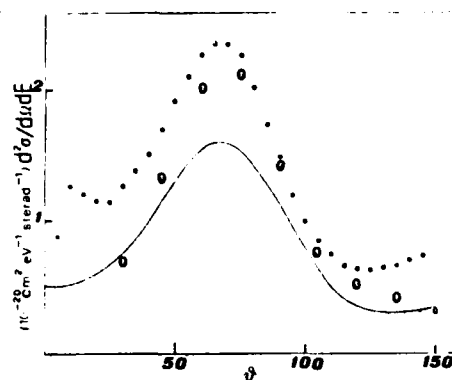
A crossed beam apparatus designed for (e,2e) experiments has been used for the present measurements. Usual working conditions were few μA current for the incident beam and $2 \cdot 10^{-6}$ torr for the residual gas pressure in the scattering chamber, corresponding approximately to a local pressure in the gas target of $p \approx 10^{-3}$ torr. The solid angle subtended by the electron analyzer is $3 \cdot 10^{-4}$ ster, while the energy resolution is .6 eV. A careful evaluation of background sources has been performed. The contribution due to change of the effective target length with the angle has been measured, comparing relative data of elastic peaks at several incident

energies (100-1000 eV) with Jansen et al.⁵ data. In addition each measurement has been repeated with the gas beam off to check for possible background counts due to the scattering of the primary beam on surfaces of the chamber. For each set of E_0 , E_B the complementary DDCS relative to $E_A = E_0 - E_B - B$ has been measured. This has been done because in the case of He, for which the contribution from double ionization is $\approx 2\%$ and the one from simultaneous excitation and ionization is below 2% for all E_0 , the following relationship is valid:

$$\int \frac{d^2\sigma}{d\Omega_B dE_B} d\Omega_B = \int \frac{d^2\sigma}{d\Omega_A dE_A} d\Omega_A$$

The DDCS for the fast scattered electrons can be given in absolute units by anchoring its optical limit (momentum transfer $K \rightarrow 0$) to the Optical Oscillator Strength (OOS) which is known by photoionization experiments within few percent. By this way it is possible to give in absolute units also the DDCS for the slow ejected electrons.

A detailed comparison with previous experimental data and with the polynomial expression suggested by Kim⁴ will be presented and discussed.



DDCS for 40 eV ejected electrons, $E_0 = 500$ eV.

(●) present data, (○) Opal et al.¹

Kim's recommended cross-section (—)

- 1) C.B. Opal, E.C. Beaty and W.K. Peterson, At. Data 4, 209 (1972)
- 2) N. Oda Radiat. Res. 64, 80 (1975) and references therein.
- 3) H. Ehrhardt, K. Jung, R. Müller-Fiedler and P. Schlemmer, (1984) to be published
- 4) Y.K. Kim Phys. Rev. A28, 656 (1983)
- 5) R.H.J. Jansen, F.J. de Heer, H.J. Luyken, B. van Wingerden and H.J. Blaauw J. Phys. B9, 185 (1976)

ENERGY PARTITIONING IN NEAR-THRESHOLD EXCITATION AND IONISATION OF HELIUM BY ELECTRON IMPACT

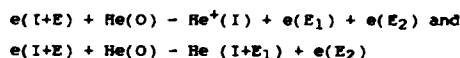
P. Hammond, P.H. Read, S. Cvejanović* and G.C. King

Schuster Laboratory, University of Manchester, Manchester M13 9PL, U.K.

*Institut za Fiziku, P.O. Box 57, 11001 Beograd, Yugoslavia

We have looked experimentally into new details of the threshold ionisation process and have found that the results agree with those of a recent computational study based on a classical treatment¹. In particular we have investigated the partitioning in energy between the two slow electrons that result from the process of near-threshold ionisation and also from the closely related process of near-threshold excitation to high-*n* states.

The two processes can be represented by



where the quantities in parentheses are the energies of the reactants or products. In the second process an electron is left bound in a high-Rydberg orbital of the atom, with an energy E_1 that is negative. In both processes one electron remains in the 1s orbital and the energies E_1 and E_2 of the other two have magnitudes that are much less than I .

According to the Wannier theory^{2,3,4}, the cross section for the near-threshold ionisation process has the form

$$\sigma_E(E_1)dE_1 \propto E^{-0.127} f(E_1/E)dE_1$$

where dE_1 represents the energy interval over which one of the outgoing electrons is observed. This equation also gives the cross section for near-threshold excitation^{1,5}, if the cross section is averaged over the closely spaced Rydberg states.

Following the computational results of Vinkalns and Gaillitis⁶, based on classical trajectory integrations, it has long been assumed that the function f is constant in the interval $E_1=0$ to E , giving a uniform partitioning in energy between the outgoing electrons. This result has also been found quantum mechanically⁷. Recently, however, the more accurate computational results¹ have indicated that the energy partitioning is not uniform. The purpose of the present work is to investigate the form of the function f for near-threshold ionisation ($E_1=0$ to E) and also for near-threshold excitation ($E_1<0$, or since the electrons are indistinguishable, $E_1>E$).

We have obtained constant residual energy (CRE) spectra, by keeping the analysing energy (E_2) fixed while the incident energy ($I+E$) is varied. To deduce the form of $f(x)$ from a CRE spectrum $Y(E, E_2)$ we use the yield (after subtraction of the background) at the point $E=2E_2$ as a normalisation point and take $f(0.5)=1.0$. Then

$$f(E_2/E) = \frac{2E_2}{E} \times \frac{Y(E, E_2)}{Y(2E_2, E_2)}$$

CRE spectra have been obtained for the following combination of E_2 and the scattering angle θ : 0.075eV, 90°; 0.150eV, 90°; 0.3eV, 90°; 0.6eV, 90°; 0.3eV, 40°; 0.6eV, 40°. The figure shows the resulting average value of $f(x)$.

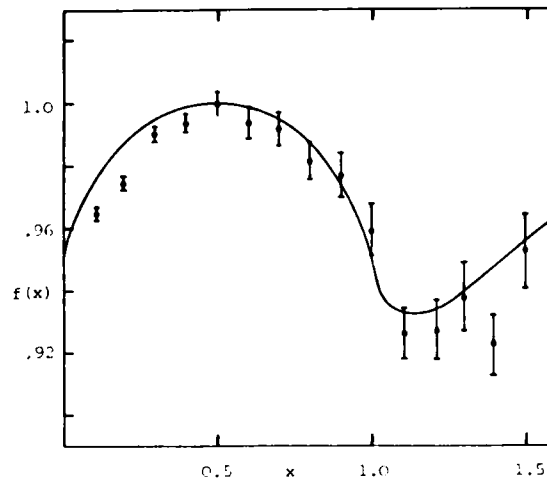


FIGURE Comparison for experimental results (points) with calculated result (full curve).

The full curve in the figure shows the function f calculated by Read¹. There is good agreement between this and the form of f that we have found experimentally.

At very low values of E_2 (0.1eV) the form of the CRE spectrum in the vicinity of $E=0$ becomes dominated by the term $E^{-0.127}$ rather than by $f(E_2/E)$, giving the "ionisation cusp" seen by Cvejanović and Read⁸ (see also Spence⁹). The yield at $E=0$ is always finite because $f(E_2/E)$ is proportional to $(E_2/E)^{-0.127}$ when E_2/E is very large¹.

In a second type of experiment, using the energy loss (EL) mode, the results are again consistent with the calculated form of f .

Results will also be presented of measurements of the form that f has when the incident energy is less than I (i.e. when $E<0$).

References

- 1 P H Read, J Phys B **17**, 3965 (1984)
- 2 Wannier G, Phys Rev **90**, 817 (1953)
- 3 Peterkop R, J Phys B **4**, 513 (1971)
- 4 Rau A R P, Phys Rev A **4**, 207 (1971)
- 5 Vinkalns I and Gaillitis M, Latvian Academy of Science Report No. 4 (1967, Riga: Zinatne) pp 17
- 6 Vinkalns I and Gaillitis M, Abstracts 5th ICPHAC, 648 (1967)
- 7 Rau A R P, J Phys B **9**, L283 (1976)
- 8 Cvejanović S and Read P H, J Phys B **10**, 1180 (1974)

EJECTED ELECTRON SPECTRA FROM AUTOIONISING STATES OF HELIUM EXCITED BY ELECTRON IMPACT

P S K Moorhead and A Crowe

Department of Pure and Applied Physics, The Queen's University of Belfast,
Belfast, United Kingdom

The ejected electron spectra due to decay of the $(2p^2)^1D$ and $(2s2p)^1P$ autoionising states of helium have been measured over the angular range 50° to 130° with respect to the incident electron beam and for incident electron energies of 70, 80, 100 and 200 eV.

The double differential cross section in the region of a particular autoionising resonance is of the form given by Balashov et al¹

$$\frac{d^2\sigma}{d\Omega_K dE} = c(K) + \frac{a(K)\epsilon + b(K)}{1 + \epsilon^2}$$

where $c(K)$ is the differential cross section for direct ionisation, $b(K)$ is the resonant differential cross section at the resonant energy E_r , and $a(K)$ is a measure of the asymmetry of the resonance. K is the ejected electron momentum and $\epsilon = 2(E - E_r)/\Gamma$, where Γ is the resonance width.

In the present work the angular dependence of each of the parameters $a(K)$ and $b(K)$ has been extracted from the measured spectra. Figure 1 shows the $a(K)$ and $b(K)$ parameters for the $(2s2p)^1P$ state from the present and previous^{2,3} experiments at an incident electron energy of 100 eV. The present data and that of Gelebart et al² have been put on the same scale by normalising the $a(K)$ parameters at 90° . The parameters of Pochat et al³ relative to the earlier data² are as discussed by them.

There is qualitative agreement for both parameters for angles $\geq 70^\circ$. However, for angles $< 70^\circ$, the $a(K)$ parameters show quite different behaviour. The present $b(K)$ parameter varies much less rapidly at both extremes of the angular range than that of the French group.

References

1. V V Balashov, S S Lipovetsky and V S Senashenko, Phys Lett **39** 103 (1972).
2. F Gelebart, R J Tweed and J Peresse, J Phys B **9** 1739 (1976).
3. A Pochat, R J Tweed, M Doritch and J Peresse, J Phys B **15** 2269 (1982).

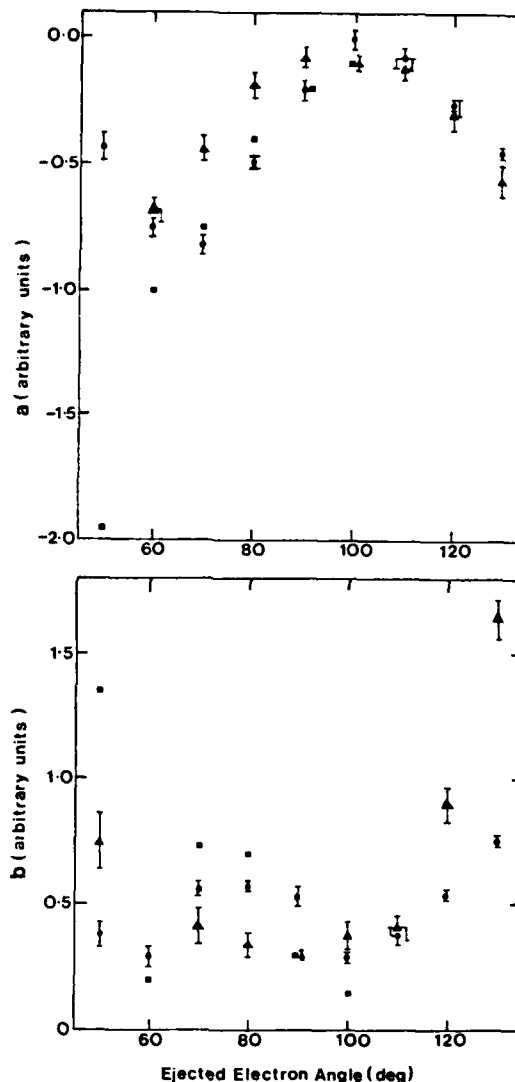


Figure 1 : $a(K)$ and $b(K)$ parameters as a function of ejected electron angle for the $(2s2p)^1P$ state of helium at an incident electron energy of 100 eV.
■ Gelebart et al², ▲ Pochat et al³, ● present data.

EXCITATION OF AUTOIONISING STATES OF HELIUM IN SPECIFIC MOMENTUM TRANSFER ELECTRON COLLISIONS

P S K Moorhead and A Crowe

Department of Pure and Applied Physics, The Queen's University of Belfast,
Belfast, United Kingdom

The autoionising states of helium excited by electron impact have been studied mostly by measuring the spectra of either the scattered or ejected electrons. Such spectra correspond to an integration over the momenta of the undetected electron. If, however, the scattered and ejected electrons are detected in a coincidence experiment, the kinematics of both outgoing electrons are completely defined. Hence information can be obtained on both the direct ionisation and autoionisation cross sections as a function of the momentum of the emitted electron for specific momentum transfer collisions. The triple differential cross section can be written in the form, Balashov et al¹,

$$\frac{d^3\sigma}{dQ_k dQ_{k_1} dE} = c(k^2, Q) + \frac{a(k^2, Q)s + b(k^2, Q)}{s^2 + 1}$$

where $c(k^2, Q)$ is the cross section for direct ionisation, $b(k^2, Q)$ is the resonance cross section and $a(k^2, Q)$ is a measure of the asymmetry of the resonance. k_0 , k and k^2 are the incident, scattered and ejected electron momenta respectively, and $Q = k_0 - k$ is the momentum transfer. $s = 2(E - E_r)/\Gamma$, where E is the ejected electron energy, E_r is the resonance energy and Γ its width.

The feasibility of this approach was first demonstrated by Weigold et al² for the $(2s2p)^1P$ and $(2p^2)^1D$ states of helium. The broad energy resolution (0.6 eV) prevented resolution of the states and the analysis of the data was based on the assumption that the 1D state could be ignored. More recently $a(k^2, Q)$, $b(k^2, Q)$ parameters for both these states have been obtained by Pochat et al³, although the features were again unresolved in the measured spectra.

In the present work, ejected electron spectra for specific momentum transfer electron collisions have been measured at an incident electron energy of 200 eV with an energy resolution ~ 100 meV for the same two states of helium. Figure 1 shows such a spectrum for a scattered electron angle of 10° and an ejected electron angle of 130° ($\phi = 0^\circ$). The 1D structure at an

ejected electron energy of 35.30 eV and the 1P at 35.54 eV are partially resolved.

Spectra obtained over a range of ejected electron angles and the $a(k^2, Q)$ and $b(k^2, Q)$ parameters derived from them will be presented.

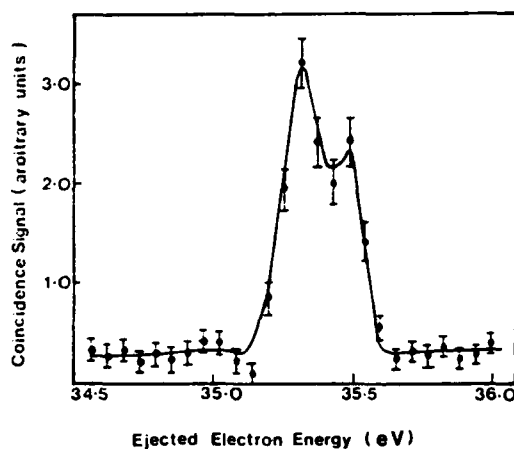


Fig 1 Coincidence electron spectrum for the $(2p^2)^1D$ (35.30 eV) and $(2s2p)^1P$ (35.54 eV) at an incident electron energy of 200 eV, a scattered electron angle of 10° and an ejected electron angle of 130° ($\phi = 0^\circ$).

References

1. V V Balashov, S S Lipovetsky and V S Senashenko, Sov Phys JETP, **36**, 858, (1973).
2. E Weigold, A Ugbabe and P J O Teubner, Phys Rev Lett, **35**, 209 (1975).
3. A Pochat, R J Tweed, M Doritch and J Peresse, J Phys B, **15**, 2269, (1982).

ELECTRON IMPACT IONIZATION CROSS SECTION MEASUREMENTS
OF THE CHLORINE, BROMINE, AND IODINE ATOMS

Todd R. Hayes, Robert C. Wetzell, and Robert S. Freund

AT&T Bell Laboratories, Murray Hill, NJ 07974 USA

Absolute cross sections for ionization of reactive atoms and molecules by electron impact are important for modeling of discharges and for quantitative mass spectrometry of neutral species extracted from discharges. We report here the first such measurements for three of the halogen atoms, over the range from threshold to 200 eV. The method uses a beam of electrons crossing a fast atomic beam, with charge state separation and complete collection of the product ions (Fig. 1).

The fast atomic beam (with a flux of about 10^{10} atoms/sec) is formed by charge transfer neutralization of a 3 kV ion beam. Chlorine ions are formed from a dc discharge in CF_2Cl_2 vapor or solid CaCl_2 in a rare gas. Bromine is formed from CF_2Br_2 vapor. Iodine is formed from solid KI in a rare gas discharge. The charge transfer gas is ethane, although many other gases would probably be equally satisfactory.

Only a single electronic state of the atom is expected to result from charge transfer with ethane; threshold measurements confirm the presence of only the ground state. Both fine structure components probably form, but the electron energy resolution is insufficient to resolve them.

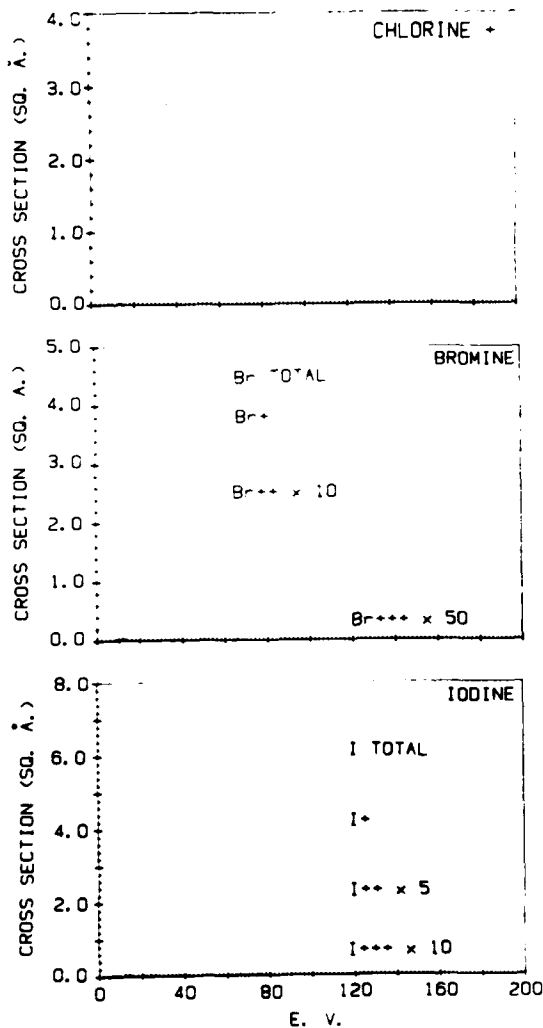
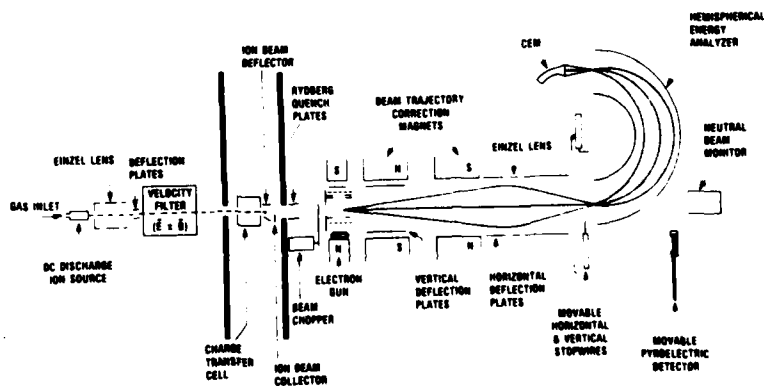
The neutral beam flux is measured absolutely by a secondary electron detector, which is calibrated against an ion beam with a pyroelectric detector. The overall absolute accuracy of the apparatus is calculated to be $\pm 15\%$. This accuracy was confirmed by remeasurements of the well-known rare gas cross sections.

Preliminary results are shown in Figs. 2, 3 and 4. For all three atoms, the maxima of the cross sections are slightly larger than those of the neighboring rare gas atoms, a trend which is consistent with calculations by Stafford¹ and by Mann².

References

1. F. E. Stafford, J. Chem. Phys. **45**, 859 (1966).
2. J. B. Mann, J. Chem. Phys. **46**, 1646 (1967)

FIGURE 1.
Apparatus



E. V.
Figures 2-4. Electron impact ionization
cross sections for Cl, Br, and I.

THE d-SHELL AUTOIONIZATION EJECTED ELECTRON SPECTRUM OF THE GROUP
IB ATOMS Cu, Ag AND Au, EXCITED BY ELECTRON IMPACT

L. F. Forrest*, G. K. James^a, M. Kurepa^b, V. Pejcev^b, K. J. Ross* and M. Wilson*

* Department of Physics, Southampton University, Southampton, England

^a Department of Physics, Chelsea College, London, England

The group IB atoms have been the subject of a number of ultraviolet absorption and arc spectra studies. The discrete spectra of these atoms above the first ionization potential are principally due to excitation of an inner d shell electron from the $nd^{10}(n+1)s$ ground state to five configurations of the form $nd^9(n+1)smp$ and $m'f(m'n+1)$, where $n = 3, 4$ and 5 and $m' = 4, 4$ and 5 for Cu, Ag and Au respectively; the np series being dominant. These series terminate at the $nd^9(n+1)s$ ion levels, and so the spectra are confined to a region within approximately 4 eV of the first ionization potential.

In the present investigations, the d-shell ejected electron spectra of Cu, Ag and Au were observed following electron impact excitation, over the range of incident electron kinetic energies 10 to 500 eV, with a beam current typically greater than 10 μ A. Velocity analysis of the ejected electrons was performed using a 180° hemispherical sector electrostatic analyser, operated in constant resolution mode. A radio-frequency heated graphite oven (high density graphite EK 986) was employed in the present work, and the metals used were 99.999% pure.

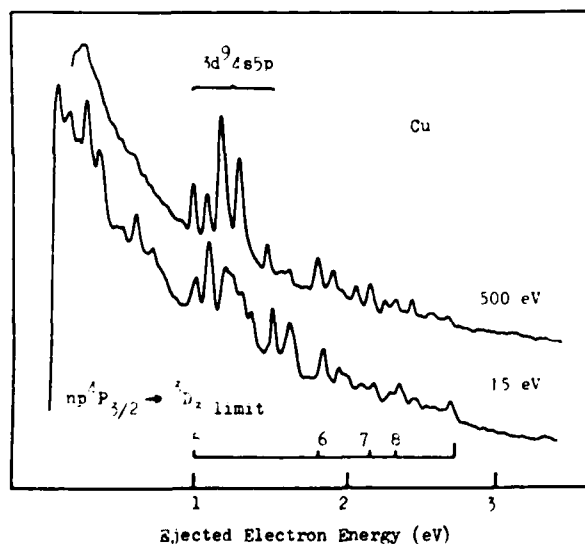


Figure 1 : The ejected electron spectrum of Cu between 0 and 3.5 eV ejected electron energy, observed with incident beam energies of 500 eV and 15 eV.

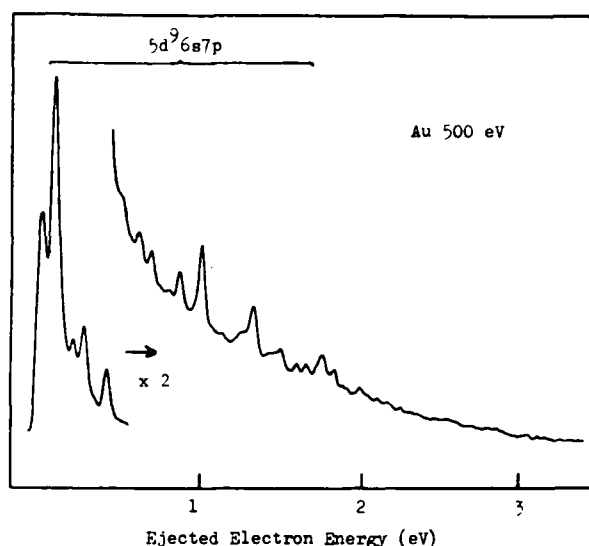


Figure 2 : The ejected electron spectrum of Au between 0 and 3.5 eV ejected electron energy, observed with a 500 eV incident electron beam energy.

The spectra of Cu obtained at 500 eV and at 15 eV, and the spectrum of Au obtained at 500 eV incident electron kinetic energy are shown in Figures 1 and 2 respectively. The corresponding spectra of Ag have been published elsewhere¹. In order to make assignments to features in our spectra which are not observable by photoabsorption we have used the results of Hartree-Fock based calculations to estimate eigenvalues for these optically disallowed levels and hence made new assignments to our spectra where possible.

References

- ¹ James G. K., Ross K. J. and Wilson M., J Phys B : At Mol Phys. 16, 4237-4247 (1983)

^a Present address : Department of Chemistry, University of British Columbia, Vancouver, Canada

^b Present address : Institute of Physics, Zemun, Yugoslavia

FORMATION AND DECAY OF AUTOIONIZATION STATES OF Sr, Ca AND Ba ATOMS
IN SLOW ELECTRON-ATOM COLLISIONS

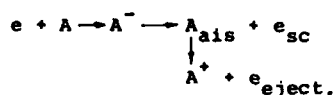
S.M.Kazakov and O.V.Khrystoforov

Physics Department, Chuvash State University, Cheboksary 428015, USSR

The electron spectrum of the autoionization states (AIS) and the energy loss spectrum of electrons scattered through 90° were investigated on the same apparatus. The electron spectrometer we used¹ is modified to permit high-temperature investigations. We studied the spectra in the primary-beam energy interval $E = 10 - 100$ eV and in the ejected-electron energy range $5 - 30$ eV.

As a result of analysis of numerous electron spectra energy dependences of the intensity for more than 40 lines have been obtained. Depending on nature of decaying autoionization states these intensities behave differently. However, for the series of lines we found the presence of one or more sharp and intense maxima on the curves near the thresholds. These maxima are caused by the additional mechanism of populating the AIS through

short-lived negative ion states of the respective atoms:

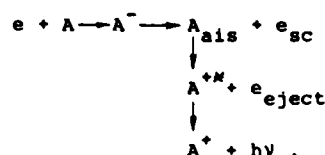


The analysis and the comparison of the energy loss and the ejected electron spectra showed that many AIS were represented by more than one line in ejected electron spectrum, as a result of multichannel decay of the AIS. The multichannel decay is best studied at small incident energies close to lowest ionization states thresholds, where the decay pattern is simple. Lines in the ejected electron spectra appear in correlated groups, each group representing decays of various AIS in a particular A^+ state. Lines within a group have different intensities, but the corresponding lines in each group have the same appearance potential, which proves the multichannel decay of AIS. Positive ion excited states in question are, most probably, the lowest 2D and 2P states of the ions Sr^+ , Ca^+ and Ba^+ . The number of the channels achieve 5-10. As a

rule, the intensities of the decays to the ground state are greater than to the excited states. Nevertheless, for all these atoms we found few decays into excited states which were several orders of magnitude stronger than the decays into the ground ionic states. We also found few transitions into the excited states which can be observed only in the narrow incident energy interval above threshold ($E_{sc} < 1$ eV), i.e. these processes are strictly resonant.

We compared our results with the results of measurement of the ionization cross sections of these atoms and the excitation functions of the spectral lines of the ions Sr^+ , Ca^+ and Ba^+ . It was found that the sharp structures on the ionization curves are the consequence of the resonance population of the AIS and their subsequent decay into different positive ion

states. The structures in the excitation function of the spectral lines are the consequence of the following process:



Reference

1. S.M.Kazakov, A.I.Korotkov, O.B.Shpenik, Sov.Phys. JETP 51, 847 (1980).

ELECTRON IMPACT IONIZATION OF LASER EXCITED BARIUM ATOMS

S. Trajmar^{*} and J. C. Nickel[†]^{*}Jet Propulsion Laboratory, California Institute of Technology, Pasadena, CA 91109[†]Department of Physics, University of California, Riverside, CA 92521

A collimated atomic Ba beam (20:1 collimation) was excited by a crossed laser beam to the $6s6p\ ^1P$ level. The tunable, single mode, cw dye laser was able to selectively pump the ^{138}Ba isotope (which has no hyperfine structure) and was linearly polarized. Radiation decay from the $6s6p\ ^1P$ level has in addition generated some population in the $6s5d\ ^1D$ metastable level of ^{138}Ba . (Branching ratio $\approx 1:700$) In the interaction region, therefore, we have a mixture of ground state Ba isotopes (in the ratio of their natural abundance), and ^{138}Ba atoms in the ground $6s^2\ ^1S$ and excited $6s6p\ ^1P$ and $6s5d\ ^1D$ states. Above the interaction region (just outside of the laser beam) only the 1D and ground state species survive (lifetime of the 1P state is $\sim 10^{-8}$ sec).

The Ba atoms in the Ba beam/laser beam interaction region or above this interaction region were ionized by a crossed electron beam. The electron beam energy was variable from a few eV to few hundred eV and the width of the electron energy distribution was about 0.4 eV. The Ba ions were mass analyzed with a monopole mass spectrometer and the $^{138}\text{Ba}^+$ ion signal was measured with and without laser pumping both in the laser/Ba interaction region and above it. (See Fig. 1 for schematic arrangement.)

$6s6d\ ^1D$ and $6s6p\ ^1P$ states. The total ionization cross sections obtained this way are averages over scattered and ejected electron distributions and do not change with laser polarization. It was found that the total ionization cross section for the $^{138}\text{Ba}(6s6p\ ^1P)$ and $^{138}\text{Ba}(6s5d\ ^1D)$ species were about 20% and 40%, respectively, larger than those of $^{138}\text{Ba}(6s^2\ ^1S)$ species in the 20 to 90 eV impact energy range. Measurements at lower electron impact energies are in progress and will be reported.

This work was performed at the Jet Propulsion Laboratory, California Institute of Technology and was supported in part by the National Aeronautics and Space Administration and in part by the National Science Foundation.

Reference:

1. S. Okudaire, J. Phys. Soc. Japan **29**, 409 (1970).

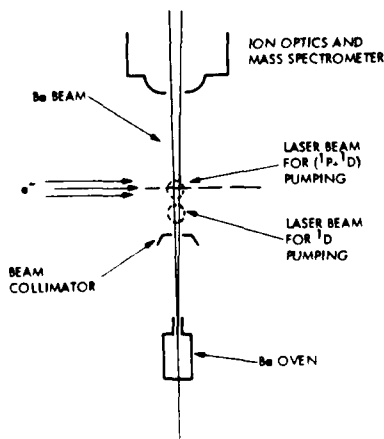


Fig. 1. Schematic experimental arrangement

From these measurements and from the known ionization cross section of ground state ^{138}Ba (which was taken equal to the ionization cross section of the naturally occurring isotope mixture)¹ we have been able to obtain ionization cross sections for ^{138}Ba in the

PRODUCTION OF EXCITED Ar II- AND Ar III-IONS BY PROTON- AND PHOTON-IMPACT*

K.-H. Scharfner, E. Kraus, H.-J. Flaig, and K. Heymann

I. Physikalisches Institut, Universität Gießen, 3500 Gießen, West Germany

There are motivations to study the population mechanism for exciting Ar II- and Ar III-levels by electron- and proton-impact: Intense transitions occur in the spectral range of the VUV which bear the potential application for an intensity calibration of spectrometer-detector systems. The configuration interaction in Ar is strong, and excitation cross sections yield information about the relative mixing coefficients. Two-electron processes are at high impact velocities dominantly determined by electron correlations.

With an experimental set-up used for studies of single and double ionization of the Ne-L shell¹ we have started to measure emission cross sections for transitions in Ar II and Ar III. In fig. 1 we present a result for the transition $3s^2 3p^4 \ ^3P_2 - 3s 3p^5 \ ^3P_1$. Included in fig. 1 are cross sections for population of the $3s^2 3p^4 \ ^3P_2$ level by Auger cascading. A problem which is so far unsolved is clearly demonstrated: The cascade channel exceeds the measured cross sections by a factor of about two, which is outside the estimated error bars of the literature data used in the analysis^{2,3}. Current experiments indicate that the Auger channel is also very strong for population of the $3s 3p^5 \ ^3P_1$ levels. This situation complicates the elimination of the weak direct two electron processes but may be helpful in consistency checks between cross sections obtained by Auger electron and by photon spectroscopy.

*Supported by Deutsche Forschungsgemeinschaft

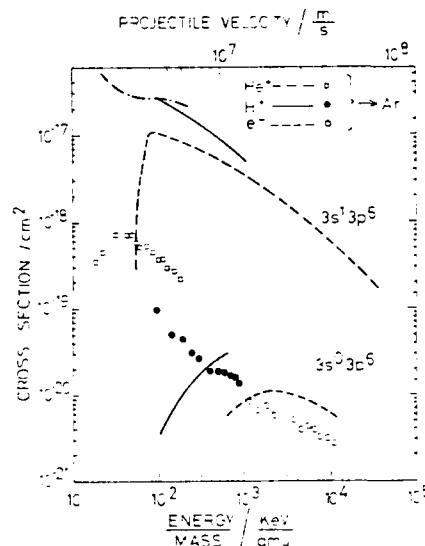


Fig. 1: Cross sections as function of the projectile energy divided by the projectile mass number. (○) electron impact, (□) proton impact, (△) He⁺ impact. A solid line: direct excitation, (---) Auger transition, (·····) Auger cascade channel.

References

1. H. Scharfner and K.-H. Scharfner, *J. Phys. A*, **11**, 1011 (1978).
2. E. J. McGuire, *Phys. Rev. A*, **11**, 1011 (1975).
3. E. J. McGuire, *J. Phys. A*, **11**, 1011 (1978).
4. A. J. Brading, *J. Phys. A*, **11**, 1011 (1978).
5. A. J. Brading, *J. Phys. A*, **11**, 1011 (1978).

ELECTRON SPECTROSCOPY OF MULTIPLY IONIZING ELECTRON-RARE GAS COLLISIONS

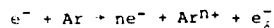
M. A. Chaudhry, A.J. Duncan, R. Hippler and H. Kleinpoppen
Atomic Physics Laboratory, University of Stirling, Stirling FK9 4LA, Scotland

INTRODUCTION

Recently the measurement of doubly differential cross sections (DDCS) for electron ejection in electron-argon collisions was reported by Hippler et al.¹ for ejected electron energies 25 eV to 300 eV, ejection angle $\theta_e = 90^\circ$ and incident electron energies of 300 eV to 8 keV. These measurements are now being extended and improved. New results are reported in argon for an incident electron energy of 1.5 keV.

APPARATUS

An energetic electron beam is injected into a dilute argon gas target. Ions produced by this process are extracted from the collision region by a small electric field (15 V/cm). Electrons ejected at 90° with respect to the incident electron direction and perpendicular to the electric field used for ion extraction are detected in a 30° parallel-plate electrostatic analyzer. Electrons ejected in an n -fold ionization process:



are identified by detection of the corresponding product ion. The ionic charge state is determined by a time-of-flight method in which the time delay of the product ion relative to the ejected electron is measured using standard coincidence electronics.

As shown in figure 1, peaks corresponding to $n=1$ up to $n=4$ are observed.

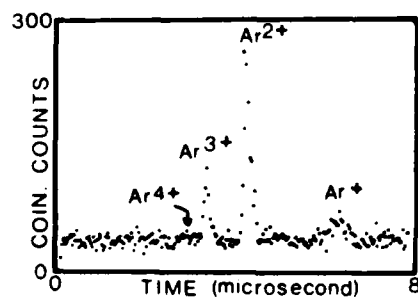


Fig. 1. Time of flight spectrum of argon ions with charge +1 to +4 in coincidence with ejected electrons of energy 200 eV.

In comparison to the earlier work of Hippler et al.,¹ improvements in energy calibration, detection efficiency and statistical accuracy have been achieved.

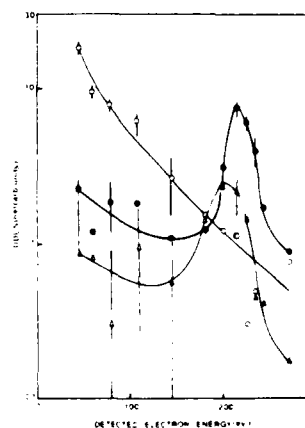


Fig. 2. Doubly differential cross sections (DDCS) for n -fold ionization versus energy of the detected electron for 1.5 keV electrons incident on argon. The ejection angle is 90° . Data are obtained in coincidence with \circ Ar^+ , \bullet Ar^{2+} , Δ Ar^{3+} , and (not shown) Ar^{4+} ions. The solid lines are only to guide the eye.

RESULTS

The DDCS for electron impact on argon at an energy of 1.5 keV is shown as a function of ejected electron energy in figure 2. With reference to the Ar^{1+} and the Ar^{2+} results, the peak in the DDCS appears to show a shift towards lower detected electron energy of about 10 eV per charge state increase, in agreement with the proton-rare gas collision results of Hippler et al.¹

The authors gratefully acknowledge the financial support of SERC and wish to thank Mr K Saeed for useful discussions.

REFERENCES

1. R Hippler, K Saeed, A J Duncan and H Kleinpoppen, Phys. Rev. A **30**, 3328 (1984).
2. R Hippler, J Bossler and H O Lutz, J Phys. B **17**, 2453 (1984).

PARTIAL CROSS SECTIONS FOR SINGLE AND MULTIPLE IONIZATION
OF Xe USING CROSSED ELECTRON-NEUTRAL BEAMS

D. Mathur and C. Badrinathan

Tata Institute of Fundamental Research, Bombay 400 005, India

It is known that ionization phenomena in heavy atoms cannot be totally explained in terms of one-electron central-field models. For instance, the strongly collective character of N shell electrons in Xe manifests itself in the totally nonhydrogenic nature of photoabsorption spectra¹. Furthermore, recent studies of electron impact ionization have established that in addition to 'direct' ionization other complex mechanisms can also make significant contributions to the ionization process. We report here high-sensitivity measurements of partial cross sections for ionization of Xe upto charge state 3, from threshold to ~ 150 eV, using crossed beams².

Fig.1 shows the single ionization cross section function for Xe; the relative cross section has been normalised against the absolute total ionization cross section of Rapp and Englander-Golden³ at 20 eV. We interpret the prominent minimum in the vicinity of 55 eV as an effect of inter-shell interactions involving virtual excitation of 4d-electrons and subsequent transfer of excitation energy to the 5p shell. Calculations using a one-electron model¹ indicate a zero in the $5p \rightarrow 4d$ contribution to single ionization in Xe at this energy. Alternative processes such as excitation-autoionization involving $5s^1 5p^5 nl nl$ or $4d^9 nl$ states are unlikely to contribute to structure at this energy.

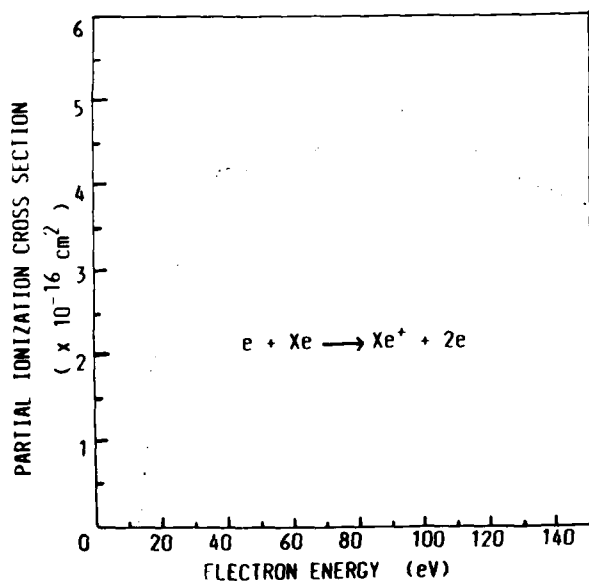


FIG.1: Cross section for single ionization of Xe.

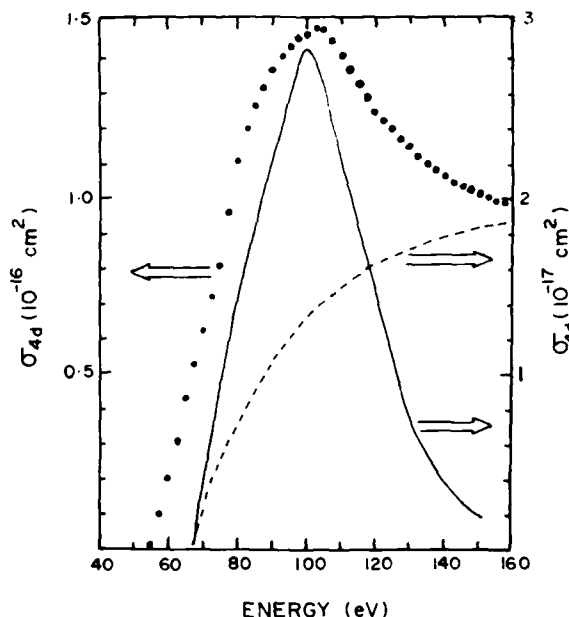


FIG.2: Ionization of 4d electrons. Circles: present data (see text); line: photoionization data (ref.4); Dashes: Lotz formula

We have also fitted the semi-empirical Lotz formula to our Xe^+ data, taking into account the 5p, 5s and 4d subshells. The difference between measured and calculated data is compared (Fig.2) with 4d photoionization cross section⁴. The surprising similarity between the two data sets demonstrates the inter-relationship between electron and photon impact ionization and indicates that concepts like electron correlations, term dependence and wavefunction collapse, which are applied extensively in photoionization, may be of relevance in electron impact ionization of high-Z atoms too.

References

1. U. Fano and J.W. Cooper, Rev. Mod. Phys. **40** 441 (1968)
2. D. Mathur and C. Badrinathan, Int. J. Mass Spectrom. Ion Proc. **57** 167 (1984)
3. D. Rapp and P. Englander-Golden, J. Chem. Phys. **43** 1464 (1965)
4. R. Haense, G. Keitel, F. J. Heuser and G. Kunz, Phys. Rev. **185** 1401 (1969)

SINGLE ELECTRON IMPACT IONIZATION CROSS SECTIONS FOR GROUNDSTATE AND METASTABLE Ar^{2+} IONS

B.A. Huber, J. Puerta and K. Wieseemann

Institut für Experimentalphysik AG II, Ruhr-Universität
D-4630 Bochum, West Germany

Partial electron impact ionization cross sections for the production of metastable multiply charged ions are of general interest on the one hand for an evaluation of metastable fractions in the primary beam of ion collision experiments on the other hand for modelling detailed ionization and excitation balances in hot plasmas.

Till now no general method for a direct access to these cross sections was available. In the case of metastable states of neutrals or singly charged ions, the difference in potential secondary electron emission from surfaces was used in order to detect metastables⁶. However, this method does not allow a separation of different excited metastable states and fails in general if the potential energy of the ground state species does not differ appreciably from that of the metastable. This is the general case for multiply charged ions and metastables with small excitation energy.

A means of distinguishing different excited states of the primary ions is the high resolution single and double translational spectrometry of secondary ions produced in electron capture reactions¹. We have used this

emitted by the source. At $E_{e1}=100$ eV, the curve was normalized to cross section values from Stephan et al.³. The agreement with experimental values of other workers^{3,4,5} over the whole energy range is quite good.

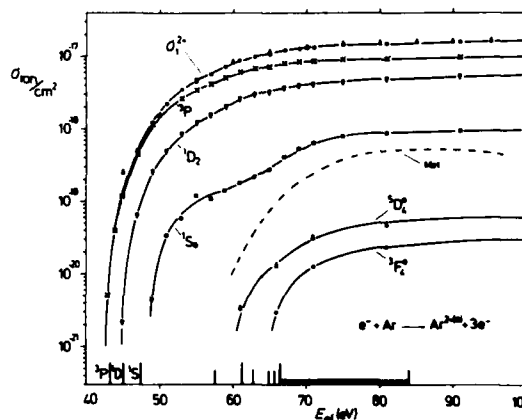


FIGURE 2 Apparent cross sections for the production of specific Ar^{2+} ion states

Fig. 2 shows some preliminary results for partial cross sections describing the production of Ar^{2+} in the $3P$, $1D_2$, $1S_0$, $5D_0$ and $3F_0$ states near threshold. The $3P$, $1D_2$ and $1S_0$ states were identified by electron capture reactions in a He target, while for the higher metastables $5D_0$ and $3F_0$ an Ar target was used. The various cross sections show a strong decrease near threshold and in some cases an additional structure at electron energies where higher excited states of Ar^{2+} become accessible.

For comparison we present the curve labeled 'met' obtained by Winter et al.⁶ by the potential emission method. This method seems to be mainly sensitive to the high lying $5D_0$ and $3F_0$ states and - to a smaller extent - to the low lying $1S_0$ state.

References

1. Huber B.A., Kahlert H.J., Wieseemann K., J. Phys. B 17 (1984) 2883
2. Kahlert H.J., Wieseemann K., Huber B.A., Annalen der Physik (Leipzig) (1985), in print
3. Stephan K., Helm H. and Märk T.D., Abstracts of Contr. Papers, XI. ICPEAC Kyoto (1979) p. 200
4. Schram B.L., Physica 32 (1966) 197
5. Nagy P., Skutlartz A., Schmidt V., J. Phys. B 13, (1980) 1249
6. Winter H., Varga P., Abstracts of Contr. Papers, XI. ICPEAC Kyoto (1979) p. 204

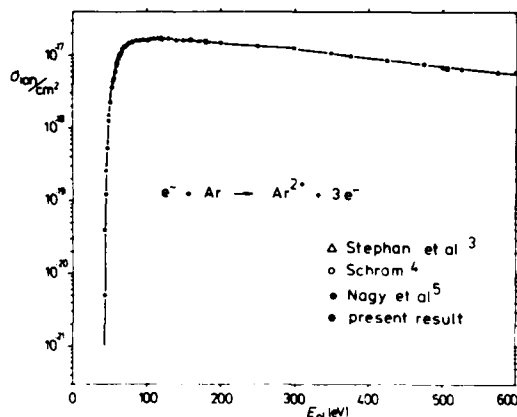


FIGURE 2 Cross section for double ionization of Ar by single electron impact

identification technique to measure metastables produced in a small electron beam ion source, where the ionizing electrons had an energetic halfwidth of less than 600meV and the electron impact energy E_{e1} could be varied between ionization threshold and 700 eV.

The total ionization cross section for Ar^{2+} given in Fig. 1 was obtained from the total Ar^{2+} current

CALCULATION OF HYDROGENIC FORMFACTORS

Siegfried Datzke* and John T. Broad**

* : Fakultät für Physik, Universität Bielefeld, F.R.G.

** : Fakultät für Chemie, Universität Bielefeld, F.R.G.

INTRODUCTION

Calculation of cross sections for processes such as inner shell ionization, multiphoton ionization, or simultaneous electron - photon excitation usually requires evaluation of matrixelements of the form :

$$f(q) = \langle f | \exp(iq \cdot r) | i \rangle \quad (1)$$

where $|i\rangle$, $|f\rangle$ are hydrogenic states with:

$$|i, f\rangle = C_{x, l} \cdot \exp(-xr) \cdot r^{-1} \cdot F_1(1 \pm i \cdot 2l \pm 2, 2xr) \cdot Y_{l, m}(\theta, \varphi) \quad (2),$$

with $x=1/n$ for bound states and $x=ik$ for free states. These integrals have been considered by many authors¹⁻³ using either parabolic or spherical coordinates; however their formulae are difficult to compute as they contain either infinite summations³ or differentiation with respect to some parameter¹. In a very recent paper, Belkić⁴ started from the integral representation of the final state to achieve a result in terms of a finite sum; yet he presents no numerical examples. We use a multipole expansion for the exponential. For each multipole order, the result is a polynomial. The total cross section for electron impact ionization is obtained by integrating the absolute square of Eq.(1) over the angles of the projectile and ejected electrons as well as over the energy distributed between them⁵:

$$\sigma_{\text{tot}} = \int_{-1}^{+1} d(\cos\theta) \int_0^{q_{\text{max}}} q^2 dq \int dQ(q) k_f/k_i |f(q)|^2 \quad (3)$$

DERIVATION OF THE FORMULAE

We start from the multipole expansion⁶. The angular integration can be performed easily⁶. The remaining radial integral is of the following form:

$$r_1 = \int_0^\infty dr r^2 \exp(-r/n_1) r^{1-1} F_1(1 \pm i \cdot n_1 \cdot 2l_1 \pm 2, 2r/n_1) \quad (4)$$

$$J_1(q) \exp(-ik_f r) r^{1-f} F_1(1 \pm i \cdot 1 \cdot 2l_f \pm 2, 2ik_f r)$$

From the definition of the Hankel functions⁷ we see that the Bessel function can be replaced by an exponential multiplied by a finite sum. Inserting this into (4), the integration can be easily carried out and gives :

$$f_r(q) = \sum_{l=0}^{\infty} i^{l+1} q^{1-l} \sum_{m=0}^{l+1/2, m} (1 \pm i/2, m) (\pm 2iq)^{-m} \Gamma(\alpha+1) \Delta^{-(\alpha+1)} \frac{a_1(\alpha)}{\Gamma(\alpha)} \frac{p}{b_1(\alpha)} \frac{z_1^p}{p!} {}_2F_1(\alpha+1, a_2, b_2, z_2) \quad (5)$$

with :

$$\begin{aligned} \alpha &= 1 \pm 1/n_1 \pm 1, p & \Delta &= 1/n_1 \pm ik \pm iq \\ a_1 &= 1 \pm 1/n_1 & b_1 &= 2l_1 \pm 2 \\ a_2 &= 1 \pm 1/n_1 \pm 1/k & b_2 &= 2l_f \pm 2 \\ z_1 &= 2/n_1 \Delta & z_f &= 2ik/\Delta \end{aligned}$$

For q smaller than .1, it is numerically propitious to expand the Bessel function in a power series⁸. Using this expansion, the integration is straightforward.

RESULTS

We will present converged triple differential cross sections for the ionization of the lowest few hydrogenic states. In addition, numerically integrated total cross sections will be given for impact energies high enough for the Born approximation to be valid.

¹ Tweed, R.J.: J.Phys. B 5; 820 (1972)

² Kocbach, L.: J. Phys. B9, 13; 2269 (1976)

³ Trautmann, D., Baur, G., Rosel, F.:

J. Phys. B 16; 3005 (1983)

⁴ Belkić, D.: J. Phys. B 17; 3529 (1984)

⁵ Bransden, B.H., Joachain, C.J.: Physics of Atoms and Molecules; New York: Longman; 1987

⁶ Messiah, A.: Quantum Mechanics Vol.2; North Holland Publishing Company; Amsterdam; 1981

⁷ Abramowitz, M., Stegun, I.A.: Handbook of Mathematical Functions; Dover Publications, Inc.; New York; 1970

⁸ Erdelyi, A.: Higher Transcendental Functions; Vol.1; New York: McGraw-Hill Book Company, Inc.; 1953

This work has been supported by the Deutsche Forschungsgemeinschaft (SFB 216).

IMPORTANCE OF HIGHER-ORDER EFFECTS IN LARGE-ANGLE COPLANAR SYMMETRIC (e,2e) PROCESSES

K.S. Baliyan and M.K. Srivastava

Department of Physics, University of Roorkee, Roorkee 247667, India

The triple differential cross sections (TDCS) measured in (e,2e) experiments provide the most sensitive probe for any model of single ionization by electron impact. In the case of coplanar asymmetric Ehrhardt-type geometry the crucial importance of second order effects, in accounting for all the main features of the TDCS measurements, is well known. In the coplanar symmetric kinematical arrangement with $\theta=45^\circ$, which is popular in (e,2e) spectroscopic studies, theories which are essentially first order in character lead to reasonable results. However, for large θ it has been recently shown by Byron et al¹ and Pochat et al² that the second-order Born term of the scattering amplitude becomes as important as and even more important than the first-order Born term.

The present paper is aimed at showing that not only the second-order effects but the contribution from still higher-order terms (n>2) are also quite important for large θ . The calculation of higher-order terms is extremely difficult. However, a workable procedure which has been used in the recent years with reasonable success is the modified Glauber (MG) approximation³. Here the

second-order term f_{G2} in the Glauber scattering amplitude f_G is replaced by the second-order Born term f_{B2} . The MG scattering amplitude is given by

$$f_{MG} = f_G + f_{B2} - f_{G2} \quad (1)$$

The authors⁴ have recently used this approximation to analyse the coplanar asymmetric data of Lohmann et al⁵ for the ionization of hydrogen. A significant enhancement in the size of the recoil peak over that predicted by the second-Born and eikonal-Born series approximations is observed particularly in situations where the momentum transfer K is not too small.

We shall consider TDCS for the ionization of

$$\text{atomic hydrogen:} \quad \frac{d^3\sigma}{d\Omega_a d\Omega_b dE_b} = \frac{k_a k_b}{k_0} |f_{MG}|^2 \quad (2)$$

The amplitude f_G in Eq.(1) is evaluated by following the method of Roy et al⁶. The amplitude f_{B2} at large θ is estimated by using the method of Byron et al¹. The procedure for evaluating f_{G2} is given in Ref. 4.

Figure 1 shows our MG results along with those obtained in the first Born (B1) and the second Born (B2) approximations at $E_0 = 500$ eV. The second-order Born contribution has been estimated throughout by using the large energy and large θ estimate given by Byron et al¹. The three results differ significantly from one another for $\theta > 90^\circ$. The dip in the B2 results at $\theta \sim 105^\circ$ depicts the interference cancellation between the first Born and the second Born amplitudes. The MG results clearly show the dominant contribution of the higher-order terms for large θ .

References

1. F.W.Byron Jr., C.J. Joachain and B. Piraux, J. Phys. B **16**, L769(1983).
2. A Pochat, R.J.Tweed, J. Peresse, C.J.Joachain, B. Piraux and F.W.Byron Jr., J. Phys. B **16**.
3. I.T.Iken, J. Phys. B **9**, 3203(1976).
4. K.S.Baliyan and M.K.Srivastava, to be published.
5. R.Lohmann, I.F.McCarthy, A.T. Stelbovics and E.Weipolt, Phys. Rev. A **30**, 758(1984).
6. A.L.Roy, A.K.Chak and N.Sil, Phys. Rev. A **23**, 1007(1981).

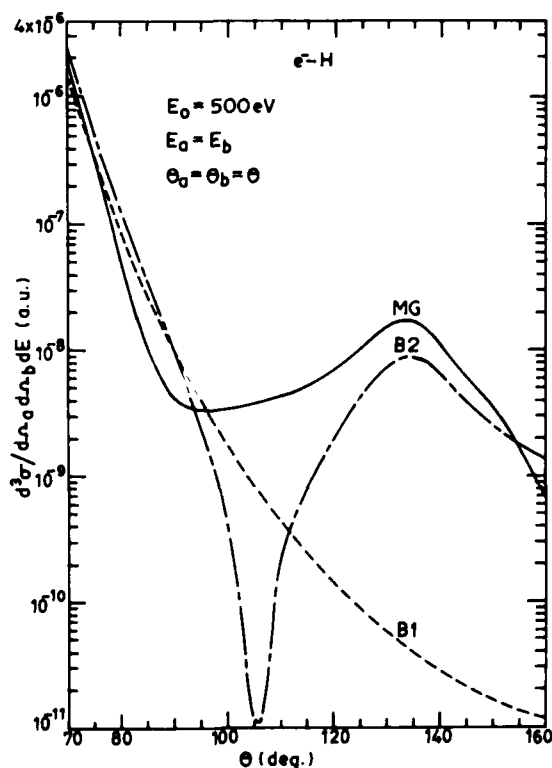


FIGURE 1

TRIPLY DIFFERENTIAL CROSS SECTIONS FOR THE $H(e,2e)H^+$ PROCESS

A.C. Roy*

School of Physical Sciences, The Flinders University of South Australia,
Bedford Park, South Australia 5042

In a previous communication¹, we reported an analytical expression for an approximate eikonal amplitude for electron-impact ionization of hydrogen. The purpose of this work is to calculate triply differential cross sections (TDCS) for the $H(e,2e)H^+$ process using that expression and to compare them with the results of other calculations and experiment. We have considered the case of coplanar asymmetric geometry, i.e. the energy of the ejected electron is small compared to the energy of the scattered electron. The direct amplitude for the present reaction has been calculated in the Glauber approximation (GA)² using the method of Roy *et al.*³ which reduces the five-dimensional Glauber amplitude for the $H(e,2e)H^+$ process to the two-dimensional form.

Table 1 shows the present Glauber results along with the first Born approximation (FBA) results

TABLE 1. Coplanar triply differential cross sections, $d^3\sigma/d\hat{k}_1 d\hat{k}_2 dE_2$, in atomic units for electron-impact ionization of atomic hydrogen for the incident energy $E = 250\text{eV}$, the ejected electron energy $E_2 = 10\text{eV}$ and the scattering angle $\theta_1 = 5^\circ$.

θ_2 (deg)	FBA ^a	GA ^b	GAE ^c	Experiment ^d
-10	0.73	0.49	0.48	
-30	2.19	1.74	1.70	
-50	3.66	3.12	3.07	2.44
-70	3.45	2.91	2.87	2.70
-90	1.83	1.42	1.40	2.38
-110	0.54	0.34	0.34	0.99
-130	0.094	0.042	0.041	
-150	0.094	0.12	0.12	
-170	0.20	0.28	0.27	
10	0.13	0.059	0.057	
30	0.078	0.091	0.091	
50	0.18	0.25	0.24	0.43
70	0.27	0.37	0.37	0.22
90	0.33	0.43	0.42	0.71
110	0.35	0.43	0.42	0.94
130	0.35	0.43	0.42	
150	0.35	0.43	0.42	
170	0.28	0.39	0.38	

^aPresent first Born approximation.^bPresent Glauber approximation.^cPresent Glauber approximation with exchange.^dReference 4.

and experiment⁴ at an incident energy $E = 250\text{eV}$, the ejected electron energy $E_2 = 10\text{eV}$ and the scattering angle $\theta_1 = 5^\circ$. The measurements are, however, relative and have been put on an absolute scale by normalizing the binary peak data at the angle of ejection $\theta_2 = 70^\circ$. $E = 250\text{eV}$, $E_2 = 10\text{eV}$ and $\theta_1 = 5^\circ$ to the second Born calculations of Byron, Joachain and Piraux⁵. An examination of the cross section values presented in Table 1 shows that the magnitudes of TDCS obtained in the GA seem to be better than the corresponding FBA values and are in reasonably good agreement with experiment. In addition, we find that the effect of exchange is not appreciable in the present case of asymmetric geometry.

The author would like to thank Professor Ian E. McCarthy for many useful discussions. Financial support for this work was provided by the Australian Research Grants Scheme.

References

- * Permanent address: Department of Physics, University of Kalyani, Kalyani 741235, West Bengal, India.
- 1. A.C. Roy and N.C. Sil, in *Abstracts of the XIII International Conference on the Physics of Electronic and Atomic Collisions, Berlin, 1983*, edited by J. Eichler, W. Fritsch, I.V. Hertel, N. Stolterfoht and U. Wille (ICPEAC, Berlin, 1983), p.164.
- 2. See, for example, E. Gerjuoy and B.K. Thomas, *Rep. Prog. Phys.* **37**, 1345 (1974).
- 3. A.C. Roy, A.K. Das and N.C. Sil, *Phys. Rev. A* **23**, 1662 (1981).
- 4. B. Lohmann, I.E. McCarthy, A.T. Stelbovics and E. Weigold, *Phys. Rev. A* **30**, 758 (1984).
- 5. See, Reference 4.

NEAR-THRESHOLD (e,2e) MEASUREMENTS IN THE
EQUATORIAL PLANE USING A NEW APPARATUS

T J Jones, S Cvejanović,* G C King, F H Read

Physics Department, Manchester University, Manchester M13 9PL, UK

*Institut za Fiziku, P O Box 57, 11001 Beograd, Yugoslavia

Many quantum mechanical treatments^{1,2,3,4} have followed in the wake of Wannier's⁵ incisive classical description of ionization events close to threshold. Their predictions vary with regard to the distributions in angle and energy of the scattered and ejected electrons. (e,2e) coincidence experiments, with their total determination of the reaction kinematics, provide a stringent test of these predictions. However, there have been only a limited number of experiments performed close to threshold.

Cvejanović and Read⁶ used a coincidence time-of-flight technique to measure the energy distribution and angular correlation functions of the two outgoing electrons. The energy distribution function was found to be uniform from 0.2 to 0.8 eV above threshold. The width of the angular correlation function, (although measured at only two angles), increased in a manner consistent with an $E^{1.4}$ dependence. This preliminary work was extended by Pichou et al⁷ who measured the energy and angular distributions close to threshold in a coplanar, non-coincidence experiment. Fournier-Lagarde et al⁸ have recently measured differential cross sections for the ionization of helium down to 1 eV above threshold using a coplanar geometry in an (e,2e) coincidence experiment. This work neatly complements the experiments of Ehrhardt et al⁹ and Schubert et al¹⁰ who had previously measured such cross sections down to a lower limit of 6 eV above threshold.

The differential cross section may be expressed as⁸

$$\frac{d\sigma}{d\Omega_1 d\Omega_2 dE_1} (E, E_1 \theta_1 \beta_1 \theta_2 \beta_2) =$$

$$(f_0^2 + f_1^2) \exp[-4 \ln 2 ((\theta_{12} - 180^\circ)/\theta_{12})^2] E^{0.127}$$

where f_0 and f_1 are the singlet and triplet scattering amplitudes respectively. θ_{12} is the width of the angular correlation function given by $\theta_{12} = 85^\circ (E(\text{eV}))^{1.4}$ and θ_{12} is the angle between the two electrons given by $\theta_{12} = \cos^{-1}(\cos\theta_1 \cos\theta_2 + \sin\theta_1 \sin\theta_2 \cos(\beta_1 - \beta_2))$.

When a non-coplanar scattering geometry is adopted with $\theta_1 = \theta_2 = 90^\circ$, then $\theta_{12} = \beta_1 - \beta_2$ and the singlet and triplet scattering amplitudes are constant. Under these circumstances, the differential cross section varies only with the relative azimuthal angle. This may be practically realised in an experiment where the two analysers rotate in the plane at 90° to the incident beam, which may be termed the equatorial plane.

A new (e,2e) coincidence apparatus has been designed for such experiments close to the threshold of

ionization. It is capable of performing coplanar or non-coplanar experiments with symmetric or asymmetric kinematics. Two coplanar analysers rotate on concentric circular tracks. The gun is carried on an arm along an arc in a perpendicular plane. The axis of rotation lies in the plane of the analysers. In a coplanar arrangement the analysers each have an angular range of $+145^\circ$ to -180° . For non-coplanar geometries, the analysers are interchangeable and the invariance of the coincidence signal may be checked. The analysers have a minimum separation angle of 37° , and may be moved back and forth under automatic control for normalisation purposes. The experiment also features a minicomputer system based on a DEC PDP 11/23 with IEEE 583 (CAMAC) and IEEE 488 (GPIB) interfaces. The computer is able not only to handle the data acquisition, but also to monitor various experimental parameters, such as the gas pressure and electron currents around the electron-optical system. Thus by having selected potentials under computer control, the spectrometer may be periodically retuned using optimization routines, and the long term stability improved. The system is interfaced in a manner that makes it possible to return the spectrometer to manual operation at any time.

The results to be presented will include measurements of differential cross sections in the equatorial plane for helium, giving information in the form of the dependence on θ_{12} and on the way in which θ_{12} varies with E .

References

1. A R P Rau, Phys Rev A **4**, 207 (1971)
2. A R P Rau, J Phys B:Atom Molec Phys **9**, L283 (1976)
3. R Klar, W Schlecht, J Phys B:Atom Molec Phys **9**, 1699 (1976)
4. A Temkin, J Phys B:Atom Molec Phys **7**, L450 (1974)
5. G R Wannier, Phys Rev **90**, 817 (1953)
6. S Cvejanović, F H Read, J Phys B:Atom Molec Phys **14**, 1841 (1974)
7. P Pichou, A Huetz, G Joyez, M Landau, J Phys B:Atom Molec Phys **11**, 3683 (1978)
8. P Fournier-Lagarde, J Mazeau, A Huetz, J Phys B:Atom Molec Phys **17**, L591 (1984)
9. H Ehrhardt, K H Hesselbacher, K Jung, K Willmann, J Phys B:Atom Molec Phys **5**, 1559 (1972)
10. E Schubert, K Jung, H Ehrhardt, J Phys B:Atom Molec Phys **14**, 3267 (1981)

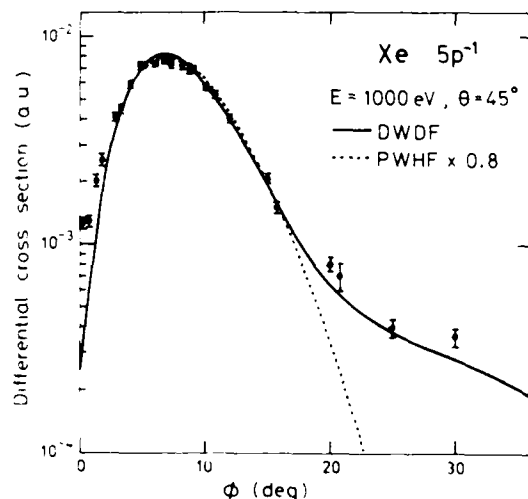
THE NONCOPLANAR SYMMETRIC (e,2e) REACTION ON THE VALENCE ORBITALS OF XENON

J.P.D. Cook*, I.E. McCarthy, J.D. Mitroy and E. Weigold

The Flinders University of South Australia, South Australia 5042, Australia
*Advanced Technology Laboratory, Bell Northern, Ottawa, Ontario, Canada

Accurate noncoplanar symmetric (e,2e) measurements have been made on xenon at $E = 1000\text{eV}$ and $\theta = 45^\circ$, and 1200eV and $\theta = 46^\circ$. Valence separation energy spectra have been obtained at 1200eV over the azimuthal angular range $\phi = 0^\circ - 30^\circ$. The $5s$ satellite structure was studied in detail as a function of the recoil momentum p from 0.3 to 1.5 a.u. The relative intensities of the different satellites remain constant within experimental error, confirming their assignment to the $5s^{-1}$ hole state. The pole strengths obtained at 1000eV and $\phi = 0^\circ$ ($p = 0.1$ a.u.) and $\phi = 8^\circ$ ($p = 0.6$) agree within experimental error with the 1200eV data. Table 1 compares the $\phi = 0^\circ$ data with a large CIHF calculation and a calculation by Hansen and Persson¹. The pole strength of the lowest state in the $5s^{-1}$ manifold is significantly overestimated in the many body calculations.

Figures 1 and 2 show noncoplanar symmetric angular correlations measured at 1000eV and $\theta = 45^\circ$ for $5p^{-1}$ and $5s^{-1}$ transitions compared with the plane- and distorted-wave impulse approximations using both DF and HF orbitals. Finite angular resolution has not been included in the calculations.

Fig. 1. The $5p^{-1}$ angular correlation.

The data have been normalized to the maximum in the DWIA $5p$ cross section using DF wave-function. The figures show that the DWIA gives an excellent description of the relative $5p:5s$ cross sections and of their shapes. The PWIA gives a good description of the

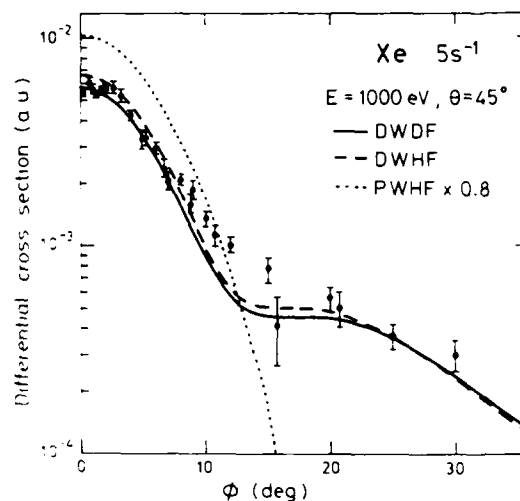


Fig. 2. The $5s$ angular correlation. shape at low momentum, where the cross section is large. It overestimates the $5s$ cross section, making no allowance for absorption in the electron waves.

TABLE 1

The normalized $5s^{-1}$ pole strengths for 1000eV and 45° .

E (eV)	Dominant Configuration of ion state	$\phi = 0^\circ$ $p = 0.1$ a.u.	Theory	
			Present	Ref. 1
23.4	$5s\ 5p^6\ ^2S$	0.36 ± 0.01	0.48	0.45
24.7	$5s^2\ 5p^4\ (^3P)\ 6s\ ^4P$	0.04	0.04	0.05
25.5	" $(^3P)\ 5d\ ^4P$	0.05	"	0.04
26.5	"	0.02	"	"
28.0	" $(^1P)\ 5d\ ^2P$	0.11	0.14	0.06
"	" $(^1S)\ 6s\ ^2S$	"	"	"
"	" $(^1D)\ 5d\ ^2S$	"	"	"
29.1	" $(^3P)\ 6d\ ^4P$	0.24	0.18	0.56
"	" $(^3P)\ 6d\ ^4P$	"	"	"
31.5	" $(^1P)\ 6d\ ^2P$	0.10	0.14	0.06
"	" $(^1P)\ 6d\ ^2S$	"	"	"
55.4		0.11	0.12	

Reference

1. I.E. Hansen and W. Persson, Phys. Rev. A 18, 1459 (1978).

POST COLLISION INTERACTION AND THE AUGER LINESHAPE

A. Russek* and W. Mehlhorn⁺

* Physics Department, The University of Connecticut, Storrs, Connecticut 06268 USA
⁺ Fakultät für Physik, Universität Freiburg, D-7800 Freiburg, FRG

The effect of a slowly receding photoelectron on the shape and location of an Auger line has been investigated for Auger transitions following photoionization of an inner shell electron. The theory of Niehaus and Morgenstern^{1,2} is reformulated and extended to take into account the time it takes for the fast Auger electron to overtake the slow electron.³ Because of this, much smaller shifts are found in the energies of the Auger peaks due to post collision interaction than those predicted by Niehaus.² The extended theory can easily be generalized to treat inner shell vacancies caused by electron impact ionization near threshold, in which case the effect on the Auger line is caused by two slowly receding electrons. Two assumptions are made in this approach:

1. The electron in the vicinity of an ion with an inner shell vacancy will not disturb the Auger process itself. At the "surface" of the ion, the Auger electron will be emitted with the same mean lifetime and Lorentzian distribution of kinetic energies with or without the presence of a nearby photoelectron. This assumption merely holds that the electric field produced by the outgoing photoelectron does not polarize the wavefunction of the residual ion sufficiently to alter the Auger process.
2. The observed energy distribution of the Auger electron differs from the emitted spectrum solely because the two outgoing electrons exchange some energy if the Auger electron passes the photoelectron. Essentially, when the fast Auger electron passes the slow photoelectron, the latter suddenly loses the electrostatic screening that the former had provided. The consequent decrease in energy of the photoelectron is compensated by an increase in energy of the Auger electron.⁴ This increase, denoted by S , is a function of the excess energy, E_1 , of the photoelectron, the energy of the Auger electron, E_A , and the time, t , that elapsed between the ejection of the photoelectron and the subsequent Auger process that fills the inner shell vacancy. In a classical picture of the Auger electron-photoelectron interaction (convenient, but not essential to the model), $S = 1/R_x$, where R_x is the radius at which the Auger electron overtakes the photoelectron. Writing $R_x = 1/S$ and denoting the time of overtaking by T_x , S is determined by equating the two alternative calculations of T_x :

$$T_x = \int_{R_1}^{1/S} \frac{dr}{v_1} = t + \int_{R_A}^{1/S} \frac{dr}{v_A}, \quad (1)$$

where $v_1(r)$ and $v_A(r)$ are the respective velocities of the photoelectron and the Auger electron:

$$v_1 = [2(E_1 + 1/r)]^{1/2} \quad (2a)$$

$$v_A = [2(E_A + 2/r)]^{1/2}, \quad (2b)$$

and R_1 and R_A are the shell radii from which the electrons originate. With S so determined, the Auger line shape is given by

$$P(E) = |a(E)|^2 \quad (3a)$$

with

$$a(E) = (\Gamma/2\pi)^{1/2} \int_0^\infty \exp(-U(t)) dt, \quad (3b)$$

$$U(t) = \int_0^t \left(\frac{\Gamma}{2} + i(E - S(t')) \right) dt'. \quad (3c)$$

It is possible to show that the distribution described by Eqs. (3) is normalized for any $S(t')$ and reduces exactly to the undistorted Lorentzian line shape when $S(t') = 0$. It is also possible to show that for all practical purposes, $S \rightarrow 0$ as $E_1 \rightarrow E_A$, and is equal to zero when $E_1 > E_A$. (Because the effective Z seen by each electron is different, S does not become identically equal to zero for all t until $E_1 > E_A + 2/R_A - 1/R_1$. However, the small range of t near $t = 0$ for which a nonzero S exists makes no significant contribution to $P(E)$.)

For the much studied $1S_0$ Auger transition in Ar at $E_A = 201$ eV, $\Gamma = 130$ meV, the shift in the Auger line when the excess energy $E_1 = 125$ eV is found to be only 4 meV, rather than the 21 meV reported by Niehaus.²

References

1. R. Morgenstern, A. Niehaus and U. Thielman, J. Phys. B **10**, 1039 (1977).
2. A. Niehaus, J. Phys. B **10**, 1845 (1977).
3. G. N. Ogurtsov, J. Phys. B **16**, L745 (1983).
4. F. H. Read, J. Phys. B **10**, L207 (1977); F. H. Read and J. Comer, Coherence and Correlation in Atomic Collisions (Edited by H. Kleinpoppen and J. F. Williams), p. 243, Plenum, N. Y..

POST-COLLISION INTERACTION (PCI) IN INNER-SHELL IONIZATION
OF ARGON K AND ARGON L AUGER SPECTRA

D. Gräf, and W. Hink

Physikalisches Institut der Universität, D-8700 Würzburg, W.-Germany

We study the PCI effect on Auger electrons following inner-shell electron impact ionization¹. Here we present measurements on the energy shift of the 2.66 keV Ar KLL(¹D₂) Auger line down to an excess energy of about 0.3% of the K-ionization threshold (3.2keV). Furthermore we report about a new experiment to evaluate the PCI shift on Ar L for high excess energy.

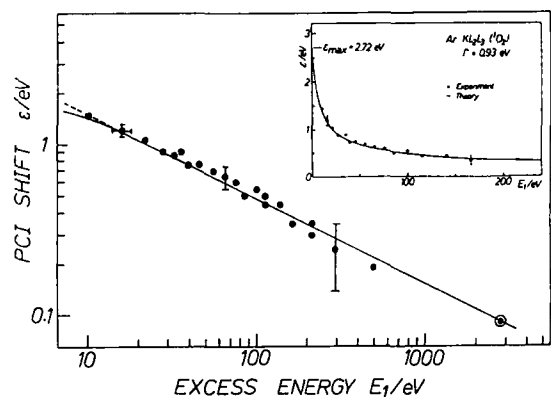


Fig. 1 PCI shift ϵ of Ar KLL(¹D₂) as function of E_1

The measured PCI shifts ϵ of the Ar KLL(¹D₂) Auger peak at various excess energies E_1 from 2.8keV down to 10eV are shown in Fig. 1. Calibration was done against the Ar LMM Auger lines. The full curve represents the theory² of strongly correlated electrons which approaches a straight line in the $\log \epsilon - \log E_1$ plot for $E_1 > 150$ eV (broken line: $\epsilon = \Gamma E_1^{-0.5}$ with $\Gamma(\text{Ar KLL}(\text{}^1\text{D}_2)) = 0.93 \text{ eV}$). The theoretical value at $E_1 = 2.8 \text{ keV}$ is added to all experimental data, a quantity small in comparison to the shifts ϵ in the small excess energy region. In this region the theory is in good agreement with the data.

For large excess energies theoretical predictions differ, depending on what kind of energy distribution is assumed for the scattered and emitted electron and how the motion of the outgoing electrons is included until the Auger electron overtakes one or both of them.

Several measurements done so far show consistent results in the low excess energy region but have rather large uncertainties relative to the PCI shift itself for high E_1 . This depends on the experimental procedure: In the case of Ar L₃ one measures the energy difference between the Ar L₃M₂₃M₂₃(¹D₂) Auger line in reference to Kr M₅N₂₃N₂₃(¹S₀). Both Auger lines have

comparable natural line width but different ionization energies. Assuming an universal function $\epsilon(\Gamma, E_1)$ for the energy shift independent of a particular inner-shell vacancy, the shifts on both Auger lines for high E_1 are almost the same. The resulting change in the energy difference Δ between the Ar L and Kr M Auger lines is therefore even less than the expected absolute shift of only some ten meV for high E_1 and is to be extracted as small difference between two nearly equal $\Delta \approx 152.18 \text{ eV}$!

In our experiment we measure the PCI shift of a diagram line in reference to a neighboured satellite line with an order of magnitude smaller Γ and $\Delta \approx 1 \text{ eV}$, thus reducing the experimental errors considerably. In Fig. 2 part of the Ar L₂₃M₂₃M₂₃ Auger spectrum is shown as an insert. The two satellite lines L₂₃M₂₃(³D₃)-M₂₃(²P) and (²D) are as predicted much narrower than the diagram lines. First results are shown in Fig. 2 (•, $\Delta E = \pm 5 \text{ meV}$) in comparison with other experiments (○ exp², □ exp³, all $\Delta E = \pm 20 \text{ meV}$, plotted relative to our data). As the experiment is still in progress we want to emphasize at this time the inherently higher accuracy of our experimental procedure and the consistency of our data, but we expect our procedure to allow for an improvement in testing theory.

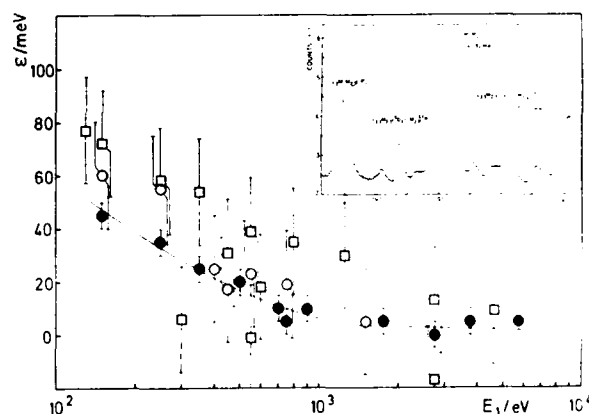


Fig. 2 PCI shift ϵ of Ar LMM as function of E_1

•: our result, ○: exp², □: exp³

References

1. D. Gräf, W. Hink, Abstr. of XI Int. Conf. (1984) 165
2. R. Huster, W. Mehlhorn, J. Phys. A 16 (1983) 67
3. E. Heidebrand et al., Phys. Rev. A 27 (1983) 21

PCI EFFECTS IN (e,e' Auger) AND (e,2e) CROSS SECTIONS: Ar 2p

G. Stefani, L. Avaldi

Istituto di Metodologie Avanzate Inorganiche del CNR
Area della Ricerca di Roma, C.P.10 00016 Monterotondo (Italy)

A. Lahmam-Bennani, A. Duguet

Laboratoire des Collisions Atomiques et Moléculaires (LA 281)
Université Paris-Sud, Bat. 351, 91405 Orsay Cedex (France)

Introduction. Inner shell ionisation and the following decay processes have been widely interpreted in terms of first Born two-step theories (B1S2). Experiments in which decay products were to be detected in coincidence with the scattered or the ejected electron have been proposed¹. They were thought to give detailed informations on the generalized alignment tensor of the ion. Coincidence experiments between scattered electron and Auger electron (e,e' Auger) were recently realised^{2,3,4}. Major findings have been the inadequacy of the two-step model at energies near the ionisation threshold. Energy shift of the Auger lines $L_3M_{2,3}M_{2,3}(1S_0)^5$ and $L_2M_{2,3}M_{2,3}(3P_{0,1,2})^6$ of Ar have been observed and ascribed to post collisional interactions (PCI). The present work will report on such an experiment on Ar and on the related (e,2e) experiments (scattered-ejected electron coincidences) which lead to the Ar $(2p^{-1})$ state parent of the studied Auger transition. Both (e,2e) and coincident Auger experiments have been performed with an incident energy of 8.2 KeV and upon identical kinematic conditions.

The (e,e' Auger) energy spectrum. The full LMM Auger spectrum has been measured in coincidence with scattered electrons at 1.5° scattering angle and for a selected energy loss of 7±6 eV above the ionisation threshold. It resulted consistently shifted by 0.15±0.07 eV toward higher energies with respect to the non coincident one which was measured contemporarely. This result is in agreement with the previous observations^{5,6}. The origin for this shift is attributed to PCI because no shift is observed in the coincident Auger spectrum measured at the same scattering angle and at energy losses well above threshold (about 60 eV). Further, the coincident spectrum evidences a satellite structure in the region from 204 to 205 eV which is present only in the spectrum taken at the lower energy loss. Clearly, none of the mentioned effect could be explained by two-step theories.

The (e,e' Auger) angular distribution. The coincident angular distribution of the $L_3M_{2,3}M_{2,3}(1S_0)$ transition has been measured in both halves of the scattering plane, for two fixed scattering angles (1.5° and 5.5°) and for two different energy losses (7±6 and 60±6 eV above the Ar 2p I.P.). The chosen kinematics ensure a negligible contribution of the indistinguishable direct (e,2e) cross-section. The present result is in disagreement with B1S2 predictions. Indeed, both the measured lobes of the

Auger distribution are not symmetric about the direction of the momentum transferred in the collision (K).

By increasing the selected energy loss (60 eV above threshold), though the energy resolution is not good enough to detect PCI energy shifts, disagreement between experiment at 1.5° scattering angle and B1S2 predictions is still found. By increasing the momentum transfer (5.5° scattering angle) even at 7 eV above threshold the agreement between B1S2 prediction and experiment is fairly good.

The (e,2e) angular distribution. To better investigate the Ar 2p decay, both Auger and ejected electrons should be measured in coincidence with the scattered electron. Coincidence experiments of this latter type are very difficult because of the very small cross-section. Nevertheless (e,e' Auger) angular correlations and (e,2e) experiments, whose final state is identical to the initial state of the Auger transition, should provide mutually complementary information on the ionization process.

The measured (e,2e) angular correlation shows a significant departure from symmetry around direction of K for the kinematic characterized by the lower values of energy loss and momentum transfer. For values of the momentum transfer which exceed 1 a.u. both lobes of the (e,2e) cross-section are fairly symmetric around the momentum transfer direction. It is worth noting that the (e,2e) cross-section for He, as measured at 1.5° scattering angle and 7eV ejected electron energy, does not show the asymmetry around K that was evident for the Ar2p ionization upon identical kinematic. Departure of the Ar (e,e' Auger) and (e,2e) angular correlations from symmetry around the K direction, could be ascribed to PCI. Further investigations along this line are under development.

Work partially supported by an Italy-France cooperative program.

- 1) E.G.Berezhko, N.M.Kabachnik & V.V.Sizov; J.Phys.B 11,1819 (1978)
- 2) E.C.Sewell & A.Crowe; J.Phys.B 15,L357 (1982)
- 3) M.Volkell & W.Sandner; XIII ICPEAC,(1983)Abstract of contributed papers p.142
- 4) A.Lahmam-Bennani, G.Stefani, A.Duguet; Lecture Notes in Chemistry 35,191 (1984)
- 5) W.Sandner & M.Volkell; J.Phys.B 17,L597 (1984)
- 6) E.C.Sewell & A.Crowe; J.Phys.B 17,L547 (1984)

THE SEMICLASSICAL APPROXIMATION FOR (e_2e) IMPULSIVE REACTIONS: MATHEMATICAL BACKGROUND

Yu.V. Popov

Institute of Nuclear Physics, Moscow State University, Moscow 119899, USSR

L. Avaldi, R. Camilloni, J. Stefani

I.M.A.I. CNR, Area della Ricerca di Roma, 00016, Monterotondo Scalo, Italy

The paper is devoted to the mathematical background of the plane wave semiclassical approximation (PWSC) proposed earlier for the explanation of some features in a triple differential cross section of an impulsive (e_2e) -experiment^{1,2}. The main idea of PWSC-model is to divide each potential

$$V_i = -e^2 z(z_i)/z_i \quad \text{and} \quad V_{12} = e^2/|\vec{r}_1 - \vec{r}_2|$$

by external and inner parts introducing the suitable cut off z_0 . For rather big energies of electrons one should expect the value z_0 to be close to a radius of the orbital ionized. Leaving the Coulomb tails of potentials in the free Hamiltonian H_0^C one can reduce the Schrodinger equation to the Faddeev set of equations for channel wave functions³. Successive iterations of these equations give us the following formal expression for a three body wave function:

$$\langle \vec{r}_1 \vec{r}_2 | \psi \rangle = \langle \vec{r}_1 \vec{r}_2 | \phi_0 \rangle + \langle \vec{r}_1 \vec{r}_2 | G_0^C(E) [1 + T^C(E) G_0^C(E)] t_{12}^C | \phi_0 \rangle$$

Here

$$T^C(E) = t_{12}^C + t_{12}^C G_0^C t_{12}^C + t_{12}^C G_0^C t_{12}^C G_0^C t_{12}^C + \dots$$

$$t_{12}^C = [V_1^{in} + V_2^{in}] + [V_1^{in} + V_2^{in}] G_0^C t_{12}^C$$

$$t_{12}^C = V_{12}^{in} + V_{12}^{in} G_0^C t_{12}^C$$

$$G_0^C(E) = (E - \hat{H}_{10} - \hat{H}_{20} - V_1^{out} - V_2^{out} - V_{12}^{out} + i0)^{-1}$$

$$(E - \hat{H}_{10} - \hat{H}_{20} - V_1 - V_2 - V_{12}^{out}) | \phi_0 \rangle = 0$$

If $e^2/E_i z_0 \ll 1$ and $\rho_i z_0 \gg 1$ ($E_{1,2}$ are energies of final electrons) then one suppose the model PWSC to be valid for $z_1, z_2 > z_0$

$$\langle \vec{r}_1 \vec{r}_2 | \psi \rangle \approx \int \frac{d^3 \vec{p}_1}{(2\pi)^3} \int \frac{d^3 \vec{p}_2}{(2\pi)^3} \langle \vec{r}_1 \vec{r}_2 | G_0^C(E) | \vec{p}_1 \vec{p}_2 \rangle \langle \vec{p}_1 \vec{p}_2 | t_{12}^C | \phi_0 \vec{p}_0 \rangle$$

The kernel $\langle \vec{r}_1 \vec{r}_2 | G_0^C(E) | \vec{p}_1 \vec{p}_2 \rangle$ can be estimated by means of semiclassical considerations⁴ or in terms of geometrical optics⁵:

$$\langle \vec{r}_1 \vec{r}_2 | \psi \rangle_{z_i \rightarrow \infty} \approx A \exp[i\sqrt{E} \chi] / \rho^{5/2} \quad (1)$$

The eikonal χ in (1) has the right Coulomb asymptotics, and an amplitude A should be calculated along the classical paths of electrons in the external Coulomb field and produces the cross section

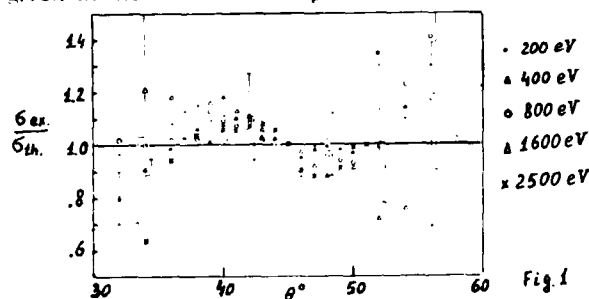
$$\frac{d^3 \sigma(\theta_1, \theta_2)}{dE d\Omega_1 d\Omega_2} = C \left[\frac{d^3 \sigma(\theta_1, \theta_2, \theta_2 - \Delta\theta_2)}{dE d\Omega_1 d\Omega_2} \right]_{PWIA}$$

$$\text{Here } C = 4\zeta/(1+\zeta)^2; \quad \zeta = 1 + \frac{2e^2}{E z_0} [2(z_0) - 1/4 \sin \zeta]$$

and the values of angle shifts $\Delta\theta_i$ are given in²:

$$\Delta\theta_i = \frac{e^2}{4E_i z_0} \frac{\rho_i \cot \zeta [|\vec{p}_1 - \vec{p}_2| + 2\rho_i \sin \zeta]}{|\vec{p}_1 - \vec{p}_2| [|\vec{p}_1 - \vec{p}_2| + (\rho_1 + \rho_2) \sin \zeta]}; \quad \zeta = \frac{1}{2}(\theta_1 + \theta_2)$$

The ratio $\sigma_{\text{exp}}/\sigma_{\text{theor}}$ for a big mass of He^{1s} data is presented on Fig. 1 σ_{exp} is given in the absolute scale.



References

1. Yu.V. Popov, J.J. Benayoun, J. Phys. B14 (1981).
2. Yu.V. Popov, V.F. Erokhin, Phys. Lett. A97, 4673, (1983) 280.
3. S.P. Merkuriev, Preprint FUB/HEP, 2/80, Inst. Theor. Phys., W. Berlin.
4. W.H. Miller, Adv. Chem. Phys., 25 (1974) 69.
5. L. Avaldi, R. Camilloni, Yu.V. Popov, J. Stefani, to be published.

STUDIES ON ASYMMETRY FOR ELASTIC SCATTERING OF SPIN-POLARISED ELECTRONS BY SPIN-POLARISED HYDROGEN ATOMS

N.S. Rao

Physical Research Laboratory, Theoretical Physics Area, Navrangpura, Ahmedabad 380 009, India

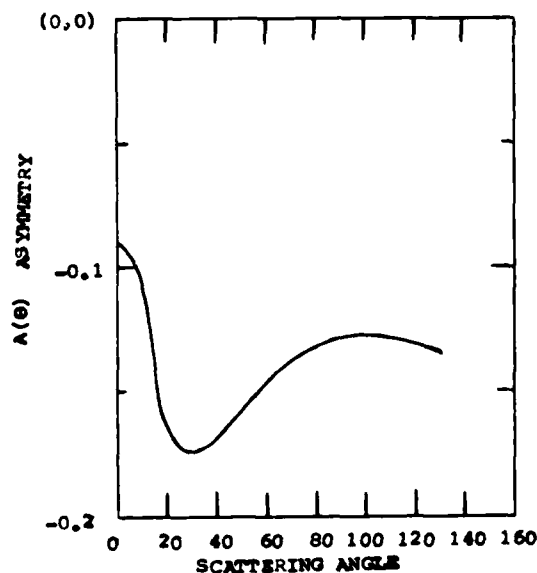
In recent years theorists¹ as well as experimentalists² have shown interest to study the angular distribution of asymmetry in scattering of spin-polarised electrons by spin-polarised hydrogen atoms at intermediate incident energy region. Few of the applied theoretical models¹ shows considerable deviations in the asymmetry $A(\Theta)$ results especially at small angles. A good comparison of the angular asymmetry is not only important in theoretical and experimental points of view but also useful to trace out better theories and experiments in the study of "Atomic Physics". Motivated to this and the encouragement of Born, Glauber eikonal series approximations^{3,4} gave me scope to improve the Born exchange results¹ to study the spin exchange effects for 1s-1s transition of electron-hydrogen interaction. Towards this improvement, second Born exchange amplitude is derived by incorporating Ochkur⁶ approximations in Born approximation. The asymmetry $A(\Theta)$ can be defined as

$$A(\Theta) = \frac{\sigma(\uparrow\downarrow) - \sigma(\uparrow\uparrow)}{\sigma(\uparrow\downarrow) + \sigma(\uparrow\uparrow)} \quad (1)$$

$A(\Theta)$ is calculated at incident energy $E \leq 300$ eV. The second Born exchange amplitude is obtained in the closed form for other elastic process⁵. The present asymmetries are found to be in good agreement with the compared theoretical¹ and experimental² results. Present results at $E = 100$ eV are shown in figure 1. As shown in the figure 1, the shape of the present curve is nearer to the shape of adiabatic and optical model curves¹ and better than the earlier Born results¹.

Finally I conclude that the present procedure is simpler and better than the earlier¹ Born exchange and static exchange results.

N.S.R. is thankful to Physical Research Laboratory, Ahmedabad, India, for the award of a Post-Doctoral Fellowship.

FIG -1 $E=100$ eV.

References

1. M.R.C. McDowell et al., J. Phys. B: **17**, 3951 (1984).
2. G.D. Fletcher et al., Phys. Rev. Lett. **48**, 1671 (1982).
3. N.S. Rao and H.S. Desai, Curr. Sci. **53**, 1271 (1984).
4. N.S. Rao and H.S. Desai, Ind. J. of Pure and Appl. Phys. **21**, 159 (1983).
5. N.S. Rao and H.S. Desai, Ind. J. of Pure and Appl. Phys. (communicated) (1984).
6. V.I. Ochkur, Zh. Eksp. Teor. Fiz. **45**, 734 (1963).

ASYMMETRY IN INELASTIC SCATTERING OF SPIN POLARISED ELECTRON WITH
SPIN POLARISED HYDROGEN ATOM

Mini Kapoor, S. Saxena and K.C. Mathur

Department of Physics, University of Roorkee, Roorkee 247667, India

The asymmetry parameter A in the scattering of spin polarised electron with spin polarised target depends mainly on the exchange contribution to the scattering process. Its measurement therefore provides a sensitive test to the various theoretical methods of obtaining the exchange scattering amplitude.

We report here the angular distribution of the asymmetry for the $1s \rightarrow 2s$ transition in the scattering of spin polarised electrons with spin polarised hydrogen atom using a two potential localised exchange approach.

The asymmetry parameter A is defined as

$$A = \frac{\sigma(\uparrow\downarrow) - \sigma(\uparrow\uparrow)}{\sigma(\uparrow\downarrow) + \sigma(\uparrow\uparrow)}$$

where $\sigma(\uparrow\downarrow)$ and $\sigma(\uparrow\uparrow)$ are the differential cross sections for spin antiparallel and spin parallel scattering respectively.

To obtain these cross-sections, we use a two potential approach.

The T matrix (including exchange) in the two potential approach for electron hydrogen inelastic scattering is given (to the first order) by

$$T_{\pm} = T_D \pm T_E$$

with

$$T_D = \langle \chi_f(\vec{r}_2) v_f(\vec{r}_1) | W | \chi_i(\vec{r}_2) v_i(\vec{r}_1) \rangle$$

$$\text{and } T_E = \langle \chi_f(\vec{r}_2) v_f(\vec{r}_1) | W | \chi_i(\vec{r}_1) v_i(\vec{r}_2) \rangle$$

The interaction potential $V = U + W$.

The distorted waves χ_n are the solutions of equation

$$H_0 + U_n \chi_n = E \chi_n$$

For the distorting potential U_n we take the static plus polarisation potential in the respective channel. To evaluate the exchange amplitude we use the local approximation, and also the Ochkur-Bonham approximation.

The results for 54.4 eV energy are presented along with the recent calculations of McDowell et al.¹. Good agreement is noted between the present two potential localised exchange approximation calculation and the ten state close coupling local exchange calculation.

Reference

1. M.R.C. McDowell, P.W. Edmonds, R.M. Potvliege, C.J. Joachain, R. Shingal and B.H. Bransden, J. Phys. B17, 3951 (1984).
2. P.W. Edmonds, M.R.C. McDowell, and J. Vande Ree, J. Phys. B16 L453 (1983).

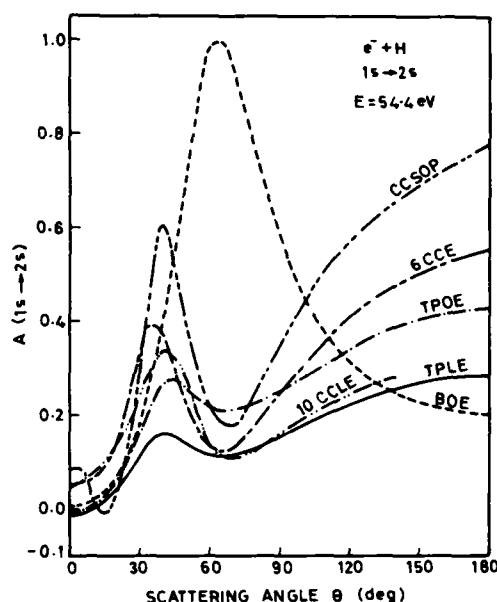


FIG. 1

Figure 1: Asymmetry A in the $1s \rightarrow 2s$ excitation of spin polarised hydrogen atom by spin polarised electron of 54.4 eV energy. — Present calculation using local exchange (curve TPLE); — Present calculation using Ochkur-Bonham exchange (curve TPOE); — Calculation in the Born-approximation with Ochkur-Bonham exchange (curve BOE); — ten-state close coupling calculation with local exchange of McDowell et al (1984) (curve 10 CCLE); — Six-state close coupling with exchange calculation of Edmonds et al² (1983) (curve 6 CCE); — Three state close coupling calculation with second order optical potential of McDowell et al (1984) (curve CCSOP).

THE THREE-BODY INTERACTION WITH LONG-RANGE FORCES: SPIN-DEPENDENT
ELECTRON HYDROGEN COLLISIONS

A. Vasilakis, M.S. Lubell, K. Rubin, and F.C. Tang
Department of Physics, City College of CUNY, New York, NY 10031, USA

J. Slevin
Department of Physics, University of Stirling, Stirling FK94LA, Scotland

M. Eminyan
Universite Paris 7, 75221 Paris, France

In order to investigate the properties of the three-body interaction with long range forces, we have developed an experimental program to study collisions between electrons and hydrogen atoms. It is well known that the three body problem cannot be solved exactly, and in the case of electron-hydrogen scattering a further complication is introduced by the symmetry properties that must be satisfied for a system containing two identical fermions. Unlike its nuclear analog, proton-deuteron scattering, the electron-hydrogen problem must contend with the infinite number of bound states that are supported by the Coulomb potential. Experience¹⁻³ has shown that extensive, detailed measurements are thus required to assist the development of reliable, predictive calculational techniques.

Our experiment utilizes spin-polarized beams to tag the electrons, thereby permitting scattering amplitudes to be probed in a more fundamental manner than is ordinarily possible. Our polarized electron source is based upon photoemission from GaAs⁵ and produces currents up to approximately 0.6 μ A with the use of 0.35 mW of power from a GaAlAs diode laser operating at 787 nm. Based upon the maximum laser power of 1 mW at our disposal we anticipate maximum source currents of at least 1.5 μ A. Although we have not yet measured the polarization of the electrons, prior experience⁵ suggests a value of approximately 0.4. (We will measure the polarization in the near future by means of Mott scattering.)

In order to allow us to observe narrow energy structures in our experiment, we have incorporated a hemispherical electron monochromator with an ultimate designed full-width-half-maximum energy resolution of 30 meV. For observation of the scattered electrons we have constructed a matched hemispherical energy-loss spectrometer which is adjustable over a range of 20° to 105° in scattering angle. We have also included in our apparatus a proton detector for ionization measurements and a Lyman-alpha detector for 2P excitation, the latter to be carried out as an electron-photon coincidence experiment.

Our polarized hydrogen beam utilizes rf dissociation⁶ and high-field state selection in a hexapole

magnet.⁷ Since we do not effect any hyperfine state selection, our low-field electronic polarization in the interaction region of the experiment is 0.5. The hydrogen beam line contains a Stern-Gerlach device and a quadrupole mass analyzer for polarimetry and dissociation measurements.

In carrying out our experimental measurements we determine the cross-section asymmetry for incident and target electron spins antiparallel and parallel. At the present time we have begun data taking in the ionization threshold region. We will report on these measurements as well as other ionization measurements.

Research supported by U.S. NSF, U.K. SERC, and NATO.

References

1. G.D. Fletcher *et al.*, Phys. Rev. Lett. **48**, 1671 (1982).
2. T.J. Gay *et al.*, Phys. Rev. A **26**, 3664 (1982).
3. G.D. Fletcher *et al.*, Phys. Rev. A (April, 1984, in press).
4. J. Slevin *et al.*, Phys. Rev. A **26**, 1344 (1982).
5. D.T. Pierre *et al.*, Rev. Sci. Instrum. **51**, 478 (1980).
6. J. Slevin and W. Stirling, Rev. Sci. Instrum. **52**, 1970 (1981).
7. V.W. Hughes *et al.*, Phys. Rev. A **5**, 195 (1972).

SPIN-DEPENDENT ELECTRON SCATTERING PHASE SHIFTS IN ATOMIC HYDROGEN

J F Williams

Department of Physics, University of Western Australia, Nedlands, WA, 6009

Differential elastic cross sections for atomic hydrogen have been measured for the scattering of electrons of energies from 9.300 to 10.300 eV over the angular range 10° to 150° with good (3 to 8 meV) energy resolution. Resonance structures associated with the $(2s^2)^1S$ (9.557 eV), $2s2p^3P$ (9.735 eV), $(2p^2)^1D$ (10.129 eV) and possibly the $(2s2p)^1P$ (10.170 eV) have been observed.

The effect of a resonance of width Γ on the differential cross section, $I(E, \theta)$ as a function of energy E is given by

$$I(E, \theta) = I_a(E, \theta) + \frac{(\varepsilon + q)^2}{(1 + \varepsilon^2)} I_b(E, \theta)$$

where $I_a(E, \theta)$ is the cross section at the resonance minimum, $I_b(E, \theta)$ is the amplitude of the resonance cross section. The total phase δ_{kr} is equal to the background phase δ_{kb} plus the resonant phase δ_{kr} where $\delta_{kr} = \cot^{-1}(-\varepsilon)$ and $\varepsilon = (E - E_r)/0.5\Gamma$. Since the resonance occurs in only one partial wave and δ_{kr} varies by π rad. over the width Γ , a measurement of the resonance profile at various scattering angles enables phase shifts to be determined. Absolute scattering cross sections are then calculated.

This method is rigorous for resonances occurring below the first inelastic channel. Since resonances occur in both the singlet and triplet partial waves, which are non-coherent, the analysis permits the determination of both the singlet and triplet phases; that is spin-dependent data has been obtained without the use of either source or detector of electron spin polarization. The following table compares the measured phases with the expected best theoretical values for $k = 0.800$ a.u. ($E = 8.7$ eV).

ℓ	Singlet		Triplet	
	Expt.	Theory	Expt.	Theory
0	0.911	0.886	1.630	1.643
1	0.002	-0.004	0.468	0.428
2	0.071	0.073	0.059	0.068

The theoretical values are obtained from variational calculations by Schwartz for $\ell=0$, by Armstead for $\ell=1$ and by Gailitis for $\ell=2$.

The measured values of the energy and widths of the two lowest resonant states are consistent within experimental accuracy with previous data by McGowan et al (1965)¹ and Williams (1975)². The present work has better precision for all measured resonances and for subsequent determination of the background phases.

1. J.W. McGowan, E.M. Clarke and E.C. Curley, Phys. Rev. Lett **15**, 917 (1965)
2. J.F. Williams in "Electron and Photon Interactions with Atoms" (ed. H. Kleinpoppen and M.R.C. McDowell, Plenum Press) 309 (1976)

MEASUREMENT OF SPIN POLARIZED ELASTIC AND INELASTIC DIFFERENTIAL SCATTERING OF ELECTRONS FROM LITHIUM ATOMS

G. Baum, M. M. M. W. Raith, W. Schroder¹, and H. Sillman
 Fakultät für Physik, Universität Bielefeld, Fed. Rep. of Germany

The spin asymmetry A is defined as $A = (I_{\uparrow} - I_{\downarrow}) / (I_{\uparrow} + I_{\downarrow})$, where I_{\uparrow} and I_{\downarrow} refer to the differential cross sections for antiparallel and parallel electron and atomic valence electron polarization, respectively. Measured is the spin asymmetry A_{2s-2p} for $2s \rightarrow 2p$ transitions, where P_e is the electron polarization and P_a the atomic polarization. In a crossed beam experiment a polarized electron beam from a GaAs cathode is scattered from a lithium atomic beam, selected by high field state selection in a Pauli trap. The electrons scattered through the angle θ are energy analyzed in a 180° spherical spectrometer with 0.3 eV resolution. During data taking the atomic polarization is frequently reversed by a spin flipper¹. P_a is measured and monitored by means of an analyzing sextupole magnet. The electron polarization can be reversed by reversing the sense of circularity of the light from the Kr^+ laser. P_e (≈ 0.3) is measured and monitored by means of 100 keV Mott scattering.

For the first measurements a scattering angle of $\theta = 107.5^\circ$ was selected and we measured A from 1.5 eV to 11 eV for elastic scattering and from 3 eV to 10 eV for the excitation of the 2p state. The values of A show for the elastic case predominantly singlet scattering in the range from 2 to 4 eV and predominantly triplet scattering above 4 eV. The comparison with theoretical calculations shows good agreement with n state² as well as with n state³ close coupling results. Modified polarized orbital calculations⁴ disagree considerably with the data. Our results for the excitation of the 2p state are shown in fig. 1 together with close coupling calculations^{5,6} and a data point from a DWBA calculation⁷.

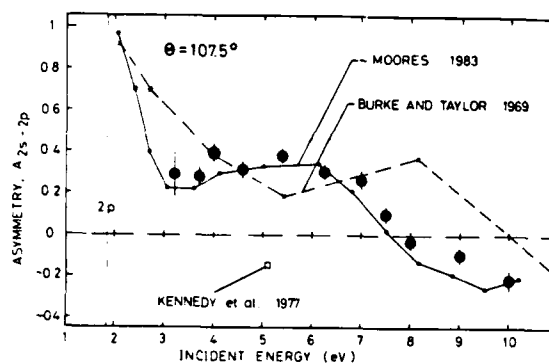


FIGURE 1 Spin asymmetry for the $2s \rightarrow 2p$ electron-lithium scattering at $\theta = 107.5^\circ$ scattering angle

REFERENCES

1. W. Schroder and G. Baum, J. Phys. E: Sci. Instrum. **16**, (1983) 52.
2. D.L. Moeres (1983) private communication.
3. P.G. Burke and A.J. Taylor, J. Phys. **B2** (1969) 869.
4. A.K. Bhatia, A. Temkin, A. Silver, and E.C. Sullivan, Phys. Rev. A **18** (1978) 1995.
5. J.V. Kennedy, V.P. Myerscough and M.P.C. McDowell, J. Phys. **B10** (1977) 2759.

¹ Present address: 11100 Station Technisch Werkel
 D-7400 Freiburg, Fed. Rep. Germany

SPIN DEPENDENCE IN ELECTRON COLLISIONS WITH SODIUM

P.J.O. Teubner, J.L. Riley and M.J. Brunger

Institute for Atomic Studies, The Flinders University of South Australia,
Bedford Park, South Australia 5042, Australia

The excitation of the 3^2P state in sodium has been studied in a series of electron photon coincidence experiments at energies of 12.1eV, 22.1eV, 54.4eV and 100eV. The polarisation of the photons emitted both normal to and in the scattering plane has been analysed before the photons are detected in coincidence with the electrons which excited the state.

For radiation emitted normal to the scattering plane, three components P_1, P_2 and P_3 of the Stokes vector can be defined. P_1 and P_2 represent the linear components of the polarisation and P_3 the circular component. The total polarisation $|P|$ is given by

$$|P| = [P_1^2 + P_2^2 + P_3^2]^{1/2}$$

It has been shown that the condition $|P| = 1$ implies coherence of the excitation process¹ and the decay of the state. In the case of the 3^2P state of sodium the significant fine and hyperfine structure results in depolarisation of the decay radiation. Thus $|P| \neq 1$ in this case which has confirmed our measurements. The influence of the FS and HFS can be accounted for by invoking the Percival-Seaton hypothesis² and by factorising out the terms arising from the structure of the excited state. This yields the reduced polarisation³, $|\bar{P}|$, which is a measure of the polarisation which would have arisen immediately after the collision and before the excited state relaxes into its HFS levels. Thus for this state in sodium the condition for coherence is $|\bar{P}| = 1$.

In the excitation of doublet states, it can be shown that $|\bar{P}| = 1$ applies only if exchange scattering processes can be ignored³. Therefore the measurement of $|\bar{P}|$ can provide information on spin dependent processes in this case even if unpolarised electrons are used to excite the state.

A series of measurements has been carried out at forward angles at the above energies and it is found that $|\bar{P}| = 1$ in each case. Thus we conclude that exchange scattering can be ignored for the electron impact excitation of the 3^2P state at forward angles at these energies.

For radiation emitted in the scattering plane, a linear component of the Stokes vector P_4 can be defined. In this case P_4 is given by

$$P_4 = \frac{I_{11} - I_{\perp}}{I_{11} + I_{\perp}}$$

the other linear component, P_5 , and the circular component, P_6 , are zero if unpolarised electrons are used⁴.

The in plane component P_4 can be combined with the out of plane component P_1 to derive the spin flip cross section which is defined in the natural coordinate frame of Hermann and Hertel⁵. Measurements of P_4 for electrons scattered through 5° at incident energies of 22.1eV, 54.4eV and 100eV show that the spin flip cross section is zero. These results are consistent with those obtained from the reduced polarisation measurements.

References

1. M.C. Standage and H. Kleinpoppen, Phys.Rev.Lett **36**, 577 (1976).
2. N. Andersen, T. Andersen, J. Ostgaard Olsen and E. Horsdal Pedersen, J.Phys.B **13**, 2421 (1980).
3. H.W. Hermann and I.V. Hertel, Comments At.Mol.Phys **12**, 61 (1982).
4. K. Bartschat and K. Blum, Z.Phys.A **304**, 85 (1982).

SCATTERING PARAMETERS FROM ELECTRON-POLARISED PHOTON COINCIDENCE EXPERIMENTS IN SODIUM

J.L. Riley and P.J.O. Teubner

School of Physical Sciences, The Flinders University of South Australia
Bedford Park, South Australia 5042, Australia

An electron-photon coincidence technique has been used to measure three components of the polarisation of the photons emitted in the decay of the 3^2P state in sodium at various incident energies. The polarisation state of the photon was determined before being detected in delayed coincidence with the inelastically scattered electron. An analysis using the reduced degree of polarisation, \overline{P} , shows that this excitation is coherent at each incident energy tested and hence a measurement of the components P_1, P_2 and P_3 normal to the scattering plane provides all of the information about the collision.

From these measurements both the parameters λ and also the absolute value of χ can be determined. More useful information can however be gained about the collision if the data is represented in the natural coordinate frame of Hermann and Hertel³. In this representation the quantisation axis is chosen to be parallel to the direction of the emitted photon, that is normal to the scattering plane. This choice of coordinate frame offers greater physical insight into the dynamics of the collision as well as minimising the unnecessary accumulation of experimental uncertainties.

The relationships between the density matrix elements in the natural frame and the polarisation components for the 3^2P state in sodium are:

$$P_1 = -0.2819 \operatorname{Re} \rho_{-11}^{\text{nat}}$$

$$P_2 = -0.2819 \operatorname{Im} \rho_{-11}^{\text{nat}}$$

$$P_3 = -0.5574 (\rho_{11}^{\text{nat}} - \rho_{-1-1}^{\text{nat}})$$

The matrix element ρ_{00}^{nat} has been shown to equal zero over the kinematic region tested. The density matrix elements ρ_{mn}^{nat} are therefore completely determined by a measurement of the three polarisation components P_1, P_2 and P_3 .

Data will be presented at incident energies of 54.4eV, 22.1eV and 12.1eV for scattering angles $\leq 15^\circ$. The data is represented in terms of both the natural coordinate frame density matrix elements and also the more commonly used scattering parameters λ and χ . In this case the errors accumulated in the natural frame are significantly less than those in the collision frame. Thus a more meaningful comparison can be made with available theories.

The data is compared to the predictions of a Born approximation, a distorted wave polarised orbital approximation⁵, a 2-state close coupling approximation⁶ and a 4-state close coupling approximation⁷. The data at 22.1eV and 12.1eV will also be compared to that obtained by Hermann et al⁸ from the laser excited atom experiments. These experiments are the time reverse of the present experiments and so should provide the same information about the dynamics of the collision.

References

1. P.J.O. Teubner, J.L. Riley, J.E. Furst and S.J. Buckman, J.Phys.B in press.
2. J.L. Riley, P.J.O. Teubner and M.J. Brunger, Phys.Rev.A **31**, Feb. (1985).
3. H.W. Hermann and I.V. Hertel, Comments At.Mol.Phys. **12**, 61 (1982)
Comments At.Mol.Phys. **12**, 127 (1982).
4. P.J.O. Teubner, J.L. Riley and M.J. Brunger, J.Phys.B to be published.
5. J.V. Kennedy, V.P. Myerscough and M.R.C. McDowell, J.Phys.B **11**, 3739 (1978).
6. D.L. Moores, Private Communication.
7. I.E. McCarthy, J.D. Mitroy and A.T. Stelbovics, J.Phys.B in press.
8. H.W. Hermann, I.V. Hertel, W. Reiland, A. Stamatovic and W. Stoll, J.Phys.B **10**, 251 (1977).

ELECTRON-ATOM COLLISION STUDIES USING OPTICALLY STATE SELECTED
BEAMS: SUPERELASTIC SCATTERING*

J. J. McClelland, M. H. Kelley, and R. J. Celotta

Radiation Physics Division
National Bureau of Standards
Gaithersburg, MD 20899

As part of an experimental program¹ to study spin dependent effects^{2,3} in low energy collisions between electrons and atoms, we have measured angle resolved spin asymmetries for superelastic scattering from the Na $3P_{3/2}$ state.

The apparatus consists of crossed beams of spin polarized electrons and spin polarized atoms with an energy selective detector for electrons scattered through some angle. A negative electron affinity GaAs photocathode, illuminated with circularly polarized light, is used as the source of spin polarized electrons. At the interaction volume, the electron beam has a diameter of 2mm with a divergence of $\pm 2^\circ$ and can be varied in energy from 2 to 40eV with a typical energy resolution of less than 150meV and a typical current of 1 μ A. The atomic sodium beam, collimated to ± 10 mrad from an effusive source, has a diameter of 5mm and a density of 10^9 - 10^{10} cm⁻³. The atoms are prepared by laser optical pumping via the $3S_{1/2}(F=2)$ to $3P_{3/2}(F=3)$ transition. By locating the optical pumping upstream from the interaction volume, one produces ground state atoms with a net electron spin polarization of 0.609 ± 0.018 .⁴ With the laser illuminating the interaction volume, one has additionally a large population of excited atoms in an oriented $3P_{3/2}$ state with spin polarization near unity. Collision studies of either ground state or first excited state targets are therefore possible.

The electron detector is a channel electron multiplier with retarding field analysis of the scattered electron's energy to distinguish between inelastically, elastically, and superelastically scattered electrons. The detector can be rotated through the angular range -100° to $+160^\circ$ and has an angular resolution of about $\pm 2^\circ$. The apparatus is thus capable of very general studies of spin dependent differential scattering cross sections for elastic, inelastic, and superelastic collisions.

Our measurements to date have focused on spin dependent effects in superelastic scattering of electrons from excited $3P_{3/2}$ sodium atoms in the angular range 10° - 30° at incident energies of 5 to 20eV.

*Work supported in part by U.S. Department of Energy, Office of Basic Energy Sciences, Division of Chemical Science.

References

1. M. H. Kelley, W. T. Rogers, R. J. Celotta, and S. R. Mielczarek, Phys. Rev. Lett. **51**, 2191 (1983).
2. J. Kessler, "Polarized Electrons", Springer-Verlag, (1976).
3. G. F. Hanne, Phys. Reports, **95**, 95 (1983).
4. J. J. McClelland and M. H. Kelley, these proceedings.

SPIN POLARIZATION AND ANGULAR DISTRIBUTION OF MNN AUGER ELECTRONS FROM KRYPTON AND XENON

U. Hahn, J. Semke, J. Kessler, H. Merz

Physikalisches Institut der WWU Münster, Domagkstr. 75, D-4400 Münster

Auger emission can often be described in a "two-step-model": in the first step the atom is ionized in an inner shell; in the second step the excited ion decays emitting the Auger electron.

The angular distribution of the Auger electrons will be anisotropic if an "alignment" is induced in the collision step /1/.

In the case of unpolarized projectiles and targets symmetry requires the spin polarization to be normal to the reaction plane spanned by the incoming projectile and the outgoing Auger electron. According to the two step model the initial hole must be aligned to transfer the direction of the projectile in the emission process:

$$\hat{P}(\cdot) = \hat{n} \left(\sum_{k=2,4} A_{k0} P_k^1(\cdot) \right) / \left(1 + \sum_{k=2,4} A_{k0} P_k(\cdot) \right) \quad (1)$$

$k = 2J$; J : angular momentum of the initial hole

A_{k0} : alignment tensor component

A_k : anisotropy parameter

The polarization parameters A_k are a product of kinematic- and interference terms between the emission matrix elements of the different channels.

Note that in (LS)J-approximation one must take into account /3/:

- the final ionic state may not be a singlet
- the average polarisation of a multiplet is zero

The angular distribution of the Auger electrons in such a non-coincidence experiment is given by /2/:

$$I(\cdot) = \frac{W}{4\pi} \left(1 + \sum_{k=2,4} A_{k0} P_k(\cos\cdot) \right) \quad (2)$$

Generally the A_k contain the emission matrix elements; in the single channel case they depend on kinematics only.

Therefore the program to study the emission step separately is:

- Determination of the alignment of the initial hole state from the anisotropy of a $1S_0$ -line
- Measurement of the spin polarization of a different line where the polarization may be non-zero
- Measurement of the anisotropy of the same line

From these experimental data the parameters A_k and A_{k0} can be evaluated.

The measurements were performed in a crossed-beam arrangement, the atoms emerging from a jet are ionised by an electron beam of an rotatable electron gun. The Auger lines are separated by a CMA analyser (resolution: $2 \cdot 10^{-3}$). The spin polarization is measured via Mott scattering /5/.

In this first measurement we investigated the following noble gas Auger lines with electrons as projectiles:

Krypton	$M_4N_1N_{2,3}$	$(^3P_2)$
	$M_5N_1N_{2,3}$	$(^3P_2)$
		$(^3P_1)$
Xenon	$M_5N_{4,5}N_{4,5}$	$(^3F_4)$
		$(^3F_{2,3})$

The evaluation of the polarization and anisotropy measurement yielded the following results for the polarization parameter β_2 and the anisotropy parameter A_2 :

Krypton $E_p = 1,5 \text{ keV}$		$M_5N_1N_{2,3}$	$M_4N_1N_{2,3}$
β_2 :	$3p_1$	-0.10 ± 0.06	(0.19 ± 0.11)
	$3p_2$	(0.10 ± 0.06)	-0.19 ± 0.11
α_2 :	$3p_1$	1.74 ± 0.83	1.79 ± 1.03
	$3p_2$	1.96 ± 0.66	1.80 ± 1.04

Xenon $E_p = 1,5$ keV

	$M_5N_{4,5}N_{4,5}$	
β_2 :	$^3F_{2,3}$	0.017 ± 0.028
	3F_4	-0.017 ± 0.028
A_2 :	$^3F_{2,3}$	0.42 ± 0.12
	3F_4	0.43 ± 0.12

The errors include the statistical errors and the uncertainty of the alignment. The values in parenthesis are concluded from (LS)J-approximation.

REFERENCES

- /1/ W. Mehlhorn in "Fundamental Processes in Energetic Atomic Collisions", Plenum (1983)
- /2/ H. Klar, J. Phys. B 13, 4741 (1980)
- /3/ N.M. Kabachnik, I.P. Sazhina, J. Phys. B 17, 1335 (1984)
- /4/ B. Lohmann, Diplomarbeit, Münster (1984)
- /5/ J. Kessler, "Polarized Electrons", Springer Verlag Berlin (1976)

IMPACT EXCITATION OF POTASSIUM AND CESIUM BY POLARIZED ELECTRONS

P. Naß, N. Ludwig, E. Reichert

Institut für Physik, Mainz, Germany

In this work the (np)-excitation of an unpolarized potassium (n=4) and cesium (n=6)-target by a longitudinally polarized electron-beam is studied. The quantity observed is the circular polarization of the (np- ns)-radiation emitted in forward direction, which gives a measure of exchange scattering in the collision process^{1,2,3,4,5}.

In Fig. 1 the observed polarization of the ($4^2P_{1/2} - 4^2S_{1/2}$)-K-resonance light as a function of collision energy is shown. Values calculated with data given by Moores³ are indicated. The agreement between theory and experiment is good for energies above 2.2 eV. The deep and narrow minimum in the theoretical data just above threshold is not observed in the experiment. May be the experimental energy resolution of our apparatus is not sufficient to resolve this structure.

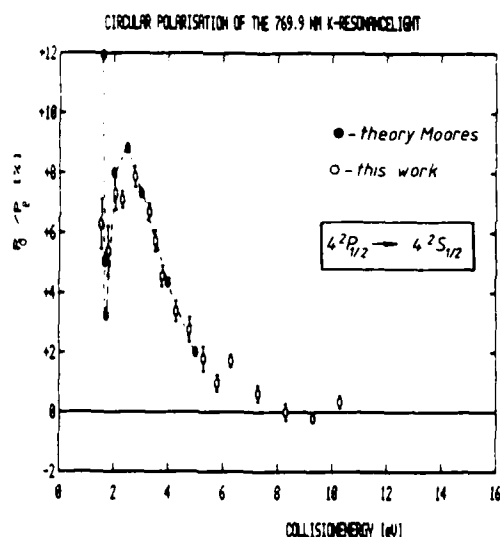


Fig. 1. Circular polarization P_{σ} of ($4^2P_{1/2} - 4^2S_{1/2}$)-K-resonance light as a function of collision energy. The dashed line, connecting the theoretical data of Moores³, are drawn to guide the eyes. P_e : electron polarization.

Fig. 2. shows similar data for the circular polarization of the ($6^2P_{3/2} - 6^2S_{1/2}$)-Cs-resonance light produced by impact with polarized electrons. The magnitude of light polarization observed just above threshold is in fairly good agreement with R-matrix calculations of Nagy et al.^{6,7}.

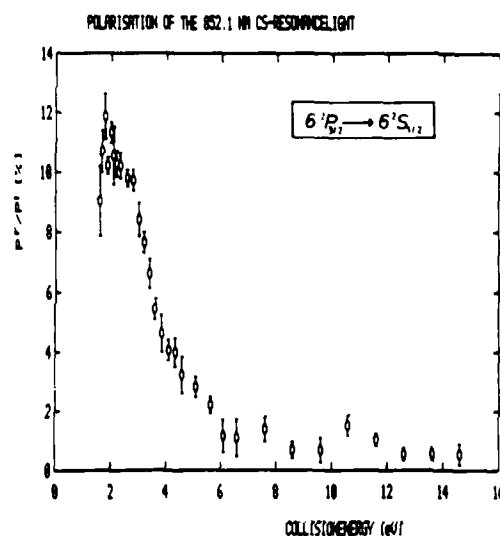


Fig. 2. Circular polarization P_{σ} of ($6^2P_{3/2} - 6^2S_{1/2}$)-Cs-resonance light as a function of collision energy. P_e : electron polarization.

REFERENCES

1. P.G. Burke, H.M. Schey, Phys.Rev. **126**, 163 (1962)
2. D.L. Moores, D.W. Norcross, J.Phys.B: Atom.Molec.Phys. **5**, 1482 (1972)
3. D.L. Moores, J.Phys.B: Atom.Molec.Phys. **9**, 1329 (1976)
4. H. Kleinpoppen, Phys.Rev. **A3**, 2015 (1972)
5. J. Kessler, "Polarized Electrons" (1976) Springer Verlag, Berlin and New York
6. D. Nagy et al., J.Phys.B: Atom.Molec.Phys. **17**, 2527 (1984)
7. D. Nagy, private communication

POLARIZATION OF ATOMIC LINE RADIATION AFTER IMPACT EXCITATION BY POLARIZED ELECTRONS

J. Goeke, G. F. Hanne, J. Kessler, M. Tushaus, and A. Wolcke

Physikalisches Institut University of Münster, D-4400 Münster, West-Germany

INTRODUCTION

For studying spin-dependent interactions in low energy electron-atom scattering the polarization of the emitted line radiation has been analyzed after excitation by polarized electrons. The excitation may be spin-dependent by the spin-orbit-interaction and by the exchange-interaction. As a result polarization components (Stokes-parameters) are obtained which only depend on the primary electron polarization. These experiments have stimulated numerical calculations¹ in which the R-matrix close-coupling method (including relativistic terms) is used to calculate the parameters which we measured. We will report on two different experiments with mercury as the target:

ELECTRON-PHOTON-COINCIDENCE EXPERIMENT

The three Stokes-parameters (η_1/P_y , η_2/P_y , and η_3) have been measured for light emitted in the direction of the electron polarization. The photons are detected in coincidence with the electrons scattered in the forward direction after excitation of the Hg 6^3P_1 -state.

The Stokes-parameters are defined as follows: $\eta_1/P_y = (I(45^\circ) - I(135^\circ))/I$, $\eta_2/P_y = (I(\sigma^+) - I(\sigma^-))/I$, and $\eta_3 = (I(0^\circ) - I(90^\circ))/I$. $I(\alpha)$ denotes the intensity of light transmitted by a linear polarization filter which is inclined to the electron beam-axis by an angle α ; η_2/P_y is the circular polarization, I the total intensity and P_y is the transverse polarization of the incident electron beam.

Only two complex scattering amplitudes are sufficient for a complete description of the excitation process studied. (With other electron scattering angles up to six different amplitudes may arise). Since we have three independent measurements, the relative phase as well as the ratio of the moduli of the two amplitudes can be extracted from the results (see figure 1.).

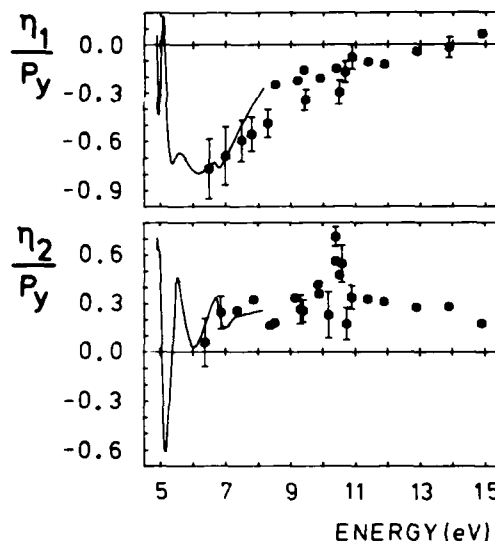


Fig. 1. Measured Stokes-parameters η_1/P_y and η_2/P_y (see text) versus electron energy. Solid line: numerical calculations of reference 1.

INTEGRATED STOKES-PARAMETERS

The polarization of line radiation measured in a non-coincidence experiment is spin-dependent as well. We measured the Stokes-parameters of several mercury transitions. Such experiments have been discussed in the literature for a calibration-free optical detector of free electron polarization². Because of many resonance states of the Hg⁻ion and the influence of the hyperfine-interaction this type of detector cannot be used without any calibration procedure. On the other hand these results have been very helpful for the classification of resonance states of the Hg⁻ion³.

REFERENCES

1. Bartschat K. Thesis Münster (1984) in collaboration with Burke P.G., and Scott N.S.
2. Wykes J.S., J. Phys. **B2** (1971) L91
3. Wolcke A., Bartschat K., Blum K., Borgmann H., Hanne G.F., and Kessler J., J. Phys. **B16** (1983) 639

SPIN EFFECTS BY ORIENTATION AND EXCHANGE IN ELASTIC ELECTRON COLLISIONS WITH HEAVY ATOMS

H.Geesmann, G.F.Hanne, F.Kaussen and J.Kessler

Physikalisches Institut der Universität Münster, D4400 Münster, W.Germany

We report on a double scattering experiment where unpolarised electrons are scattered on unpolarised heavy atoms and the spin polarisation of elastically scattered electrons is analysed by Mott scattering. The purpose of the present investigation is to study the differences in the polarisation effects when targets with different angular momenta are used. We compare scattering of electrons with Hg ($6s^2\ ^1S_0$), Tl ($6s^2 6p\ ^2P_{1/2}$) and Pb ($6s^2 6p^2\ ^3P_0$) at low collision energies of 1....20 eV.

If target atoms have nonzero orbital angular momentum (like Tl and Pb) this can be oriented by electron impact /1/ as shown in a semiclassical picture in fig.1.

If the fine structure interaction is sufficiently large the atoms will be found after elastic scattering in their ground state with well defined total angular momentum quantumnumber J. This means however that the atomic spin is also oriented after elastic collision as is shown in fig. 2 for a "one-electron-atom" like Tl. The ground state of Tl has $J=1/2$ and is separated from the (excited) state with $J=3/2$ by approximately 1 eV.

This spin orientation of the atoms might influence the polarisation of the scattered electrons if exchange collisions are involved /2/. Figure 2a e.g. demonstrates that spin down electrons are preferred to be built in the atom by exchange collision since spin up electrons cannot form a $J=1/2$ state. Thus the differential cross section for spin up and spin down electrons are different when exchange is important. This leads to polarisation phenomena like in Mott scattering but the mechanism for producing them are very different. In Mott scattering the spin polarisation is caused by the spin orbit interaction of the continuum electron with the nucleus. Instead, the effect just discussed results from an L-orientation of the atomic electrons which is transferred to the spins of the scattered electrons by the atomic fine structure interaction and exchange.

In order to investigate these different processes, we measure the polarisation of elastically scattered electrons for Hg, Tl and Pb. The Hg atoms have zero spin and orbital angular momentum and can only show Mott scattering effects, whereas Tl and Pb can also produce

spin effects by orientation and exchange. It is expected that the sequence of target atoms with $Z = 80, 81, 82$ (Hg, Tl, Pb) shows very similar behavior with respect to Mott scattering, but differences with respect the other effect when exchange collisions are involved.

First theoretical results are now available by a R-matrix calculation of the Belfast group /3/.

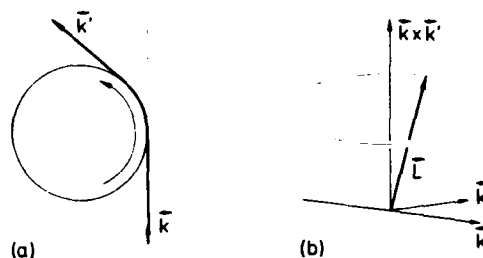


Figure 1. Semiclassical model of orientation by collision. (a) Orientation in the scattering plane caused by a grazing collision. (b) Orientation described by the vector model.

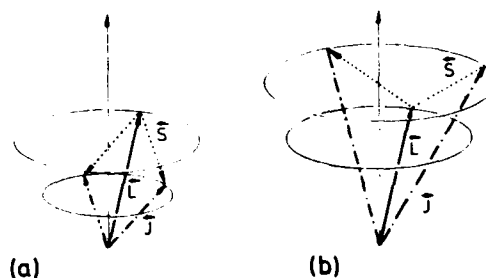


Figure 2. Semiclassical vector model for $L=1$ and $S=1/2$. (a) Total angular momentum $J=1/2$: Only spin vectors S antiparallel to the given orbital angular momentum vector L can form a $J=1/2$ state. (b) Same for $J=3/2$, illustrating that only spin vectors S parallel to the given L can form a $J=3/2$ state.

REFERENCES:

- /1/ M.Kohmoto and U.Fano, J.Phys.B 14 (1981) L447
- /2/ G.F.Hanne, Comments At.Mol.Phys. 14 (1984) 163
- /3/ K.Bartschat, K.Blum, P.G.Burke, G.F.Hanne and N.S.Scott, J.Phys.B 17 (1984) 3797

ASYMMETRY OF POLARIZED ELECTRONS SCATTERED INELASTICALLY FROM MERCURY ATOMS

H.Borgmann, J.Goeke, G.F.Hanne, C.Hölscher, J.Kessler and A.Wolcke

Physikalisches Institut, Universität Münster, Domagkstraße 75, D-4400 Münster, W.-Germany

The electron impact excitation of heavy atoms is strongly influenced by various spin-dependent interactions (spin-orbit interaction, fine-structure interaction, exchange). For studying these interactions we measured the asymmetry of polarized electrons scattered inelastically from mercury atoms for collision energies from the excitation threshold up to 50eV. The excitation of various target states (Hg 6^3P_1 , 6^3P_2 and 6^1P_1) has been studied by measuring the angular distribution of asymmetry.

A scheme of the apparatus is shown in figure 1.

The vector of the spin polarization of an electron beam which results from a GaAsP photocathode (illuminated with circularly polarized light) is rotated by magnetic coils to be perpendicular to the scattering plane which is defined by two electron detectors. From the number of electrons scattered to the left (N_L) and right (N_R) the scattering asymmetry $A = (N_L - N_R)/(N_L + N_R) = S_A(\theta) P$ is calculated. As an example of our measurements the asymmetry function S_A is plotted as a function of the scattering angle θ in figure 2a,b for excitation of the 6^3P_1 and 6^3P_2 states of Hg for a collision energy of 7.5eV. The opposite sign of $S_A(\theta)$ for the different excitations indicates that exchange is the dominant spin-dependent process here [1/].

Results for various target states and collision energies are presented and compared with new theoretical data (R-matrix close-coupling/2/ and DWBA calculations/3/).

References

- /1/ G.F.Hanne, Phys.Rep.95 (1983) 95
- /2/ K.Bartschat, K.Blum, P.G.Burke, G.F.Hanne and N.S.Scott J.Phys.B.17 (1984) 3797
- /3/ K.Bartschat, D.H.Madison and G.F.Hanne to be published

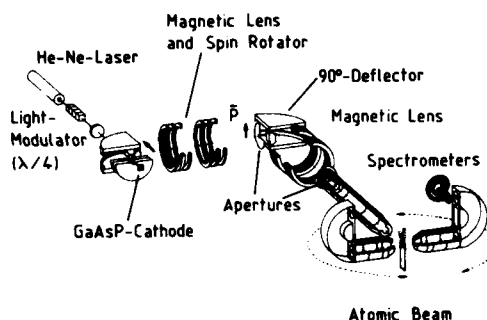
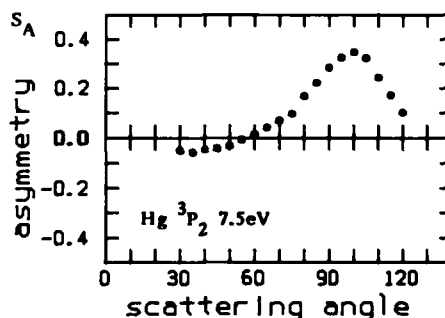
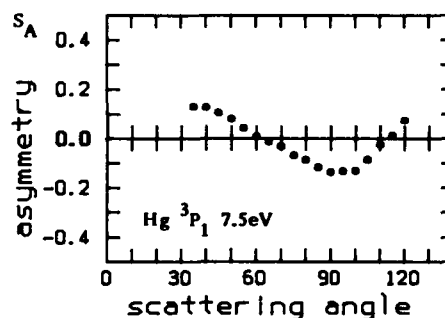


Fig. 1 scheme of apparatus

Fig. 2a,b scattering asymmetry S_A as a function of the scattering angle θ

ELASTIC SCATTERING OF POLARISED ELECTRONS FROM MERCURY AND XENON FOR COMPLETE EVALUATION OF THE SCATTERING AMPLITUDES

O. Berger and J. Kessler

Physikalisches Institut der Universität Münster, D-4400 Münster, W.-Germany

The elastic electron scattering from spinless atoms can be described completely by two complex scattering amplitudes if Coulomb interaction and spin-orbit interaction in the continuum are taken into account. Complete elastic scattering experiments are feasible in the sense that the moduli and the relative phase of the two scattering amplitudes can be determined /1/.

Experiments in which the differential cross-section or the Sherman-function S are measured do not contain all the information on the scattering process due to the fact that unpolarised electrons are scattered and the effect of the electron spin in the scattering process is not accessed completely. The missing information can only be obtained by scattering polarised electrons and measuring the additional parameters T and U describing the change of the polarisation in the scattering process /2/.

In the experiment we report here the angular dependence of the polarisation parameters S , T and U has been measured at various fixed energies between 25 and 150 eV for mercury and xenon. The polarised electrons are produced in a GaAsP source. After a first 90° deflection the electrons are focused into a rotatable deflection system which allows to vary the scattering angle continuously. A beam of 50-200 nA with a polarisation of typically 32% is obtained in the target region. The elastically scattered electrons from a target consisting of either mercury vapour or xenon gas are transmitted through a filter lens and a Wien-filter. Thereafter they are accelerated and enter a Mott-detector for polarisation analysis (Fig. 1). Two pairs of counters in the Mott-detector allow a simultaneous analysis of the transverse polarisation components. From the measured polarisation components the polarisation parameters S , T and U are derived. In the special case where the primary polarisation \vec{P} lies in the scattering plane, as in our experiment, the polarisation \vec{P}' of the scattered electrons can be described by

$$\vec{P}' = S\vec{n} + T\vec{P} + U(\vec{n} \times \vec{P}) \quad (1)$$

where \vec{n} is the unit normal vector of the scattering plane.

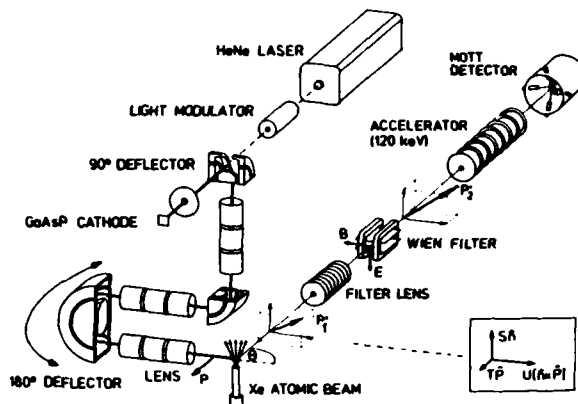


Fig. 1: Schematic diagram of the apparatus

The experimental results are shown in comparison with several theoretical calculations /3/, /4/, /5/.

From the measured polarisation parameters S , T and U together with the absolute differential cross-section, which has been investigated by different groups, a complete evaluation of the scattering amplitudes in terms of the moduli and the relative phase is presented.

REFERENCES:

- /1/ R Möllenkamp, W Wübker, O Berger, K Jost and J Kessler, J. Phys. B: At. Mol. Phys. **17**, 1107 (1984)
- /2/ J Kessler, *Polarized Electrons* (Springer, Berlin) (1976)
- /3/ D Walker, Adv. Phys. **20**, 257 (1971)
- /4/ B Awe, F Kemper, F Rosicky and R Feder J. Phys. B: At. Mol. Phys. **16**, 603 (1983) and private communication
- /5/ IE McCarthy, CJ Noble, BA Phillips and AD Turnball, Phys. Rev. A **15** 2173 (1977) and private communication

SEMI-RELATIVISTIC CALCULATIONS OF ELASTIC
SCATTERING OF ELECTRONS FROM XE AND HG

R.P. McEachran and A.D. Stauffer

Physics Department, York University, Toronto, Canada M3J 1P3

We present results for the elastic scattering of electrons from xenon and mercury using a model which includes relativistic effects as well as exchange and polarization. The relativistic potential is derived from relativistic Dirac-Fock wave functions¹ while the polarization potential is the accurate non-relativistic polarized-orbital potential used previously.^{2,3} Differential and total elastic scattering cross sections are given and compared to existing relativistic and non-relativistic calculations as well as to experimental data over the energy range from threshold to a few hundred electron volts.

Since relativistic effects are included in our model the spin polarization of the scattered electrons can also be calculated. We show results for the polarization parameters S, T and U which can be measured in a 'perfect' scattering experiment.⁴ These quantities are compared to recent theoretical and experimental results and are in general in good agreement with the experimental data. Special attention is paid to situations where disagreements have arisen in the past.

References

1. I.P. Grant, B.J. McKenzie, P.H. Norrington, D.F. Mayers and N.C. Pyper, *Computer Phys. Comm.* **21**, 207 (1980).
2. R.P. McEachran and A.D. Stauffer, *J. Phys. B* **16**, 255 (1983).
3. R.P. McEachran and A.D. Stauffer, *J. Phys. B* **17**, 2507 (1984).
4. W. Wübker, R. Möllenkamp and J. Kessler, *Phys. Rev. Letts.* **49**, 272 (1982).

ELECTRON SCATTERING ON HEAVY ATOMS*

K. Bartschat, P. G. Burke and N. S. Scott

Department of Applied Mathematics and Theoretical Physics
The Queen's University of Belfast, Belfast BT7 1NN, Northern Ireland.

Electron scattering by heavy atoms has been studied both experimentally and theoretically for many years. Experimentally, not only can total and differential elastic and inelastic cross sections be measured, but the use of high resolution polarised electron and atom beams enable observables such as the spin polarisation, asymmetry functions and the Stokes' parameters to be determined. Theoretically, new developments in methods and computer programs have enabled the combined influence of resonances, electron exchange and relativistic effects, to be accurately included.

In this paper we present recent results for elastic and inelastic scattering of electrons by Cs, Hg, Tl and Pb targets using the relativistic R-matrix method¹. These calculations include for the first time all the effects mentioned above within the framework of the Breit-Pauli Hamiltonian. The influence of electron correlation on resonances in e^- -Hg scattering and the role of the one-body spin orbit, mass correction and Darwin operators will be discussed.

Fig. 1 shows the influence of the Darwin term and the mass correction term on the spin polarisation function S_p and the asymmetry function S_A for the electron impact excitation of the $(6s6p)^3P_1$ state of Hg from the $(6s^2)^1S_0$ ground state. It can be seen that the additional terms in the Hamiltonian clearly change the results of an earlier R-matrix calculation^{2,3}, where only the spin-orbit interaction was included. The structure of the curves and the overall agreement with the experimental data⁴ remains essentially unchanged. This indicates that other effects like core polarisation and electron

correlation are also important and have to be taken into account for further improvement of the theoretical results.

Electron correlation on the $(6s6p^2)$ -resonances in e^- -Hg scattering has been studied by including additional correlation functions in the R-matrix expansion. The most important change to the original R-matrix calculation^{3,5} is a split in the energy positions of the $(6s6p^2)^2D$ -resonances. This effect can be simulated by shifting the corresponding R-matrix poles and in fig. 2 we show the results of the integrated Stokes' parameter σ_2/ρ_V , which describes the circular polarisation of the light emitted after excitation with transversally polarised electrons. The agreement with the experimental data⁶ has clearly improved, a tendency which is also found for other observables which strongly depend on the position of these resonances.

The R-matrix calculations for e^- -Hg scattering will also be compared with recent DWBA results⁷ and new experimental data of the Münster group.

References

1. N. S. Scott and P. G. Burke (1980), J. Phys. B, **13**, 4299.
2. K. Bartschat, N. S. Scott, K. Blum and P. G. Burke, (1984), J. Phys. B, **17**, 269.
3. N. S. Scott, P. G. Burke and K. Bartschat (1983), J. Phys. B., **16**, L361.
4. K. Bartschat, G. F. Hanne, A. Wolke and J. Kessler, (1981), Phys. Rev. Lett., **47**, 997.
5. K. Bartschat, K. Blum, P. G. Burke, G. F. Hanne and N. S. Scott (1984), J. Phys. B, **17**, 3797.
6. A. Wolke, K. Bartschat, K. Blum, H. Bergmann, G. F. Hanne and J. Kessler (1983), J. Phys. B, **16**, 639.
7. K. Bartschat, D. H. Madison and G. F. Hanne (1985), J. Phys. B, (to be published).

* This work was supported by the Deutsche Forschungsgemeinschaft and the British Council.

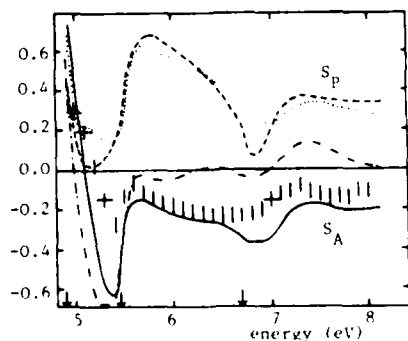


Fig. 1: Spin polarisation function S_p and scattering asymmetry function S_A for the $(6s^2)^1S_0 \rightarrow (6s6p)^3P_1$ transition in Hg. Comparison of the old (--- and ----) and the new (.... and .-. .) R-matrix calculations (see text) with the experimental data (Bartschat et al 1981) for an electron scattering angle $\theta = 90^\circ$.

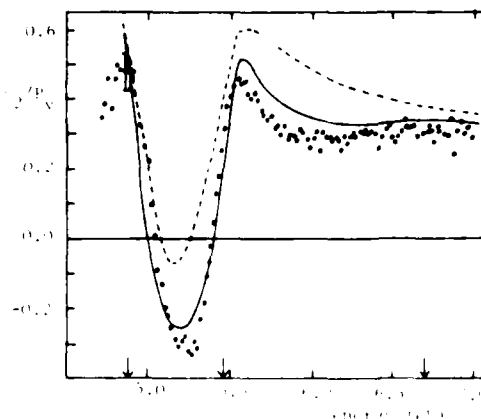


Fig. 2: Results for the integrated Stokes' parameter σ_2/ρ_V in the old (---) and the new (—) R-matrix calculations (see text) compared to the experimental data (Bartschat et al 1985).

RELATIVISTIC EFFECTS IN ELASTIC SCATTERING OF ELECTRONS FROM HEAVY ATOMS

K. Hasenburger, D. Madison*, K. Bartschat**, K. Blum

* Institut f. Theoretische Physik I, Universität Münster, D-4400 Münster, W. Germany

† Dept. of Physics and Astronomy, Drake University, Des Moines, Ia 50311, USA

** present address: Dept. of Applied Mathematics and Theoretical Physics, Queen's University, Belfast BT7 1NN, Northern Ireland

Relativistic effects in elastic scattering between electrons and heavy spinless atoms (Hg, Xe) are investigated in an energy range of 20 to 700 eV. Results will be presented which show the influence of the various relativistic effects on the electron polarization vector and cross-section.

We have performed the following calculations:

- completely relativistically as discussed in ref.¹,
- taking relativistic effects up to α^2 into account,
- including only spin-orbit coupling.

In the numerical calculations we have used various local exchange potentials^{2,3}, a polarization potential⁴ and an imaginary absorption potential⁵. For Xenon we used the relativistic wave functions of Walker and for Hg Bissner's semi-relativistic wave functions.

We have calculated the differential cross-section and the S (polarization), T and U parameters⁶, that describe the change of the polarization vector completely. S, T, U values and differential cross-sections are compared with experiment in an energy range of 20 - 700 eV. Preliminary results are shown in figs. 1 and 2.

References

- H.J. Meister, H.F. Weiss, Z. Phys. **216**, 165 (1968)
- B. Awe, F. Kemper, F. Rosicky, R. Feder, J. Phys. B **10**, 605 (1977)
- C.B. Furness, I.E. McCarthy, J. Phys. B **6**, 2240 (1973)
- L.T. Sin Fui Lam, J. Phys. B **14**, 3543 (1981)
- G. Staszewska, D.W. Schwenke, D. Thirumalai, D.G. Truhlar, Phys. Rev. A **29**, 1740 (1984)
- J. Kessler, "Polarized Electrons", chap. 3.3.1, Springer-Verlag, Berlin, Heidelberg, New York, 1976
- W. Eitel, Z. Phys. **241**, 355 (1971)
- J. Kessler, C.B. Lucas, L. Vučković, J. Phys. B **10**, 147 (1977)

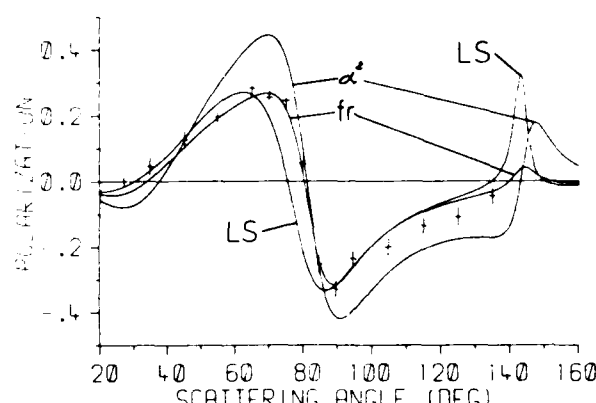


Fig. 1: Spin polarization versus scattering angle for elastic e^- - Hg scattering at 50 eV. Experimental data of Eitel⁷, fr: full-relativistic calculation, α^2 : see b), LS: only spin-orbit coupling.

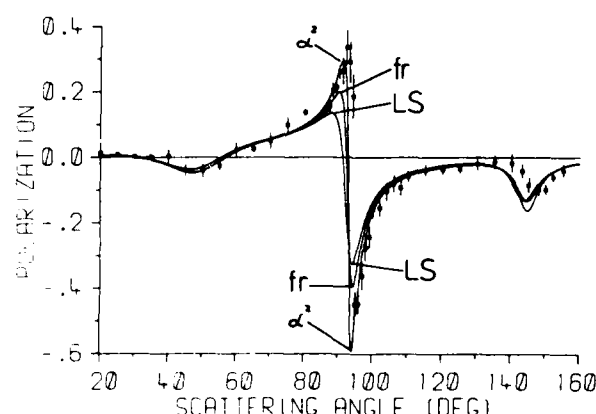


Fig. 2: Scattering from Xe at $E=400$ eV. Experimental data of Kessler, Lucas and Vučković⁸.

POLARIZATION PHENOMENA IN ELECTRON-ATOM COLLISION PROCESSES*

Keh-Ning Huang

Institute of Atomic and Molecular Sciences, Academia Sinica
P. O. Box 23-166, Taipei, Taiwan 107, Republic of China
and

Department of Physics, National Taiwan University
Taipei, Taiwan 107, Republic of China

Particle collision on a many-particle target has been one of the most fruitful probes of elementary interactions and the target structure. Electron-atom collision, in particular, has also important applications in astrophysics, plasma physics, and radiation physics. Most of previous works on electron-atom collision are about the total cross section. Nevertheless, the spin polarization and angular distribution of the scattered electron can reveal a wealth of information about the atomic structure. Furthermore, valuable new information about electron-atom collision processes can be obtained from experiments with polarized electron beams. Formulas for spin polarization and angular distribution of elastically scattered electrons are well-known^{1,2} and depend only on the incident energy and the phase shifts of partial waves. On the other hand, for inelastically scattered electrons, the spin polarization and angular distribution depend on the energies of the incident and scattered electrons, on the phase shifts, and on the transition amplitudes involving both the projectile and target. In this paper, we report the kinematics of inelastic electron-atom collisions including the radiative and Auger transitions of the target after the collision. A relativistic approach is used in the present formulation, and therefore the spin polarization of the electron and fine structures of the atom are built in from the outset. The spin polarization and angular distribution of the scattered electron are presented in concise parametrized expressions. For low-energy electron-atom collisions, where only a few partial waves suffice, these angle-independent parameters provide a convenient classification of dynamical effects and facilitate comparisons between different calculations. In addition, the present approach is formulated in such a way that any single-channel or multichannel dynamical theory can be used to calculate pertinent parameters.

Electron-atom scatterings can be summarized by the scattering equation as

$$c_{u'v} = \sum_{u_i v_i} c_{u_i v_i} I(u_i v_i; u'v), \quad (1)$$

where $c_{u'v}$ and $c_{u_i v_i}$ are the density matrices of the scattered and incident electrons, respectively, and

$I(u_i v_i; u'v)$ is the appropriate interaction matrix. To write the angular distribution and spin polarization of the scattered electron in vector forms, we define three orthogonal unit vectors $(\hat{t}, \hat{n}, \hat{k}_i)$ as $\hat{k}_i = \vec{k}_i / |\vec{k}_i|$, $\hat{n} = \vec{k}_i \times \vec{k}_s / |\vec{k}_i \times \vec{k}_s|$, $\hat{t} = \hat{n} \times \hat{k}_i / |\hat{n} \times \hat{k}_i|$, where \vec{k}_i and \vec{k}_s are the momenta of the incident and scattered electrons, respectively, \hat{n} is normal to the scattering plane, and \hat{t} is on the scattering plane and perpendicular to \hat{k}_i . The angular distribution of the scattered electron can be written as

$$\frac{d\sigma(\theta, \phi)}{d\Omega} = \frac{\sigma}{4\pi} F(\theta, \phi), \quad (2)$$

where the distribution function is

$$F(\theta, \phi) = 1 + a + b(\hat{p} \cdot \hat{n}), \quad (3)$$

Here \hat{p} is the spin polarization of the incident electron. The spin polarization of the scattered electron is given as

$$p_x(\theta, \phi)F(\theta, \phi) = c(\hat{p} \cdot \hat{k}_i) + d(\hat{p} \cdot \hat{t}), \quad (4)$$

$$p_y(\theta, \phi)F(\theta, \phi) = e + f(\hat{p} \cdot \hat{n}), \quad (5)$$

$$p_z(\theta, \phi)F(\theta, \phi) = g(\hat{p} \cdot \hat{k}_i) + h(\hat{p} \cdot \hat{t}). \quad (6)$$

Here a, b, c, d, e, f, g , and h are eight independent functions of the polar angle θ . It is clear from (3)-(6) that the analyzing power of the target, $b/(1+a)$, does not equal the polarizing power, $e/(1+a)$, even when the interaction involved in the scattering conserves parity. Only when the scattering can be approximated by the potential scattering, can we equate the analyzing power to the polarizing power because $b=e$. The kinematics of coincidence measurements of the scattered electron and excited target will also be studied, and the triply differential cross section of electron-impact ionization³ will be discussed.

References

1. N. F. Mott, Proc. Roy. Soc. A124, 425 (1929).
2. J. Kessler, Polarized Electrons (Springer, Berlin, 1976).
3. K.-N. Huang, Phys. Rev. A28, 1869 (1983).

* Work supported in part by the National Science Council and Academia Sinica, Republic of China.

ON SPIN-POLARIZATION OF AUGER ELECTRONS

K. Blum, B. Lohmann, E. Taute

Institut f. Theoretische Physik I, Universität Münster, D-4400 Münster, W. Germany

The polarization of Auger electrons has been studied by Klar¹ and by Kabachnik². These authors developed formal theories, based on symmetry considerations and derived necessary conditions for the occurrence of spin polarization for processes with unpolarized initial particles. In particular, Kabachnik² showed that spin-orbit coupling in the continuum is not necessary for obtaining spin polarization, provided individual components of the ionic fine structure levels are separated out.

Kabachnik² made some predictions for Auger lines where a noticeable polarization may be expected. These conditions are not sufficient to explain recent experimental data³.

In order to obtain additional criteria one has to consider dynamical factors. The physical mechanism, responsible for the spin polarization, is the final-state interaction experienced by the electron when it leaves the target. A significant spin polarization can only be obtained if the dynamical conditions are such that the ejected electron is significantly influenced by short-range effects. This requires in particular that its kinetic energy is not too high.

Results of model calculations will be presented which show the influence of the final-state interactions.

References

- ¹ H. Klar, J. Phys. B **13**, 4741 (1980)
- ² N.M. Kabachnik, J. Phys. B **14**, L227 (1981)
- ³ U. Hahn, H. Merz, private communication

MULTICHANNEL EIKONAL THEORY OF EXCITATION IN ELECTRON-METASTABLE ATOM COLLISIONS

E. J. Mansky and M. R. Flannery

School of Physics, Georgia Institute of Technology, Atlanta, Georgia 30332 USA

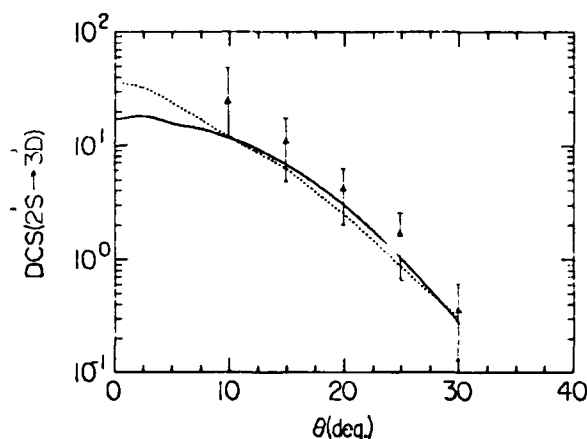
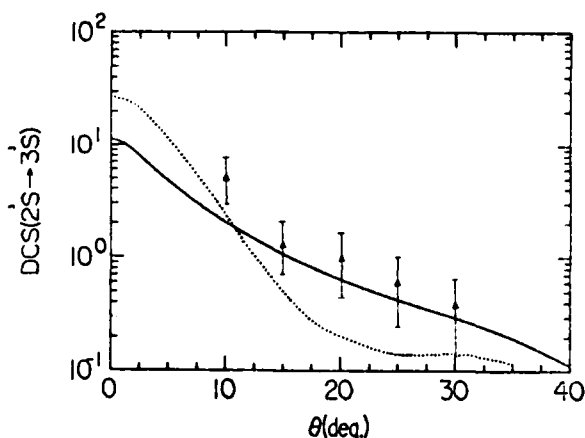
The multichannel eikonal theory^{1,2} has been modified analytically so as to incorporate directly the effect at distant impact parameters ($\rho_{\max} \rightarrow \infty$) of the various dipole couplings which are important in collisions of electrons with metastable atoms. Differential and integral cross sections are then obtained for $e\text{-H}(2s, 2p)$ and for $e\text{-He}(2^1 3s, 2^1 3p)$ for collision energies E (eV) in the range $[E_1, E_2]$ which is $[5, 500]$ for H^* and He^* , is $[17, 500]$ for $\text{H}(1s)$ and $[40, 2000]$ for $\text{He}(1^1s)$. All ten sublevels (nine for $\text{He}(2^3s)$) corresponding to the principal quantum numbers $n \leq 3$ are retained in the basis set for the target states of $\text{H}(n\ell)$ and $\text{He}(1s\ n\ell)$.

Very good agreement with experiment^{3,4} and with close-coupling calculations⁵ are obtained for integral and differential cross sections DCS (see representative results in Table 1 and Figures 1-3).

Polarization fractions for transitions $3p \rightarrow 2s$ and $2p \rightarrow 1s$ in H and for $3^1 3p \rightarrow 2^1 3s$ and $2^1 p \rightarrow 1^1 s$ in He are also calculated and compared with experiment. The first theoretical predictions for parameters (λ, u, x and ψ) are provided for transitions $\text{H}(3d \rightarrow 2p)$ and for $\text{He}(3^1 3p \rightarrow 2^1 3p)$ in the energy range $[E_1, E_2]$ and are found to be consistent with the low-energy ($E < 45.6$) experimental data.

Table 1: Theoretical and experimental values for the DCS($1s \rightarrow 2p$) in H at $E = 54.40$ eV. (in units of a_0^2/sr).

(deg.)	present results	close-coupling results ⁵	experiment ³
0	38.34	39.0	-
10	7.542	7.81	7.54
20	1.103	1.18	1.04
30	0.1716	0.199	0.157
40	0.0329	0.0471	0.0436



Figures 1 and 2: DCS (a_0^2/sr) for $e\text{-He}(2^3s + 3^3L)$ at $E = 20$ eV. Present Results —; Previous Results (ref. 2) ----; Experiment (ref. 4) Δ .

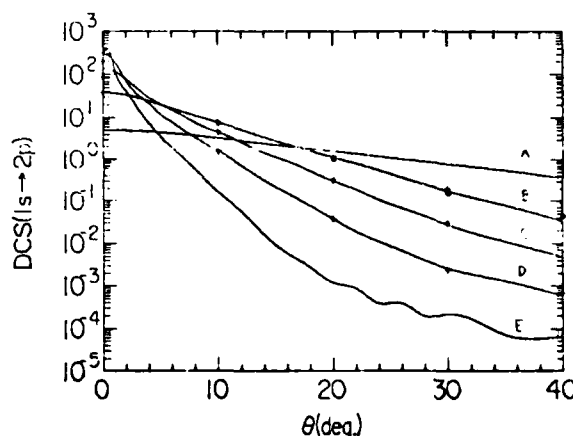


Figure 3: DCS (a_0^2/sr) for $e\text{-H}(1s + 2p)$ at E (eV) = 20, 54.4, 100, 200 and 500 (curves A-F, respectively). Present results —; \circ [ref. 3]; $+$ [ref. 5].

This research is supported by U.S. AFOSR Grant No. AFOSR-84-0233.

References

1. M. R. Flannery and K. J. McCann, *J. Phys. B* **7**, 2518 (1974), **8** 1716 (1975).
2. M. R. Flannery and K. J. McCann, *Phys. Rev. A* **12** 846 (1975).
3. J. F. Williams, *J. Phys. B* **14**, 1197 (1981).
4. R. Müller-Fiedler, P. Schlemmer, K. Jung, H. Hotop, and H. Ehrhardt, *J. Phys. B* **17**, 259 (1984).
5. A. J. Kingston, W. C. Fon, and P. G. Burke, *J. Phys. B* **9**, 605 (1976).
6. H. B. van Linden van den Heuvell, E. M. van Gasteren, J. van Erck, and H. G. M. Heideman, *J. Phys. B* **16**, 1619 (1983).

A NEW APPROACH TO SCATTERING BY MULTI-CENTRAL INTERACTIONS

D.P. Dewangan and S.B. Khadkikar

Physical Research Laboratory, Navrangpura, Ahmedabad 380 009, India.

In the theory of scattering of many-body complex systems the approximate scattering by multicentered potentials is a convenient starting point. The implied sudden approximation is expected to hold especially at high energies when the fermi-motion of the particles can be neglected. However the problem of multi-centre scattering which is equivalent to an infinite set of coupled ordinary differential equations defies an exact solution. The purpose of this note is to give an approximate solution which will be amenable to further extension to the many-body scattering formulation.

Let us consider scattering by two potentials V_1 and V_2 centered at O_1 and O_2 . Let us Green's functions be denoted by G_0^+ , G_1^+ , G_2^+ and G^+ with no potential, V_1 , V_2 , $V_1 + V_2$ and the corresponding wave functions $\phi_{i,f}$, ξ_2^+ and ξ_1^+ , + denoting outgoing boundary conditions. Then using the usual equations for Green's function and Lipmann-Schwinger equations, it is easy to show

$$\psi^+ = \phi_i^{-1} \cdot \xi_1^+ \cdot \xi_2^+ + (G^+ V_2 \xi_1^+ - \phi_i^{-1} \cdot \xi_1^+ \cdot (G_0^+ V_2 \xi_2^+)) \quad (1)$$

Here . dot denotes ordinary product which is commutative. The terms in the bracket cancel in Born-approximations upto second order and can be shown to be exactly zero in eikonal approximation. Hence one can use the approximation:

$$\psi^+ = \phi_i^{-1} \cdot \xi_1^+ \cdot \xi_2^+ \quad (2)$$

This ansatz was already used by Dewangan¹ for electron-atomic collisions. We can obviously generalize the above expression for any number of potentials - these need not act from different centres,

$$\psi^+ = \phi_i^{-1} \cdot \prod_{m=1}^n \xi_m^+ \quad (3)$$

It can be shown that in the case of two potentials the total T-matrix is given by

$$T = T_1 + T_2 + \langle \phi_f | V_1 | G_0^+ V_2 \xi_2^+ \rangle + \langle \phi_f | V_2 | G_0^+ V_1 \xi_1^+ \rangle + \langle \phi_f | V_1 + V_2 | \phi_i^{-1} \cdot G_0^+ V_1 \xi_1^+ \cdot G_0^+ V_2 \xi_2^+ \rangle \quad (4)$$

where T_1 , T_2 are T-matrices for potentials V_1 and V_2 respectively. Only the last term in (4) is approximate and replaces the following terms in the exact expression for T:

$$\langle \phi_f | V_1 | G_2^+ C_0^+ V_1 \xi_1^+ \rangle + \langle \phi_f | V_1 | G_2^+ V_1 G^+ V_2 \xi_1^+ \rangle + \{1 \leftrightarrow 2\} \quad (5)$$

Clearly our transition amplitude includes exactly all those terms in which the particle is scattered from the same potential any number of times, and also those terms in which the incident particle, after being multiply scattered by one potential, is scattered finally once by the second potential.

It appears that the first term in (1), that is ansatz(2) is quite satisfactory to explain the $e^- + H(1s) \rightarrow e^- + H(2s)$ differential cross-section¹ as shown in the figure 1.

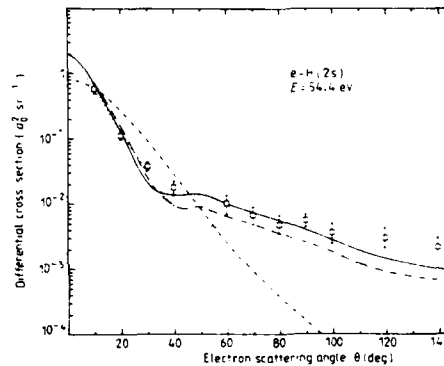


Figure 1. Differential cross sections for $e^- + H(1s) \rightarrow e^- + H(2s)$ at 54.4 eV ($k_0 = 2$ au): —, the present model not including exchange; ···, the Glauber approximation; —, the first Born approximation; — · —, the present model including exchange through the Ochkur approximation; ○, experimental data of Williams.²

This means there is large cancellation among the last terms of (1). Further applications are being considered.

References

1. D.P. Dewangan, J.Phys.B. **16** (1983), L595.
2. J.F. Williams, J.Phys.B. **14** (1981) 1197.

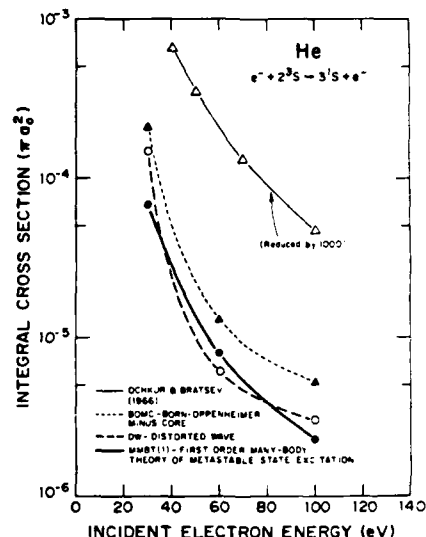
ELECTRON-IMPACT EXCITATION FROM THE 2^3S METASTABLE STATE OF HELIUM TO HIGHER ELECTRONIC STATES

David C. Cartwright and G. Csanak
University of California, Los Alamos National Laboratory
Los Alamos, New Mexico 87545

Metastable electronic states are now known¹ to play an important role in determining the degree of ionization and the flow of energy in plasmas containing inert gas atoms, but relatively little is currently known about the cross sections for excitation and ionization from these states. Although data are now becoming available on the density^{2,3} of metastable species, and their influence on the net ionization,¹ under certain plasma conditions, relatively little is known about excitation from atoms initially in metastable electronic states to higher electronic states. The only direct measurement of the differential cross section (DCS) for excitation from a metastable atomic state that has been reported to date is the recent work of Müller-Fiedler et al.⁴ From a theoretical standpoint, the only DCSs that have been reported to date are Born and Glauber results by Khayrallah et al.⁵ for the $2^3S + 3^3S$ transition, and the ten-channel eikonal results by Flannery and McCann⁶ for spin-conserved transitions.

The many-body formulation, previously used with good success for treating excitation from ground-state closed-shell targets, has been extended to treat excitation from targets in excited electronic states. In the first-order formulation of this many-body theory for metastable targets, the excitation process can occur by a two-step de-excitation-excitation process, as well as by the usual "direct" excitation mechanism. If only the "direct" excitation mechanism is considered, the customary distorted-wave approximation is obtained.

Figure 2 shows a comparison of integral cross sections obtained by various approximations with that reported by Ochkur and Bratsev,⁸ for the transition $e^- + \text{He}(2^3S) \rightarrow \text{He}(3^3S) + e^-$. Comparisons with the other experimental and theoretical results will be presented.



REFERENCES

1. C. M. Ferreira, J. Loureiro, and A. Ricard, *J. Appl. Phys.* **57**, 82 (1985).
2. M. Iino, I. Tachikawa, Y. Takubo, and M. Shimazu, *Jap. J. App. Phys.* **22**, 1422 (1983).
3. Y. Ichikawa and S. Teii, *J. Phys. D: Appl. Phys.* **13**, 1243 (1980).
4. R. Müller-Fiedler, P. Schlemmer, K. Jung, H. Hotop, and H. Ehrhardt, *J. Phys. B: At. Mol. Phys.* **17**, 259 (1984).
5. G. A. Khayrallah, S. T. Chen, and J. R. Rumble, *Phys. Rev.* **A17**, 513 (1978).
6. M. R. Flannery and K. J. McCann, *Phys. Rev.* **A12**, 846 (1975).
7. N. T. Padial, G. D. Meneses, F. J. da Paixão, G. Csanak, and D. C. Cartwright, *Phys. Rev.* **A23**, 2194 (1981); L. E. Machado, E. P. Leal and G. Csanak, *Phys. Rev.* **A29**, 1811 (1984).
8. V. I. Ochkur and V. F. Bratsev, *Sov. Astron. AJ* **9**, 797 (1966).

SMALL ANGLE "SUPERELASTIC" $3^2P \rightarrow 3^2S$ (e^- , Na) SCATTERING IN THE 10-25 eV RANGE

G. F. Shen*, J.-L. Cai*, B. Jaduszliwer* and B. Bederson*

*New York University, Department of Physics, New York, New York 10003

*The Aerospace Corporation, Los Angeles, CA 90009

Collision experiments involving scattering by laser-excited atoms is a matter of considerable current interest^{1,2}. Hertel et al.³ have studied in detail the dependence of inelastic scattering by $3^2P_{1/2}$ sodium atoms on the plane of polarization of the laser light. An experimental program is in progress⁴ at New York University to measure reliable absolute cross sections for elastic, inelastic, and superelastic electron collisions with laser-excited sodium atoms.

This paper reports on atomic recoil studies of small angle "superelastic" scattering of electrons by sodium atoms at intermediate energies, performed using a new atomic beams apparatus at NYU. The atom, electron and laser beams are mutually perpendicular and intersect in a well-defined interaction volume. The atom beam is recoil-scattered by both many-photon resonant absorption and by electron scattering, ionized by surface ionization with mass spectrometric selection with channeltron detection. The detector is 3m downstream from the interaction region, in order to obtain high angular resolution. The photon-deflected atom beam profile can be used to obtain the relative populations of ground and excited states: the electron-scattered atom can then be analyzed, in two dimensions, to determine absolute cross sections, both differential and integral, for specific state-to-state reactions. In the experiment the effusive atomic sodium beam is state-selected by hexapole electromagnet, before laser excitation, in the $F=2$, $M_F=-1,0,1,2$ states. The right-circularly polarized laser is tuned to the $3^2S_{1/2}$, $F=2 \leftrightarrow 3^2P_{3/2}$, $F=3$ transition. The atomic detector is displaced from the undeflected beam axis to the peak of the photon-recoiled atomic beam. The atomic beam signals are measured by having the channeltron output fed into a high-sensitivity electrometer. The analog output is sampled by an ADC of a PDP 11/03, programmed to operate as a multichannel analyzer.

Fig. 1 shows detector signal vs detector position, at $E_0 = 20$ eV. The effective superelastic cross section σ_s is proportional to the ratio A_s/A_0 , where A_s is the area under the superelastic scattering peak and A_0 is the area under the deflected atomic beam. Fig. 2 shows the ratio A_s/A_0 at electron energies ranging from 10 to 25 eV.

We also have measured the ratio at electron energy

of 20 eV with both circularly and linearly polarized laser light. The ratio of effective superelastic cross section for Na atoms excited by σ light and π light is 1.3. Comparison with available computations will be presented.

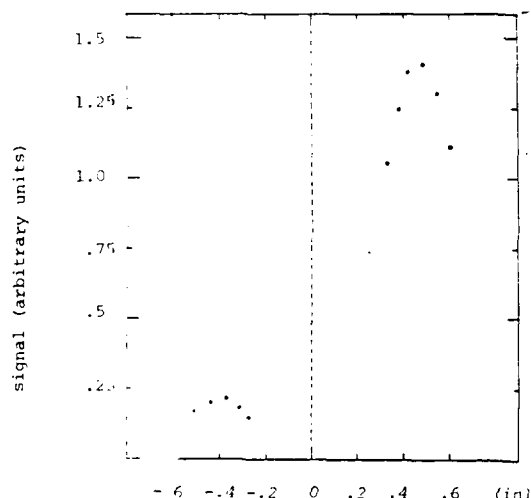


FIGURE 1. Detector signal vs detector position at $E_0 = 20$ eV. 0 represents the position of the undeflected atomic beam. The left prominent peak is the signature of superelastic scattering and the right prominent peak is the signature of forward inelastic scattering. Direction of electron beam is left to right.

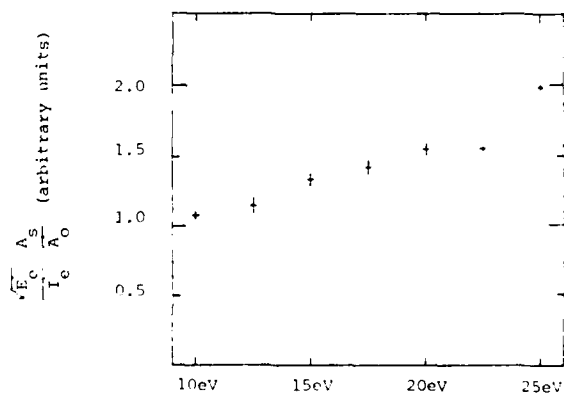


FIGURE 2. The ratio A_s/A_0 at electron energies ranging from 10 to 25 eV.

Reference

1. I.V. Hertel and W. Stoll, *Advances in Atomic and Molecular Physics* Vol. 13 p. 113 (1977)
2. D.F. Register et al, *Phys Rev A* **28**, 151 (1983)
3. W. Reiland et al, *Z. Phys. A* **307**, 51 (1982)
4. B. Jaduszliwer et al, *Phys Rev A* **30**, 1255 (1984)

ELECTRON IMPACT EXCITATION OF ALKALI ATOMS

C. E. Bielschowsky and H. G. P. Lins de Barros

Centro Brasileiro de Pesquisas Físicas, CBPF/CNPq 22290-Rio de Janeiro-RJ-Brasil

We have applied the Glauber approximation (GA) to the study of the following excitation processes:

$e^- + X(ns) \rightarrow e^- + X(ms)$ and $e^- + X(ns) \rightarrow e^- + X(mp)$ where X is Li, Na or K. The interaction potential between the incident electron and the atom has been approximated by:

$$V_I = - \frac{e^2}{|\vec{r}_1|} + \frac{1}{|\vec{r}_1 - \vec{r}_V|} + A \frac{e^{-\lambda|\vec{r}_1|}}{|\vec{r}_1|} \quad (1)$$

where \vec{r}_1 and \vec{r}_V are the coordinates for the incident and valence electrons respectively. The last term represents the averaged spherical potential which describes the interaction between the incident electron and the core electrons plus $N-1$ nuclear charges, where N is the atomic number. The parameters A and λ were obtained by fitting a numerical potential generated through a Hartree-Fock- $X\alpha$ program.

Applying (1), the Glauber phase is:

$$X = \frac{2}{k_0} \ln \frac{|\vec{b} - \vec{s}|}{b} + \frac{2A}{k_0} K_0(\lambda b) \quad (2)$$

where \vec{k}_0 is the linear momentum to the incident electron, \vec{b} is the classical impact parameter, \vec{s} is the projection of \vec{r}_1 on the plane perpendicular to \vec{k}_0 and K_0 is a Bessel function. We have called this approximation Yukawa-Frozen-Core (YFC). When $A=0$ the Inert-Frozen-Core¹ (IFC) approximation is obtained.

The atomic wave functions have been described by orthogonal Slater-type orbitals. Applying the method proposed by Thomas and Chan² and using explicitly the orthogonality of the spin-orbitals, after some further analytical developments, we have been able to express the scattering amplitude, for the processes described above, in terms of one-dimensional integrals.

Figure 1 shows typical results for the differential cross sections. Our results show that GA predicts reasonable cross sections in the intermediate scattering angle region, also for alkali atoms, as long as the core contribu-

tion is considered.

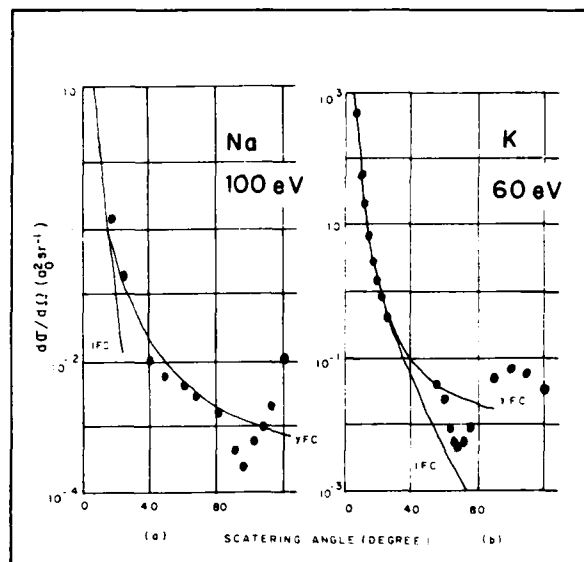


FIGURE 1 - a) Scattering Cross Section for the process $e^- + Na(3s) \rightarrow e^- + Na(3p)$ at 100 eV. YFC = Yukawa-Frozen-Core approximation. IFC = Inert-Frozen-Core approximation. = Experimental results³.

b) Scattering Cross Section for the process $e^- + K(4s) \rightarrow e^- + K(4p)$ at 60 eV. IFC = Yukawa-Frozen-Core approximation. IFC = Inert-Frozen-Core approximation. = Experimental results⁴ (54.4 eV)

REFERENCES:

- 1) Walters, H.R.J. - J. Phys. B: Atom. Molec. Phys. **6** (1973), 1003
- 2) Thomas, B.K. and Chan, F.T. - Phys. Rev. A **8** (1973), 252
- 3) Buckman, S.J. and Teubner, P.O.J. - J. Phys. B: Atom. Molec. Phys. **12** (1979), 1741
- 4) Buckman, S.J.; Noble, C.J. and Teubner, P.J. O. - J. Phys. B: Atom. Molec. Phys. **12** (1979) 3077

This work was supported by Brazilian Agency X CNPq.

INELASTIC ELECTRON SCATTERING FROM SODIUM AND MAGNESIUM

M.J. Brunger, S.J. Buckman, J.L. Riley, R. Scholten and P.J.O. Teubner

School of Physical Sciences, The Flinders University of South Australia,
Bedford Park, South Australia 5042, Australia

The recent development and application of a coupled channels optical theory to electron scattering from light metal vapours by McCarthy, Mitroy and Stelbovics¹ has demonstrated the need for reliable differential cross section measurements in the energy range from 10eV to 40eV.

We have measured differential cross sections for the excitation of the 3^2P state in sodium at 22.1eV and 54.4eV over the angular range from 2° to 140° . A major effort has been made at 54.4eV to resolve the discrepancy between earlier results from this laboratory² and those of Srivistava and Vuskovic³. In a series of experiments we have been able to demonstrate the dominant role which data for scattering angles less than 10° play in the determination of the absolute value of the cross sections for intermediate energy inelastic scattering in sodium. This forward angle behaviour has implications not only for the absolute value but also for the shape of the differential cross section at backward angles. This point will be explored in detail as it is particularly relevant to the recent theory of McCarthy et al¹ where the calculations overestimate the cross sections for scattering angles greater than 60° . Our measurements at 22.1eV show the same disagreement with the data of Srivistava and Vuskovic³ and with the theory¹.

A modulated crossed beam technique was used to measure the angular distributions of the inelastically scattered electrons. The absolute values were determined by integrating the angular distribution and normalising the data to the known total cross section⁴. A generalised oscillator strength formalism has also been used to provide absolute cross sections. The comparison of the two techniques has consequences for the validity of the First Born approximation at these energies.

A modulated crossed beam technique has also been used to measure angular distributions for the excitation of the 3^1P state in magnesium over the angular range from 3° to 130° at incident electron energies of 10, 20 and 40eV. The absolute values of the differential cross sections have been assigned by integrating the angular distributions of the 3^1P state of Leep and Gallagher⁵. The data are compared with previous experimental values of Williams and Trajmar⁶. In general there is good agreement between the previous

data and the present results in absolute value but we find significant difference in the shapes of the cross sections at all energies. For example at both 40eV and 20eV we find structure in the cross section at middle angles which is similar to that observed in elastic scattering⁶. Thus our data demonstrate that a distorted wave calculation would be profitable. No theory exists with which we can compare our data.

References

1. I.E. McCarthy, J.D. Mitroy and A.T. Stelbovics, *J.Phys.B* in press.
2. S.J. Buckman and P.J.O. Teubner, *J.Phys.B:Atom. Molec.Phys.* **12**, 1741 (1979).
3. S.K. Srivistava and L. Vuskovic, *J.Phys.B:Atom. Molec.Phys.* **13**, 2633 (1980).
4. E.A. Enemark and A. Gallagher, *Phys.Rev.A* **6**, 192 (1972).
5. D. Leep and A. Gallagher, *Phys.Rev.A* **13**, 148 (1976).
6. W. Williams and S. Trajmar, *J.Phys.B:Atom.Molec. Phys.* **11**, 2021 (1978).

Excitation of Core in Li

S. N. Tiwary*+

*Department of Physics, Morehouse College
Atlanta, Georgia 30314, USA

+Adjunct Professor, Department of Physics, Atlanta University
Atlanta, Georgia 30314, USA

We^{1,2} have explored the possibility of using the asymptotic Green function approximation (AGFA) to study elastic and inelastic collision processes in atoms and ions by electron impact in the low, intermediate and high energy range employing single-configuration Hartree-Fock (HF) wave function. Our investigation indicates that the AGFA is capable of producing reasonably good results but one should employ adequate wave function of the target specially for the heavy systems.

The primary purpose of this work is to see the impact of using the configuration interaction (CI) wave function within the AGFA in the analytic form as in our earlier work³ on the cross section of the excitation of core-electron in Li by electron impact. The result will be discussed.

References

1. S. N. Tiwary, Phys. Rev. A 28, 751 (1983)
2. S. N. Tiwary, J. Phys. B: 14, 2951 (1981)
3. S. N. Tiwary, A. E. Kingston and A. Hibbert, J. Phys. B: 16, 2457 (1983)

A LEAST-SQUARES APPROACH TO ELECTRON SCATTERING

A. L. Merts* and L. A. Collins*

*Group T-4, MS B212, Los Alamos National Laboratory, Los Alamos, NM 87545 USA

We have applied a least-squares (LS) technique¹ to the solution of sets of coupled differential equations that commonly arise in electron scattering from atoms and molecules. We formulate the LS prescription by invoking the following steps. First, we expand the scattering wavefunction in a basis of radial functions. Second, we substitute this expansion into the radial Schrödinger equation and derive a system of matrix equations for the linear expansion coefficients. These matrix equations are of dimension $N_e \times N_p$ by $N_c \times N_l$, where the number of channels, radial mesh points, and basis functions are given by N_c , N_p , and N_l respectively. Third, we impose the LS constraint that the square of the error be a minimum with respect to variations of the linear expansion coefficients. This constraint leads to a second set of linear equations in terms of square matrices of order $N_l \times N_c$. We solve this system of equations by standard linear algebraic techniques. One particular advantage of the LS approach is the ability to extract the error in the solution at each radial point rather than as an averaged quantity. This allows a systematic evaluation of the validity of the basis in each region of space and can lead to a better choice of expansion functions.

We have applied the procedure to local sets of coupled differential equations in various scattering regions. In the internal region ($R < 10 a_0$), we performed calculations on the Huck model of coupled square wells. We obtained excellent agreement with the exact results by employing a basis of four or five simple polynomials and radial meshes of ten to twenty points.

We also applied the technique to the intermediate-asymptotic scattering regime ($R > R_a \approx 10 a_0$). Our basis resembled the standard Burke-Shey² form, consisting of inverse powers of the radial variable modulated by a Bessel or Coulomb function. The LS solutions at the inner boundary were matched to the R-matrix (function and derivative) obtained from a linear algebraic calculations³ in the internal region ($R \leq R_a$) in which exchange and correlation effects were included. Since the correct asymptotic form is contained in the LS solutions, this matching leads directly to the determination of the reactance matrix K . We have applied the LS formulation to inelastic scattering of electrons by Li, Be⁺, and O⁵⁺ and to elastic scattering from H₂, N₂, and LiF. Radial meshes of fifty points

and expansions of five or six terms were sufficient to produce accurate scattering information. The computational times are comparable to those for new asymptotic methods involving the combination of propagation and accelerated expansions⁴ and generally much faster than pure propagation prescriptions.

Work performed under the auspices of the U.S. Department of Energy through the Los Alamos National Laboratory.

References

1. A. L. Merts and L. A. Collins, J. Phys. B **18**, L59 (1985).
2. P. G. Burke and H. M. Shey, Phys. Rev. **126**, 147 (1962).
3. L. A. Collins and B. I. Schneider, Phys. Rev. A **27**, 101 (1983).
4. C. J. Noble and R. Nesbet Comp. Phys. Comm. **33**, 399 (1984).

EXCITATION OF THE $3^{1,3}P$ STATES OF MAGNESIUM BY ELECTRON IMPACT*G.D. Menezes⁺, C.B. Pagan⁺ and L.E. Machado⁺⁺⁺Instituto de Física "Gleb Wataghin", Universidade Estadual de Campinas, 13100 Campinas, SP BRAZIL⁺⁺Departamento de Física, Universidade Federal de São Carlos, 13560 São Carlos, SP BRAZIL

Total and differential cross sections for the inelastic scattering of electrons off Magnesium atoms are calculated for the excitation of the $3^{1,3}P$ atomic levels at intermediate incident electron energy. The general method used was the First Order Many Body Theory of Csanak et al.¹. Previous studies^{2,3} have shown some instabilities in the calculation of the Mg scattering orbitals. Using the Linear Algebraic technique, Collins and Schneider⁴ have developed a computer code that does not show these instabilities. We used that code in obtaining the scattering solutions. The relevance of the inclusion of correlation effects in the ground and excited states is discussed. Also we calculated the orientation and alignment parameters λ and χ that can be measured by coincidence experiments. Our results are compared with both theoretical⁵ and experimental⁶ results available in the literature.

References

1. G. Csanak, H.S. Taylor and R. Yaris, Phys. Rev. **A3**, 1322 (1971)
2. P.G. Burke and W.D. Robb, Adv. At. Mol. Phys. **11**, 143 (1975)
3. Unpublished results of G. Csanak, L.E. Machado and E.P. Leal (1980)
4. L.A. Collins and B.I. Schneider, Phys. Rev. **A24**, 2387 (1981)
5. I.I. Fabrikant, J. Phys. B: At. Mol. Phys. **13**, 603 (1980)
6. W. Williams and S. Trajmar, J. Phys. B: At. Mol. Phys. **11**, 2021 (1978)

*Work partially supported by Conselho Nacional de Desenvolvimento Científico e Tecnológico (CNPq), Brazil, under grant No. 1.01.10.033/83.

ANGULAR MOMENTUM TRANSFER IN ELECTRON-HELIUM COLLISIONS

J.P.M. Beijers, J. van Eck, P.A. Zeijlmans van Emmichoven, H.G.M. Heideman

Fysisch Laboratorium, Rijksuniversiteit Utrecht, Princetonplein 5,
3584 CC Utrecht, The Netherlands.

In this contribution we will report on the 2^1P and 3^1P excitation of helium by electron impact. We measured angular correlations between the scattered electrons and emitted photons, which yields the absolute value $|\langle L \rangle|$ of the transferred angular momentum. In fig. 1a $|\langle L \rangle|$ is plotted as a function of the electron scattering angle for 2^1P excitation at 80 eV. There is a clear indication for a node in $|\langle L \rangle|$ at an angle of 60° . This gives strong evidence for a sign reversal of $\langle L \rangle$ at that angle, in agreement with a circular polarisation measurement of the $2^1P \rightarrow 1^1S$ VUV-photons¹. We also performed² the same measurements at incident beam energies of 50 and 60 eV, where no sign reversal was found.

For 3^1P excitation we measured angular correlations between the scattered electrons and the $3^1P \rightarrow 1^1S$ coincident VUV-photons at 80 eV. The contributions of 3^1S and 3^1D scattered electrons, due to the insufficient energy resolution, to the coincidence signal can be neglected at this energy. In fig. 1b a compilation of the existent data at 80 eV is given. The data points of Beyer et al.³ were obtained with a circular polarization analysis of the $3^1P \rightarrow 2^1S$ photons, so they got the sign as well (a positive sign for angles smaller than 73° and a negative sign for larger angles). From our measurements we conclude that a sign reversal occurs at an angle of about 65° . Beyer³ also performed a circular polarization measurement at 50 eV, in which case they also found a sign reversal.

We can understand these results qualitatively with a classical grazing model⁴, in which a positive $\langle L \rangle$ is associated with an attractive electron-atom interaction and a negative $\langle L \rangle$ with a repulsive interaction. A zero-crossing of $\langle L \rangle$ thus reflects a sign reversal of the interaction potential. From a quantummechanical analysis⁵ it follows that $\langle L \rangle$ changes sign if the interaction between the electron and the atom changes sign. However, an attractive potential does not necessarily lead to a positive $\langle L \rangle$ and vice versa, as is the case in the classical model. The following picture now emerges. At 80 eV and large impact parameters (small scattering angles) the attractive polarization force dominates the electron-atom interaction and leads to a positive $\langle L \rangle$. As the scattering angle increases the collisions become more violent and the repulsive interaction with the core-electrons will become more and more important, finally

dominating the electron-atom interaction at the larger angles. Thus at some scattering angle we may expect a sign reversal in $\langle L \rangle$. Due to the larger polarizability of the 3^1P state this sign reversal will probably occur at a larger scattering angle than in the 2^1P case. For lower energies the incident electrons will on the average approach the atom less closely so that it may be expected that the attractive polarization force can dominate the interaction over the full angular range and no sign reversal occurs. Measurements for 3^1P at 50 and 60 eV are in progress now.

We wish to thank Dr. H.J. Beyer who send us his results prior to publication.

References

- ¹J.F. Williams in 'Proc. 13th Int. Conf. on the Physics of Electronic and Atomic Collisions, (Berlin, 1983).
- ²J.P.M. Beijers, J. van Eck, and H.G.M. Heideman, J. Phys. B **17**, L265 (1984).
- ³H.J. Beyer, private communication.
- ⁴N.C. Steph and D.E. Golden, Phys. Rev. A **21**, 1848 (1980).
- ⁵M. Kohmoto and U. Fano, J. Phys. B **14**, L447 (1981).

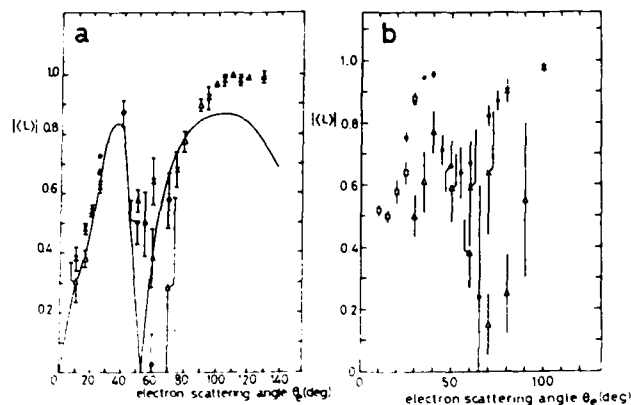


FIGURE 1 Variation of $|\langle L \rangle|$ as a function of electron scattering angle at 80 eV. a) 2^1P excitation. ●, present data; Δ, Hollywood et al. (1979) at 81.2 eV; ×, Slevin et al. (1980); —, R-matrix calculation of Fon et al. (1980) at 81.6 eV. b) 3^1P excitation. ●, present data; □, Emyan et al. (1975); ×, McAdams et al. (1982); Δ, Beyer.

ANGULAR DEPENDENCE OF THE ENERGY LOSS SPECTRA FOR ARGON BY INTERMEDIATE ENERGY ELECTRON IMPACT

G. Gerson B. de Souza, Heloisa M.B. Roberty, C.A. Lucas and C.E. Bielschowsky

Instituto de Química da Universidade Federal do Rio de Janeiro
Cidade Universitária - 21.910 - Rio de Janeiro - RJ - Brasil

As an initial step to the determination of doubly differential cross sections for the scattering of intermediate energy (1.0 keV) electrons by Argon atoms we have obtained an extensive set of energy-loss spectra in the angular range of 2 to 20 degrees.

We have used a crossed-beam type electron energy-loss spectrometer which has been described earlier¹. It features a Mollenstedt electron velocity analyzer and a triode gun as the electron source.

In figure 1 we present two typical spectra, measured at 4° and 12°. The incident energy is 1.0 keV, the energy resolution is approximately 1.4 eV and the energy-loss range is 0-100 eV.

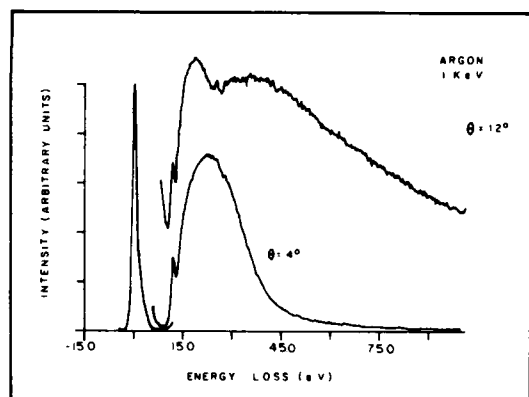


FIGURE 1 - Electron energy-loss spectra of argon at 1 keV

The differential cross section for the excitation to the $3p^5(4s,4s')$ unresolved levels (11.8 eV energy loss) has also been measured and normalized to the elastic absolute values of Jansen et al². The corresponding generalized oscillator strengths are shown in figure 2 along with the Born-type calculations of Ganas and Green³.

Assuming a 10% experimental error one can see a quantitative agreement with the theoretical values for $K^2 < 0.4$ u.a. For larger K^2 values, however, a poor agreement is observed.

This could in principle be related to a possible failure of the Born Approximation or to an inadequate representation of the involved excited states. There can also be some contribution to the measured intensity at 11.8 eV from the $3p^5(4p, 4p')$ states.

A very interesting angular behaviour can also be observed (Fig.1) for the autoionizing states of Argon which appear around 27 eV energy-loss

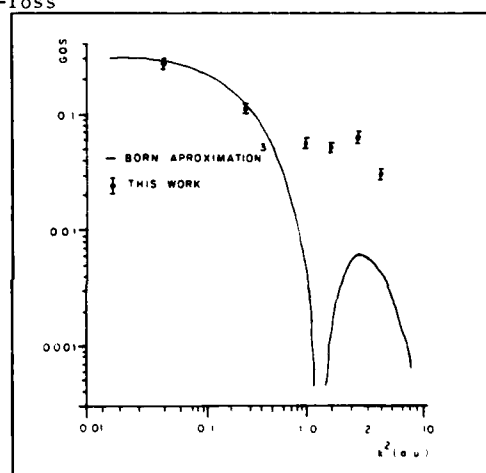


FIGURE 2 - GOS for the excitation to the $3p^5(4s,4s')$ levels.

Financial support from the CNPq, FINEP and FUJB is gratefully acknowledged.

REFERENCES:

- 1) G.G.B. de Souza, A.C.A. e Souza, R. de B.Faria, in Electronic and Atomic Collisions, J. Eichler, W. Fritsch, I.V. Hertel, N.Stol Terfoht and U. Wille, editors. North-Holland Amsterdam, Oxford, New York and Tokyo 1983 (page 707)
- 2) Jansen R.H.J. de Heer F.J., Luyken H.J., Van Wingerden B and Blaauw H.J. 1976 J. Phys.B: At. Mol. Phys. 9, 185-212
- 3) P.S. Ganas and A.E.S. Green, Phys. Rev. A4, 182 (1971).

A STEPWISE ELECTRON AND LASER EXCITATION STUDY OF THE 6^3P_2 METASTABLE STATE OF Hg

C.J. Webb, W.R. MacGillivray and M.C. Standage

School of Science, Griffith University, Nathan, 4111, Queensland, Australia

In a series of papers (1-4) we have reported on experimental and theoretical studies of stepwise excitation processes which use a combination of electron excitation followed by laser excitation of atoms to determine atomic collision parameters. Here, experimental results are reported for a stepwise excitation study of the 6^3P_2 metastable state of Hg in which the relative partial total cross-sections have been determined for the Zeeman substates. The use of a single-mode c.w. dye laser and atomic beam techniques allowed information to be obtained for particular isotopes of Hg, in this case the 200 isotope.

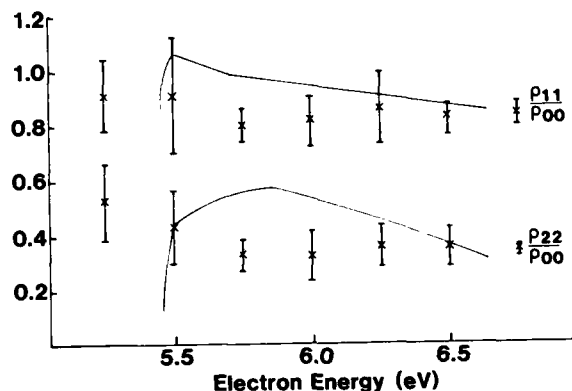
The excitation scheme used in this experiment involved electron impact excitation of ground state Hg atoms to the 6^3P_2 state followed by further excitation using 546.1 nm laser radiation to the 7^3S_1 state. Fluorescence is monitored from stepwise excited atoms decaying to the 6^3P_0 state. Details of the experimental arrangement are given elsewhere^(2,6). The excitation geometry consists of anti-collinear electron and linearly polarized laser beams (polarised at angle α to the vertical) with the fluorescence being detected at right angles. Polarisation measurements were performed with a linear polariser at angle β to the horizontal. Care was taken to eliminate sources of systematic error. Because the 6^3P_2 state is metastable the laser excited 6^3P_2 - 7^3S_1 (546.1 nm) transition saturates at low power. These effects were eliminated by working at very low laser power (0.2 mWmm^{-2}). Radiation trapping effects were found to be negligible, however, because of the long 6^3P_2 state lifetime, determined by the transit time of the atoms through the laser beam ($\sim 5 \mu\text{s}$), polarisation measurements were found to be very sensitive to small magnetic fields.

Stepwise fluorescence line polarisations were measured over a range of electron beam energies from 5.25 to 6.75 eV. The line polarisation is related to the partial total cross-sections of the 6^3P_2 state by⁽³⁾

$$P(\alpha) = \frac{6\sigma_{11}/\rho_{00} - 6\sigma_{22}/\rho_{00} - (1 + \cos 2\alpha)}{6\sigma_{11}/\rho_{00} + 6\sigma_{22}/\rho_{00} + (1 + \cos 2\alpha)} \quad (1)$$

where σ_{xx} are the partial total cross-sections for the Zeeman substates. Measurements of $P(\alpha)$ for two values of laser polarisation angles $\alpha = 0^\circ$ and $\alpha = 90^\circ$ enables the ratios of the partial total cross-sections to be

determined. Experimental values are shown in the figure for the 200-isotope 6^3P_2 state. Measurements are compared with the results of a recent close coupling calculation by Scott et al⁽⁵⁾. Agreement is reasonable with the energy spread of the electron beam precluding observation of the sharp rise in the theoretical curves at threshold.



References

1. McLucas, C.W., MacGillivray, W.R. and Standage, M.C. 1982a, Phys. Rev. Lett. **48**, 88.
2. McLucas, C.W., Wehr, H.J.E., MacGillivray, W.R. and Standage, M.C., 1982b, J. Phys. B. **15**, 1883.
3. Webb, C.J., MacGillivray, W.R. and Standage, M.C., 1984a, J. Phys. B. **17**, 1675.
4. Webb, C.J., MacGillivray, W.R. and Standage, M.C., 1984b, J. Phys. B. **17**, 2577.
5. Scott, N.S., Burke, P.G. and Bartschat, K., 1983, J. Phys. B. **16**, L361.
6. Webb, C.J., MacGillivray, W.R. and Standage, M.C., submitted, J. Phys. B., 1984.

STUDY OF ELECTRON IMPACT EXCITATION OF METASTABLE MERCURY STATES
USING STEPWISE ELECTRON-PHOTON EXCITATION

GF Hanne, V Nickich, and M Sohn

Physikalisches Institut, Universität Münster, Domagkstr. 75, D-4400 Münster, West Germany

The population of the metastable Hg ($6^3P_{0,2}$) states which have been excited by electron impact with unpolarized electrons has been studied using stepwise electron-photon excitation and observation of fluorescence emission. The excitation-emission scheme is illustrated in figure 1.

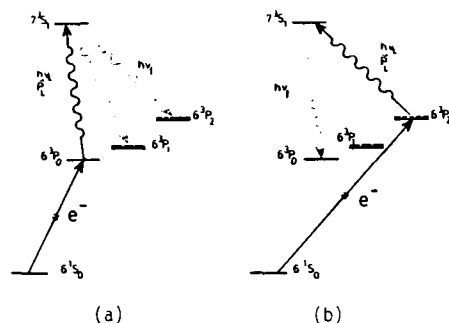


Fig. 1

Mercury atoms are excited from the ground state to the 6^3P_0 state (a) or 6^3P_2 state (b) by electron impact. The electron beam was produced by a directly heated LaB₆ cathode followed by a monochromator and a lens system which enabled the electron beam to operate at collision energies between 4 and 8 eV. The second step was a laser transition ($h\nu_L$) from e.g. Hg (6^3P_0) to Hg (7^3S_1) (Fig. 1(a)). The laser photons were produced by a pulsed excimer/dye laser system. The fluorescence emission ($h\nu_F$) from Hg (7^3S_1) to Hg (6^3P_2) was detected by a photon analyzer system which consisted of a linear polarization analyzer, an interference filter to select one of the $7^3S_1 \rightarrow (6^3P_{0,1,2})$ transitions and a photomultiplier tube.

The intensity of fluorescence emission is given by:

$$I_f \propto \sum_M c_M Q_M$$

where Q_M is the total excitation cross section of a magnetic sublevel with quantum number M , and the c_M depend on geometry, the laser polarization \vec{P}_L and the position of the polarization analyzer described above. The intensity of fluorescence emission is a measure of the excitation function, and by rotating the linear laser polarization as well as the polarization analyzer the ratios Q_2/Q_0 , Q_1/Q_0 and Q_2/Q_1 can be obtained.

The results are shown in fig. 2. The excitation functions are compared with calculations of Scott et al.¹ (R-matrix approach with spin-orbit interaction terms in the Hamiltonian). The results for Q_2/Q_0 , Q_1/Q_0 and Q_2/Q_1 for electron impact excitation of the 6^3P_2

state are compared with calculations of Bartschat². The experimental ratios are larger than the calculated ones but the general behaviour is reproduced. The sharp decrease of the theoretical values close to excitation threshold could not be observed in the experiment because of the limited energy resolution of the electron beam (about 180 meV).

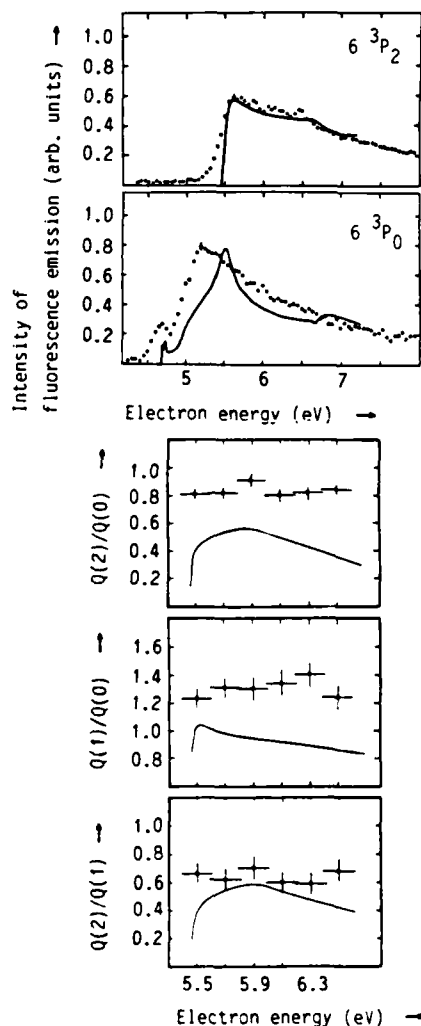


Fig. 2

REFERENCES

1. NS Scott, PG Burke, and K Bartschat, J. Phys. B **16**, L361 (1983)
2. K Bartschat, thesis, Universität Münster (1984)

A DENSITY FUNCTIONAL APPROACH TO ELECTRON-MOLECULE RESONANT SCATTERING

L. Malegat, M. Le Dourneuf, N. Tronc

* Laboratoire de Chimie Physique, Université PARIS VI, 75005 Paris, France
 ** Observatoire de Paris, 92100 Meudon, France

- Accurate methods have been developed for treating exchange and correlation effects in electron scattering by simple atomic or molecular targets. However, the need for simple models remains obvious, especially for developing extended calculations at a qualitative level of accuracy on series of molecules including heavy ones.

- Density functional theory provides a very attractive description of exchange and correlations in the ground state of any N-electron system. For a closed shell molecule a one electron effective potential $V_{\text{eff}}(\vec{r})$ may be derived by minimising the total energy with respect to the density $n(\vec{r})$:

$$V_{\text{eff}}(\vec{r}) = V_{\text{nuc}}(\vec{r}) + \int \frac{n(\vec{r}') d\vec{r}'}{|\vec{r}-\vec{r}'|} + \frac{dE_{\text{xc}}}{dn}$$

Exchange and correlation are represented by the first derivative of an unknown functional of the density. Within the 'local density approximation', we use the exchange-correlation functional calculated for a paramagnetic free electron gas (\vec{r}) , and evaluate it at each point \vec{r} from the density $n(\vec{r})$ occurring in the real system at this point. For an open shell molecule, a one electron effective potential $V_{\text{eff}}^{\sigma}(\vec{r})$ is similarly derived for each spin orientation σ , by minimising the total energy with respect to the spin density 2×2 matrix whose diagonal elements we note $\rho_{\sigma}(\vec{r})$:

$$V_{\text{eff}}^{\sigma}(\vec{r}) = V_{\text{nuc}}(\vec{r}) + \int \frac{\rho_{\sigma}(\vec{r}') d\vec{r}'}{|\vec{r}-\vec{r}'|} + \frac{dE_{\text{xc}}}{d\rho_{\sigma}}$$

$$n(\vec{r}) = \rho_{\uparrow}(\vec{r}) + \rho_{\downarrow}(\vec{r})$$

Within the 'local spin density approximation', we use the exchange correlation functional calculated for a

spin polarized free electron gas, and evaluate it at each point \vec{r} from the spin densities $\rho_{\sigma}(\vec{r})$ occurring in the real system at this point.

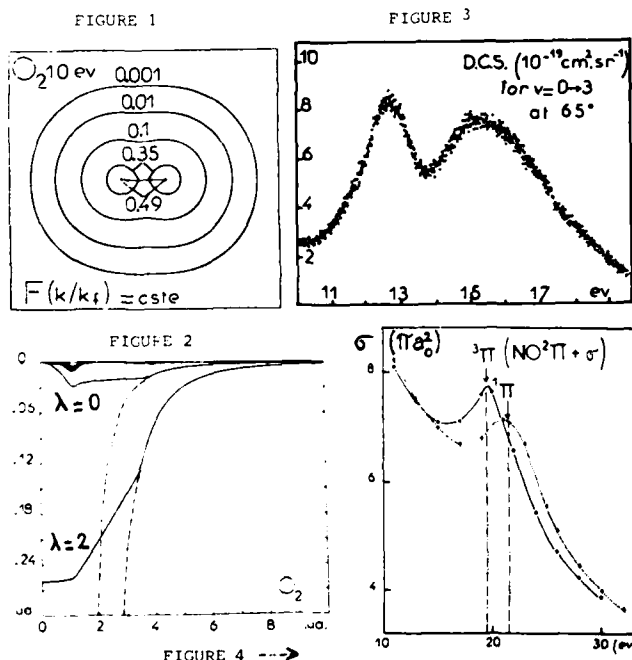
- Following previous work from Padial⁽³⁾, we are then studying the use of these exchange correlation potentials in electron scattering by molecules.

- The limitations of the method are threefold: the only channel of interest in the collision process must be the molecular ground state. The colliding electron must have sufficiently low energy to be approximately equivalent to an 'average' target electron. We can relax this constraint a bit by multiplying the exchange correlation potential by the energy dependent factor $F(k_0/k_F)$ which is derived from Slater's calculation of the exchange potential in a plane-wave model, and evaluating it in a local density approximation (figure 1). The method provides the short range part of the correlation potential only, which must then be joined to the well known long range part often referred to as the polarisation potential (figure 2).

- The density functional model has considerable advantages compared to other simple models: it provides a parameter-free correlation-polarisation potential. Exchange and correlation are described coherently. Open shell targets may be treated very simply by the use of the spin polarized formalism. We will study the validity of the correlation polarisation model by comparing exact exchange calculations of the 2,3 eV π g resonance in N_2 without correlation, and with the present model, in its plain or energy-dependent form. We will assess similarly the reliability of the exchange potential by comparing the location obtained for the N_2 π g resonance using our best correlation potential and various representations for exchange: the quasi exact 'separable approximation', the Hara free electron gas model, and the present one again in its plain or energy-dependent form. We will compare the results of the spin-independent and spin-polarized formalisms in the case of the π , 15eV resonance in the open shell NO molecule (figure 3). Preliminary results in an 'extended Hara exchange + energy independent correlation-polarisation' model are displayed in figure 4. Detailed results will be presented at the Conference.

References:

1. W.Kohn, L.J. Sham, Phys. Rev. **140** A 1133 (1965)
2. W.J. Carr, R.A. Coldwell-Horsfall, A.E. Fein, Phys. Rev. **124** 747 (1961)
3. N.T. Padial, D.W. Norcross, Phys. Rev. A **29** 1742 (1984)



TRANSITIONS OF MOLECULES BETWEEN HIGH-ANGULAR-MOMENTUM STATES

Isao Shimamura and Amulya C. Roy

RIKEN (The Institute of Physical and Chemical Research), Wako, Saitama 351-01, Japan

Recent developments in experimental techniques have led to measurements of an increasing number of cross sections for electron-molecule collisions to an increasing accuracy. The cross sections for state-to-state rotational transitions, rather than the averaged cross section, are, however, extremely difficult to measure directly. This is because the energy resolution of electron spectrometers is too low to resolve rotational lines, which are closely spaced, in the energy-loss spectra. Reliable theoretical calculations are too cumbersome to carry out for many different initial and final rotational states; molecules are normally distributed among many different rotational states. One of the present authors, however, has noted that most molecules occupy high-lying rotational states J , and has derived simple formulas for the cross sections for transitions of linear and spherical-top rotators from high rotational states J to high rotational states $J'=J\pm\Delta J$.^{1,2} The main virtue of these formulas is that they give the cross sections for the transitions $J\rightarrow J\pm\Delta J$ for any high J in terms of a single unknown parameter independent of J . The present work is a generalization of these formulas for transitions of symmetric-top rotators.

Main results for the transitions of linear rigid rotators are first summarized. Assume that the collision time is much shorter than the rotational period, which is of the order of $\sim 10^{-12}$ s. This assumption, namely, the sudden collision assumption is equivalent to the assumption that the electron temperature be higher than the rotational temperature. Without any further approximations it follows for $J \gg |\Delta J|$ that^{1,2}

$$d\sigma(J \rightarrow J \pm \Delta J)/d\omega = C(|\Delta J|)[1 \pm (\Delta J/2)J^{-1} + O(J^{-2})]. \quad (1)$$

The two cross sections $d\sigma(J \rightarrow J \pm \Delta J)/d\omega$ plotted versus J approach a value $C(|\Delta J|)$ common to both as $J \rightarrow \infty$, one from above and the other from below in a manner nearly symmetric with respect to the horizontal line that aims at the limiting value. The sum of the two cross sections $d\sigma(J \rightarrow J \pm \Delta J)/d\omega$ is $2C(|\Delta J|)[1 + O(J^{-2})]$ and is nearly independent of J for high J . This partial-sum rule is to be compared with Drozdov's sum rule that the sum of $d\sigma(J \rightarrow J')$ over all J' is a constant independent of J .³

Because the rotational energy $E_r(J)$ is $BJ(J+1)$, B being the rotational constant, the transition energies ΔE for a fixed value of ΔJ are linear in J . Therefore,

the cross sections $(\Delta E)d\sigma(J \rightarrow J \pm \Delta J)/d\omega$ for energy loss by the electron increases with J in proportion to J for high J . The sum of the two energy-loss cross sections for $J' = J \pm \Delta J$, however, is nearly constant for high J .^{1,2} This is to be compared with the recently proven sum rule for the energy-loss cross section.^{4,5}

We have generalized these results for symmetric-top rotators. They have a well-defined quantum number K ($-J \leq K \leq J$) for the projection of the rotational angular momentum onto the body-fixed symmetry axis. We have proved the following high- J formulas:

$$d\sigma(JK \rightarrow JK \pm \Delta J, K')/d\omega = C(|\Delta J|)[1 \pm (\Delta J/2)J^{-1} + O(J^{-2})] \quad (2)$$

for transitions with $K = K'$ and

$$d\sigma(JK \rightarrow JK')/d\omega = A(\Delta K)[1 + O(J^{-2})], \quad (3)$$

$$d\sigma(JK \rightarrow J \pm \Delta J, K')/d\omega = A(|\Delta J|, K) \times [1 \pm (\Delta J/2)J^{-1} + 2s(K \cdot K')A'(|\Delta J|, K)[1 + O(J^{-2})]] \quad (4)$$

for any K and K' , where $s = \text{sign}(K - K')$. If the rotator has a plane of symmetry, $A(\Delta K)$, $A(|\Delta J|, K)$, and $A'(|\Delta J|, K)$ are independent of the sign of $\Delta K = K' - K$. Equation (2) involves only one parameter that is common to all values of J and K . Equation (3) depends only on ΔK and not on J or on K . Equation (4) expresses all cross sections in terms of only two parameters that depend only on $|\Delta J|$ and K and not on J or K . In all of these cases the two cross sections for $J' = J \pm \Delta J$ approach the same limit as $J \rightarrow \infty$, one from above and the other from below in a nearly symmetric way, as in the case of linear rotators.

These results are applicable to rotational transitions, in the sudden approximation, due to collisions with electrons, positrons, atoms, and ions, to photoabsorption, and to photoionization.

References

1. I. Shimamura, Symposium on Electron-Molecule Collisions, Invited Papers, eds. I. Shimamura and M. Matsuzawa (Univ. Tokyo, 1979); Chem. Phys. Lett. **73**, 328 (1980).
2. I. Shimamura, Phys. Rev. A **28**, 1357 (1983).
3. S. I. Drozdov, Sov. Phys. JETP **1**, 591 (1955); *ibid.* **3**, 759 (1956).
4. I. Shimamura, Phys. Rev. A **23**, 3350 (1981).
5. I. Shimamura, Electron-Molecule Collisions, eds. I. Shimamura and K. Takayanagi (Plenum, New York, 1984) Chap. 2.

ELECTRON SCATTERING FROM POLYATOMIC AND DIATOMIC TARGETS
VIA A FULLY AB INITIO TREATMENT OF INTERACTION

F. A. Gianturco⁺, U. T. Lamanna*, A. Palma⁺ and L. Pantano⁺

⁺ Department of Chemistry, University of Rome, Rome, Italy.

^{*} Department of Chemistry, University of Bari, Bari, Italy.

The accurate treatment of electron-molecule interactions starting from first principles has been so far a rather elusive result unless simple diatomics were considered. Even for such cases, however, the computational efforts have been rather massive and limited, as a consequence, the range of energies which could be considered during the scattering process.

A few years ago we begun^{1,2} a series of studies on polyatomic molecules by performing a parameter-dependent calculation of the full interaction and found reasonable agreement with the available experimental data. More recent efforts³ have modified in the model the way in which polarisation and correlation forces are included so that both molecules of the AH_n type⁴ and diatomics⁵ can be treated via a fully ab-initio potential form.

In the present study we have addressed the problem by performing the following steps:

- (i) The target wavefunctions were generated at the SCF level by using a one-centre-expansion (OCE) of a large set of Slater orbitals, so that a fairly realistic description of the static interaction was obtained⁶;

- (ii) The exchange interaction was obtained from the Hara and the asymptotically adjusted versions of the free electron-gas (FEGE) exchange approximation introduced earlier for polyatomic targets⁷;
- (iii) The polarisation-correlation potential was generated via the molecular density obtained in (i), within the local electron-gas theory for the short-range region and via the asymptotic form of the polarisation potential in the long-range region.⁸
- (iv) Rotationally inelastic cross sections, integral and differential, were obtained at high collision energies (above 20 eV) in the lab. frame and via the IOS decoupling scheme. In the low energy region (down to < 1 eV), total cross sections were computed within the Fixed Nuclei approximation. Some of the preliminary results are shown in Figure 1 for the HF molecule, where one sees the direct bearing that molecular charge distributions have on the behaviour of the exchange potential at various collision energies. Further results on CH_4 and H_2O will be presented at the Conference.

References

1. F. A. Gianturco and D. G. Thompson, J. Phys B **9**, L 383 (1976).
2. idem, J. Phys B **13**, 613 (1980).
3. A. Jain and D. G. Thompson, J. Phys B **15**, L631(1982).
4. idem, J. Phys B **16**, 1113 (1983).
5. N. T. Padial and D. W. Norcross, Phys. Rev. **A29**, 1742 (1984).
6. F. A. Gianturco and D. G. Thompson, Chem. Phys. **14**, 111 (1976).
7. S. Salvini and D. G. Thompson, J. Phys B **14**, 3797 (1981).
8. J. O'Connell and N. F. Lane, Phys. Rev. **A27**, 1893 (1983).

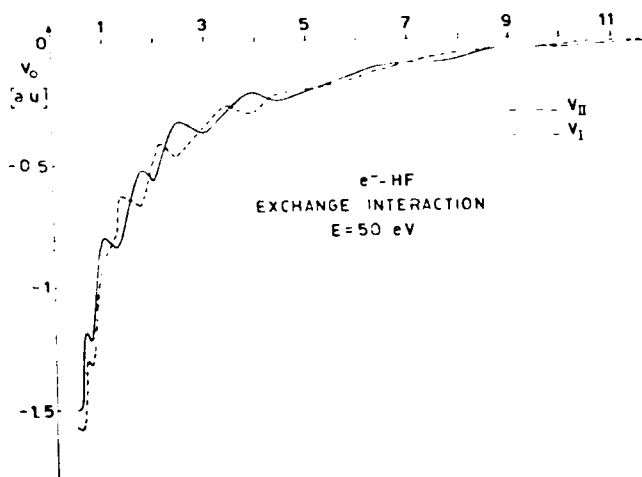


FIGURE 1

EFFECTS OF COMBINED MANIFESTATION OF DIRECT AND RESONANT INTERACTION
IN SLOW ELECTRON-MOLECULE COLLISIONS

G.K.Ivanov and G.V.Golubkov

Institute of Chemical Physics, Academy of Science, Moscow USSR

The dissociative attachment (DA) and scattering of slow electrons on molecules are considered with help of Heitler-type equation for the collision T-operator

$$T = K - iK \sum_{\nu} |l\nu\rangle \langle l\nu| T \quad (1)$$

Here $|l\nu\rangle = \varphi_e X_\nu$, $\varphi_e = \pi^{1/2} R_{e,e} Y_{em}$, $R_{e,e}$ is the radial wave function of the free electron normalized to the δ -function of energy, Y_{em} is its angular function with the quantization axis directed along the molecule XY, X_ν is the vibrational wave function, ϵ_ν is the electron energy in ν -th channel. The sum in (1) is taken only over open channels ($\epsilon_\nu > 0$).

For the K-matrix we use such representation which provides to establish the direct connection of the phenomenological parameters of the dynamic theory with the molecular adiabatic terms

$$K = K^{(0)} + \sum_{\beta} V | \psi_{\beta}^e \rangle g_{\beta} \langle \psi_{\beta}^e | V = \bar{K} - i \sum_{\beta} V | \beta d \rangle \langle \beta d | V \quad (2)$$

V is the operator of electron-molecule interaction, ψ_{β}^e and g_{β} are the electron wave function and Green's function which describes the nuclear motion in β -th dissociative channels. The sum \sum_{β} refers to dissociative channels, $|\beta d\rangle = \pi^{1/2} \psi_{\beta}^e X_d^A$, where the nuclear function is taken at the energy E , received by the nuclei in accordance with the energy conservation law. The eq.(1) is equivalent, as may be shown, to equation

$$T = \bar{K} - i \bar{K} \sum_{\nu} |l\nu\rangle \langle l\nu| T - i \bar{K} \sum_{\beta} |\beta d\rangle \langle \beta d| T \quad (3)$$

which takes into account the dissociative channels on equal grounds with the scattering ones. Here

$$\langle \beta d | \bar{K} | \beta d \rangle = 0, \quad \langle \beta d | \bar{K} | l\nu \rangle = \langle \beta d | V | l\nu \rangle$$

The following relation between the function $|\beta d\rangle$ and $|\beta d'\rangle$ takes place $\bar{K} |\beta d'\rangle = V |\beta d'\rangle$.

The scattering and DA of slow electrons are described by the amplitudes $T_{e\nu, e\nu'}$ and

$T_{e\nu, ad}$, and collisional transitions

$$X^- + Y \rightarrow (e^- + XY) \rightarrow X + Y^-$$

by $T_{ad, \beta d}$ respectively. While neglecting of the inelastic background processes when

$$K_{e\nu, e\nu'}^{(0)} = K_{e\nu, e\nu}^{(0)} \delta_{\nu\nu'}$$

we get from eq.(1) (at fixed ℓ) the Bardsley equation [1] with nonlocal optical potential

$$U = -i \sum_{\nu} V_{\ell \beta} | \nu \rangle \frac{1}{1 + i K_{e\nu, e\nu}^{(0)}} \langle \nu | V_{\ell \beta} \quad (4)$$

$$(V_{\ell \beta} = \langle \varphi_e | V | \psi_{\beta}^e \rangle).$$

It is important, however, to point out that the potential U gains an additional (shift) term due to background scattering which is lacking in the configuration interaction theory.

To illustrate the role of inelastic background scattering let us take the expression for amplitude of DA of electron to a non-excited molecule at $\omega < E < 2\omega$ (ω is the vibrational quantum of XY, $\hbar = m_e = e = 1$)

$$T_{e\nu, ad} = \frac{\bar{K}_{e\nu, ad} (1 + i \bar{K}_{e\nu, e\nu}) - i K_{e\nu, e\nu} \bar{K}_{e\nu, ad}}{(1 + i K_{e\nu, e\nu}) (1 + i \bar{K}_{e\nu, e\nu}) + K_{e\nu, e\nu}^2}$$

It is shown the inelastic background scattering may increase the probability of DA by means of direct vibrational excitation of molecule and its subsequent decay off this state.

Reference

1. J.Bardsley, J.Phys., B1, 405 (1968)

SCATTERING OF LOW ENERGY ELECTRONS BY HCN AND CO

A. Jain and D. W. Norcross*

Joint Institute for Laboratory Astrophysics, University of Colorado and
National Bureau of Standards, Boulder, Colorado 80309 USA

We have recently used a parameter-free *ab initio* model to study low energy electrons with linear molecules.^{1,2} In this model, the total interaction potential is composed of an exact static potential plus a parameter-free correlation-polarization potential. Exchange is treated exactly through a separable exchange approximation. This model has been highly successful in reproducing shape resonances, in particular the well-known Π_g resonance in N_2 .¹

This model applied to the isoelectronic molecule HCN yielded a similar Π resonance,³ which is consistent with experiments.⁴ The shape of the Π resonance as a function of internuclear distance is qualitatively very similar to that of the N_2 Π_g resonance. Its position at equilibrium (in linear geometry) is about 0.4 eV above the measured position, suggesting that the geometry of the HCN^- is substantially bent. A broad Σ resonance is obtained when the CH or CN bonds are stretched well beyond R_e ; the former appears to cross the neutral curve at about 2.7 a.u., i.e., about 0.5 eV below the $H + CN^-$ asymptote, the latter to approach the neutral curve much more slowly and tangentially.

Another isoelectronic diatomic molecule is CO, which is also known to have a Π structure at 1.8-1.9 eV; the width of this resonance, as estimated from measurements⁵ of the vibrational excitation cross section, is roughly 1.0 eV. There have been several proof-of-principle static-exchange calculations for CO, but these fail to predict the correct position or width of the Π resonance. Neglect of correlation and/or polarization effects in the interaction potential was presumed responsible. The Π resonance was also obtained in earlier calculations,⁶ in which its position was used to tune the cut-off parameter in a semiempirical polarization potential. In that work, the exchange interaction was approximated by enforcing orthogonality of bound and continuum orbitals of like symmetry. Recent calculations⁷ employing an *ab initio* treatment of exchange and short-range polarization effects yielded much better agreement ($E_r = 1.72$ eV and $\Gamma = 0.75$ eV) with measurements.

The present work is the first for CO to include both an exact treatment of exchange and a parameter-

free model of the correlation-polarization interaction (both long- and short-range effects). We used a large GTO basis set in order to get a Hartree-Fock level wave function for the CO molecule. This basis gave a total energy of -112.7707 a.u. and a dipole moment of 0.099 a.u. Our scattering results were first checked against earlier work⁸ at the static-exchange level; excellent agreement was obtained. The position and width of the Π resonance (converged to better than 1%) were found to be 3.30 eV and 1.90 eV, respectively. When the correlation-polarization potential was added, the resonance position and width changed to 1.85 eV and 0.95 eV, respectively.

Results for the resonance parameters as a function of internuclear distance, and for total, momentum transfer, and differential cross sections in the energy range 10^{-3} to 10 eV will be presented and compared with earlier theoretical and experimental work at the conference. The agreement with the latter is generally good, even at low energies. The one exception is the integral cross section at the resonance, for which our result is about a third larger than measured values.⁹ This may be due to the fact that the differential cross section is strongly forward peaked at the resonance,¹⁰ an observation confirmed by our calculations. The measurement was taken using a transmission technique, which discriminates against forward scattering.

This work was supported by the U. S. Dept. of Energy (Office of Basic Energy Sciences).

References

1. N. T. Padial and D. W. Norcross, Phys. Rev. A **29**, 1742 (1984).
2. N. T. Padial and D. W. Norcross, Phys. Rev. A **29**, 1590 (1984).
3. A. Jain and D. W. Norcross, Phys. Rev. A (submitted).
4. M. Inoue, J. Chimie Physique (Fr.) **63**, 1061 (1966); P. D. Burrow (see L. Ng, U. Balaji and K. D. Jordan, Chem. Phys. Lett. **101**, 171 (1983); M. Tronc, private communication.
5. M. Tronc, R. Azria and Y. Le Coat, J. Phys. B **13**, 2327 (1980).
6. N. Chandra, Phys. Rev. A **16**, 80 (1977).
7. S. Salvini, P. G. Burke and C. J. Noble, J. Phys. B **17**, 2549 (1984).
8. L. A. Collins and B. I. Schneider, private communication cited in Ref. 7.
9. Ch. K. Kwan, Y. F. Hsieh, W. E. Kauppila, S. J. Smith, T. S. Stein, M. N. Uddin, and M. S. Dababneh, Phys. Rev. A **27**, 1328 (1983).
10. K. Jung, Th. Antoni, R. Müller, K.-H. Kochem and H. Ehrhardt, J. Phys. B **15**, 3535 (1982).

* Staff Member, Quantum Physics Division, National Bureau of Standards.

THE INTERACTION OF LOW ENERGY ELECTRONS WITH HCL - ELASTIC SCATTERING, VIBRATIONAL EXCITATION, AND ANION STATES

A. Jain,* D. W. Norcross,** S. V. O'Neil,* N. T. Padial† and P. Rosmus‡

*Joint Institute for Laboratory Astrophysics, University of Colorado and National Bureau of Standards, Boulder, Colorado 80309 USA

‡Institute for Modern Optics, Department of Physics and Astronomy, University of New Mexico, Albuquerque, New Mexico 87131 USA

§JILA Visiting Fellow (1984-1985); Fachbereich Chemie der J. W. Goethe Universität, D-6000 Frankfurt FGR

Close-coupling calculations of vibrationally elastic and inelastic scattering have been carried out in the multipole-extracted adiabatic-nuclei (MEAN) approximation,¹ employing a new parameter-free model² of the correlation-polarization interaction and an exact treatment of exchange.³ Calculated differential cross sections for $vv' = 00$ provide a new absolute normalization for measurements⁴ of cross sections for vibrational excitation. Vibrational excitation is quite sensitive to the treatments of both correlation-polarization and exchange -- the notations in Figure 1 are: FBA, first Born approximation; SE, with a free-electron-gas model of exchange; ESE, with exact exchange; COP, with correlation-polarization.

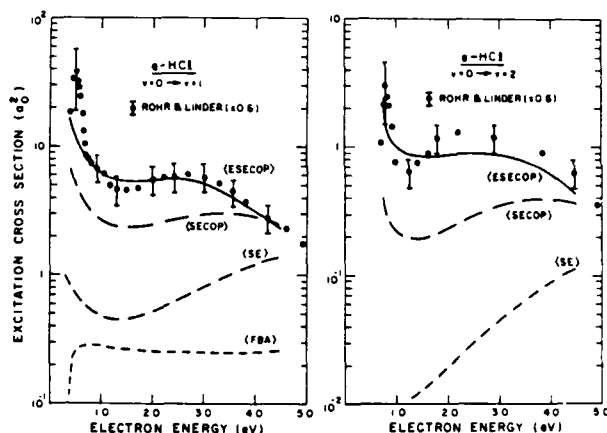


Figure 1. Vibrational excitation cross sections.

The calculated eigenphase sums for sigma symmetry as a function of internuclear distance are completely consistent with a model⁵ postulating a single electronic state of HC^- responsible for both a bound state at large internuclear distances and a resonance near equilibrium. According to this model, the bound state correlates asymptotically with the lowest dissociation state ($\text{H} + \text{Cl}^-$), and is attractive near the neutral curve. The

merging with the neutral curve is strongly influenced by the long-range dipole tail of the potential, causing a cusp in the real part of the fixed-nuclei potential energy curve of the anion state. The threshold peaks in vibrational excitation are therefore a direct consequence of the polar nature of the molecule.

The present scattering calculations indicate that the anion state merges with the neutral curve at about 2.6 a.u., thus 0.7-0.8 eV below the $\text{H} + \text{Cl}^-$ asymptote. This is in sharp contrast to molecular structure calculations⁶ of the bound anion potential, which yielded curves that are essentially repulsive, crossing the neutral curve roughly 0.2 eV above the asymptote.

In an attempt to resolve the difference between the qualitative behavior of the 1^2 potential curve consistent with the scattering results and that found in bound state calculations,⁶ O'Neil and Rosmus are undertaking very large scale *ab initio* Born-Oppenheimer calculations on the HC^-/HC^- system. The calculations are based upon a flexible Gaussian orbital basis, multi-configuration SCF, and a multi-reference CI. In parallel with this study, we are in the course of modifying the scattering code to calculate bound states of the $\text{HC}^- + e$ system; i.e., a direct extension of the scattering calculations to negative energies in the fixed-nuclei approximation. Both calculations will focus on internuclear separations between 2.6 and 3.8 a.u., the region in which the 1^2 and 1^1 potential curves intersect; results will be presented at the conference.

This work was partially supported by the U.S. Dept. of Energy (Office of Basic Energy Sciences).

References

1. D. W. Norcross and N. T. Padial, *Phys. Rev. A* **25**, 226 (1982).
2. N. T. Padial and D. W. Norcross, *Phys. Rev. A* **29**, 1742 (1984).
3. B. I. Schneider and L. A. Collins, *Phys. Rev. A* **24**, 1264 (1981); T. V. Rescigno and A. F. Orel, *Phys. Rev. A* **24**, 1267 (1981).
4. K. Rohr and F. Linder, *J. Phys. B* **9**, 2521 (1976).
5. W. Domcke and L. S. Cederbaum, *J. Phys. B* **14**, 149 (1981).
6. M. Krauss and W. L. Stevens, *J. Chem. Phys.* **74**, 570 (1981); M. Bettendorff, P. J. Bunker and S. D. Peyerimhoff, *Mol. Phys.* **50**, 1363 (1981).
7. W. Domcke and G. Mündel, *J. Phys. B* (in press).

†Staff Member, Quantum Physics Division, National Bureau of Standards.

ABSOLUTE ELASTIC DIFFERENTIAL ELECTRON SCATTERING CROSS SECTIONS FOR CARBON MONOXIDE

C. Mott and J. Nickel
University of California, Riverside, California 92521 USA

A program has been initiated at Riverside to measure absolute electron impact differential scattering cross sections for molecular targets. The first spectrometer which has been constructed is a cross beam device utilizing hemispherical energy analyzers and cylindrical electrostatic optics. The instrument has an energy range of 5-100 eV, and angular range of -10^0 - 120^0 , and an energy resolution of 60 mV. It will be used to measure elastic cross sections of diatomic molecules.

Since we wish to use the relative flow technique^{1,2} to place the molecular cross sections on an absolute scale, considerable effort is being invested to explore the limits of accuracy of this technique in our apparatus. In the relative flow technique, the cross section of species 1 is compared to species 2 through the relation

$$\frac{\sigma_1(\psi)}{\sigma_2(\psi)} = \frac{\dot{N}_{e1}}{\dot{N}_{e2}} \left(\frac{m_2}{m_1} \right)^{1/2} \frac{\dot{N}_2}{\dot{N}_1} \quad (1)$$

$\sigma(\psi)$ is the DCS, m is the mass of the molecular species, \dot{N} is the gas flow rate, and \dot{N}_e is the scattered electron count rate at the detector. Theoretical considerations^{3,4} show that the above relation is valid provided that the flow rate condition

$$\dot{N}_2 = \left(\frac{\dot{N}_1}{\dot{N}_2} \right)^2 \left(\frac{m_1}{m_2} \right)^{1/2} \dot{N}_1 \quad (2)$$

holds and that the mean free path of the gas behind the capillary is of the order of the individual capillary diameter or larger. λ is the molecular diameter. Experiments suggest that under appropriate experimental conditions, equation 1 is valid even for combinations of flow rates which violate equation 2.

Results of the relative flow investigation comparing neon and helium will be presented. To give a measure of how well our experimental technique works, these results will be compared with those of Register and Trajmar.⁵ In addition, preliminary results of the elastic cross sections of CO⁶ in the incident energy range of 20-100 eV and angular range 10^0 - 120^0 will be presented.

References

1. S.K. Srivastava, A. Chutjian, and S. Trajmar, J. Chem. Phys. 63, 2659 (1975)
2. S. Trajmar and D.F. Register in Electron-Molecule Collisions, eds. I. Shimamura and K. Takayanagi, Plenum Press, New York (1984)
3. J. A. Giordmaine and T.C. Wang, J. Appl. Phys. 31, 463 (1960)
4. R.H. Jones, D.R. Olander, and V.R. Kruger, J. Appl. Phys. 40, 4641 (1979)
5. D.F. Register and S. Trajmar, Phys. Rev. A 29, 1785 (1984)
6. H. Tanaka, S.K. Srivastava, and A. Chutjian, J. Chem. Phys. 69, 5329 (1978)

R-MATRIX METHOD FOR VIBRATIONAL EXCITATION AND DISSOCIATIVE ATTACHMENT

P.G. Burke*, L.A. Morgan* and C.J. Noble†

*Queen's University, Belfast, N. Ireland.

†Royal Holloway College, Egham, England.

‡SERC Daresbury Laboratory, Warrington, England.

We have extended the R-matrix theory of vibrational excitation and dissociative attachment described by Schneider et al¹. The formalism has been applied to the case of electron impact on N₂, F₂ and H₂⁺ targets using generalized versions of the multi-centre R-matrix method with numerically defined continuum basis functions which we have previously used for calculations at fixed internuclear separations². In the generalised R-matrix approach the full Hamiltonian of the scattering system including nuclear kinetic energy and Bloch terms is diagonalized within a finite hypersphere in configuration space corresponding to values of the scattering electron coordinate r_{e} and to values of the internuclear coordinate R such that $A_{\text{in}} < R < A_{\text{out}}$. The Hamiltonian matrix is calculated by expanding the scattering wavefunction in the form

$$\Psi_{\text{e}} = \sum_{ij} \chi_i(1\dots N+1; R) \theta_{ij}(R) C_{ijk}$$

where χ_i denotes a fixed-nuclear R-matrix state, θ_{ij} is a nuclear basis function and the C_{ijk} are variational constants. Generalized R-matrices are constructed on the boundaries of the internal region and are then used to solve both the electronic and nuclear problems in the external region.

We have used this approach to calculate low energy vibrational excitation cross sections for both vibrational excitation and dissociative attachment cross sections for e⁻ - F₂ scattering. Eigenphase sums are also calculated. In these calculations we use a static exchange plus polarization model³ and so include both resonant and non-resonant effects. Our results will be compared to previous calculations and where possible to experiment.

In the N₂ and F₂ cases, crossings of the (N+1)-electron R-matrix states are either absent at low energies (this was the situation found by Schneider et al⁴ in their single-centre R-matrix calculations for the e⁻ - N₂ system) or infrequent. By way of contrast, we find for e⁻ - H₂⁺ scattering, using a two-state model^{5,6}, such crossings are extremely numerous and simple extensions of the basic theory are not adequate. We conjecture that this situation will be encountered

frequently in multistate calculations. We will describe the methods we have evolved to overcome these difficulties and present those results which are available by the time of the conference. Another feature which has emerged from the calculations already completed is that in many cases it is important to make at least some explicit allowance for dissociation processes if the appearance of spurious resonances is to be avoided.

References

1. S.I. Schneider, M. LeDourneuf and P.G. Burke, J.Phys. B: At. Mol. Phys. **12**, L365 (1979).
2. P.G. Burke, C.J. Noble and S. Salvini, J.Phys. B: At. Mol. Phys. **16**, L113 (1983).
3. L.A. Morgan and C.J. Noble, J.Phys. B: At. Mol. Phys. **17**, L369 (1984).
4. S.I. Schneider, M. LeDourneuf and Vo Ky Lan, Phys. Rev. Lett. **43**, 1926 (1979).
5. J. Tennyson, C.J. Noble and S. Salvini, J.Phys. B: At. Mol. Phys. **17**, 905 (1984).
6. J. Tennyson and C.J. Noble, J.Phys. B: At. Mol. Phys. **18**, 155 (1985).

THE APPLICATION OF COHERENT RENORMALIZED MULTICENTER POTENTIAL MODEL (CRMPM) WITH INTRAMOLECULAR MULTIPLE SCATTERING (IMS) TO VIBRATIONALLY ELASTIC AND INELASTIC ELECTRON-H₂ SCATTERING*.

Lee Mu-Tao, L.F.C. Botelho* and L.C.G. Freitas

Departamento de Química, Universidade Federal de São Carlos, 13.560, São Carlos, SP, Brasil

Recently, the coherent version of renormalized multicenter potential model¹ including multiple scattering effect has been applied to study the elastic scattering of electron by several molecules²⁻³ at the intermediate and high energies (20-1500 eV). Despite its simplicity, this theoretical model proves its efficiency to treat the elastic e⁻-molecule problem particularly at the higher incident energies. In this abstract, we report the extension of CRMPM-IMS to obtain the cross sections of the vibrationally elastic and inelastic (0 → 1) scattering of electron by H₂ in the 20-81.6 eV energy range.

In this calculation, the static interaction potential is derived from the Wang's⁴ valence-bond type wavefunction. The initial and final vibrational wavefunctions are of Morse type. The intramolecular multiple scattering is taken in account along the formalism of Hayashi and Kuchitsu⁵; we include in this calculation up to double scattering.

Our theoretical result are compared with the experimental measurements of Trajmar et. al.⁶⁻⁷. There is an agreement in the vibrationally elastic cross sections in the covered energy range. Our vibrational excitation (0 → 1) cross sections also agree qualitatively with experiments, however, our theory overestimates the magnitude of the cross sections.

* Work supported by CNPq, grant nº 40.4585/82-QU.

* L.F.C. Botelho thanks CNPq for the scholarship.

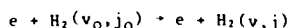
References

1. M.T. Lee and L.C.G. Freitas, *J. Phys. B: At. Mol. Phys.* **14** 4091 (1981).
2. A. Jain, L.C.G. Freitas, Lee Mu-Tao and S.S. Tayal, *J. Phys. B: At. Mol. Phys.* **17** L185 (1984).
3. L.F.C. Botelho, L.C.G. Freitas, Lee Mu-Tao, A. Jain and S.S. Tayal, *J. Phys. B: At. Mol. Phys.* **17** L641 (1984).
4. W. Wang, *Phys. Rev.* **21** 579 (1928).
5. H. Hayashi and K. Kuchitsu, *J. Phys. Soc. Japan* **21** 1154 (1966).
6. S. Trajmar, P. Trajmar and J.K. Rice, *J. Chem. Phys.* **52** 4502 (1970).
7. S. Trajmar, P. Trajmar, J.K. Rice and A. Kupperman, *J. Chem. Phys.* **52** 4515 (1970).

THEORETICAL CROSS SECTIONS FOR LOW-ENERGY $e-H_2$ SCATTERING*

A. N. Feldt, T. L. Gibson†, M. A. Morrison, and B. C. Saha
Dept. of Physics & Astronomy, Univ. of Oklahoma, Norman, Okla. 73069 USA

We have calculated cross sections for the electronically elastic scattering processes



for target vibrational quantum numbers $v_0 = 0, 1$ and $v = 0, 1, 2$, and for rotational quantum numbers $j_0 = 0, 1$ and $j = 0, 1, 2, 3$. Scattering energies studied range from near each excitation threshold to 10.0 eV.

These calculations were based on laboratory-frame close-coupling (LFCC) theory.¹ At low energies, the computationally simpler adiabatic nuclei (AN) theory² could not be used, as it yields inelastic cross sections that are in error by hundreds of percent.³ In the LFCC calculations, sufficient channels were included to converge the cross sections to better than 1%. Vibrational wave functions were determined by numerical solution of the nuclear Schrodinger equation.

Static, exchange, and polarization terms in the electron-molecule interaction potential were based on newly-determined near-Hartree-Fock $X^1\Sigma_g^+$ wave functions at 11 internuclear separations from 0.5 to 2.6 a_0 . The static contribution was calculated from the H_2 charge distribution by numerical quadrature. Exchange was treated via a local, free electron gas model potential⁴; to obtain an exchange potential best suited to inelastic $e-H_2$ scattering, this potential was tuned in the Σ_u electron-molecule symmetry. Polarization effects were incorporated using a variationally-determined, parameter-free potential⁵ that takes account of non-adiabatic effects via a non-penetrating approximation.⁶

Figure 1a shows integrated LFCC cross sections for the vibrational excitation $(v_0 = 0) \rightarrow (v = 1)$: the sums over final rotational states of ro-vibrational cross sections for $(v_0 = 0, j_0 = 0) \rightarrow (v = 1, j)$. These theoretical results are compared to cross sections derived from beam⁶ and swarm⁷ experiments.

Theoretical and experimental differential cross sections at 4.5 eV scattering energy^{8,9} are compared in Fig. 1b. Agreement with beam data at other energies⁶ studied is comparable to that in this figure.

For completeness, we show in Fig. 2 total integrated cross sections (summed over rovibrational states).^{10,11} The elastic contributions to these results were taken from AN calculations in which exchange was included exactly via an iterative method¹²; the inelastic contributions came from the LFCC model-exchange study described above.

References:

1. A. M. Arthurs and A. Dalgarno, Proc. Roy. Soc. (London) A256, 540 (1960); R. J. W. Henry, Phys. Rev. A 2, 1349 (1970).
2. See M. A. Morrison, Austr. J. Phys. 36, 239 (1983) and refs. therein.
3. M. A. Morrison, A. N. Feldt, and B. C. Saha, Phys. Rev. A 30, 2811 (1984).
4. T. L. Gibson and M. A. Morrison, Phys. Rev. A 30, 2497 (1984).
5. A. Temkin, Phys. Rev. 107, 1004 (1957).
6. H. Ehrhardt, L. Langhans, F. Linder, and H. S. Taylor, Phys. Rev. 173, 222 (1968).
7. R. W. Crompton, D. K. Gibson, and A. G. Robertson, Phys. Rev. A 2, 1386 (1970).
8. S. F. Wong and G. J. Schulz, Phys. Rev. Lett. 32, 1089 (1974).
9. F. Linder and H. Schmidt, A. Naturforsch. 26a, 1603 (1971).
10. J. W. Ferch, W. Raith, and K. Schroder, J. Phys. B 13, 1481 (1980).
11. Robert Jones (private communication, 1984).
12. L. A. Collins, D. W. Robb, and M. A. Morrison, Phys. Rev. A 21, 488 (1980).

*This research was supported by the Office of Basic Energy Sciences, U. S. D.O.E., and by a grant (to MAM) from the Research Corporation.

†Current Address: Cal Tech, Pasadena, CA 91125, U.S.A.

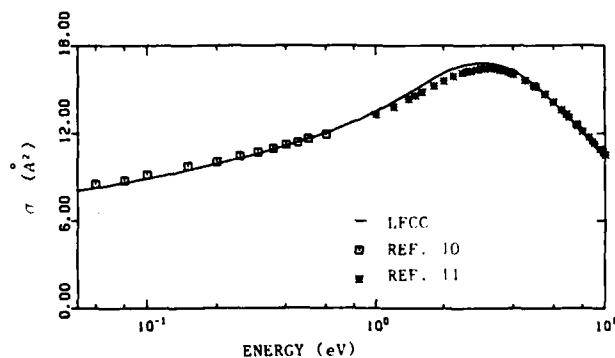
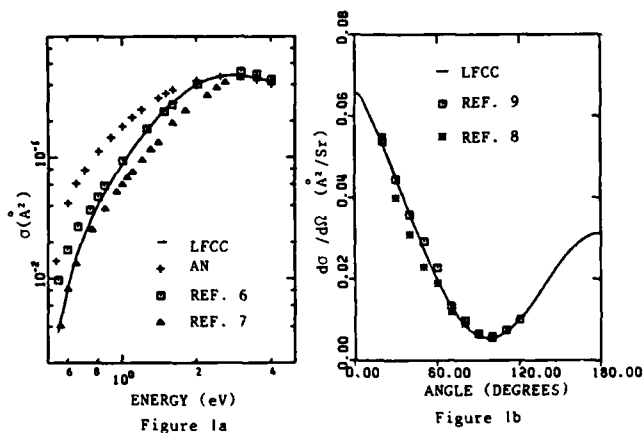


Figure 2.

SCATTERING OF ELECTRONS BY HYDROGEN MOLECULE IN INDEPENDENT UNITED ATOM MODEL

N.S. Rao* and H.S. Desai**

* Physical Research Laboratory, Theoretical Physics Area, Navrangpura, Ahmedabad 380 009, India

** Physics Department, Faculty of Science, M.S. University, Baroda 390 002, India

In recent years, theoreticians¹ (Khare and Jhansar) have proposed an "independent united atom model" (IUAM) to study the molecular problems in terms of atomic problems. This model is similar to IAM (independent atom model) and more reliable than IAM. Using this IUAM we studied the collisional cross sections for elastic scattering of electrons by hydrogen molecule in the incident energy range from 100 to 800 eV. The present results are found to be in good agreement with the compared data².

According to the IUAM¹ the scattering is considered in terms of the scattering by independent atoms again centered at the various nuclei of the molecule but the atom is obtained by reducing internuclear distance (R) to zero. In the present paper, \bar{e} -H₂ scattering is considered in terms of two helium like atoms, centered at the two nuclei, each scattering independently. Half of the scattering amplitude³ from each atom is added coherently to obtain scattering amplitude due to molecule.

$$\bar{f}(H_2) = 0.5 f(He) \left[1 + \frac{\sin 2 qR}{2 qR} \right] \quad (1)$$

In the present work, the Born scattering amplitude for helium atom³ is improved⁴ by including third Born term in the scattering amplitude to study the collisional cross sections for hydrogen molecule through (1). The differential and total cross sections (DCS, TCS) are calculated at $E \leq 800$ eV. The TCS results are shown in table 1 along with the other data². These results are found to be in good agreement with the compared experimental results².

The present TCS can be further improved by the inclusion of exchange corrections⁵. The DCS results will be presented at the time of Conference.

N.S.R. is thankful to Physical Research Laboratory, Ahmedabad, India, for the award of a Post-Doctoral Fellowship.

Table 1. Total Cross Sections in a.u., for elastic scattering of electron by H₂.

E eV	Present	Others ²	
100	9.88	9.01	9.25
200	5.86	5.76	5.89
300	4.28	4.36	4.48
400	3.38	3.45	3.56
500	2.84	2.97	2.98
600	2.44	2.55	2.57
700	2.16	2.28	2.24
800	1.93	-	2.00

References

1. S.P. Khare and B.L. Jhanwar, XIII I.C.P.E.A.C., 225 (1983).
2. B. Van Wingerden et al., J. Phy. B **13**, 3481 (1980)
3. N.S. Rao and H.S. Desai, Pramana **17**, 309 (1981)
4. N.S. Rao and H.S. Desai, J. Phy. B **16**, 863 (1983)
5. N.S. Rao and H.S. Desai, V-N.W.A.N.P., 69 (1984)

VIBRATIONAL AND RO-VIBRATIONAL DIFFERENTIAL CROSS SECTIONS FOR ELECTRON SCATTERING FROM H_2

J. E. Furst, M. Mahgerefteh and D. E. Golden

Department of Physics and Astronomy, Univ. of Okla., Norman, Oklahoma 73019 USA

We have recently measured differential cross sections for the elastic scattering of electrons from He^1 and H_2^1 , using a time-of-flight (TOF) technique, with an energy resolution of 0.5 eV. We have now combined the TOF technique with an electrostatic hemispherical monochromator, to obtain a higher energy resolution. The electron gun gives an electron pulse of width < 5 nS. The stationary detector views electrons scattered from the background gas. The count rate in this detector is used to normalize the count rates in the rotating detector, allowing for variations in electron beam current and molecular beam density. This normalization procedure is especially important at low energies and together with the monochromator allows us to measure vibrational ($v = 0 \rightarrow 1, \Delta j = 0$) and ro-vibrational excitation cross sections for H_2 , from about 1 to 10 eV.

We have measured relative differential cross sections over the range 30° to 120° . These have been placed on an absolute scale by normalization to our standard He cross sections, which have been put on an absolute scale by phase shift analysis. Total and momentum transfer cross sections have then been obtained from these measurements.

References

1. D. E. Golden, J. E. Furst and M. Mahgerefteh, Phys. Rev. A 30 1247 (1984).
2. J. E. Furst, M. Mahgerefteh and D. E. Golden, Phys. Rev. A 30 2256 (1984).

AB INITIO POLARIZATION POTENTIALS FOR e^- -MOLECULE SCATTERING.

E. Ficocelli Varracchio and U.T. Lamanna.

Department of Chemistry, University of Bari, Via Amendola 173,
70126 Bari, ITALY.

An accurate theoretical study of low energy e^- -molecule scattering requires a detailed knowledge of the dynamical polarization, induced on the target molecule by the electric field of the colliding charged projectile. Such a quantity is expected to be, in general, non local, energy (or velocity) dependant and, at the same time, it should also contain in its structure an exchange contribution, deriving from the identity of the projectile and target electrons.

A completely ab initio approach to the above interaction can be obtained, in principle, by using the mathematical techniques of many-particle systems, based on the Green's function formalism. While such an approach has already been implemented, a few years ago, for atomic targets¹, it is only more recently that the first few numerical applications have appeared in the literature for the e^- -molecule problem². It should be pointed out, anyway, that the formulation of Ref. [2] is completely perturbative in its structure, while it is very likely that in actual applications of the theory it might prove necessary to go beyond such a perturbative scheme. It can be readily shown that a basic ingredient of the non perturbative theory is represented by the so called Bethe-Salpeter amplitude, defined as

$$X_m(i, i') = \langle \Psi_m | T [\Psi(i) \Psi^\dagger(i')] | \Psi_0 \rangle \quad (1)$$

where Ψ (Ψ^\dagger) are electron destruction (creation) field operators and T is Wick's time ordering operator (see Ref. [1] for more details). The quantity in (1) physically represents the transition amplitude between the Ψ_0 (ground) and Ψ_m (excited) target states and it is then intuitive to foresee that the dynamic polarization potential will be represented in terms of such quantities.

We have recently shown that the above X_n amplitudes can more simply be evaluated within numerical schemes of the order of complexity of Hartree-Fock calculations, but that are at the same time able to sum up infinite classes of diagrams, corresponding to the R.P.A. formulation of many-body theories³. We are presently applying such formulation to the e^- -H₂ system, for which we are

eventually interested into a determination of the vibro-rotational excitation cross sections.

The full equations of the theory, relating the Bethe-Salpeter amplitudes of eq. (1) to the dynamical polarization potential, along with explicit numerical results for the e^- -H₂ system, will be illustrated in detail at the Conference.

References

1. Gy. Csanak, H.S. Taylor and R. Yaris, Adv. At. Mol. Phys. **7**, 287 (1971).
2. A. Klonover and U. Kaldor, J. Phys. B **11**, 1623 (1978).
3. E. Ficocelli Varracchio, J. Phys. B **17**, L611 (1984).

LOW-ENERGY SCATTERING OF ELECTRONS FROM Li_2

N. T. Padial

Institute for Modern Optics, University of New Mexico, Albuquerque, New Mexico 87131, USA

We present theoretical results of electron- Li_2 scattering cross sections in the fixed-nuclei approximation employing an exact treatment of the static and the exchange interactions. The static potential is augmented by a parameter-free model¹ of the correlation-polarization interaction. This model, which uses the free-electron gas correlation for short distances and the asymptotic form of the polarization, has a simple dependence on the molecular charge densities and polarizabilities.

Earlier applications of this approximation for H_2 , N_2 , HCl , and HCl_2 gave very satisfactory results. In those cases, the short-range part of the model correlation-polarization potential was much smaller than the static potential. For Li_2 the model polarization part represents a much larger contribution to the total potential and, consequently, poses a more stringent test to the theory.

The scattering equations are solved using an integral equations formulation of the close-coupling approximation. We incorporated exchanged effects through a separable-potential formulation. All calculations were carried out at the equilibrium internuclear separation and in the molecular body-fixed frame within the fixed-nuclei approximation.

The scattering equations were solved for eight collisional symmetries from Σ_g^+ to Π_u for incident electron energies below 1 eV. For higher energies, we increased this number to $M_L = 7$, at 10 eV. We completed our calculations for the entire energy range with the unitarized-Born approximation values for symmetries up to $L_L = 38$. The maximum order of channel angular momentum is 38 for gerade and 37 for ungerade symmetries.

The theoretical cross section includes the elastic and rotational contributions and is compared to the experimental results² that include elastic, rotational, vibrational, inelastic, and ionization cross sections. Except near resonances, the effect of vibrational contributions will probably be small. Due to the neglect of the inelastic and the ionization processes in theory, our results are considerably smaller than the experimental data in the higher energy range. A comparison with the electron-Li scattering gives some validity to this explanation. In this case, a two-state close-coupling calculation³ shows that the contribution of the 2s-2p transition increases the total cross sections to more than twice the elastic 2s-2s part at 10 eV.

In the intermediate energy regime (1-5 eV) the results are in reasonable agreement with the experiment. At low-energies (<1 eV), the cross sections are sensitive to the model polarization as is demonstrated by considering several cutoff forms.

References

1. N. T. Padial and D. W. Norcross, Phys. Rev. A **29**, 1742 (1984); we used Eq. 9 of this paper.
2. T. G. Miller, A. Kasdan and B. Bederson, Phys. Rev. A **25**, 1777 (1982).
3. D. W. Norcross, private communication; see also J. Phys. B **4**, 1458 (1971).

ELECTRON ELASTIC CROSS SECTIONS MEASUREMENTS FOR O_2
AT INTERMEDIATE ENERGY (300 - 1000 eV) RANGE*.

Ione Iga, Lee Mu-Tao, J.C. Nogueira, R.S. Barbieri[†] and Maria Cristina A. Lopes^{*}

Departamento de Química, Universidade Federal de São Carlos, 13.560, São Carlos, SP, Brasil

Although the oxygen molecule is one of the major constituent of the earth's atmosphere and the $e^- - O_2$ interaction is one of the most important aim in the atmospheric physics, there are relatively few measurements of the elastic and excitation cross sections for the electron- O_2 scattering. In this communication, we report the differential, integral and momentum transfer cross sections (DCS) for electrons elastically scattered by O_2 . In our experiments¹ we use the crossed electron beam-molecular beam scattering method. The scattered electrons are energy-selected by a Möllenstedt velocity analyzer² and counted by a channeltron. The energy resolution was 1.5 eV and the angular resolution is about 0.2° . The pressure of the target beams of N_2 and O_2 was calibrated by a McLeod gauge.

The measurements were made for scattering angles from 5 to 120° and incident energies of 300, 400, 500, 800 and 1000 eV. The absolute values of the DCS were obtained by the relative flow technique³, where absolute differential cross sections for N_2 ^{4,5} were used as secondary standards. Errors in our DCS were estimated to be 16%.

Fig. 1 shows some of the absolute values of the DCS for O_2 in comparison to experimental values of Daimon⁶ et. al. with excellent agreement. Comparison with the theoretical results from Independent Atom Model (IAM) also shows fairly good agreement.

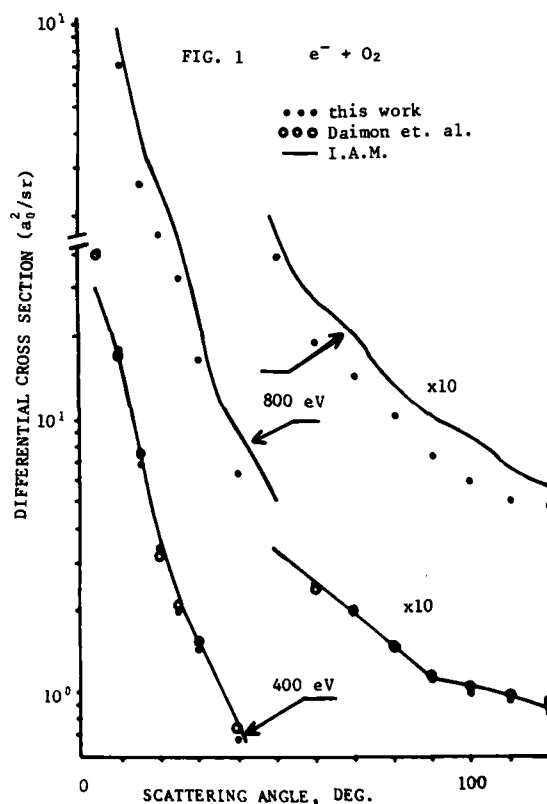
* Work supported by CNPq, grant nº 40.3582/82.

[†] R.S. Barbieri and Maria C.A. Lopes thank CNPq for the scholarship.

References

1. I. Iga, J.C. Nogueira and Lee Mu-Tao, J. Phys. B: Atom. Molec. Phys. **17**, L185 (1984).
2. G. Möllenstedt, Optik **9**, 473 (1952).
3. S.K. Srivastava, A. Chutjian and S. Trajmar, J. Chem. Phys. **63**, 2659 (1975).
4. R.H.J. Jansen, F.J. de Heer, H.J. Luyken, B. van Wingerden and H.J. Blaauw, J. Phys. B: Atom. molec. Phys. **9**, 185 (1976).
5. R.D. DuBois and M.E. Rudd, J. Phys. B: Atom. Molec. Phys. **9**, 2657 (1976).
6. Hiroshi Daimon, Shigeo Hayashi, Tomotsu Kondow and Kozo Kuchitsu, J. Phys. Soc. of Japan **51**, 2641

(1982).



INCLUSION OF EXCHANGE IN THE NON-ITERATIVE PDE METHOD: APPLICATION TO e-N₂ SCATTERING

C. A. Weatherford,* K. Onda,* A. Temkin

Atomic Physics Office
 Laboratory for Astronomy and Solar Physics
 NASA/Goddard Space Flight Center
 Greenbelt, Maryland 20771 USA

* Permanent address: Dept. of Physics, Florida A&M University, Tallahassee, FL

+ Present temporary address: ISAS, Tokyo 153, JAPAN

We have developed a method of including exchange exactly¹ in the framework of the noniterative partial differential equation (PDE) technique². The method has been checked by comparing results in the static-exchange approximation. Σ_g partial wave results are given in Table I.

Table I: e-N₂ Σ_g static-exchange results^a

k^2	b.	c.	present
0.1	18.86 (2.311)	15.16 (2.406)	14.95 (2.417)
0.3	-- (1.308)	-- --	9.76 (1.983)
0.5	6.97 (1.524)	6.83 (1.723)	6.81 (1.747)
1.0	3.09 (1.043)	3.17 (1.296)	3.50 (1.350)

a. Entries are cross section in Å², and (eigenphase sums, in radians)

b. Results of Collins, Robb, & Morrison, Phys. Rev. A **21**, 488 (1980)

c. Collins & Schneider (unpublished).

Given the entirely different analytic and numerical techniques used in these calculations, we consider the agreement to be satisfactory-particularly with the new unpublished results of Collins and Schneider.

Our second calculation included a static polarization potential originally adjusted using an HFEGE approximation for exchange³. Use of that potential with the present incorporation of exact exchange showed that exact exchange requires a diminution in strength of that polarization potential. Wishing to retain its qualitative features, however, we have now used a scaled version of that polarization potential. Results are given in Fig. 1 compared to various experiments and calculations.

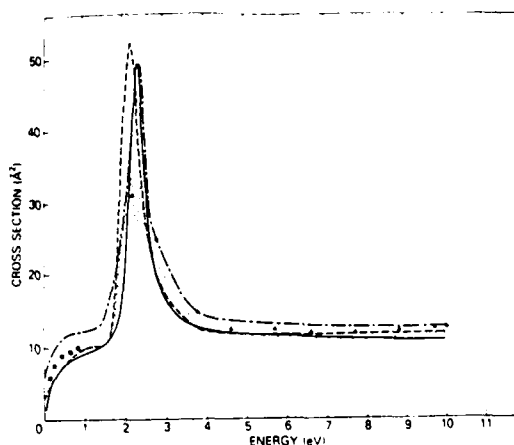


Fig. 1 Present SEP results (solid curve) compared to other calculations and experiments. References and details are given in Ref. 1.

The overall agreement with experiment and other SEP calculations is very good. At higher energies ($k^2 \leq 10$ eV) and particularly at low energies ($k^2 < 1.5$ eV), however, our results are somewhat lower than experiment. It is significant that such an increase was found by Rumble et al⁴ when a static potential based on a multi-configuration (MCSF) N₂ ground state was used. We are therefore implementing a calculation with the better ground state⁵ to test these changes in the presence of exact exchange. Results will be presented at the meeting.

References

1. C. A. Weatherford, K. Onda, A. Temkin, Phys. Rev. A (submitted).
2. E. C. Sullivan and A. Temkin, Comp. Phys. Comm. **25**, 97 (1982).
3. K. Onda and A. Temkin, Phys. Rev. A **28**, 621 (1983).
4. J. R. Rumble, W. J. Stevens, D. G. Truhlar, J. Phys. B **16**, L113 (1984).
5. J. R. Rumble, C. A. Weatherford, K. Onda, A. Temkin, (work in progress).

EXPERIMENTAL MEASUREMENTS OF SHAPE RESONANCES
USING A POSITION SENSITIVE DETECTOR

Fred Currell, Tim Reddish and John Comer

Physics Department, Manchester University, Manchester M13 9PL, UK

An electron spectrometer has been employed to observe resonances in the differential cross sections for the excitation of vibrational levels of the ground states of N_2 , CO and CO_2 . A position sensitive detector has been used in order to measure many cross sections simultaneously and so produce a significant gain in sensitivity¹. Many energy-loss spectra are collected, each at a different electron impact energy and a surface is produced representing the differential cross section as a function of the two variables. An example of the results obtained using this technique is illustrated in figure 1. Taking a section in the energy-loss direction shows peaks corresponding to the excitation of the $v=2-10$ levels of the $X^1\Sigma_g^+$ state. A section in the

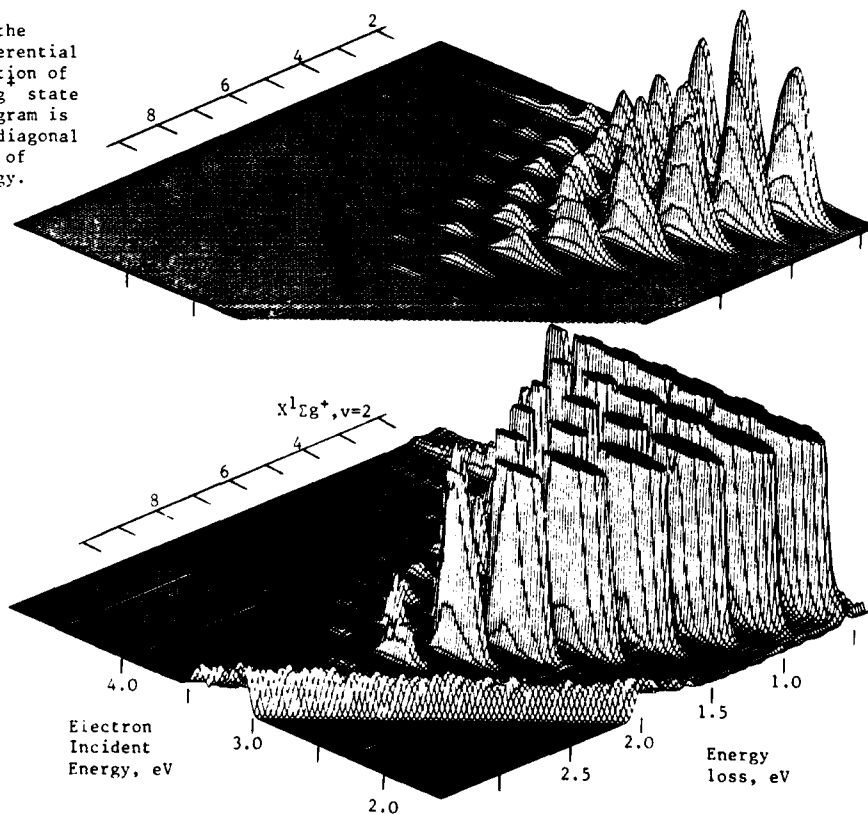
impact energy direction, however, shows the differential cross section for the excitation of specific vibrational levels. These contain intense features due to the $2^1\Sigma_g$ shape resonance in N_2 .

This resonance has been the subject of intense experimental and theoretical work. Measurements of the differential cross sections as a function of scattering angle will be presented together with corresponding measurements in other systems.

Reference

1. P J Hicks, S Daviel, B Wallbank and J Comer, J Phys E:Sci Instrum, **13**, 713 (1980)
T Reddish, B Wallbank and J Comer, J Phys E:Sci Instrum, **17**, 100 (1984)

FIGURE 1 The surface shows the experimentally measured differential cross section for the excitation of the $v=2-10$ levels of the $X^1\Sigma_g^+$ state of N_2 at 60° . The lower diagram is expanded vertically and the diagonal ridge is due to a background of electrons close to zero energy.



VIBRATIONAL EXCITATION OF N_2 by ELECTRON IMPACT

S.Yagi, T.Takayanagi, K.Wakiya and H.Suzuki
Department of Physics, Sophia University, Chiyoda-ku, Tokyo 102, Japan

Y.Fujita, K.Hoshiba, S.S.kano and H.Takuma
Institute for Laser Science, University of Electro-Communications, Chofu-shi, Tokyo 182, Japan

The vibrational excitation of N_2 by electron at the incident energy of 1.8eV to 4eV is known to be affected by the resonance with the $N_2^-(^2\Pi_g)$. We report the cross sections for the vibrational excitations up to $V=11$ at this region of the impact energies. Also, the differential cross section for the $V=1$ excitation at 1eV - 1.5eV is reported.

The experimental apparatus is the same as described in the proceeding of the XIII ICPEAC¹. The energy resolution is 30 meV (FWHM) with the incident electron current of 5nA and the electron beam crosses the N_2 beam at the collision center at 90 deg. For the collection of the low energy electrons, we utilized an additional "collecting" electrode and the overall transmission efficiency of electrons are measured by the loss spectrum of He. The measured differential cross section were normalized by the elastic scattering signal at 30 deg to derive the absolute values. Figure 1 shows the energy dependence of the vibrational excitation to the $V=11$ level at the scattering angle of 30 deg. The solid curve in Fig.1 is the back ground to be subtracted. Much more precise information on the coupling between N_2 and N_2^- states will be given by this experiment.

Below the incident energy of 1.5eV, we have not much data on the excitation function of N_2^2 . Figure 2 is the data of the absolute DCS to the $V=1$ level at the impact energy of 1.5eV. Normalization was performed based on the data reported by Shyn et al³. The dotted curve in the figure is the angular dependence of the pure resonance ($^2\Pi_g$) scattering normalized at 30 deg. It is known that, at 2.2eV of the incident energy, the resonance ($^2\Pi_g$) scattering is dominant. In the present experiment at 1.5eV, the resonance ($^2\Pi_g$) still plays an important role but the contribution from non resonance (mainly Σ_g) is apparent. A detailed discussion will be given at the conference.

This work is supported by the Grant-in-aid for Fusion Research of Ministry of Education.

References

- 1) S.Ito et al. Abstracts of Contributed papers XIII ICPEAC P.247C Berlin (1983)
- 2) A.G.Engelhardt, A.V.Phelps, and C.G.Risk, Phys.Rev.135 A 1566, (1964)
- 3) T.W. Shyn and G.R.Carignan, Phys.Rev. A 22, 923 (1980)

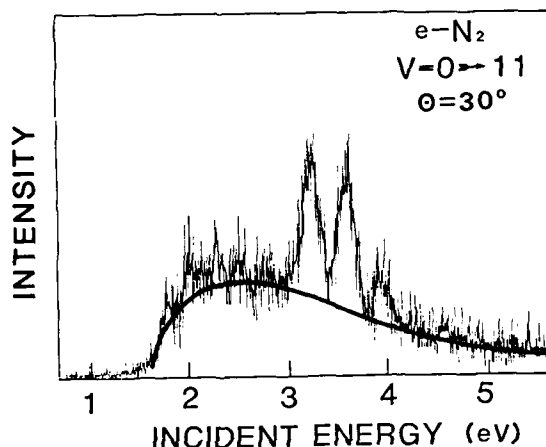


FIG.1

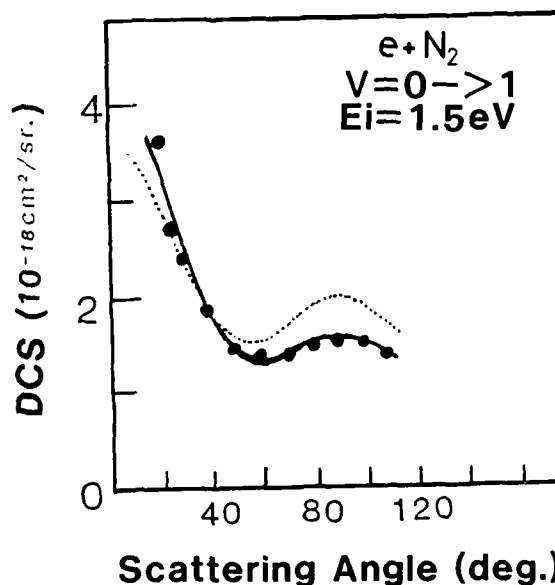
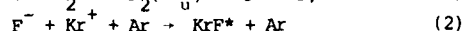
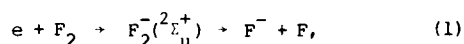


FIG.2

OBSERVATION OF VIBRATIONAL EXCITATION OF F_2 BY ELECTRON IMPACT

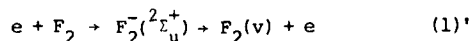
Y.Fujita, K.Hoshiba, S.S.Kano and H.Takuma
 Institute for Laser Science, University of Electro-Communications, Chofu-shi, Tokyo 182 Japan
 S.Yagi, T.Takayanagi, K.Wakiya and H.Suzuki
 Department of Physics, Sophia University, Chiyoda-ku, Tokyo 102 Japan

It is important to elucidate the vibrational excitation of F_2 by low energy electron impact from both the pure and applied scientific viewpoints. This is because the process is closely related to dissociative electron attachment, which is highly important for the kinetics of the electron beam pumped excimer lasers such as KrF or XeF. In the laser medium of KrF



are suggested to be the dominant processes for the fuel production. Ab initio calculations¹⁾ show that the potential curve of the intermediate state, $F_2(^2\Sigma_u^+)$, of dissociative electron attachment crosses near the equilibrium internuclear separation of $F_2(^1\Sigma_g^+)$. Consequently this process is supposed to have large cross section at very low incident electron energy (< 1eV), which has been confirmed by recent measurements²⁾.

In the vibrational excitation by low energy electron impact (< 2eV), the same intermediate state, $F_2(^2\Sigma_u^+)$, as that of the dissociative attachment is concerned, and the resonant scattering



is expected to play the dominant role. These dissociative attachment and the vibrational excitation cross sections are calculated by the same resonant scattering theory. Thus, once the cross section for the process (1)' is measured by experiments, we will be able to predict the cross section for the process (1) or v.v. Semiempirical calculations have been made by Hall³⁾ and Bardsley et al.⁴⁾ to know these cross sections by the use of different methods. The obtained values for the cross sections are almost the same for the dissociative attachment. However, the cross sections for vibrational excitation by Hall (about 10^{-16} cm² for v=1 peak value) are larger by almost one order of magnitude than that by Bardsley. Wong et al.⁵⁾ also calculated these cross sections by R-matrix method for several sets of the resonance parameters. Considering the present status of these theories of vibrational excitation of F_2 , the measurement are highly important to test these calculations.

The experimental apparatus was the same as we

reported in the XIII ICPEAC⁶⁾. Because of extremely corrosive nature of F_2 , the energy selector and analyzer systems are differentially pumped separately. The sample, delivered from Central Glass Co, is F_2 (10%) in He buffer. The overall resolution of our apparatus is about 30 meV (FWHM) at the incident electron current of 5 nA.

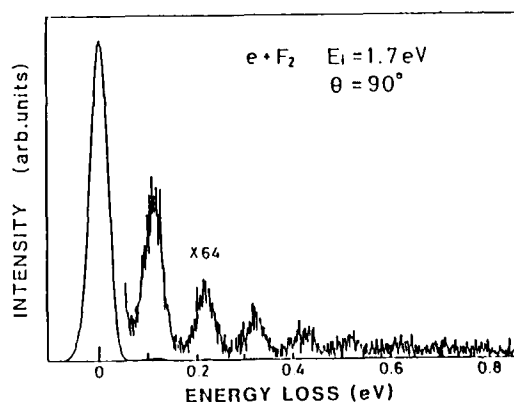
Typical energy loss spectrum of F_2 at the impact energy 1.7 eV and scattering angle 90° is shown in the figure. The vibrational peaks (v=0 through 7) are observed and the peak intensity as a function of v does not decrease drastically. Also, the angular distributions of v=1,2 vibrational excitations show the Σ_u partial wave characteristics. These facts are considered to be the evidence of the resonant scattering. It must be noted that the elastic peak of the figure contains the signals of elastic scattering by He.

The differential cross sections of vibrational excitation of F_2 at the impact energy less than 2 eV will be discussed at the conference.

This work is supported by the Grant-in-aid for Fusion Research of Ministry of Education.

References

- 1) T.N.Rescigno and C.F.Bender, J.Phys. B9,1329 (1976)
- 2) P.J.Chantry, Bul.Am.Phys.Soc. 24,134 (1979)
- 3) R.J.Hall, J.Chem.Phys. 68,1803 (1978)
- 4) J.N.Bardsley and J.M.Wadehra, J.Chem.Phys. 78,7227 (1983)
- 5) C.F.Wong and J.C.Light, Phys.Rev.A 30,2264 (1984)
- 6) S.Ito et al. Abstracts of Contributed papers XIII ICPEAC P.274 (Berlin 1983)



ELECTRON ATTACHMENT TO H₂O, SO₂ and C₃F₈ in Ar, N₂, and CH₄W. C. Wang,^{*} M. A. Fineman,⁺ and L. C. Lee^{*}^{*} Department of Electrical & Computer Engineering, San Diego State University, San Diego, California 92182 USA⁺ Department of Physics, San Diego State University, San Diego, California 92182 USA

Electron attachment processes for electronegative gases (H₂O, SO₂ or C₃F₈) in trace amounts in a few hundred torr of buffer gas (Ar, N₂, or CH₄) were investigated using a parallel-plate drift-tube apparatus. Electron attachment rate constants for the electronegative gases were measured as a function of E/N (or the mean electron energy) in various buffer gases.

In this experiment, electrons were produced by irradiation of the cathode with ArF (193 nm) or KrF (248 nm) excimer laser photons. The transient current induced by the electron motion between the electrodes under an applied electric field was observed. This current is equal to

$$i(t) = eN_e W/d \quad (1)$$

where N_e is the number of electrons between the electrodes, W is the electron drift velocity in the buffer gas, and d is the electrode spacing.

When an electronegative gas is added to the buffer gas, electrons will be attached and the current will be reduced to

$$i'(t) = eN_e' W' e^{-v_a t}/d \quad (2)$$

Using the data from a run without electronegative gas (Eq. 1) and one of same buffer gas but with electronegative gas (Eq. 2), we can plot $\ln(i'/i)$ versus t , and we can determine the electron attachment rate v_a , and the attachment rate constant for a two-body process $k_a = v_a/[M]$, where $[M]$ is the concentration of the electron attachers. The N_e' and W' values can be different from the values of N_e and W . The data were analyzed at sufficient times after the laser pulses such that N_e , N_e' , W and W' are independent on time.

With this newly developed method, we have measured the electron attachment rate constants for several electronegative gases (H₂O, SO₂ and C₃F₈) in several buffer gases (Ar, N₂, and CH₄) that are frequently used in diffuse-discharge switches. For H₂O in Ar, the electron attachment rate constant, k_a , increases with increasing E/N from 2-15 Td. At E/N = 15 Td, $k_a = 1.3 \times 10^{-10}$ cm³/s. For H₂O in N₂, the electron attachment rate constants are very small for E/N in the 8-24 Td region. At E/N ≤ 8 Td, electron attachment due to the formation of a "temporary" negative ion is observed. The "temporary" negative ion has also been observed in the electron attachment to H₂O in CH₄. The lifetime of the "temporary" negative ion is about 200 ns. The

"apparent" electron attachment rate constant for H₂O in CH₄ decreases with increasing E/N, for example, $k_a = 1.6 \times 10^{-11}$ cm³/s at E/N = 1 Td and $k_a = 0$ at 15 Td.

The electron attachment to C₃F₈ in Ar has also been investigated. The electron attachment rate constant decreases with increasing E/N. At E/N = 1 Td, $k_a = 6 \times 10^{-10}$ cm³/s. For C₃F₈ in N₂, the k_a value increases with increasing E/N. At E/N = 25 Td, $k_a = 1.2 \times 10^{-10}$ cm³/s. We also find that the k_a value increases with increasing E/N for C₃F₈ in CH₄, for which $k_a = 4 \times 10^{-10}$ cm³/s at E/N = 30 Td.

The electron attachment due to SO₂ in Ar is currently under investigation. The electron attachment rate constant increases with increasing E/N. We have used both the ArF (193 nm) and the KrF (248 nm) excimer laser photons for producing the photoelectrons in this experiment. Since the laser photons are absorbed by SO₂, it is interesting to study the effect of photodissociation fragments on the observed electron attachment process. At 193 nm, SO₂ has a large absorption cross section and the photoexcitation at this wavelength can lead to dissociation into SO + O. The electron attachment rate constants measured at 193 nm will be not only due to SO₂ but also due to these photofragments. This problem can be avoided by producing the conduction electrons with the less energetic KrF (248 nm) excimer laser photons. In other words, the electron attachment rate constant measured with the 248 nm laser line should be due mainly to SO₂. Note, however, that by comparing the attachment rate constants measured at these two wavelengths, we may obtain information for the electron attachment rate constants of radicals. We will report in more detail the results of this investigation at the conference.

This work is supported by U. S. Air Force Office of Scientific Research under Grant No. AFOSR-82-0314.

TOTAL CROSS SECTION MEASUREMENTS FOR ELECTRON SCATTERING BY OCS AND SO₂

M.S. Dababneh*, Y.-F. Hsieh, W.E. Kauppila, C.K. Kwan, and T.S. Stein

Department of Physics and Astronomy, Wayne State University, Detroit, Michigan 48202 USA

In this paper we report absolute total cross section measurements for low energy electrons scattered by the triatomic molecules, OCS and SO₂. The experimental approach (beam transmission through a gas scattering region) and apparatus are the same as has been used recently for electron and positron total scattering cross section measurements by other molecules.¹ The electron beam originates from a thermionic cathode and has a measured energy width (FWHM) of about 0.15 eV.

The present total cross section measurements for OCS are shown in Figure 1 along with the prior total cross section measurements of Szymtkowski² and the continuum multiple-scattering model calculations of Lynch et al.³ for integrated elastic cross sections. The present results are considerably lower than Szymtkowski at the low energy (1.15 eV) shape resonance, and generally lower at higher energies, except at the minimum in the vicinity of 2 eV where both measurements are in good agreement. The large difference at the 1.15 eV shape resonance could be explained by the narrower energy spread of the electron beam used by Szymtkowski.

In Figure 2 are displayed the present total cross section results for SO₂, which indicate a narrow shape resonance in the vicinity of 1 eV and a broader bump around 10 eV. Due to the lack of any other readily available total cross sections that could be used for comparison,⁴ we show some measurements of elastic scattering,⁵ electronic excitation,⁶ and ionization cross sections, which do not collectively account for the total cross sections reported here.

This work is supported by the National Science Foundation. One of us (MSD) also acknowledges receipt of a research grant from Yarmouk University.

*Physics Department, Yarmouk University, Irbid, Jordan

References

1. Ch.-K. Kwan, Y.-F. Hsieh, W.E. Kauppila, Steven J. Smith, T.S. Stein, M.N. Uddin, and M.S. Dababneh, Phys. Rev. Lett. **52**, 1417 (1984); Phys. Rev. A **27**, 1283 (1983).
2. Cz. Szymtkowski, Abstracts of Contributed Papers for ICPEAC XIII (Berlin, 1983) p. 242.
3. M.G. Lynch, D. Dill, J. Siegel, and J.L. Dehmer, J. Chem. Phys. **71**, 4249 (1979).
4. O.J. Orient, I. Iga, and S.K. Srivastava, J. Chem. Phys. **77**, 3523 (1982).

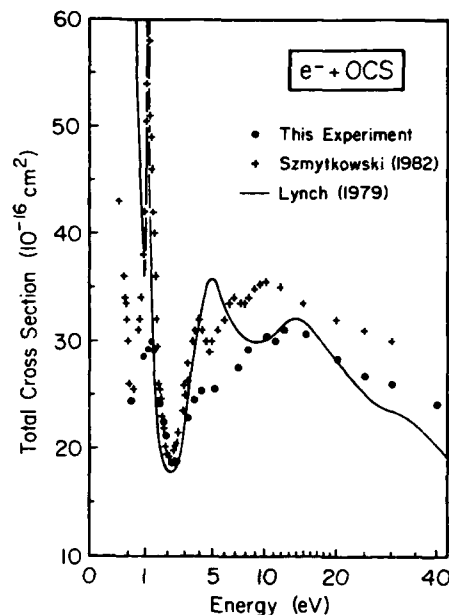
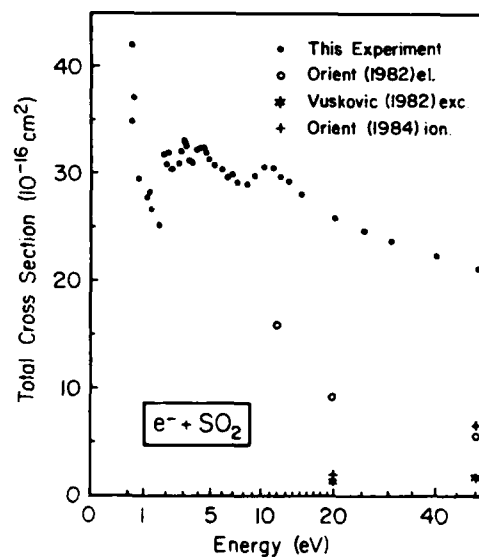


FIGURE 1 Electron-OCS scattering cross sections.

FIGURE 2 Electron-SO₂ scattering cross sections.

5. L. Vuskovic and S. Trajmar, J. Chem. Phys. **77**, 5436 (1982).
6. O.J. Orient and S.K. Srivastava, J. Chem. Phys. **80**, 140 (1984).

SCATTERING OF HIGH ENERGY ELECTRON FROM MOLECULES

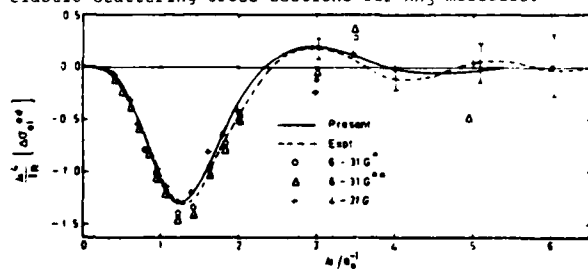
Mukesh Kumar, A.N.Tripathi and V.H.Smith, Jr*

Department of Physics, University of Roorkee, Roorkee 247667, India

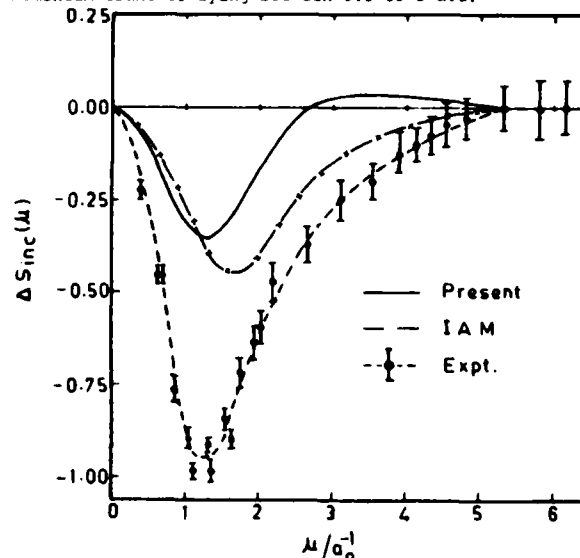
*Department of Chemistry, Queens University, Kingston, Ontario, Canada

The study of high energy electron-molecule scattering¹⁻² are of great potential value for examining the quality of molecular wave functions and for studying the chemical binding effects if the first Born approximation is valid. The elastic scattering is well predicted by the Hartree-Fock (HF) wave function but the inelastic scattering cross-section which relates the two electron distribution function (intracule), are found to be quite sensitive to electron correlation effects and are not accounted by HF theory. The experimental data resulting from high energy electron scattering measurements are mostly confined to total scattering cross section (elastic + inelastic) which limits the comparison between the experiment and theory. However, in recent years some efforts are being made to measure both elastic and inelastic components³ separately.

Recently Thakkar⁴ has demonstrated that one can calculate both, the elastic and inelastic scattering cross-sections at the self-consistent field (SCF) level on the same footing which is better than the independent atom model (IAM) result for the inelastic contribution, as these are strongly affected by the formation of chemical bond. Therefore, it is worth presenting, the calculation of total, elastic and inelastic high energy electron scattering cross-section from molecular systems. We have chosen the ten electron systems (Ne, HF, H₂O, NH₃, CH₄). A simple SCF molecular wave function constructed from a double zeta quality basis set of contracted Gaussian orbitals⁵ is employed. Various trends and systematics in the electron intensities (elastic and inelastic) for the ten electron systems have been examined. The effect of molecular bonding has also been examined with the help of difference functions computed between present electron scattering intensity and that for IAM. The figures 1 (a-b) present our difference functions elastic and inelastic scattering cross-sections for NH₃ molecule.



The elastic scattering results (fig.1a) are in good agreement with the recent data in the region of momentum transfer lying between 0.3 to 3 a.u.



However, the present calculation of inelastic scattering (fig.1b) using the present SCF molecular wave function show a large deviation compared to the measurement³ in the same angular region. The details of the result for this along with the other molecules will be presented in the conference.

References:

1. R Benesch and V.H.Smith Jr. in wave Mechanics: The First Fifty years edited by W.C.Price et al (Butter Worths, London 1973) p 357-377.
2. R.A. Bonham and M. Fink, High energy electron scattering (Van Nostrand, New York 1974).
3. A Duguet, A Lahman-Bennani and M.Rouault J. Chem. Phys. **78**(1983), 6595.
4. A.J. Thakkar J. Chem. Phys. **81**(1984) 943.
5. L.C.Snyder and H. Basch, Molecular wave functions and properties, 1972 (New York; Wiley).

VIBRATIONAL EFFECTS ON ELECTRON-MOLECULE SCATTERING FOR POLYATOMICS: H_2O

Martin Breitenstein, Richard J Mawhorter,* Hermann Meyer, and Armin Schweig

Fachbereich Physikalische Chemie der Philipps Universität
Hans-Meerwein-Strasse, D-3550 Marburg/Lahn, Federal Republic of Germany

The comparison of experimental and theoretical cross sections for high energy electron scattering from a wide range of molecules has significantly furthered our understanding of molecular charge distributions. Only for H_2 and D_2 ,¹ however, where both vibrational and correlation effects can be treated fully, is there good agreement between theory and experiment. While it has become clear that electron correlation causes the most discrepancy between theory and experiment, vibrational effects are another possible source of disagreement. These have been studied for several diatomics² in addition to H_2 and D_2 . It was found that these vibrational effects were small, which encouraged the direct comparison of inherently averaged experimental results with theoretical calculations done at a single fixed geometry. The purpose of this work is to see if they remain small for a polyatomic such as H_2O .

To provide as sensitive a comparison of cross sections as possible, the results are presented in terms of $\Delta\sigma$, the difference between the actual cross section σ_{IOL} and a reference cross section σ_{IAM} based on the independent atom model. $\Delta\sigma$ is the representation in scattering space of the rearrangement of charge to form the molecular bonds.

For a polyatomic molecule, the effects of the different vibrational modes must be taken into account. For each of the 3 H_2O vibrational modes Q_i , 26 molecular geometries (40 for Q_2) were determined at uniform intervals in Q_i , and a 4-31G+BF SCF wave function was computed for each geometry. Our program DSIGMA,³ which calculates the scattering in the first Born approximation analytically from a given wave function, was then used to determine σ_{IOL} , σ_{IAM} , and $\Delta\sigma$ at small intervals in the scattering variable s for total, elastic, and inelastic scattering. Near Hartree-Fock $\Delta\sigma$ curves were also calculated for the equilibrium geometry, and the excellent qualitative agreement of the 4-31G+BF results is more than adequate for a study of this nature. Repeated calculations for each step in Q_i resulted in values for each cross section as a function of Q_i and s , e.g. $\Delta\sigma^i(Q_i, s)$. At each s -value, s_0 , a quadratic polynomial in Q_i was then fitted in the least squares sense to the smooth functions $\Delta\sigma(Q_i, s_0)$. Such a function is shown in the inset in Figure 1. The averaging was completed by evaluating the integrals $\langle \Delta\sigma(s) \rangle_{vib} = \int_{-\infty}^{\infty} P(Q) \Delta\sigma(Q, s) dQ$ for each value of s and for both harmonic and anharmonic distribution functions $P^h(Q_i)$ and $P^a(Q_i)$. The fitting procedure enabled

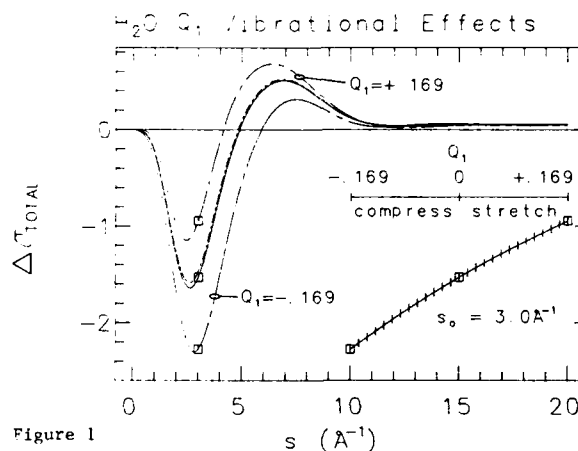


Figure 1

analytic evaluation of these integrals and ensured the convergence of the functions $\Delta\sigma(Q)$.

The results confirm that the bending motion of Q_2 has little effect on the charge distribution, in contrast to the stretching motions of Q_1 and Q_3 . There is substantial cancellation for the antisymmetric Q_3 mode, so the effects are largest for the symmetric stretch Q_1 . Q_1 has a large anharmonicity, and illustrates the importance of using the best available anharmonic distribution functions. Figure 1 shows the $\Delta\sigma_{eq}$ ($Q_1=0$) curve (—) and those calculated at the maximum Q_1 displacements. These deviate significantly from $\Delta\sigma_{eq}$, but when all 27 curves (represented by hash marks in the inset) are averaged, the difference from $\Delta\sigma_{eq}$ is very small, as shown by the fourth curve (— · —). Hence even the largest correction is well within current experimental error limits, and these results for a polyatomic molecule lend further credence to the practice of comparing cross sections calculated at a fixed geometry with (averaged) experimental data.

The efficacy of the standard formula used to account for vibrational averaging in the IAM has also been examined. Discrepancies are small, roughly half the size of the vibrational corrections themselves.

RJM would like to acknowledge a fellowship from the German Academic Exchange Service (DAAD).

1. K. Szalewicz, W. Kofos, H.J. Monkhorst, & C. Jackson, J. Chem. Phys. **80**, 1435 (1984); *ibid.* **77**, 1323 (1982).
 2. J. Epstein & R.F. Stewart, *ibid.* **70**, 5515 (1979).
 3. M. Breitenstein, A. Endesfelder, H. Meyer, A. Schweig, & W. Zittlau, Chem. Phys. Lett. **97**, 403 (1983).
- *Present address: Jet Propulsion Laboratory, 4800 Oak Grove Drive, Pasadena, CA 91109.

Low-Energy Electron Scattering on Methane

J. Ferch, B. Granitza, and W. Raith

Fakultät für Physik, Universität Bielefeld, D-4800 Bielefeld, Fed. Rep. of Germany

We measured the absolute total electron scattering cross section of CH_4 in the energy region between 0.085 and 12 eV in a transmission experiment performed with our improved high-resolution time-of-flight spectrometer /1/. The results show a pronounced Ramsauer minimum at 0.401(20) eV with an absolute total cross section value of $1.356(37) \times 10^{-16} \text{ cm}^2$. Computation of the forward-scattering cut-off solid angle, averaged over the length of the target, yielded a value of $1.5 \times 10^{-3} \text{ sr}$, corresponding to 1.2×10^{-4} of the sphere. Thus for s-waves the undiscriminated forward scattering is completely negligible compared with the total uncertainty of the cross section measurements of several percent. Only if forward scattering were enhanced by a factor of 100 or more, its influence would exceed the 1% level.

Our results are in good agreement with the early measurements of Brüche /2/ as well as Ramsauer and Kollath /3/ and the recent results of Floeder et al /4/, obtained with a technically quite different apparatus. They disagree with the published data of Barbarito et al /5/ as can be seen from Fig.1. We obtained a considerably higher cross section in the whole energy range studied. The most noticeable discrepancies are in the vicinity of the Ramsauer minimum, where our cross section is about five times higher than that of Barbarito et al. Those authors located the Ramsauer minimum at an electron energy of 0.215 eV whereas we found it at 0.401 eV, in excellent agreement with the early measurement /3/.

Fig.1 shows a comparison of our results with other experimental data. The data of Tanaka et al /6/ and of Sohn et al /7/ are derived from differential cross section measurements in the range of 30 to 140° and 30 to 120° , respectively. Barbarito et al pointed out, that the Ramsauer minimum of argon, measured by Golden and Bandel /8/ deviated from the earlier measurement of Ramsauer and Kollath /9/ in a similar way. This suggestion, however, does not help in understanding the discrepancy because our recent measurement of the argon cross section /1/ confirm the old measurements.

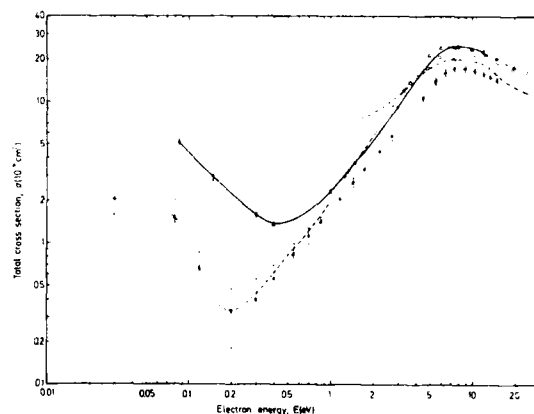


Fig. 1. Absolute total cross section of CH_4 :
 —, This work; —, Brüche /2/;
 ---, Ramsauer and Kollath /3/; Δ , Floeder et al /4/; ---, Barbarito et al /5/;
 O, Tanaka et al /6/; —, Sohn et al /7/;
 ---, Brode /10/; \square , Griffith et al /11/.

REFERENCES

- /1/ Ferch, J., Granitza, B., Masche, C. and Raith, W., submitted to J. Phys. B (1984)
- /2/ Brüche, E., Ann. Phys. Lpz. **4** (1930) 387
- /3/ Ramsauer, C. and Kollath, R., Ann. Phys. Lpz. **4** (1930) 91
- /4/ Floeder, K., Fromme, D., Raith, W., Schwab, A., and Sinapius, G., Abstracts 2nd ECAMP, Amsterdam 1985
- /5/ Barbarito, E., Basta, M., Calicchio, M. and Tessari, G., J. Chem. Phys. **71** (1979) 54
- /6/ Tanaka, H., Okada, T., Boesten, L., Suzuki, T., Yamamoto, T. and Kubo, M., J. Phys. B **15** (1982) 3305
- /7/ Sohn, W., Jung, K. and Ehrhardt, H., J. Phys. B **16** (1983) 891
- /8/ Golden, D.E. and Bandel, H.W., Phys. Rev. **149** (1966) 58
- /9/ Ramsauer, C. and Kollath, R., Ann. Phys. Lpz. **3** (1929) 536
- /10/ Brode, R.B., Phys. Rev. **25** (1925) 636
- /11/ Griffith, T.C., Charlton, M., Clark, G., Heyland, G.R. and Wright, G.L., Positron Annihilation, ed. P.G. Coleman, S.C. Sharma and L.M. Diana, North Holland, Amsterdam 1982, p. 61

ROTATIONAL AND ROVIBRATIONAL EXCITATION OF CH_4 BY ELECTRON IMPACT BETWEEN 0.5 eV AND 10 eV

R. Müller, K. Jung, and H. Ehrhardt

Fachbereich Physik der Universität Kaiserslautern, D-6750 Kaiserslautern, West Germany

Cross sections for the electron impact rotational excitation of CH_4 have been measured in a crossed beam spectrometer for the impact energies 0.5 eV, 5 eV, 7.5 eV, and 10 eV. Absolute state-to-state cross sections are deduced from the broadened energy loss peaks by using the method of analysis given by Shimamura¹. The results (angular dependencies) are compared with calculations of Jain and Thompson² and of Abusalbi et al.³. In some cases comparison with experimental work of Tanaka et al.⁴ is possible.

For an impact energy of 0.5 eV the pure rotational excitation is rather weak. For $j = 0 \rightarrow 3$ the differential cross section is between 10^{-20} and 10^{-22} cm^2/sr with the larger values at large scattering angles, whereas for $j = 0 \rightarrow 4$ it is relatively constant with respect to the scattering angle ($d\sigma/d\omega(j = 0 \rightarrow 4) = 10^{-19}$ cm^2/sr). At the same impact energy, but with simultaneous excitation of the ν_2 vibrational mode the rotational branches with $\Delta j = 0, 1$, and 2 have also been measured. The cross sections are of the order of 10^{-19} cm^2/sr for $\Delta j = 0$ and 1 and 10^{-20} to 10^{-21} cm^2/sr for $\Delta j = 2$. For the simultaneous excitation of the infrared active vibrational mode ν_4 only rotational transitions $\Delta j = 1$ are found with increasing cross sections in forward direction ($\sim 10^{-17}$ cm^2/sr at angles below 15°).

In the range of impact energies between 5 eV and 10 eV a short living negative ion state is formed and the rotational excitation of the molecule is strongly influenced by this resonance. Therefore all angular dependencies for each $j \rightarrow j'$ -transition have similar shapes and are practically independent of the impact energy. The cross section for the $j = 0 \rightarrow 0$ transition has a deep minimum close to 110° scattering angle. Here the cross section drops from ca. 10^{-16} cm^2/sr to less than 10^{-17} cm^2/sr , whereas for $j = 0 \rightarrow 3$ and $j = 0 \rightarrow 4$ the cross sections remain constant over the measured angular range having a value of ca. 10^{-17} cm^2/sr . The nearly isotropic cross section is to be expected for collisions in which a large amount of momentum has been transferred (i.e. $j_t = 3, 4$).

This work was supported by the Deutsche Forschungsgemeinschaft (SFB 91).

References

1. J. Shimamura, Phys. Rev. A 28(3) (1983) 1357-1362
2. A. Jain and D.G. Thompson, J. Phys. B 16 (1983) 3077-3098
3. N. Abusalbi, R.A. Eades, T. Nam, D. Thirumalai, D.A. Dixon, D.G. Truhlar, M. Dupuis, J. Chem. Phys. 78(3) (1983) 1213-1227
4. H. Tanaka, M. Kubo, N. Onodera, A. Suzuki, J. Phys. B 16 (1983) 2861-2869

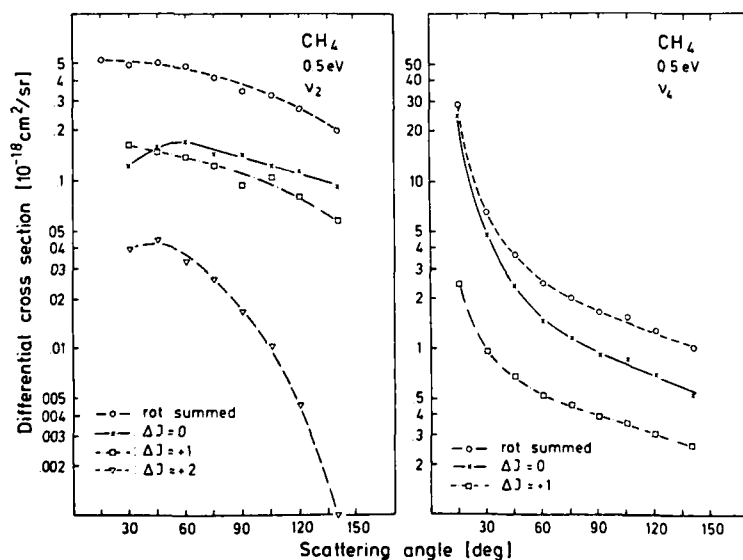


Fig. 1:
Differential cross sections for the rotational branches with $\Delta j = 0, 1$, and 2 and rotationally summed differential cross sections for the simultaneous excitation of the vibrational modes ν_2 and ν_4 at the electron impact energy $E_0 = 0.5$ eV.

MULTICHANNEL SCHWINGER VARIATIONAL CALCULATIONS OF
 LOW-ENERGY ELECTRON-MOLECULE COLLISIONS^a

Marco A. P. Lima,* Thomas L. Gibson,* Winifred Huo,+ and Vincent McKoy*

*A. A. Noyes Laboratory of Chemical Physics, California Institute of Technology, Pasadena, California 91125 USA

+Radiation Laboratory, University of Notre Dame, Notre Dame, Indiana 46556 USA

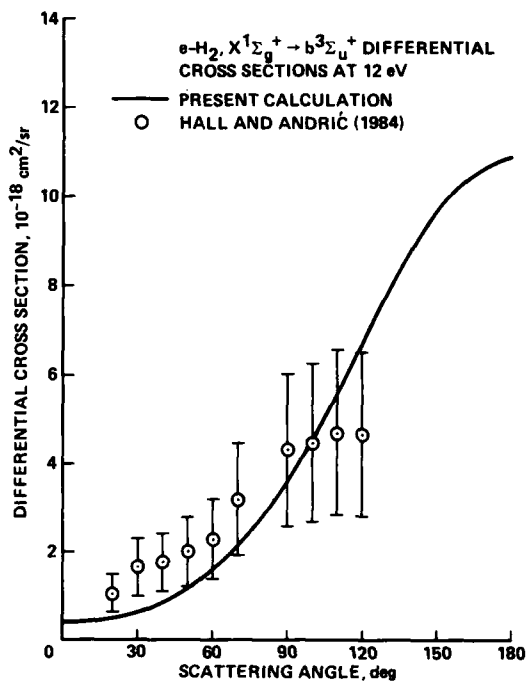
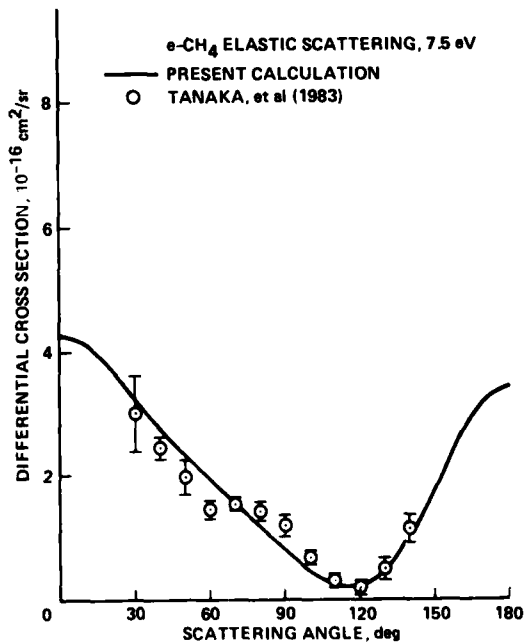
The multichannel Schwinger variational method, as developed by Takatsuka and McKoy,¹ has been applied to study elastic and inelastic low-energy electron-molecule collisions. An earlier study² on the electron-impact excitation cross sections of the $b^3\Sigma_u^+$ state in H_2 has been substantially extended. Calculations based on the two-state approximation have been carried out, using a (6s4p) Gaussian basis set on each nucleus. The calculated cross sections are found to be stable when the size of the basis set is further increased. Figure 1 compares the calculated differential cross section at 12 eV incident energy with a recent measurement of Hall and Andrić.³ At this energy, the measured integral cross section is $5.4 \times 10^{-17} \text{ cm}^2$, versus our calculated value of $5.42 \times 10^{-17} \text{ cm}^2$. At higher energies, the calculated differential and integral cross sections are in significant disagreement with the measurements of Khakoo, McAdams, and Trajmar.⁴ This aspect, as well as our calculations on the $a^3\Sigma_g^+$ state, will be discussed.

Elastic $e\text{-CH}_4$ scattering cross sections, at incident energies from 3 to 20 eV, have been calculated at the static exchange level using a (12s8p4d,7s) Gaussian basis set for C and H, respectively. The differential cross section calculated at 7.5 eV incident energy, together with the experimental data of Tanaka, et al.,⁵ are presented in Figure 2. The calculated total cross section is $18.14 \times 10^{-16} \text{ cm}^2$, versus the experimental value of $19.6 \times 10^{-16} \text{ cm}^2$. It is seen from Figure 2 that the static exchange approximation is capable of reproducing the minimum in the differential cross section. However, the shoulder in the experimental spectrum near 60° appears to be a polarization effect, and is not reproduced in the present level of approximation. Polarization studies are currently under way to see if they can reliably reproduce this aspect of the experiment.

Low-energy $e\text{-N}_2$ scattering is also being studied using a large Gaussian basis set, 11s8p3d on each nucleus. The results will be presented at the meeting.

References

- a. Work supported by the National Science Foundation under Grant No. PHY-8213992.
- ¹K. Takatsuka and V. McKoy, Phys. Rev. A30, 1734 (1984).
- ²M.A.P. Lima, T.L. Gibson, K. Takatsuka, and V. McKoy, Phys. Rev. A30, 1741 (1984).
- ³R.I. Hall and L. Andrić, J. Phys. B17, 3815 (1984).
- ⁴M.A. Khakoo, R. McAdams, and S. Trajmar, Phys. Rev. A (to be published).
- ⁵H. Tanaka, T. Okada, L. Boesten, T. Suzuki, T. Yamato, and M. Kubo, J. Phys. B15, 3305 (1982).


 Figure 1 Differential cross section of H_2 $X^1\Sigma_g^+ \rightarrow b^3\Sigma_u^+$ excitation by electron impact.

 Figure 2 Differential cross section of $e\text{-CH}_4$ elastic scattering

RAMSAUER-TOWNSEND EFFECT IN ELECTRON-SiH₄ ELASTIC SCATTERING

A. Jain* and D. G. Thompson†

*Joint Institute for Laboratory Astrophysics, University of Colorado and National Bureau of Standards, Boulder, Colorado 80309 USA

†Department of Applied Mathematics and Theoretical Physics, The Queen's University of Belfast, Belfast, N. IRELAND

An understanding of low energy electron scattering by silane (SiH₄) molecules is required in plasma chemistry and plasma processing for thin-film deposition or surface treatment.^{1,2} Pollock³ has given values for the momentum transfer for e-SiH₄ elastic scattering below 4 eV (swarm data). Estimates of the various e-SiH₄ cross sections have recently been made from measured and theoretical cross section data and measured electron swarm data, with the aid of a set of cross sections for CH₄.^{4,5} The well-known Ramsauer-Townsend (RT) minimum was estimated to be at about 0.3 eV, the same as in CH₄, but with about five times larger cross section.⁴ There is considerable difference between the estimates of various cross sections by Hayashi⁴ and Garscadden *et al.*⁵

Unfortunately, there is no *ab initio* calculation on the e-SiH₄ system in this low energy region. Our earlier work on CH₄ in a parameter-free model-potential theory^{6,7} predicted quite satisfactory results for the position of RT minimum and the cross section. In order to investigate the utility of this model for a heavier system such as the SiH₄, we have studied e-SiH₄ scattering in precisely the same model.

We generated a single-center (at the Si atom) basis with 47 expansion terms (total energy -- 290.45 a.u.). Results with a smaller basis (33 terms) were also obtained. The value of the spherical polarizability calculated in our polarization potential (Pople-Schofield method⁶) is 44.7 a.u.; 32% larger than the experimental value (30.4 a.u.).⁸

In brief, the total interaction potential is composed of a near Hartree-Fock static term, a parameter-free polarization potential and a free-electron-gas exchange (FEGE; Hara⁶ type) potential (plus orthogonalization of the bound and the continuum orbitals). The number of terms in the single-center expansion of the static and the exchange potentials were kept up to

$l_{\text{max}} = 6$. The same value of l was used for the K-matrix size. We include A₁, A₂, E and T₂ symmetries only in our final cross sections.

The position of our RT minimum was found around 0.12 eV (with the 33 term basis set, it occurs at about 0.09 eV) in the A₁ symmetry. We also found (similar to CH₄) a T₂ enhancement in the cross section around 4 eV. The A₁ state also has a broad structure around 2.5 eV. This means that in the final cross sections a shape resonance structure occurs around 3-4 eV, which is mainly due to T₂ symmetry.

We are also trying to generate a much bigger basis set in order to improve convergence; this might push the RT minimum toward higher energy, consistent with experiment and also with the CH₄ results.

We plan to present complete results at the time of conference.

This work was supported by the U.S. Dept. of Energy (Office of Basic Energy Sciences). A part of the calculation was done at the Queen's University of Belfast. One of the authors (AJ) is thankful to D. W. Norcross and A. V. Phelps for helpful discussions.

References

1. J. Perrin, J. P. M. Schmitt, G. De Rosny, B. Drevillon, J. Huc and A. Lloret, *Chem. Phys.* **73**, 383 (1982).
2. J. Perrin and J. P. M. Schmitt, *Chem. Phys.* **80**, 351 (1983).
3. W. J. Pollock, *Trans. Faraday Soc.* **64**, 2919 (1968).
4. M. Hayashi, VI Dry Process Symposium, Oct. 11-12 (1984, Tokyo), p. 127.
5. A. Garscadden, G. L. Duke and W. F. Bailey, *Appl. Phys. Lett.* **43**, 1012 (1983).
6. A. Jain and D. G. Thompson, *J. Phys. B* **15**, L631 (1982).
7. A. Jain, Ph.D. Thesis (The Queen's University of Belfast, 1983).
8. A. A. Maryott and F. Buckley, U. S. NBS Circular No. 537 (1953).

ELASTIC DIFFERENTIAL SCATTERING AND VIBRATIONAL EXCITATION OF C_2H_6 BY LOW ENERGY ELECTRONS

H. Tanaka and L. Boesten

Departments of General Sciences and Physics, Sophia University,
7-1 Kioicho, Chiyoda-ku, Tokyo 102, Japan

Elastic and vibrationally inelastic differential, integral, and momentum-transfer cross sections for electrons scattered by C_2H_6 are reported in the energy range from 2 to 20 eV. Scattering angles were covered from 10° to 130° . With the help of the relative flow technique¹, the elastic cross sections are placed on an absolute scale. From the measured energy loss-spectrum of the lowest normal modes in C_2H_6 , the ratios of the area under the peaks of the vibrational excitation and the elastic scattering as well as their heights were determined. The resulting relative intensities were then converted to absolute values by calibration against the known DCS for elastic scattering.

In previous measurements², we have used a spectrometer with a 172° cylindrical analyser and a gas beam effusing from a nozzle. In the present measurements with a new vacuum system, hemispherical electrostatic dispersion elements and tube lenses are used. The lenses follow the design proposed by Chutjian³, but their driving voltages were recalculated with a new matrix program as well as a beam tracing program to obtain improved focussing at the lower end of the energies considered by Chutjian and to achieve better adjustments to the particular geometry of our apparatus. The main voltages of the zoom lenses are driven by a personal computer in accordance with the energy loss being measured. Also this time, the C_2H_6 beam is formed by a small capillary array. Thus, the geometrical experimental conditions are considerably improved when compared with the previous measurements. The over-all resolutions used were 50 meV for elastic scattering (to increase intensity), and 30 meV for the vibrational measurements. The over-all errors were estimated to be 10-20% for elastic scattering and 30-40% for vibrational excitations.

The new measurements for the angular distribution for the elastic scattering now show the σ -wave characteristic much more clearly than in the previous measurements. A similar feature appears in the DCS of the vibrational excitation on a much smaller scale. At lower angles, the angular distributions are nearly flat. The total cross sections for scattering of slow electrons by the saturated hydrocarbons, CH_4 , C_2H_6 , and C_3H_8 show a broad maximum centered around 7.5 eV.

In the case of CH_4 ⁴, this maximum was due to a short-lived shape resonance of the T_d symmetry. To confirm this, further measurements of the excitation function for the electron impact energy are under way.

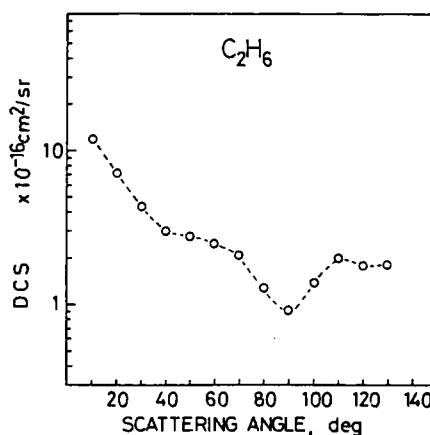


Figure 1. Vibrationally elastic DCS at 7.5 eV.

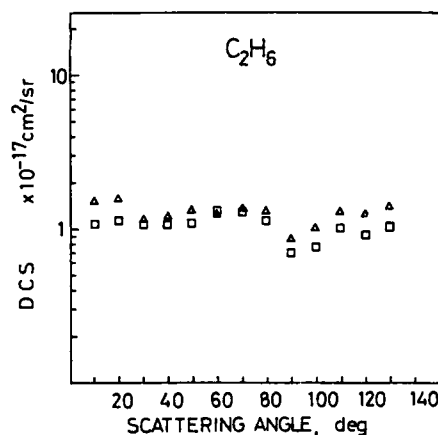


Figure 2. Vibrationally inelastic DCS at 7.5 eV.

— Δ 3 and 25 modes, — \square 14 modes.

Reference

1. S. K. Srivastava, A. Chutjian, and S. Trajmar, *J. Chem. Phys.* **63** 2659 (1975).
2. D. Matsunaga et al., in *Abstracts of the XII ICPEAC*, Gatlinburg, Tennessee, 1981, edited by S. Datz, p.358.
3. A. Chutjian, *Rev. Sci. Instr.* **50** 347 (1979).
4. H. Tanaka et al., *J. Phys.* **B 15** 3395 (1982).

TEMPORARY NEGATIVE IONS IN COMPLEX MOLECULES: DIBENZENE CHROMIUM

P.D. Burrow,* A. Modelli,[†] M. Guerra,[#] and K.D. Jordan,[@]^{*} Department of Physics & Astronomy, University of Nebraska, Lincoln, NE 68588 USA[†] Istituto Chimico "G. Ciamician", Università di Bologna, 40126, Bologna, Italy[#] C.N.R. Ozzano Emilia (Bologna) Italy[@] Department of Chemistry, University of Pittsburgh, Pennsylvania 15260 USA

The variety of geometries and molecular orbital symmetries available in hydrocarbon compounds and their derivatives make such systems attractive for studies of temporary negative ions in spite of their greater complexity. Because of the close connections between the properties of the normally unoccupied orbitals and the energies and lifetimes of temporary ions,¹ resonances with a number of different characteristics can often be observed in the total scattering cross section of a given compound.

The interpretation of scattering data in complex molecules is, of course, greatly facilitated by high molecular symmetry. As an example of such a system we describe here our results in dibenzene chromium, a "sandwich" molecule consisting of two parallel benzene rings on opposite sides of a chromium atom. The data in curve (a) of Fig. 1 were taken using the electron transmission method devised by Sanche and Schulz² and show the derivative with respect to energy of the electron beam current transmitted through a gas cell as a function of the impact energy. Curve (b) illustrates a portion of the data on a more sensitive scale. In curve (c) the transmission spectrum is shown with reduced discrimination against scattered electrons, the electron beam attenuation deriving primarily from electrons rejected by elastically scattering back into the monochromator.³

The major features in curve (a) are typical of "shape" resonances formed by binding the impacting electron temporarily into the unoccupied orbitals of the ground state molecule. The molecular orbitals of dibenzene chromium may be derived from the π orbitals of two benzene molecules (face to face) and the 3d atomic orbitals of Cr. A careful examination of the appropriate interactions leads to the assignment given in the figure. Furthermore, the experimental energies and symmetries are in excellent agreement with the results of an X α calculation similar to those carried out on other organometallic compounds.⁴

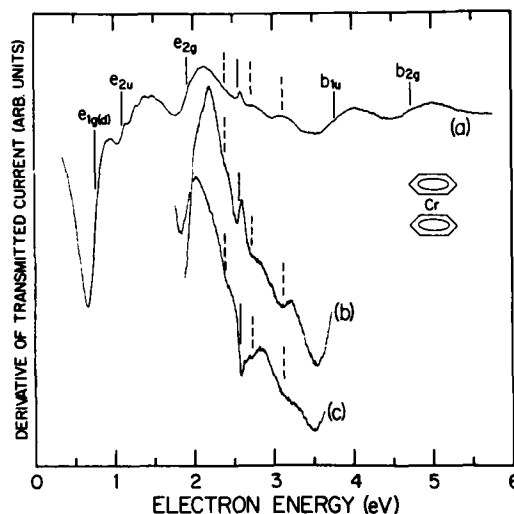


Figure 1

The remaining features in the spectrum are too narrow to be ascribed to shape resonances. Rather, their characteristics suggest core-excited states of the neutral compound. In particular the very narrow resonances at 2.4 and 2.57 eV are characteristic of Feshbach resonances commonly found in atoms and small molecules, in which two electrons in Rydberg orbitals are bound to the positive ion core. The profiles of these resonances are substantially altered in curve (c), reflecting the angle-dependent interference effects characteristic of such negative ion states.

Acknowledgements

This work was supported in part by NSF and by NATO grant #1829.

References

1. K.D. Jordan and P.D. Burrow, *Accts. of Chem. Res.* **11**, 341 (1978).
2. L. Sanche and G.J. Schulz, *Phys. Rev. A* **5**, 1672 (1972).
3. A.R. Johnston and P.D. Burrow, *J. Electr. Spectrosc. and Relat. Phenom.* **25**, 119 (1982).
4. A. Modelli, A. Foffani, M. Guerra, D. Jones and G. Distefano, *Chem. Phys. Letters* **99**, 58 (1983).

SHAPE RESONANCES ASSOCIATED WITH THE BONDING OF THE HYDROGEN
ATOM WITH FIRST ROW ATOMS IN SIMPLE MOLECULES

M. TRONC, L. MALEGAT and M. BEN ARFO

Laboratoire de Chimie Physique, Université Pierre et Marie Curie
11 Rue Pierre et Marie Curie 75231 PARIS Cedex 05 France

Differential cross sections have been obtained, with a crossed-beams electron-impact spectrometer for the excitation of H-M (M=C,N,O) stretching motion in a series of polyatomic molecules: HCN, C_2H_2 , C_3H_4 , CH_4 , H_2O , NH_3 . All these cross sections are dominated by a 1-2 eV broad shape resonance centered at 6-8 eV which was not detected in transmission experiments¹ because it is too short lived.

The extra electron is trapped in an antibonding σ^* valence orbital, and the concentration of electron in this σ^* orbital elongates the H-M bond which leads to prominent excitation of stretching vibrational modes of the electronic ground state in the auto-detaching process. Figure 1 shows an energy loss spectrum for the HCN molecule at an electron energy of 6.7 eV center of the $^2\Sigma^+$ resonance. Figure 2 shows an energy loss spectrum for the C_2H_2 molecule at 6.2 eV center of the $^2\Sigma^+$ resonance. The two spectra show prominent resonant excitation of the Hydrogen-Carbon stretching motion (nv_1 modes in HCN; nv_1 , (nv_3) modes in C_2H_2).

The characteristics of shape resonances depend on purely geometrical factors², and on dynamical effects: it will be shown that the resonance energy can be related to the H-M bond length and bond strength.

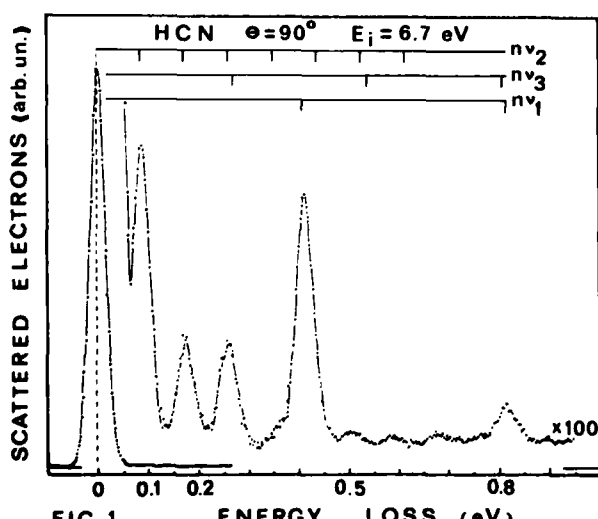


FIG. 1

The angular distributions of the scattered electron show the contribution of the s ($l=0$) partial wave, (which can-

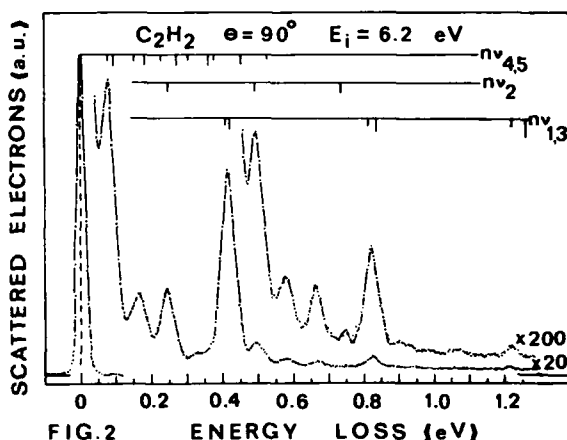


FIG. 2

not by itself support a shape resonance) together with the d ($l=2$) or the p ($l=1$) partial wave in the trapping, depending on the characteristic charge distribution of the σ^* orbital in each molecule.

Most of these molecules are known to produce H^- ions by dissociative attachment through Feshbach resonances lying in the same energy range as the shape's. As these dissociating resonant states can also lead to vibrational excitation of high vibrational levels³, they can interfere with the shape resonances.

Moreover, it will be shown that the counterpart of these low energy electron-scattering shape resonances are observed in K-shell photoionisation where they appear in the discrete part of the spectrum on account of the more attractive coulomb field between the positive-ion and the ejected electron, which shifts by roughly 10 eV to lower energy the resonance position in the ejected-electron kinetic energy scale.

REFERENCES

- 1) K.D. JORDAN and P.D. BURROW Accounts of Chem. Res. **11**, 391 (1978)
- 2) M. TRONC and L. MALEGAT in Proceeding of the 38th international meeting "Photophysics and Photochemistry above 6 eV. Bombannes 1984. Eds LAHMANN Elsevier Scientific Pub. Co. (Amsterdam) in press.
- 3) F. GRETEAU, R.I. HALL, A. HUETZ, D. VICHON, J. MAZEAU, J. Phys. B: Atom. Mol. Phys. **12**, 2925 (1979).

$e^- - O_3$ COLLISIONS AT LOW ENERGIES

K. N. Joshipura* and H. S. Desai**

* N. B. P. Science College, ANAND 388 001, India

** Physics Department, Faculty of Science, M. S. Univ. Baroda, India

Studies on electron collision with O_3 are rare¹. Presently, rotational excitation of O_3 by slow electrons, below 0.1 eV, is considered. O_3 possesses a small dipole moment, hence at low energies, the first Born approximation is reasonably good. Considering only the dominant dipole interaction, we take into account the asymmetric top^{2,3} nature of the O_3 molecule. Its rotational levels are defined by angular momentum quantum no. J and its sublevels τ . Total or integrated cross-sections are calculated for various allowed transitions, $J_\tau \rightarrow J'_\tau$. Also calculated are momentum transfer cross-sections, by employing two methods^{4,5}. At 0.01 eV incident energy, the cross-section are of the order of 10^{-14} cm^2 , for the most dominant

transition, $0_0 \rightarrow 1_0$. The effects of shorter ranged interactions may be small enough to be neglected, in the energy range considered here.

References

1. Joshipura K. N., Ind. J. Pure Appl. Phys. 22, 167 (1984)
2. Herzberg G. 'Molecular Spectra and molecular structure' Vol. II, III. Van Nostrand Reinholder (1966)
3. Itikawa Y. J. Phys. Soc. Japan 32, 217 (1972)
4. Crawford O. H. J. Chem. Phys. 47, 1100 (1967)
5. Rudge K. R. H. J. Phys. B7, 1323 (1974)

A LINEAR ALGEBRAIC APPROACH TO ELECTRONIC EXCITATION OF ATOMS AND MOLECULES BY ELECTRON IMPACT

B. I. Schneider* and L. A. Collins*

*Theoretical Division, Los Alamos National Laboratory, Los Alamos, New Mexico 87545 USA

We have extended our linear algebraic (LA) technique¹ to treat electronic excitations of atoms and molecules by electron impact. The total system wavefunction ψ has the form

$$\psi(\vec{R}, \vec{r}) = \sum_{c=1}^n \phi_c(\vec{R}) f_c(\vec{r}) + \sum_{\alpha} d_{\alpha} \chi_{\alpha}(\vec{R}, \vec{r}), \quad (1)$$

where ϕ_c is an eigenfunction of the target atomic or molecular hamiltonian, F_c is the wavefunction for the scattered electron in channel c , and χ_{α} is a "correlation" function added for completeness and may represent orthogonality constraints or excited states not included in the first term. We utilize the Feshbach formalism to derive a set of coupled, nonlocal Lippman-Schwinger equations for F_c . The channels included in the first part of (1) appear in direct and exchange coupling terms while the correlation functions give rise to an effective optical potential.² These integral equations are converted to a set of matrix equations by introducing a discrete quadrature for the integrals. We make a further simplification by invoking a separable expansion in terms of an L^2 basis for the off-diagonal direct and all of the exchange and optical potential terms. This prescription reduces the coupled integral equations to a set of uncoupled inhomogeneous equations³ and greatly reduces the order of the matrix equations that must be solved. For cases involving strongly dipole-coupled transitions for which the separable expansion becomes large, we have developed an efficient iterative procedure for solving the coupled direct equations. The separable expansion is retained for the exchange and correlation contributions.

We have applied the technique to electron scattering from He, H_2^+ , and H_2 at the two-state close-coupling (2cc) level. Results for He and H_2^+ are in very good agreement with other calculations. In the Table, we present total cross sections for the $X^1\Sigma_g^+$ to $b^3\Sigma_u^+$ excitation in H_2 . Our results without correlation agree well with those of Chung and Lin;⁴ however, we note that correlation effects are very important for this transition. This result is confirmed by comparison with new R-matrix⁵ and Schwinger⁶ variational calculations.

Table $e+H_2 \ X^1\Sigma_g^+ \rightarrow b^3\Sigma_u^+$

E(eV)	$\sigma(a_0^2)$	
	a	b
12.0	0.85	1.92
15.0	1.19	2.08
20.0	0.53	0.68

Work performed under the auspices of the U.S. Department of Energy and NATO Scientific Exchange Grant 687/84.

References

1. B. I. Schneider and L. A. Collins, Phys. Rev. A **24**, 1264 (1981).
2. B. I. Schneider and L. A. Collins, Phys. Rev. A **30**, (1984)
3. L. A. Collins and B. I. Schneider, J. Phys. B **17**, L235 (1984).
4. S. Chung and C. C. Lin, Phys. Rev. A **17**, 1874 (1978).
5. C. J. Noble, private communication.
6. V. McKoy, private communication.

ELECTRONIC EXCITATION OF DIATOMIC MOLECULES BY ELECTRON IMPACT

K.L. Baluja*, P.G. Burke*, C.J. Noble* and J. Tennyson*

*SERC Daresbury Laboratory, Warrington, England.

†Queen's University, Belfast, N. Ireland.

We report recent results which we have obtained using a multi-centre R-matrix method with numerically defined continuum orbitals for the electronic excitation of a range of diatomic molecules. These include the first R-matrix results which have been obtained for open-shell homonuclear and heteronuclear targets. The theory underlying these calculations and the numerical methods have both been described previously^{1,2}. Briefly, we use a modified version of the IBM ALCHEMY code³ to construct the Hamiltonian in the internal region of configuration space and solve the single-centre external problem using R-matrix propagator⁴ and accelerated Gailitis expansion methods⁵.

We have carried out two-state calculations for the $X\ ^1\Sigma_g^+ + b\ ^3\Sigma_u^+$ transition for H_2 excitation using both a static exchange model and a static exchange with polarisation (SEP) model in which short range polarisation effects are accounted for by including two particle - one hole L^2 terms in the expansion of the scattering wavefunction. The results which we obtain both for elastic scattering and for electronic excitations are in good agreement with results obtained by Collins and Schneider using the Linear Algebraic method⁶.

We have also investigated the application of the R-matrix method to open-shell targets by considering the electronic excitation of H_2^+ , O_2 and NO. In the case of O_2 and NO the target ground state is represented by an SCF wavefunction and the excited states by single-particle excitations. In these cases we find there is increased sensitivity to polarisation effects which are better represented by adding coupled states rather than by using a single-state with an optical potential. For O_2 we used a three-state model and calculated cross sections for the transitions $X\ ^3\Sigma_g^- - a\ ^1\Sigma_g^+$ and $X\ ^3\Sigma_g^- - b\ ^1\Sigma_g^+$. For NO we have used a six-state model and calculated the positions and widths of a number of low-lying resonances. Some examples of these results are illustrated in the table below.

Resonance parameters for low-lying states of NO^- .Six-state R-matrix calculations assuming an internuclear separation of 2.1747 a_0 .

Symmetry	E res	(Ryd)	Γ res	(Ryd)	
$^1\Sigma^+$	0.178	0.037	SE, SEP		
	> 0.15				Zecca et al ⁹
	0.082				Tronc et al ¹⁰
$^1\Delta$	0.086	0.031	SE		
	0.085	0.030	SEP		
	> 0.15				Zecca et al ⁹
	0.057				Tronc et al ¹⁰
					Burrow ¹¹

References

1. P.G. Burke, I. Mackey and I. Shimamura, J.Phys. B: At. Mol. Phys. **10**, 2497 (1977).
2. P.G. Burke, C.J. Noble and S. Salvini, J.Phys. B: At. Mol. Phys. **16**, L113 (1983).
3. A.D. McLean, Proc. Conf. on Potential Energy Surfaces in Chemistry, p.87, (1971) (published by IBM Research Laboratory, San Jose, California, ed. W.A. Lester, Jr.).
4. K.L. Baluja, P.G. Burke and L.A. Morgan, Comp. Phys. Commun. **27**, 299 (1982).
5. C.J. Noble and R.K. Nesbet, Comp. Phys. Commun. **33**, 399 (1984).
6. L.A. Collins, private communication (1985).
7. J. Tennyson, C.J. Noble and S. Salvini, J.Phys. B: At. Mol. Phys. **17**, 905 (1984).
8. J. Tennyson and C.J. Noble, J.Phys. B: At. Mol. Phys. **18**, 155 (1985).
9. A. Zecca, I. Lazzizzera, M. Krauss and C.E. Kuyatt, J.Chem. Phys. **61**, 4560 (1974).
10. M. Tronc, A. Huetz, M. Landau, F. Pichou and J. Reinhardt, J. Phys. B: At. Mol. Phys. **8**, 1160 (1975).
11. P.D. Burrow, Chem. Phys. Lett. **26**, 265 (1974).

INELASTIC SCATTERING OF ELECTRONS BY HYDROGEN MOLECULE

N.S. Rao

Physical Research Laboratory, Theoretical Physics Area, Navrangpura, Ahmedabad 380 009, India.

Independent atom model (IAM)^{1,2} is the simplest model to study the molecular problems in terms of respective atomic problems. IAM has been used extensively to study the elastic collisional cross sections for hydrogen molecule². Though the electron-molecule problem is the simplest, none of the workers studied the electronic excitation in electron-hydrogen molecule scattering. Motivated to this and the encouragement of my earlier work^{3,4}, gave me scope to extend our studies³ to inelastic scattering of electrons by hydrogen molecule. IAM can be used¹ to study the inelastic collision process. The averaged overall differential cross sections (DCS) for the present study can be written as¹

$$\bar{I}_M(\Theta) = 2 I_A(\Theta) \left[1 + \frac{\sin qR}{qR} \right] \quad (1)$$

where $I_M(\Theta)$ and $I_A(\Theta)$ are the hydrogen molecule and atomic DCS. Using Born and Glauber eikonal series approximations, $I_A(\Theta)$'s are calculated earlier³ for hydrogen 1s-2s transition. These $I_A(\Theta)$'s are used for the present study of hydrogen molecule through (1). And DCS are calculated at incident energy $E \leq 400$ eV. These results ($\bar{I}_M(\Theta)$) are shown in table 1 at $E = 200$ eV and 400 eV.

Table 1. \bar{e} -H₂ inelastic DCS in units of $a_0^2 \text{ Sr}^{-1}$ at $E = 200$ and 400 eV.

Θ	$E = 200 \text{ eV}$	$E = 400 \text{ eV}$
0	4.208 + 0	3.541 + 0
5	1.836 + 0	1.203 + 0
10	7.262 - 1	2.833 - 1
20	8.217 - 2	1.320 - 2
30	1.581 - 2	2.157 - 3
40	5.345 - 3	6.552 - 4
50	2.299 - 3	2.626 - 4
60	1.136 - 3	1.282 - 4
70	6.333 - 4	7.061 - 5
80	3.887 - 4	4.334 - 5
90	2.584 - 4	2.889 - 5
100	1.825 - 4	2.055 - 5

Unfortunately no other data is available for the comparison of present results. The present results will be compared nicely in near future at scattering angles $\Theta \leq 60^\circ$. The present results can be further improved by including third Born term instead of third Glauber

term in the scattering amplitude.

N.S.R. is thankful to Physical Research Laboratory, Ahmedabad, India, for the award of a Post-Doctoral Fellowship.

References

1. H.S.W. Massey et al. "Electronic and Ionic Impact Phenomena", Vol.2 (Oxford) (1969).
2. B.L. Jhanwar et al. *Phy. Rev. A*, **22**, 2451 (1980).
3. N.S. Rao and H.S. Desai, *Curr. Sci.* **52**, 480 (1983).
4. N.S. Rao and H.S. Desai, *Proc. of VIIth I.C.P.A.* (accepted) D-19 (1985).

AD-A163 497

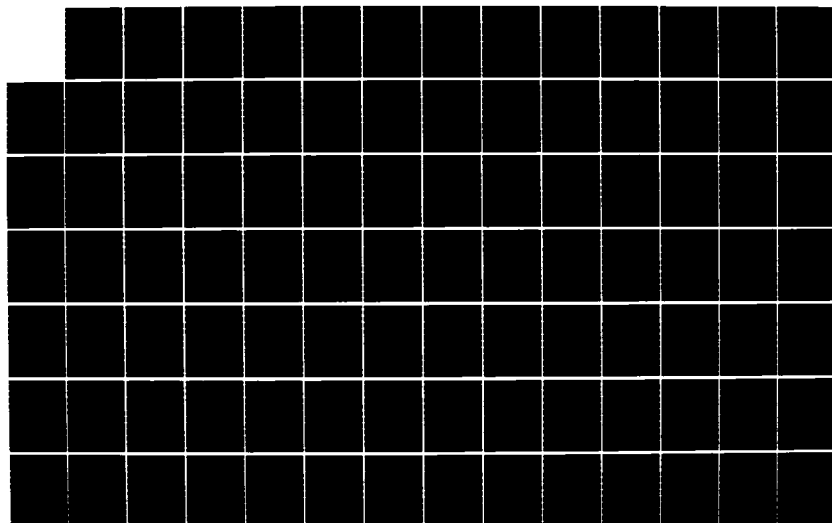
ELECTRONIC AND ATOMIC COLLISIONS ABSTRACTS OF
CONTRIBUTED PAPERS INTERNAT. (U) SRI INTERNATIONAL
MENLO PARK CA MOLECULAR PHYSICS CENTER
M J COGGIOLA ET AL. 1985

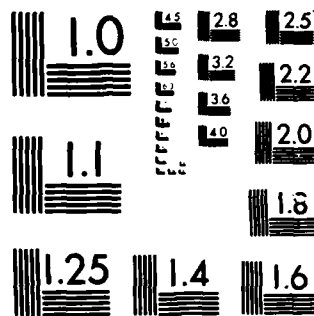
4/8

UNCLASSIFIED

FFB 7/4

NL





MICROCOPY RESOLUTION TEST CHART
NATIONAL BUREAU OF STANDARDS-1963-A

THE LOWEST $1\epsilon_u^+$ AUTOIONIZING STATE OF H_2

S. Hara* and H. Sato†

* Institute of Physics, University of Tsukuba, Ibaraki 305, Japan

† Department of Physics, Ochanomizu University, Otsuka, Bunkyo-ku, Tokyo 112, Japan

The energy width Γ and the energy shift Δ of the autoionizing state of two-electron diatomic molecular system at internuclear distance R are given in atomic units (a.u.) by

$$\Gamma = 2\pi\Gamma(k)/k, \quad k = \{2(E - \epsilon)\}^{1/2}, \quad (1)$$

$$\Delta = P \int \Gamma(k)/(E - \epsilon - k^2/2) dk \quad (2)$$

$$E = E^0 + \Delta, \quad (3)$$

where,

$$\Gamma(k) = \int |\langle \phi_k(1,2) | 1/r_{12} | \psi(1,2) \rangle|^2 dk. \quad (4)$$

In the above expressions, ϕ_k is the eigenfunction of PHP and ψ that of $(1 - P)H(1 - P)$ with the eigenvalue E^0 , ψ and E^0 being interpreted as the zeroth order wavefunction and energy of the autoionizing state. The projection operator P projects all the two-electron wavefunctions onto the subspace in which one of the electrons is in the bound state of the one-electron system with energy ϵ , and H is the Hamiltonian. The function ϕ_k can be expressed as the following form,

$$\phi_k(1,2) = \chi(1)F_k(2) \pm F_k(1)\chi(2). \quad (5)$$

The function χ represents the wavefunction of the one electron system and F_k is the continuum wavefunction with wave number k . Integration in eq. (4) is performed over angular part of k .

We have calculated the potential energy curves for several autoionizing states of H_2 and He_2^{2+} .¹⁻⁴ For the lowest $1\epsilon_u^+$ autoionizing state, the energy widths and the energy shifts are calculated adopting the Coulomb, the static and the static exchange wavefunctions for F_k and it is found that the energy widths are not very sensitive to the choice of the continuum wavefunction F_k . The accuracy of the energy widths depends mainly on that of ψ .

The $1\epsilon_u^+$ autoionizing states are interesting since they are related to photoionization and photodissociation. We have calculated the energy widths, the energy shifts, and the resonance energies

$$E_{res} = E - \epsilon \quad (6)$$

for the lowest $1\epsilon_u^+$ autoionizing state of H_2 . Results are

shown in Table 1. The zeroth order energy widths Γ^0 and resonance energies E_{res}^0 are obtained by using the approximation $\Delta = 0$. In Table 1, the contributions from p and f waves to Γ^0 are denoted by Γ_p^0 and Γ_f^0 , respectively. The contribution from f wave is small enough to be neglected. The present resonance energies agree well with those obtained by others.⁵⁻⁹ Work is now in progress on the autoionizing states of different symmetries.

Table 1. Results for the lowest $1\epsilon_u^+$ autoionizing state of H_2 in a.u.

R	E_{res}^0	Γ_p^0	$\Gamma_f^0 \times 100$	Γ^0	$\Delta \times 100$	Γ
1.0	0.7365	0.0082	0.0001	0.0082		
1.2	0.6292	0.0113	0.0002	0.0113		
1.4	0.5328	0.0143	0.0003	0.0143		
1.6	0.4478	0.0172	0.0004	0.0172		
1.8	0.3726	0.0199	0.0007	0.0199		
2.0	0.3085	0.0226	0.0006	0.0226	-0.1667	0.0226
	0.3087	0.0210	0.0002	0.0210	-0.1783	0.0211
2.2	0.2472	0.0234	0.0002	0.0234		
2.4	0.2051	0.0264	0.0002	0.0264		
2.6	0.1641	0.0299	0.0003	0.0299		
2.8	0.1287	0.0337	0.0003	0.0337	-0.3467	0.0340
3.0	0.0983	0.0378	0.0004	0.0378	-0.5365	0.0382
3.2	0.0723	0.0427	0.0003	0.0428	-0.7009	0.0433
3.6	0.0303	0.0485	0.0028	0.0486		

Thirty basis functions were used for the calculations in the region $R \leq 2.0$, and 38 basis functions in the region $R \geq 2.0$.

1. S. Hara and H. Sato, J. Phys. B, **11**, 955 (1978).
2. H. Sato and S. Hara, J. Phys. B, **13**, 4457 (1980), corrigendum **15**, 1305 (1982).
3. H. Sato and S. Hara, Abstracts of XII ICPEAC, p775 (Gatlingburg, 1981).
4. S. Hara and H. Sato, J. Phys. B, **17**, 4301 (1984).
5. A. Hazi, Electron-Molecule and Photon-Molecule Collisions, ed. by T. Rescigno, V. McKoy, and B. Schneider, p281 (Plenum, New York, 1979).
6. H. Takagi and H. Nakamura, Phys. Rev. A, **27**, 691 (1983).
7. L. A. Collins and B. I. Schneider, Phys. Rev. A, **27**, 101 (1983).
8. S. L. Guberman, J. Chem. Phys., **78**, 1404 (1983).
9. J. Tennyson and C. J. Noble, private communication.

THE ELECTRON MOMENTUM SPECTROSCOPY OF H_2^{**}

M.A. Coplan,* A.D. Smith,* D.J. Chornay,* J.H. Moore,*
J.A. Tossell,* V.H. Smith, Jr.,[†] and J.W. Liu[‡]

* Institute for Physical Science and Technology, University of Maryland, College Park, MD 20742 USA

† Department of Chemistry, University of Maryland, College Park, MD 20742 USA

‡ Department of Chemistry, Queen's University, Kingston, Ontario, Canada K7L 3N6

§ Division of Physics, National Research Council, Ottawa, Ontario, Canada K1A 0R6

The cross section in electron momentum or (e,2e) spectroscopy factorizes under appropriate conditions into an electron collision term and a structure term.¹ Precise experimental cross sections coupled with accurate structure calculations can lead to a better understanding of the scattering dynamics which in turn can be used to obtain more detailed knowledge of the target's electronic structure.

We have obtained precise (e,2e) data for H_2 at four incident electron energies and have compared the results with calculations which take into account the overlap of the $1s_g$, $2p_u$, $2p_u$ and $2s_g$ H_2^+ final state wave functions with a high quality CI wave function for the $1s_g$ ground state of the H_2 target.² For the $1s_g$ final state, the differences between experiment and theory are mainly due to the inadequacy of the simple plane wave description of the collision process; for the $2p_u$, $2p_u$ and $2s_g$ final states, discrepancies between the data and calculations can be attributed to deficiencies in the H_2 CI wave function.

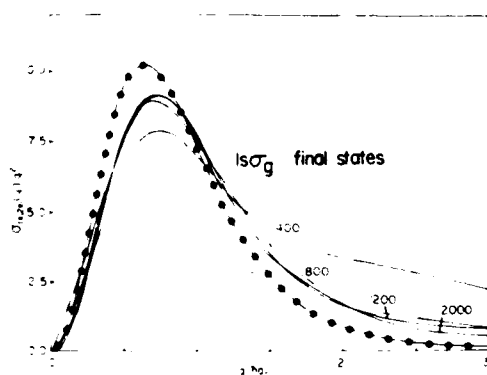


Fig. 1

Fig. 1 shows the relative (e,2e) cross section, $\sigma(e,2e)/q^2$, weighted by q^2 as a function of q for electron impact ionization of H_2 leading to H_2^+ in the $1s_g$ ground state. The solid lines are fits to the experimental data at incident electron energies of 400, 800, 1200 and 2000 eV. The curve labeled CI is a calculation based on a CI wave function² and agrees best in the large q region with the 2000 eV data. This is the expected result when distortion effects

assume a role. These effects can be accounted for by substituting distorted waves for plane waves in the formulation of the collision process.³

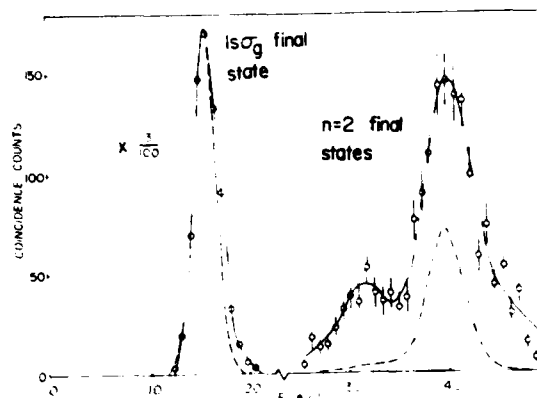


Fig. 2

Fig. 2 shows a separation energy spectrum obtained by summing (e,2e) cross sections over the q range from 0.2 to 3.0 atomic units at electron binding energies from 10 to 50 eV. The peak at 15.8 eV corresponds to the transition to the $1s_g$ ground state of H_2^+ , the dominant ionization process. The unresolved peaks covering the range from 25 to 50 eV correspond to the $n = 2$ final states of H_2^+ . The difference between experiment (full line) and calculations (broken line) in the $n = 2$ region is well outside of experimental error and is especially large around 30 eV corresponding to the $2p_u$ state.

References

1. E. Weigold and I.E. McCarthy, *Advances in At. and Mol. Phys.*, **14** 172 (1978)
2. J.W. Liu and V.H. Smith, Jr., *Phys. Rev. A*, submitted for publication
3. M.A. Coplan, D.J. Chornay, J.H. Moore, J.A. Tossell and N.S. Chant, *Lecture Notes in Chemistry*, **35** 156 (1984)

** Research supported by NSF Grant CHE8205884 and the Computer Science Center of the University of Maryland

ROTATIONALLY RESOLVED ELECTRON-PHOTON COINCIDENCE STUDY
 OF THE $H_2(d^3\sigma_u^-)$ EXCITATION

 J. W. McConkey,^a S. Trajmar,^b J. C. Nickel^c and G. Csanak^x
^aDepartment of Physics, University of Windsor, Windsor, Ontario, Canada

^bJet Propulsion Laboratory, California Institute of Technology, Pasadena, CA 91109

^cDepartment of Physics, University of California, Riverside, CA 92507

^xLos Alamos National Laboratory, Los Alamos, NM 87545

Only three electron-photon coincidence measurements have been reported so far on molecules.¹ In these measurements no attempt was made to resolve the rotational structure of the band being studied and, therefore, no detailed information about individual angular-momentum states could be obtained. The work reported here represents the first attempt to isolate and study by coincidence techniques an ensemble of molecules excited by electron impact into a specific rotational state. The polarization character of the radiation from the decay of the excited state was measured at 90° with respect to the scattering plane. 3000 hours of continuous data acquisition were required to obtain the present data. Figure 1 shows a typical coincidence spectrum. The three normalized Stokes' parameters were determined for the $H_2(X^1g^+; v_0 = 0, N_0 = 1 \rightarrow d^3\sigma_u^-, v_1 = 0, N_1 = 1)$ excitation at 25 eV electron impact energy and 20°, 40° and 60° scattering angles followed by the $(d^3\sigma_u^-, v_1 = 0, N_1 = 1 \rightarrow a^3g^+, v_f = 0, N_f = 1)$ radiation decay.

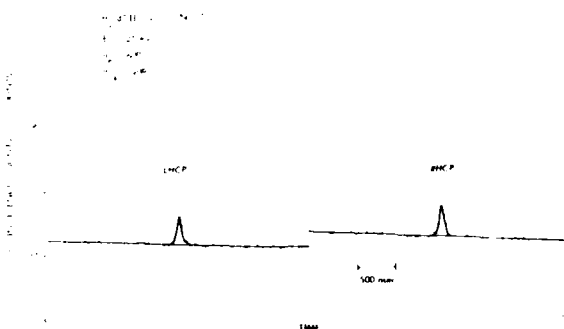


Fig. 1. Coincidence peaks obtained for left and right circularly polarized photons.

The circular polarization measurements indicate that no net angular momentum perpendicular to the scattering plane is transferred to the molecule in these collisions. Averaging over unresolved ground state magnetic sublevels in the electron impact process and the perturbing effects of fine and hyperfine fields in the radiation process could cause significant reduction of the coherence of the emitted radiation. In spite of

all these effects, we found considerable degree of linear polarization and coherence. Figure 2 shows the linear polarization of the coherent part of the radiation field for impact energy of 25 eV and scattering angle of 60°. The Stokes' parameters and the degree of polarization are listed in Table I.

Table I. Stokes' Parameters at $E_0 = 25$ eV.

(deg)	$P_C(\text{circ})$	$P_C(0^\circ)$	$P_C(45^\circ)$	P
20	-0.04 ± 0.10	-0.08 ± 0.14	$+0.02 \pm 0.10$	0.09 ± 0.20
40	$+0.04 \pm 0.18$	-0.03 ± 0.17	$+0.04 \pm 0.19$	0.06 ± 0.31
60	$+0.01 \pm 0.13$	$+0.30 \pm 0.17$	$+0.15 \pm 0.14$	0.34 ± 0.26

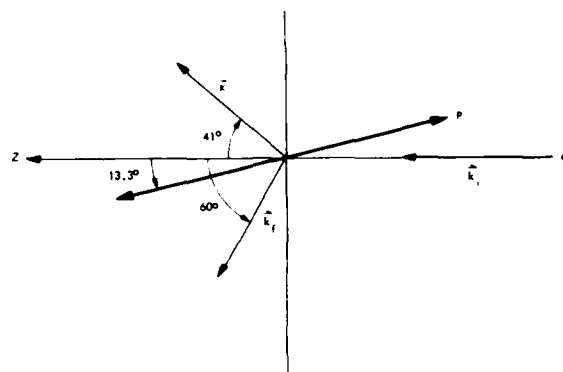


Fig. 2. Schematic representation of the observed radiation field ($E_0 = 25$ eV, $\theta = 60^\circ$).

The Stokes' parameters can be analyzed in terms of state multipoles characterizing the excited state with the help of the formalism given by Blum and Jakubowicz.² The interpretation and implication of these results will be discussed.

This work was performed at the Jet Propulsion Laboratory, California Institute of Technology and was supported in part by the National Aeronautics and Space Administration and in part by the National Science Foundation.

References

1. I. C. Malcolm and J. W. McConkey, J. Phys. B 12, L67 (1979); K. Becker, H. W. Dasser, and J. W. McConkey, J. Phys. B 16, 1177 (1983) and 17, 2535 (1984).
2. K. Blum and H. Jakubowicz, J. Phys. B 11, 9909 (1978).

ELASTIC AND INELASTIC ELECTRON SCATTERING CROSS SECTIONS FOR H_2

M. Khakoo^a and S. Trajmar

^aJet Propulsion Laboratory, California Institute of Technology, Pasadena, CA 91109
Physics Department, University of Windsor, Windsor, Ontario, Canada N9B 2Z2

A beam-beam scattering arrangement was used to measure differential elastic and inelastic electron scattering cross sections for H_2 in the 15 to 100 eV impact energy and 10° to 125° angular regions. The relative flow method^{1,2} was utilized with the known differential elastic scattering cross sections of He^3 to obtain the absolute cross sections. The calibration procedure was checked out on Ne for which elastic cross sections are known.

The H_2 elastic cross sections obtained in the 15 eV to 100 eV impact energy region will be presented and compared with other experimental and theoretical results.

Excitation to the $b^3\sigma_u^-$ continuum state was studied at impact energies ranging from 20 to 100 eV. A typical spectrum is shown in Fig. 1. The continuum energy-loss

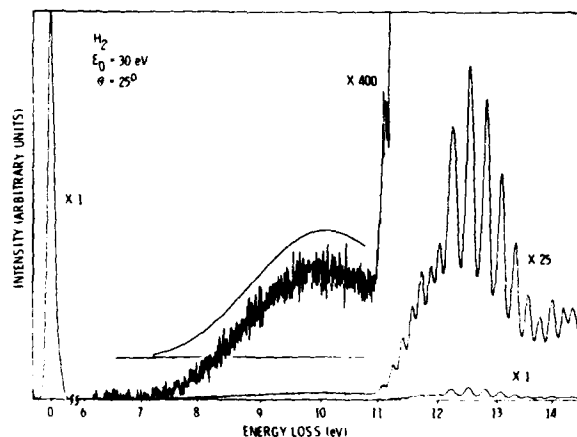


Fig. 1. Energy-loss spectrum for H_2 showing the $b^3\sigma_u^-$ continuum

profile was fitted to the Franck-Condon envelope determined by Gibson⁴ to obtain the total scattering intensity associated with this transition. From the measured inelastic to elastic scattering intensity ratios, we obtained the absolute excitation cross sections for the $b^3\sigma_u^-$ state by utilizing the elastic cross sections. The present results will be discussed and compared to other experimental and theoretical data.

Excitations of the $B^1\sigma_u^+$, $c^3\sigma_u^-$, $a^3\sigma_g^+$, $C^1\sigma_u^-$ and $E^1\sigma_g^+$ discrete states were also studied at 20, 30, 40 and 60 eV impact energies. A typical spectrum is shown in Fig. 2. The overlapping vibrational band structure of the various electronic transitions were unfolded using a computer code described earlier.⁵ The scattering

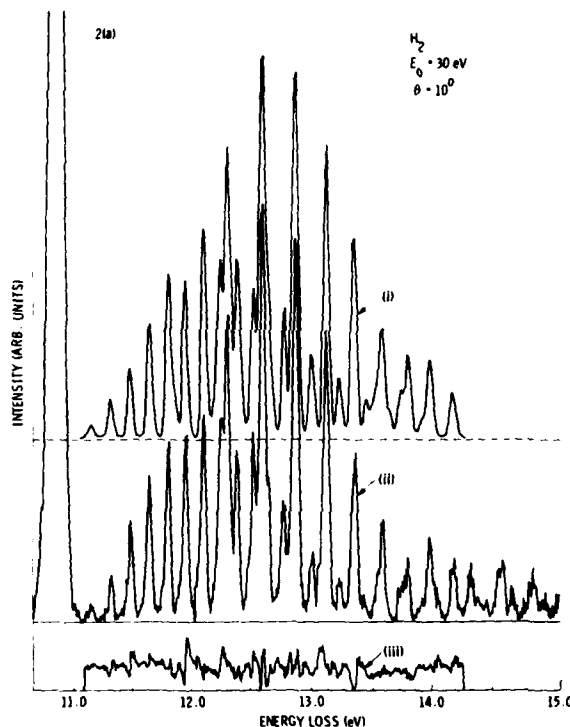


Fig. 2. Energy-loss spectrum for H_2 showing the overlapping band structure of the various discrete electronic transitions. (i) computer fit (ii) experimental spectrum, (iii) difference spectrum.

intensities were then transformed into absolute cross sections by the same procedure which was employed for the $b^3\sigma_u^-$ excitation. The results will be presented and compared to other available data.

This work was performed at the Jet Propulsion Laboratory, California Institute of Technology and was supported in part by the National Aeronautics and Space Administration and in part by the National Science Foundation.

References

1. S. K. Srivastava, A. Chutjian and S. Trajmar, J. Chem. Phys. **63**, 2659 (1975).
2. S. Trajmar and D. F. Register, in *Electron Molecule Collisions*, eds. K. Takayanagi and I. Shimamura, Plenum Press, New York, 1984.
3. D. F. Register, S. Trajmar and S. K. Srivastava, Phys. Rev. **A21**, 1134 (1980).
4. T. L. Gibson, private communication (1984).
5. D. C. Cartwright, A. Chutjian, S. Trajmar and W. Williams, Phys. Rev. **A16**, 1013 (1977).

RECENT ADVANCES IN ELECTRON IMPACT EMISSION EXPERIMENTS OF H_2 , He, N_2 AND Ar

J. M. Ajello^{*} and D. E. Shemansky[†]

^{*}Jet Propulsion Laboratory, California Institute of Technology, Pasadena, CA 91109
[†]Lunar and Planetary Laboratory, University of Arizona, Tucson, Arizona 85713

We have completed experimental studies of electron impact cross section measurements of H_2 , He, N_2 and Ar and have found the following fundamental results: 1) the benchmark dissociative cross section of H Ly- γ produced by electron dissociation of H_2 , widely used as a calibration standard in the VUV, needs to be revised downward by 0.69; 2) experimental H_2 Rydberg state cross sections at low energies are lower than theoretical calculations; 3) the H_2 ($a^3_g \rightarrow b^3_u$) continuum is an important uv emission process at low energy (< 20 eV); 4) ionization excitation cross sections of He, the simplest gas for this type of two electron excitation process, show energy dependences different from theoretical calculations; 5) the low energy vibrational cross sections of both the $H_2(B)$ and $N_2(a)$ states show departures from Franck-Condon distribution due to differences in excitation threshold of the vibrational levels; 6) emission studies of the Ar resonance lines at 104.8 and 106.6 nm can be compared to electron energy loss experiments which measured direct and cascade cross sections with good agreement.

We have revised the Lyman- γ cross section¹ based on previously measured Lyman- γ /Lyman bands and Lyman-Werner bands electronic cross section ratios.² The revised value is $8.18 \pm 1.2 \times 10^{-18}$ cm² at 100 eV. Also, the cross sections for the H_2 Rydberg states at < 100 eV are now lower than theoretical calculations.³ This is of fundamental importance since H_2 is the simplest molecule for theoretical calculations of electronic excitation. The differences in energy dependence are shown in Fig. 1. We show in Fig. 2 the first relative emission cross section measurement of the a-b continuum compared to other important H_2 cross sections.

Simultaneous ionization-excitation of He leads to emissions at 121.51 nm and 164.04 nm. We find that all experimental data is in agreement in respect to the shape of the excitation functions of the HeII emissions. The failure of the theory to describe the experimental results stems from the neglect of electron correlation effects between two orbital electrons.

The cross section of the $a^1_g \rightarrow x^1_g$ band system has been measured. The energy dependence of each vibrational level, is shown in Fig. 3. At energies > 20 eV, the relative a^1_g vibrational cross sections gradually converge on the Franck-Condon distribution. The threshold shift effect on vibrational cross sections

has not been recognized in the literature and is important for other molecules, especially N_2 , H_2 , HD, D_2 , CO, O_2 .

Work was performed at JPL-Caltech and was sponsored by AFOSR and NASA.

References

1. M. J. Mumma and E. C. Zipf, J. Chem. Phys. **55**, 1661 (1971).
2. J. M. Ajello, D. E. Shemansky, Y. L. Yung, and D. Kwok, Phys. Rev. A **29**, 336 (1984).
3. G. P. Arrighini, F. Biondi, C. Guidotti, A. Biagi, and F. Marinelli, J. Chem. Phys. **53**, 133 (1980).

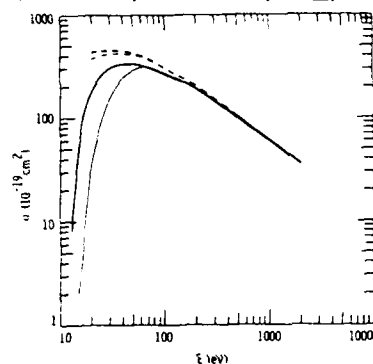


Fig. 1. The heavy curve is the $H_2(B)$ and the light line the $H_2(C)$ direct cross sections. The dashed curves are theoretical cross sections.³

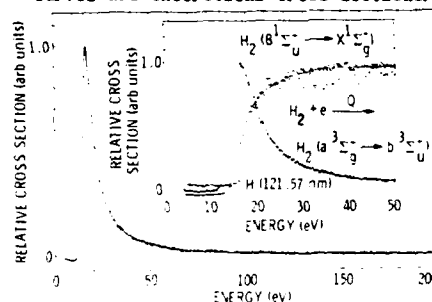


Fig. 2. Relative emission cross section of the H_2 ($a^3_g \rightarrow b^3_u$) continuum.

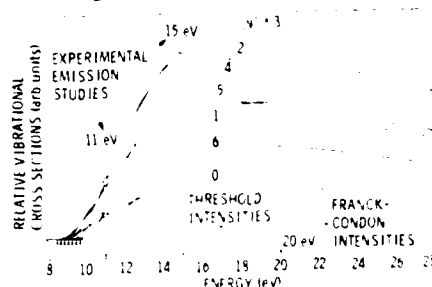


Fig. 3. The relative emission cross section of each vibrational level in the threshold region.

ELECTRON IMPACT EXCITATION OF N_2 IN THE NEAR THRESHOLD REGIONT. Antoni¹, S. Trajmar² and D. C. Cartwright³¹National Research Council Resident Research Associate²Jet Propulsion Laboratory, California Institute of Technology, Pasadena, CA 91109³Los Alamos National Laboratory, Los Alamos, New Mexico 87545

Electron scattering by molecular nitrogen has been the subject of the most extensive studies among all molecules. In spite of all these efforts our knowledge of electron collision cross sections for N_2 is rather fragmentary. In the area of electron impact excitation of the electronic states of N_2 the major problems are: 1) non-availability of differential (and in many cases integral) cross section data at low impact energies (threshold to few eV above threshold); 2) large discrepancies in the available cross sections at intermediate impact energies. On the other hand there is a need for accurate cross sections for practical applications and for guiding the development of theoretical methods for the interpretation of such data.

In our laboratory, we are in the process of measuring electron impact excitation cross sections for the electronic states of N_2 at low impact energies. One encounters two major experimental problems with low-energy absolute cross section measurements: 1) in analyzing data associated with various bands of a given electronic state the cross section dependence has to be explicitly considered for each band (because the excitations occur at different impact energies above the respective thresholds); 2) special calibration procedures are required to compensate for the dependence of the detector efficiency on the residual energy of the electrons and to place the measurement on the absolute scale. A new computer code for analyzing the electron energy-loss spectra and a procedure for the absolute calibration of the cross sections were developed and will be described.

We have now determined absolute cross sections for elastic scattering and electron-impact excitation of the lower triplet states of N_2 in the near threshold region. Results will be presented for impact energies ranging from 7.5 to 20 eV and scattering angles between 15° and 120° . The measurements are performed with a crossed-beam spectrometer using single hemispherical energy selectors. At 1.5 nA primary beam intensity the overall energy resolution is 27 meV.

Two examples of energy loss spectra for 10 eV impact energy and 15° and 120° scattering angles are given in Fig. 1. Even from these unprocessed data it can be seen, that the intensity ratios for elastically and inelastically scattered electrons vary drastically with angle for the excitation of some bands (e.g. the

peak associated with the $X^1_g - B^3_g$, $v = 1$ transition at $E = 7.564$ eV) whereas in other cases they change only smoothly (for instance for the process $X^1_g - A^3_u$, $v = 6$ at $E = 7.184$ eV). The elastic DCS's are nearly isotropic at this energy.

This work was performed at the Jet Propulsion Laboratory, California Institute of Technology and was supported in part by the National Aeronautics and Space Administration and in part by the National Science Foundation.

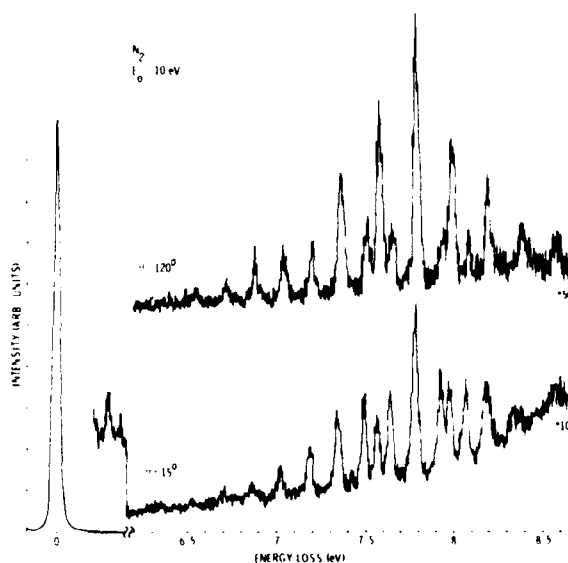


Fig. 1. Electron impact energy-loss spectra for N_2 obtained at 10 eV impact energy and 15° and 120° scattering angles.

ROTATIONALLY-RESOLVED IONIZATION OF N_2 BY ELECTRON IMPACT

P. W. Zetner, W. B. Westerveld* and J. W. McConkey

Physics Department, University of Windsor, Ontario, N9B 3P4 Canada

* Physics Department, University of N. Carolina, Raleigh, NC 27650 USA

Recently there has been an increasing interest in non dipole effects¹⁻³ following collisions of low energy electrons with simple molecules. Excitation of the $B^2_{\pi_u}+$ state of N_2 has been particularly widely studied⁴⁻⁸ because of the wide use of the resultant First-Negative bands in plasma diagnostics. The development of supersonic beam techniques has allowed rotationally-specific target preparation so that non-dipole effects in the excitation (ionization) process become much more obvious. Excited state rotational populations have generally been deduced from emission spectra following the initial excitation process. Considerable rotational warming of the $N_2^+ B^2_{\pi_u}+$ state has been observed as the incident electron energy was decreased and various models have been put forward to explain the observations. DeKoven et al.⁷ suggest that an interaction occurs between the ion and the ejected electron thus causing a breakdown of the $\Delta K = \pm 1$ dipole selection rule. Becker et al.³ looked at the excitation of the $N_2 C^1_{\pi_u}+$ state, where no ejected electron was involved and observed similar rotational warming effects which increased as the incident electron energy was reduced towards threshold.

In the present study laser fluorescence techniques⁵ are used to probe the rotational population of the $N_2^+ (X^2_{\pi_g}+)$ state following electron collisions with a cold N_2 beam from a pulsed supersonic jet. The operation of the system was as follows. $N_2^+ X^2_{\pi_g}+$ molecules were formed using a pulsed electron gun. After allowing sufficient time for the decay of any excited ionic species the interaction region was probed with the 10 ns pulse output from a molelectron N_2 -laser-pumped dye laser system. Suitable choice of dye allowed different vibrational levels of the $X^2_{\pi_g}+$ state to be investigated. Following absorption of a laser photon to the $B^2_{\pi_u}+$ ($v = 0$) state, the resulting 3914 Å fluorescence was detected using a cooled photo-multiplier. Typical scans of the R-branch region of the (0,1) vibrational transition are shown in Figure 1. Clear differences in the two spectra taken at 300 and 50 eV impact energies can be seen with more rotational development apparent in the 50 eV spectrum.

Detailed studies are being made of the effect of collisions involving secondary electrons from the ionization process or from beam-aperture interactions. Relative cross sections for different ΔK transitions in

the ionization process as a function of incident electron energy will be presented at the Conference.

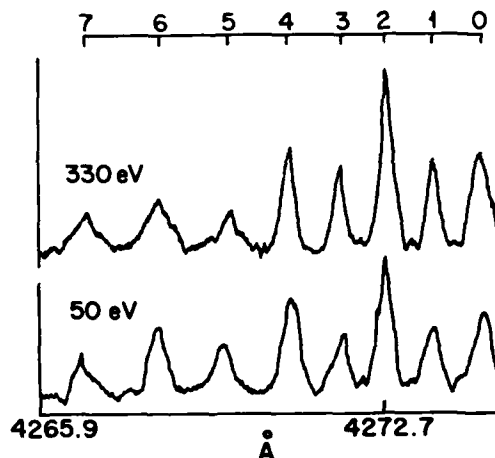


Figure 1. Variation of 3914 Å (0,0) output fluorescent intensity as a function of input laser wavelength. The R-branch members of the $X^2_{\pi_g}+$ ($v = 1$) - $B^2_{\pi_u}+$ ($v = 0$) transition are indicated.

This work was supported by the Natural Sciences and Engineering Research Council of Canada (NSERC).

References

1. S. P. Hernandez, P. J. Dagdigan and J. P. Doering, *J. Chem. Phys.* **77**, 6021 (1982); *Chem. Phys. Lett.* **91**, 409 (1982).
2. P. J. Dagdigan and J. P. Doering, *J. Chem. Phys.* **78**, 1336 (1983).
3. K. Becker, I. L. Forand, P. W. Zetner and J. W. McConkey, *J. Phys. B* **17**, 1915 (1984).
4. G. Culp and A. T. Stair, Jr., *J. Chim. Phys.* **54**, 37 (1967).
5. J. Allison, T. Kondow and R. N. Zare, *Chem. Phys. Lett.* **64**, 202 (1979).
6. A. Carrington and R. P. Luckett, *Chem. Phys. Lett.* **74**, 19 (1980).
7. B. M. DeKoven, D. E. Levy, H. H. Harris, R. R. Zeparski and T. A. Miller, *J. Chem. Phys.* **74**, 5659 (1981).
8. G. I. Sukhinin and R. G. Sharatutdinov, *Sov. Phys. Tech. Phys.* **28**, 204 (1983).

PARTIAL GENERALISED OSCILLATOR STRENGTH FOR IONISATION OF THE NITROGEN MOLECULE BY 1-KEV ELECTRON IMPACT

K.Kuroki*, F.Nishimura, N.Oda and T.Ichimori

Research Laboratory for Nuclear Reactors, Tokyo Institute of Technology, Meguro-ku, Tokyo, Japan

Generalised oscillator strengths (GOS) have been derived from measurements of double-differential cross sections (DDCS) for ionising collisions by electron impact on various kinds of atoms and molecules. However, in the DDCS measurements one cannot determine the initial and final states of the transitions of interest when many orbitals take part in these transitions.

The aim of this study is to obtain more detailed information on the structures of the GOS, that is, partial generalized oscillator strength (PGOS) corresponding to the specified transitions by using electron-electron coincidence (e-2e) method.

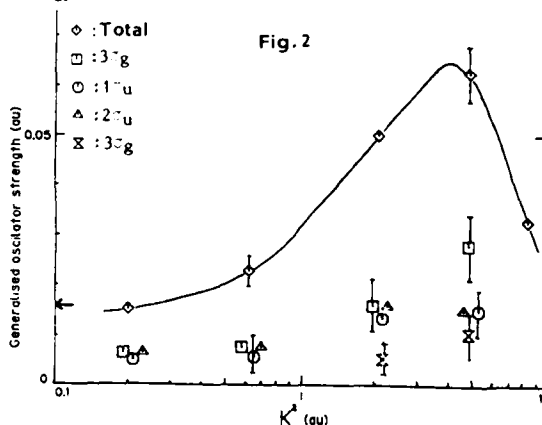
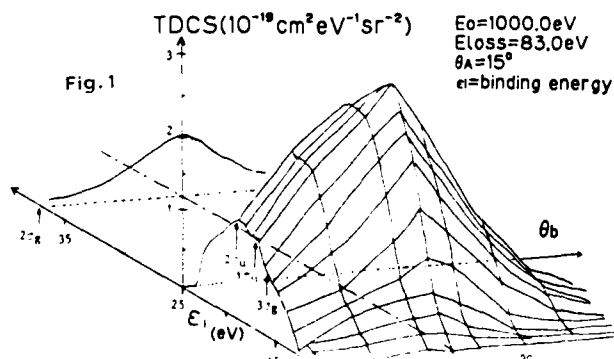
The GOS becomes approximately equal to the optical oscillator strength when the momentum transfer of the incident electron tends to zero. Van der Wiel, Brion and their coworkers (Brion and Hammett 1981 and references therein) have measured the partial optical oscillator strengths by using electron-electron and electron-ion coincidence methods in the case of 0° scattering of incident electrons. In our measurements the scattering angle of the incident electrons is not limited to the 0° angle and therefore the momentum transfer of the incident electrons can be varied.

In the present work, TDCS have been measured for a nitrogen molecule bombarded by 1 keV electrons using a crossed-beam method. The (e-2e) spectrometer system consists of a cylindrical mirror analyzer ($\Delta\theta=0.5^\circ$, $\Delta E/E=0.3\%$) for the scattered electrons, a 45° parallel-plate mirror analyzer ($\Delta\theta=4^\circ$, $\Delta E/E=1.0\%$) for the ejected electrons, fast coincidence circuits and microcomputers. In measurements of the GOS, when the energy loss of the incident electrons is fixed, the energy of the ejected electrons varies, corresponding to the individual molecular orbital taking part in the ionising collisions. The TDCS and partial DDCS were normalised to the absolute scale with respect to the

absolute DDCS which were previously measured using a static gas target in our laboratory, by integrating the relative TDCS over all ejection directions, assuming a cylindrical symmetry about the direction of the momentum transfer.

The TDCS measurements to derive the GOS were performed under coplanar geometry where the azimuthal angle ϕ equals 0 or π . The scattering angle was varied from $+5^\circ, +2^\circ, -2^\circ$ to -20° , corresponding to momentum transfer from 0.21 to 4.9 au, and the ejected angle from $+40^\circ$ to $+120^\circ$. Figure 1 shows the angular distributions and the energy spectra of the ejected electrons for the scattering angle $\theta_a=15^\circ$, in the form of TDCS. The incident electron energy is 1000.0 eV, and the energy loss is 83.0 eV. The four orbitals indicated by arrows in the figure, correspond to the molecular orbitals of $3\sigma_g$ (15.59 eV, $X^2\Sigma_g^+$), $1\pi_u$ (16.96 eV, $A^2\Pi_u$), $2\sigma_u$ (18.78 eV, $B^2\Sigma_u$) and $2\sigma_g$ (37.3 eV, $^2\Sigma_g$).

In the normalisation procedure we ignored the contributions of the $1\sigma_g$ and $1\sigma_u$ (409.9 eV) orbitals and the configuration-interaction state (28 eV). The contribution of the recoil peak to the TDCS was 20% at $\theta_a=5^\circ$, 40% at $\theta_a=2^\circ$. Figure 2 shows the total and partial GOS plotted against the square of the momentum transfer (K) for the energy loss of 83.0 eV. An arrow on the ordinate indicates the value for an energy loss of 83 eV at $K=0$ which was estimated by extrapolation of the experimental data obtained by Weight et al (1976) for energy losses less than 69 eV.



References

1. Brion C E and Hammett A Advances in Chemical Physics vol 45 (New York: Wiley 1981) pp 1-80
2. Wight G R, Van der Wiel M J and Brion C E J. Phys. B: At. Mol. Phys. 1974 9 675-89
3. Hammett A, Stoll W and Brion C E J. Electron Spectrosc. Relat. Phenom. 1976 8 367-76

* Permanent address: National Research Institute of Police Science, Chiyoda-ku, Tokyo, 102 Japan.

GENERALIZED OSCILLATOR STRENGTH FOR THE $X^1\Sigma_g^+ \rightarrow a^1\Pi_g$ TRANSITION
IN MOLECULAR NITROGEN AT 1 keV INCIDENT ELECTRON ENERGY

G. G. B. de Souza and C. A. Lucas

Instituto de Química da Universidade Federal do Rio de Janeiro
Cidade Universitária - 21910 - Rio de Janeiro - RJ - Brasil

Generalized oscillator strength (GOS) for the dipole-forbidden quadrupole-allowed transition $X^1\Sigma_g^+ \rightarrow a^1\Pi_g$ (Lyman-Birge-Hopfield band) in molecular nitrogen has been obtained at 1 keV electron incident energy.

We have used a crossed-beam type electron energy-loss spectrometer which has been described earlier¹. An extensive set of energy-loss spectra have been obtained in the angular range 2 to 20 degrees. In figure 1 we present a typical electron energy-loss spectrum, measured at 2°. The energy resolution is approximately 0.6 eV and the energy-loss range is 0 - 35 eV.

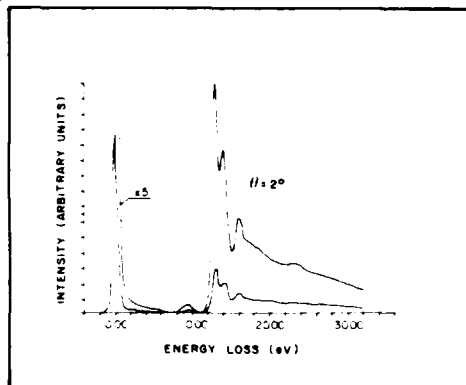


FIGURE 1 - Electron energy-loss spectrum of nitrogen at 1 keV.

The relative differential cross section for the Lyman-Birge-Hopfield band (9.2 eV energy-loss) has been measured and made absolute by comparison with the absolute elastic differential cross section of Jansen et al².

The corresponding GOS is presented in figure 2. There is a good agreement with the experimental results of Oda and Osawa³ and Skerbelle et al⁴. A poor agreement is observed, however, with the results published by Wong et al⁵. The theoretical calculations based on the Born Approximation⁶ agree with the experimental results only in the range $0 < K^2 < 0.3$ a.u.; the calculations based on the Random Phase and Tamm-Dancoff Approximations⁷

on the other hand, show a reasonable agreement only for $K^2 > 1$ a.u.

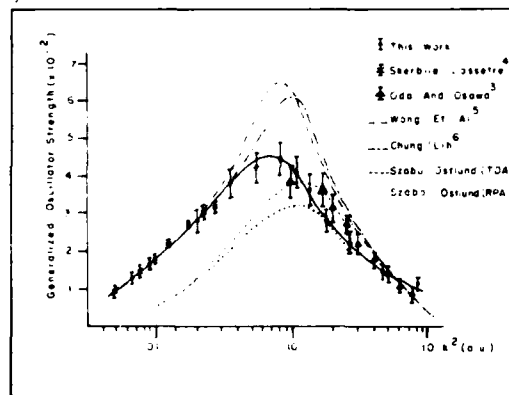


FIGURE 2 - Generalized Oscillator Strength for the Lyman-Birge-Hopfield Band.

Financial support from the CNPq, FINEP and FUJB is gratefully acknowledged.

REFERENCES:

- 1) G.G.B. de Souza, A.C.A. e Souza, R. de B. Faria, in *Electronic and Atomic Collisions*, J. Eichler, W. Fritsch, I.V. Hertel, N. Stolterfoht and U. Wille, editors - North-Holland Amsterdam, Oxford, New York and Tokyo 1983 (page 707).
- 2) Jansen, R.H.J., de Heer, F.J., Luyken, H.J., Van Wingerden, B., Blaauw, H.J., *J. Phys. B*, **9**, 185 (1976)
- 3) Oda, N., Osawa, T., *J. Chem. Phys. B*, **14**, L563 (1981)
- 4) Skerbelle, A., Lassetre, E.N., *J. Chem. Phys.*, **53**, 3806 (1970)
- 5) Wong, T.C., Lee, J.S., Wellenstein, H.L., Bonham, R.A., *J. Chem. Phys.*, **63**, 1538 (1975)
- 6) Chung, S., Lin, C.C., *Physical Review A*, **6**, 988 (1972)
- 7) Szabo, A., Ostlund, N.S., *Chem. Phys. Lett.*, **17**, 163 (1972)

LOW-LYING RESONANCES IN ELECTRON-LITHIUM MOLECULE SCATTERING

H. H. Michels*, R. H. Hobbs* and L. A. Wright**

*United Technologies Research Center, East Hartford, Connecticut 06108 USA

**Mission Research Corporation, Albuquerque, New Mexico 87106 USA

The resonance structure associated with electron scattering by the hydrogen molecule has been the subject of many theoretical and experimental studies¹⁻³. In contrast, electron scattering by Li_2 has received relatively little attention. Miller, et al.⁴ have measured total cross sections for $e + \text{Li}_2$ scattering in the 0.5–10.0 eV region and find a very large ($\sim 500 \text{ \AA}^2$) and rising total cross section for the low-energy region. These results suggest that some sort of shape resonance may be found in this system corresponding to a low-lying state of Li_2^- . Such resonant states have been observed in electron impact excitation of Na_2 ⁵.

The location of the low-lying electronic states of Li_2^- is also required for an analysis of Li^- formation by dissociative attachment (DA) of $e + \text{Li}_2$ and for studies of collisional vibrational excitation of Li_2 .⁶ McGeoch, et al.⁷ have commented on the possibility of Li^- formation through a series of reactions similar to those found for $e + \text{H}_2$.

In order to clarify the electronic structure of the Li_2^- anion, a series of *ab initio* calculations of the parent $^1\Sigma_g^+$ state of Li_2 and of several possible symmetries of the anion were undertaken. The calculational framework that was chosen was a configuration-interaction (CI) expansion built from orthonormal Slater-type orbitals (STO's). An extended (14 σ , 6 π , 2 δ) basis was optimized using several methods of approach. Complete orbital optimization was possible only for Li_2 and the ground $X^2\Sigma_u^+$ state of Li_2^- since the excited anion states are either autodetaching at some critical internuclear separation or are pure resonant states. The lowest $^2\Sigma_g^+$ state of Li_2^- , which is the principle channel for DA of $e + \text{Li}_2$, is variationally stable for large internuclear separations, and a smooth extrapolation of optimized orbital exponents for this state was carried out into the autodetaching region. The purely resonant states of Li^- and Li_2^- were treated using a modified nuclear charge hamiltonian, similar to that described by Nestmann, et al.⁸. In this method the resonant states are variationally stabilized by an increased nuclear charge and an analytic extrapolation is carried out to determine the real part of the expectation value of the unperturbed hamiltonian.

The calculated results are shown in Fig. 1 for several low-lying electronic states of Li_2^- . Our calculated electron affinity for Li_2 , derived from our

location of the $X^2\Sigma_u^+$ state of Li_2^- , is 0.42 eV, in good agreement with previous theoretical studies.

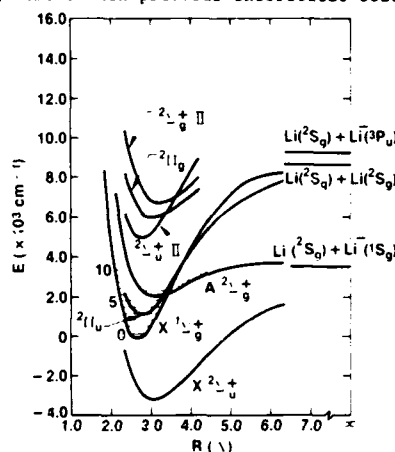


FIGURE 1 Low-Lying Resonant States of Li_2^- .

The $A^2\Sigma_g^+$ state of Li_2^- exhibits a complex potential energy for internuclear separations smaller than 3.45 Å, where a crossing with the $X^1\Sigma_g^+$ state of Li_2 is found. This resonant state of Li_2^- is mainly of the Feshbach type with a small width for decay to the ground state of Li_2 . Of special interest is the low-lying $^2\Pi_u$ resonant state which lies approximately 150 meV above the ground state of Li_2 . This anion state has a dominant MO configuration of $(1\sigma_g^2 1\sigma_u^2 2\sigma_g^2 1\pi_u)$, indicating a relatively large capture width for low-energy electron scattering, and is probably responsible for the large scattering cross sections observed by Miller, et al.⁴ for low collisional energies. The character of this $^2\Pi_u$ state is similar to the $^2\Pi_g$ resonant state of N_2^- in that the anion state lies lower than the corresponding neutral parent for a wide region of internuclear separations (3.5 $\lesssim R \lesssim 9.0 \text{ \AA}$).

References

1. G. J. Schulz, Rev. Mod. Phys. **45**, 422 (1973).
2. "Electron-Molecule and Photon-Molecule Collisions", eds. T. N. Rescigno, et al, Plenum Press, NY (1979).
3. "Resonances in Electron-Molecule Scattering", ed. D. G. Truhlar, ACS Symp. Series 263, (1984).
4. T. M. Miller, A. Kasdan and B. Bederson, Phys. Rev. A **25**, 1777 (1982).
5. D. Teillet-Billy, L. Bouby and J. P. Ziesel, Abst. 13th ICPEAC, ed. J. Eichler, et al, **294** (1983).
6. J. M. Wadehra and H. H. Michels, Chem. Phys. Lett., in press.
7. M. W. McGeoch and R. E. Schlier, "Production and Neutralization of Negative Ions and Beams", AIP Conf. Proc. **111**, 291 (1984).
8. B. Nestmann and S. D. Peyerimhoff, to be published.

Supported in part by AFOSR, Contract F49620-83-C-0094.

OBSERVATION OF $f^3_{g,u}$ OF F_2 MOLECULE BY ELECTRON ENERGY LOSS SPECTROSCOPY

K.Hoshiba⁺, Y.Fujita⁺, S.S.Kano⁺, H.Takuma⁺
T.Takayanagi⁺⁺, S.Yagi⁺⁺, K.Wakiya⁺⁺ and H.Suzuki⁺⁺

⁺ Institute for Laser Science, University of Electro-Communications, Chofu-shi, Tokyo 182 Japan.
⁺⁺ Department of Physics, Sophia University, Chiyoda-ku, Tokyo 102 Japan

Recent years molecular fluorine has been of great interests because of its wide application to the high power UV lasers such as rare gas halide or F_2 lasers. We performed high resolution electron energy loss spectroscopy of F_2 to find the upper level, $f^3_{g,u}$, of F_2 laser. In the pioneering work of Nishimura and his collaborators, the lower level of the laser transition, $a^3_{u,u}$, has been reported,¹ which we also confirmed by the use of "contamination-free" sample.

The experimental apparatus was the same as we reported in the XIII ICPEAC.² The overall resolution was 30-50 meV. The incident electron beam was crossed at 90 deg. at the collision center. The sample gas contained 10 % of F_2 in He, which was delivered from Central Glass Co. The purity of the sample was satisfactory: we observed only the feature of N_2 at/around 13.14 eV in the energy loss spectrum (air 0.04%, CF_4 less than 0.0002%).

Fig.1 shows the energy loss spectrum of F_2 at the incident electron energy of 18 eV. In the energy loss region of 11.5 eV to 12 eV, the vibrational structure $f^3_{g,u}$ is observed at the smaller scattering angle. It is evident that, for the larger scattering angle, a new feature becomes apparent near 11.6 eV. We assign these feature as $f^3_{g,u}$, the predicted upper laser level.³ The separation between two adjacent vibrational peaks is

almost the same as that of $F^1_{g,g}$, which is expected by the analogy with the case of Cl_2 .⁵

Above 12 eV, our high resolution spectrum (0.05 eV FWHM) is identical with the reported one by Hitchcock et al.⁶

As for the lower laser level of F_2 laser, $a^3_{u,u}$, we confirmed the assignment of Nishimura et al.¹ The scattering angle dependence of the broad feature near 9 eV is shown in Fig.2 and is considered to be a superposition of the triplet and the singlet state. On the other hand, another broad feature near 7 eV, which is considered to be $3^3_{g,u}$, $3^1_{g,u}$, $1^3_{g,u}$ and $3^1_{g,u}$, does not show any drastic change in the scattering angle dependence at the incident energy of 30 eV. Detailed analysis will be discussed.

This work was supported by grant-in-aid for the Fusion Research of Ministry of Education.

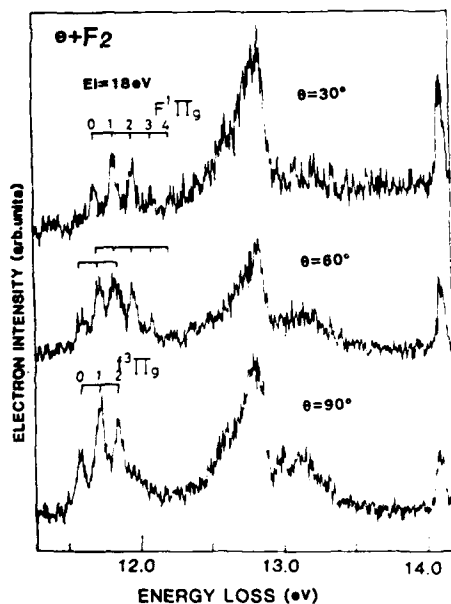


Fig.1

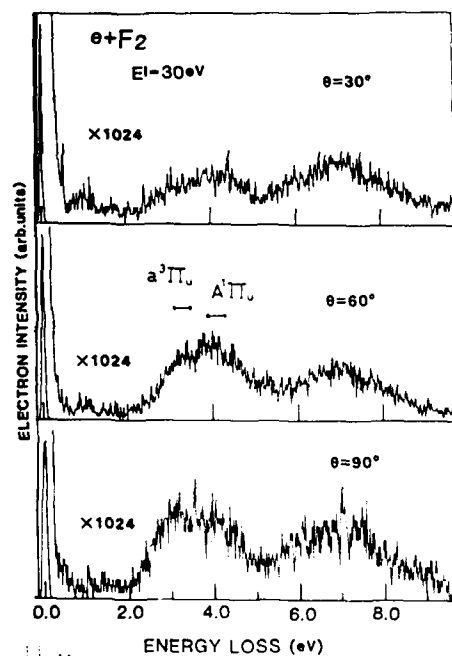


Fig.2

1. H.Nishimura, T.Yamashita, and Y.Tsugan, J. Chem. Phys. **51**, 1001 (1970).
2. H.Hitchcock et al., Abstract of International Symposium XIII ICPEAC, 1984, Berlin, 1984.
3. A.Kishino, A.Kishino and J.W. Edwards, Appl. Phys. Lett. **21**, 41 (1972).
4. T.Yamashita and H.Nishimura, J. Chem. Phys. **51**, 1010 (1970).
5. H.Nishimura, T.Yamashita, Y.Akai, and Y.Tsugan, J. Chem. Phys. **51**, 1001 (1970).
6. A.Hitchcock, G.L. Fisher, J. A. A. Reilly, and P.A. Hitchcock, J. Chem. Phys. **71**, 40 (1979).

LOW ENERGY ELECTRON - CH MOLECULE COLLISION

V. H. CHHAYA

Department of Physics, Saurashtra University, Rajkot 360 005 India

Various interstellar molecular species are being discovered. Their study can help much to understand the mechanism of the formation of stars and the cooling of interstellar gas.

When the gas is very thin, the rotationally excited polar molecule decays mostly via an emission of radiation. This leads to a loss of thermal energy of the gas as a whole. Dalgarno and Mc Gray¹ discussed the possibility of this type of cooling in the interstellar gas. Collisions of free electrons, if any, with such molecules may be an important mechanism to cool the interstellar gas containing them.

One of the many molecules found in the interstellar gas is CH molecule. It is also one of the cometary molecules. In the present investigation rotational excitation cross sections are calculated using the close coupling approximation for low energy ($< 10\text{ eV}$) electron collision with CH molecule. The results are compared with those of other investigators. Further rate of the electron cooling due to rotation excitation is calculated.

References.

1. A. Dalgarno and R. A. Mc Gray, Ann. Rev. Astron. Astrophys, 10 (1972) 375.

ELECTRON MOMENTUM SPECTROSCOPY OF CHLORINE

C.E. Brion, L. Frost and E. Weigold

The Flinders University of South Australia, South Australia 5042, Australia

The valence region of chlorine has been examined in detail using noncoplanar symmetric electron coincidence spectroscopy at 1000eV. The experiments were carried out on a coincidence spectrometer employing a new five element retarding lens with improved angular resolution, and position sensitive detectors mounted on the hemispherical energy analysers. The energy resolution was set at 1.3eV FWHM. Complete binding energy spectra from 9eV to 50eV were measured over a range of azimuthal angles corresponding to electron momenta of 0.1 a.u. to 2.2 a.u. The pole strengths for the various transitions and the individual orbital momentum distributions were obtained by fitting the peaks in the measured separation energy spectra with the measured transmission function suitably broadened in some cases to allow for the natural widths of the states.

The ground state MO configuration of Cl_2 is

$$(\text{core}) (4z_g)^2 (4\sigma_u)^2 (5\sigma_g)^2 (2\pi_u)^4 (2\pi_g)^4$$

Spherically averaged momentum distributions of all five valence states have been obtained, and the inner $4\pi_u$ and $4z_g$ transitions have been clearly identified for the first time.

The results are compared with the manybody Green's function calculation of Bieri et al.¹. This calculation is in poor agreement with the data in the inner valence region. Although it predicts splitting of these orbitals, it underestimates the severity of the splitting and obtains incorrect positions for the dominant poles. Figure 1 shows typical binding energy spectra at $\phi = 0^\circ$ ($q=0.1$ a.u.) and $\phi = 7^\circ$ ($q=0.5$ a.u.). The measured momentum distributions show that the peak at about 27eV binding energy must be assigned to the $4z_g$ orbital which also shows considerable strength in the 35eV to 40eV region. The peak at about 24eV must be assigned to the $4\pi_u$ orbital, as must most of the strength in the 20 - 22.5 and 30 - 35eV binding energy regions.

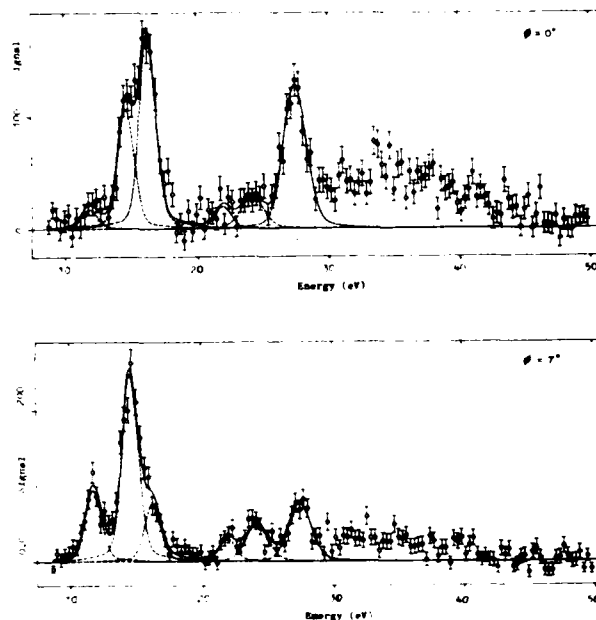


Figure 1. Separation energy spectra of Chlorine at $\phi = 0^\circ$ ($q=0.06$ a.u.) and $\phi = 7^\circ$ ($q=0.5$ a.u.). The curves are the results of Gaussian fits to the data using the experimental transmission function and natural line widths.

Reference

1. G. Bieri, L. Åbrink and W. von Niessen, J. Electron Spectrosc. 27, 129 (1982).

LOW ENERGY ELECTRON-IMPACT EXCITATION OF HF

S. Cvejanović and J. Jureta

Institute of Physics, P.O. Box 57, 11001 Belgrade, Yugoslavia

We present the first low energy electron-impact excitation study of HF, obtained using a field-penetration threshold spectrometer¹. The apparatus is a crossed beam electron impact spectrometer whose analyser is sensitive to very slow electrons ($0 \leq E_e \leq 10$ meV), produced at the scattering center during incident beam energy scan. The overall resolution is 40 meV.

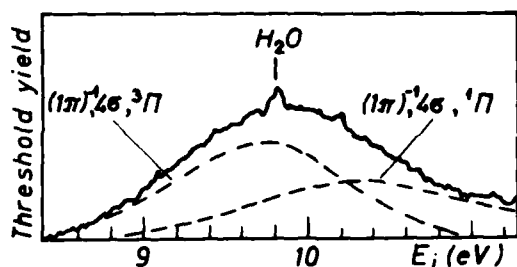


FIGURE 1 Lowest energy continuum in HF

The lowest energy structure is a broad continuum having a maximum at 9.9 eV. Considering the high energy electron-impact data² on the $^1\Pi$ continuum, a decomposition of the threshold yield, as indicated below the spectrum of Fig. 1, shows the dominant contribution of previously undetected $^3\Pi$ component with a maximum at 9.9 ± 0.1 eV, 0.6 eV below the $^1\Pi$, in general agreement with calculations³.

There is no detectable excitation of HF between the continua from Fig. 1 and Rydberg excitation region shown in Fig. 2. Almost all prominent peaks in this region are neatly represented by a single Rydberg series of six levels whose mean quantum defect is 1.0, and only the first member shows notable vibrational excitation. We identified this state, whose quantum defect is slightly smaller ($\delta = 0.91$) than the rest of the series, with $(1\pi)^{-1}3p\sigma, ^3\Pi$, whose existence was indicated in the photo-absorption work⁴. Following this and intensity distribution arguments, we attribute the dominant contribution to other members of the series shown on Fig. 2 to $np\sigma, ^3\Pi$ excitations, despite the fact that the integer value of quantum defect indicates ns Rydberg series.

The rest of the smaller peaks below 14 eV, starting with a doublet feature at 12.74/12.80 eV, can consistently be described by selective resonant excitation of $v = 24/25, 30$ and 37 vibrational level of otherwise unnoticed $B^1\Sigma$ state. The resonance series in question was detected in transmission⁵ at energies which are about 40 meV above the mentioned B-state levels, which

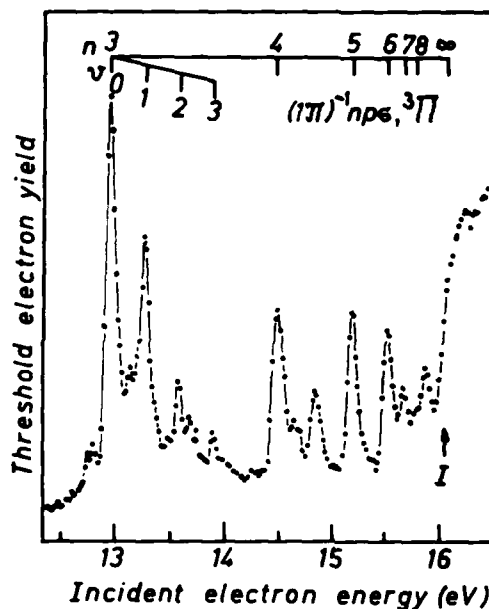


FIGURE 2 Threshold spectrum in the Rydberg region

is within the error bar of its energy calibration, although this energy difference may lose any significance in light of large width of the resonance⁵. One small peak at 13.68 eV is coincident with $v=2$ level of $(1\pi)^{-1}np\sigma, ^1\Pi$ state whose other vibrational levels are masked by stronger nearby contributions.

The last peak below ionisation rise and the structure in the beginning of the ionisation continuum probably correspond to the lowest Rydberg levels converging to the excited ionic state 2Σ at 19.12 eV.

References

1. S. Cvejanović, J. Jureta and D. Cvejanović, J. Phys. B18, (1985), in press.
2. A.P. Hitchcock and C.E. Brion, Chem. Phys. 61, 281 (1981).
3. C.F. Bender and E.R. Davidson, J. Chem. Phys. 49, 4989 (1968), and T.H. Dunning Jr., J. Chem. Phys. 65, 3854 (1976).
4. A.E. Douglas and F.R. Greening, Can. J. Phys. 57, 1650 (1979).
5. D. Spence and T. Noguchi, J. Chem. Phys. 63, 505 (1975).

ELECTRON ENERGY-LOSS STUDIES USING A MULTIDETECTOR SPECTROMETER:
THE SPECTRUM OF Cl_2

Richard J Stubbs, Trevor A York and John Comer

Physics Department, The University, Manchester M13 9PL, UK

The energy-loss spectrum of Cl_2 has been studied up to the second ionization potential $A^2\Pi_u$ at 14.2eV. Approximately 70 new transitions have been seen and in addition new information is revealed regarding many that have been previously reported¹⁻⁵. By employing a variety of scattering conditions, transitions which are forbidden by electric dipole selection rules and are consequently absent from photoabsorption spectra can be enhanced relative to those that are allowed. In the present work a monochromatic beam of electrons with energy in the range 5 to 120eV is scattered by a target gas which effuses from a narrow tube. Electrons scattered in the range of angles from 0° to 90° have been detected.

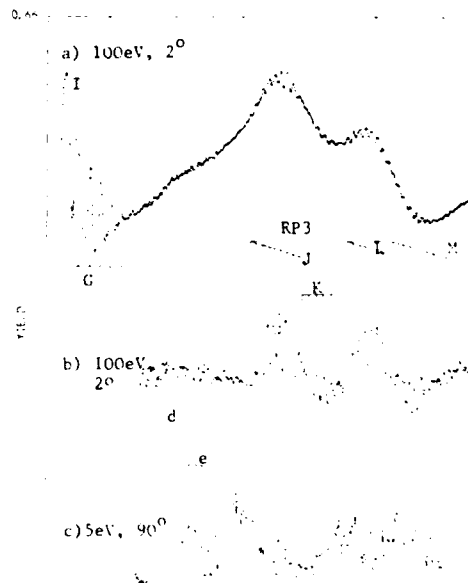
In order to minimise effects due to corrosion the spectrometer incorporates two special features. Firstly, a position-sensitive multidetector like the one described by Hicks et al⁶ is employed to greatly improve the detection efficiency of scattered electrons and consequently high quality spectra can be accumulated in relatively short times. Secondly, differential pumping is used to reduce the background gas pressure in the vicinity of vulnerable components.

The spectrum of Cl_2 between the first and second ionization potentials has not been previously discussed in experimental reports and is shown in figure 1. The top spectra displays the new data obtained in this region and it is evident that many small undulations are superimposed on a slowly changing background. By subtracting this background the undulations become more apparent as shown in the lower two spectra. The majority of the transitions that are seen in this region form six vibrational series, four of which are allowed and two spin-forbidden. Following consideration of the effective principal quantum numbers of the series three may form a Rydberg progression converging on the second ionization potential. The series display a quantum defect of 2.2 and the progression may represent $^1\Sigma_u^+$ states having configuration $3p\sigma_g^2 3p\pi_u^3 3p\pi_g^4 ns\sigma_g$.

References

1. R P Iczkowski, J C Margrave and J W Green, *J Chem Phys* **33**, 1261 (1960)
2. A E Douglas, *Can J Phys* **59**, 835 (1981)
3. J Jureta, S Cvejanovic, M Kurepa and D Cvejanovic, *Z Phys A* **304**, 143 (1982)
4. T Moeller, B Jordan, P Gurtler, G Zimmerer, D Haaks, J Le Calve and M C Castex, *Chem Phys* **76**, 295 (1983)
5. D Spence, R H Huebner, H Tanaka, M A Dillon and R G Wang, *J Chem Phys* **80**, 2989 (1984)
6. P J Hicks, S Daviel, B Wallbank and J Comer, *Phys E:Sci Instrum* **13**, 713 (1980)

FIGURE 1 Spectrum of chlorine between the first and second ionization potentials 1(a) displays raw data, (b) and (c) are the result of subtracting a smoothed background. Seven vibrational series are indicated.



AN ELECTRON ENERGY-LOSS INVESTIGATION OF FREE RADICALS

Richard J Stubbs, Trevor A York and John Comer

Physics Department, Manchester University, Manchester M13 9PL, UK

Free radicals such as SO , CH_3 and S_2 comprise an important group of molecules that are not available to the experimentalist under normal laboratory conditions. They are chemically unstable and have lifetimes in some cases of less than a millisecond. However, they are physically stable since they have a non-zero dissociation energy and, if undisturbed by collisions, do not spontaneously decompose. The study of free radical spectra has contributed greatly to the knowledge of molecular structure, but it has been mainly limited to photon-related techniques such as photoabsorption and photoemission. Even relatively long-lived radicals such as SO are unexplored by electron impact methods.

An electron spectrometer incorporating a position-sensitive multidetector¹ which has been previously used for electron energy-loss investigations of corrosive gases^{2,3} has been modified for the study of free radical spectra. Radicals are produced by a 2450MHz discharge in a low pressure gas flow through a $\frac{1}{4}$ " diameter pyrex tube. The discharge products pass into the spectrometer through a 1mm diameter nozzle and the resulting molecular beam is crossed with a monochromatic electron beam.

An energy-loss study has been made of SO , produced by a discharge in a mixture of sulphur dioxide and argon. Spectra have been collected at impact energies of between 12eV and 100eV above the excitation threshold and at scattering angles between 2° and 75° . The energy-loss range covered extends from 0.5eV to 9.5eV. A typical discharge spectrum is shown in figure 1a and is compared to an undischarged SO_2 spectrum in figure 1b. In addition to the expected SO transitions, features due to the transient molecule S_2 are also observed. Spectra collected under optical scattering conditions are in agreement with photoabsorption studies^{4,5} and contain new SO Rydberg states.

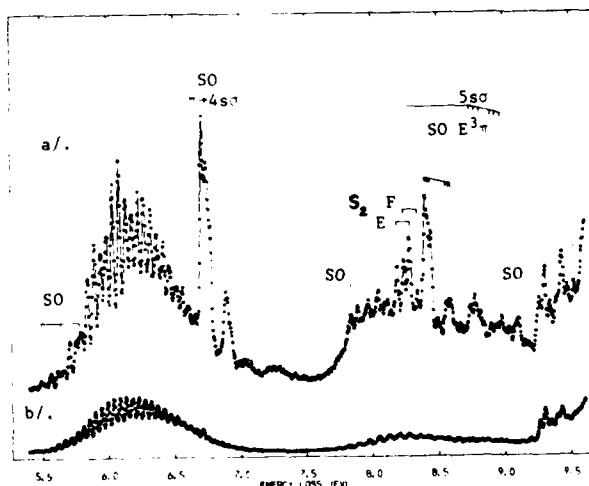
At low impact energies the low-lying spin-forbidden states $a^1\Delta_g$, $b^1\Sigma^+_g$ have been observed in SO , S_2 and O_2 and compared to the results of chemiluminescence studies^{6,7}. A superelastic scattering spectrum of the $a^1\Delta_g$ state in S_2 has been obtained. Two new quadrupole transitions in SO are also proposed.

References

1. P J Hicks, S Daviel, B Wallbank, J Comer, J Phys E **13**, 713 (1980)
2. T A York, J Comer, J Phys B, **16**, 3627 (1983)
3. T A York, J Comer, J Phys B, **17**, 2563 (1984)
4. R J Donovan, D Husain, P T Jackson, Trans Far Soc, **65**, 2930 (1969)
5. R J Donovan, D Husain, C D Stevenson, Trans Far Soc, **66**, 1 (1970)
6. I Barnes, K H Becker, E H Fink, Chem Phys Lett, **67**, 310 (1979)
7. I Barnes, K H Becker, E H Fink, Chem Phys Lett, **67**, 314 (1979)

FIGURE 1 Spectra accumulated at an impact energy of 100eV above the excitation threshold and scattering angle 2°

a/ discharge on
b/ discharge off



THRESHOLD EXCITATION OF N_2O

D. Čubrić, J. Jureta, S. Cvejanović, D. Cvejanović*, P. Hammond**, G.C. King**, and F.H. Read**

Institute of Physics, P.O. Box 57, Belgrade, Yugoslavia

*Faculty of Natural Sciences and Mathematics, Department of Physics and Meteorology, P.O. Box 550, Belgrade, Yugoslavia

**Physics Department, University of Manchester, Manchester M13 9PL, England

An electron impact threshold spectrometer of the field penetration type¹ has been used to study the spectrum of N_2O . The spectrum is obtained in the energy range from 1.6 eV to 20 eV and with an overall resolution of 45 meV.

The spectrum on figure 1 corresponds to the excitation of the lowest valence states. The structures corresponding to the excitation of optically allowed $^1\Delta$, $^1\Pi$ and $2^1\Sigma^+$ states, previously observed in both high energy electron impact² and photoabsorption³ experiments, are indicated by solid vertical bars above the spectrum. Positions of optically forbidden $^3\Sigma^+$ and $^3\Pi$ states observed in present experiment are in agreement with previous low energy experiment⁴. There is no evidence of the excitation of $^3\Delta$, $^3\Sigma^-$ and $^1\Sigma^-$ in threshold spectrum and dashed lines indicate their calculated positions⁵.

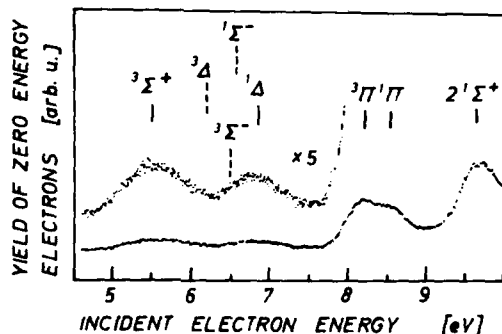


FIGURE 1

The spectrum on figure 2 presents threshold excitation of Rydberg states. Rydberg series converging to the ground $X^2\Pi$ state of ion are indicated in the figure. The dominant features correspond to the excitation of the $ns\sigma$, $np\sigma$, and $np\pi$ Rydberg series. In the same energy range the excitation of the lowest $ns\sigma$ Rydberg state with $A^2\Sigma^+$ ion core is observed. Besides, a number of new structures, possibly belonging to an optically forbidden Rydberg series, has been observed. New structures are indicated in figure 2 by NS.

At impact energies between 2 and 3 eV a broad structure caused by the resonant vibrational excitation

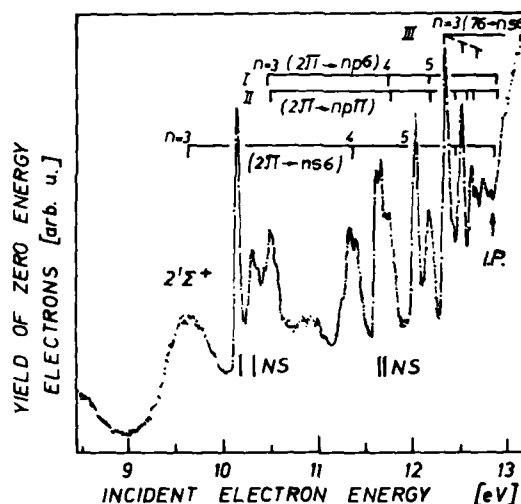


FIGURE 2

of the ground state is observed. It corresponds to the decay of two shape resonances, known to be present in this energy region.

References

1. S. Cvejanović, J. Jureta and D. Cvejanović J. Phys. B 18, (1985), in press.
2. R.H. Huebner, R.J. Celotta, S.R. Mielczarek and C.E. Kuyatt, J. Chem. Phys. 63, 4490 (1975)
3. J.W. Rabalais, J.M. McDonald, V. Scherr and McGlynn, Chem. Rev. 71, 73 (1971)
4. R.I. Hall, A. Chutjian and S. Trajmar, J. Phys. B 6, L111 (1973)
5. N.W. Winter, Chem. Phys. Lett. 33, 300 (1975)

MOMENTUM DISTRIBUTIONS AND BINDING ENERGIES
OF H_2O AND NH_3 BY HIGH MOMENTUM RESOLUTION BINARY $(e,2e)$ SPECTROSCOPY

A.O. Bawagan, R. Müller-Fiedler, K.T. Leung[†] and C.E. Brion

Department of Chemistry, The University of British Columbia, Vancouver,
B.C., V6T 1Y6, Canada.

High momentum resolution $(O,1a_1^{-1})$ binary $(e,2e)$ spectroscopy, in the symmetric non-coplanar geometry ($E_0 = 1200\text{eV}$), has been used to measure the binding energy spectra and momentum distributions (MDs) of the valence orbitals of H_2O and NH_3 . Representative results for H_2O are shown in Figures 1 and 2. The binding energy spectra (Fig.1a) show considerable satellite structure in the 25-45eV region which can be attributed to final state configuration interaction (many-body) effects involving the $(2a_1)^{-1}$ hole state. This result is in general accord with the predictions of a variety of theoretical studies¹⁻³. However, the best quantitative agreement (in terms of both peak positions and intensities) has been obtained with the SAC-CI NV calculation² shown in Fig.1b.

It can be seen from Fig.2 that there are significant discrepancies between the measured and calculated MDs for the $1b_1$ and $3a_1$ orbitals. The calculations have been done with a range of literature SCF wavefunctions⁴⁻⁶. A comparison of theoretical MDs calculated from even more sophisticated wavefunctions⁷⁻⁸ (ie. with total energies extremely close to the Hartree-Fock limit) with the experimental MDs, will be presented. In addition, the effect of vibrational motion on momentum distributions is currently under investigation.

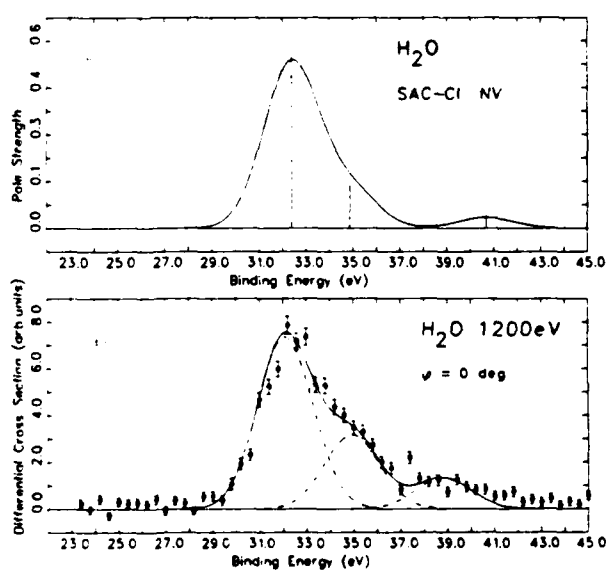


Figure 1 Binding energy spectra of the inner valence region of water.

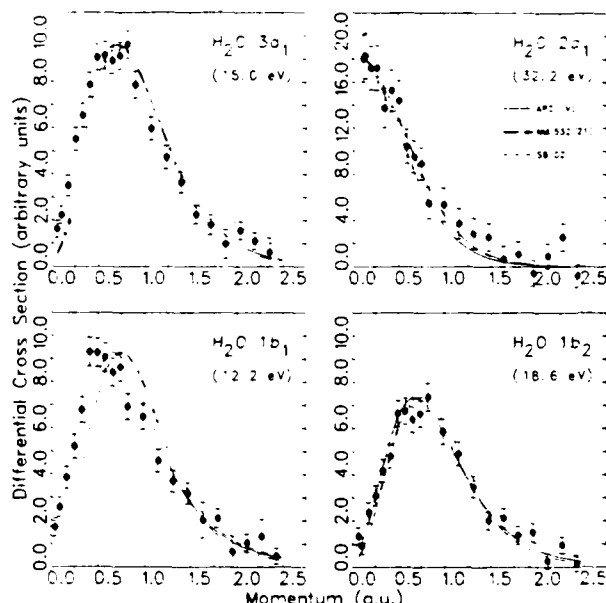


Figure 2 Experimental and calculated momentum distributions for the outer valence orbitals of water.

This work received financial support from NSERC (Canada) and Deutsche Forschungsgemeinschaft (Post-doctoral Fellowship for RMF).

[†]Present Address, Lawrence Berkeley Laboratory

References

1. H. Nakatsuji and T. Yonezawa, Chem. Phys. Lett. **87** (1982) 426.
2. W. Von Niessen, L.S. Cederbaum, J. Schirmer, G. Diercks and W.P. Kraemer, J. Elect. Spect. **28** (1982) 45.
3. H. Agren and H. Siegbahn, Chem. Phys. Lett. **69** (1980) 424.
4. L.C. Snyder and H. Basch, Molecular Wavefunctions and Properties (Wiley, New York, 1972).
5. S. Aung, R.M. Pitzer and S.I. Chan, J. Chem. Phys. **49** (1968) 2071.
6. D. Neumann and J.W. Moskowitz, J. Chem. Phys. **49** (1968) 2056.
7. B.J. Rosenberg and I. Shavitt, J. Chem. Phys. **63** (1975) 2162.
8. E.R. Davidson and D. Feller, Chem. Phys. Lett. **104** (1984) 54.

INNER-SHELL ELECTRON ENERGY LOSS SPECTROSCOPY OF PCl_3 and SO_2

C.E. Brion, R.N.S. Sodhi and K.H. Sze

Department of Chemistry, University of British Columbia
Vancouver, B.C. V6T 1Y6, Canada

Core electronic excitation spectra of PCl_3 (Phosphorus 2p, 2s; Chlorine 2p, 2s) and SO_2 (Sulfur 2p, 2s; Oxygen 1s) have been measured using inner-shell electron energy loss spectroscopy at high impact energy and small scattering angles.

The measurements for PCl_3 were made using an earlier described spectrometer¹ at $E_0 = 1500\text{eV}$ and over the range $\theta = 0.9$ to 4.8 degrees. The energy resolution is in the

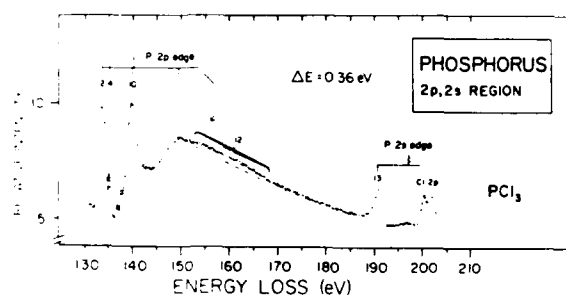


Figure 1 Energy Loss Spectrum of PCl_3

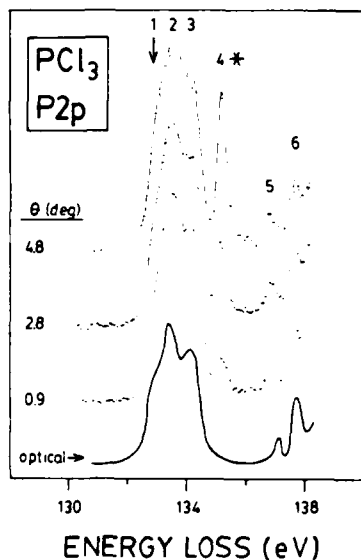


Figure 2 P 2p Spectrum of PCl_3

range $0.18\text{--}0.36\text{eV}$ (FWHM). A wide range spectrum (Fig.1) shows the P 2p, 2s spectra and the Cl 2p edge. Figure 2 shows the P 2p region in detail. The original ISEELS spectrum, run at $\theta = 0.9^\circ$, showed a small peak (4*) not present in the previously published soft X-ray spectrum².

It is unusual to observe such intense forbidden transitions under the present conditions of momentum transfer ($K^2 = 0.25$). Spectra have been run at a series of scattering angles to investigate this evidently π -dipole transition. From figure 2 it can be seen that the transi-

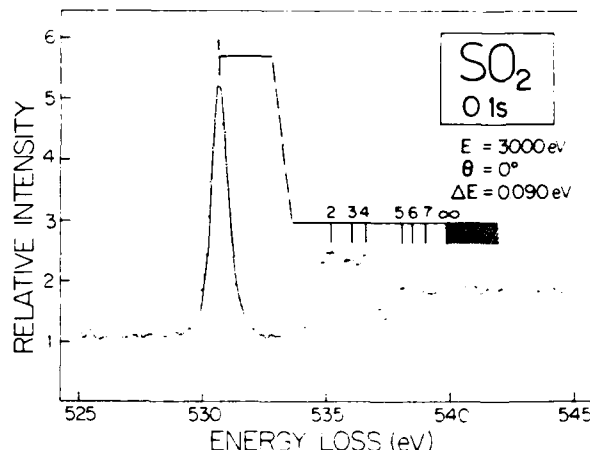


Figure 3 O 1s Spectrum of SO_2

ition (4*) becomes relatively large by $\theta = 4.8^\circ$ compared to neighbouring dipole allowed transitions (1,2,3). A detailed investigation of this forbidden transition will be reported together with the other PCl_3 spectra³.

A new high resolution electron energy loss spectrometer⁴ has been used to study core electronic excitation spectra of SO_2 (Sulfur 2p, 2s; Oxygen 1s). These spectra were obtained at $E_0 = 3000\text{eV}$ and $\theta = 0^\circ$. Figure 3 shows the O 1s excitation spectrum of SO_2 , obtained at an energy resolution of 0.09eV (FWHM). This corresponds to an equivalent $\Delta\lambda$ of 0.004\AA at 23\AA which compares very favourably with resolution obtainable by optical methods in this region. These results and the sulfur spectra⁵ will be reported.

This work received financial support from The Natural Sciences and Engineering Research Council of Canada.

References

1. A.P. Hitchcock and C.E. Brion, J. Electron Spectrosc. 13 (1978) 193.
2. L.N. Mazilov and A.V. Kondratenko, Proc. 6th Int. Conf. on Vacuum UV Radiation Physics, II-71 (Charlottesville, 1980).
3. R.N.S. Sodhi and C.E. Brion, J. Electron Spectrosc., in press 1985.
4. S. David, C.E. Brion and A.P. Hitchcock, Rev. Sci. Instrum. 5 (1984) 182.
5. K.H. Sze and C.E. Brion, to be published.

ELECTRON ENERGY LOSS SPECTROSCOPY
OF NH_3 IN THE 5.5-11 eV ENERGY RANGE

D. Roy*, M. Furlan, M.-J. Hubin-Franskin, J. Delwiche, and J.E. Collin

Laboratoire de Spectroscopie d'Electrons; Université de Liège B6,
Sart-Tilman, 4000 par Liège 1, Belgium.

We report a study of the singlet states of ammonia in the 5.5-11 eV energy range by means of high resolution electron energy loss spectroscopy. Spectra measured at 50 eV incident electron energy and various scattering angles (4° - 40°), with an energy resolution of 15 or 20 meV, allowed us to determine further accurate data on the vibrational progressions and electronic states. Previously published electron impact measurements^{1,2} were obtained at medium energy resolution.

The instrument is a VG LEELS 400 electron spectrometer modified for the study of gases. The electrostatic deflectors for the energy selection and analysis are 150° hemispherical condensers. The target gas is introduced through a needle, around which the analyzer system can be rotated from -35° to -120° with respect to the direction of the incoming beam. All this set-up is enclosed in a mumetal vessel, pumped by turbomolecular and cryogenic pumps.

in a UV spectrum, while the relative intensities of the different electronic bands are somewhat different. But dramatic changes occur when the scattering angle is increased, depending on the character of the transitions.

The dominating A state progression exhibits 15 vibrational levels involving out-of-plane vibration. The region above shows the two overlapping progressions of the B and C states, the latter being much stronger in electron impact excitation than in photoabsorption.³ Inspection of the D state region at high resolution reveals an underlying state classified as the D' state. Above 9.5 eV, many members of the progressions arising from E, F, and G states are identified and can be compared to photoabsorption data.³

The study of the angular dependences of the differential cross sections of these states reveals that some assignments proposed before may have to be revised. Further details will be presented at the Conference.

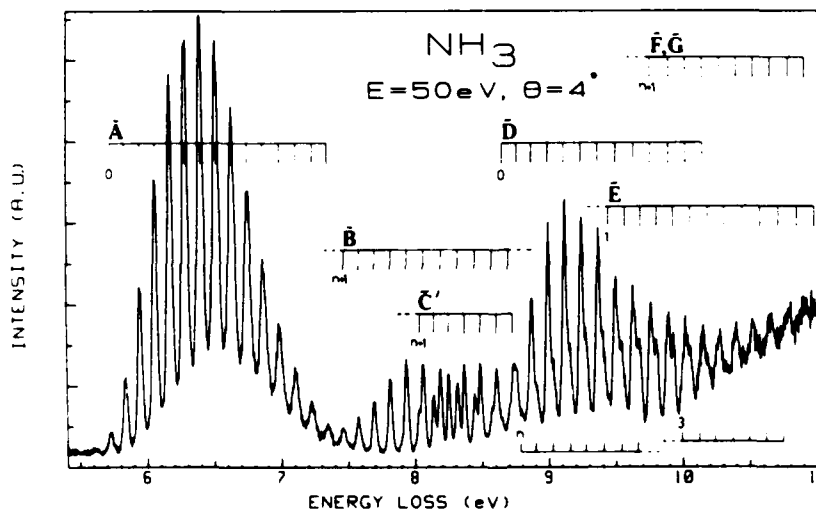


Fig.1 Electron energy loss spectrum of NH_3

Figure 1 shows the energy loss spectrum in the region studied, for 50 eV incident electron energy and 40° scattering angle. Inspection of this and other spectra obtained at various angles allowed us to determine eight electronic transitions accompanied by a large number of vibrational levels. The overall shapes of the extended vibrational progressions are similar to what is found

*Permanent address: CRAM and Département de Physique, Université Laval, Québec, QC G1K 7P4, Canada

†"Chercheur qualifié" of FNRS of Belgium.

1. E.N. Lassettre, A. Skerbele, M.A. Dillon, and K.J. Ross, *J. Chem. Phys.* **48**, 5066 (1968).
2. W.R. Harshbarger, *J. Chem. Phys.* **54**, 2504 (1971).
3. K. Watanabe and S.P. Sood, *Sci. Light (Tokyo)* **14**, 36 (1965).

SMALL-ANGLE, INTERMEDIATE ENERGY (1.0 keV)
ELECTRON ENERGY LOSS SPECTRA OF ETHYLENE

Ana C. A. e Souza, G. Gerson B. de Souza

Instituto de Química da Universidade Federal do Rio de Janeiro
Cidade Universitária - 21.910 - Rio de Janeiro - RJ - Brasil

Electron energy-loss spectra, covering the elastic and inelastic region up to 75 eV energy-loss, have been obtained for the ethylene molecule at 1.0 keV impact energy.

The measurements were carried out using the electron impact spectrometer described by Souza et al¹. The scattered electron intensities were measured as a function of energy (LE) in the angular range 2 to 8 degrees. The energy resolution, as determined by the full width at half maximum (fwhm) of the elastic peak, was approximately 1.5 eV. In figure 1 we present typical spectra, obtained at 3, 4 and 5 degrees. The results have been normalized to the elastic data of Fink et al² and converted to double differential cross sections.

Financial support from the Conselho Nacional de Desenvolvimento Científico e Tecnológico (CNPq), Fundação Universitária José Bonifácio (FUJB) and Financiadora de Estudos e Projetos (FINEP) is gratefully acknowledged.

REFERENCES:

- 1) G. Gerson B. de Souza, A.C.A. e Souza, R. de B. Faria, in *Electronic and Atomic Collisions*, J. Eichler, W. Fritsch, I.V. Hertel, N. Stol Terfoht and U. Wille, editors, North-Holland, Amsterdam, Oxford, New York and Tokyo, 1983 (page 707)
- 2) M. Fink, K. Jost and D. Herrmann, *J. Chem. Phys.*, **63**, 1985 (1a75)

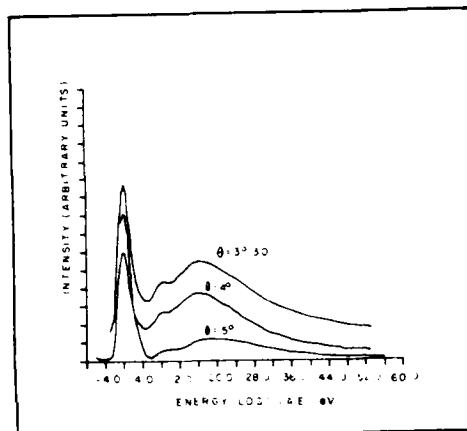


FIGURE 1 - Electron Energy loss Spectra for Ethylene at 1 keV Incident Energy.

ELECTRON MOMENTUM SPECTROSCOPY OF CHLOROMETHANES

A.M. Grisogono, W. von Niessen* and E. Weigold

The Flinders University of South Australia, South Australia 5042, Australia
 *Technische Universität Braunschweig, D-3300 Braunschweig, West Germany

The molecular orbital structure of the chloromethanes ($\text{CH}_n\text{Cl}_{4-n}$, $n = 0, \dots, 4$) has been studied by electron momentum spectroscopy via the noncoplanar symmetric ($e, 2e$) reaction. This technique generates electron binding energy spectra at various values of azimuthal angle (corresponding to different bound electron momenta), and hence the electron momentum distributions of valence molecular orbitals may be determined.

The experiments were performed at 1000 and 1200 eV incident electron energy over a range of 8 to 45 eV in binding energy with an energy resolution of 1.2 eV. Azimuthal angles of 0° to 27° provided an electron momentum range up to 2 a.u. with a resolution of 0.1 a.u.

The data are analysed by fitting the experimental resolution function to the observed peaks (matched to high resolution photoelectron spectra where available in the outer valence region). The resulting pole strengths for the various transitions are compared to theoretical pole strengths calculated by a combination of the outer valence Green's function methods (OVGF) and an extended two particle-hole Tamm-Dancoff Green's function approximation (2ph-TDA) for the inner valence region. The measured electron momentum distributions are compared with those given by the SCF MO wavefunctions used in the Green's function calculation. Since the present data provide relative rather than absolute cross-section measurements the data are normalized to the theory at one of the outer valence states, for which the pole strength is close to unity and the theoretically predicted momentum distribution provides a good fit to the shape of the data. Comparisons of theory and experiment for the other states then allow the predicted symmetry assignments and pole strengths to be checked against the data.

The 2ph-TDA model predicts a breakdown of the molecular orbital picture at binding energies $\gtrsim 20$ eV, and this is experimentally verified by a complicated satellite structure which in effect "smears out" the strengths over a range of energies. The calculated strengths are generally too high in this energy range, e.g. the $1e$ transition of CHCl_3 at 25 eV and the $2a_1$ transition of CCl_4 at 20 eV both fall experimentally well below the theoretical cross-sections, but there is an appreciable cross-section observed over the

whole higher energy range where no molecular orbitals can be individually identified. In the case of the $1t_2$ state of CCl_4 at 25 eV not only is the observed strength an order of magnitude below theory, but the shape of the distribution also suggests that the symmetry assignment of the state is not correct.

Even where two or more states close in energy are not experimentally resolved the technique allows some verification of symmetry assignments, by comparison of the summed theoretical distributions with the shape of the data, since the shape of the summed distribution is sensitive to the symmetry types of its components. This is particularly useful in the outer valence region where accidental and near degeneracies are not infrequent. For example the $2e$ and $3a_1$ states of CHCl_3 , being of different symmetries, add to a complex distribution, which is supported by the data.

In general the manybody calculations underestimate the degree of splitting of the higher energy states, but provide good models of the outer valence states.

Both momentum and position density maps have been produced from the theoretical molecular orbital calculations for all the orbitals of the chloromethanes in the energy range, and will be available for display.

PARTIAL AND TOTAL ELECTRON IMPACT IONIZATION CROSS SECTIONS FROM THRESHOLD UP TO 180 eV

K. Leiter and T.D. Märk

Institut für Experimentalphysik, Leopold Franzens Universität, A 6020 Innsbruck, Austria

Recently, there has been a growing interest in quantitative knowledge on electron impact ionization cross sections¹ of halocarbon compounds used for plasma etching². Therefore we have recently measured partial and total ionization cross sections of CF_4 and CCl_4 ^{3,4}. The present study is an extension to CF_2Cl_2 , however, using an improved deflection mass spectrometer method⁵. This new method allows the quantitative detection of fragment ions with excess kinetic energy, thereby eliminating possible discrimination effects for the detection of these ions.

Using this method, we have obtained absolute partial ionization cross section functions in CF_2Cl_2 from threshold up to 180 eV for the production of the following ions:

CF_2Cl_2^+ , CFCl_2^+ , CF_2Cl^+ , CCl_2^+ , Cl_2^+ , CFCl^+ , FCl^+ , CF_2^+ , CCl^+ , Cl^+ , CF^+ , F^+ , C^+ and $\text{CF}_2\text{Cl}^{2+}$, CFCl_2^{2+} , CFCl^{2+} , CCl_2^{2+} , CCl^{2+} , Cl^{2+} .

It is interesting to note, that in contrast to CF_4 and CCl_4 ^{3,4} stable parent ions exist in CF_2Cl_2 with a cross section maximum of $1.1 \times 10^{-22} \text{ m}^2$ at 100 eV.

The absolute total ionization cross section function is obtained by summing up the weighted partial cross section functions (summation method¹). Fig. 1 shows a comparison between present experimental results, previous experimental results^{6,7} and values calculated using the classical binary encounter approximation (full line in Fig. 1). It can be seen, that there is good agreement in magnitude between present results and values determined by Beran and Kevan⁶, however, that the results of Pejcev et al.⁷ and the theoretical values are much higher in the vicinity of the maximum cross section. However, it is interesting to note, that the theoretical values approach at high energies the present results and that the shape of the curve as measured by Pejcev et al. is in very good agreement with the present determination.

Work supported by Österreichischer Forschungsfonds.

References

1. T.D. Märk and G.H. Dunn, *Electron Impact Ionization*, Springer, Wien (1985)
2. D.L. Flamm and V.M. Donnelly, *Plasma Chem. Plasma Proc.*, 1 (1981) 317
3. K. Stephan, K. Leiter, H. Deutsch and T.D. Märk, *Proc. 13th ICPEAC*, Berlin (1983) 276
4. K. Leiter, K. Stephan, E. Märk and T.D. Märk, *Plasma Chem. Plasma Proc.*, 4 (1984) 235
5. K. Leiter, K. Stephan and T.D. Märk, *Proc. 10th Intern. Conference Mass Spectrometry*, Swansea (1985)
6. J.A. Beran and L. Kevan, *J. Phys. Chem.*, 73 (1969) 3866
7. V.M. Pejcev, M.V. Kurepa and I.M. Cadez, *Chem. Phys. Lett.*, 63 (1979) 301

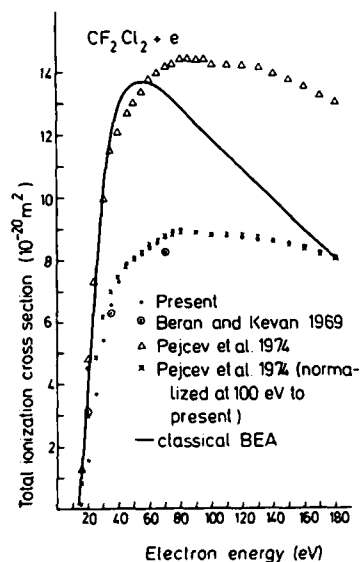


Fig. 1 Total ionization cross section function of CF_2Cl_2 . See text.

ELECTRON IMPACT SPECTROSCOPY OF SILANE AND GERMANE

David Spence, R.-G. Wang,* and M. A. Dillon

Argonne National Laboratory, Argonne, Illinois 60439 U.S.A.

Electronic spectra of the group IV_A hydrides, silane (SiH₄), and germane (GeH₄) have been investigated by means of electron energy loss spectroscopy in an energy range that includes all single-electron excitation from the valence shell. Electron impact spectra of both gases recorded using electrons of 200-eV incidence are displayed in Figure 1. The conditions employed have been chosen to favor the excitation of states by direct scattering and to exclude those transitions requiring an exchange mechanism. Hence, all features in Figure 1 are related to vertical transitions which terminate in symmetry allowed and forbidden singlet states.

The ground-state configuration and ordering of both molecules is $(1a_1)^2 \dots (ma_1)^2 (nt_2)^6 1A_1$ in Td symmetry. The lowest manifold of excited states arise from orbital transitions of the type s, p, d + t₂. The promotion of a bonding t₂ valence electron to non-bonding Rydberg orbitals expands the molecular framework of these molecules, rendering their electronic spectra dissociative below the first ionization limit. Thus, the spectra below the first IP in Figure 1, which we designate region 1, consist almost entirely of diffuse structures. Provisional identification of salient features in this energy range are indicated by labels in the figure. The lowest lying Rydberg configurations are consistent with those suggested in an analysis of the electronic spectrum of methane.¹ In addition, evidence is presented for the existence of valence (v)

and mixed valence-Rydberg (σ^*) states.

The ~ 4 eV energy interval preceding the second IP, designated region 2, is the range of optically allowed autoionizing Rydberg series p, d, + a₁ converging to the $2A_1$ ground state ion in both molecules. At larger scattering angles, members of the forbidden autoionizing

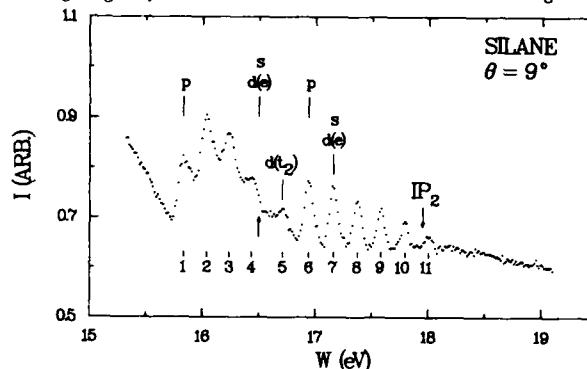


FIGURE 2. Energy loss spectra from 15 eV to 19 eV of silane. Similar structures appear in the same energy region of germane, shown in Fig. 1.

series s, d, + a₁ are expected to substantially overlap those of the allowed series. The 9° spectra in Figure 1 reveal the presence of much discrete structure converging to the respective $2A_1$ ion states. The region of the silane spectrum containing the structure has been recorded independently and is displayed in Figure 2. The spectrum appears to consist of at least two progressions and an underlying continuum. The peaks, numerically labelled to facilitate identification are broadened considerably by both autoionization and instrumental resolution (~ 40 meV). Term value locations of selected peaks measured relative to $2A_1(v' = 0)$ at 17.95 eV are included in the figure, together with the appropriate terminating orbitals. Peak positions correspond fairly well to those reported using threshold photoelectron spectroscopy.² However, the angular behavior depicted in Figure 1 suggests the substantial contribution of optically forbidden transitions.

This work is supported by the U.S. Department of Energy.

References

1. M. A. Dillon, R.-G. Wang, and D. Spence, J. Chem. Phys. **80**, 5581 (1984).
2. T. Heinis, K. Borlin, and M. Jurgen, Chem. Phys. Lett. **110**, 429 (1984).

*Visiting Foreign Scholar. Permanent address: Dept. of Physics, Chengdu University of Science & Technology, Chengdu, Sichuan, People's Republic of China.

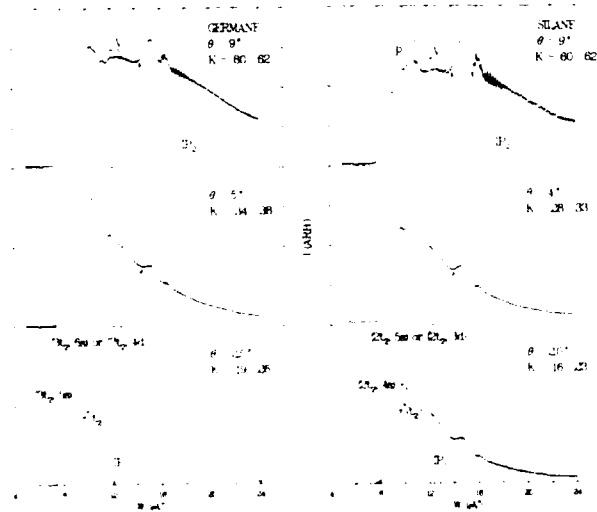


FIGURE 1. Energy loss spectra from 4 eV to 24 eV of silane (right) and germane (left).

(e, 2e) SPECTROSCOPY OF SILICON COMPOUNDS: IONIZATION POTENTIALS AND ELECTRON
MOMENTUM DISTRIBUTIONS FOR VALENCE SHELL ORBITALS OF SiF_4

R. Fantoni, A. Giardini-Guidoni, R. Tiribelli, P. Cambi⁺, M. Paoi⁺ and P. Tarantelli⁺
ENEA, TIB - Divisione Fisica Applicata, C.R.E. Frascati, C.P. N. 65, 00044 Frascati (Rome), Italy

The binary (e,2e) spectroscopy or momentum spectroscopy allows the analysis of the electronic structure, the determination of the ionization potentials (and of the relevant satellite structure, if any) and the momentum distribution of the one electron orbitals of a molecular system⁽¹⁾. In this spectroscopy the two outgoing electrons from a ionization process are detected in coincidence, after careful measurement of energy and momentum at different separation energies satisfying the energy balance: $E_i - E_f = E_A + E_B$ where E_i , E_A and E_B are respectively the incoming and the outgoing electron energies and E_f is the final energy of the electron ejected from the target. Momentum conservation equation $k_i = k_A + k_B + k_r$, where k_i , k_A and k_B are respectively the electron momenta and k_r is the recoil momentum of the residual ion. In case of high incident energy and high momentum transfer, k_r is nearly opposite to the momentum of the bound electron, the scattering process becomes similar to that of free electrons. The cross section is proportional to⁽²⁾ the square product of two factors: the Fourier transform (averaged over the orientation of \mathbf{q}) of the orbital of the ejected particle, and the overlap between the final ionic state $|\psi_{N-1}^+\rangle$ and that of the remainder of the molecule $|\psi_{N-1}^-\rangle$ after an ionization process which has left any other orbital frozen. From this point of view, $|\psi_{N-1}^+\rangle$ is to be read as the product of a free particle state and an ion eigenfunction. We thus have

$$S(\epsilon, q) = F_\phi(q) |\langle \psi_{N-1}^+ | \psi_{N-1}^- \rangle|^2$$

being ϕ the HF eigenstate of the struck electron and $F_\phi(q)$ the electron momentum distribution (EMD).

The (e,2e) experiments were carried out with an electron coincidence spectrometer at quite high incident energy (1600 eV) and in out-of-plane symmetric kinematics⁽²⁾.

Previous measurements performed on methane and fluoro-substituted methanes⁽³⁾ showed the importance of chemical environment on the electron momentum distribution. This effect can be tested going from carbon to silicon. The momentum space investigation of fluoro-silicon compounds presents in fact a noticeable interest because fluorine p orbitals have size and energy favoring a large participation in the bond. In Fig. 1 energy spectra of SiF_4 measured at different q-momentum values are shown and compared with the deconvolution based on PES data⁽⁴⁾. Preliminary results obtained for the EMD distribution of SiF_4 taken at $\epsilon_i = 16.5$ eV and $\epsilon_f = 400$ eV are reported in Fig. 2 and compared with momentum

space molecular orbitals as calculated from a Gaussian basis set.

These results indicate that the Gaussian basis set fairly well predicts the momentum distribution and IF of external valence shell orbitals. Further work is in progress to measure other e.m.d.

FOOTNOTE AND REFERENCES

(⁺) Università di Perugia (Italy)

1) J.B. McCarthy et al.: Phys.Rept. **37C**, 375 (1976)

2) R. Camilloni et al.: Phys.Rev. **17**, 1434 (1978)

3) R. Cambi et al.: Chem.Phys.Lett. **70**, 445 (1980)

4) G. De Alti et al.: Chem.Phys. **25**, 283 (1978)

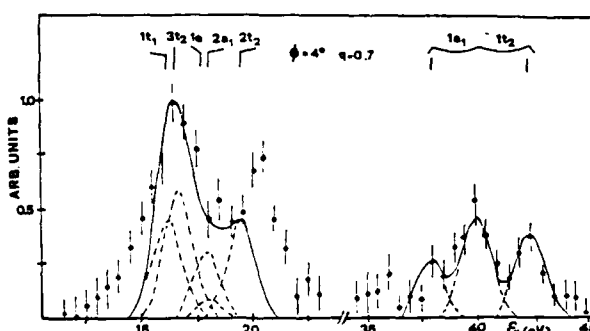


Fig. 1 - Ionization energy spectra of SiF_4 compared with calculations (see text).

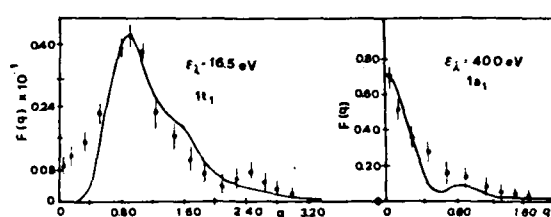


Fig. 2 - EMD of SiF_4 measured at different q values and compared with the calculated ones (see text).

INNER-SHELL SPECTRA OF BENZENE, PYRIDINE AND CYCLOHEXANE
STUDIED BY keV ELECTRON IMPACT

A. P. Hitchcock*, D. C. Newbury*, A. L. Johnson^o, J. A. Horsley[†] and J. Stöhr[‡]

* Department of Chemistry, McMaster University, Hamilton, Canada L8S 4M1

^o Materials and Molecular Research Division, Lawrence-Berkeley Laboratory,
University of California-Berkeley, California 94720

[†] Corporate Research Science Laboratory, Exxon, Annandale, NJ 08801

A differentially pumped, inelastic electron scattering spectrometer¹ has been constructed at McMaster University for systematic studies of the inner-shell spectra of gaseous molecules. The spectrometer is operated under single scattering conditions with 3 keV incident electron energy and 1-2° scattering angles such that primarily electric dipole transitions are excited. Recently we have recorded the spectra of a number of cyclic saturated and unsaturated organic molecules including cyclohexane (Fig. 1) and pyridine (Fig. 2). The interpretation of these spectra is aided by comparison to the photoelectron yield spectra of the same molecules in oriented monolayers or condensed films recorded with soft x-ray synchrotron radiation (SSRL) and by the results of SCF-X_α calculations. The condensed phase spectra distinguish valence and Rydberg transitions while the polarization dependence of the spectrum of the oriented molecule allows unambiguous assignment of π or σ character².

A comparison of the pyridine and benzene free molecule and condensed phase spectra has allowed a definitive reassignment of the previously reported gas phase benzene carbon K-shell spectrum³. The feature at 288.0eV (#3) in benzene is clearly the b_{2g}^{*} valence state, not a 3p Rydberg state as previously assigned³.

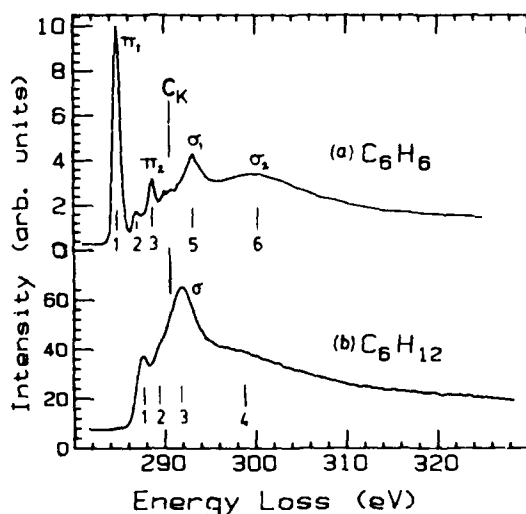


Fig. 1: Electron energy loss spectra of (a) benzene³ and (b) cyclohexane in the region of carbon K-shell excitation.

The σ resonance intensity in the continuum of both pyridine and benzene is split into two features, 3 and 10eV above the K-shell IP. The continuum shape obtained from the SCF-X_α calculation of benzene shows two features arising from promotions of carbon 1s electrons to σ^* orbitals of e_{1u} and a_{2g} symmetry. The position, relative intensity and polarization dependence of these features are in good agreement with the experimental results.

Research supported by NSERC (Canada) and Exxon Research and Engineering Company.

References

1. A.P. Hitchcock, S. Beaulieu, T. Steel, J. Stöhr and F. Sette, J. Chem. Phys. **80**, 3927 (1984).
2. J. Stöhr and R. Jaeger, Phys. Rev. B **26**, 4111 (1982).
3. A.P. Hitchcock and C.E. Brion, J. Electron Spectrosc. Relat. Phenom. **10**, 317 (1977).

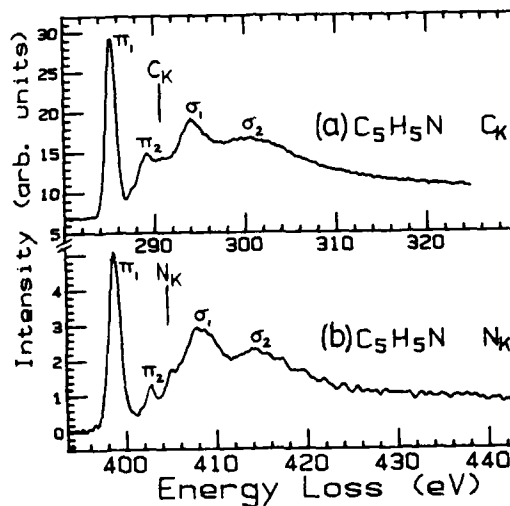


Fig. 2: Electron energy loss spectra of pyridine recorded with 3 keV impact energy in the region of (a) carbon K-shell and (b) nitrogen K-shell excitation.

MOLECULAR GEOMETRY FROM K-SHELL RESONANCES IN
 INELASTIC ELECTRON SCATTERING SPECTRA

A. P. Hitchcock* and J. Stöhr†

* Department of Chemistry, McMaster University, Hamilton, Canada L8S 4M1

† Corporate Research Science Laboratories, Exxon, Annandale, NJ 08801

In recent years inelastic scattering of keV electrons has been used to record electron energy loss spectra in the region of K-shell excitation of molecules containing C, N, O and F¹. These spectra exhibit resonance features around the K-shell ionization threshold. The resonances of a particular molecule are also observed essentially unchanged in the solid state either in a low temperature condensed film or when the molecule is chemisorbed on a surface under conditions where the geometry does not change appreciably. The polarization dependence of the synchrotron K-shell electron yield spectra of chemisorbed molecules² clearly indicates the resonance symmetry. The invariance of near-edge resonances with physical state (free, surface-chemisorbed or solid) shows these resonance states are highly localized and only dependent on the intramolecular potential and geometry.

Recently, we have shown that for one class of molecular K-shell features, π shape resonances, the position of the resonance relative to the K-shell ionization threshold (δ) varies systematically with intramolecular distance (R)^{3,4}. The resonance position changes by up to 25 eV for a given combination of core excited atom and adjacent species. If an association is made between a resonance and a particular set of core-excited and adjacent, back-scattering atoms then a remarkably good linear relationship (Fig. 1) is observed between δ and R within classes of resonances characterized by the same Z_T , the sum of atomic numbers of the

pair of atoms involved (for example $Z_T = 14$ for B-F, C-O and N-N bonds). This empirical relationship has been used to estimate intramolecular bond lengths to within ± 0.05 Å for both free⁴ and chemisorbed⁵ molecules.

The evidence for the R-dependence of resonance positions will be presented along with a comparison to recent theoretical treatments of near-edge core excitation resonances. In addition, recent studies of the inner-shell spectra of a variety of sulfur containing molecules will be reported. These investigations seek to determine if the $\delta(R)$ approach can be applied to features in the core spectra of third row atoms and thus enable determinations of bond lengths to silicon, phosphorus, sulfur and chlorine.

Research supported by NSERC (Canada) and Exxon Research and Engineering Company.

References

1. C.E. Brion, S. Daviel, R.N.S. Sodhi and A.P. Hitchcock, AIP Conf. Proc. **94**, 426 (1982); A.P. Hitchcock, J. Electron Spectrosc. **25**, 245 (1982).
2. J. Stöhr and R. Jaeger, Phys. Rev. **B26**, 4111 (1982).
3. F. Sette, J. Stöhr and A.P. Hitchcock, Chem. Phys. Lett. **110**, 517 (1984) J. Chem. Phys. **81**, 4906 (1984).
4. A.P. Hitchcock, S. Beaulieu, T. Steel, J. Stöhr and F. Sette, J. Chem. Phys. **80**, 3927 (1984).
5. J. Stöhr et al. Phys. Rev. Lett. **51**, 2414 (1983); Chem. Phys. Lett. **105**, 332 (1984).

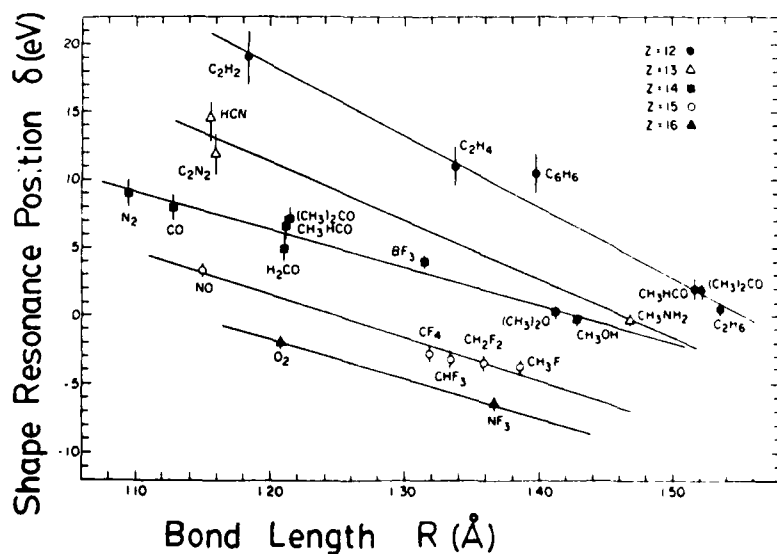


Figure 1: K-shell π shape resonance position ($\delta = E_T - IP$) versus bond length. For molecules such as CO the point is the average of the resonance position in both core spectra (C1s, O1s). The lines are linear least squares fits to points in the same class of Z_T , the sum of atomic numbers of the bonded atoms.

THE STUDY OF ELECTRIC DIPOLE FORBIDDEN INNER SHELL
TRANSITIONS BY ELECTRON IMPACT EXCITATION

I Harrison and G C King

Physics Department, Manchester University, Manchester M13 9PL, UK

In the study of inner shell transitions in atoms and molecules the electron energy loss technique has some important advantages over photon absorption studies using synchrotron radiation. Thus for states with high values of excitation energy ($>200\text{eV}$) electron impact can provide superior energy resolution^{1,2}. A second and perhaps more important advantage of electron impact excitation is its ability to induce electric-dipole forbidden transitions. This can occur when the value of incident energy is reduced to a value close to that of the state, and the optical selection rules are relaxed. Recently the electron energy loss technique has been used to observe for the first time an inner shell electric dipole forbidden transition³.

A new electron spectrometer using an unselected electron beam has been constructed specifically for the study of these electric dipole forbidden transitions. The principal advantages of the new spectrometer are the large incident electron currents available at the target (typically several hundred nano amps) and the ability to go to low values of incident energy (typically 100eV above the threshold energy of the state of interest). For example, in the case of CO the dipole forbidden transition from $1s$ to $2p\pi^*_{3/2}$ state has been studied closer to threshold than ever before and with improved sensitivity.

The spectrometer has been used to study electric dipole transitions in a range of molecules. In most cases new states have been observed. The data yields directly the values of singlet-triplet splittings and hence an understanding of the exchange interactions which involve the inner shell hole. The data also allows recent theoretical predictions⁴ to be tested.

New experimental results in a range of molecules, including CO, COS, CO_2 , CS_2 and N_2O will be presented and discussed. For example a value of $(.98 \pm .02)\text{eV}$ has been obtained for the $1,^3\Pi,^3\Sigma^-(1s\text{N}_c)^{-1}$ singlet-triplet splitting in N_2O .

References

1. G C King, M Tronc, F H Read and R C Bradford, *J Phys B:Atom Molec Phys* **10**, 2479 (1977)
2. M Tronc, G C King and F H Read, *J Phys B:Atom Molec Phys*, **12**, 137 (1979)
3. D A Shaw, G C King, F H Read and C Cvejanovic, *J Phys B:Atom Molec Phys*, **15**, 1785 (1982)
4. A V Kondratenko, L N Mazalov, F Kh Gel'Mukhanov, V I Avdeev and E A Saprykhina, *J Struct Chem*, **18**, 437 (1977) (1977 *Zh Strukt Khim* **18**, 546)

CROSS SECTIONS FOR H^- AND Cl^- PRODUCTION FROM HCl BY DISSOCIATIVE ELECTRON ATTACHMENT

O. J. Orient and S. K. Srivastava

Jet Propulsion Laboratory, California Institute of Technology, Pasadena, CA 91109

Dissociative electron attachment cross section measurements for the production of Cl^- and H^- ions from HCl have been performed utilizing a crossed target beam-electron beam collision geometry and a quadrupole mass spectrometer. The relative flow technique is employed to determine the absolute values of cross sections. The experimental apparatus and techniques used in the present measurements have been described earlier.¹ Our dissociative electron attachment cross section data for Cl^-/HCl as a function of the electron beam energy are shown in Fig. 1 and our dissociative electron attachment cross section data for H^-/HCl as a function of the electron beam energy are shown in Fig. 2. In Table I we have summarized our results, together with data found in the literature.

Table I

Ion	Peak (eV)	Peak Cross Section cm^2	References and Methods
H^-/HCl	6.9	$(5.2 \pm 0.4) \times 10^{-19}$	Azria et al. ² (Static gas)
	9.2	$(2.8 \pm 0.2) \times 10^{-19}$	Azria et al. ² (Static gas)
	7.1 ± 0.1	$(2.1 \pm 0.42) \times 10^{-18}$	Present Work (Cross beam)
	9.05 ± 0.1	$(0.93 \pm 0.19) \times 10^{-18}$	Present Work (Cross beam)
Cl^-/HCl	-1.5	-	Gutbier and Neuert ³ (Static gas)
	0.66 ± 0.02	-	Fox ⁴ (Static gas)
	0.77 ± 0.1	-	Frost and McDowell ⁵ (Swarm)
	0.46 ± 0.02	3.9×10^{-18}	Buchelnikova ⁶ (Static gas)
	0.81	19.8×10^{-18}	Christophorou et al. ⁷ (Swarm)
	0.84 ± 0.005	-	Ziesel et al. ⁸ (Static gas)
	0.84	$(8.9 \pm 0.7) \times 10^{-18}$	Azria et al. ² (Static gas)
	-0.8	-25.0×10^{-18}	Sze et al. ⁹ (Swarm)
	0.82 ± 0.04	-	Allen and Wong ¹⁰ (Static gas)
	0.85 ± 0.02	$(26.6 \pm 5.3) \times 10^{-18}$	Present Work (Cross beam)

This work was performed at JPL-Caltech and supported by AFOSR and NASA.

References

- O. J. Orient and S. K. Srivastava, J. Chem. Phys. **78**, 2949 (1983).
- R. Azria, L. Roussier, R. Paineau and M. Tronc, Rev. Phys. Appl. (Paris) **9**, 469 (1974).
- H. Gutbier and H. Neuert, Z. Naturforsch. **9A**, 335 (1954).
- R. E. Fox, J. Chem. Phys. **26**, 1281 (1957).

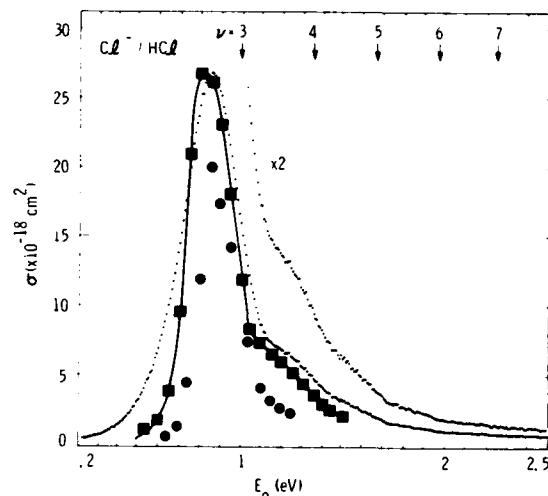


Fig. 1. The arrows indicate the position of the vibrational levels of the $\text{HCl}^+_{v=0}$ ground state. \bullet Tillet-Billy and Gauyacq.¹¹ \blacksquare Allen and Wong¹⁰ normalized to our peak cross section.

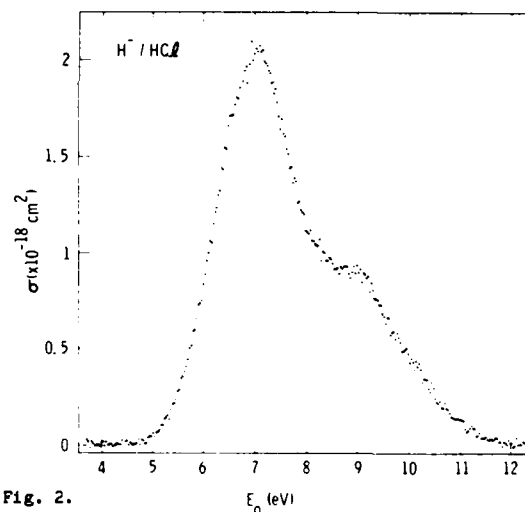


Fig. 2.

- D. C. Frost and C. A. McDowell, J. Chem. Phys. **29**, 503 (1958).
- I. S. Buchelnikova, Sov. Phys. JETP **35**, 783 (1959).
- L. G. Christophorou, R. N. Compton, G. S. Hurt and P. W. Reinhardt, J. Chem. Phys. **43**, 4273 (1965).
- J. P. Ziesel, J. Nenner and G. J. Schulz, **63**, 1943 (1975).
- R. C. Sze, A. E. Greene and C. A. Braw, J. Appl. Phys. **53**, 1312 (1982).
- M. Allen and S. F. Wong, J. Chem. Phys. **74**, 1687 (1981).
- D. Tillet-Billy and J. P. Gauyacq, J. Phys. B: At. Mol. Phys. **17**, 4041 (1984).

IONIZATION AND DISSOCIATIVE IONIZATION OF CO, CO₂ AND CH₄ BY ELECTRON IMPACT

O. J. Orient and S. K. Srivastava

Jet Propulsion Laboratory, California Institute of Technology, Pasadena, CA 91109

Cross sections for ionization and dissociative ionization of CO, CO₂, and CH₄ by electron impact are of considerable interest for the various plasma systems and are also important from the theoretical point of view. We have measured these cross sections by utilizing a crossed electron beam-molecular beam technique. A quadrupole mass spectrometer was employed for detecting the various fragments. A detailed description on the experimental setup, procedures and normalization method can be found in a publication by Orient and Srivastava.¹

Cross section data on these molecules are presented in Figures 1 through 4. We estimate that the accuracy of these cross sections is about 15%. Comparisons have been made with the previously published results. In general, within the error limits our data agree well with those published by Rapp and his co-workers.²

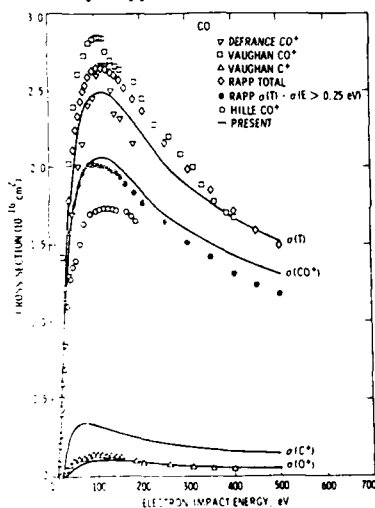


Fig. 1

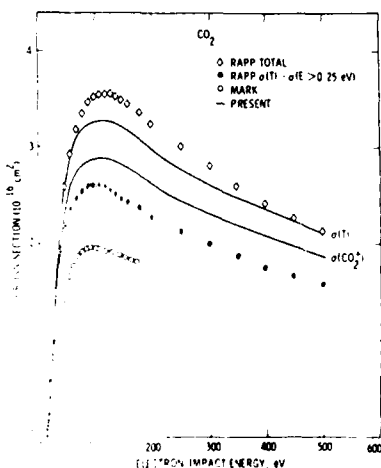


Fig. 2

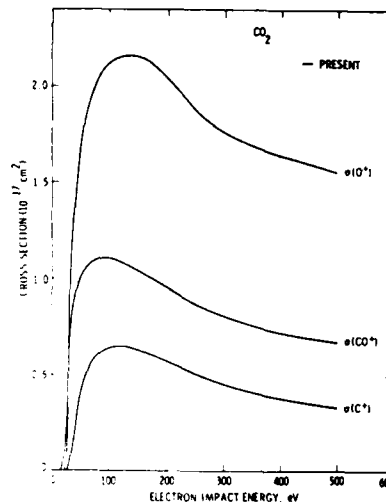


Fig. 3

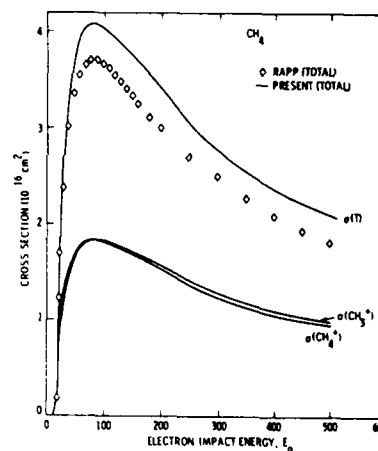


Fig. 4

Work was performed at JPL-Caltech and was sponsored by AFOSR and NASA.

References

1. O. J. Orient and S. K. Srivastava, *J. Chem. Phys.* **80**, 140 (1984).
2. D. Rapp and P. E. Golden, *J. Chem. Phys.* **43**, 1464 (1965).
3. A. L. Vaughan, *Phys. Rev.* **38**, 1687 (1931).
4. E. Hille and T. D. Mark, *J. Chem. Phys.* **69**, 4600 (1978).
5. M. M. DeFrance and J. C. Gomet, *Methods Physiques D'Analyse (GAMS) July-Sept.*, 205 (1966).
6. T. D. Mark and E. Hille, *J. Chem. Phys.* **69**, 2492 (1978).

ELECTRON IMPACT IONIZATION AND DISSOCIATIVE IONIZATION
OF AMMONIA

O. J. Orient and S. K. Srivastava

Jet Propulsion Laboratory, California Institute of Technology, Pasadena, CA 91109

We have utilized a crossed electron beam-molecular beam collision geometry and a quadrupole mass spectrometer to study the ionization and dissociative ionization processes in ammonia. The incident electron energies were chosen from threshold of the ionization to 500 eV. Experimental apparatus and normalization procedures are described in a previous publication by Orient and Srivastava.¹

It was observed that upon electron impact NH_3 ionizes into NH_3^+ and dissociatively ionizes into NH_2^+ , NH^+ , and N^+ fragments. The cross sections for all these processes were measured. Total cross sections, which are the sum of all individual cross sections connected with the above mentioned processes, are presented in Fig. 1 along with previously published data. It is clear from this figure that there is a large disagreement between the present measurements and some of the previous ones. The present results are uncertain by about 15%.

Cross sections for ionization into NH_3^+ , NH_2^+ , NH^+ , and N^+ are presented in Fig. 2. Due to the limited space here a comparison with all the previously measured data can not be given. In general there are large differences between the various measurements and again this is due to different methods of normalization. However, we have one major difference from the previously published data. It is connected with the ratio of $\text{NH}_2^+/\text{NH}_3^+$. Past results^{4,5} show that this ratio is less than 1. However, our measurements indicate that the ratio is greater than 1 which is consistent with the findings of Brion et al.¹¹ by the methods of photoelectron spectroscopy.

Work was performed at JPL-Caltech and was sponsored by AFOSR and NASA.

References

- O. J. Orient and S. K. Srivastava, *J. Chem. Phys.* **80**, 140 (1984).
- J. C. Gomet, *C. R. Acad. Sci., Ser. B* **281** 627 (1975).
- M. Djuric-Preger, D. Belic and M. Kurepa, *Proc. VIIIth Symp. Phys. Ionized Gases*, Dubrovnik, p. 54 (1976).
- T. D. Mark, F. Egger and M. Cheret, *J. Chem. Phys.* **67** 3795 (1977).
- A. Crowe and J. M. McConkey, *Int. J. Mass Spectrom. Ion Phys.* **24**, 181 (1977).
- D. K. Jain and S. P. Khare, *J. Phys.* **B9**, 1429 (1976).
- K. Bederski, L. Wojcik and B. Adamczyk, *Int. J. Mass Spectrom. and Ion Phys.* **35**, 171 (1980).
- G. DeMaria, L. Malaspina and V. Piacente, *Ric. Sci., Parte 2, Sez A3*, 681 (1963).

- L. E. Melton, *J. Chem. Phys.* **45**, 4414 (1966).
- F. W. Lampe, J. C. Franklin and F. H. Field, *J. Am. Chem. Soc.* **79**, 6129 (1957).
- C. E. Brion and A. Hammett, *Jour. Elec. Spectr. and Rad. Trans.* **12**, 323 (1977).
- J. C. Gomet, *C. R. Acad.* **281**, 627 (1975).

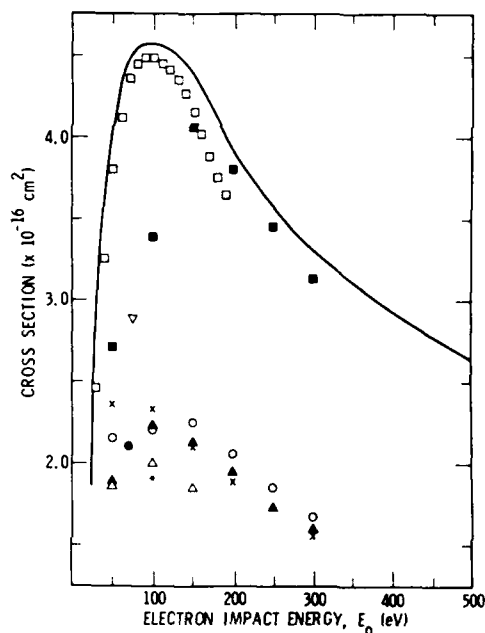


Fig. 1. Total ionization cross sections for NH_3 . present measurements; \square Djuric-Preger et al.³; \circ Mark et al.⁴; \times Crowe and McConkey⁵; \triangle Jain and Khare⁶; \diamond Bederski et al.⁷; \bullet DeMaria et al.⁸; \blacksquare Melton⁹; and \blacktriangle Lampe et al.¹⁰; \blacksquare Gomet¹².

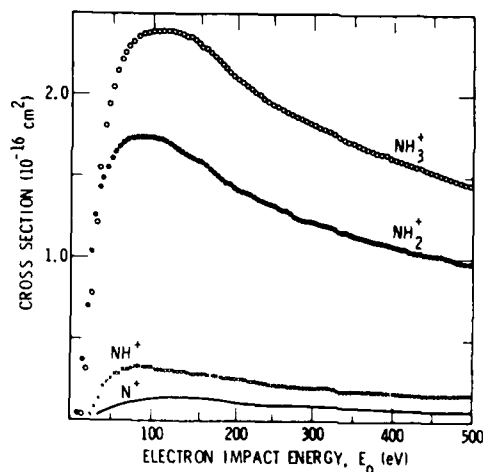


Fig. 2. Fragment ion production from NH_3 .

ABSOLUTE MEASUREMENT OF THE PHOTOEMISSION CROSS SECTION
FOR LYMAN- α RADIATION PRODUCED IN $e^- + H_2$ COLLISIONS

R. C. G. Ligtenberg, Armon McPherson, N. Rouze
W. B. Westerveld, and J. S. Risley

Department of Physics
North Carolina State University
Raleigh, North Carolina 27695-8202 USA

We have developed a technique and apparatus for the measurement of absolute electron impact photoemission cross sections in the vacuum ultraviolet (vuv) wavelength region. Well-parametrized synchrotron radiation is used to simulate the radiative emission of decaying atoms excited along an electron beam. A multi-adjustable manipulator is used to precisely position a spectrometer-detector system in front of the radiometric calibration port of SURF II (National Bureau of Standards, Gaithersburg, Maryland). The spectrometer-detector system used consists of a Minuteman 302VM Seya-Namioka type spectrometer with a Jobin-Yvon holographic grating and an EMI 9642/4B venetian blind photomultiplier. The manipulator has two axes of rotation, one of which coincides with the spectrometer entrance slit, the other with the exciting electron beam. These two rotations allow synchrotron radiation to be scanned across the grating surface in such a way that the angles of emission encountered in the electron atom source are accurately duplicated. In this way point-to-point variations in the detection efficiency, see Fig. 1, and geometrical factors, such as collection solid angle and length of electron beam viewed, are determined in an integral fashion. We anticipate an

ultimate overall accuracy of 5% for cross sections obtained with this system.

A preliminary measurement of the photoemission cross section for Lyman- α radiation produced in 100 and 300 eV $e^- + H_2$ collisions has been performed. A MgF_2 window was placed in front of the photomultiplier to block contributions from multiple order dispersion of synchrotron radiation. An emission spectrum produced by collisions of 100 eV electrons with H_2 is shown in Fig. 2. The use of a spectrometer allows an accurate determination of the Lyman- α signal arising from dissociative excitation of H_2 separate from the molecular emission in this wavelength region. Our preliminary measurements indicate that the accepted value for the Lyman- α emission cross section¹ is too high. This conclusion is substantiated by a recent absolute measurement by Van Zyl et al.²

This work was supported in part by the Aeronomy Program of the National Science Foundation, Grant No. ATM-81-21724.

References

1. See, for example, M. J. Mumma and E. G. Zipf, *J. Chem. Phys.* **55**, 1661 (1971).
2. B. Van Zyl, M. W. Gealy, and H. Neumann, submitted to *Phys. Rev. A*.

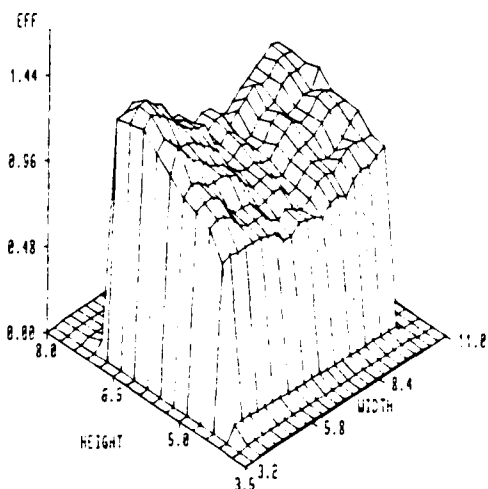


FIG. 1. Map of the relative detection efficiency as a function of position on the grating surface for a spectrometer setting of 121.6 nm. The synchrotron radiation was polarized perpendicular to the grating grooves.

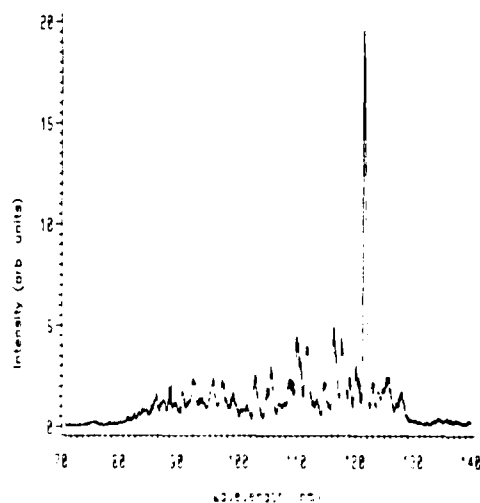


FIG. 2. Emission spectrum produced by collisions of 100 eV electrons with H_2 . No MgF_2 was used for this measurement, nor for the efficiency scan in Fig. 1.

ANGULAR INTENSITY DISTRIBUTION OF BALMER- α AND LYMAN- α EMISSION EXCITED BY ELECTRON IMPACT ON H_2

S.Arai, M.Morita, K.Hironaka, N.Kouchi*, N.Oda* and Y.Hatano

Department of Chemistry, Tokyo Institute of Technology, Meguro-ku, Tokyo 152, Japan

*Research Center for Nuclear Science and Technology, University of Tokyo, Tokai-mura, Ibaraki 319-11, Japan

+Research Laboratory of Nuclear Reactors, Tokyo Institute of Technology, Meguro-ku, Tokyo 152, Japan

Observation of optical emission from excited fragment atoms produced by dissociative excitation of molecules is of great importance in understanding highly excited molecular states and their dissociation processes.¹ Translational spectroscopy of dissociation fragments has been successfully carried out by observing the Doppler profile of optical emissions from fragment atoms.¹ It has been shown theoretically that the Doppler profiles depend not only on the kinetic energy and the spatial distribution of fragment atoms² but also on the population into their magnetic sublevels, i.e., the polarization of atomic radiation.³ The Doppler profile should be, therefore, affected by the observing direction,² and it has been known that optical emission from excited atoms by electron impact on molecules is anisotropic⁴ and it has been confirmed experimentally for Balmer- α emission by electron impact on H_2 .⁵ This paper presents the anisotropy of Balmer- α and Lyman- α emission excited by electron impact on H_2 .

The anisotropy of optical emission has been mainly described as the polarization degree, Π , which is defined as, $\Pi = (I_{\parallel} - I_{\perp}) / (I_{\parallel} + I_{\perp})$ (1), where I_{\parallel} and I_{\perp} are emission intensities whose electric vectors orient parallel and perpendicular, respectively, to the incident electron beam. The value of Π is also obtained from eq.(2) by measuring the angular distribution of optical emission intensity $I(\theta)$,⁵

$$I(\theta)/I(90^\circ) = 1 - \Pi \cos^2 \theta \quad (2),$$

where θ is the detecting angle with regard to the electron beam. Since the correction of the polarization sensitivities of devices which have been used to detect the optical emission is the serious problem especially in the measurement of I_{\parallel} and I_{\perp} , the latter method based on eq.(2) has an advantage for obtaining the value of Π .⁵

Balmer- α emission was detected through an interference filter with a photomultiplier, while Lyman- α emission was detected through a MgF_2 - O_2 filter with a continuous dynord electron multiplier (Ceratron). Using a static gas target, the correction of the apparatus function was made accurately than that of a crossed beam method. Anisotropy of optical emission has been obtained from the angular distribution measurement and expressed by Π using eq.(2). Energy dependence of Π for Balmer- α and Lyman- α emission is shown in Fig.1 and Fig.2, respectively. Large discrepancies with the results obtained by different groups from I_{\parallel} and I_{\perp} measurements may reflect the difficulty in determining the detecting efficiency of

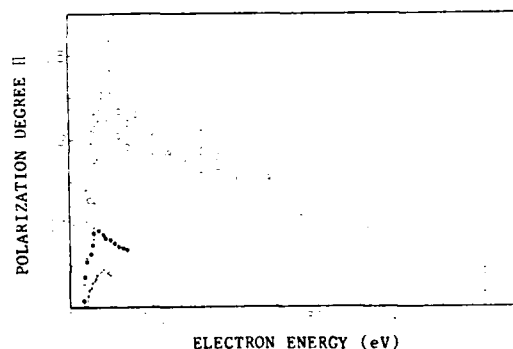
 I_{\parallel} and I_{\perp} .

Fig.1 Polarization degree Π of Balmer- α emission. \circ : this work, \bullet : Karolis and Harting (ref.6), \times : Glass-Maujean (ref.7). \bullet and \times are obtained from I_{\parallel} and I_{\perp} measurement.

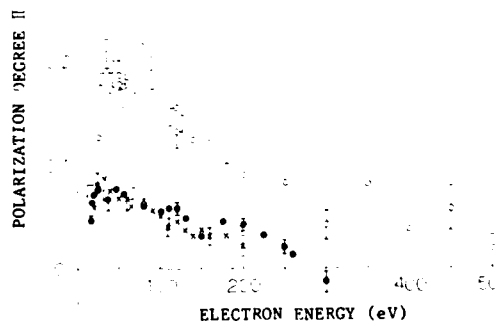


Fig.2 Polarization degree Π of Lyman- α emission. \circ : this work, \bullet : Malcolm et al (ref.8), \times : Ott et al (ref.9). \bullet and \times are obtained from I_{\parallel} and I_{\perp} measurement.

Reference

1. Y.Hatano, Comments on At.Mol.Phys., **13**, 259 (1983) and references cited therein.
2. K.Ito, N.Oda, Y.Hatano and T.Tsuboi, Chem.Phys., **17**, 35 (1976).
3. N.Kouchi, K.Ito, N.Oda and Y.Hatano, Chem.Phys., **70**, 105 (1982).
4. R.J.van Brunt and R.N.Zare, J.Chem.Phys., **48**, 4304 (1968).
5. N.Takahashi, S.Arai, N.Kouchi, N.Oda and Y.Hatano, J.Phys., **B16**, L547 (1983).
6. C.Karolis and E.Harting, J.Phys., **B11**, 357 (1978).
7. M.Glass-Maujean, J.Phys., **B11**, 431 (1978).
8. I.C.Malcolm, H.W.Dassen and J.W.McConkey, J.Phys., **B12**, 1003 (1979).
9. W.R.Ott, W.E.Kaupilla and W.L.Fite, Phys.Rev., **A1**, 1089 (1970).

ANGULAR DISTRIBUTION OF FRAGMENTS FROM DISSOCIATIVE ELECTRON ATTACHMENT*

Andrew U. Hazi

Physics Department, Lawrence Livermore National Laboratory
University of California, Livermore, California 94550 USA

The formalism¹ describing the angular distribution of products that result from the dissociative attachment of electrons to diatomic molecules has been extended to include the cases where the fragments possess internal angular momenta. The present theory, just as the earlier work, is based on the customary projection operator treatment² of the electronic resonance states of molecular anions. In addition, the theory makes extensive use of frame transformations³ applied within the adiabatic nuclei approximation.⁴ The expressions for the total scattering wavefunction, the equation governing the nuclear motion and the scattering amplitude for dissociative attachment have been derived using several different body-fixed representations of the total scattering wavefunction. Formal difficulties associated with each of these representations have been examined and found not to be significant in those cases where the effects of rotational motion can be neglected.

The theory takes on its simplest form when the projection operator formalism is applied to that body-fixed scattering wavefunction which is a simultaneous eigenstate of \tilde{H} , \tilde{J}_z and \hat{R} ($= \hat{\phi}$), where \tilde{H} and \tilde{J}_z are the Hamiltonian and the z-component of the total angular momentum operator, respectively. Both \tilde{H} and \tilde{J}_z refer to the body-fixed frame in which the z-axis is taken along the internuclear axis. The eigenvalues of the "operator" \hat{R} specify the orientation of the internuclear axis relative to the z-axis of the space-fixed frame.

For heteronuclear diatomic molecules, the present expression for the angular distribution of fragments reduces to the previously derived results¹ provided the rotational period is small compared to the time required for dissociation. However, I also find that in cases where more than one partial wave contributes to the attached electron's wavefunction, not only the total width of the resonance, but also the decay amplitude for each partial wave is required for calculating the angular distribution of fragments. This result holds even when one uses the "local" or "boomerang" approximation⁶ for treating the nuclear motion.

The extension of the present theory required for describing dissociative electron attachment to homonuclear diatomic molecules will be discussed.

* This work was performed under the auspices of the U. S. Department of Energy by Lawrence Livermore National Laboratory under contract No. W-7403-Eng-48.

Reference

1. T. F. O'Malley and H. S. Taylor, Phys. Rev. **176**, 207 (1968).
2. T. F. O'Malley, Phys. Rev. **150**, 14 (1966).
3. E. S. Chang and U. Fano, Phys. Rev. **A6**, 173 (1972).
4. M. Shugard and A. U. Hazi, Phys. Rev. **A12**, 1903 (1975).
5. M. Shugard, Ph.D. Thesis, Univ. of California at Los Angeles, 1977.
6. D. Birtwistle and A. Herzenberg, Phys. Rev. **A4**, 53 (1971).

ANGULAR DIFFERENCE DOPPLER PROFILES: DYNAMICS OF FORMATION OF H* IN ELECTRON-H₂ COLLISIONS

Teiichiro Ogawa, Keiji Nakajima, and Hirofumi Kawazumi

Department of Molecular Science and Technology, Kyushu University, Kasuga-shi, Fukuoka 816, Japan

A high resolution measurement of the Doppler profile of the Balmer lines produced in electron-molecule collisions and its differentiation has disclosed the translational energy distribution of H*, D* and N*.¹ This method is very useful if the dissociation is approximately isotropic. However, recent studies have disclosed an angular dependence of the Balmer lines.² Thus, more accurate analysis with a due consideration for anisotropy has to be made for a further study of dissociation dynamics.

The angular distribution has in general a dipolar form and depends on an asymmetry parameter b . The probability for an atom to emit toward an angle θ with respect to the dissociation axis depends on its magnetic sublevel; J_p is a parameter for polarization in the sublevel:

$$J_p = (J_{||} - J_{\perp}) / (J_{||} + J_{\perp}). \quad (1)$$

The Doppler profile observed at angle θ with respect to the electron beam is obtainable with these two parameters:

$$F(\theta, \nu) = (3\sigma/16\pi^2 \nu) (J_{||} + J_{\perp}) (1 - J_p \cos^2 \theta) + (1 + b P_2(\cos \theta) P_2(\cos \theta)) \quad (2)$$

There are usually more than one dissociation processes for the production of the excited atom. Each of them may have a set of different anisotropy parameters. In such case estimation of the two key parameters can be carried out by taking the difference of the two Doppler profiles measured at two different angles θ and θ' . If we take θ as 90° and θ' as 45° :

$$F(\theta, \nu) = F(\theta, 90^\circ, \nu) - F(\theta, 45^\circ, \nu) = - (b + (1 + J_p \cos^2 \theta) (J_{||} + J_{\perp}) (1 - J_p \cos^2 \theta)) b P_2(\cos \theta) \quad (3)$$

for an excited atom with a uniform velocity v . The angular difference Doppler profile, $\Delta F(\theta)$, should be obtained by the integration over ν . Typical simulated angular difference Doppler profiles for atoms with large translational energies is shown in Fig. 1.

The hydrogen was collided with a beam of electron in a collision chamber. The Doppler profile of the

Balmer lines was measured with a Fabry-Perot interferometer with an optical resolution of about 0.065 Å.

There are four major dissociation processes for the hydrogen molecule as are shown in the potential energy diagram (Fig. 2).³ They are divided into a fast and a slow group (a peak and a wing in the Doppler profile).

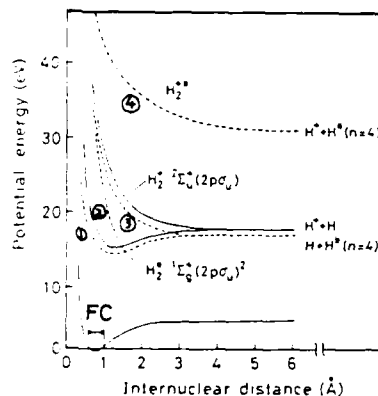


Fig. 2.
Potential energy diagram
— H_2, H_2^+
--- H_2^*
① - ④: major dissociation processes.

Typical Doppler profiles of the Balmer-β line taken at 90° and 45° and their angular difference Doppler profiles are shown in Fig. 3. A comparison of the observed profile with the simulated one indicates that $b > 0$ and $J_p > 0$ for the major component of the fast group. Since this component was assigned to the direct dissociation through $(2p\sigma_g)(4i)$ Rydberg states (4i denotes correlation with $H^*(n=4)$ in the dissociation limit), the symmetry of this Rydberg states has to be Σ_g and the excited hydrogen atom has to be either p^+ or d^+ .

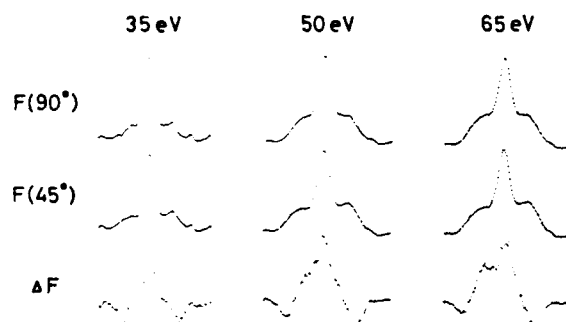


Fig. 4. Observed Doppler profiles and their differences.

References

1. M. Higo, S. Kamata & T. Ogawa, Chem. Phys., **66**, 243 (1982); T. Ogawa, S. Ishibashi, J. Kurawaki & H. Kawazumi, JCP, in press.
2. J. Kurawaki and T. Ogawa, Chem. Phys. Lett., **98**, 12 (1983).
3. K. Nakajima, H. Kawazumi & T. Ogawa, Chem. Phys., submitted.

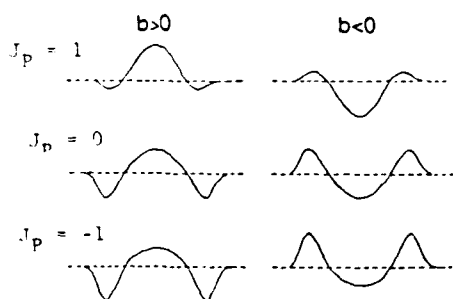


Fig. 1. Simulated angular difference Doppler profiles

AN AB-INITIO STUDY OF THE DISSOCIATIVE ATTACHMENT TO H_2 OF ELECTRONS OF ENERGIES 6 eV to 12 eV

S. Bhattacharyya*, L. Chatterjee and K. Basu

*Gokhale College, Calcutta 700020, India
Jadavpur University, Calcutta 700032.

An ab-initio dissociative attachment (DA) cross section for H^- ion formation is obtained after allowing some modification over our previous field theoretic calculation¹ and with a more realistic type of molecular and ionic wave function. The result fits well with other experimental and theoretical findings.

The phenomena is treated as a recombination process. The leptonic field of the projectile electron interacts with the fields of the particles constituting the target molecule via longitudinal photon exchange. The energy range considered here is much above DA threshold (3.7 eV). The velocity of the target molecule in thermal equilibrium is assumed to be negligible compared to the speed of the projectile electron. However, situation will be different if $E_1 \leq 3.7$ eV, and the thermal velocity of H_2 with Maxwellian distribution cannot be ignored resulting in an increased phase space.

Our computation with hydrogen molecule in the ground electronic and vibronic state gives for the cross-section

$$\sigma_{DA} = \frac{4}{(2\pi)^6} \left| \frac{M_{fi}}{P_1} \right|^2 2M_p(E_1 - \epsilon)^{3/2}, \quad M_{fi} = M_{ee} + M_{ep}$$

where, E_1 and P_1 are the energy and momentum of the projectile. $M_p = \text{mass of hydrogen atom}$

Although one may question here the Born type of interaction, yet the interference term between M_{ee} and M_{ep} gives rise to peak in the cross-section near 10 eV, the threshold for H_2^- ion formation in the $2\Sigma_g^+$ state

$$M_{fi} = \frac{9}{4\pi(2\pi)^9} \delta^3(P_c - Q_c) H_2(X_1 X_2 r)$$

$$\Psi_1(X_3) \times L(r) \sum_{i=1}^{12} (2D_1^{ee}(X_1 X_2 X_3 r) - G_1^{ep}(X_1 X_2 X_3 r))$$

$H_2(X_1 X_2 r)$ and $\Psi_1(X_3)$ are respectively the wave functions of the target and the projectile.

$D_1^{ee}(X_1 X_2 X_3 r)$ and $G_1^{ep}(X_1 X_2 X_3 r)$ are the product of the wave function of H atom and H^- ion along with the Coulomb part of e-e interaction and e-p interaction respectively.

For example,

$$D_1^{ee}(X_1 X_2 X_3 r) = H(X_3 - r) H^-(X_1 + 2r, X_2) / |X_3 - X_2 - r|$$

$$G_1^{ep}(X_1 X_2 X_3 r) = H(X_3 - r) H^-(X_1 + 2r, X_2) / |X_3 + r|$$

$L(r)$ gives the wave function of the motion of the atom and ion.

All the peaks in the summation arise because of the indistinguishability of the identical particles. The integrals in the DA cross-section are evaluated analytically.

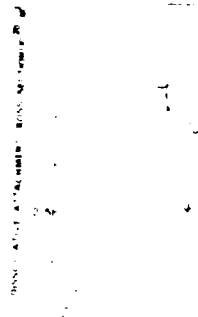


FIGURE 1 Energy dependence of H^- ion formation cross-section due to dissociative attachment of H_2 by electron.

-- Experimental result Schultz³,
--- Experimental result Rapp et al.²,
— Present theoretical calculation.

Reference

1. S. Bhattacharyya, L. Chatterjee, T. Roy, Indian J. Phys. **57B** (1983) 104.
2. D. Rapp, T. E. Sharp, D. Brack, Phys. Rev. Letter **14** (1965) 533.
3. G. J. Schulz, Phys. Rev. **170** (1969) 816.

DISSOCIATIVE ELECTRON ATTACHMENT TO MOLECULAR LITHIUM

J. M. Wadehra* and H. H. Michels*

*Department of Physics, Wayne State University, Detroit, Michigan 48202 USA
 †United Technologies Research Center, East Hartford, Connecticut 06108 USA

The fact that both molecular lithium (Li_2) and molecular hydrogen (H_2) are isoelectronic in the valence region suggests that the rates of electron attachment to these two molecules might also be quite similar. In fact, to the contrary, results of recent experiments¹ indicate that the maximum rate for electron attachment to Li_2 is about $10^{-17} \text{ cm}^2 \text{ sec}^{-1}$ which is comparable to the measured value for H_2 .

Both experimental observations as well as theoretical calculations for H_2 indicate² that vibrational excitation of the molecule can enhance the electron attachment rate by several orders of magnitude. One of the aims of present studies is to investigate whether a similar strong enhancement of the attachment rate occurs for Li_2 on increasing the vibrational energy.

Figure 1 shows the potential curves of some low vibrational levels of Li_2 and Li_2^- . The lowest two states of atomic Li_2 , namely the $X^2\Sigma_g^+$ and the $A^2\Sigma_g^+$ states, have the same electronic symmetry as the lowest two states of H_2 . However, due to large

polarizability and weak bond strength, the $X^2\Sigma_g^+$ state of Li_2^- is a true bound state for all internuclear separations. The $A^2\Sigma_g^+$ state, on the other hand, is bound only for $R > 6.51 \text{ a.u.}$ For smaller internuclear separations, this state is the lowest resonance of Li_2^- .

A semiclassical approach utilizing the local-width resonance model is used to obtain the cross sections and rates for dissociative attachment to Li_2 . The resonance width for the $A^2\Sigma_g^+$ state is parametrized in atomic units as $\Gamma(R) = 0.0143 k(R)$, where $k(R)$ is the local wave number of the attached electron. The behavior of the attachment cross section is investigated both as a function of the incident electron energy for a given rovibrational state of the molecule Li_2 and as a function of the internal energy of the molecule for a fixed incident electron energy.

This research is supported by AFOSR under Grant AFOSR-84-0143 and Contract F49620-83-C-0094.

References

1. M. W. McGeoch and R. E. Schlier, in *Proceedings of the Third International Symposium on the Production and Neutralization of Negative Ions and Beams*, edited by K. Prelec (American Institute of Physics, New York, 1984), p. 291.
2. J. M. Wadehra, *Phys. Rev. A* **29**, 106 (1984).

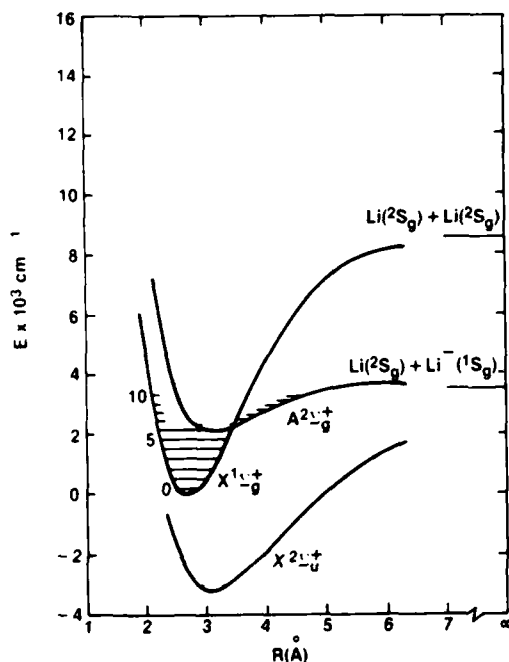


FIGURE 1 Potential energy curves for dissociative electron attachment to Li_2 .

VUV FLUORESCENCE PRODUCED BY DISSOCIATIVE ELECTRON-IMPACT EXCITATION OF SF₆J.L. Forand⁺, K. Becker⁺, and J.W. McConkey⁺ Department of Physics, University of Windsor, Windsor, Ontario, Canada N9B 3P4
Department of Physics, Lehigh University, Bethlehem, Pennsylvania, USA 18015

Collisions between electrons and sulphur-hexafluoride (SF₆) molecules are of great practical interest due to the importance of the molecule in high voltage insulators and spark gaps. Although several studies utilizing different techniques have been performed to investigate e⁻ - SF₆ collisions¹, little is known about the dissociative excitation of SF₆ by electron impact and virtually no absolute cross-sections for the various resultant fragment emissions are available to date. Data are particularly scarce for emissions in the extreme ultraviolet region of the spectrum.

We have studied the VUV fluorescence (400 - 2000Å) produced by electrons incident on SF₆ under single collision conditions. A crossed electron-gas beam set-up was employed in conjunction with a 0.5 m Seya-Namioka VUV monochromator. Detection of the VUV radiation was made using either a Mullard 419 BL channel electron multiplier or a caesium-iodide coated Galileo Electro-Optics BX 7600-4413 photon counter tube (above 1200Å). Wavelength scans from 400 - 2000Å for various incident electron energies displayed a variety of emission features which could be identified as arising from neutral or singly ionized fluorine and sulphur. No emissions from more highly ionized species were found. Excitation functions were measured for the most prominent features from threshold (typ. 30-50 eV) to 600 eV and they were put on an absolute scale by comparison with well-known benchmark cross sections^{2,3}. In separate runs the threshold region of each line was scanned to determine the onset potential which can yield information about the underlying dissociation mechanism(s). A detailed analysis of the data will be presented at the Conference, but the main results may be summarized as follows:

1) The neutral fluorine emissions were found to be the most prominent features. Intense emissions were observed around 975, 955, 806, 795 and 780Å and weak emissions were detected all the way to the ionization limit of F I at 711Å. The major transitions arise from upper 2s² 2p⁴ ns, md electron configurations (n=3,4,5,6; m=3,4,5) and terminate in the 2s² 2p⁵ 2p⁰ ground state. The 955Å line has the largest emission cross section of all observed fragment emissions with 2.3×10^{-18} cm² at 200 eV impact energy. The excitation functions of all the FI lines display a smooth increase from a single onset to a broad maximum around 200 eV. No indications were found that processes with different dissociation limits were occur-

ring.

2) Emissions from singly ionized fluorine were observed in the spectrum below appr. 600Å, but were extremely weak. Only the line at 606Å (transition 2s 2p⁵ 3p⁰ - 2s² 2p⁴ 3p) was intense enough to be studied in some detail. Onset potentials were found to occur at approximately 45 and 59 V. Subtraction of the FI ionization potential (17.4 eV) and the photon energy corresponding to 606Å (20.5 eV) results in residual energies necessary to break up the SF₆ molecule of 7 and 21 eV respectively.

3) The major neutral sulphur emissions occur at 1425, 1433, 1474, 1483, 1666, 1807 and 1820Å. The lines correspond to two series of emissions, from upper 3s² 3p³ 3d, 4s electron configurations to the 3s² 3p⁴ 3p ground state and from the 3s² 3p³ 4s 3p, 1D⁰ states to the 3s² 3p⁴ 1D state respectively. The strongest emission is the feature centred at 1474Å with an emission cross section of 3.2×10^{-19} cm² at 200 eV. For all S I emissions smooth excitation functions were measured with a maximum slightly below 200 eV and appearance potentials around 35 V. This yields residual energies around 27 eV, which is 9 eV higher than the residual energy observed in connection with the formation of excited fluorine fragments.

4) The emissions identified as arising from excited S II fragments lie between 900 and 1260Å with intense lines around 910, 937, 995-1030, 1047, 1100, 1203 and 1256Å. The spectrum is very complex and a variety of excited states - some of which are unidentified or unclassified - are involved. Typically, emission cross sections for S II features range from $1-10 \times 10^{-19}$ cm² at 200 eV. Measured onset potentials yielded residual energies close to 24 eV.

This work was supported by the Natural Sciences and Engineering Research Council of Canada (NSERC).

References

1. See S. Trajmar and A. Chutjian, *J. Phys. B* 10, 2943 (1977) and references given therein.
2. K. Becker et al., *Plan. Space Sci.* 31, 197 (1983).
3. K. Becker and J.W. McConkey, *Can. J. Phys.* 62, 1 (1984).

OBSERVATIONS AND CROSS SECTIONS FOR ELECTRON ATTACHMENT
IN MOLECULES AT ULTRALOW ELECTRON ENERGIES

A. Chutjian and S. H. Alajajian

Jet Propulsion Laboratory, California Institute of Technology, Pasadena, CA 91109

Extremely sharp, resolution limited onsets have been observed in electron attachment and dissociative attachment (DA) to a large number of molecules. The onsets are observed at electron energies less than 10 meV, and the resolutions attained to date using the Kr photoionization technique^{1,2} are $\Delta E = 4-8$ meV (FWHM). The threshold onset is a general phenomenon, and has been observed by us so far in SF_6 ,¹ CCl_4 ,¹ CFC_3 ,² $2\text{-C}_4\text{F}_6$, $2\text{-C}_4\text{F}_8$, C_5F_8 , C_6F_6 , C_7F_8 , C_6F_{10} and $1,1,1\text{-C}_2\text{C}_3\text{F}_3$ --all molecules known to have neutral-negative ion curve crossings at zero electron energy. The phenomenon is not observed in CF_2C_2 --a molecule known to have a curve crossing near 70 meV. The lineshape for the DA channel $\text{C}_2\text{F}_3^-/\text{CFC}_3$ is shown in Fig. 1 at a resolution of 4 meV (FWHM).

The experimental results are interpreted in terms of the s-wave behavior of the attachment cross section $\sigma_A(E)$ in the limit $E \rightarrow 0$, namely $\sigma_A(E) \sim E^{-1/2}$ for $E \rightarrow 0$. Attachment cross sections are obtained by normalization through the absolute attachment rate constant.¹ Results in CCl_4 and SF_6 are shown in Fig. 2 where comparison is also made with other swarm (o and),⁴ collisional ionization (\square)⁵ and earlier photoionization (---)⁶ results. There is very good agreement of the present data in SF_6 with theory,^{7,8} in particular with a prediction of the sharp onset in an earlier calculation by us.⁷ Experimental lineshapes and attachment cross sections will be

presented for the above molecules, and comparisons given with theory in the case of SF_6 .

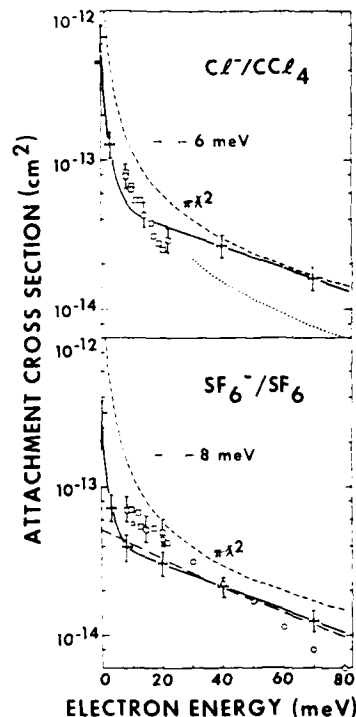


Fig. 2. Cross sections for electron attachment to CCl_4 and SF_6 . Present results are given as solid line (—). The maximum s-wave capture cross section ($\pi\lambda^2$, ---) is indicated.

This work was carried out at JPL-Caltech, and was supported by the AFOSR, DOE and NSF under agreement with NASA.

References

1. A. Chutjian and S. H. Alajajian, *Phys. Rev. A*, in press.
2. A. Chutjian, S. H. Alajajian, J. M. Ajello and O. J. Orient, *J. Phys. B* **17**, L745 (1984).
3. E. P. Wigner, *Phys. Rev.* **71**, 1002 (1948).
4. L. G. Christophorou et al., *J. Chem. Phys.* **51**, 4691 (1971) (CCl_4); *J. Chem. Phys.* **72**, 4049 (1980) (SF_6).
5. G. W. Foltz et al., *J. Chem. Phys.* **67**, 1352 (1977).
6. A. Chutjian, *Phys. Rev. Letters* **46**, 1511 (1981); erratum **48**, 289 (1982).
7. A. Chutjian, *J. Phys. Chem.* **86**, 3518 (1982).
8. J. P. Gauyacq and A. Herzenberg, *J. Phys. B* **17**, 1155 (1984).

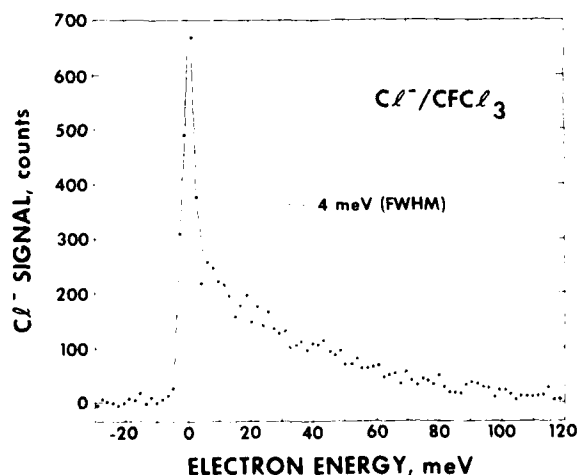


Fig. 1. Attachment lineshape for the process $\text{C}_2\text{F}_3^-/\text{CFC}_3$ at 4 meV (FWHM) resolution.

PHOTOENHANCED ELECTRON ATTACHMENT IN C_2H_3Cl AND C_3F_3H AT 193 nm

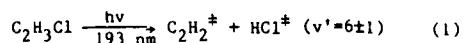
M. J. Rossi, H. Helm and D. C. Lorents

Chemical Physics Laboratory, SRI International, Menlo Park, CA 94025

From the temperature dependence of the electron attachment coefficients cross sections for rotationally and vibrationally excited attachers can be derived, that are significantly larger than the ones found for the corresponding ground states. The goal of the present study was to investigate the electron attachment properties of vibrationally excited HCl and HF using photoelimination at 193 nm from the above mentioned precursors as the method of preparation.

Our experiment involves the measurement of the electron attachment coefficient of an electron swarm in a drift cell, whose gap between the parallel plate electrodes was irradiated with 1 mJ/cm^2 of 193 nm laser radiation following the method of Gruenberg.

Figure 1 shows our results for unexcited C_2H_3Cl in 500 Torr He, whose attachment coefficient as a function of reduced electric field strength E/N shows a maximum $\eta/P=34 \text{ cm}^{-1}\text{Torr}^{-1}$ at 2.2 Td. When the gas mixture (500 Torr He) is excited with $.9 \text{ mJ/cm}^2$ at 193 nm the upper attachment curve which is based on the density of ground state vinylchloride (2% excitation) results. The photoenhancement of the electron attachment coefficient (η/P) is quite impressive and amounts to 20000 at .1 Td and to 500 at 2.2 Td. We attribute this result to the presence of vibrationally excited HCl, which is generated according to equation (1). The concentration



dependence reveals fast quenching of the excited attacher by the precursor (C_2H_3Cl), and the pertinent results are given in Table 1. The power dependence of η/P is linear up to to 2.3 mJ/cm^2 , after which it shows a "plateau", so that we must conclude that an unknown deactivation process becomes important. The dependence of η/P on total pressure is weak.

In the case of trifluoroethylene the results are very similar. The photoenhancement of the electron attachment coefficient based on the excited density of trifluoroethylene amounts to a factor of 60000 at .1 Td and to 11000 at 6 Td with a ground state attachment coefficient of $1.0 \text{ cm}^{-1}\text{Torr}^{-1}$ and $1.8 \text{ cm}^{-1}\text{Torr}^{-1}$, respectively. For C_2F_3H the amount of precursor excitation (.0036) is much smaller than in the vinylchloride case. Characteristic data are given in

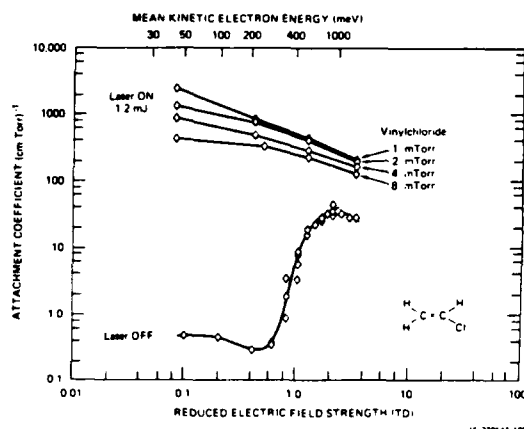


Figure 1 Experimental Result for Photoenhanced Electron Attachment of Vinylchloride.

Table 1 and this effect is thought to be due to the presence of vibrationally excited HF according to equation (2).

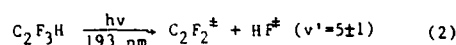


Table 1

Vinylchloride (C_2H_3Cl) ($\alpha = 1.7 \times 10^{-17} \text{ cm}^2$)

$\frac{E}{N}$ (Td)	f	σ (cm^2)	k_a ($\text{cm}^3 \text{ s}^{-1}$)	k^d ($\text{cm}^3 \text{ s}^{-1}$)
0.082	0.01984	4.1×10^{-14}	5.7×10^{-7}	2.0×10^{-9}
1.23	0.01984	9.7×10^{-14}	4.2×10^{-7}	4.0×10^{-9}

Trifluoroethylene (C_2F_3H) ($\alpha = 2.44 \times 10^{-18} \text{ cm}^2$)

0.82	1.75×10^{-3}	4.3×10^{-14}	1.5×10^{-6}	4.5×10^{-10}
4.10	1.74×10^{-3}	2.3×10^{-14}	1.8×10^{-6}	8.0×10^{-10}

Experimental data for the 193 nm photoenhanced electron attachment of vinylchloride ($.9 \text{ mJ/cm}^2$) and of trifluoroethylene $.75 \text{ mJ/cm}^2$. (f is the fractional excitation of the precursor, σ is the averaged attachment cross section, k_a is the attachment rate constant.

Acknowledgment: Research supported by ARO is gratefully acknowledged.

ELECTRON SCATTERING BY EXCITED HYDROGENIC IONS USING AN OPTICAL POTENTIAL APPROACH

D. H. Oza and J. Callaway

Department of Physics, Louisiana State University, Baton Rouge, LA 70803 U.S.A.

In this work, we are primarily interested in the scattering of electrons by hydrogenic ions in excited states at low energies. Particularly for ions in the excited states, the coupling between various states is very strong. A direct calculation using the close-coupling method with a basis of real atomic states supplemented by pseudostates, as has been successfully done in the case of the scattering by ions in the ground state, may be inadequate due to the large number of channels which must be included.

In order to describe the target atom adequately, including the excited bound states as well as the continuum, a basis of real atomic states supplemented by a rather large number of pseudostates is employed. But we consider only a small number of channels explicitly. A set of coupled integro-differential equations are solved for this set of channels. The effects of channels not explicitly included are incorporated through a complex, energy dependent, optical potential. This optical potential describes the energy dependent polarizability of the initial target state, and also includes the loss of flux to other open channels not explicitly included.

The set of coupled integrodifferential equations are converted to the integral form using appropriate two-particle Green's functions. The resulting set of coupled integral equations for the scattering functions describing the motion of the scattered electron are

$$\begin{aligned} \phi_{ia}(r) = & \frac{1}{r} F_{\lambda}(k_i r) \delta_{ia} - \sum_{j=1}^N \int \Omega_j(r, x) \left\{ V_{ij}(x) - \frac{e^2}{r} \delta_{ij} \right\} \phi_{ja}(x) \\ & + \int dy y^2 \left[u_i(y) \left\{ W_{ij}(y, x) - (k_i^2 - E_j) \delta_{i_1 i_2} \delta_{j_1 j_2} \right\} u_j(x) \right. \\ & \left. + U_{ij}(x, y) \right] \phi_{ja}(y) x^2 dx \end{aligned} \quad (1)$$

where F_{λ} is the regular Coulomb function for the incident channel, the sum in the second term is over explicitly included channels, Ω_j is the two-particle

Green's function, u_i is the target state function, V_{ij} and W_{ij} are direct and exchange potentials respectively and U_{ij} is the complex, energy dependent, optical potential.

$$U_{ij}(r, x) = - \sum_m \int y^2 dy \int z^2 dz K_{im}(r, y) \gamma_m(y, z) K_{mj}(z, x) \quad (2)$$

In this expression, the indices i and j run over all the channels explicitly included whereas the index m is over all the channels we wish to include via the optical potential. In this way it is possible to include a large basis set without having to consider the dynamics of the pseudostates in detail. Here K_{im} is the non-local kernel which includes the direct and exchange potential and γ_m is the appropriate Green's function.

$$\begin{aligned} K_{ij}(r, x) = & \left[V_{ij}(r) - \frac{e^2}{r} \delta_{ij} \right] \frac{\delta(r-x)}{r^2} \\ & + (-1)^{S_{ij}} u_i^*(x) \left[W_{ij}(x, r) - (k_i^2 - E_j) \delta_{i_1 i_2} \delta_{j_1 j_2} \right] u_j(r) \end{aligned} \quad (3)$$

Eq.(1) is solved numerically by a linear algebraic method. The Green's function, Ω_j , is adapted to obey the K matrix boundary conditions. Due to the complex optical potential, the resulting K-matrix is also complex. It is determined by fitting the numerical solution at large distances to the asymptotic form. From the complex K-matrix, the other scattering information is obtained in the usual way.

We have been able to reproduce the 3-state (1s, 2s, 2p) close-coupling results for the scattering of electrons by hydrogen atom in the ground state in the literature using our computer code. In the conference, we will present the elastic scattering cross-sections by hydrogen atom and singly ionized helium ions from their lower excited states.

This work is supported in part by the U.S. National Bureau of Standards.

P-WAVE PHASE SHIFTS AND RESONANCES FOR ELECTRON SCATTERING BY He^+

D. H. Oza

Department of Physics, Louisiana State University, Baton Rouge, LA 70803-4001 U.S.A.

Accurate calculations have been performed with an algebraic variational method¹ for the scattering of electrons by He^+ at energies below the $n=2$ threshold of the target in the close-coupling pseudostate expansion approximation. The continuum functions in the $1P$ -wave are relevant to the final state functions for the photoionization of He atoms in their ground state, for which rather accurate experimental data exists. In addition, there are three series of resonances, of which nine members of the $(2snp + 2pns)$ series have been experimentally observed². Also, there is interesting recent experimental work on the lowest $3P$ resonance³.

In this work, we have used three different basis sets for the description of the target ion. One set, which we call the 6-state set (3-3), consists of $1s, 2s$ and $2p$ bound eigenfunctions of the ion and one s -type pseudostate and two p -type pseudostates. The 14-state (6-5-2-1) basis set consists of all the real bound states up to $n=3$ and three s -type, three p -type, one d -type and one f type pseudostates. The 14-state basis set is supplemented by one s -type, one d -type, one g -type and one f -type pseudostates to make the 18-state (7-5-3-2-1) basis set. The parameters of the larger basis sets are given in Ref. 1.

Selected and representative results are presented in three tables below. The phase-shifts in the non-resonant region at an incident electron energy of 2.0 Ry are given in Table 1. We also include the three-state close-coupling results of Burke and McVicar⁴ (all real states) and Jacobs⁵ (1s real, and other pseudostates) to notice the significant improvement in the present phase-shifts. Due to a lower bound on the phase-shifts¹ in this case, one can judge the accuracy of results.

The resonance parameters for the lowest $3P$ resonance are given in Table 2. We compare our results with that of Ho⁶ by complex coordinate rotation method and with the experiment³. The experimental result quoted here is the one with the least error.

To demonstrate the fact that the essential physics of the scattering problem is adequately represented in the present approach in a practically tractable way, we present in Table 3 the resonance

parameters for a very narrow resonance for which no other ab initio theoretical results exist in the literature, although the experimental resonance energy has been known for two decades².

This work is supported in part by the U.S. National Bureau of Standards.

Table 1. $1P$ Phase-shift for $k^2=2.0$ Ry.

Basis	δ
1s-2s-2p (Ref. 4)	-0.0447
1s-2s-2p (Ref. 5)	-0.0285
6 states (3-3)	-0.0249
14 states (6-5-2-1)	-0.02419
18 states (7-5-3-2-1)	-0.02400

Table 2. $2s2p\ 3p^0$ Resonance

	Energy (Ry)	$\Gamma/2$ (Ry)
6 states (3-3)	-1.520593	0.000300
14 states (6-5-2-1)	-1.520902	0.000301
18 states (7-5-3-2-1)	-1.520913	0.000301
Complex Rotation (Ref. 6)	-1.520985	0.000299
Experiment (Ref. 3)		0.000307

Table 3. $(2s7p + 2p7s)\ 1p^0$ Resonance

	Energy (Ry)	$\Gamma/2$ (Ry)
6 states (3-3)	-1.02114	0.0000245
14 states (6-5-2-1)	-1.02135	0.000025
Experiment (Ref. 2)	-1.0215	

References

1. J. Callaway, Phys. Repts., 45, 89(1978).
2. R. P. Madden and K. Codrington, Ap. J., 141, 364(1965).
3. H. Cederquist, et. al., J. Phys. B, 16, L479(1983).
4. P. G. Burke and D. U. McVicar, Proc. Phys. Soc. (Lon.), 86, 989(1965).
5. V. Jacobs, Phys. Rev. A3, 289(1971).
6. Y. K. Ho, J. Phys. B, 17, L695 (1984).

ELECTRON IMPACT EXCITATION OF OPTICALLY ALLOWED TRANSITIONS IN C-LIKE IONS

K.M. Aggarwal

Department of Applied Mathematics and Theoretical Physics,
The Queen's University of Belfast,
Belfast BT7 1NN, Northern Ireland.

The optically allowed transitions in carbon-like ions have been observed in the solar spectrum by many workers. The experimentally observed line intensity ratios help in the determination of composition, density and temperature of the solar plasma if the atomic parameters are known. These parameters are energy levels, transition probabilities and collision strengths. The first two parameters are known fairly well, but the information available about the collision strengths

is not very accurate. Hence, in this paper, the results for Ω are reported for the optically allowed transitions in C-like ions.

The electron impact excitation of transitions among the $1s^2 2s^2 2p^2$, $1s^2 2s 2p^3$ and $1s^2 2p^4$ configurations of C-like ions has been studied using the R-matrix code and the results have already been reported for the optically forbidden transitions.¹⁻³ The results for the optically allowed transitions were not reported earlier because of the limited number of partial waves considered ($L \leq 9$). These partial waves are insufficient for the convergence of Ω in such transitions. Hence, the contribution of $L > 9$ has now been calculated from the Coulomb-Born program and values of Ω for allowed transitions are reported here for 4 ions viz. O III, Ne V, Mg VII and Si IX. The calculations are in progress for Ca XV and Fe XXI.

The wavefunctions used in the calculations of Ω for $L > 9$ are the same as used for $L \leq 9$ in the R-matrix program. These have been computed from the CIV3 program. The contribution to Ω of $L > 9$ has found to be significant in comparison to that of $L \leq 9$ and in fact increases with the increase of incident energy of the electrons.

The values of Ω are listed at a few energies in Table I for 6 optically allowed transitions (among the $2s^2 2p^2$ and $2s 2p^3$ configurations) for each ion. From these Ω , the excitation rate coefficients can be easily calculated because contrary to the forbidden transitions, these are not dominated by resonances. However, the resonances in these transitions are not completely ruled out and we do observe these for some transitions in the threshold energy region as is also evident from results listed in Table I.

The earlier results available for these transitions are mainly from the Distorted Wave calculations and are at energies well above the excitation thresholds. On comparison the present results for Ω are found to be

lower, in general, by as much as a factor of 1.5. This is mainly due to the choice of different wavefunctions employed in different calculations and partly due to the scattering methods used i.e. R-matrix and Distorted Wave.

Table I.

Collision strengths for optically allowed transitions as a function of energy (w.r.t. the ground state) between the $1s^2 2s^2 2p^2$ and $1s^2 2s 2p^3$ configurations of C-like ions.

Energy (keV)	Transition					
	$2p \rightarrow 3p^0$	$2p \rightarrow 3p^2$	$3p \rightarrow 3s^0$	$1p \rightarrow 1p^0$	$1p \rightarrow 1p^2$	$1s \rightarrow 1p^0$
a) O III						
2.00	8.012	6.535	3.592	4.713	2.030	0.798
2.50	8.507	7.455	4.602	5.958	2.592	1.091
3.00	8.721	7.800	4.789	6.740	3.265	1.259
4.00	9.190	8.512	6.191	8.086	4.149	1.589
5.00	9.583	8.980	7.162	8.914	4.785	1.769
b) Ne V						
3.00	4.819	4.460	3.962	4.788	2.316	0.980
4.00	4.962	4.515	4.047	4.999	2.632	1.022
5.00	5.137	4.626	4.170	4.957	2.618	1.035
10.00	6.210	5.336	4.692	5.700	2.922	1.170
20.00	8.100	7.013	5.831	7.305	3.634	1.515
30.00	9.401	8.258	6.802	8.607	4.269	1.763
40.00	10.61	9.338	7.641	9.712	4.838	2.000
c) Mg VII						
4.0	3.200	2.909	2.750	3.380	1.745	0.6866
5.0	3.310	2.918	2.722	3.252	1.716	0.6780
7.5	3.606	3.098	2.778	3.343	1.687	0.6868
10.0	3.933	3.354	2.936	3.569	1.772	0.7372
20.0	5.025	4.272	3.500	4.451	2.224	0.9540
30.0	5.917	5.307	4.098	5.247	2.620	1.151
40.0	6.457	5.650	4.526	5.831	2.897	1.239
50.0	7.044	6.092	4.921	6.353	3.092	1.315
60.0	7.676	6.636	5.329	6.912	3.360	1.431
d) Si IX						
5.0	3.038	2.586	1.899	2.457	1.186	0.5030
7.5	3.179	2.827	2.185	2.855	1.361	0.5873
10.0	3.262	2.926	2.367	3.052	1.433	0.6095
20.0	3.577	2.961	2.436	3.139	1.484	0.6208
30.0	4.165	3.480	2.782	3.495	1.664	0.7048
50.0	4.649	4.044	3.293	4.191	2.025	0.8620
70.0	5.297	4.563	3.679	4.795	2.314	0.9961
90.0	5.969	5.125	4.091	5.341	2.575	1.106

References

1. K.M. Aggarwal, *Astrophys. J. Suppl.* **52**, 387 (1983).
2. K.M. Aggarwal, *Astrophys. J. Suppl.* **54**, 1 (1984).
3. K.M. Aggarwal, *Astrophys. J. Suppl.* **56**, 303 (1984).

COLLISION STRENGTHS FOR THE FORBIDDEN TRANSITIONS AMONG THE GROUND-STATE CONFIGURATION OF SIII*

Y. K. Ho and Ronald J. W. Henry

Department of Physics and Astronomy
Louisiana State University, Baton Rouge, LA USA 70803

Observations of the extreme-ultraviolet spectrum of the Jupiter satellite Io during the Voyager 1 and 2 encounters revealed bright emission lines of some sulphur and oxygen ions.¹ Atomic data such as collision strengths for various sulphur ions are needed to interpret the physical conditions of the Io plasma torus. For example, it has been deduced that the temperature of the torus is 80,000K. Electron impact excitation rate coefficients at that temperature are hence of interest.

We present calculations of collision strengths for the forbidden transitions among the ground-state configuration of SIII ions. Electron impact excitations for $3p-1D$, $3p-1S$, and $1D-1S$ transitions are calculated by use of a three-state close coupling approximation. Configuration-interaction type wave functions are used to represent the target ground states. The configurations are of $3s^2 3p^2$, $3p^4$, $3s 3p^2 3d$, $3s^2 3d^2$, and $3s^2 3p 4f$. The optimization of the excited orbitals has been discussed in a previous publication.² The scattering wave functions are solved by use of a non-iterative integral equation method.³ Results for the thermally averaged effective collision strengths are shown for temperatures ranging from 20,000 to 140,000K.

Calculations are being extended to investigate convergence behaviour by including more states in the close coupling expansion. Resonance effects on the collision strengths are also being investigated. We will present the latest results at the meeting. A comparison with the other close coupling calculation⁴ at temperatures less than 20,000K will also be presented.

*Supported in part by NASA grant NAGW-48.

1. D. E. Shemansky and G. R. Smith, *J. Geophys. Res.* **86**, 9179 (1981).
2. Y. K. Ho and R. J. W. Henry, *Ap. J.* **282**, 816 (1984).
3. R. J. W. Henry, S. P. Rountree, and E. R. Smith, *Comput. Phys. Comm.* **23**, 233 (1981).
4. C. Mendoza, *J. Phys. B* **15**, 867 (1982).

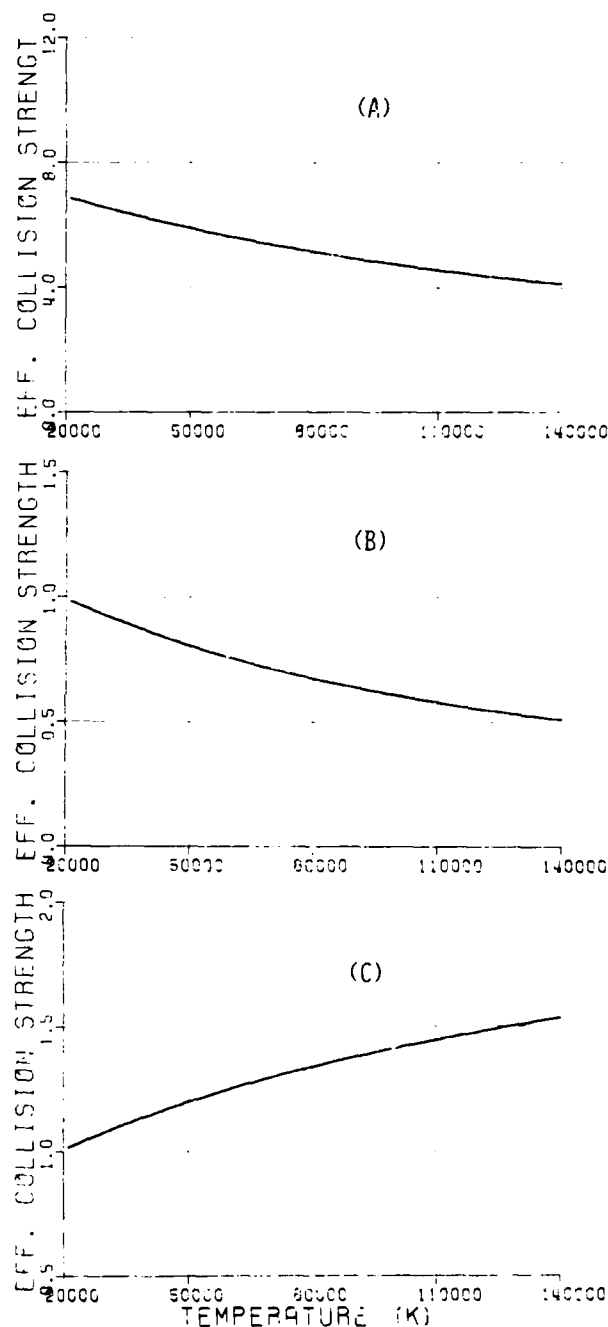


Fig. 1 Thermally averaged collision strengths as a function of temperatures;

- (a) $3p-1D$ transition;
- (b) $3p-1S$;
- (c) $1D-1S$.

DIFFERENTIAL ELECTRON SCATTERING CROSS SECTIONS FOR THE $3s^2S_{1/2} + 3p^2P_{1/2,3/2}$ TRANSITIONS IN MgII: COMPARISON OF EXPERIMENT AND THEORY

I. D. Williams, A. Chutjian, A. Z. Msezane^{*} and R. J. W. Henry[†]

Jet Propulsion Laboratory, California Institute of Technology, Pasadena, CA 91109
Atlanta University, Atlanta, Georgia 30314

^{*}Louisiana State University, Baton Rouge, Louisiana 70803

Experimental and theoretical angular differential cross sections will be reported for the inelastic $3s^2S_{1/2} + 3p^2P_{1/2,3/2}$ transitions in MgII at electron energies of 35 and 50 eV.¹ Experimentally, measurements have been made in the range of electron scattering angles of $8^\circ \leq \theta \leq 17^\circ$, using the newly developed electron energy loss technique in a 90° crossed electron-ion beam geometry.² A five-state close coupling approximation has been used to obtain theoretical values in the angular range $0^\circ \leq \theta \leq 180^\circ$.³ These measurements find application in the diagnostics of high temperature plasmas as found in solar flares, stellar atmospheres, and the interstellar medium.

A velocity analyzed beam of MgII ions, generated in a Mg vapor discharge, was electrostatically focussed onto the collision region. A transverse electric field prior to the collision region deflected MgII ions away from any neutral Mg atoms or photons present in the incident beam. An electron beam of low angular divergence was focussed onto the ions, and inelastically scattered electrons were detected by an electrostatic analyzer and lens system, which could be rotated relative to the incident beam direction.² Energy loss spectra were obtained at 1° intervals for a range of forward scattering angles, corresponding to excitation of the unresolved $3s^2S_{1/2} + 3p^2P_{1/2,3/2}$ fine structure transitions in MgII at 4.42 eV ($j = 1/2$) and 4.43 eV ($j = 3/2$). The overall resolution in the energy loss spectra was 0.55 eV (FWHM). Relative differential cross sections were determined by calculating the area under the peaks in the energy loss spectra.

Theoretically, Msezane and Henry³ previously calculated cross sections for the $4s + 4p$ excitation in ZnII in a five-state close-coupling approximation in which the $4s$, $4p$, $3d^94s^2$, $5s$, and $4d$ states were retained. Very good agreement with measurements of the absolute emission cross sections⁴ was obtained at electron energies E in the energy range $15 \leq E \leq 100$ eV, when cascade contributions were included; and with the differential energy-loss measurements⁵ at 75 eV. We use reactance matrices obtained by Msezane and Henry³ to calculate differential cross sections in MgII at 35 and 50 eV in which $3s$, $3p$, $3d$, $4s$ and $4p$ states are included.

Results at an electron energy of 35 eV are

presented in Figs. 1(a) and (b). To compare the shape of the measured differential cross sections to theory, the experimental values are normalized to the theoretical values at $\theta = 12^\circ$. Good agreement in shape is observed between experiment and theory, although experimental results show a slight shoulder feature not present in the calculations. The optically forbidden MgII $3s^2S + 4s^2S$, $3d^2D$ transitions have also been detected experimentally for the first time anywhere,⁶ and results on these features will also be presented.

The experimental work was carried out at JPL-Caltech, under contract with NASA; RJWH and AZM were supported by the DOE Office of Basic Energy Sciences. One of us (IDW) thanks the NRC for their support.

References

1. I. D. Williams, A. Chutjian, A. Z. Msezane and R. J. W. Henry, submitted to *Astrophys. J.*
2. A. Chutjian, *Phys. Rev. A* **29**, 64 (1984).
3. A. Z. Msezane and R. J. W. Henry, *Phys. Rev. A* **25**, 692 (1982).
4. W. T. Rogers, G. H. Dunn, T. Østgaard-Olsen, M. Reading and G. Stefani, *Phys. Rev. A* **25**, 681 (1982).
5. A. Chutjian, A. Z. Msezane and R. J. W. Henry, *Phys. Rev. Lett.* **50**, 1357 (1983).
6. I. D. Williams and A. Chutjian, unpublished results.

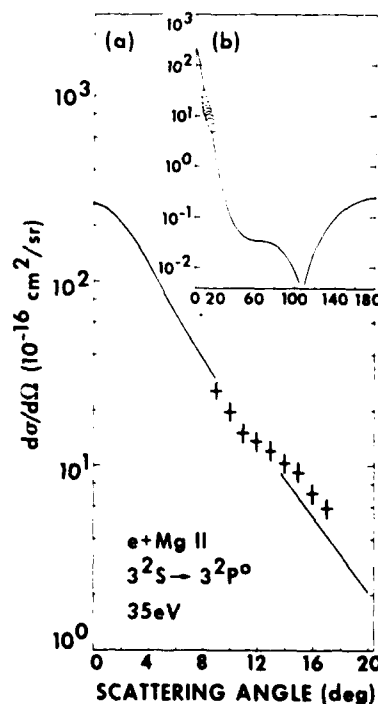


Figure 1.

ELECTRON IMPACT EXCITATION OF THE $5p\ 2P$ AND $5s^2\ 2D$ STATES IN CdII

Alfred Z. Msezane* and Ronald J. W. Henry†

*Department of Physics, Atlanta University, Atlanta, Georgia 30314 USA

†Department of Physics, Louisiana State University, Baton Rouge, Louisiana 70803 USA

Electron impact excitation of the lower $5p\ 2P$ and upper $5s^2\ 2D$ laser states in the He-CdII hollow-cathode laser, one of the most stable and useful metal ion lasers, is of current experimental and theoretical interest. The upper and lower states are populated via the following stepwise excitation processes¹

$$e + Cd \rightarrow Cd^+ + 2e$$

$$e + Cd^+ \rightarrow Cd^+(5s^2\ 2D) + e \quad (1)$$

$$e + Cd^+ \rightarrow Cd^+(5p\ 2P) + e \quad (2)$$

Absolute crossed-beam emission cross section measurements for processes (1) and (2) have been reported²⁻⁵ with the surprising result that the cross section for process (1) is comparable to or even exceeds that for process (2). The surprise stems from the consideration that the e-CdII system involves the excitation of the next higher resonance transition to ZnII for which experimental and theoretical data have been reported. The result in e-ZnII collision indicates that the resonance cross section ($4s\ 2S \rightarrow 4p\ 2P$) is at least an order of magnitude larger than the inner-shell ($4s\ 2S \rightarrow 4s^2\ 2D$). Evidently, though ZnII and CdII are similar, yet different trends are possible which require careful theoretical and experimental investigations.

Recently, Chutjian⁶ has obtained from energy-loss spectra both the differential and integral cross sections for the resonance transition $5s\ 2S \rightarrow 5p\ 2P$ in CdII and contrasted the differential cross section with that for the ($4s\ 2S \rightarrow 4p\ 2P$) transition in ZnII. The semiempirical Gaunt factor expression of Mewe⁷ is the only theory that has been used for comparison with measurement.

Electron impact excitation of CdII from ground state to excited $5p\ 2P$ and $5s^2\ 2D$ is investigated in two and three state close-coupling approximation from threshold to 60eV. Accurate target wave functions are employed which yield the experimentally observed energy splittings. The Hartree-Fock orbitals of Clementi and Roetti⁸ for the ground state of CdII are used as basis.

Program CIV39 is used to modify some orbitals and to generate the excited orbitals $6s$, $5p$, $6p$, $5d$ and $4f$.

In the $5s\ 2S - 5p\ 2P$ two-state calculation, for example, the $5s\ 2S$ state is represented by (omitting terms with coefficients < 0.01)

$$0.99844\ 4d^{10}\ 5s + 0.00795\ 4d^{10}\ 6s - 0.03819\ 4d^9\ 5s(3D)5d + 0.00257\ 4d^9\ 5p(3P)6p - 0.03982\ 4d^9\ 5p(1F)4f$$

and the $5p\ 2P$ state by

$$0.88269\ 4d^{10}\ 5p - 0.46943\ 4d^{10}\ 6p - 0.02202\ 4d^9\ 5p(3D)5d$$

The resulting energy splitting of 0.202a.u. compares well with the experimentally observed value¹⁰ of 0.201a.u. Also, the dipole length and dipole velocity oscillator strengths are the same and equal to 1.21. This value contrasts with the beam-foil¹¹ result of 0.62. We do not yet understand the factor of two discrepancy between our result and the measurement.

Our cross section maxima for $5p\ 2P$ and $5s^2\ 2D$ differ by at least an order of magnitude. This difference is consistent with that found in ZnII¹² but is in disagreement with emission measurement. Two and three-state close-coupling results are compared with crossed-beam measurements from energy-loss spectra and absolute emission and with semi-empirical calculation.

*Supported in part by the U. S. Department of Energy, Office of Basic Energy Sciences.

References

1. M. Mori, M. Murayama, T. Goto and S. Hattori, IEEE J. Quantum Electron. **14**, 427 (1978)
2. K. Hane, T. Goto and S. Hattori, Phys. Rev. A **27**, 124 (1983)
3. T. Goto, J. Phys. D: Appl. Phys. **15**, 421 (1982)
4. K. Hane, T. Goto and S. Hattori, J. Phys. D **15**, L82 (1982)
5. K. Hane, T. Goto and S. Hattori, J. Phys. B: At. Mol. Phys. **16**, 629 (1982)
6. A. Chutjian, Phys. Rev. A **29**, 64 (1984)
7. R. Mewe, Astron. Astrophys. **20**, 215 (1972)
8. E. Clementi and C. Roetti, Atomic Data and Nuclear Data Tables **14**, 177 (1974)
9. A. Hibbert, Comput. Phys. Commun. **9**, 141 (1975)
10. C. E. Moore, "Atomic Energy Levels" NBS Circular No. 467 (Washington, D. C.: U. S. Government Printing Office) (1952)
11. T. Andersen and G. Sorensen, J. Quant. Spectrosc. Radiat. Transfer **13**, 369 (1973)
12. A. Z. Msezane and R. J. W. Henry, Phys. Rev. A **25**, 696 (1982)

INNERSHELL EXCITATION OF Ti^{3+} BY ELECTRON IMPACT: EFFECTS OF TARGET
WAVE FUNCTIONS AND COUPLING

A. Z. Msezane* and Ronald J. W. Henry†

*Department of Physics, Atlanta University, Atlanta, Georgia 30314 USA

†Department of Physics, Louisiana University, Baton Rouge, Louisiana 70803 USA

The dominance of excitation-autoionization to electron impact ionization cross sections in Ti^{3+} has been demonstrated experimentally^{1,2} and calculated using a Distorted-Wave³ approximation and a 10-state R-matrix⁴ expansion. The disturbing discrepancy between the earlier Distorted-Wave calculation and measurement has been attributed mainly to the scattering approximation rather than the poor target wave functions employed⁵.

The number of states included in the close-coupling expansion and the description of the atomic states are the two major limiting factors on the accuracy achieved by a close-coupling approximation. We report here our investigation in Ti^{3+} for electron impact energies greater than the $3p^5 3d^2 2D^0$ threshold: a) Wave function effects on innershell excitation cross sections from ground $3p^5 3d^2 2D$ to $3p^5 3d^2 2p^0$, $2D^0$, $2F^0$ using the Hartree-Fock (HF) wave functions employed by Griffin et al³ and our constructed configuration interaction (CI) wave functions in a two-state close-coupling approximation; b) Coupling among the dominant autoionizing states by including the four target states $2D$, $2p^0$, $2D^0$ and $2F^0$ in a four-state close-coupling approximation.

A ten term expansion is used for the ground $2D$ state. The $2p^0$ and $2F^0$ states are each represented by 7 term expansions, while a 6 term expansion represents the $2D^0$ state.

For tractable calculations, we retain only terms with coefficients of magnitude <0.01 in the expansions. Hartree-Fock orbitals of Clementi and Roetti⁶ are used as starting point for $1s$, $2s$, ---, $3d$ orbitals. Program CIV3⁷ is used to modify some orbitals and to generate excited $4s$, $4p$, $4f$, and $5s$ orbitals. The calculated dipole length, f_L and dipole velocity, f_v oscillator strengths and the energy splittings, ΔE for the $2D-2p^0$ transition are given below as an example and compared with those of Hibbert et al⁸.

Present			Hibbert et al ⁸		
$\Delta E(a.u.)$	f_L	f_v	$\Delta E(a.u.)$	f_L	f_v
1.8592	0.754	0.756	1.847	0.721	0.731

The CI wave functions were constructed using the same ionic core to facilitate estimation of importance of the REDA⁹ mechanism. Various combinations of orbitals were tested and they led essentially to the same ΔE , f_L and f_v obtained above.

Notable features of our calculation are:

- (i) The cross sections $\sigma(2p^0)$, $\sigma(2D^0)$ and $\sigma(2F^0)$ obtained using the HF wave function exceed those from the CI wave functions by less than 10%, 12% and 15% respectively (ii) The difference in $\sigma(2p^0)$, $\sigma(2D^0)$ and $\sigma(2F^0)$ calculated in (a) using the CI wave functions and in (b) is insignificant.

We conclude that for excitation-autoionization calculations in Ti^{3+} for impact energies above the $2D^0$ threshold: (i) coupling among the dominant states is unimportant i.e. the two-state close-coupling approximation is adequate, (ii) the use of the HF wave functions yields reasonable results provided that the appropriate scattering approximation is employed. Below the $2D^0$ threshold resonances appear to be important⁴ and contribution of the REDA mechanism may be estimated as described in reference 9.

Our cross sections will be compared with those from measurements and other calculations.

*Supported in part by The U. S. Department of Energy, Office of Basic Energy Sciences

References

- 1R. A. Falk, G. H. Dunn, D. C. Gregory and D. H. Crandall, Phys. Rev. **A27**, 762(1983)
- 2R. A. Falk, G. H. Dunn, D. C. Griffin, C. Bottcher, D. C. Gregory, D. H. Crandall and M. S. Pindzola, Phys. Rev. Lett. **47**, 494(1981)
- 3D. C. Griffin, C. Bottcher and M. S. Pindzola, Phys. Rev. **A25**, 1374(1982)
- 4P. G. Burke, W. C. Fon and A. E. Kingston, J. Phys. **B**, **17**, L733(1984)
- 5A. Z. Msezane and R. J. W. Henry, unpublished (1983)
- 6E. Clementi and C. Roetti, Atomic Data and Nuclear Data Tables, **14**, 177(1974)
- 7A. Hibbert, Comput. Phys. Commun. **9**, 141(1975)
- 8A. Hibbert, A. E. Kingston and S. N. Tiwary, J. Phys. **B15**, L643(1982)
- 9R. J. W. Henry and A. Z. Msezane, Phys. Rev. **A26**, 2545(1982)

DISTORTED-WAVE-METHOD CALCULATION OF ELECTRON-IMPACT EXCITATION OF ATOMIC IONS

Yukikazu Itikawa and Kazuhiro Sakimoto

Institute of Space and Astronautical Science, Komaba, Meguroku, Tokyo 153, Japan

Electron-impact excitations of atomic ions are fundamental processes in high temperature plasmas in laboratory and astrophysical systems. The difficulty of the measurement of the excitation cross sections makes it necessary to develop a theoretical method reliably applicable to various collision systems. Here an approach is proposed, in which i) the target ion is represented by as accurate a wave function as possible and iii) a distorted-wave (DW) method is employed to treat collision dynamics. As a test of the approach, cross sections are calculated for ions of He-, Be- and C-like isoelectronic sequences and compared with other theoretical results.

Introducing a distortion potential, U^{DW} , and regarding the difference between the true interaction and U^{DW} as a perturbation, we adopt the standard theory of first-order perturbation. We assume U^{DW} to be a spherical average of the electrostatic potential formed by the target ion in its initial state. The same potential is used for the calculation of DW of both the initial and the final states. Furthermore, an electron exchange is taken into account only between the interacting electrons. Thus we have the direct and exchange parts of the transition matrix elements in the form

$$T^{(d)}_{i \rightarrow f} = N \int \psi_f^* (1..N) F_2^{(-)}(N+1) r_{N,N+1}^{-1} \psi_i (1..N) F_1^{(+)}(N+1) \\ T^{(ex)}_{i \rightarrow f} = -N \int \psi_f^* (1..N-1, N+1) F_2^{(-)}(N) r_{N,N+1}^{-1} \psi_i (1..N) \\ F_1^{(+)}(N+1) \cdot$$

Here ψ is the target wave function, F is the distorted wave, and N is the number of the target electrons.

Assuming the L-S scheme of the angular momentum coupling and taking account of configuration mixing in the target function, we can use the procedure of Smith and Morgan¹ to evaluate the angular-momentum part of $T(i \rightarrow f)$.

As an example of the results, Figs. 1 and 2 show the collision strength for the transition $1^1S \rightarrow 2^1S$ for Li II and O VII, respectively. The electron energy is expressed in the threshold units. The present result is compared with the close-coupling (CC) calculation by van Wyngaarden et al.² Also shown are the results of the Coulomb-wave approximation (with (CBXA) and without (CB) electron exchange), where the DW is replaced by the corresponding Coulomb wave. The same CI target wave function has been used in all the calculations. We conclude that the present approach, though being very simple, gives good results unless the energy of the incident or scattered electron is very low. For a higher nuclear charge, the present DW method is very good even near the threshold. More details will appear.³

References

1. K. Smith and L.A. Morgan, Phys. Rev. **165** 110 (1968)
2. W.L. van Wyngaarden, K. Bhadra and R.J.W. Henry, Phys. Rev. A **20** 1409 (1979)
3. Y. Itikawa and K. Sakimoto, Phys. Rev. A **31** (1985) (in press)

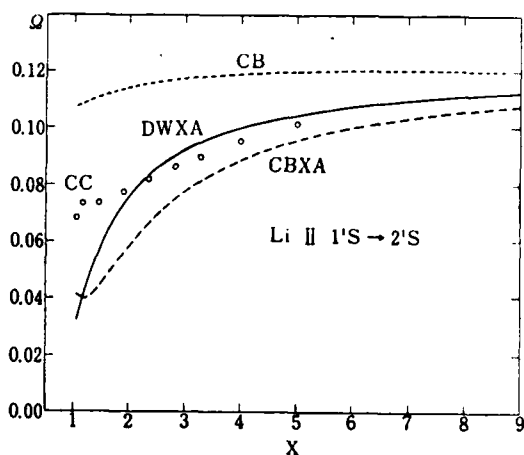


Fig. 1

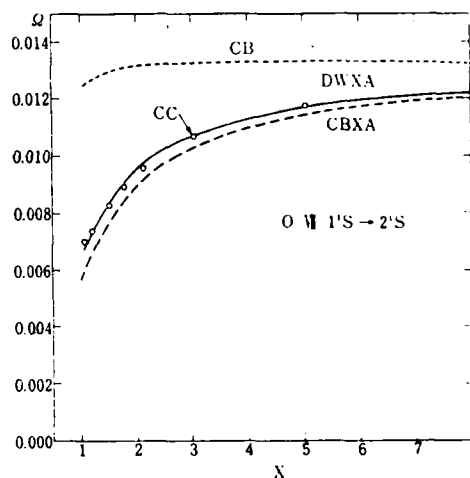


Fig. 2

EXCITATION OF DOUBLY EXCITED AUTOIONIZATION STATES IN IONS

Rajesh Srivastava and A.K.Katiyar

Physics Department, University of Roorkhee, Roorkhee, INDIA

The ionization of atoms and positive ions by electron impact is one of the most important atomic collision processes relevant to controlled thermo nuclear fusion research¹. Theoretical models which allow the calculation of the contributions to the electron impact ionization cross-sections arising from both direct and indirect contributions such as excitation - autoionization are currently being developed. In fact, the mechanism where excitation of an ion to an electronic state of energy higher than the ionization potential followed by autoionization allows a few specific excitation transitions to contribute significantly to the total ionization cross-section. Our interest, therefore, is at present, mainly confined to the most important issue of excitation - autoionization contribution.

Doubly excited states with two electrons are the most fundamental atomic species which autoionize. Such doubly states are not only in neutral species (like helium and alkaline earths etc.) but also recently being analysed in ions also². A first step towards the study of excitation - autoionization contribution due to these doubly excited states therefore, would be to find first, the cross-sections for their production by electron. In view, we shall present in this conference for the first time our extensive study in obtaining electron impact excitation cross-sections for doubly excited states in heliumlike ions. We have calculated the cross-sections for the excitation of $(2p)^3\ ^3P$, $2p3p\ ^1P$, $2p3d\ ^1D$ and $2p3d\ ^3D$ states from the ground state $(1s)^2\ ^1S_g$ of Li^+ ion. The calculations are performed in an improved distorted wave Born approximation (DWBA)³ where distortion effects due to static, Coulomb, exchange and polarization effects are taken in both the initial and final channels.

As a sample, we present in the Table I our present results for $(2p)^2\ ^3P$ excitation only, while rest of the results for other

excitations would be presented and discussed along with theory in the conference. Except our earlier calculation⁴ in Coulomb Born Oppenheimer approximation (CBO) for only $(2p)^2\ ^3P$ excitation, unfortunately, no other theoretical and experimental results are available for comparison. However, looking the success of our present DWBA model as applied to single³ and double⁵ excitations in helium, we hope our results for Li^+ to be quite reliable.

Reference

1. D H Crandall, Phys. Scr. **23**, 153(1980).
2. R Bruch, Phys. Scr. **26**, 381 (1982).
3. R Srivastava et al. J.Chem. Phys.(1984) (in press).
4. B Padhy et al. Phys. Rev.A **28** 1825(1983).
5. R Srivastava et al. Phys. Rev. A (1984) (in press).

TABLE I Total cross-sections for $(2p)^2\ ^3P$ excitation in Li^+ ion

Impact electron energy (eV)	Present DWBA σ (a.u.)	CBO approximation (Ref.4) σ (a.u.)
148.25	0.5293E-04	0.5402E-04
149.00	0.5320E-04	0.5476E-04
150.00	0.5336E-04	0.5556E-04
152.00	0.5318E-04	0.5654E-04
155.00	0.5120E-04	0.5680E-04
165.00	0.4354E-04	0.5160E-04
170.00	0.3864E-04	0.4744E-04
175.00	0.3386E-04	0.4303E-04
200.00	0.1613E-04	0.2400E-04
250.00	0.3421E-05	0.6823E-05
300.00	0.2045E-06	0.2086E-05
400.00	0.5878E-07	0.2629E-06
500.00	0.1840E-07	-

COLLISION STRENGTHS FOR CII

K.A. Jerjian* and R.J.W. Henry*

*Dept of Physics & Astronomy, University of Nebraska at Lincoln, Lincoln, NE 68588 USA

*Dept of Physics & Astronomy, Louisiana State University, Baton Rouge, LA 70803 USA

A close coupling calculation and the multichannel quantum-defect theory¹ for determining the positions and the widths of resonances have been applied to calculate the collision strengths of the electron impact excitation of singly ionized carbon. Five states ($2p^0$, $4p$, $2D$, $2S$, $2P$) have been used in the expansion of the scattering wave function. The effect of the resonances that converge to the $2S$ and $2P$ thresholds on the $2p^0 - 2D$ transition is evaluated.

Since it is essential for collision strength calculations to have a good representation for the various states of the target ions, we first carry out a somewhat extensive configuration interaction calculation for the CII ions using the computer program CIV3 of Hibbert² to extract an optimum and yet manageable set of configuration interaction wave functions. The results for the oscillator strengths of the dominant configurations of the various excited states - $2s2p^2$ - relative to the dominant configuration of the ground state - $2s^22p$ - and the energy differences are shown in Table 1.

The close coupling calculations were performed using the non-iterative integral equation code of Henry et al.³, at four energies, all of them above the highest target state considered. The different reactance matrices were then extrapolated below some of the thresholds with the use of the computer program RANAL⁴ to obtain the resonance enhanced collision strengths and the resonance parameters. As an example, the detailed collision strength and the resonances in the $2p^0 - 2D$ transition for $3p^0$ symmetry are shown in Fig. 1.

Table 1. Oscillator strengths for the various $2s2p^2$ excited states of CII relative to the $2s^22p$ $2p^0$ ground state.

	f_L	f_V	$\Delta E(a.u)$ (theory)	$\Delta E(a.u)$ (exp)
$2D$	0.133	0.136	0.348	0.341
$2S$	0.112	0.118	0.462	0.439
$2P$	0.521	0.525	0.518	0.504

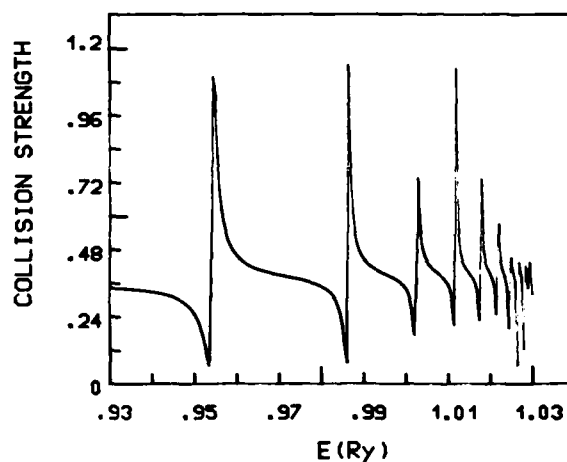


FIGURE 1. Collision strength vs energy showing the presence of resonances in the $2p^0 - 2D$ transition in CII. $3p^0$ symmetry, above the $2S$ threshold.

References

1. M.J. Seaton, J. Phys. B 2, 5 (1969).
2. A. Hibbert, Comp. Phys. Commun. 9, 141 (1975).
3. R.J.W. Henry, S.P. Rountree and E.R. Smith, Comp. Phys. Commun., 23, 233 (1981).
4. A.K. Pradhan and M.J. Seaton (unpublished).

ELECTRON IMPACT COLLISION STRENGTHS FOR THE FINE STRUCTURE TRANSITIONS IN FE XII

S. S. Tayal and Ronald J. W. Henry

Department of Physics and Astronomy, Louisiana State University, Baton Rouge, Louisiana 70803-4001 USA

Fe XII forbidden lines due to fine structure transitions within the ground $3s^2 3p^3$ configuration are observed in the emission ultraviolet spectrum of the sun obtained by the Naval Research Laboratory slit spectrograph on Skylab¹. Certain line ratios of the Fe XII ion may be usefully employed for determining the physical conditions in solar corona^{2,3}. In order to calculate these line ratios accurately a detailed knowledge of the atomic data, especially the oscillator strengths and electron excitation rate coefficients for transitions among ground $3s^2 3p^3$ configuration and many more low lying excited levels, is needed.

We have calculated the configuration-interaction (CI) wavefunctions for the seven lowest target states: $3s^2 3p^3 4s^0$, $2d^0$, $2p^0$, $3s 3p^4 4p$, $2d$, $2p$ and $2s$. The CI wavefunctions are constructed from $1s$, $2s$, $2p$, $3s$, $3p$, $3d$ and $4f$ orthonormal basis orbitals. The $1s$, $2s$, $2p$, $3s$ and $3p$ orbitals are those of the ground state $3s^2 3p^3 4s^0$ given by Clementi and Roetti⁴ and $3d$ and $4f$ are obtained with CIV3⁵ minimizing the energies of $3s^2 3p^3 4s^0$ and $2d^0$ states respectively. The relativistic effects are incorporated by means of Breit-Pauli Hamiltonian which includes the spin-orbit, spin-other-orbit, spin-spin, one-body mass correction and one-body Darwin terms.⁶ The wavefunctions are used to calculate oscillator strengths for transitions among the fine structure levels. Good agreement with the experimental energy splittings and between length and velocity formulations for the oscillator strengths is obtained.

We have included these seven target states in our close-coupling scattering calculations.⁷ The collision strength calculations including the effects of intermediate coupling and autoionization is in progress and should be available by the time of the conference. These will be compared with the other available theoretical calculations.

References

- ¹U. Feldman and G. A. Doschek, J. Opt. Soc. Am. **67**, 726 (1977).
- ²U. Feldman and G. A. Doschek, Ap. J. **273**, 822 (1983).
- ³G. L. Withbroe and J. C. Raymond, Ap. J. **285**, 347 (1984).
- ⁴E. Clementi and C. Roetti, At. Nucl. Data Tables **14**, 177 (1974).
- ⁵A. Hibbert, Comput. Phys. Commun. **9**, 141 (1975).
- ⁶R. Glass and A. Hibbert, Comput. Phys. Commun. **16**, 19 (1978).
- ⁷R. J. W. Henry, S. P. Rountree, and E. R. Smith, Comput. Phys. Commun. **23**, 233 (1981).

COLLISION STRENGTHS FOR FINE STRUCTURE TRANSITIONS
IN Ne II AND Mg IV

A E Kingston and C T Johnson

Department of Applied Mathematics and Theoretical Physics
The Queen's University of Belfast
Belfast BT7 1NN
Northern Ireland

The $2s^2 2p^5 \ ^2P_{1/2}^0 - \ ^2P_{3/2}^0$ transition in the ground state of NeII is observed from HII regions and planetary nebulae. The neon abundance in these objects can be estimated from the line flux if the collision strength and transition probability are known. The corresponding transition in MgIV has been detected recently¹. We are calculating these collision strengths using the R-matrix method.

We represented the two target states $2s^2 2p^5 \ ^2P_{1/2}^0$ and $2s2p^6 \ ^2S^e$ by configuration interaction wave functions using the CIV3 program of Hibbert². The expansion included the principal $2s\text{-}3l$ and $2p\text{-}3l$ ($l=s,p,d$) singly excited configurations, plus $2s2p - 3s3p$, $2p^2 - 3p^2$, $3d^2$ double electron excitations. We retained the $2p^2 - 3l^2$ configurations when optimising the $3s, 3p$ and $3d$ correlation orbitals, as this gave significant improvements in the energy and fine structure splitting of the ground state. To obtain an accurate value for the $2p^0 - ^2S^e$ oscillator strength we optimized an additional $3d$ orbital on the $^2S^e$ state. In Table 1 we compare the oscillator strengths derived from our scattering target wave functions (a) with those from more sophisticated calculations (b) including further orbitals, with the previous theoretical calculations of Westhaus and Sinanoglu³, and with experiment. Examination of the convergence of the configuration expansion suggests that the experimental values for NeII may be too low.

TABLE 1

Theory			
	Ref 3	Present (a)	Present (b)
NeII: Length	0.073	0.090	0.095
Velocity	0.091	0.090	0.098
MgIV: Length	0.081	0.089	0.087
Velocity		0.085	0.089
Experiment			
	Ref 4	Ref 5	Ref 6
NeII: 0.076 ± 0.008		0.077 ± 0.003	0.071 ± 0.014
MgIV:		Not Available	

Resonances converging on the $2s2p^6 \ ^2S^e$ state have been observed experimentally for both NeII and MgIV. We show preliminary values for quantum defects in the MgIV $2S2p \ ^6P^0$ series in Table 2. They are in good

agreement with those derived from the measurements of Esteve and Mehman⁷, using a more recent value for the series limit⁸.

TABLE 2

	Theory		Experiment
Resonance	Ref 9	Present	Refs 7,8
$2s2p \ ^6P_{3/2}$	0.549	0.567	0.571
$2s2p \ ^6P_{4/2}$	0.530	0.548	0.555
$2s2p \ ^6P_{5/2}$	0.521	0.528	0.563
$2s2p \ ^6P_{6/2}$	0.517	0.519	0.504

Collision strengths for the $2p^0 - ^2P_{3/2}^0$ transition are calculated using the JAJOM program of Saraph¹⁰.

References

- 1 S Beckwith, N J Evans, A Natta, F W Russell, and J Wyant, Ap J 277, 207(1984).
- 2 A Hibbert, Comput Phys Commun 9, 141(1975).
- 3 O Sinanoglu, Nucl Instrum Methods 110, 193(1973).
- 4 E J Knystautas and R Doolin, Astron Astrophys 37, 145(1974).
- 5 D J G Irwin, A E Livingston, and J A Kernahan, Can J Phys 51, 1948(1973).
- 6 L J Curtis and W H Smith, Phys Rev A9, 1537(1974).
- 7 J M Esteve and G Mehman, Ap J 193, 747(1974).
- 8 W C Martin and R Zalubas, J Phys Chem Ref Data 9, 20(1980).
- 9 D Petrini and E Kislak, J Phys B 16, 491(1983).
- 10 H E Saraph, Comput Phys Commun 15, 247(1978).

ELECTRON IMPACT EXCITATION OF O^+

B.M. McLaughlin and A.E. Kingston

Department of Applied Mathematics and Theoretical Physics
The Queen's University of Belfast,
Belfast BT7 1NN, Northern Ireland.

The R-matrix method as described by Burke and Robb¹ has been applied to the electron impact excitation of the lowest lying eight states of the O^+ ion. Collision strengths and the excitation rate coefficients are calculated for transitions involving these eight states of the O^+ ion, i.e. $1s^2 2s^2 2p^3 \ ^4S^o, \ ^2D^o, \ ^2P^o, \ 1s^2 2s^2 2p^2 \ ^3P^o, \ ^3D^o, \ ^3S^o$ and $1s^2 2s^2 2p^2 \ ^1D^o, \ ^1S^o$.

Elaborate configuration interaction wave functions are used to describe the target state wave functions which are constructed from the seven orthonormal basis orbitals $1s, 2s, 2p, 3s, 3p, 3d, 4f$. The $1s, 2s, 2p$ orbitals are those obtained by Clementi and Roetti² for the $1s^2 2s^2 2p^3 \ ^4S^o$ ground state in the Ne $^4S^o$ isoelectronic series. The remaining orbitals are optimised in the $1s^2 2s^2 2p^3 \ ^4S^o$ state of the O^+ ion using the CIV3 program of Hibbert³.

The collision calculations are carried out at a very fine energy mesh in the region between all thresholds using the R-matrix package of Harrington et al.⁴ It is seen that the collision strengths exhibit complicated resonance structure for all the transitions of interest. Fig. 1 is a plot of the total collision strength for the forbidden transition $1s^2 2s^2 2p^3 \ ^4S^o - 1s^2 2s^2 2p^3 \ ^2D^o$ in the energy range from the $^2D^o$ threshold to the $^4S^o$ threshold. Between all thresholds shown there is a complicated structure of resonances. Table 1 gives a sample comparison of our results on total collision strengths with the previous calculations of Saraph et al.⁵ and Pradhan⁶ for the forbidden transition $1s^2 2s^2 2p^3 \ ^4S^o - 1s^2 2s^2 2p^3 \ ^2D^o$.

For astrophysical purposes the quantity which is of interest is the effective collision strength as a function of electron temperature. These are obtained by averaging the total cross sections over a Maxwellian distribution.

Our results are compared with the previous calculations of Pradhan⁶ for the forbidden transitions $1s^2 2s^2 2p^3 \ ^4S^o - 1s^2 2s^2 2p^3 \ ^2D^o, \ ^2P^o$ and with 20 and Henry⁷ for the allowed transitions $1s^2 2s^2 2p^3 \ ^4S^o - 1s^2 2s^2 2p^3 \ ^2P^o, \ ^2D^o, \ ^2S^o$ and $1s^2 2s^2 2p^3 \ ^4S^o - 1s^2 2s^2 2p^3 \ ^3S^o$.

Our calculations for the above forbidden and allowed transitions show improvement on previous calculations. Further transitions will be presented at a later date along with the above comparison on collision strengths.

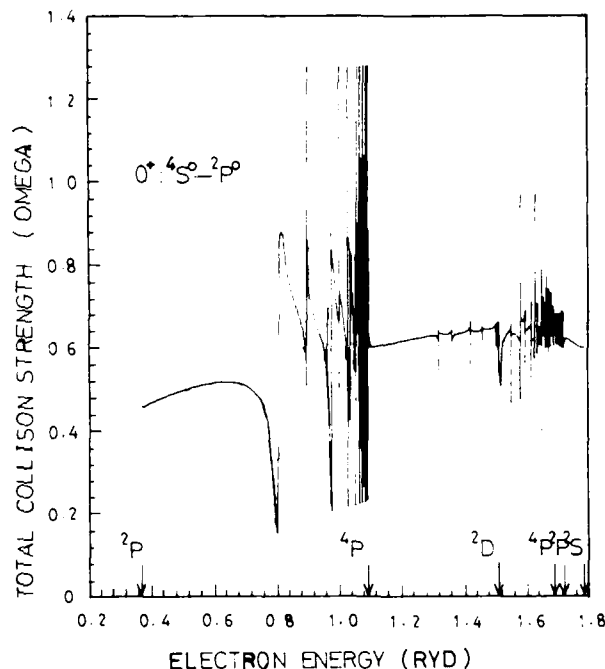


Figure 1: The total collision strength for the forbidden transition $1s^2 2s^2 2p^3 \ ^4S^o - 1s^2 2s^2 2p^3 \ ^2D^o$ in O^+ .

Energy (Ryd)	Saraph et al	Pradhan	Present Results
0.87	1.47	1.353	1.458
0.919	1.46	1.363	1.407
1.009	1.48	1.392	1.439

Table 1: Total collision strengths for the $1s^2 2s^2 2p^3 \ ^4S^o - 1s^2 2s^2 2p^3 \ ^2D^o$ transition in O^+ between the $^2D^o$ and the $^4S^o$ threshold.

References

1. E.J. Burke and W.D. Robb, Adv. At. Mol. Phys. **11**, 133 (1975).
2. E. Clementi and C. Roetti, At. Data & Nucl. Data Tables **14**, 107 (1974).
3. A. Hibbert, Comp. Phys. Commun. **9**, 14 (1975).
4. G.A. Harrington, E.J. Burke, M. McDouneut, W.D. Robb, P.J. Taylor and V. Poljan, Comp. Phys. Commun. **14**, 207 (1977).
5. B.L. Saraph, B.L. Selton and J. Sherrington, Phil. Trans. Roy. Soc. Lond. A **264**, 77 (1969).
6. A. Pradhan, J. Phys. B: At. Mol. Phys. **9**, 433 (1976).
7. T.R. Ho and R.L.K. Henry, Ap. J. **264**, 733 (1983).
8. A. Pradhan, M.N.R.A.S. **177**, 91 (1976).

ELECTRON IMPACT EXCITATION-AUTOIONIZATION OF LITHIUM-LIKE IONS

Defrance P, Rachafi S. and Chantrenne S.

Université Catholique de Louvain, Institut de Physique, Chemin du cyclotron, 2
B1348 Louvain-la-Neuve - BELGIUM

The electron impact excitation-autoionization of the doubly excited ($1s, 2i, 2i'$) states plays an important role for Lithium-like ions. For this process the theory (1-2) assumes that the radiative decay of "autoionizing" states is negligible for $Z < 10$. On the other hand, lifetime calculations and plasma observations has well established that importance for high Z .

We have estimated the total excitation-autoionization cross-section $\sigma(E)$ in a way which includes the probability of auto-ionization and radiative decay A_{ia} and A_{ir} respectively :

$$\sigma(E) = \sum_i \sigma_i(E) \frac{A_{ia}}{A_{ia} + A_{ir}}.$$

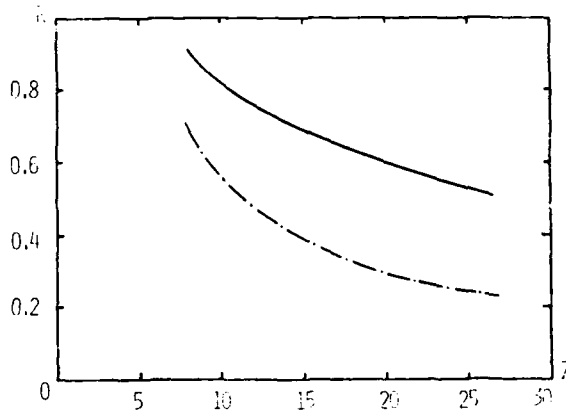
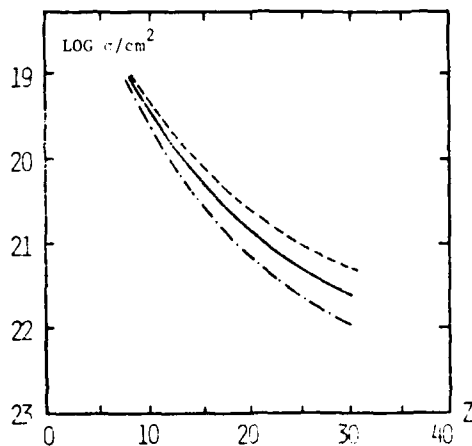
E is the electron energy and $\sigma_i(E)$ is the electron impact excitation cross-section from the ground state to the particular state i belonging to one of the configurations ($1s, 2i, 2i'$).

The branching ratio R is defined as :

$$R = \frac{\sigma(E)}{\sum_i \sigma_i(E)}.$$

In the case of Lithium-like ions, we used data of Goett and Sampson (2) for $\sigma_i(E)$ obtained in a scaled Coulomb-Born approximation.

Values of A_{ia} and A_{ir} are available in two approximations. In the first one (3) Coulomb wave functions are used in a Z -expansion method. In the second one (4) relativistic effects are included and Dirac-Hartree-Slater functions are used. For each ion, we have calculated $\sigma(E)$ at its maximum σ_m (Fig. 1). The three curves are : --- : for $R=1$ for all i and Z , --- and — for the data of references (3) and (4) respectively.



It is seen that σ_m decreases as Z^{-4} , Z^{-5} and $Z^{-4.5}$ in the three cases respectively.

The total branching ratio R (Fig. 2) is constant in the first case, and decreases as Z^{-1} and $Z^{-1/2}$ in the two approximations respectively. This means that relativistic effects affects strongly the Z dependance of R .

This also indicates that the radiative decay of doubly excited Lithium-like ions is significantly competitive with autoionization for $Z > 7$.

References.

1. Jakubowicz H. and Moores D.L., J. Phys. B **14**, p. 3733, (1981).
2. Goett S.J. and Sampson D.H., At. Data, Nucl. Data Tables **29**, p. 535-572, (1981).
3. Vainshtein L.A. and Safronova V.I., At. Data, Nucl. Data Tables **21**, p. 49, (1978).
4. Chen M.H., Crasemann B. and Mark H., Phys. Rev. A **24**, p. 1832, (1981); **26**, p. 1441, (1982) and **27**, p. 524, (1983).

ELECTRON IMPACT IONISATION OF Ne^{7+} .

S. Chantrenne, P. Defrance, S. Rachafi, D. Belic* and F. Brouillard

Université Catholique de Louvain, Institut de Physique, Chemin du cyclotron, 2
B 1348 Louvain-la-Neuve, Belgium

* Institute of Physics, Beograd, Yugoslavia.

A measurement of the total ionisation cross section
for the process :



has been performed, using the ECR source of the University
of Louvain in conjunction with the "animated crossed beam"
method (ref. 1).

The beam, extracted by a voltage of a few kilovolt,
is charge analysed by a wien filter and crossed at 90°
with an electron beam. A magnet subsequently separates
the primary ions from ions in a higher charge state.
The intensities of the ion beam and of the electron beam
are collected in Faraday cups while the ionisation
products are detected by means of channelplates.
First, results have been obtained for the single ionisation
of lithium-like ions N^{4+} and O^{5+} (ref. 2). In
the same isoelectronic sequence, results have been obtained
for Ne^{7+} for which experimental data are not available.
The figure shows that our results follow rather
exactly the prediction of Jakubowicz who uses the Coulomb-
Born approximation without exchange (ref. 3). The excitation-
autoionisation structure is clearly resolved and
the threshold is seen to be very close to the theoretical
value (908.01 eV).

References

- (1) F. Brouillard and P. Defrance (Physica Scripta, Vol. T3, 68, 1983).
- (2) P. Defrance, S. Chantrenne, S. Rachafi, D. Belic, D. Gregory, F. Brouillard (2nd ECAMP, Amsterdam, 1985).
- (3) B. Jakubowicz and D.L. Moores (J. Phys. B : At. Mol. Phys. 14, 3733, 1981).

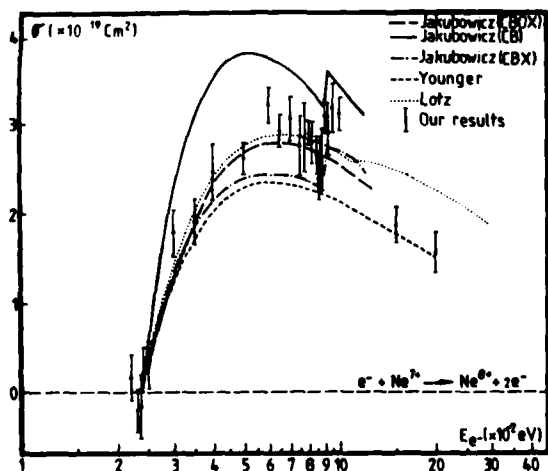


Fig. 1

IONIZATION OF Ti^+ , Ti^{2+} AND Ar^{2+} BY ELECTRON IMPACT*M J Diserens⁺, M F A Harrison⁺⁺, and A C H Smith⁺

* Department of Physics and Astronomy, University College London, London WC1E 6BT, U.K.

++ Culham Laboratory, Abingdon, Oxon, OX14 3DB, U.K. (Euratom/UKAEA Fusion Association)

Within our programme of measurements of electron impact ionization cross sections relevant to fusion research, we have measured absolutely the cross sections for single ionization of Ti^+ , Ti^{2+} , and Ar^{2+} in the energy range from threshold to 2000, 2200 and 1250 eV respectively.

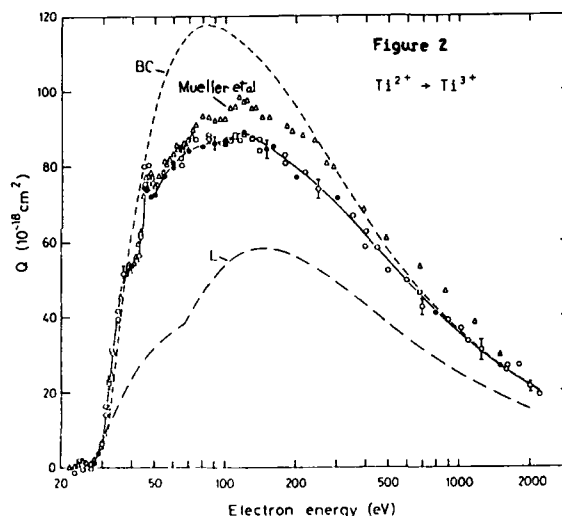
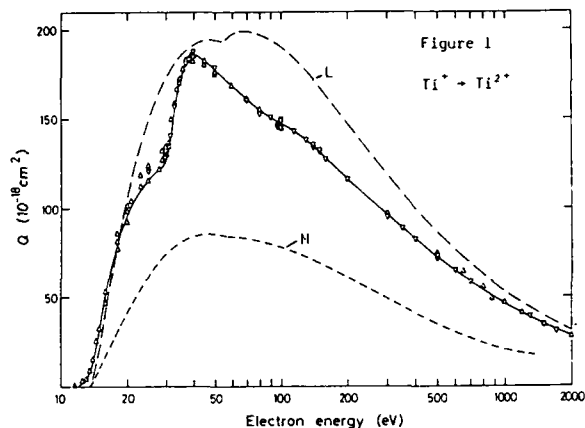
For these measurements the fast crossed beams technique described by Montague and Harrison¹ and by Montague et al² was used. The target ion energies were between 2 and 6 keV. The ions were generated in a sputter ion source and consequently the cross sections presented represent ionization from an unknown distribution ground and metastable excited states. Nevertheless the measured cross sections are of practical relevance because impurity ions in a fusion plasma are formed in a similar manner to those extracted from our sputter source.

In figure 1 the cross section for $Ti^+ + Ti^{2+}$ is compared with the cross sections calculated by means of the semi-empirical Lotz formula³(L) and the scaled-Born approximation of McGuire⁴(M). The fair agreement of the Lotz cross section is fortuitous since excitation-autoionization is not correctly included in the formula and clearly forms a large contribution in this case. The observed autoionization threshold at 31 eV suggests that the excitation-autoionization process is $Ti^+ (3p^6 3d^2 4s) \rightarrow Ti^+ (3p^5 3d^2 4s nl) \rightarrow Ti^{2+} (3p^6 3d^2) + e$ where $nl = 3d, 4s$ or $4p$.

In figure 2 our measured cross section for $Ti^{2+} + Ti^{3+}$ is compared with the measurements of Mueller et al⁵. The small discrepancy in magnitude and the small additional peak below the main threshold in the latter case are probably symptoms of different metastable state populations in target beams. The semi-empirical formula of Burgess and Chidichimo⁶, which includes the contribution of excitation-autoionization, rather over-estimates the magnitude, while the Lotz formula is in poor agreement.

Our measured cross section for $Ar^{2+} + Ar^{3+}$ is 15% larger than that of Müller et al⁷ and 15% smaller than that of Mueller et al⁵ over most of the energy range.

One of us (MJD) was in receipt of a SERC-CASE Postgraduate Studentship when this research was performed.



REFERENCES

1. Montague R G and Harrison M F A, J. Phys. B 16, 3045 (1983)
 2. Montague R G, Harrison M F A and Smith A C H, J. Phys. B 17, 3295 (1984)
 3. Lotz W, Z. Phys. 220, 466 (1969)
 4. McGuire E J, Phys. Rev. A 16, 73 (1977)
 5. Mueller D W, Morgan T J, Dunn G H, Gregory D C and Crandall D H, Abstracts 13ICPEAC, Berlin 1983, p204
 6. Burgess A and Chidichimo M C, Mon. Not. R. Astr. Soc. 203, 1296 (1983)
 7. Müller A, Salzborn E, Frodl R, Becker R, Klein H and Winter H, J. Phys. B 13, 1577 (1980)
- * work performed at Culham Laboratory

SINGLE AND MULTIPLE IONIZATION OF MULTIPLY CHARGED IONS BY ELECTRON IMPACT

A.Müller, K.Tinschert, Ch. Achenbach, E.Salzborn

R.Becker*, and M.S.Pindzola[†]

Institut für Kernphysik, Universität Giessen, D-6300 Giessen, West Germany

^{*}Institut für Angewandte Physik, Universität Frankfurt, D-6000 Frankfurt, West Germany[†]Atomic Theory Group, Physics Division, Oak Ridge, Nat. Lab. Oak Ridge, Tenn. 37830, U.S.A.

Employing an improved crossed-beams technique based on the 'animated-beams method' first described by De-france et al.¹ cross sections for electron impact ionization of multiply charged ions for electron energies from threshold to 1000 eV have been measured. This alternative technique does not require a separate measurement of the so-called form factor and since both beams are always 'on' background pressure modulation effects cannot occur. To assure the reliability of the applied experimental technique several test measurements were performed².

Ionization measurements performed include cross sections $\sigma_{q,q+2}$ for electron impact double ionization of Ar^{q+} ($q = 1, 4$) ions³. In both cases contributions of L-shell ionization-autoionization could be identified. Calculations based on semiempirical and semiclassical theories were made to compare the relative strengths of direct double ionization and inner-shell ionization with subsequent autoionization. Obviously direct double ionization decreases rapidly with increasing charge state, while the contribution of L-shell ionization-autoionization nearly remains constant. Thus $\sigma_{4,6}$ for Ar^{4+} ions is almost completely dominated by the indirect L-shell contribution above 350 eV.

An extraordinary behavior of the cross section $\sigma_{q,q+1}$ was observed for Sb^{q+} and Bi^{q+} ($q = 1, 2$) ions⁴. At energies greater than 200 eV the cross sections for Sb^{2+} ($4d^{10}5s^25p$) and Bi^{2+} ($5d^{10}6s^26p$) (Fig. 1), $\sigma_{2,3}$, are larger than the corresponding cross sections, $\sigma_{1,2}$, for Sb^{1+} and Bi^{1+} ions, respectively. This behavior is a consequence of the effect that the 4d(5d) hole configuration goes from autoionizing to bound when the charge state of the Sb(Bi) ions is increased from +1 to +2. The collision strength of the 4d(5d) subshell missing in the cross section $\sigma_{1,2}$ for single ionization can be found in the cross section $\sigma_{1,3}$ for double ionization which as a result attains very large values.

Furthermore, measurements of electron impact single and multiple ionization of Kr^{q+} ($q = 1, 2, 3, 4$) ions have been performed. Some general trends concerning the contributions of direct and indirect ionization processes could be extracted.

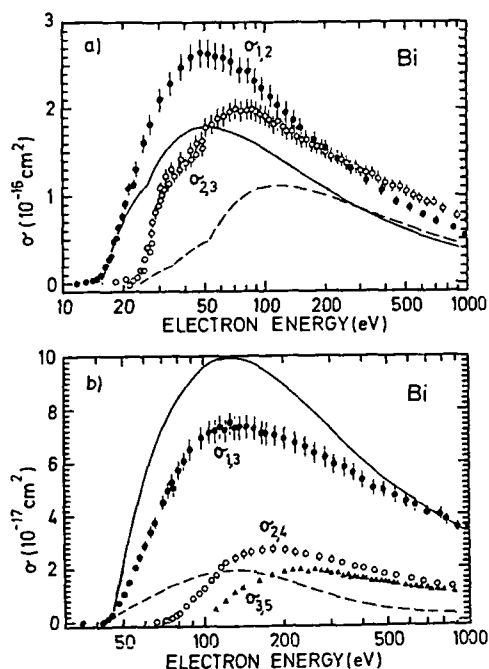


Fig. 1: Electron impact single and double ionization cross sections for Bismuth ions. (a) closed circles, experimental $\sigma_{1,2}$; open circles, experimental $\sigma_{2,3}$; solid curve, $\sigma_{1,2}$ calculated from the Lotz formula⁵ with contributions from 6p and 6s subshells; dashed curve, $\sigma_{2,3}$ calculated from the Lotz formula⁵ with contributions from 6p, 6s and 5d subshells. (b) closed circles, experimental $\sigma_{1,3}$; open circles, experimental $\sigma_{2,4}$; triangles, experimental $\sigma_{3,5}$; dashed curve, direct double ionization cross section $\sigma_{1,3}$ calculated from binary encounter theory⁶; solid curve, total calculated $\sigma_{1,3}$ including the indirect 5d ionization-autoionization contribution.

References

1. P. De-france, F. Brouillard, W. Claeys, G. van Wassenhove, *J. Phys. B: At. Mol. Phys.* **14**, 103 (1981)
2. A. Müller, K. Huber, K. Tinschert, R. Becker and E. Salzborn, *J. Phys. B.*, in print
3. A. Müller, K. Tinschert, C. Achenbach, R. Becker and E. Salzborn, *J. Phys. B.*, in print
4. A. Müller, K. Tinschert, C. Achenbach, E. Salzborn, R. Becker and M. S. Pindzola, *Phys. Rev. Lett.* **54**, 414 (1985)
5. W. Lotz, *Z. Physik* **216**, 241 (1968)
6. M. Gryzinski, *Phys. Rev.* **138** A, 336 (1965)

ELECTRON IMPACT EXCITATION OF Kr^{+28*} A. Z. Msezane,[†] J. Lee,[†] R. J. W. Henry,^{**} and K. J. Reed^{***}[†]Atlanta University, Atlanta, GA^{**}Louisiana State University, Baton Rouge, LA^{***}Lawrence Livermore National Laboratory, University of California, Livermore, CA

Multi-state close coupling calculations have been performed to obtain electron collision cross sections for oxygen-like krypton. Configuration interaction type wave functions were employed, and oscillator strengths and energy levels were calculated for the target ion. The cross sections were computed for electron impact energies ranging from near threshold to 10 keV.

Spectral lines due to oxygen-like krypton have been observed in laboratory plasmas¹ and may be useful for purposes of plasma diagnostics. Accurate electron collision cross sections are required for interpretation of spectroscopic data obtained from the plasmas. Calculation of electron impact excitation cross sections for some transitions in O-like Kr have been reported.² We have extended the earlier work to include more of the transitions from the ground state $2p^4(^3P^e)$ to levels arising from the $n = 2$ and $n = 3$ excited states of the ion. We have also retained the $2p^4(^1D^e)$ and $2p^4(^1S^e)$ states together with the $2p^4(^3P^e)$ state in order to investigate the effect of coupling between the terms of the ground state configuration.

Hartree-Fock orbitals of Clementi and Roetti³ were used as a starting point for the $1s$, $2s$, and $2p$ orbitals of the target ion. The Program CIV3⁴ was used to generate the excited $3s$, $3p$, $3d$, $4s$, $4p$, $4d$ and $5s$ orbitals. These orbitals were used to construct configuration-interaction type wave functions after extensive investigation of the effects of C.I. upon oscillator strengths and energy levels of the target states. The program NIEM⁵ was used to solve the resulting integro-differential equations.

*This work was performed under the auspices of the U. S. Department of Energy by Lawrence Livermore National Laboratory under contract No. W-7405-Eng-48.

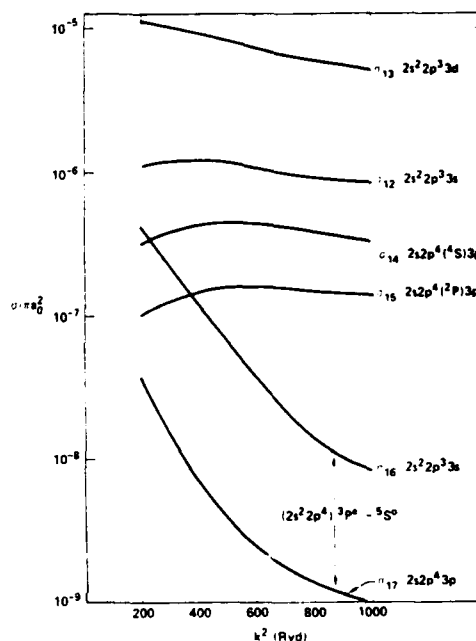


FIGURE 1. Excitation cross sections for O-like Kr $(2s^2 2p^4) 3P^e - 3S^e$

Reference

1. S. Wong, et al., *PIIR* 15498, Sept. 1984.
2. A. Z. Msezane, J. Lee, R. J. W. Henry and K. J. Reed, 5th Topical Conference on Atomic Processes in High Temperature Plasmas, Asilomar, CA (1985).
3. E. Clementi and C. Roetti, *Atomic Data and Nuclear Data Tables* **14**, 177 (1974).
4. A. Hibbert, *Comput. Phys. Commun.* **9**, 141 (1975).
5. R. J. W. Henry, S. P. Rountree, and L. R. Smith, *Comp. Phys. Commun.* **24**, 233 (1981).

MEASUREMENTS OF CROSS SECTION FOR SINGLE AND DOUBLE IONIZATION FOR Na^+ , K^+ AND Ba^+

T.Hirayama, K.Oda, Y.Morikawa, T.Ono, Y.Ikezaki, S.Kobayashi, T.Takayanagi, K.Wakiya and H.Suzuki

Department of Physics, Sophia University, Kioicho 7-1, Chiyoda-ku, Tokyo 102 JAPAN

Cross section data for electron-ion collision processes can provide important informations in the study of high temperature plasmas relevant to the thermonuclear fusion and astrophysics. We have measured ionization cross sections for Na^+ , K^+ and Ba^+ by electron impact using the crossed beam technique.

The experimental apparatus, techniques and conditions used for these measurements are the same as described by Hirayama et al.^{1,2)} except for Ba^+ ion source. A compact surface ionization type ion source designed by Sakai et al.³⁾ is used to obtain Ba^+ ions.

Results for single ionization cross section of Na^+ and K^+ are shown in Fig.1 and Fig.2 with the experimental results of Hooper et al.⁴⁾ and Peart et al.⁵⁾, and semi-empirical Lotz formula⁶⁾. Our results are in good agreement with the previous data within the experimental uncertainties. In the results of K^+ , our data show more rapid rise near the threshold than the Lotz calculation. There exist some autoionizing states above 5.28 eV (1-electron excitation) and 11.29 eV (2-electron excitation) above the ionization potential of K^+ ion⁷⁾, which are designated by arrows in Fig.2. Therefore this feature is

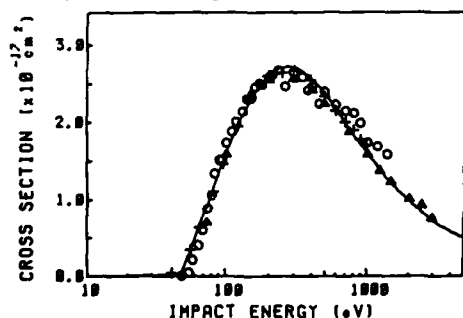


Fig.1. Single ionization cross section of Na^+ . Open circle - present, cross - Hooper et al.⁴⁾, triangle - Peart et al.⁵⁾, full curve - Lotz calculation (This curve is multiplied to reproduce the experimental results.)

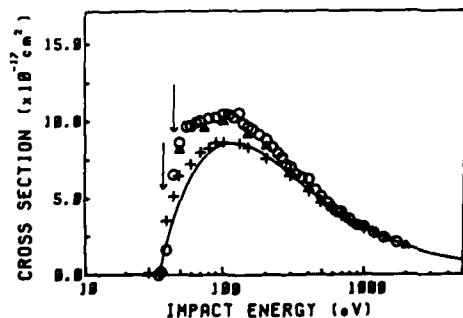


Fig.2. Single ionization cross section of K^+ . Symbols are the same as in Fig.1. Arrows represent the autoionization thresholds. (See text)

believed to be indirect ionization processes due to excitation-autoionization.

Results for double ionization cross section of Na^+ and K^+ are shown in Fig.3 together with results of the other alkali ions⁸⁻¹⁰⁾. In the results of K^+ , there is an evidence of structure around impact energy 350 eV. L-shell ionization potential of neutral potassium atom is about 310 eV (2p electron) and 390 eV (2s electron)¹¹⁾. Inner shell ionization potential of K^+ ion is not so far from these values, therefore this structure is attributed to the contribution from the L-shell ionization-autoionization (Auger effect).

Measurements of ionization cross section of Ba^+ are now in progress.

REFERENCES

1. T.Hirayama, K.Oda, T.Ono, Y.Morikawa, K.Wakiya and H.Suzuki, Abstracts of Contributed Papers, XIIIth ICPEAC (Berlin, 1983) pp.201
2. T.Hirayama, K.Oda, Y.Morikawa, T.Ono, Y.Ikezaki, T.Takayanagi, K.Wakiya and H.Suzuki, to appear in J. Phys.Soc.Jpn. (1985)
3. Y.Sakai, I.Katsumata and T.Oshio, Jpn.J.Appl.Phys. 22 1048 (1983)
4. J.W.Hooper, W.C.Lineberger and F.M.Bacon, Phys.Rev. 141 165 (1966)
5. B.Peart and K.T.Dolder, J.Phys. B1 240 (1968)
6. W.Lotz, Z.Phys. 216 241 (1968)
7. H.Aizawa, K.Wakiya, H.Suzuki, F.Koike and F.Sasaki, J.Phys.B (1985) in press.
8. B.Peart and K.T.Dolder, J.Phys. B2 1169 (1969)
9. D.W.Hughes and R.K.Feeney, Phys.Rev. A23 2241 (1981)
10. D.R.Hertling, R.K.Feeney, D.W.Hughes and E.Sayle II J.Appl.Phys. 53 5427 (1982)
11. Roothaan-Hartree-Fock calculation by E.Clementi and C.Roetti, Atomic Data and Nuclear Data Tables 14 177 (1974)

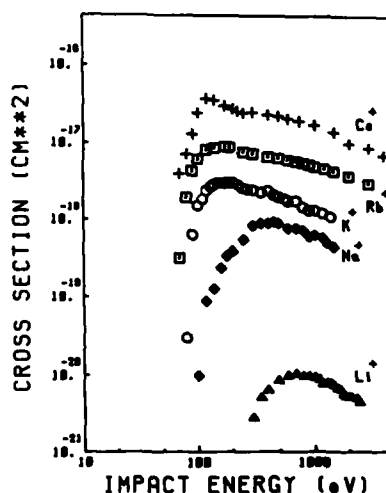


Fig.3. Double ionization cross section of alkali ions. Li^+ - Peart et al.⁸⁾, Na^+ , K^+ - present, Rb^+ - Hughes et al.⁹⁾, Cs^+ - Hertling et al.¹⁰⁾

DISTORTED-WAVE CROSS SECTIONS FOR ELECTRON-IMPACT IONIZATION OF THE LITHIUM-LIKE IONS

R.I.Câmpeanu, L.Nagy

Department of Physics, University of Cluj-Napoca, Romania

In the last few years the electron-impact ionization of atomic ions received great attention, especially in connection with fusion plasma studies. Beam measurements¹ and elaborate calculations^{2,3} were employed recently by Bell et al⁴ to compile recommended cross sections and rates for light ions.

From the existing theories the distorted wave method of Younger³ is extremely attractive, as it produces quite reliable data at low computing cost, and this in spite of an "unphysical" inclusion of the electron exchange⁵. In the present paper we investigate two new ways of including the exchange in the distorted-wave approximation.

We obtain the exchange scattering amplitude g by employing the standard definition

$$g(E_e, E_f) = f(E_f, E_e) \quad (1)$$

where f is the direct scattering amplitude and E_e and E_f are the energies of the ejected and scattered electrons respectively. We denote by DWT the model without exchange, by DWE1 the model with the exchange amplitude given by (1) and by DWE2 a variant, also based on (1), in which from the two emerging electrons the one with the higher energy is always computed in the static potential of the target ion, while the slower electron sees the residual ion. From this point of view DWE2 is similar to Younger's DWE.

Ion	I(Ry)	DWT	DWE1	DWE2	Ref3	Ref2	Ref4
B III	2.780	1.91	1.66	2.51	-	-	1.65
C IV	4.742	1.99	1.80	2.07	1.74	1.83	1.74
N V	7.182	2.04	1.86	2.02	1.82	-	1.86
O VI	10.156	2.10	1.93	1.97	1.84	-	1.98

Table 1. Scaled total cross sections $\sigma_{\text{tot}}^{\text{Li}} u^{1/2}$ (in units of $\pi a_0^2 \text{Ry}^2$) for electron-impact ionization of lithium like ions at $u=2.25$

Table 1 contains our scaled cross sections at the relative impact energy $u=E_1/I=2.25$ (I is the ionization energy), where the effect of the electron exchange is maximum.

For N IV our model DWE1 is in perfect agreement with the recommendation⁴ based on the accurate measurements of Crandall et al¹.

In the case of O VI our DWE models agree better with the experiment-based recommendation⁴ than any other theory, but we should also note the large error bars for this measurement.

For C IV the experiment gives too low cross sections⁴ and our model DWE1 agrees best with the sophisticated calculation of Jakubowicz and Moores².

For B III the model DWE1 is again in very good agreement with the recommendation of Bell et al⁴.

On the other hand, Table 1 shows clearly that our model DWE2 gives increasingly bad results as one goes to lower values of Z . For O VI, where the nuclear field dominates the distortion of the electron waves, our two DWE models yield similar results, but for B III it becomes obvious that only the correct account of the electronic potentials can give accurate results.

The present data indicate that for lithium-like ionic targets our model DWE1 produces better results than Younger's DWE³, at roughly the same computing cost.

References

1. D.H.Crandall, R.A.Phaneuf, B.E.Hasselquist, D.C.Gregory, ORNL-TM-7020 and J.Phys.B **12**, L249(1979)
2. H.Jakubowicz, D.Moores, J.Phys.B **14**, 3733 (1981)
3. S.M.Younger, Phys.Rev.A **22**, 111(1980)
4. K.L.Bell, H.B.Gilbody, J.G.Hughes, A.E.Kingston, T.J.Smith, J.Phys.Chem.Ref.Data **12**, No.4(1984)
5. M.R.C.McDowell, Atomic and Molecular Physics of Controlled Thermonuclear Fusion (eds.C.J.Joachain, D.E.Post), Plenum, 1983

THE ATOMIC DATABANK AT BELFAST AND DARESBURY

K.M. Aggarwal and K.A. Berrington

Department of Applied Mathematics and Theoretical Physics,
The Queen's University of Belfast,
Belfast BT7 1NN, Northern Ireland.

A database to collect, store and display numerical atomic data has been developed at the Queen's University of Belfast in collaboration with the Daresbury Laboratory of UK/SERC. The database stores data for collision processes such as electron-atom/ion excitation, ionization, photoionization and free-free transitions. The database is divided in two parts. The first part holds basic collision data such as reactance matrices which come directly from large computer codes such as RMATRIX and IMPACT. These data are bulky and are required in machine readable form, and hence are not appropriate for publication in scientific journals but it is still necessary to store the data for further processing, such as computations of collision cross sections, rate coefficients, resonance analysis, angular distribution etc. The second part of the database stores the data at a more processed level. This is mainly for collision cross sections and rate coefficients and comes from three sources: (i) from processing the basic data stored in the first part of the database; (ii) from the literature; and (iii) from recommendations of specialists (both theoreticians and experimentalists). Such recommended data often involve some manouvering of primary data such as taking combinations of two or more sets of data in different energy regions for the same transition, use of scaling laws and interpolation/extrapolation etc.¹⁻³ Both parts of the database are stored on demountable disks and tapes and in two locations, i.e. at Belfast and Daresbury. Potential users are invited to contact the authors for further information on access. The present paper concerns the data stored in the second part of the database.

Excitation rate coefficients as a function of electron temperature are currently stored for over 100 ions in the databank. A complete list of ions for which data are stored is given in Table 1. These data are primarily from the published literature. However, for the majority of the ions the data are published in the form of collision strengths instead of the rate coefficients. These are calculated from the available data for as many as 5 different sources for each ion and are compared with one another. The rate coefficients are collected and calculated for as many as 190 transitions for an ion and are both in LS and intermediate coupling schemes. The comparisons as well as the recommended values in both the numerical and graphical forms, together with a complete list of references will be available during the conference.

Table 1 Contents of Belfast and Daresbury Atomic Databank on March 1, 1985.

Sequence	Ions
H	H I, He II, Li III, C VI, Ne X, Si XIV, Ar XVIII, Fe XXVI.
He	He I, Li II, Be III, B IV, C V, O VII, Ne IX, Mg XI, Si XIII, S XV, Ar XVII, Ca XIX, Ti XXI, Cr XXIII, Fe XXV, Ni XXVII, Zn XXIX, Se XXXIII, Kr XXXV, Mo XLI, Cd XLVII, Xe LIII, Gd LXIII, W LXXIII.
Li	Li I, Be II, C IV, N V, O VI, Ne VIII, Mg X, Si XII, Ar XVI, Ca XVIII, Ti XX, Cr XXII, Mn XXIII, Fe XXIV, Zn XXVIII, Kr XXXIV, Mo XL, Xe LII, Gd LXII, W LXXII.
Be	C III, N IV, O V, Ne VII, Mg IX, Si XI, S XIII, Ar XV, Ca XVII, Ti XIX, Cr XXI, Mn XXII, Fe XXIII, Ni XXV, Zn XXVII, Kr XXXIII, Mo XXXIX, Cd XLV, Xe LI, Gd LXI, W LXXI.
B	C II, N III, O IV, Ne VI, Si X, S XII, Mn XXI, Fe XXII, Mo XXXVIII.
C	C I, N II, O III, Ne V, Mg VII, Si IX, S XI, Ca XV, Mn XX, Fe XXI.
N	N I, O II, Ne IV, Na V, Mg VI, Si VIII, Ca XIV, Mn XIX, Fe XX.
O	O I, Ne III, Na IV, Mg V, Al VI, Si VII, Ca XIII, Mn XVIII, Fe XIX.
F	Ne II, Na III, Mg IV, Al V, Si VI, Mn XVII, Fe XVIII.
Ne	Na II, Mg III, Al IV, Fe XVII.
Na	Na I, Mg II, Si IV, S VI, Ar VIII, Ca X, Ti XII, Fe XVI, Zn XX, Kr XXVI, Mo XXXII.
Mg	Mg I, Al II, Si III, S V, Fe XV, Mo XXXI.
Al	Si II, S IV, Ca V, Ar VI, Fe XIV.
Si	Si I, S III, Ca IV, Ar V.
P	S II, Cl III, Ar IV, K V.
S	Cl II, Ar III, K IV, Ca V, Fe XI.
Cl	Ar II, K III, Ca IV, Fe X.
Ar	Ar I, Fe IX.
K	K I, Ca II, Fe VIII.
Ca	Fe VII.

References

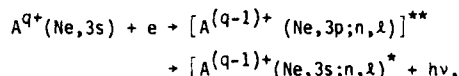
- 1) K.M. Aggarwal, Mon. Not. R. Astr. Soc. **202**, 15P (1983).
- 2) K.M. Aggarwal, A.E. Kingston and M.R.C. McDowell, Astrophys. J. **278**, 874 (1984).

DIELECTRONIC RECOMBINATION MEASUREMENTS OF P^{4+} , S^{5+} , AND Cl^{6+}

P. F. Dittner, S. Datz, P. D. Miller, and P. L. Pepmiller

Oak Ridge National Laboratory,* Oak Ridge, TN 37831 USA

Dielectronic recombination (DR) via 3s-3p excitation in the Na-like ions P^{4+} , S^{5+} , and Cl^{6+} has been measured. The DR process investigated for these ions is



where Ne represents the neon core ($1s^2, 2s^2, 2p^6$), n and l are the quantum numbers of the captured electron, and ν is the frequency of the emitted radiation due to the 3p-3s relaxation. A merged beam approach¹ was used to take advantage of our ability to produce high charge state, MeV/amu ions, and a high current, high energy electron beam. The merged beam apparatus is constructed such that in the interaction region, the ion beam (~ 0.5 -mm dia.) is coaxial with and embedded within the electron beam (~ 3 -mm dia.) for a distance of 84 cm.

We observed the amount of electron capture attending the passage of the ions through the electron beam as a function of relative energy which is varied by changing the ion energy. After exiting the interaction region, the ion beam is subjected to charge state analysis using electrostatic deflection field of ~ 4 kV/cm. The A^{Q+} is deflected into a Faraday cup and ions that have picked up an electron, $A^{(Q-1)+}$, are deflected onto a solid-state position-sensitive detector, allowing them to be counted.

The $A^{(Q-1)+}$ ions are due to signal, the sought-after DR, and background due to electron pickup from the residual gas or slit edge scattering. To measure the pure background level ($\sim 5X$ signal), we modulated the electron energy such that the relative energy, E_r , alternated between $0 < E_r = E_1 < 1.5E_m$ and $E_r = E_2 > 1.5E_m$, where E_m is the 3p-3s transition energy. This energy modulation was accomplished by applying an 11-Hz square wave voltage to an 8-mm diameter cylinder which surrounds the electron beam. Since no DR signal is expected above E_m , one can subtract the $A_2^{(Q-1)+}$ rate ($E_r = E_2$) from the $A_1^{(Q-1)+}$ rate ($E_r = E_1$), at the same ion energy, to extract the signal. The ratio, $R_S = (A_1^{(Q-1)+} - A_2^{(Q-1)+})/A^{Q+}$ at an ion velocity, v_i , is related to the DR cross section, $\sigma(v_r)$ by

$$R_S = (\rho_e L / v_i) \int v_r \sigma(v_r) f(v_r) dv_r = (\rho_e L / v_i) \langle v_r \sigma \rangle$$

where ρ_e is the electron density, L is the length of the interaction region, v_r is the relative velocity, and $f(v_r)$ is the relative velocity distribution function.

Although we cannot determine $f(v_r)$ independently, we constructed an $f(v_r)$ such that a fold of the theoretically calculated rate² for Cl^{6+} had the same shape (but

not magnitude) as our Cl^{6+} data. This $f(v_r)$ was used to convolute the calculated rate for P^{4+} and S^{5+} and was found to be a reasonable fit to the data for these ions as well (see Fig. 1). Data for the three ions indicate a higher cross section than the calculation which assumes no field in the interaction region (lower curve in Fig. 1), but a lower cross section than the calculation which assumes complete Stark mixing of the n, l states (upper curve in Fig. 1).

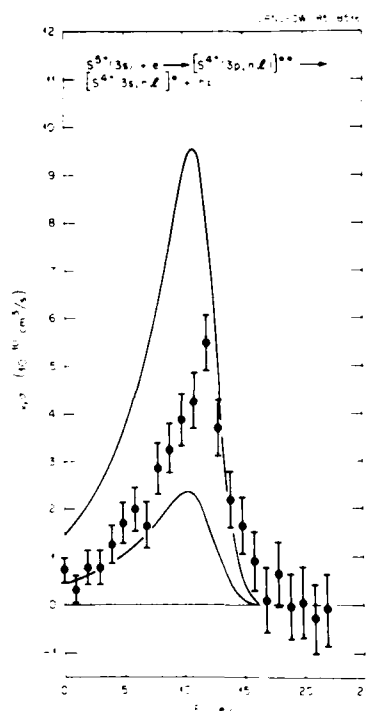


FIGURE 1. DR rates $\langle v_r \sigma \rangle$ for S^{5+} vs. relative energy. Our results (\bullet) compared to calculations (Ref. 2); no field-lower curve, complete Stark mixing-upper curve.

References

- * Research sponsored by the U.S. Department of Energy, Division of Basic Energy Sciences under Contract No. DE-AC05-84OR21400 with Martin Marietta Energy Systems, Inc.
1. P. F. Dittner, S. Datz, P. D. Miller, C. D. Moak, P. H. Stelson, C. Bottcher, W. B. Dress, G. D. Alton, and M. Meskovic, Phys. Rev. Lett. **51**, 31-34 (1983).
2. D. Griffin, M. Pindzola, and C. Bottcher, "The Effect of External Electric Fields on the Dielectronic Recombination Cross Section of Li- and Na-like Ions," ORNL/TM-9473, April 1985.

FINAL RYDBERG STATE DISTRIBUTION FROM DIELECTRONIC RECOMBINATION

D. Mueller, A. Müller, C. Timmer, D. S. Belić, B. D. DePaola, N. Djurić, and G. H. Dunn*

Joint Institute for Laboratory Astrophysics, University of Colorado and
National Bureau of Standards, Boulder, Colorado 80309 USA

Serious disagreements between theory and experiments for dielectronic recombination (DR) have been reported.¹⁻⁴ It has been recognized for some time that mixing of angular momentum states by such mechanisms as collisions,⁵ plasma microfields,⁶ and magnetic fields⁷ may affect DR. More recently, in an effort to rationalize the above-mentioned experiment-theory dilemma, the effects of extrinsic electric fields have been treated.⁸⁻¹⁰ It has been found that angular momentum mixing by the external fields can in effect add many participating resonances to the collision, thus leading to a substantial enhancement of the cross section. This also results in a strong dependence of cross section versus n , where n is the principle quantum number of the Rydberg state of the product particle.

To more fully understand the DR process, we have continued experiments on $\text{Mg}^+(3s) + e \rightarrow \text{Mg}(3p, n\ell) + \text{Mg}(3s, n\ell) + h\nu$. Measurements have now been made and are reported here of cross section versus n_f for two different values of electric field in the collision region, and of cross section versus electron energy for the small n_f range $32 \leq n_f \leq 35$. Here n_f is defined operationally in terms of the field E_1 at which the state field ionizes by $n_f = (3.2 \times 10^8/E_1)^{1/4}$, and is close to -- but not identical to -- the principal quantum number n .

A 2 keV mass analyzed beam (~ 300 nA) of $^{24}\text{Mg}^+$ traveling in the z direction intersects a magnetically confined (0.02 or 0.0065 T, x direction) beam of electrons (2 mm \times 4 mm, 15 μA). In the collision region the colliding ions see an effective electric field $\vec{E}_c = \vec{v} \times \vec{B}$ in the y direction. This field and an applied field a few centimeters down beam serve to

separate the ion and product Rydberg atom beams. The product Rydberg atoms continue into a region with electric field in the x - z plane and given by $E_1 = V/(8R)$, where $\pm V$ volts are applied to plane plates at an angle 28° with respect to each other and R is the distance from the apex of the wedge. Because the field changes with z , Rydberg atoms with different n_f are field ionized at different values of z . Electrons (or ions) are detected on a position sensitive detector, and by varying V the cross section versus n_f can be measured over the range $18 \leq n_f \leq 55$.

The resulting curve has a maximum near $n_f = 33$, and the sum $\sigma_T = \sum_{n_f} \sigma_{n_f}$ is consistent with the total cross section previously reported² using a coincidence technique.

Similar work on DR for Li^+ is in progress, and will be discussed.

This work was supported in part by the Office of Fusion Energy, U. S. Department of Energy.

References

1. J. B. A. Mitchell, C. T. Ng, J. L. Foraud, D. P. Levac, R. E. Mitchell, A. Sen, D. B. Miko and J. Wm. McGowan, *Phys. Rev. Lett.* **50**, 335 (1983).
2. D. S. Belić, G. H. Dunn, T. J. Morgan, D. W. Mueller and C. Timmer *Phys. Rev. Lett.* **50**, 339 (1983).
3. P. F. Dittner, S. Datz, P. D. Miller, C. D. Heath, P. H. Stelson, C. Bottcher, W. R. Dress, G. D. Alton and N. Nešković, *Phys. Rev. Lett.* **51**, 31 (1983).
4. J. F. Williams, *Phys. Rev. A* **29**, 2936 (1984).
5. A. Burgess and H. P. Summers, *Astrophys. J.* **157**, 1007 (1969).
6. V. L. Jacobs, J. Davis and P. C. Kepple, *Phys. Rev. Lett.* **37**, 1390 (1976).
7. W. A. Huber and C. Bottcher, *J. Phys. B* **13**, L399 (1980).
8. K. LaGattuta and Y. Hahn, *Phys. Rev. Lett.* **51**, 558 (1983).
9. A. P. Hickman, *J. Phys. B* **17**, L101 (1984).
10. D. C. Griffin, M. S. Pindzola and C. Bottcher, private communication (1985).

*Staff Member, Quantum Physics Division, National Bureau of Standards.

THEORETICAL CALCULATIONS OF ELECTRIC FIELD EFFECTS ON
DIELECTRONIC RECOMBINATION BY MATRIX DIAGONALIZATION

D. C. Griffin*, M. S. Pindzola⁺ and C. Bottcher

Atomic Physics for Fusion Group, Physics Division,
Oak Ridge National Laboratory, Oak Ridge, TN 37831

External electric fields can have a pronounced effect on dielectronic recombination cross sections. They not only can field ionize high Rydberg states, but they can also cause a redistribution of the angular momentum among the doubly-excited, intermediate states which may significantly enhance the total dielectronic recombination cross section. This field enhancement has been demonstrated by a number of approximate theoretical calculations.^{1,2,3} However, all of these employed some variation of the configuration-average approximation, and they do not properly take into account the field mixing between individual levels within the doubly-excited configurations that are populated during the recombination process.

We will present the results of intermediate-coupled calculations of dielectronic recombination cross sections associated with the $2s+2p$ excitation in several Li like ions and the $3s+3p$ excitation in several Na like ions in the presence of an external electric field. The eigenvectors for the doubly-excited, intermediate states, were determined in these calculations by diagonalizing a Hamiltonian which includes the internal electrostatic and spin-orbit terms as well as the Stark matrix elements. However, only doubly-excited configurations with the same principal quantum number n for the Rydberg electron were included in a given matrix, so that the effects of field induced n mixing were neglected.

The variation of the cross sections with the external electric field will be presented as a function of principal quantum number and electron energy, and the results of the calculations will be compared with recent crossed electron-ion beam measurements of the dielectronic recombination cross sections.

* Permanent address: Department of Physics, Rollins College, Winter Park, Florida 32789.

⁺ Permanent address: Department of Physics, Auburn University, Auburn, Alabama 36849.

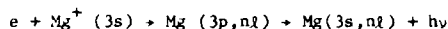
1. V. L. Jacobs, J. Davis, and P. C. Kepple, Phys. Rev. Lett. 37, 1390 (1976).
2. K. LaGattuta and Y. Hahn, Phys. Rev. Lett. 51, 558 (1983).
3. D. C. Griffin, M. S. Pindzola and C. Bottcher Oak Ridge National Laboratory Technical Report TM 9478 (1985).

DIELECTRONIC RECOMBINATION OF Mg^+

A. P. Hickman

Chemical Physics Laboratory, SRI International, Menlo Park, CA 94025 USA

There has been considerable interest in the dielectronic recombination (DER) of the magnesium ion,



A discrepancy arose because the first measurements¹ turned out to be about a factor of five larger than the earlier calculations of LaGattuta and Hahn². Subsequently, LaGattuta and Hahn³ suggested that small electric fields (< 24 volts/cm) present in the experiment would make the cross sections an order of magnitude larger. The present work shows that a more detailed calculation of DER in the field-free limit also leads to significantly larger cross sections. The increase occurs because we include the fine structure of the ionic core, and also use more accurate autoionization rates for states of large angular momenta.

To include fine structure, it is convenient to use the pair coupling scheme⁴ for the angular momenta. Then the orbital and spin angular momenta of the incident electron are \vec{l} and \vec{s} ; the orbital and spin angular momenta of the Mg^+ valence electron are \vec{L}_1 and \vec{S}_1 and $\vec{J}_1 = \vec{L}_1 + \vec{S}_1$, $\vec{K} = \vec{l} + \vec{J}_1$, and $\vec{J} = \vec{K} + \vec{s}$. One then expresses the autoionization rates of the core-excited Rydberg states $Mg(3p_{j_1}; n\ell)$ in terms of the autoionization rates of the states $Mg(3p; n\ell)$ calculated in LS coupling. Making the further approximation, valid for large L , that the rates are independent of the spin of the Rydberg electron, one obtains

$$\Gamma^K(3p_{j_1}; n\ell) = (2J_1+1) \sum_{L=\ell \pm 1} \left\{ \begin{matrix} S_1 & L_1 & J_1 \\ l & K & L \end{matrix} \right\}^2 \Gamma^L(3p; n\ell)$$

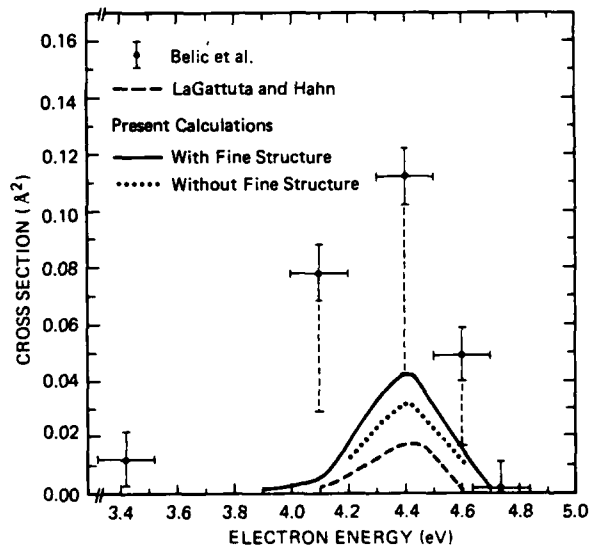
The autoionization rates have been evaluated by using Multichannel Quantum Defect Theory⁵ to extrapolate scattering calculations performed above the threshold for electron impact excitation of $Mg^+(3s \rightarrow 3p)$, to the Rydberg series of autoionization states below the threshold. Using the Coulomb-Bethe approximation⁶, and evaluating certain integrals using the method of reference 7, the rates may be obtained analytically.

Results are shown in the figure. The present calculation is more than a factor of two larger than the previous calculation of LaGattuta and Hahn². There is about 30% difference between the peak values of the results with and without fine structure. The difference between the dotted curve and the dashed curve of

LaGattuta and Hahn² is due to our use of more accurate autoionization rates for $L \geq 5$.

We conclude that it is very important to include all the distinct autoionization rates that may contribute to the recombination. Because of a saturation effect, the contribution of a manifold of degenerate autoionizing states is limited. However, if these states are split by fine structure, each state may contribute separately, and the total cross section may increase. Thus the splitting of several zeroth order states that has been attributed to external fields is already present to some degree in the zero field case. Our results indicate that the zero field case should be treated as thoroughly as possible before introducing external fields.

This work was supported by NSF Physics.



References

1. D. S. Belic, G. H. Dunn, T. J. Morgan, D. W. Mueller, and C. Timmer, *Phys. Rev. Lett.* **50**, 339 (1983).
2. K. LaGattuta and Y. Hahn, *J. Phys. B* **15**, 2101 (1982).
3. K. LaGattuta and Y. Hahn, *Phys. Rev. Lett.* **51**, 558 (1983).
4. H. E. Saraph and M. J. Seaton, *Phil. Trans.* **271**, 1 (1971).
5. M. J. Seaton, *Rep. Prog. Phys.* **46**, 167 (1983).
6. M. J. Seaton and P. J. Storey, in *Atomic Processes and Applications* (North Holland, 1976).
7. A. Burgess, D. G. Hummer, and J. A. Tully, *Phil. Trans.* **266A**, 225 (1970).

ANGULAR DEPENDENCE OF DIELECTRONIC RECOMBINATION CROSS SECTIONS

K. J. LaGattuta

Department of Physics, University of Connecticut, Storrs, CT 06268 USA

Past calculations of dielectronic recombination total cross sections (σ^{DR}), for singly charged target ions^{1,2}, have compared poorly with the results of recent crossed beam coincidence measurements^{3,4}. The experimental σ^{DR} is now known to be ~ 5 (Mg^{1+}) to ~ 10 (Ca^{1+}) times larger than the theory, for these ions. By contrast, calculations of σ^{DR} for few times charged ions⁵ have compared more favorably with results of merged beam noncoincidence experiments⁶. It has been suggested that electric field induced mixing⁷ of high Rydberg states levels, in the interaction region, could be responsible for the enhancement of measured σ^{DR} values. One expects that such mixing should occur most readily in the lowest charge state, $Z = 1$, but detailed Z dependent calculations are still lacking. Meanwhile, other possibilities may exist.

In this context, it is worth pointing out that the coincidence data was accumulated at fixed geometry; i. e., the outgoing stabilizing photon was detected at fixed angle with respect to the incoming electron beam. Further, in the Mg^{1+} experiment, both the electron beam and the stabilizing photon made fixed angles with respect to the direction of the static electric field which existed in the interaction region. Hence, these data may reflect an angular dependence, while the total σ^{DR} values, of course, do not.

For select ions, we shall calculate σ^{DR} differential in θ , the angle made by the outgoing stabilizing photon with a space fixed direction, and dependent on photon polarization. The space fixed direction will be either the electron beam axis or, when there is an applied electric field, the direction of this field. In the latter case, explicit dependence of σ^{DR} on the angle made by the incoming electron beam, θ_e , and the space fixed axis will be included. The isolated resonance approximation will be invoked in a single-configuration, no-coupling, distorted-wave formalism.

Preliminary results for Mg^{1+} , with an applied electric field of magnitude 24 V/cm in the interaction region, show changes in σ^{DR} of $\lesssim 50\%$, when both θ and θ_e are varied; i. e., this is the difference between the maximum and minimum σ^{DR} values.

This work was supported in part by the US DOE

References

1. K. LaGattuta and Y. Hahn, J. Phys. B15, 2101 (1982)
2. I. Nasser and Y. Hahn, Phys. Rev. A30, 1558 (1984)
3. D. Belic et al, Phys. Rev. Lett. 50, 339 (1983).
4. J. Williams, Phys. Rev. A29, 2936 (1984)
5. D. McLaughlin and Y. Hahn, Phys. Rev. A27, 1389 (1983)
6. P. Dittner et al, Phys. Rev. Lett. 51, 31 (1983)
7. K. LaGattuta and Y. Hahn, Phys. Rev. Lett. 51, 558 (1983)

DIELECTRONIC RECOMBINATION SATELLITE STRUCTURE OF
LITHIUM-LIKE IONS*

L. J. Roszman and A. W. Weiss

National Bureau of Standards
Gaithersburg, Maryland 20899

The total rate of dielectronic recombination is critically important for modelling the ionization balance in high temperature plasmas. However, this recombination process also gives rise to spectral lines which are usually satellitic to lines of the recombining ion, and which are often useful for diagnostic purposes.

We have carried out calculations of the dielectronic recombination lines for the process $e + \text{Ar}^{15+}$ and $e + \text{Fe}^{23+}$, i.e. the recombination of lithium-like ions to form beryllium-like ions. In particular, we concentrate on the $\Delta n \neq 0$ transitions where the principal quantum number change is $3 \rightarrow 2$. The bound orbital basis was computed in the Hartree-Fock approximation. The dielectronic and bound state wave function calculations themselves included all intra-complex configuration interaction as well as Pauli approximation relativistic corrections, i.e. intermediate coupling. The continuum functions were computed in the distorted wave approximation using the semiclassical approximation for exchange with the ion core.

Wavelengths were estimated by referring the calculated energy levels to the relevant levels of the lithium-like ion, a procedure which we expect to compensate for most of the residual correlation and relativistic errors.^{1,2} Unfortunately, configuration interaction and intermediate coupling sometimes make this procedure ambiguous. While selection was always made on the basis of dominant configurations, in these cases we expect our accuracy to be somewhat degraded. We should note that strong configuration mixing also leads to a number of transitions which are not satellitic to any transition in the Li-like ion. For instance, the transition $3s^2 - 2s3p$ is made allowed by configuration interaction but cannot be construed as a lithium-like satellite.

Intensities depend on the dielectronic capture (autoionization) rate as well as the radiative rate and these have been computed in the conventional 'isolated resonance' approximation as a function of temperature. We also investigate, for selected cases, the competition between direct radiative recombination and dielectronic recombination, by including the coherent interference between dielectronic and direct matrix elements.

*This work was supported in part by the Department of Energy, Office of Magnetic Fusion Energy.

References

1. A. H. Gabriel and C. Jordan, *Nature* **221**, 947 (1969).
2. A. H. Gabriel, *Mon. Not. Roy. Astron. Soc.* **160**, 99 (1972).

DIABATIC STATES OF THE H_2 MOLECULE FOR THE DESCRIPTION OF
 $H_2^+ + e$, $H^- + H^+$, and $H(1s) + H(n\ell)$ COLLISIONS

P. Quadrelli and K. Dressler

Physical Chemistry Laboratory, ETH-Zentrum, CH-8092 Zurich, Switzerland

The properties of the excited states of the H_2 molecule are related to the cross sections of a variety of collision processes involving as initial or final states the systems $H_2^+ + e$, $H^- + H^+$, and $H(1s) + H(n\ell)$.

For the first three excited $1\sigma_g^+$ states of H_2 accurate ab initio wavefunctions, electronic energy curves and nonadiabatic coupling functions are available in the adiabatic electronic basis, covering a wide range of internuclear distances R .¹ In order to solve the coupled oscillator problem for the vibrationally bound excited states in a nonadiabatic representation, the electronic states are transformed into a diabatic electronic basis which is defined by zero dynamical coupling at all R values and by the unit transformation matrix for $R \rightarrow \infty$ (Fig. 1a). Comparison between theory and experiment shows that the resulting nuclear dynamical energies of the bound states are accurate within a few cm^{-1} for the lowest levels and within 50 cm^{-1} for the levels involving the largest nuclear kinetic energy.

Nevertheless the ab initio diabatic states generated by this definition have no resemblance with the diabatic states needed in the description of, e.g., dissociative recombination $H_2^+ + e \rightarrow H(1s) + H(2s,2p)$. We have constructed a diabatic basis (Fig. 2a) similar to the one discussed by Hazi, Derkits and Bardsley² by fitting the lowest three of the diagonalized adiabatic energy curves (Fig. 2b) to the corresponding ab initio electronic energies of the EF, GK, and $H 1\sigma_g^+$ states in the interval $R=1-6$ au.

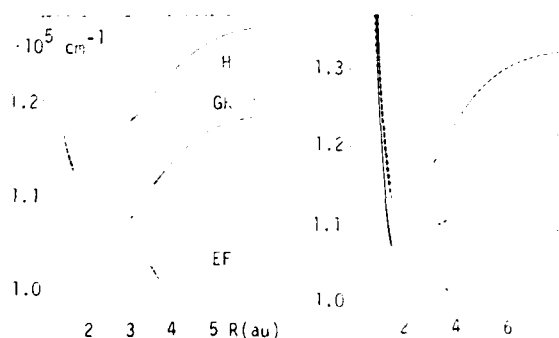


FIGURE 1a. Ab initio

diabatic (solid) and adiabatic (dashed) energies.

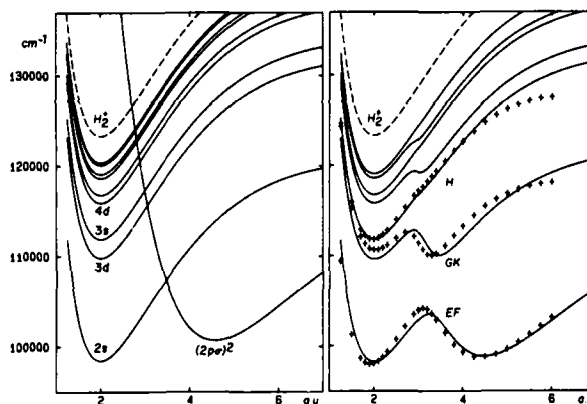


FIGURE 2a. Fitted
 diabatic energies

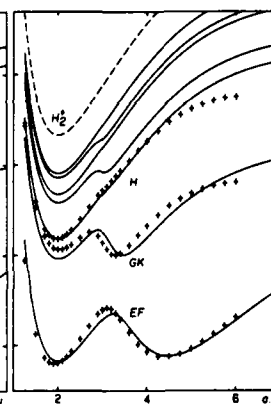


FIGURE 2b. Ab initio (+) and
 fitted adiabatic energies

Using the fitted adiabatic energy curves (Fig. 2b) we can simulate the diabaticizing transformation which was applied to the three ab initio adiabatic states (Fig. 1a) by selecting only the lowest three of the diagonalized electronic states and their dynamical coupling functions: The diabatic states generated by back transformation of this artificial adiabatic basis of dimension three (Fig. 1b) differ greatly from the corresponding ones in the original set (Fig. 2a), but they are qualitatively similar to the diabatic curves generated from the ab initio data (Fig. 1a).

We conclude that (i) a small number of accurately known adiabatic electronic states with associated coupling functions suffices for an adequate description of the vibrationally bound states, (ii) empirically chosen diabatic electronic states may be useful for calculations of collision cross sections, (iii) simultaneous accurate descriptions of the vibrationally bound states and of the collision processes which take place in the energy continuum above $H(1s) + H(2\ell)$ require an electronic basis of large dimension even if the individual electronic wavefunctions are very accurate.

References

1. L. Wolniewicz and K. Dressler, *J. Chem. Phys.* **82** (1985, in press).
2. A.G. Hazi, C. Derkits, and J.H. Bardsley, *Phys. Rev. A* **27**, 1751 (1983).

THE DETERMINATION OF INTERNAL ENERGIES OF MOLECULAR IONS
FROM ELECTRON IMPACT DISSOCIATION MEASUREMENTS

J.B.A. Mitchell, H. Hus*, and R. Janssen†

Department of Physics, The University of Western Ontario,
London, Ontario, Canada N6A 3K7

*Permanent Address: Dept. de Physique, Université Catholique de Louvain,
Louvain-la-Neuve, Belgium.

†Permanent Address: Technical University, Eindhoven, The Netherlands.

The dissociative recombination of molecular ions with electrons is influenced strongly in some cases by the initial excitation state of the recombining ion. Indeed for certain ions, a change of a few tenths of an eV of internal energy can lead to a change in the reaction cross section of several orders of magnitude. This situation occurs when the potential energy curve for the neutral dissociating state does not intersect the ion state in the vicinity of the ground vibrational level. Such is believed to be the case for H_2^+ , H_3^+ , HeH^+ and He_2^+ . For other ions the effects of vibrational excitation are less well understood.

The Merged Electron-Ion Beam Experiment (MEIBE) at UWO has been used recently for measurements of the dissociative recombination of $CO^+(1)$ and $H_3^+(2)$. In such studies it is important that the internal energy of the molecular ions is well characterized. The ions in this experiment are produced in a radiofrequency ion source mounted in the terminal of a Van de Graaff accelerator.

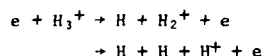
Electron impact dissociation cross sections were measured as a function of centre of mass energy for both ions. This process involves an electronic transition from the bound ground state of the ion to a higher repulsive state and so it exhibits a threshold, the energy of which depends on the internal energy of the initial ions. A Franck-Condon analysis of the ionization of CO to form CO^+ was performed and the relative populations of the vibrational levels of the CO^+ ions used in the experiment were calculated.

This analysis predicted that vibrational states up to $v = 10$ should be populated in the beam. This was confirmed by the measurement of the threshold for CO^+ dissociation.

H_3^+ is formed indirectly by the reaction:



and so the vibrational population of the ions cannot be estimated from Franck-Condon considerations. Measurements of the electron impact dissociation reactions:



have allowed a direct determination of the internal energy of the H_3^+ ions to be made. Preliminary studies indicate that the r.f. source under normal operating conditions produces H_3^+ ions which are very excited

These measurements will be discussed in more detail.

Reference

1. J.B.A. Mitchell and H. Hus. J. Phys. B **18**, 547, 1985.
2. J.B.A. Mitchell, C.T. Ng, L. Forand, R. Janssen and J. Wm. McGowan. J. Phys. B **17**, L909, 1984.

THE POPULATION DISTRIBUTIONS AMONG THE EXCITED LEVELS OF
HYDROGEN-LIKE IONS IN THERMAL PLASMAS

R.J. Hutcheon¹, N.N. Ljepojevic², S. Volonté³, R.W.P. McWhirter⁴

¹ The Nuclear Development Corporation, Pretoria, South Africa

² The Institute of Physics, Belgrade, Yugoslavia

³ The University de Mons, Mons, Belgium

⁴ The Rutherford Appleton Laboratory, Oxfordshire, United Kingdom

For hydrogen-like ions of nuclear charge greater than about 10 their main resonance lines (Lyman lines) are sufficiently narrow from a range of emitting plasma conditions that the two components can be separately resolved spectroscopically. They have been observed from the solar atmosphere, tokamak plasmas used in fusion research and from laser produced plasmas. In most cases their intensity ratio is about 0.5 as would be expected for a statistical population distribution between the $2p^2P_{1/2}$ and $2p^2P_{3/2}$ levels. However there is evidence that significant departures from the 0.5 statistical ratio do occur and it is the purpose of the work reported in this paper to carry out a calculation to explore the circumstances and processes where such departures could take place.

We have done a collisional-radiative calculation where we have taken account of the usual radiative decay processes and electron-collision induced transitions between the principal quantum levels up to $n = 50$ where the sub-levels (l, j) are assumed to be relatively statistically populated down to level $n = 5$. For levels $n = 2, 3$ and 4 separate account is taken of the (n, l, j) sub-levels including in particular the effect of collisional-transitions induced by electrons and ions where the principal quantum number does not change ($\Delta n = 0$ collisions). It is these $\Delta n = 0$ collisions that are largely responsible for the departures of the population of the sub-levels from their statistical distributions. For those transitions induced by ion collision we have included the possibility that various ions of any charge or mass be present in order to cover solar plasmas, fusion plasmas as well as laser produced plasmas. For ions of nuclear charge greater than about 15 the helium-like satellite lines in the neighborhood of the Lyman lines need also to be taken into account. We show how these satellites modify the apparent intensity ratio of the components of the Lyman doublet. Results are presented for a wide range of ions and plasma conditions.

The calculation is also capable of predicting the intensity distributions among other multiplets of hydrogen-like ions such as the HeII λ 1640Å Balmer multiplet for which we also present results. In addition

the usual collisional-radiative ionization and recombination coefficients are calculated and a selection of these are compared with some earlier results.

Finally some experimental data is reviewed and compared with the predictions of the calculation.

ELECTRON-ION RECOMBINATION STUDIES OF CADMIUM

R K Thareja and A Khare

Department of Physics, Indian Institute of Technology, Kanpur-208016, India

Preliminary experimental investigation of the effect of inert gases, in our case helium, at various pressures on the intensity of Cd I and Cd II transitions is presented.

A high voltage, high current pulse is used to produce the cadmium plasma. The plasma expands at low pressure and recombines to produce the population in the next lower ionization stage. The visible spectrum was recorded on an ordinary film, using a three prism spectrograph (Carl Zeiss). In addition to the earlier report¹, we have observed the following cadmium transitions in the presence of helium gas at a pressure of 15 Torr.

Cd I (632.5 nm); $5d\ 2D_{3/2} - 4f\ Cd\ II(533.7nm)$;

Cd I (508.5 nm); $5d\ 2D_{5/2} - z\ 4F_{3/2}$

Cd II (502.5 nm); $5d\ 2D_{3/2} - z\ 4F_{5/2}$

Cd II (488.1 nm); Cd I (467.8 nm).

A strong dependence of the intensity of the emitted spectrum on pressure of background gas is observed, indicating electron-ion recombination in the expanding plasma. An extensive study on the recombination behavior of the transition at 537.8 nm and 533.7 nm, laser transitions² is reported. The variation of line intensity as a function of helium pressure and distance from the metal surface is shown in Fig.(1). It is observed that at certain critical pressure ~ 2.6 Torr of helium, the intensity is maximum. The enhancement of the intensity implies that probably the density of plasma at this point satisfies the conditions for recombination laser³. The results are in agreement with the experimental observations on a similar system for IR transitions⁴.

In addition, it is observed that at a pressure of 5.8 Torr of helium, the emitted cadmium spectrum is weak. The work is in preliminary stages and needs further investigations. These studies will be helpful in optimizing the conditions for plasma recombination laser having the similar electrode

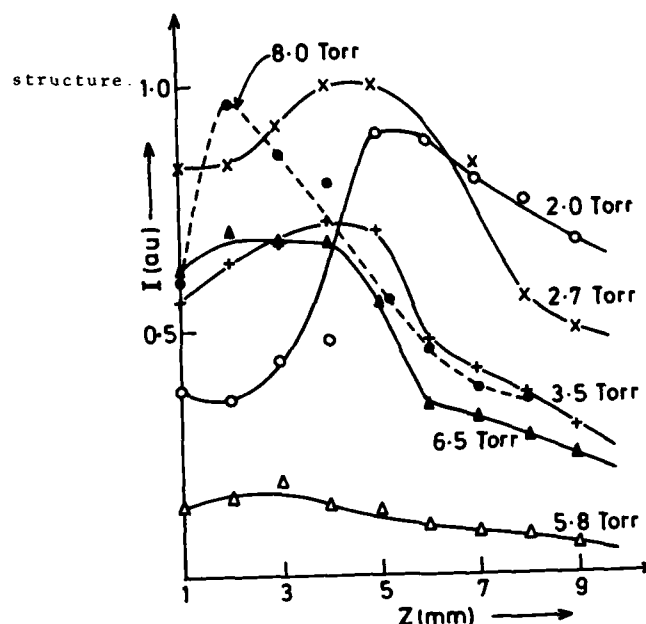


Fig.1 : The variation of line intensity of the transitions at 533.7 nm and 537.8 nm in the presence of helium gas and the distance from the metal surface. The discharge parameters are: Capacitor charging voltage = 14.25 KV, total storage capacitance = 0.166 F.

The project is partially financed by Department of Science and Technology, New Delhi.

References

1. S Goldsmith, S Shalev, R L Boxman Physica DE 13 (1980)
2. O R Wood II and W T Silfvast, J. de Phys C-9-439, 29 (1980)
3. W T Silfvast, L H Szeto and O R Wood II Opt. Lett. 7, 34 (1982)
4. W T Silfvast, L H Szeto and O R Wood II Appl. Phys. Lett. 36, 615 (1980)

DISSOCIATIVE RECOMBINATION OF H_2^+ BY COLLISIONS WITH SLOW ELECTRONS

Hidekazu Takagi and Hiroki Nakamura*

Physics Lab., School of Medicine, Kitasato Univ., Sagami-hara, Kanagawa 228, Japan

*Division of Theoretical Studies, Institute for Molecular Science, Okazaki 444, Japan

I. Introduction

The title process via the $1^1\Sigma_g(2p\sigma_u)^2$ resonance state is studied by the multichannel quantum defect theory (MQDT). Our analysis is different from that of Giusti et al.¹ mainly in two respects: the values of the quantum defect and the two-step MQDT treatment. The main purpose of this work is to investigate the effect of these differences on the cross sections.

II. Method

The basic information necessary for the MQDT treatment is the potential energy curve $E_d(R)$ of the dissociative state, the width $\Gamma(R)$ of this state, and the quantum defect $\mu(R)$. These quantities are obtained from our previous calculations of the elastic scattering of electrons from H_2^+ .² The quantum defect $\mu(R)$ is obtained by subtracting the resonance contribution from the total d-wave phase shift and is fitted by a Padé approximant. The values are shown in Fig.1 in comparison with those used by Giusti et al. Their

quantum defect seems to be a little too large and incorrect. In the actual calculations of the cross sections we have followed the procedure formulated by Seaton.³ The basic quantity in this treatment is

$$R = S e^{-i\pi} = \begin{pmatrix} R_{oo} & R_{oc} \\ R_{co} & R_{cc} \end{pmatrix},$$

where the suffix o(c) indicates the open(closed) channel. The matrices S and C are the same as those in ref.1. The advantage of this Seaton's procedure consists in the fact that the unitarity of the scattering matrix is simply guaranteed by the symmetry of the matrix R .

III. Results

The calculated cross sections are shown in Fig.2. The number of channels included and the convolution procedure to obtain the smoothed cross sections are the same as in ref.1. Our results agree with the experiment⁴ in respect to the general energy dependence at low energies. Especially the position of the first dip at $E \approx 0.1$ eV agrees with the experiment better than that of Giusti et al. This better agreement is attributed to the effect of the proper quantum defect employed here. The effect of the difference in the

two-step MQDT treatment was found to be small. In respect to the magnitude of the cross sections there still remains, unfortunately, a discrepancy between the present result and the experiment. As a byproduct, we have also obtained the d-wave partial cross sections for vibrational excitation of H_2^+ .

Fig. 1

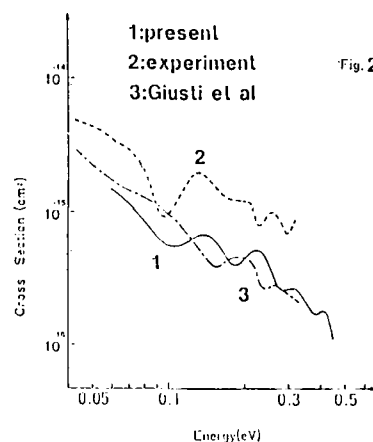
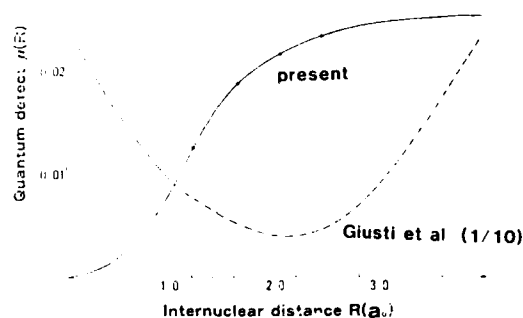


Fig. 2

References

1. A. Giusti-Suzor, J.N. Bardsley, and D.C. Derkits, Phys. Rev. **A28**, 682 (1983).
2. H. Takagi and H. Nakamura, Phys. Rev. **A27**, 691 (1983).
3. M.J. Seaton, Rep. Prog. Phys. **46**, 167 (1983).
4. D. Auerbach et al, J. Phys. **B10**, 3797 (1977).

APPLICATION OF SCHWINGER-TYPE VARIATIONAL METHODS TO THE
COLLISIONS OF POSITRONS WITH ATOMS AND MOLECULES :
AN L^2 - FORMALISM*

M. A. ABDEL-RAOUF
ACHALM STRASSE 13, 7406 MÖSSINGEN, WEST-GERMANY.

STARTING FROM THE SEPARABLE APPROXIMATION FORMALISM¹ OF THE SCHWINGER-TYPE VARIATIONAL METHODS, WE FORMULATE A HIERARCHY OF VARIATIONAL FUNCTIONALS FOR THE SCATTERING AMPLITUDES. WE ALSO DERIVE A PRACTICAL TECHNIQUE IN WHICH A HIERARCHY OF METHODS ARE PRESENTED. THE METHODS ARE APPLICABLE TO MANY-CHANNEL SCATTERING PROBLEMS. ALL TRIAL FUNCTIONS REQUIRED IN THIS TECHNIQUE ARE EXPANDED IN TERMS OF L^2 - VECTORS AND, THEREFORE, IT COINCIDES WITH THE APPROACH INTRODUCED BY MCKOY AND COLLABORATORS² FOR TREATING ELECTRON-MOLECULE SCATTERING WITHIN THE FRAMEWORK OF SCHWINGER'S VARIATIONAL METHOD. THE FIRST THREE MEMBERS OF THE HIERARCHY ARE APPLIED TO THE TWO CHANNEL HUCK PROBLEM. IN THIS CASE, WE INVESTIGATE THE CONVERGENCE OF THE REACTANCE MATRIX ELEMENTS AS THE BASIS SET INCREASES DIMENSIONALLY, AS WELL AS THEIR CONVERGENCE WHEN THE ORDER OF THE VARIATIONAL METHOD IN THE HIERARCHY INCREASES.

THE MAIN PURPOSE BEHIND THIS INVESTIGATION IS TO PROPOSE A PRACTICAL AND REASONABLE APPROACH FOR TREATING COLLISION PROCESSES WITH SPHERICAL AND AXIAL SYMMETRICAL POTENTIALS IN WHICH EXCHANGE EFFECTS DO NOT SHOW UP DURING THE COLLISION AND REARRANGEMENT CHANNELS ARE ALLOWABLE.

THE PROPOSED APPROACH IS APPLIED TO THE INELASTIC SCATTERING OF POSITRONS BY HYDROGEN ATOMS AND THE POSITIVE ION OF THE HYDROGEN MOLECULE.

REFERENCES

1. M. A. ABDEL-RAOUF, PHYS. REPT 108, (1984) 1-163;
PHYS. REV. A30, (1984) 2794.
2. SEE E.G. K. TAKATSUKA AND V. MCKOY, PHYS. REV. A30, (1984) 1734; T. L. GIBSON, M.A.P. LIMA, K. TAKATSUKA AND V. MCKOY, PHYS. REV. A30, (1984), 3005; D.K. WATSON AND V. MCKOY, PHYS. REV. A20, (1979) 1474.

THE THEORY OF THE COLLISIONS OF POSITRONS WITH ALKALI-ATOMS AND ALKALI-LIKE IONS

M. A. Abdel-Raouf
Achalm Straße 13, 7406 Mössingen, West-Germany

It is well known that alkali atoms and alkali-like ions are quantum mechanical systems of extremely high polarizabilities and that their collisions with positrons are at least two-channel problems in which both elastic and rearrangement processes take place even if the scattering energies are zero. This fact makes it reasonable, in any treatment of these problems, to consider frozen core models for the targets and assume that the total collisional cross-sections are predominated by elastic and positronium formation cross-sections to a wide region of incident energies. An excellent approximation, however, can be obtained by switching on the polarization potential of the first channel.

The one valence-electron model of the target q has the total Hamiltonian, (Rydberg units are used):

$$H_V^q = -\nabla_r^2 - \frac{2Z_{\text{eff}}^q}{r} + V_c^q(r), \quad (1)$$

where Z_{eff}^q is the effective charge of the nucleus plus the core of the target, i.e. $Z_{\text{eff}}^q = Z^q - N_c^q$, N_c^q is the number of core electrons. For neutral atoms $Z_{\text{eff}}^q = 1$, for alkali-like ions of one positive charge, i.e. $^{12}\text{Mg}^+$, $^{20}\text{Ca}^+$, $^{38}\text{Sr}^+$, $^{56}\text{Ba}^+$ and $^{88}\text{Ra}^+$, $Z_{\text{eff}}^q = 2$ and for Li-isoelectronic ions from $5\text{B}(2+)$ to $10\text{Ne}(7+)$ $Z_{\text{eff}}^q = 2, 3, \dots, 7$.

The core potentials V_c^q are defined by

$$V_c^q(r) = \sum_i \langle \phi_i^q | \frac{2}{|r-r_i|} - \frac{2Z_{\text{eff}}^q}{r} | \phi_i^q \rangle$$

$$\text{or } V_c^q(r) = -8\pi \sum_j \frac{M_j^q}{j} \sum_{p,s} \frac{m_{p,s}^q}{r} \left(\frac{1}{(\alpha_{ps}^q)^{j_{ps}^q+1}} \right) A_p^q A_s^q$$

$$\begin{aligned} & \frac{A_p^q A_s^q \exp(-\alpha_{ps}^q r) (j_{ps}^q)!}{\sum_{i=1}^{j_{ps}^q-1} i! r^{j_{ps}^q-i} (\alpha_{ps}^q)^{j_{ps}^q-i}} - \\ & - \frac{2Z_{\text{eff}}^q (j_{ps}^q-1)!}{r}, \end{aligned} \quad (2)$$

where M_j^q is the number of core orbitals, j_{ps}^q is the number of electrons in the j th orbital of the target q , A_p^q 's, A_s^q 's, α_{ps}^q 's are given in the tables by Clementi and Roetti¹, and j_{ps}^q is equal to $j_p^q + j_s^q$, $j_{ps}^q = k_p^q + k_s^q + 2$, where k_p^q are integers presented in the tables.

The ground-state energies of the targets are determined by

$$E_V^q = -4\pi \sum_{p,s} A_p^q A_s^q \alpha_{ps}^q \left(\frac{(\alpha_{ps}^q)^2 (j_{ps}^q)!}{(\alpha_{ps}^q)^{j_{ps}^q+1}} \right) -$$

$$\begin{aligned} & - 2(\alpha_{ps}^q)^{-j_{ps}^q} (k_p^q \alpha_p^q + \alpha_s^q - (N^q+1)Z_{\text{eff}}^q + N^q)(j_{ps}^q-1)! \\ & + (\alpha_{ps}^q)^{-j_{ps}^q+1} k_p^q (k_p^q+1)(j_{ps}^q-1)! + 8\pi \sum_{j=1}^{j_{ps}^q} \sum_{p,s} \frac{m_{p,s}^q}{r} A_p^q A_s^q \\ & \frac{A_p^q A_s^q \exp(-\alpha_{ps}^q r) (j_{ps}^q)!}{\sum_{i=1}^{j_{ps}^q-1} i! r^{j_{ps}^q-i} (\alpha_{ps}^q)^{j_{ps}^q-i}} - \\ & - \frac{2Z_{\text{eff}}^q (j_{ps}^q-1)!}{r} \end{aligned} \quad (3)$$

Considering the partial wave expansions of the scattering wave functions of the elastic and rearrangement channels, the coupled static treatment provides us with the coupled integro-differential equations²

$$\{d^2/dx^2 - \ell(\ell+1)/x^2 + (\kappa_1^q)^2\} f_\ell^q(x) = V_\ell^q(x) f_\ell^q(x) + \int_0^\infty K_{12}^q(y,x) f_\ell^q(y) dy \quad (4)$$

$$\begin{aligned} & \{d^2/dy^2 - \ell(\ell+1)/y^2 + (\kappa_2^q)^2\} g_\ell^q(y) = \\ & = 2 \int_0^\infty K_{21}^q(y,x) f_\ell^q(x) dx, \end{aligned} \quad (5)$$

where x is the position vector of the positron relative to the nucleus of the target, and y is defined by $y = \frac{1}{2}(r+x)$. K_{12}^q and K_{21}^q are the coupled kernels of the first and second channels. $U^q(x)$ is the static potential given by

$$\begin{aligned} U^q(x) = & 8\pi \sum_{j=1}^{j_{ps}^q+1} \sum_{p,s} \frac{m_{p,s}^q}{r} (\alpha_{ps}^q)^{j_{ps}^q+1} \frac{A_p^q A_s^q}{(\alpha_{ps}^q)^{j_{ps}^q+1}} \\ & \frac{A_p^q A_s^q \exp(-\alpha_{ps}^q x) (j_{ps}^q)!}{\sum_{i=1}^{j_{ps}^q-1} i! x^{j_{ps}^q-i} (\alpha_{ps}^q)^{j_{ps}^q-i}} \\ & + 2(N^q+1)(Z_{\text{eff}}^q-1)/x. \end{aligned} \quad (6)$$

$(\kappa_1^q)^2$ and $(\kappa_2^q)^2$ are related by $(\frac{1}{2})^2 - 2(\kappa_1^q + \kappa_2^q)^2 + 1$. (Note that all electrons of the targets are assumed here to be of $l=0$ -type). The polarization potential of the target can be switched on by replacing $U^q(x)$, e.g., by $U^q(x) + U_{\text{pol}}^q(x)$, U_{pol}^q is determined using the l -state wave functions of the valence electrons, i.e.

$$U_{\text{pol}}^q = -\frac{4\pi}{3} \sum_{p,s} A_p^q A_s^q \alpha_{ps}^q \left(\frac{(\alpha_{ps}^q)^2 (j_{ps}^q)!}{(\alpha_{ps}^q)^{j_{ps}^q+1}} \right) -$$

In our computer program we calculated the elastic and positronium formation cross-sections for all partial waves corresponding to $\ell \leq 10$, where ℓ is the total angular momentum quantum number.

References

1. Clementi and Roetti, *At. Data and Anal. Tables*, 14, 107 (1974).
2. M.A. Abdel-Raouf, *J. Chem. Phys.*, 61, 1288 (1974); A.J. Stauffer, *Phys. Rev. A*, 10, 1000 (1974); F.P. Moynihan and A.J. Stauffer, *Phys. Rev. A*, 10, 1000 (1974).

NEW THEORY OF THE ANNIHILATION PARAMETER FOR e^+ - ATOM (MOLECULE) SYSTEMS.

E. Ficocelli Varracchio

Department of Chemistry, University of Bari, Via Amendola 173,
70126 Bari, ITALY.

The effective number of annihilation electrons (Z_a), in e^+ - atom (molecule) systems, is defined by the integral

$$Z_a = \langle k_i, \psi_i^N | \sum_{j=1}^N \delta(y - z_j) | k_i, \psi_i^N \rangle \quad (1)$$

whose evaluation characteristically requires a knowledge of the $|k_i, \psi_i^N\rangle$ full system wave function. In the spirit of a recent approach to the problem of e^+ - atom (molecule) collisions, we wish to reformulate the matrix element (1) in the language of Field Theoretic (FT) Green's functions. The formal advantage of the FT formulation derives from the fact that the final amplitudes involved will depend on a smaller number of coordinates, than the full system wave function. Such an aspect should, therefore, make them more readily amenable to numerical calculations.

By using the FT approach it is not difficult to show that the knowledge of Z_a , in (1), can be completely reduced to the determination of the following two-particle propagator

$$K(\tau y, \tau' y') = \frac{1}{i^2} \langle \psi_i^N | T[\psi(\tau) \psi(y) \psi^\dagger(y') \psi^\dagger(\tau')] | \psi_i^N \rangle \quad (2)$$

where ψ (ψ^\dagger) and Ψ (Ψ^\dagger) are the destruction (creation) field operators for the electron and positron, respectively, T is Wick's time ordering operator (see Ref. [1] for more details) and $|\psi_i^N\rangle$ represents the target state wave function. The amplitude in (2) describes the fully correlated motion of a positron-electron pair and, in the present FT formalism, it is the quantity in terms of which the annihilation parameter can be completely expressed.

It can be shown that the K amplitudes, in (2), obeys the following (Bethe-Salpeter) equation

$$K = \Delta S + S \frac{\delta \Sigma}{\delta U} S \quad (3)$$

where Δ and S are the one-particle propagators for the electron and the positron, respectively, while Σ is an "optical potential" of the theory, completely presiding over elastic scattering processes in the system. The first term on the r.h.s. of (3) ($\Delta \cdot S$) represents the lowest order (Hartree) approximation to the K propaga-

tor, that completely neglects correlation effects in the motion of the pair. Correlation effects are fully contained in the second term on the r.h.s., involving the functional derivative of the optical potential.

Details of the formalism and explicit numerical applications to the e^+ - H system will be illustrated at the Conference.

References

1. E. Ficocelli Varracchio, Ann. Phys., (N.Y.) 145, 131 (1983).

POSITRONIUM FORMATION IN D-WAVE POSITRON-HYDROGEN SCATTERING

C.J. Brown and J.W. Humberston

Department of Physics and Astronomy, University College London

The Kohn variational method has been used to calculate the d-wave contribution to the elastic scattering and positronium formation cross-sections for positrons in collision with hydrogen atoms in the Ore gap (the energy interval between the positronium formation threshold, 6.8 eV, and the threshold for excitation of the $n = 2$ level of the hydrogen atom, 10.2 eV). The general technique and form of the trial function is very similar to that used by the present authors for s- and p-wave scattering (Humberston 1982, 1984; Brown and Humberston 1984) except that there are now short range correlation terms of three symmetries. Thus,

$$\begin{aligned} \psi_1 = & Y_{2,0}(\hat{r}_1) \phi_H(r_2) k^{\frac{1}{2}} \left[j_2(kr_1) - K_{11}^t n_2(kr_1) [1 - \exp(-\lambda r_1)] \right]^5 \\ & - Y_{2,0}(\hat{r}_1) \phi_{Ps}(r_3) K_{21}^t (2\kappa)^{\frac{1}{2}} n_2(\kappa\rho) [1 - \exp(-\mu\rho)]^7 \\ & + Y_{2,0}(\hat{r}_1) r_1^2 \sum_i a_i g_i + \bar{Y}_{2,0}(\hat{r}_1, \hat{r}_2) r_1 r_2 \sum_i b_i g_i \\ & + Y_{2,0}(\hat{r}_2) r_2^2 \sum_i c_i g_i \\ \psi_2 = & Y_{2,0}(\hat{r}_1) \phi_{Ps}(r_3) (2\kappa)^{\frac{1}{2}} \left[j_2(\kappa\rho) - K_{22}^t n_2(\kappa\rho) [1 - \exp(-\mu\rho)] \right]^7 \\ & - Y_{2,0}(\hat{r}_1) \phi_H(r_2) k^{\frac{1}{2}} K_{12}^t n_2(kr_1) [1 - \exp(-\lambda r_1)]^5 \\ & + Y_{2,0}(\hat{r}_1) r_1^2 \sum_i d_i g_i + \bar{Y}_{2,0}(\hat{r}_1, \hat{r}_2) r_1 r_2 \sum_i e_i g_i \\ & + Y_{2,0}(\hat{r}_2) r_2^2 \sum_i f_i g_i \end{aligned}$$

where $g_i = \exp \left[-(\alpha r_1 + \beta r_2 + \gamma r_3) \right] r_1^{k_i} r_2^{l_i} r_3^{m_i}$

The nomenclature is the same as that used previously and the summation over i for each symmetry includes all terms with

$$k_i + l_i + m_i \leq \omega$$

where k_i, l_i, m_i and ω are non-negative integers.

Results have been obtained at four positron energies corresponding to $k = 0.71, 0.75, 0.80$ and 0.85 (in units of a_0^{-1}) for a sequence of trial functions with $\omega = 1, 2, \dots, 6$ (4, 10, 20, 35, 56 and 84 terms of each symmetry). From the variation of the results with respect to ω we can be reasonably confident that the cross-sections given in the tables (with $\omega = 6$), have

converged to within 10% of their exact values. However, the convergence is not quite as rapid as we would wish, most probably because the results are not yet fully optimised with respect to the non-linear parameters in the trial functions.

Also given in the tables are the well converged s- and p-wave cross-sections obtained by the present authors. The present p-wave results are slightly different from those published by Brown and Humberston, having been obtained with an improved choice of values of the non-linear parameters which gives much more rapid convergence with respect to ω .

One of us (C.J.B.) acknowledges the award of a SERC Research Studentship.

Table 1 Elastic scattering cross-sections (in units of πa_0^2)

$k(a_0^{-1})$	s-wave	p-wave	d-wave
0.71	0.026	0.800	0.32
0.75	0.043	0.724	0.41
0.80	0.065	0.622	0.42
0.85	0.086	0.547	0.41

Table 2 Positronium formation cross-sections (in units of πa_0^2)

$k(a_0^{-1})$	s-wave	p-wave	d-wave
0.71	0.0041	0.027	0.0006
0.75	0.0044	0.365	0.33
0.80	0.0049	0.482	0.81
0.85	0.0058	0.561	1.10

References

- Brown C.J. and Humberston J.W. 1984 J. Phys. B: Atom. Molec. Phys. **17** L423
- Humberston J.W. 1982 Can. J. Phys. **60** 591
- 1984 J. Phys. B: Atom. Molec. Phys. **17** 2353

ELECTRON CAPTURE BY INTERMEDIATE ENERGY POSITRONS FROM ALKALI ATOMS

J. M. Wadehra and Sultana N. Nahar

Department of Physics, Wayne State University, Detroit, Michigan 48202 USA

Alkali atoms are isoelectronic, in the valence shell, with the hydrogen atom and in most collision processes it is reasonably accurate to treat alkali atoms as being hydrogenlike. For example, the cross sections for positronium formation in alkali atoms can be obtained by first reducing the alkali atom to a hydrogenlike system by averaging over the motion of the core electrons. The valence ns electron is then the only possible actively transferring electron. However, unlike hydrogen, in the case of alkali atoms the process of positronium formation is exoergic since the ionization potential of all alkali atoms is smaller than the binding energy of positronium (6.8 eV). The purpose of this study is to investigate the cross sections for positronium formation by impact of positrons in the intermediate energy range where the Born approximation becomes applicable.

The static potential of the ion core, as experienced by either the active electron or the projectile positron, can be most conveniently obtained by integrating over the core electrons using the wave functions of Li^+ (or Na^+ etc.). In some calculations,

the static potential is replaced, for computational ease, by an appropriately chosen pseudopotential. The cross sections for the process of electron transfer in alkali atoms are then calculated by using the distorted wave Born approximation (DWBA) in a manner similar to its use for atomic hydrogen.¹

Figure 1 shows the differential cross sections using the plane wave Born approximation for positronium formation in Li for impact energies of 100 eV and 200 eV. The post-prior discrepancy for this rearrangement process is observed to be small. A number of checks on the computer code have been made to ensure its correctness. The deep minimum in the differential cross section, arising due to the cancellation of the contributions to the scattering amplitude from the attractive and repulsive parts of the positron-atom interaction, appears only in the first Born calculations.

Both differential and total cross sections for positronium formation in heavier alkali atoms (Na, K, Cs, Rb) have also been obtained using the DWBA. However, for computational economy, the positron-atom interactions for these alkali atoms have been replaced by a judicious choice of pseudopotentials.

This research has been supported by the National Science Foundation.

Reference

1. R. Shakeshaft and J. M. Wadehra, Phys. Rev. A22, 968 (1980).

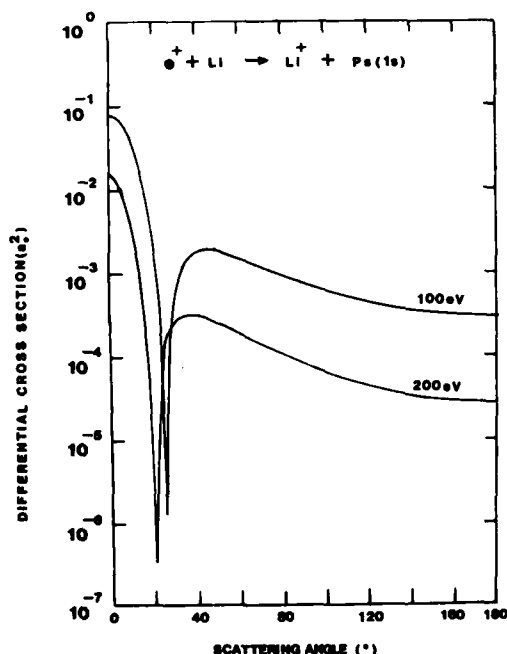


FIGURE 1 Differential cross sections for positronium formation for positron impact energies of 100 eV and 200 eV.

POSITRON- AND ELECTRON-ALKALI (SODIUM AND POTASSIUM) TOTAL CROSS SECTION MEASUREMENTS*

T.S. Stein, C.K. Kwan, R.D. Gomez, Y.-F. Hsieh, W.E. Kauppila, and Y.J. Wan

Department of Physics and Astronomy, Wayne State University, Detroit, Michigan 48202, USA

We have set up an experimental system to measure absolute total scattering cross section (Q_T) values for positrons and electrons colliding with alkali atoms using a beam transmission technique. Prior to the present experiments, Q_T measurements have been reported in the literature for positrons colliding with only room-temperature gases (the inert gases and various molecules).

Our positrons are produced by an ^{11}C source created by the $^{11}\text{B}(p,n)^{11}\text{C}$ reaction using a 4.75 MeV proton beam from a Van de Graaff accelerator. Low energy positrons emitted by the ^{11}C source are guided by a curved axial magnetic field to our alkali scattering apparatus shown schematically in Fig. 1.

We have recently completed measurements of $e^+-\text{K}$ and $e^--\text{K}$ Q_T values¹ and have now measured $e^--\text{Na}$ Q_T values in preparation for the corresponding measurements with positrons in the same apparatus and using the same technique. Our initial $e^--\text{Na}$ Q_T measurements are shown in Fig. 2 along with other experimental²⁻⁴ and theoretical⁵ results.

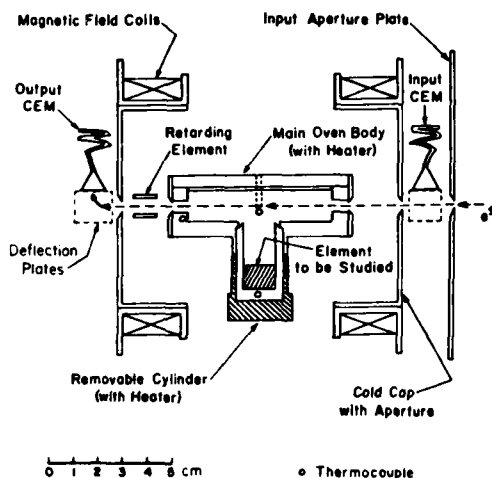
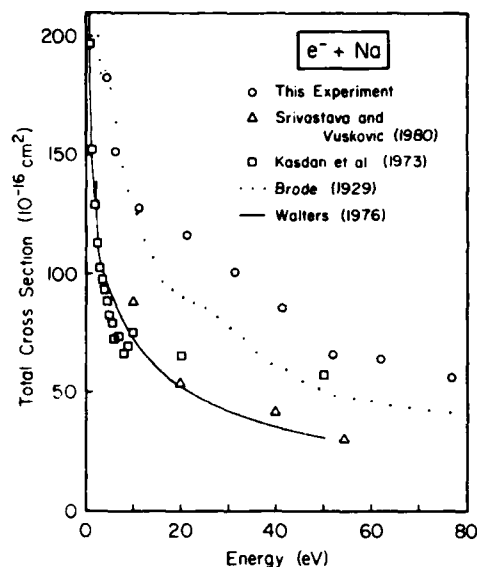


FIGURE 1 Schematic diagram of alkali scattering system.

The preliminary indications are that although there are considerable differences between existing experimental electron Q_T results for both Na and K, we are observing some consistent patterns in these measurements. Our measurements and those of Brode² tend to be in good

FIGURE 2 $e^--\text{Na}$ total scattering cross sections.

agreement at low energies and the general shapes of Brode's Q_T curves are quite similar to ours over the entire energy range of overlap for both Na and K, although we have higher values than Brode at the higher energies. Our Q_T curves differ in shape from those of Kasdan et al.³, with our Q_T values being about twice as large as those of Kasdan et al. at low energies, but tending to merge with their results at higher energies.

Comparisons of our $e^+-\text{K}$ and $e^--\text{K}$ measurements indicate an overall degree of similarity between positron and electron scattering that has not been observed for any other target atoms or molecules.

*This work supported by the National Science Foundation.

References

1. T.S. Stein, R.D. Gomez, C.K. Kwan, Y.-F. Hsieh, and W.E. Kauppila, to be published.
2. R.B. Brode, Phys. Rev. **34**, 673 (1929).
3. A. Kasdan, T.M. Miller, and B. Bederson, Phys. Rev. A **8**, 1562 (1973).
4. S.K. Srivastava and L. Vuskovic, J. Phys. B **13**, 2633 (1980).
5. H.R.J. Walters, J. Phys. B **9**, 227 (1976).

POSITRONIUM FORMATION IN LOW-ENERGY POSITRON-H⁻ COLLISIONS

Richard J. Drachman

Laboratory for Astronomy and Solar Physics, Goddard Space Flight Center, Greenbelt, MD 20771 USA

Positronium (Ps) formation in collisions between e⁺ and H⁻ ions is an especially interesting process since it is exothermic and the lowest three levels of Ps can be formed even at zero incident energy. In addition, the Coulomb attraction between the initial particles gives a formation rate that increases like 1/v as the incident energy decreases. Because of this attraction, many partial waves must be retained in the calculation even at zero energy.

We have begun a program to compute the cross-sections for formation into all the open Ps channels at very low energy, using a series of increasingly accurate approximations. These are based on the two-state trial function

$$\Psi = F(\vec{x})\phi(r_1, r_2) + G(\vec{R}_1)\phi(\rho_1)\psi(r_2) + G(\vec{R}_2)\phi(\rho_2)\psi(r_1),$$

where ϕ is the H⁻ wave function, ϕ and ψ represent Ps and H respectively, and F and G are the wave functions of the incident e⁺ and the outgoing Ps center of mass.

In the simplest approximation, the incident e⁺ moves in a pure Coulomb potential, giving rise at zero energy to Bessel functions for the partial-wave components of F:

$$F_L(x) = \sqrt{\left(\frac{\pi}{kx}\right)} J_{2L+1}(\sqrt{8}x),$$

and the outgoing Ps atom is in a plane wave state; exchange is neglected in the final state. This Coulomb-Born approximation has been shown to give partial cross-sections in serious violation of the unitarity limits. In the next approximation, the e⁺ moves in the more realistic potential of the frozen H⁻ ion, which is repulsive at short distances but attractive at large. Our preliminary result for s-waves is much more reasonable:

$$\sigma_0 = \frac{0.15}{k^2} \pi a_0^2$$

More complete results in this approximation will be reported at the Conference.

We expect eventually to solve the coupled equations resulting from the two-state trial function above, but in the meantime an estimate of the plausibility of this result can be obtained using a complex quantum-defect method¹. To do this, we relate the cross-section to the parameters of the Rydberg resonances in the Ps + H system². These resonances are produced by the coupling of the Ps + H open channel to the e⁺H⁻ Coulomb bound states of the closed channel. If we represent the complex energies of these bound states in terms of quantum defects we can write

$$E(NL) = E(\text{res}) - i\frac{\Gamma}{2} = E(H^-) - \frac{1}{(N - \mu_N)^2},$$

where μ is the quantum defect and is expected to vary slowly with N. Using the relation¹ for the phase shift $\delta = \pi\mu$ we can get an estimate for the complex phase shift just above threshold in the e⁺ + H⁻ channel, and from that can derive a value for the Ps formation cross-section. The best values for the position and width of the lowest s-wave resonance are those of Ho²:

$$E(\text{res}) = -1.205 \text{ Ry and } \Gamma = (5.5 \pm 1.8) \times 10^{-3} \text{ Ry.}$$

From these we derive the result

$$\sigma_0 = \frac{0.26 \pm .08}{k^2} \pi a_0^2,$$

where we have assumed that the quantum defect is actually independent of N. This estimate is fairly consistent with our distorted-wave result, and gives us some confidence in the reasonableness of that approximation.

References

1. M. J. Seaton, Rep. Prog. Phys. **46**, 167 (1983).
2. R. J. Drachman and S. K. Houston, Phys. Rev. A **12**, 885 (1975); Y. K. Ho, Phys. Rev. A **17**, 1675 (1978).

PARTIAL CROSS SECTIONS FOR POSITRON SCATTERING FROM HELIUM

L. M. Diana,* D. L. Brooks,* S. C. Sharma,*
P. G. Coleman,* P. K. Pendleton,*
B. E. Seay,* and L. S. Fornari*

* Center for Positron Studies, Department of Physics, University of Texas at
Arlington, Arlington, Texas 76019 USA

+ School of Mathematics and Physics, University of East Anglia, Norwich NR4 7TJ,
U.K.

There has been considerable recent activity in the measurement of inelastic cross sections for positrons scattered from helium. Total positronium formation cross sections, Q_{ps} , have been reported by both the Texas^{1,2} and the University College London³ group. Diana *et al.*⁴ and Sueoka⁵ have reported total ionization cross sections, Q_{ion} , and Coleman and Hutton⁶ and Sueoka⁵ have measured cross sections for the excitation to the 2^1s state. In addition Coleman *et al.*⁷ have published cross sections for excitation plus ionization for positrons scattered into a forward cone of 60° half-angle.

However, total excitation cross sections, Q_{ex} , have yet to be measured, and it is for this reason, in part, that a partitioning of the total cross section, Q_{tot} , is of interest.

The result is shown in Figure 1. The Q_{tot} curve is a smoothed rendition of the available data.⁸ Q_{el} is extrapolated from below the first inelastic threshold to meet calculated values at about 150 eV and above. It is unlikely that this Q_{el} is in error by more than 10%; therefore, since Q_{el} is such a small part of Q_{tot} between 25 and 250 eV, the consequent uncertainty in the total inelastic cross section should not exceed a few percent. Q_{ps} is a smooth

Similarly, the dashed curve serves as a guide through the Q_{ion} values from reference 4. This curve indicates that expectations for Q_{ex} are about $0.08\pi a_0^2$ at about 100 eV increasing to about $0.17\pi a_0^2$ in the neighborhood of 200 eV. Sueoka⁵ finds Q_{ex} to be approximately $0.065\pi a_0^2$ at 100 eV. Sueoka's values for Q_{ion} , which agree within experimental uncertainty with those obtained for electron scattering, if used in this way, would predict Q_{ex} ranging from about 0.37 to $0.45\pi a_0^2$ between 60 and 100 eV.

References

1. L. S. Fornari, L. M. Diana, and P. G. Coleman, *Phys. Rev. Lett.* **51**, 2276 (1983).
2. L. M. Diana, S. C. Sharma, L. S. Fornari, P. G. Coleman, P. K. Pendleton, D. L. Brooks, and B. E. Seay, in *Positron Annihilation -- Proceedings of the 7th International Conference on Positron Annihilation*, Jan. 6-11, 1985, New Delhi, India, edited by P. C. Jain, R. M. Singru, and K. P. Gopinathan (World Scientific Publishing Co. Pte. Ltd., Singapore, to be published).
3. M. Charlton, G. Clark, T. C. Griffith, and G. R. Heyland, *J. Phys. B* **16**, L465 (1983).
4. L. M. Diana, L. S. Fornari, S. C. Sharma, P. K. Pendleton, and P. G. Coleman in *Positron Annihilation -- Proceedings of the 7th International Conference on Positron Annihilation*, Jan. 6-11, 1985, New Delhi, India, edited by P. C. Jain, R. M. Singru, and K. P. Gopinathan (World Scientific Publishing Co. Pte. Ltd., Singapore, to be published).
5. O. Sueoka, *J. Phys. Soc. Jpn.* **51**, 3757 (1982).
6. P. G. Coleman and J. T. Hutton, *Phys. Rev. Lett.* **45**, 2017 (1980).
7. P. G. Coleman, J. T. Hutton, D. R. Cook, and C. A. Chandler, *Can. J. Phys.* **60**, 584 (1982).
8. W. E. Kauppila and T. S. Stein, *Can. J. Phys.* **60**, 471 (1982).

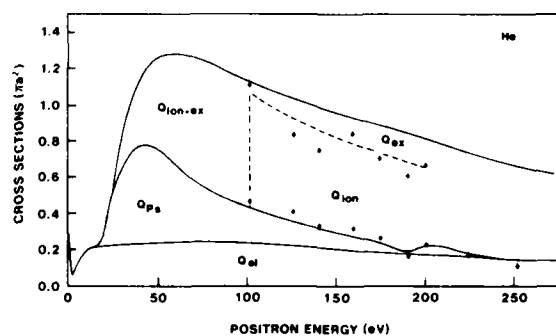


FIGURE 1 Partial cross sections for positron-helium scattering. See text for discussion.

curve through the data of reference 1 and a curve to guide the eye through the plotted data from reference 2.

IONISATION OF HELIUM BY POSITRON IMPACT

D. Fromme, W. Raith and G. Sinapius

Fakultät für Physik, Universität Bielefeld, D-4800 Bielefeld, Fed. Rep. of Germany

Ionisation of helium by positron impact may be accomplished by two processes: ionisation by positronium formation (threshold $E_{ps} = 17.8$ eV; cross section σ_{ps}) and ionisation without simultaneous positronium formation (threshold $E_{ion} = 24.6$ eV; cross section σ_{ion}). Knowledge of both σ_{ps} and σ_{ion} is necessary - in addition to the elastic (σ_{el}) and the excitation (σ_{ex}) cross sections - for partitioning the positron total cross section σ_t into its contributions and for detailed comparisons with electron cross sections. However, for both cross sections there is only insufficient information available up to now: Measurements were performed for restricted energy ranges only. Positronium formation cross sections were measured by two groups^{1,2} with essentially different results. The first measurements of $\sigma_{ex} + \sigma_{ion}$ were performed by Coleman et al³ and actually are differential cross sections integrated from 0° to 60° . The results of Sueoka⁴ agree with measurements for ionisation of helium by electron impact⁵, except for the lowest energies above threshold.

We built up an apparatus which enables measuring of both, σ_{ps} and σ_{ion} . To our knowledge this is the first experimental set-up allowing detection of the ions produced by positron impact. The whole apparatus is surrounded by coils providing a longitudinal magnetic field of up to 200 G. Positrons are emitted by a ^{22}Na -source and moderated by an annealed tungsten foil installed obliquely in front of the source. Slow positrons are accelerated towards the scattering tube. The scattering tube consists of a 50 cm long narrow glass tube lined with a spiral of tungsten wire on the inside. The tungsten spiral serves two purposes: It defines the potential of the scattering tube and, by feeding a direct current through the wire, it maintains a longitudinal electric field inside the tube to extract the ions produced in $e^+ - \text{He}$ collisions. Gas is continuously supplied through two holes in the middle of the tube and pumped at both ends. Behind the scattering tube the charged particles are accelerated towards the microchannel plate detectors. Positrons and ions are separated by a crossed electric and magnetic field (ExB) analyser and reach detectors 1 and 2, respectively. The velocities of positrons and ions differ substantially because of their different masses.

For measurements of σ_{ion} , those ions are counted reaching detector 2 with an appropriate delay after detection of a positron by detector 1. The time-delay spectrum is analysed using a time-to-amplitude converter and a multichannel analyser. For measurements of $\sigma_{ps} + \sigma_{ion}$ all the ions reaching detector 2 are counted.

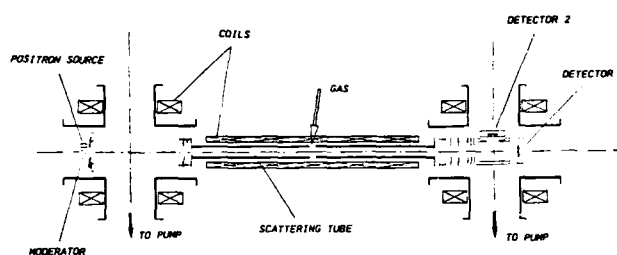


FIGURE 1 Schematic diagram of the apparatus.

The construction of the apparatus was finished recently. First measurements of helium-ion production rates were performed in the σ_{ion} -mode⁶. They indicate an energy dependence slightly different from electron ionisation cross sections⁵. At present various tests are performed in order to learn about possible systematic errors.

REFERENCES

1. M. Charlton, G. Clark, T. C. Griffith and G. R. Heyland, *J. Phys.* B 16 (1983) L465
2. L. S. Fornari, L. M. Diana and P. G. Coleman, *Phys. Rev. Lett.* 51 (1983) 2276
3. P. G. Coleman, J. T. Hutton, D. R. Cook and C. A. Chandler, *Can. J. Phys.* 60 (1982) 584
4. O. Sueoka, *J. Phys. Soc. Jpn.* 51 (1982) 3757
5. R. G. Montague, M. F. A. Harrison and A. C. H. Smith, *J. Phys.* B 17 (1984) 3295
6. D. Fromme, W. Raith and G. Sinapius, in 'Positron Annihilation' Proc. of 7th ICPA 1985 ed P. C. Jain, R. M. Singru and K. P. Gopinathan (Singapore: World Scientific) in press

POSITRON EXCITATION OF THE 2^1P STATE OF HELIUM

R.P. McEachran,* L.A. Parcell† and A.D. Stauffer*

* Physics Department, York University, Toronto, Canada M3J 1P3

† School of Mathematics and Physics, Macquarie University, North Ryde, N.S.W. 2113, Australia

We present results for differential and total cross sections for the excitation of the 2^1P state of helium by positron impact. We use a distorted wave approximation similar to that employed in our earlier calculation of the excitation of the 2^1S state.¹

In the present work there is a long range contribution to the T-matrix and we discuss some novel numerical methods used to accurately evaluate this contribution.

The main purpose of this calculation is to provide a theoretical analysis of some recent experimental measurements.^{2,3} Thus we examine the angular range over which the differential cross section has an appreciable magnitude. In addition the relative magnitudes for excitation of the 2^1S and 2^1P states are presented. An analysis is made of the various contributions to the experimentally measured data.

References

1. L.A. Parcell, R.P. McEachran and A.D. Stauffer, J. Phys. B 16, 4249 (1983).
2. P.G. Coleman, J.T. Hutton, D.R. Cook and C.A. Chandler, Can. J. Phys. 60, 584 (1982).
3. O. Sueoka, J. Phys. Soc. Jap. 51, 2381 (1982).

A RELIABLE CALCULATION FOR 2^1S EXCITATION OF HELIUM ATOM BY POSITRON IMPACT

Rajesh Srivastava, Mukesh Kumar and A.N.Tripathi

Department of Physics, University of Roorkee, Roorkee 247667, India

Theoretical study on positron impact excitation (ionization) has become of considerable importance particularly due to the availability of intense positron beam experiments¹. Among the atomic excitation studies by positron, helium is one of species which has been widely studied²⁻⁵. On the experimental side, Coleman et al⁶ have measured the total excitation cross-sections for 1^1S-2^1S of helium only in the near threshold region (23-29eV). For this excitation, a number of theoretical attempts have been made. Among them the work of Willis et al² in close-coupling approximation and Parcell et al³ and Mandal et al⁴ in distorted wave approximation are worth mentioning. Parcell et al have described the distortion in both the channels and included the polarization in final channel whereas Mandal et al⁴ have used a version of distorted wave in which the incident channel wave function satisfies the adiabatic equation.

One observes that there exists reasonable differences among the different results obtained in various theoretical models. In general, it has been found that there are two very common uncertainties involved in evaluating the cross-sections.

- (i) The adoption of a theoretical approximation.
- (ii) The use of approximate wave function of target as input for explicit evaluation of the scattering amplitude (in that particular model).

We have carried out a reliable calculation in the distorted wave model where distortion effects due to polarization and static potentials are taken in both the ingoing and outgoing positron distorted waves. The polarization is taken in dipole approximation⁷.

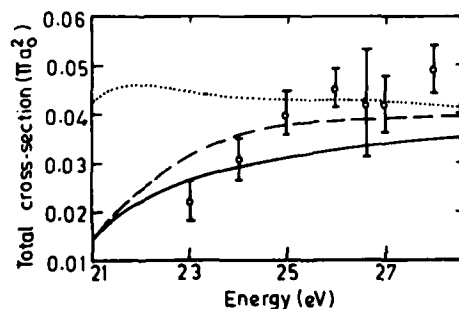


Fig.1 1^1S-2^1S excitation cross-section. — present calculation; Parcell et al

(Ref.3); - - - Mandal et al (Ref.4); \circ Coleman et al (Ref.6).

Accurate wavefunctions of the many parameter correlated type⁵ are employed through the introduction of Fourier transform of interaction potential and consequent follow up of a fitting procedure to obtain a suitable algebraic expression for the transition form factor.

The details about the theoretical procedure and various differential and total cross-section results would be presented in the conference. In table I as well as in figure 1, we have shown some of our results along with others. Looking the success of our similar approach⁸ in e^- -He scattering, we believe the present results to be quite reliable

Table I Calculated cross section (πa_0^2) for 1^1S-2^1S

Energy eV	5cc (i)	5cc (ii)	Mandal et al	Parcell et al	Present
40	5.94-2	2.65-2	3.81-2	3.56-2	3.41-2
60	4.34-2	3.69-2	3.01-2	- - -	2.83-2
80	3.29-2	3.17-2	2.41-2	2.26-2	2.35-2
100	2.63-2	2.68-2	2.01-2	1.89-2	1.87-2
200	1.28-2	1.41-2	1.07-2	1.05-2	1.10-2

References

1. T.S.Stein and W.E.Kaupplia, Adv. At. Molec. Phys. **10** 53 (1983).
2. S.L.Willis, J.Hata, M.R.C.McDowell, C.J. Joachain and F.W.Byron Jr., J. Phys. B **14** 2687 (1981).
3. L.A.Parcell, R.P.McEacharn and A.D.Stanffer J. Phys. B **16** 4249 (1983).
4. Mandal et al 1985 (Private Communication).
5. Mukesh Kumar, R.Srivastava and A.N. Tripathi. VIIth International Conf. on Positron Annihilation Delhi, Jan.1985, D31.
6. P.G.Coleman, J.D.McNutt, L.M.Diana and J.T.Hutton Phys. Rev. A **22** 2290 (1980).
7. A. Temkin and J.C.Lamkin, Phys. Rev **121** 788 (1961).
8. R.Srivastava, Mukesh Kumar and A.N.Tripathi, J. Chem. Phys. (in press) 1985.

INTERMEDIATE ENERGY POSITRON (ELECTRON)-ARGON DIFFERENTIAL ELASTIC SCATTERING CROSS SECTION MEASUREMENTS*

W.E. Kauppila, G.M.A. Hyder, M.S. Dababneh**, Y.-F. Hsieh, C.K. Kwan, and T.S. Stein

Department of Physics and Astronomy, Wayne State University, Detroit, Michigan 48202 USA

Relative differential cross sections for the elastic scattering of intermediate energy positrons (and electrons) by argon atoms are being measured using a crossed-beam setup, which is shown in Figure 1. The origin of the slow positron beam (intensity $>20,000/\text{sec}$ at 100 eV with a FWHM of about 1.5 eV) is a 50 millicurie sodium-22 radioactive source with an annealed tungsten cylinder, which serves as a back-scattering moderator for a small fraction of the high energy positrons emerging from the source. The atom beam source consists of a multichannel capillary array. In order to achieve suitable background pressures for operation of the channeltron detectors for the primary beam and scattered positrons, differential pumping is used for the scattering and detector regions, and only one exit port for the scattered particles is open at a time. The retarding element preceding detector #2 is used to reject any inelastically scattered positrons, while the collimators restrict the field of view of detector #2 to within 5° of the desired scattering angle, and the trap (consisting of a stack of knife-edged plates) diminishes the reflection of positrons from the scattering chamber wall into detector #2. Detector #1 is offset from the primary beam direction so that it will not respond to any high energy positrons that may be coming directly from the sodium-22 source. The retarding element preceding detector #1 is tuned to maximize transmission of the primary beam through the scattering chamber and to slow down the positrons prior to being electrostatically deflected toward the channeltron. The relative nature of the measurements made for the different scattering angles is achieved by maintaining a constant "head" pressure on the capillary array atom source (by using an automatic pressure controller) and compensating for any changes in the primary beam intensity, which has also been staying remarkably constant. Special efforts have been made to minimize stray magnetic fields. Electron measurements are being made to test the experimental system, since they can be compared with other measurements.

Our initial differential cross section measurements for 100 eV positrons elastically scattering from argon for angles ranging from 30° to 120° are displayed in Figure 2 along with the results of a polarized-orbital approximation calculation by Stauffer and McEachran.¹ In this figure the present measurements are normalized to the theory at 45° . The relative shape of the present results are in good agreement with the theory.

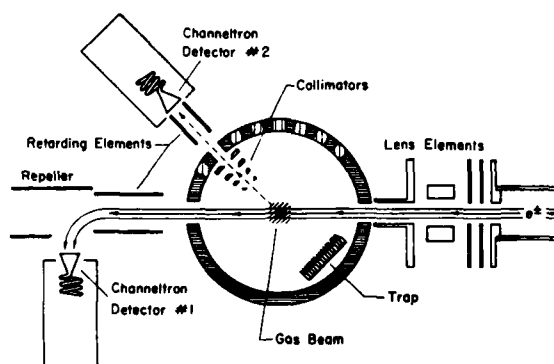


FIGURE 1 Experimental setup.

* This work supported by the National Science Foundation

**Present address: Department of Physics, Yarmouk University, Irbid, Jordan.

Reference

1. A.D. Stauffer and R.P. McEachran, private communication.

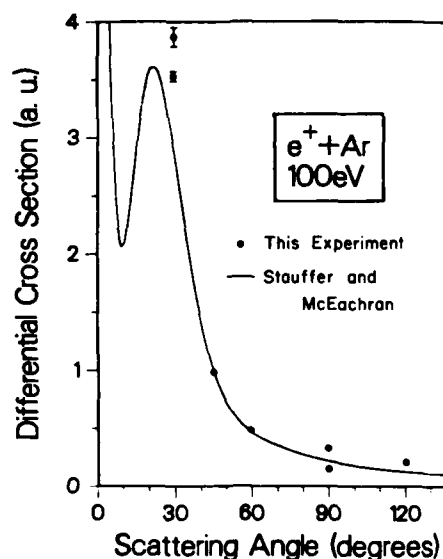


FIGURE 2 Comparison of experimental and theoretical differential cross section results for elastic scattering of 100 eV positrons by argon.

COMPUTATION OF MOMENTUM TRANSFER AND ANNIHILATION
CROSS-SECTION OF POSITRONS IN NOBLE GASES

A. S. GHOSH*, P. S. GROVER+ AND K. V. SINHA+

*Department of Theoretical Physics, Indian Association for
Cultivation of Science, Jadavpur, Calcutta - 700 032, INDIA.

+Department of Physics & Astrophysics, University of Delhi,
Delhi - 110 007, INDIA.

The interaction of slow positrons, energy less than positronium formation threshold in noble gases (H, He, Xe and Kr) have been investigated using the recent technique developed by Ghosh and Co-workers. We have computed the positron-atom momentum transfer Cross-section and e^+ annihilation cross-section for energies varying upto positronium formation threshold (17.8 eV for He, 6.7 eV for H, 7.2 eV for Kr and 5.3 eV for Xe). Only elastic scattering have been considered. The calculation have been further used to estimate the positron life time in gases. We have compared our computed results with the available experimental data. The details of the calculation and result will be reported in the conference.

A CALCULATION OF THE LOWEST PARTIAL WAVE IN LOW ENERGY POSITRON HYDROGEN MOLECULE SCATTERING

E.A.G. Armour

Department of Mathematics, University of Nottingham, Nottingham NG7 2RD, England

A generalization of the Kohn method is applied to the calculation of an approximation to the lowest partial wave in low energy positron hydrogen molecule scattering. The calculation is an extension of work already carried out on this subject¹; an account has been submitted for publication².

The nuclei in the target hydrogen molecule are taken to be fixed in their equilibrium position with internuclear separation, $R = 1.4$ bohr. The target wavefunction, ψ_G , is taken to be intermediate in accuracy between the SCF wavefunction and the very accurate wavefunction of Kołos and Roothaan³.

The trial wavefunction, ψ_T , in the generalized Kohn method is a generalization of the wavefunction used by Massey and Ridley⁴ and is of the form

$$\psi_T = \frac{N}{(\lambda_3-1)} \{ \sin[c(\lambda_3-1)] \cos \tau + \cos[c(\lambda_3-1)] \times (1 - \exp[-\gamma(\lambda_3-1)]) \sin \tau + a [\cos[c(\lambda_3-1)] (1 - \exp[-\gamma(\lambda_3-1)])] \times \cos \tau - \sin[c(\lambda_3-1)] \sin \tau \} \psi_G + \sum_{i=1}^M g_i \chi_i \psi_G \quad (1)$$

N and γ are constants and τ , a and $\{g_i\}$ are variable parameters. Particles 1 and 2 are the electrons in the target hydrogen molecule and particle 3 is the incident positron

$$c = \frac{1}{2} k R \quad (2)$$

where k is the wavenumber of the positron in atomic units. λ_3 and the associated coordinate, μ_3 , are the confocal elliptical (prolate spheroidal) coordinates

$$\lambda_3 = \frac{r_{3A} + r_{3B}}{R} \quad (3)$$

$$\mu_3 = \frac{r_{3A} - r_{3B}}{R} \quad (4)$$

where r_{3A} and r_{3B} are the distances of the positron from nuclei A and B, respectively.

The $\{\chi_i\}$ are short-range correlation functions to take into account the interaction between the positron and the hydrogen molecule.

$$\chi_1 = \frac{N}{(\lambda_3-1)} \cos[c(\lambda_3-1)] \{ 1 - \exp[-\gamma(\lambda_3-1)] \} \exp[-\gamma(\lambda_3-1)] \quad (5)$$

and

$$\chi_i = (\lambda_1 \lambda_2 \mu_1 \mu_2)^{p_i} [M_{13} \cos(\phi_1 - \phi_3)]^{b_i} + \lambda_1 \lambda_2 \mu_1 \mu_2^{s_i} \times [M_{23} \cos(\phi_2 - \phi_3)]^{c_i} e^{-\beta(\lambda_1 + \lambda_2)} \frac{r_i s_i}{\lambda_3 \mu_3} e^{-\gamma \lambda_3} \quad i > 1 \quad (6)$$

where

$$M_{13} = [(\lambda_1^2 - 1)(\lambda_3^2 - 1)(1 - \mu_1^2)(1 - \mu_3^2)]^{\frac{1}{2}} \quad (7)$$

and ϕ_1 is the azimuthal angle of electron 1. a_i , b_i , c_i , d_i , p_i , r_i and s_i are non-negative integers chosen so that the $\{\chi_i\}$ have the Σ_g^+ symmetry of the lowest partial wave. p_i was taken to have the values 0 and 1. When $\mu_i = 1$, χ_i contains factors like $M_{13} \cos(\phi_1 - \phi_3)$ which are of the form

$$M_{13} \cos(\phi_1 - \phi_3) = \frac{4}{R^2} (x_1 x_3 + y_1 y_3) \quad (8)$$

in terms of the Cartesian coordinates with origin midway between the nuclei and Z axis along the internuclear axis. Thus when $p_i = 1$, χ_i is made up of products of 1 particle functions of σ and π symmetry. Up to 64 short range correlation functions, of which 32 are of electronic symmetry, are used in the calculation.

The parameter, τ , in ψ_T is varied to avoid the anomalous singularities⁵ which can affect the accuracy of the results of the calculation. The parameters a and $\{g_i\}$ are determined by the generalized Kohn method. Results for the phase shift and the associated contribution to the total cross section are presented and compared with experiment⁶. The contribution to Z_{eff} , the effective number of electrons per hydrogen molecule available to the positron for annihilation, is also calculated and compared with experiment⁷.

References

1. E.A.G. Armour, J. Phys. B **17**, L375 (1984)
2. E.A.G. Armour, submitted to J. Phys. B.
3. W. Kołos and C.C.J. Roothaan, Rev. Mod. Phys. **32**, 219 (1960).
4. H.S.W. Massey and R.O. Ridley, Proc. Phys. Soc. A **69**, 659 (1956).
5. C. Schwartz, Ann. Phys., NY **16**, 36 (1961).
6. T.C. Griffith and G.R. Heyland, Phys. Rep. **39**, 169 (1978).
7. J.D. McNutt, S.C. Sharma and R.D. Brisbon, Phys. Rev. A **20**, 347 (1979).

A CALCULATION OF THE LOWEST Σ_u^+ PARTIAL WAVE IN LOW ENERGY POSITRON HYDROGEN MOLECULE SCATTERING

E.A.G. Armour and D.J. Baker

Department of Mathematics, University of Nottingham, Nottingham NG7 2RD, England

The generalization of the Kohn method, which has previously been applied to the calculation of an approximation to the lowest (Σ_g^+) partial wave^{1,2}, is applied to the calculation of an approximation to the lowest partial wave of Σ_u^+ symmetry.

The nuclei in the target hydrogen molecule are taken to be fixed in their equilibrium position with internuclear separation, $R = 1.4$ bohr. The target wavefunction, ψ_G , used in the calculation is intermediate in accuracy between the SCF wavefunction and the very accurate wavefunction of Kołos and Roothaan³.

The trial wavefunction, ψ_T , in the generalized Kohn method is taken to be of the form

$$\begin{aligned} \psi_T = & N[\Omega_1(\lambda_3)\cos\tau + \Omega_2(\lambda_3)(1-\exp[-\gamma(\lambda_3-1)])\times\sin\tau \\ & + a[\Omega_2(\lambda_3)(1-\exp[-\gamma(\lambda_3-1)])\cos\tau - \Omega_1(\lambda_3)\sin\tau]] \\ & \times P_1(\mu_3)\psi_G + \sum_{i=1}^M g_i x_i \psi_G \end{aligned} \quad (1)$$

N and γ are constants and τ , a and $\{g_i\}$ are variable parameters. Particles 1 and 2 are the electrons in the target hydrogen molecule and particle 3 is the incident positron

$$c = \frac{1}{2}kR \quad (2)$$

where k is the wave number of the positron in atomic units. λ_3 and μ_3 are the confocal elliptical (prolate spheroidal) coordinates,

$$\lambda_3 = \frac{r_{3A} + r_{3B}}{R} \quad (3)$$

$$\mu_3 = \frac{r_{3A} - r_{3B}}{R} \quad (4)$$

where r_{3A} and r_{3B} are the distances of the positron from nuclei A and B, respectively.

The functions, $\Omega_1(\lambda_3)$ and $\Omega_2(\lambda_3)$, are chosen so that ψ_T is regular at $\lambda_3 = 1$ and

$$\psi_T \sim_{\lambda_3 \rightarrow \infty} N[\Omega_1'(\lambda_3) + a\Omega_2'(\lambda_3)]P_1(\mu_3)\psi_G \quad (5)$$

where

$$\Omega_1'(\lambda_3) = \cos\tau\Omega_1(\lambda_3) + \sin\tau\Omega_2(\lambda_3) \quad (6)$$

$$\Omega_2'(\lambda_3) = -\sin\tau\Omega_1(\lambda_3) + \cos\tau\Omega_2(\lambda_3) \quad (7)$$

has the asymptotic form appropriate to the lowest Σ_u^+ partial wave.

The $\{x_i\}$ are short-range correlation functions to take into account the interaction between the positron and the hydrogen molecule

$$x_1 = N\Omega_2(\lambda_3)(1-\exp[-\gamma(\lambda_3-1)])\exp[-\gamma(\lambda_3-1)] \times P_1(\mu_3) \quad (8)$$

The remaining $\{x_i\}$ are of the same form as in the previous calculation² except that the indices are chosen so that the functions are of Σ_u^+ symmetry. A similar number of short range correlation functions, of both Σ^+ and Π electronic symmetries, are used as in the previous calculation.

The parameter, τ , in ψ_T is once again used to avoid anomalous singularities⁴ and the parameters a and $\{g_i\}$ determined by the generalized Kohn method. The results for the phase shift and associated contribution to the total cross section enable a more realistic comparison to be made with experiment⁵ than was possible earlier². The contribution to Z_{eff} , the effective number of electrons per hydrogen molecule available to the positron for annihilation, is also calculated to see if it becomes significant in the energy range below the positronium formation threshold at 8.63 eV.

It is also hoped to include results for cross sections for rotational excitation and de-excitation obtained using both the calculated Σ_g^+ and Σ_u^+ wavefunctions and the method of Ficocelli Varracchio⁶.

References

1. E.A.G. Armour, J. Phys. B **17**, L375 (1984).
2. E.A.G. Armour, submitted to J. Phys. B. and Abstracts of the XIVth ICPEAC.
3. W. Kołos and C.C.J. Roothaan, Rev. Mod. Phys. **32**, 219 (1960).
4. C. Schwartz, Ann. Phys., NY **16**, 36 (1961).
5. T.C. Griffith and G.R. Heyland, Phys. Rep. **39**, 169 (1978).
6. E. Ficocelli Varracchio, J. Phys. B **14**, L511 (1981).

POSITRON AND ELECTRON TOTAL CROSS-SECTION MEASUREMENTS FOR MOLECULAR OXYGEN

C.K. Kwan, Y.-F. Hsieh, W.E. Kauppila, Steven J. Smith, and T.S. Stein

Department of Physics and Astronomy, Wayne State University, Detroit, Michigan 48202 USA

Total cross-sections have been measured for positrons and electrons scattered by O_2 in the range of 1-500 eV using a transmission technique. Positrons are produced by bombarding a boron target with a 4.75 MeV proton beam from a Van de Graaff accelerator. Approximately 10^{-6} of the "fast" positrons produced are moderated in the target itself and the energy width of the positron beam is about 0.1 eV. The electron beam is produced by thermionic means and has an energy width typically of 0.15 eV.

The total cross-sections are deduced from the attenuation of the transmitted beam, the target gas pressure and the length of the scattering region. The gas pressure is measured by a capacitance manometer. For every energy, the total cross-section is measured in at least six runs with varying target gas pressures. The experimental errors, excluding the effect of small angle scattering, is estimated to be 6% for positrons and 5% for electrons.

Fig. 1 shows the present results for positrons and electrons scattered by O_2 . The electron measurements are shown along with the measurements of Sunshine et al.¹ and Dalba et al.² The positron data are shown along with the measurements of Charlton et al.^{3,4} and Coleman et al.⁵ An overall observation is that electron total cross-sections are everywhere larger than the positron cross-sections reflecting the absence of an exchange interaction for positron scattering and the fact that static and polarization potentials have opposite signs resulting in an overall weaker interaction for positrons than for electrons. Another feature in the comparison between positron and electron total cross-sections is a tendency for merging of the cross-section curves at higher energies due to the fact that at these energies the static interaction is the dominant interaction.

The present positron results are in quite good agreement with the measurements of Charlton et al.^{3,4} although some of the features between 8 and 13 eV mentioned by the latter authors are not evident from our measurements. We also observe no significant rise in the total cross-sections in the vicinity of the positronium formation threshold. The present electron total cross-section results are about 20% larger than those of Sunshine et al.¹ from 12 to 100 eV. We are unable to confirm the "bump" of the electron total cross-sections between 11 and 13 eV observed by earlier

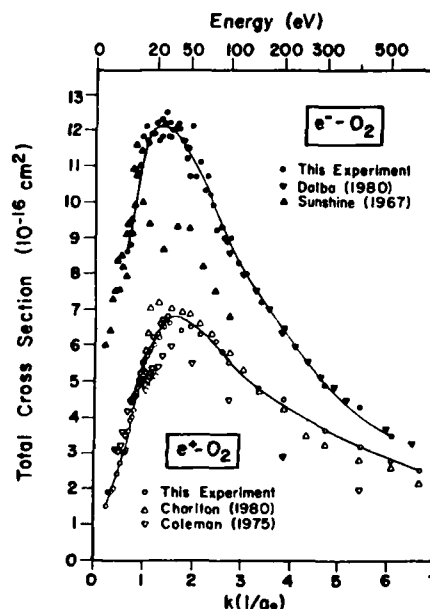


FIGURE 1 Comparison of positron and electron total cross-sections for molecular oxygen.

Our present results, however, agree remarkably well with those of Dalba et al.² where the energies overlap.

This work is supported by the National Science Foundation under Grant No. PHY 83-11705.

References

1. G. Sunshine, B.B. Aubrey and B. Bederson, Phys. Rev. **154**, 1 (1967).
2. G. Dalba, P. Fornasini, R. Grisenti, G. Ranieri and A. Zecca, J. Phys. B **13**, 4695 (1980).
3. M. Charlton, T.C. Griffith, G.R. Heyland and G.L. Wright, J. Phys. B **13**, L352 (1980).
4. M. Charlton, T.C. Griffith, G.R. Heyland and G.L. Wright, J. Phys. B **16**, 323 (1983).
5. P.G. Coleman, T.C. Griffith, G.R. Heyland and T.L. Killeen, *Atomic Physics* vol. 4 (New York: Plenum, 1975) PP. 355-371.

POSITRON SCATTERING BY NITROGEN MOLECULE

N. Bhattacharya and D.N. Tripathi

Dept. of Physics, Banaras Hindu University VARANASI - 221005 (INDIA)

Theoretically¹ calculated total cross sections for the positron scattering by nitrogen molecule (12-g) vis-a-vis experimentally² determined values are far from satisfactory. Hence the present study. The earlier work³ has been extended with the following objectives; 1. to explain the observed total scattering cross sections in the entire energy range, 2. to emphasize the fact that in the close coupling approach with the integral equation algorithm the value of r_{\min} (i.e. the lower limit of the integration) is very sensitive to the total cross section (but not the rotational excitation) and hence is important in determining its value, 3. lastly, to point out the discrepancies between the present and the previously reported theoretical studies in so far giving values of various cross sections (rotational excitation etc.) and hence the need of the experimental measurements.

Interaction potential has been improved over the one used earlier by accurate calculation of polarization potential using the Hartree-Fock SCF wave functions for N_2 -molecule. In addition it contains the static component. The singularity of the interaction potential appearing at the origin has been avoided by taking the solution of the scattering equation to be zero out to the point r_{\min} , a point determined by the requirement that the interaction potential is equal or greater than the kinetic energy of the impinging positron. This is the value taken for the lower limit of the integration and, naturally, it varies with the incident energy. The possibility of the annihilation or positronium formation has not been included.

The reported results of the total scattering cross sections (Table) are in excellent agreement with the experimentally measured cross sections in the entire energy range. Therefore, it can be safely concluded that the positronium formation cross section has no marked influence at least over the total scattering cross sections. It is found to be sensitive with the values of r_{\min} (the respective values of r_{\min} are given in the table). Rotational excitation cross sections for the $0 \rightarrow 2$ and $0 \rightarrow 4$ transitions are also reported (Table) which are in disagreement with the previously reported results. However, on the basis of the good agreement between the observed and the present values of total cross section, it is contended that the reported rotational excitation cross sections are reliable. Various other cross sections, in addition, viz; differential, momentum transfer cross sections etc. are also calculated but are not reported in the absence of any comparable experimental results. Finally, it is concluded that in order to resolve the existing discrepancies and clarify the collision dynamics the experimental determination of the differential cross sections is essential.

ACKNOWLEDGEMENT: We are grateful to Prof. D.K. Rai for his fruitful discussions and encouragements during the course of this work.

TABLE

Inc. Energy (eV)	Total Cross Section (a_0^2)		Rot. Excit. Cross Section (a_0^2)		r_{\min} (a_0)
	Present	Expt.	0 2	0 4	
0.1	83.9	--	0.24	0.16 (-5)	4.0
1.0	11.4	a) 13.2	0.30	3.10 (-5)	4.0
4.0	9.3	a) 11.4 b) 12.4	0.21	8.10 (-5)	3.0
10.0	18.5	a) 16.0 b) 17.6	0.26	3.07 (-4)	2.0
100.0	23.8	a) 23.2	0.18	1.41 (-3)	1.0

a). Reference 2b, b). Reference 2c, (-5) means 10^{-5}

References:

- 1.a) E.S. Gillespie and P.G. Thompson, J. Phys. B.8, 2858 (1975)
- b) J.W. Darewych and P. Baille, J. Phys. B.7, L1 (1974)
- c) J.W. Darewych, P. Baille and S. Hara, J. Phys. B.7, 2407 (1974)
- 2.a) P.G. Coleman, T.C. Griffith and G.R. Heyland, Appl. Phys. 4, 89 (1974)
- b) K.R. Hoffman, M.S. Dababneh, Y.F. Hsieh, W.E. Kauppi, V. Pol, J.H. Smart and T.S. Stein, Phys. Rev. A25, 1393 (1982)
- c) M. Zharlton, T.C. Griffith, G.R. Heyland and G.L. Wright, J. Phys. B 16, 323 (1983)
- 3.a) A.K. Pandey and D.N. Tripathi, Abstracts of Contributed Papers XIII ICPEAC, Berlin 306 (1983)
- b) N. Bhattacharya and D.N. Tripathi, J. Phys. B. (communicated)

A HYPERSPHERICAL STUDY OF THE POSITRONIUM NEGATIVE ION

J. Botero and C. H. Greene

Department of Physics and Astronomy, Louisiana State University, Baton Rouge, LA 70803-4001

In order to investigate the quasiseparability of the few-particle wave function in hyperspherical coordinates¹, and in particular its dependence on the particle masses, we have treated the positronium negative ion ($e^+e^-e^-$) adiabatically² using these coordinates. The fact that the center of mass of the system does not coincide with the position of any of the particles makes a major difference in the structure of the wave function and in the treatment of the problem.

We describe the three-particle configuration space in terms of symmetric Jacobi coordinates which in turn are replaced by hyperspherical coordinates:

$$R = [r_1^2 + (\gamma r_2)^2]^{1/2}, \quad \alpha = \tan^{-1}(\gamma r_2/r_1),$$

where r_1 is the electron-electron separation and r_2 is the distance from the positron to the center of mass of the electron pair. The factor $\gamma=(3/4)^{1/2}$ is needed to make R^2 the total moment of inertia.

The adiabatic treatment² consists of finding eigenvalue $U_\mu(R)$ and eigenstates $\phi_\mu(R, \Omega)$ of the Hamiltonian at fixed R , and approximating the total wave function by the product of a radial function $F_\mu(R)$ and the $\phi_\mu(R, \Omega)$ obtained before. In this work we have solved for the ϕ_μ variationally, expanding it in a nonorthogonal basis of hydrogenic wavefunctions of positronium. The $1s, 2s, 2p$ and $3s$ basis functions were used. Solution of the radial equation gave then a lower and upper bound on the ground state energy. Our first results give an upper bound of $E_u = -0.2597$ and a lower bound $E_l = -0.2646$, which bracket the best calculated value $E_{\text{exact}} = -0.2620$ (in atomic units).³

Figures 1 and 2 show the lowest two $1s^e$ adiabatic potential curves of the positronium negative ion. We conclude that the effect of the different reduced mass of the electrons with respect to the positive charge in Ps^- and H^- is simple: to a good approximation all distances are doubled and all energies are halved in the ground and first excited states of Ps^- .

This work was supported in part by the National Science Foundation. J. B. was also supported by the

"Escuela Colombiana de Ingenieria". C. H. G. received support in the form of an Alfred P. Sloan Foundation Fellowship.

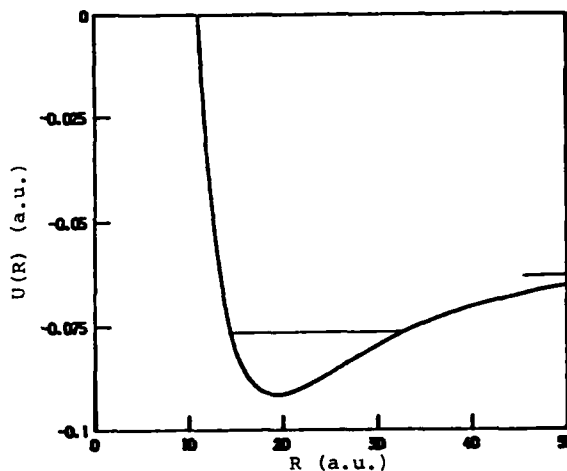


Figure 1: Potential curve of the first excited state.

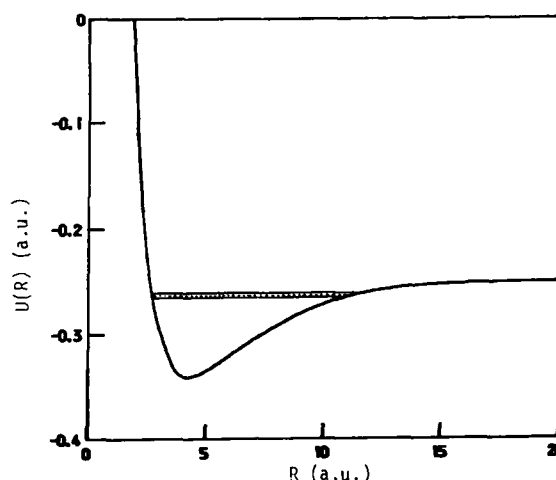


Figure 2: Ground state potential curve

References

1. U. Fano, Rep. Prog. Phys. **46**, 97(1983) and references therein.
2. J. H. Macek, J. Phys. **B1**, 831(1968).
3. Y. K. Ho, J. Phys. **B16**, 1503(1983).

COLLISIONS OF e^{\pm} WITH Ps^{\pm}

M. A. Abdel-Raouf
Achalm Straße 13, 7406 Mössingen, West-Germany

The fact that Ps^+ and Ps^- are two stable ions with ground-state energies¹ equal to -0.5024 Ryd. raises the questions about their elastic and inelastic (if it exists) scattering by electrons and positrons, respectively, as well as their dissociation into two positronium atoms or one positronium atom and two (or three) photons in various scattering problems. In this work we restrict ourselves to the investigation of the S-wave elastic scattering of electrons(positrons) by the positronium positive(negative) ions. The calculations are carried out by virtue of a least-squares variational method². We are intended to evaluate the scattering phase shifts for a wide region of incident energies, $0 \leq k^2 \leq 0.51$ where k is the wave number of the projectile, and we hope that the used method, which is almost anomaly free, could provide us with some indications about resonances or the existence of higher bound-states of the targets.

Let us assume that 1,2 be the two identical particles of each ion, a being its third particle and b refers to the incident projectile.

Let us also assume that a is fixed and r_{12} does not play any role in the target wave function. Therefore, we may write the total wave function in the form

$$\Psi = (\phi_T(s_1, t_1) + \phi_T(s_2, t_2)) \psi(kr_{ab}) + \phi_S \sum_i C_i \chi_i, \quad (1)$$

where ϕ_T represents the ground-state of the considered ion to be chosen in the Hylleraas' form

$$\phi_T(s, t) = e^{-s/2} \cosh(0.33t/2), \quad E_T = -0.50133 \text{ Ryd.} \quad (2)$$

The functions ϕ_S and χ_i are expressed by

$$\phi_S = e^{-\alpha(s_1+s_2)} (\cosh(\beta(t_1-t_2)) + \cosh(\gamma(s_1-s_2))) \quad (3)$$

$$\text{and } \chi_i = v^{k_i} (s_1^{n_i} s_2^{n_i} t_1^{p_i} t_2^{q_i} + s_1^{m_i} s_2^{m_i} t_1^{q_i} t_2^{p_i}) \quad (4)$$

The scattering wave function $\psi(kr_{ab})$ is defined by

$$\psi = \sin(kv - \eta_c) + \tan(\eta_0) (1 - e^{-\alpha v}) \cos(kv - \eta_c) \quad (5)$$

where s_i, t_i, v are Hylleraas' vectors satisfy the relations

$$s_i = r_{ia} + r_{ib}, \quad t_i = r_{ia} - r_{ib}, \quad v = r_{ab} \quad (6a)$$

$$+v \leq s_i \leq \infty, \quad -v \leq t_i \leq +v, \quad 0 \leq v \leq \infty \quad (6b)$$

The parameters $\alpha, \beta, \gamma, C_i, \tan(\eta_0)$ are variational parameters. η_0 is the S-wave phase shift and η_c is the Coulomb phase shift.

The total Hamiltonian H , is expanded by

$$H = H_1 + H_2 + H_a + H_b + \tilde{V}, \quad (7)$$

where H_i is given by

$$H_i = -\frac{4}{(s_i^2 - t_i^2)} \left\{ (s_i^2 - v^2) \frac{\partial^2}{\partial s_i^2} + (v^2 - t_i^2) \frac{\partial^2}{\partial t_i^2} + 4s_i \frac{\partial}{\partial s_i} + 4t_i \frac{\partial}{\partial t_i} + 2s_i \right\}, \quad i=1,2$$

$$H_a = -\frac{4}{(s_a^2 - t_a^2)} \left\{ (s_a^2 - u^2) \frac{\partial^2}{\partial s_a^2} + (u^2 - t_a^2) \frac{\partial^2}{\partial t_a^2} + 4s_a \frac{\partial}{\partial s_a} - 4t_a \frac{\partial}{\partial t_a} \right\} - \left\{ \frac{\partial}{\partial v} + \frac{2}{v} + 2(\cos(\theta_{1a,v}) + \cos(\theta_{2a,v})) \frac{\partial}{\partial s_a} + 2(\cos(\theta_{1a,v}) - \cos(\theta_{2a,v})) \frac{\partial}{\partial t_a} \right\} \frac{\partial}{\partial v},$$

H_b is obtained from H_a by replacing a with b ,

$$v = \frac{2}{u} + \frac{2}{v}, \quad \text{and}$$

$$s_a = r_{1a} + r_{2a}, \quad s_b = r_{1b} + r_{2b}, \quad t_a = r_{1a} - r_{2a}, \quad t_b = r_{1b} - r_{2b}.$$

Defining the set of projections

$$\langle \chi_{-1} | H - E | \Psi \rangle = P_1,$$

$$\langle \chi_0 | H - E | \Psi \rangle = P_2,$$

$$\text{and } \langle \chi_i | H - E | \Psi \rangle = P_i, \quad i=1, \dots, N$$

where χ_{-1} and χ_0 are the sin and cosin parts of ψ , the variational parameters can be determined by virtue of the variational principle

$$\delta \sum_i^{N+2} P_i^2 = 0.$$

References

1. A.K. Bhatia and R.J. Drachman, Phys. Rev. A25, (1981) 2523.

2. The method and its applications in atomic and nuclear scattering are reviewed by M. A. Abdel-Raouf, Phys. Rept 108, (1984) 1-163.

ACCURATE CALCULATIONS OF THE BOUND-STATES OF THE POSITRONIUM IONS AND MOLECULES

M. A. ABDEL-RAOUF

ACHALM STRAßE 13, 7406 MÖSSINGEN, WEST-GERMANY

THE EXISTENCE OF A BOUND-STATE COMPOSING OF TWO POSITRONIUM ATOMS, OR A POSITRONIUM NEGATIVE (POSITIVE) ION AND A POSITRON (ELECTRON), I.E. OF TWO ELECTRONS AND TWO POSITRONS, IS INVESTIGATED. THE ACCURATE VARIATIONAL ENERGIES AND VARIATIONAL PICTURES OF THIS QUANTUM MECHANICAL SYSTEM, THE POSITRONIUM MOLECULE (USUALLY REFERRED TO AS Ps_2), ARE OBTAINED BY EMPLOYING A LARGE NUMBER OF VECTORS, DEPENDING ON ALL RELATIVE COORDINATES OF THE FOUR PARTICLES, FOR CONSTRUCTING A TRIAL EXPANSION SPACE IN WHICH THE PREVIOUSLY MENTIONED THREE SUBCLUSTERS ARE REPRESENTED. THE RESULTANT VARIATIONAL PICTURES ARE USED FOR CALCULATING THE ANNIHILATION PROBABILITIES OF Ps_2 INTO TWO (OR THREE) PHOTONS AND ONE POSITRONIUM ATOMS, AS WELL AS THE EVALUATION OF THE EXPECTATION VALUES OF SOME ASSOCIATED OPERATORS.

THE USE OF ARBITRARY MASSES IN THE COMPUTING PROGRAMM ENABLES US TO INVESTIGATE OTHER FOUR BODY SYSTEMS, LIKE $e^+u^-e^+u^-$ AND $e^-u^+e^-u^+$. IN ORDER TO LOCALIZE THE EXACT GROUND STATES OF Ps^- , Ps^+ AND Ps_2 WITHIN ARBITRARY NARROW GAPS, THE TEMPLE FORMULA¹ IS USED FOR DETERMINING EFFECTIVE LOWER BOUNDS TO THE BOUND-STATES OF THESE SYSTEMS. THE RESULTS PROVIDE US WITH EXTREMELY VALUABLE INFORMATIONS ABOUT THE EXISTENCE (OR ABSENCE) OF THE HIGHER EXCITED STATES OF THE SYSTEMS UNDER CONSIDERATION.

THE CAREFUL EXPERIMENTS BY MILLS², IN WHICH THE GROUND STATE OF Ps^- WAS ACCURATELY DETECTED, HAVE ENCOURAGED THE THEORETICAL INVESTIGATION OF VARIOUS 3 BODY SYSTEMS WHERE THE HAMILTONIANS ARE PREDOMINATED BY THE MUTUAL INTERACTIONS BETWEEN THE PARTICLES AND NONE OF THEM CAN HAVE AN INFINITE MASS. THE ELABORATE TREATMENT³ OF Ps^- WAS ABLE TO CONFIRM THE EXISTENCE OF A $1S^e$ STATE, BUT FAILED IN PROVIDING US WITH ANY INFORMATION ABOUT HIGHER STATES. IN FACT, ALL THESE DEVELOPMENTS HAVE SHED LIGHT ON THE PIONEERING WORK BY JOHN A. WHEELER⁴ IN WHICH HE SHOWED THAT Ps^+ ARE STABLE IONS AND Ps_2 IS UNSTABLE. ONLY HYLLERAAS AND ORE⁵ SUCCEEDED IN PROVING THAT THE HAMILTONIAN OF Ps_2 SUPPORTS A BOUND-STATE WITH BINDING ENERGY 0.11 eV, WHICH HAS BEEN INCREASED BY ORE⁶ TO 0.135 eV.

RECENTLY, TISENKO⁷ HAS USED HYLLERAAS-ORE'S WAVE FUNCTION IN ORDER TO CALCULATE THE ANNIHILATION

PROBABILITIES OF Ps_2 INTO TWO OR THREE PHOTONS.

IN THIS WORK WE USE, FOR THE FIRST TIME, A WAVE FUNCTION WHICH DEPENDS ON THE RELATIVE DISTANCES BETWEEN THE SIMILAR PARTICLES OF Ps_2 AND ALLOWS FOR THE EXISTENCE OF VARIOUS SUBCLUSTERS OF THIS MOLECULE.

THE TOTAL HAMILTONIAN OF A FOUR BODY SYSTEM CAN BE WRITTEN AS

$$H = \sum_{i < j} \left\{ -\frac{1}{2} \left(\frac{1}{m_i} + \frac{1}{m_j} \right) \left(\frac{\partial^2}{\partial r_{ij}^2} + \frac{2}{r_{ij}} \frac{\partial}{\partial r_{ij}} \right) + \frac{e_i e_j}{r_{ij}} \right\} - \sum_{i \neq j, k; j < k} \left(\frac{1}{m_i} \right) \cos(\theta_{ij, ik}) \frac{\partial^2}{\partial r_{ij} \partial r_{ik}} \quad (1)$$

WHERE e , m AND r , REFER TO THE CHARGES, MASSES AND RELATIVE COORDINATES OF THE PARTICLES. CONSIDERING THAT $i, j=1, 2$ DENOTE THE ARGUMENTS OF THE NEGATIVE PARTICLES, IT IS EASY TO SHOW THAT H CAN BE REDUCED, AT $e_i=2$, $m_i=1/2$, $i=1, \dots, 4$, TO THE FORM

$$H = H_{hyd} + H' \quad (2)$$

WHERE H_{hyd} IS THE HAMILTONIAN OF THE HYDROGEN MOLECULE AND H' IS A KINETIC ENERGY OPERATOR DEPENDS ON m_3 AND m_4 AND VANISHES WHEN THESE MASSES ARE INFINITE.

THE TOTAL WAVE FUNCTION IS CHOSEN IN THE FORM

$$\Psi = \sum_i C_i \chi_i \quad (3)$$

WHERE THE χ_i 'S ARE DEFINED BY

$$\chi_i = u^{l_i} v^{l_i} e^{-\alpha(s_1 + s_2)} \{ \cosh(\beta(t_1 - t_2)) + \cosh(\gamma(s_1 - s_2)) \} \{ s_1^{n_i} s_2^{n_i} t_1^{p_i} t_2^{q_i} + s_1^{n_i} s_2^{n_i} t_1^{q_i} t_2^{p_i} + \dots \} \quad (4)$$

AND $s_1 = r_{13} + r_{14}$, $t_1 = r_{13} - r_{14}$, $u = r_{12}$ AND $v = r_{34}$.

REFERENCES

1. M. A. ABDEL-RAOUF, PHYS. REPORTS 84, (1982) 163; PHYSICA C97, (1979), 103.
2. A. P. MILLS, PHYS. REV. LETT. 50, (1983) 671.
3. Y. K. HO, J. PHYS. B16, (1983) 1503; A. K. BHATIA AND R. J. DRACHMAN, PHYS. REV. A28, (1983) 2523.
4. J. A. WHEELER, ANN. N. Y. ACADEM. SCI. 48, (1946), 219.
5. E. A. HYLLERAAS AND A. ORE, PHYS. REV. 71, (1947) 493.
6. A. ORE, PHYS. REV. 71, (1947) 913.
7. YU. A. TISENKO, IZV. VUZ, 24, (1981), 3-6, ENG. TRANS. SOV. PHYS. J. 24, (1981) 99-102.

AUTOIONISATION STATES OF THE POSITRONIUM MOLECULES

M. A. Abdel-Raouf

Achalm Straße 13, 7406 Mössingen, West Germany

The method of the complex coordinate¹ is used for calculating the autoionisation states of the positronium molecules, (Fig. 1).

The total Hamiltonian H , can be written as

$$H = T_1 + T_2 + T_a + T_b + V, \quad (1)$$

where the kinetic energy operators T_1 , T_2 , T_a and T_b have the following forms, respectively

$$T_1 = -\frac{1}{2m_1} \left\{ \frac{\partial^2}{\partial r_{1a}^2} + \frac{2}{r_{1a}} \frac{\partial}{\partial r_{1a}} + \frac{\partial^2}{\partial r_{1b}^2} + \frac{2}{r_{1b}} \frac{\partial}{\partial r_{1b}} + \frac{\partial^2}{\partial r_{12}^2} + \frac{2}{r_{12}} \frac{\partial}{\partial r_{12}} + 2(\cos(\theta_{1a,1b}) \frac{\partial^2}{\partial r_{1a} \partial r_{1b}} + \cos(\theta_{1a,12}) \frac{\partial^2}{\partial r_{1a} \partial r_{12}} + \cos(\theta_{1b,12}) \frac{\partial^2}{\partial r_{1b} \partial r_{12}}) \right\}. \quad (2a)$$

$$T_2 = -\frac{1}{2m_2} \left\{ \frac{\partial^2}{\partial r_{2a}^2} + \frac{2}{r_{2a}} \frac{\partial}{\partial r_{2a}} + \frac{\partial^2}{\partial r_{2b}^2} + \frac{2}{r_{2b}} \frac{\partial}{\partial r_{2b}} + \frac{\partial^2}{\partial r_{12}^2} + \frac{2}{r_{12}} \frac{\partial}{\partial r_{12}} + 2(\cos(\theta_{2a,2b}) \frac{\partial^2}{\partial r_{2a} \partial r_{2b}} + \cos(\theta_{2a,12}) \frac{\partial^2}{\partial r_{2a} \partial r_{12}} + \cos(\theta_{2b,12}) \frac{\partial^2}{\partial r_{2b} \partial r_{12}}) \right\}. \quad (2b)$$

$$T_a = -\frac{1}{2m_a} \left\{ \frac{\partial^2}{\partial r_{1a}^2} + \frac{2}{r_{1a}} \frac{\partial}{\partial r_{1a}} + \frac{\partial^2}{\partial r_{2a}^2} + \frac{2}{r_{2a}} \frac{\partial}{\partial r_{2a}} + \frac{\partial^2}{\partial r_{ab}^2} + \frac{2}{r_{ab}} \frac{\partial}{\partial r_{ab}} + 2(\cos(\theta_{1a,2a}) \frac{\partial^2}{\partial r_{1a} \partial r_{2a}} + \cos(\theta_{1a,ab}) \frac{\partial^2}{\partial r_{1a} \partial r_{ab}} + \cos(\theta_{2a,ab}) \frac{\partial^2}{\partial r_{2a} \partial r_{ab}}) \right\}. \quad (2c)$$

$$T_b = -\frac{1}{2m_b} \left\{ \frac{\partial^2}{\partial r_{1b}^2} + \frac{2}{r_{1b}} \frac{\partial}{\partial r_{1b}} + \frac{\partial^2}{\partial r_{2b}^2} + \frac{2}{r_{2b}} \frac{\partial}{\partial r_{2b}} + \frac{\partial^2}{\partial r_{ab}^2} + \frac{2}{r_{ab}} \frac{\partial}{\partial r_{ab}} + 2(\cos(\theta_{1b,2b}) \frac{\partial^2}{\partial r_{1b} \partial r_{2b}} + \cos(\theta_{1b,ab}) \frac{\partial^2}{\partial r_{1b} \partial r_{ab}} + \cos(\theta_{2b,ab}) \frac{\partial^2}{\partial r_{2b} \partial r_{ab}}) \right\}. \quad (2d)$$

The potential energy V is given by

$$V = -\frac{e^2}{r_{1a}} - \frac{e^2}{r_{1b}} - \frac{e^2}{r_{2a}} - \frac{e^2}{r_{2b}} + \frac{e^2}{r_{12}} + \frac{e^2}{r_{ab}} \quad (3)$$

(Setting $m_1 = m_2 = m_a = m_b = 1/2$ and $e^2 = 2$ means that H is given in Rydberg atomic units).

In our calculation we use the Hylleraas' vectors

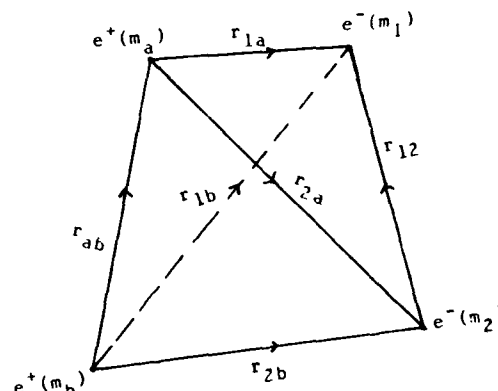


Fig. 1

$$s_i = r_{ia} + r_{ib} \quad \text{and} \quad t_i = r_{ia} - r_{ib}, \quad i=1,2$$

$$u = r_{12} \quad \text{and} \quad v = r_{ab} \quad \text{with} \quad 0 \leq v \leq \infty, \\ +v \leq s_i \leq \infty \quad \text{and} \quad -v \leq t_i \leq v. \quad (4)$$

We also assume that r_{ab} is fixed in space and the total wave function is independent of r_{12} . This assumption reduces the volume element $d\tau$ to the form $d\tau = (1/16) (s_1^2 - t_1^2)(s_2^2 - t_2^2) dv ds_1 ds_2 dt_1 dt_2$.

The following forms of the wave function are tested:

- 1) $\psi_1 = e^{-1/2(s_1+s_2)} \cosh(\beta(t_1 - t_2))$,
- 2) $\psi_2 = e^{-\alpha(s_1+s_2)} (\cosh(\beta(t_1 - t_2)) + \cosh(\gamma(s_1-s_2)))$,
- 3) $\chi_i = \psi_2 (s_1^{n_i} s_2^{q_i} t_1^{p_i} t_2^{q_i} + s_1^{n_i} s_2^{m_i} t_1^{q_i} t_2^{p_i})$, $\psi_3 = \sum_i c_i \chi_i$.

The autoionisation states are obtained by setting $r_{kj} + r_{kj} e^{i\theta}$, where k, j and $j=3,4$ refer to the positrons, in the reduced Hamiltonian and determining the negative eigenvalues of the complex part of the spectrum of H using Rayleigh-Ritz method, i.e. by solving the eigenvalue problem²

$$(\mathcal{H} - \epsilon_k) \mathbf{c} = 0, \quad \mathbf{c} = (c_1, c_2, c_3, c_4)^T, \quad k=1,2,3,4$$

Γ_k is the width of the autoionisation state.

References

- ¹The mathematical aspects of the method of complex coordinate are reviewed by C.S.Sharma, Phys.Rept.,26,(1976)1-64. The physical aspects of the method and its applications to Atomic Collisions are compiled in the work by V.K.Ho, Phys.Rept.,22,(1983)1-68.
- ²See e.g. F.Balslev and J.D.Combes, Commun. Math. Phys.,22,(1971)280 and B.Simon, Commun. Math. Phys., 27,(1972)1.

ORTHOPOSITRONIUM LOCALIZATION IN GASES BY DENSITY FLUCTUATION SCATTERING

C. V. Heer

Department of Physics, Ohio State University, Columbus, Ohio 43210 USA

The enhanced lifetime of orthopositronium, o-Ps, in helium is attributed to the formation of a cavity surrounding the o-Ps atom. This cavity formation is explained in terms of a balancing of the zero point kinetic pressure of the o-Ps atom and the hydrostatic pressure of the surrounding gas, and this explanation requires a repulsive interaction potential between the o-Ps atom and the helium atoms. A similar enhanced lifetime has been observed in ethane^{1,2} in which the interaction potential may be attractive. It is the purpose of this paper to develop a model in which the attenuation α of the coherent wave by elastic fluctuation scattering of matter waves

$$\alpha = a^2 \int d\Omega \int d^3x e^{-i\vec{k} \cdot \vec{r}} \langle \Delta n(0) \Delta n(\vec{r}) \rangle$$

$$= 2\pi a^2 k^{-2} v \int_0^{2k} K dK \langle |\Delta n_K|^2 \rangle$$

provides localization of the o-Ps. The s-wave scattering length $a > 0$ for a repulsive and $a < 0$ for an attractive potential, and the wave number in the gas or liquid is $k^2 = k_0^2 - 4\pi a n$. This damping constant α is used to form a phenomenological Schrodinger equation whose wave function is damped in the surrounding gas. The kinetic pressure of this localized o-Ps atom is balanced by the hydrostatic pressure of the surrounding gas and yields the probability p of being outside the cavity and in the gas. Near the critical point the Ornstein-Zernike relationship

$$v \langle |\Delta n_K|^2 \rangle = \frac{n(n\mu/\beta)}{1 + \xi^2 K^2}$$

is used. $\xi^2/R_c^2 = n\mu/\beta$ where μ is the isothermal compressibility and $\beta = 1/k_B T$. It is assumed these equations remain valid for matter waves. Well away from the critical point $R_c^2 = R_0^2(n\mu/\beta - 1)/(n\mu/\beta)$ and for an ideal gas $n\mu/\beta = 1$. The values of $n\mu/\beta$ were taken from the experimental equation of state for ethane. The decay rate λ is plotted in the form $(\lambda - \lambda_{vac})/b = Dp$ against D in Figure 1. The curves which are shown are for $a = -0.70 \times 10^{-10}$ m and $R_0 = 1.5 \times 10^{-10}$ m.

The model used in this paper is controversial. If correct it applies also to electron and positron localization in gases and liquids. Recent theoretical work³ on electrons in solids suggest that localization occurs when the elastic free path is comparable to the deBroglie

wavelength and an extension to high density gases would seem appropriate.

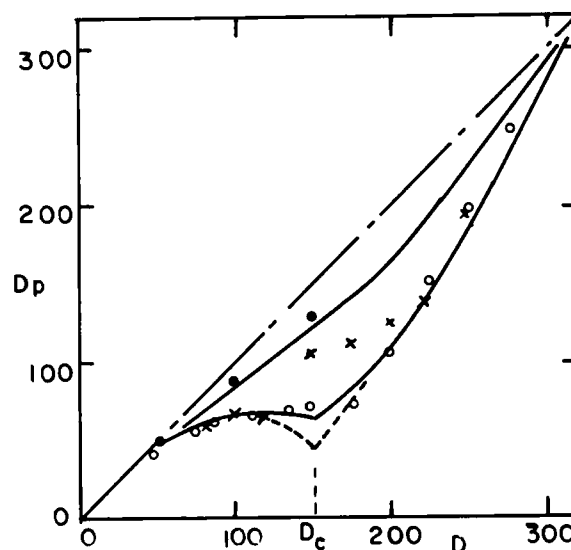


Figure 1. Orthopositronium lifetime $(\lambda - \lambda_{vac})/b = Dp$ in ethane as a function of the number density $n = 2.68 \times 10^{25} \text{ D m}^{-3}$. p is the probability that the o-Ps atom is outside the cavity. The solid curves follow from the theory at $T = 377 \text{ K}$ and $T - T_c = 0.9$, and the dashed curve at $T - T_c = 0.07 \text{ K}$. Solid circles are taken from the experimental curve at $T = 377^\circ$ and the open circles at 306.4 K of Ref. (1). The x are taken from the experimental data at $305.45 \pm 0.1 \text{ K}$ of Ref. (2) and may be in the vapor-liquid region.

References

1. S. C. Sharma, A. Eftekhari, and J. D. McNutt, Phys. Rev. Lett. **48**, 953 (1982).
2. S. C. Sharma, S. R. Kafle, and J. S. Hart, Phys. Rev. Lett. **52**, 2233 (1984).
3. S. John, Phys. Rev. Lett. **53**, 2169 (1984).

INTERACTIONS OF POSITRONIUM WITH CH_4 AND C_2H_6 MOLECULES

Suresh C. Sharma, Michael H. Ward, Charles A. Dark, and Eric M. Juengerman

Center for Positron Studies, Department of Physics
The University of Texas at Arlington, Arlington, Texas 76019

Recent advances in the investigations of the scattering and annihilation of low-energy positrons in simple molecular gases have shown several new and interesting features. For example, i) the cross sections for the pickoff annihilation of orthopositronium atom formed in gaseous C_2H_6 at low densities where one positronium-one molecule interactions dominate show a significant variation with the temperature of the gas¹, ii) the probabilities of positronium formation in CH_4 and C_2H_6 show marked changes with density², and iii) the pickoff annihilation rates of orthopositronium atoms exhibit remarkable sensitivity to density fluctuations in these gases.³⁻⁵

In this paper we present detailed new results from analyses of our data on the formation and annihilation of positronium in CH_4 and C_2H_6 gases. We show that the observed temperature dependence of the cross sections for pickoff annihilation of orthopositronium in C_2H_6 does not result primarily from a velocity dependence of the collision cross section, the subexcitation positron model of positronium formation⁶ provides a reasonably good fit to the electric field dependence of the positronium yields in CH_4 , and that the annihilation behavior of positronium seen in C_2H_6 provides information useful to the equation of state.

References

1. S. C. Sharma, J. D. McNutt, A. Eftekhari, and R. A. Hejl, *J. Chem. Phys.* **75** 1226 (1981).
2. S. C. Sharma, J. D. McNutt, A. Eftekhari, and Y. J. Ataiyan, *Can. J. Phys.* **60** 610 (1982).
3. S. C. Sharma, S. R. Kafle, and J. S. Hart, *Phys. Rev. Lett.* **52**, 2233 (1984).
4. S. C. Sharma, A. Eftekhari, and J. D. McNutt, *Phys. Rev. Lett.* **48**, 953 (1982).
5. J. D. McNutt and S. C. Sharma, *J. Chem. Phys.* **68**, 130 (1978).
6. W. Brandt and H. Feibus, *Phys. Rev.* **174** 454 (1968).

AD-A163 497

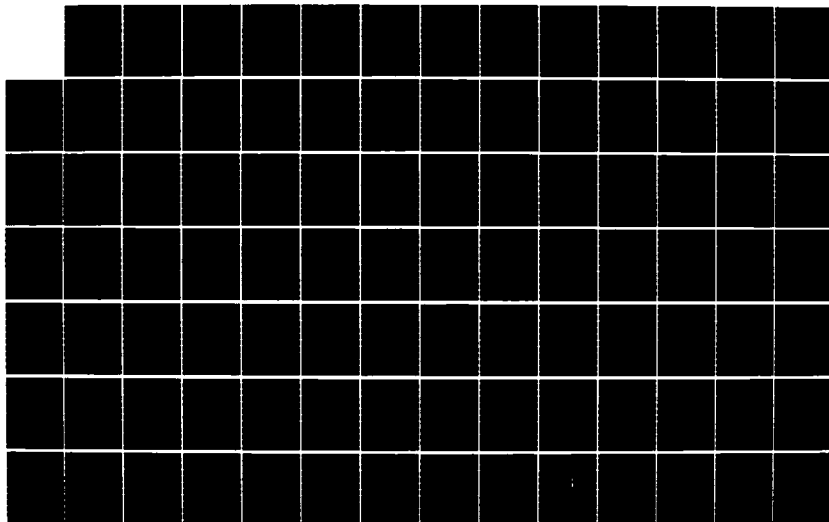
ELECTRONIC AND ATOMIC COLLISIONS ABSTRACTS OF
CONTRIBUTED PAPERS INTERNAT. (U) SRI INTERNATIONAL
MENLO PARK CA MOLECULAR PHYSICS CENTER
M J COGGIOLA ET AL. 1985

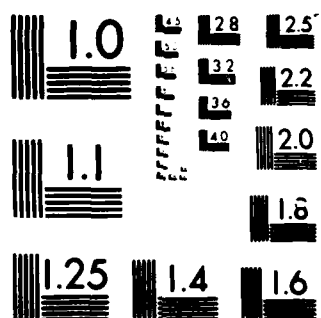
5/8

UNCLASSIFIED

FFG 7/4

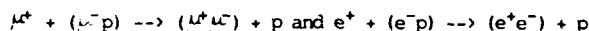
NL



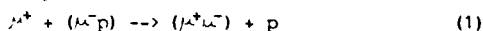


MICROCOPY RESOLUTION TEST CHART
NATIONAL BUREAU OF STANDARDS-1963-A

CLASSICAL TRAJECTORY MONTE CARLO CALCULATION FOR

K. Nakanishi,[†] T. Watanabe,[§] A. Ohsaki,^{*} and K. Iguchi^{*}[†] Department of Chemistry, Waseda University, Ohkubo, Shinjuku-ku, Tokyo 160 Japan[§] Atomic Process Laboratory, The Institute of Physical and Chemical Research (RIKEN), Wako, Saitama 351-01 Japan^{*} Institute for Molecular Science, Okazaki, Aichi 444 Japan

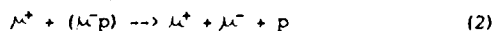
The formation of $(\mu^+\mu^-)$ has not yet been succeeded experimentally, but it is highly desired from the viewpoint of exotic atom physics.¹ One of the possible way for $(\mu^+\mu^-)$ production is to make use of the collision process of



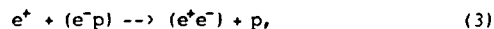
Process (1) can be considered as a similar process of proton-hydrogen charge transfer; $p + (e^-p) \rightarrow (e^-p) + p$. In the comparison of Process (1) with the

proton-hydrogen charge transfer process, there are some difficulties to make a theoretical formulation mainly from the following points; (a) mass ratio of μ -meson to proton is not so small as that of electron to proton, and (b) highly endothermic property of the reaction. In heavy particle collisions, relative motion can be determined independently from other interactions and can often be treated by a almost unperturbed description. This is the reason why we can avoid a real three-body problem in the formulation of charge transefer process by taking into account an nearly unperturbed relative motion. As one of the method to solve a three-body problem, the classical trajectory Monte Carlo (CTMC) method has been developed and applied to many cases.^{2,3} We can treat completely three-body problem and solve them in the limit of classical mechanics. Particularly in the cases of Coulomb interacting three-body collision problems such as charge transfer processes and ionization processes by ion-atom collisions, CTMC method has been applied and been proved to give proper results empirically.² Probably this is supposed to be due to the identity of two-body scattering cross section formulas for Coulomb potential between classical mechanics and quantum mechanics.

Under these theoretical background, we have made a CTMC calculation for Process (1) together with a breakup process of $\mu^+-(\mu^-p)$ collision as



and positron impact process on hydrogen as



for comparison of the accuracy of the method. We take similar coordinate systems as those by Olson and Salop²; C_i ($i=1,2,\dots,9$) represent the Cartesian coordinates particle μ^- (or e^-) ($i=1,2,3$) with respect to p , the

Cartesian coordinates of particle μ^+ (or e^+) ($i=4,5,6$) with respect to the center of mass of (μ^-p) (or (e^-p)), respectively. We can obtain Hamiltonian canonical equations for the system and C_i with $i=7,8,9$ can be substracted from these equations because they are in constant motion. By solving twelve sets of simultaneous equations for C_i and its canonical conjugated variables P_i , with the initial conditions which are relevant to the initial quantum state and are randomly selected by Monte Carlo method, we can obtain the probability, where the final state is found either in the classical bound state (Kepler's orbit) of $(\mu^+\mu^-)$ (or of (e^+e^-)) or not.

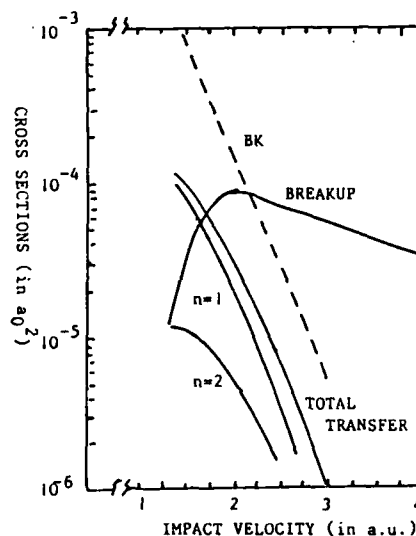


Fig. 1. The cross section for Process (1) and (2), as function of impact velocity of μ^+ . $n=1$ indicates the process in which $(\mu^+\mu^-)$ is formed into the ground state and $n=2$ indicates the process to form into $n=2$ excited states of $(\mu^+\mu^-)$. BK means the cross section by Brinkmann-Kramers approximation.

Reference

- 1) K. Nagamine, Invited talk at IIIrd LAMPF II Workshop (Los Alamos, July, 1983).
- 2) R. E. Olson and A. Salop, Phys. Rev., **A16** 531 (1977).
- 3) Reference cited in Ref. 2

QUANTUM MECHANICAL STUDY FOR THE PROCESS OF $\mu^+ + (\mu^- p) \rightarrow (\mu^+ \mu^-) + p$

Q.Ma, X.Cheng, Z.Liu, Y.Liu, and T.Watanabe*

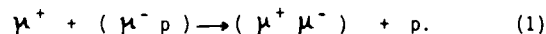
* Department of Modern Physics, China University of Science and Technology, Hefei, Anhui Province China.
Atomic Process Laboratory, The Institute of Physical and Chemical Research (RIKEN),
Wako-shi, Saitama-ken 351-01, Japan.

Recently classical trajectory Monte Carlo (CTMC) method has been applied to the process of $\mu^+ + (\mu^- p) \rightarrow (\mu^+ \mu^-) + p$ and $e^+ + H \rightarrow (e^+ e^-) + p^1$.

We will make a calculation in quantum mechanical way for

$\mu^+ + (\mu^- p) \rightarrow (\mu^+ \mu^-) + p$ in order to compare the results with those by CTMC method. This process has been suggested by Nagamine²⁾ as one of the possible way to produce $(\mu^+ \mu^-)$ atom from experimental point of view.

The atomic structures of exotic particles draw much attention from the viewpoint of quantum electrodynamics (QED). They will give us many information concerning QED because the interaction there is direct and they need not to use complex perturbation calculations. As one of the possible way to produce $(\mu^+ \mu^-)$, one can consider the process as



Here we are formulating and calculating the cross sections for process (1) by using quantum mechanical way. The process (1) is characterized by the large mass transfer between initial and final states and consequently the center of mass of incident particle is greatly varied. Furthermore, there exist large endothermic energy difference (1.13 KeV) between initial and final states. In this sense, this is considered to be typical three-body collision problem. CTMC method treats three-body problem rigorously in classical mechanics. We can obtain the characteristic feature of the three-body problem in the limit of classical mechanics. On the other hand, the quantum mechanical method may show the characteristic feature of quantal effects. For this reason if we can obtain similar results for the same process by the first Born approximation or by some improved approximation with those by CTMC, the cross section can be considered reliable.

The first order Born approximation (FBA) and the first order distorted wave approximation (DWBA) have been applied for the process (1)³⁾. Using the initial relative coordinate \vec{R} (relative coordinate of μ^+ with respect to the center of mass of $(\mu^- p)$) and the initial inner coordinate \vec{r} and the final relative coordinate \vec{R}' (relative coordinate of p with respect to the center of mass of $(\mu^+ \mu^-)$) and the final inner coordinate \vec{r}' , the total Hamiltonian of the system can be written as

$$H = -\frac{\hbar^2}{2\mu} \nabla_R^2 - \frac{\hbar^2}{2\nu} \nabla_r^2 - \frac{e^2}{r} + H'_i(\vec{r}, \vec{R})$$

$$\text{and } H = -\frac{\hbar^2}{2\mu'} \nabla_{R'}^2 - \frac{\hbar^2}{2\nu'} \nabla_{r'}^2 - \frac{e^2}{r'} + H'_f(\vec{r}', \vec{R}')$$

where μ and μ' are reduced masses of the relative motion in the initial and a final state, and ν and ν' reduced masses of composite atom in the initial and a final state, respectively. $H'_i(r, R)$ and $H'_f(r', R')$ are the interaction Hamiltonian in the initial and final state.

We assume the total wave function of colliding system as

$$\Psi = F_i(\vec{R}) \psi_i(\vec{r}) + F_f(\vec{R}') \psi_f(\vec{r}'),$$

where $\psi_i(\vec{r})$ and $\psi_f(\vec{r}')$ are the ground state eigenfunction of composite particles in the initial and a final state and $F_i(\vec{R})$ and $F_f(\vec{R}')$ the corresponding wavefunction of relative motions.

The equations for $F_f(\vec{R}')$ in FBA and in DWBA are

$$\left(-\frac{\hbar^2}{2\mu'} \nabla_{R'}^2 + E_f - E \right) F_f^{FBA}(\vec{R}') + \langle \psi_f(\vec{r}') | H'_i | F_i^0(\vec{R}) \psi_i(\vec{r}) \rangle_{\vec{r}} = 0$$

where $F_i^0(\vec{R})$ is a plane wave in the initial state, and

$$\left(-\frac{\hbar^2}{2\mu'} \nabla_{R'}^2 + E_f - E \right) F_f^{DW}(\vec{R}') + \langle \psi_f(\vec{r}') | \left(-\frac{\hbar^2}{2} \nabla_R^2 + E_i - E \right) | F_i^{DW}(\vec{R}) \psi_i(\vec{r}) \rangle_{\vec{r}} + \langle \psi_f(\vec{r}') | H'_i | F_i^0(\vec{R}) \psi_i(\vec{r}) \rangle_{\vec{r}} = 0$$

From these $F_f^{FBA}(\vec{R}')$ and $F_f^{DW}(\vec{R}')$, the scattering amplitude $f(\theta)$ and the total cross section with these $f(\theta)$ can be obtained as

$$\sigma = \frac{V_f}{V_i} \int |f(\theta)|^2 d\Omega,$$

where V_i and V_f are the velocities of initial and final states, respectively. This results show that DWBA's result is not so much different from FBA's result and these are 30~50% larger value than CTMC results in the impact velocity region 1.75~3.0 a.u.. Brinkmann-Kramers results are about five times as much as that of FBA.

CTMC results are considered more reliable than those of FBA and DWBA in the velocity region below 1.7 a.u.. From these results we can conclude that the maximum of cross section lies around 1. a.u. impact velocity (2.0~3.0 KeV impact energy) and its magnitude is $3.5 \sim 5.0 \times 10^{-4} a_0^2$ (a_0 being the hydrogen Bohr radius) or $2.7 \sim 4.0 \times 10^{-20} \text{ cm}^2$.

References

1. A.Ohsaki, T.Watanabe, K.Nakanishi and K.Iguchi, Abstract of XIV ICPEAC (1985).
2. K.Nagamine, Proceeding of 3rd LAMPF II Workshop, eds., J.C.Allred, T.S.Bhatia, K.Ruminer and B.Talley (LA-9933-C, 1983)p.258.
3. P.Mandal and S.Guha, J.Phys. B12,1603(1979).

RATIO OF THE CROSS-SECTION FOR LEPTON AND ANTI-LEPTON SCATTERING FROM HYDROGEN ATOM
- A FIELD THEORETIC APPROACH

Sujata Bhattacharyya*, Lali Chatterjee and Keka Basu Choudhury

*Gokhale College, Calcutta 700020, India.
Department of Physics, Jadavpur University, Calcutta 700032, India.

A comparative study of the same generation lepton and anti-lepton scattering from hydrogen atom is done. The ratio of the elastic differential cross-section for the first generation species (e^-, e^+) is found to be a function of scattering angle and energy of the projectile. Whereas in the case of second or third generation leptons the ratio is found to be unity with second order S-matrix.

Here we try to extend the technique of Feynman diagrams without further modification to free-bound interactions. The philosophy behind the approach is to take the S-matrix expansion for the free interacting particles. The S-matrix is then operated upon by the initial and final physical states. The bound wave function¹ which is a solution of Dirac equation in Lorentz gauge, takes into account exchange of Coulomb photon of all orders. The effect of binding on the amplitude comes through these bound state vectors.

The amplitude for the processes

$$H+L^{-(+)} \rightarrow H+L^{-(+)}$$

is determined from the sum of three Feynman diagrams with one virtual photon exchange in each case. The direct and exchange interaction diagrams of $L^{-(+)}$ (Lepton (Antilepton)) with bound-electron of the hydrogen atom are added to the nucleus-lepton (anti-lepton) interaction diagram. For the second and third generation leptonic pairs (μ^\pm, τ^\pm) the exchange interaction do not arise. In the case of atomic collision in the non-relativistic energy range the proton form-factor is found to have negligible contribution. So that nucleus behaves as a lepton of heavy mass.

With low target momentum contribution from lepton (anti-lepton)-bound-electron interaction (direct) and lepton (anti-lepton)-nucleus interaction are found to be same. Interference of lepton-nucleus term with both the exchange and direct term vanishes identically because of vanishing trace between odd number of γ -matrices involved. With higher order diagram it is worth searching for the contribution towards such interferences.

In the case of positron interaction with bound electron the exchange term arises from pair annihilation. Contribution of the annihilation diagram is very low in the case of free-free interaction in the nonrelativistic limit. But here the annihilation diagram is found to modify the cross-section through interference with direct term because of the integrals over bound wave functions.

The ratio $\frac{\sigma^-(\theta)}{\sigma^+(\theta)}$ is always greater than one. This shows the scattering of electron off hydrogen target is favoured more than that of the positron. But hydrogen atom does not show this difference in behaviour for the second and third generation leptons (μ^\pm, τ^\pm) for which the ratio is always one. This may be attributed to the fact that the target and projectile leptons are of different generations. Other existing results also yield the ratio $\frac{\sigma^-(\theta)}{\sigma^+(\theta)}$ to be greater than one. However, although in those cases, $\frac{\sigma^-(\theta)}{\sigma^+(\theta)}$ varies slightly with angle near the forward direction, after that it remains almost independent of angle for a particular energy. Our result is compared with other model¹ calculations. After initial rise in the forward direction the ratio $\frac{\sigma^-(\theta)}{\sigma^+(\theta)}$ is found to decrease with angle and energy. There is a scope to improve our result by including higher order radiation correction and distortion of the projectile wave function. Ratio $\frac{\sigma^-(\theta)}{\sigma^+(\theta)}$ for 40° lab. scattering angle. UEBS is the unitarised Eikonal Born Series of Ref. (2).

Energy (ev)	100	200	300	400
$\sigma^-(\theta)/\sigma^+(\theta)$				
Present	1.535	1.311	1.225	1.183
UEBS	1.645	1.367	1.252	1.189

Reference

1. I. Harris and C.M. Brown, Phys. Rev. **105**, No. 5, p.1656 (1957)
2. F.W. Byron, C.J. Joachain, R.M. Potvliece, J. Phys. **B15**, P.3915 (1982).

AUGER FORMATION OF $(\text{PuH})^+$ MUO-MOLECULAR ION

L. Chatterjee and S. Bhattacharyya*

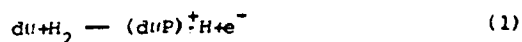
Jadavpur University, Calcutta 700032, India

*Gokhale College, Calcutta 700020, India.

The $(\text{PuH})^+$ auger formation rate is calculated for the $V=0$, $J=0$, and $J=1$ levels and the values compared with other existing ones. Distortion effects are discussed.

The non-resonant Auger-muo-molecular formation process has been proved in a field theoretic manner, using QED in the Coulomb gauge. The low energies involved justify the use of the Coulomb gauge - but the justification of using Born type approximations at these energies remains questionable. We can however introduce distorted wave functions for the initial state to improve accuracy. For a simple estimate we may also use the Sommerfeld factor to weigh the effect of distortion. However, as muonic atoms are dimensionally 200 times smaller than the target host molecules, their interaction is neutronlike, so distortion effects are expected to be small. We discuss this aspect.

We assume that the Auger formation process for muonic atoms incident on Hydrogen molecules



is not noticeably different from formation of the corresponding atoms. This is mainly because the neutron-like mesic atom can penetrate freely through the molecule, and interact with one or other of the target nuclei. The spectator nucleus is left behind in a neutral atomic state with one electron. This spectator atom is further not expected to recoil, so that the effective kinematics remains same as in the atomic case. This was observed in 1957 by Jackson¹.

Further, hydrogen atoms may be formed in the chamber due to dissociation of target molecules by Auger mesomolecule formations. Free nucleons, present in the system could also participate in molecule formation, a nearby spectator electron carrying away the energy release. We thus obtain the $(\text{PuH})^+$ formation rate as $4.87 \times 10^6 \text{ sec}^{-1}$. This is in excess of our previous computation² and includes the $J=1$ final state which was neglected then.

The rate of formation of $(\text{PuH})^+$ muomolecular ion computed by us is in good agreement with experiment and lies between the two exist-

ing theoretical values. Table 1.

The methodology involved utilises a Born-type expansion of the scattering matrix in powers of the electromagnetic coupling constant. While this is retained to first order for the interaction, the exchange of Coulomb photons is accounted for to all orders through the initial and final bound state wavefunctions. The inclusion of both μ -p and μ -d interactions in the matrix element, and their resultant interference distinguishes it from simple first Born calculations. The contraction of the field operators in the Hamiltonian with the creation and annihilation operators in the state Vectors yield momentum relations between the interacting particles. This approach may also be used to study the resonant molecule formation process.

Table 1. Values are from ref. (3)

	Con- forte et al.	Ble- ser et at.	Eys- tri- ta- kie	Co- hen	Zal- devish and Gers- tain	Pono- morev and Faif- man	Pre- sent
(10^6 s^{-1})	6.82	5.6	5.53	3.0	1.3	5.91	4.87
	\pm	\pm	\pm				
	0.25	0.03	0.16				

References

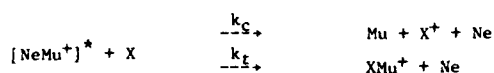
1. M. Leon, Phys. Rev. Lett. 52, Page 605
2. L. Chatterjee and S. Bhattacharyya, Phys. Letters 93A, No. 7, P. 360 (1983).
3. L. I. Ponomarev, N. P. Faifman, Sov. Phys. JETP 886 (1976).

REACTIONS OF POSITIVE MUON MOLECULAR IONS IN THE GAS PHASE

I.D. Reid, M. Senba, D.J. Arseneau, D.M. Garner, and D.G. Fleming

TRIUMF and Department of Chemistry
University of British Columbia
4004 Wesbrook Mall, Vancouver, B.C., Canada, V6T 2A3

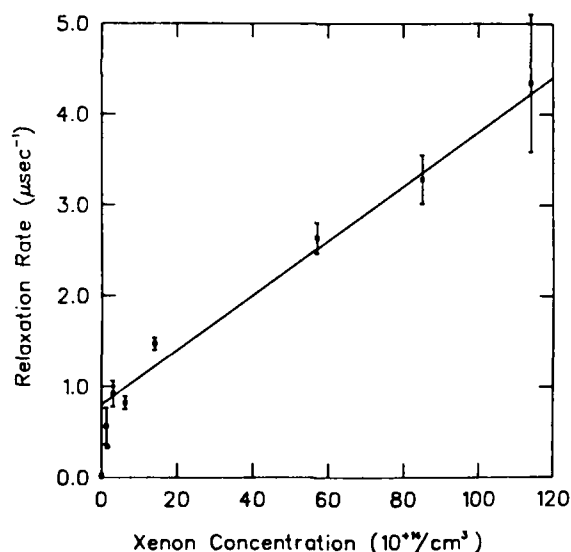
The diamagnetic muon spin rotation signal from positive muons stopped in the noble gas moderators He, Ne and Ar is due to the formation of μ^+ molecular ions (e.g. $[\text{HeMu}^+]^*$) in ro-vibrationally excited states.¹ This signal is very long-lived, with $T_2 \sim 50 \mu\text{s}$. Upon the addition of some reactant gas X thermal charge exchange may cause the formation of muonium ($\text{Mu}=(\mu^+e^-)$), depolarizing and hence relaxing the signal, in competition with muon transfer: e.g.



where k_c and k_t are the rate constants for charge exchange and muon transfer, respectively. The competition produces two relaxations, a fast component due to charge exchange, and a slow component due to muon transfer where the muons, remaining in a diamagnetic environment, maintain their polarization.

We have studied k_c at room temperature for a variety of reactants X (Xe, Kr, CH_4 , C_2H_6 , C_2H_4 , CH_3F , NH_3 and N_2O) in He and Ne, and for Xe, NH_3 and CH_4 in Ar. Relaxation was not seen in Ar for any dopant, nor for CH_4 or C_2H_6 dopants in He or Ne. A fast relaxation component was seen with all the other reactants in both He and Ne, although the reactions with C_2H_4 and Kr were measureable only in Ne. The Kr reactions are surprising since Mu formation with Kr should be endothermic, even for a bare muon.

Figure 1 shows recent and previously published¹ data for the relaxation rate λ vs Xe concentration for the $[\text{NeMu}^+]^* + \text{Xe}$ reaction. The new data extends to much lower concentrations, showing a pronounced curvature in λ at these concentrations which was not established previously; all reactants show similar behaviour at low concentrations. Within errors, all the high-concentration data can be fitted to a linear dependence (e.g. Fig. 1) from which a rate constant k_c is determined. Preliminary values for k_c are given in Table 1, compared with theoretical calculations from simple Langevin theory (Xe, Kr, CH_4 , C_2H_4) or from the Average Dipole Orientation (ADO) theory (CH_3F , NH_3). Given present uncertainties about the reaction mechanism, the agreement between theory and experiment is good, with the notable exception of CH_4 , suggesting that muon transfer (k_t) dominates over charge exchange in this case. This may be related to tunnelling-enhanced

FIGURE 1 $[\text{NeMu}^+]^*$ Reaction with Xe

fragmentation of metastable ions,² particularly if an intermediate complex is formed, as in current work on ion-molecule reactions.³

Reactant	He moderator		Ne moderator	
	$k_c(\text{exp})$	$k_c(\text{theory})$	$k_c(\text{exp})$	$k_c(\text{theory})$
Xe	12 ± 4	23.5	3.0 ± 0.5	11
CH_4	< 0.02	20.5	< 0.02	12.5
NH_3	60 ± 20	36	26 ± 3	21
CH_3F	29 ± 5	37	7 ± 2	20
N_2O	20 ± 2	—	11 ± 1	—
C_2H_4	?	25	20 ± 4	14
Kr	?	19	7.2 ± 0.9	9.1

TABLE 1 $[\text{HeMu}^+]^*$ and $[\text{NeMu}^+]^*$ Molecular Ion Reaction Rates (10^{-10} cc/Sec)

References

1. D.G. Fleming et al., Chem. Phys. **82**, 75 (1983).
2. M.F. Jarrold, A.J. Illies and M.T. Bowers, Chem. Phys. Letts. **92**, 653 (1982); J.E. Moryl and J.M. Farrar, J. Phys. Chem., **86**, 2020 (1982).
3. M. Durup-Ferguson, H. Bohringer, D.W. Fahey and E.E. Ferguson, J. Chem. Phys. **79**, 265 (1983); W. Dobler et al., *ibid.*, **79**, 1543 (1983).

DYNAMICS OF MUON SPIN POLARIZATION DURING CYCLIC CHARGE EXCHANGE IN NOBLE GASES

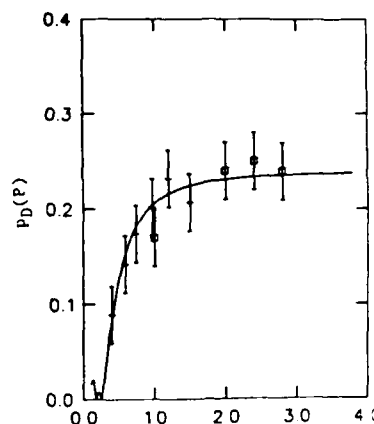
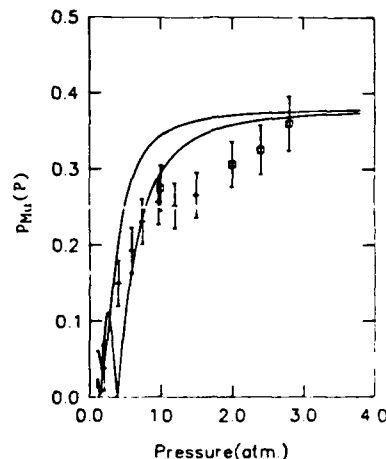
M. Senba, R.E. Turner, I.D. Reid, D.M. Garner, D.J. Arseneau, and D.G. Fleming

TRIUMF and Department of Chemistry
University of British Columbia
4004 Wesbrook Mall, Vancouver, B.C., Canada, V6T 2A3

A beam of 4.2 MeV positive muons (100% spin polarized) was stopped in noble gas targets and the spin polarizations of muons thermalized as triplet muonium and in diamagnetic chemical environments have been measured as a function of pressure, $p_{\text{Mu}}^t(P)$ and $p_D(P)$, respectively. A set of coupled quantal rate equations for muon spin dynamics, based upon quantal Boltzmann equations, have been developed^{1,2} to calculate $p_{\text{Mu}}^t(P)$, $p_{\text{Mu}}^s(P)$, and $p_D(P)$ where $p_{\text{Mu}}^s(P)$ is for singlet muonium which is unobservable in this experiment. The dynamics of the muon spin is generated by the muonium hyperfine interaction between the positive muon and the electron and by the electron pickup and loss rates ($k_p(t)$ and $k_e(t)$) of muon and muonium, respectively.

Energetic charged particles undergo three broad regimes of energy loss as they thermalize in gases. At high energies where slowing-down is mainly via ionization of atomic electrons (Bethe-Bloch regime), no significant muonium formation occurs. In the second regime the muon passes through a series of charge exchange cycles, $\mu^+ + e^- \longleftrightarrow \text{Mu}$, where it spends an appreciable amount of time as a muonium atom. Muons emerge from the charge exchange regime in one of these chemical environments, the probability of which depends upon $k_p(t)$ and $k_e(t)$. In the last stage the thermalization process is dominated by elastic, inelastic and reactive collisions and there are no further charge exchange cycles. Due to the presence of the hyperfine interaction there may be a significant muon depolarization in the charge exchange region. That is, during free flight of muonium between collisions there is an exchange of polarization between the muon and the electron which is mediated by the hyperfine interaction ($\nu=4463.3$ MHz). If the time between collisions approaches the order of the hyperfine period ($1/\nu=0.22$ nsec) then the electron can carry away an appreciable portion of the polarization when it is lost in the next charge exchange reaction.

In order to solve the coupled rate equations, the following assumptions have been made: (1) $k_p(t)$ and $k_e(t)$ are nonzero only in the charge exchange regime and (2) they are time independent. There are three adjustable parameters, i.e. k_p , k_e and a constant which relates the pressure to the time span of the charge exchange regime (t_c). Figures 1 and 2 show fits to the data taken in Ar. A set of parameters was obtained through a fit of $p_D(P)$ shown in Fig. 1, and these parameters were used to calculate $p_{\text{Mu}}^t(P)$ which is the

FIGURE 1 $p_D(P)$ in Ar. Pressure(atm)FIGURE 2 $p_{\text{Mu}}^t(P)$ (upper) and $p_{\text{Mu}}^s(P)$ (lower) in Ar, the superscripts t and s refer to triplet and singlet muonium spin states, respectively.

upper curve at high pressures shown with data points in Fig. 2. The lower curve is $p_{\text{Mu}}^s(P)$. The time span for the charge exchange regime (t_c) in 760 Torr Ar has been determined to be 0.04 nsec, in good agreement with earlier studies.³ The quantity t_c is difficult to obtain in proton charge exchange studies. It is interesting to note that, $p_{\text{Mu}}^t(P)$ and $p_{\text{Mu}}^s(P)$ are, in general, not equal and the p's could be oscillating functions of pressure.

Reference

1. R.E. Turner, Phys. Rev. **A28**, 3300 (1983).
2. R.E. Turner and M. Senba, Phys. Rev. **A29**, 2541 (1984).
3. D.G. Fleming et al., Phys. Rev. **26**, 2527 (1982).

TEMPERATURE DEPENDENCE OF MUONIUM SPIN EXCHANGE WITH O₂

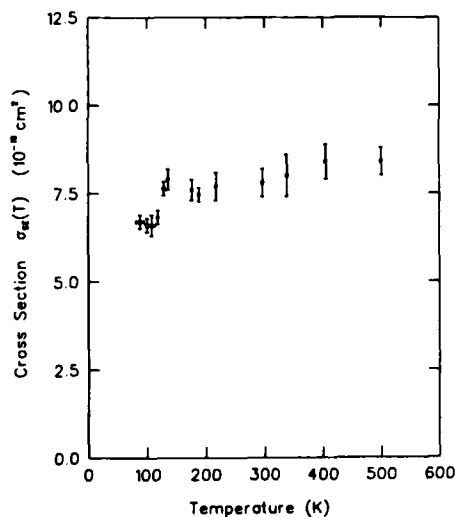
M. Senba, I.D. Reid, D.M. Garner, D.J. Arseneau, and D.G. Fleming

TRIUMF and Department of Chemistry
University of British Columbia
4004 Wesbrook Mall, Vancouver, B.C., Canada, V6T 2A3

Muonium (Mu) is a bound state of a positive muon (μ^+) and an electron and can be regarded as an ultra light isotope of hydrogen atom with a mass ratio of $m(\text{Mu})/m(\text{H})=1/9$. We have measured the temperature dependence of the spin exchange cross section of Mu with O₂ from 88 K to 500 K using the muon spin rotation technique (MSR).

Details of the MSR technique can be found in Refs. 1-3. Muons produced in the decay process $\pi^+ \rightarrow \mu^+ \nu_\mu$ are 100% longitudinally spin-polarized due to parity violation in the weak interaction. These muons are stopped in a moderator (typically 800 Torr N₂ or Ar) doped with a known amount (typically of order 0.1%) of O₂. A muonium atom in its triplet state precesses in a weak transverse magnetic field with a frequency of 1.39 MHz/Gauss. The MSR-technique observes the time evolution of the muon spin precession by time-differentially detecting positrons which are emitted preferentially along the muon spin direction at the instant of muon decay ($\mu^+ \rightarrow e^+ \bar{\nu}_\mu \nu_e$). Exchange of electrons with opposite spin directions between Mu and O₂ disturbs the precession of muon spin and removes this muonium atom from the spin-coherent Mu ensemble. This spin exchange process manifest itself as damping of the MSR signal defined as $S(t) = A e^{-t/\lambda} \sin(\omega t + \phi)$ where A is the initial asymmetry, ω is the Larmor frequency of triplet muonium in a transverse applied field, ϕ is the initial phase, and λ is the relaxation rate which is related to the spin-exchange cross section $\sigma_{se}(T)$ via $\lambda = \lambda_0 + [O_2](1/2)fV\sigma_{se}(T)$ where $[O_2]$ is the concentration of O₂, f is 8/9 for spin 1 oxygen, and V is the average relative velocity of O₂ and Mu. The relaxation rate was measured at various O₂ concentration, and the cross section was determined from the slope of the λ vs $[O_2]$ curve.

The result of the measurements is shown in Fig. 1. $\sigma_{se}(T)$ is found to be independent of temperature from 125 K to 500 K within the accuracy of this experiment, which is consistent with a simple random phase approximation with a cut-off interaction length. Below 118 K, $\sigma_{se}(T)$ decreases to another constant value. The cause of this drop in the cross section is not yet

FIGURE 1 Spin exchange cross section of Mu with O₂

established. To rule out the possibility of O₂ condensation on the surface of the aluminum target vessel, off-beam tests have been performed and no sign of condensation of O₂ was seen down to 87 K. Condensation of O₂ or possible presence of cold spots in the vessel is inconsistent with the observation that even below 118 K the observed relaxation rate is a linear function of O₂ concentration. As for the possible formation of dimers (O₂)₂, these would presumably be formed via termolecular processes and the absence of definite moderator pressure dependence of $\sigma_{se}(T)$ excludes this possibility. The quantity $\sigma_{se}(T)$ is the thermal average of energy dependent cross section $\sigma_{se}(E)$. Therefore the observed strong temperature dependence in $\sigma_{se}(T)$ at low temperature could be attributed to possible resonance structure in $\sigma_{se}(E)$ for Mu-O₂.⁴

References

1. D.G. Fleming et al., J. Chem. Phys. **73**, 2751 (1980).
2. R.J. Mikula et al., J. Chem. Phys. **75**, 5362 (1981).
3. D.G. Fleming et al., Phys. Rev. **26**, 2527 (1982).
4. M. Senba et al., Hyperfine Interactions **17-19**, 703 (1984).

PIONIUM IN QUANTUM ELECTRODYNAMICS

A. Karimkhodzhaev*, A. Karich†, R.N. Faustov**

*Institute of Physics, P.O. Box 57, Belgrade, Yugoslavia
Tashkent State University, Tashkent, USSR

†Institute of Physics, P.O. Box 57, Belgrade, Yugoslavia

**VNIICPV, Moscow, USSR

In recent years there has been a constantly growing interest on the structure of the S.C. exotic atoms like $(\pi\mu)$, (πe) , $(\pi\pi)$ physical systems. The energy levels of the $(\pi\mu)$ atomic system¹ have been calculated up to the two-photon exchange approximation including the hadronic vacuum polarization effects². It is to be pointed out that the Lamb-shift measurement of such system would provide an alternative information on the π -meson radius. In the previous publication³ it has been shown that it would be possible in high energy accelerators to create $(\pi^+\pi^-)$ atomic systems and to measure the lifetime, the absolute square of the wave function at the origin, and the Lamb-shift.

In the present note we show the result of the calculation of the energy levels of pionium in the framework of the quasipotential approach of the Logunov-Tavkhelidze⁴ using one-photon exchange approximation. The second order effects in the point like pion vertex function and the electron-positron vacuum polarization effects are included.

The Lamb-shift of the pionium reads

$$\begin{aligned} \Delta W(2S) - \Delta W(2P) = & - \frac{\alpha^4 \mu}{12} \left(1 - \frac{3\mu}{2(m_a + m_e)} \right) + \\ & + \frac{\alpha^5 \mu^3}{72\pi} \left[\frac{1}{m_a^2} + \frac{1}{m_e^2} \right] + \frac{\alpha^5 \mu^3}{6\pi} \left[\frac{1}{m_a^2} \ln \frac{m_a}{2W_{2,0}^{av}} + \right. \\ & + \left. \frac{1}{m_e^2} \ln \frac{m_e}{2W_{2,0}^{av}} - \left(\frac{1}{m_a^2} + \frac{1}{m_e^2} \right) \ln \frac{R_y}{W_{2,1}^{av}} \right] - \\ & - \frac{\alpha R_y}{3\pi} \int_0^1 \frac{c^2 \sqrt{1-x} \left(1 + \frac{x}{2} \right)}{(\sqrt{x} + c)^4} dx. \end{aligned}$$

where $m_a = m_{\pi^-}$, $m_e = m_{\pi^+}$, $\mu = \frac{m_a m_e}{m_a + m_e}$

$$c = \frac{2m_e}{\alpha\mu}, \quad R_y = \frac{\alpha^2 \mu}{2}$$

$W_{n,l}^{av}$ - is the average of the excitation energy with the reduced mass used and m_e is the electron mass.

In this approximation the hadronic effects are not included. Their contribution would appear through the S-wave of the π - π scattering and the measured value of the Lamb-shift would provide a more precise value for the scattering length.

The numerical value Lamb-shift is

$$\Delta W(2S) - \Delta W(2P) \approx - 11? \cdot 10^{-3} \text{ eV.}$$

References:

1. Combes R. et al. Phys.Rev.Lett. v. 37, p. 249, 1976
Aronson S.H. et. al. Phys.Rev.Lett. v. 48, p. 1048, 1982.
2. Karimkhodzhaev A., Faustov R.N. Yad.Fiz. v. 29, p. 463, 1979.
3. Nemenov L.L. JINR P1-84-285, Dubna, 1984.
4. Logunov A.A., Tavkhelidze A.N. Nuov. sim. v.39, p. 580, 1963.
Faustov R.N. Fizika elementarnih sostoyaniy i atomnogo jadra, v.3, p. 283, 1972, Atomizdat.

TOTAL SCATTERING CROSS-SECTIONS AND INTERATOMIC POTENTIALS
FOR NEUTRAL HYDROGEN AND HELIUM ON SOME NOBLE GASES

David N. Ruzic* and Samuel A. Cohen

Princeton Plasma Physics Laboratory, Princeton, NJ 08544, USA

Present address: Fusion Studies Laboratory, University of Illinois, Urbana, IL 61801 USA

Measurements of the total scattering cross-section for 30 to 1800 eV D incident on He, Ne, Ar and Kr, and from 40 to 850 eV He incident on He, Ar and Kr are presented. They provide a way to extract the interatomic potential over a narrow range in interatomic distances. The potentials thus determined are in the repulsive wall region, roughly 0.5 Å to 2.0 Å depending on the pair. Knowledge of the cross-sections increase understanding of edge effects, improve designs and models of divertors and pumped limiters, and refine calculations of neutral density profiles in fusion devices.

The cross-sections are determined by passing energetic neutral atoms through a gas-filled scattering cell and monitoring the attenuation as a function of pressure in the cell. A complete description of the apparatus and techniques can be found in reference 1. The source of the energetic neutrals is the charge exchange efflux from the Princeton Large Torus (PLT) tokamak. The PLT tokamak proves 1-second "shots" of nearly constant 2×10^{15} atoms/cm² efflux. The great advantage of using the PLT tokamak is the purity of the efflux and the "brightness" of the emission in the desired energy range. The energy spectrum is roughly Maxwellian with an average energy of 250 eV. No other source of neutrals has comparable brightness over this broad energy range. For this reason tokamaks offer a unique method for studying certain atomic processes.

The detector of the energetic neutrals is the Low-Energy Neutral-Atom Spectrometer (LENS)². The LENS is a time-of-flight spectrometer with an energy range of 10 eV to 2000 eV for deuterium. The minimum detectability threshold for deuterium at 100 eV is 1.0×10^{10} atoms/cm² eV s ster when the time resolution is 1 msec. Since the flux over a wide energy range is measured virtually simultaneously, and since elastic neutral-neutral collisions dominate at these energies, the dependence of cross-section on energy for a particular pair of atoms can be determined during one PLT "shot".

What is actually measured is $\bar{S}_{sc}(E)$, the averaged effective-angle-dependent total scattering cross-section. It is an averaged quantity because the scattering cell has finite dimension; it is effective-angle dependent because deflections smaller than a certain angle are still detected. Further complications arise from scattering events that add particles into the beam. Variation of pressure along the scattering path, beam divergence, scattering that adds to

the beam, and quantum-mechanical corrections for small-angle scattering were all taken into account in the effective-angle calculation.

If the problem is treated classically an analytic expression for \bar{S}_{sc} can be found assuming the interaction is governed by a spherical potential $V(r) = Kr^{-s}$.³

$$\bar{S}_{sc} = \pi \left(\frac{KF(\theta)}{E} \right)^2 \langle \theta^{-2} \rangle \quad (1)$$

and

$$\langle \theta^{-2} \rangle \equiv \frac{1}{2\pi b} \frac{\int \int_0^{2\pi} \theta_d^{-2} d\phi d\vec{r} - \int \int_{\phi_{min}}^{\phi_{max}} (\theta_{dmin}^{-2} - \theta_{dmax}^{-2}) d\phi d\vec{r}}{\int d\vec{r}} dz \quad (2)$$

where θ_{min} , θ_{max} , θ_d , θ_{dmin} , and θ_{dmax} refer to scattering angles in the gas cell that are generally functions of position, incident and azimuthal scattering angles¹, and $F(s) = \pi^{1/2} \Gamma(s/2 + 1/2) / \Gamma(s/2)$. Note that \vec{r} has four dimensions: two angles to define the incident beam's direction, and the x and y dimensions of the scattering cell. The effective scattering angle, θ_{ef} , can now be defined: $\theta_{ef} = \langle \theta^{-2} \rangle^{-1/2}$. To find s from the data, equation (1) can be put into linear form and solved graphically. In principal K can also be found but the error associated with the extrapolation to find the intercept value of a logarithmic quantity is quite large. The validity limits for the interatomic potential's range from the minimum and maximum scattering cross-sections observed. The table below summarizes the data:

Incident, target atoms	θ_{ef} (mrad)	s	K(max) Å ^s eV	K(min) Å ^s eV	r_{max} Å	r_{min} Å	\bar{S}_{sc} (Å ²) at 200eV
D,He	19.5±2.7	2.60	4.02	.662	1.3	.33	1.4±.1
D,Ne	22.1±4.0	3.45	14.2	3.96	2.3	.71	4.7±.3
D,Ar	23.9±5.4	4.45	14.9	5.06	2.20	.81	4.8±.3
D,Kr	24.7±6.4	5.20	12.4	4.53	1.30	.84	4.6±1.0
He,He	19.5±2.7	2.60	5.74	.946	1.2	.38	2.0±.3
He,Ar	22.64±4.2	3.70	28.4	8.6	2.4	1.1	6.5±1.0
He,Kr	24.1±5.9	4.90	47.5	16.9	2.2	1.2	7.5±1.0

Acknowledgements: This work was supported by the Fannie and John Hertz foundation and DOE contract #DOEC02-76-CHO-3073.

References:

- David Neil Ruzic, Ph.D. Thesis, Princeton University, (1984).
- D. E. Voss and S. A. Cohen, *Rev. Sci. Instrum.*, **53**, 1696 (1982).
- I. Amdur and J. E. Jordan, *Advan. Chem. Phys.*, **10**, 29 (1966).

BOUND STATES OF COMPOSITE PARTICLES USING QUANTUM FIELD THEORY

D. N. Tripathy

Institute of Physics, Sachivalaya Marg, Bhubaneswar-751005, India.

There has been a great success in using the methods of quantum field theory to the study of bound states of elementary particles both in relativistic¹ and nonrelativistic² quantum mechanics. This has been achieved by solving the Bethe-Salpeter equation for two-body problems. However, very little progress has been made on the application of the field theoretic techniques to study the bound states of composite particles. Quite sometime back Girardeau, through a series of papers³, has developed a second quantized formulation of a system of composite particles by defining the creation and annihilation operators for the atomic species. In this formalism he has arrived at an expression for a projected Hamiltonian which contains the interatomic (Coulomb) interactions V plus some effective interatomic exchange interactions arising out of exchanges of electrons and nuclei. In the present work we apply Girardeau's formalism with appropriate modifications to study the bound state of two neutral hydrogen atoms, the simplest composite particle.

We start with the Hamiltonian for the system of composite particles without the exchange term, which is written in the form :

$$H = H_0 + V, \quad (1)$$

where V denotes the interatomic Coulomb interaction whose expression in terms of the atomic field operators has been given by Girardeau³. The matrix element $\mathcal{V}_{\beta\beta'}^{(0)}(\vec{r}-\vec{r}')$ that appears in the expression for V is given by

$$\mathcal{V}_{\beta\beta'}^{(0)}(\vec{r}-\vec{r}') = \int d\vec{r}_e d\vec{r}_p \phi_{\beta}^*(\vec{r}_e) \phi_{\beta'}(\vec{r}_e) W(\vec{r}_e, \vec{r}_p) \phi_{\beta'}^*(\vec{r}_p) \phi_{\beta}(\vec{r}_p), \quad (2)$$

where $W(\vec{r}_e, \vec{r}_p, \vec{r}_e', \vec{r}_p') = e^2 \left[\frac{1}{|\vec{r}_e - \vec{r}_e'|} + \frac{1}{|\vec{r}_e - \vec{r}_p'|} + \frac{1}{|\vec{r}_p - \vec{r}_e'|} + \frac{1}{|\vec{r}_p - \vec{r}_p'|} \right]$. ϕ_{β} denote the wave functions for the hydrogen atom, $a = m/(M+m)$ and $b = M/(M+m)$, m and M being the masses of the electron and proton respectively.

Let us define the Bethe-Salpeter amplitude $\chi_{\vec{r}\vec{r}'}(\vec{r}_1, \vec{r}_1', t_1; \vec{r}_2, \vec{r}_2', t_2)$ for the two composite particle system (here two hydrogen atoms) as

$$\chi_{\vec{r}\vec{r}'} = \sum_{\beta_1, \beta_2} \beta_{\vec{r}\vec{r}'}^{(\beta_1 \beta_2)}(\vec{r}_1, t_1, \vec{r}_2, t_2) \phi_{\beta_1}(\vec{r}_1') \phi_{\beta_2}(\vec{r}_2'), \quad (3)$$

$$\beta_{\vec{r}\vec{r}'}^{(\beta_1 \beta_2)} = \langle 0 | T [\psi_{\beta_1}(\vec{r}_1, t_1) \psi_{\beta_2}(\vec{r}_2, t_2)] | 2\vec{P}E \rangle. \quad (4)$$

In this equation T denotes the Wick time-ordering

operator, $|0\rangle$, the vacuum state and $|2\vec{P}E\rangle$, the state vector for the two composite particles having total momentum \vec{P} and energy E . We now define a differential operator $S_{\vec{r}\vec{r}'}$ as

$$S_{\vec{r}\vec{r}'} \equiv i \frac{\partial}{\partial t_1} + \frac{1}{2\mu} \frac{\partial^2}{\partial \vec{r}^2}; \quad \vec{r} = 1, 2. \quad (5)$$

It can be shown that

$$(S_{1\vec{r}_1} - \epsilon_1)(S_{2\vec{r}_2} - \epsilon_2) \beta_{\vec{r}\vec{r}'}^{(\beta_1 \beta_2)}(\vec{r}_1, t_1, \vec{r}_2, t_2) = i \delta(t_1 - t_2) \sum_{\beta_1, \beta_2} \mathcal{V}_{\beta_1 \beta_2}^{(0)}(\vec{r}_1 - \vec{r}_2) \beta_{\vec{r}\vec{r}'}^{(\beta_1 \beta_2)}(\vec{r}_1, t_1, \vec{r}_2, t_2). \quad (6)$$

Following Eq.(7) one obtains

$$\{S_{1\vec{r}_1} + \frac{1}{2\mu} \frac{\partial^2}{\partial \vec{r}_1^2} - V(\vec{r}_{1e})\} \{S_{2\vec{r}_2} + \frac{1}{2\mu} \frac{\partial^2}{\partial \vec{r}_2^2} - V(\vec{r}_{2e})\} \chi_{\vec{r}\vec{r}'} E = i \delta(t_1 - t_2) W(\vec{r}_{1e}, \vec{r}_{2e}, \vec{r}_1, \vec{r}_2) \chi_{\vec{r}\vec{r}'} E, \quad (7)$$

μ being the reduced mass of the electron-proton system. Introducing the relative and center of mass times, and using the translational invariance property of the system, the left hand side of Eq.(7) is simplified. Further introducing the relative and center of mass coordinates and confining ourselves to the center of mass frame of the two composite particle system we arrive at the equation

$$\left[\frac{1}{2\mu} \frac{\partial^2}{\partial \vec{r}^2} - \frac{1}{2M} \frac{\partial^2}{\partial \vec{R}^2} - \frac{1}{2\mu} \frac{\partial^2}{\partial t^2} - V(\vec{r}_{1e}) - V(\vec{r}_{2e}) + W(\vec{r}_1, \vec{r}_2, \vec{r}_{1e}, \vec{r}_{2e}) - E \right] \chi_E(\vec{r}, \vec{r}_{1e}, \vec{r}_{2e}) = 0. \quad (8)$$

If we now ignore the momentum variable (conjugate to \vec{R}), Eq.(8) reduces to the Schrödinger equation for hydrogen molecule with fixed nuclei having its energy E depending parametrically on R . In the limit of $(R/\lambda) \rightarrow 0$, R can be identified with the internuclear separation.

We, therefore, notice that the projected Hamiltonian obtained by Girardeau for a system of composite particles is correct, but one has to define the Bethe-Salpeter amplitude properly in order to arrive at the Schrödinger equation for the hydrogen molecule. The effect of the interatomic exchange interactions that have been neglected by us from the projected Hamiltonian, is under investigation.

References

1. H. Gell-Mann and F. Low, Phys. Rev. **84**, 350 (1951).
2. S. D. Schwinger, Ann. Phys. (N.Y.) **20**, 454 (1962).
3. L. D. Girardeau, J. Math. Phys. **4**, 1 (1963), ibid. **12**, 1799 (1971).

ATOMIC BEAM SCATTERING WITH MAGNETIC ANALYSIS,
AND THE STRUCTURE OF RARE GAS OXIDES AND FLUORIDES.

V. Aquilanti, E. Luzzatti, F. Pirani and G.G. Volpi
Dipartimento di Chimica dell'Università, 06100 Perugia, Italy.

The study of the interaction between a rare gas atom and an oxygen or fluorine atom is of large interest for the applications and for the understanding of the role of P atoms in the van der Waals bonding. However these interactions are very difficult to be characterized, in particular for the important case when ground state atoms are involved.

In our laboratory we measure total scattering cross sections as a function of velocity in the thermal energy range for collisions of velocity selected and magnetically analyzed oxygen and fluorine atomic beams with rare gases.

By measuring the behaviour of oxygen and fluorine beams as a function of the magnetic field strength at a given velocity, it is possible to analyze the distribution of atomic states in the beam under various experimental conditions and to determine the population of the relative magnetic sublevels. In particular metastable oxygen atoms are not present in conditions used for our scattering experiments.

We use basically the same experimental apparatus previously described,^{1,2,3} with a modification which has been recently introduced to avoid negative effects of casual fluctuations of general experimental conditions, such as the ground pressure and, in particular, those in the microwave discharge where atoms are produced. In this way a significant improvement of quality of the scattering data can be achieved, especially in the experiments involving oxygen atoms. The cross sections for oxygen-rare gas systems are obtained in a wider velocity range and with lower uncertainty than in previous experiments.^{1,2} The analysis of the present data allows a characterization of the six lowest lying states of the rare gas oxides around the equilibrium region.

Finally, the present total cross section measurements with magnetic selection, analyzed together with previously measured differential cross sections⁴ and total cross sections obtained at lower energies,⁵ allow to derive a systematic picture of the interactions between fluorine atoms and the heavy rare gases.

For the three lowest lying states of the fluorides of argon, krypton and xenon,³ the table shows well depth and equilibrium distances r_m , the accuracy being of the order of 1 meV for ϵ and of 0.1 Å for r_m .

It is interesting to stress that, for analysis of data for the three rare gas fluorides, we were guided by the considerations about coupling schemes described in Ref.6

Table

	$3/2, 1/2 >$	$3/2, 3/2 >$	$1/2, 1/2 >$
F-Xe	151.0	5.6	8.1
r_m	2.31	3.85	3.65
F-Kr	36.0	5.5	7.0
r_m	2.78	3.75	3.55
F-Ar	6.7	5.5	6.3
r_m	3.25	3.60	3.50

ϵ in meV, r_m in Å

The transition between cases a) and c) occurs for F-Ar in the repulsive region, and for F-Xe in the attractive region. The F-Kr case is intermediate, the transition taking place in the well region for the ground state: this region governs the rainbow structure in differential cross sections, and therefore a further analysis of the experimental data in Ref. 4 is required.

Besides the interest of these results for the characterization of weak chemical bonds, the knowledge of these interactions, when used jointly with the previously developed theory of angular momentum coupling schemes⁷ and decoupling approximations⁸ for atoms in P-states, allows the computation of intramultiplet mixing and depolarization cross sections.⁹

REFERENCES

1. V. Aquilanti, G. Liuti, F. Pirani, F. Vecchiocattivi and G.G. Volpi, J. Chem. Phys. **65**, 4751 (1976).
2. V. Aquilanti, E. Luzzatti, F. Pirani and G.G. Volpi, J. Chem. Phys. **73**, 1181 (1980).
3. V. Aquilanti, E. Luzzatti, F. Pirani and G.G. Volpi, Chem. Phys. Letters **90**, 392 (1982).
4. C.H. Becker, P. Casavecchia and Y.T. Lee, J. Chem. Phys. **69**, 2377 (1978); **70**, 1936 (1979).
5. K. Müller, Dissertation, Max-Planck-Institut für Strömungsforschung Bericht 1/1984, Göttingen (1984).
6. V. Aquilanti, G. Grossi and F. Pirani, in "Electronic and Atomic Collisions" Invited Papers, XIII ICPEAC (North Holland 1983) 441.
7. V. Aquilanti and G. Grossi, J. Chem. Phys. **73**, 1165 (1980).
8. V. Aquilanti, P. Casavecchia, G. Grossi and A. Laganà, J. Chem. Phys. **73**, 1173 (1980).
9. V. Aquilanti, G. Grossi and A. Laganà, Nuovo Cimento **63** B, 7 (1981).

RADIATIVE RECOMBINATION OF KR $1_u(3P_1)$ EXCIMERS

H. Schmoranzer, P. Wollenweber, K. Barzen

Fachbereich Physik, Universität Kaiserslautern
D-6750 Kaiserslautern, W.-Germany

With the view of a spectroscopic determination of the interatomic potentials of rare gas excimers the vacuum-ultraviolet emission of krypton has been investigated previously in the spectral region of the second continuum¹ and the modulated first continuum² in the red wing of the $3P_1 - 1S_0$ atomic line. At present further details of the Kr emission spectrum observed in the blue wing of the first atomic resonance line will be discussed.

20 keV-electrons at a beam current of 250 μ A were utilized for cw excitation of the krypton gas at 50 mbar with impurities less than 30 ppm. The spectral resolution attained was 0.01 nm. The blue wing of the atomic emission line at 123.584 nm exhibits three structures of which the spectral positions agree with Tanaka's "unanalyzed absorption bands"³ and more recent absorption measurements⁴. The emission structures are displayed in Fig. 1 as a difference spectrum obtained by subtracting an exponential background. The weak structure at shortest wavelengths (labelled 1) is observed at 300 K while it disappears at 150 K.

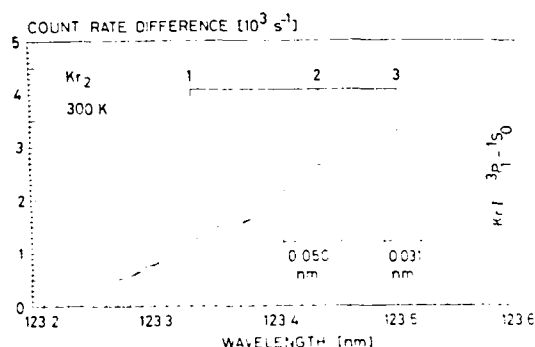


FIGURE 1 Emission spectrum of blue wing of KrI first resonance line (exponential background subtracted)

It is concluded that the modulated blue wing spectrum observed arises from the repulsive $1_u(3P_1)$ state. $O_g^+(3P_1)$ as a hypothetical initial state can be excluded since a hump, necessary for explaining structure 1, in the O_g^+ potential curve is contradicted by experimental and ab initio results⁴. Consequently a simulation of the free-bound emission spectrum $1_u(3P_1) - O_g^+(1S_0)$ was performed by calculating Franck-Condon factors from the $1_u(3P_1)$ continuum to all bound vibrational levels of $O_g^+(1S_0)$ and by superposing the free-bound FCFs weighted according to different thermal population distributions

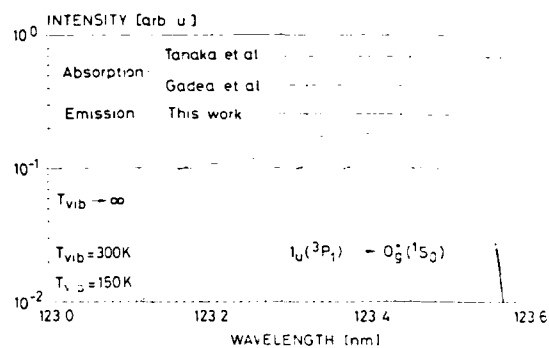


FIGURE 2 Calculated $1_u(3P_1) - O_g^+(1S_0)$ free-bound emission spectra in comparison with experimental spectral positions

of continuum states assumed (Fig. 2). As input data the ground state potential known⁵ and the excited state potential described by point pairs⁴ were used, and a variation of the electronic transition moment was neglected within the relevant interval of internuclear distance.

The calculated spectra can be seen to reproduce the experimental spectral positions of maxima rather well. An additional broad structure around 123.17 nm is predicted by the calculations which may be found at higher temperature.

The structured continuous emission observed in the krypton excimer spectrum on the short wavelength side of the first atomic resonance line can be interpreted to manifest the radiative recombination of an excited Kr $5s\ 3P_1$ atom colliding with a Kr atom in the ground state. After emission of a vuv photon a dimer in the weakly bound ground state is formed. Furthermore the agreement stated between experimental and calculated spectra corroborates the interatomic potential employed in describing the excimer state.

Financial support from the Deutsche Forschungsgemeinschaft under Sonderforschungsbereich 91 is gratefully acknowledged.

References

1. H. Schmoranzer, R. Wanik, H. Krüger, Abstracts XI ICPEAC (ed. K. Takayanagi, N. Oda; Kyoto 1979), p.416
2. P. Wollenweber, K. Barzen, H. Schmoranzer, Abstracts XIII ICPEAC (ed. J. Eichler et al.; Berlin 1983), p.339
3. Y. Tanaka, K. Yoshino, D.E. Freeman, J. Chem. Phys. 59, 5160 (1973)
4. F.X. Gadea, F. Spiegelmann, M.C. Castex, M. Morlais, J. Chem. Phys. 78, 7270 (1983)
5. R.A. Aziz, Mol. Phys. 35, 177 (1979)

THE COLLISIONAL RELAXATION OF EXCITED-STATE ZEEMAN COHERENCES IN ATOMIC YTTERBIUM VAPOR

A. G. Yodh, J. Golub, and T. W. Mossberg

Department of Physics, Harvard University, Cambridge, Massachusetts 02138

We have employed a tri-level photon echo technique¹ to study the effects of collisions on excited-state Zeeman coherences in atomic Yb. Some collisions are found to destroy (depolarize) the Zeeman coherences. Others leave the coherence intact, while changing the velocity of the atom as a whole. Both Yb-He and Yb-Ar collisions were studied. In the former case, cross-sections for depolarization and velocity changes were measured, as was the spectrum of collisionally induced velocity changes. Our experiment² together with two others recently reported^{3,4}, provides the first quantitative look at the role of velocity changes in the collisional relaxation of Zeeman coherences.

We use three linearly polarized laser pulses to create an echo signal. The pulses excite different Zeeman components of the $\lambda = 556\text{nm}$, $(6s^2)^1S_0 - (6s6p)^3P_1$ Yb transition. Effective collisional relaxation cross-sections, $\sigma_{\text{eff}}^z(t_{21})$, for the excited-state Zeeman coherence were measured by monitoring the intensity of the echo signal as a function of perturber pressure for various values of t_{21} and t_{32} . Here t_{ij} represents the time interval between the i th and j th pulses.

The first two laser pulses generate eight non-zero spherical tensor moments in the 3P_1 state. The $q=1$ components of the orientation and alignment are created with amplitudes that are modulated as a function of axial velocity with period $v_m = \lambda/t_{21}$. The echo is generated as a result of the interaction of the third laser pulse with the velocity modulation in these quantities.

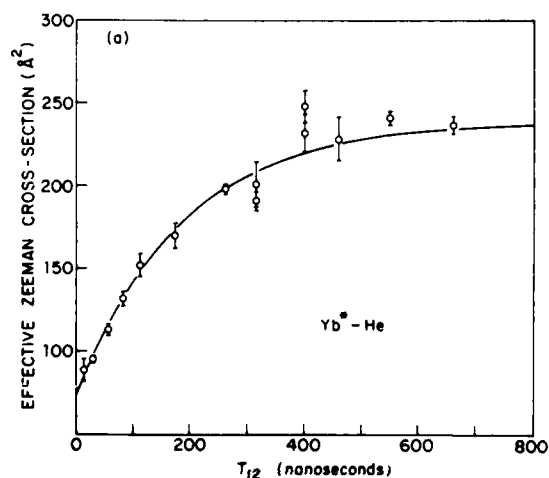


FIGURE 1 $\sigma_{\text{eff}}^z(t_{21})$ vs. t_{21} for Yb-He collisions

TABLE 1

Perturber	$\sigma_D^z (\text{\AA}^2)$	$\sigma_{\text{vcc}}^z (\text{\AA}^2)$	$\sigma_{\text{tot}}^z (\text{\AA}^2)$
He	89(7)	150(8)	239(9)
Ar	150(10)	$\geq 681(25)$	$\geq 836(25)$

During t_{32} , collisions that thermalize the population of the 3P_1 manifold (depolarizing collisions) or that thermalize the atomic velocities (velocity-changing collisions) can reduce the echo amplitude. A velocity-changing collision that changes an atom's velocity by an amount larger than the modulation period, v_m , will prevent that atom from contributing to the echo signal. Our measured effective relaxation cross-sections, $\sigma_{\text{eff}}^z(t_{21})$, represent the effect of collisions that depolarize or induce velocity changes larger than λ/t_{21} .

In figure 1 we show $\sigma_{\text{eff}}^z(t_{21})$ characteristic of the Yb-He system for various t_{21} . Only depolarizing collisions, contribute to the measured cross-section, σ_D^z , in the short t_{21} limit. For longer t_{21} , both depolarizing and velocity-changing collisions contribute to $\sigma_{\text{eff}}^z(t_{21})$. For long t_{21} , σ_{eff}^z represents the state's total quantum mechanical cross-section, σ_{tot}^z . The cross-section for velocity-changing collisions, σ_{vcc}^z is the difference between σ_{tot}^z and σ_D^z . A summary of our measurements is given in Table 1.

In closing we note that our measurements, representative of the rank one and rank two tensor moments of the 3P_1 state show interesting differences with data obtained in similar studies³ sensitive to the rank zero moment of the same state. Future work is planned on this subject.

This work was supported by the National Science Foundation under grant PHY-8207080, and the Joint Services Electronics program under contract N00014-84-K-0415. A.G.Y. gratefully acknowledges support of Army fellowship DAAG19-83-0008.

REFERENCES

1. T.W. Mossberg, R. Kachru, S.R. Hartmann, and A.M. Flusberg, Phys. Rev. A 20, 1976 (1979).
2. A.G. Yodh, J. Golub, and T.W. Mossberg, to be published in Phys. Rev. A.
3. J.C. Keller and J.L. Le Gouet, Phys. Rev. Lett. 52, 2034 (1984).
4. A.P. Ghosh, C.D. Nabors, M.A. Attili, J.E. Thomas, and M.S. Feld, Phys. Rev. Lett. 53, 1333 (1984).

SCATTERING OF ORIENTED Ne^* ATOMS IN ONE $^3J=2, M_J$ STATE

Ch. Bender, W. Beyer, H. Haberland, D. Hausmann, and H.P. Ludescher

Fakultät für Physik, Universität Freiburg, Germany

One M_J level of the $\text{Ne}(2p^5 3s, J=2)$ state can be selected, given any desired orientation, and scattered from another atom by the apparatus shown schematically in Fig. 1. An electron impact excited supersonic neon beam is crossed with a CW single mode dye laser beam in a homogeneous magnetic field. The laser pumps a neon $3s \rightarrow 3p$ transition, which is followed by cascade to the ground state. The Zeeman splitting - indicated above the figure - allows the selective removal of 3M_J state. In the scattering center there is a rotatable magnetic field. The quantisation axis of the M_J sublevels follows the local magnetic field adiabatically. The differential cross section is either measured as a function of the scattering angle or the direction of the quantisation axis of the 3M_J states.

During the scattering event, the magnetic field direction is no longer a good quantisation axis. Instead the initially prepared state couples to the internuclear axis. The detector sees over all final M_J states. Their transition with respect to the magnetic field could, in principle, be measured, by using the same combination of laser and magnetic field in front of the detector.

Fig. 2 shows the differential cross section, when the magnetic field is perpendicular to the initial asymptotic velocity vector. Very large differences can be seen, depending on which M_J state is selected. The fast regular oscillations result from the nuclear symmetry of the problem. The other structure is caused by interference from different potentials.

The orientation dependence of the cross section at a scattering angle of $\theta_{\text{cm}} = 150^\circ$ is shown in Fig. 3. The angle θ is the direction of the initial orientation with respect to the direction of the Ne^* beam as indicated in Fig. 1. The solid lines have been calculated from a simplified "locking-radius" model, which has been fitted at $\theta = 90^\circ$. Note the strong M_J and orientation dependence of the differential cross sections, which is up to a factor of 7. The locking radius obtained from these data is not much different from the classical turning point, much smaller than that for the excited alkali case. A simple physical picture will be presented, which is able to explain this unexpected difference.

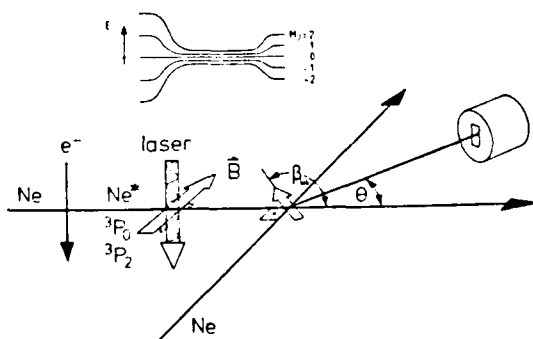


FIGURE 1 Principle of the experiment. The rotatable magnetic field in the scattering center allows to vary the orientation of the 3M_J states continuously.

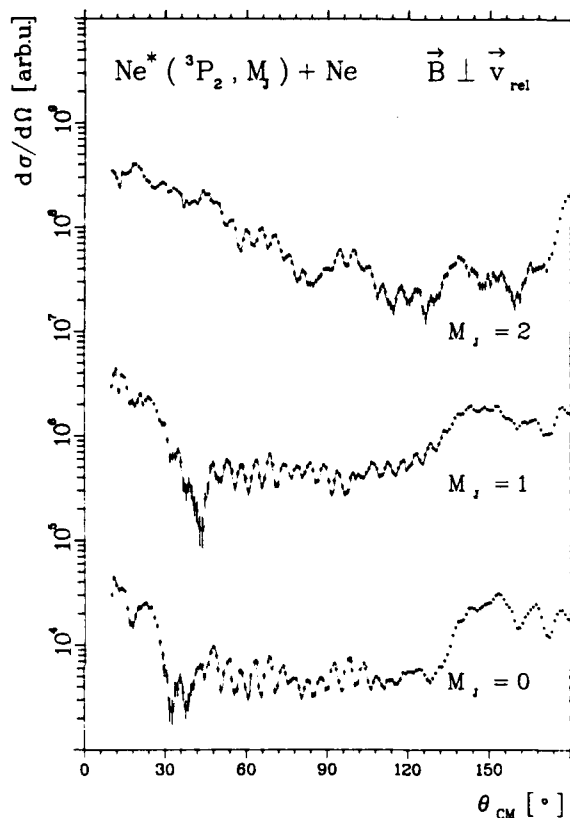


FIGURE 2 Differential cross section at $E_{\text{cm}} = 66$ meV for the different M_J states and one fixed orientation.

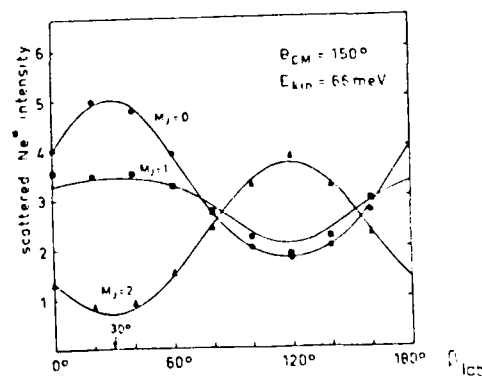


FIGURE 3 Orientation dependence of the differential cross section.

THE INFLUENCE OF THE COLLISIONS OF
METASTABLE ATOMS ON THE OPTOGALVANIC EFFECTS

HE Maoqi, WANG Guoyi, and WANG Zhaoyong

Department of Physics, Fudan University, Shanghai, CHINA

In hollow cathode discharge, the signals of optogalvanic effect depend on if there are the collisions with metastable atoms. We studied systematically, in the range of 5604Å to 6340Å, the change of optogalvanic signals in sodium transitions without metastable atoms and neon transitions with metastable atoms respectively, observed that the convert current needed for changing the optogalvanic signals from positive into negative will be decreased gradually when the lower state is a metastable state to far from a metastable state. There are also the saturation and non-saturation phenomena in sodium and neon signals respectively.

Considering the various aspects of collisional transfer, collisional ionization, optical excitation, collisional relaxation and spontaneous emission of the upper, lower and metastable states, we established an analytical expressions for the optogalvanic effect and discussed various situations of the experiments with these expressions.

If the lower state of transition is not relevant to a metastable state, i.e. far from metastable state, we can neglect the collisional exchange with the metastable atoms. The $2p \rightarrow 3s$, $4d$ transitions of neon atom and all the transitions of sodium atom belong to this category. In this case, the optogalvanic effects are negative.

In the second case, the lower state of transition itself is a metastable state. For instance, the $1s_3$, $1s_5$ states of neon atom and the $3d^9 4s^2 2D_{3/2}$ state of copper atom are metastable states in corresponding transitions. Then, the optogalvanic effects are positive when the discharge current is small enough. But with the increase of the discharge currents, the optogalvanic signals will be changed into negative one by one according to the collision and lifetime of the metastable atoms.

If the lower state of transition is not a metastable state but there exists couplings with the nearby metastable states in some extent due to the collisions, the optogalvanic signals of those transitions in which the lower state is a little bit far from metastable states will be changed firstly from positive into negative with the increase of the discharge current. The magnitude of the convert current needed for such change depends on how far the lower state is from the metastable state. The closer from the metastable state, the larger convert current are needed.

The expressions we established for the optogalvanic effect are coincidence with these experiments satisfactory. This means the collisions with the metastable state atoms play an important role in the optogalvanic effect.

Na⁺-NOBLE GAS DIFFERENTIAL CROSS SECTIONSM. O'Callaghan and A. Gallagher⁺Joint Institute for Laboratory Astrophysics, University of Colorado and
National Bureau of Standards, Boulder, Colorado 80309 USA

Two-step optical excitation with co-propagating laser beams is used to obtain differential cross section information for $\text{Na}(3P_{1/2}) \rightarrow \text{Na}(3P_{3/2})$ transfer due to noble gas collisions. Na atoms of a particular v_z velocity are optically excited to the $3P_{1/2}$ state, with $v_z = 0$ to $2\bar{v}_{\text{thermal}}$. A second laser excites to the 4D state atoms that have been collisionally transferred to the $3P_{3/2}$ state, and vice versa. 330 nm, 4D \rightarrow 4P \rightarrow 3S cascade fluorescence is then detected. As shown diagrammatically in Fig. 1, the v_z distribution of $\text{Na}(3P_{3/2})$ atoms resulting from the inelastic collision is observed by scanning the second laser. In Fig. 2 an example spectrum is shown for He perturbers and 0 and -2.0 GHz detuning of ω_1 from $3S_{1/2}(F=2)$ to $3P_{3/2}(F=3)$, ω_2 scans the region of the $3P_{1/2} \rightarrow 4D_{3/2}$ transition.

This method of obtaining differential cross section information has previously been used¹ to study a rotationally inelastic cross section in CO_2 . Due to the angular and collision-velocity averaging in such a cell experiment, the data represent an average over differential cross sections. In an atomic beam experiment, currently under construction, the differential cross section for elastic and inelastic excited-state collisions can be observed directly. Beam experiments based on similar methods have been used to measure product-state distributions in atom-molecule collisions.²

This work was supported in part by National Science Foundation grant PHY82-00805.

References

1. W. K. Bischel and C. K. Rhodes, Phys. Rev. A **14**, 176 (1976).
2. I. V. Hertel, in *Dynamics of the Excited State*, K. P. Lawley, Ed. (Wiley, New York, 1982).

⁺Staff Member, Quantum Physics Division, National Bureau of Standards.

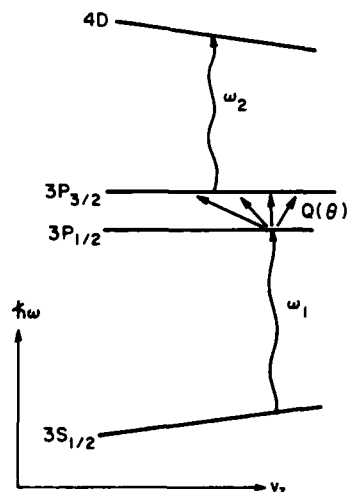


Figure 1. Schematic diagram of the spectroscopy used to observe the collisional deflection.

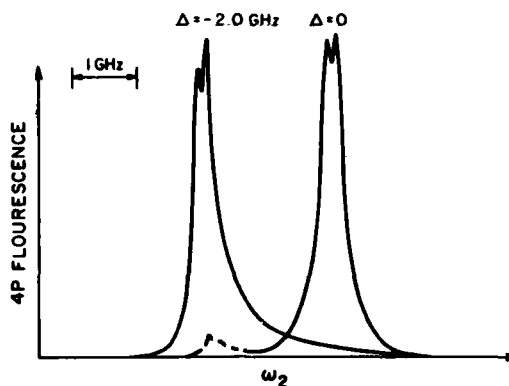


Figure 2. 4P fluorescence versus ω_2 for ω_1 detunings of 0 and -2.0 GHz from the $3S_{1/2} \rightarrow 3P_{3/2}$ transition and 0.5 Torr He. Data influenced by 3S hyperfine structure are dashed.

FINAL STATE DISTRIBUTION FOR $\text{Na}(3P_J) + \text{Na}(3P_{J'}) + \text{Na}(nL_{J''}) + \text{Na}(3S_{1/2})$

Steven A. Davidson, J. F. Kelly and A. Gallagher*

Joint Institute for Laboratory Astrophysics, University of Colorado and
National Bureau of Standards, Boulder, Colorado 80309 USA

Relatively good agreement exists^{1,2} for measurements of the total rate coefficient for $3P + 3P + 3S + (5S \text{ or } 4D)$. Those measurements did not, however, take into account the effect of the J values of the $3P$ reactants, nor did they determine the product states' J value. In the current research, we have measured the relative rate coefficients for producing the $5S_{1/2}$, $4D_{3/2}$, $4D_{5/2}$, $4F_{5/2}$, and $4F_{7/2}$ states from different combinations of $\text{Na}(3P_J) + \text{Na}(3P_{J'})$ collisions.

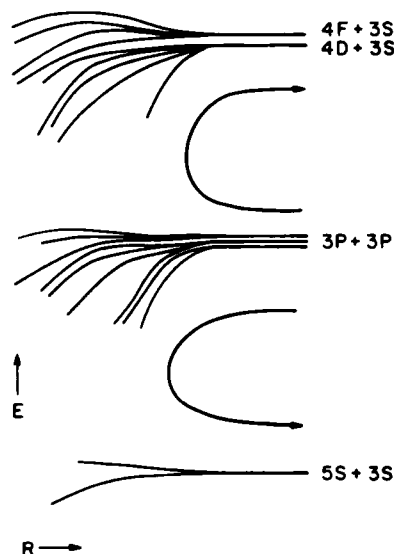
The experiment was done in three steps. Step one involved populating $3P_{1/2}$ or $3P_{3/2}$ and measuring intensity ratios of $4D + 3P_{1/2,3/2}$, $(4F+3D) + 3P_{1/2,3/2}$, and $5S + 3P_{3/2}$ fluorescence at $[\text{Na}] = 2.8, 6.4, \text{ and } 16 \times 10^{12} \text{ cm}^{-3}$. In the next step, conditions were the same and we measured the $4D + 3P$ fluorescence intensity from a known ratio of $3P_{1/2}$ and $3P_{3/2}$ density. In the third step we raised the sodium density to $>2.5 \times 10^{14} \text{ cm}^{-3}$ where an essentially statistical mixture of the $3P_{1/2}$ and $3P_{3/2}$ states occurred, and thus a large fraction of collisions ($\sim 45\%$) are between $3P_{1/2}$ and $3P_{3/2}$ atoms. Intensity ratios were taken as in step one.

The observed rate coefficients appear in Tables 1 and 2; typical uncertainties are on the order of 10%. All measurements were made at $T_{\text{cell}} = 640^\circ\text{K}$ in a stainless steel cell with hot sapphire windows.¹ At the sodium densities used, the vapor is optically thick and substantial resonance-radiation diffusion occurs. This was not a problem since in steps one and three the intensity ratios are independent of $3P$ -atom distribution and in interpreting the data of step two we used (and confirmed) the ratio of infinite slab D-line effective decay rates,³ as our cell has an infinite slab internal architecture.

Cascades from higher states have a negligible effect on the $4D$ and $4F$ fluorescence intensities, but the rate coefficient for the $5S$ state include $0.5 k_{5P}$. This is expected to be a small correction to k_{5S} due to the large $5P$ state activation energy.

This work was supported in part by National Science Foundation grant PHY82-00805.

*Staff Member, Quantum Physics Division, National Bureau of Standards.

Stylized potentials for Na_2 .Table 1. Ratio of rate coefficients relative to $k_{5S}(3/2, 3/2)$.

J	J'	$5S_{1/2}$	$4D_{3/2}$	$4D_{5/2}$	$4F_{5/2}$	$4F_{7/2}$
1/2	1/2	3.2	1.3	1.9	0.96	1.4
3/2	3/2	1	0.91	1.3	0.39	0.44

Table 2. Ratio of rates from statistical mixture of $3P_{1/2}$ and $3P_{3/2}$.

$5S_{1/2}$	$4D_{3/2}$	$4D_{5/2}$	$4F_{5/2}$	$4F_{7/2}$
1	0.64	0.88	0.37	0.43

References

1. J. Huennekens and A. Gallagher, Phys. Rev. A **27**, 771 (1983).
2. M. Allegrini, P. Bicchi, and L. Moi, Phys. Rev. A **28**, 1338 (1983).
3. T. Holstein, Phys. Rev. **72**, 1212 (1947); **83**, 1159 (1951).

COLLISIONAL TRANSITIONS BETWEEN ATOMIC STATES
INTERACTING VIA RYDBERG CONTINUUM

G.K.Ivanov and G.V.Golubkov

Institute of Chemical Physics, Academy of Science, Moscow USSR

To describe atomic processes involving molecular Rydberg states

$$X + Y - (e^- + XY^+) - X' + Y' \quad (1)$$

the equation for the collision T-operator obtained in [1] is generalized in the following way ($\hbar = m_e = e = 1$)

$$T = \bar{K} + \bar{K} \sum_{\nu} \langle \nu | T | \nu \rangle \langle \nu | T - i \bar{K} \sum_{\beta} | \beta \rangle \langle \beta | T \quad (2)$$

Here $\nu = [2(E_\nu - E)]^{1/2}$, E_ν is the nuclei vibrational energy and E ($|E| \ll 1$) is the relative energy of atoms X and Y (which are measured from the zero vibrational level of XY^+),

$|\nu\rangle = \varphi_e \chi_\nu$, $\varphi_e = \pi^{1/2} R_{ee} Y_{em}$, R_{ee} is the Coulomb radial wave function of zero energy, Y_{em} is the electron angular function (in body-fixed frame), χ_ν is the vibrational wave function of the ion XY^+ ,

$$\bar{K} = K^{(0)} + \sum_{\beta} V | \psi_{\beta}^e \rangle \bar{g}_{\beta} \langle \psi_{\beta}^e | V \quad (3)$$

where V is the operator of the interaction between the electron and the ion core, \bar{g} is the real part of the Green's function which describes the nuclear motion in the $X + Y$ (β -th) channel, ψ_{β}^e is the electron wave function of this channel, $K | \beta \rangle \langle \beta | = V | \beta \rangle \langle \beta |$, $\langle \beta | = \pi^{1/2} \varphi_{\beta}^e \chi_{\beta}^{\beta}$, where χ_{β}^{β} is the nuclear wave function of β -state at the energy E .

The first term in (3) is responsible for the direct interaction, the following ones - for the resonant (configuration) interaction.

The eq.(2) ensures the unitarity of the S-matrix ($S = 1 - 2iT$). The T-matrix is expressed through the K-matrix elements defined as

$$\bar{K}_{ee'e\nu} = \langle \chi_\nu | \bar{K}_{ee} | \chi_{e\nu} \rangle, \bar{K}_{ee,\beta d} = \pi^{1/2} \langle \chi_\nu | V_{e\beta} | \chi_d^{\beta} \rangle,$$

$$\bar{K}_{\beta d,\beta d} = 0; \bar{K}_{ee} = \langle \varphi_e | \bar{K} | \varphi_e \rangle, V_{e\beta} = \langle \varphi_e | V | \psi_{\beta}^e \rangle$$

Here, as well as in [1], all the necessary parameters of the theory are reconstructed from the adiabatic picture of terms.

For the process (1) proceeding through Rydberg states with $\nu = 0$ and fixed ℓ at energy $E < 0$ we obtain

$$T_{\beta d,\beta d} = \frac{\bar{K}_{\beta d,e0} \bar{K}_{e0,\beta d}}{i \pi \nu - \bar{K}_{ee,e0} + \sum_{\alpha} \bar{K}_{e\alpha,\alpha d}^2} \quad (4)$$

In the neighbourhood of the isolated $\nu=0$ resonance (4) assumes a familiar Breit-Wigner form.

At the energy $0 < E < \omega$ (ω is the vibrational quantum of XY^+) when the simultaneous population of the continuum with $\nu = 0$ and the Rydberg series with $\nu = 1$ occurs, we obtain

$$T_{\beta d,\beta d} = \frac{\bar{K}_{\beta d,e0} \bar{K}_{e0,\beta d}}{i - \bar{K}_{ee,e0}} + \frac{\bar{K}_{\beta d,e1} \bar{K}_{e1,\beta d}}{i \pi \nu - \bar{K}_{ee,e1} + \delta_1} \quad (5)$$

$$\text{where } \delta_1 = \sum_{\alpha} \bar{K}_{e\alpha,\alpha d}^2 + \bar{K}_{ee,e1}^2 / (1 + \bar{K}_{ee,e0}^2),$$

$$|\bar{K}_{ee,\beta d}|^2 \ll 1.$$

It is suitable to introduce the probabilities averaged over the resonances

$$W = |T_{\beta d,\beta d}|^2 = \frac{1}{1 + \bar{K}_{ee,e0}^2} (\delta_{\beta d} \delta_{\beta d} + \frac{\delta_{\beta d} \delta_{\beta d}}{\delta_1}) \quad (6)$$

where

$$\delta_{\beta d} = \bar{K}_{e0,\beta d}^2.$$

According to (6) the double interconfiguration transition is necessary for the repopulation of the continuous spectrum (the first term in (6)) and for the population of quasilocalized Rydberg levels and interconfiguration transition is enough.

Reference

1. G.K.Ivanov and G.V.Golubkov, Chem.Phys. Lett., 107, 261 (1984)

TWO ELECTRON MODEL CALCULATIONS OF Li(2s-2p) AND Na(3s-3p) EXCITATION
IN Li-Na HIGH ENERGY COLLISIONS

Svend Erik Nielsen,⁺ Martin Larsen⁺ and John S. Dahler⁺⁺

⁺Chemistry Laboratory III, H.C.Ørsted Institute, University of Copenhagen, 2100 Copenhagen Ø, Denmark

⁺⁺Department of Chemistry, University of Minnesota, Minneapolis, Minnesota 55455, USA

A two-electron model of direct excitation in Li-Na collisions has been developed¹ based upon one-electron model eigenstates of the separated atoms. The electronic scattering state is expanded in a valence-bond type, antisymmetrized and translational phase factor modified, two-electron atomic basis. The time-dependent Schrödinger equation is solved by the impact parameter method assuming a rectilinear trajectory and constant relative velocity of the heavy particle motion. Solutions of the resulting close-coupled equations for the expansion coefficients have been obtained in the high energy limit for various sets of basis functions Li(2s/2p)Na(3s/3p), involving single and double (simultaneous) excitation of the alkali atoms. The aim has been to obtain first estimates of Li(2s-2p) and Na(3s-3p) excitation cross sections and polarizations as functions of collision energy, and to probe the details of the direct excitation mechanism² for quasi-two-electron systems.

Experimental studies of the Li-Na collision system³ have shown double-maximum structures for the Li(2p) and Na(3p) emission cross sections (●/▲ in figure 1) as functions of energy, tentatively interpreted as Massey-maxima for single and double excitation. In figures 1 and 2 we compare the predictions of 5-state close-coupling calculations (S) including single excitation states only (Li(2p)Na(3s) and Li(2s)Na(3p)), 6-state close-coupling calculations (D) including double excitation states only (Li(2p)Na(3p)), and 10-state close-coupling calculations (SD) including single as well as double excitation states.

We notice (figure 2) the long range behaviour of the double excitation probability (X), and at small impact parameters the strong enhancement of the double excitation probability at the expense of Li (O) and Na (+) single excitation (compare S/D and SD), indicating an effective two-step mechanism for double excitation.

The 5-state single excitation calculations (S) predict the relative magnitudes of Li(2s-2p) and Na(3s-3p) excitation cross sections (O/+ in figure 1) in fair agreement with the experimental results above 10 keV. The absolute magnitudes, however, are too large by a factor of two to three. The 10-state (SD) single excitation cross sections shown in figure 1 match the experimental results at 50 keV within the experimental uncertainty. We may expect the present 10-state calculation to overestimate the Li(2p)Na(3p) double excitation

contribution for two reasons, the high energy model itself discarding the phase factor modified exchange couplings, and the neglect of close-lying higher excited states competing with the Li(2p)Na(3p) channels.

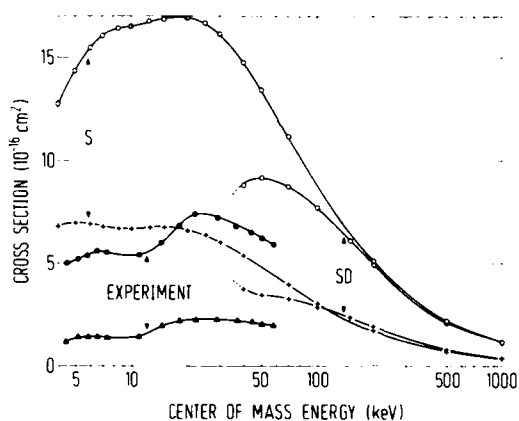


Figure 1

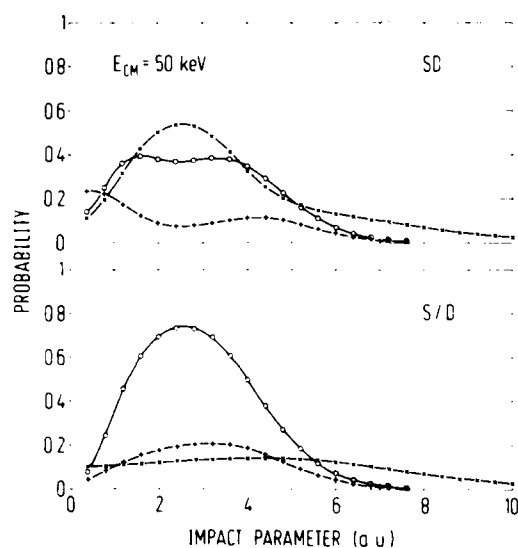


Figure 2

References

1. S.E.Nielsen, M.Larsen and J.S.Dahler, Abstracts XIII ICPEAC (Berlin 1983), 336
2. N.Andersen and S.E.Nielsen, Adv.Atom.Molec.Phys. 18 265 (1982)
3. B.Bisgaard, T.Andersen, B.V.Sørensen, S.E.Nielsen and J.S.Dahler, J.Phys.B 13 4441 (1980)

EXCITATION AND DEEXCITATION OF ORIENTED ATOMS IN ENERGETIC COLLISIONS:
THE ROLE OF THE MASSEY PARAMETER

Nils Andersen⁺ and Svend Erik Nielsen⁺⁺

⁺ Institute of Physics, University of Aarhus, and Physics Laboratory II, H.C.Ørsted Institute, Copenhagen, Denmark
⁺⁺ Chemistry Laboratory III, H.C.Ørsted Institute, University of Copenhagen, 2100 Copenhagen Ø, Denmark

In recent years there has been considerable speculation about production/destruction of oriented atomic states in electron-atom¹ and atom-atom² collisions, and the physical origin of this orientation. For electron-atom collisions this has been done in terms of repulsive and attractive forces.¹⁻³ Low-energy atom-atom collisions may be interpreted by molecular models.^{2,4} This contribution addresses the excitation and deexcitation of oriented atomic states in energetic atom-atom collisions.

In quasi-one-electron systems the excitation at large impact parameters dominantly takes place via direct transitions among the involved states.⁵ For the simple case of alkali ground state - resonance state (ns-np) transitions in alkali - rare gas collisions one may as a first approximation limit the basis to the three (lab-fixed) states ($|s\rangle$, $|C\rangle$, $|D\rangle$) = ($|ns\rangle$, $2^{-1/2}(|np_z\rangle - i|np_x\rangle)$, $2^{-1/2}(-|np_z\rangle - i|np_x\rangle)$). In this basis³ the mathematics and physics take a simple and transparent form: Denoting by θ the rotation angle of the internuclear axis (figure 1) one obtains the close-

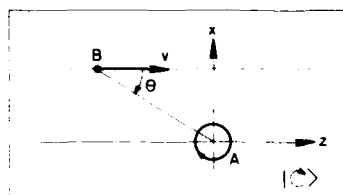


Figure 1

coupled equations $i\frac{d}{dz}\underline{a} = \underline{A}\underline{a}$ for the scattering amplitudes $\underline{a} = (a_s, a_C, a_D)$, where in usual notation

$$\underline{A} = U_{0s} \begin{pmatrix} 0 & cc & cc \\ \exp i(\frac{\Delta E}{v}z - \theta) & 0 & 0 \\ -\exp i(\frac{\Delta E}{v}z + \theta) & 0 & 0 \end{pmatrix} + U_{10} \begin{pmatrix} 0 & 0 & 0 \\ 0 & 0 & cc \\ 0 & e^{i2\theta} & 0 \end{pmatrix}$$

$$\Delta E = (e_{np} - e_{ns}) + \frac{1}{v} \int_{-\infty}^z \{ \frac{1}{2}(U_{11} + U_{00}) - U_{ss} \} dz,$$

$$\text{and } U_{0s} = 2^{-1/2} \langle np_0 | V | ns \rangle^{\text{mol}}$$

$$U_{10} = \frac{1}{2} \langle np_1 | V | np_1 \rangle^{\text{mol}} - \langle np_0 | V | np_0 \rangle^{\text{mol}} = \frac{1}{2} (U_{11} - U_{00})$$

are matrix elements of the electron - rare gas interaction V in the molecular frame of reference.

From these equations we can read several things:

The excitation probability has its maximum when the phase $(\frac{\Delta E}{v}z - \theta)$ is stationary during the collision.

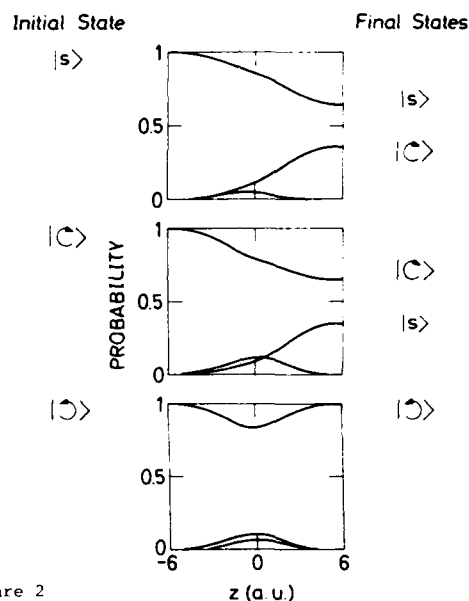


Figure 2

Since θ changes by π this implies $\frac{\Delta E}{v}a \approx \pi$ (a being the effective interaction length of V) which is the Massey maximum rule. So when this criterion is fulfilled, the $|C\rangle$ state is excited with nearly maximum probability, $\frac{1}{\sqrt{2}}(\int_{-\infty}^{\infty} U_{0s} dz)^2$, while the $|D\rangle$ state is suppressed since the phase $(\frac{\Delta E}{v}z + \theta)$ changes by 2π .

This and other observations are illustrated in figure 2 for excitation and deexcitation in Na-He collisions, followed along the trajectory. Initial conditions correspond to $\frac{\Delta E}{v}a \approx \pi$, $b = 2.2$ a.u., $E_{cm} = 2.0$ keV, and V is the Baylis model potential.⁵ With the present choice of basis functions 1. order estimates have a surprisingly large range of validity.

A detailed discussion based on the formalism above of excitation and deexcitation processes as function of impact parameter and energy will be presented at the conference.

References

1. M. Kohmoto and U. Fano, X ICFEAC (1977), Abstracts, p. 516, and J. Phys. B 14 1447 (1981)
2. I.V. Hertel, H. Schmidt, A. Bähring and E. Meyer, Ber. Prog. Phys. (1985), in press
3. N. Andersen, I.V. Hertel and H. Elmergreen, J. Phys. B 17 L901 (1984)
4. A. Bähring, I.V. Hertel, E. Meyer and H. Schmidt, J. Phys. A 16 293 (1983)
5. N. Andersen and S.E. Nielsen, Abstracts of the 1982, p. 265 (1982)

H(2s) FORMATION IN NON-ADIABATIC GROUND STATE HYDROGEN ATOM COLLISIONS

B.M. McLaughlin and K.L. Bell

Department of Applied Mathematics and Theoretical Physics
The Queen's University of Belfast
Belfast BT7 1NN Northern Ireland

Recently McLaughlin and Bell¹ have performed non-exchange and first order exchange calculations on total cross sections for H(2s) and H(2p) production in collisions between ground state hydrogen atoms. The non-exchange close coupling impact parameter calculations confirmed that coupling via higher intermediate states was unimportant. Whereas the first order exchange calculations performed within the Bates, Crothers, Rudge-Ochkur approximation confirmed that electron exchange was important below about 100 keV. These calculations of McLaughlin and Bell¹ confirmed that below about 15 keV a more refined theory is required for the treatment of electron exchange. In addition it is necessary to consider the effect of the rotation of the internuclear axis during the collision. This is necessary in order to account for the reluctance of the electrons to follow the rapid rotation of the internuclear axis leaving the electrons localised in space, especially at small impact parameters b , i.e. close collisions.

To formulate and carry out calculations for a non-adiabatic theory on cross sections for H-H collisions present a formidable task. We have therefore employed a simple two-state symmetrised travelling atomic basis set, with Bates and McCarroll² electron translational factors within the time dependent impact parameter formalism. We have used a travelling atomic basis set at present as opposed to the more natural and sophisticated travelling molecular basis set having variationally optimised switching functions, (cf Crothers and Hughes^{3,4}, Crothers and Todd⁵) so as to provide a benchmark for future calculations.

For H(2s) formation the cross sections depends on the evaluation of the electron exchange matrix elements "exactly" which are computationally difficult to evaluate. The most difficult of these exchange matrix elements being the two electron r_{12}^{-1} exchange matrix elements. These r_{12}^{-1} two electron exchange matrix elements may be evaluated exactly using the method of Green et al⁷ unlike their earlier "approximate" evaluation made by Ritchie^{8,9} in his calculations for H(2s) production in H-H collisions.

We concentrate on the single excitation process

$$H_A(1s) + H_B(1s) \rightarrow H_A(2s) + H_B(1s)$$

The basis set for the singlet and triplet states are then given by

$$\psi_0^\pm = \frac{1}{\sqrt{2}} (\psi_{1s}(r_A) \psi_{1s}(r_B) \pm \psi_{1s}(r_B) \psi_{1s}(r_A))$$

$$\psi_0^\pm = \frac{1}{N_0^\pm} [\psi_{1s}(r_{A1}) \psi_{1s}(r_{B2}) \exp(\frac{1}{2} i v (s_2 - s_1)) \pm \psi_{1s}(r_{A2}) \psi_{1s}(r_{B1}) \exp(-\frac{1}{2} i v (s_2 - s_1))] \times \exp[-it(\epsilon_{1s}^A + \epsilon_{1s}^B + \frac{1}{4} v^2)]$$

$$\psi_0^\pm = \frac{1}{N_1^\pm} [\psi_{2s}(r_{A1}) \psi_{1s}(r_{B2}) \exp(\frac{1}{2} i v (s_2 - s_1)) \pm \psi_{2s}(r_{A2}) \psi_{1s}(r_{B1}) \exp(-\frac{1}{2} i v (s_2 - s_1))] \times \exp[-it(\epsilon_{2s}^A + \epsilon_{1s}^B + \frac{1}{4} v^2)]$$

with N_0^\pm, N_1^\pm being appropriate normalization factors, $\psi_j(r)$ are the bound hydrogenic states.

The cross section for $1s \rightarrow 2s$ excitation is then given by

$$Q(1s \rightarrow 2s) = \frac{1}{4} Q^{(+)} + \frac{3}{4} Q^{(-)}$$

where

$$Q^{(\pm)} = 2\pi \int_0^\infty |a_1^\pm(b)|^2 b db \quad a_0^2$$

Calculations are in progress and results will be presented at the conference.

References

1. B.M. McLaughlin and K.L. Bell, J. Phys. B.: At. Mol. Phys. **16**, 3797 (1983).
2. B.M. McLaughlin (1983) Ph.D. thesis, The Queen's University of Belfast, Northern Ireland.
3. D.R. Bates and R. McCarroll, Proc. Roy. Soc. Lond. **A245**, 294 (1958).
4. D.S.F. Crothers and J.G. Hughes, Comments At. Mol. Phys. **15**, 15 (1984).
5. D.S.F. Crothers and J.G. Hughes, Proc. Roy. Soc. Lond. **A359**, 345 (1978).
6. D.S.F. Crothers and N.R. Todd, J. Phys. B.: At. Mol. Phys. **14**, 2233 (1981).
7. Green T.A., Stanley H.E. and Chiang You-Chien, Helv. Phys. Acta **38**, 109 (1965).
8. B. Ritchie, Phys. Rev. **A2**, 759 (1970).
9. B. Ritchie, Phys. Rev. **A3**, 656 (1971).

LYMAN-ALPHA EMISSION FROM LOW-ENERGY H COLLISIONS WITH RARE-GAS ATOMS*

B. Van Zyl, M. W. Gealy, and H. Neumann

Department of Physics, University of Denver, Denver, Colorado 80208, USA

Excitation of ground-state hydrogen atoms (H) to the 2p state in collisions with rare-gas atoms was examined by observation of the Lyman-alpha (L_α) emission resulting from the interactions. The H-atom energy range extended from below 0.05 to 2.5 keV.

The H atoms were produced by photodetachment of electrons from H^- ions, which were collimated into a beam of the desired energy and trajectory prior to the photodetachment region. The light source employed was a yttrium-aluminum-garnet laser (1064 nm) operated in a 50% duty-cycle mode, with the H^- ions traversing the laser cavity.¹ After deflecting the remaining H^- ions into a collector, the fast H atoms entered a target cell containing low-density rare-gas atoms.

The L_α photons were observed at 90° to the H-beam axis with an absolutely-calibrated detector consisting of a LiF gathering lens, a broad bandpass interference filter, a narrow bandpass O_2 -gas-cell filter, and a solar-blind photomultiplier with a MgF_2 window. The polarization of the emitted L_α was measured by inserting a Brewster-angle-mounted LiF window in front of the photomultiplier tube.

The photon detector was calibrated absolutely by observing L_α from H + Ne collisions as a function of distance into the target cell. For H-atom energies in the 1.5 keV range, collisionally excited H atoms from this reaction are formed primarily in ns states.² For $n \geq 3$, these ns states have long radiative lifetimes and decay preferentially to the 2p state, causing the L_α signal from such cascade processes to increase with distance into the target cell. Because the cross sections for excitation to the 3s and 4s states have been measured previously,³ and those for higher ns states can be estimated by extrapolation with a simple model, the absolute amount of this L_α signal increase with distance can be calculated. Comparison of this calculated result with the measured L_α signal increase with distance into the target cell gives the total detector efficiency to within $\pm 14\%$ uncertainty.

The cross sections for Balmer-alpha and Balmer-beta emissions, which result largely from $ns \rightarrow 2p$ and $nd \rightarrow 2p$ hydrogenic transitions, for H-atom collisions with all rare-gas atoms were reported earlier.³ Thus, the cross sections for 2p-state population via these cascade processes can be computed. Subtraction of

these cross-section values from the measured results for total L_α emission reported here allows the direct 2p-state-excitation cross sections to be determined.

For H + He collisions, more than 90% of the observed L_α emission results from direct excitation of the 2p state for all H-atom energies. The 2p-state-excitation cross section is about $5 \times 10^{-17} \text{ cm}^2$ for H-atom energies above 0.1 keV, below which it drops rapidly with decreasing energy.

However, for the other rare-gas targets, cascade population of the 2p state is an important contributor to the total L_α emission. For H + Ne collisions, cascade population of the 2p state from higher ns states accounts for about 40% of the total L_α emission for H-atom energies in the 1 keV range. The 2p-state-excitation cross section for this reaction is the smallest observed.

For Ar, Kr, and Xe targets, cascade population of the 2p state from higher nd states is the dominant source of L_α for H-atom energies below about 0.5 keV. For these reactions, the 2p-state-excitation cross sections reach maxima close to 10^{-16} cm^2 for H-atom energies near 2 keV but exhibit secondary maxima at energies below 0.1 keV as well.

The polarizations of the L_α emissions generally ranged between about 0 and 0.1 for most reactions and did not exhibit a strong H-atom-energy dependence. The exception was H + Ne collisions, where the polarization exceeded 0.2 for H-atom energies below 0.2 keV. These positive polarization values indicate that the $m_l = 0$ sublevel of the 2p state is more heavily populated in the collisions than the $m_l = \pm 1$ sublevels.

References

1. B. Van Zyl, N. G. Utterback, and R. C. Amme, *Rev. Sci. Instrum.* **47**, 814 (1976).
2. B. Van Zyl, M. W. Gealy, and H. Neumann, *Phys. Rev. A* (to be published).
3. B. Van Zyl, M. W. Gealy, H. Neumann, and R. C. Amme, *Proceedings of the Thirteenth International Conference on the Physics of Electronic and Atomic Collisions* (Berlin, 1983), p. 335.

*Supported by the Aeronomy Program, Division of Atmospheric Sciences, National Science Foundation.

ELECTRON-SPIN SPECTROSCOPY IN PENNING IONIZATION WITH He(2³S) METASTABLE ATOMS[†]

L. G. Gray, R. S. Keiffer, J. M. Ratliff, F. B. Dunning and G. K. Walters
Department of Physics, Rice University, Houston, Texas 77251 USA

Studies of spin dependences in Penning ionization reactions of the type



are being used to probe the dynamics of this process, and to identify the channels through which ionization occurs. In the present work the electrons on the He(2³S) atoms are spin labelled and the polarization of the ejected electrons is determined.

The apparatus is described in detail elsewhere.^{1,2} Briefly, a microwave discharge is used to generate He(2³S) atoms in a flowing helium afterglow. The 2³S atoms are optically pumped to preferentially populate either the $M_J(M_S) = +1$ or -1 state. Target gas is then introduced downstream into the afterglow leading to Penning reactions. The resultant electrons are extracted from the afterglow through a differentially-pumped aperture and their polarization measured using a Mott polarimeter.

The polarization of the 2³S atoms resulting from optical pumping is determined by injecting argon into the flow tube and measuring the polarization of the Penning electrons. Since Penning reactions involving argon are known to conserve spin, the extracted electron polarization equals the initial polarization of the 2³S atoms, typically 30%.

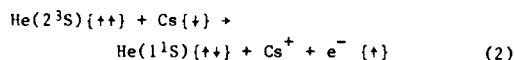
The polarizations of the electrons produced in Penning reactions with a number of target species, normalized to an initial metastable atom polarization of 100%, are shown in Table I.

Table I. Polarization of electrons produced in Penning reactions involving polarized He(2³S) atoms

K	Rb	Cs	O ₂	Cl ₂	CF ₃ Cl
93	71	100	31	74	90
± 7%	± 9%	± 5%	± 5%	± 3%	± 4%

Consider initially the data for the alkalis. In the case of Cs the ejected electron polarization is equal, within experimental error, to that of the 2³S atoms. This indicates that Penning

reactions must proceed via the so-called exchange channel



in which the Cs valence electron tunnels into the core hole of the 2³S atom with simultaneous ejection of the 2s electron. For Rb the ejected electron polarization is significantly lower indicating that other, non-spin-conserving, ionization channels must be operative. This confirms the conjecture of Johnson et al.³ who noted that a number of Rb autoionizing levels of configuration 4p⁵sn lie close in energy to the 2³S level and suggested that Penning reactions might proceed via energy transfer to a core-excited state followed by autoionization. Spin-orbit coupling in the 4p⁵ core can lead to a loss of spin polarization through polarization of the orbital moment, resulting in a reduction in ejected electron polarization. Penning ionization via autoionizing channels may also be possible for K, although only a few K autoionizing states lie sufficiently close in energy to the 2³S level. The data suggest that such a channel might be operative for K, but to a much lesser extent than for Rb.

The molecular targets listed in Table I were selected because energy distribution measurements⁴ showed that Penning reactions involving these species can proceed via an ionic channel. The present data show that reactions do proceed by other than the exchange channel and further work is in progress to determine the relative importance of the exchange and ionic channels.

References

1. L. G. Gray, K. W. Giberson, Chu Cheng, R. S. Keiffer, F. B. Dunning and G. K. Walters, *Rev. Sci. Instr.*, **54**, 271 (1983).
2. J. Keiffer, F. B. Dunning, M. R. O'Neill, R. D. Rundel and G. K. Walters, *Phys. Rev. A*, **11**, 1271 (1975).
3. C. E. Johnson, C. A. Tipton, and H. G. Robinson, *J. Phys. B*, **11**, 927 (1978).
4. O. Leisn, H. Morgner and W. Müller, *Z. Phys. A*, **304**, 23 (1982).

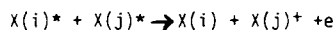
[†]Research supported by NSF under grant #PHY84-00709.

RARE GAS METASTABLE-METASTABLE MODEL POTENTIALS AND
ASSOCIATED PENNING IONIZATION CROSS SECTIONS

DAVID HUDSON

White Oak Laboratory, Naval Surface Weapons Center,
10901 New Hampshire Avenue, Silver Spring, MD 20903-5000

The interaction potential and Penning cross sections for processes of the type:



are of considerable scientific and technological interest. The case where the X's are rare gas metastables, are the only reactions, which to the author's knowledge, have been experimentally and theoretically studied. Several pairs have been studied experimentally by Neynaber and collaborators (1,2) yielding not only cross sections but, also an indication of the potential well depth. Theoretically, the situation is worse. Apparently the only quantum calculation to yield a reasonable cross section and potential curve is the work on $\text{He}^* + \text{He}^*$ by Garrison et.al.(3). However, many years ago, Ferguson observed (4) that the classical momentum transfer cross section assuming a modified Buckingham potential gave an unexpectedly good value for the $\text{He}^* + \text{He}^*$ reaction.

The present work first directly applied Ferguson's technique, where the necessary data in the form of scalar dipole polarizability was available, to cases where experimental results existed. Again, agreement is found to be unexpectedly good. The discrepancies lie in the 10-50 percent range.

Next, by taking advantage of the available well depth information from Neynaber's work and the one potential curve from Garrison et.al., various model potentials were created.

These model potentials are used to compute a semi-classical momentum transfer cross section. The phase shifts are evaluated by the Clenshaw-Curtis quadrature technique.

A comparison of these results, the primitive results and experimental values is presented. An attempt is made to explain why such good agreement with experiment is obtained. Empirical rules for the region of safe use for this approach are considered. Finally, a discussion of the extension of the method to other atoms and excitation states along with preliminary results are presented.

References

1. Neynaber, R. H. and S. Y. Tang, J. Chem. Phys. 72 5783 (1980).
2. Neynaber, R. H. and S. Y. Tang, J. Chem. Phys. 72 6176 (1980) and references therein.
3. Garrison, G. J., W. H. Miller and H. F. Schaefer, J. Chem. Phys. 59, 3193 (1973).
4. Ferguson, E. E., Phys. Rev. 128, 210 (1962).

THE ANGULAR DISTRIBUTION OF PENNING ELECTRONS: STRONG DEPENDENCE ON THE ELECTRON ENERGY FOR $\text{He}(2^1\text{S}) + \text{Ar}, \text{Kr}, \text{Xe}$.

Alfred Hertzner, Harald Morqner, Klaus Roth, and Günther Zimmermann

Fakultät für Physik, Hermann Herder-Str. 3, D-7800 Freiburg

The angular distribution of electrons from Penning ionization processes:



has been studied before by Ebding and Niehaus [1]. There, the angular distribution is given as the angle dependent intensity integrated over the entire electron energy range associated with a particular final state of the ion B^+ . The underlying assumption is that the angular distribution depends at most only mildly on the electron energy. A theoretical study [2] made use of the same concept.

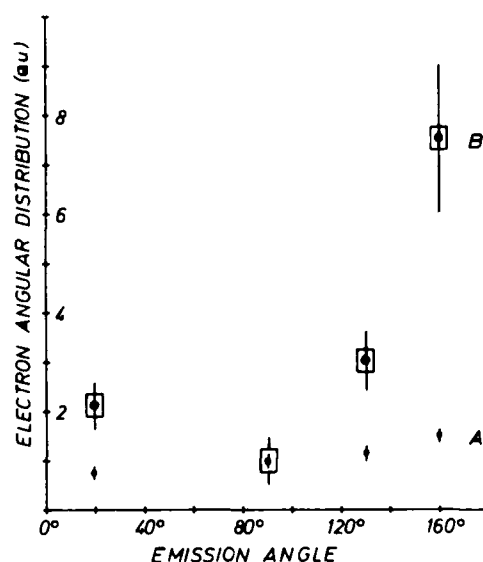
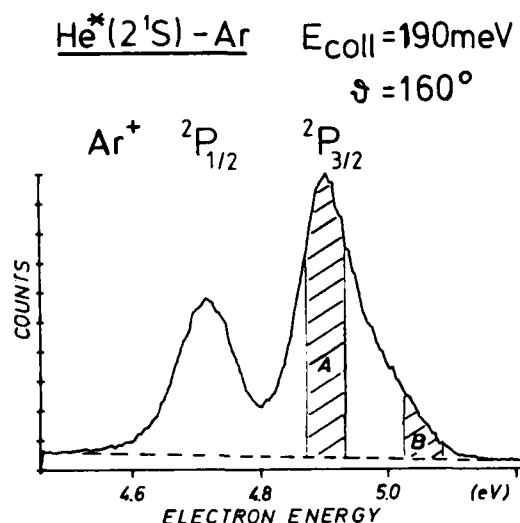
In the present study we find for the first time that experimental angular distributions of Penning electrons show a drastic dependence on the electron energy. The effect occurs for $\text{He}(2^1\text{S})$ colliding with the target atoms Ar, Kr, and Xe in a range of collision energies between 70 meV and 300 meV. At lower collision energies this effect is very small as found by Bregel and Hotop [3].

In fig. 1 we show an electron energy spectrum for $\text{He}(2^1\text{S}) + \text{Ar}$ with an averaged collision energy of

190 meV. For this spectrum the electron spectrometer was set to an angle of 160° with respect to the $\text{He}(2^1\text{S})$ beam velocity. In the spectrum two intervals of electron energy are marked A and B. The intensity integrated over A varies by a factor of roughly two as a function of emission angle. On the other hand, the intensity within interval B is strongly peaked for backward emission, i.e. $\theta=180^\circ$ and drops to 1/8 of its backward intensity when measured under 90° . A similar result is obtained for the other target atoms Kr and Xe. It is noteworthy that no comparable effect could be found for Penning ionization by the other metastable species $\text{He}(2^3\text{S})$.

The interpretation of these findings is in progress.

Support of this work by the Deutsche Forschungsgemeinschaft is gratefully acknowledged.



References

1. Ebding L., and Niehaus A., Z.Phys. 270 (1974) 43
2. Hoffmann A., and Morqner H., J.Phys. B 12 (1979) 2857
3. Bregel Th., and Hotop H. (1984) priv. communication

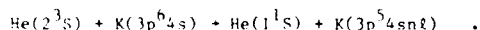
PENNING IONIZATION CROSS SECTIONS FOR COLLISIONS OF $\text{He}(2^1,^3\text{S})$ WITH ALKALI ATOMS:
COMPARISON OF THEORY AND EXPERIMENT

K. F. Scheibner,* J. S. Cohen,[†] R. L. Martin[†] and N. F. Lane^{*§}

*Physics Department, Rice University; present address: Joint Institute for Laboratory Astrophysics, University of Colorado and National Bureau of Standards, Boulder, Colorado 80309 and University of Colorado, Colorado Springs, Colorado 80933 USA

[†]Los Alamos National Laboratory, Los Alamos, New Mexico 87545 USA

Experimental measurements¹ of ionization rates for collisions of $\text{He}(2^3\text{S})$ atoms with alkali atoms show a trend of increasing ionization rate in the series sodium, potassium, rubidium, in marked contrast to the much smaller rate observed for cesium. Johnson *et al.*¹ suggest that the measured ionization rates for K and Rb may contain important contributions from indirect processes such as core excitation followed by atomic autoionization:



Some such core-excited states are nearly degenerate with the separated-atom states of $\text{He}(2^1,^3\text{S})$ and ground-state K or Rb. For Na, however, the energies of these core-excited states lie 10 to 20 eV higher and thus are not expected to participate in the ionization process. Furthermore, for Cs this entire series [i.e., $\text{Cs}(5p^56snl)$] lies about 5 eV below the initial electronic energy of the system and is therefore out of resonance (at least initially). Of course, there are other core-excited states of Cs which could become involved including the energetically accessible first excited state of Cs^+ .

The experimental observations raise interesting basic questions about the relative roles and physical dynamics of two types of ionization processes, i.e., those involving molecular autoionizing states and those involving atomic autoionizing states.

A previous study² of the $\text{He}(2^1,^3\text{S}) + \text{Na}$ system, which successfully combined modern L^2 methods with Stieltjes imaging techniques, yielded optical potentials for the relevant states and theoretical cross sections that agree well with experiment.

Encouraged by the favorable results of this earlier study (where the core-excited states are not important to the ionization process) we undertook the

present study to consider the more difficult problem of $\text{He}(2^1,^3\text{S}) + \text{K}$. In this case there are several core-excited, atomic autoionizing states which can have an important effect of the measured ionization rates. The techniques of Cohen *et al.*² are modified to correctly include the influence of these additional channels.

The calculation of the cross sections involves five steps: (1) a spin and symmetry Hartree-Fock calculation of the ground state of KHe; (2) a CI calculation of the resonance states which dissociate into the appropriate atoms and ions [e.g., into $\text{He}(2^1,^3\text{S}) + \text{K}^+$]; (3) partitioning of the Hamiltonian to define a resonance space and a continuum space followed by construction of the L^2 width matrix elements; (4) Stieltjes imaging which yields continuum normalized widths; (5) use of the resulting optical potentials to calculate complex phase shifts which yield the absorption cross sections.

By selective modification of the partitioning scheme [cf. step (3) above] we are able to explicitly examine the role of the core-excited atomic autoionizing states.

As a corollary to the above study we have also calculated the electron energy distributions predicted by the optical potentials for both the $\text{He}(2^1,^3\text{S}) + \text{Na}$ and $\text{He}(2^1,^3\text{S}) + \text{K}$ systems.

[†]Work supported by U. S. Dept. of Energy.

[§]Work supported in part by U. S. Dept. of Energy (ORNS).

References

1. C. F. Johnson, C. A. Tipton and H. G. Robinson, I. Phys. **4** 11, 927 (1978).
2. J. S. Cohen, R. L. Martin and N. F. Lane, Phys. Rev. A **31**, 152 (1985).

IONIZATION OF NEON IN COLLISIONS WITH $\text{He}^*(2^3\text{S})$ Toshio Tsuboi,^{*,†} and Keith T. Gillen[†]^{*} International Academic Center, Tokyo 2-12-5, Japan[†] Chemical Physics Laboratory, SRI International, Menlo Park, CA 94025 USA

The excitation energy of $\text{He}^*(2^3\text{S})$ is not sufficient for Penning ionization of Ne at thermal energies. However, for higher collision energies, calculations¹ using diabatic state correlation diagrams show the incoming potential to cross into the continuum at internuclear separations of ~ 1.5 Å. This could yield substantial ionization of the Ne target in an electron exchange process akin to Penning ionization.

We have examined Ne ionization processes in this system using a delayed coincidence technique to measure the double-differential scattering of the fast product He. A fast $\text{He}^*(2^3\text{S})$ beam, produced by near-resonant charge transfer of He^+ in Na vapor, crossed an effusive Ne beam; around the intersection volume rotated a Channeltron that measured the angular distribution of scattered fast atoms. In a direction perpendicular to both beams product Ne^+ ions were accelerated to a second Channeltron. The time delay spectrum between the particles detected on the two Channeltrons yielded for each scattering angle θ of the He a time-of-flight spectrum for the He product of the ionizing collision



Elastically and inelastically scattered $\text{He}^*(2^3\text{S})$ from non-ionizing collisions was not time-correlated with the Ne^+ signal and yielded only a uniform background in the coincidence spectra.

Measurements have been made over the laboratory energy range $100 \text{ eV} \leq E_0 \leq 400 \text{ eV}$. Below a reduced scattering angle $\tau (=E_0\theta)$ of $\sim 4000 \text{ eV-degrees}$, there are only two major observed features in the coincidence spectra. The most prominent feature at all scattering angles occurs at a heavy particle energy loss (endothermicity) of $\sim 3 \pm 1 \text{ eV}$, implying the release of a low energy (1-2 eV) electron in the ionization process. An additional feature separates in energy from the 3 eV feature at small angles and shifts gradually to higher endothermicities as the scattering angle increases. The reduced angular distribution $\rho (= \theta \sin \theta \frac{d\sigma}{d\Omega})$ for ionization is relatively flat for $50 \leq \tau \leq 1000$ and decreases gradually for larger scattering angles; any angular threshold for the ionization process must occur below 50 eV-degrees.

In supplementary experiments we have also measured the ratios of total slow ion production rates for $\text{He}^*(2^3\text{S})$ collisions with various target gases including Ne, He, and Ar. The cross section for ionization of Ne is substantial, varying from $\sim 15\%$ to $\sim 30\%$ of the cross section for Penning ionization of Ar over the energy range 100 eV - 500 eV. Penning ionization of Ar is thought to be the dominant component of the $\sim 10 \text{ Å}^2$ total destruction cross section² for $\text{He}^*(2^3\text{S}) + \text{Ar}$ in this energy range. The cross section for ionization of He is at least an order of magnitude smaller than that of Ne.

The ionization process can be understood in analogy to the system $\text{He}^*(2^3\text{S}) + \text{He}$ studied³ previously with different techniques. The incoming $\text{He}^* + \text{Ne}$ diabatic¹ state cuts through the lowest $\text{He} + \text{Ne}^+ + e^-$ continuum state at ~ 1.5 Å; the high density of Ne excited states (relative to the $\text{He}^* + \text{He}$ case) increases the probability for diabatic transit into the continuum where ionization can occur; this results in the larger total ionization cross section for Ne. The major feature at $\Delta E \sim 3 \text{ eV}$ can result either from ionization at the passage into the continuum or from population of $\text{He}^-(1s^2 2s) + \text{Ne}^+$ states, with the He^- stabilized in the field of the Ne^+ until the asymptotic region where the ion-pair curve rises above the $\text{He} + \text{Ne}^+ + e^-$ continuum and autodetaches. As in the $\text{He}^* + \text{He}$ system, the observed scattering at small angles can result from attractive interactions in the outgoing product ion channel that partially compensate for the repulsion in the incoming channel. The second (shifting) feature is consistent with ionization peaked at the inner turning point of the collision on the incoming diabatic state; both the scattering angle and the electron energy (and resultant energy loss) increase as the distance of closest approach decreases.

This work received financial support from the National Science Foundation.

References

1. J. C. Brenot, D. Dhucq, J. P. Gauyacq, J. Pommier, V. Sidis, M. Barat, and E. Pollack, *Phys. Rev. A* **11**, 1933 (1975).
2. J. T. Moseley, J. R. Peterson, D. C. Lorents, and M. Hollstein, *Phys. Rev. A* **6**, 1025 (1972).
3. K. T. Gillen, J. R. Peterson, and R. E. Olson, *Phys. Rev. A* **15**, 527 (1977).

LASER-ASSISTED IONIZATION ON $\text{He}(2^1, 2^3\text{S}) + \text{He}(1^1\text{S})$
COLLISION SYSTEM

P. Pradel, P. Monchicourt, D. Dubreuil, J. Heuzé

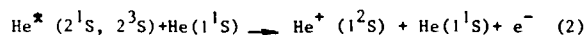
J.J. Laucagne and G. Spiess

Service de Physique des Atomes et des Surfaces, CEN/SACLAY
91191 Gif-sur-Yvette Cedex, France

Laser-assisted collisions can be defined /1/ as processes where photon absorption is made possible only in the course of a collision between two atoms, whereas it is not possible when these two atoms are far apart.

The observed bound-free assisted process is :
 $\text{He}^*(2^1\text{S}, 2^3\text{S}) + \text{He}(1^1\text{S}) + h\nu \rightarrow \text{He}^+(1^2\text{S}) + \text{He}(1^1\text{S}) + e^-(1)$
 The photon energy $h\nu = 3.49$ eV is chosen so as not to be resonant with any atomic transition. The $\text{He}(1^1\text{S})$ atom acts only as a perturber which shifts the He^* levels and allows photon absorption. Figure 1 shows the potential curves of He_2^* and He_2^+ systems /2, 3/ together with the field-dressed curves for one photon absorption. Ionization becomes possible for approximately $R \approx 2\text{\AA}$.

Our working energies allow field-free collisional ionization via a diabatic channel /4/ :



The value of the cross-section σ_d of reaction (2) permits a determination of the cross-section σ_a for the reaction (1). The experimental work is performed for 2 kinetic energies 50 eV and 35 eV in the center-of-mass system.

The He^* beam comes from a charge-exchange reaction between an He^+ beam colliding on a cesium target /5/. Charged particles emerging with He^* atoms from the Cs cell are removed out off the beam by a transverse electric field. This neutral beam is then incident on the He gas target cell. He^+ resulting from reactions (1) or (2) are charge-analysed by a transverse electric field and then are incident on a detector. In the interaction chamber, the He^* beam is crossed with an orthogonal laser light beam (3rd harmonic of a Nd:YAG laser.), $\lambda = 355$ nm, $I \approx 8 \times 10^6 \text{ W cm}^{-2}$. The ions correlated with the laser shot (via the process (1)) are superimposed on the background diabatic signal from reaction (2). For $E_{\text{CM}} = 50$ eV the laser correlated ion peak is equal to the diabatic signal. In the same way for $E_{\text{CM}} = 35$ eV the assisted ion peak is 2.5 times larger than the diabatic one. σ_d increases with increasing energy by approximately a factor 1.7; on the contrary σ_a decreases by a factor ≈ 0.5 showing that the colliding system exhibits a completely different kinematics when illuminated by the laser light. Competing reactions such as i) two photon-ionization ii) photoexcitation of He^* followed

by collisional ionization and iii) collisional excitation of He^* followed by photoionization, have been investigated and cannot account for the measured additional ion contribution.

The energetic dependence of the two cross-sections σ_d and σ_a have been obtained in the energy range of 25-100 eV in the center-of-mass system, and have been compared with their theoretical behaviour; these results will be presented at the conference.

1. L.I. Gudzenko and S.I. Yakovlenko, Sov. Phys. JETP **35**, 877 (1972).
2. R.P. Saxon, K.T. Gillen and B. Liu, Phys. Rev. A **15**, 543 (1977).
3. S.L. Guberman and W.A. Goddard III, Phys. Rev. A **12**, 1203 (1975).
4. K.T. Gillen, J.R. Peterson and R.E. Olson, Phys. Rev. A **15**, 527 (1977).
5. P. Pradel and J.J. Laucagne, J. Phys.(Paris) **44**, 1263 (1983).

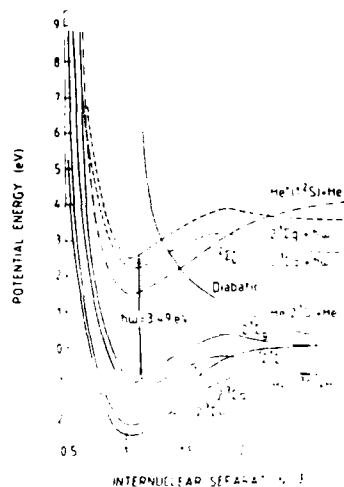


Figure 1 - Relevant potential curves for He_2^* and He_2^+ . Broken lines represent the field dressed potential curves.

ELECTRON SPECTROMETRIC STUDY OF IONIZING THERMAL ENERGY COLLISIONS OF Ne(4s,4p,4d) ATOMS WITH Ar ATOMS

T. Bregel, W. Bußert, J. Ganz, K. Harth, M. Raab, M.-W. Ruf, and H. Hotop

Fachbereich Physik, Universität Kaiserslautern, 6750 Kaiserslautern, FRG

In our program to study in detail ionizing thermal energy collisions of excited rare gas atoms with atoms and molecules, we have previously reported on reactions involving state-selected metastable Ne(3s $^3P_{2,0}$) and laser excited Ne(3p J=1,2,3) atoms¹⁻⁶. We have now extended these studies to the higher excited short lived states Ne(4s,4p,4d); here, we report our first results obtained in thermal energy ($E_{rel}=60$ meV) collisions with Ar.

A collimated metastable Ne(3s 3P_2) atom beam is transversely excited by two anticollinear single mode cw dye lasers, both linearly polarized parallel ($\pi_{||}$) or perpendicular (π_{\perp}) to the relative collision velocity, to the Ne(4s 3F_4) state via the Ne(3p 3D_3) state. Spontaneous emission from Ne(4d) leads to significant populations of the Ne(4p 3D_3) and Ne(4s 3P_2) state. The relative time-integrated excited state densities N are estimated from the rate equations and A-coefficients to be $N(4d):N(4p):N(4s) \approx 4.8:4.4:1$. Electrons released in ionizing collisions of the various excited states with Ar are energy analyzed with a high resolution electron spectrometer. Fig. 1 shows the resulting spectrum due to reactions of the Ne(4d,4p,4s) states. Their contributions are fully resolved and the spectrum shows three distinct components due to Ar $^+(^2P_{3/2, 1/2})$ ionization. The resolution of the low energy edge^{1,2,3/2} of the spectrum allows to obtain rather direct information on the well depths of the entrance channel potential curves. Since they represent Rydberg states to the Ne $^+$ -Ar ionic potentials, one expects well depths of comparable size. In agreement with recent results for Ne $^+$ -Ar⁷, the well depth for Ne(4d)+Ar is found to be close to 160 meV; those for Ne(4s,4p)+Ar are about 30 meV smaller. These findings are in good qualitative agreement with the behaviour of the Na(4s,4p,4d)+Ar potentials, calculated by Duren et al.⁸. Only the Ne(4p)+Ar spectrum shows a significant polarization effect, rather similar to the one found for Ne(3p 3D_3)+Ar^{5,6} and compatible with expectations on the basis of the Na(4p)+Ar interactions⁸.

The areas for the three different spectra should reflect the relative excited state densities, if the respective cross sections were the same. We find relative polarization-averaged spectral areas $I(4d):I(4p):I(4s) = 0.67:3.8:1$ indicating that the apparent Ne(4s)- and Ne(4p)-cross sections agree within 20 %, whereas the Ne(4d)-cross section is much smaller. This result probably reflects unfavourable coupling of the 4d-Rydberg

electron to the continuum. Electron angular distribution effects, now under investigation, may also, at least in part, be responsible for the low Ne(4d) signal at our detection angle of 60° relative to the neon beam direction in the plane of the neon and laser beams.

This work has been supported by the Deutsche Forschungsgemeinschaft (SFB 91).

References

1. H. Hotop, Electronic and Atomic Collisions, N.Oda and K. Takayanagi (Eds.), p.271, North Holland Publ., 1980
2. H. Hotop, J. Lorenzen, and A. Zastrow, J. Electron Spectrosc. Rel. Phen. **23**, 347 (1981)
3. J. Lorenzen, H. Morgner, W. Bußert, M.-W. Ruf, and H. Hotop, Z. Physik A **310**, 141 (1983)
4. W. Bußert, J. Ganz, H. Hotop, M.-W. Ruf, A. Siegel, H. Waibel, P. Botschwina, and J. Lorenzen, Chem. Phys. Lett. **95**, 277 (1983)
5. W. Bußert, T. Bregel, J. Ganz, K. Harth, A. Siegel, M.-W. Ruf, H. Hotop, and H. Morgner, J. de Physique (Conf. Series), Proc. of "Collisions in a Laser Field" March 27-30, 1984, in press
6. W. Bußert, T. Bregel, R.J. Allan, M.-W. Ruf, and H. Hotop, Z. Physik A **320**, 105 (1985)
7. D. Hausmann and H. Morgner, Mol. Phys. (in press)
8. R. Duren, E. Hasselbrink, and G. Moritz, Z. Physik A **307**, 1 (1982)

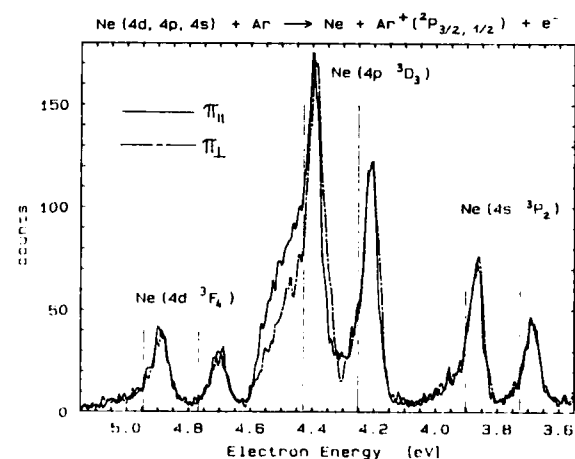


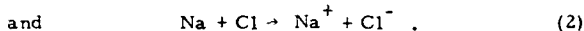
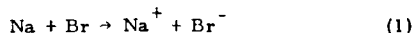
Fig. 1 Electron energy spectra due to ionizing thermal energy collisions of Ne(4d,4p,4s) atoms with Ar atoms. The vertical lines indicate the positions of the respective asymptotic excited-ionic state difference energies.

ION-PAIR PRODUCTION IN COLLISIONS OF Na WITH Cl AND Br[†]

R. H. Neynaber, S. Y. Tang, and D. P. Wang

University of California, San Diego, La Jolla, CA 92093, USA and
La Jolla Institute, La Jolla, CA 92038, USA

Experimental studies of ion-pair production in atomic alkali-halogen systems are rare. To increase the data base of these important processes we have used merging-beams techniques to examine Na-Cl and Na-Br. Absolute and relative cross sections, Q , have been measured (by detecting the negative product ion) for the reactions



When the reactants and products are in the ground states, the endoergiticities of reactions (1) and (2) are 1.78 and 1.52 eV, respectively. The reactions were investigated in a range of relative kinetic energy of the reactants, W , from threshold to 500 eV for (1) and threshold to 10 eV for (2).

Only two systems have previously been studied; these are Na-I and Li-I.¹ The cross-sectional behavior of these systems with W has successfully been predicted by various curve-crossing theories including the Landau-Zener-Stueckelberg (LZS) approximate model.²⁻⁴ This behavior, and especially that around threshold, is strongly related to the degree of adiabaticity of the reactant and product potential curves. These two systems are the most adiabatic of the alkali-halogens and behave similarly. Specifically, the Q -curves exhibit a step function at threshold rising from zero to some finite value. Then, Q continues to rise above this finite value as the relative velocity of the reactants, v , increases above the threshold velocity, v_t , until a maximum is reached and a decline begins. For Na-Br and Na-Cl, a step function is again predicted at v_t , but the finite value at the peak of the step function is also the maximum Q . One of the purposes of the present experiments is to determine if this actually describes the behavior around threshold. Further, the measurements will be a useful test of ion-pair production theories in general. Finally,

these systems are of interest in seeded, fossil-fuel reaction kinetics for reducing soot and as a means for measuring the population of ground-state (GS) Na in a mixture of ground and excited-state Na atoms. Actually, reaction (2) has already been used to measure the GS Na content in laser-excited Na vapor.⁵

The Na atom beam for these experiments is generated by charge-transferring Na^+ (from a surface ionization source) in Na vapor. This ensures a virtually pure GS beam. The Br beam is formed by charge-transfer-ring Br^+ from an electron impact source (which contains CFBr_3 vapor) in a vapor of CFCl_3 . The Cl is produced by electron detachment of Cl^- in O_2 . The Cl^- , in turn, is formed from CCl_4 in an electron impact source. Both the Br and Cl beams have atoms in the $np^5 2P_{3/2}$ GS and the $np^5 2P_{1/2}$ excited state. The separation of these states is 0.46 and 0.11 eV, respectively, for Br and Cl. The population ratio for these states is presumably that of the statistical weights and is 2. The contribution to ion-pair production by atoms in these states depends strongly, however, on the crossing radii of the associated reactant covalent and the product ionic potential curves. The net result is a negligible contribution for $\text{Br}(^2P_{1/2})$ and about 20% for $\text{Cl}(^2P_{1/2})$.

When these factors are considered, our results for both systems are in reasonable agreement with the slightly modified LZS theory of Faist and Levine.⁶ Also, the threshold behavior agrees with the predictions described above.

References

1. A. M. C. Moutinho, J. A. Aten and J. Los, *Physica* **53**, 471 (1971).
2. L. D. Landau, *Phys. Z. Sowjetunion* **2**, 46 (1932).
3. C. Zener, *Proc. Roy. Soc. A* **137**, 696 (1932).
4. E. C. G. Stueckelberg, *Helv. Phys. Acta* **5**, 370 (1932).
5. D. P. Wang, S. Y. Tang and R. H. Neynaber, *XIV ICPEAC* (1985).
6. M. B. Faist and R. D. Levine, *J. Chem. Phys.* **64**, 2953 (1976).

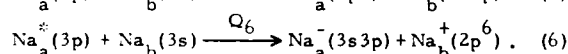
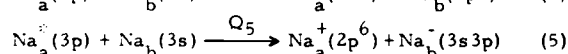
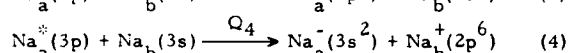
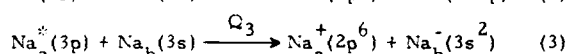
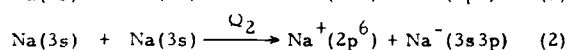
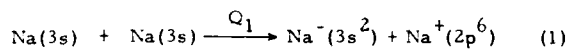
[†] Supported by NSF CPE83-10965 and the Air Force Office of Scientific Research (AFSC) under Contract No. F49620-84-C-0058.

ION-PAIR PRODUCTION AND THE EFFECT OF LASER EXCITATION IN Na-Na COLLISIONS*

S. Y. Tang, D. P. Wang, and R. H. Neynaber

University of California, San Diego, La Jolla, CA 92093, USA and
La Jolla Institute, La Jolla, CA 92038, USA

A review of experimental research in ion-pair production for two-body reactions shows a preponderance of effort devoted to processes in which an alkali is one of the reactants. The other reactant is often a halogen atom or molecule and sometimes a hydrogen atom. Prior to the present effort, however, no work on alkali-alkali systems has been reported. This is probably due to small reaction cross sections, Q , resulting from unfavorable curve crossing radii, R_c , for ground-state (GS) atoms although exceptions to this are alkali systems in which Cs is a partner. Here we describe our beam-gas efforts in studying (either directly or by deduction) the following alkali-alkali reactions in a range of relative kinetic energy, W , of the reactants from 500 to 2750 eV:



The subscripts a and b identify a specific atom and relate each product to its parent. An abbreviated electron configuration is shown above. A more complete identification of states is as follows: GS Na $\text{Na}(3s)$; $\text{Na}(3s^2S)$; GS Na^- $\text{Na}^-(3s^2) = \text{Na}^-(3s^2^1S)$; GS Na^+ $\text{Na}^+(2p^6) = \text{Na}^+(2p^6^1S)$; excited Na^- = shape resonance $\text{Na}^-(3s3p) : \text{Na}^-(3s3p^3P)$ - the energy of this state is 0.08 eV above that of GS Na; and excited Na^+ $\text{Na}^+(3p) : \text{Na}^+(3p^2P_{3/2})$. Other shape resonances such as the $3s3p^1P$ state are not included because they have not been proven to exist¹ and would likely have unfavorable crossing radii, R_c . Feshbach resonances definitely have unfavorable R_c . The $\text{Na}^*(3p)$ is produced by a laser. In some of our studies the $\text{Na}^*(3p)$ is in the fast beam and the hyperfine level $F = 3$; in others the $\text{Na}^*(3p)$

is in the stationary gas and the distribution of F is undefined.² We assume that the Q for each reaction is independent of the F distribution. The studies were made by measuring product currents of Na^+ or Na^- originating from atoms in the fast beam.

Some of the most interesting observations will now be discussed under the assumption that the Landau-Zener-Stueckelberg (LZS) curve-crossing model can be applied for qualitative explanations. First in our range of W , all Q increase with W . This is consistent with operating on the rising portion of the LZS universal curve (sugarloaf shape) of $Q/4 - R_c^2$ versus v/K , where v is the relative collision velocity and K is inversely related to R_c , as is the coupling potential, ΔV . We can conclude that all ΔV for the reactions are relatively large and that curve crossings, or transitions, are fairly adiabatic. Next, Q_2 is negligible compared with Q_1 . This is due to the energy of the GS of Na^- being smaller than that of the resonant state of Na^- and thus a larger separation at R_∞ (internuclear distance at infinity) of the ionic (product) and covalent (reactant) potential curves for reaction (2) than (1). This, in turn, results in a smaller R_c , larger K , and (from the universal curve) smaller Q for (2). Similarly, $Q_1 < 0.02 Q_3$ and $Q_1 < 0.02 Q_4$ ($Q_3 \approx Q_4$) because of the smaller energy of GS Na than $\text{Na}^*(3p)$ and thus the larger separation of potential curves for (1) than (3) and (4). This is a direct result of the laser excitation. Next, for a given W , the slope of the Q_1 - W curve is greater than that of the Q_4 - W curve. This is the result of the larger K for reaction (1) and a steeper slope on the universal curve. Complicating the above analyses, although not changing our qualitative conclusions, is multiple curve crossing due to the existence of neutral-neutral exit channels other than the reactant channel. Finally, $Q_3 < Q_5$ and $Q_4 > Q_6$. A discussion of these results is too involved to be presented here. (For reference, $Q_1 \approx 1 \times 10^{-3} \text{ \AA}^2$ at $W = 1500 \text{ eV}$.)

References

1. A. R. Johnston and P. D. Burrow, *J. Phys.* B15, L745 (1982).
2. D. P. Wang, S. Y. Tang and R. H. Neynaber, XIV ICPEAC (1985).

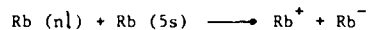
*Supported by NSF CPE83-10965 and the Air Force Office of Scientific Research (AFSC), under Contract No. F49620-84-C-0058.

ION PAIR FORMATION BY THE COLLISIONAL REACTION
 $\text{Rb}(nl) + \text{Rb}(5s) \longrightarrow \text{Rb}^+ + \text{Rb}^-$

M. Cheret, L. Barbier and M. Djerad

Service de Physique des Atomes et des Surfaces, CEN/SACLAY
 91191 Gif-sur-Yvette Cedex, France

Negative ions are observed in a Rb vapour when highly excited $\text{Rb}(nl)$ levels are populated /1,2/ (nl : 5d to 11s). Experimental observations give evidence that they are formed via the following reaction :



Some of the studied levels (5d to 8s) lie below the limit of the ionic curve Rb^+, Rb^- (energy defect ΔE 4070 cm^{-1} to 725 cm^{-1}) and others (7d to 11s) above this limit. The rate coefficients deduced from the measurements are represented on fig.1 :

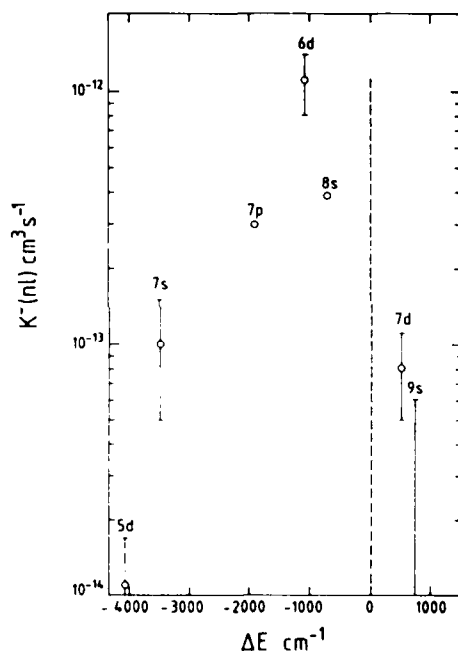


Figure 1 : Rate coefficients against the energy defect of the reaction.

The corresponding cross sections (fig.2) are calculated assuming a maxwellian distribution of the velocity and constant value of the cross section above the energy threshold.

It is shown that a Landau Zener calculation at the crossing point R_c between the unperturbed covalent and ionic curves explains the result obtained for level 5d and 7s ($R_c=54$ and 63 a.u.). The R.K. Janev and A.Salin /3/ model is used to calculate the coupling $H_{12}(R_c)$. This factor is ten times higher than the value predicted by

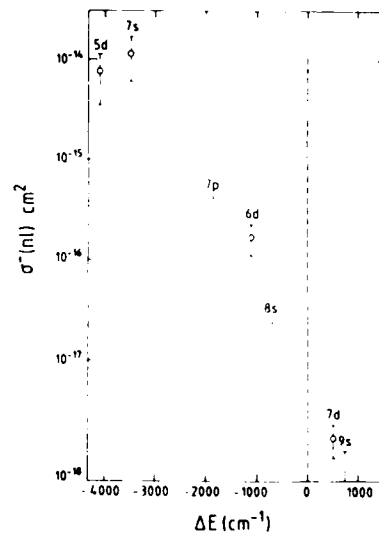


Figure 2 : Cross sections for ion pair formation (n) against the energy defect of the reaction.

the Olson phenomenological law /4/.

For the other levels the crossing point is passed diabatically or does not exist (level 7d and 9s). An other mechanism involving crossings at shorter distances is proposed (fig.3) and evidences for its validity are given. 1).

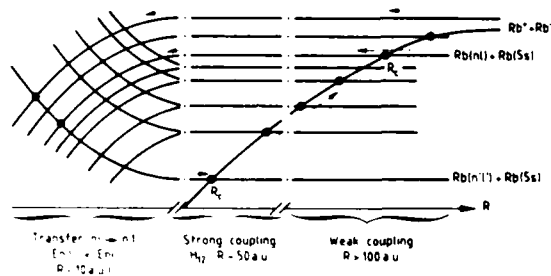


Figure 3 - Mechanisms for ion pair formation. Levels 5d and 7s R_c 50 a.u. strong coupling direct formation. Levels 6d, 8s R_c 200 a.u. weak coupling transfer to lower levels (5d, 6d) at short distance. Level 7d, 9s no crossing with (Rb^+, Rb^-) transfer to lower levels.

References

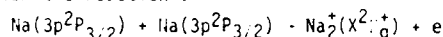
1. M. Cheret and L. Barbier, Phys. Rev. **30**, 1132 (1984).
2. L. Barbier, Thèse d'Etat, Orsay (déc. 1984).
3. R.K. Janev and A. Salin, J. Phys. B **5**, 177 (1972).
4. R.E. Olson, F.T. Smith and E. Bauer, Appl. Opt. **10**, 1848 (1971).

A CORRELATED ORBITAL METHOD FOR MODEL POTENTIAL CALCULATIONS OF THE EXCITED STATES OF Na₂ UP TO THE Na(3p) + Na(3p) DISSOCIATION LIMIT.

A. Henriët*, F. Masnou-Seeuws* and C. Le Sech*

*Laboratoire des Collisions Atomiques et Moléculaires, Bât. 351, Université Paris-Sud, 91405 ORSAY Cedex FRANCE
+Laboratoire d'Astrophysique Fondamentale, Observatoire de Meudon, 92190 MEUDON FRANCE

During the past few years, many experiments¹⁻³ have been devoted to the study of the associative ionisation of two laser excited sodium atoms, involving as a possible mechanism the reaction :



Most theoretical calculations concerning the Na₂ molecule have been limited to the ground and low lying excited states⁴⁻⁵. However, recent *ab initio* calculations⁶ predict a crossing at R=9 a.u. between the Na₂⁺ X²Σ_g⁺ curve and the Na₂ 1¹Σ_g⁺ curve correlated to the Na(3p)-Na(3p) dissociation limit.

We have recently⁷ proposed a method which is a generalisation both of model potential calculations⁸ for one active electron systems and of the Pluvillage method for two electron systems⁹. The energies of the Na₂ molecule are obtained by computing the matrix elements of a model hamiltonian on a basis of a limited (20) number of correlated configurations such as :

$$\Psi_{ab} \Omega(1,2) = [\phi_a(1)\phi_b(2) \pm \phi_b(1)\phi_a(2)] \Omega(1,2) \quad (1)$$

In Eq(1) we have denoted by (1) and (2) the coordinates of the two electrons. $\phi_a(i)$ is an eigenfunction of a one electron model hamiltonian describing the motion of the electron (i) in the field of the two Na⁺ cores. ϵ_a is the associated eigenenergy. $\Omega(1,2)$ describes the collision of two free electrons in the absence of an external field. We have used in the present work :

$$\Omega(1,2) = u_0(kr_{12})/r_{12} \quad (2)$$

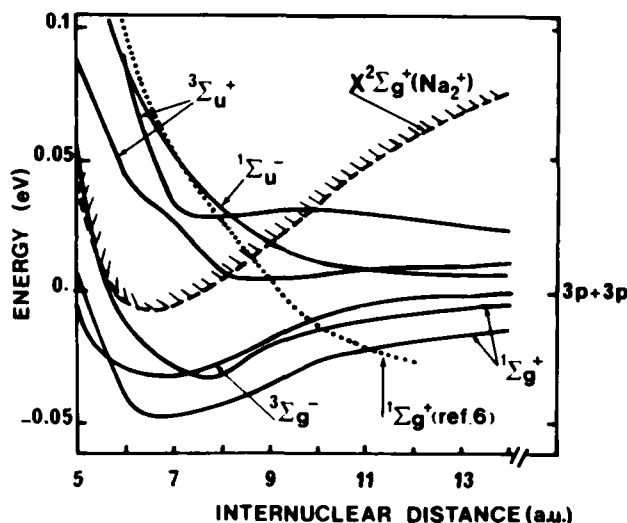
where u_0 is a regular spherical coulombic function and r_{12} the interelectronic distance. The matrix element of the hamiltonian are then easily obtained from the independent electron energy $\epsilon_a + \epsilon_b$, the collision energy k^2 , and bielectronic integrals involving a cross kinetic term and the dielectric operator V_{die} .

The collision energy is optimised so as to minimize the energy of the lowest state of a given symmetry. The molecular energies are obtained after diagonalisation of the hamiltonian for various internuclear distances.

On the table are presented the values obtained for the depth (De, Te) and position R_e of the well in the ground state and in some excited states. Good agreement is obtained with experiment and with the pseudo-potential calculations of Jeung⁵.

On the figure are displayed the Σ curves correlated to the 3p+3p dissociation limit together with the Na₂⁺ ground state curve. Our results differ from previous work⁶.

RESULTS			
	De(10 ³ cm ⁻¹)	Re(a.u.)	
X ² Σ _g ⁺	5.89	5.8	Present work
	6.02	5.8	Jeung ⁵
	6.024	5.82	Exp ¹⁰
	5.1		Montagnani et al. ⁶
	Te(10 ³ cm ⁻¹)	Re(a.u.)	
3 ¹ Σ _g ⁺	25.8	6.5	Present work
	25.8	6.6	Jeung ⁵
	25.7	6.7	Exp ¹⁰
2 ¹ Σ _g ⁺	29.1-27.0	7.2-12.6	Present work
	28.5-23	6.9-12.7	Jeung ⁵
	28.45-27.87	6.97-12.73	Exp ¹⁰
2 ³ Σ _g ⁺	27.6	7.5	Present work
	27.3	7.3	Jeung ⁵
2 ³ Σ _g ⁺	25.7	6.6	Present work
	25.6	6.6	Jeung ⁵



References

1. T. Roussel, B. Carré, P. Breger and G. Spiess, J.Phys. E 14 (1981) L313
2. R. Bonnano, J. Boulmer and J. Weiner Phys.Rev. A28 (1983) 604
3. J.G. Kircz, R. Morgenstern and G. Nienhuis Phys.Rev. Lett. 48 (1982) 610
4. D.D. Konowalow, M.E. Rozenkrantz and J. Olson J.Chem. Phys. 72 (1980) 2612
5. G.H. Jeung J.Phys.B 16 (1983) 4289
6. R. Montagnani, P. Riani and O. Salvetti Theoret.Chim. Acta 64 (1984) 431
7. A. Henriët, M. Aubert-Frecon, C. Le Sech and F. Masnou-Seeuws J.Phys.B 17 (1984) 3417
8. A. Henriët and F. Masnou-Seeuws Chem.Phys.Lett. 101 (1983) 535
9. P. Pluvillage J.Phys.Radium 12 (1951) 789
10. J. Vergès, C. Effantin, J. d'Incan, D.L. Cooper and R.F. Barrow Phys.Rev.Lett 53 (1984) 46 and references therein

HOMONUCLEAR ASSOCIATIVE IONIZATION IN COLLISIONS BETWEEN He(5³P) AND He(1¹S) ATOMS

S. Runge, A. Pesnelle, M. Perdrix, G. Watel and J.S. Cohen*

Service de Physique des Atomes et des Surfaces, CEN/SACLAY, 91191 Gif-sur-Yvette Cedex, France

* Theoretical Division, Los Alamos National Laboratory, Los Alamos, New Mexico 87544 - U.S.A

A characteristic feature of homonuclear associative ionization, also known as the Hornbeck-Molnar ionization (HMI)



is that the potential energy of the system at the separated limit is lower in the incoming channel than in the outgoing channel (fig.1). In the thermal range, the relative kinetic energy E_k of the reactants is not sufficient for the total energy to reach the ionic asymptotic limit ($A^+ + A$) and the nuclei remain bound, forming an associative ion A_2^+ . The origin of the ionization must be sought in the couplings between the potential energy curves for the excited neutral molecule A_2^* and the ground state of the molecular ion A_2^+ .

HMI has been investigated in a crossed-beam experiment for the collision He(5³P)+He using a time-of-flight (TOF) technique. Excited states were produced from metastable He(2³S) using a tunable CW source of coherent light at 294 nm produced by second harmonic generation in a ring laser. The density distribution of the He(5³P) atoms in the interaction zone was investigated by a highly sensitive photo-ionization method with a krypton laser tuned to the red lines (647 and 752 nm). The combination of these techniques with a crossed-beam geometry allowed the kinetic energy dependence of the cross-section to be investigated with a good resolution in the range 20-200 meV, via the TOF spectra of He₂⁺ ions resulting from HMI and of He⁺ ions produced by photoionization of He(5³P)¹. The experimental points are represented by rectangles on figs.2.

Nielsen et al.² and later Koike et al.³ for H₂^{*} considered the vibronic coupling between attractive adiabatic H₂^{*} curves and the ionic one in a region such as (I) in fig.1. The cross sections exhibit values of about 10⁻¹⁸ cm² at 300°K and a monotonic decrease with increasing E_k which is not observed here.

V(R)

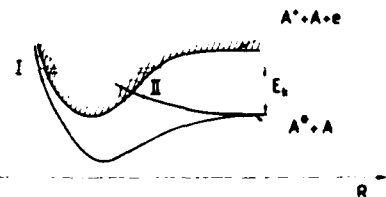


Figure 1

Later, Cohen developed the MSCC model⁴; he considered repulsive diabatic states He₂^{*} penetrating into the continuum of He⁺ + e, and interacting with the attractive ones by electronic coupling. The ionization occurs in a region such as (II) in fig.1. The cross sections for HMI were calculated for He^{*} (n=3,4)+He; they exhibit structures and values close to 10⁻¹⁶ cm².

We had first developed a model potential method for He₂^{*} and used it to calculate the ³Π_u diabatic states and couplings between them. The interpretation of our results has been performed by an extension of the MSCC model to the present case n=5: broken line on figs 2a and 2b is the result of MSCC model¹. Improvement of the agreement between experiment and theory at low energies is possible, considering two effects. (a) The effect of a small inaccuracy in the energies calculated by the model potential method; a 14 meV shift of the crossing energies of the 5P channel is made (full line on fig.2a). (b) The effect of adding long range couplings between asymptotically nearly degenerate potential curves (full line on fig. 2b).

The shape of the experimental curve is well reproduced by the ³Π_u symmetry, which is found to be preponderant and the validity of the MSCC model is thus shown.

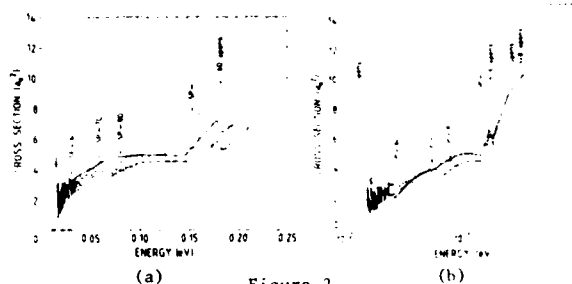


Figure 2

References

1. S. Runge, A. Pesnelle, M. Perdrix, G. Watel and J.S. Cohen, submitted to Phys. Rev. A.
2. S.E. Nielsen and R.S. Berry, Phys. Rev. A **4**, 865 (1971)
3. F. Koike and H. Nakamura, J. Phys. Soc. Japan **33**, 1426 (1972).
4. J.S. Cohen, Phys. Rev. A **13**, 99 (1976).

VELOCITY DEPENDENCE OF ASSOCIATIVE AND DISSOCIATIVE
IONIZATION OF RARE GAS ATOMS AND SIMPLE MOLECULES BY $\text{He}2^3\text{S}$ ATOMS

P.A. Jerram and A.C.H. Smith

Department of Physics and Astronomy, University College London, London, WC1E 6BT, U.K.

Velocity dependence of ionization branching ratios with velocity for collisions of $\text{He}2^3\text{S}$ with various atomic and molecular species are reported for the velocity range 1.5×10^3 to $4 \times 10^4 \text{ m s}^{-1}$ (0.0 to 4eV). These ratios were combined with our absolute total ionization cross sections to give the partial cross sections for all the various channels (i.e. chemi-ionization). The branching ratios have been measured for Ar, Kr, Xe, H_2 , D_2 , O_2 , H_2 , CO, CO_2 , H_2O , NH_3 , CH_4 , C_2H_2 and C_2H_4 .

The branching ratios are measured using a double time-of-flight (TOF) technique. Both the velocity selection of the incident metastable atoms and the identification of the ion fragments are now made using TOF analysis. This is done by simultaneously collecting 16 mass spectra in 16 velocity ranges. A chopper wheel positioned in front of the metastable beam source provides a pulsed beam. The beam is generated in a hot cathode constricted arc source and contains metastable atoms with velocities of up to 20 km s^{-1} . The metastables are mainly 2^3S but also about 9% of 2^1S are present which are removed with a He discharge quench lamp.

In the TOF mass spectrometer the ions are accelerated to about 3keV and then detected with an electron multiplier. The detection efficiency of this multiplier was measured as a function of ion mass. The relative efficiency was similar to that measured by Krebs³ showing a maximum for a mass number of 18.

Selected results for two distinct gases are shown in fig. 1. In (a) the only competing processes in Ar and CO are Penning and associative ionization. The percentage of associative ionization rapidly decreases to less than 1% as the velocity increases. For most diatomic and polyatomic molecules Penning ionization and dissociative ionization are found to be the chief processes, as shown in (b) for CH_4 . Our results for Ar compare well with those of Pesnelle et al⁴. Other groups^{2,5} have measured branching ratios for unselected beams but comparison is difficult as the velocity distributions of the metastable atom beams are unknown.

One of us (PAJ) is in receipt of a SERC postgraduate studentship and some aspects of this work have been funded in the past by the SERC.

Reference:

1. Jerram P.A. and Smith A.C.H., This conference. Velocity dependence of chemi-ionization of rare gas atoms and simple molecules (1985)
2. Hotop H, Niehaus A. and Schmeltekopf A.L., Z. Phys. 229, 1-13 (1969).
3. Krebs K.H., Fortschritte der Physik, 16, 419 (1968).
4. Pesnelle A., Watel G. and Manus C., J. Chem. Phys. 62, 3590 (1975).
5. West W.P., Cook T.B., Dunning F.B., Rundel R.D. and Stebbings R.F., J. Chem. Phys. 63, 1237 (1975)

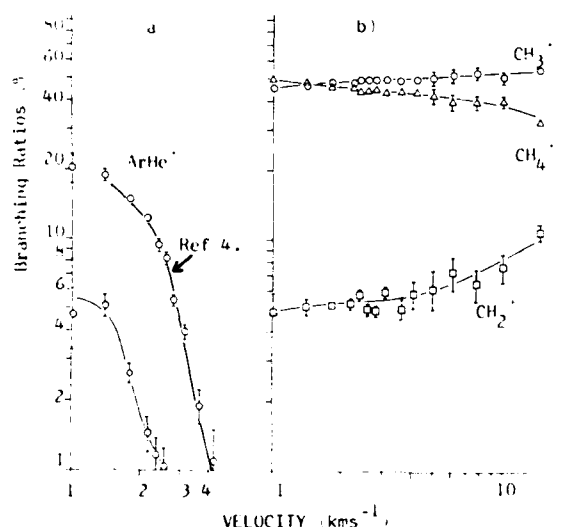


Figure 1

VELOCITY DEPENDENCE OF CHEMI-IONIZATION OF RARE GAS ATOMS AND SIMPLE MOLECULES

P.A. Jerram and A.C.H. Smith

Department of Physics and Astronomy, University College London, Gower Street, London WC1 6BT, UK.

Measurements have been made of the variation of ionization cross section with velocity for $\text{He}(2^3\text{S})$ with various atomic and molecular species. These measurements cover the wide velocity range $1\text{--}19\text{ km s}^{-1}$ (kinetic energy range $0.02\text{--}7.5\text{ eV}$).

Relative variations of cross sections have been measured for Ar, Kr, Xe, H_2 , D_2 , O_2 , H_2 , CO, CO_2 , NH_3 , H_2O , CH_4 , C_2H_6 & C_2H_2 . These relative cross sections are then normalised to our previously measured absolute cross sections, or in some cases to other absolute data^{2,3}. Where comparisons can be made, the data from these other groups agreed with our absolute cross sections (see Figure 1).

The relative cross sections are measured using a TOF technique. A chopper wheel placed in front of the arc source gives pulses of metastable atoms $\sim 1\text{ ns}$ wide. The time of this start pulse is accurately identified by the intense photon peak from the source. Two TOF spectra are then collected, one by means of a channeltron 1.06 m from the source showing the velocity distribution of $\text{He}(2^3\text{S})$ atoms emitted from the source and the other by means of a TOF mass spectrometer located 0.54 m from the source showing the mass spectrum of the product ions. The TOF mass spectrometer views the interaction volume of the metastable and target beams and selects the ions of interest while eliminating any ions due to background gases. Dividing the second spectrum by the first gives the variation with velocity of the relative ionization cross section which is then normalised to an absolute cross section one at particular velocity. The results given here are for $\text{He}(2^3\text{S})$ only, as the $\text{He}(2^1\text{S})$ component of the beam was too small ($\sim 9\%$) for making useful measurements. The $\text{He}(2^3\text{S})$ component was removed with an optical quench lamp.

A sample result is shown for the variation of cross section with velocity of $\text{He}(2^3\text{S})$ on argon. As can be seen our cross section agrees well with the other relative and absolute data shown^{4,5,6,7} in the normalisation used.

One of us (PAJ) is in receipt of a SERC Postgraduate Studentship and some aspects of this work have in the past been funded by the SERC.

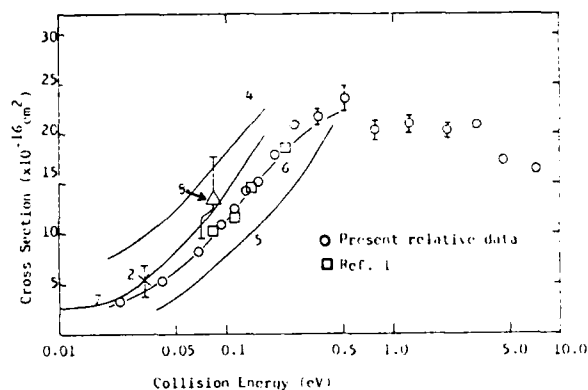


Figure 1

References:

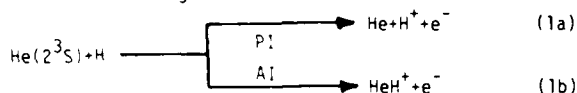
1. Jerram PA and Smith ACH, *J. Phys. B*, **10**, 1985.
2. Schmeltekopf AL and Fehsenfeld EC, *J. Chem. Phys.*, **53**, 3173 (1970).
3. Ueno T, Yokoyama A, Takao S and Hatano Y, *Chemical Physics*, **45**, 261 (1980).
4. Woodard HR, Sharp RC, Sealy D and Haseblitz EE, *J. Chem. Phys.*, **69**, 2275 (1978).
5. Besonelle A, Wateil G and Harris C, *J. Chem. Phys.*, **62**, 3590 (1975).
6. Hellenberger E and Michals A, *Z. Physik*, **B**, **20**, 33 (1975).
7. Bordeniski S, Feltgen R, Lichtenfeld E and Pohl H, *Chem. Phys. Lett.*, **78**, 226 (1981).
8. Lindinger W, Schmeltekopf AL and Fehsenfeld EC, *J. Chem. Phys.*, **61**, 2890 (1975).

ASSOCIATIVE IONIZATION IN THERMAL ENERGY COLLISIONS OF $\text{He}(2^3\text{S})$ ATOMS WITH HYDROGEN ATOMS

H. Waibel, W. Bußert, M.-W. Ruf, and H. Hotop

Fachbereich Physik der Universität, D-6750 Kaiserslautern, FRG

The ionizing reaction



is a model system for Penning (PI) and associative (AI) ionization studies, both experimentally [1-3] and theoretically [3-6]. We have carried out the first electron spectrometric study of reaction (1) with sufficiently high resolution to partially resolve the rotational structure due to formation of rovibrationally excited $\text{HeH}^+(\text{v}, \text{J})$ ions in path (1b).

A well collimated beam of state-selected $\text{He}(2^3\text{S})$ metastables from a differentially-pumped dc discharge source crosses a quasi-beam of hydrogen atoms from a microwave discharge in a field-free region. Product electrons ejected perpendicularly to both beams are energy analyzed in a double hemispherical condenser with an effective resolution of 35 meV (FWHM). The relative collision energy distribution ranges from 20 to 120 (7 to 50) meV with a maximum at 45(17) meV for room temperature (liquid nitrogen temperature) of both beam sources. Electron energy spectra are measured by multichannel scaling techniques.

Fig. 1A shows the result at room temperature, as accumulated over 30 hours. The spectrum clearly exhibits rotational-vibrational structure, which is even better resolved in our low temperature data. For comparison we have carried out quantum mechanical calculations using the program due to Hickman and Morgner [7], modified to include changes of the rotational quantum number during electron emission, the $\text{He}(2^3\text{S}) + \text{H}$ potential of Morgner and Niehaus [3], and the HeH^+ potential given by Bishop and Cheung [8]. It is found that the main J-dependent contributions stem from $v = 1-4$. Fig. 1B shows the total calculated AI spectrum for $T=300$ K, which includes the formation of quasi-bound HeH^+ states, but leaves out Penning ionization to free $\text{He} + \text{H}^+$ states. Therefore, Fig. 1A and Fig. 1B can only be compared for energies above 6.26 eV. Good overall agreement between experiment and theory is observed at both collision temperatures lending strong support to the idea that the local complex potential method provides a satisfactory description of $\text{He}(2^3\text{S}) + \text{H}$ ionizing collisions.

We acknowledge support of this work by the Deutsche Forschungsgemeinschaft (SFB 91).

References

1. H. Hotop, E. Illenberger, H. Morgner, and A. Niehaus, *Chem. Phys. Lett.*, **10**, 493 (1971)
2. J. Fort, J.J. Laucagne, A. Pesnelle, and G. Watel, *Phys. Rev.*, **A18**, 2063 (1978)
3. H. Morgner and A. Niehaus, *J. Phys.*, **B12**, 1805 (1979)
4. W.H. Miller, C.A. Slomcomb, H.F. Schaefer III, *J. Chem. Phys.*, **56**, 1347 (1972)
5. A.P. Hickman, A.D. Isaacson, and W.H. Miller, *J. Chem. Phys.*, **66**, 1483 (1977)
6. R.J. Bienenek, *Phys. Rev.*, **A18**, 392 (1978)
7. A.P. Hickman, and H. Morgner, *J. Phys.*, **B9**, 1765 (1976)
8. D.M. Bishop, and L.M. Cheung, *J. Mol. Spectrosc.*, **75**, 1719 (1979)

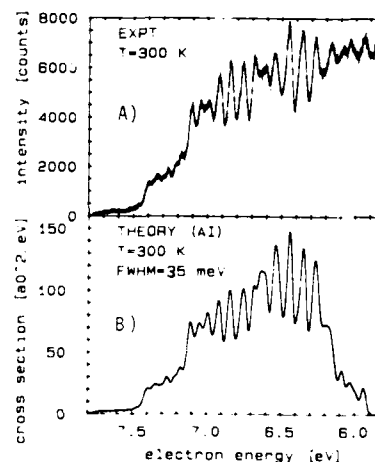
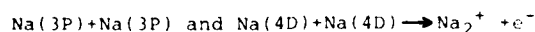


Fig. 1: Comparison between measured high energy part of the electron energy spectrum of reaction (1) at room temperature (A) and quantum mechanical calculation (B) of the spectrum due to AI (reaction 1b, including quasi-bound states). The calculation represents an average over collision energies for $T=300$ K and was convoluted with a Gaussian of 35 meV FWHM; it includes changes of the rotational quantum number during electron emission up to $J=3$.

A NEW LOOK AT ASSOCIATIVE IONIZATION BETWEEN TWO EXCITED ALKALI ATOMS:



E. Meyer, H. Schmidt, R. Witte and I.V. Hertel

Institut für Molekülphysik, Freie Universität Berlin, D-1000 Berlin 33, West Germany

Discrepancies between experimental results of Morgenstern et al.¹ and Rothe et al.² on associative ionization of excited Sodium emphasize the need to reinvestigate these processes. Both groups have measured the dependence of $\text{Na}(3\text{P}) + \text{Na}(3\text{P}) \rightarrow \text{Na}_2^+ + \text{e}^-$ on the polarization angle of the exciting light. Their results differ in a phase factor of 2.

We use a well-collimated Na-beam, which is intersected at right angles with a linear polarized laser beam tuned to the $\text{Na}(3^2\text{S}_{1/2}, F=2) \rightarrow \text{Na}(3^2\text{P}_{3/2}, F=2)$ transition. The entrance windows of the apparatus are carefully checked so that they do not destroy the linear polarization of the exciting light. This could be a possible explanation for the discrepancy between the previous experiments.

As shown in Fig. 1 we observe a strong dependence of the ion signal from the direction of the polarization vector. At $\theta=0^\circ$ ($\mathbf{E} \perp \text{Na beam}$) the ion rate has its minimum, while at $\theta=90^\circ$ ($\mathbf{E} \parallel \text{Na beam}$) the maximum is observed in agreement with the results of Morgenstern¹. The simultaneously measured fluorescence intensity is also depicted in Fig. 1 to show the correct excitation and alignment of the Sodium atoms. In addition the position of the atomic p-orbital is schematically shown in Fig. 1.

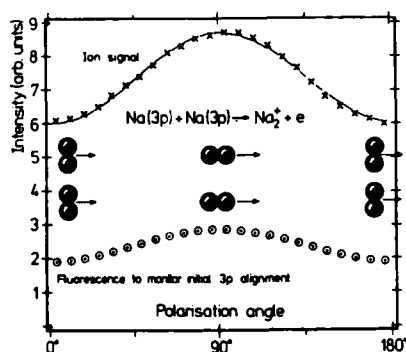


Fig. 1 Polarization dependence of the ion rate for $3\text{P}_{3/2}$ excitation (statistical error $\approx 2\%$)

We use a $\cos(2\theta)$ -function which best fits to our data. No improvement is found by adding a $\cos(4\theta)$ term to the fit-function. In order to extend our studies to higher excited states we use a second laser, directed antiparallel to the first one. We excite the $4^2\text{D}_{5/2}$ state of sodium with linear and the 3P state with circular polarization.

The ion-rate is drastically increased by a factor of 5000-10000 and we observe a slight polarization dependence of the ion-production shown in Fig. 2.

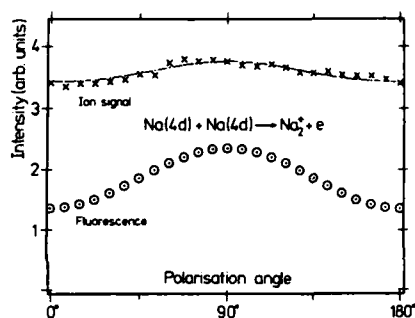


Fig. 2 Polarization dependence of the ion rate for $4\text{D}_{5/2}$ excitation

Details will be reported at the conference.

References

1. J.G. Kircz, R. Morgenstern and G. Nienhuis, Phys. Rev. Lett. **48**, 610 (1982)
2. E.W. Rothe and R. Theyanni, G.P. Rock and C.C. Tung, Phys. Rev. A, submitted

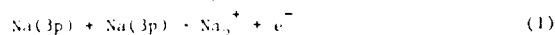
One of us (E.M.) wishes to thank the Welsh Foundation for financial support.

POLARIZATION DEPENDENCE OF ASSOCIATIVE IONIZATION
IN $\text{Na}(3p) + \text{Na}(3p)$ COLLISIONS

Harro A.J. Nijler, Berko P.v.d. Meulen, Henk G.M. Heideman, Gerard Nienhuis, Reinhard Morgenstern

Fysisch Laboratorium, Princetonplein 5, 3584 CC Utrecht, The Netherlands

We have investigated associative ionization of laserexcited $\text{Na}(3p)^2P_{3/2}$ atoms, i.e. the process



by measuring the total ion yield as a function of the angle θ between the relative velocity of the two excited Na-atoms and the electric polarization vector of the laserlight. In an earlier investigation^{1,2} we found that the ion-signal can be described by

$$I = 1 + r_1 \cos^2 \theta + r_2 \cos^4 \theta \quad (2)$$

with $r_1 = 0.27$ and $r_2 = 0.10$. Some doubt however was shed on these results by new experiments by Rothe et al.³ which disagree with our earlier results: they found $r_1 = -0.01$ and $r_2 = 0.38$, which means an essentially different periodicity of the ion signal.

We now report our more recent results that were obtained under modified experimental conditions.

- the ion-multiplier was sometimes arranged such that no fluorescence photons from the scattering center could reach the first dynode. By this we could rule out a possible fluorescence-dependent sensitivity of the ion detection.
- We used two counterpropagating Na beams instead of one. This leads to higher relative velocities and an even better defined direction of the relative velocity.
- Shape and size of the laserspot were varied in a wide range.

By blocking one of the Na beams we could again investigate collisions of atoms within one beam (at considerable lower kinetic energy). Fig. 1 shows the results for head-head (h-h) collisions from the counter-propagating beams and head-tail (h-t) collisions within one beam. The new data mainly confirm our earlier results. We obtain $r_1 = 0.304$, $r_2 = 0.066$ for h-h collisions and $r_1 = 0.225$, $r_2 = 0.032$ for h-t collisions. It is interesting to see that a stronger polarization dependence arises for the higher-energy h-h collisions. Also the h-h cross-section is at least 1.5 times higher than the h-t cross section.

As described earlier we have analyzed these data to obtain rate constants $k(m_1, m_2)$ for associative ionization of atoms that before the collision are in magnetic substates m_1 and m_2 respectively (z-axis along the relative velocity direction). The results are summarized in table 1.

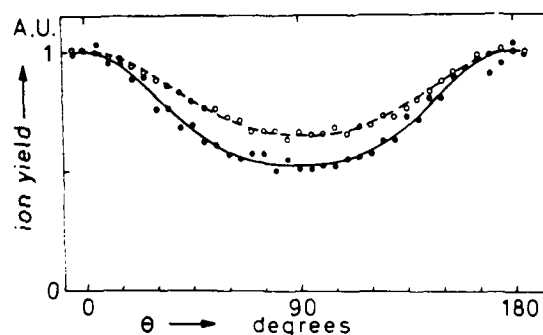


Fig. 1. Polarization dependence of the ion yield of process (1), with: \bullet higher collision energy (h-h), \circ lower collision energy (h-t).

Different from our earlier results an analysis in terms of both the $j m_j$ - and the $i m_i$ -descriptions yields non-negative rate constants, i.e. neither of the two descriptions can be ruled out.

A discussion of the results in terms of potential curves as e.g. performed by Jones and Dahler⁴ will be given at the conference.

m_j, m_j'	$3/2, 3/2$	$3/2, 1/2$	$1/2, 1/2$	
$k(m_j, m_j')$	1.12 ± 0.03	0.373 ± 0.024	2.140 ± 0.020	h-h
	0.872 ± 0.003	0.72 ± 0.03	1.703 ± 0.009	h-t
m_i, m_i'	1 1	1 0	0 0	
$k(m_i, m_i')$	1.12 ± 0.03	0.01 ± 0.05	4.53 ± 0.07	h-h
	0.872 ± 0.003	0.65 ± 0.05	2.93 ± 0.10	h-t

Table 1 Values for the relative rate constants in the $j m_j$ - and $i m_i$ description for higher (h-h) and lower (h-t) energy collisions. k values are normalized such that $k = 1$ for polarisation-independent ionization.

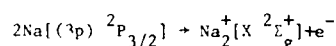
- J.G. Kircz, R. Morgenstern, G. Nienhuis, Phys.Rev. Lett. 48 610 (1982)
- G. Nienhuis, Phys. Rev. A26 3137 (1982)
- E.W. Rothe, R. Theyunni, C.P. Reck, C.C. Tung, to be published
- D.M. Jones, J.S. Dahler, Phys. Rev. A31 210 (1985)

POLARIZATION DEPENDENCE OF ASSOCIATIVE IONIZATION
AND OF LASER-INDUCED CHEMI-IONIZATION AND EXCITATION TRANSFER

Dumont M. Jones and John S. Dahler

Departments of Chemistry and Chemical Engineering, University of Minnesota, Minneapolis, MN 55455 U.S.A.

Our theory has been designed to aid in interpreting experimental studies of inelastic collisions involving laser-prepared reactant atoms and/or laser-induced electronic transitions. Recent thermal beam experiments by Kircz, Morgenstern and Nienhuis¹ and by Rothe, Theyunni, Reck and Tung² fall into the first of these categories. These investigators have measured the dependence of the rate of the associative ionization process



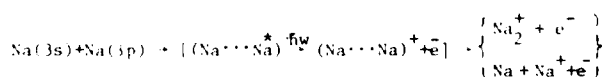
on the angle θ between the direction of relative motion of the colliding atoms and the polarization axis of the laser used to prepare the sodium atoms in the reactive $(3p) \ ^2P_{3/2}$ states. The integral cross section for this process can be written in the form³

$$\sigma(E, \theta) = \sum_n \sigma_n(E) \rho_{nn}(\theta)$$

with E the kinetic energy of relative motion of the reactant atoms and $\sigma_n(E)$ the cross section for reaction of an adiabatic Born-Oppenheimer state. Finally, $\rho_{nn}(\theta)$ is an easily computable diagonal matrix element of the

electronic density operator representative of the laser-prepared initial state. By comparing this formula with the data of Kircz et al, we have been able to conclude that at least two adiabatic Born-Oppenheimer states contribute to the experimentally observed process. The most reactive of these is the $1\Sigma_g^+$ state with the asymptotic form $\frac{1}{g} \frac{1}{u}$. The next most reactive is either $1\Sigma_g^+$ or $3\Sigma_g^-$, both with the asymptotic form $\frac{1}{u} \frac{1}{g}$.

Our method of analysis also can be applied to a two-color experiment⁴ such as that in which a resonant D-line laser pumps the $3p$ state and a second, high-intensity non-resonant laser drives the chemi-ionization process.



The situation is more complicated here, not only because there are two laser intensities and two laser polarizations, but because the individual state-to-state cross sections for the laser-induced chemi-ionization events are themselves dependent on the polarization of the non-resonant laser⁵. The differences between the intensity and polarization dependences of competing ionization processes, e.g. the chemi-ionization events described above and photoionization of neutral dimers, are

identifying characteristics which can be used to extract cross section information about the individual processes.

References

1. G. Kircz, R. Morgenstern, and G. Nienhuis, Phys. Rev. Lett. **48**, 610(1982); G. Nienhuis, Phys. Rev. A **26**, 3137(1982).
2. E. W. Rothe, R. Theyunni, G. P. Reck and C. C. Tung, Phys. Rev. A (in press).
3. D. M. Jones and J. S. Dahler, Phys. Rev. A **31**, 210 (1985).
4. P. Polak-Dingels, J. F. Delpack, and J. Weiner, Phys. Rev. Lett. **44**, 1663(1980); J. Weiner and P. Polak-Dingels, J. Chem. Phys. **74**, 508(1981).
5. H. P. Saha, J. S. Dahler and S. E. Nielsen, Phys. Rev. A **28**, 1487(1983); H. P. Saha and J. S. Dahler, Phys. Rev. A **28**, 2859(1983).

EXCITATION OF HELIUM BY H^+ AND H IMPACT : A DISTORTED WAVE APPROACH

Indira Khurana, Rajesh Srivastava and A.N. Tripathi

Department of Physics, University of Roorkee,
Roorkee (INDIA)

In recent years, the study on collisional excitations of Helium atom by proton and hydrogen gained impetus experimentally and theoretically because of well known practical applications of their cross-section data. A couple of calculations for excitation of helium¹ in H^+ - He and only a few calculations for H - He collisions^{2,3} are available for the evaluation of total cross-section in literature. On the experimental side⁴ only total cross-section measurements for excitation of helium by proton impact are known for specific energies.

There have been rare differential measurements because of practical difficulties. However, recently, Park et al⁴ have reported the differential cross-sections for excitation of the helium target to the $n=2$ level at certain energies of proton impact. We also know the angular differential cross-section measurements offer the cleanest test for any theoretical approach. Although calculations for DCS using Born and multistate eikonal approximations for p-He scattering are available but as pointed out by Park et al themselves that theoretical studies using other approximations are desirable and a little feasible as the Collision processes with H^+ and H are concerned are not fully understood.

TABLE I: DCS results for 2^1S excitation of helium atom by H^+ and H at impact energy of 100 keV

	H ⁺ -He collisions		H-He collisions	
	FBA	DWBA	FBA	DWBA
σ_{total}	3.41(5)*	6.36(4)	3.87(3)	1.75(4)
σ_{exc}	4.56(4)	2.89(4)	1.38(4)	1.11(3)
σ_{ion}	2.47(3)	1.42(4)	1.73(3)	2.33(4)
σ_{el}	4.83(2)	3.74(2)	4.79(-2)	1.94(3)
σ_{ex}	5.20(-6)	1.49(1)	1.87(-6)	4.70
σ_{ex}	2.81(-8)	2.52	1.37(-7)	7.94(-1)
σ_{ex}	8.79(-17)	5.65(-3)	2.12(-11)	3.16(-3)
σ_{ex}	1.51(-15)	5.60(-4)	1.40(-11)	2.18(-4)
σ_{ex}	5.46(-18)	2.54(-4)	1.61(-11)	4.01(-4)

* The number in parenthesis denotes the power of ten by which the quantity should be multiplied.

In view of the above facts, we thought it worth while to study p-He scattering in distorted wave Born approximation (DWBA) which has proved to be quite useful and great success in the work on e-He scattering⁵. We also realize that DWBA hardly much have been done in the scattering of atoms. To explore such applications of DWBA, we report, in the conference proceedings on proton impact excitations of helium in helium and also to begin with excitation of helium by impact of a structured atom like H^+ hydrogen. In order to minimize the errors in the results a consistent version of DWBA where distortion effects are included in both the channels has been used. To avoid further uncertainties in the results the wave functions of helium atom are taken to be of the most accurate many-parameter correlated (MPC)⁵ type.

We have also performed parallel calculations using these MPC wave functions in first Born approximation (FBA) for both the transitions to facilitate comparison. The detailed theoretical analysis along with various results, fully compared and discussed would be presented in the conference itself. However in the table I we present our different theoretical results for 2^1S excitation of He only.

References

1. Sur et. al Phys. Rev A 24 2465(1981)
(See other references therein)
2. MM Felden Physica 84C 439(1976)
3. D S F Crothers and R P McEachran J.Phys.B 3 976 (1970)
4. Park et.al Phys. Rev A 18 48(1978)
(See other references therein)
5. M Kumar, R Srivastava and A N Tripathi Phys. Rev.A 1984(in press).

PROTON-HYDROGEN EXCITATION AT HIGH AND INTERMEDIATE ENERGIES

Carlos O. Reinhold and Jorge E. Miraglia

Instituto de Astronomía y Física del Espacio, C.C.: 67, Suc.: 28, 1428 Buenos Aires, Argentina

So far, the continuum distorted wave (CDW) theoretical method has been used to calculate electron capture processes¹. However, this method can be straightforwardly extended to calculate direct processes². We have computed the proton-hydrogen excitation with the CDW method. The results are shown in the figure. Good agreement with the experiments is found for proton energies larger than, say, 75 KeV. But at intermediate projectile energies the CDW largely overestimate the experiments.

For the present reactions the Coulomb peaking impulse approximation (CPIA) should be more appropriate³. This method consists of replacing the electron-projectile continuum interaction in the entrance channel, within the CDW formalism, by the Coulomb logarithmic phase factor. Results with this approximation are also shown in the figure. Better agreement with the experiments is found.

References

1. Dž. Belkic, R. Gayet and A. Salin, Phys. Report **56**, 279 (1979).
2. J.E. Miraglia, J. Phys. B **15**, 1092 (1982) Eq.(4.2).
3. J.E. Miraglia, Phys. Rev. A **30**, 1721 (1984).
4. J.T. Park, J.E. Aldag, J.M. George and J.L. Peacher, Phys. Rev. A **14**, 608 (1976).
5. T.J. Morgan, J. Geddes, H.B. Gilbody, J. Phys. B **6**, 2118 (1973).

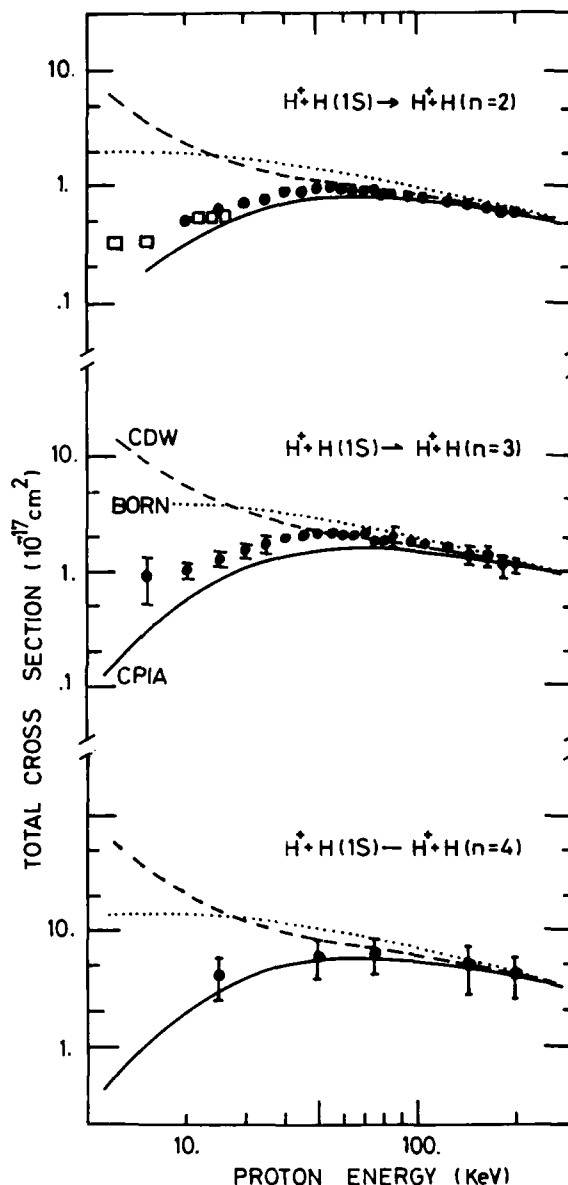


FIGURE: Total cross sections of excitation levels $n = 2, 3$ and 4 of hydrogen by proton impact, theory: as indicated

experiment: \bullet ; Park et al.⁴ (1976).

\square ; Morgan et al.⁵ (1973).

DIFFERENTIAL CROSS SECTIONS FOR THE EXCITATION OF ATOMIC HYDROGEN
BY LITHIUM IONS AT INTERMEDIATE ENERGY*

J. L. Peacher and G. Bhattacharya

University of Missouri-Rolla, Rolla, Missouri 65401 USA

Differential cross sections for the excitation of atomic hydrogen from its ground state to its first excited state in collision with singly charged lithium ions were recently measured.¹ The Glauber approximation has been quite successful in describing a variety of atomic collision processes in the intermediate to high-energy range.² Franco³ presented a modified Glauber approximation to describe collisions between intermediate to high-energy atoms or ions and atomic hydrogen. Franco applied the theory to the excitation of atomic hydrogen from its ground state to its first excited state by singly charged helium ions. The theoretical results were in good agreement with experimental data. Recently Peacher *et al.*⁴ presented a modified Glauber approximation with the same simple analytical structure as the first Born approximation to describe collisions between complicated atom or ion projectiles and atomic hydrogen. Peacher *et al.* applied the theory to the excitation of atomic hydrogen from its ground state to its first excited state by a hydrogen molecular ion. Again the theoretical results for the differential cross section were in good agreement with experimental data.

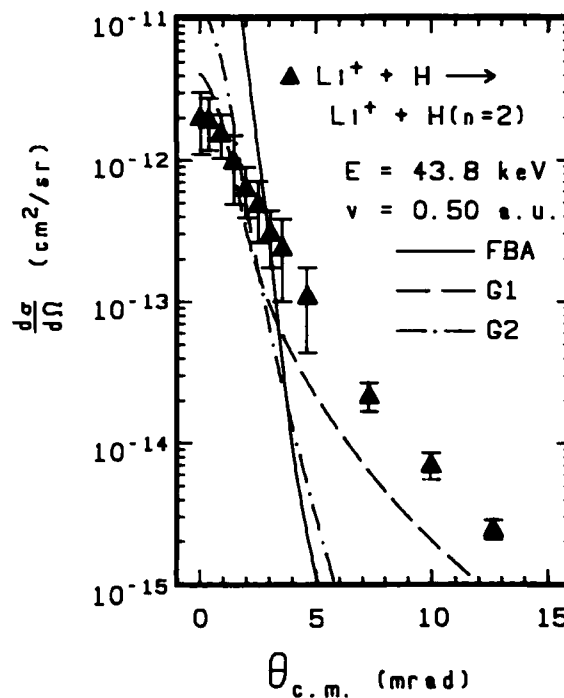
The collision studied here is $\text{Li}^+(1s^2) + \text{H}(1s) \rightarrow \text{Li}^+(1s^2, \theta) + \text{H}^*(n=2)$, where θ is the scattering angle. Angular differential cross sections have been calculated for this collision system using the modified Glauber approximation developed by Peacher *et al.* (G1) and the modified Glauber approximation developed by Franco (G2). A simple one parameter variational wave function was used to represent the ground state of the lithium ion. The results are shown in the figure for an incident laboratory energy of 43.8 keV for the lithium ion. First Born approximation results are shown for comparison. The G1 results are in reasonable agreement with the available experimental results. This energy corresponds to a velocity of 0.5 a.u. which is low for a Glauber-type approximation. Presumably the agreement would improve at higher incident energies. However at present this is the only energy at which experimental results are similar. Both results fall well below the experimental data at large scattering angles. The G1 results have nearly the same shape as the experimental results at large scattering angles but are a factor of ~ 3.5 low. In the modified Glauber approximation (G1) developed by Peacher *et al.* the angular distribution

of the scattered ion is basically determined by the angular distribution that would be obtained by scattering a bare particle with the mass and charge of the ion. This angular distribution is multiplied by the form factor of the incident ion.

*Supported in part by the National Science Foundation.

References

1. J. T. Park, E. Redd, J. T. Kvale, D. M. Blankenship, P. J. Martin and J. L. Peacher, *Bull. Am. Phys. Soc.* **26**, 1306 (1981).
2. E. Gerjuoy and B. K. Thomas, *Rep. Prog. Phys.*, **37**, 1345 (1974); F. W. Byron, Jr. and C. J. Joachain, *Phys. Rep.*, **34C**, 233 (1977).
3. V. Franco, *Phys. Rev. A*, **25**, 1358 (1982).
4. J. L. Peacher, P. J. Martin, D. G. Seely, J. E. Aldag, T. J. Kvale, E. Redd, D. Blankenship, V. C. Sutcliffe, and J. T. Park, *Phys. Rev. A* **30**, 729 (1984).



THE SEARCH FOR THE $2p^2\ ^3P^e$ STATE OF THE H^- ION

A. van Wijngaarden, J. Patel, K. Becker*, and G.W.F. Drake

Department of Physics, University of Windsor, Windsor, Ontario, CANADA N9B 3P4

*Present address: Physics Department, Lehigh University, Bethlehem, PA 18105 USA

The H^- ion has only two bound states, the $1s^2\ ^1S_0$ ground state and a $2p^2\ ^3P^e$ excited state. The properties of the bound excited state were predicted by Drake¹ and confirmed by Jacobs et al.^{2,3}, but have not been firmly established experimentally. The $2p^2\ ^3P^e$ state, which has a binding energy of only 9.5 meV, decays spontaneously with a lifetime of 1.73 ns into a neutral H(1s) ground state atom, a photon and an electron. It is the only known atomic state where the energy is partitioned among the decay products. The decay leads to a broad continuum on the long wavelength side of Lyman α . Although satellite observations in stellar atmospheres suggested the existence of the excited H^- state⁴, previous attempts to observe it under controlled laboratory conditions have failed^{5,6}.

We made an attempt to detect the $2p^2\ ^3P^e$ state of the H^- ion by observing the H(1s) decay product. A highly collimated beam of ground state H^- ions (energy below 140 keV) is crossed with a thermal Hg beam inside a static electric field. The excited H^- ions which are presumably formed in glancing collisions with Hg atoms survive long enough as charged particles to be noticeably deflected by the electric field before they decay. The decay-in-flight of the excited H^- ions is expected to result in an asymmetric feature on the angular distribution of the neutrals formed by direct neutralization of the ground state H^- ions. Although no sound evidence of the $2p^2\ ^3P^e\ H^-$ ions was found in our experiment, we were able to establish a limit: from the statistical analysis of our data it was found that our search would have been successful, if the cross section for formation of $2p^2\ ^3P^e\ H^-$ ions in collisions of ground state H^- ions with Hg atoms had been larger than $1 \times 10^{-20}\text{ cm}^2$. It is conceivable, though rather unlikely that the lifetime of the $2p^2\ ^3P^e$ state of the H^- ion is somewhat shortened in our experiment by the static electric field of 1-1.5 kV/cm.

As a by-product of our experiment, we have obtained the first differential (in angle) charge transfer cross sections for hydrogen ions colliding with mercury atoms for scattering angles in the range 3° to 15° and for small angle forward scattering. Details of the cross section measurements will be presented at the Conference.

References

1. G.W.F. Drake, *Astronhys. J.* **184**, 145 (1973)
2. V.L. Jacobs et al., *Astrophys. J.* **191**, 785 (1974)
3. V.L. Jacobs et al., *Astronhys. J.* **242**, 1278 (1980)
4. S.R. Heap and P. Sticker, *Astrophys. J.* **187**, 127 (1974)
5. J.S. Risley et al., *Abstracts IAU 1973* (1973)
6. J.S. Risley et al., *Abstracts IAU 1973* (1973)

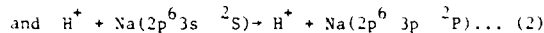
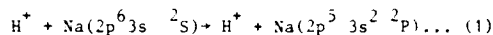
This work was supported by the Natural Sciences and Engineering Research Council of Canada (NSERC).

THE EXCITATION OF SODIUM ATOMS BY PROTON IMPACT

O. Schöller and J.S. Briggs

Fakultät für Physik, University of Freiburg, W. Germany

The excitation of neutral sodium atoms in collision with protons has been calculated using an atomic state expansion impact-parameter method in the energy range from a few keV to a few MeV. Specifically the excitation processes



have been studied. In a target-based expansion the time-dependent Schrödinger equation has been solved in the following approximations, of decreasing sophistication.

- i) In treating the processes (1) and (2) all seven $2p^6 3s$ electrons are retained in an expansion of the wavefunction in 25 Na-states.¹
- ii) Only the initial and final states of transition (1) or (2) respectively are retained, when the close-coupling problem reduces to a one-electron problem.
- iii) The coupled equations are solved in a first order (Born) approximation. The results for transition (1) are identical to those obtained by Theodosiou et al.² using the PWBA.

whose validity in this range is indicated by agreement with electron impact data (v is the velocity of the proton and $v_{2p} = 1.67$ a.u. is the orbital velocity of the $2p$ -electron).

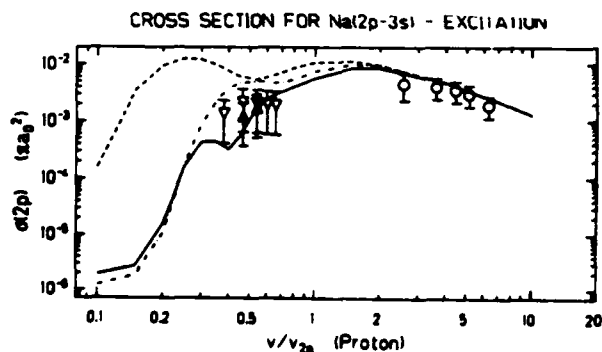


FIGURE 1 Total cross section for Na(2p) excitation. Theory:— 25 state close coupling (i), -.- 4 state close coupling (ii), --- Born approximation (iii): Experiment: Hintermayer et al.³ (proton impact), Keßler⁴ (electron impact).

In Fig. 1 results for process (1) are compared with the experimental data of the Freiburg group for proton³ and electron⁴ impact. It turns out that in the energy regime from 10 to 30 keV, the $2p$ -shell excitation is well described only by method (i). In the higher energy range all approximations converge to the first Born result

CROSS SECTION FOR Na(3s-3p) - EXCITATION

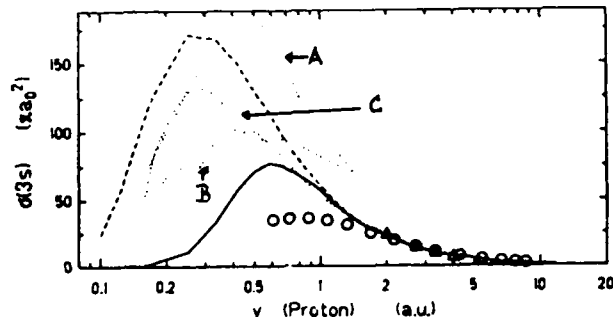


FIGURE 2 Total cross section for Na(3s) excitation. Theory:—, -.-, --- see Fig. 1: curve A, Born approximation⁵; B, close coupling⁵; C, Born approximation⁶: Experiment: electron impact, Enemark et al.⁷ Buckman et al.⁸

Fig. 2 shows our results for process (2) in comparison to other calculations^{5,6} and to the experimental data of Enemark et al.⁷ and Buckman et al.⁸ for electron impact. The results of method i) and ii) coincide. The excitation of the $3s$ -electron is not affected by the Na-core— as expected.

1. O. Schöller and J.S. Briggs, in "Fundamental Processes in Atomic Collision Physics" (H.O. Lutz, J.S. Briggs and H. Kleinpoppen, eds.) NATO-ASI Series, Plenum Press, 1985
2. C.E. Theodosiou and W. Mehlhorn, (private communication)
3. R. Hintermayer, G. Keßler, I. Passarge and W. Mehlhorn, this volume
4. G. Keßler, Diplom thesis, Freiburg 1984
5. R.J. Bell, B.G. Skinner, Proc. Phys. Soc. **80**, 404 (1962)
6. K.C. Mathur, A.N. Tripathi, S.K. Joshi, Phys. Lett. **35A**, 139 (1971)
7. E.A. Enemark, A. Gallagher, Phys. Rev. A **6**, 192 (1972)
8. S.J. Buckman, P.J.O. Teubner, J. Phys. **B12**, 1741 (1979)

The support of the DFG is gratefully acknowledged.

EXCITATION OF THE Na(3d) LEVEL BY H^- , H^+ , H_2^+ , or H_3^+ IONS

L. W. Anderson, James S. Allen, Chun C. Lin and R. E. Miers

Department of Physics, University of Wisconsin, Madison, WI 53706 USA

We report measurements of the apparent excitation cross sections of Na atoms by incident H^- , H^+ , H_2^+ , or H_3^+ ions with energies in the range 1-25 keV for the reaction H^- (or H^+ or H_2^+ or H_3^+) + Na + Na(3d). The apparent cross section is the sum of the cross sections for both the excitation of the Na(3d) level directly and by cascade from higher levels.

Our apparatus has been described previously.^{1,2} An ion beam is extracted, accelerated, focussed, momentum analyzed and collimated. The collimated beam enters a Na vapor target. A Na reservoir is connected to the target by a 1.8 cm i.d. tube. Both the Na reservoir and the target are heated. The Na density in the target is governed by the temperature of the Na in the reservoir and by the temperature of the target. Inside the Na vapor target is an electron gun and a suppressed Faraday cup. The electron gun and Faraday cup are coaxial with the ion beam. The electron gun cathode rotates in and out of the beam axis. Thus either an electron beam or an ion beam can pass through the Na vapor interaction region and enter the Faraday cup. Since the interaction geometry of the electron beam is identical to that of the ion beam, it is possible to measure directly the ratio of the apparent cross section for Na(3d) production by ions to the apparent cross section for Na(3d) production by electron impact from the corresponding intensity ratio of the 3d + 3p emission, which exits the target through a sapphire window. The light passes through an interference filter and is focussed onto the cathode of a photomultiplier tube. The photocurrent in the photomultiplier, I_{PM} , is measured simultaneously with the ion or e^- current, I_0 . For low Na target density, n , the apparent cross section Q^A is given by $Q^A = kI_{PM}/nI_0$, where k is a constant depending on the transmittance of the window, lens and filter, the efficiency of the photomultiplier, the geometry of the collision region viewed by the phototube, and other factors.

The relative values of Q^A as a function of energy are found by comparing I_{PM}/I_0 for different ion energies while n is held fixed. We measure and compare I_{PM}/I_0 for 15 keV H^+ ions with I_{PM}/I_0 for 100 eV electrons keeping n fixed. The value of k/n is determined using the known value of Q^A for electrons incident on Na.³

The absolute values of Q^A for H^- , H^+ , H_2^+ , or H_3^+ incident on Na are shown in Fig. 1. The apparent

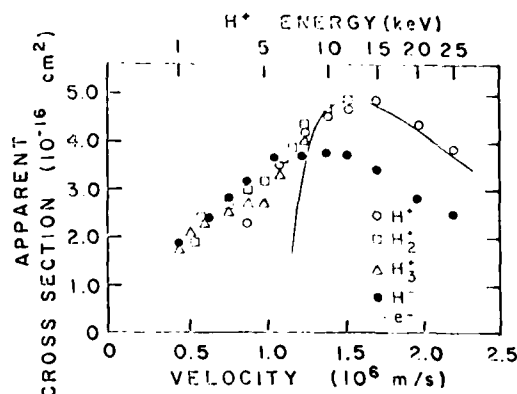


FIGURE 1 Experimental cross sections for Na(3d) excitation by H^- , H^+ , H_2^+ or H_3^+ ions as a function of the velocity of the incident ion. Also shown are the Na(3d) electron excitation cross sections.

cross sections for the excitation of the Na(3d) level by ions are large being $4.7 \times 10^{-16} \text{ cm}^2$ for H^+ ions with an incident velocity of $1.5 \times 10^6 \text{ m/s}$ and $3.8 \times 10^{-16} \text{ cm}^2$ for H^- ions at the same velocity. The cross sections for excitation by H^+ , H_2^+ , and H_3^+ ions are nearly identical functions of the ion velocity. The cross section for excitation by H^+ ions is nearly the same as the electron excitation cross section at high velocities. The cross section for excitation by H^- ions is about 20% lower than the H^+ ion cross section at high velocities. The cross sections are about an order of magnitude smaller than the corresponding Na(3p) cross sections. The Na(3d) cross sections are expected to be large because the principal quantum number is unchanged in the excitation.

References

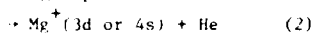
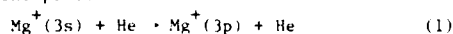
1. A. I. Howard, et al., Phys. Lett. **32A**, 423 (1972).
2. A. I. Howard, et al., Phys. Rev. Lett. **51**, 2029 (1983).
3. J. O. Phelps and C. C. Lin, Phys. Rev. **A24**, 1299 (1981).

INELASTIC DIFFERENTIAL SCATTERING CROSS SECTIONS FOR EXCITING 30, 66.7, AND 150 keV Mg^+ IN COLLISION WITH He:
 $\text{Mg}^+(3s) + \text{He} \rightarrow \text{Mg}^+(3p) + \text{He}$ and $\text{Mg}^+(3d \text{ or } 4s) + \text{He}$ #

E. Redd, D. M. Blankenship, D. G. Seely, T. J. Gay, J. L. Peacher, and J. T. Park

University of Missouri-Rolla, Rolla, Missouri 65401 USA

Quasi-One-Electron (QOE) collision systems have been studied extensively in the 1 to 15 keV energy range.¹ Recent absolute differential cross section measurements at 30, 66.7, and 150 keV have been performed using the University of Missouri-Rolla Ion Energy-Loss Spectrometer (UMRIELS). Data was obtained for the processes



for center of mass angles less than 35 mrad. A multi-state impact parameter calculation² for the first process has been converted to differential cross sections for comparison to the present results.

The UMRIELS has an energy resolution of 0.8 eV and center of mass angular resolution of 0.8 mrad for this system. The energy resolution is sufficient to easily resolve the excitation of Mg^+ to the 3p state at 4.42 eV energy-loss. The circles in the Figure represent the differential cross section for this process at 66.7 keV. Integration gives a total cross section of $3.3 \pm 1.0 \times 10^{-16} \text{ cm}^2$. The 3d and 4s states could not be resolved, but energy-loss spectra⁴ reached a local maximum nearest to the value expected for exciting the $\text{Mg}^+(3d)$ state at 8.86 eV. That was the energy-loss value used in obtaining the differential cross section at 66.7 keV represented by the squares in the Figure. Integration of this differential cross section over angle gives a total cross section of $9.9 \pm 3.0 \times 10^{-17} \text{ cm}^2$. These total cross sections are larger than those reported by N. Andersen, *et al.*⁵ Our experiment differed from that of N. Andersen, *et al.* in that our measurements were unaffected by cascade and did not depend on detector calibration.

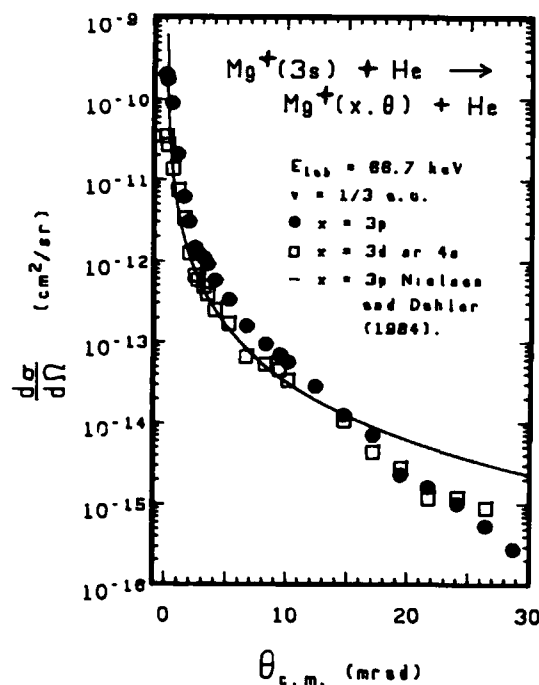
The solid line in the Figure represents the three-state (3s, 3p₀, 3p₁) impact parameter calculation of Nielsen and Dahler.² The calculated result was presented as probability vs. impact parameter. It was converted into an angular differential cross section vs. angle using a potential given by Sondergaard and Mason.⁶ The total cross section calculated by Nielsen and Dahler is $1.474 \times 10^{-16} \text{ cm}^2$.

The calculation underestimates the total cross section by a factor of two. The differential cross section is underestimated at the angles which contribute most significantly to the total cross section. The calculation overestimates the differential cross

section at larger angles. Comparisons at 30 and 150 keV are similar. Considering the simplicity of the three-state calculation and the complexity of this system, the agreement is relatively good.

#Supported in part by the National Science Foundation.

1. N. Andersen and S. E. Nielsen, *Adv. At. Mol. Phys.* **18**, 265 (1982) and references therein.
2. S. E. Nielsen and J. S. Dahler, *J. Phys. B* **13**, 2435 (1980), and private communication (1984).
3. J. T. Park, J. M. George, J. L. Peacher, and J. E. Aldag, *Phys. Rev. A* **18**, 48 (1978).
J. T. Park, J. E. Aldag, J. L. Peacher, and J. M. George, *Phys. Rev. A* **21**, 751 (1980).
T. J. Kvale, D. G. Seely, D. M. Blankenship, E. Redd, T. J. Gay, M. Kimura, E. Rille, J. L. Peacher, and J. T. Park (submitted to *Phys. Rev. A*).
4. E. Redd, D. M. Blankenship, T. J. Kvale, T. J. Gay, J. L. Peacher, and J. T. Park, *Bull. Am. Phys. Soc.* **29**, 812 (1984).
5. N. Andersen, T. Andersen, and K. Jensen, *J. Phys. B* **9**, 1373 (1976).
6. N. A. Sondergaard and E. A. Mason, *J. Chem. Phys.* **62**, 1299 (1975).

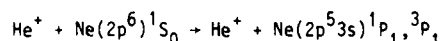


ORBITAL AND SPIN ANGULAR MOMENTUM ANALYSIS OF THE PRODUCTS OF He^+ Ne INELASTIC COLLISIONS

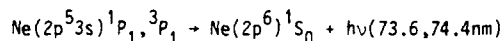
J. Grosser, R. Hasse, H. P. Neitzke and H. Pfeiffer

Institut für Atom- und Molekülphysik, Universität Hannover, Federal Republic of Germany

The angular distribution of the photons, which are emitted from an excited atom, carries information about the angular momentum polarization of the emitter. We use this relationship for an investigation of the processes



The excited atoms radiate after the collision,



We detect the photons in coincidence with the scattered He^+ ions. There are two aspects, in which such a coincidence experiment is superior to an analysis of all photons emitted: (1) The information to be derived is related to a well defined scattering angle, and (2), using the conservation law for the reflexion symmetry of the electronic wave function at the scattering plane, it is possible to derive properties of the second collision product (He^+) from measured properties of the first one (Ne). As the electronic spin takes part in the operation of reflexion, we are able to distinguish between processes, in which the He^+ spin direction remains unaltered in the collision ($\uparrow\uparrow$ or $\downarrow\downarrow$) and processes, in which the spin is reversed ($\uparrow\downarrow$ or $\downarrow\uparrow$)¹.

We use the y-axis, which is at right angles to the collision plane, as the quantization axis. When the He^+ spin before the collision points upward, the asymptotic form of the wave function is

$$e^{ikr} |\uparrow\rangle |^1S_0\rangle + \quad (1)$$

$$e^{ikr}/r [f_1 |\uparrow\rangle |m_j=1\rangle + f_{-1} |\uparrow\rangle |m_j=-1\rangle + f_0 |\uparrow\rangle |m_j=0\rangle]$$

The kets refer to the He^+ ion and to the Ne atom, respectively. For this initial condition, other combinations of angular momentum quantum numbers than those occurring in eq.1 are forbidden by reflexion symmetry. When the He^+ spin before collision points downward, the allowed wave functions are obtained from eq.1 by reversing all spin quantum numbers. In both cases, an inverted He^+ spin is accompanied by an excitation of the Ne atom to a state with $m_j=0$, an uninverted spin by an excitation to $m_j=\pm 1$. The quantities $|f_0|^2$, $|f_1|^2 + |f_{-1}|^2$ and $f_1 f_{-1}^*$ can be derived from our experiments. Because the He^+ ions are not polarized in the actual experiment, and because we do not distinguish between 1P_1 and 3P_1 emission, the actual experimental results are averages, which is indicated by a bar over the symbols.

As an example for our experimental results, the black circles in fig.1 show the fraction of He^+ -spin inverting collisions as a function of the collision energy. The im-

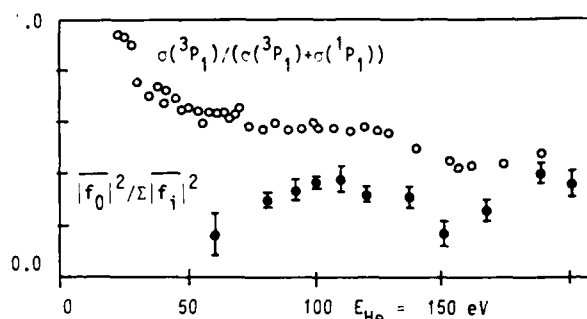


Fig.1 Black circles: percentage of He^+ -spin inverting collisions for a fixed value of the impact parameter $E_{\text{CM}}^{\text{CM}} = 1070 \text{ eVdeg}$. Open circles: percentage 3P_1 products integrated over all impact parameters.

act parameter, measured by the reduced scattering angle θ , was held constant. The open circles show the fraction of 3P_1 radiation in the total emission (Isler²).

In a model in which the spin-orbit interaction is neglected for the time of the collision, the following relation can be shown to hold

$$|f_0|^2 / \Sigma |f_i|^2 = 1/2 \sigma(^3P_1) / (\sigma(^3P_1) + \sigma(^1P_1)) \quad (2)$$

The cross sections occurring at the right hand side are the differential cross sections, which are not known; when the differential triplet to singlet ratio may be replaced by the integral one, eq.2 requires that the upper curve in fig.1 is twice the lower curve. This is not what we observe experimentally. We conclude therefore that the spin orbit interaction must be taken into account. The argument would be much more conclusive, when our results were separated into their singlet and triplet contributions. We are performing experiments, in which the collisions occur in a weak magnetic field. The field rotates the light angular distributions. Because the optical lifetimes of the triplet and singlet states are different, they are differently rotated, allowing to separate their contributions.

1) J. Grosser, H.-P. Neitzke, Z. Phys. A 304 (1981) 49

2) R.C. Isler, Phys. Rev. A10 (1974) 2093

OPTICAL MODEL THEORY OF ELASTIC $H^+ - H$
AND $H^+ - He$ SCATTERING AT INTERMEDIATE VELOCITIES

R.M. Potvliege⁺, C.J. Joachain⁺ and F. Furtado^{*}

⁺Physique Théorique, Université Libre de Bruxelles, Belgium
^{*}Departamento de Física, Universidade Nova de Lisboa, Portugal

Recently, angular distribution measurements have become available for elastic proton scattering by atomic hydrogen¹ and helium² at intermediate relative velocities $1 \leq v \leq 2$ (in a.u.). In this work, we have calculated the corresponding differential cross sections, using an ab-initio optical potential approach. We first evaluate the second Born amplitude, by using the closure approximation, including exactly the contribution of low-lying states. We then obtain the corresponding complex eikonal phase by Fourier-Bessel transformation. The resulting eikonal optical scattering amplitude provides an all order unitarisation of the two first terms of perturbation theory, taking into account an infinite number of channels in an approximate way.

In the above-mentioned treatment it is difficult to take into account the influence of charge-exchange channels on the elastic scattering process, since charge exchange corresponds to an all-order rearrangement of the Born series. This effect is negligible at large enough collision energies but should be incorporated in the theoretical description at intermediate velocities.

In order to investigate this problem, we have extracted a correction to the elastic optical model amplitude from the elastic amplitude obtained in a two-state charge-exchange approximation, in which we have minimised the double countings arising from the piece of the Born series present in both amplitudes. As an example, we show in Fig. 1 our second-order optical potential results (short dashed curve) together with our results corrected for the presence of the charge-exchange channel (full curve), for the case of $H^+ - H$ scattering at a proton laboratory energy of 25 keV ($v = 1$). The corrected results are seen to be in very close agreement with the multistate Sturmian expansion calculation of Shakeshaft³, represented by the long-dashed curve, and with the experimental data¹. As expected, we find that the difference between our two sets of theoretical results decreases as the relative velocity increases. Results will also be presented for the case of proton-helium elastic scattering.

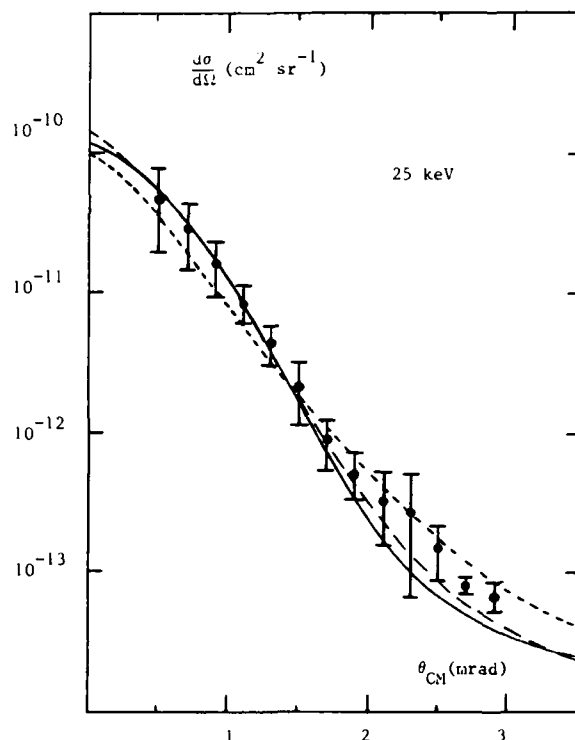


Fig. 1. Differential cross sections for the elastic scattering of protons by atomic hydrogen, at a laboratory collision energy of 25 keV ($v = 1$). --- : second order optical potential results, — : second order optical potential results, corrected for the presence of the charge exchange channel, - - - : multistate Sturmian expansion calculation of Shakeshaft³. The experimental data are those of Rille et al¹.

References

1. E. Rille, J.L. Peacher, E. Redd, T.J. Kvale, D.G. Seely, D.M. Blankenship, R.E. Olson and J.T. Park, Phys. Rev. A 29, 521 (1984).
2. J.L. Peacher, T.J. Kvale, E. Redd, P.J. Martin, D.M. Blankenship, E. Rille, V.C. Sutcliffe and J.T. Park, Phys. Rev. A 26, 2476 (1982).
3. R. Shakeshaft, Phys. Rev. A 18, 1930 (1978).

AB INITIO CALCULATION OF POTENTIAL CURVES FOR THE
GROUND AND EXCITED STATES OF C_2 AND C_2^+

Cui Zuolin

Pan Shoufu

Institute of Atomic and Molecular Physics
Jilin University Changchun, P. R. China

The potential curve between atom-atom and atom-ion is an important physics quantity in all of science, especially in collision theory. In order to calculate scattering cross sections, one must have the knowledge about the potential curve of the system questioned. In this paper, using MONSTERGAUSS¹ which has been transplanted on H-16 M computer by us, we have calculated the potential curves of the ground and excited states of C_2 and C_2^+ . In our calculation, we have used 6-31G and 6-311G basis sets. The calculated results are listed in Table I and II.

Table I potential curves of C_2 (6-311G)

R(Å)	$1\Sigma_g^+$	
	E(a.u.)	E(a.u.)
0.6	-72.711827	-72.322691
0.8	-74.561885	-74.223070
1.0	-75.205283	-74.905906
1.2	-75.358025	-75.090899
1.4	-75.342664	-75.093111
1.6	-75.282540	-75.035711
1.8	-75.220064	-74.965502
2.0	-75.165603	-74.901926

Table II potential curves of C_2^+ (6-31G)

R(Å)	$4\Sigma_g^-$	
	E(a.u.)	E(a.u.)
0.6	-71.329553	-71.740723
0.8	-73.617812	-73.920413
1.0	-74.874335	-74.696123
1.2	-75.003920	-74.915267
1.4	-75.056152	-74.939614
1.6	-75.035713	-74.908792
1.8	-74.998226	-74.870513
2.0	-74.960477	-74.836166

We have also made the geometry optimization calculations, obtaining the equilibrium positions of C_2 and C_2^+ and the lowest values of the potential curves. Our results are listed in Table III and IV.

Table III R_e and E_e of C_2

	$1\Sigma_g^+$		
	present work	other work ²	expt. ³
$R_e(\text{Å})$	1.258	1.253	1.242
$E_e(\text{au})$	-75.363100	-75.26497	-

	$3\Pi_u$		
	present work	other work ²	expt. ³
$R_e(\text{Å})$	1.305	1.298	1.312
$E_e(\text{au})$	-75.447729	-75.35438	-

Table IV R_e and E_e of C_2^+

	$4\Sigma_g^-$		
	present work	Pople ²	Vernaegen ³
$R_e(\text{Å})$	1.404	1.456	1.412
$E_e(\text{au})$	-75.056167	-74.97681	-

	$2\Pi_u$		
	present work	Pople ²	Vernaegen ³
$R_e(\text{Å})$	1.345	1.358	1.312
$E_e(\text{au})$	-74.941994	-74.85908	-

We have also performed configuration interaction calculations(CI) for $1\Sigma_g^+$ (C_2) at $R=1.2$ Å and for $4\Sigma_g^-$ (C_2^+) at $R=1.4$ Å, obtaining correlation energies and total CI energies. They are -0.05 and -75.5196311 hartree, -0.16 and -75.1038139 hartree respectively. Our CI calculation is direct CI method. It has been made by two steps. At first, we have made SCF calculation under a single reference configuration, obtaining MO coefficients and MO energies. Then we have classified the MO according to valid point group symmetry. In our calculation, they are C_{2v} for C_2 and D_{2h} for C_2^+ respectively. Next the integral transformation from AO basis to MO basis are made and configurations are generated. Then multi-configuration SCF calculation is made and correlation energy is calculated. In our calculation, we have included single, double excitation with respect to the reference configuration and 500 configurations at most.

Reference

1. Program MONSTERGAUSS, M. R. Peterson and R. A. Poirier, University of Toronto, Ontario, Canada, 1981.
2. W. A. Lathan, W. J. Hehre, and J. A. Pople, J. Am. Chem. Soc. 93, 608 (1971).
3. G. Vernaegen, J. Chem. Phys. 49, 4698 (1968).

SEMICLASSICAL CALCULATION OF WAVE-FUNCTIONS IN n DIMENSIONS

J. B. Delos*, C. E. Knaison* and D. W. Reid†

*College of William and Mary, Williamsburg, Virginia 23185

†Oak Ridge National Laboratory, Oak Ridge, Tennessee

A semiclassical theory for calculating quantum-mechanical wave-functions for systems with any number of degrees of freedom was developed by Maslov and Fedorink (MF).¹ This theory is being implemented in the present authors to solve the Schrödinger equation for simple systems including: (1) two-dimensional scattering on a Morse potential; (2) three-dimensional scattering; (3) a beam two-dimensional non-linear oscillator. The theory is now being extended to consider tunneling in n dimensions.

Consider also representative n -dimensional scattering as shown in Fig. 1. Associated with these trajectories is a smooth surface or Lagrangian manifold in phase-space; it has a generating function $S(q)$ such that $p_i = \partial S / \partial q_i$, and surfaces of constant S represent wave-fronts, which are perpendicular to the trajectories (Fig. 1).

In "regular" regions of space, the wave function is approximately given by a combination of terms of the form

$$\Psi(q) = [c(q)]^{1/2} \exp[i\phi(q)/\hbar - \mu\pi/\epsilon] \quad (1)$$

where c is a density function and μ is an integer called the Maslov index, which is calculated by examining the signs of certain derivatives. Higher-order equations can also be obtained.

Near the caustic (the boundary between allowed and forbidden regions), $c(q)$ diverges and eq. (1) fails, but it can be calculated by transformation into momentum space. A Lagrange manifold always has a smooth projection into some set of canonical coordinates and momenta (p_α, q_α) , and an associated generating function $S(p_\alpha, q_\alpha)$; and density $[c(p_\alpha, q_\alpha)]$ is calculable from the trajectories. In this space, the wave-function is

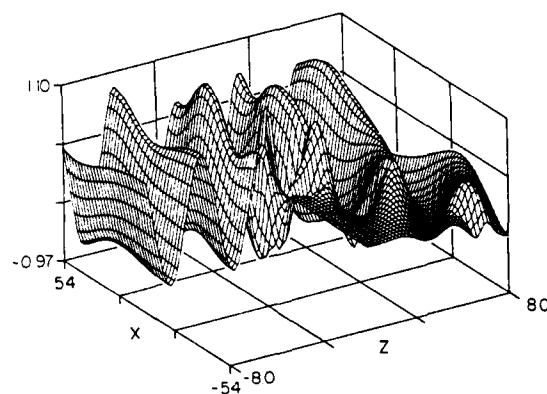
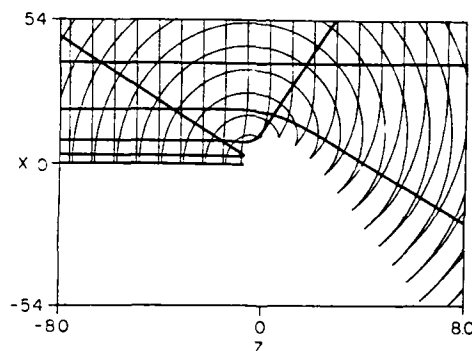
$$\Psi(p_\alpha, q_\alpha) = [c(p_\alpha, q_\alpha)]^{1/2} \exp[i\phi(p_\alpha, q_\alpha)/\hbar - \mu\pi/\epsilon] \quad (2)$$

and $\phi(p)$ is obtained by Fourier-transformation of (1).

The resulting wave-function is shown in Fig. 2; it is a combination of incoming plane waves, outgoing circular waves and (near the caustic) an Airy function. The MF method is straightforward, mathematically sound, and should be valuable for many semiclassical calculations.

References

1. V. I. Maslov and M. V. Fedorink, *Semiclassical Approximation in Quantum Mechanics*, Reidel, Boston, 1961.
2. Papers submitted to J. Chem. Phys. and Phys. Rev.



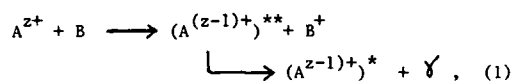
SIMULTANEOUS TRANSFER-EXCITATION IN HIGH ENERGY ION-ATOM COLLISIONS

D. McLaughlin* and Y. Hahn†

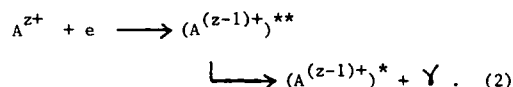
* Physics Department, University of Hartford, Hartford, CT 06117 USA

† Physics Department, University of Connecticut, Storrs, CT 06268 USA

When high energy ions collide with a target atom, a multitude of processes can take place, leading to excitation, ionization and charge transfer. One particular mode of reactions, the resonant transfer-excitation (RTE), is of special interest, not only because of its exotic nature, but also for its relationship to the dielectronic recombination (DR) in electron-ion collision. It is schematically described by



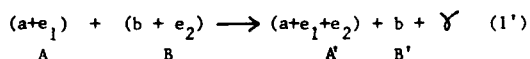
which may be compared with the DR,



The target B in (1) is assumed to play the role of providing the 'free electrons' in the process (2). These two processes are related in the impulse picture. For a proper analysis of (1) in terms of (2), therefore, a reliable unfolding of the binding effect of the electrons in B is required.

The experimental data of Tanis et al.¹ and Clark et al.² were analyzed³ previously in terms of the DR cross sections^{4,5} and the target electron profile of B. Recently, Feagin et al.⁶ made an attempt to provide a theory of (1) from the ion-atom collision point of view, in which both the RTE and the additional non-resonant (NTE) amplitudes were considered. A more complete formulation has been given⁷, in which the interactions responsible for the DR-like process in (1) are properly incorporated, with the full effect of the radiation channels. In addition, the NTE amplitude was also constructed, identifying the interactions that cause this process. The overlap between the non-orthogonal electron orbitals for the initial and final states plays an important role.

In order to simplify notation, consider a two-electron system



The scattering amplitude for (1') is

$$T_{fi} = T_{fi}^{RTE} + T_{fi}^{NTE}, \quad (3)$$

where, assuming the impulse approximation and the plane wave approximation for the ion cores to be valid,

$$T_{fi}^{RTE} \approx \sum_d \int d\mathbf{q}_{22} T_{fi}^{DR} \int d\mathbf{q}_{21} \hat{\psi}_B \quad (4)$$

and

$$T_{fi}^{NTE} \approx \sum_d \int d\mathbf{q}_{22} \langle f|D|d \rangle \frac{1}{E - E_{N+1} - i\Gamma/2} C_{BA2} t_{fi}^{xt} \quad (5)$$

In (4) and (5), T_{fi}^{DR} is the off-shell DR amplitude, t_{fi}^{xt} is the excitation amplitude for the projectile electron in A, and C_{BA2} is the overlap between the initial and final states for electron 2. A closure approximation is used in (5) for the non-resonant part.

We will present a detailed numerical calculation of the amplitudes (4) and (5), and the resulting cross sections for a number of systems for which experimental data are already available^{1,2}. Dependence of the cross sections on the number of electrons N_A and on the core charge Z_A will be carefully examined. Our study will focus on the ions with $N_A = 2, 3$ and 4.

This work was supported in part by a DOE grant.

References

1. J. A. Tanis et al, Phys. Rev. Lett. **49**, 1325 (1982) and **53**, 2551 (1984).
2. M. Clark et al, Phys. Rev. Lett. **54**, 544 (1985).
3. D. Brandt, Phys. Rev. A **27**, 1314 (1983).
4. D. McLaughlin and Y. Hahn, Phys. Lett. **88A**, 394 (1981).
5. D. McLaughlin, I. Nasser and Y. Hahn, Phys. Rev. A (1985).
6. J. M. Feagin et al, J. Phys. **B17**, 1057 (1984).
7. Y. Hahn, Phys. Rev. A (1985).

TRANSFER AND EXCITATION TO THE L-SHELL: THEORETICAL STATE SELECTED CROSS-SECTIONS

Tricia M. Reeves*, James M. Feagin†, Eugen Merzbacher*

*Department of Physics and Astronomy, The University of North Carolina, Chapel Hill, NC 27514

†Department of Physics, California State University-Fullerton, Fullerton, CA 92634

The process of transfer and excitation (TE) can best be understood by sorting out the possible interactions, concentrating separately on the dominant ones, and thus producing a model which explains, and agrees qualitatively, with the experimental evidence so far.¹ The highly charged projectile has usually a much greater nuclear charge than the target, making the impulse approximation appropriate. The three interactions important in bringing about the transition are the repulsion between the two active electrons, and the forces between the nuclei and the electrons. At the proper projectile velocity, the energy exchange is confined to the two active electrons, and as a result of the electron-electron interaction the transfer and excitation takes place. This process, called resonance transfer and excitation (RTE), becomes more important as the nuclear charge of the projectile increases. On the other hand, if the target nucleus excites the projectile electron at the same time the target electron is captured, the final state is reached but the two processes are uncorrelated. This non-resonance transfer and excitation (NTE) dominates in projectiles with lower atomic number and is always important at a lower projectile velocity than RTE. Recent experiments have shown clearly distinct NTE and RTE peaks.^{2,3}

Our calculations, based upon the above model (reference 1) using hydrogenic wave functions, predict the general shape of the total TE curve for all transitions to the L level as a function of the ratio of projectile velocity to its K-shell electron velocity for various projectiles (Figure 1). Our results show well the general trend of TE with projectile atomic number and of RTE with velocity. The theoretical NTE peak, however, occurs at a higher energy than that observed in experiments.^{2,3}

We find that the most interesting interference effects are discernible only when individual final states are examined. For a given final state there may be many pathways which can interfere. For example, a final state $2s2p$ (either singlet or triplet) can be achieved either by excitation of the projectile electron to the $2s$ state and capture of the target electron to the $2p$, or the reverse. Each combination can happen either through NTE or RTE, giving a total of four amplitudes and thus six possible interference terms.

The exchange-type interference is very important for NTE and gives rise to interesting effects (Fig. 3). Here it can be seen that the energy dependence for NTE is quite characteristic of the final state, whereas all transitions in RTE have essentially the same behavior (Fig. 2). When the amplitudes for the two processes are added properly and squared to give the probability for TE, distinctive behavior is shown for each final state (Fig. 4). The triplet $2s2p$, not shown, follows the singlet and is about ten percent greater.

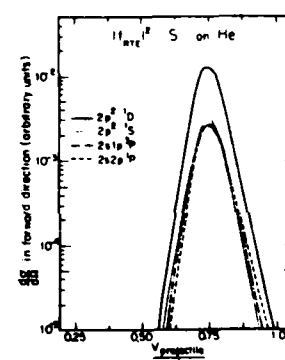
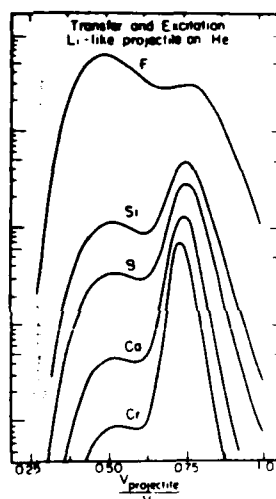


Fig. 2

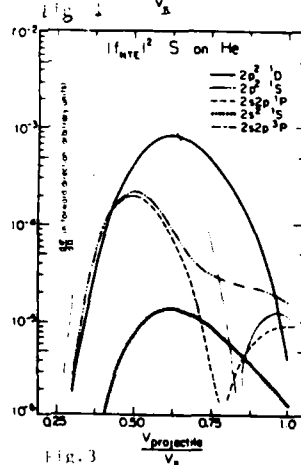


Fig. 3

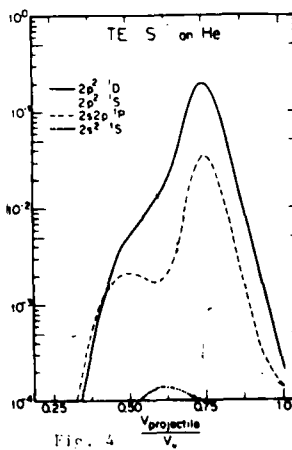


Fig. 4

*Acknowledge support US DoE, No ASOR-76ER02408

References:

1. Feagin J M, Briggs J S, Reeves T, J Phys. B, **17**, 1057-1068 (1984)
2. Clark M, et al, Phys Rev Let, **54**, 544 (1985)
3. Tans J A, et al (to be published)

L-SHELL RESONANT-TRANSFER-AND-EXCITATION FOR $\text{La}^{40+} + \text{H}_2$ COLLISIONS

M. W. Clark^a, E. M. Bernstein^a, J. A. Tanis^a, K. H. Berkner^b, P. Gohil^b, W. G. Graham^c,
R. H. McFarland^d, T. J. Morgan^e, A. Muller^f, A. S. Schlachter^b, J. W. Stearns^b, and M. P. Stockli^g

^aDepartment of Physics, Western Michigan University, Kalamazoo, Michigan 49008 USA

^bLawrence Berkeley Laboratory, Berkeley, California 94720 USA

^cDepartment of Physics, University of Ulster, Coleraine BT52 1SA, NORTHERN IRELAND

^dDepartment of Physics, University of Missouri, Rolla, Missouri 65401 USA

^eDepartment of Physics, Wesleyan University, Middletown, Connecticut 06457 USA

^fUniversity of Giessen, Giessen, FEDERAL REPUBLIC OF GERMANY

^gDepartment of Physics, Kansas State University, Manhattan, Kansas 66506 USA

Previous experimental studies^{1,2} have shown the existence of resonant-transfer-and-excitation (RTE) involving electron capture coincident with projectile K-shell excitation. Calculated³ RTE cross sections for lithiumlike ions based on theoretical dielectronic recombination cross sections,⁴ give good agreement with the measurements for sulfur, calcium, and vanadium ions incident on helium targets.^{1,2} Additional measurements⁵ for $\text{Ca}^{17+} + \text{H}_2$ collisions are also in good agreement with theory.

It is expected that RTE should also occur in the L-shell, i.e. for electron capture coincident with projectile L-shell excitation. To investigate this process we have measured projectile L x-ray emission coincident with single electron capture for 455-710 MeV $^{139}\text{La}^{40+} + \text{H}_2$ collisions. This work was done at the Lawrence Berkeley Laboratory using the SuperHILAC. The results are shown in Fig. 1 in which $\sigma_{\text{La}\beta}$ denotes the total cross section for $\text{La}\beta$ x-ray emission while $\sigma_{\text{La}\beta}^{q-1}$ is the cross section for $\text{La}\beta$ x-rays coincident with single electron capture. (The La and $\text{L}\beta$ lines were not resolved in this work).

In the figure it is seen that $\sigma_{\text{La}\beta}^{q-1}$ exhibits a pronounced resonant behavior with a maximum near 550 MeV. In addition, $\sigma_{\text{La}\beta}$ also shows a maximum near the same energy. Since $\sigma_{\text{La}\beta}^{q-1}$ is equal to nearly two-thirds of $\sigma_{\text{La}\beta}$ at 550 MeV, this observation of resonant behavior in the singles x-ray yield $\sigma_{\text{La}\beta}$ is expected.

At present there are no DR cross section calculations with which to compare these L-shell RTE results. In the figure we show the calculated⁶ Auger electron energies for La^{40+} transformed to the electron rest frame for three of the strongest transitions⁷ in singly ionized La. These calculations show that the maximum in $\sigma_{\text{La}\beta}^{q-1}$ occurs at an energy consistent with that expected on the basis of specific allowed Auger transitions.

This work was supported in part by the U. S. Department of Energy, Division of Chemical Sciences and the Office of Fusion Energy, and the Science and Engineering Research Council, Great Britain.

REFERENCES

1. J.A. Tanis, E.M. Bernstein, W.G. Graham, M.P. Stockli, M. Clark, R.H. McFarland, T.J. Morgan, K.H. Berkner, A.S. Schlachter, and J.W. Stearns, Phys. Rev. Lett. **53**, 2551 (1984).
2. J.A. Tanis, E.M. Bernstein, C.S. Oglesby, W.G. Graham, M. Clark, R.H. McFarland, T.J. Morgan, M.P. Stockli, K.H. Berkner, A.S. Schlachter, J.W. Stearns, B.M. Johnson, K.W. Jones, and M. Mehan, Nucl. Inst. Meth., in press.
3. C.S. Oglesby, E.M. Bernstein, and J.A. Tanis, Bull. Am. Phys. Soc. **29**, 743 (1984).
4. D.J. McLaughlin and Y. Hahn, Phys. Lett. **88A**, 394 (1982); J. Nasser and Y. Hahn, JOSTT **29**, 1 (1983).
5. E.M. Bernstein, J.A. Tanis, K.H. Berkner, M.W. Clark, W.G. Graham, R.H. McFarland, T.J. Morgan, A. Muller, A.S. Schlachter, and J.W. Stearns, Abstracts, This conference.
6. J.P. Desclaux, Comput. Phys. Commun. **9**, 31 (1975).
7. F.J. McGuire, Phys. Rev. **A3**, 1801 (1971).

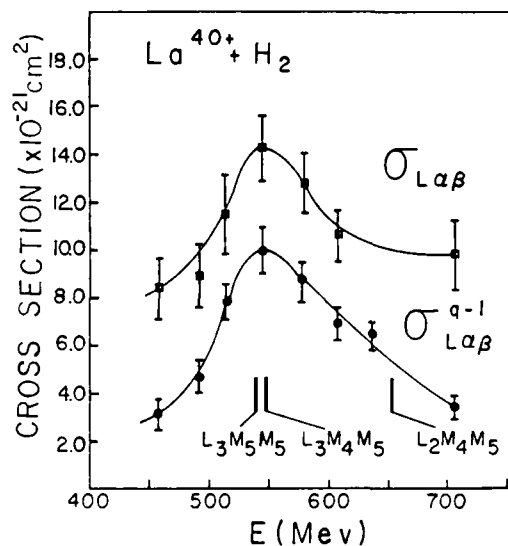


FIGURE 1. Projectile x-ray cross sections for $\text{La}^{40+} + \text{H}_2$. Selected Auger transition energy are denoted by $\text{L}_3\text{M}_5\text{M}_5$, etc.

CORRELATED AND UNCORRELATED ELECTRON CAPTURE AND K-SHELL EXCITATION IN $S^{13+} + He$ COLLISIONS

J. A. Tanis^a, F. M. Bernstein^a, M. W. Clark^b, W. G. Graham^c, R. H. McFarland^d, T. J. Morgan^e,
B. M. Johnson^f, K. W. Jones^f, and M. Meron^f

^aDepartment of Physics, Western Michigan University, Kalamazoo, Michigan 49008 USA

^bDepartment of Physics, University of North Carolina, Chapel Hill, North Carolina 27514 USA

^cPhysics Department, University of Ulster, Coleraine, BT52 1SA NORTHERN IRELAND

^dDepartment of Physics, University of Missouri, Rolla, Missouri 65401 USA

^eDepartment of Physics, Wesleyan University, Middletown, Connecticut 06457 USA

^fBrookhaven National Laboratory, Upton, New York 11973 USA

Recent experimental studies^{1,2} have provided strong evidence for resonant-transfer-and-excitation (RTE)³ in ion-atom collisions in which electron capture and inner-shell excitation occur together as a correlated electron-electron process in a single encounter. A related question is whether electron capture and projectile excitation can occur in a single encounter by means of separate uncorrelated electron-nucleus interactions. This two-step process is called non-resonant-transfer-and-excitation (NTE).^{3,4} Experimental evidence for NTE has recently been obtained in $Si^{11+} + He$ collisions.⁵

We report new evidence for NTE in 15–200 MeV $_{16}S^{13+} + He$ collisions obtained using the Brookhaven Tandem Van de Graaff. Fig. 1a shows the cross section for total projectile K x-ray emission, $\sigma_{K\alpha\beta}$, and the cross section for projectile K x rays coincident with single electron capture, $\sigma_{K\alpha\beta}^{q-1}$. It is seen that $\sigma_{K\alpha\beta}^{q-1}$ exhibits a maximum near 130 MeV due to RTE and a maximum near 30 MeV attributed to NTE. The dashed curve is the calculated³ RTE cross section (multiplied by 0.85) and the solid curve is a calculated NTE cross section obtained from the product of the K-shell excitation cross section and the probability for capture to the L-shell.⁶ This product has been normalized to the data near 30 MeV.

Fig. 1b shows the *ab initio* calculations of Reeves and Feagin⁷, for the $1s^2 2s \rightarrow 1s 2s^2 2p$ and $1s^2 2s \rightarrow 1s 2s 2p^2$ transitions only, which include both the uncorrelated (NTE) and correlated (RTE) contributions to charge transfer and excitation. These calculations, in which the lower energy maximum arises from the uncorrelated amplitude (NTE) and the higher energy maximum arises from the correlated amplitude (RTE), provide substantial qualitative agreement with the measured energy dependence of $\sigma_{K\alpha\beta}^{q-1}$. The narrower RTE width in Fig. 1b compared to the corresponding $\sigma_{K\alpha\beta}^{q-1}$ width in Fig. 1a is due to the fact that only the two transitions mentioned above have been included in the calculations.

This work was supported in part by the U.S. Department of Energy, Division of Chemical Sciences and the Office of Magnetic Fusion Energy, and the Science and Engineering Research Council, Great Britain.

References

1. J. A. Tanis, E. M. Bernstein, W. G. Graham, M. Clark, S. M. Shafroth, B. M. Johnson, K. W. Jones, and M. Meron, Phys. Rev. Lett. **49**, 1325 (1982).
2. J. A. Tanis, E. M. Bernstein, W. G. Graham, M. P. Stockli, M. Clark, R. H. McFarland, T. J. Morgan, K. H. Berkner, A. S. Schlachter, and J. W. Stearns, Phys. Rev. Lett. **53**, 2551 (1984).
3. D. Brandt, Phys. Rev. A **27**, 1314 (1983).
4. P. L. Pepmiller, P. Richard, J. Newcomb, R. Dillingham, J. M. Hall, T. J. Gray, and M. Stockli, IEEE Trans. Nucl. Sci. **NS-30**, 1002 (1983).
5. M. W. Clark, D. Brandt, J. K. Swenson and S. M. Shafroth, Phys. Rev. Lett. **54**, 544 (1985).
6. T. McAbee, Nucl. Inst. Meth. **214**, 89 (1983); D. Brandt, Nucl. Inst. Meth. **214**, 93 (1983).
7. T. M. Reeves and J. M. Feagin, private communication. J. M. Feagin, J. S. Briggs, and T. M. Reeves, J. Phys. B **17**, 1057 (1984).

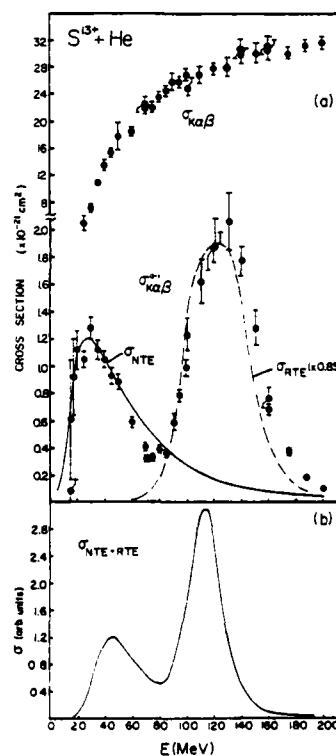


FIGURE 1. Projectile cross sections for $S^{13+} + He$.

CORRELATIONS BETWEEN CHARGE CHANGING EVENTS AND K
X-RAY EMISSION IN $\text{Ca}^{q+} + \text{H}_2$ COLLISIONS

E. M. Bernstein^a, J. A. Tanis^a, K. H. Berkner^b, M. W. Clark^c, W. G. Graham^d,
R. H. McFarland^e, T. J. Morgan^f, A. Muller^g, A. S. Schlachter^b, and J. W. Stearns^b

^aDepartment of Physics, Western Michigan University, Kalamazoo, Michigan 49008 USA

^bLawrence Berkeley Laboratory, Berkeley, California 94720 USA

^cDepartment of Physics, University of North Carolina, Chapel Hill, North Carolina 27514 USA

^dDepartment of Physics, University of Ulster, Coleraine BT52 1SA, NORTHERN IRELAND

^eDepartment of Physics, University of Missouri, Rolla, Missouri 65401 USA

^fDepartment of Physics, Wesleyan University, Middletown, Connecticut 06457 USA

^gUniversity of Giessen, Giessen, FEDERAL REPUBLIC OF GERMANY

In single collisions between ions and atoms inner-shell vacancies may be created by excitation, ionization, and charge transfer. These processes may be isolated by measuring coincidences between K x-ray emission and projectile charge-changing events. Recent work^{1,2} has also shown that excitation and charge transfer can occur together in a single encounter due to a correlated electron-electron interaction, a process referred to as resonant-transfer-and-excitation (RTE).

We have measured cross sections for calcium K-shell x rays coincident with electron capture and loss for 180-302 MeV $\text{Ca}^{q+} + \text{H}_2$ collisions ($q = 16+, 17+, 18+, 19+$). In addition, cross sections for total K x-ray emission and total electron capture and loss cross sections were obtained at the same time. This work was performed at the LBL SuperBILAC.

Figure 1 shows the K x-ray cross sections obtained for $\text{Ca}^{17+} + \text{H}_2$ collisions. $\sigma_{\text{K}\alpha\beta}$ is the total calcium K x ray (i.e. $\text{K}\alpha + \text{K}\beta$) emission cross section, $\sigma_{\text{K}\alpha\beta}^{q-1}$ is the cross section for calcium K x rays coincident with single electron capture, and $\sigma_{\text{K}\alpha\beta}^{q+1}$ is the cross section for calcium K x rays coincident with single electron loss. The measured cross sections for K x rays coincident with double electron capture and loss were negligible. Results similar to those shown for Ca^{17+} were obtained for the other charge states investigated.

From the figure it is seen that $\sigma_{\text{K}\alpha\beta}$ exhibits a rising trend over the energy range investigated with some indication of structure. On the other hand, $\sigma_{\text{K}\alpha\beta}^{q-1}$ is strongly resonant with two maxima and $\sigma_{\text{K}\alpha\beta}^{q+1}$ is generally flat except for a suggestion of minima near 205 MeV and 260 MeV.

The maxima in $\sigma_{\text{K}\alpha\beta}^{q-1}$ are attributed to RTE as seen by comparison with the calculated RTE cross section³ (dashed curve). The "resonant" widths are narrower than those obtained previously for $\text{Ca}^{17+} + \text{He}$ collisions due to the smaller electron momentum distribution in the H_2 target. For the same reason the minimum between the peaks is considerably deeper for the H_2 target. For energies ≥ 260 MeV the discrepancy between experiment and theory is very similar to that observed² for $\text{Ca}^{17+} + \text{He}$ collisions; the origin of this discrepancy is not understood at present.

The data suggest that the structure in both $\sigma_{\text{K}\alpha\beta}$ and $\sigma_{\text{K}\alpha\beta}^{q+1}$ are correlated to the maxima in $\sigma_{\text{K}\alpha\beta}^{q-1}$. This is the first time we have observed such structure in $\sigma_{\text{K}\alpha\beta}$ in the RTE resonance region. Since $\sigma_{\text{K}\alpha\beta}^{q-1}/\sigma_{\text{K}\alpha\beta} \sim 0.20$ and since $\sigma_{\text{K}\alpha\beta}^{q-1}$ contributes to $\sigma_{\text{K}\alpha\beta}$ it might be expected that the resonant behavior in $\sigma_{\text{K}\alpha\beta}^{q-1}$ would affect $\sigma_{\text{K}\alpha\beta}$. It is more difficult, however, to explain the apparent structure in $\sigma_{\text{K}\alpha\beta}^{q+1}$ since one would expect this cross section to be independent of $\sigma_{\text{K}\alpha\beta}^{q-1}$.

This work was supported in part by the U.S. Department of Energy, Division of Chemical Sciences and the Office of Fusion Energy, and the Science and Engineering Research Council, Great Britain.

References

1. J. A. Tanis, E. M. Bernstein, W. G. Graham, M. Clark, S. M. Shafroth, B. M. Johnson, K. W. Jones, and M. Meron, Phys. Rev. Lett. **49**, 1325 (1982).
2. J. A. Tanis, E. M. Bernstein, W. G. Graham, M. P. Stockli, M. Clark, R. H. McFarland, T. J. Morgan, K. H. Berkner, A. S. Schlachter, and J. W. Stearns, Phys. Rev. Lett. **53**, 2551 (1984).
3. C. S. Oglesby, E. M. Bernstein, and J. A. Tanis, Bul. Am. Phys. Soc. **29**, 743 (1984).

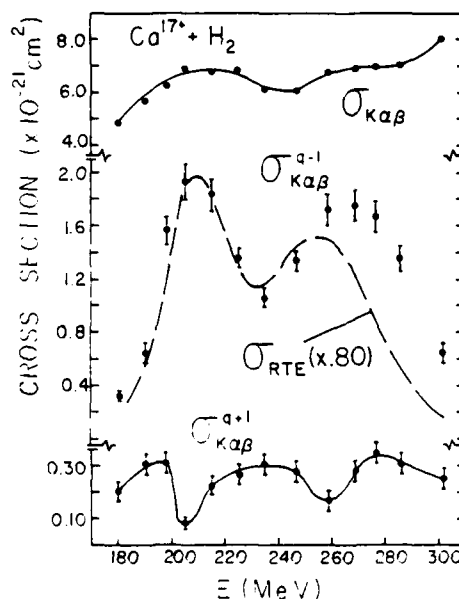


FIGURE 1. Projectiles cross sections for $\text{Ca}^{17+} + \text{H}_2$.

STRUCTURE IN HIGH ENERGY, MULTIPLY-CHARGED ION-ATOM ELECTRON-CAPTURE CROSS SECTIONS

W.G. Graham^{†††}, J.A. Tanis*, E.M. Bernstein*, M. Clark*, R.H. McFarland[‡], T.J. Morgan[‡], K.H. Berkner**, A.S. Schlachter**, J.W. Stearns** and A. Müller^{§§§}.

^{†††} Physics Department, University of Ulster, Coleraine, N. Ireland; *, Physics Department, Western Michigan University, Kalamazoo, U.S.A.; [‡], Physics Department, University of Missouri, Rolla, U.S.A.; [‡], Physics Department, Wesleyan University, Middletown, U.S.A.; **, Lawrence Berkeley Laboratory, Berkeley, U.S.A.; ^{§§§}, University of Giessen, West Germany.

In theoretical calculations of single-electron capture in high-energy, multiply-charged ion-atom collisions, the cross sections are found to vary monotonically with the projectile energy.

Evidence of structure in the energy dependence of single-electron-capture cross sections has been found in the present measurements of electron capture in 180 to 365 MeV Ca^{q+} ($q=16$ to 19) collisions in H_2 .

Results for Ca^{16+} and Ca^{17+} are shown in the figure 1. (The results for Ca^{18+} and Ca^{19+} are similar.)

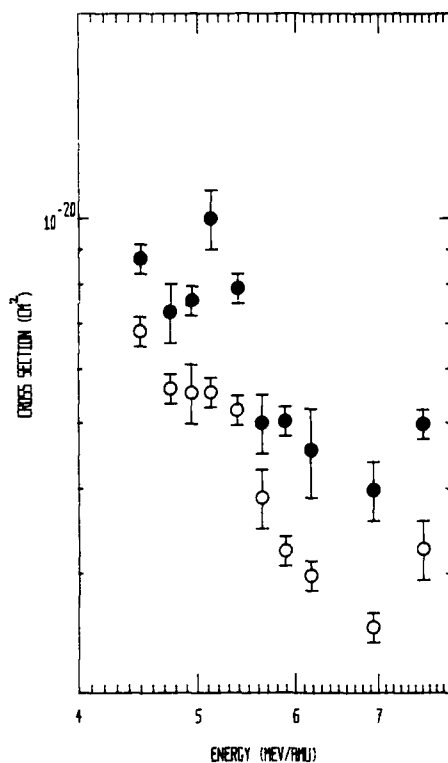


Figure 1. Single-electron capture cross sections for Ca^{16+} and Ca^{17+} in H_2 . The error bars indicate the relative uncertainties.

For all charge states there is a distinct increase in the electron-capture cross section at around 5.4 MeV/amu. This can be attributed to a contribution from resonant-transfer and excitation (RTE)¹ to the electron-capture channel. This structure occurs at the same energy as the first maximum in the RTE cross section for these collision partners. Assuming a monotonically

decreasing background, the increase in the electron-capture cross section is approximately $2 \times 10^{-21} \text{ cm}^2$, which is of approximately the same magnitude as the RTE cross section.

A second broader maxima in the RTE cross section is observed at 6.9 MeV/amu. In the present electron-capture cross sections no distinct structure is observed. However there are indications that RTE is contributing to the electron-capture cross section in that the energy dependence in this region is not as pronounced as might be expected. In the present measurements the energy dependence in this region varies from about E^0 to E^{-2} , whereas the electron capture cross section might normally be expected² to decrease at around E^{-4} .

The results illustrate the necessity to include RTE in theoretical formulations of ion-atom collision interactions.

Acknowledgements

This work was supported in part by the U.S. D.O.E., Division of Chemical Sciences and Office of Fusion Energy; by the S.E.R.C. G.B. and by the Research Council U.S.A.

References

1. J.A. Tanis, E.M. Bernstein, M. Clark, W.G. Graham, R.H. McFarland, T.J. Morgan, K.H. Berkner, A.S. Schlachter, J.W. Stearns and A. Muller. Abstracts of this meeting.
2. A.S. Schlachter, J.W. Stearns, W.G. Graham, K.H. Berkner, R.V. Pyle and J.A. Tanis, Phys. Rev. A.27, 3372 (1983).

CAPTURE, RTE- AND NTE-PROCESSES INTO HIGHLY-CHARGED 3.6 MeV/u Sm^{q+} PROJECTILES

W.A. Schönfeldt, P.H. Mokler, D.H.H. Hoffmann, A. Warczak*

GSI, P.O. Box 110541, D-6100 Darmstadt, FRG

*Permanent Address: Jagellonian University, Cracow, Poland

The transfer of electrons from rare gases (He, Ar, Xe) into 3.6 - 4.7 MeV/u Sm^{q+} projectiles was studied for high incoming charge states q with $33 \leq q \leq 54$. The L- and M-x-ray emission of the projectile was used to extract information on different electron capture processes. Additionally, to a pure capture of target electrons, a projectile core excitation may occur. These transfer and excitation processes can be of resonant and of non-resonant type, called RTE and NTE, respectively (Refs. 1 and 2). Information on all three processes - capture, RTE, and NTE - will be extracted from the q dependent x-ray spectra.

Transfer and excitation processes have been found recently by measuring the K x-ray emission for Li-like projectiles in coincidence with charge changed projectiles. The impact energy dependence of the cross sections gave the signature for RTE and NTE^{1,2}. In decelerating highly charged Sm projectiles - for the ASD method see Ref. 3 - we were able to study L-shell RTE and NTE processes without any coincidence requirements. This is due to the fact, that at high projectile charge states and correspondingly low projectile velocities electron capture processes dominate strongly any pure excitation or ionization processes in the projectile. The signature for RTE and NTE is here the charge state dependence of the x-ray cross sections.

Figure 1 summarizes some of the measured x-ray cross sections as a function of projectile charge state. The Sm-M radiation reflects the capture to excited projectile states. After opening of the projectile L-shell - $q > 52$ - the captured electrons can cascade down to the L shell giving rise to the tremendous L x-ray emission. From a detailed analysis of the total L x-ray spectra the original n, l distribution of captured electrons could be extracted. For one incoming projectile L vacancy, for example, the capture into the 4f level dominates.

The Sm ($L_L + L_{\alpha}$) x-ray cross section in Fig. 1 reflects in some way the number of L_3 -shell vacancies after a collision. In the charge state range $46 \leq q \leq 52$ (closed incoming L shell) we find a hump in the $L_L + L_{\alpha}$ x-ray cross section. We attach this hump to the $L_M M_j$ - RTE process with a total maximum cross section of $\sigma_{\text{RTE}}^L \sim 2 \times 10^{-19} \text{ cm}^2$. This is about two orders of magnitude larger than σ_{RTE}^K reported in the literature². In detail the observed hump is due to

the increase of the projectile binding energies E_n with the charge state q . Only for q around 48 the RTE condition $|E_{L_3}| - |E_{M_j} + E_{M_j}| = m_e v_{\text{proj}}^2/2$ can be fulfilled for the various $M_{i,j}$ -subshells, resulting in the cross section enhancement.

The NTE process was observed for excitation between L subshells of the Sm projectile for incoming L vacancies. Incoming L-vacancies ($q \geq 53$) are certainly in the L_3 -subshell and not in the L_2 shell at the beginning of the collision. This is due to the short lifetimes in such a high atomic number projectile. All the x-ray transitions to the L_2 shell, called L_{β} in Fig. 1, are therefore caused by a non-resonant excitation of a L_2 electron into the open L_3 shell in connection with a capture of a target electron into higher shells. The NTE cross section was found for this process to be $\sigma_{\text{NTE}} = 2 \times 10^{-18} \text{ cm}^2$ for $q \approx 54$. This value has to be compared to the single electron capture cross section extracted to be for $q = 54$ $\sigma_{\text{capt}} = 8 \times 10^{-17} \text{ cm}^2$.

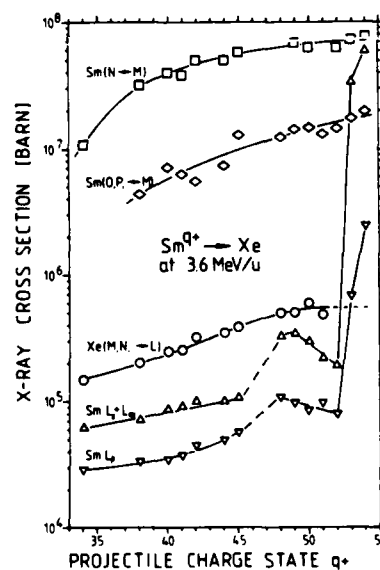


Figure 1 L and M x-ray emission cross section.

References

1. J.A. Tanis et al., Phys. Rev. Lett. **49** (1982) 1325
2. J.A. Tanis et al., Phys. Rev. Lett. **53** (1984) 2551
3. P.H. Mokler et al., Nucl. Instr. Meth. **B4** (1984) 34

EXCITATION AND IONIZATION IN $\text{Si}^{11+} + \text{He}$ COLLISIONS

M. Clark*, J. Anthony†, J. K. Swenson and S. M. Shafroth

Department of Physics and Astronomy, The University of North Carolina, Chapel Hill, N.C. 27514
and Triangle Universities Nuclear Laboratory, Durham, N.C.

Using an experimental arrangement illustrated and described in a recent paper by Clark et. al.¹, we have measured Si K x-ray excitation cross sections (Fig. 1), Si^{11+} to Si^{12+} single ionization cross sections (Fig. 2) and Si K x-rays in coincidence with Si^{12+} ions (Fig. 3) arising from Si^{11+} on He over the energy ranges shown in the figures. Work is in progress to extend these measurements to H_2 , Ne and Ar target gases. We conclude, based on these results and those of reference 1, where Si^{11+} on He for the case of electron capture and K x-ray excitation were measured, that the primary process giving rise to K x-ray production in this energy range is the $1s-2p$ excitation of the Si^{11+} projectile without either capture or loss of an electron taking place. This is because the coincidence cross sections for either capture or loss are less by an order of magnitude than the x-ray excitation cross sections. Also theory is in agreement with this assumption. The solid curve in Fig. 1 is a $1s-2p$ excitation cross section calculation of McAbee². To compare it with the data a fluorescence yield must be included, and this would bring the theory well below experiment since it is thought to be of order 0.3.

Furthermore it appears that in the case of the coincidence data shown in Fig. 3, the primary process is L-electron ionization and $1s-2p$ projectile excitation rather than K-electron ionization and $2s-2p$ excitation leading to a K x-ray in coincidence with the ion beam which lost one electron. This conclusion is based on theoretical calculations of McAbee², as well as the fact that L-shell ionization is far more probable in the energy regime for this experiment. The solid curve in Fig. 3 shows a scaled ECPSSR calculation for K-shell ionization and the dotted curve shows a scaled $1s-2p$ excitation calculation. Neither of these is quite appropriate, because the observed process is a double one i.e. excitation and ionization. More precisely, impact parameter dependent excitation and ionization probabilities should be convoluted to obtain the theoretical cross section for the double process. Nevertheless the data does follow the trend with energy for the excitation calculation.

As for the electron loss data (Fig. 2), the absolute values of the cross sections are more than 10 times the singles K_α x-ray cross section at 60 MeV and much more at lower projectile energies. The rise in

ionization cross section at 25 MeV is suggestive of L-shell velocity matching which should occur at ~ 34 MeV. (K-shell velocity matching occurs at ~ 136 MeV).

In the light of the new information obtained here and progress in the theory, it would be interesting to reanalyze the 1978 work of Doyle et. al.³, who calculated the charge-state dependence of the mean K-shell fluorescence yields of Si^{9+} ions on He.

This work was supported by the Chemical Sciences Division, U.S. D.O.E.

* Present address, Physics Department, Western Michigan Univ, Kalamazoo, MI 49008

† Physics Department, North Carolina State University and TUNL

Fig. 1

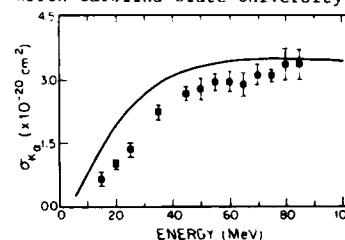


Fig. 2

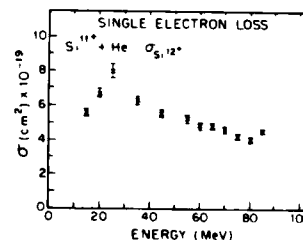
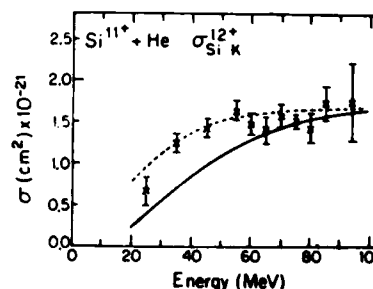


Fig. 3



References:

1. M. Clark, D. Brandt, J. K. Swenson and S.M. Shafroth, Phys. Rev. Lett. **54**, 544 (1985).
2. T. L. McAbee, Nucl. Instrum. Methods **214**, 89 (1983).
3. B. L. Doyle, U. Schiebel, J. R. Macdonald, and L. D. Ellsworth, Phys. Rev. A **17**, 523 (1978).

TARGET-THICKNESS DEPENDENCE OF THE Au L X-RAY YIELDS
PRODUCED BY 2.5 MeV/amu SULPHUR IONS

A.Berinde, C.Ciorte, Al.Enulescu, Daniela Flueraşu, I.Piticu and V.Zoran
Central Institute of Physics, P.O.Box HG-6, Bucharest, Romania

In energetic ion-atom collisions the electron capture (EC) to the bound states of the projectile shows up e.g. as projectile-charge-state dependence and (solid) target-thickness dependence of the observed X-ray yields. Compared to the K X-rays, its influence on the L X-ray yields is by far less studied¹. Part of an effort to obtain reliable L-subshell ionization cross sections², this work provides the first investigation of target-thickness dependence of the heavy partner L X-ray yields in asymmetric collisions.

By means of two HPGe X-ray detectors located at 18° and 90° relative to the beam axis we measured the absolute X-ray yields by 80 MeV, 9+ S ions bombarding 0.3-250 µg/cm² Au targets. The overall experimental uncertainty is of the order of 10%. The results are shown in Fig.1.

To the measured L X-ray yields we fitted as a function of the target thickness t the two-component model of Betz et al³:

$$\sigma_{xi}(t) = a_i - (b_i/t) [1 - \exp(-\tau t)] \quad i = \alpha, \beta, \gamma \quad (1)$$

$$a_i = \sigma_i^d + \sigma_i^c(\sigma_v/\sigma); \quad b_i = \sigma_i^c(\sigma_v/\sigma^2)$$

Here σ is the sum of the cross sections for K-vacancy production (σ_v) and quenching in the projectile. The

contribution to the thin target X-ray yields of EC to the outer shells has been estimated to be less than 5% and has been neglected. Thus σ^d and σ^c are the target X-ray production cross sections by direct ionization and EC to the projectile K-shell, respectively. In deriving eqs.(1) we also assumed constant degree of excitation in the Au outer shells along the target. Indeed within the errors we have found the same X-ray energy shift and L_β/L_α ratio for all targets. The fit gives $\sigma = 1.30(12) \times 10^4$ kb and the results shown in Table 1.

Table 1. Result of fitting eqs.(1) to the data.
All values in kbarns

	α	β	γ
$\sigma^c(\sigma_v/\sigma)$	1.39(6)	0.64(6)	0.053(6)
σ^d	2.71(25)	1.33(13)	0.19 (2)

The cross sections for EC from the target L-subshells to the projectile K-shell have been calculated with the formulae of Nikolaev⁴, by using for Au the experimental binding energies and for S the binding energy for an average charge state $q = 13$. When multiple ionization is taken into account (according to ref.2), the ratios $(\sigma_\beta/\sigma_\alpha)^c = 0.35$ and $(\sigma_\gamma/\sigma_\alpha)^c = 0.031$ are lower than the experiment by only about 20%. From σ^c and Table 1, an equilibrium fraction $\sigma_v/\sigma = 0.02$ of S ions with one K-vacancy within the target could be inferred. Scaling σ^c by a semiempirical factor would bring this value in closer agreement to the corresponding post-foil fraction⁵.

From the X-ray angular distribution in the range $\theta_x = 15^\circ - 90^\circ$ we obtained the L_β -vacancy alignment parameter $\kappa A_{20} = -0.12(3)$ and $-0.095(4)$ for 6.3 and 136 µg/cm², respectively. Even after correcting for the Coster-Kronig attenuation ($\lambda = 0.8 - 0.9$), the alignment remains independent of the target thickness, at variance with the predictions of the 1st order EC theory⁶. Also, its thin target value, like σ^d of Table 1, is in disagreement to advanced SCA calculations⁷.

REFERENCES

1. F.D.Mc Daniel et al., Phys.Rev. A19, 1517 (1979)
2. A.Berinde et al., these Abstracts (XIV ICPEAC) p.400
3. H.-D.Betz et al., Phys.Rev.Lett. 33, 807 (1974)
4. V.S.Nikolaev, Zh.Eksp.Teor.Fiz. 51, 1263 (1966)
5. U.Scharfer et al., Nucl.Instr.Meth. 146, 573 (1977)
6. E.G.Berezhko et al., J.Phys. 814, 2635 (1981)
7. F.Rösel et al., Z.Phys. A304, 75 (1982)

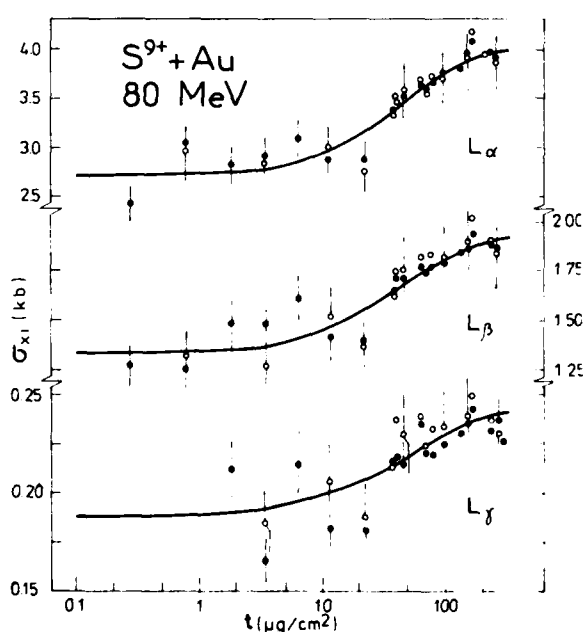


Figure 1. Absolute Au L X-ray yields σ_{xi} ($i = \alpha, \beta, \gamma$) vs the target thickness for $\theta_x = 180^\circ$ (o) and 90° (•). Full line: fit to the data according to eqs.(1).

L-SUBSHELL VACANCY PRODUCTION AND MULTIPLE IONIZATION EFFECTS IN S+Au COLLISIONS

A. Berinde, C. Ciortea, Al. Enulescu, Daniela Flueraşu, I. Piticu, and V. Zoran

Central Institute of Physics, P.O. Box MG-6, Bucharest, Romania

In order to investigate the influence of the multiple ionization upon the ratios of the L-subshell vacancy production cross sections as obtained from the X-ray yields, we bombarded a 70 $\mu\text{g}/\text{cm}^2$ selfsupported Au target with 0.5-2.5 MeV/amu S ions and detected the X-rays at 55° relative to the beam axis by using a HPGe detector.

Assuming a multiple binomial distribution for outer shell vacancies and using the scaling rule of Larkins¹, we have found for the LX-ray yields the well known relations², where the (effective) atomic parameters are expressed in terms of those for the singly-ionized atom and of the probabilities p_i of single-electron ejection from the $i=M-, N-,$ and $O-$ shells simultaneously with L-shell ionization, we checked that this procedure is valid for p_M values at least as high as 0.2. Compared to our previous work for lighter ions³, the present results take into account the blocking of the $L_1-L_3M_{4,5}$ Coster-Kronig transition in the presence of an M-vacancy.

The probabilities p_M and p_N entering the effective atomic parameters were obtained from the L_α/L_{β_1} and L_γ/L_{β_1} yield ratios, respectively, measured under S bombardment and compared to the corresponding ones measured with

2.5 MeV protons. The latter are considered to be characteristic for singly-ionized atoms. Thus, the present method of investigating the outer-shell ionization is a method of "yield shifts". Knowing p_N , we extracted p_O from $L_{\gamma_{2,3,6}}/L_{\beta_1}$ vs $L_{\gamma_{4,4}}/L_{\beta_1}$. In the energy range 0.5-2.5 MeV/amu p_M is increasing from 0.038 to 0.128, $p_N = 0.43$ and p_O is decreasing from 0.45 to 0.42. These probabilities give the number of the spectator vacancies in the subshells involved in the L-vacancy decay, irrespective how they were produced (ionization, rearrangement, shake-off, etc.).

The multiple ionization reduces f_{23} by about 30% relative to its singly-ionized atom value, while ω_2 and ω_3 are increased by about 20% up to 30% when the projectile energy varies from 16 to 80 MeV. Mostly affected by the blocking of the $L_1-L_3M_{4,5}$ transition are ω_1 and f_{12} . Their values relative to the unperturbed ones are compared in Fig.1 to the corresponding ones when blocking is neglected. The increasing difference between the two sets of values reflects the increase in the average number of M-vacancies.

Starting from the atomic parameters of Krause⁴ and the radiative partial widths of Scofield⁵ and taking into account the multiple ionization, we extracted from the measured X-ray yields the ratios $\sigma_{L_1}/\sigma_{L_2}$ and $\sigma_{L_2}/\sigma_{L_3}$. They are compared to the values obtained with unperturbed atomic parameters in Fig.2. The multiple ionization effects, and for $\sigma_{L_1}/\sigma_{L_2}$ especially the blocking of the $L_1-L_3M_{4,5}$ Coster-Kronig transition, bring the energy dependence of the cross section ratios in qualitative agreement to that observed for lighter projectiles. The dichotomy suggested in ref.6 becomes thus superfluous.

At 80 MeV, the target thickness dependence⁷ of the $\sigma_{L_1}/\sigma_{L_2}$ ratio is negligible, while the value of $\sigma_{L_2}/\sigma_{L_3}$ extrapolated to zero thickness is by only 18% higher than the equilibrium value. Thus, neither multiple ionization nor electron capture to the projectile can explain the discrepancy between the experiment and the predictions of the ECPSSR theory for direct ionization (Fig.2).

REFERENCES

1. F.P. Larkins, J. Phys. B4, 129 (1971)
2. T.J. Gray, in "Methods of Experimental Physics" vol.17 (Academic Press: New York 1980) p.196
3. A. Berinde et al., X84, Leipzig 1984, Abstracts p.48
4. M. Krause, J. Phys. Chem. Ref. Data 8, 307 (1979)
5. J.H. Scofield, At. Nucl. Data Tables 14, 121 (1979)
6. W. Jitschin et al., J. Phys. B16, 4405 (1983)
7. A. Berinde et al., these Abstracts (XIV ICPEAC) p.399

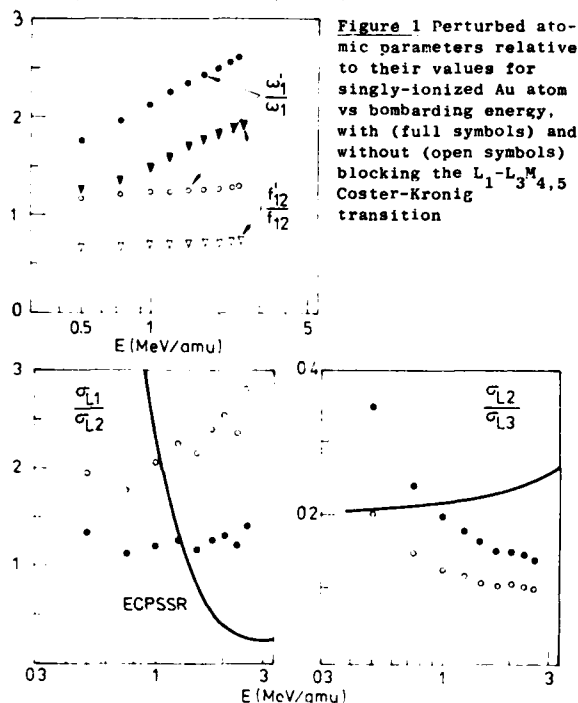


Figure 2. Ionization cross section ratios evaluated with unperturbed (o) and perturbed (*) atomic parameters.

PROJECTILE DEPENDENCE OF Au IONIZATION AT 0.5 AND 1 MeV/amu

A.Berinde, C.Ciortea, Al.Enulescu, Daniela Flueraşu, I.Piticu and V.Zoran

Central Institute of Physics, P.O.Box MG-6, Bucharest, Romania

Previously^{1,2} we studied the energy dependence of the multiple ionization (MI) effects upon the Au L-shell X-ray yields using F and S as projectiles. In the present work we extend these studies for more projectiles between C and S, at bombarding energies of 0.5 and 1 MeV/amu.

In order to obtain information on the outer-shell ionization we used the method of yield shifts². The single-particle ionization probability of the M-shell denoted p_M , is small at the impact velocities studied. Its value has been obtained with sufficient accuracy for F and S only^{1,2}. We checked for these two cases that within 15% p_M varies with the projectile atomic number as Z_1^2 . Therefore we used this scaling to deduce p_M for C, O, F, Mg and Si from p_M for S (0.038 at 16 MeV and 0.069 at 32 MeV). The value of p_N has been obtained from the L_{γ}/L_{γ_1} intensity ratio for protons relative to that for the heavier projectile. The corresponding ratio R has the form $[1-p_N(Z_1)]/[1-p_N(1)] = 1+p_N(1) - p_N(Z_1)$ if one is assuming that the M-vacancies are concentrated in the $M_{4,5}$ subshells. The values of R are plotted in Fig.1 against $Z_1^2 - 1$. The Z_1^2 scaling rule predicts a linear

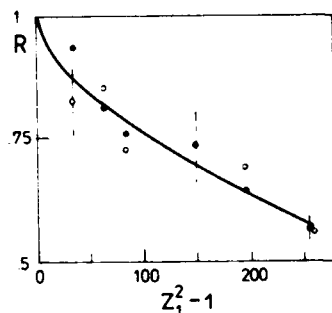


Figure 1. The ratio R (\circ , 0.5 MeV/amu; \bullet , 1 MeV/amu) vs $Z_1^2 - 1$. Full line: polynomial fit in $Z_1^2 - 1$.

dependence of R on this variable, while the data favour a weaker decrease, in qualitative agreement to the prediction of Becker et al.³. From a polynomial fit to the experimental values of R we obtained $p_N(Z_1) - p_N(1) = (-2.387 + 2.36 Z_1 + 0.027 Z_1^2) \times 10^{-2}$. Finally, from the relation between $L_{Y_{2,3,6}}/L_{Y_1}$ and $L_{Y_{4,5}}/L_{Y_1}$ intensity ratios we extracted $(1 - p_0)/(1 - p_N)$. We have found that this probability ratio is approximately independent of projectile and energy and in what follows we took an average value of 0.78.

Using the above outer-shell ionization probabilities to modify for MI the atomic parameters of the singly-ionized atom^{4,5}, we evaluated from the measured yields the cross section ratios $\sigma_{L_1}/\sigma_{L_2}$ and $\sigma_{L_2}/\sigma_{L_3}$. The importance of the MI effects is expressed in Fig. 2, in terms

of the factors C_{12} and C_{23} by which these cross section ratios differ from the corresponding ones calculated with unperturbed atomic parameters.

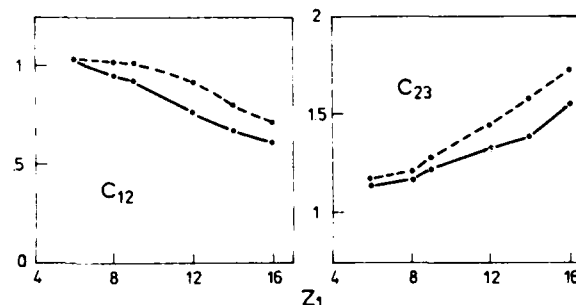


Figure 2. Variation of the MI effects upon the L-subshell ionization with projectile atomic number and energy (---, 0.5 MeV/amu; —, 1 MeV/amu).

Our results for Au L-subshell ionization are compared to the predictions of the united-atom version of SCA⁶ in Fig. 3. A similar comparison with ECPSSR has been done by Jitschin⁷, however without taking into account the multiple ionization. Even after considering it in the present work, the subshell cross-section ratios remain in gross disagreement to the available direct ionization theories.

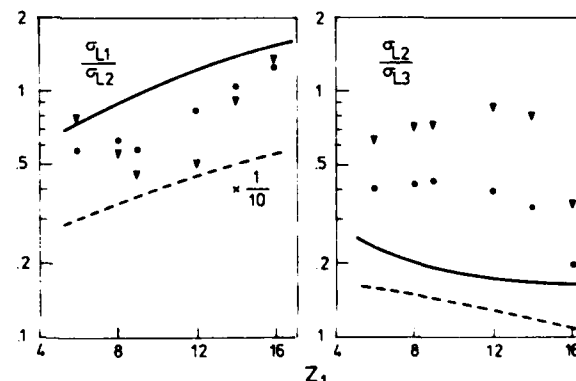


Figure 3. Au L-subshell ionization cross section ratios vs Z_1 compared to SCA calculations (∇ , ---, 0.5 MeV/amu; \bullet , —, 1 MeV/amu).

REFERENCES

1. A.Berinde et al., X84, Leipzig 1984, Abstracts p.48
2. A.Berinde et al, these Abstracts (XIV ICPEAC) p.400
3. R.L.Becker et al., Nucl.Instr.Meth.232[B4], 271 (1984)
4. M.Krause, J.Phys.Chem.Ref.Data 8, 307 (1979)
5. J.H.Scofield, At.Data Nucl.Data Tables 14, 121 (1979)
6. F.Rösel et al., Z.Phys. A304, 75 (1982)
7. W.Jitschin, Nucl.Instr.Meth. 232 [B4], 292 (1984)

COMPILATION AND ANALYSIS OF K-SHELL X-RAY PRODUCTION
BY HYDROGEN AND HELIUM IONS IN ELEMENTS FROM BERYLLIUM TO URANIUM

G. Lapicki

Department of Physics, East Carolina University, Greenville, North Carolina 27834, USA

Rutledge and Watson¹ originated extensive tabulations of inner-shell cross sections by ionic projectiles in atomic targets; their compilation was restricted to K-shell ionization by H and He ions and reported some 600 x-ray production cross sections in 1973. In a 1978 sequel,² this compilation was extended to about 1200 x-ray production cross sections by H and He ions and covered, as well, K-shell ionization cross sections by ions heavier than helium; compilations of L-shell ionization data also exist.³ In one of his most recent analysis,⁴ Paul uses some 3200 cross sections for protons alone and normalizes these data to predictions of the ECPSSR theory.⁵ In our original analysis,⁵ we have scaled about 2600 K-shell x-ray production cross sections to the results of this theory. The deviations of experiment from the ECPSSR theory were found to be, on the average, within 10%. Analogous analyses by Paul⁴ revealed, however, that this theory systematically overestimates the data in the slow collision regime; progressively so with the decreasing projectile velocity.

As of February 1985, I have compiled some 5400 K x-ray production cross sections by protons, deuterons, and He ions. After conversion to K-shell ionization cross sections σ_K^{expt} , these data are divided by the predictions of the first Born approximation⁶ σ_K^{FBORN} and the ECPSSR theory,⁵ σ_K^{ECPSSR} , which goes beyond the first Born calculations. For each projectile, the ratios so obtained were grouped, arbitrarily, in equal (0.2 in length) intervals on the $\log(v_1/v_{2K})$ scale; v_1 and v_{2K} are the projectile and K-shell target electron velocities, respectively. An arithmetic average of all cross sections in each group so defined is found, all data within the group are rejected if they differ by more than a factor of 2 from this mean, a new average is found, and the rejection is made again from all data in the group by the same criterion. Typically in two but no more than three iterations, the averages converge to constant values which are plotted in Figure 1.

Only proton data are analyzed in this figure; the data for other projectiles exhibit similar trends. The failure of the first Born approximation and the relative success of the ECPSSR theory are confirmed here.

Residual deviations of the ECPSSR theory from the data are statistically significant. While the data for moderately heavy and light target elements are in agreement with the averages of all data and with this theory, the cross sections for the lightest and heaviest

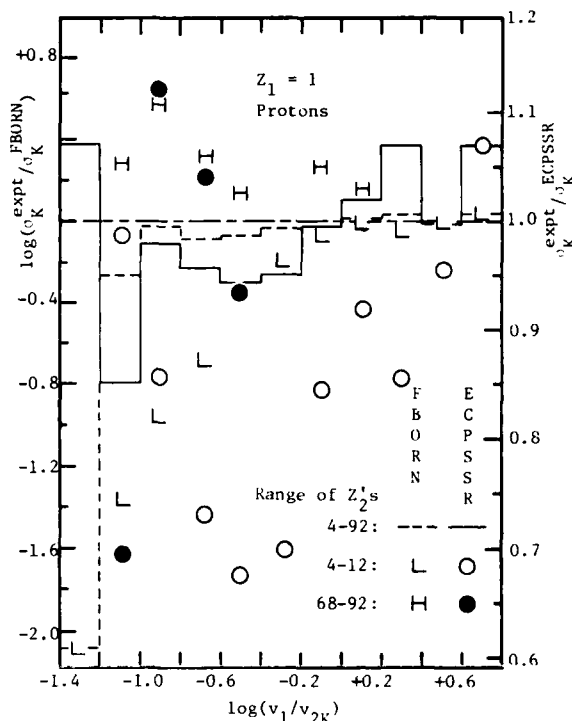


Fig. 1. Ratios based on circa 3600 experimental cross sections to the first Born approximation (left-hand side logarithmic ordinate) and to the ECPSSR theory (right-hand side linear ordinate) calculations; Z_2 is target's atomic number.

target atoms oscillate in opposite directions around these averages. Reasons behind nearly complementary discrepancies, in collision systems with the largest ($Z_1/Z_2 \approx 1/8$) and the smallest ($Z_1/Z_2 = 1/80$) projectile-to-target atomic number ratios, will be discussed.

This is a preliminary report on the work supported by the National Bureau of Standards Grant NB82NADA3033.

References

1. G. H. Rutledge and R. L. Watson, *At. Data Nucl. Data Tables* **12**, 195 (1973).
2. R. K. Gardner and T. J. Gray, *At. Data Nucl. Data Tables* **21**, 515 (1978) and erratum, *ibid.* **24**, 281 (1979).
3. T. L. Hardt and R. L. Watson, *At. Data Nucl. Data Tables* **17**, 107 (1976); R. S. Sokhi and D. Crumpton, *ibid.* **30**, 49 (1984).
4. H. Paul, *Nucl. Instr. Meth. B* **213**, 5 (1984) and references therein to his previous analyses.
5. W. Brandt and G. Lapicki, *Phys. Rev. A* **23**, 1717 (1981).
6. G. S. Khandelwal, B. -H. Choi, and E. Merzbacher, *At. Data Tables* **1**, 103 (1969).

CHARACTERISTIC FEATURES OF EJECTED ELECTRON SPECTRA FOR 5-25 keV He⁺ IMPACT ON NEON

N. Tokoro, N. Oda and T. Ichimori

Research Laboratory for Nuclear Reactors, Tokyo Institute of Technology, Tokyo 152, Japan

Although detailed information concerning electron production processes of ion-atom collisions can be obtained from measurements of ejected electrons as functions of the angle and energy of the electrons, such experimental investigations in the intermediate energy region (a few keV to several tens of keV) have been rather scarce so far. More data for various collision systems are still needed to study electron production mechanisms from the viewpoint of quasimolecular approach. Recently, we have reported¹⁾ strong collision-velocity-dependent features for both target and projectile autoionization peaks in the He⁺-Ne collision system. For neon lines, autoionizing states with 2p vacancies such as K2s²2p⁴(¹D)nln'¹ are dominant for incident energies less than 10 keV, whereas those with 2s vacancy such as K2s2p⁶(²S)n1 or K2s2p⁵(^{1,3}P)n1 are dominant for higher incident energies. In this work, measurements have been performed at extended electron energy region to investigate continuum part of spectra for the He⁺-Ne collision system. Ejected electron spectra at 90° from 5, 15 and 25 keV He⁺-Ne collisions are shown in Fig. 1. As can be seen in Fig. 1, the energy distributions of continuum electrons are well represented by the exponential functions of the electron energy. Since the exponential energy dependence of ejected electrons having such a functional form as $\exp(-E \cdot b/v)$, where E is the electron energy, b is a constant, and v is the internuclear velocity, is theoretically expected²⁾ to result from the direct transition to continuum states from bound states of quasimolecule, we determined parameters A and B in the function $A \cdot \exp(-B \cdot E)$ so that

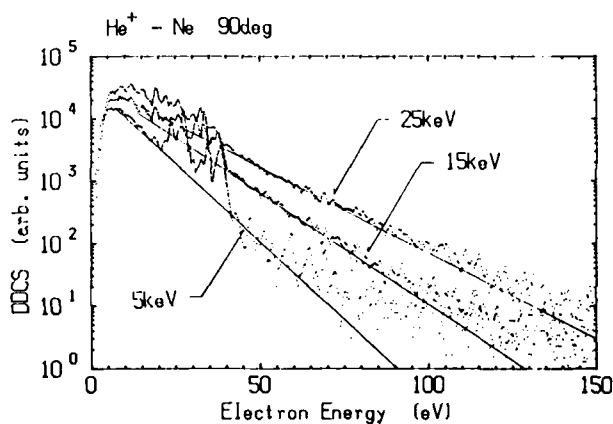


Fig. 1 Doubly differential cross sections for production of electrons in 5, 15 and 25 keV He⁺-Ne collisions

the best fit to the experimental continuum spectra is obtained, and reciprocals of B as functions of the internuclear velocity are plotted in Fig. 2. As can be seen in Fig. 2, the reciprocal B is closely proportional to the internuclear velocity in accordance with theoretical formula. On the other hand, similar dependence of energy distribution of ejected electrons has been reported in a few keV/amu to several tens of keV/amu H⁺ impacts on hydrogen and nitrogen molecules by Rudd³⁾ and Neⁿ⁺ impacts on neon by Woerlee et. al.,⁴⁾ and interpreted as a result of the so-called direct MO ionization. Thus, the electron production mechanism for the continuum part in the present He⁺-Ne collision system may be also attributed to the direct transitions to continuum states from bound states of quasimolecule which rapidly promote during collision.

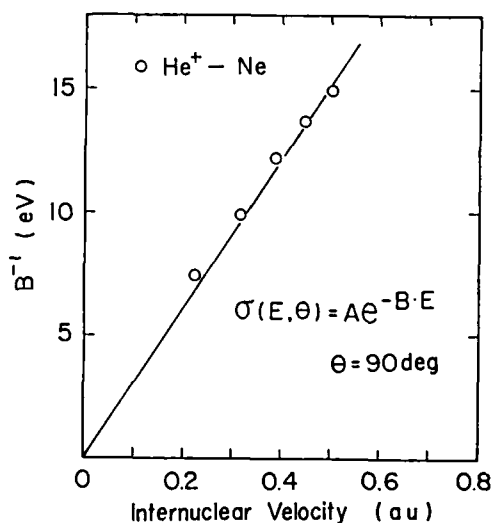


Fig. 2 Reciprocals of B plotted as functions of the internuclear velocity

References

- 1) N. Tokoro and N. Oda, J. Phys. B **17**, L871 (1984)
- 2) T. Watanabe, P. H. Woerlee, and Yu. S. Gordeev, Proc. 11th Int. Conf. on the Physics of Electronic and Atomic Collisions (Kyoto, North-Holland) p.652 (1979)
- 3) M. E. Rudd, Phys. Rev. A **20**, 787 (1979)
- 4) P. H. Woerlee, Yu. S. Gordeev, H. de Waard, and F. W. Saris J. Phys. B **14**, 527 (1981)

ELECTRON EMISSION IN COLLISIONS OF C^+ IONS WITH ATOMIC AND MOLECULAR TARGETS*

L.H. Toburen

Pacific Northwest Laboratory
Richland, WA 99352

Although extensive data exists regarding the details of ionization in collisions of bare ions with atomic and molecular targets, there have been few studies of the energy and angular distributions of electrons produced in heavy ion-atom collisions. Studies for low energy collisions, i.e., $\lesssim 1$ au, indicate that the primary mechanism responsible for electron emission in light collision systems is direct coupling between the bound and continuum states of the quasimolecule.^{1,2} In high energy collisions the dominant process is coulomb ionization which can be scaled from proton results if proper account is taken of the effects of screening.^{3,4}

The present study addresses the intermediate energy range to investigate the features of the electron spectra in the region where the ionization process is in transition from predominantly molecular processes to those of a coulomb nature. Data were obtained from singly charged carbon ions with energies from 800 keV to 4200 keV (~ 1.3 to 7 au) for He, Ar, and CH_4 targets and for 800 keV to 2400 keV for neon targets. Electron spectra were recorded at 13 angles from 15° to 130° for ejected electron energies from approximately 10 eV to 1200 eV.

The electron spectra obtained for ionization of neon by C^+ are remarkably similar in shape and magnitude to previous results for neon ions.¹ This is illustrated in Fig. 1. In all cases the spectra approach an exponential shape at the higher electron energies. This is consistent with electron emission

via coupling between bound and continuum states as discussed by Woerlee et al.¹ and Rudd².

It must be emphasized that the data of Fig. 1 are for electron emission at 90° ; additional spectral features are observed at other emission angles, see Fig. 2. The exponential shape of the spectra is still

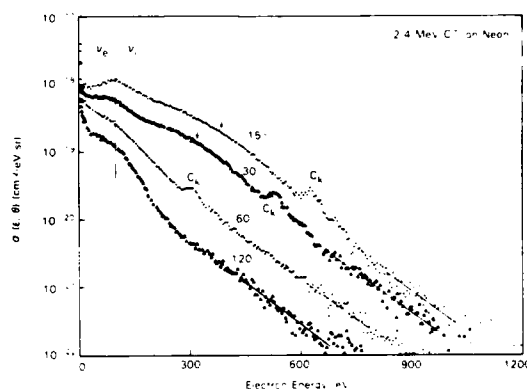


FIGURE 2.

evident at the high energy end of each spectrum, but features resulting from coulomb processes are now present at lower electron energies. In particular one observes a broad peak at $v_e = v_i$ due to electrons stripped from the moving ion, a broad distribution representative of a binary encounter peak (the kinematic position is indicated by the arrows in the 15° and 30° spectra), and Auger peaks resulting from inner shell ionization of the incident carbon ion. It is expected that the broad range of data developed in this study will enable evaluation of the relative significance of the different mechanisms responsible for ionization in this energy range.

*Work supported by U.S. DOE Contract DE-AC06-76RL01830.

1. P.H. Woerlee, Yu. S. Gordeev, H. de Waard and F.W. Saris, *J. Phys. B* **14**, 527 (1981).
2. M.E. Rudd, in *High-Energy Ion-Atom Collisions*, ed. by D. Berenyi and G. Hock (Elsevier, New York, 1982).
3. L.H. Toburen, N. Stolterfoht, P. Zeim, D. Schneider, *Phys. Rev. A* **24**, 1741 (1981).
4. S.T. Manson and L.H. Toburen, *Phys. Rev. Letters* **46**, 529 (1981).

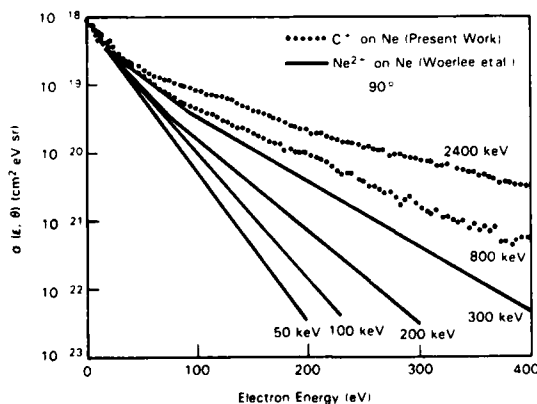


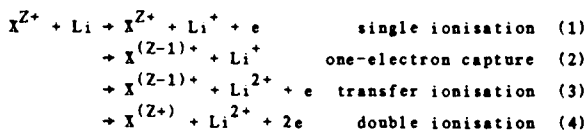
FIGURE 1.

IONISATION AND CHARGE TRANSFER IN COLLISIONS OF H^+ AND He^{2+} IONS WITH Li ATOMS

M B Shah, D S Elliott and H B Gilbody

Department of Pure and Applied Physics, The Queen's University of Belfast,
Belfast, United Kingdom

A crossed beam coincidence technique incorporating time-of-flight spectroscopy of the collision products¹ has been applied to studies of



Cross sections for the separate processes 1 - 4 have been separately determined for X^{Z+} ions of H^+ and He^{2+} at impact energies within the ranges 43-2100 $keV amu^{-1}$ and 22-1400 $keV amu^{-1}$ respectively. The results provide a valuable assessment of a number of recent theoretical predictions and are relevant to schemes for plasma diagnostics in fusion devices.

The primary ion beam was arranged to intersect (at right angles) a beam of Li atoms effusing from a soft iron furnace. Slow ion and electron collision products were collected by a transverse electric field and separately counted by multipliers. Li^+ or Li^{2+} product ions were distinguished from background gas ions by their characteristic times of flight to the multiplier. Ionisation and charge transfer events were recorded by separately counting slow Li product ions in coincidence with electrons and a coincidence of the ions with a third multiplier used to detect fast charge analysed $X^{(Z-1)+}$ collision products². All cross sections were normalised by reference to our previously measured absolute He^{2+} impact cross sections³ for (2) in the range 22-200 $keV amu^{-1}$ and are subject to an uncertainty of $\pm 20\%$ in absolute magnitude.

Our cross sections for process (1) are compared with other data in figure 1. Previous measurements for equivelocity electron impact^{4,5} are rather smaller than our H^+ impact cross sections even at the highest velocities, but the agreement is still within maximum combined uncertainties of 35%. Classical impulse calculations⁶ for H^+ impact and CTMC calculations⁷ for both H^+ and He^{2+} impact are in excellent agreement with our measurements. Born estimates^{8,9} for H^+ impact all lie below our measured values.

In the case of one-electron capture, our measurements show an excellent agreement with the total cross sections σ_{11} measured by McCullough et al³ for

He^{2+} impact over a wide range of energies. For H^+ impact, values of σ_{11} measured by Il'in et al¹¹ are about a factor of two larger than our values.

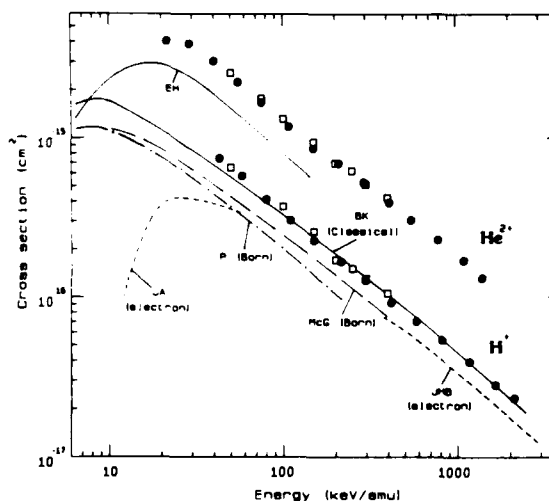


Figure 1 : Cross sections for single ionisation of Li by H^+ and He^{2+} impact (process 1)

● present data : Theory, ○ CTMC Method⁷, P. Born⁸, McG. Born⁹, EH, Close coupling¹⁰, BK Classical impulse⁶ : Equivelocity electron impact, JA⁴, JHB⁵.

Our measurements show that the transfer ionisation process (3) contributes up to 5% of σ_{11} for H^+ impact and up to about 25% of σ_{11} for He^{2+} impact. The double ionisation process (4) is the main Li^{2+} production mechanism; at 550 $keV amu^{-1}$ the ratio $\sigma(4)/\sigma(3)$ is 34.0 and 7.4 for H^+ and He^{2+} respectively.

References

1. M B Shah and H B Gilbody, *J Phys B*, **14**, 2361 (1981).
2. M B Shah and H B Gilbody, *J Phys B*, **15**, 3441 (1982).
3. R W McCullough, T V Goffe, M B Shah, M Lennon and H B Gilbody, *J Phys B*, **15**, 111 (1982).
4. I P Zapesochnyi and I S Aleksakhin, *Sov Phys JETP*, **28**, 41 (1969).
5. R Jalin, R Hagemann and R Botter, *J Chem Phys*, **52**, 952 (1973).
6. D R Bates and A E Kingston, *Adv in Atom and Molec Phys*, **6**, 269 (1970).
7. R E Olson, *J Phys B*, **15**, L167 (1982).
8. G Peach, *Proc Phys Soc (London)*, **85**, 709 (1965).
9. E J McGuire, *Phys Rev A*, **13**, 267 (1971).
10. A M Ermolaev and R N Hewitt, *Nuc Inst Methods*, in course of publication.
11. R N Il'in, V A Oparin, E S Solov'ev and N V Fedorenko, *Sov Phys JETP*, **11**, 921 (1967).

CROSS SECTIONS FOR IONIZATION AND ELECTRON TRANSFER FOR 5-300 KEV/u He^{2+} IONS IN GASES

Akio Itoh, M.E. Rudd, and T.W. Goffe*

University of Nebraska-Lincoln, Lincoln, Nebraska 68582-0111 USA

Comprehensive measurements of total cross sections for ionization and electron transfer have been performed over a wide energy range of He^{2+} ions for a variety of atomic and molecular targets. Projectile energies used for ionization and charge transfer were 10-300 keV/u and 5-150 keV/u, respectively, and the target gases were He, Ne, Ar, Kr, H_2 , N_2 , O_2 , CO, CO_2 , CH_4 and H_2O . The cross sections σ_+ and σ_- corresponding respectively to the production of positive and negative charge were measured by the transverse field method using a parallel plate electrode apparatus.^{1,2} Single and double electron capture cross sections, σ_{21} and σ_{20} , were measured by electrostatic separation of the charge components of the beam after passing through a known length of the target gas at a measured pressure.³ Since the total charge of the collision partners must be conserved, the corresponding four cross sections have the following interrelationship derived by neglecting three-electron capture cross sections.

$$\sigma_+ = \sigma_- + \sigma_{21} + 2\sigma_{20}.$$

The most reliable cross sections were then deduced in a self-consistent manner by making a weighted least-square adjustment of the four measured cross sections to satisfy the above relation at each impact energy. Uncertainties of the final cross sections obtained in this way were typically about 15 %.

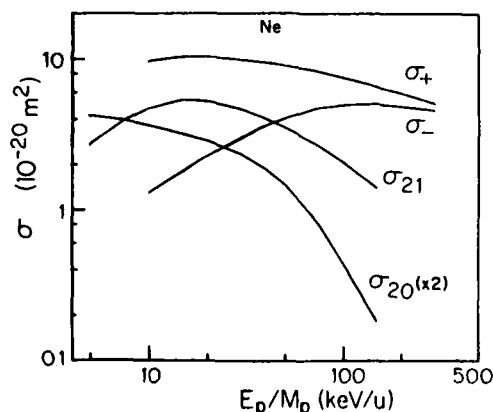


Fig. 1 Present cross sections for Ne target obtained by the adjustment procedure (see text).

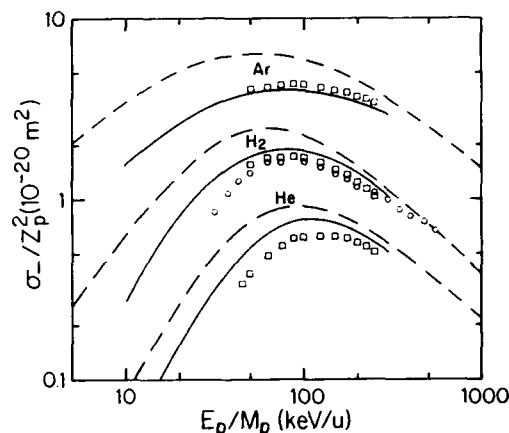


Fig. 2 Comparison of present σ_- data (solid lines) with other data. σ_- (ref.1); σ_- (ref.4). Dashed lines represent proton impact data (ref.4).

Fig. 1 presents four cross sections for Ne target atoms. The results show a well-known tendency that the positive ion production σ_+ is dominated by ionization channel at high impact energies and by electron transfer at low energies. In Fig. 2 the electron production cross sections σ_- for He, Ar and H_2 targets are compared with proton impact data denoted by dashed lines.⁴ The cross sections are plotted according to a Z_p^{-2} scaling predicted by the Born approximation. The helium impact data are considerably smaller than the corresponding proton impact data over the whole energy range investigated, while the other sections begin to converge with increasing projectile energies as expected. Further studies will be undertaken to investigate each contributing mechanism such as direct ionization and transfer-ionization.

Reference

- *present address: 3 Belvedere Park, Hilltown, Pa., 17033 Down BTR, CHL, North Ireland.
1. L.J. Fiskett, S.L. Taylor and J.L. Garvin, *Trans. Faraday Soc.* **67** (1971) 171.
2. M.E. Rudd, P.J. Ffolkes, M.L. Williams, M. Kessler and T.W. Goffe, *Trans. Faraday Soc.* **67** (1971) 171.
3. M.E. Rudd, T.W. Goffe, *J. Chem. Phys.* **54** (1971) 171, submitted to *Phys. Rev.*
4. M.E. Rudd and M.L. Williams, *J. Chem. Phys.* **54** (1971) 171.

IONIZATION OF RARE GAS ATOMS IN 1.05 MEV/AMU FULLY STRIPPED ION IMPACT

H. Shibata, S.H. Be, T. Tonuma, H. Kumagai, M. Kase, T. Kambara, I. Kohno and H. Tawara*

The Institute of Physical and Chemical Research (RIKEN), Hirosawa, Wako-shi, Saitama 351, Japan

*Institute of Plasma Physics, Nagoya University, Nagoya 464, Japan

In order to investigate the systematic behavior of ionization processes by fully stripped ions, we measure total apparent ionization cross sections σ_+ ($=\sum i\sigma_i$ where σ_i is the cross section for production of recoil ions with charge i , B^{i+}) using a condenser plate method. The yields of recoil ions produced in ion impact are measured as a function of the target gas pressure up to about 10^{-4} Torr, ensuring single collision conditions.

The present experimental results for ionization of He, Ne and Ar atoms in 1.05 MeV/amu He^{2+} , C^{6+} , O^{8+} and Ne^{10+} ion impact are shown in Fig. 1, together with the experimental results by Rudd et al.¹ in proton impact. The electron impact data with equivalent velocity (~ 572 eV) (Rapp and Englander-Golden²) are also plotted at $Z = 1$ projectiles which are in good agreement with proton data. Data in other projectile ion impact by Schlachter et al.³, Hvelplund et al.⁴ and Knudsen et al.⁵ are also shown. Some of these data have been taken at slightly different impact energies. Therefore, a correction is made for

these data to obtain the cross sections at 1.05 MeV/amu impact energy, assuming that the ionization cross section at this energy region decreases inversely proportional to the impact energy. The present data are also found to be in good agreement with these data presently available.

To find the dependence of the ionization cross sections on the atomic number of the fully stripped ions, a least-square fitting in the form of $\sigma_+ = \sigma_0 Z^\alpha$ is made including all these data. The following results are obtained at 1.05 MeV/amu ion impact:

Target	α	σ_0 ($\times 10^{-16}$ cm ²)
He	1.84	0.23
Ne	1.69	0.61
Ar	1.68	1.52

In Fig. 1 are plotted with the dotted lines the results calculated by Olson⁶ using the classical trajectory Monte Carlo method. The agreement between the present data and this calculation is generally good for He and Ar, but the discrepancy in Ne is significant.

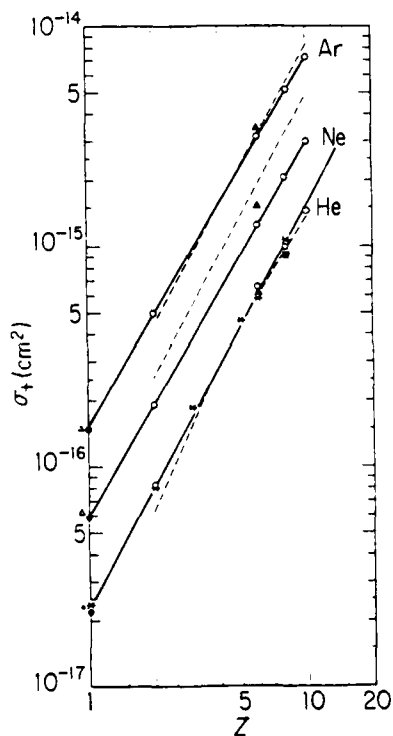


FIGURE 1. Total apparent ionization cross sections for He, Ne and Ar atoms plotted against the nuclear charge Z of 1.05 MeV/amu fully stripped ions. open circles: present data. closed circles: Rudd et al. (Ref. 1). crosses: Knudsen et al. (Ref. 5). closed triangles: Schlachter et al. (Ref. 3). closed squares: Hvelplund et al. (Ref. 4). open triangles at $Z = 1$: electron data of Rapp and Englander-Golden (Ref. 2). The dotted lines represent the calculation by Olson (Ref. 6) and the solid lines the least-square fitting to experimental data.

References

1. M.E. Rudd, R.D. DuBois, L.H. Toburen, C.A. Ratcliffe, and T.V. Goffe, Phys. Rev. A **28** 3244 (1983).
2. D.Rapp and P. Englander-Golden, J. Chem. Phys. **43** 1464 (1965).
3. A.S. Schlachter, K.H. Berkner, W.G. Graham, R.V. Pyle, P.J. Schneider, K.R. Stalder, J.W. Stearns, J.A. Tanis, and R.E. Olson, Phys. Rev. A **23** 2331 (1981).
4. P. Hvelplund, H.K. Haugen, and H. Knudsen, Phys. Rev. A **22** 1930 (1980).
5. H. Knudsen, L.H. Andersen, P. Hvelplund, G. Astner, H. Cederquist, H. Danared, L. Liljeby, and K.G. Rensfelt, J. Phys. B: At. Mol. Phys. **17** 3545 (1984).
6. R.E. Olson, J. Phys. B: At. Mol. Phys. **12** 1843 (1979).

ELECTRON EJECTION IN $\text{He}^+ - \text{He}$ COLLISIONS: EXPERIMENT AND THEORY*

R. D. DuBois[#] and S. T. Manson[†]

[#] Pacific Northwest Laboratory, Richland, WA 99352 (USA)

[†] Georgia State University, Atlanta, GA 30303 (USA)

Ionization of atoms by fast bare ions can be fairly well represented theoretically within the framework of the Born approximation. Fast structured ions, on the other hand, arrive at the collision center containing bound electrons of their own. These electrons partially screen the incoming nuclear charge. In addition new electron ejection channels are introduced. Thus the theoretical calculation is far more complicated.

Past experiments measured only the total electron emission as a function of emission angle and energy. Thus the individual components of the theoretical model needed to be summed in order to compare with experiment.¹

Recently preliminary measurements of the electron emission measured in coincidence with an ionized projectile were reported.^{2,3} The system studied was $\text{He}^+ - \text{Ar}$ for which no theoretical information was available. Here we present additional data for a simpler system $\text{He}^+ - \text{He}$ and compare it with theoretical calculations made in the Born approximation.

The data are for 1.6 MeV He^+ impact and electron emission at 30° . In order to reduce the experimental uncertainties, the data are presented as the fraction of the electron emission in coincidence with an ionized projectile with respect to the total electron emission. These fractions were measured from approximately 10-1000 eV as shown in Fig. 1. The experimental uncertainties for these data are dominated by statistical uncertainties (10-20% for the coincidence data and <10% for the total electron emission data).

The experimental data are compared with theoretical calculations that assume four electron ejection channels: a) target ionization with the projectile remaining in the ground state, b) target ionization with the projectile being excited (excitation includes ionization), c) projectile ionization with the target remaining in the ground state and d) projectile ionization with the target being excited. Processes (c+d) and (b+c+d) should be lower and upper limits, respectively, for the measured fractions.

As can be seen, in the region of the peak theory slightly overestimates experiment. Here the

dominant contribution to the measured fractions are processes (c+d). At lower energies the theory underestimates the measured fractions however the importance of process b is clear. For the highest energies shown, theory is again too small, although here the calculations are difficult to perform.

Additional experimental and theoretical details will be presented. In addition, a similar comparison will be available for $\text{He}^+ - \text{Ar}$ collisions.

*DOE Contract DE-AC06-76RLO 1830 and U.S. Army Research Office Contract DAAG-29-83-K-0054

1. S.T. Manson and L.H. Toburen, Phys. Rev. Lett. **46**, 529 (1981).
2. R.D. DuBois, Second Workshop on High Energy Ion-Atom Collision Processes, Debrecen, Hungary (1984).
3. R.D. DuBois, Bull. of Am. Phys. Soc. **29**, 1091 (1984).

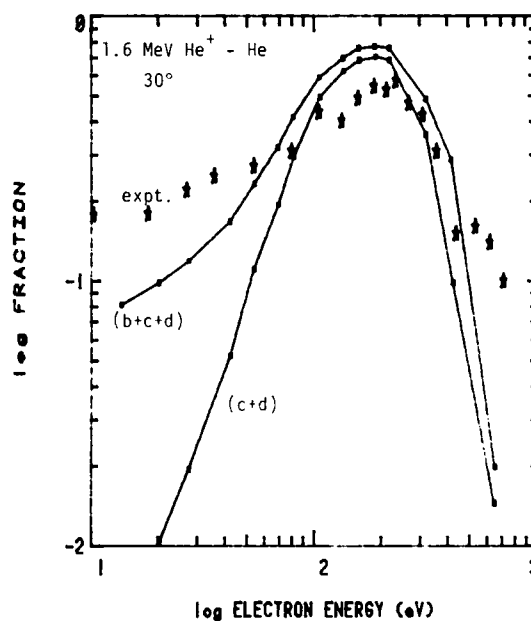


FIGURE 1.

IMPACT PARAMETER DEPENDENT EMISSION OF ELECTRONS IN ION-ATOM COLLISIONS

G. Schiwietz, T.J.M. Zouros, U. Stettner, N. Stolterfoht

Hahn-Meitner-Institut für Kernforschung Berlin GmbH
Glienickerstr. 100, D-1000 Berlin 39, West Germany

Target electron ionization was measured as a function of impact parameter in collisions of 100 keV $H^+ + Ar$ and 400 keV $Ar^+ + Ar$. The electrons were detected in coincidence with the scattered projectile. The time-of-flight method was used to determine the electron spectra.

Low intensity beams (typically less than 10 nA), provided by an AN 400 electrostatic Van-de-Graaff accelerator, were used to reduce random coincidences. Care was taken to maintain single collision conditions in the Ar jet target utilized. The unscattered ion beam was less than 0.5 mm in diameter and was dumped in a Faraday cup. The scattered projectiles were detected in a 7-ring position sensitive channelplate detector. The channelplate was made up of two plates sandwiched together to provide sufficient amplification of the weak signal detected. The fast timing signal produced from each ring (better than 3 ns) was further tagged by a digital bit identifying the ring. The particle detector was placed at a distance of 35.6 cm from the target enabling the measurement of the probability of electron ionization at impact parameters between 0.13 and 0.5 a.u. for proton and 0.35 and 0.95 a.u. for Ar projectiles respectively. The timing signal was connected to the stop side of a time-to-amplitude converter (TAC). The count rate in each ring never exceeded 200 kHz.

A large solid angle (28 msr) analyzer equipped with a channel plate was used to detect the electrons. A fast timing pulse was produced and it was used to start a coincidence unit and the TAC. Thus the time of flight of the measured electrons was determined.

Count rates were kept low enough to avoid second order effects due to random signals which could change the shape of the true coincidence spectrum. The true coincidences were deduced by normalizing and subtracting a purely random spectrum. This was obtained by supplying one channel of the coincidence unit with random stop pulses. A microprocessor supporting a two-dimensional memory array was used to collect the data.

Fig. 1 shows the time of flight spectra for impact parameters between 0.35 and 0.95 a.u. for the system 400 keV $Ar^+ + Ar$. Moliere potentials were used to convert scattering angle to impact parameter. All spectra were normalized to the same accumulated charge after the random coincidences were subtracted. The prominent peak which increases with decreasing impact parameter is produced by Ar-L-Auger electrons. The small peak to the right of this peak, visible at all impact parameters is due to ion-photon coincidences. This peak allows an accurate time zero determination. The flat structure at 50 - 80 ns can be associated with the decay of autoionizing states involving outer shell electrons.

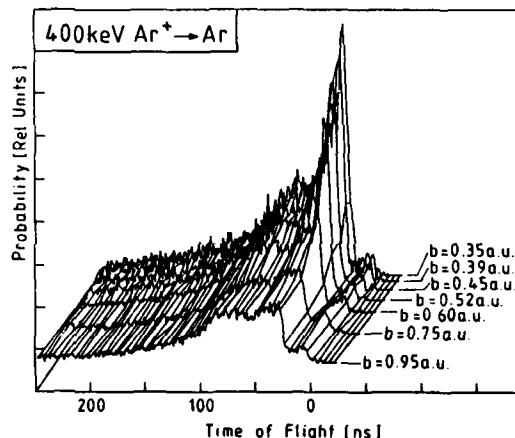


Fig. 1 Time of flight spectra of electrons from $Ar^+ + Ar$ collisions for specific impact parameters.

Total cross sections determined by integrating over impact parameter were in good agreement with known cross sections¹. The impact parameter dependence of the Ar-L-Auger peak is well explained within the Kessel model² for the promotion of the $4f$ MO.

¹T. Schneider, diplom thesis (FU Berlin, 1983) unpublished.

²R.K. Cacak, Q.C. Kessel and M.E. Rudd, Phys. Rev. **A2**, 1327 (1970).

ELECTRON EJECTION IN ION-ATOM COLLISIONS: BETHE-BORN THEORY FOR STRUCTURED INCIDENT IONS

Steven T. Manson* and John H. Miller*

*Department of Physics and Astronomy, Georgia State University, Atlanta, Georgia 30303 USA
 *Radiological Sciences Department, Pacific Northwest Laboratory, Richland, Washington 99352 USA

Cross sections for excitation or ionization of an atom or molecule by a fast, structureless charged particle, e.g., H^+ or e^- , can generally be quite well predicted by first Born approximation.¹ For an inelastic collision in which a bare incident particle of mass M , velocity v , and charge z loses energy ΔE , the Born cross section can be approximated very well by the Bethe-Born asymptotic cross section¹ which is an expansion in $\Delta E/T$ with $T=mv^2/2$, m being the electron mass. This cross section, for a process in which the target is excited from state o (usually the ground state) to state n (which may be an excited or ionized state), is given by¹

$$\sigma_{on} = \frac{4\pi a_o^2}{T/R} \left[z^2 \frac{f_{on}}{\Delta E/R} \ln\left(\frac{4T}{R}\right) + b_{on} + O\left(\frac{\Delta E}{T}\right) \right] \quad (1)$$

where a_o is the Bohr radius, R is the Rydberg energy (13.6eV), f_{on} is the optical oscillator strength of the target at $h\nu=\Delta E$, and b_{on} is a target property which is a function of ΔE alone. Roughly speaking, the first term in Eq. (1) is due to glancing collisions while the second results from knock-on collisions. Much use has been made of Eq. (1) recently in the modelling of electron ejection cross sections.^{2,3}

Lately, interest has risen in collisions where the incident ion of nuclear charge Z also contains N electrons. In this case the electron spectrum is more complicated owing to the extra possible channels: electrons can be ejected from the target with the projectile remaining in the ground state or with simultaneous projectile excitation, as well as, electron ejection from the projectile with the target either remaining in the ground state or excited. A Bethe-Born differential cross section was derived for each of these channels; total cross sections were treated previously.⁴ For target excitation with the projectile remaining in the ground state,

$$\sigma_{on} = \frac{4\pi a_o^2}{T/R} \left[(z-N)^2 \frac{f_{on}}{\Delta E/R} \ln\left(\frac{4T}{R}\right) + b_{on} + O\left(\frac{\Delta E}{T}\right) \right] \quad (2)$$

Note the $(z-N)^2$ of the leading term as compared to z^2 for bare incident particles. This shows that the projectile is fully screened by its electrons in glancing collisions, as we expect. The second term is far more complicated and depends upon both target and

projectile internal properties. For target ionization with simultaneous projectile excitation, the Bethe-Born cross section has no glancing term and the form of the second term differs from the "no excitation" case.

Electron ejection from the projectile can be treated in exactly the same way in the projectile frame. The projectile, however, "sees" a neutral particle so that, while Eq. (2) applies for electron ejection by the projectile with the target remaining in the ground state, the first term vanishes. Ejection with simultaneous target excitation is just like the target ionization case with the role of projectile and target reversed.

The detailed forms of each of these terms will be presented, along with the next term in the Bethe-Born expansion. Finally, a comparison of $He^+ + Ar$ experimental results and a semi-empirical model based on the Bethe-Born asymptotic cross section will be presented.

*Work supported by the U. S. Department of Energy Contract No. DE-AC06-76RL0-1830 and the U. S. Army Research Office Contract No. DAAG-29-83-K-0054.

References

1. M. Inokuti, Rev. Mod. Phys. **43**, 297 (1971).
2. J. H. Miller, L. H. Toburen, and S. T. Manson, Phys. Rev. A **27**, 1337 (1983).
3. W. E. Wilson, J. H. Miller, L. H. Toburen, and S. T. Manson, J. Chem. Phys. **80**, 5631 (1984).
4. G. H. Gillespie and M. Inokuti, Phys. Rev. A **22**, 2430 (1980) and references therein.

CALCULATIONS OF ELECTRON ENERGY DISTRIBUTION EJECTED IN ION-ATOM COLLISIONS BY PSEUDOSTATE METHOD

Takeshi Mukoyama,^{*} Chii-Dong Lin,⁺ and Wolfgang Fritsch[#]^{*} Institute for Chemical Research, Kyoto University, Kyoto 606 Japan⁺ Department of Physics, Kansas State University, Manhattan, Kansas 66506 USA[#] Hahn-Meitner-Institut für Kernforschung Berlin, D-1000 Berlin 39 West Germany

In ion-atom collisions the pseudostate method has achieved great success for calculations of K-shell ionization cross sections.¹⁻³ However, applications of this method are limited to the calculations for total ionization cross sections. In the present work, we have calculated the energy distributions of ejected electrons in ion-atom collisions by the use of pseudostates.

Using the Slater-type orbital (STO) as a basis function, we expand the atomic wave functions in terms of STO's and diagonalize the atomic Hamiltonian with this base set. The electron transition probabilities to continuum states are given by those to discrete states with positive energy eigenvalues; i.e. the pseudostates. The calculations of the transition probabilities are made within the framework of the semiclassical approximation (SCA), assuming the straight-line trajectory.

Following the method widely used in photoionization,⁴ the energy spectrum of ejected electrons at energy E , $\sigma(E)$, is obtained from

$$\sigma\left(\frac{E_i + E_{i+1}}{2}\right) = \frac{f(E_i) + f(E_{i+1})}{2(E_{i+1} - E_i)}, \quad (1)$$

where $f(E_i)$ is the transition probability of the electron to the pseudostate with energy E_i .

We have tested the present method for protons on hydrogen. The impact-parameter-dependent energy spectra for 25-, 100-, and 400-keV protons were calculated and transitions with $l = 0, 1$, and 2 were considered. As has been pointed out already,³ the precise form of the STO is not important and the results obtained with the different choice of the base sets lie on a smooth line.

Comparison of the present results with the SCA values with exact continuum wave functions shows that in low-energy region of the ejected electron spectra both values are in good agreement with each other, but at energies higher than about 40 eV the pseudostate method gives larger values than the SCA. This discrepancy at high energies comes from the fact that the continuum wave function in this energy region oscillates too rapidly to be represented as superposition of a few STO's.

In Fig. 1, we show the energy distribution of electrons integrated over all impact parameters for 30-keV protons on He. The calculations were made in the manner similar to the previous case for hydrogen, except that we used the Hartree-Fock-Slater potential⁵

in atomic Hamiltonian. The experimental values and the Born Hartree-Fock calculations of Rudd and Madison⁶ are also plotted in the figure. For low-energy electrons the present results agree with their experimental and theoretical values, but at high energies the pseudostate method overpredicts the experimental and the Born Hartree-Fock energy distributions.

In conclusion, we have shown that the pseudostate method can well represent the electron spectrum in low-energy region, but overpredicts at high energies. For practical applications, the pseudostate approach is quite adequate since the ionization cross sections are dominated in low-energy electron region.

References

1. A. L. Ford, E. Fitchard, and J. F. Reading, Phys. Rev. A **16**, 133 (1977).
2. R. Shakeshaft, Phys. Rev. A **18**, 1930 (1973).
3. W. Fritsch and C. D. Lin, Phys. Rev. A **27**, 3361 (1983).
4. R. F. Stewart, C. Laughlin, and G. A. Victor, Chem. Phys. Lett. **29**, 353 (1974).
5. F. Herman and S. Skillman, *Atomic Structure Calculations* (Prentice-Hall, Englewood Cliffs, N.J., 1963).
6. M. E. Rudd and D. H. Madison, Phys. Rev. A **14**, 128 (1976).

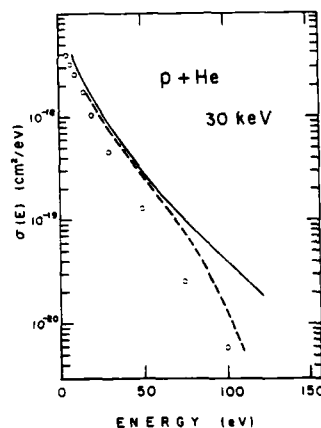


Fig. 1. Energy distribution of electrons ejected from helium atom by 30-keV protons. The solid curve represents the present results and the dashed curve indicates the Born Hartree-Fock calculations (Ref. 6). The circles are the experimental data taken from Ref. 6.

MOLECULAR-STATE CLOSE-COUPPLING THEORY INCLUDING CONTINUUM STATES:
III. DETAILED CONTINUUM SCATTERING AMPLITUDES

W. R. Thorson and G. Bandarage

Department of Chemistry, University of Alberta, Edmonton, Alberta CANADA T6G-2G2

Recently^{1,2} we have developed a theory of close-coupling in low/intermediate energy ion/atom collisions, based on molecular-state expansions and including electronic continuum channels. The continuum is represented by a discrete set of packet states which span it locally (in the interaction region), and are constructed from exact adiabatic continuum states. An essential feature of any such formulation is that effects of escape of the unbound electrons from the subspace spanned by the basis must be included in the equations for the close-coupled propagator. Using an approach similar to that used by Reading and Ford³ in a slightly different context, we have derived close-coupled integral equations for a propagator exhibiting these effects. This propagator is non-unitary, i.e. does not conserve probability: this is physically correct, since unbound electrons are continually escaping from the interaction region over times short compared to the duration of the collision. Previous formulations which claim to include the continuum (either by simple projection on packet states or by approximate numerical quadratures over continuum energies) give no account of these escape effects.^{4,5}

In formulation of these integral equations it is also necessary to construct an accurate subspace representation of the nonadiabatic couplings which cause transitions in a molecular state description. We have exhibited these matrix elements for couplings between continuum states. They are singular when the energies of the states coupled are degenerate. These singularities occur because an adiabatic description cannot possibly be appropriate for the full continuum: a distant unbound electron cannot really "follow" the nuclear motion adiabatically. However, we have proved that the effect of these singularities within the packet state basis is finite, and therefore an adiabatic close-coupling formalism is valid for describing continuum states in the interaction region---always provided that the effects of escape from this region are correctly included.

In the work reported here, we have formulated the theory of asymptotic continuum scattering amplitudes resulting from escape of unbound electrons from the close-coupled system described above. A state vector generated by the close-coupling propagator describes only the amplitudes of states localized in the interaction region. As is physically correct, such a state vector does not satisfy the time-dependent Schrodinger equation: the residual

term arises from the time-derivatives of the decaying continuum packet state amplitudes, i.e. the loss-rate due to escape. This term serves as an inhomogeneous source term for a separate propagator describing the time evolution of unbound electrons escaping from the system, that is, propagation outside the subspace described by the close-coupling propagator. This new propagator is not adiabatic in character, but "sudden": It generates scattering amplitudes at a detector, at a time $t \rightarrow \infty$, arising from sources at times t' during the collision, in terms of expansions in adiabatic continuum eigenstates for the system configuration at the source time, t' . The complete continuum scattering amplitude (for given electron orbital angular momentum (L,M) and energy ϵ , but integrated over angles) is then given by a coherent superposition of contributions arising at all times t' throughout the collision⁶.

In the present work we have used collisional ionization in the two-center one-electron systems (e.g., H^+ - $H(1s)$ impact ionization) as a prototype model for the theory. However, with certain restrictions the theory may be extended to treat collisional detachment of negative ions: the essential requirement is that the detaching state (or any other quasi-discrete levels embedded in the continuum) should be related adiabatically to the continuum, and that couplings linking it to the continuum be potential couplings of *finite range*.

References

1. W. R. Thorson (ms. submitted for publication, Phys. Rev. A).
2. W. R. Thorson and G. Bandarage (ms. submitted for publication, Phys. Rev. A).
3. J. F. Reading and A. L. Ford, J. Phys. B: Atom. Mol. Phys. **12**, 1367 (1979); J. F. Reading, A. L. Ford, G. L. Swafford and A. Fitchard, Phys. Rev. **A20**, 130 (1979).
4. D. A. Micha and R. D. Piacentini, Phys. Rev. **A25**, 204 (1982).
5. G. Soff, J. Reinhardt, B. Muller and W. Greiner, Zeits. f. Phys. **A294**, 137 (1980); G. Soff, W. Greiner, W. Betz and B. Muller, Phys. Rev. **A20**, 169 (1979); J. Reinhardt, B. Muller and W. Greiner, Phys. Rev. **A24**, 103 (1980).
6. A similar propagator is described in W. R. Thorson and H. Levy II, Phys. Rev. **181**, 232 (1969).

AUTOIONIZATION RESONANCE PROFILES IN ELECTRON EMISSION SPECTRA OF HELIUM PRODUCED BY FAST IONS

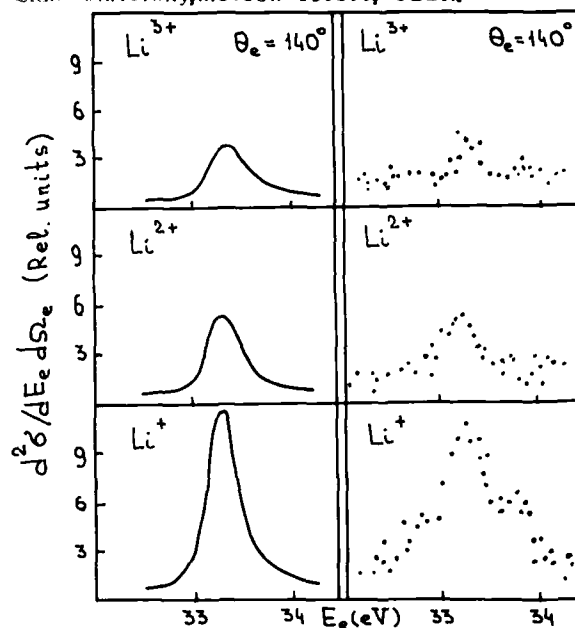
A.L. Godunov, V.S. Senashenko

Institute of Nuclear Physics, Moscow State University, Moscow 119899, USSR.

The problem of the electron emission spectra in the region of autoionization resonances attracts much attention in the ion-atom collision physics because the observed electron spectra contain rich information concerning the collision dynamics and the structure of colliding atomic systems. The theory of resonance ionization of atoms by heavy charged particles, taking into account final-state interactions^{1,2,3} has proved to be successful in explaining most of the experimental data on ionization of helium by protons.

The present work continues the theoretical study of the principal regularities in the behaviour of the autoionization resonance parameters of helium ionized by the nuclei with $Z > 1$ and by the H- and He-like ions of various ionization degree. The effect of the projectile charge and of the bound electrons on the target electron spectrum has been examined. At small ejection angles and a low relative velocity of a scattered heavy particle with respect to an ejected electron the behaviour of the resonance parameters is determined mainly, by the final-state interactions in both proton-atom and ion-atom collisions. At large ejection angles the resonance profiles are nearly symmetric and can be properly described by allowing for two-step transitions in the amplitude of autoionization state excitation. As the projectile charge increases the resonance intensity rises with respect to the background formed by direct transitions to continuum. Under the ionization of helium by the H- and He-like ions, the screening of the projectile nuclear charge has significant influence on the autoionization line profiles. At small ejection angles, for example the intensity of resonances increases with the projectile ionization degree, whereas with increasing the ejection angle the pattern reverses, namely, the resonances related to ions of lower ionization degree show a higher intensity.

Figure 1 illustrates the results of calculating the electron emission spectra of helium produced by 2200 keV lithium ions of various ionization degree. Experimental data of⁴ are also presented in the figure. The calculations seem to be in agreement with the observed behaviour of the electronic spectrum in the region of the lowest autoionization state of helium excited by the ionization collisions with



heavy charged particles.

References.

1. A.L. Godunov, V.S. Senashenko, Proc. of the All-Union Conf. on the Theory of Atoms and Atomic Spectra, Minsk, 1983, p.60.
2. A.L. Godunov, V.N. Mileev, V.S. Senashenko, Zh. T. Fiz., 53, 1898 (1983).
3. A.L. Godunov, V.S. Senashenko, Proc. IX All-Union Conf. on the Physics of Electronic and Atomic Collisions, Abstr. of Paper, Riga, 1984, p. 90.
4. D. Schneider, P. Arcuni, R. Bruch, W. Stöffer, Proc. XIII ICPEAC, Abstr. of Paper, Berlin, 1983, p.383.

He^{**} EXCITATION BY Li^+ IMPACT: A COINCIDENCE INVESTIGATION

P. van der Straten, P.M. Koenraad and R. Morgenstern

Fysisch Laboratorium, Rijksuniversiteit Utrecht, Princetonplein 5,
3584 CC Utrecht, The Netherlands.

We have investigated the excitation of He^{**} autoionizing states in $\text{Li}^+ + \text{He}$ collisions at collision energies between 1.4 and 3 keV by analyzing the ejected electrons in coincidence with the scattered Li^+ projectiles. For one thing this allows to clarify the reason for the large width¹ of the earlier measured non-coincident electron spectra, which in the past were ascribed to quasimolecular effects^{2,3}. Secondly this allows a detailed description of the excited He^{**} atom directly after the excitation in terms of complex population amplitudes for the various excited states. This yields information about the excitation mechanisms and the time-development of the excited electron cloud.

In fig. 1 one can see that the coincident electron energy spectra are much narrower than the non-coincident ones. They can quantitatively be explained without invoking quasimolecular effects as e.g. energy variations of the excited states as a function of internuclear distance or Doppler shifts of the emitted electron's energy corresponding to velocities of the quasimolecular system. Only the He^{**} recoil velocity and post collision interaction (PCI) in the field of the receding Li^+ ion have to be taken into account properly.

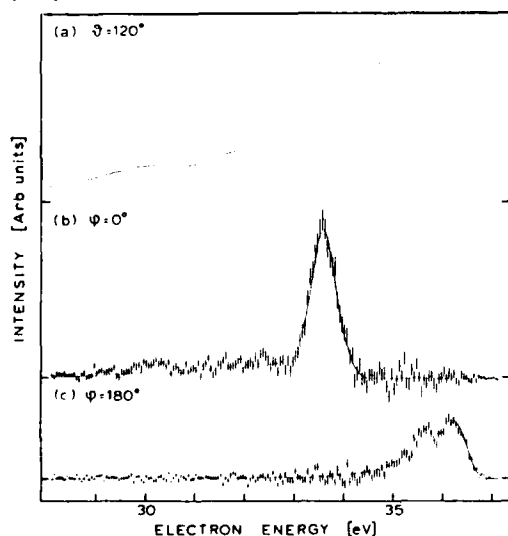


FIGURE 1 Energy spectra of electrons from 2 keV $\text{Li}^+ + \text{He}$ collisions measured at electron emission angles $\theta = 120^\circ$. Non-coincident spectrum (a) and spectra, measured in coincidence with Li^+ -ions scattered through $\theta_p = 10^\circ$ and azimuth angles of $\phi = 0^\circ$ (b) and $\phi = 180^\circ$ (c).

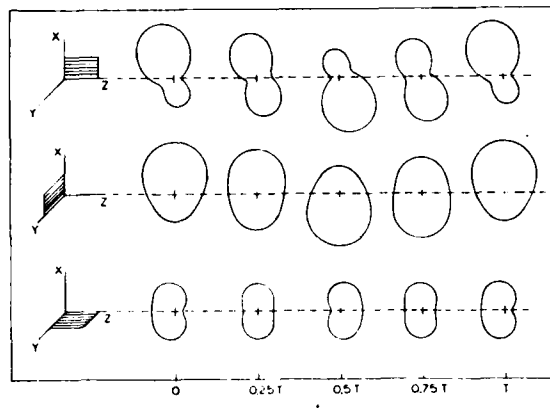


FIGURE 2 Charge density of the excited electron cloud in three different planes at different times after the collisions (z in the beam direction, y perpendicular to the scattering plane). The period T of the oscillations is ~ 800 a.u.

As opposed to $\text{He}^+ + \text{He}$ collisions, where mainly $\text{He}^{**}(2p^2)^1D$ is excited, Li^+ impact causes a considerable excitation also of $\text{He}^{**}(2s2p)^1P$ and $(2s^2)^1S$. The coherence between states of different parity causes asymmetries in the angular electron distributions. Analysis of the observed asymmetries allows in turn to determine the phases between autoionization amplitudes. After taking into account the relative phases of autoionization matrix elements - essentially the Coulomb phases of the emitted electron wave functions - this yields in turn the phases between the initial population amplitudes for the contributing states. With this knowledge one can reconstruct the charge density of the excited electron cloud immediately after the collision and its time dependence. An example is shown in fig. 2. One can see that the electron cloud is initially "attracted" by the Li^+ projectile. The connection between this macroscopic collective picture with the most important radial and rotational couplings will be discussed in terms of the $\text{Li}^+ - \text{He}$ correlation diagram.

References

- ¹P. van der Straten, P.M. Koenraad, R. Morgenstern, and A. Niehaus, *Z. Phys. A* **320**, 81 (1985).
- ²A. Yagishita in 'Electronic and Atomic Collisions', edited by J. Eichler, I.V. Hertel, N. Stolterfoht (Elsevier, 1984), p.253.
- ³C.J. Zwakhals, R. Morgenstern, and A. Niehaus, *Z. Phys. A* **307**, 41 (1982).

AN EXPERIMENTAL INVESTIGATION OF THE METASTABLE STATES OF BERYLLIUM ANIONS

T. J. Kvale,* G. D. Alton,* R. N. Compton,* D. J. Pegg,*† and J. S. Thompson†

*Oak Ridge National Laboratory, Oak Ridge, Tennessee 37831, U.S.A.

†The University of Tennessee, Knoxville, Tennessee 37916, U.S.A.

We report the first experimental measurements of the energy levels of the metastably bound states of Be^- . State and eigenenergy identifications were made by measuring the difference in energy between the collisionally induced and autodetaching peaks which appear in the ejected spectra from decaying Be^- ion beams. More detailed results of this investigation are to be published.

The Negative Ion Source Test Facility (NISTF), located at Oak Ridge National Laboratory, was modified in order to perform the Be^- state energy measurements. Be^+ ions were accelerated to 50- to 60-keV and were focused through a recirculating Li charge-exchange cell situated immediately prior to the experimental chamber. This arrangement permits the generation and study of relatively short lived ($\tau > 10^{-7}$) negative ion states. Detached electrons accompanying the Be^- ion beam were energy analyzed with a spherical sector energy analyzer operated in the fixed pass energy mode. (For details of the electron spectroscopy, see Ref. 1.)

A typical electron energy spectrum is shown in Fig. 1. This spectrum was obtained with ~ 2 mTorr in a gas cell preceding the electron energy analyzer in order to enhance the collisional detachment cusp electron signal. The peak corresponding to the autodetached electrons from Be^- occurred at a center-of-mass energy of 2.53 eV. The latest theoretical calculations predict the $\text{Be}^- (1s^2 2s 2p^2) ^4P$ state energy to be 2.56 eV above the ground state of Be. This value was derived from separate calculations of the total energies of the $\text{Be}^- (^4P)$ state² and the $\text{Be} (1s^2 2s^2) ^1S$ state.³ Due to the close proximity in energy, it is reasonable to conclude that we have determined the energy of $\text{Be}^- (1s^2 2s 2p^2) ^4P$. Lifetime measurements for the various J levels of this ion are in progress and will further serve to identify the state of this anion. If the theoretically predicted $\text{Be}^- (1s^2 2p^3) ^4S^0$ state does exist the allowed radiative decay channel to the $\text{Be}^- (^4P)$ state would most likely prohibit us from observing an autodetachment peak in the electron energy spectrum.

This research was supported in part by grants from the Office of Naval Research (ONR 393-071) and by the U.S. Department of Energy through The University of Tennessee (DE-AS05-83ER13097) and Postgraduate Research Training administered by the Oak Ridge Associated Universities. Oak Ridge National Laboratory is operated by Martin Marietta Energy Systems, Inc. with the U.S. Department of Energy under contract DE-AC05-84OR21400.

References

1. G. D. Alton, R. N. Compton, and D. J. Pegg, *Phys. Rev. A* **28** 1905 (1983).
2. D. R. Beck and C. A. Nicolaides, *Int. J. Quan. Chem.* **S18** 467 (1984).
3. C. F. Bunge, *Phys. Rev. A* **14** 1965 (1976).

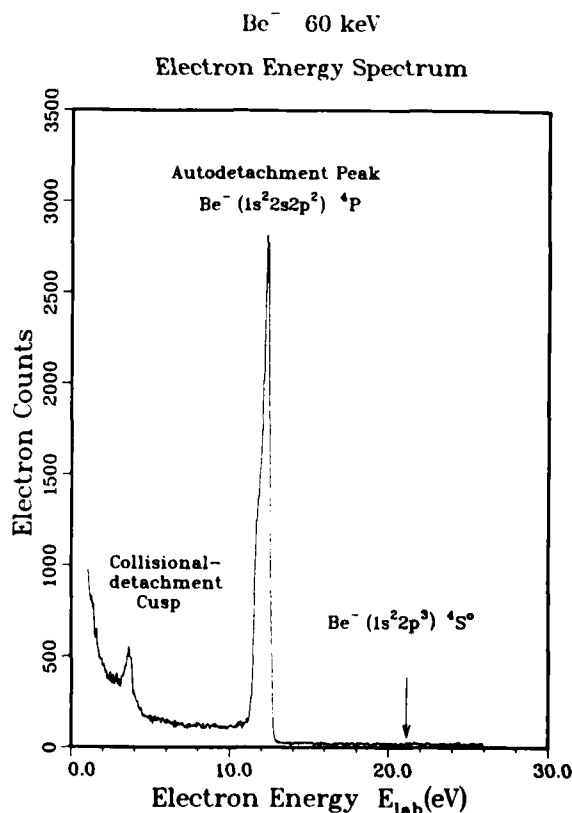


Fig. 1. A typical energy spectrum of electrons ejected from a 60 keV Be^- beam.

CALCULATION OF PROBABILITY OF AUTOIONIZATION IN LOCALLY EXCITED He AND Li⁺

J. P. Mohanty*, C. S. Singh and D. K. Rai

Department of Physics, Banaras Hindu University, Varanasi-221005, India
 *Department of Physics, F.M. College, Balasore, Orissa-756001, India

The effect of using distorted wave function for the continuum electron while calculating the probability of autoionization of $2s^2\ ^1S$, $2s2p\ ^1,^3P$, $2p^2\ ^1D$ and $2S^2\ ^1S$ states of He and Li⁺ has been studied. Separate calculations have been performed using distorted wavefunction (with and without exchange) and pure coulombic wavefunction for the continuum electron.

The calculation is based on the method suggested by Wu¹ using the formula given by Wentzel² from time independent perturbation theory. The radial equation of the distorted wavefunction of the continuum electron is solved by a non-iterative procedure of Harriot and Percival³, the normalization being obtained by comparison with the JWKB solution⁴.

From the comparison of our results among themselves and with other accurate theoretical results we infer the following two points:

- (i) The simple perturbation approach due to Wentzel is worth using to obtain the decay probability of the autoionizing states of atoms and ions where other accurate results are not available.
- (ii) In case of atoms distorted wavefunction with exchange must be used to represent the continuum electron.

References

1. T.Y. Wu, Phys. Rev. 66, 291 (1944).
2. W. Wentzel, Z. Phys. 43, 524 (1927).
3. R. Harriot, Proc. Phys. Soc. 72, 121(1958).
4. A. Burgess, Proc. Phys. Soc. 21, 442(1953).

CROSS SECTIONS FOR ELECTRON AUTOIONIZATION IN LOW ENERGY $\text{Li}^+ - \text{Ne}$ COLLISIONS

Y. Ikezaki, M. Katano, H. Ono, T. Takayanagi, K. Wakiya and H. Suzuki

Department of Physics, Sophia University, Kioicho 7-1, Chiyoda-ku, Tokyo 102 JAPAN

In the low energy Ion-Atom collision, the excitation mechanism described by quasimolecular effect is generally predominant. Doubly-excited autoionizing states in Ne are selectively excited by low energy Li^+ ion impact. In present work, the energy and angular distribution of the ejected electrons are measured and cross section for the autoionization is determined by simultaneous-collision technique¹⁾.

Ejected-electron spectra are measured in the impact energy range below 8 Kev and at observation angle from 10 deg. to 135 deg. with respect to the incident ion beam. Fig.(1) shows electron spectra at the observation angle 30 deg. for the impact energy 4 Kev. Assignments of autoionizing states in Ne are those of Andersen and Olsen²⁾. Cross sections for excitation of peak a, d, e, and f are determined by the following method. Electron spectrum is obtained by the simultaneous-collision technique, with 20 eV electrons. The spectrum gives a superposition of an elastic-scattering peak caused by e-Ne collisions and autoionization peaks caused by $\text{Li}^+ - \text{Ne}$ collisions. We denote the $\text{Li}^+ - \text{Ne}$ and electron-Ne cases by subscripts i and e, and we obtain a expression for cross section

$$\sigma_i = \frac{\sum_i I_i f_i(\theta_i)}{\sum_e I_e f_e(\theta_e)}$$

Where I_i is the elastic differential cross section for e-Ne scattering³⁾, S the area of the peak, I the current, and $f(\theta)$ represents the angular dependence of collision volume and we determined it from Kr MNN Auger spectrum⁴⁾.

Tentative results are shown in Fig.(2) and Fig.(3). Fig.(2) shows cross sections for excitation of lines a, e, and f. In Fig.(3) present results are compared with the data of P. Bisgaard et al.⁵⁾.

Fig(1) A typical ejected-electron spectrum at the observation angle 30 deg. for the impact energy 4 Kev.

Fig(2) Excitation cross section vs impact energies of Li^+ ion.

Fig(3) Sum of integrated cross sections for $2s^2 2p^4 n l n' l'$ states as a function of internuclear velocity. \circ - P. Bisgaard et al., \bullet - present.

References

- 1) A. Yagishita, K. Wakiya, T. Takayanagi, H. Suzuki, S. Ohtani and F. Koike, Phys. Rev. A22, 118 (1980)
- 2) N. Andersen and J. Østgaard Olsen, J. Phys. B10, L719 (1977)
- 3) J. F. Williams and A. Crowe, J. Phys. B8, 2233 (1975)
- 4) L. O. Werne, T. Bergmark and K. Siegbahn, Physica Scripta 6, 141 (1972)
- 5) P. Bisgaard, J. Østgaard Olsen and N. Andersen, J. Phys. B13, 1403 (1980)

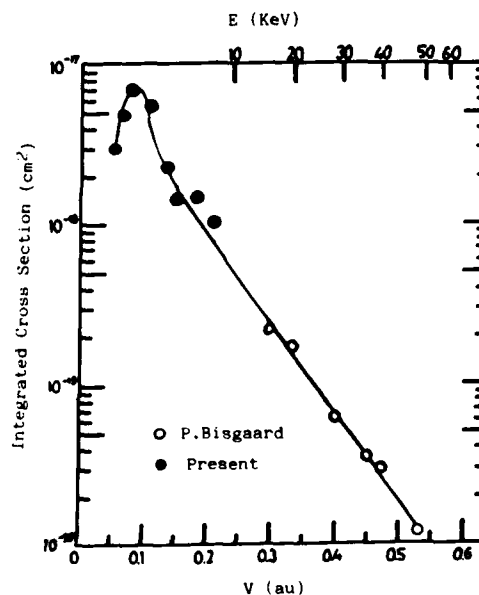
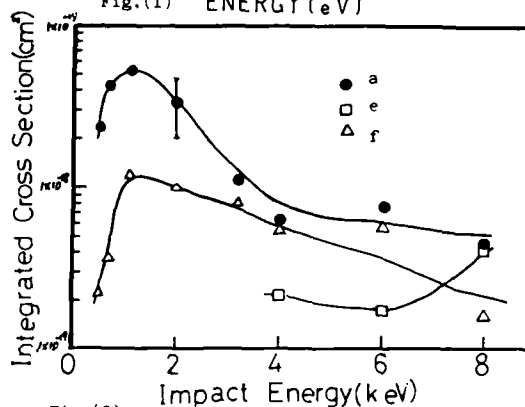
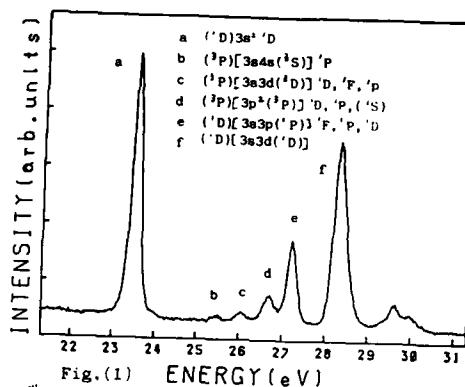


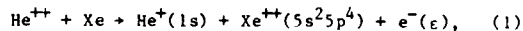
Fig. (3)

SPECIAL FEATURES OCCURRING IN DOUBLE DIFFERENTIAL CROSS SECTIONS
FOR TRANSFER IONIZATION COLLISIONS

A. Niehaus and A.G. Kuiper

Fysisch Laboratorium, Rijksuniversiteit Utrecht, Princetonplein 5,
3584 CC Utrecht, The Netherlands.

We consider the transfer ionization (TI) system



which has been studied earlier¹. In fig. 1 the relation between the energy of ejected electrons and the inelastic energy gain Q is shown in a potential curve model. It is seen that, in a (TI)-collision, a certain value of Q can be realized by transitions leading to different final Xe^{++} -states, and to the corresponding different electron energies. The double differential cross section $\Sigma(\theta, Q)$ therefore is an incoherent sum of partial cross sections $\sigma(\theta, Q)$. For cases such as the He^{++}/Xe -system, where the potential curves belonging to the different ion-states run approximately parallel, the dependence on Q will be approximately the same for all partial cross sections, so that the "shape" of $\Sigma(\theta, Q)$ will closely resemble the "shape" of the $\sigma(\theta, Q)$. In fig. 2 we show a series of normalized $\Sigma(\theta, Q)$ for a collision energy of $E_0 = 50$ eV. The spectra are measured by a parallel-plate electrostatic analyser with position sensitive detection allowing simultaneous measurement at different energies. As evident from fig. 1, each partial cross section contains contributions from four types of transitions: at the two crossings 1 and 2, and at each of the crossings "on the way in" or "on the way out". To these four types of transitions there correspond four branches of the classical deflection function (Q, b). In fig. 3 we show ($Q = 8$ eV, b) for $E_0 = 50$ eV, calculated numerically from adapted potentials V_i and V_f . The dominant feature of the spectra at low angles is the stationary peak at the high- Q edge. It is caused by coalescence of the crossings 1 and 2, and can be described by an Airy-function¹. The dominant feature at larger angles is a broad peak at the low Q -edge which shifts with observation angle. It is caused by transitions close to the turning point, where the "in"- and "out"-amplitudes become identical. Also this feature can be approximately described by an Airy-function in both energy scale², and angle variable. The corresponding rainbow angle θ_r is indicated in fig. 3. Further details of the observed spectra will be discussed, and approximate relations to the model quantities will be given.

References

- ¹A. Niehaus, Comments Atom. Mol. Phys. **9**, 153 (1980).
- ²A.Z. Devdariany, U.N. Ostroskii, and A. Niehaus, J. Phys. P **18** (1985) in press.

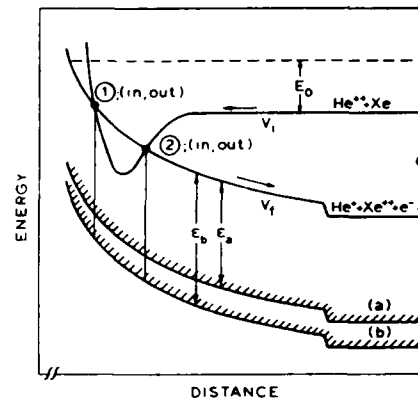


FIGURE 1

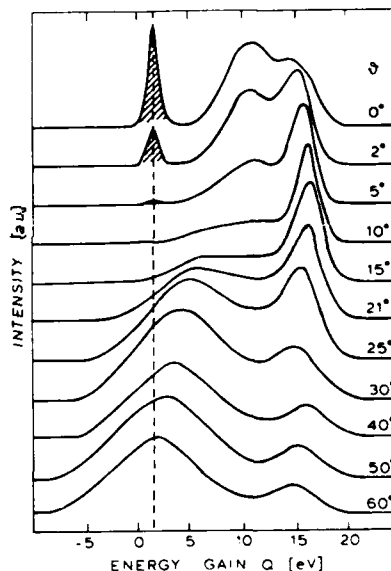


FIGURE 2

The shaded peaks belong to charge transfer.

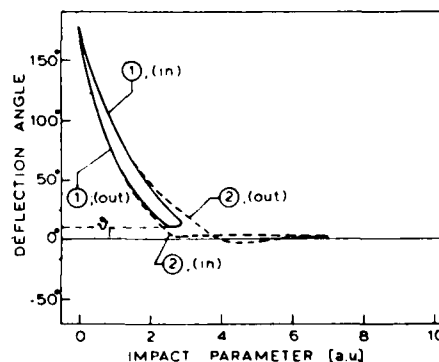


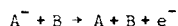
FIGURE 3

FURTHER DEVELOPMENT OF THE DYNAMICAL COMPLEX POTENTIAL THEORY OF ELECTRON DETACHMENT

M. L. Du, S. E. Haywood and J. B. Delos

Physics Department, College of William and Mary, Williamsburg, Virginia 23185

In earlier work¹ we have developed a theory of electron detachment in collisions of negative ions with atoms



This theory is now being extended in the following ways.

(1) The energy spectrum of detached electrons is being calculated. (2) Calculations of total cross sections for electron detachment are being extended over a large energy range. (3) A theory of associative detachment is being developed.

The theory is based upon a semiclassical close-coupling model in a "diabatic" representation. Let $\psi_b(r;t)$ represent a state in which the active electron is bound to (AB) and let $\{\phi_e(r;t)\}$ be a set of states in which it is free, with asymptotic kinetic energy ϵ . Expansion of the full wave function in such a basis,

$$\Psi(r,t) = c_b(t)\phi_b(r;t) + \int_0^\infty c_e(t)\phi_e(r;t)\rho(\epsilon)d\epsilon$$

leads to a set of coupled differential equations for the coefficients. Defining

$$\mathcal{E}(t) = i\hbar \frac{d}{dt} \ln[c_b(t)]$$

the quantity $\mathcal{E}(t)$ plays the role of a dynamical complex potential. It obeys an integral equation which is easy to solve by iteration, and a typical result is shown in Fig. 1.

Presently we have calculations of electron-energy-spectra for model systems. For a case in which the energy gap between the bound and free states $\Delta(t)$ varies quadratically with time, $\Delta(t) = E_0 - Bt^2$, then a representative electron-energy-spectrum is shown in Fig. 2.

1. T. C. Wang and J. B. Delos, Phys. Rev. A **29**, 542, 552 (1984); J. Chem. Phys. **79**, 4306 (1983); R. D. Taylor and J. B. Delos, Proc. Roy. Soc. (London) A **37a**, 179, 209 (1982).

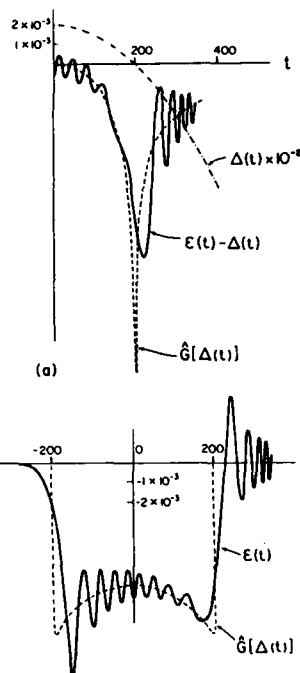


FIG. 1. (a) Comparison of static and dynamical complex potentials. Here we show the real part for $t > 0$. Dotted-dashed line is the energy gap between the discrete state and the continuum, $\Delta(t) \times 10^{-3}$. Dashed line is $\text{Re}[\mathcal{E}(t)] \equiv \text{Re}[F_1(t)]$, part of the static or local complex potential. Solid line is $\text{Re}[\mathcal{E}(t) - \Delta(t)] \equiv \text{Re}[F_2(t)]$, the corresponding part of the dynamical complex potential. (b) As in (a), but here is the imaginary part.

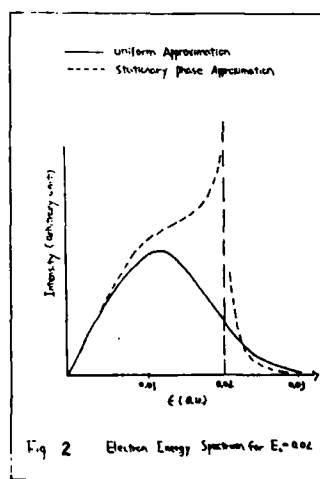


Fig. 2 Electron Energy Spectrum for $E_0 = 0.02$

COLLISIONAL ELECTRON DETACHMENT OF ALKALI ANIONS

D. Scott, M. S. Haq, R. L. Champion, and L. D. Doverspike

Department of Physics, College of William and Mary, Williamsburg, Virginia 23185 USA

Absolute total cross sections for electron detachment have been measured for collisions of Na^- and K^- with rare gases at relative collision energies ranging from a few eV to about 200 eV. These alkali anions, which are characterized by angularly-correlated s-electrons, are observed to be extremely stable with respect to collisional electron detachment. Figure 1 gives the total electron detachment cross sections, $\sigma_e(E)$, for collisions of K^- with Ar and Ne, as a function of relative collision energy. The remarkable feature of these measurements is that K^- , with its small electron affinity (EA), is extremely stable against collisional detachment for relative collision energies up to about eighty times the EA of potassium. At 35 eV, $\sigma_e(E)$ for K^- -Ar is a factor of approximately 160 times smaller than that for H^- -Ar. Similar results have been observed for collisions of Na^- -He and K^- -Kr, Xe systems. These small cross sections are presumably due to an ability of the M^- -X (where $\text{M}^- \equiv \text{Na}^-, \text{K}^-$; $\text{X} = \text{Ne}, \text{Ar}, \text{Kr}, \text{Xe}$) electronic wave function to adjust adiabatically during the collision, causing the electronic energy of M^- -X to remain below that of $\text{M}+\text{X}$ down to relatively small internuclear separations.

The above features can be described by a curve crossing model. Figure 2 shows a schematic diagram of the potential energies of various states of the reactants and products which are relevant to the K^- -Ar collision. If the incoming K^- -Ar state remains approximately parallel to and slightly below the X^0Z^+ continuum of $\text{K}+\text{Ar}+\text{e}$, then the detachment probability will remain small, until the crossing A is reached.

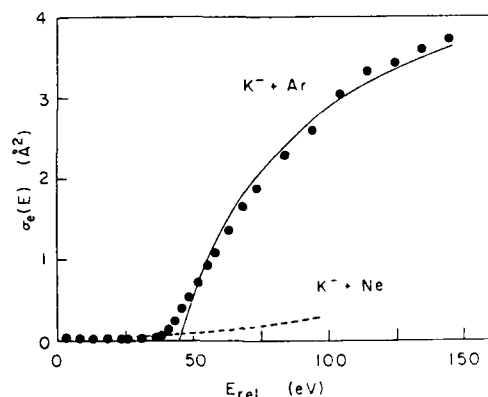


Fig. 1 Total cross sections for electron detachment.

Within this curve-crossing formalism, a simple model is used to describe the observed $\sigma_e(E)$. In this model, it is assumed that the probability for detachment is zero for impact parameters $b > b_x$ and is unity for $b < b_x$, where b_x is the impact parameter for which the classical turning point of the nuclear motion is R_x . The total cross section for electron detachment is then given by

$$\sigma_e(E) = \pi R_x^2 (1 - V_x/E) \quad \text{for } E > V_x$$

where V_x is the threshold energy for detachment as indicated in Fig. 2. A two-parameter fit was made to $\sigma_e(E)$, and the best fit (with $V_x = 45.6$ eV and $R_x = 2.5 a_0$) is shown as a solid line in Fig. 1. The success of this simple model suggests that the detachment probability at the crossing is large and may approach unity.

Measurements of $\sigma_e(E)$ for Na^- -He, Ar, Kr, Xe and K^- -He, Ne exhibit no distinct onsets for detachment and remain small ($< 0.5 \text{ \AA}^2$) throughout the energy range studied, indicating the absence of a curve crossing in this energy range. Striking similarities are observed between the energy dependence of $\sigma_e(E)$ for all the systems reported here and that of the cross sections for projectile excitation which result from corresponding neutral alkali-rare gas collisions.

Total cross sections for electron detachment and heavy ion production for collisions of Na^- and K^- with various molecular targets have been completed and will also be presented.

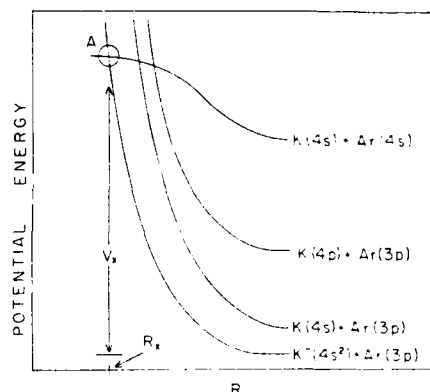


Fig. 2 Schematic diagram of potential energy curves for the K^- -Ar collision. The vertical axis is potential energy and the horizontal axis is internuclear distance.

THEORY OF ELECTRON DETACHMENT IN SLOW NEGATIVE IONS IMPACT ON ATOMS,
APPLICATION TO $H^- + He \rightarrow H + He + e$

Fumihiro Koike

School of Medicine, Kitasato University, Sagami-hara, Kanagawa 228, Japan

A new method was proposed^{1,2} for solving the time-dependent semiclassical Schrodinger-equations including the couplings between a discrete state and continuum states. In the present paper, this formalism is applied to the following process:



The result of CI calculation by Olson and Liu³ has been adopted for the internuclear electrostatic potential energies $U_i(R)$ for H^-+He and $U_n(R)$ for $H+He$, where R is the internuclear distance. For the coupling matrix element at R between the discrete H^-+He state and the continuum $H+He+e$ state with a free-electronic kinetic energy ϵ , $V(\epsilon, R)$, the following has been adopted:

$$V(\epsilon, R) = (M_p + i v_R M_d) \exp(-\frac{R}{R_c}) \epsilon^{1/4} \exp(-\frac{\epsilon}{\epsilon_c}), \quad (2)$$

where the first term including M_p represents the electrostatic (potential) coupling and the second represents the radial coupling, and v_R is the internuclear radial velocity. The quantities M_p , M_d , R_c , and ϵ_c are the parameters, which have been determined empirically.

Due to the coupling with the continuum, the ionic state shifts in energy from the original position U_i and obtain a "resonance energy" U_r that may be a complex number. The pole of the ionic-space Green's function gives U_r , i.e., it satisfies

$$U_r - U_i - \int_{U_n}^{\infty} \frac{V V^*}{E' - U_r} dE' = 0. \quad (3)$$

Because U_r depends on both v_R and R , eq.(3) has been solved numerically at a number of time points for each impact parameter and collision energy.

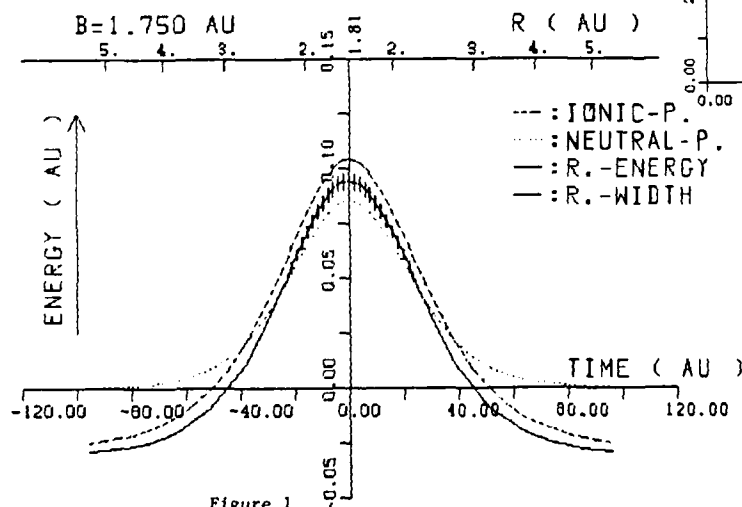


Figure 1

Figure 1 shows the result for the case that the impact parameter is 1.75au and the center-of-mass collision energy is 2 au. We find from this figure that the radius from which U_r starts to have an imaginary part, which is illustrated by vertical bars, is not the radius of the crossing between U_i and U_n but that between the real part of U_r and U_n .

The detachment probability evaluated in the lowest order, $P_d^{(0)}$, is given by

$$P_d^{(0)} = 1 - \exp[2 \int_{-\infty}^{\infty} \text{imaginary part of } U_r \cdot dt], \quad (4)$$

where t is the time, and the detachment probability including the first order correction, $P_d^{(1)}$, is given by

$$P_d^{(1)} = \int_0^{\infty} d\epsilon \left| \int_{-\infty}^{\infty} V^* \exp[-i \int_{-\infty}^t (\epsilon + U_n - U_r) dt'] dt \right|^2. \quad (5)$$

Figure 2 shows the neutralization cross sections DCS0 and DCS1, which are obtained by multiplying the elastic scattering cross sections to $P_d^{(0)}$ and $P_d^{(1)}$, respectively. The sharp rise in DCS1 at the forward angles is consistent with the experimental result by Hege et al.⁴

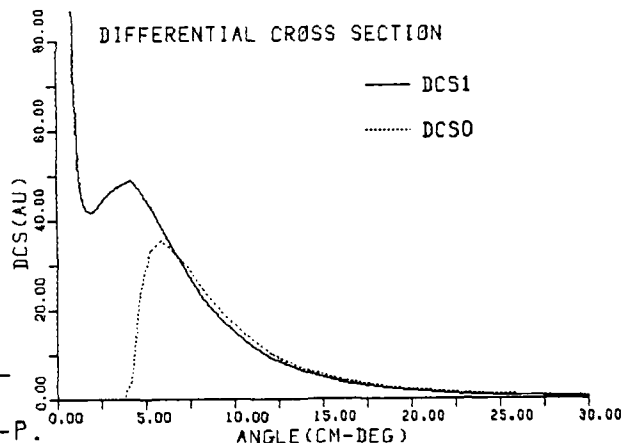


Figure 2

References

1. F.Koike, XIII ICPEAC Book of Abstracts, 405 (1983)
2. F.Koike, XIII ICPEAC Book of Abstracts, 571 (1983)
3. R.E.Olson and B.Liu, Phys. Rev. A22, 1389(1980)
4. U.Hege, Y.Itoh, and F.Linder, XIII ICPEAC Book of Abstracts 398(1983)

ELECTRON DETACHMENT OF H^- IN THE LABORATORY FORWARD DIRECTION

M. G. Menendez, C. R. Mauldin, M. M. Duncan and J. L. Hopkins

Department of Physics and Astronomy, University of Georgia, Athens, GA 30602

Collisionally induced electron loss of H^- occurs via the two general processes of single electron loss (SEL) and double electron loss (DEL). We shall refer to the double differential cross section (DDCS) measured without process selection as the combined-DDCS and, accordingly, refer to the DDCS measured with process selection as SEL-DDCS and DEL-DDCS. Previous measurements of the combined-DDCS for electron detachment of H^- upon collisions with He and other targets at ion energies from 0.15 MeV/amu to 0.7 MeV/amu and comparisons with theoretical calculations have established the importance of target excitations.¹ Recent measurements and preliminary calculations of the DDCS further suggest that excitation of the projectile in the final state might be manifest in the combined-DDCS.^{2,3} These results can be summarized as follows:

- (1) the combined-DDCS is composed of two components;
 - (a) a target-dependent, double peaked structure due to the interference between $\ell = 0$ and $\ell > 0$ partial waves of electrons ejected via the SEL process, and
 - (b) a sharp peak centered about the electron energy equivalent to the velocity of the incident ion
- (2) on the basis of process selective measurements⁴ of SEL-DDCS and DEL-DDCS both components of the combined-DDCS are attributable to the SEL process which dominates over the DEL process⁵
- (3) the sharp peak displays forward-backward symmetry in the projectile rest frame
- (4) the sharp peak has been tentatively assigned to SEL events which leave the H atom in excited states.

Since the assignment of the sharp peak is only tentative and because there is interest in including final state H atom excitations in the theoretical calculations^{3,6} we have measured the angular distribution of this peak in detail. The sharp peak from 0.5 MeV H^- collisions with He was extracted from the combined-DDCS in the manner previously described.²

The angular distribution of the sharp peak was measured in the range $0^\circ \leq \theta_{lab} \leq 2.6^\circ$ in steps of 0.1° from $\theta_{lab} = 0^\circ$ to $\theta_{lab} = 0.6^\circ$ and in steps of about 0.2° for $\theta_{lab} > 0.6^\circ$. These data were transformed to the projectile frame and account was taken of the finite energy and angular resolutions. The data in the projectile frame show that electrons in the range 0 to 0.1 eV provide the main contribution to the sharp peak and that these electrons are essentially isotropically distributed.

This work was supported by AFOSR Grant No. 83-0264.

References

1. J. Macek, M. G. Menendez and M. M. Duncan, Phys. Rev. A29, 516 (1984)
2. M. M. Duncan, M. G. Menendez and J. L. Hopkins, Phys. Rev. A30, 655 (1984)
3. L. A. Wright, T. C. Genoni and M. R. Franz, Bull. Am. Phys. Soc. 28, 797 (1983)
4. The experimental configuration used for these measurements is described in M. M. Duncan, J. L. Hopkins, and M. G. Menendez, Nuclear Instruments and Methods in Physics Research (May 1985)
5. For further details on the DEL-DDCS see M. M. Duncan, M. G. Menendez, J. L. Hopkins and C. R. Mauldin, contributed paper, this conference
6. A. Starace, private communication

PROCESS SELECTIVE EXPERIMENTS: THE DOUBLE ELECTRON LOSS OF H^- IN COLLISIONS WITH HE

M. M. Duncan, M. G. Menendez, J. L. Hopkins and C. R. Mauldin

Department of Physics and Astronomy, University of Georgia, Athens, GA 30602

We have measured at $\theta_{lab} = 0^\circ$ electrons which were time correlated with protons produced by double electron loss of H^- in collisions with He at an ion energy of 0.5 MeV. The experimental configuration which provides access to the final charge states H^- , H and H^+ as well as to the electrons is described elsewhere.¹ In order to increase the electron count rate our best energy and angular resolutions were not used; for these measurements $\Delta E/E = 0.016$ FWHM and $\Delta\theta = \pm 0.9^\circ$. The signal-to-noise ratio (that is, the ratio of correlated events to uncorrelated events) as measured from the output of the time-to-amplitude converter was about 2. The electron energy spectrum obtained by requiring a specific time correlation contains true as well as accidental events. Thus the appropriate uncorrelated (accidental) spectrum, obtained simultaneously with the above spectrum, was subtracted from the above spectrum in order to obtain the "true" correlated spectrum.

The $(e-H^+)$ - correlated electron energy spectrum at $\theta_{lab} = 0^\circ$ shows: (1) a peak at an energy of 272 eV, the energy of an electron moving with the same velocity as the incident ion; (2) no evidence of the double-peaked structure seen in the uncorrelated electron spectra from H^- collisions with He and other targets² and in the $(e-H)$ - correlated electron energy spectra;³ (3) a forward (0° in the projectile frame) - backward (180° in the projectile frame) asymmetry which persists after the finite resolutions of the detection system were taken into account. The interpretation of this asymmetry is that the electron ejection in the projectile frame has an angular distribution involving an odd power of $\cos\theta$, perhaps $\cos\theta$ itself.

This work was supported by AFOSR Grant No. 83-0264.

References

1. M. M. Duncan, J. L. Hopkins and M. G. Menendez, Nuclear Instruments and Methods in Physics Research (May 1985)
2. J. Macek, M. G. Menendez and M. M. Duncan, Phys. Rev. A29, 516 (1984)
3. For further details see M. G. Menendez, C. R. Mauldin, M. M. Duncan and J. L. Hopkins, contributed paper, this conference

UNITED ATOM ROTATIONAL COUPLING IN $H^+ + He$ COLLISIONS

Chiling Wang and Joseph Macek

Behlen Laboratory of Physics, The University of Nebraska,
Lincoln, NE 68588-0111 USA

For highly asymmetric collisions it is necessary to supplement the $2p\sigma \rightarrow 2p\pi$ rotational coupling equations to incorporate transitions to the $2s\sigma$ state near the united atom limit. The avoided crossing of the $2s\sigma \rightarrow 2p\sigma$ is usually treated diabatically¹ for nearly symmetric collisions. We have made three state calculations to test this prescription for highly asymmetric systems using the $H^+ + He$ system as a prototype. Molecular energy levels and coupling matrix elements calculated by Green and co-workers² were used as input data for the three-state dynamical calculations.

The probability vs. impact parameter for transitions from the 2σ to the 3σ adiabatic molecular state near the united atom limit is shown in Fig. (1) for relative velocities of 0.2 and 0.5 atomic units. The large and nearly energy independent peak in the probability near $b=0.5$ au. represents a marked departure from diabaticity for this system.

The small, but non-negligible and energy dependent, probability at large b is due to indirect $2\sigma \rightarrow 1\pi \rightarrow 3\sigma$ rotational coupling. The energy dependence of this component reflects the energy dependence of the dominant $2\sigma \rightarrow 1\pi$ rotational transition. The indirect or two step coupling occurs because the $2\sigma \rightarrow 3\sigma$ crossing is not completely diabatic. The mixing angle $\alpha(R)$ of Taulbjerg and Briggs¹ is found to equal -1.365 rather than $-\pi/2$ at large R . As a consequence both the 2σ and 3σ states couple to the 1π state, and the 3σ state takes some of the intensity that goes to the 2σ state in a purely diabatic treatment.

Support for this research by the National Science Foundation under grant number 8203400 is gratefully acknowledged.

References

1. K. Taulbjerg and J. S. Briggs, J. Phys. B 8, 1895 (1975).
2. T. A. Green, J. C. Browne, H. H. Michels, and M. M. Madsen, J. Chem. Phys. 1, 5198 (1974).

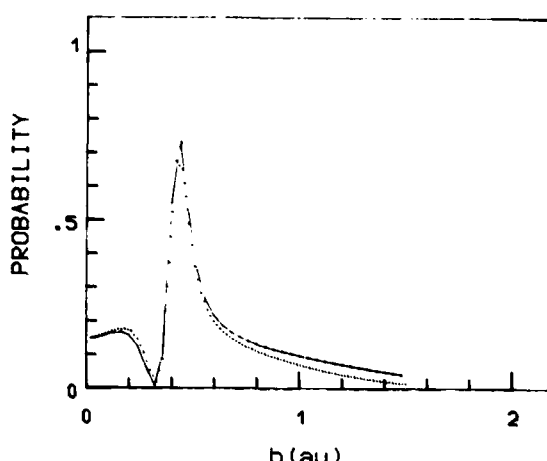


FIGURE 1 Probability as a function of impact parameter b for a $2\sigma \rightarrow 3\sigma$ transition near the united atom limit. The solid curve corresponds to a relative velocity of 0.5 au and the dotted curve to a velocity of 0.2 au.

PRODUCTION AND DECAY OF 2p VACANCIES IN
LOW-ENERGY Ar IONS STOPPING IN Mg

Sam J. Cipolla and Larry Hicks

Physics Department, Creighton University, Omaha, Nebraska 68178 USA

The 2p vacancy production cross section σ_{2p} was measured for 200–380 keV Ar^{2+} ions stopping in thick Mg targets. The cross sections were obtained from analysis of the Ar L x-ray yields measured with a thin-window gas-flow proportional counter. The product of the counter efficiency and the 2p fluorescence yield was obtained by normalizing our results to the Ar-Si 2p vacancy production cross sections measured by Schneider, et al.¹ after they were scaled to Ar-Mg using the Kessel model. Our results are consistent with the $3d\sigma-3d\pi-3d\delta$ rotational coupling as the cause of 2p electron promotion into unoccupied molecular orbitals in the Ar-Mg collision quasimolecule.

Combined with our previous measurements⁴ of the total Mg K-vacancy production cross section σ_K in these collisions, information was obtained on the projectile energy dependence of the Ar 2p-vacancy lifetime τ and the collisional quenching cross section σ_q . From the rate equations for the fraction of Ar projectiles that possess a 2p vacancy while traveling through a solid, the equilibrium fraction f_{eq} is found to be,

$$f_{eq} = \sigma_{2p} / (\sigma_{2p} + 1/Nv\tau + \sigma_q) \quad (1)$$

where N is the target atom density and v is the incident speed of the Ar projectile. We have calculated f_{eq} for different incident Ar energies E from the Ar-Mg vacancy transfer cross section σ_K :

$$\sigma_K = (1/3) f_{eq} \sigma_{rot} \quad (2)$$

where σ_{rot} is the theoretical $2p\sigma-2p\pi$ rotational coupling cross section.³ Equations (1) and (2) were used to determine τ as a function of E , assuming no quenching ($\sigma_q = 0$), and also to determine σ_q as a function of E assuming τ is equal to the constant free-atom value of 4×10^{-15} s for Ar possessing a single 2p vacancy.

The results indicate that σ_q is negligible compared with the spontaneous decay cross section $1/Nv\tau$. This conclusion is in agreement with the experimental results of Garcia, et al.⁴ for Ar traveling in carbon.

The figure gives the results for τ vs E in these experiments. Errors for each measurement were on the order of 10–20%.

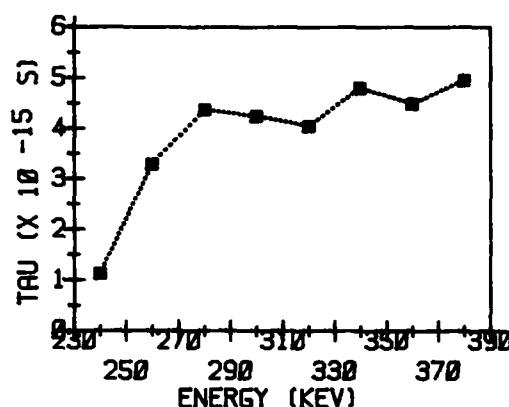


FIGURE 1. The Ar 2p-vacancy lifetime τ as a function of projectile energy for Ar traveling in and stopping in Mg.

References

1. D. Schneider, G. Nolte, U. Wille, and N. Stolterfoht, Phys. Rev. A **28**, 161 (1983).
2. S. J. Cipolla and M. E. Mildebrath, Nucl. Instr. Meth. Phys. Res. **218**, 777 (1983).
3. K. Taulbjerg, J. S. Briggs, and J. Vaaben, J. Phys. B **9**, 1351 (1976).
4. J. D. Garcia, R. J. Fortner, H. C. Werner, D. Schneider, N. Stolterfoht, and D. Ridders, Phys. Rev. A **22**, 1884 (1980).

L-SHELL EXCITATION IN FAST COLLISIONS OF $\text{Ne}^+-\text{Ne}^{\S}$

H.J. Hoffmann, U. Lais and R. Brenn

Fakultät für Physik, Universität Freiburg, Hermann-Herder-Str. 3, 7800 Freiburg, FRG

Inner shell excitation is well understood in the limiting cases of the quasimolecular model (slow, symmetric or level matching collisions) or direct Coulomb excitation in perturbative treatment (fast, asymmetric collisions). The transition region between both models or the corresponding outer shell processes are however much less tested experimentally or studied theoretically.

The present experiments extend our earlier work¹ on K-shell excitation in $\text{Ne}^{n+}-\text{Ne}$ collisions to (single and double) 2s-shell excitation processes and extend similar data by Hippler and Schartner² and Beyer et al.³ to higher velocities, well into the transition region between both models. The aim is to test the range of validity of MO calculations for these systems, e.g. by Albat et al.⁴ and Fritsch and Wille⁵.

Excitation cross sections for the production of several excited states in NeII and NeIII with one or two 2s shell vacancies in 1 to 4.5 MeV Ne^+-Ne collisions were studied by measuring the UV emission between 38 and 53 nm with a novel grazing incidence spectrometer. The instrument utilizes high precision x-y-translational stages driven by stepping motors under computer control and incremental measuring devices for a high precision absolute position readout of the optical elements to move the exit slit with the channeltron multiplier on a calculated or computer optimized focal curve.

The spectrometer can be positioned at angles between 0° and 150° to the beam direction, offering the possibility to measure UV angular distributions in order to study alignment processes or to Doppler separate projectile from target emission lines in symmetric collision systems. An instrument with these facilities has, to our knowledge, not been available in fast ion-atom collision experiments although one instrument with computer calculated and controlled scan path has recently been described in the literature⁶.

In fig. 1, the UV emission from the decay of the $(1s^2 2s 2p^5)^3P^0$, $J=0,1,2$ multiplet, separated for projectile and target, is shown for 3 MeV Ne^+-Ne collisions. The resolution of 0.04 nm, obtained in first order for a gold coated 600 1/mm grating of 2.2 m radius at 83.22° grazing angle with the spectrometer positioned at 120° to the beam direction, is limited by the 40 μm entrance and exit slit widths. The difference between target and projectile line intensities is in contrast to the predictions of the MO model and shows its breakdown for

these velocities.

By normalizing our cross sections to the 1 MeV values by Beyer et al.³ we extract absolute cross sections for the production of the $(2s 2p^5)^1P_1, ^3P_{0,1,2}$ and $(2s 2p^6)^1S_0$ excited states in NeII and NeIII, separately for projectile and target. Their velocity dependences are found to deviate from predictions of available model calculations.

References

1. K. Holzer and R. Brenn, Progress Report "Energie-reiche Atomare Stöße", EAS-1,24 (1980) J. Eichler, B. Fricke, R. Hippler, D. Kolb, H.O. Lutz, P. Mokler eds.
2. R. Hippler and K.-H. Schartner, J.Phys. B8, 2528 (1975)
3. H.-F. Beyer, R. Hippler and K.-H. Schartner, Z.Physik 292, 353 (1979)
4. R. Albat, N. Gruen, B. Wirsam, J.Phys. B8, 2520 (1975)
5. W. Fritsch and U. Wille, J.Phys. B11, 4019 (1978)
6. E. Gilberg, M.J. Hanus and B. Foltz, Rev.Sci.Instr. 52, 662 (1981)

The authors acknowledge the assistance of D. Charalambidis, H. Götz, W. Haas, K.J. Koulen and J. Schmäzlin in the experiments.

[§]Supported in part by Deutsche Forschungsgemeinschaft

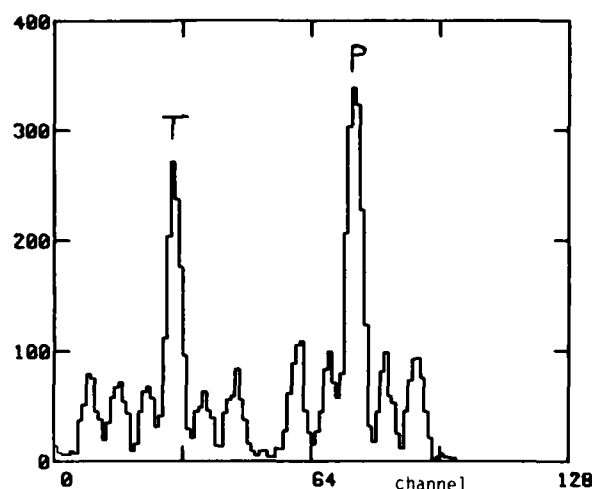


Figure 1 Decay of the $(2s 2p^5)^3P^0$ multiplet; the spectral range is 48.65 to 49.65 nm. P: Group of Doppler shifted projectile lines; T: Target lines

VELOCITY DEPENDENCE OF QUASIMOLECULAR AUGER EMISSION IN Kr-Kr COLLISIONS

A. P. Shergin^{*}, R. Bilau, R. Stötzl, H. O. LutzFakultät für Physik, Universität Bielefeld, 4800 Bielefeld 1, FRG
A. F. Ioffe Physicotechnical Institute, Leningrad, USSR

Electronic processes in slow atomic collisions are determined by the electron orbitals evolving in the transiently formed molecule. The spectroscopy of collisionally emitted continuum electrons has been used as a tool to study these quasimolecular (MO) states.¹ An interesting feature of this electron emission has been seen by Liesen et al.² who observed oscillation-like structures in the MO Auger spectrum. They were attributed to the interference of decay amplitudes along the incoming and outgoing parts of individual collision trajectories.

In the work to be reported here we have studied the continuum electron emission in 150 keV and 450 keV Kr-Kr collisions. Electrons were energy analyzed (energy E_e) in an electrostatic spectrometer perpendicular to the primary ion beam direction. They were detected in coincidence with Kr ions scattered through 15° after interaction with a dilute Kr gas target.

The results are shown in Fig. 1. No oscillations have been found in the coincident MO Auger spectra although we tried to closely reproduce the experimental conditions of ref. 2. The spectra can be decomposed into an exponential component and a broad maximum. The behaviour of the exponential component (broken lines) with ion energy indicates the increasing significance of direct transitions to the continuum with increasing ion energy.³ Writing the exponent as $(-aE_e/Mv_0)$ with v_0 the collision velocity, the value $a = 0.14$ a.u. gives good agreement with experiment between 50 and 450 keV ion energy. The broad maximum has previously been associated with MO Auger emission¹ and provides information on collision broadening Γ and MO level energy. For example, Γ is found to scale with $v_0^{2/3}$ in agreement with previous work.¹

This work has been supported by the Deutsche Forschungsgemeinschaft.

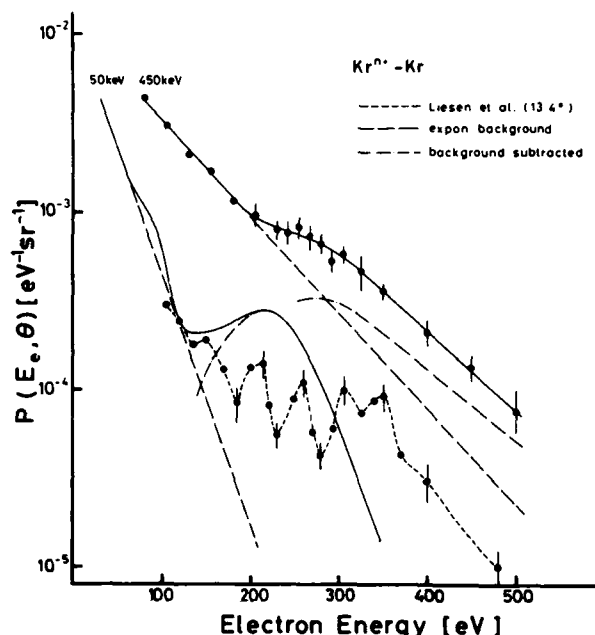


Fig. 1: Electron spectra coincident with ions scattered through 15° . 50 keV data from ref. 1, Liesen et al. from ref. 2; 450 keV \diamond present data ($n=2, 4$).

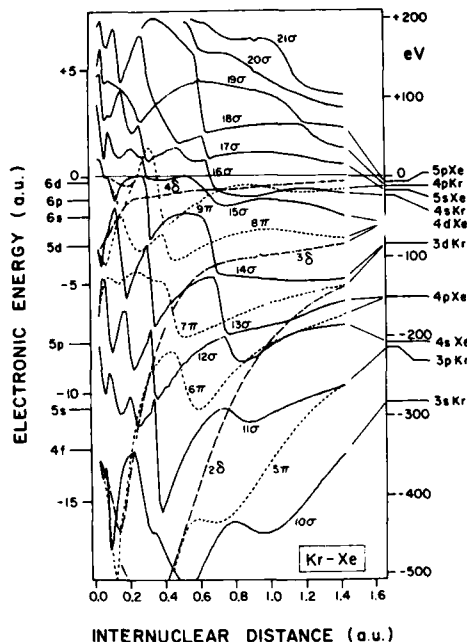
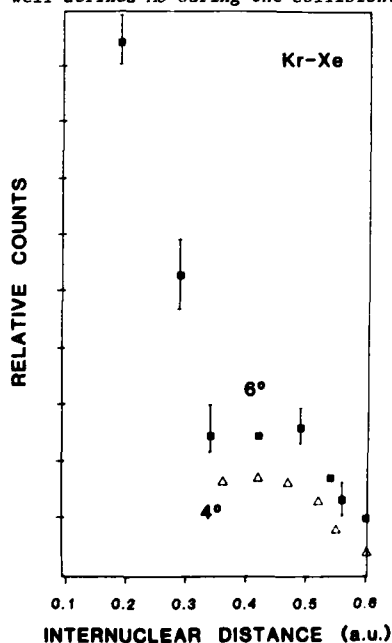
- 1 V. V. Afrosimov, G. G. Meshki, N. N. Tsarev, and A. P. Shergin, Zh. Eksp. Teor. Fiz. **84**, 454 (1983).
- 2 D. Liesen, A. N. Zinoviev, and F. W. Saris, Phys. Rev. Lett. **47**, 1392 (1981).
- 3 P. H. Woerlee, Y. S. Gordeev, H. de Waard, and F. W. Saris, J. Phys. **B14**, 527 (1981).

CONTINUUM ELECTRON EMISSION FROM COLLISIONS OF 0.1-3.2 MeV Kr IONS WITH Xe TARGETS

P. Clapis,* R. Roser,* K. J. Reed[†] and Q. C. Kessel*

*Department of Physics and Institute of Materials Science, University of Connecticut, Storrs, CT 06268 USA
[†]Lawrence Livermore National Laboratory, Livermore, CA 94550 USA

A band of electrons with energies in the range of 150 to 600 eV have been observed from collisions of Kr with Xe targets. Coincidence measurements between these electrons and the scattered ions determine the impact parameter dependence for this electron emission and show this dependence and the electron energies to be consistent with the promotion of M- and N-shell electrons. Figure 1 shows sharp increases in the electron production cross section for distances of closest approach of 0.6 and 0.3 a.u. An extension of the calculations of Eichler and coworkers¹ is shown in Figure 2 where a series of avoided crossings appear for each of these internuclear distances. The threshold behavior for the production of these continuum electrons, together with the agreement with Figure 2, indicates that two specific promotions are responsible for the production of vacancies which may be produced in any of a number of orbitals. The filling of these vacancies can take place from outer-lying orbitals which, during the collision, may be poorly defined because of uncertainty broadening and dynamic coupling. The observed band of electrons is consistent with such an excitation-decay process. This is in contrast to an explanation for continuum electrons from Kr-Kr collisions wherein they were attributed to the filling of a single, well defined MO during the collision.^{2,3}



This research has been supported by National Science Foundation grant PHY-8406117. We also acknowledge the use of computational facilities at LLNL; work there performed, in part, under the DOE by LLNL under contract No. W-7405-ENG-48.

References

1. J. Eichler, U. Wille, B. Fastrup and K. Taulbjerg, Phys. Rev. A **14**, 707 (1976).
2. Yu. S. Gordeev, P. H. Woerlee, H. de Waard and F. W. Saris, J. Phys. B **13**, 513 (1981).
3. V. V. Afrosimov, G. G. Meskhi, N. N. Tsarev and A. P. Shergin, Zh. Eksp. Teor. Fiz. **84**, 454 (1983); (English Trans: Sov. Phys. JETP **57**, 263 (1983)).

LARGE ANGLE MEASUREMENTS OF K-SHELL VACANCY PRODUCTION IN COLLISIONS OF Ne AND Ar IONS WITH Ar TARGETS

A. A. Antar[†] AND Q. C. KESSEL*

*Department of Physics and Institute of Materials Science, The University of Connecticut, Storrs, CT 06268 USA

[†]Department of Physics, Central Connecticut State University, New Britain, CT 06050 USA

The final charge state of Ne and Ar projectiles scattered through angles ranging from 1 to 45° by single collisions with Ar targets have been measured.

The product of the target gas pressure times the path length in the gas is kept small enough ($2 \sim 6 \times 10^{-4}$ Torr-cm) to minimize multiple collisions. The projectile Ne and Ar ions are produced in the terminal of a Van de Graaff accelerator. The energy of these projectiles ranged from 0.15 to 1.50 MeV using single Ne and Ar ions and up to 3.0 MeV using doubly ionized projectiles. For each set of an ion energy, E_0 , and scattering angle θ , the number of ions having charge state m , N_m , are counted after passing through an electrostatic analyzer. The probability of the ions having charge state m (for each set of E_0 & θ) is given by $P_m = N_m / \sum N_m$. The average charge \bar{m} of the scattered ions was then determined from the values of P_m from the relation $\bar{m} = \sum m P_m$.

The data are compared with inelastic energy loss measurements obtained by Kessel and coworkers^{1,2} for the same collision pairs at lower energies. For the Ne⁺-Ar collision the final charge states range from 2 to 6 show an excitation for a distance of closest approach $R_0 = 0.2\text{\AA}$ where m increases from 2 to 4. A comparison of these data with the molecular-potential calculations of Eichler and coworkers^{3,4} show this excitation may be attributed to Ar L-shell vacancy production. For the Ar⁺-Ar collision, the final charge states range from 4 to 10 show an increase in the average charge state of the scattered ions from 7 to 8 when the distance of the closest approach, R_0 is changing from 0.03 to 0.015\AA. Lutz and coworkers observed K-shell excitation⁵ for similar collision conditions and therefore this increase in ionization may be attributed to the production of K-shell vacancy in one of the argon atoms.

This research has been performed at the University of Connecticut, supported by National Science Foundation grant number PHY-8406117.

References

1. Q. C. Kessel, in Proceedings of the 5th International Conference on Physics of Electronic and Atomic Collisions, Leningrad, USSR, 1967, pp. 94.
2. Q. C. Kessel, P. H. Rose and L. Grodzins, Phys. Rev. Lett. 22 1031 (1969).
3. J. Eichler and U. Wille, Phys. Rev. A 11, 1973 (1975).
4. J. Eichler, U. Wille, B. Fastrup and K. Taulbjerg, Phys. Rev. A 14, 707 (1976).
5. H. O. Lutz, W. R. McMurray, R. Pretorius, R. J. van Reenen and J. J. van Heerden, Phys. Rev. Lett. 40 1133 (1978).

K-SHELL EXCITATION AND KK ELECTRON CAPTURE IN SYMMETRIC HEAVY ION COLLISIONS

E. Morenzoni*, R. Anholt, W.E. Meyerhof

Department of Physics, Stanford University, Stanford, California 94305 USA

In several asymmetric heavy ion collision experiments it has been found that the induced x-ray production does not depend linearly on the target thickness¹⁻⁴. This behaviour depends on the build up of K- and L-shell vacancies in the projectile when it moves through the foil. K-shell excitation and ionization is then no longer simply related to the K x-ray yields. For instance a projectile K-shell vacancy created in a first collision can be quenched by a process whereby a target K-electron is transferred to the projectile K-shell (KK electron capture), before a radiative or non-radiative decay takes place. KK electron capture should manifest itself even in symmetric ($Z_p = Z_t$) collisions by enhancing the target K-vacancy production cross section relative to that of the projectile. The enhancement depends on the cross section for KK electron capture and on the fraction of projectiles carrying a K-vacancy. K-vacancy production in symmetric collisions occurs predominantly via the $2p\pi-2p\sigma$ molecular orbitals, when a previously created $2p\pi$ vacancy is transferred to the $2p\sigma$ orbital at small internuclear distances and then shared between target and projectile K-shell⁵. This process depends on the L-shell population of the projectile.

In order to study the various competing processes responsible for projectile and target K-vacancy production in symmetric systems, we measured the separated target and projectile K x-ray emission in Ni-Ni, Cu-Cu, Nb-Nb, Ag-Ag as a function of the target thickness. The target thickness ranged from 5 to 200 $\mu\text{g}/\text{cm}^2$, the beam energy between 75 and 105 MeV. The K x-rays were detected with a SiLi detector set at 30° and 150° with respect to the beam direction. In this way the Doppler shifted projectile lines could be separated from the target lines. K_α and K_β energy shifts and K_α/K_β ratios for target and projectile were also determined as a function of the target thickness and used to determine the average L and M shell populations during the K-vacancy decay and the K-shell fluorescence ω_K . The projectile and target K-vacancy production cross sections so obtained for Cu-Cu collisions at 90 MeV are displayed in fig. 1 as a function of the target thickness. By analyzing these cross sections with a model which takes into account the evolution of the projectile L- and K-shell inside the target, the cross sections of the K-shell excitation in target and projectile and of KK electron transfer in symmetric collisions could be determined. We found that K-shell excitation in target and projectile (σ_K) is equal consistently with the

MO model prediction of K-vacancy production via $2p\pi-2p\sigma$ rotational coupling and equal sharing probability between target and projectile. The KK electron capture cross section is larger than σ_K . Its magnitude is in strong disagreement with predictions from the OBK theory⁶. A description of KK-electron capture in terms of a two pass $2p\sigma-1s\sigma$ radial coupling is in better agreement with the experimental values.

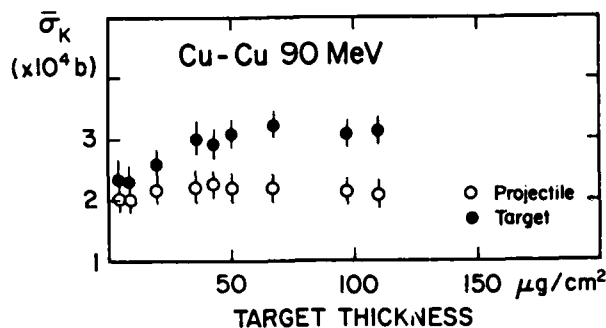


FIGURE 1 K-vacancy production cross sections for target and projectile as a function of target thickness in Cu-Cu collisions at 90 MeV

References

1. H.D. Betz et al., Phys. Rev. Lett. **33**, 807 (1974)
2. R.K. Gardner et al., Phys. Rev. **A15**, 2202 (1977)
3. A. Tanis et al., Phys. Rev. **A22**, 483 (1980)
4. J.P. Rozet et al., J. Phys. **B14**, 73 (1981)
5. W.E. Meyerhof, Phys. Rev. Lett. **31**, 1341 (1973)
6. V.S. Nikolaev, Sov. Phys. JETP **24**, 847 (1967)

*Present address: Institut für Mittelenergiephysik, ETH-Zürich, CH-8093 Zürich-Honggerberg, Switzerland

SPECTROSCOPY OF QUASIMOLECULAR ORBITALS
FROM INTERFERENCES IN $1s\sigma$ - $2p\pi$, $2p\sigma$ X RAY TRANSITIONS*

R. Schuch, R. Hoffmann, E. Justinjano, J. Konrad, P.M. Mokler^x, A. Oppenländer,
W. Schadt[†], H. Schmidt-Böcking

Physikalisches Institut der Universität, D-6900 Heidelberg, FRG

^xGSI, D-6100 Darmstadt, FRG

[†]Institut für Kernphysik, D-6000 Frankfurt, FRG

In recently performed collision experiments of decelerated hydrogenlike Cl^{16+} ions with Ar atoms an interference structure in the spectra of quasimolecular K- α rays (MO x rays) for fixed impact parameters was found¹⁾. It was possible to extract in a direct way $1s\sigma$ - $2p\pi$ quasimolecular transition energy from this structure²⁾. We want to report here about new experiments with light (S^{15+} -Ar) and intermediate heavy (Ge^{31+} -Kr, Kr^{35+} -Mo) collision systems with the following goals:

1. A better understanding of the interference structure and more precise spectroscopic information
2. Extending the studies to heavier systems and also to the use of solid targets.

The spectra of MO x rays contains a superposition of transitions from mainly the $2p\sigma$ and $2p\pi$ states into the $1s\sigma$ state. Although the transition from $2p\pi$ should dominate, the contribution from $2p\sigma$ influences the spectroscopic result. With respect to the first point we searched for possibilities to separate the two contributions in the MO x ray spectra.

According to theoretical predictions e.g. by Briggs et al.³⁾, the interference structure in the MO x rays should be shifted in the photon energy for observation at two different polar angles (0° and 90°). We therefore performed an experiment with 12.8 MeV S^{15+} on Ar (gas target) and observed MO x rays in coincidence with scattered particles at two emission angles (20° and 90°) with respect to the beam axis. A small shift in the interference structure at the two emission angles is observed, which will be compared with theoretical predictions.

With respect to the second point we report about results from measurements with decelerated (2.6 MeV/u) Ge^{31+} on a Kr gas target and 4.6 MeV/u Kr^{35+} on a Mo solid target. The fig.1 shows a two-dimensional spectrum of x ray energy versus coincidence time at a small impact parameter of 820 fm from the Ge^{31+} -Kr experiment. In the part of the spectrum above the characteristic x rays the time peak for the MO x rays

is clearly seen. Subtracting the random background one can already see from the two-dimensional spectrum the existence of an interference minimum and a maximum in the MO x ray continuum. This structure is utilized to obtain $1s\sigma$ - $2p\pi$, $2p\sigma$ quasimolecular transition energies also in these intermediate heavy systems.

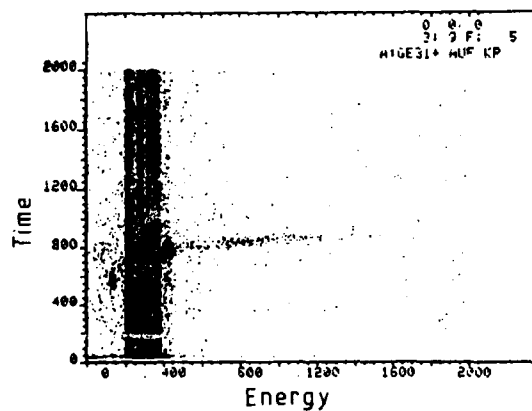


Fig. 1: Two-dimensional coincidence spectrum: time versus x ray energy for impact parameters around 820 fm.

*supported by Bundesministerium für Forschung und Technologie.

References

1. I. Tserruya, R. Schuch, H. Schmidt-Böcking, J. Barrette, Wang Da-Hai, B.M. Johnson, K.W. Jones, M. Meron, Phys. Rev. Lett. **50**, 30 (1983)
2. R. Schuch, H. Schmidt-Böcking, I. Tserruya, B.M. Johnson, K.W. Jones and M. Meron, Z. Phys. **A320**, 185 (1985)
3. J.S. Briggs, J. Macek and K. Taulbjerg, J. Phys. **B12**, 1457 (1979)

K-VACANCY PRODUCTION IN HIGH ENERGY $U + U$ AND $U + Pb$ COLLISIONS AT SMALL IMPACT PARAMETERS*

J. D. Molitoris, R. Anholt, W. E. Meyerhof, O. K. Baker, S. Andriamonje,[†] and E. Morenzoni[‡]
Department of Physics, Stanford University, Stanford, CA 94305

Extending our earlier investigation of the Pb K -shell vacancy production in elastic $Xe + Pb$ collisions near and above the nuclear Coulomb barrier,¹ we have determined the Pb and U K -shell ionization probabilities in elastic $U + Pb$ and $U + U$ collisions at 4.6, 5.8, and 7.3 MeV/a.m.u. In these heavy-ion - atom collisions, the molecular model is appropriate, according to which the ionization of an inner (K) shell can be described in terms of the ionization of the molecular orbitals ($1s\sigma$, $2p\sigma$) leading to that shell.²

In this work we investigate $2p\sigma$ ionization in symmetric and asymmetric collisions and $1s\sigma$ ionization in asymmetric $U + Pb$ collisions. We used projectile energies near and above the Coulomb barrier because of their interest in related, but more complex studies, such as the determination of atomic positron production in heavy-ion collisions³ and the study of nuclear time delay effects in deep inelastic nuclear reactions.⁴ In the former of these, the $1s\sigma$ ionization probability plays an important role, whereas in the latter, use is made of the much larger $2p\sigma$ ionization probability. Our work directly tests calculations which have been made of these ionization probabilities.^{5,6}

We determined these K -shell vacancy probabilities by detecting the K x-rays of the collision partners in coincidence with scattered particles. A major difficulty at projectile energies above the Coulomb barrier is the production of K x-rays by the internal conversion (IC) of γ -rays, from inelastic nuclear reactions. To overcome this problem we made use of a γ -ray anticoincidence method described in our earlier work.¹ The technique worked well in the determination of the K -vacancy production probability from U x-rays as it helped to eliminate some IC due to Coulomb excitation in addition to IC from nuclear γ -ray cascades connected with near-elastic and deep-inelastic reactions. The method made negligible difference in the measurement of Pb x-rays.

Comparison of the experimental data with theory is made slightly more complicated because of the need to consider vacancy sharing between the $2p\sigma$ and $1s\sigma$ MO's.⁷ Judging from the measured impact parameter dependence of the K -vacancy sharing factor⁸ (w), for our purposes w should be nearly independent up to several hundred fm. In that case, the measured Pb and U K -vacancy production probabilities can be written in terms of the theoretical $2p\sigma$ and $1s\sigma$ vacancy production probabilities as:

$$P_{Pb} = (1 - w)P_{2p\sigma} + wP_{1s\sigma} \quad (1)$$

$$P_U = wP_{2p\sigma} + (1 - w)P_{1s\sigma} \quad (2)$$

If we take w from theory,⁷ we can calculate the expected values of $P_{2p\sigma}$ and $P_{1s\sigma}$ from the experimental values of P_{Pb} and P_U :

$$P_{2p\sigma} = [(1 - w)P_{Pb} - wP_U]/(1 - 2w) \quad (3)$$

$$P_{1s\sigma} = [(1 - w)P_U - wP_{Pb}]/(1 - 2w) \quad (4)$$

These values are shown in Fig. 1 for 7.3 MeV/a.m.u. $U + Pb$ collisions and are compared with coupled channel calculations⁶ and a scaling law description.⁹ Figure 1 also shows a similar comparison for 7.3 MeV/a.m.u. $U + U$ collisions. Here the $P_{1s\sigma}$ contribution was estimated by the scaling law description and was subtracted from the data. We will also present results for projectile energies of 5.8- and 4.6-MeV/a.m.u. Comparison is made with theory and other available data.

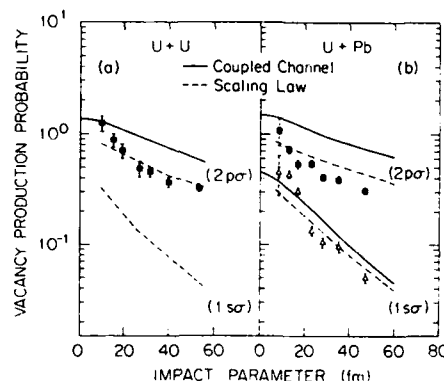


Fig. 1. $1s\sigma$ (Δ) and $2p\sigma$ (\blacksquare) vacancy production probabilities versus impact parameter for 7.3 MeV/a.m.u. (a) $U + U$ and (b) $U + Pb$ collisions compared with theory.

References

- * Supported in part by the NSF (Grant PHY-83-13676).
- [†] Permanent address: C.E.N.B.G., Bordeaux, France.
- [‡] Permanent address: E.T.H., CH-8093 Zürich, Switzerland.
- 1. R. Anholt *et al.*, *Z. Phys. A* **308**, 189 (1982).
- 2. W. E. Meyerhof and K. Taulbjerg, *Ann. Rev. Nucl. Sci.* **27**, 279 (1977).
- 3. U. Müller *et al.*, *Z. Phys. A* **313**, 263 (1983).
- 4. Ch. Stoller *et al.*, *Phys. Rev. Lett.* **53**, 14, 1329 (1984).
- 5. T. deReus *et al.*, *J. Phys. B: At. Mol. Phys.* **17**, 615 (1984).
- 6. U. Müller and T. deReus, (Private communication) (1984).
- 7. W. E. Meyerhof, *Phys. Rev. Lett.* **31**, 1341 (1973).
- 8. R. Schuch *et al.*, *Phys. Rev. Lett.* **39**, 79 (1977).
- 9. F. Bosch *et al.*, *Z. Phys. A* **296**, 11 (1980).

Z-DEPENDENCE OF POSITRON PEAK STRUCTURE IN SUPERHEAVY COLLISION SYSTEMS

H. Bokemeyer, H. Folger, H. Grein (GSI, Darmstadt),
 T. Cowan, J.S. Greenberg, J. Schweppe (Yale University),
 A. Balanda*, K. Bethge, A. Gruppe,
 K. Sakaguchi, K.E. Stiebing (Univ. Frankfurt),
 D. Schwalm (Univ. Heidelberg), P. Vincent** (Rutgers Univ.),
 H. Backe, M. Begemann, M. Klüver, N. Trautmann (Univ. Mainz)

We have pursued a series of experiments to study positron creation in the collision systems $^{238}\text{U} + ^{248}\text{Cm}$, $^{232}\text{Th} + ^{248}\text{Cm}$, $^{238}\text{U} + ^{238}\text{U}$, $^{238}\text{U} + ^{232}\text{Th}$, $^{232}\text{Th} + ^{232}\text{Th}$ where supercritical binding can be achieved with the beams and targets available. Both ^{238}U and ^{232}Th projectiles were used to avoid the possibility of a collision partner common to all the systems. The measurements were motivated especially by the anomalous appearance¹ of a narrow positron peak in $^{238}\text{U} + ^{248}\text{Cm}$ collisions. This peak displayed many of the properties that could be associated with spontaneous positron emission from a giant dinuclear system, in particular a peak energy consistent² with the energy of a supercritically bound 1s state for a system composed of the two nuclear charges ($Z_U=188$) marginally touching. The measurements noted above were carried out to search for peak structures in other supercritical systems with special emphasis on exploring two distinguishing features that could identify the spontaneous positron excitation process: 1) a very strong dependence of the peak energy on the total nuclear charge Z_U and 2) emission from the combined system.

The general features of all the collision systems studied were found to be similar, with a pronounced peak appearing above the continuous background in each case. As found in the $\text{U} + \text{Cm}$ system¹, the peaks appear to be produced in a narrow interval of bombarding energy near the Coulomb barrier, they cannot be identified with any trivial nuclear source, and the very similar Doppler-broadened line widths are all compatible with emission by a system moving with the center-of-mass velocity. However, a near degeneracy in peak energies is observed for all the systems, which contrasts with the $\sim Z_U^{20}$ dependence expected² for spontaneous positron emission from systems of constant nuclear charge distribution and state of ionization. Figure 1 illustrates that to account for this near constancy in peak energies within the context of spontaneous positron emission, it is necessary to invoke very radically different charge distributions for the metastable giant nuclear systems. It bears emphasis that the very similar peak energies and widths are notable features of the spectra and suggest a common source.

Because of these findings, we recently have also pursued the question of whether the peaks are uniquely associated with only supercritical systems by studying the subcritical system $^{232}\text{Th} + ^{181}\text{Ta}$ ($Z_U=163$). As shown in Figure 2, a narrow peak with an energy consistent with the peaks in the supercritical systems is also observed in this case. In this system we have also detected γ -ray transitions which could contribute structure to the positron spectrum in the region of the peak through internal pair creation. The extent to which the nuclear transitions can account for the peak in Figure 2 is presently being investigated.

* On leave from IF UJ, Krakow, Poland

** Present address: BNL, Upton, NY, USA

¹ J. Schweppe et al., Phys. Rev. Lett. 51(1983)2261

² J. Reinhardt et al., Z. Phys. A303(1981)173

Figure 1

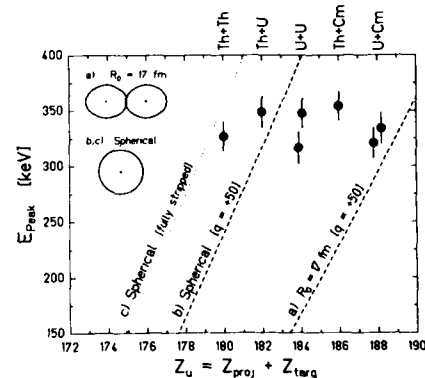
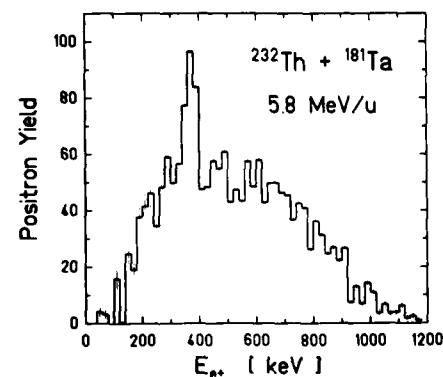


Figure 2



ACCURACY OF MEASURED $H(n=3)$ DENSITY MATRICES FOR
 H^+ -He AND H^+ , H_2^+ , AND H_3^+ -CARBON FOIL COLLISIONS

W. B. Westerveld, N. Rouze, and J. S. Risley

Department of Physics
 North Carolina State University
 Raleigh, North Carolina 27695-8202 USA

We have developed an experimental technique to determine the density matrix of fast excited hydrogenic systems. The technique has been applied to measure the density matrix of $H(n=3)$ atoms formed in 40-80 keV H^+ -He electron transfer collisions^{1,2} and 40-160 keV H^+ , H_2^+ , and H_3^+ collisions with carbon foils.^{3,4} In the experiment, the excited hydrogen atoms are allowed to radiatively decay in the presence of externally applied axial or transverse electric fields. These fields produce Stark mixing of the different ℓ -levels, thereby changing the intensity and polarization of the observed light. The electric fields can be kept sufficiently small (<1000 V/cm) so that the collision itself is unaffected.

The data are analyzed by modeling the time evolution of the excited hydrogen atoms from their formation until their decay. Statistical fitting of calculated signals to experimental observations allows the determination of a linear superposition of the calculated signals which "best" fits the measured signals and yields the $H(n=3)$ density matrix at the time of the formation of the hydrogen atom. The obtained density matrix specifies the charge and current distribution of the excited atom, thus facilitating an intuitive understanding of the collision process², see Fig. 1.

An attractive feature of this experiment lies in the almost exact analysis which is possible. The modeling of the experiment relies on the calculable time evolution of excited hydrogen atoms in external homogeneous fields and, in the experiment considered,

the essential forward scattering with a known velocity of the formed atoms. In principle, therefore, high accuracies are possible for the derived density matrices. However a number of small systematic effects has not been taken into account, such as cascade from higher lying levels and the energy dependence of the density matrix for speeding up (slowing down) of the charged projectiles on passing through a gaseous target in axial electric fields. At very low velocity the angular distribution of the emerging hydrogen atoms should be taken into account in the analysis. Turn-on effects associated with the electric fields are difficult to evaluate quantitatively. The highest demands are put on the optical system with respect to polarization sensitivity and accuracy. Specifically, errors due to the solid angle subtended and the length of beam viewed need to be considered. We are currently in the process of exploring the above systematic effects in order to incorporate them in the analysis or, where possible, to minimize them.

This work was supported in part by the Atomic, Molecular, and Plasma Physics Program of the NSF, Grant No. PHY-82-08905.

References

1. C. C. Havener et al., Phys. Rev. Lett. **48**, 926 (1982).
2. C. C. Havener et al., Phys. Rev. Lett. **53**, 1049 (1984) and submitted to Phys. Rev. A.
3. N. Guilbert, M. S. thesis North Carolina State University (1984).
4. R. Cline et al., Bulletin of the Am. Phys. Soc. **29**, 1504 (1984).

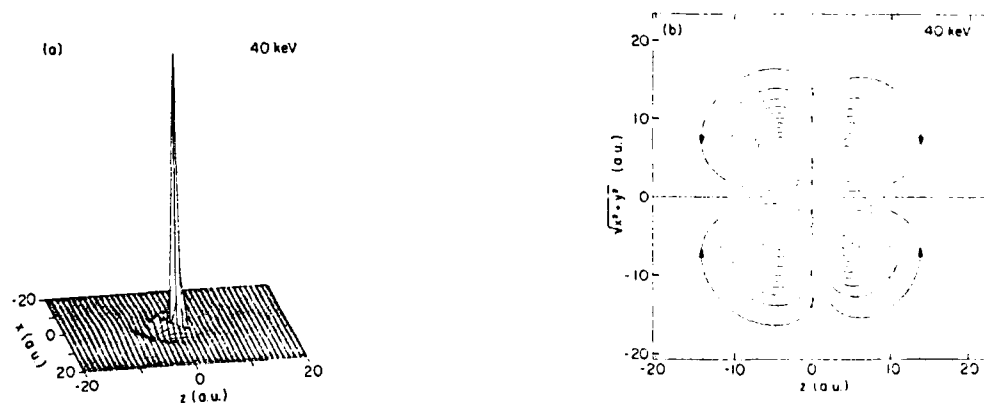


Fig. 1. Density (a) and current distribution (b) of $H(n=3)$ atoms formed in 40 keV H^+ + He electron-transfer collisions.² In the figure, the He^+ ion is to the left.

THE Na $2p^5 3s^2 2p_{1/2,3/2}$ STATES EXCITED BY PROTON IMPACT: ABSOLUTE CROSS SECTIONS AND ALIGNMENT.

R. Hintermayer, G. Keßler, T. Passarge and W. Mehlhorn

Fakultät für Physik, Universität Freiburg, D-7800 Freiburg, FRG

We have measured absolute excitation cross sections $Q(^2P)$ of Na $2p^5 3s^2 2p$ and the alignment parameter A_2 of Na $2p^5 3s^2 2p_{3/2}$ for proton impact in the energy range $E_{H^+} = 10 \dots 30$ keV or range of reduced velocity $v_{rel}/v_{2p} = 0.38 \dots 0.66$ ($v_{rel} = v_{H^+}$ and v_{2p} are the velocities of the proton and the $2p$ electron of Na, respectively).

Experimentally, the proton beam passed through a metal vapor oven and excited the Na atoms inside the oven. Electrons from the autoionisation of the $2p^5 3s^2 2p_{1/2,3/2}$ states were measured for different ejection angles θ relative to the proton beam. For the cross section measurements the magic angles $\theta = 54.7^\circ$ or 125.3° were used.

The cross sections for proton impact were determined on an absolute scale by fitting them to the absolute cross section for elastic scattering of electrons¹ by Na atoms at the incident energy of 500 eV. To achieve this, the intensity of autoionization electrons following proton impact and the intensity of electrons elastically scattered by the same Na target were measured intermittently, thereby the density of the Na target and the transmission of the electron spectrometer need not be determined.

The alignment parameter A_2 , with $A_2 = [Q(2p_0) - Q(2p_1)] / [Q(2p_0) + 2Q(2p_1)]$ and $Q(2p_m)$ the excitation cross section of a $2p_m$ electron to a $3s_0$ state, was determined via the angular distribution of autoionization electrons

$$I_{3/2}(\dots) = (I_{3/2}/4\pi) [1 + A_2 P_2(\cos\theta)].$$

In Fig. 1 and 2 the present experimental values of the absolute cross sections $Q(^2P)$ and the alignment parameter A_2 (here also earlier values are included) are compared to theoretical results obtained for different approximations². It is interesting to note, that best agreement for the cross sections occurs for a 25 state SCA calculation, where backcoupling and polarization effects of the target atom has been taken into account, whereas for the alignment parameter A_2 best agreement occurs for the PWBA. This rather good but unexpected agreement with the PWBA results has been found already earlier³.

The support by the Deutsche Forschungsgemeinschaft is gratefully acknowledged.

References

1. M. Fink and D. Gregory, At. Data Nucl. Data Tables **14**, 39 (1974).
2. O. Schöller and J.S. Briggs, in "Fundamental Processes in Atomic Collision Physics" (H.O. Lutz, J.S. Briggs and H. Kleinpoppen, eds.) NATO-ASI Series, Plenum Press, 1985.
3. C.E. Theodosiou, E. Breuckmann, B. Breuckmann and W. Mehlhorn, J. Phys. B **12**, L689 (1979).
4. P. Ziem, R. Morgenstern and N. Stolterfoht, Proc. X. ICPEAC, Paris 1977, p. 1002.
5. R. Ruckteschler and W. Mehlhorn, Proc. XII. ICPEAC, Gatlinburg 1981, p. 748.

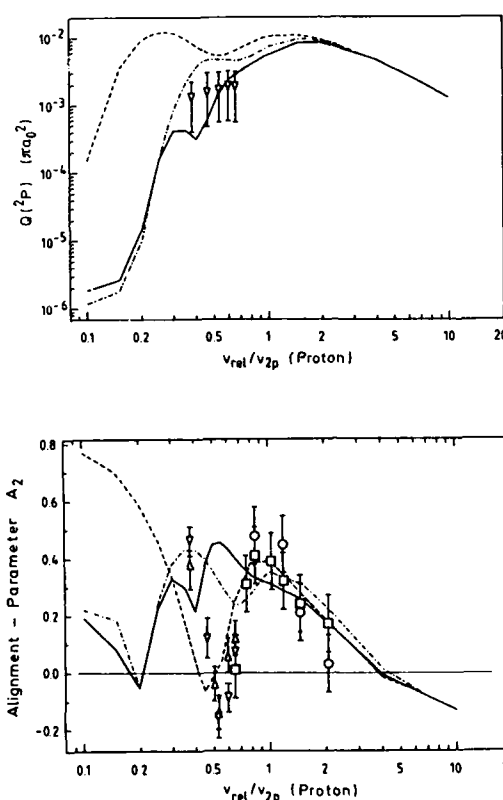


Fig. 1 and 2. Absolute excitation cross sections $Q(^2P)$ of Na $2p^5 3s^2 2p$ and alignment parameter A_2 of Na $2p^5 3s^2 2p_{3/2}$ for proton impact as function of v_{rel}/v_{2p} . Experiment: ∇ = present values, Δ = Theodosiou et al.³, \circ = Ziem et al.⁴, \square = Ruckteschler and Mehlhorn⁵. Theory²: — = 25 state close coupling calculation (SCA), - - - = 4 state close coupling calculation (SCA), . . . = PWBA (identical to the results of Theodosiou et al.³).

AD-A163 497

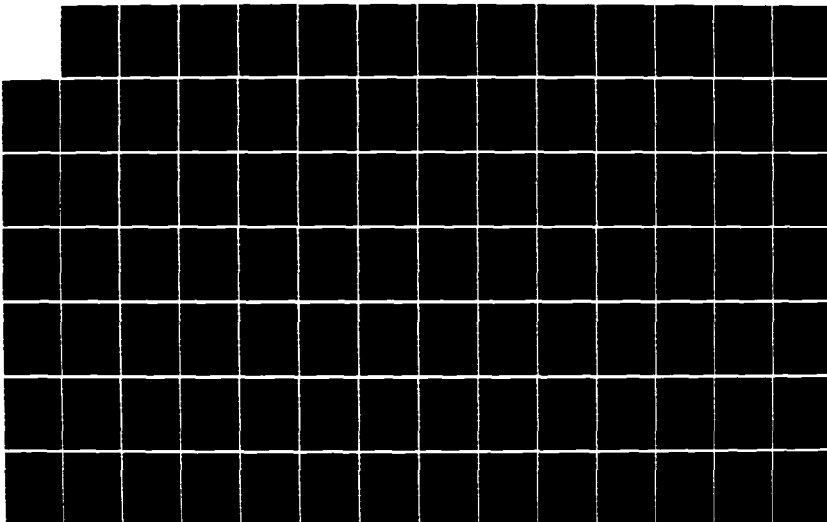
ELECTRONIC AND ATOMIC COLLISIONS ABSTRACTS OF
CONTRIBUTED PAPERS INTERNAT. (U) SRI INTERNATIONAL
MENLO PARK CA MOLECULAR PHYSICS CENTER
M J COGGIOLA ET AL. 1985

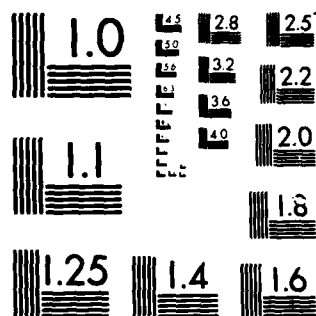
678

UNCLASSIFIED

FFQ 7/4

NL





MICROCOPY RESOLUTION TEST CHART
NATIONAL BUREAU OF STANDARDS 1963-A

APPLICATION OF THE QUASI-COINCIDENCE TECHNIQUE TO EXCITED STATE CAPTURE BETWEEN ALKALI IONS AND INERT GAS ATOMS

K. NEHER, B. STAUDENMAYER, Fakultät Physik, Universität Freiburg, D-7800 Freiburg
V. KEMPTER, Phys. Institut TU Clausthal, D-3392 Clausthal

INTRODUCTION

The shape and the orientation of the charge cloud of an atom excited in collisions will reflect details of the underlying excitation mechanisms.¹ Analysis of the polarization properties of the light emitted by the excited atom has developed into a powerful tool for the test of predictions concerning the physics of the collision process. We have studied excited state capture of Li^+ and Na^+ colliding with inert gases by using the quasi-coincidence technique.² So far the quasi-coincidence technique has been applied only to excited state capture in collisions of He^+ and Ne^+ with inert gases.^{3,4} Even in the simplest case He^+-He the measured reduced degree of polarization $|P|$ was far from unity, and information on the shape and orientation of the excited state's charge cloud could not be obtained.

We have carried out a complete polarization analysis of the $\text{Li}(2p \rightarrow 2s)$ and $\text{Na}(3p \rightarrow 3s)$ photons emitted after excited state capture in collisions of Li^+ and Na^+ with the inert gases. The reduced degree of the polarization for this class of collision processes is indeed unity except for very small scattering angles. Thus the polarization results can be used to deduce the shape and orientation of the excited state's charge cloud.

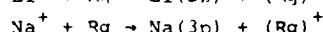
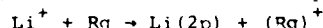
EXPERIMENT

Li^+ and Na^+ ion beams are produced by evaporating the appropriate alkali metals, and by ionizing a small fraction of the evaporated atoms by collisions with hot metal surfaces. A stable beam current density of 10^{-7} A/mm² at 1 m distance from the ion source can be maintained at 2.5 keV beam energy. The monoenergetic ion beam collides with inert gas atoms in a short collision cell of 3 mm length. The photon detector consists of a polarization analyzer, an interference filter, and a photomultiplier and detects photons from the transitions $\text{Li}(2p \rightarrow 2s)$ and $\text{Na}(3p \rightarrow 3s)$. Photons are only registered if the emitting atom is scattered into the desired angle and decays after it has left the collision cell. The angular resolution is about 1 degree FWHM. Both the linear polarizations P_1 and P_2 ,

and the circular polarization P_3 are measured as a function of the scattering angle.

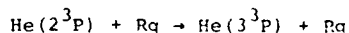
RESULTS AND INTERPRETATION

A complete polarization analysis of the emitted photons from the capture processes



where $\text{Rg} = \text{He, Ne, Ar, Kr, Xe}$, will be presented for scattering angles θ between 1 and 4 degs at 2.5 keV impact energy. Full coherence is found for $\theta > 2$ degs except for Li^+-Ne and Na^+-Ne . The results for Li^+-He are in qualitative agreement with previous results.¹ In general P_3 is small in the studied θ -range at 2.5 keV. The ($m=\pm 1$) substates of $\text{Li}(2p)$ and $\text{Na}(3p)$ are dominantly populated. We can conclude that the $\text{Li}(2p)$ and $\text{Na}(3p)$ charge clouds are oriented almost perpendicular to the internuclear axis under these conditions. These results can be understood on the basis of one-electron orbital correlation diagrams⁵ which predict that the dominant excitation mechanism under the studied conditions should be rotational coupling at small internuclear distances (1 a.u.).

In an auxiliary experiment we have studied



with the quasi-coincidence technique at the same impact energy. As in the case



studied in ^{3,4} the reduced degree of polarization is well below unity, and there is no complete coherence.

REFERENCES

1. T. Andersen, H.P. Neitzke, VIII ICPEAC Berlin, Invited Papers, 667 (1983).
2. W. Wittmann, H.J. Andrä, Z. Phys. A288, 335 (1978).
3. H. Winter, Phys. Scripta T6, 136 (1983).
4. R.W. Michaels, C.S. Lee, D.A. Church, Nucl. Instr. Meth. 202, 223 (1983).
5. M. Barat, NATO Adv. Sci. Series 103, 359 (1983).

POLARISATION STUDIES OF RESONANT ELECTRON EXCHANGE IN $\text{Na}^+-\text{Na}^*(3p)$ COLLISIONS

A. Bähring, R. Witte, H. Schmidt and I.V. Hertel

Institut für Molekülphysik, Freie Universität Berlin, D-1000 Berlin 33, West Germany

The merging of atomic and molecular description in low energy ion-atom scattering has extensively been discussed in previous publications¹ where we studied inelastic collisions in the model system $\text{Na}^+-\text{Na}^*(3p)$. The simple picture arising from these measurements of the polarisation dependent differential cross sections was that of a finite internuclear distance R_L , where the main axis of the $3p$ -charge cloud changes from space-fixed to body-fixed behaviour thus being locked to the molecular axis. Of course, the measured value of R_L is marking an effective locking range rather than a definite radius. Moreover, to be roughly constant R_L must be appreciably smaller than the impact parameter b . This is also seen from semiclassical calculations of $R_L(b)$ shown in Fig. 1. Indeed the condition $b < R_L$ is fully satisfied in the case of collisional $3p$ - $3s$ deexcitation and $3p$ - $3d$ excitation, for both processes proceed via rotational coupling at quasi-fixed impact parameters $b \approx 5a.u.$ In contrast, the recently studied resonant charge transfer in

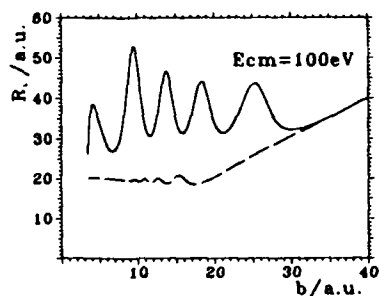


Fig.1 Locking radius R_L as a function of impact parameter b , calculated for gerade

—, ungerade --- potentials

the excited channels² is observed under collision angles peaking at $\theta_{CM}=0^\circ$ and hence taking place mainly at large impact parameters. There we reach the limits of our simple locking model, the processes becoming very complicated as indicated in Fig. 2. Since we are no longer able to disentangle the numerous possible transitions each leading to different trajectories there is no more defined impact parameter and therefore even the semiclassical picture becomes dubious. Moreover, the huge amount of partial waves taking part in the small angle scattering makes calculations very difficult.

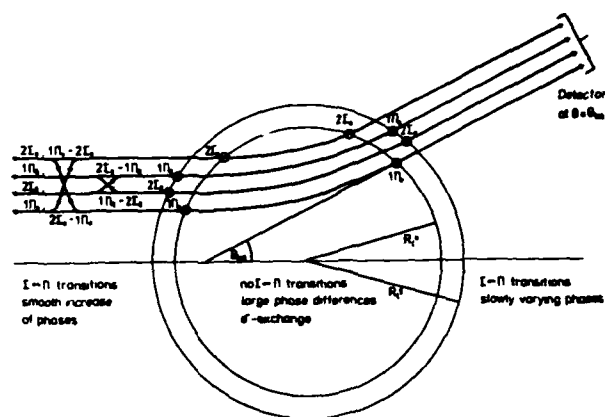


Fig.2 Scheme of the interaction regions in elastic scattering

This is demonstrated in Fig. 3, where we compare a measured angular dependency of the circular asymmetry P_3 with semiclassical calculations. According to the limited resolution of our apparatus the theoretical curve had to be averaged over the angular interval $\Delta\theta_{CM} = \pm 0.1^\circ$ resulting in a much smoother behaviour and damped to a magnitude that agrees well with

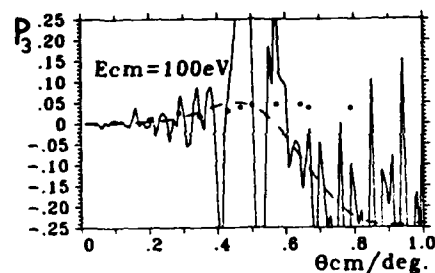


Fig.3 Angular dependent circular asymmetry P_3

• exp., — theory, --- averaged theory

experiment. Further effort is being made towards considerable improvement of the angular resolution employing multichannel detectors.

References

- 1 A.Bähring, I.V.Hertel, E.Meyer, H.Schmidt, Z.Phys. A **312**, 293 (1983); A.Bähring, I.V.Hertel, E.Meyer, W.Meyer, N.Spies, H.Schmidt, J.Phys.B **17**, 2859 (1984); A.Bähring, E.Meyer, I.V.Hertel, H.Schmidt, Z.Phys.A **320**, 141 (1985)
- 2 A.Bähring, I.V.Hertel, E.Meyer, H.Schmidt, Phys. Rev.Lett. **53**, 1433 (1984); R.J.Allan, A.Bähring, H.Schmidt, R.Witte, to be published

SPIN-DEPENDENT INTERACTION IN keV $\text{Ne}^+ + \text{Na}$ COLLISIONS

W. Jitschin, S. Osimitsch, H. Reihl, D. Mueller,
H. Kleinpoppen, and H.O. Lutz

Fakultät für Physik, Universität Bielefeld, 4800 Bielefeld, West Germany
Atomic Physics Laboratory, University of Stirling, Stirling FK9 4LA, Scotland

The spin polarization of an electron is influenced in a collision by:

case 1) interaction between spin and other angular momentum;

case 2) exchange of individual electrons.

Both interaction mechanisms may be active in collision systems with at least two electrons.

As a first step towards experiments in which the spins of all collision partners are known before and after the collision we investigated the Na 3s to 3p excitation by Ne^+ ions with spin preparation and analysis of Na only:



The Na atoms had an initial spin polarization $P = 0.205$, and the spin polarization of the excited final Na 3p state was derived from the circular polarization P_3 of the fluorescence light which is affected by hyperfine relaxation after the collision.¹ The observed polarization values P_3 (Fig. 1) are compatible with spin-conservation at high impact energies; however, with decreasing impact energy P_3 becomes smaller indicating the increasing influence of spin-changing interactions during the collision.

As a possible explanation for the observed depolarization we suggest the following simplified mechanisms: Excitation of Na presumably occurs via quasi-resonant charge-exchange from the 3s state to the 4p state at large internuclear distances and subsequent rotational coupling to the 3p state (Fig. 2). The 4p

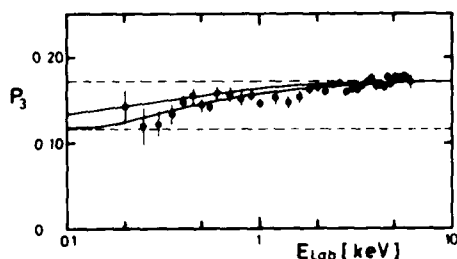


Fig. 1: Circular polarization P_3 of the Na 3p fluorescence light. The upper dashed curve ($P_3=0.171$) corresponds to spin-conservation during the collision, the lower dashed curve ($P_3=0.117$) corresponds to an unpolarized Na 3p electron immediately after the collision. Solid curves take spin-precession calculated for pure coupling cases into account; upper curve: jj-coupling, lower curve: electron-exchange.

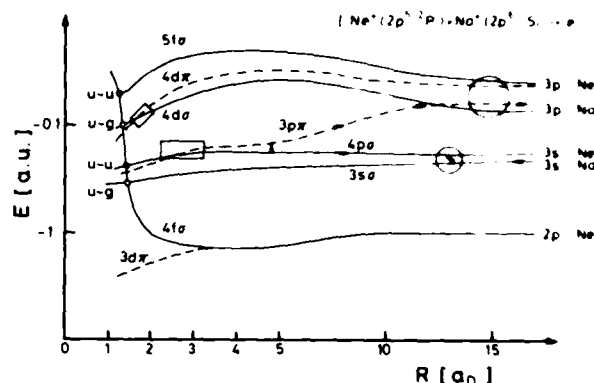


Fig. 2: Molecular orbital diagram of the $\text{Na}^+\text{Ne}^+\text{e}^-$ system (based on diagrams of Olsen et al.³).

state correlates to the atomic $\text{Ne}(2p^5 3s)$ state in which the 3s electron interacts with the $2p^5$ core. The actual interaction results in intermediate coupling of the angular momenta involved. In order to estimate the depolarization of the 3s electron by the interaction one may calculate the depolarization for the limiting cases of jj-coupling (case 1 above) and LS-coupling (case 2 above). In jj-coupling the 3s spin couples with the $2p^5_j$ state where j is (statistically) either $3/2$ or $1/2$ (resulting splitting 417 cm^{-1} and 1070 cm^{-1} , respectively). In LS coupling the spin of the 3s electron is affected by exchange of 3s and $2p^5$ electrons due to the electrostatic interaction (interaction energy $2/3 G^1 = 970 \text{ cm}^{-1}$). With known interaction energies the spin-precession can be calculated.²

The curves obtained by assuming an interaction time $t = 11 a_0/v$ (v denotes the impact velocity) are in qualitative agreement with the experimental data (Fig. 2).

This work has been supported by the Deutsche Forschungsgemeinschaft in Sonderforschungsbereich 216.

¹ W. Jitschin, S. Osimitsch, H. Reihl, H. Kleinpoppen, and H. O. Lutz, J. Phys. B 17, 1899 (1984)

² K. Blum and H. Kleinpoppen, Phys. Rep. 52, 203 (1979)

³ J. O. Olsen, T. Andersen, M. Barat, C. Courbin-Gaussorgues, V. Sidis, J. Pommier, J. Agustí, N. Andersen, and A. Russek, Phys. Rev. A 19, 1457 (1979)

PROTON-INDUCED L X-RADIATION:
STRONG DEPENDENCE OF POLARIZATION ON TARGET NUCLEAR CHARGE

U. Werner, W. Jitschin, and H. O. Lutz

Fakultät für Physik, Universität Bielefeld,
4800 Bielefeld 1, Fed. Rep. of Germany

The polarization and anisotropy of X-radiation originates from the anisotropy (alignment) of the collisionally induced vacancy state. For the proton-induced L-shell radiation of heavy target atoms ($Z_2 > 47$) existing data are in reasonable agreement with advanced theories and, if scaled properly, depend only weakly on the target nuclear charge.^{1,3} In contrast, for light target atoms ($Z_2 = 30$) only two experimental points are available.⁴

In our measurements we recorded the L-spectra of the 3d transition elements Co, Ni, Cu, and Zn ($Z_2 = 27-30$) with a plane-crystal X-ray spectrometer.⁵ The various L lines are well resolved allowing a determination of the L polarization (Fig. 1); measured values were corrected for the polarization sensitivity of spectrometer. At high impact velocities the observed polarization values are small in all targets studied (Fig. 2). At small velocities polarization values of considerable size are

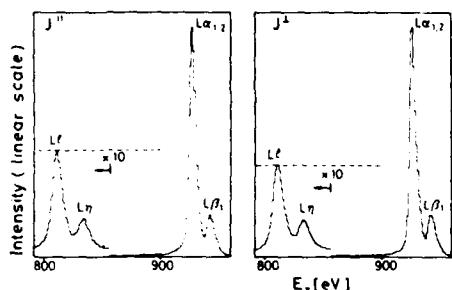


Fig. 1: Recorded L X-ray spectra for 212 keV H_2^+ impact on solid Cu taken for two perpendicular components of the linear polarization.

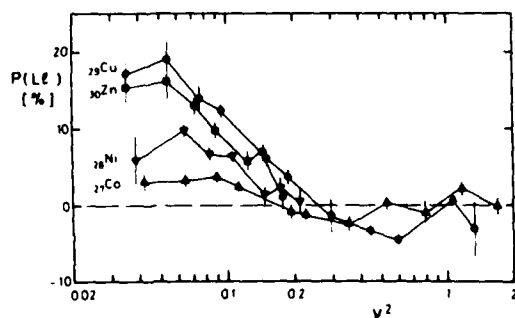


Fig. 2: Measured polarization of the L_γ line corrected for the polarization sensitivity of the spectrometer. v denotes the impact velocity in terms of the classical L_γ electron orbiting velocity. Curves are guides for the eye.

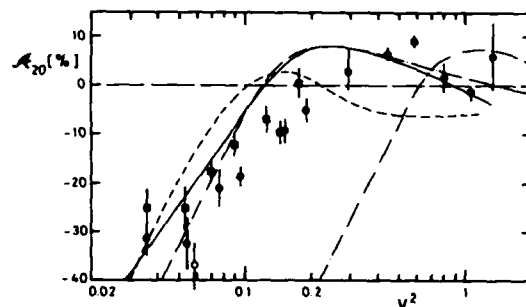


Fig. 3: L_γ -subshell alignment of Cu and Zn. Experiment: \bullet Cu, \blacksquare Zn, present work; \circ Cu, ref. 4. Theory: --- CPSSR with hydrogenic wavefunctions, -.- CPSSR with screened wavefunctions, — SCA with relativistic Hartree-Fock-Slater wavefunctions³, - - - SCA with screened relativistic hydrogenic wavefunctions.³

found for Cu and Zn. In contrast, for Co and Ni considerably smaller polarization values are observed which are attributed to an efficient dealignment after the collision caused by angular momentum coupling of the L_γ vacancy with the unfilled $M_{4,5}$ level in Co and Ni.⁶ Solid-state effects in the metallic targets used are not expected to be serious since the $M_{4,5}$ state is rather well localized.⁷

For Cu and Zn the dealignment is presumably small, and the collisional-induced alignment has been derived from the measured polarization taking corrections for deceleration of the projectile in the target and Coster-Kronig cascades into account (Fig. 3). The results agree qualitatively with scaled data for heavy atoms as well as theoretical calculations.

The work has been supported by the Minister für Wissenschaft und Forschung Land Nordrhein-Westfalen.

¹B. Cleff, *Acta Physica Polonica A* **61**, 285 (1982).

²W. Jitschin, *Nucl. Instrum. Meth.* **232**, 292 (1984).

³A. Jakob, D. Trautmann, F. Rösel, and G. Baur, *Nucl. Instr. Meth.* **232**, 218 (1984) and priv. comm.

⁴A. Schöler and F. Bell, *Z. Phys. A* **286**, 163 (1978).

⁵W. Jitschin, B. Wisotzki, U. Werner, and H. O. Lutz, *J. Phys. E* **17**, 137 (1984).

⁶W. Jitschin, *J. Phys. B* **17**, 4179 (1984).

⁷I. R. Holton, P. Weightman, and P. T. Andrews, *J. Phys. C* **16**, 3607 (1983).

ALIGNMENT AND ORIENTATION OF H(2p) EXCITATION IN H⁺- AND H-RARE GAS COLLISIONS

R. Hippler, W. Harbich, M. Faust, H. Kleinpoppen, M. O. Lutz

Fakultät für Physik, Universität Bielefeld, 4800 Bielefeld 1, FRG

In a previous investigation we have studied H(2p) excitation in H⁺-He. At charge changing collisions at incident energies of a few keV.¹ Using the polarized photon-scattered projectile coincidence technique detailed information about the underlying mechanism for these collision systems was obtained. We have now extended the method to higher incident energies and to quasi-one electron systems, such as H-He. Results for the integrated (i.e. integrated over the scattering angle) alignment for the H⁺-He collision system show a pronounced incident energy dependence as displayed in Fig. 1. From these data some information about the collision dynamics may be extracted. At low incident energies H(2p) excitation may proceed via a two-step process in the transiently formed quasi-molecule. The first step couples the (H-He)⁺ ground state to the charge exchange channel, followed, in a second step, by rotational (o-o) or radial coupling with higher-lying molecular orbitals (MO). The small integral alignment observed at low incident energies indicates that both couplings contribute with about equal probability to the total H(2p) excitation. At large incident energies H(2p) excitation is the result of a one-step process. Coulomb-distorted wave (CDW) calculations predict a large negative alignment A₂₀ around 100 keV incident energy, in qualitative agreement with the experimental data.

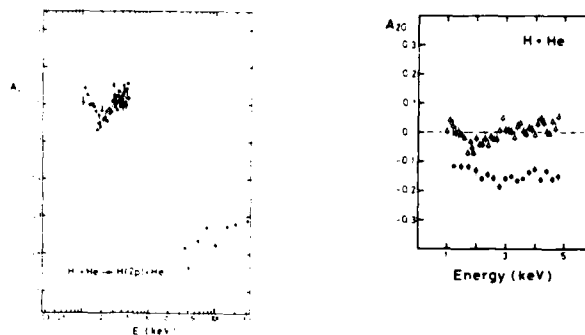
A different energy dependence of the integrated alignment A₂₀ is observed for the quasi-one electron system H-He (Fig. 2). Over the range of incident energies studied, the integrated alignment A₂₀ is almost constant, and amounts to about -0.15. A similar behaviour was also observed for other collision systems, H-He and H-Ar. This negative alignment contrasts sharply to the alignment observed for H⁺-He collisions, where at the same incident energies A₂₀ ≈ 0 was observed.

Pronounced differences between H-He and H⁺-He collisions were also observed for the differential alignment. Measuring the linear and circular polarizations of emitted light in coincidence with scattered projectiles, the alignment tensor components A₂₀ (Q=0,1,2) and the orientation vector were obtained. In comparison to the H⁺-He collision system the following differences were observed:

(1) In H-He collisions the relative population of H(2p₀) is small (< 0.2) and, over the limited range of impact parameters investigated so far, decreases with decreasing impact parameter. This differs from the H⁺-He

collision in so far as, particularly at small impact parameters, a pronounced H(2p₀) excitation was observed.

(ii) The total polarization $P = [(7 P_1/3)^2 + (7 P_2/3)^2 + P_3^2]^{1/2}$ is close to unity, within the experimental uncertainty, in marked difference to H⁺-He, where P averaged only 60-70 %.



Figs. 1 and 2: Integrated alignment A₂₀ versus incident energy for H⁺-He and H-He collisions, respectively.

Fig. 1: ● present results, □ Teubner et al.³

Fig. 2: Present results for ● H-He and Δ H⁺-He collisions

The above differences give evidence that different excitation mechanism may be responsible for H(2p) excitation in H⁺-He and H-He collisions. The strong increase of H(2p₀) excitation in H⁺-He collisions has been attributed to a radial o-o coupling operating at small impact parameters. Obviously, from the present data, such a coupling is of minor importance in H-He collisions.

¹ R. Hippler, M. Faust, R. Wolf, H. Kleinpoppen, M. O. Lutz, Phys. Rev. A, in press

² L. Dube private communication (1984)

³ P. J. O. Teubner, W. E. Kaupilla, W. L. Fite, R. J. Girnius Phys. Rev. A **2**, 1763 (1970)

THE COUPLING OF ELECTRONIC ANGULAR MOMENTUM TO THE MOLECULAR AXIS IN AN ATOM - ATOM COLLISION

J. Grosser

Institut für Atom- und Molekülphysik, University of Hannover, Federal Republic of Germany

More and more atom-atom collision experiments involve a detailed control of the state of polarization of the product or reactant atoms. They require for their interpretation a good understanding of the interaction between the electronic angular momentum of the atoms and the molecular axis, which is formed by the atoms during the collision. For the comparatively simple case of a $^1S + ^1P$ collision, the transition from the atomic to the molecular motion has been completely analysed¹. The P wave function remains space fixed for atomic distances larger than a "locking radius" r_1 and rotates with the axis at smaller distance (The possible uncoupling at very small distance near the united atom limit is not considered here). The transition between the two types of motion is accompanied by a transfer of angular momentum between the electronic and nuclear degrees of freedom. Recent experiments² have fully confirmed the theoretical predictions.

The theory has now been extended to the cases $^1S + ^2S$,¹ L... Fig.1 shows schematically, which types of motion are expected for different combinations of the atomic distance r and the relative velocity v of the atoms. The angular momenta indicated in the various regions are conserved. L, S, and J are the electronic orbital, spin, and total angular momentum. The z- and z'-coordinate axes are fixed in space and to the molecular axis, respectively. The boundaries in fig.1 correspond to zones of radial or rotational coupling. The theory involves the following steps: (1) an eigenfunction expansion of the total wave function in the form

$$\Psi = e^{iM\varphi} \sum_{K, M} \frac{1}{M} (J) F_{KM}(r) u_{KM}(r) \quad (1)$$

where r, φ , and φ are polar coordinates describing the relative motion of the atoms, and K, M, and J are the quantum numbers describing the absolute value and the z and z'-components of the total electronic + nuclear angular momentum; (2) the derivation of the coupled equations for the radial functions $F_{KM}(r)$; (3) the approximate solution of the coupled equations and the summation of eq.1 over K, using semiclassical methods. The theory allows a rigorous discussion of the conservation laws for parity and planar reflexion and a comparison with results obtained for stable molecules.

We discuss a collision $^1S + ^2P$ as the simplest example. The transition from J_1 to J_2 conservation at low velocity is quite similar to the transition from L_1 to L_2 conservation in the case without spin. There exists a

locking radius r_1 , at which the wave function ceases to rotate with the axis. Angular momentum is transferred between the nuclear and electronic degrees of freedom when the system passes through the locking region. For a system with, for example

$$V_{J_1=3/2} - V_{J_2=1/2} = C r^{-3}, \quad (2)$$

the locking radius is

$$r_1 = \sqrt{C/2\hbar v} \quad (3)$$

Simple expressions for the angular momentum balance are obtained, when the wave function has a well defined reflection symmetry, including spin, with respect to the xz-(scattering) plane. In a situation, in which the system dissociates from a state $J^2=3/2, J_z=3/2$ or $J^2=3/2, J_z=1/2$, the expectation value of J_y increases or decreases by an amount

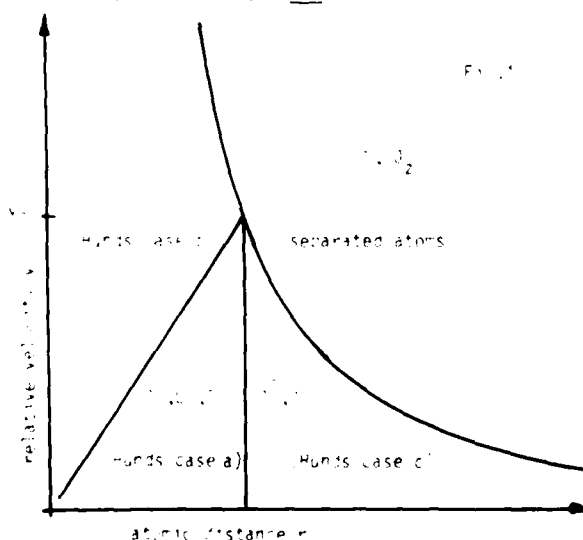
$$\pm \frac{3}{2} \mp \frac{b}{r_1} \quad (4)$$

when the system goes through the locking region. b is the impact parameter, eq.4 holds to the first order in b.

The decoupling process at higher collision energy ($v \gg v_0$) in fig.1 can to a first approximation be described by neglecting the spin. A closer inspection shows that the spin orbit interaction causes a transfer of reflection symmetry between the electronic orbital and spin degrees of freedom. Model calculations for all transitions occurring in fig.1 will be presented.

1) J.Grosser, J.Phys.B14, 1449(1981)

2) A.Bähring et al., Z.Phys.A312, 293(1983)



DIAGONAL AND NONDIAGONAL ELEMENTS OF THE INTEGRAL CROSS SECTION MATRIX FOR
 $H(1s) + Ne, Ar \rightarrow H(nl)$ COLLISIONS AT LOW ENERGY

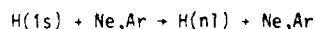
S. Debus, J. Grosser, W. Krüger

Institut für Atom- und Molekülphysik, Universität Hannover, Hannover, Federal Republic of Germany

We report measurements of the quantities

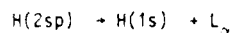
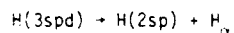
$$\sigma_{nlm/nl'm} = \int f_{nlm} f_{nl'm}^* d\Omega \quad (1)$$

for the inelastic collision processes



for $n=2$ and 3 at collision energies from 40 to 1600 eV. The f_{nlm} are the inelastic scattering amplitudes, the integral is over the scattering angles. The σ with $l=l'$ are the integral cross sections, the nondiagonal terms describe a coherent excitation of, for instance, s and p states ("s-p-coherence"). Practically, the matrix σ is the density matrix for the ensemble of excited atoms produced in the collision.

The experimental method consists of the measurement of the light emitted from the excited atoms,



and of the variation of the light intensities under the influence of an external electric field. The L_{α} intensity, for instance, is related to the cross section matrix as follows:

$$I(L_{\alpha}) = \text{const} \sum_{nlm/nl'm} \sigma_{nlm/nl'm} a_{nlm/nl'm}(F) \quad (2)$$

The sum is over all $n \geq 2$, the $n > 2$ terms are cascade contributions. The σ do not depend upon the field strength, the field dependence of the weighting factors $a(F)$ can be calculated numerically. Some of the functions $a(F)$ are shown in fig.1. It is assumed in eq.2 and in the figure that the quantization axis is the field direction. The weighting factors have an important symmetry property under the reversion of the field direction,

$$a_{nlm/nl'm}(-F) = (-1)^{l+l'} a_{nlm/nl'm}(F) \quad (3)$$

This allows to evaluate the data in two steps. The first one is the evaluation of the experimental values $I(F) + I(-F)$, it yields essentially the cross sections. The second one is the evaluation of $I(F) - I(-F)$, giving nondiagonal (coherence) terms.

We fit the data to the theoretical curves by a least squares procedure, in general the fit covers both H_{α} and L_{α} data. Cascade contributions from $n=4$ are not taken into account, but cascades from $n=3$ are fully taken care of. The table shows preliminary results for a combined H_{α}/L_{α} -evaluation for $H+Ar$ at 300 eV collision energy. The cross sections are summed over the magnetic quantum num-

bers. Our data are compared to data obtained by time resolved H_{α} measurements¹. The last column has been used to normalize our data, but the good agreement of the $3s$ results is conclusive. Our $2s$ and $2p$ results have the same order of magnitude as the results of Birely and McNeal² obtained above 1 keV without cascade corrections, and they are within the limits, which we obtained earlier from an evaluation of the L_{α} measurements alone³.

	2s	2p	3s	3p	3d	3d+0.123p
Our work	3.4	2.9	0.8	0.0	3.5	$3.5 \cdot 10^{-17} \text{cm}^2$
ref.1	-	-	0.8	-	-	$3.5 \cdot 10^{-17} \text{cm}^2$

Table Integral production cross sections, $H+Ar$, 300 eV

The evaluation of the difference signals gives comparatively large values for the $2s/2p$ -coherence term. Other coherences have not yet been found. The coherence terms are limited in their magnitude by the requirement

$$|\sigma_{nlm/nl'm}| \leq \sqrt{\sigma_{nlm/nl'm} \sigma_{nl'm/nl'm}} \quad (4)$$

The typical values found for $\text{Re} \sigma_{2s/2p}$ are not much below the limit. The sign of $\sigma_{2s/2p}$ carries a simple geometric information about the wave function produced in the collision. We can conclude for $H+Ar$ at high energy that the excited electron has its center of charge behind the proton, that is, it points back to the collision partner. This behaviour is reversed at low collision energy.

- 1) B. VanZyl, H. Neumann, H. L. Rothwell Jr., R. C. Amme, Phys. Rev. A **21**, 716 (1980)
- 2) J. H. Birely, R. McNeal, Phys. Rev. A **5**, 257 (1971)
- 3) J. Grosser, W. Krüger, Z. Phys. A **320**, 155 (1985)

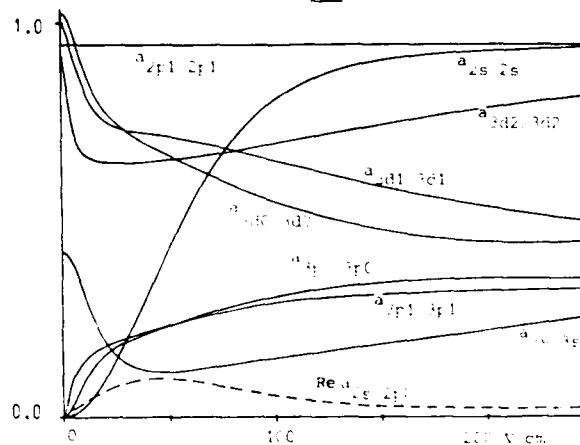


Fig.1 Field dependence of L_{α} weighting factors

EXCITATION OF LOW-ENERGY H TO ns STATES IN COLLISIONS WITH RARE-GAS ATOMS*

B. Van Zyl, M. W. Gealy, and P. S. Ormsby

Department of Physics, University of Denver, Denver, Colorado 80208, USA

Excitation cross sections of ground-state hydrogen atoms (H) to the 2s, 3s, and 4s states in collisions with rare-gas atoms are reported and compared. The H-atom energy range extended from 0.1 to 2.5 keV.

The cross sections for excitation to the long-lived 3s and 4s states were measured previously¹ by observing the increase in the Balmer-alpha and Balmer-beta emissions from $3s \rightarrow 2p$ and $4s \rightarrow 2p$ transitions as a function of distance along the H-beam axis into a target cell containing low-density rare-gas atoms. The 2s-state-excitation cross sections were measured by observing the changes in Lyman-alpha (L_α) emission when an electric field parallel to the H-beam axis was applied in the interaction region viewed by the photon detector.

The basic technique for generation of the H-atom beam, a description of the absolutely-calibrated L_α detector, and the cross sections for L_α emission from H + rare-gas-atom collisions are given elsewhere at this conference.² The electric field was applied by two plates perpendicular to the H-beam axis having 1 cm dia apertures through which the H atoms could pass, and centered about the L_α detector's optical axis.³ Most measurements were made with an applied field of 700 V/cm. The polarizations of the L_α emission observed in the presence of the applied field were also measured. Both the L_α signal and the polarization were found to be independent of the field polarity.

The 2s-state-excitation cross sections could not be simply obtained by subtraction of the L_α emission cross sections measured with the field on and off. Indeed, the field-on cross sections were sometimes smaller than the field-off cross sections. This results from the changes in the cascade population of the $n = 2$ states from higher n states, which can be quite large, when the field is applied. It was thus necessary to undertake an analysis of these cascade effects to properly estimate the 2s-state-excitation cross sections.

The cross sections for these ns-state excitations exhibit a remarkable similarity for all rare-gas-atom targets. They are characterized by broad maxima at H-atom energies near 0.5 keV for 2s-state excitation, the maxima for 3s- and 4s-state excitation occurring at slightly higher H-atom energies. The cross-section ratios for H-atom energies above 1 keV are in reason-

able agreement with the predictions of an n^{-3} scaling law and exhibit a systematic departure from these predictions for lower H-atom energies. This similarity in the ns-state-excitation cross sections for all rare-gas targets is in sharp contrast to the profound differences among these targets for other $n\ell$ -state-excitation processes.

The H + Ne reaction provided an opportunity to examine ns-state excitations in considerable detail. While the reason is not understood, ns-state excitations dominate over other $n\ell$ -state excitations for this reaction.³ It is not that ns-state excitations are here more probable than for other rare-gas atoms, but rather that other $n\ell$ -state excitations are less probable.

The polarizations of the total L_α emissions observed when the electric field was applied were generally smaller than those measured with no field.² For some reactions, the polarizations were slightly negative. However, the polarization of quench-induced L_α from 2s-state decay is a function of electric-field magnitude,⁴ and is near zero for a 700 V/cm field.

The polarization of quench-induced L_α was investigated as a function of electric-field magnitude by observing L_α from H + Ne collisions for an H-atom energy of 0.4 keV. Here, about 67% of the total L_α observed when the electric field was applied resulted from 2s-state excitation. The theoretical dependence of the quench-induced L_α polarization on the electric-field magnitude⁴ was verified for fields between about 200 and 2000 V/cm.

References

1. B. Van Zyl, M. W. Gealy, H. Neumann, and R. C. Amme, Proceedings of the Thirteenth International Conference on the Physics of Electronic and Atomic Collisions (Berlin, 1983), p. 335.
2. B. Van Zyl, M. W. Gealy, and H. Neumann, presented at this conference.
3. B. Van Zyl, M. W. Gealy, and H. Neumann, *Phys. Rev. A* (to be published).
4. D. H. Crandall, unpublished Ph.D. dissertation, University of Nebraska (1970).

*Supported by the Aeronomy Program, Division of Atmospheric Sciences, National Science Foundation.

BRANCHING RATIOS FOR THE DECAY OF $n=3$ HYDROGEN ATOMS IN AXIAL AND TRANSVERSE ELECTRIC FIELDS

N. Rouze, C. C. Havener,* W. B. Westerveld, and J. S. Risley

Department of Physics
North Carolina State University
Raleigh, North Carolina 27695-8202 USA

The branching ratios for the $n=3$ to $n=2$ Balmer- α decay of hydrogen atoms in axial and transverse electric fields in the range 0 - 1000 V/cm have been calculated using a density matrix formalism^{1,2} to take into account the time evolution of the atomic states in the presence of the electric field. The branching ratios are useful when it is desired to measure the cross section for the production of metastable 2s hydrogen atoms by applying an electric field to mix the 2s and 2p states, thereby allowing the atoms to decay by emitting Lyman- α radiation. To correct for cascade contributions from the $n=3$ level, branching ratios for the $n=3$ to $n=2$ decay in an electric field are needed. An example of the use of these branching ratios is provided in the study of H + Ne collisions by Van Zyl, Gealy, and Neumann.³

Branching ratios were calculated for each of the 14 independent elements of the axially symmetric $H(n=3)$ density matrix. An interesting result is that the branching ratios depend on the off-diagonal density matrix elements which give the coherent excitation of the hydrogen atoms in addition to the diagonal density matrix elements which give the cross sections for producing individual excited states. This result emphasizes the need to determine the complete $n=3$

density matrix including the off-diagonal elements.

Results for some of the density matrix elements are shown in Fig. 1. For the off-diagonal s_0p_0 , p_0d_0 , and $p_{\pm 1}d_{\pm 1}$ density matrix elements, the branching ratios change sign for axial fields directed in the $+z$ and $-z$ directions. For transverse fields, only the real and imaginary parts of the s_0d_0 off-diagonal density matrix element have non-zero branching ratios and the magnitude of these ratios are one half the ratios for an axial field. Thus, if the values of the off-diagonal density matrix elements are not known, it is preferable to use transverse electric fields since the contributions to the $n=3$ to $n=2$ branching ratio from these elements is less.

This work was supported in part by the Atomic, Molecular, and Plasma Physics Program of the NSF, Grant No. PHY 82-08905.

References

- *Present address: ORNL, Oak Ridge, Tennessee.
1. C. C. Havener, W. B. Westerveld, J. S. Risley, N. H. Tolk and J. C. Tully, Phys. Rev. Lett. **48**, 926 (1982).
2. C. C. Havener, N. Rouze, W. B. Westerveld and J. S. Risley, Phys. Rev. Lett. **53**, 1049 (1984), and submitted to Phys. Rev. A.
3. B. Van Zyl, M. W. Gealy, and H. Neumann, submitted to Phys. Rev. A.

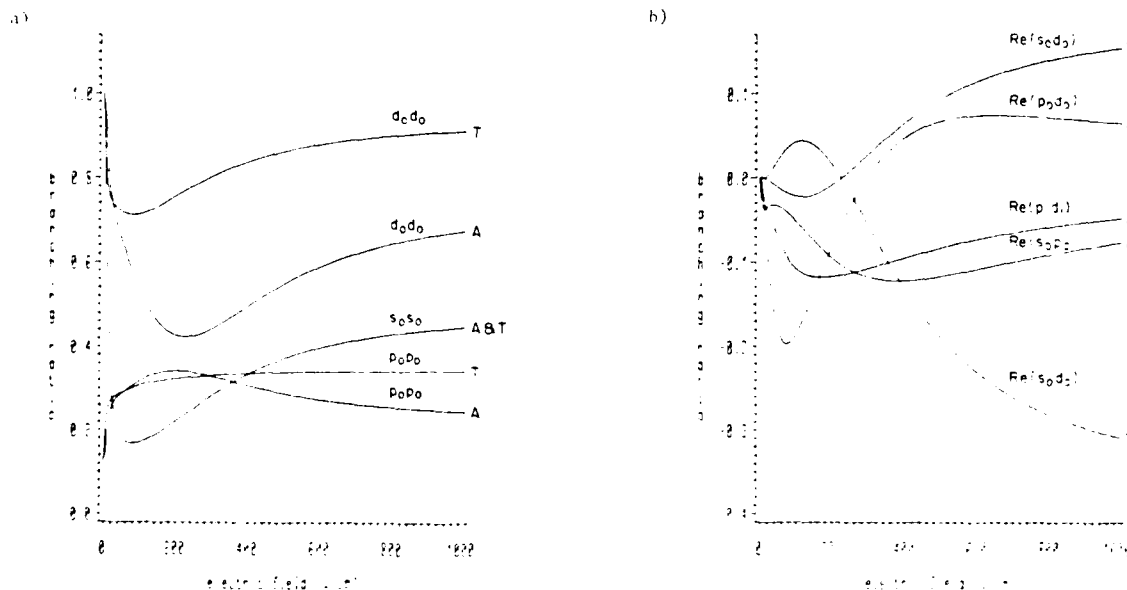


FIG. 1. Branching ratios for the $n=3$ to $n=2$ decay of hydrogen atoms in axial (A) and transverse (T) electric fields for a) three of the diagonal density matrix elements and b) the real parts of the off-diagonal density matrix elements. Axial fields are directed to the $+z$ direction.

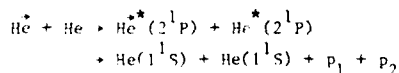
CORRELATIONS AND STATISTICAL DISTRIBUTIONS IN THE SIMULTANEOUS EXCITATION OF BOTH ATOMS IN He-He, H-H₂ AND Ne-Ne COLLISIONS

L. Moorman, J. van Eck, H.G.M. Heideman and G. Nienhuis

Fysisch Laboratorium, Rijksuniversiteit Utrecht, Princetonplein 5,
3584 CC Utrecht, The Netherlands.

THE EXPERIMENT

We measured photon-photon angular distributions resulting from the simultaneous excitation of two colliding helium atoms to the 2^1P state i.e.:



where the fast projectile is indicated by an arrow and the target atoms have thermal velocities. The angular correlation between the emitted photons p_1 and p_2 , which are measured in coincidence provides information on the excitation of the different magnetic-substate combinations of two simultaneously excited atoms. For instance it reflects the probabilities to find the system after the collision in the state $|M_1 M_2\rangle$, where one atom is in the substate $|M\rangle = |M_1\rangle$ and the other in the substate $|M_2\rangle$. The quantization axis is chosen along the beam axis. In our experiment apart from the usual symmetries we have the so called strong symmetry, which means that an interchange of the two final substates leaves the excitation amplitudes the same if the initial ground state is non-degenerate. Apart from a normalization constant the density matrix G is determined by the relative partial cross sections:

$$\begin{aligned} \alpha &= N\langle 00 | G | 00 \rangle & \beta &= N\langle 10 | G | 10 \rangle \\ \lambda &= N\langle 1-1 | G | 1-1 \rangle & \mu &= N\langle 11 | G | 11 \rangle \\ \chi &= N\langle 1-1 | G | 00 \rangle \end{aligned}$$

and the coherence integral: $\chi = N\langle 1-1 | G | 00 \rangle$. We measured them as a function of the kinetic energy in the energy range 0.5 to 3.5 keV.

CORRELATIONS

If a complete experiment is performed every type of atomic-state correlation leads to correlations in the polarization of the two simultaneously emitted photons. However, notice the following:

- 1) We do not detect the direction of the relative final velocity. This leads to an additional axial symmetry around the beam axis.
- 2) We measure angular correlations in stead of polarization correlations, so we cannot measure all independent parameters which exist.
- 3) The density matrix is necessarily anisotropic. This is a direct consequence of the strong symmetry.
- 4) The two atoms get excited with respect to one and the same collision plane (not fixed in our experiment). The mirror symmetry with respect to this

plane is a type of atomic-state correlation.

We find that not every type of atomic-state correlation leads to correlation in the angular distribution. By using the assumption of quasi uncorrelated excitation taking only into account note 4, we derive an inequality for mutually different diagonal elements e.g. $\beta^2 < \alpha(\lambda + \mu)$. Above 1 keV our experimental results do not satisfy this inequality and therefore indicate a real dynamical correlation between atomic substates.

STATISTICAL DISTRIBUTIONS

We define a statistical distribution by the situation where all basis states, with respect to which the state of the system is expanded, have equal probabilities and no coherence. This leaves open the exact choice of the basis set. We choose the magnetic substates of the total orbital angular momentum (L_t) as a base and require a "weighted statistical" assumption. The strong symmetry leads to the rule that no $L_t = 1$ state can be created. The distribution where all the magnetic substates of the total angular momentum get the same weight, including the strong symmetry, fits the low energy data.

OTHER SYSTEMS

We have also searched for double atom excitation in other systems. In $\text{H} + \text{H}_2$ no double excitation leading to two coincident UV photons could be detected. In case of $\text{Ne} + \text{Ne}$ we measured two visible light photons emitted in coincidence due to the decay of the $(2p^5 3p)$ to the $(2p^5 3s)$ state. Search for simultaneous excitation of two $\text{Ne}(2p^5 3s)$ states, namely $3s'[1/2]$, or $3s[3/2]$;

with mean lifetimes of 1.8 ns and 28 ns, respectively were without success. We will compare this with TOF measurements of Brenot et al.¹ and Gerber et al.², who measured emitted electrons of (Atomic or Molecular) Autoionizing states (AAI, MAI) or Intermediate Negative Ions (NI).

References

- ¹J.C. Brenot, D. Dhruicq, J.P. Gauyacq, J. Pommier, V. Sidis, M. Barat, and E. Pollack, Phys. Rev. A **11**, 1245 (1975).
- ²G. Gerber, R. Morgenstern, and A. Niehaus, J. Phys. B **6**, 493 (1973).

MULTIPLE IONIZATION OF Ne, Ar, Kr, AND I BY RELATIVISTIC URANIUM IONS

J. Ullrich,* S. Kelbch,* and H. Schmidt-Böcking,* S. Hagmann,** R. Anholt,† W. Rauch,†† A.S. Schlachter,‡
A. Müller,* P. Richard,** Ch. Stoller,† C.L. Cocke,** and R. Mann‡

*University of Frankfurt, Frankfurt, Federal Republic of Germany

**Department of Physics, Kansas State University, Manhattan, Ks. 66502

†Department of Physics, Stanford University, Stanford, California

††University of Marburg, Marburg, F.R.G.

‡Lawrence Berkeley Laboratory, Berkeley, California

‡Joint Institute of Laboratory Astrophysics, Boulder, Colorado

‡GSI-Darmstadt, F.R.G.

Multiple ionization cross sections $\sigma(q)$ for 425-MeV/amu U ions incident on Ne, Ar, Kr, and I targets were measured at the Lawrence Berkeley Laboratory BEVALAC. The incoming U beam was collimated by an Al-Hb collimator to a beam-spot size of 6-mm diameter. A coincidence between two scintillators in front and behind the target chamber defined the path of the relativistic projectile and therefore the target region. This part of the target area could be viewed by a recoil-ion detector (channel plate) and an electron detector (channeltron) mounted opposite to each other, perpendicular to the beam direction. The gas-target pressure was varied between 7×10^{-5} and 6×10^{-4} torr. The recoil-ion charge state q , which is the degree of multiple ionization, was determined by measuring the q -dependent time-of-flight of the extracted recoil ions between their creation in the target region and their arrival at the channel plate. Additionally, a recoil-ion-electron coincidence was required for a "true" multiple ionization process. This multiple coincidence suppressed background originating from the high flux of δ -electrons and x rays produced by the relativistic heavy ions.

Figure 1 shows ratios between measured Ar charge-state cross sections using 425-MeV/amu and 15.5-MeV/amu U ions.¹ As expected from simple binary-encounter ionization theories, the cross sections should fall off as v^{-2} , where v is the ion velocity (shown by the dashed line in Fig.1). The strong enhancement of $\sigma(q=1)$ over $\sigma(q=2)$ in the 425-MeV/amu data is probably due to a high contribution of target single ionization by δ electrons and x rays created by the projectiles. These data have not been corrected for these additional non-separable coincidences.

References

- * Supported by GSI-Darmstadt and BMFT.
- ** Supported by the Department of Energy.
- † Supported by NSF grant No. PHY-83-13676.
- ‡ Supported by the Department of Energy.

1. S. Kelbch, R. Mann, P. Richard, H. Schmidt-Böcking, J. Ullrich, J. Phys. B18, 323 (1975).

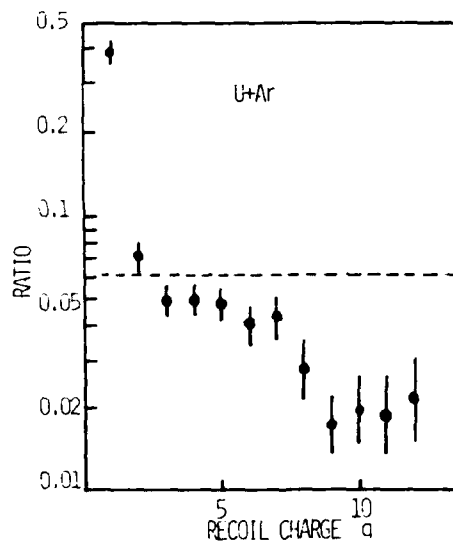


Figure 1. Cross-section ratios $\sigma(q)/\sigma(q=1)$, 425-MeV/amu U/Ar, 15.5-MeV/amu U for Ar multiple ionization. The error bars show statistical uncertainties only. In this preliminary analysis, the absolute uncertainty in the cross-section ratio is estimated to be a factor of three.

PICOAMPERE CURRENTS OF HIGHLY IONIZED SLOW RECOIL IONS PRODUCED BY 70 MEV Br^{18+} IMPACT.*

C. Stoller, L. Lembo, K. Danzmann* and W.E. Meyerhof

Physics Department, Stanford University, Stanford CA 94305

*Physikalisch-Technische Bundesanstalt, 1000 Berlin 10

Energetic heavy ions impinging on solid or gaseous targets can produce slow, highly ionized recoil ions. First evidence of this effect was seen in line shifts of x-rays following a heavy ion collision¹. In 1979, Cocke² reported the direct observation of highly charged Ne recoil ions produced by the impact of 1 MeV/amu C^{6+} , N^{7+} , O^{8+} , F^{9+} and Cl^{11+} ions on a Ne gas target. The slow recoil ions can be extracted from the target with electric fields and because of their small initial kinetic energy (< 10 eV) the resulting beam can have a very small energy spread. Such beams are very useful if precision studies of transitions in the highly charged ions are to be done.

We would like to report here first results obtained with our source of slow recoil ions. The experimental set up is shown in fig. 1. The apparatus is placed at the high energy end of the Stanford FN Van-de-Graaff accelerator, i.e. at a place where the different charge states emerging from the accelerator are not yet completely separated. We used a Br beam as the 'hammer' for producing the Ne recoil ions. The Br beam is focused on the Ne gas jet with a magnetic quadrupole doublet which only focuses well for one charge state. We found Br^{18+} at an energy of 70 MeV to be the optimum beam, significant fractions of both the 63 MeV Br^{18+} and the 77 MeV Br^{19+} beam also hit the target.

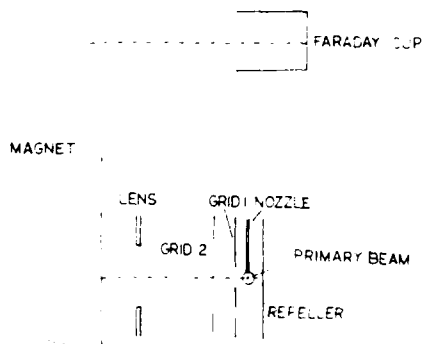


FIGURE 1 Apparatus to extract the slow recoil ions from the gas target and to determine the resulting charge state fractions. The Br is directed out of the plane of the paper.

Four centimeters upstream from the target the incident beams are stripped to an average charge of $18+$ before impinging on the target gas. This poststripping significantly enhances the production of highly charged recoil

ions. The recoiling ions are accelerated by a system of parallel grids, focused by an electrostatic lens and deflected by a 180° magnet similar to the one used by Mann et al³. The recoil ion current is measured in a Faraday cup.

Fig. 2 shows a typical distribution of the different charge states emerging from the target obtained by varying the magnetic field in the magnet. The total accelerating voltage is approximately 500 V (including the potential difference between the nozzle and the first accelerating grid). We have measured currents of up to 1 pA of Ne^{10+} and up to 600 pA of Ne^{5+} with an incident beam of less than 100 particle-nA of Br.

In view of the above results, we are now starting to investigate possibilities of doing optical spectroscopy on H- and He-like Ne by measuring the spectrum after the Ne^{10+} or Ne^{5+} ion has captured an electron in a Na vapor target at the exit of the 180° magnet.

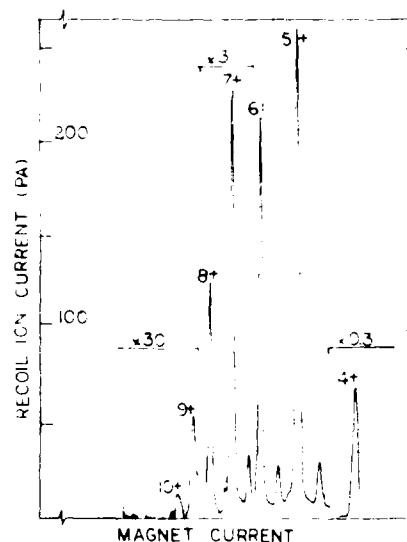


FIGURE 2 Ne recoil ion current (charge) versus magnetic field. Note changes of scale.

References:

* Supported by NSF (Grant PHY 83-13676) and ONR (Grant No 0014-78-C-0403).

1. see e.g. M.D. Brown, J.R. MacDonald, P. Richard, J.R. Mowat, and I.A. Sellin, Phys. Rev. **A9**, 1470 (1974).
2. C.L. Cocke, Phys. Rev. **A20**, 749 (1979)
3. R. Mann, C.L. Cocke, A.S. Schlachter, M. Prior, and R. Marrus, Phys. Rev. Lett. **49**, 1329 (1982).

PRODUCTION OF MULTIPLY CHARGED IONS FROM MOLECULAR TARGETS IN HEAVY ION IMPACT

H.Tawara,[#] T.Tonuma,^{*} S.H.Be,^{*} H.Shibata,^{*} H.Kumagai,^{*} M.Kase,^{*} T.Kambara,^{*} and I.Kohno^{*}[#] Institute of Plasma Physics, Nagoya University, Nagoya 464, Japan^{*} Institute of Physical and Chemical Research (RIKEN), Wako-shi 351-01, Japan

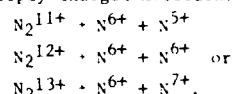
Recently a number of the investigations on mechanism for production of multiply-charged recoil ions in energetic, heavy ion impact have been reported. We have already reported some results on total ionization cross sections by heavy ion impact including He^{2+} , C^{6+} , O^{8+} , Ne^{10+} and Ar^{14+} ions and partial ionization cross sections by Ar^{4+} - Ar^{14+} impact at 1.05 MeV/amu.¹

Following these works on atomic targets, we extend our measurements to molecular targets. In the present work is used an apparatus similar to that described previously.² Typical charge spectra of recoil ions from molecular N_2 targets in 1.05 MeV/amu Ar^{4+} and Ar^{12+} ion impact are shown in Fig.1. In these spectra, we can see a number of peaks corresponding to multiply-charged nitrogen ions including a weak trace of N^{6+} ions, as well as a dominant peak of N_2^{2+} ions which are produced in soft collisions. It is clearly seen from these spectra that the production of multiply-charged atomic recoil ions such as N^{4+} , N^{5+} and N^{6+} ions are significantly enhanced with increasing the projectile charge q . Unfortunately it is impossible to identify the naked N^{7+} ions as $^{14}\text{N}_2$ gas is used in this experiment, though a small amount of N^{7+} ions might be produced in the present collisions.

It is interesting to compare these data with those in electron impact. However, very few measurements of the cross sections for production of multiply-charged ions from molecular targets by electron impact have been reported. N^{3+} ions are the highest charge state directly observed in electron impact.³ Though no direct comparison can be made as the collision velocities in both projectiles are not the same, it is found that production ratio $\text{N}_2^{2+}/\text{N}_2^{+}$ ions are apparently similar in both collisions. However, the production of atomic ions, particularly multiply-charged ions, is significantly enhanced in Ar^{q+} ion impact. Mechanisms responsible in production of multiply-charged atomic ions from molecular targets could be different from those in single atom targets. By comparing the collision time (10^{-17} s) with the dissociation time of molecular ions (10^{-14} - 10^{-15} s), the multiply-charged atomic ions (for example N^{6+}) are thought to be produced through a process of production of multiply-charged molecular ions (for example N_2^{12+}) followed by dissociation into two atomic ions with fairly symmetric charge ($\text{N}^{6+} + \text{N}^{6+}$). In electron impact, only singly- and

doubly- charged molecular ions (N_2^{+} and N_2^{2+}) have been observed but no molecular ions with higher charge. Even in ion impact, no trace of triply-charge molecular ions (N_2^{3+}) corresponding to $M/e=9.33$ is seen in Fig.1. This may imply that the life times of these multiply-charged molecular ions are too short that these ions are not detected even though these ions are produced in collisions.

From this discussion, we can infer that the multiply-charge atomic ions, for example N^{6+} the highest charge state observed in the present work, are produced via the following dissociation processes of multiply-charged molecular ions:

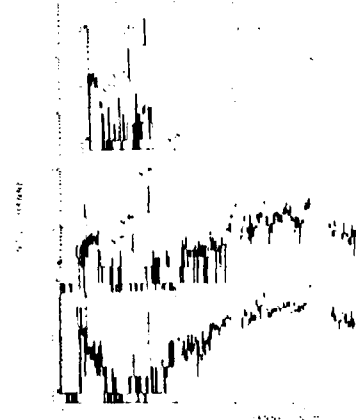


Of course there should be other possibilities for productions of these multiply-charged atomic ions as well. To understand the whole mechanisms for production of these multiply-charged atomic ions from molecular targets, it would be necessary to measure the energy and charge distributions and possibly the angular distributions of two dissociated ions in coincidence, in addition to measurements of total productions cross sections of these ions and theoretical investigations on the level schemes and their life times of multiply-charged molecular ions such as $\text{N}_2^{12+} \sim \text{N}_2^{14+}$ ions.

References

1. S.H.Be et al., to be published
2. T.Tonuma et al., *J. Phys. B* **17**, L317 (1984)
3. N.R.Daly and K.E.Powell, *Proc. Phys. Soc.* **89**, 273 (1966)

Fig.1



STORAGE OF HEAVY-ION GENERATED MULTIPLY-CHARGED RECOIL IONS IN A RADIO-FREQUENCY QUADRUPOLE ION TRAP

C.S. O, R.T. Short, S.D. Berry, S.B. Elston, M. Breinig, R. DeSerio, I.A. Sellin, and B. Thomas*
University of Tennessee and Oak Ridge National Laboratory

D.A. Church, H.M. Holzschelter, and R.A. Kenefick
Texas A&M University

Multiply-charged recoil ions, produced by impact of 1 MeV chlorine ions having mean charge state near ten with target gas, were stored in a radio-frequency quadrupole ion trap. The radio-frequency quadrupole ion trap was mounted in front of the Penning ion trap on the ARND EN Tandem uHV beam line [1]. The heavy ion beam passed through apertures in the trap ring electrode to ionize the target gas atoms near the equatorial plane of the ion trap. The trap was operated at a trapping RF angular frequency of $\omega = 2\pi \times 8.4$ MHz with peak amplitude adjustable to over one thousand volts. An axial motion resonance method was used to detect the ions. After a chosen time delay, the DC voltage applied to the ring electrode was swept to successively bring the ion axial oscillation angular frequencies into resonance with the detection frequency $\omega_{z0} = 2\pi \times 280$ kHz. Both neon and methane were used as target gases. Neon ions Ne^{q+} ($2 \leq q \leq 8$) and C^{q+} ($2 \leq q \leq 4$) were observed. For lower charged states the ions of mass 22 and 20 neon isotopes were well resolved. The charge state of the stored ions was also identified through harmonic radial motion resonance removal by exciting the parametric resonance. Different combinations of trap operating voltages, both RF and DC, were used to produce a mean potential well depth varying from as low as 1 eV up to about 100 eV depending on the charge state of the ions. Stability conditions were investigated and found to be in agreement with theoretical prediction. Storage times of the stored ions were limited by charge exchange with the background gas atoms. Storage times of over one second were realized for Ne^{3+} and C^{2+} ions in target gas partial pressures over 3 and 6 $\times 10^{-6}$ Torr, respectively. Experimental loss time constants for decay of the stored neon ion number were measured at several partial pressures of the neon target gas. The charge exchange rate constants so obtained were in good agreement with earlier measurements in other types of ion traps [1,2].

These data indicate that RF traps will be useful for both collision and spectroscopy experiments on multiply-charged ions at low energies. The advantages of this trap type arise particularly when low ion energies, the absence of a magnetic confining field, and a simplified introduction of external beams into the relatively small ion confinement region are desired.

Research supported by the National Science Foundation;

Texas A&M CEMR, and Oak Ridge Associated Universities and by the U.S. Department of Energy, under contract no. DE-AC05-84OR21400 with Martin Marietta Energy Systems, Inc.

References

- [1] D.A. Church, R. A. Kenefick, W.S. Burns, C.S. O, R. Holmes, S. Hultdt, S.D. Berry, M. Breinig, S.B. Elston, J.-P. Rozet, I.A. Sellin, D. Taylor and B. Thomas, Phys. Rev. Lett. **51**, 1636 (1983).
- [2] M.H. Prior, R. Marrus, and C.R. Vane, Phys. Rev. **A28**, 141 (1983).

*Permanent address: Carleton College, Northfield, MN.

ELECTRON STRIPPING CROSS SECTION FROM MULTI-CHARGED IONS BY H AND He

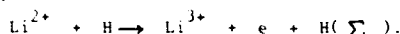
S.Karashima, T.Watanabe,* and Y.Liu†

* Department of Electrical Engineering, Faculty of Engineering, Science University of Tokyo, Shinjuku-ku, Tokyo 162 Japan

† The Institute of Physical and Chemical Research (RIKEN), Wako-shi, Saitama-ken 351 Japan

‡ China University of Science and Technology, Hefei, Anhui Province, China

Electron stripping cross sections for energetic highly charged C, Ne, and Ar ions passing through atomic hydrogen and helium target are calculated using the method of the binary encounter approximation (BEA). It is found that the stripping cross section can be obtained by the plane-wave Born approximation¹⁾ as well as BEA in the case of



We treat the electron loss process of multi-charged ion A^{q+} (atomic number Z_1) in the collision with a neutral atom B (atomic number Z_2):



where $B(\Sigma)$ means all possible electron states of B. In the process of electron stripping from A^{q+} , the interaction of electron in A^{q+} with nucleus B is usually screened by the surrounding electrons. In the present paper, we confine ourselves to the case where this effect can be ignored, i.e. $Z_2 \ll q$. For the time being, we treat $Z_2 = 1, 2$ and $q \geq 3 Z_2$.

The process (1) is characterized by the large magnitude of momentum, transferred to the electrons in the ion A^{q+} by collision with the neutral atom B. Such collision with large momentum transfer can well be approximated by the classical description supporting the use of BEA. An electron in A^{q+} is assumed to be ejected into the continuum if the energy transferred to the electron exceeds its binding energy E_i .

The momentum distribution $f(p)dp$ for an electron having momentum between p and $p + dp$ and the probability $I_r(p)dp$ for finding an electron in this momentum range at a distance r from the projectile nucleus in a potential $V(r)$ are both obtained by the Thomas-Fermi (TF) model:

$$f(p)dp = \int_0^{E(p)} I_r(p)dp n(r)r^2(p,E) \frac{dr}{dp}(p,E)dE \quad (2)$$

and

$$I_r(p)dp = 3 p^2 dp / p_{\max}^3 \quad \text{for } p \leq p_{\max}, \quad (3)$$

where $r(p,E)$ is determined with relation $(p^2/2m) + V(r) = E$ and $n(r) = (8\pi/3h^3)p_{\max}^3(r)$ is the number of electron per unit volume at r . The value of the maximum momentum p_{\max} is given through the TF equation.

When we define ionization cross section $\sigma_n^{(i)}(v,w)$ in the laboratory frame for the collision between a nucleus with a velocity w , the cross section $\sigma_n(v)$ for electron stripping from A^{q+} by collision with the target nucleus is defined as

$$\sigma_n(v) = \int_0^\infty \sigma_n^{(i)}(v,w) f(w) dw, \quad (4)$$

where $f(w)$ denotes a momentum distribution function determined in eq.(2). On the other hand, $\sigma_n^{(i)}(v,w)$ for projectile ion is derived from the Vriens theory^{2,3)}.

We have carried out integration in eq.(4) taking the binding energy which corresponds to each electronic states in shell-structure such as K-, L-, or M-shell. In the calculation for $f(w)$ in eq.(2), we have used three values of the K, L, and M shells, i.e. $f_K(w)$, $f_L(w)$, $f_M(w)$. The description for these functions $f(w)$ is made such that the integration over E to a certain $E(p)$ and over p from 0 to ∞ in eq.(2) equals the number of electrons, i.e. 2 ($q_1 \leq Z_1 - 2$) and 1 (otherwise) for the K-shell electrons.

The calculated results of σ_n for $C^{q+} + H$ are shown in the figure. The comparison with experimental data for C^{q+} is also made.

References

1. T.Watanabe, J.Phys. B18(1985) in press.
2. L.Vriens, Case Studies in Atomic Collision Physics I, ed., E.W.McDaniel and M.R.C.McDowell (North-Holland, Amsterdam 1967)p.335.
3. L.Vriens, Proc. Phys. Soc. 90,935(1967).

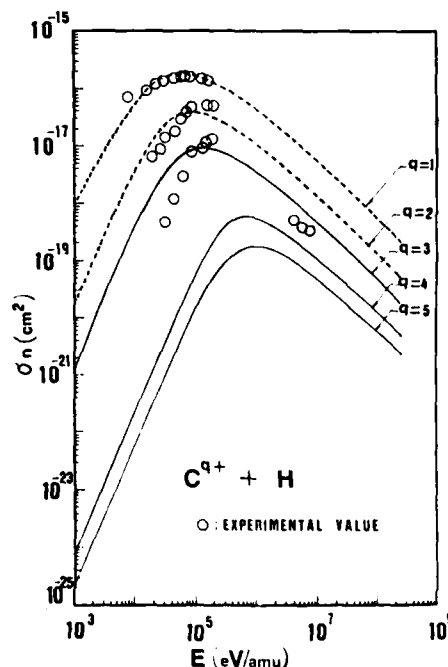


Fig.1 Electron stripping cross sections

HIGH RESOLUTION MEASUREMENT OF $K\beta$ AND $K\alpha$ X RAYS FROM 33 MeV Ar IONS IN SOLID TARGETS

T. Kambara, Y. Awaya, M. Kase, H. Shibata and H. Kumagai

The Institute of Physical and Chemical Research (RIKEN), Hirosawa, Wako, Saitama 351-01, Japan

We have been measuring K X rays from Ar ions passing through various solid targets with high resolution to study target atomic number (Z_2) dependence of multiple inner-shell ionization process. We have reported that the L-shell ionization probability of the Ar ions (P_L) at the time of the $K\alpha$ transition and the hypersatellite to satellite intensity ratio of the $K\alpha$ X rays depend on Z_2 systematically.^{1, 2)}

In the present report, we present the result of measurement of the relative intensity of the $K\beta$ X rays to the $K\alpha$ X rays as a function of Z_2 . We have found that the ratio has a dependence similar to that of P_L . This implies that the electronic transition from the outer shell is affected by the ionization in the L-shell.

The experimental set up is the same as that reported previously;^{1, 2)} the energy of the incident Ar ions from the RIKEN heavy-ion linac is about 33 MeV and the X rays are measured by a broad range crystal spectrometer. The target species are Be, C, Mg, Al, Ca, Ti, Cr, V, Fe, Co, Ni, Cu, Zn, Y, Nb, Tb, Ta, and Au. In order to assign the L-shell hole numbers for the $K\beta$ satellite peaks, the result of energy calibration using fluorescent L-X rays of In and Sn is compared with the estimated values of $K\beta$ transition energies.

The L-shell ionization probability at the time of $K\alpha$ transition is deduced from the intensity distribution of the $K\alpha$ satellites, as reported previously,^{1, 2)} and it shows oscillatory dependence on Z_2 with the first minimum at $Z_2=22$ and the second one at $Z_2=45$. This dependence is shown in Fig. 1(a), where the ionization probability is denoted by $P_L(K\alpha)$. This fact is described as a result of level matching between the L-shell of Ar ion and the L and M shell of target atoms.²⁾ The ionization probability at the time of $K\beta$ transition, $P_L(K\beta)$, estimated from the average energy of the $K\beta$ satellites is shown in Fig. 1(b). It has the same dependence as that of the $P_L(K\alpha)$ on Z_2 at small Z_2 's but the dependence is not clear at large Z_2 's. The first minimum of P_L is seen in both $K\alpha$ and $K\beta$ transitions but the second one is not clear for $K\beta$ one.

The intensity ratio among the $K\alpha$ satellites, $K\beta$ hypersatellites, and $K\beta$ satellites is strongly dependent on the target species. The Z_2 dependence of the intensity ratio between $K\beta$ satellites and the $K\alpha$ hypersatellites has been discussed previously.^{1, 2)} The Z_2 dependence of the intensity ratio between the $K\beta$ and $K\alpha$ X rays, shown

in Fig. 1(c), is similar to the Z_2 dependence of the ionization probability $P_L(K\alpha)$ shown in Fig. 1(a). This may be explained as a result of the increase in electron capture cross section to M-shell according to

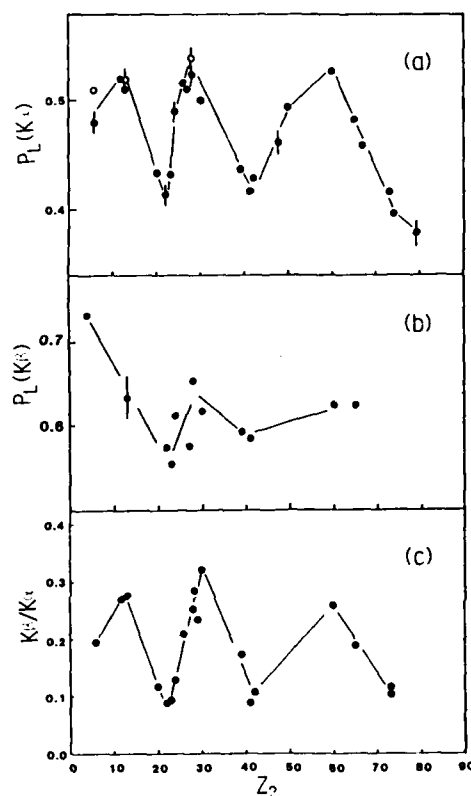


Fig. 1. The target atomic number Z_2 dependence of (a) probability of L-shell holes at the $K\alpha$ -ray emission, (b) probability of L-shell holes at the $K\beta$ -ray emission and (c) intensity ratio between Ar $K\beta$ X rays and $K\alpha$ X rays.

the level matching and increase in the transition probability of the $K\beta$ transitions for ions with more L-shell holes if the number of electrons in the M-shell is independent of the number of L-electrons.

References

1. Y. Awaya, T. Kambara, M. Kase, H. Kumagai, J. Urakawa, H. Shibata, T. Matsuo, J. Takahashi and M. Namiki: Abstract of XIII ICPEAC (Berlin, 1983), P. 470.
2. Y. Awaya, T. Kambara, M. Kase, H. Shibata, H. Kumagai, K. Fujima, J. Urakawa, T. Matsuo and J. Takahashi: to be published in Nucl. Instr. Methods.

HIGH RESOLUTION MEASUREMENT OF Cu K X RAYS FROM COLLISION SYSTEMS OF Cu IONS ON C TARGET AND C IONS ON Cu TARGET

Y. Awaya, T. Kambara, M. Kase, H. Kumagai, H. Shibata, T. Mizogawa, and K. Shima*

The Institute of Physical and Chemical Research (RIKEN), Hirose, Wako, Saitama 351-01, Japan

* Tandem Accelerator Center, University of Tsukuba, Ibaraki 305, Japan

In order to study the difference in ionized states between target atoms and projectile ions, we have measured the K X rays from the Cu ions passing through C foil and that from Cu target atoms excited by C ions under the condition that the relative velocity between the target atoms and the projectiles is same.

The 0.83-MeV/amu Cu^{4+} and C^{2+} ions were accelerated by the RIKEN heavy-ion linac and momentum analyzed. Targets used were 80 $\mu\text{g}/\text{cm}^2$ carbon foil for Cu ions and 0.22 mg/cm^2 Cu foil for C ions. The Cu K X rays were measured by using a broad range X-ray crystal spectrometer¹⁾ with a crystal of LiF(220) ($2d=2.848 \text{ \AA}$).

An estimated value of the average charge of incident Cu ions is $17.3^{+2)}$ and Cu ions are considered to reach a charge equilibrium state after they traverse the carbon target of a few $\mu\text{g}/\text{cm}^2$.

This means that if a Cu ion loses its electrons successively from low to high binding energies, the ion does not bear L vacancies when it collides with a target C atom. Therefore, the configurations of L and K shells are considered to be nearly the same for the projectile Cu ion and the target Cu atom. On the other hand, the effective charges felt by a projectile Cu ion from a target C atom and that felt by a target Cu atom from a projectile C ion is deemed to be $6+$ when a K electron of Cu ion/atom is ionized. The difference between the spectra of Cu K X rays from the projectile Cu ions and that of the target Cu atoms reflects mainly the density effect in collision system.

The Cu K X-ray spectra obtained from Cu ions and the Cu target are shown in Fig. 1 in comparison with the fluorescent Cu X rays. KL^n denotes the initial state vacancy configuration with single K and n -multiple L holes. Figure 1 shows that a Cu ion has about two more L vacancies than a target Cu atom does when they emit K X rays. This is because a Cu ion collides successively with target C atoms whereas a target Cu atom interacts once with a projectile C ion during the K vacancy exists. When a projectile loses one K-electron and multiple L-electrons in a collision with a small impact parameter, then it can collide with other target atoms with larger impact parameters and captures or loses outer shell electrons before K X rays are emitted.

Further measurements of Cu K X rays from both the projectile Cu ions and the target Cu atom excited by carbon at the different collision energies will be reported and discussions will be made about the collision process or the state of the Cu projectile and the atom.

References

- 1) A. Hitachi, H. Kumagai, and Y. Awaya; Nucl. Instr. Methods 195, 631 (1982)
- 2) K. Shima, T. Ishihara, and T. Mikumo; Nucl. Instr. Methods 200, 605 (1982)

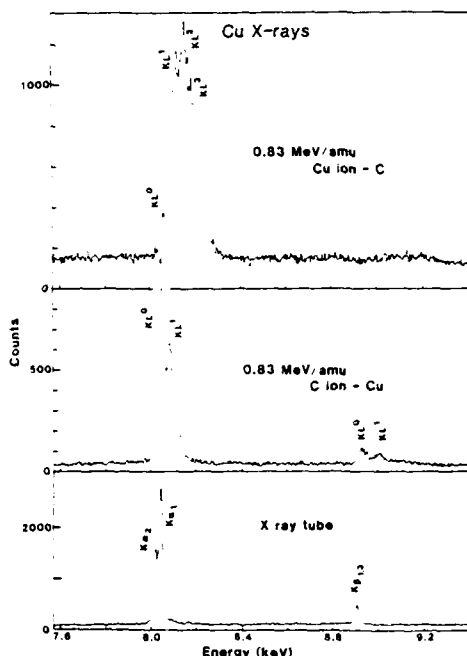


Fig. 1. Spectra of Cu K X rays from projectile Cu ions passing through C foil and from target Cu foil induced by C-ion bombardment. Fluorescent Cu X rays are also shown for comparison. The incident energy of Cu ions and C ions is 0.83 MeV/amu.

IMPACT PARAMETER DEPENDENCE OF MULTIPLE IONIZATION IN 15 MeV F^{6+} ON Ne COLLISIONSS. Kelbch^{*}, C. L. Cocke⁺, S. Hagmann⁺, H. Schmidt-Böcking^{*}, and R. Schuch[†]^{*} On leave from: Institut f. Kernphysik, University of Frankfurt, D6000, Frankfurt/FRG⁺ J. R. Macdonald Laboratory, Kansas State University, Manhattan, Kansas 66506, USA[†] On leave from: Physikal. Institut, University of Heidelberg, 69 Heidelberg, FRG

In fast heavy ion atom collisions, multiple electron processes incorporating both target and projectile usually dominate single excitation or ionization reactions. These processes can be separated into pure multiple ionization (MI), electron capture or projectile electron loss accompanied by MI (CI or LI, respectively). Theoretical interest in those many-body problems grew recently since more and more experiments of the total production cross sections of recoil ions by heavy ion impact have been performed and have shown that highly charged target ions are created with very large cross sections. Already from these total cross section experiments a strong influence of the different impact parameter dependencies of pure MI, CI and LI have been derived (see e.g. refs. 1,2). Detailed tests of the theoretical concepts currently available - as e.g. the statistical model³ can be made only by comparison of impact parameter dependencies rather than cross sections. Therefore, we have measured the scattering angle (or impact parameter) dependence of the multiple ionization probability $P^{MI}(\theta)$ as well as $P^{CI}(\theta)$ and $P^{LI}(\theta)$ in collisions of 15 MeV F^{6+} with Ne and Ar.

The multiply-charged recoil ions were charge-state analyzed by a time-of-flight technique and measured in coincidence with the magnetically charge-state-analyzed projectiles scattered by an angle θ perpendicular to the magnetic deflection

plane. The detection of the projectiles was performed with a position-sensitive channel plate detector with a bow-tie-shaped aperture. To measure the extremely small scattering angles involved in such collisions ($5 \cdot 10^{-5} - 10^{-3}$ rad) a very tight collimation of the beam was necessary resulting in a collimation length of 7m before the target, a beam spot diameter of below 0.2mm and a flight path of the projectiles of 7m downstream of the target region.

In qualitative agreement with the statistical model a shift of the maximum in the recoil ion production probability $P^q(\theta)$ towards larger projectile scattering angles with increasing recoil ion charge state q was observed (Fig. 1). However, at large θ (small impact parameters), deviations from this model are observed since the $P^q(\theta)$ do not decrease rapidly to zero as would be predicted by the statistical model.

This work was supported by the U. S. Department of Energy, Division of Chemical Sciences, and the Bundesministerium für Forschung und Technologie.

REFERENCES

1. T. J. Gray, C. L. Cocke, E. Justiniano, Phys. Rev. A2, 849 (1980).
2. S. Kelbch, H. Schmidt-Böcking, J. Ullrich, R. Schuch, E. Justiniano, H. Ingwersen, C. L. Cocke, Z. Phys. A317, 9 (1984).
3. J. H. McGuire, L. Weaver, Phys. Rev. A16, 41 (1977).

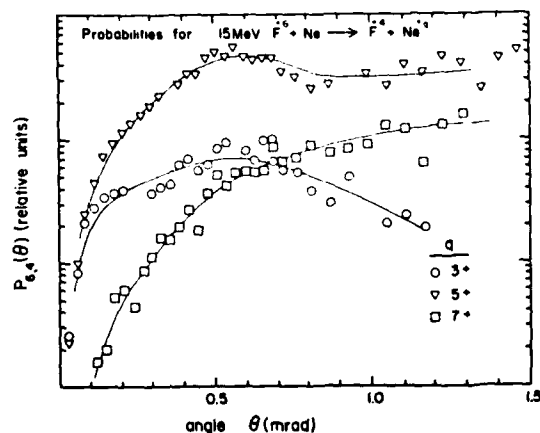


Fig. 1: Scattering angle dependence of the multiple ionization accompanied by double electron capture for 15 MeV $F^{6+} \rightarrow Ne$.

MULTIPLE-ELECTRON PROCESSES IN $H^+ + (He, Ne)$ COLLISIONS AT 300 keV

Richard L. Becker

Physics Division, Oak Ridge National Laboratory*, Oak Ridge, TN 37831 USA

Pauli exchange terms (PET's) play an important role in the Hartree-Fock Independent-Fermi-particle model (IFPM) of atomic structure, but are usually neglected in ion-atom collisions. We have developed the IFPM formulation of collision theory over the past few years.¹ It was applied first to close collisions: (a) K-vacancy production in coincidence with charge transfer,² in which the PET's strongly correct the single-particle-model (SPM),^{1,3} leading to a cross section close to that of the single-electron-transition (SET) model;^{4,3} and (b) $K_m L^v$ multiple-vacancy distributions for K_α satellites ($m = 1$) and hypersatellites ($m = 2$), where the sum of PET's is small because of a tendency toward random phases in the transition amplitudes⁵ so that the distributions are determined by the mean L-shell vacancy per electron, $\bar{p}_L^{(m)}$. More recently we have applied the IFPM to more distant collisions, corresponding to coincidence measurements (summarized in Ref. 6) of the final projectile and target charges, in which target K-shell vacancies are not detected. The calculations were done with the coupled-channels method in the single-center-expansion approximation (see Ref. 2) or with our "one-and-a-half center" expansion (OHCE).⁷ The cross sections will be denoted⁶ by $\sigma_{qq'v}$ where q and q' are the initial and final ionic charges of the projectile and v is the final number of vacancies in the target. We also define cross sections for inclusive electron ejection,

$$\sigma_{11}^{e-} = \Sigma v \sigma_{11v}, \quad \sigma_{10}^{e-} = \Sigma (v-1) \sigma_{10v}, \quad \sigma^{e-} = \sigma_{11}^{e-} + \sigma_{10}^{e-},$$

single-electron capture, $\sigma_{10} = \sum_{v=1}^N \sigma_{10v}$, and non-capture ("direct") ionization, $\sigma_{11} = \sum_{v=1}^N \sigma_{11v}$ ($N = 2$ for He and 8 for Ne).

Hippler *et al.*⁸ have measured the energy and angle of an ejected energetic ("δ") electron in $H^+ + (He, Ne, Ar)$ at 300 keV together with the final charge v of the recoiling target, obtaining values of

$$\frac{d^2 \sigma_v^{e-}}{d\Omega_\delta dE_\delta} = v \frac{d^2 \sigma_{11v}}{d\Omega_\delta dE_\delta} + (v-1) \frac{d^2 \sigma_{10v}}{d\Omega_\delta dE_\delta}$$

for $v = 2$ and 3 (Ne) relative to $v = 1$. Additional unpublished work in which q' instead of v is measured gives the ratio of ejection plus transfer to total ejection,

$$\frac{d^2 \sigma_{10}^{e-}}{d\Omega_\delta dE_\delta} / \frac{d^2 \sigma^{e-}}{d\Omega_\delta dE_\delta}.$$

They have suggested that the cross sections differential in E_δ could give information on the impact-parameter dependence of the transition probabilities, and proposed that ejection at energy E_δ comes predominantly from $b = \hbar v_p / (I + E_\delta)$, where I is the ionization potential.

We have calculated the impact-parameter dependent IFPM probabilities for all of the above processes. The PET terms are important for all transitions involving charge transfer. Integration over b gives good agreement with measured σ_{10} , σ^{e-} , and the cross section for non-v-weighted vacancy production, $\sigma_{11} + \sigma_{10}$. In neon our K_α -satellite \bar{p}_L value, 0.100, is close to the experimental 0.105.⁹ The impact-parameter dependence suggests that electrons of high energy E_δ correspond to values of b larger than those of the equation above by factors of two or more. Calculations for argon are in progress.

References

- *Research sponsored by the U.S. Department of Energy, Division of Basic Energy Sciences under Contract No. DE-AC05-84OR21400 with Martin Marietta Energy Systems, Inc.
- ¹R. L. Becker, J. F. Reading, and A. L. Ford, IEEE Trans. Nucl. Sci. NS-29, 1092 (1981); R. L. Becker, A. L. Ford, and J. F. Reading, Phys. Rev. A29, 3111 (1984).
- ²R. L. Becker, A. L. Ford, and J. F. Reading, J. Phys. B13, 4059 (1980).
- ³R. L. Becker, A. L. Ford, and J. F. Reading, Proc. 8th Conf. Applic. of Accelerators in Research and Industry, Nucl. Instrum. and Meth. (May, 1985), to be published.
- ⁴R. L. Becker, A. L. Ford, and J. F. Reading, Proc. 2nd Intern. Seminar on High Energy Ion-Atom Collisions, ed. by G. Hock and D. Berényi (Akadémiai Kiadó, Budapest, 1985), to be published.
- ⁵R. L. Becker, A. L. Ford, and J. F. Reading, Nucl. Instrum. and Meth. B4, 271 (1984).
- ⁶R. D. DuBois, Phys. Rev. Lett. 52, 2348 (1984).
- ⁷J. F. Reading, A. L. Ford, and R. L. Becker, J. Phys. B14, 1905 (1981).
- ⁸R. Hippler, J. Rossler, and H. O. Lutz, J. Phys. B17, 2453 (1984).
- ⁹J. O. Christensen and Finn Folkmann, Intern. Symp. on Produc. and Phys. of Highly Charged Ions (Stockholm, 1982), contrib. papers, p. 55.

GENERATION OF CONTINUUM PSEUDOSTATES FOR COUPLED-STATES CALCULATIONS OF ION-ATOM COLLISIONS

A. L. Ford and J. F. Reading

Physics Department, Texas A&M University, College Station, Texas 77843 USA

Diagonalization of the target atom hamiltonian H_T in a finite square-integrable basis gives a discrete set of eigenfunctions that represent the lowest few target bound states and provide a discrete representation of the ionization continuum. We have previously shown that K-shell ionization probabilities and cross sections for ion-atom collisions can be calculated accurately by using this discrete set of pseudostates in coupled-states calculations, at collision velocities near the K-shell orbital velocity.¹ These calculations used the independent particle model and either a hydrogenic (for one-electron systems) or a Hartree-Fock target atom potential. We have recently used similar two-electron continuum pseudostates to calculate excitation and single ionization cross sections in correlated two-electron collision systems.² Such calculations are in excellent agreement with both experiment and Born calculations of Bell and Kingston done using explicitly correlated wavefunctions for high energy p+He collisions.

At lower collision velocities we have found that pseudostates generated by diagonalization of H_T are inadequate. At low collision velocities the transition matrix elements depend critically on the slope of the wave functions near the target nucleus, and in the diagonalization of H_T this region of coordinate space receives insufficient weight. The problem is solved by diagonalizing powers of H_T . For a hydrogenic target potential we compare our continuum pseudostates from diagonalization of various powers of H_T to exact continuum Coulomb wave functions, and show the improvement obtained at small distances due to diagonalization of higher powers of H_T . Comparison between cross sections from the exact hydrogenic PWBA and our Born calculations with pseudostates shows the dramatic

improvement in cross section accuracy obtained at low collision velocities when diagonalization of higher powers of H_T is used.

Diagonalization of powers of H_T has also been implemented for Hartree-Fock target potentials and applied to coupled-states calculations of ion-atom collision ionization cross sections at low collision energies.³ Such calculations are used to test current models of Coulomb deflection, target recoil, and increased binding; inaccuracies in the widely used Brandt model are indicated.

Finally, diagonalization of powers ($H_T - E$) has been used as part of a new method for solving the electron-ion scattering problem, for the purpose of separating two-electron continuum pseudostates into single and double ionization components. Results of application of this method to p+He and e+He collisions at high collision velocities will be given.

This work was supported by the NSF under grant PHY-8407263 and by the Texas A&M CEMR.

References

1. A. L. Ford, E. Fitchard, and J. F. Reading, Phys. Rev. A 16, 133 (1977); A. L. Ford, J. F. Reading, and R. L. Becker, Phys. Rev. A 23, 510 (1981); J. F. Reading, A. L. Ford, and R. L. Becker, J. Phys. B 14, 1995 (1981).
2. J. F. Reading, A. L. Ford, J. S. Smith, and R. L. Becker, in Electronic and Atomic Collisions, edited by J. Eichler, I. V. Hertel, and N. Stolterfoht (Elsevier, Amsterdam, 1984), p. 201; A. L. Ford and J. F. Reading, Proceedings of the 8th Conf. on the Application of Accelerators in Research and Industry, 1984, to be published.
3. J. F. Reading, A. L. Ford, J. S. Smith, J. Alexander, and R. L. Becker, Nucl. Instr. Meth. B4, 266 (1984).

THEORY OF EQUILIBRIUM CHARGE-STATE DISTRIBUTIONS

T. Åberg*, A. Blomberg* and O. Goscinski†

*Helsinki University of Technology, SF-02150 Espoo, Finland
 †Department of Quantum Chemistry, Uppsala University, Box 518
 75120 Uppsala, Sweden

The variation of the charge distribution of ions penetrating through gases is usually described by a system of master equations involving cross-sections of all relevant charge-changing processes.¹ Since information on these quantities for many-electron atoms is scarce, this approach does not allow for a derivation of the equilibrium distribution $P(q)$. Previously, using information-theoretical arguments² and a statistical analysis³ $P(q)$ has been shown to be well described by either a distribution normal in $\ln(q+2)$ (the lognormal distribution) or the gamma-distribution in $q+2$, the χ^2 -distribution also used by Baudinet-Robinet et al.⁴ The former corresponds to cases with heavy projectiles and targets in which both multiple electron capture and loss are appreciable.²

For a better understanding of the origin and implications of these distributions it is necessary to consider the underlying microscopic processes more in detail than previously. The basic assumption leading to a lognormal distribution is that the random variable X in each single process obeys

$$X_i = X_{i-1} \cdot \tau_{i-1} \quad (1)$$

where all the variables τ_i have the same probability distribution $P_\tau(\tau)$. The resulting asymptotic ($i \rightarrow \infty$) solution is, however, not stationary since the variance becomes infinite.

If one considers processes with either only increase ($\tau \in [1, \infty)$) or only decrease ($\tau \in (0, 1]$) of X and imposes boundaries on X ($x \in [0, x_0]$), the stochastic process has a stationary distribution given by $P(x) \propto x^{p-1}$ or $\propto (x_0 - x)^{p-1}$ (the parameters $p, x_0 > 0$). In the case of ionization collisions Eq. (1) with $x=q+2$ and $x_0=\infty$ could thus describe processes with only electron loss or only electron capture. In the information-theoretical derivation² $P(x)$ was in fact used as an a priori distribution describing only loss.

The simplest way to take into account both capture and loss processes is to introduce a small negative correlation dependent on X_{i-1} in Eq. (1), i.e.,

$$X_i = X_{i-1} f(X_{i-1}) \tau_{i-1} \quad (2)$$

where $f(X_{i-1})$ is some function of X_{i-1} . In terms of $y_i = \ln x_i$ Eq. (2) becomes

$$\Delta y_i = \ln f(e^{y_{i-1}}) + \ln \tau_{i-1}. \quad (3)$$

Replacing the collision index i by a continuous time-variable t Eq. (3) takes the Langevin form⁵

$$\frac{dy}{dt} = \ln f(e^y) + F(t) + m \quad (4)$$

where $F(t)$ is white noise, and m is the average of $\ln \tau_i$. The corresponding stationary Fokker-Planck solution for X is

$$P^*(x) = (1/x) \exp \left\{ -\frac{\sigma^2}{2} \int_0^x \frac{x' (m + \ln f(x'))}{x'^2} dx' \right\} \quad (5)$$

where σ is the variance of $\ln \tau_i$. Without correlation ($f(x)=1$) $P_0(x)$ is recovered, the lognormal distribution is obtained for $f(x)=x^{-1/2} (x_0^{-1/2} + 1)$, whereas $f(x) = e^{-x/2}$ yields the gamma distribution. Thus the problem has been reduced to the determination of the correlation function $f(x)$ in Eq. (2) from single-collision dynamics. Defining $Z_{i-1} = X_{i-1} f(X_{i-1})$ in Eq. (2) implies that the probability $P(x_i | x_{i-1})$ for a charge-state transition from x_{i-1} to x_i in a single collision is of the form $P(x_i | x_{i-1}) = Z_{i-1}^{-1} P_\tau(x_i Z_{i-1})$, where P_τ is a universal probability density. This could be verified by future experiments.

References

1. J.-D. Betz, Rev. Mod. Phys., **42**, 407 (1970).
2. O. Goscinski, T. Åberg and M. Jönsson, Phys. Lett., **A90**, 464 (1982).
3. T. Åberg, A. Blomberg, T. Jönsson and M. Jönsson, to be published.
4. Y. Baudinet-Robinet, Phys. Rev., **A22**, 96 (1980), and references therein.
5. G. E. Uhlenbeck and H. N. Callen, The Principles of Statistical Mechanics (Gordon, London, 1963).

ANOMALIES IN THE FINAL-CHARGE-STATE DEPENDENCE OF FOIL-EXCITED,
FAST HEAVY RYDBERG ATOMS*

W. Koenig,** A. Faibis,** E. P. Kanter,** D. Maor,† I. Plesser,*
J. Sokolov,* B. J. Zabransky,** and Z. Vager‡

** Physics Division, Argonne National Lab., Argonne, IL 60439

† Dept. of Physics, Technion, Haifa, Israel 32000

‡ Physics Department, Weizman Institute of Science, Rehovot, Israel

Studies of foil-excited fast (MeV/amu) heavy ions have demonstrated large yields of high- n Rydberg atoms formed in such beams. In an effort to better understand these results, we have measured the yields of Rydberg atoms ($n \sim 100-200$) in foil-excited ^{32}S and ^{28}Si beams at incident energies of 3.9 MeV/amu (S, Si) and 3 MeV/amu (Si). Target-thickness ($2 \mu\text{g}/\text{cm}^2$ - $140 \mu\text{g}/\text{cm}^2$) as well as both final and incident charge-state (9^+ - 16^+ for ^{32}S , 7^+ - 14^+ for Si) dependences were measured. The Rydberg atoms were field-ionized in a longitudinal electric (stripper) field and the detached electrons were detected in coincidence with the remaining charge-state-analyzed ionic cores. The stripping field was preceded by another longitudinal (cut-off) field and a transverse (clean-up) field. This arrangement permitted definition of independent lower and upper limits for the range of main quantum numbers (n) for the detected Rydberg atoms.

The experiments show that the production probability of foil-excited Rydberg atoms depend strongly on the mean core charge within the target which varies as a function of the incident charge state (for thin targets) and target thickness (for non-equilibrium incident charge states). The dependences on the target thickness and on the final charge state—in particular for thick targets—are less pronounced (see FIGURE 1). These features show the importance of bulk processes over surface effects.

Beside the above mentioned general trends, certain charge states exhibit a rather anomalous behaviour. For ^{32}S the production probability for $q_{\text{final}} = 14^+$ increases much more rapidly with target thickness than the q -averaged probability. It does not show any saturation even at $100 \mu\text{g}/\text{cm}^2$ where it is nearly a factor 2 above the mean probability (see FIGURE 1). On the other hand for the thinnest targets the Rydberg production probability for $q_{\text{final}} = 13^+$ is significantly lower (\sim factor 2) than for the neighboring final charge states. This effect vanishes completely for thicker targets (see FIGURE 1). Both anomalies are independent of the incident charge state (9^+ or 13^+). For ^{28}Si a similar behavior (although less pronounced) appears for ions with the same number

of core electrons indicating the importance of shell effects. Possible explanation of these effects (e.g. excitation mechanism into Rydberg states following cascade processes or core-charge changing e^- -emission of the foil-excited ions) will be discussed.

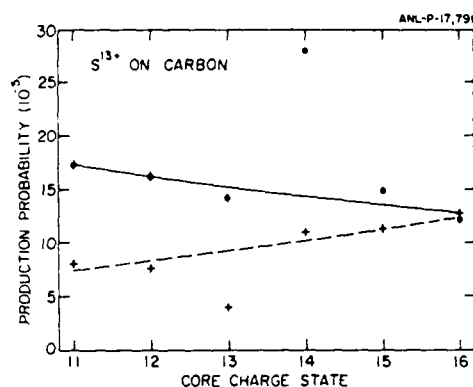


FIGURE 1 Production probability P of foil excited Rydberg atoms ($n \sim 100-200$) as a function of the final charge state of the ion core. The incident beam was 3.9 MeV/amu $^{32}\text{S}13^+$ on carbon targets with thicknesses of $100 \mu\text{g}/\text{cm}^2$ (o) and $2 \mu\text{g}/\text{cm}^2$ (+). The full line shows a fit to the data points assuming $P \propto q_{\text{final}}^m$ with $m = -0.8 \pm 0.2$ ($100 \mu\text{g}/\text{cm}^2$) and $m = 1.4 \pm 0.3$ ($2 \mu\text{g}/\text{cm}^2$). The data are not corrected for the dependence of the ionization thresholds on the final charge state. The corrected m -values are $+0.7$ ($100 \mu\text{g}/\text{cm}^2$) and 2.9 ($2 \mu\text{g}/\text{cm}^2$) respectively.

*Work supported by the U. S. DOE, Office of Basic Sciences under Contract W-31-109-ENG-38.

X-RAY PRODUCTION WITH ATOMIC AND MOLECULAR BEAMS IN THIN FOILS

E. Morenzoni, P. Fumagalli, G. Bonani, W. Wolfli

Institut für Mittelenergiephysik, ETH-Zürich, CH-8093 Zürich-Honggerberg, Switzerland

X-ray production by atomic beam bombardment has been studied intensively over a wide range of projectile energies and for various projectile-target combinations, whereas there have been few investigations with molecular beams¹⁻². When a fast (MeV) molecule penetrates a thin foil, the valence electrons are immediately stripped and the molecule breaks up (Coulomb explosion)³. Due to the Coulomb repulsion the molecule fragments begin to depart from each other, but for sufficiently small times after the molecule entrance in the target they remain spatially and temporally correlated. The vicinity of the molecule ions has been found to manifest itself in several ion-atom interaction processes. For instance the electron loss per atom is generally larger for molecules than for atoms having the same velocity⁴. This implies that the clustered ions behave at small internuclear distance with an effective charge number larger than that of the atomic ions. Since inner-shell ionization depends quadratically on the projectile nuclear charge (Z_p) and electron capture on the fifth power of Z_p ⁵, one expects the target X-ray production to be enhanced by the passage of projectiles in the form of closely correlated clusters. On the other hand the larger energy loss per atom experienced by clustered projectiles should reduce the X-ray yields. The penetration of clustered projectiles in thin foils influences more sensitively the ionization of electrons, whose orbital radius r is at least of the order of magnitude of the mean interatomic distance R in the exploding molecule. Also the time $\Delta t = R/v$ (v : projectile velocity) which is the time difference between the passage of two molecule fragments should be comparable to or smaller than the orbit time $T = 1/\omega$ ⁶.

In order to study the role played by different cluster effects, we measured the low energy X-rays produced in collisions of C, C₂, C₃ projectiles impinging on thin Al and Au targets of different

thickness. The projectile energy ranged from 1 to 11 MeV. With the target thickness the maximum inter-ionic distance reached by the molecule fragments inside the foil could be controlled. We present results of X-ray production cross sections for atomic and molecular beams at the same velocity and a comparison of these results with different theoretical predictions for inner-shell ionization.

References

1. F.K. Chen et al., Phys. Rev. **A15**, 2227 (1977)
2. A. Lurio et al., Phys. Rev. **A17**, 90 (1978)
3. D.S. Gemmel, Physics of Electronic and Atomic Collisions p. 841, S. Datz ed., North-Holland 1982
4. W. Brandt et al., Phys. Rev. Lett. **22**, 1325 (1974)
5. V.S. Nikolaev, Sov. Phys. JETP **24**, 847 (1967)
6. G. Basbas, R.H. Ritchie, Phys. Rev. **A25**, 1943 (1982)

A NEW VARIATIONAL TREATMENT OF DIRECT EXCITATION OF
ATOMS BY BARE NUCLEI AT INTERMEDIATE VELOCITIES

B. Brendlé and R. Gayet

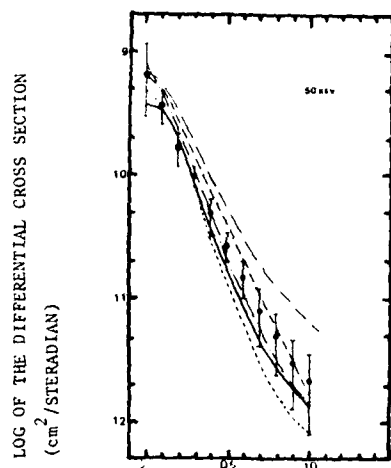
Laboratoire des Collisions Atomiques (ER 260 du CNRS)
Université de Bordeaux I, 33405 Talence, France

The well known Schwinger variational amplitude between states α and β of a system

$$T_{\alpha\beta} = \sum_{i,j} \langle \beta | V | i \rangle (D^{-1})_{ij} \langle j | V | \alpha \rangle$$

$$D_{ij} = \langle j | V - V G_T^+ V | i \rangle$$

is used in the impact parameter formalism for the excitation of hydrogenlike ions by bare nuclei at intermediate velocities¹. The target propagator is evaluated on the target eigenfunction basis set hereafter limited to $1s \dots 5g$. As a check of the method, differential and total cross sections for excitation of the $n = 2$ level of H atoms by H^+ impact is calculated and compared with experimental data² and previous theoretical results of Bransden and Noble (BN) and Shakeshaft (S). Our results (referred to as BG) are obtained by limiting the intermediate states i and j to the target states $1s, 2s, 2p_0, 2p_{\pm 1}$. The first (BI) and second (BII) Born approximations are obtained as by-products of our calculations. The variational procedure makes $T_{\alpha\beta}$ converges very fast on i and j . A reasonable convergence is found on the basis used to evaluate the propagator.



SCATTERING ANGLE (10^{-3} Radian) IN THE
CENTRE OF MASS FRAME

FIGURE 1 - Excitation of H ($n = 2$) by 50 keV H^+
impact
Experiment² - Theory : BG — ;
BN --- ; S . . . ; BI - . - ;
BII - - - -

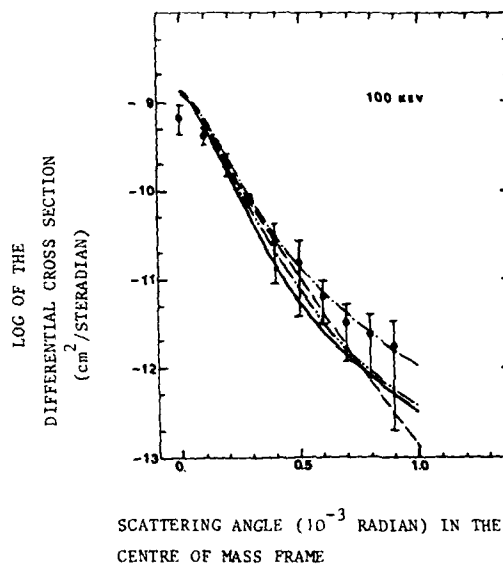


FIGURE 2 - Same legend as figure 1 but the laboratory
 H^+ energy is 100 keV

Our results agree well with previous data, which gives confidence in further applications to direct excitation collisions.

E(keV)	BI	BII	BDN ³	S	BG	Experiment ²
50	14.97	19.08	11.92	8.67	9.20	10.53 ± 0.64
105	10.14	11.23	9.32	8.4	8.54	8.88 ± 0.29

Total cross sections (10^{-17} cm²) for excitation of
H ($n = 2$) by H^+ at two laboratory impact energies E

References

1. B. Brendlé and R. Gayet, to be published ; B. Brendlé, Thèse de 3e cycle, (Université de Bordeaux I, 1984, unpublished).
2. J.T. Park in "Advances in Atomic and Molecular Physics", ed. by D.R. Bates and B. Bedersen, (Ac. Press, N. Yo, 1983) p. 83-8 ; references to data cited here can be found therein.
3. B.H. Bransden, D.P. Dewangan and C.J. Noble, J. Phys. B 12, 3563 (1979).

DIRECT EXCITATION OF 400 MeV - Fe^{24+} BY BARE NUCLEI OF CHARGE Z_p
EVIDENCE FOR FINITE LIMITS OF CROSS SECTIONS WHEN $Z_p \rightarrow \infty$

B. Brendlé and R. Gayet

Laboratoire des Collisions Atomiques (ER 260 du CNRS)
Université de Bordeaux I, 33405 Talence, France

The variational method of Brendlé and Gayet, derived in the impact parameter formalism¹, is applied to the excitation of hydrogenlike ions by bare nuclei. The long-range projectile-target Coulomb interaction which does not contribute to the transition is omitted. Thus the true perturbing potential is

$$V = \left(\frac{Z_p Z_T}{R} - \frac{Z_p}{R-X} \right) - \frac{Z_p (Z_T - 1)}{R} = Z_p \left(\frac{1}{R} - \frac{1}{R-X} \right)$$

where R is the internuclear distance and X the distance between the electron and the target nucleus. Z_p and Z_T are respectively the projectile and target charges. The amplitude of transition from the state i to the state j is :

$$T_{ji} = \langle j | V | i \rangle \langle j | (D^{-1})_{ij} \rangle \langle j | V | i \rangle$$

$$D_{ji} = \langle j | V - V G_T^+ V | i \rangle$$

here, i and j are eigenfunctions of the unperturbed target hamiltonian, including χ and ϕ . In the straight line impact parameter formalism, it is easily seen that, for a given target and a given transition at a given impact velocity, matrix elements $\langle j | V | i \rangle$, $\langle j | (D^{-1})_{ij} \rangle$ and $\langle j | V | i \rangle$ are exactly $\propto Z_p$, while matrix elements $\langle j | V G_T^+ V | i \rangle$ are exactly $\propto Z_p^2$. These scaling laws are noticeable computational advantages of our method. It turns out that when Z_p is large enough, $(D^{-1})_{ij}$ is $\propto Z_p^{-2}$. Then T_{ji} admits a finite limit when $Z_p \rightarrow \infty$. As a result differential and total direct excitation cross sections tend to be constant, as functions of Z_p , when $Z_p \rightarrow \infty$. This important conclusion holds as long as the straight line

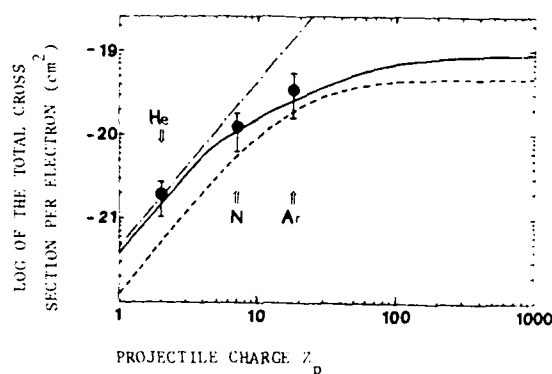


FIGURE 1 - Excitation cross section of the sublevels n of Fe^{24+} for $n=2$ and $\ell=0,1$.

- $n\ell = 2p$: Experiment² - Theory : present results
- ; first Born approximation - - -
- $n\ell = 2s$: Present theoretical results : - - -

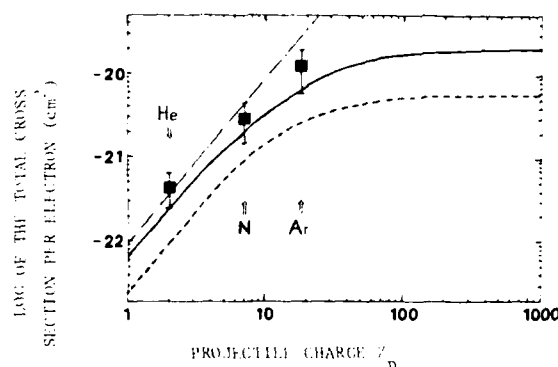
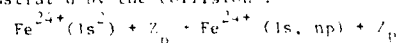


FIGURE 2 - same legend as figure 1 but $n=3$

■ experiment² for $n\ell = 3p$

impact parameter approximation is valid. The situation is illustrated by the collision :



Experimental data² were obtained for $n=2,3$. The Fe^{24+} ions impinge on various atoms of nuclear charges $Z_p < 26$ at a laboratory energy of 400 MeV (intermediate velocity regime). Because of the small relative velocity, direct excitation of Fe^{24+} by the atomic electrons is very unlikely. Rather, the K shell of Fe^{24+} is compact enough to consider that excitation is only due to the nuclear charge Z_p . In our calculations the orbitals of Fe^{24+} are considered as hydrogenlike orbitals around a charge $Z_T = 25$. The set of states i and j are $1s, ns, np_{\sigma}, np_{\pi}$ for the excitation of the ns and np subshells ($n=2,3$). The states m with $n=1, \dots, 5$ and $\ell=0,1,2$ are used to expand the propagator. The upper limit predicted by our theory is clearly confirmed by the measurements. The first Born approximation gives reasonable results only for $Z_p \approx Z_T$ where the matrix elements $\langle j | V G_T^+ V | i \rangle$ are negligible with respect to $\langle j | V | i \rangle$. Thus, excitation cross sections are $\propto Z_p^2$ when $Z_p \approx Z_T$.

References

1. B. Brendlé and R. Gayet, proceedings of XIV ICPEAC (1983) and to be published ; B. Brendlé, these de docteur Université de Bordeaux I, 1984, unpublished.
2. J.P. Rozet, K. Wöhrer, A. Chetoui, A. Jolly and C. Stephan, private communication and to be published.

THEORY OF THE EXCITATION OF HIGHLY-STRIPPED PROJECTILE IONS

U. Thumm, J.S. Briggs and O. Schöller

Fakultät für Physik, University of Freiburg, W. Germany

The standard non-relativistic first Born theory¹ of projectile excitation in collision with a neutral target atom considers the separate influence of target nucleus and target electrons upon the projectile electron to be excited. Normally the electron-electron exchange interaction and the nucleus-nucleus interaction are neglected. This approximation and the assumption that the target atom remains undisturbed in zeroth-order approximation limits the validity of the first Born approximation to collision speeds v greater than the orbital speeds of the electrons involved. Roughly speaking, this requires that the ratios Z_p/v , Z_T/v both be small, where Z_p , Z_T are the effective nuclear charges felt by the electrons taking part in the collision. For light targets and loosely-bound projectile electrons this condition is not difficult to achieve. However, increasingly, projectile-electron excitation is observed under conditions where Z_p/v is not small for non-relativistic velocities and so for these cases the existing first Born formulation is never valid. When $Z_p \gg Z_T$, i.e. one is concerned with excitation of inner-shell electrons on highly-stripped projectile ions in collision with light neutral targets, then a consideration of the effect of the target atom on the projectile electron to first order is valid but it is not valid to assume that the target atom is undisturbed by the projectile Coulomb field. Rather the target atom will be strongly polarised by the projectile field. At large distances the distortion is a direct polarisation effect which can be represented by virtual excited states of the target itself. By contrast at short distances, "exchange" polarisation is more important, where the target electron occupies virtual states of the projectile. In the limit $Z_p \gg Z_T$ the latter effect is more important. A strong potential expansion of the 4-body (two colliding one-electron ions) Coulomb collision problem has been made in which the distortion of the target electron to all orders in the projectile potential occurs but projectile excitation occurs by a single interaction with target nucleus or electron. The main result is that the transition matrix element for simultaneous excitation of the projectile and target from initial states i to final states f is given by

$$T_{fi} = 1/(2\pi^2) \int d\mathbf{q} d\mathbf{k} q^{-2} e_{if}^P(-\mathbf{q}) \psi_{\mathbf{k},i}^+ (\mathbf{K}+\mathbf{k}+\mathbf{q}) \psi_{\mathbf{k},f}^T(\mathbf{K}+\mathbf{v}+\mathbf{k}) - Z_T \psi_{\mathbf{k},f}^T(\mathbf{K}+\mathbf{v}+\mathbf{k}+\mathbf{q}) \quad (1)$$

Here $\psi_{\mathbf{k},i}^+$ is the momentum space off-shell Coulomb wavefunction in the projectile field. The Born result is recovered by replacing this wavefunction by $\delta(\mathbf{K}+\mathbf{q})$. The expression (1) has been evaluated approximately and some preliminary results for helium-like ions are shown in fig. 1.

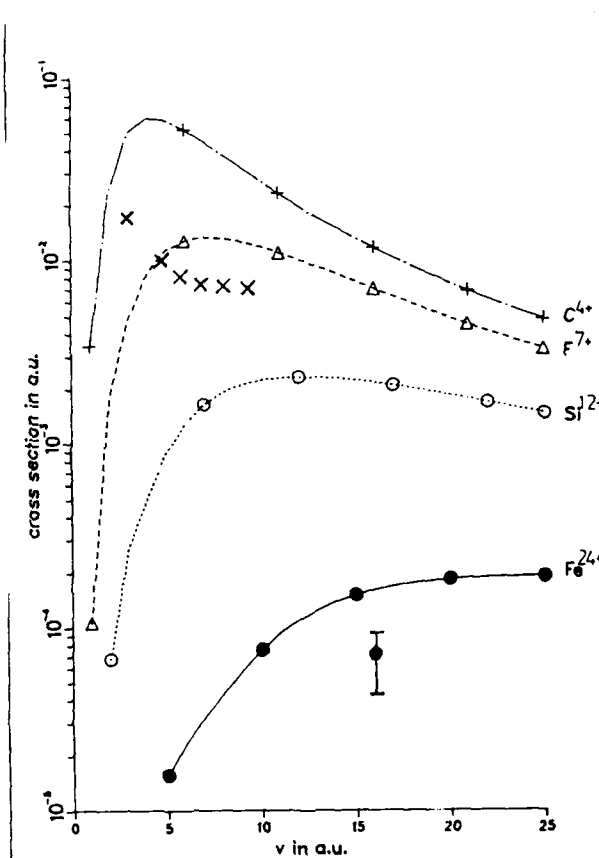


FIGURE 1 Total cross-sections for $(1s^2)^1S + (1s2p)^1P$ excitation of helium-like projectile in collision with helium

x experiment from ref. 3 (F^{7+})
 • experiment from ref. 2 (Fe^{24+})

Reference

1. J.S. Briggs and K. Taulbjerg in "Topics in Current Physics Vol. 5 Ed. I.A. Sellin (Springer: Berlin) 1978, p. 105
2. A. Chetoui and K. Wöhrer (private communication)
3. M. Terasawa, T.J. Gray, S. Hagmann, J. Hall and J. Newcomb Phys. Rev. A27 2868 (1983)

HYDROGEN EXCITATION IN ENERGETIC STRIPPED-ION HYDROGEN ATOM COLLISIONS

A. Salop⁺ and J. Eichler^{**}⁺ Varian Associates, 611 Hansen Way, Palo Alto, California 94306 USA^{**} Hahn-Meitner Institut für Kernforschung, Berlin 39, West Germany

Excitation of atomic hydrogen by collisions with energetic fully-stripped ions is being studied using a method incorporating both a sudden (modified first Magnus) approximation^{1,2} and a first order Born approximation.³ An impact parameter approach is used in which a projectile is assumed to follow a classical rectilinear trajectory. At the smaller impact parameters for which the effective projectile-target electron interaction is strong but of brief duration, the Born approach is invalid and the sudden approximation is employed to calculate the relevant transition amplitudes and excitation probabilities. At the larger impact parameters for which the collisional interaction becomes weak and extended in time, the sudden approximation breaks down and the Born theory becomes appropriate for these calculations.

The amplitude in the sudden approximation (SUA) corresponding to the transition from the 1s ground state to an n,m excited state during a given trajectory corresponding to an impact parameter b is given by

$$a(b, 1s \rightarrow n, m) = \langle n, m | \exp(-i \int_{-\infty}^{\infty} V(t) dt) | 1s \rangle \quad (1)$$

where $V(t)$ is the time-dependent Coulomb interaction between the projectile and the target electron. By following a procedure similar to that detailed in Refs. 1 and 2, one can derive a closed form expression for the transition amplitude as a finite sum over complex ${}_1F_2$ hypergeometric functions. The corresponding impact parameter Born approximation (IPBA) transition amplitudes are obtained by appropriately scaling the analytic expressions for $H^+ + H$ collisions derived by van den Bos and de Heer.³

For fast $H^+ + H$ collisions (for example, a projectile velocity of 25 a.u.), the integrated interaction is weak enough for the IPBA to be adequate even at the smallest parameters. This is therefore a case where the SUA computations can be checked directly against reliable IPBA values, and indeed, the excitation probabilities obtained with the two approximations are in precise agreement over an extended range of impact parameters.

The situation is quite different however in the regime of heavier projectiles and lower velocities. In Table 1 are listed both SUA and IPBA 1s-2s excitation

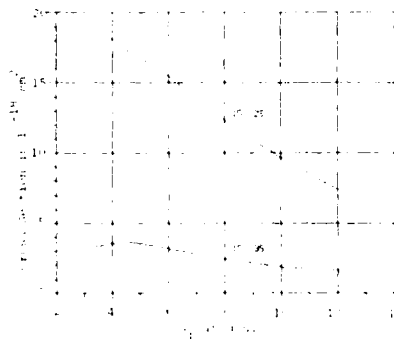
probabilities $P(b)$ for $C^{6+} + H$ collisions at projectile velocities of 3 a.u. ($E_p = 2.7$ Mev) and 25 a.u. ($E_p = 188$ Mev). At the high velocity, the collisional perturbation to the system is still small enough for the IPBA to be a fair approximation even at low-b values, and the two sets of calculations are in fairly close agreement up to $b = 2.5$ a.u. For the low velocity case, it is clear that the non-unitary IPBA results are anomalously large for the close collisions, whereas the SUA is a good approximation in this region. At the larger impact parameters, the SUA breaks

Table 1

1s-2s excitation probabilities for $C^{6+} + H$ collisions.

b(a.u.)	v _p = 3 a.u.		v _p = 25 a.u.	
	IPBA	SUA	IPBA	SUA
0.0	1.21	3.49(-3)	1.79(-2)	1.57(-2)
0.5	9.43(-1)	4.16(-3)	1.40(-2)	1.25(-2)
1.0	5.19(-1)	8.05(-3)	7.71(-3)	7.07(-3)
2.0	9.14(-2)	2.00(-2)	1.37(-3)	1.40(-3)
3.0	1.10(-2)	2.58(-2)	1.67(-4)	2.48(-4)
4.0	1.08(-3)	2.43(-2)	1.66(-5)	6.53(-5)
5.0	9.33(-5)	1.97(-2)	1.45(-6)	2.62(-5)

down, and the IPBA becomes the valid theory. The total excitation cross section at each energy is estimated by integrating over a composite excitation probability curve $P(b)$ obtained by smoothly merging the low-b SUA and high-b IPBA excitation probabilities. Total 1s-2s and 1s-3s excitation cross sections obtained for $C^{6+} + H$ collisions over a range of projectile velocities using the combined SUA-IPBA approach are presented in Fig. 1.

Fig. 1. Total excitation cross sections for $C^{6+} + H$.

⁺ Formerly at Molecular Physics Laboratory, SRI International, Menlo Park, CA where work was performed.

1. J. Eichler, Phys. Rev. A15, 1856 (1977).

2. A. Salop and J. Eichler, J. Phys. B12, 257 (1979).

3. J. van den Bos and F.J. de Heer, Physica 31, 333 (1967).

EXPERIMENTAL Z_T DEPENDANCE OF $1s \rightarrow 2p3p$ EXCITATION CROSS SECTIONS OF TWO ELECTRONS IRON IONS
COLLIDING WITH TARGET ATOMS

K. Wohrer*, J.P. Rozet*, A. Chetoui* and C. Stephan**

* Institut Curie and Université Pierre et Marie Curie, 11, rue Pierre et Marie Curie
75231 Paris Cédex 05 - France

** Institut de Physique Nucléaire, B.P. n° 1, 91405 Orsay - France

Excitation mechanism in ion-atom collisions is known to be well described by the first Born approximation when the perturbation induced by the exciting partner is small (high collision velocity or very asymmetric system). The energy dependance of excitation cross sections has been widely studied in the past, especially for the most simple cases $p \rightarrow H$, He . By contrast, very few has been done concerning the incoming charge state dependance. Deviations to the Z^2 law predicted by first order treatments have been observed in the case of ionization (1) but no systematic study has been performed.

In experiments reported here, projectile excitation of 400 MeV Fe^{24+} ions impinging on target atoms has been measured. By only changing the target (here the exciting partner), the dependance of the cross section on the incoming charge state can be studied in a simple manner and for a fixed collision velocity. Beams of Fe^{24+} ions have been obtained at the CEVIL in Orsay. The target is an effusive gaseous jet with a known profile operating under single collision condition. Heliumlike $n = 2$, $3p \rightarrow 1s$ transitions following excitation into $2p$ and $3p$ states are detected by a $Si(Li)$ detector (resolution of about 180 eV at 6 keV). Branching ratios $nP \rightarrow 1s/nP \rightarrow all$ are known ((2) and (3)) so that population cross sections of these excited states can be determined; corresponding values are reported, for the case of $n = 2$, in the figure I (open circles). Direct excitation cross sections are extracted after subtraction of the cascade contribution and of a double process contribution (target ionization accompanied by capture from the target) both evaluated as indicated in (4).

Uncorrected (open circles) and corrected values (full circles) are shown in figure I in connection with various theoretical predictions: first Born approximation (----), large basis set of target centred coupled state calculations (.) (5) and a new analytical method based on the Schwinger variational method (—) (6). In the calculations, the exciting partner is a bare ion but the charge transfer channel is not considered so that comparison with the experiment (transfer channel is also closed in that case since target atoms are carrying electrons) makes sense.

When looking at the results, two essential features are worth to mention:

. The first Born approximation is valid for the

most asymmetric system even though the collision relative velocity is rather low ($V/V_{1s} \sim 0.6$). When increasing the asymmetry of the collision deviations to the Born results are more and more pronounced

. An effect of saturation at high Z_T is clearly exhibited by the experiment in agreement with the theoretical prediction of the variational method. A similar behaviour has also been observed in the case of excitation into $1s3p$ states.

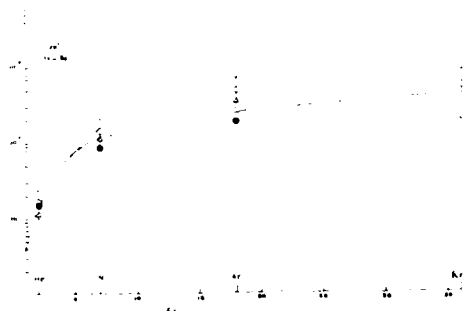


Figure I - Experimental and theoretical $1s^2 \rightarrow 1s2p$ excitation cross sections for 400 MeV $Fe^{24+} + Z_T$. See text for the explanation of the symbols.

References

1. Berkner *et al.*, J. Phys. B **11** (1978) 875.
2. Lin *et al.*, Phys. Rev. A **15** (1977) 154.
3. J.P. Desclaux, private communication (1984).
4. K. Wohrer, Thesis, Paris (1984).
5. J. Reading, private communication (1982).
6. Brendlé and Gayet, submitted to Phys. Rev. Lett. (1985).

AUTOIONISATION OF $N^{3+}(1s^2 3ln'l')$ FORMED BY TWO-ELECTRON CAPTURE
IN $N^{5+}(1s^2)+H_2$ COLLISION, AT 3.4 keV/amu.

A. Gleizes*, P. Benoit-Cattin*, A. Bordenave-Montesquieu*, S. Dousson** and D. Hitz**

CENG, AGRIPPA-CEA-CNRS, 85X, 38041 Grenoble Cédex, France
* Centre de Physique Atomique, UA-CNRS n° 770, Université Paul Sabatier
118 route de Narbonne, 31062 Toulouse Cédex, France.
** Centre d'Etudes Nucléaires, Grenoble, France.

The electron spectrum shown in the figure results from two-electron capture by $N^{5+}(1s^2)$ ions into $N^{3+}(1s^2 3ln'l')$ autoionising states, which decay by electron emission into $1s^2 2l'l'$ continua. Capture processes with the metastable ions $N^{5+}(1s2s^3S)$ cannot contribute to this spectrum since the corresponding reactions are very exothermic; in this case Li-like $1s2ln'l'$ autoionising states are mainly excited, by one-electron capture¹. The Be-like configurations formed by charge exchange in $N^{5+}(1s^2)+H_2$ collisions have also been observed, using translational energy spectroscopy², in $F^{7+}+He$ system. With nitrogen such states cannot be seen using an helium target since this capture process becomes endothermic; even with hydrogen target, only capture into $n'=3$ terms is observable with high intensity, electron transfer into $n'=3$ configurations being a much less probable endothermic reaction.

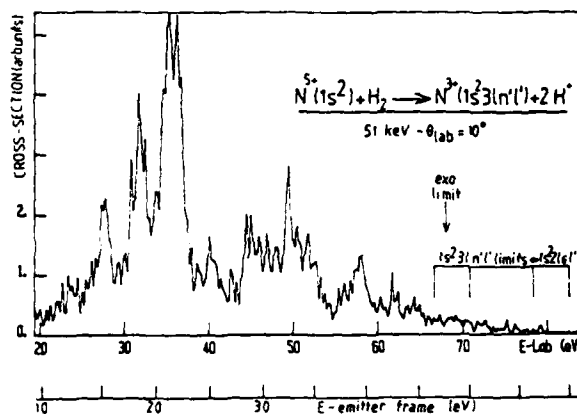
To be sure that our identification is correct, the electron energy has been estimated using an effective nucleus charge $Z=5$ for the two excited electrons; the $(Z=5, 3s^2)$ energy has then been taken in ref. 3; it results an electron energy equal to 28.8 or 18.8 eV depending whether autoionisation occurs into $1s^2 2s 1$ or $1s^2 2p \pm 1$ continua respectively. These values, together with the series limits are in good agreement with our electron spectrum.

Below 20 eV structures were observed which might be due to two-electron capture into $1s^2 2pn'l$, $n \geq 5$ but possible spurious electron background makes this identification ambiguous; more experimental work is necessary.

It is worth emphasizing that theoretical work will be very useful to identify the numerous structures seen in figure 1.

References.

1. A. Bordenave-Montesquieu, P. Benoit-Cattin, A. Gleizes, S. Dousson and D. Hitz 1985, J. Phys.B. Letters **18**, to be published.
2. H. Tawara, T. Iwai, Y. Kaneko, M. Kimura, N. Kobayashi, A. Matsumoto, S. Ohtani, K. Okuno, S. Takagi and S. Tsurubuchi 1983, Proc. 13 th ICPEAC, Berlin, p.542.
3. Y. K. Ho, 1979, J. Phys. B **12**, 387; H. Bachau 1984, J. Phys. B **17**, 1771.



ELECTRON ANGULAR DISTRIBUTIONS AND TOTAL CROSS SECTIONS FOR TWO-ELECTRON
CAPTURE PROCESSES OBSERVED IN $N^{6,7+} + He$ COLLISIONS BY ELECTRON SPECTROSCOPY AT 10.2 qkeV.

A. Bordenave-Montesquieu*, P. Benoit-Cattin*, A. Gleizes*, S. Dousson** and D. Hitz**

CENG, AGRIPPA-CEA-CNRS, 85X, 38041 Grenoble Cédex, France

* Centre de Physique Atomique, UA-CNRS n° 770, Université Paul Sabatier

118 route de Narbonne, 31062 Toulouse Cédex, France.

** Centre d'Etudes Nucléaires, Grenoble, France.

Angular distributions for the $1sn1n'1'$ ($n=2,3$ and $n'>n$) and $n1n'1'$ ($n=3$ and $n'>n$) lines have been measured in $N^{6+} + He$ and $N^{7+} + He$ respectively (figures 1 and 2). Cross sections and angles are given in the emitter frame. It can be seen that these distributions are often non-isotropic and in some cases asymmetrical with respect to 90° . This means that an estimate of total cross-sections from only one-angle measurement¹ may lead to erroneous values. After integration over the angles and summation over all the lines, the following total autoionisation cross sections have been obtained²:

$$N^{7+} + He : \sigma_{\text{auto}} = 7.2 \pm 2.2 \cdot 10^{-20} \text{ m}^2$$

$$N^{6+} + He : \sigma_{\text{auto}} = 3.9 \pm 1.2 \cdot 10^{-20} \text{ m}^2$$

For $q = 0$, σ_{n1} values measured by Gordeev et al³ are consistent with our value only when lowered by at least 20 % in order that the sum $(\sigma_{n1} + \sigma_{\text{auto}})$ agrees with the $\sigma_{q,q-1}$ value measured by Iwai⁴.

For $q = 7$, our value seems to be high compared to the $\sigma_{q,q-1}$ value published by Bliman et al⁵ but better agrees with the largest $\sigma_{q,q-1}$ cross sections measured by other authors^{4,6}. For this system measurement of the σ_{n1} value would be important to check the consistency of all these cross sections.

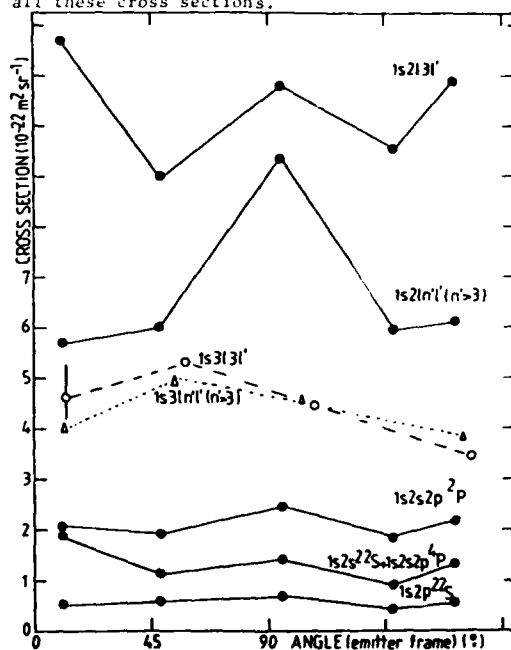


Fig. 1 - $N^{6+} + He$

References.

1. A. Bordenave-Montesquieu, P. Benoit-Cattin, A. Gleizes, A.I. Marrakchi, S. Dousson and D. Hitz 1985, International Conf. Physics of Highly Ionised Atoms. Oxford (1984) to appear in Nucl. Instr. Meth. B.
2. In ref.1 a systematic error in the cross section calculation has led to values which are too low by about a factor ten.
3. Yu.S. Gordeev, D. Dijkkamp, A.C. Drentje and F.J. De Heer 1983, Phys. Rev. Lett. 50, 1842.
4. T. Iwai, Y. Kaneko, M. Kimura, N. Kobayashi, S. Ohtani, K. Okuno, S. Takagi, H. Tawara and S. Tsurubuchi 1982, Phys. Rev. A 26, 105.
5. S. Bliman, M. Bonnefoy, J.J. Bonnet, S. Dousson, A. Fleury, D. Hitz and B. Jacquot 1983, Physica Scripta T3, 63.
6. V.V. Afrosimov, A.A. Basalae, E.D. Donets, K.O. Lozhkin and M.N. Panov 1981, Proc. 12 th ICPEAC, Gatlinburg, p. 690.

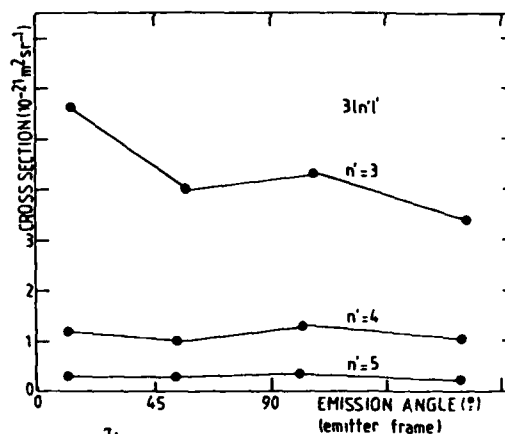


Fig. 2 - $N^{7+} + He$

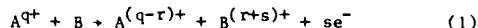
TRIPLE COINCIDENCE STUDIES OF SLOW COLLISIONS OF HIGHLY
 CHARGED IONS WITH ATOMS: ELECTRON SPECTRA

M. Mack, A.G. Drentje* and A. Niehaus

 Fysisch Laboratorium, Rijksuniversiteit Utrecht, Princetonplein 5,
 3584 CC Utrecht, The Netherlands.

*Kernfysisch Versneller Instituut, Groningen, The Netherlands.

In collisions of highly charged ions with atoms the capture of one or more electrons is a very important process.¹ Very little, however, is known about the mechanisms governing multi-electron capture from gas targets, i.e. processes of the kind



Such information can be obtained, as one measures the ejected electrons in coincidence with the charge selected projectile ion $A^{(q-r)+}$ and the charge selected target ion $B^{(r+s)+}$. We have built an experimental set-up to perform such measurements: main part of the set-up is an electrostatic cylindrical mirror analyzer (CEMA), accepting electrons emitted at a polar angle $\theta = 50^\circ \pm \Delta$ with respect to the beam axis. We report here on non-coincident electron spectra, which already revealed specific details of the processes (1). As examples, we show spectra of Ar^{9+} (0.9 keV/amu) on Ar (fig. 1) and of O^{6+} (6.75 keV/amu) on Ar (fig. 2).

Common features of these spectra are:

- they consist only of projectile autoionization peaks.
- No target electron peaks were found so far. All peaks exhibit a corresponding dopplershift.
- lifetimes τ of the excited states seem to be not too short: so far we found no indication for molecular autoionization ($\tau < \text{collision time}$).

Further details of interpretation will be given at the conference: the electron peaks can be ascribed to certain specific charge changing processes only if one takes the coincidence measurement into account.

Still, we can comment on a special feature of the O^{6+} -Ar spectrum (fig. 2): two peak regions are distinctly separated by about 400 eV (all electron energies refer to the emitter frame). The low energy region (20-60 eV) shows projectile autoionization within or to

the L-shell of the $O^{(6-r)+}$ ion; the high energy electrons (350-475 eV), however, can only be emitted if there exists a K-shell hole in $O^{(6-r)+}$. One measures the identical spectrum, only dopplershifted, at 2.25 keV/amu; therefore one wonders, whether this slow ($v = 0.25$ a.u.) impact really can excite the $(1s^2)$ configuration to $(1s2l \dots)$. Possibly the O^{6+} -beam contains a large fraction of metastable ions, e.g. $O^{6+}(1s2s^3S)$. The occurrence of different metastable states could explain the differences between our electron spectrum and the high energy part measured by Schmidt-Boecking².

References

- ¹H.W. Drawin, Phys.Scr. **24**, 622 (1981).
- ²H. Schmidt-Boecking, private communication, 1985.

fig. 1

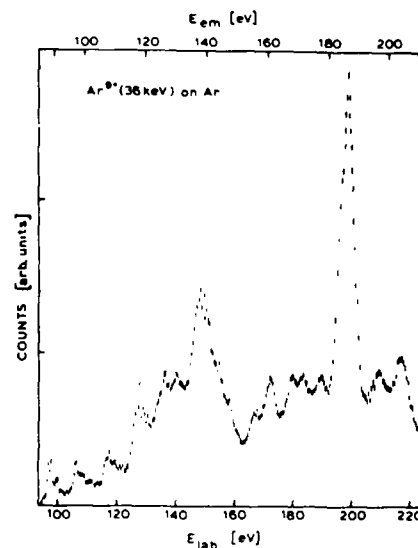
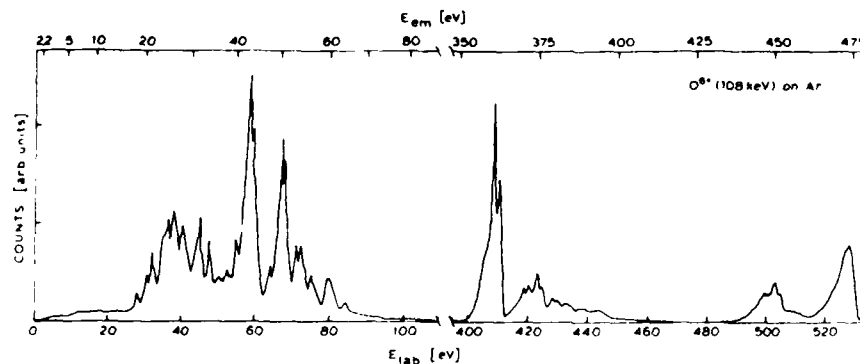


fig. 2



ANALYSIS OF HIGH RESOLUTION L-AUGER SPECTRA FROM MULTIPLY IONIZED Ar PROJECTILES

N.Stolterfoht, Th.Schneider, D.Schneider, and A.Itoh

Hahn-Meitner-Institut für Kernforschung Berlin GmbH
Glienickestr. 100, D-1000 Berlin 39

Recently, we have measured L-Auger electrons from highly ionized Ar projectiles utilizing the method of zero degree Auger spectroscopy.¹ Thus, Doppler broadening effects could essentially be reduced so that the spectra were measured with relatively high resolution. Light target gases such as He have been used to minimize outer shell excitation in addition to the L-shell ionization. Hence, Auger spectra for individual charge states of the projectile could be studied. In Fig.1 an example is shown referring to 91.6 MeV Ar⁵⁺ projectiles in He. In our previous study,¹ the interpretation of various spectral structures remained unclear.

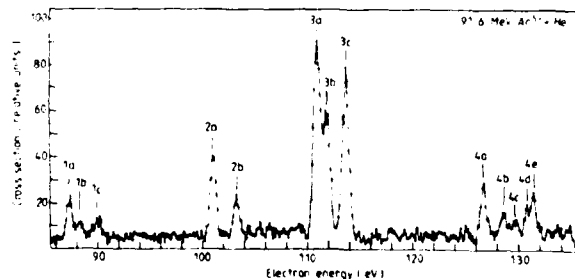


Fig.1 Spectrum of Ar-L Auger electrons ejected in collisions with 91.6 MeV Ar⁵⁺ on He. From Ref.1 where also line energies are given.

To verify the spectral structures, Ar-L Auger transition energies were calculated using a multi-configuration Dirac-Fock (MCDF) program.² For the cases studied, the term splitting and the fine structure splitting are of the same order so that intermediate coupling schemes are suitable for the calculations. The results are summarized in Fig.2. When the projectile is singly ionized in the 2p orbital in the collision, Ar⁶⁺ is created. When the 3p electron is removed in addition to the 2p ionization, Ar⁷⁺ is obtained.

In Fig.2 the Auger transitions for Ar⁶⁺ and Ar⁷⁺ are indicated by arrows labelled in accordance with the notation of the peak groups (Fig.1). The peaks 2a and 2b are attributed¹ to the initial configuration $1s^2 2s^2 2p^5 3s^2$ forming the doublet $^2P_{3/2,1/2}$. The peak groups 1, 3, and 4 are due to the initial configuration $1s^2 2s^2 2p^5 3s^2 3p$ and the final configurations $1s^2 2s^2 2p^6$ with an additional 3d, 3p, and 3s electron, respectively. Here, term splitting and fine structure splitting is important only for the initial configuration which implies

10 individual states. The branching ratios of these states determine the peak structure in the groups 1, 3, and 4. For instance, note the peak 4a which is attributed to the lowest lying J=1 state. The corresponding lines are seen to be missing in the groups 1 and 3.

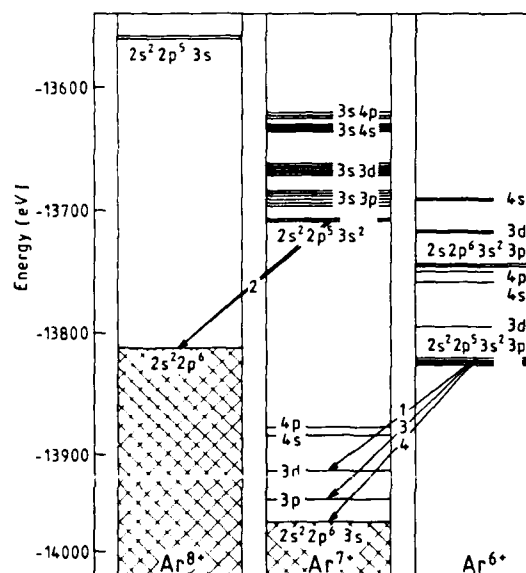


Fig.2 Energy diagram for Ar⁶⁺, Ar⁷⁺, and Ar⁸⁺.

The peak group 1 is particularly interesting, since it is produced by three-electron transitions which cannot be initiated by the two-body Coulomb interaction operator in first order. Also, shake-up effects or configuration interaction in the final state of the residual ion should not be important. Here, higher order effects such as interchannel interaction have to be considered.

We are much indebted to Drs. I.P.Grant, F.Folkmann, and W.Menzel for their support to install the MCDF program. We thank Dr. A.Salin for valuable discussions.

- 1) A.Itoh, T.Schneider, G.Schiwietz, Z.Roller, H.Platten, G.Nolte, D.Schneider, and N.Stolterfoht, J.Phys.B **16**, 3965 (1983).
- 2) I.P.Grant, B.J.McKenzie, P.H.Norrington, D.F.Mayers, and N.C.Pypar, Comp.Phys.Comm. **21**, 207 (1980).

STUECKELBERG OSCILLATIONS IN C^{4+} -He DOUBLE-CAPTURE CROSS SECTION AT LOW ENERGY

A. Bárány* and H. Danared**

*Institute of Theoretical Physics, S-752 38 Uppsala, Sweden

**Research Institute of Physics, S-104 05 Stockholm, Sweden

In a recent state-selective study of single- and double-capture processes in slow C^{4+} -He, Ne, Ar and Xe collisions, performed by means of translational energy-gain spectroscopy at the University of Aarhus¹, structures reminiscent of interference oscillations have been detected in the C^{4+} -He double-capture energy-gain spectra. The structures show up as extra peaks in all spectra taken at projectile collision energies between 300 eV and 700 eV (cf. Fig. 1). Such peaks could result from capture to excited states, but an inspection of the relevant C^{2+} states shows that one would have to invoke several *ad hoc* arguments as to the populating mechanisms. Instead the structures were provisionally interpreted as due to angular scattering and Stueckelberg interference oscillations, as discussed by Olson and Kimura² for the system C^{6+} -H at similar collision energies. That such angular scattering intensity oscillations can show up as distinct structures in the energy-gain spectra is due to the kinematic energy shift and the non-vanishing acceptance angle of the experimental set-up³. A strong support for the given interpretation was the correct inverse velocity dependence of the wavelength of the observed structures.

To further investigate the Stueckelberg oscillation interpretation we are presently generating model energy-gain spectra to compare with the experimental ones. The differential cross section per unit angle is constructed from a classical deflection function according to the prescriptions of Olson and Smith⁴. It is then transformed into a differential cross section per unit energy gain using the kinematical relationships. The Landau-Zener probabilities are evaluated with the coupling matrix element derived by Grozdanov and Janev⁵. A synthetic energy-gain spectrum at 500 eV projectile collision energy is shown in Fig. 2. We also note that the rather crude semiclassical approximation used may be improved⁶.

References

1. H. Cederquist, L.H. Andersen, A. Bárány, P. Hvelplund, H. Knudsen, E.H. Nielsen, J.O.K. Pedersen, and J. Sørensen, J.Phys.B, to be published
2. R.E. Olson and M. Kimura, J.Phys.B 15, 4231 (1982)
3. E.H. Nielsen, L.H. Andersen, A. Bárány, H. Cederquist, J. Heinemeier, P. Hvelplund, H. Knudsen, K.B. MacAdam, and J. Sørensen, J.Phys.B 18, in print
4. R.E. Olson and F.T. Smith, Phys.Rev. A3, 1607 (1971)
5. T.P. Grozdanov and R.K. Janev, J.Phys.B 13, 3431 (1980)
6. A. Bárány, J.Phys.B 12, 2841 (1979)

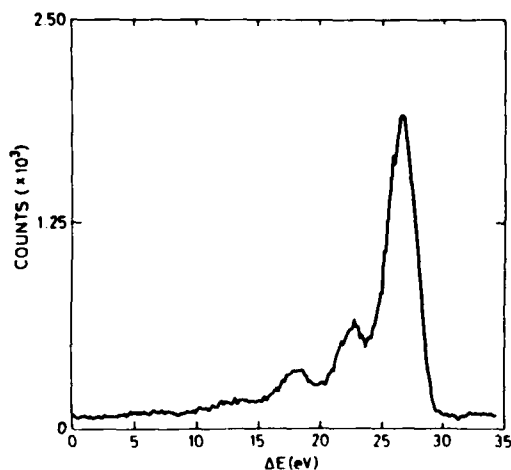


FIGURE 1 Experimental energy-gain spectrum of 500 eV C^{4+} capturing two electrons from He^1 .

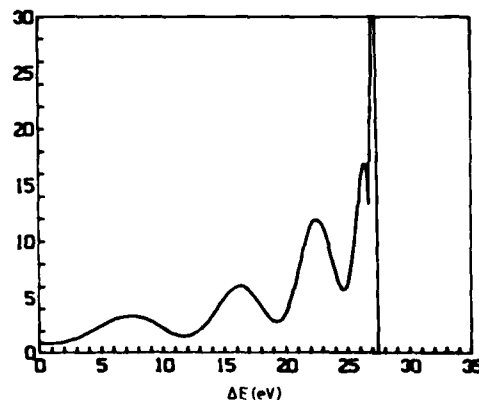


FIGURE 2 Theoretical differential cross section per unit energy-gain for 500 eV C^{4+} capturing two electrons from He into the ground state. Scale on vertical axis is in atomic units.

AN EXTENDED CLASSICAL BARRIER MODEL FOR MULTI-ELECTRON TRANSFER REACTIONS

A. Bárány* and P. Hvelplund**

*Institute of Theoretical Physics, S-752 38 Uppsala, Sweden

**Institute of Physics, DK-8000 Aarhus, Denmark

While single-electron capture by slow multiply charged ions have received much attention during the last decade and several useful theoretical models have been proposed, the situation has been different for multi-electron transfer processes. The recent availability of fresh experimental coincidence¹ and state-selective² data, however, has now made it possible to formulate and test some new theoretical ideas. We here describe a recent extension of the classical barrier model for single-electron capture to multi-electron transfer reactions^{3,4}. This extension follows along the lines proposed by Janev and Presnyakov⁵, but our prescription differs significantly from theirs.

Our extension of the classical barrier model treats a multi-electron transfer process as a consecutive progression of one-electron transfers. This progression leaves the target ion in a distinct charge state but does not predict the final charge state of the projectile, since autoionisation of multiply excited projectile states may occur during or after the collision. The model thus predicts cross sections for target loss of a specific number of electrons (m) given the projectile charge state (q). The actual computational scheme is

$$\sigma_q^m = -(\kappa_m^2 - \kappa_{m+1}^2)$$

$$\kappa_m = -2(q-m+1)^{1/2} m^{1/2} + m/I_m,$$

where I_m is the m th ionisation potential of the target.

The model also predicts internal energy defects associated with the transfer of m electrons from the target to (possibly later autoionising) excited states of the ion. These defects Q_m are defined through the recursive relations

$$Q_1 = (q-1)/R_1$$

$$Q_m = (q-(2m-1))/R_m + Q_{m-1}.$$

In Fig. 1 energy-gain spectra of 1 keV $\text{Xe}^{q+} + \text{Ar} \rightarrow \text{Xe}^{(q-1)+}$ are shown together with the model estimates of internal energy defects (corrected for kinematical shifts) for one-, two- and three-electron loss from the target and for $q = 12, 14$ and 18.

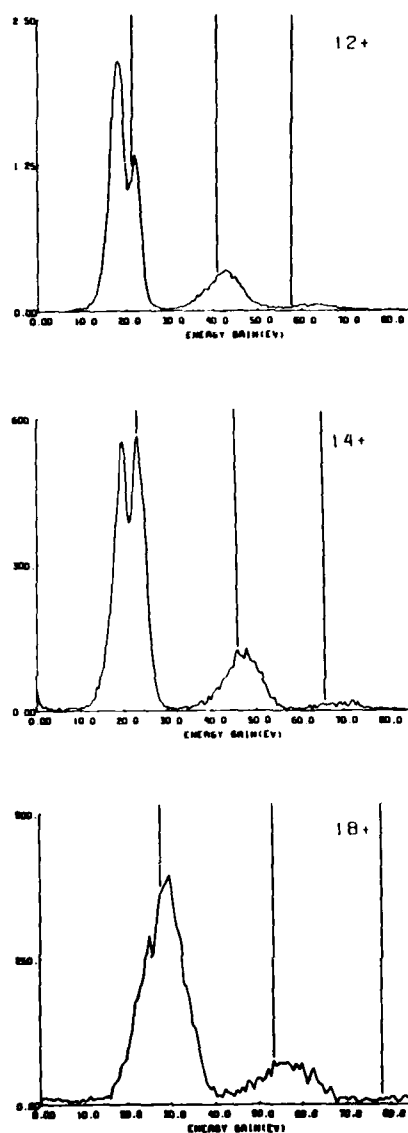
References

1. G. Astner, A. Bárány, H. Cederquist, H. Danared, S. Hult, P. Hvelplund, A. Johnson, H. Knudsen, L. Liljeby, and K.-G. Rensfelt, J.Phys.B 17, L877 (1984)
2. E.H. Nielsen, L.H. Andersen, A. Bárány, H. Cederquist, J. Heinemeier, P. Hvelplund, H. Knudsen, K.B. MacAdam,

and J. Sørensen, J.Phys.B 18, in print

3. A. Bárány, G. Astner, H. Cederquist, H. Danared, S. Hult, P. Hvelplund, A. Johnson, H. Knudsen, L. Liljeby, and K.-G. Rensfelt, Nucl.Instr.Meth.B, to be published
4. P. Hvelplund, L.H. Andersen, A. Bárány, H. Cederquist, J. Heinemeier, H. Knudsen, K.B. MacAdam, E.H. Nielsen, and J. Sørensen, Nucl.Instr.Meth.B, to be published
5. R.K. Janev and L.P. Presnyakov, Phys.Reports 70, 1 (1981)

FIGURE 1



MULTI-ELECTRON PROCESSES IN SLOW COLLISIONS OF Ar^{q+} WITH Ne, Ar, Kr

L. Liljeby, C. Astner, A. Bárány*, H. Cederquist, H. Danared, S. Huldt**,
P. Hvelplund***; A. Johnson, H. Knudsen***; K.-G. Rensfelt

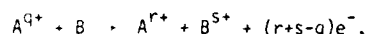
Research Institute of Physics, S-104 05 Stockholm, Sweden

*Institute of Theoretical Physics, S-752 38 Uppsala, Sweden

**Institute of Physics, S-223 62 Lund, Sweden

***Institute of Physics, DK-8000 Aarhus, Denmark

We report results from a study of slow charge-changing collisions of the general type



where the multiply charged projectiles have been produced as recoil ions using the Stockholm cyclotron to give a "hammer" beam¹. The recoils are accelerated to an energy of 1.8q keV and collide with the target in a gas cell. By coincident time-of-flight charge-state analysis of projectiles and secondary target ions, absolute cross sections for specific reactions are determined. We have used Ar ions as projectiles and Ne, Ar, Kr as target gases. A rather detailed presentation of the experimental set-up and results for the Ar-Ar collisions have recently been published². Here we briefly present the Ar-Kr system, but a more thorough discussion and comparison of all three collisional systems will be published³.

Due to the large potential energy carried by the projectile into the collision, a great variety of processes may occur. Fig. 1 shows the absolute summed cross sections σ_q^s for production of a secondary target ion of charge state s. We see that even the cross section for detaching s = 6 electrons from the target is appreciable if only the projectile charge state q is large enough.

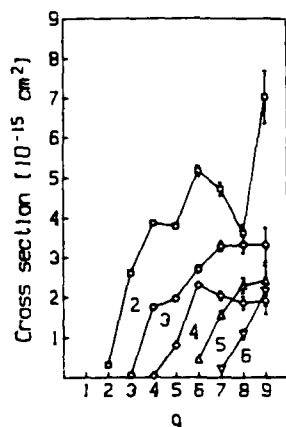


FIGURE 1 Cross sections σ_q^s for production of target ions of charge state s = 2,...,6 in collisions of 1.8q keV Ar^{q+} with Kr.

Fig. 2 shows in more detail the absolute cross sections σ_{qr}^s for production of secondary target ions of charge state s = 3 split up into different final projectile charge states r. Transfer ionisation dominates completely, the competing channels being ejection of one or two electrons, respectively.

References

1. G. Astner, A. Bárány, H. Cederquist, H. Danared, P. Hvelplund, A. Johnson, H. Knudsen, L. Liljeby, and L. Lundin, *Physica Scripta* **13**, 163 (1983)
2. G. Astner, A. Bárány, H. Cederquist, H. Danared, S. Huldt, P. Hvelplund, A. Johnson, H. Knudsen, L. Liljeby, and K.-G. Rensfelt, *J. Phys. B* **17**, L877 (1984)
3. L. Liljeby et al, *Physica Scripta*, to be published

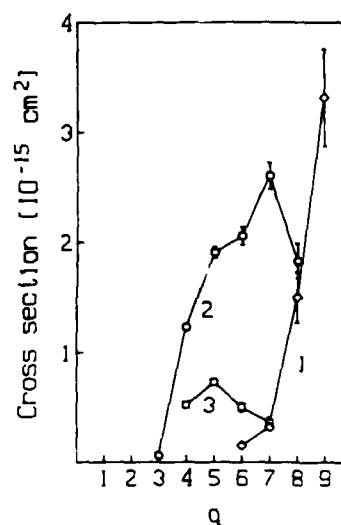


FIGURE 2 Cross sections σ_{qr}^s for s = 3 in coincidence with projectile final charge states r = q-3, q-2 and q-1. Same system as in Fig. 1.

ELECTRON CAPTURE BY STATE-SELECTED IONS IN THE Ar^{2+}/Ar COLLISION SYSTEM

J. Puerta, B.A. Huber and K. Wieseemann

Institut für Experimentelle Physik AG II, Ruhr-Universität
D-4630 Bochum, West Germany

One of the main complications in the experimental investigation of electron capture by multiply charged ions is the possible presence of various excited metastable states in the used primary beam. A direct determination

of the metastable fraction is possible only when the ion beam is well defined. Metastable primary ions are the cause of various difficulties and discrepancies in the experimental results. This was demonstrated in the investigation of state-selected electron capture [1].

Thus, in order to avoid the difficulties caused by the presence of metastable states in the ion beam, the investigation of electron capture by state-selected ions is preferred to be possible, in order to avoid these difficulties. Thus an unambiguous state-selected translational spectroscopy becomes feasible.

With this aim in mind, the present investigation of the electron capture by state-selected ions of Ar^{2+} is presented. The specific states is proved to be possible, in order to avoid these difficulties. Thus an unambiguous state-selected translational spectroscopy becomes feasible.

The experimental setup used to study the system

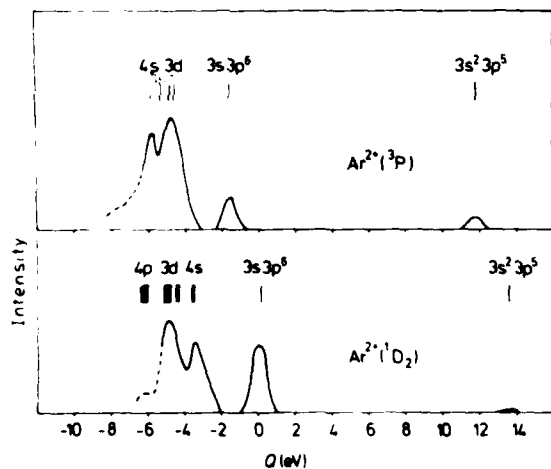


Fig. 2. Translational spectra of Ar^+ ions produced in $\text{Ar}^{2+} 3p_{3/2}/\text{Ar}$ collisions. $E = 600 \text{ eV}$, $\theta = 10^\circ$, $\phi = 0^\circ$.

Ar^{2+}/Ar collision have been studied by many workers with quite different results. Different states of the Ar^{2+} ions are populated in Ar^{2+}/Ar collisions. Figures 1 and 2 show spectra of tertiary Ar^+ ions produced in electron capture reactions of prepared Ar^{2+} ions in an Ar target. Vertical lines indicate the position of possible final

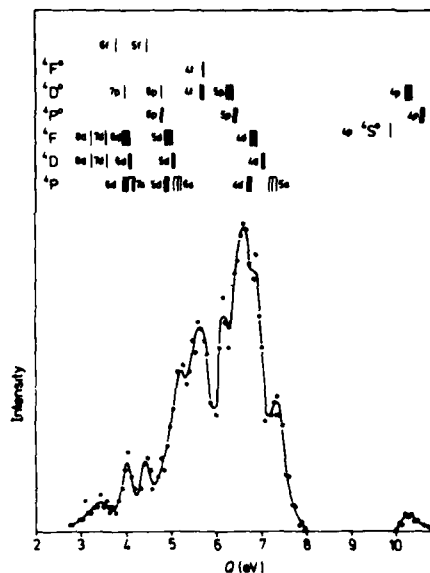


Fig. 3. Energy gain spectrum of Ar^+ ions produced in $\text{Ar}^{2+} 5p_{3/2}/\text{Ar}$ collisions. $E = 600 \text{ eV}$, $\theta = 10^\circ$, $\phi = 0^\circ$.

states of the Ar^+ ions. One can see that groundstate ($4s$) and weakly excited metastables ($1D_2$) produce Ar^+ ions with low excitation energy, while highly excited Ar^{2+} metastables ($5p_{3/2}$) produce strongly excited Ar^+ ions: dominantly $n = 4, 5, 6$ levels with large angular momentum are populated.

From these spectra a rough estimate (within a factor of 2) of electron capture cross sections is possible. At 600 eV one obtains: ($3P$) $2 \cdot 10^{-17} \text{ cm}^2$, ($1D$) $2 \cdot 10^{-17} \text{ cm}^2$, ($3S$) $2 \cdot 10^{-17} \text{ cm}^2$, ($5p_{3/2}$) $5 \cdot 10^{-15} \text{ cm}^2$, ($3F_{7/2}$) $2 \cdot 10^{-15} \text{ cm}^2$. These findings are in agreement with estimates from the above crossings involved in these reactions.

In an electron beam ion source with a typical electron energy of about 500 eV , the highly excited ($5p_{3/2}$), ($3F_{7/2}$) states contribute less than 1% to the Ar^{2+} beam, nonetheless they give the major contribution to the total electron cross section. A slight variation of the beam composition with the ion source condition is a plausible reason of the discrepancy of the results of different workers. The results stress the necessity of cross section measurements with state selected projectiles especially if low charge states are considered.

J. Huber, B.A., Kahlert H.J. and Wieseemann K., J. Phys. B 17 (1984) 2883

J. Huber, B.A., Puerta J. and Wieseemann K., these proceedings

DIFFERENTIAL CROSS SECTIONS FOR ELECTRON TRANSFER IN $\text{Ne}^{4+} + \text{He}$ COLLISIONS

L. N. Tunnell, C. L. Cocke, W. T. Waggoner, J. P. Giese

J. R. Macdonald Laboratory, Kansas State University, Manhattan, Kansas 66506

An apparatus has been designed and tested to measure the differential electron transfer cross section for low velocity, highly ionized projectiles impinging on neutral targets. Measurements have been taken for $\text{Ne}^{q+} + \text{He}$ ($q = 3, 4, 5$), at energies ranging from approximately 70 to 180 eV/q.

A 30 MeV bromine beam from the Kansas State University EN tandem Van de Graaff was used to ionize neon gas, thus producing several charge states. An acceleration system and magnet were used to extract, charge analyze, and momentum analyze selected neon charge states and energies. This secondary beam was then passed through the helium gas cell and detected downstream by a position sensitive detector. Using a retarding grid system, the neon ions which had undergone single charge exchange were separated from the direct and elastic components of the beam. The overall resolution of the system was approximately 5 milliradians (FWHM).

The energy-gain for single electron transfer of $\text{Ne}^{4+} + \text{He}$ was measured by Schmeissner *et al.*¹ It was observed that population of the 3s state dominated the spectrum. The Ne^{4+} beam had the additional advantage of being sufficiently intense to measure differential cross sections.

In Fig. 1 the differential capture cross section for $\text{Ne}^{4+} + \text{He}$ as a function of τ , ($\tau = \theta\theta$), is presented. The forward peak is a notable feature of these spectra. There is considerable population within the angle which would correspond to a collision with an impact parameter equal to the crossing radius.² The position of the maxima and minima, however, do move with τ in such a way as to suggest that they can be observed as Stueckelberg oscillations. These oscillations are attributed to interference between the probability amplitudes for capture occurring near the crossing radius on the incoming and outgoing paths.

This work is supported by the U. S. Department of Energy, Division of Chemical Sciences.

References

1. C. Schmeissner, C. L. Cocke, R. Mann, and W. Meyerhof, Phys. Rev. A **30**, 1661 (1984).
2. R. Mann, C. L. Cocke, A. S. Schlachter, M. Prior, and R. Marrus, Phys. Rev. Lett. **49**, 1329 (1982).

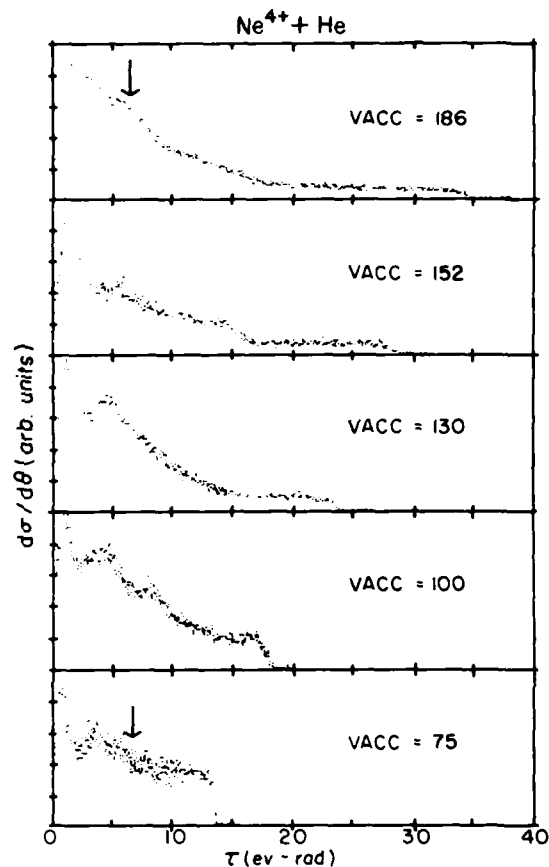


Fig. 1: Differential electron capture cross sections for $\text{Ne}^{4+} + \text{He}$. Laboratory collision energies, τ (in eV), are given by $4 \times V_{\text{acc}}$. The abrupt cut-off in each of the spectra is due to the finite diameter of the detector. Arrows indicate the first minima predicted by the half-pass scattering model.

ENERGY GAIN SPECTROSCOPY OF LOW ENERGY Ar^+ AND Ne^+ ON ATOMIC AND MOLECULAR HYDROGEN

J. P. Giese, C. L. Cocke, S. L. Varghese,* and L. Tunnell

J. K. Macdonald Laboratory, Kansas State University, Manhattan, Kansas 66506
University of South Alabama, Mobile, Alabama 36688

The study of electron capture by low-energy highly charged ions from atomic and molecular hydrogen targets is motivated both by the basic physics of such collisions and by the role these collisions play in the energy balance of high-temperature plasma devices. The specific final state populations of these systems can be determined by ion-lateral energy spectroscopy of the product ions. We have measured the energy gain of Ar^{5+} ($q=5$) and Ne^{5+} ($q=5$) projectiles in single electron capture events.

The apparatus used is described in detail elsewhere,¹ but will be briefly outlined here. The projectile ions were produced in a recoil ion source pumped by a fast fluorine beam from the FSI tandem. The recoil ions were charge-state and momentum analyzed in a double-focussing magnetic spectrometer. The ions were then accelerated to their incident energies and directed through the target gas cell. The atomic hydrogen target was produced in a thermal dissociation oven, which when cold, also served as the molecular hydrogen target. After exiting the oven, the product ions are analyzed in a hemispherical double-focussing electrostatic spectrometer.

Energy gain spectra for Ne^{5+} on H and H_2 are shown here. The energy resolution of the main peak was 0.3 eV/q. However, the resolution of the single capture peaks was limited by the inherent kinematics of the reaction system. At the scattering angles other than 0° , some energy is given to the target atom. Thus, the energy gained by the projectile is a function of scattering angle. As an estimate of this effect, kinematic lines were calculated from standard two-body kinematics and are shown in the figure. If the electron capture is assumed to proceed at a localized crossing between the incident and final potential curves, then there is a scattering angle corresponding to an impact parameter equal to the crossing radius. This angle is indicated by a blackened triangle on the appropriate kinematic line. The Q-values of the possible final states were calculated assuming the projectile was in its ground state and that capture occurred without exciting the projectile core.

Analysis of the Ne^{5+} on H spectrum shown here indicates that the final state of the product ion is $1s^2 2s^2 2p n l$. Similarly, the major peak in the Ne^{5+} on H_2 spectrum appears to be due to population of the $n=4$ final states. However, there are features at high energy gain in the H_2 spectrum which are

entirely absent in the H spectrum. Kinematic lines for the 3p and 3d final states are shown. Neither of these lines can explain the feature at 19 eV. Also, because of the small difference in binding energies of H and H_2 , we consider it unlikely that these states would be strongly populated in the H_2 system and not at all in the H system. Another explanation for these features which we favor is double capture into an excited state of the product ion followed by autoionization. The final state is then $1s^2 2s^2 2p n l n' l'$. The Q-value for two typical states is indicated in the figure using the notation $(n l, n' l')$.

Similar analyses have been made for the other systems mentioned above. Population of the feature at high energy gain increases with the charge state of the projectile. It should be noted that it is not possible in all cases to unambiguously identify the final state populations.

This work was supported by the U. S. Department of Energy, Division of Chemical Sciences.

References

1. J. P. Giese, C. L. Cocke, S. L. Varghese, W. Waggoner, L. Tunnell, NIMS, to be published April 1985.

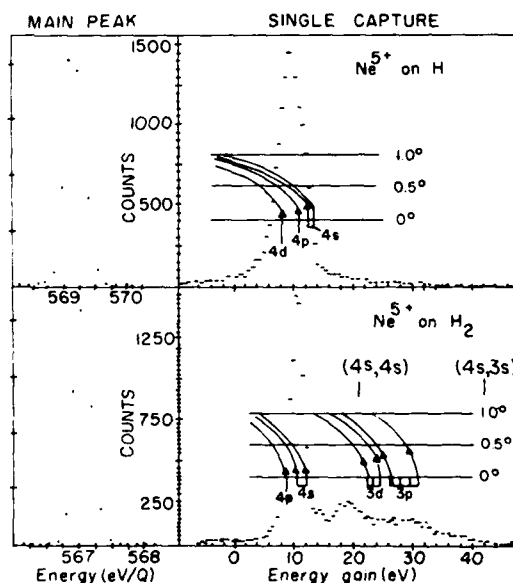


Fig. 1: Energy gain spectra for Ne^{5+} on H and H_2 . Kinematic lines for the possible final states are shown. The scattering angle corresponding to an impact parameter equal to the crossing radius is indicated by a blackened triangle.

TRANSLATIONAL ENERGY GAIN SPECTROSCOPY STUDIES OF MULTIPLY CHARGED ION ATOM COLLISIONS

P. Hvelplund, L.H. Andersen, A. Bárány*, H. Cederquist*, H. Knudsen and J.O.K. Pedersen.

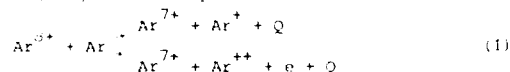
*Institute of Physics, University of Aarhus, DK 8000 Aarhus C, Denmark
Research Institute of Physics (AFI), S-104 05 Stockholm, Sweden

*Institute of Theoretical Physics, S-752 38 Uppsala, Sweden

During the last two years we have performed experimental investigations of state selective electron capture for a variety of multiply charged ions colliding with atoms and molecules. Parts of this investigation is published already¹⁾²⁾³⁾⁴⁾ but new results are currently obtained.

Multiply charged ions of charge state q are created as "recoil ions" in collisions between high energy (35 MeV) $\text{Cl}^{5+,11+}$ ions and various neutral species. The recoil ions are accelerated to an energy of approximately 20q eV and momentum analysed before they are accelerated to the collision energy of typically 100 - 2000 eV. The ions which have experienced a charge-exchange collision are then decelerated and analysed in a hemispherical electrostatic analyser and finally detected by a channel electron multiplier. An energy gain spectrum is obtained by sweeping the decelerating voltage; the resolution is $\approx 0.25q$ eV.

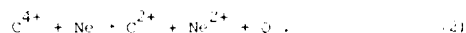
An example of a measured energy gain spectrum is shown in fig.1 for the process



where Q is the internal energy defect in the collision. Due to recoil of the target atom, the energy gain ΔE of the projectile is slightly smaller than Q , but this small kinematic shift can easily be corrected for. The narrow peaks are identified as single capture to the designated final states of the Ar^{7+} ion whereas the broad peak (TI) is attributed to transfer ionisation processes. The broadening of this peak is caused by recoil from the ejected

electron. This effect prevents a precise assignment of excited levels for the TI-process.

Besides transfer ionisation, we observe "true" double capture in some low q collisions such as



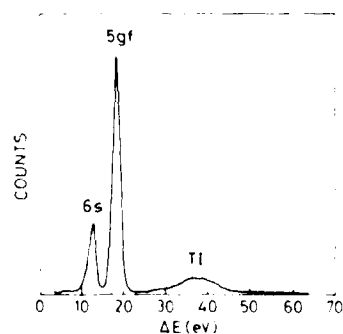
Shown in fig.2 is an energy gain spectrum for this process where several collision channels are identified.



State selective electron capture cross sections are until now obtained for ions ranging from C^{4+} to Xe^{20+} in various atomic and molecular gases. The paper will show examples of spectra obtained and we will discuss simple models which explain general findings such as the position of the "reaction window" and the variation of cross sections with energy and charge state.

References

1. E.H. Nielsen, L.H. Andersen, A. Bárány, H. Cederquist, P. Hvelplund, H. Knudsen, K.K. MacAdam, and J. Sørensen, J.Phys.B **17** (1984) L119.
2. E.H. Nielsen, L.H. Andersen, A. Bárány, H. Cederquist, J. Heinemeier, P. Hvelplund, H. Knudsen, E.H. MacAdam, and J. Sørensen, J.Phys.B, in press.
3. H. Cederquist, L.H. Andersen, P. Hvelplund, H. Knudsen, E.H. Nielsen, J.O.K. Pedersen, J. Sørensen, and A. Bárány, Preprint.
4. P. Hvelplund, L.H. Andersen, A. Bárány, H. Cederquist, J. Heinemeier, H. Knudsen, E.H. MacAdam, E.H. Nielsen, and J. Sørensen, Nucl. Instrum. Methods, in press.



ELECTRON CAPTURE CROSS SECTIONS AND n, l -LEVEL POPULATIONS FOR HIGHLY CHARGED SLOW RECOIL IONS

R. Mann, C.L. Cocke*

GSI, P.O. Box 110541, D-6100 Darmstadt, FRG
*KSU, Manhattan, Kansas 66506

Ar^{q+} and J^{q+} ($5 \leq q \leq 26$) recoil ions were produced in 1.4 MeV u U^{32+} , Kr^{18+} , Si^{11+} collisions with Ar, HJ targets. Total one electron capture cross sections σ_c from He and H_2 targets into 200 eV/q extracted recoil ions are measured by the decelerating method¹ (Fig. 1). The σ_c -dependence on q (Fig. 2) is

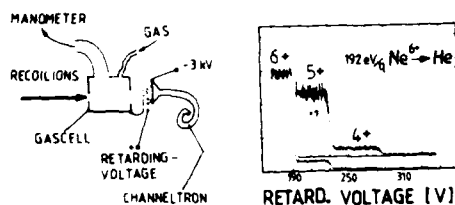


Figure 1

in better agreement with the peak values of the classical barrier model² (CB) than with the absorbing sphere model³ (AS). Besides a general smooth increase of $\sigma_c(q)$ significant fluctuations in neighbored q values are observed which are not simply reproduced by any existing theory. Such fluctuations may reveal the electron transfers to be strongly dependent on the individual electronic level structure of the system even for high charge states. Indeed, the Q-value spectroscopy¹ indicate that subshells are selectively populated (Fig. 3). For certain charge states

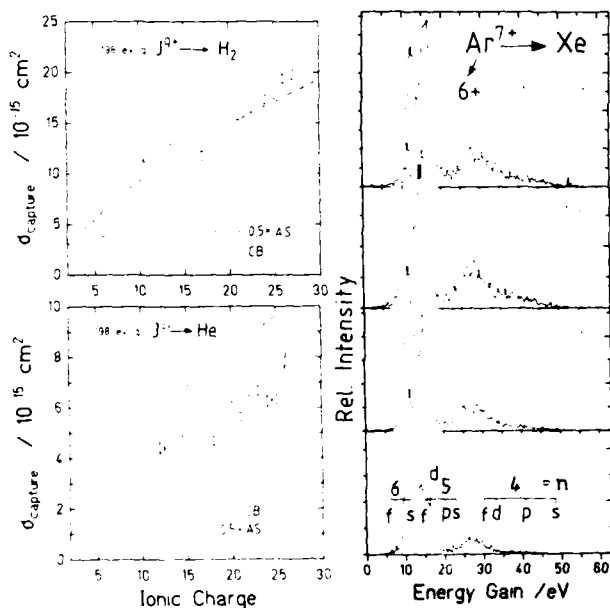


Figure 2

Figure 4

($10+, 11+$) the energy range of subshell levels calculated by a Dirac Fock program overlap for different main shells n . Energy gain spectra of Ar^{q+} ions (Fig. 4) indicate a strong dependence on the collision energy for selectively populated subshells. This can be qualitatively understood³ from adiabaticity criteria of the capture process.

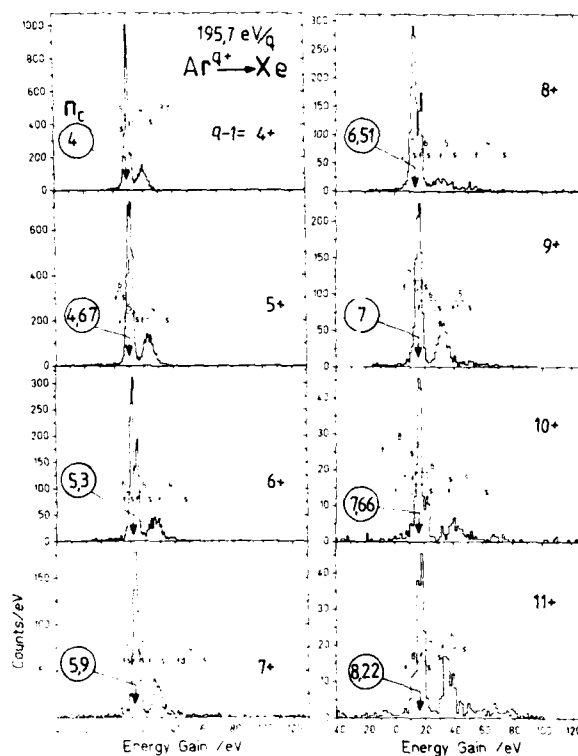


Figure 3

References

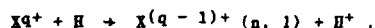
1. R. Mann, C.L. Cocke, A.S. Schlachter, M. Prior, and R. Marrus, Phys. Rev. Lett. **49** (1982) 1329
2. R. Mann, F. Folkmann, and H.F. Beyer, J. Phys. **B14** (1981) 1161
3. C. Schmeissner, C.L. Cocke, R. Mann, W. Meyerhof, Phys. Rev. **A30** (1984) 1661

STATE-SELECTIVE ELECTRON CAPTURE BY SLOW MULTIPLY CHARGED IONS IN ATOMIC HYDROGEN

R W McCullough, F G Wilkie and H B Gilbody

Department of Pure and Applied Physics, The Queen's University of Belfast,
Belfast, United Kingdom

Translational energy spectroscopy in conjunction with a tungsten tube furnace has been used in this laboratory to carry out the first measurements of their type for the electron capture process



In our energy range corresponding to velocities $v < 1$ a.u. where a quasi-molecular description of the collision is appropriate selective capture into a limited number of product ion states occurs via pseudo-crossings of the adiabatic potential energy curves of the molecular system. In particular moderately exothermic reaction channels provide the main contribution to the total one electron capture cross section.

The feasibility of the technique was demonstrated at the single impact energy of 8 keV for the $N^{2+} + H$ collision system¹. Subsequent apparatus improvements enabled the first detailed comparison between experiment and theory for the $C^{3+} + H$ system² in the energy range 0.6 - 18 keV and more recently for the $N^{2+} + H$ system³ in the energy range 0.6 - 8 keV. In both of the above cases the agreement with theory was good for the dominant reaction channels.

A new position sensitive detector system with microchannel plates, phosphor screen and CCD camera has recently been installed in our product ion energy analyser. This detection system has enabled higher resolution FWHM 1.5 eV combined with increased detection efficiency to be achieved. Fig. 1 shows an energy change spectrum for C^{2+} ions formed in single collisions between 12 keV C^{3+} and atomic hydrogen. The main features of this spectrum are in good agreement with those observed in our previous work and predicted by theory⁴. The major reaction channels are indicated by full vertical lines and are labelled according to the C^{2+} product ion state formed. These channels are listed below together with their energy defects and associated pseudo-crossings.

Reaction	ΔE (eV)	R_c (a.u.)
$C^{3+}(1s^2 2s)2S + H$		
$+ C^{2+}(1s^2 2s 3p)3p^0 + H^+$	2.05	26.5
$+ C^{2+}(1s^2 2s 3s)3S + H^+$	4.72	11.5
$+ C^{2+}(1s^2 2p^2)1S + H^+$	11.63	4.68
$+ C^{2+}(1s^2 2p^2)1D + H^+$	16.17	3.36

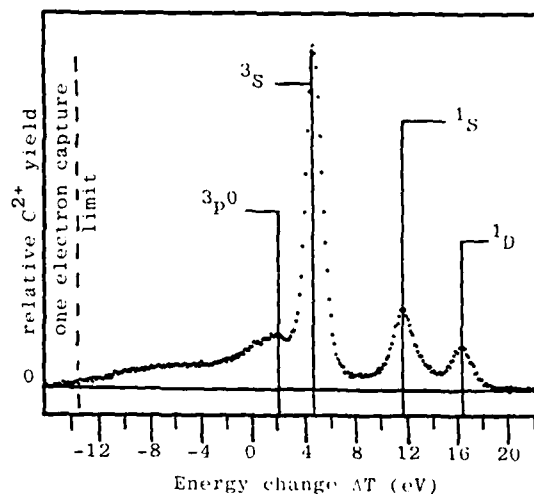


Figure 1 : Energy change spectrum for C^{2+} ions produced in one electron capture collisions by 12 keV C^{3+} ions in atomic hydrogen.

However these new measurements clearly indicate the presence of other minor reaction channels resulting in the formation of higher excited states of C^{2+} between $3p^0$ and the continuum. The unresolved channels account for approximately 24% of the total C^{2+} of the total C^{2+} product ion signal. Further measurements at other collision energies for the $C^{3+} + H$ system will be presented at the conference together with those for other collision systems.

References

1. R W McCullough, M Lennon, F G Wilkie and H B Gilbody. *J Phys B* **16**, L173, 1983.
2. R W McCullough, F G Wilkie and H B Gilbody. *J Phys B* **17**, 1373, 1984.
3. F G Wilkie, F B Yousif, R W McCullough, J Geddes and H B Gilbody. *J Phys B* **18**, 479, 1985.
4. S Bienstock, T G Heil, C Bottcher and A Dalgarno. *Phys Rev A* **25**, 2850, 1982.

ON NEUTRALISATION OF HIGHLY CHARGED IONS NEAR METAL SURFACES

M. Delaunay*, S. Dousson* and R. Geller*
and

P. Varga*, M. Fehrer* and H. Winter*

AGRIPPA, C.E.N. Grenoble, 85 X, 38041 Grenoble CEDEX, France

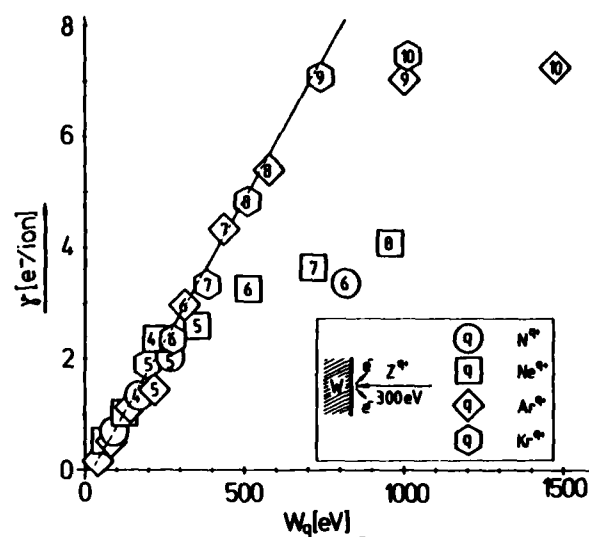
*) Service d'Ionique Generale, C.E.N. Grenoble, France

*) Institut für Allgemeine Physik, TU Wien, Austria

Experience on neutralisation of slow multi-charged ions at metal surfaces [1,2] suggests the following processes. At distances of typically 10 \AA from the surface, resonance capture of one or several electrons produces highly excited or autoionizing [3] particles, which during their further approach are rapidly deexcited in a series of Auger processes, each of them bridging an energy gap of about $15 - 30 \text{ eV}$ [2,4]. Each step will last typically $10^{-15} - 10^{-14} \text{ s}$ and can lead to electron ejection. The corresponding electron yield γ should therefore be roughly proportional to the overall potential energy W_q released by an ion Z^{q+} until its neutralisation has been completed. This picture is also confirmed by all so far available experimental results [1,2,5]. During 10^{-14} s , ions with a kinetic energy of $E/M = 7.5 \text{ eV/amu}$ (e.g. 300 eV Ar^{q+}) travel about 4 \AA . Therefore, even such rather slow highly charged ions will reach the surface before their above described neutralisation/deexcitation processes have been terminated. This is supported by measured γ , which decrease with E the faster the higher q [1]. Furthermore, with given Z beyond a certain q value the gaps between adjacent states involved in the Auger deexcitation cascades may become so large, that the related Auger transition probabilities are drastically decreased. This is especially to be expected for H-, He- and Ne-like configurations, for which the respectively lowest excited states are widely separated from the corresponding ground states. For few electron-ions with higher Z , radiative deexcitation may become comparably important as Auger deexcitation, because the probability of the radiative processes increases rapidly with Z . In this context, we refer to Ar K_α emission observed for impact of Ar^{17+} on CuBe [6].

In conclusion, a correspondingly smaller contribution to electron ejection and thus a deviation from linear γ vs. W_q characteristics should be found for high q -values as above defined.

Applying decelerated ions from an ECR source [7], we have started systematic investigations of electron emission due to impact of slow highly charged ions on metal surfaces.



The figure shows results obtained for contaminated tungsten (background pressure ca. 10^{-8} mbar) bombarded by 300 eV N^{q+} ($q \leq 6$), Ne^{q+} ($q \leq 8$), Ar^{q+} and Kr^{q+} ($q \leq 10$). We clearly find deviations from linear γ vs. W_q plots, most notably at $q = 9$ for Ar and $q = 6$ for N, in agreement with our expectations.

At smaller ion impact energies (i.e. 100 or 200 eV) less pronounced deviations have been found, which suggests more efficient electron ejection, if enough time for the respective neutralisation/deexcitation sequences is provided.

Studies for impact of ions with higher q and also lower E on atomically clean target metals are in progress.

Acknowledgement

Austrian participation in this work has been supported by Kommission zur Koordination der Kernforschung at the Austrian Academy of Sciences.

References

- 1) H.D. Hagstrum, Phys.Rev. **96**(1954)325
- 2) U.A. Arifov, L.M. Kishinevskii, E.S. Mukhamadiev and E.S. Parilis, Sov.Phys.-Tech.Phys. **18**(1973)118
- 3) H.D. Hagstrum and G.E. Becker, Phys.Rev.B **8**(1973)107
- 4) P. Varga, W. Hofer and H. Winter, Surf. Sci. **117**(1982)142
- 5) P. Varga and H. Winter, Phys.Rev. A **18**(1978)2453
- 6) E.D. Donets, Physica Scripta T **3**(1983)11
- 7) R. Geller and B. Jacquot, Nucl.Instr.Meth. **202**(1982)399

A PRACTICAL CRITERION TO DETERMINE TRANSLATION FACTORS. APPLICATION TO $\text{He}^{2+} + \text{H}$ COLLISIONS.

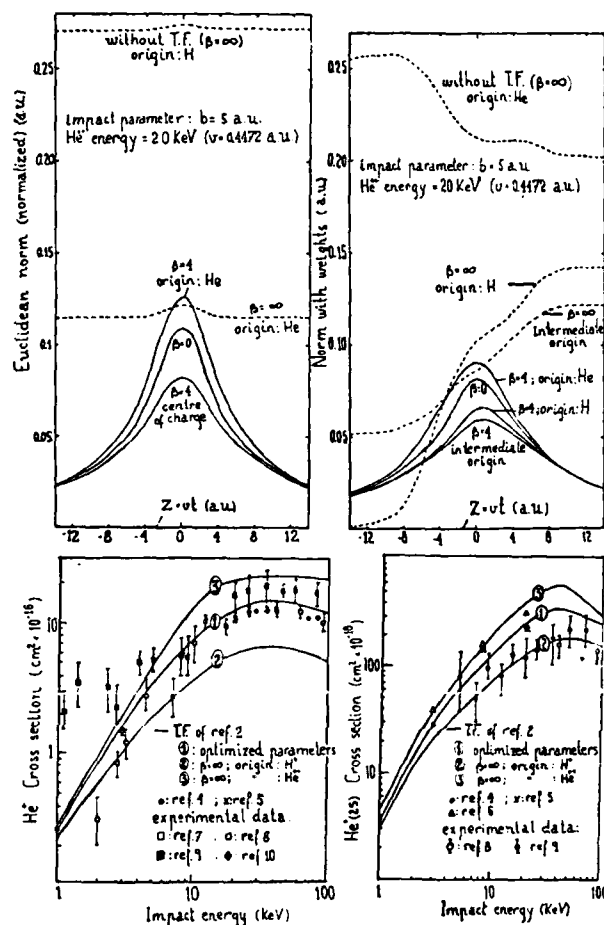
J.M. Gómez Llorente, L.F. Errea, L. Méndez and A. Riera

Departamento de Química Física y Química Cuántica,
Universidad Autónoma de Madrid, 28049 MADRID (Spain)

We present results of applying the Euclidean norm method¹ to determine a common translation factor for $\text{He}^{2+} + \text{H}(1s)$ collisions. Norms with and without weights are presented. The parameters determined are the cut-off parameter β of ref. 2 and the so-called privileged origin. Our conclusion is that the norm method, which is an extension of the criterion of Rankin and Thorson³, provides a simple and useful procedure to determine translation factor parameters.

REFERENCES

- 1.- Riera, A., Phys. Rev. A., **30**, 2304 (1984).
- 2.- Errea, L.F., Méndez, L. and Riera, A., J. Phys. B, **15**, 101 (1982).
- 3.- Rankin, J. and Thorson, W.R. Phys. Rev. A., **18**, 1990 (1978).
- 4.- Winter, T.G. and Hatton, G.J. Phys. Rev. A., **21**, 793 (1980).
- 5.- Kimura, M. and Thorson, W.R., Phys. Rev. A., **24**, 3019 (1981).
- 6.- Crothers, D.S.F. and Todd, N.R., J. Phys. B., **14**, 2251 (1981).
- 7.- Fite, W.L., Smith, A.C.H. and Stebbings, R.F., Proc. R. Soc., A, **268**, 527 (1962).
- 8.- Shah, M.B. and Gilbody, H.B., J. Phys. B., **7**, 630 (1974).
- 9.- Bayfield, J.E. and Khayrallah, G.A. Phys. Rev. A., **12**, 869 (1975).
- 10.- Olson, R.S. Salop, A., Phaneuf, R.A. and Meyer, F. W., Phys. Rev. A., **16**, 1867 (1977).



CROSS SECTION FOR $\text{He}^{2+} + \text{H}(1s)$ COLLISIONS	
Our results with 4-state calculations: $2s\sigma$, $2p\sigma$, $3d\sigma$ and $2p\pi$.	
- No translation factor, origin on H^+	
- No translation factor, origin on nuclear centre of charge	
Use of euclidean norm	
- $w_n = 1$	
- w_n = transition probabilities of previous case	
- w_n = transition probabilities chosen by iteration procedure	
Other results with translation factors.	
- Results of Winter and Hatton ⁴ using plane wave T.F. (four states calculation)	
- Id. (ten states calculation)	
- Results of Kimura and Thorson ⁵ with optimized T.F.'s (four states calculation)	
- Id. (ten states calculation)	
- Results of Crothers and Todd ⁶ with variationally optimized T.F.'s. Five states calculation ($2s\sigma$, $2p\sigma$, $2p\pi$, $3d\sigma$ and $3d\pi$).	
Interpolated experimental data	
- Fite et al. ⁷	
- Shah and Gilbody ⁸	
- Bayfield and Khayrallah ⁹	
- Olson et al. ¹⁰	

FOR 20 KeV He^{2+} IMPACT ENERGY			
σ_{2s}	$\sigma_{2p\sigma}$	$\sigma_{2p\pi}$	σ_{tot}
1.36	2.21	2.45	6.02
3.88	7.97	7.35	19.20
2.90	5.72	5.01	13.63
2.62	5.0	4.35	11.97
2.51	4.81	4.16	11.48
2.91	4.16	3.76	10.8
2.37	4.88	4.14	12.3
2.65	3.97	3.76	10.40
2.18	4.66	3.70	11.23
2.90	-	-	10.36
-	-	-	15 ± 1
1.5 ± 0.3	-	-	10 ± 1
1.3 ± 0.5	-	-	15 ± 5
-	-	-	10

INFLUENCE OF ROTATIONAL COUPLING ON CHARGE TRANSFER
BETWEEN MULTIPLY CHARGED IONS AND NEUTRAL ATOMS AT LOW ENERGIES

M. Gargaud*, R. McCarroll*, P. Valiron* and G. Zannoli*

*Laboratoire d'Astronomie et d'Astrophysique (UA 352 du CNRS), Observatoire de l'Université de Bordeaux I,
33270 Floirac, France

*Groupe d'Astrophysique (ERA 961 du CNRS), Université de Grenoble I, B.P. 68, 38402 Saint-Martin-d'Hères, France

The aim of this work is to clarify the relative importance of radial and rotational coupling in the quasi-molecular model of charge transfer of multiply charged ions with neutral targets.

The dynamics of the collision is treated by a quantum mechanical formalism, which allows us to cover the range of thermal eV to keV energies. A model potential method^{1,2} is used to compute the required molecular energies and the corresponding dynamical coupling. Provision is made to account for translation effects by the introduction of appropriate reaction coordinates^{3,4}.

The results presented in this abstract concern the C^{4+}/H system which has been the subject of much recent investigation^{1,2,5-10}. The essential features can be most simply understood in terms of the diabatic representation² (figure 1) in which the matrix elements vary smoothly with R in contrast to their complex structure in the adiabatic representation. It is observed that the only important rotational coupling matrix elements are these between states converging to the same dissociation limit. It is found that rotational coupling contributes to the charge transfer process in two specific ways. At low energies (< 40 eV/amu), its influence appears to be localized to the vicinity of the crossing radius R_X . The pure sinusoidal character of the partial wave cross-sections is then preserved (figure 2a). At higher energies (≥ 50 eV/amu) the electronic states tend to decouple from the internuclear axis even for $R < R_X$, which produces an additional peak in the partial wave cross-sections. Interference effects tend to attenuate the sinusoidal character associated with purely radial coupling (figure 2b).

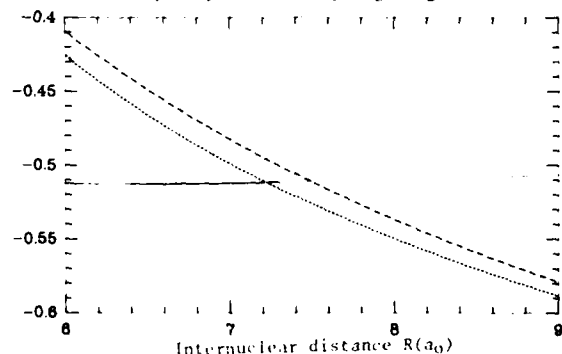


Figure 1. Diabatic diagonal matrix elements (in atomic units) pertaining to the $1s_H$ entry channel (—) and the $3p_C$ (.....) $\pi 3p_C$ (----) exit channels in C^{4+}/H collision.

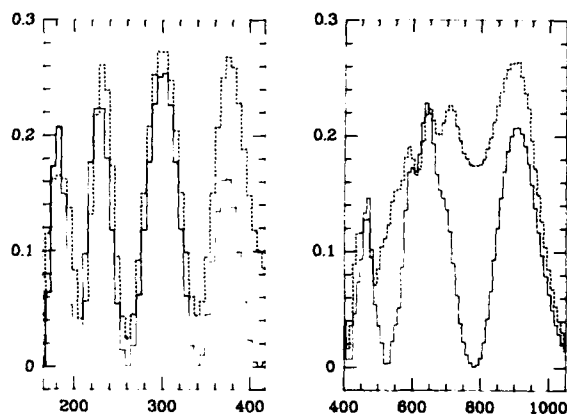


Figure 2a,b. Partial wave cross sections (a_0^2) for capture into $C^{3+}(3p)$ with (---) and without (—) rotational coupling for collision energies of 29.5 eV/amu (fig. 2a) and 147.3 eV/amu (fig. 2b).

The overall effect of rotational coupling on charge transfer is confined to a relatively narrow energy range around 150 eV/amu. At energies lower than 50 or higher than 300 eV/amu, the effect is much less marked, becoming negligible for energies less than 10 eV/amu. The inclusion of translation effects does not appreciably modify the results for energies below 1 keV/amu.

Our results are in good agreement with Phaneuf *et al.*⁸ at energies less than 50 eV/amu. At higher energies, however, our computed cross-sections, in common with other calculations^{6,7}, lie somewhat (by about 50%) above the experimental data.

Results for other systems will be presented at the conference.

1. Valiron P., Gayet R., McCarroll R., Masnou-Seeuws F. and Philippe M. 1979, *J. Phys. B: At. Mol. Phys.* **12**, 53
2. Gargaud M., Hanssen J., McCarroll R. and Valiron P. 1981, *J. Phys. B: At. Mol. Phys.* **14**, 2259
3. Thorson W.R. and Delos J.B. 1978, *Phys. Rev. A* **18**, 135
4. Errea L.F., Méndez L. and Riera A. 1982, *J. Phys. B: At. Mol. Phys.* **15**, 101
5. Gargaud M. and McCarroll R. 1985, *J. Phys. B: At. Mol. Phys.* **18**, 463
6. Olson R.E., Shipsey E.T. and Browne J.C. 1978, *J. Phys. B: At. Mol. Phys.* **11**, 699
7. Hanssen J., Gayet R., Harel C. and Salin A. 1984, *J. Phys. B: At. Mol. Phys.* **17**, L323
8. Phaneuf R.A., Alvarez I., Meyer F.W. and Crandall D.H. 1982, *Phys. Rev. A* **26**, 1892
9. Bottcher C. and Heil T.G. 1982, *Chem. Phys. Lett.* **86**, 506
10. Fritsch W. and Lin C.D. 1984, *J. Phys. B: At. Mol. Phys.* **17**, 3271

LOW ENERGY CHARGE TRANSFER IN ONE ELECTRON SYSTEMS*

G.J. Bottrell and T.G. Heil

Department of Physics and Astronomy, University of Georgia, Athens, Georgia 30602

We have examined the total cross-sections for charge transfer in the one electron systems He^{2+} , Li^{3+} , Be^{4+} , B^{5+} , and C^{6+} colliding with hydrogen. The collision energies are up to 100 eV. The approach used is fully quantum mechanical and uses a diabatic representation that is a generalization of that of F. Smith. Our basis set size ranged from two to thirteen states (all σ states), in an effort to study the convergence of the cross-sections and diabatic states with respect to the molecular basis set. Convergence studies with respect to angular couplings are in progress.

*Supported by the National Science Foundation.

POTENTIAL CURVES AND COUPLING ELEMENTS FOR CHARGE TRANSFER IN $Al^{+3} + H$ COLLISIONS*K. Kirby⁺ and T.G. Heil⁺⁺⁺Harvard-Smithsonian Center for Astrophysics, Cambridge MA 02138⁺⁺Department of Physics and Astronomy, University of Georgia, Athens GA 30602

Adiabatic potential curves, electronic wavefunctions and radial coupling matrix elements have been computed for four states in the 2_{-}^{+} manifold leading to the separated atom limits $Al^{+3} + H$ and $Al^{+2} ({}^2S, {}^2P, {}^2D) + H^{+}$. The basis set of Slater-type functions was optimized for the specific atomic limits. In order not to prejudice the calculations to describe only the ground state accurately, a single-excitation configuration interaction (CI) calculation to obtain natural orbitals n ; for the four 2_{-}^{+} states was devised. These natural orbitals were then treated equivalently in a first-order CI calculation. The asymptotic energy splittings are within 1-2% of the experimental values which indicates that the calculated crossing-points of these potential curves should be very accurate. Electric dipole transition moments, and radial coupling matrix elements computed using the one-electron operator $\sum_{i=1}^N \frac{Z_i}{r_i^3}$ are given as functions of internuclear separation, R . These curves and matrix elements have been transformed to a Galilean invariant diabatic representation. Quantal scattering calculations are in progress using these diabatic curves and couplings to predict cross-sections for forming $Al^{+2} ({}^2S, {}^2P, {}^2D)$ ions in collisions of Al^{+3} and H .

*Supported by United States Department of Energy, Fundamental Interactions Branch.

CROSSED-BEAM STUDY OF THE SINGLE-CHARGE TRANSFER PROCESS $\text{Hg}^{++}(^1\text{S}) + \text{Kr}(^1\text{S}) \longrightarrow$
 $\text{Hg}^+(^2\text{S}) + \text{Kr}^+(^2\text{P}_{3/2}, ^2\text{P}_{1/2})$ AT eV COLLISION ENERGIES

B. Friedrich, J. Vančura, M. Sadílek¹, Z. Herman

J. Heyrovský Institute of Physical Chemistry and Electrochemistry,
 Czechoslovak Academy of Sciences, Máchova 7, 121 38 Prague 2, Czechoslovakia

As a part of a systematic scattering investigation of the single-charge transfer processes of doubly-charged ions^{2, 3}, we undertook a crossed beam study of the title processes where the spin-orbit states of the $\text{Kr}^+(^2\text{P})$ product could be resolved. The experiments were carried out on the scattering apparatus EVA II⁴ and the range of collision energies covered was 0.9 through 2.7 eV. Because of kinematic reasons, the Hg^+ product ions were measured, although the signals of Kr^+ could be detected also.

The large spin-orbit splitting of the $\text{Kr}^+(^2\text{P})$ states, 0.65 eV, made it possible to distinguish the regions of scattering of Hg^+ due to the formation of $\text{Kr}^+(^2\text{P}_{3/2})$ and $\text{Kr}^+(^2\text{P}_{1/2})$ as separate features in the scattering diagrams of Hg^+ . Using standard procedures, CM angular distributions pertinent to the formation of these two states of Kr^+ (state-selected relative differential cross sections) were evaluated together with the ratio of the total cross sections $\sigma(3/2)$ and $\sigma(1/2)$ of forming $\text{Kr}^+(^2\text{P}_{3/2})$ and $\text{Kr}^+(^2\text{P}_{1/2})$, respectively, in de-

pendence on collision energy.

Figs. 1 and 2 show the relative differential cross sections, $\sigma_{\text{diff}}(\vartheta)$, at collision energies $T=0.92$ and 2.71 eV, respectively. The areas under the curves at a given collision energy are normalized to the ratio of $\sigma(3/2)$ and $\sigma(1/2)$.

The formation of both $\text{Kr}^+(^2\text{P}_{3/2})$ and $\text{Kr}^+(^2\text{P}_{1/2})$ results in strong forward peaking of Hg^+ .

A preliminary quasiclassical calculation for $\text{Kr}^+(^2\text{P}_{1/2})$ based on the ion-induced dipole, V_{ID} , and Coulomb potentials between the reactant and product pairs, respectively, leads to an adequate description of the strong forward peaking of Hg^+ due to the $\text{Kr}^+(^2\text{P}_{1/2})$ formation.

The value of the ratio $\sigma(3/2)/\sigma(1/2)$ at $T=2.71$ eV compares well with that of $b_{\text{max}}^2(3/2)/b_{\text{max}}^2(1/2)$ where $b_{\text{max}}=(1+V_{\text{ID}}(R_{\text{cr}})/T)^{1/2} \cdot R_{\text{cr}}$; $R_{\text{cr}}(3/2)=3.4$ Å and $R_{\text{cr}}(1/2)=3.8$ Å are the respective crossing separations of the diabatic terms. With decreasing collision energy the cross section ratio increases faster than the ratio of b_{max}^2 .

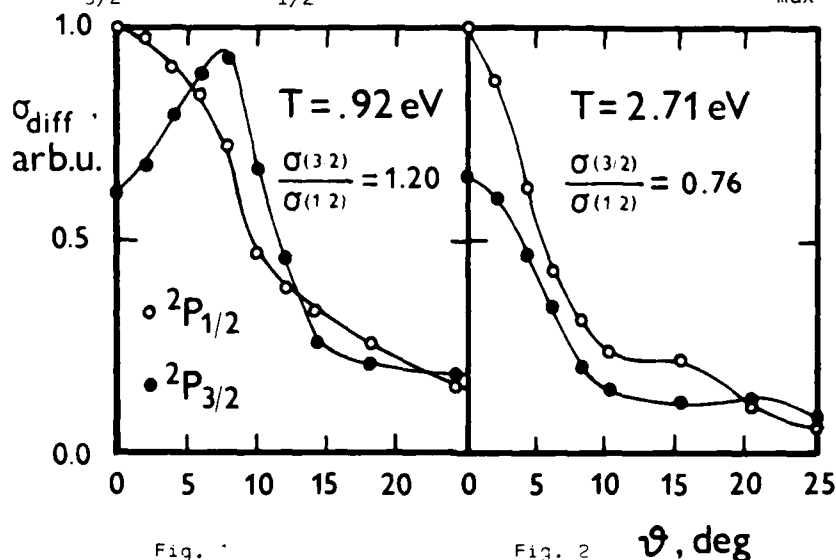


Fig. 1

Fig. 2

ϑ , deg

References:

1. Predoctoral Student, Charles University, Prague
2. B. Friedrich, Z. Herman, Chem. Phys. Lett. **107**, 375 (1984)
3. B. Friedrich, Š. Pick, L. Hládek, Z. Herman, E. Nikitin, A. Reznikov, S. Umanskii, J. Chem. Phys.
4. Z. Herman, K. Birkinshaw, Ber. Bunsenges. Physik. Chem. **77**, 566 (1973)

RESONANCE STATES OF MULTIPLY-CHARGED MOLECULAR IONS

S. Preston and A. Dalgarno

Harvard-Smithsonian Center for Astrophysics, Cambridge, MA 02138 USA

Multiply-charged molecular ions XA^{n+} may be created by the approach of a highly-ionized atomic system X^{n+} and a neutral atom A if the potential well arising from the attractive long range polarization interaction is deep enough to contain bound vibrational levels. In a diabatic representation, one potential energy curve is crossed by the repulsive potential of a lower-lying electronic state which separates into the charged products $X^{(n-1)+}$ and A^+ . The bound levels are properly characterized as diabatic Feshbach resonances whose decay widths give the rates of predissociation into the vibrational continuum of the repulsive diabatic electronic state.

In the alternative adiabatic representation, the two potential curves undergo an avoided crossing. A potential well may be induced in the lower-lying electronic state by its interaction with the higher-lying state. The bound levels are then characterized as shape resonances whose lifetimes are determined by the rates of tunnelling through the potential barrier.

An exact treatment requires the solution of the coupled equations of nuclear motion in the interacting electronic states in which one channel is closed and the others open. We have solved the equations for several of the molecular systems involved in the charge transfer of doubly and trebly charged ions of carbon, nitrogen and oxygen with atomic hydrogen¹. To avoid the loss of linear independence that occurs in classically forbidden regions we used an orthonormalization technique similar to that described by Scott and Watts².

Depending on the strength of the coupling, the diabatic or the adiabatic representation may produce a more satisfactory zero order description of the bound states. Examples will be presented.

References

1. T. G. Heil, S. E. Butler and A. Dalgarno, Phys. Rev. A **27**, 2365 (1983).
2. M. R. Scott and H. A. Watts, Siam J. Numer. Anal., **14**, 40 (1977).

CHARGE TRANSFER OF HELIUM IONS IN NEON

B. Zygelman and A. Dalgarno

Harvard-Smithsonian Center for Astrophysics, Cambridge, Massachusetts 02138, U.S.A.

Charge transfer of He^+ ions in collisions with neon atoms may occur by a radiative process in which a photon is emitted during the collision and by a non-radiative process driven by the action of the nuclear kinetic energy. Experimental evidence for the radiation process has been obtained at thermal energies¹ and a detailed theoretical model has been developed². At thermal energies, the non-radiative process is slow but at some higher energy it will become more rapid than radiative charge transfer.

Calculations will be reported of the cross sections for the charge transfer processes driven by the nuclear radial coupling of the $X^{2\pi^+}$ and $B^{2\pi^+}$ states of the HeNe^+ molecule. The adiabatic potential energy curves were constructed by the RKR method². The adiabatic coupling matrix elements, corresponding to an origin at the center of mass of the nuclei has been calculated by Barat et al.³. In order to explore the sensitivity of the cross section to the coordinate origin we used the transition dipole moment of Cooper et al.² to derive the coupling for an origin on either one of the two nuclei.

The cross sections were obtained by transforming to a diabatic basis⁴ and solving the resulting pairs of coupled equations. At very low energies the cross sections are sensitive to the choice of origin but are also negligible compared to the radiative cross sections. At higher energies, the choice of origin has little effect. The radiative and non-radiative cross sections become equal at a relative energy of 40eV with a value of about $3 \times 10^{-21} \text{ cm}^2$. At 1300eV, the non-radiative cross section has increased to $2 \times 10^{-16} \text{ cm}^2$, orders of magnitude larger than the radiative cross section.

References

1. R. Johnsen, Phys. Rev. A28, 1460(1983).
2. D. L. Cooper, K. Kirby and A. Dalgarno, Can. J. Phys. 62, 1622(1984).
3. M. Barat, J. C. Brenst, D. Dhulicq, J., Pommier, V. Sidis, P. E. Olson, E. J. Shipsey and J. C. Browne, J. Phys. B. 9, 269(1976).
4. T. G. Heil, S. E. Butler and A. Dalgarno, Phys. Rev. A23, 1100(1981).

THE CHARGE TRANSFER CROSS SECTION FOR $\text{Xe}^+(^2P_{3/2})$ IONS IN
Xe OVER THE ENERGY RANGE 0.4 to 4.5 eV (LAB)

P. Larsen* and M.T. Elford†

* Dept. of Physics, University of Trondheim, Trondheim, Norway, NTH-7034
† Res. School Phys. Sciences, A.N.U., Canberra, Australia, 2600

The analysis of ion mobility data enables the cross section for resonant charge transfer to be obtained at low ion energies where alternative beam techniques are either difficult or subject to large uncertainty. In the present work measurements were made of the mobility of Xe^+ ions in Xe using a variable length drift tube of the Tyndall-Powell four-gauze type¹. The E/N and pressure ranges used were from 50 to 10,000 Td (where E is the electric field strength, N the gas number density; 1 Td = 10^{-21} volt m^2) and from 3.5 to 92 Pa. The ions were produced by electron impact using electrons obtained by α -particle ionization.

Due to spin orbit coupling two Xe^+ species are observed [$\text{Xe}^+(^2P_{1/2})$ and $\text{Xe}^+(^2P_{3/2})$] in the arrival time spectrum. The ion current maxima due to each species was obtained by deconvolution and their identity established by comparison with the data of Helm².

Particular care was taken to minimize errors due to the shutter open time effect noted by Hegerberg et al.³ The estimated absolute error of the mobility values is $\pm 1\%$ over the full E/N range for the $\text{Xe}^+(^2P_{3/2})$ ions, and $\pm 1.5\%$ for the $\text{Xe}^+(^2P_{1/2})$ ions for E/N ≤ 190 Td rising to $\pm 6\%$ at 900 Td. This was the highest E/N value for which the deconvolution procedure for the $\text{Xe}^+(^2P_{1/2})$ ion was considered reliable. Over the common E/N range the present data agree to within the stated experimental errors with the only previous high precision mobility data for Xe^+ ions in Xe, those of Helm.²

The resonant charge transfer cross section for $\text{Xe}^+(^2P_{3/2})$ ions in Xe was derived using the theory of Skullerud⁴ and the procedure described by Hegerberg et al.³ Only data for E/N values greater than 2500 Td were used in the analysis in order to conform to the assumptions of the Skullerud mobility formula. It is for this reason that it was not possible to derive the charge transfer cross section for $\text{Xe}^+(^2P_{1/2})$ ions by this procedure.

The charge transfer cross section shown in Figure 1 (curve P) is estimated to have an absolute error of $\pm 5\%$ and to extend over the energy range 0.4 to 4.5 eV (lab). The present cross section agrees with the quantum mechanical calculation of Sinha and Bardsley⁵ to within the experimental error. Over the common energy range the present cross section agrees with previous experimental cross sections to within the quoted uncertainties.

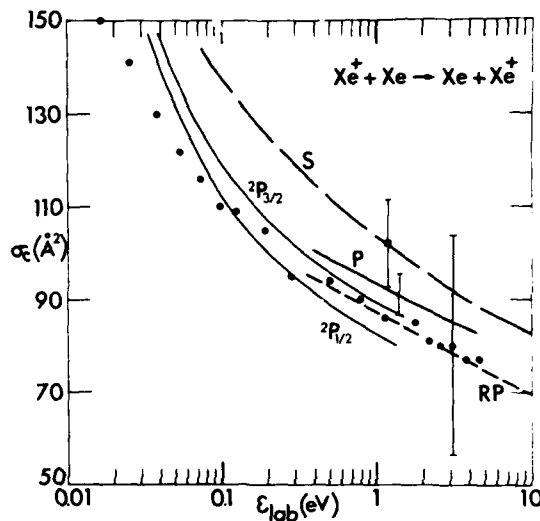


FIGURE 1. The resonant charge transfer cross section for Xe^+ ions in Xe: (P) — Present ($^2P_{3/2}$); ● Koizumi et al.⁶ (injected ion-drift tube); ■ Ziegler⁷ (beam experiment); — ($^2P_{1/2}$), ($^2P_{3/2}$), Sinha and Bardsley⁵ (theoretical); — (S), Sheldon⁸ (theoretical); — (RP) Rapp and Francis⁹ (theoretical). The quoted errors bars of the experimentally derived cross sections are as shown.

References

1. M.T. Elford, J. Chem. Phys. **79**, 5951 (1983).
2. H. Helm, J. Phys. B. **9**, 2931 (1976).
3. R. Hegerberg, M.T. Elford and H.R. Skullerud, J. Phys. B. **15**, 797, 1982.
4. H. Skullerud, J. Phys. B. **2**, 86 (1969).
5. S. Sinha and N. Bardsley, Phys. Rev. A, **14**, 104 (1976).
6. I. Koizumi, O. Kazuhiko, N. Kobayashi and Y. Kaneko, J. Phys. Soc. (Japan) **51**, 2650 (1982).
7. B. Ziegler, Z. Physik **136**, 108 (1953).
8. J.W. Sheldon, Phys. Rev. Lett. **8**, 64 (1962).
9. D. Rapp and W.A. Francis, J. Chem. Phys. **37**, 2631 (1962).

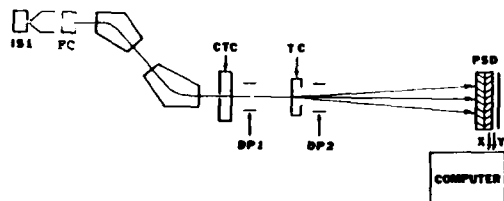
DIFFERENTIAL CHARGE-TRANSFER CROSS SECTIONS FOR $O^+(^4S)$ and $O^+(^2D)$ IONS WITH ATMOSPHERIC GASES

D. A. Schafer, J. H. Newman, K. A. Smith, and R. F. Stebbings

Space Physics and Astronomy Department, Rice University, Houston, TX USA

Energetic O^+ ions precipitate into the earth's atmosphere during periods of geomagnetic activity.¹ These ions collide with the ambient atmospheric particles, resulting in thermospheric heating and production of a flux of upward-moving neutral particles that may escape the atmosphere. Differential cross sections for the atomic collision processes involved are required to make accurate models of these precipitation events.

Absolute differential cross sections for charge transfer of 1.5 and 5 keV $O^+(^4S)$ and $O^+(^2D)$ ions with He, H_2 , N_2 , O_2 , CO_2 and SO_2 are presented for laboratory-frame scattering angles between 0.05° and 5° . The apparatus is shown below.



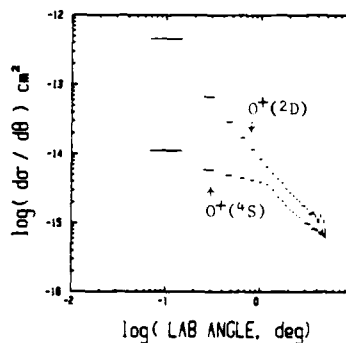
Ions produced in an electron-impact-sustained plasma ion source are formed into a beam that is momentum-analyzed by a pair of 60° sector magnets. Two 25-micron diameter holes separated by 10 cm collimate the beam before it enters the target cell. All ions exiting the cell are deflected by plates DP2, and neutral products of charge-transfer reactions in the target cell impact the position-sensitive detector (PSD). The PSD determines the location of particle impacts on its surface to an accuracy of about 100 microns, and an LSI-11 microprocessor accumulates the position information until the angular distribution of reaction product is determined.

Absolute cross sections are found by measuring both the primary ion beam and the scattered neutral product with the PSD, after determining the relative efficiency of that detector for ions and neutrals of the same species and energy. The PSD calibration for neutrals is made by: (1) measuring the primary ion beam flux at the PSD, (2) converting a large, but known, fraction of that beam to fast neutrals by charge exchange in the target cell, and (3) measuring the resulting count rate at the detector. This calibration procedure is effective because the PSD

subtends a relatively large solid angle when viewed from the target cell, so that virtually all of the collision product is collected.

The ion beam initially contains O^+ in both ground (4S) and excited (2D) states. The attenuation method developed by Turner et al.² is used to determine the fraction of ions in each state. We use a similar technique to produce a pure ground-state ion beam. The cell labelled FC in the figure above is filled with N_2 , which has a much larger charge-transfer cross section for $O^+(^2D)$ than for $O^+(^4S)$. The N_2 pressure in this cell is adjusted to remove the excited species from the beam by charge exchange, leaving a relatively-pure ground-state beam. Differential charge-transfer cross sections are then measured for both the pure ground-state beam and for a beam containing both ground and excited states. Since the fraction of ions in each state is known, the excited-state differential charge transfer cross section is determined by subtracting the pure-ground-state data from the mixed-state data.

The results presented below represent the first measurements of differential charge-transfer cross sections for excited-state O^+ ions with N_2 . As expected, the differential cross section for the nearly-resonant $O^+(^2D)$ reaction is much more strongly forward-peaked than that for the ground state.



This work was supported by National Science Foundation grant ATM 8023219 and by National Aeronautics and Space Administration grant NSG 7386.

References

1. M. R. Torr and D. G. Torr, *Geophys. Res. Lett.*, **6**, 700 (1979); J. Kozyra, T. E. Cravens, and A. F. Nagy, *J. Geophys. Res.*, **87**, 2481 (1980).
2. B. R. Turner, J. A. Rutherford, and D. M. J. Compton, *J. Chem. Phys.*, **48**, 1602 (1968).

ELECTRON CAPTURE FROM Li(2s) BY 2 - 20 keV C⁺, N⁺ AND O⁺

F. Aumayr, G. Lakits and H. Winter

Institut für Allgemeine Physik, TU Wien, Austria

C⁺, N⁺ and O⁺ each have low lying excited states, some of them being metastable. If, as usual, metastable ion beam fractions are not known, collisional studies with such ions are subject to considerable uncertainty. We are interested whether a recently developed technique for measuring multi-charged metastable ion beam fractions (so-called X3C method for excitation by core-conserving electron capture [1]) is also applicable to singly charged ion species. To this purpose, the extent of core conservation during electron capture from suitable atoms as Li(2s) has to be investigated.

Earlier work on state-selective capture from Li(2s) by protons [2] or Ne⁺ ions [3] revealed a dominant population of such excited states, for which the reaction energy defects are smallest. For capture by C⁺, N⁺ or O⁺ from Li(2s), electron transfer into respective 3s neutral states should be most probable, because corresponding energy defects are smaller than for the other possible capture channels. Cross sections for such near-resonant capture processes can be calculated by semiempirical methods [4], the success of which is of general interest for other similar capture processes. Apart from this, C, N and O are prominent fusion plasma impurities, which can possibly be detected by means of Li beam-activated charge exchange spectroscopy [5], which demands knowledge of corresponding state-selective electron capture cross sections.

For the present studies, C⁺, N⁺ or O⁺ ion beams have been produced with a plasma source supplied by various gases or vapours. It is known that metastable ion beam fractions can critically depend on the ion source feeding substance, cf. e.g. [6].

Fig. 1 shows total cross sections for electron capture from Li(2s) by C⁺, N⁺ and O⁺ respectively, which have been measured in the same way as for H⁺-Li collisions [7], using the latter data at 10 keV for calibration. So far, within the presently achieved accuracy of about 25 %, no difference in the cross sections showed up when producing the primary ions from different source feeding gases, which seems to support our hypothesis of ion core conservation in capture from Li(2s). With the latter assumption, we have been able to explain our data shown in fig. 1 with semiempirical

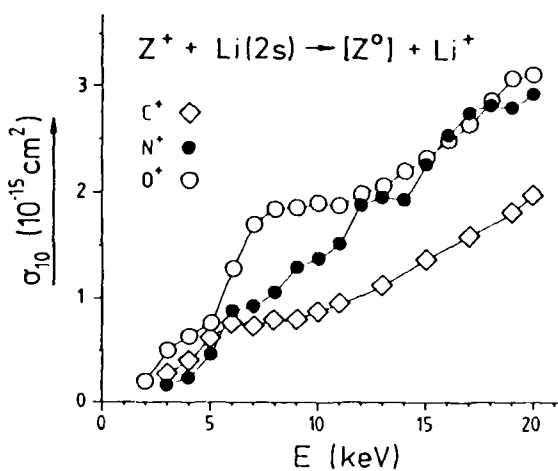


Fig. 1: Total single electron capture cross sections for impact of C⁺, N⁺ or O⁺ on Li(2s), vs. impact energy E.

calculations [4] as earlier referred to, taking into account the slightly different energy defects for the three ion species.

Further investigations along these lines together with vuv spectroscopy in view to state-selective electron capture and metastable ion beam fraction measurements by means of X3C are in progress.

Acknowledgments

This work has been supported by Fonds zur Förderung der wissenschaftlichen Forschung (Proj. Nr. 4376), and by Kommission zur Koordination der Kernfusionsforschung at the Austrian Academy of Sciences.

References

- 1) A. Brazuk et al., J.Phys.B: At.Mol.Phys. **17**(1984)2489
- 2) F. Aumayr, H. Fehring and H. Winter, J.Phys.B: At.Mol.Phys. **17**(1984)4185,4201
- 3) E. Rille and H. Winter, J.Phys.B: At.Mol.Phys. **15**(1982)3489
- 4) Yu. Derikov, Sov.Phys.-JETP **18**(1964)134
P.E. Olson, Phys.Rev. A **6**(1972)1822
P.E. Olson and F.T. Smith, Phys.Rev. A **2**(1973)1529
G.E. Ice and P.E. Olson, Phys.Rev. A **11**(1975)111
- 5) H. Winter, Comm.At.Mol.Phys. **12**(1982)165
- 6) B.H. Hughes and T.O. Tierman, J.Chem.Phys. **55**(1971)3419
- 7) Aumayr F and Winter H, Phys.Rev. A **31**(1985)67

STATE SELECTIVE AND TOTAL ELECTRON CAPTURE IN $H^+Li(2s)$ COLLISIONS (2 - 20 keV)

Friedrich AUMAYR and Hannspeter WINTER
Institut für Allgemeine Physik, TU Wien, Austria

Recently, the first extensive experimental study of total and state selective electron capture in $H^+Li(2s)$ collisions at impact energies of 2 - 20 keV has been presented¹⁻³. The investigations involved $Li(2p)$ excitation, state - selective electron capture into $H(2p)$ and $H(3, \ell)$ subshells, and direct determination of total capture cross sections.

Electron transfer in relatively slow ($v < 1$ a.u.) $H^+Li(2s)$ collisions can be described as a quasi - one electron process, and a comparison between our experimental results and respective calculations⁴⁻⁶ is of considerable interest. There is also a practical application of this collision system for Li - beam - activated charge exchange spectroscopy of magnetically confined plasmas (see e.g. ref.1).

For the sake of completeness and to check the consistency of our previous measurements, electron capture into the metastable $H(2s)$ subshell has now been investigated at impact energies between 2 - 20 keV:



For detection of $H(2s)$ atoms, the use of both electrical field quenching and dye laser fluorescence spectroscopy has been considered, finally using the first method. Results of these measurements are shown in fig. 1.

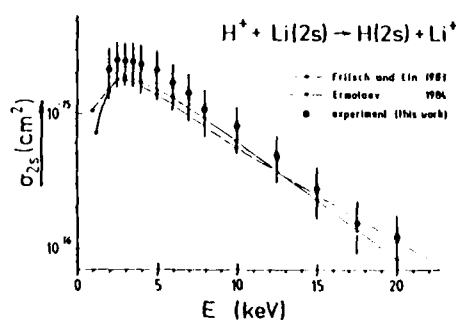


Fig. 1. Absolute cross sections for capture into $H(2s)$ subshell for $H^+Li(2s)$ collisions.

Since all significant partial capture cross sections for $H^+Li(2s)$ collisions are now

available, the sum of these can be compared with the total single electron capture cross section σ_{10}^3 as shown in fig. 2. Satisfactory agreement within the combined error limits is found and thus proves the consistency of our measurements.

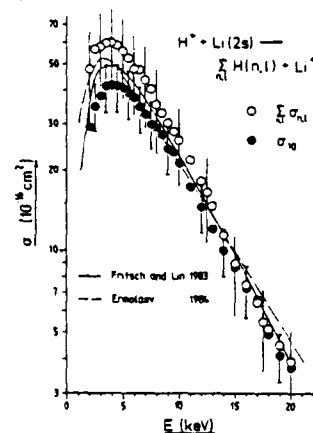


Fig. 2. Comparison of total capture cross sections obtained by either summing up of significant state - selective capture cross sections or from direct measurements.

In the present contribution a detailed comparison of our cross section data for various inelastic channels with all available calculations will be presented and discussed.

Acknowledgement

This work has been supported by Fonds zur Förderung der wissenschaftlichen Forschung (Proj. No. 4376).

References

- 1) Aumayr F, Fehrer M and Winter H, J.Phys.B:At.Mol.Phys. **17** (1984) 4185
- 2) Aumayr F, Fehrer M and Winter H, J.Phys.B:At.Mol.Phys. **17** (1984) 4201
- 3) Aumayr F and Winter H, Phys.Rev.A **31** (1985) 67
- 4) Fritsch W and Lin C D, J.Phys.B: At.Mol.Phys. **16** (1983) 1595
- 5) Sato H and Kimura N, Phys.Lett. **96A** (1983) 286
- 6) Ermolaev A M, J.Phys.B:At.Mol.Phys. **17** (1984) 1069

DIFFERENTIAL CROSS SECTIONS FOR 30, 66.7, AND 150 keV Mg^+ ELECTRON CAPTURE FROM He⁺

E. Redd, D. M. Blankenship, D. G. Seely, T. J. Gay, J. L. Peacher, and J. T. Park

University of Missouri-Rolla, Rolla, Missouri 65401 USA

Differential electron capture cross sections have been obtained for 30, 66.7, and 150 keV Mg^+ colliding with He using the University of Missouri-Rolla Ion Energy-Loss Spectrometer (UMRIELS).¹ The cross section measurement at 66.7 keV is absolute. The cross sections have structure consistent with qualitative descriptions of Quasi-One-Electron (QOE) collision systems. The structure is most marked at 30 keV and is least marked at 150 keV.

$^{24}\text{Mg}^+$ ions were produced in a Colutron ion source. The ions were accelerated to the desired energy and collimated prior to the scattering region. The accelerator and entrance collimation were rotated about the scattering center to determine angular scattering dependence. After the scattering region a magnet steered the ions to the desired detector while fast neutrals resulting from electron capture were undeflected and struck the neutral detector. The ions were normally deflected to the ion energy-loss detector but if undeflected, the ions struck the neutral detector. Relative differential electron capture cross sections were obtained by measuring the angular dependence of the neutral detector signal.

If the detector efficiencies for ions and neutrals are the same, absolute cross sections will be obtained. Using the neutral detector in four ways has the possibility of showing the detector efficiencies to be equal. Integration of the angular distributions were performed for: current mode fast neutrals, current mode ions, pulse mode fast neutrals, and pulse mode ions. Since the quotient from dividing current mode neutrals by current mode ions is the same as dividing pulse mode neutrals by pulse mode ions, the detection efficiency is assumed to be the same for both fast neutrals and ions. These equal quotients can then be divided by the number of scatterers to determine the total electron capture cross section.

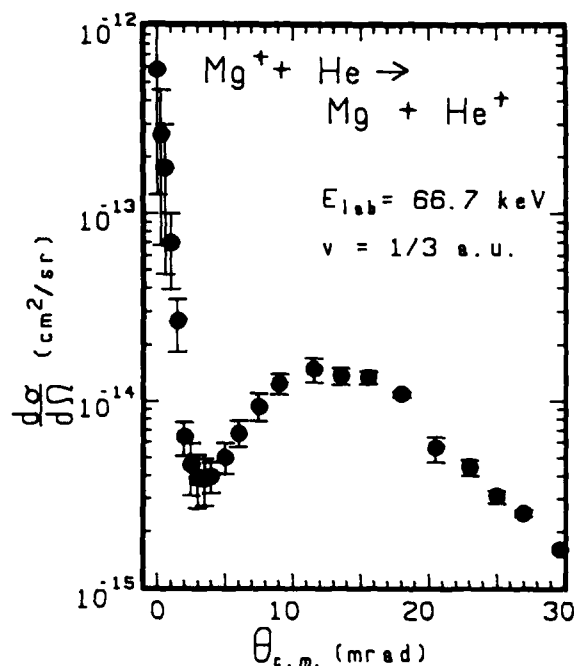
The above procedure was used to obtain the total cross section value of $1.76 \pm 0.44 \times 10^{-17} \text{ cm}^2$ for the 66.7 keV differential electron capture cross section shown in the Figure. The analog and pulse mode measurements implied the detection efficiencies were equal for Mg ions and neutrals at this energy.

The differential cross section shows a definite structure. The cross section falls to a local minimum value of $3.8 \pm 1.1 \times 10^{-15} \text{ cm}^2/\text{sr}$ at 3.4 mrad. The cross section has local maxima of $5.8 \pm 4.6 \times 10^{-13} \text{ cm}^2/\text{sr}$

at 0 mrad and $1.5 \pm 0.2 \times 10^{-14} \text{ cm}^2/\text{sr}$ at 11.5 mrad. This behavior is consistent with the qualitative QOE scattering explanations,² i.e. excitation to the electron capture states requires the cores to interpenetrate. For the Mg^+ - He system this should occur for $R < 1.9 \text{ a.u.}$ By using a potential given by Sondergaard and Mason³ the differential cross section can be converted into probability vs. impact parameter. The probability reaches a maximum of 0.31 at impact parameter of 0.92 a.u. The probability has a broad maximum at impact parameters less than 1.3 a.u. The differential electron capture cross section structure further implies the validity of the qualitative QOE scattering explanations even though no quantitative calculations are available for comparison.

[†]Work supported in part by the National Science Foundation.

1. P. J. Martin, K. Arnett, D. M. Blankenship, T. J. Kvale, J. L. Peacher, E. Redd, V. C. Sutcliffe, J. T. Park, C. D. Lin, and J. M. McGuire, Phys. Rev. A **23**, 2858 (1981).
2. N. Andersen and S. E. Nielsen, Adv. At. Mol. Phys. **18**, 265 (1982) and references therein.
3. N. A. Sondergaard and E. A. Mason, J. Chem. Phys. **62**, 1299 (1975).



DOUBLE TARGET IONIZATION RESULTING FROM SINGLE CHARGE TRANSFER IN H^+ , He^{++} - NEON, SODIUM AND MAGNESIUM COLLISIONS*

R. D. DuBois

Pacific Northwest Laboratory, Richland, WA 99352 (USA)

Electron transfer is an effective method of producing target ionization in slow ion-atom collisions. Most experimental studies of charge transfer observe only the final projectile charge states - hence only total single electron transfer cross sections are measured. By measuring, in addition, the final target ionization charge state in coincidence with the final projectile charge state the pure charge transfer process σ_{10} can be separated from the processes where additional ionization occurs $\sigma_{2,3}^{10}$. Here the superscripts refer to the projectile initial and final target charge states while the subscript gives the final target charge state. It has been previously observed¹ that in very low energy collisions the double target ionization channel can be as large or larger than the single target ionization channel. This is due to the limited channels that are energetically available.

In the present work, neon, sodium and magnesium targets are investigated. They have a filled outer shell, a single outer shell electron, and two outer shell electrons respectively. Data are presented for target ionization charge state production due to single electron transfer to the projectile. Impact energies are less than 200 keV.*

Figure 1 shows spectra of magnesium ions produced by 15 keV (lower curve) and 100 keV (upper curve) proton impact. Note that for the lower impact energy Mg^+ production dominates while at higher energies Mg^{2+} dominates. The cross sections shown in Figure 2 indicate that the relative amount of double ionization increases dramatically in going from neon to magnesium. This is because single ionization of neon occurs via 2p capture while double ionization is by simultaneous 2p capture and 2p ionization. For magnesium, however, single ionization occurs via 3s capture whereas double ionization occurs via 3s capture plus 3s ionization, 3s capture plus 2p ionization, 2p capture plus 3s ionization or 2p capture followed by an Auger decay. For lower energies double ionization is via 3s capture plus 3s ionization while at higher energies it is probably via 2p capture and an Auger process.

He^{++} impact data will also be presented.

*DOE Contract DE-AC06-76RLO 1830

Reference: I. W. Groh, A.S. Schlachter, A. Müller & E. Salzborn, J.Phys.B Lett.15 L207 (1982) and references therein.

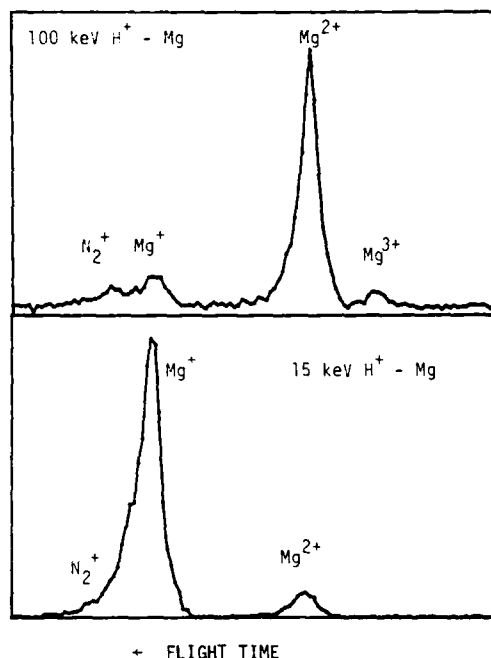


FIGURE 1.

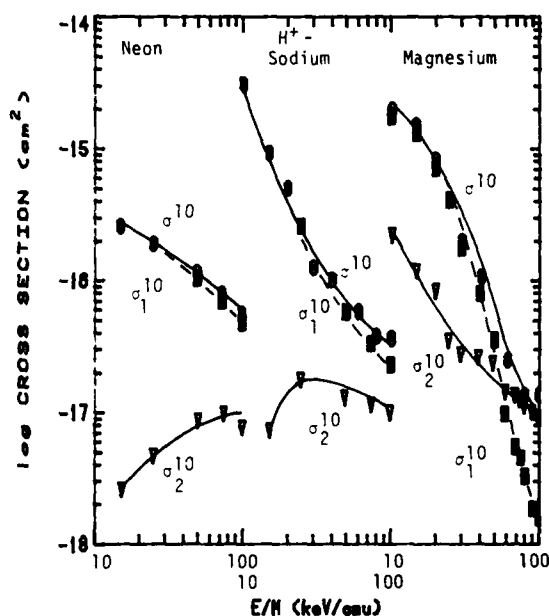


FIGURE 2.

LOW ENERGY ELECTRON CAPTURE BY FULLY STRIPPED LIGHT IONS FROM H AND H₂

F. W. Meyer, A. M. Howald, C. C. Havener, and R. A. Phaneuf

Physics Division, Oak Ridge National Laboratory*
Oak Ridge, Tennessee 37831 USA

Measurements of total electron capture cross sections for fully stripped and H-like C, N, O, F, and Ne ions incident on H and H₂ have been performed in the energy range 0.2 to 10 keV/amu using ion beams produced by the ORNL ECR multicharged ion source.¹ The experiment employs the ORNL atomic hydrogen gas target, a directly heated tungsten tube in which molecular hydrogen is thermally dissociated. A collimation section preceding the target limits the magnetically charge analyzed incident beam to a divergence of ± 1.7 mr, and 1 mm cross section inside the target. Immediately downstream of the collision target cell, charge analysis occurs in an electrostatic parallel-plate analyzer. A single CEM operated in pulse-counting mode is employed for particle detection. The electron-capture signal and primary beams are measured alternately for a preselected number of cycles under computer control, and the total electron capture cross section is deduced from the fraction of ions which capture an electron at a known (calibrated) target thickness.

Figure 1 shows the experimental electron capture cross section results obtained for the measured fully stripped light ions incident on atomic and molecular hydrogen. The error bars shown reflect random uncertainty in terms of reproducibility of the measurements at two standard deviations. Systematic uncertainties are estimated to be $\pm 9\%$.

In the case of the fully stripped C, N, and O projectiles incident on H, the present measurements can be compared to theoretical calculations. Very good agreement is found between the present results for C⁶⁺, N⁷⁺, and O⁸⁺ incident on H, and the close-coupling calculations of Fritsch and Lin² employing a modified atomic-orbital (AO) expansion. While falling systematically below the AO calculations, the discrepancy is less than 20% at energies above 1.5 keV/amu, and approaches 40% at the lowest energies measured. For C⁶⁺ and O⁸⁺ incident on H, close coupling calculations by Green et al.³ and Shipsey et al.⁴, respectively, employing a molecular-orbital (MO) expansion are also in reasonable accord with the present results. The MO results lie systematically above the AO calculations by about 10% above 1.0 keV/amu, and by as much as 40% at 0.2 keV/amu.

References

*Operated by Martin Marietta Energy Systems, Inc., for the U.S. Department of Energy under contract No. DE-AC05-84OR21400.

1. F. W. Meyer, to be published in NIM (March 1985).
2. W. Fritsch and C. D. Lin, Phys. Rev. A **29**, 3039 (1984).
3. T. A. Green, E. J. Shipsey, and J. C. Browne, Phys. Rev. A **25**, 1364 (1982).
4. E. J. Shipsey, T. A. Green, and J. C. Browne, Phys. Rev. A **27**, 821 (1983).
5. R. K. Janev, D. S. Belic, and B. H. Brandsen, Phys. Rev. **28**, 1293 (1983).
6. M. N. Panov, A. A. Basalev, and K. O. Lozhkin, Phys. Scr. **T3**, 124 (1983).
7. R. A. Phaneuf, I. Alvarez, F. W. Meyer, and D. H. Crandall, Phys. Rev. A **26**, 1892 (1982).

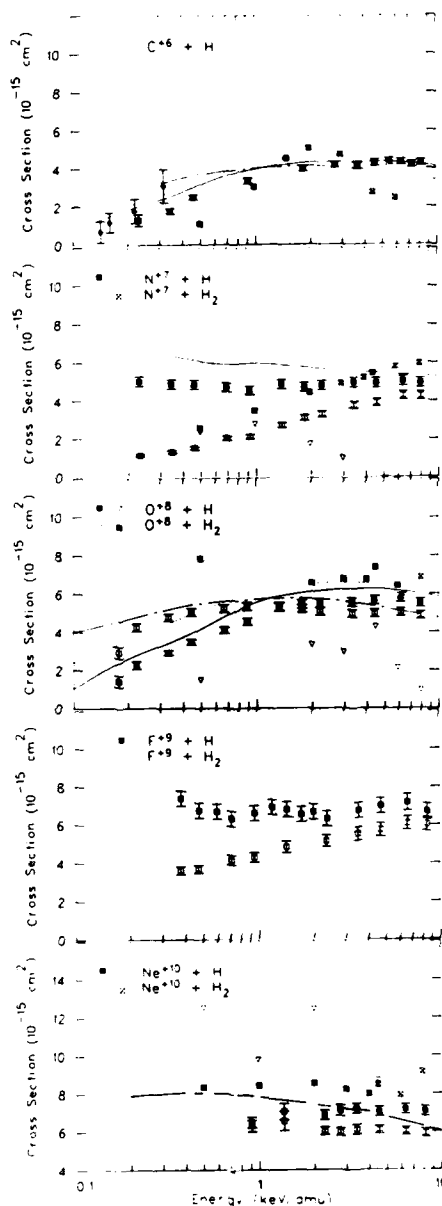


FIGURE 1. Total electron capture cross sections for fully stripped C, N, O, F, and Ne ions incident on H and H₂; data points with error bars — present results (solid diamonds from Ref. 7); data points without error bars — experimental results of Ref. 6. Theory curves are for atomic hydrogen; solid curves — AO calculation (Ref. 2); dotted curves — MO calculation (Refs. 3, 4); chain-dashed curves — multichannel Landau Zener calculations (Ref. 5).

10 KeV/q Al^{12+} COLLISIONS WITH H_2 AND He : MOST POPULATED n STATE AND MEAN \bar{n} VALUE FROM LYMAN SPECTROSCOPY*

D. Vernhet, A. Touati, P. Bouisset, A. Chetoui, J.P. Rozet, K. Wohrer

Institut Curie and Université P & M Curie, 11, rue P & M Curie, 75231 Paris Cedex 05, France

and C. Stephan

Institut de Physique Nucléaire, BP n°1, 91405 Orsay, France

Highly charged ions (Al^{12+} , Al^{13+}) have been recently produced at the ECR Minimax source in Grenoble. Ion beam intensities (respectively 1nA and 50pA) are not high enough to allow high resolution spectroscopy of Lyman, Balmer... series which provides the full $P(n)$ distribution. However information about n values can be obtained by recording Lyman spectra emitted after capture with a high efficiency Si(Li) detector :

- (i) The most populated n state can be identified by the n_m value of the most intense direct Lyman X ray since coupled state calculations (2) predict always that $P(n)$ and $P(np)$ distributions maximize for the same n values.
- (ii) The proportion of p states populated by capture is given by the intensity ratio I (direct Lyman X rays) / I (all Lyman X rays). Indeed every n state decays either directly (in the case of $n=1$) or after a cascade to the $1s$ state through a Lyman emission with a nearly unit probability as shown from helium-like branching ratios (3).
- (iii) The mean \bar{n} value can be extracted from the intensity ratio of Lyman β and Lyman α X rays which result from cascade events (4).

Figure 1 shows helium-like Lyman spectra recorded for Al^{12+} collisions with H_2 target and Table 1 shows experimental values for n_m , percentage of p states and \bar{n} . Corresponding coupled state calculations for $P(n)$ distributions are now under performance (5). However one should notice that since two-electron targets are used, transfer ionization and autoionizing double capture processes are allowed and contribute to the Lyman X-ray spectrum. Calculations should include these two-electron processes for the comparison with experiment to be valid.



Figure 1 : Lyman spectrum emitted in $Al^{12+} + H_2$ collisions.

target	n_m	% p	\bar{n}
H_2	6	2.4 ± 0.7	3.4 ± 0.3
He	6	2.4 ± 0.8	2.9 ± 0.1

Table 1 : Experimental values of n_m , % p, \bar{n} , for Al^{12+} collisions.

References :

1. R. Geller and B. Jacquot, Nucl. Instrum. Methods **184**, 293 (1981).
2. T.A. Green, E.J. Shipsey and J.C. Browne, Phys. Rev. A **25**, 1364 (1982).
3. W.L. Wiese, M.W. Smith and B.M. Glennon, Atomic Transition Probabilities, Vol I, NBS 4, 1966.
4. A. Chetoui, J.P. Rozet, K. Wohrer, D. Vernhet, P. Bouisset, A. Touati and S. Stephan, to be published in Nucl. Instrum. Methods (1985).
5. A. Salin and C. Harel, private communication.

* Work performed at CENG AGRIPPA, CEN-CNRS, 85X, 38041 Grenoble Cedex.

Measurement of Charge Exchange Cross Sections for $H^+ + He \rightarrow He^+ + H(n=3, \ell, m_\ell)$

M. C. Brower and F. M. Pipkin

Lyman Laboratory of Physics, Harvard University, Cambridge, MA 02138

A microwave-resonance optical detection technique was used to measure the partial cross sections for charge capture into the individual ℓ, m_ℓ states of the $n=3$ manifold of hydrogen by 50 keV protons passing through a helium target. The method is similar to that used earlier for measurements of charge capture by protons from N_2 and H_2 targets.¹ A number of improvements were made so that one could determine with greater precision the small partial cross sections for capture into the D states.

Figure 1 shows a schematic diagram of the experiment. Neutral hydrogen atoms formed in the target pass through a radiofrequency interaction region which can drive transitions among the states in the $n=3$ manifold. After emerging from the rf region, the Balmer- α light emitted at right angles to the beam by the atoms is observed with a detector consisting of a narrow-band interference filter, a rotatable polarizer, and a cooled RCA 8852 photomultiplier tube. The fractional change in light detected when the rf field is switched on is proportional to the difference in population of the states coupled by the field.

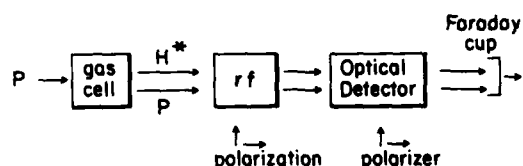


Fig. 1. Schematic diagram of the microwave resonance optical detection experiment used to study charge exchange collisions.

Two principal transitions are studied, the $3^2S_{1/2} - 3^2P_{3/2}$ transition near 2940 MHz and the $3^2P_{3/2} - 3^2D_{5/2}$ transition near 1080 MHz. The rf region is designed to be rotated so that the electric field is either parallel or perpendicular to the beam direction (the axis of quantization), making it possible to drive either $\Delta m = 0$ or $\Delta m = \pm 1$ transitions. The rf region can also be rotated close to or far away from the target with the field remaining parallel to the beam. In addition, the optical polarizer in the Balmer- α detector can be rotated parallel or perpendicular to the beam direction in order to distinguish between $\Delta m = 0$ and $\Delta m = \pm 1$ decays. The total of twelve independent measurements (two transitions, three rf configurations, two optical polarizations) provide sufficient information to determine the relative cross sections for capture into

each of the angular momentum substates of the $n=3$ manifold.

The velocity of a 50 keV proton is roughly uc . The scattering at this energy lies midway between the low energy regime described by molecular orbital methods and the high energy regime described by the Born approximation. The measured cross sections decrease as ℓ increases and for each ℓ they decrease as m_ℓ increases. This qualitatively confirms the results of coupled state calculations^{2,3} and of other more conventional calculations^{4,5} if one includes the Burgdorfer⁶ post-collision interaction corrections. Detailed comparisons will be made with the theories and measurements of the density matrix for charge capture into the $n=3$ state by Havener, et al.⁷

This research was supported by National Science Foundation Grant PHY84-10330.

References

1. R. J. Knize, S. R. Lundeen, and F. M. Pipkin, Phys. Rev. A **29**, 1114 (1984).
2. T. G. Winter and C. C. Lin, Phys. Rev. A **10**, 2141 (1974).
3. R. Shakeshaft, Phys. Rev. A **18**, 1930 (1978).
4. M. Lieber, University of Arkansas (private communication).
5. L. J. Dubé, Albert-Ludwigs-Universität (private communication).
6. J. Burgdorfer, Phys. Rev. A **24**, 1756 (1981).
7. C. C. Havener, N. Rouze, W. B. Westerveld, and J. S. Risley, Phys. Rev. Lett. **53**, 1049 (1984).

CHARGE TRANSFER IN $H^+ + Na$ COLLISIONSR. Shingal, C.W. Newby, C.J. Noble⁺, D.R. Flower and B.H. BransdenDepartment of Physics, University of Durham, South Road, Durham DH1 3LE, U.K.
Daresbury Laboratory, Daresbury, Warrington WA4 4AD, U.K.

A number of theoretical¹⁻³ and experimental⁴⁻⁶ results have been reported in the literature for charge transfer in collisions of protons with sodium atoms. The theoretical studies are based either on travelling molecular (MO) or atomic (AO) orbitals. The calculations differ markedly in the energy range over which they overlap, as is also the case of the experimental data.

We have reinvestigated the $H^+ + Na$ collision process using a semi-classical impact parameter method⁷. An atomic state expansion centred on the two nuclei was used to represent the wave function of the system. Plane-wave translation factors were included in the calculation. The valence electron of the sodium atom is assumed to move in an effective potential representing the core electrons. The Hamiltonian for the system can thus be written as

$$H = -\frac{1}{2}\nabla^2 - \frac{Z_A}{r_A} - V_{\text{eff}}(r_B)$$

where A and B are the projectile and the target nuclei, respectively. The effective potential, $V_{\text{eff}}(r)$, is taken to be of the form

$$V_{\text{eff}}(r) = \frac{Z_B - \sum_s z_s}{r} + \sum_{s=1}^2 \sum_{k=0}^3 \frac{z_s (\gamma_s r)^k (4-k)}{4k!r} e^{-\gamma_s r}$$

Here, z_1 and z_2 are the K and L shell charges. The parameters γ_s are variationally determined. A basis set consisting of a large number of Slater type orbitals is used to represent the target atom states. This ensures that given the choice of effective potential, the Slater orbitals are able to represent a considerable number of bound states of the sodium atom. A model potential due to Peach⁸ was also used. Preliminary calculations of charge transfer cross-sections for the impact energy range 0.5 - 20 keV, using an expansion consisting of $n = 3$ states on the target and $n = 1-3$ states on the projectile show a good agreement with the experimental data of Anderson et al.⁶ (Fig. 1) but not with the experimental data of Gruebler et al.⁹.

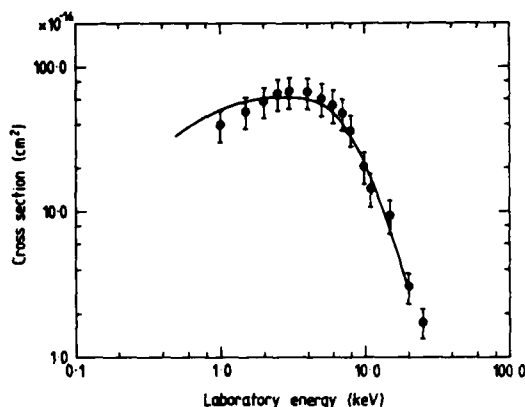


FIGURE 1 Total cross-sections for $H^+ + Na \rightarrow H + Na^+$. Theoretical cross-sections: —, 16-state atomic expansion, present work. Experimental cross-sections: ●, Anderson et al.⁶

References

1. M. Kimura, R.E. Olson and J. Pachale, Phys. Rev. A26, 3113 (1982).
2. C. Kubach and V. Sidis, Phys. Rev. A23, 110 (1981).
3. W. Fritsch, Phys. Rev. A30, 1135 (1984).
4. T. Nagata, J. Phys. Soc. Jpn. 48, 2068 (1980).
5. J.K. Berkowitz and J.C. Zorn, Phys. Rev. A29, 611 (1984).
6. C.J. Anderson, A.M. Howald and L.W. Anderson, Nucl. Instrum. and meths. 165, 583 (1979).
7. B.H. Bransden, 'Atomic Collision Theory', 2nd Edn. (Benjamin Cummings, N.Y.) (1983).
8. G. Peach, Comments At. Mol. Phys. 11, 101 (1982).
9. W. Gruebler, P.A. Schmelzbach, V. Konig and H. Marmier, Helv. Phys. Acta 43, 254 (1970).

"HEISENBERG CORE" IN CLASSICAL TRAJECTORY MONTE-CARLO CALCULATIONS OF IONISATION AND CHARGE EXCHANGE

D. Zajfman and D. Maor

Department of Physics, Technion, Haifa, Israel

The classical trajectory Monte Carlo (CTMC) method has yielded results for ionization and charge exchange in a single electron collision system (bare nucleus on H atom) which are in good agreement with experiment within a defined range of projectile velocities^{1,2}. For targets containing more than one electron, usually the so-called independent electron approximation has been applied³. In this approach, electron-electron interactions are neglected, except for an average screening of the nucleus. Agreement with experiment is not very good.

We report on full four body CTMC calculations of cross sections for single and double ionization and charge exchange in collisions of bare nuclei (p , He^{++}) with He atoms. Following the work of Kirschbaum and Wilets⁴, we add to the target nucleus the potential:

$$V(p_i, r_i) = \left(\frac{\xi^2}{4\alpha r_i} \right) \exp \left[\alpha \left(1 - \left(\frac{r_i p_i}{\xi} \right)^4 \right) \right] \quad (1)$$

where p_i, r_i represent the values of the momentum and distance of each electron relative to the target nucleus. This potential causes $r_i p_i \geq \xi$, with the equality sign holding for the ground state. The reason for imposing this constraint, which is practically the Heisenberg principle, is that the ground state of the He atom is classically unstable⁴. The value of ξ is obtained from Hartree-Fock calculations for the He ground state. α is called the hardness parameter and we find our results to be independent of it for $\alpha > 50$.

Fig. 1 displays the "apparent cross section" for target ionization (charge integral of target ions) for the collision $He^{++} \rightarrow He$ measured by Puckett et al.⁵ and calculated here. The agreement is seen to be very good.

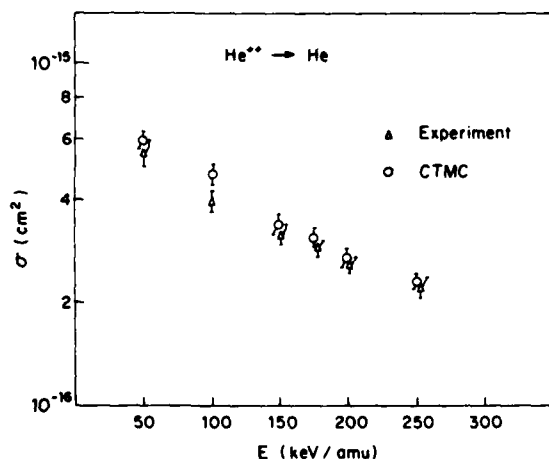


Fig. 1 "Apparent cross section" for target ionization

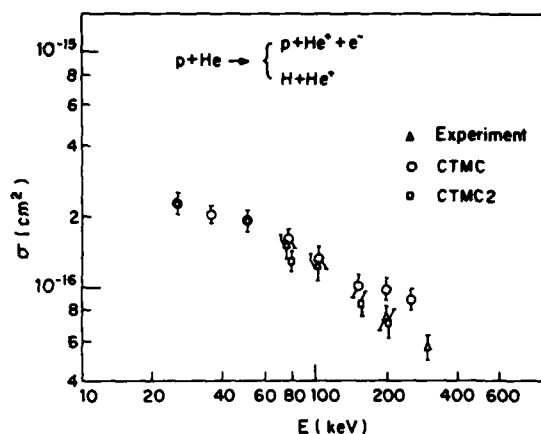


Fig. 2 Single electron loss cross section for $p + He$

Similar calculations were performed for $p + He$. In compliance with available experimental data, we show in Fig. 2 results from the experiment of Du Bois et al.⁶ and present calculations (CTMC) for the single electron loss cross section. Good agreement is obtained up to ~ 100 keV, above that the calculated results are too high. Fig. 2 contains three additional points designated CTMC2. These were obtained when a potential of the form (1) was also added to the proton. The reason for this is: the physical meaning of the constraint imposed by (1) is to prevent binding of electrons below the quantum-mechanical ground state. It thus constitutes a "Heisenberg core" around the nucleus (in analogy with the Pauli core in identical fermion interactions). As can be seen in the Figure, adding this potential to the proton reduces the calculated cross section, seemingly in better agreement with the data. Additional results of calculations using the "Heisenberg core" will be shown.

References

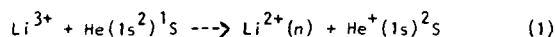
1. R. Abrines and I.C. Percival, Proc. Phys. Soc. **88**, 861 (1966).
2. R.E. Olson and A. Salop, Phys. Rev. **A16**, 531 (1977).
3. R.E. Olson, J. Phys. B: At. Molec. Phys. **15**, L163 (1982).
4. C.L. Kirschbaum and L. Wilets, Phys. Rev. **A21**, 834 (1980).
5. L.J. Puckett, G.O. Taylor and D.W. Martin, Phys. Rev. **178**, 271 (1969).
6. R.D. Du Bois, L.H. Toburen and M.L. Rudd, Phys. Rev. **A29**, 70 (1984).

SINGLE ELECTRON CAPTURE IN Li^{3+} - He COLLISIONS

L. Opradolce, C. Falcón and I. Casaubon

Instituto de Astronomía y Física del Espacio, C.C.: 67, Suc.: 28, 1428 Buenos Aires, Argentina

We have calculated total cross sections for the collisional reaction,



in the impact energy range of the Li^{3+} projectile $1.5 \cdot 10^{-4}$ - 43 KeV. We have adopted a molecular description of the system in which only one electron is active. This electron is supposed to move in a combined field of a bare Li^{3+} nucleus and a $\text{He}^+(1s)$ core. We have represented the electron- He^+ core interaction by a model potential¹.

The electronic eigenenergies and eigenfunctions of the $(\text{LiHe})^{3+}$ molecule were obtained by a variational method^{2,3} using a basis set of Slater-type functions. Close coupling calculations employing a seven-state diabatic molecular basis were then performed in order to compute the exchange cross sections. For energies greater than 90 eV the transitions amplitudes were computed using the impact parameter approximation. Below this energy a full quantum mechanical method was employed to calculate the scattering S-matrix. The diabatic basis considered includes, other the entry channel, two molecular states

(Σ_2, Π_1) leading at large nuclear separations to $\text{Li}^{2+}(n=2)$ and four states $(\Sigma_5, \Sigma_6, \Pi_2, \Delta_1)$ connected in the same limit with $\text{Li}^{2+}(n=3)$. For the energies here investigated, electron capture takes place, predominantly, into the $\text{Li}^{2+}(n=2)$ atomic state. At very low energies the reaction occurs via the avoided crossing at $8.5 a_0$ between the entry channel Σ_4 and the Σ_2 state. However for the energies considered in the experimental work by Wirkner-Bott et al.⁴ we have found that an interpretation of the capture mechanism in terms of the crossing is not valid due to the diabatic behaviour of the transition amplitude at that point. In the figure we show a Landau-Zener calculation including the two states involved in the crossing to illustrate this behaviour. This explains the apparent contradiction pointed out by those authors when experimental cross sections for the present system and for $\text{Li}^{3+} - \text{H}_2$ are compared. Our close coupling results are shown in the figure. A very good agreement is found with the experiment.

References

1. Opradolce L., Varillon P. and McCarroll R. 1983 J. Phys. B: At. Mol. Phys. **16** 2017.
2. Varillon P, 1976 These, Université de Bordeaux I, n° d'ordre 1279.
3. Hanssen J. 1980 These, Université de Bordeaux I, n°

d'ordre 1602.

4. Wirkner-Bott I., Seim W., Muller A., Kester P., and Salzborn E. 1981 J. Phys. B **14** 3987.
5. Susuki H., Kajikawa Y., Toshima H., Ryufuku H and Watanabe T. 1984 Phys. Rev. A **29** 525.

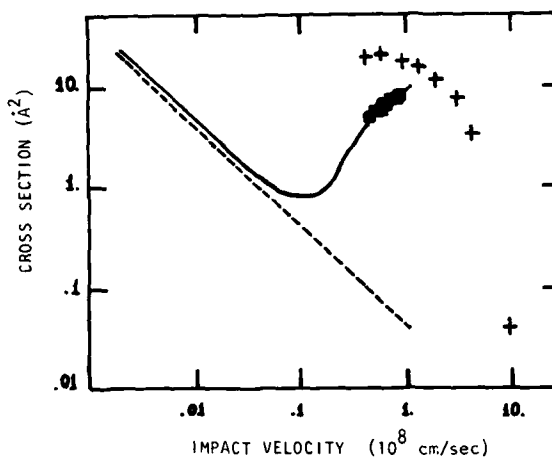


Figure 1: Total cross section for single electron capture in Li^{3+} - He collisions.

- 7-state calculation (this work)
- Landau-Zener (this work)
- + U.D.W.A. ref (5)
- Experiment ref (4)

EIKONAL CROSS SECTION IN PROTON-HELIUM ELECTRON CAPTURE PROCESSES

K. Kobayashi, N. Toshima and T. Isnihara

Institute of Applied Physics, University of Tsukuba, Sakura, Ibaraki 305, Japan

The eikonal approximation has been applied successfully to various fields of high energy collision processes. Recently it has also achieved great success in electron capture processes of bare ions colliding with a hydrogenic target. Application to multielectron targets has been made using a rather crude approximation of a single-electron model,¹ in which the electronic orbitals are described by hydrogenic wave functions with a fractional effective nuclear charge.

We calculate the electron capture cross sections for $H^+ + He \rightarrow H + He^+$ treating the passive electron (not transferred) explicitly in a distorted-wave formalism based on the eikonal approximation. The distorted wave χ_f satisfies the time-dependent Schrödinger equation

$$(H_f + V_D - i\frac{\partial}{\partial t})\chi_f = 0$$

H_f is the channel Hamiltonian corresponding to the final state and the distortion potential V_D is chosen as the common part of the interactions in the initial and the final channels. V_D consists of two terms, the internuclear interaction and the interaction between the passive electron and the proton. The transition amplitude at an impact parameter b is given by

$$A_{fi}(b) = -i \int_{-\infty}^{\infty} dt \langle \chi_f | V_f - V_D | \psi_i \rangle$$

where ψ_i is the total wave function derived from the initial state at $t = -\infty$. We apply the eikonal approximation to both χ_f and ψ_i .

In Fig. 1, we present the differential cross sections at energy of 293 keV. The agreement with the experimental data² is very good. In order to see the effects of the passive electron we have carried out a calculation omitting its interaction with the incident proton in V_D . The results are also shown in this figure. The shape of the differential cross section is affected appreciably by this interaction. On the other hand, the integrated total cross sections are not sensitive to this interaction, the neglect of which increases them by 25 %, 12 % and 5 % at incident energies of 100 keV, 250 keV and 1 MeV, respectively. Comparison with the CDW approximation³ is also made in this figure. In this calculation, a distorted wave approach similar to ours is employed but the static potential averaged over the initial electronic state is used in place of the pure Coulombic interactions in V_D .

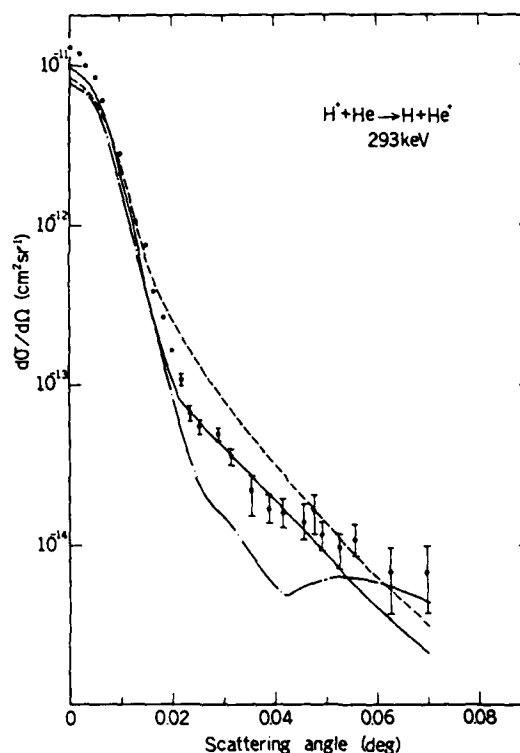


Figure 1. Differential cross sections at 293 keV. — eikonal (with full interactions), --- eikonal (without the interaction between the passive electron and the proton), - · - CDW (Ref. 3), · · · CDW (Ref. 3).

The integrated cross sections agree well with available experimental data for the incident energy higher than 250 keV. Though the eikonal approximation does not include the Thomas double scattering process, the agreement is excellent even at 10 keV.

References

1. T. R. Ho, M. Lichten, R. T. Jordan and G. W. Bardeen, *Phys. Rev. A* **21**, 1777 (1980).
2. T. R. Bratton, M. L. Lichten and G. W. Bardeen, *J. Phys. B* **12**, L107 (1979).
3. R. D. Rivarola, R. D. Tennyson, A. Fausto and G. Belkacem, *J. Phys. B* **16**, 1611 (1983).

2p - 2s VACANCY TRANSFER IN $\text{Ne}^+ + \text{Ne}$ COLLISIONS
IN THE ENERGY RANGE OF 5 - 500 keV

A. Toepfer, H.J. Lüdde, B. Jacob R.M. Dreizler
Institut für Theoretische Physik der Universität
Frankfurt am Main, Federal Republic of Germany

We suggest to solve ion(atom)-atom scattering problems involving a larger number of electrons by a two step procedure:

In a first step we determine the effective screening during the collision process by solution of quasimolecular extended Thomas-Fermi equations.¹ With the aid of effective (Hartree-Fock type) single particle potentials constructed from these solutions we then calculate the time development of the orbitals, which are initially occupied in both target and projectile.

In practice the second step is carried through by diagonalisation of h_{eff} as a function of the internuclear separation² in order to generate correlation diagrams and a suitable quasimolecular basis. The time dependent problem (including the effects of radial and rotational couplings) is then solved in terms of the basis (augmented by translational factors) generated.³ In order to extract relevant physical information from the solution a projection of the total final wavefunction, given in the form of a Slater determinant, onto wavefunctions representing final channels is required. Transition probabilities can be calculated in terms of determinants of the one particle density matrix.⁴ Inclusive probabilities can be discussed in turn.

In figure 1 we indicate the results obtained for the system $\text{Ne}^+ + \text{Ne}$ in comparison with experimental information available^{5,6,7} for a basis set of 18 molecular orbitals, from which in the separated atom limit the atomic orbitals 1s, 2s, 2p, 3s, 3p of both target and projectile can be constructed. The initial state is specified by the configuration

$$i = (1s^2 2s^2 2p^3)_p (1s^2 2s^2 2p^6)_T,$$

where the initial 2p-hole in the projectile is distributed statistically in the magnetic quantum number.

The theoretical cross sections given, correspond to the following situation: σ_{channel} : We assume that the full final configuration of the 19 electrons is identified as

$$f_1 = (1s^2 2s^1 2p^6)_p (1s^2 2s^2 2p^6)_T$$

$$f_2 = (1s^2 2s^2 2p^6)_p (1s^2 2s^1 2p^6)_T$$

and we calculate $\sigma_{\text{channel}} = \sigma(i \rightarrow f_1) + \sigma(i \rightarrow f_2)$.

σ_{inc} : We assume that instead of f_1 only the projectile subconfiguration $(2s^1 2p^6)_p$ is identified by measurement of the radiative 2p-2s transition, while the target can be in any state. Correspondingly instead of f_2 only the target subconfiguration $(2s^1 2p^6)_T$ is measured. We thus calculate the inclusive cross sections

$$\sigma_{\text{inc}} = \sigma(i \rightarrow (2s^1 2p^6)_p) + \sigma(i \rightarrow (2s^1 2p^6)_T).$$

Experimental cross sections⁵⁻⁷ are normalised to the value at 200 keV of Ref. 5, in order to circumvent the question of absolute cross sections which does not seem to be settled. Our calculated cross section σ_{inc} (reduced by a factor of 0.33 to fit the experiment at 200 keV) reproduces the energy variation of the experimental cross section very reasonably and somewhat better than σ_{channel} (reduction factor 0.41). The discrepancy in absolute value remains to be discussed, however.

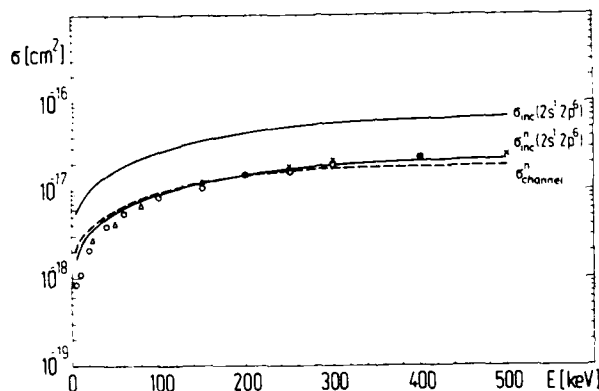


Fig. 1: Cross section for the 2p-2s vacancy transition in the $\text{Ne}^+ + \text{Ne}$ system. Experimental points from Ref. 5-7, calculated cross sections: see text.

References

1. E.K.U. Gross, R.M. Dreizler, Phys. Rev. A20(1979)1798
2. A. Toepfer, E.K.U. Gross, R.M. Dreizler, Phys. Rev. A20(1979)1808
3. A. Toepfer, B. Jacob, H.J. Lüdde, R.M. Dreizler, Phys. Lett. 93A(1982)18
4. H.J. Lüdde, R.M. Dreizler, J. Phys. B18(1985)107
5. R. Hippler, K.A. Schartner, J. Phys. B8(1975)2528
6. T. Andersen, E. Bøving, P. Hedegard, O.J. Østgaard, J. Phys. B11(1978)1449
7. E. Bloemen, H. Winter, F.J. de Heer, R. Fortner, A. Salop, J. Phys. B11(1978)4207.

COMMENT ON $H^+ + He \rightarrow H^0 + He^{i+}$

J. H. McGuire

Department of Physics, Kansas State University, Manhattan, KS 66506 USA

Since the double ionization of helium is a two electron transition, understanding of few body transition mechanisms is required to analyze double ionization data. Furthermore, since single ionization is fairly well understood at high projectile velocities, it is both natural and sensible to consider the double ionization of two electron targets such as helium.

Studies of double ionization by photons have lead to a final state rearrangement (R) or shakeoff picture for double ionization. In this picture, after the first electron is removed, the wavefunction of the second electron readjust itself and there is a finite probability that the second electron ends up in a continuum state, i.e. double ionization. In this picture at high photon energies, the cross section for double ionization, σ^{ii} , is proportional to the cross section for single ionization, σ^i , namely $\sigma^{ii} = R \sigma^i$. For photoionization of helium $R \approx 3.0$.

In double ionization by charged particles, e.g. $H^1 + He \rightarrow H^+ + He^{+2} + 2e^-$, it is possible for the projectile to interact directly with each electron, so that (in the simplest picture) the probability for double ionization P^{ii} is equal to the product of the probabilities for ionization of each electron, $P^{ii} = P_1^i P_2^i$. This is called direct double ionization (D). The rearrangement mechanism (R) is also possible, and at sufficiently high velocities R dominates over D. Furthermore since R and D lead to the same final state, interference between R and D is possible. We also note that in helium due to final state correlation the value of R for charged particles is about an order of magnitude lower than for photons.

In the original studies of $H^+ + He \rightarrow H^0 + He^{+2} + e$ by Horsdal-Pedersen and Larsen,¹ it was found that above 50 keV σ^{ii}/σ^i is independent of energy suggesting that the R mechanism is operative. Furthermore the value of R is about 3.0, i.e. the same as for photons. Horsdal-Pedersen and Larsen point out that in both photoionization and capture at high energies, one electron is rapidly removed from the system so that final state correlation is minimized. Hence it may not be surprising that R is the same for photons as for the capture channel.

In our opinion, the analysis of Horsdal-Pedersen and Larsen is quite sensible. However, a simple estimate of mechanism D indicates that D may not be negligible, as illustrated in the figure. Since in the ratio σ^{ii}/σ^i mechanism D scales as the square of the projec-

tile charge, Z_p^2 , while R is independent of Z_p , we suggest that the ratio σ^{ii}/σ^i may have a different energy dependence for incident alpha particles than for incident H^+ . Furthermore, at the higher energies shown in the figure, interference between R and D mechanisms may occur for alpha particle impact. Studies of differential cross sections in momentum transfer or ejected electron energy may also be useful in sorting out these double transition mechanisms.

I gratefully acknowledge discussion with E. Salzborn and A. Muller, who have recent data for $H^+ + He \rightarrow H^0 + He^{+1}$. This work was supported by the Division of Chemical Sciences, U.S. Department of Energy.

Reference

1. F. Horsdal-Pedersen and L. Larsen, J. Phys. B. **12**, 4085 (1979).

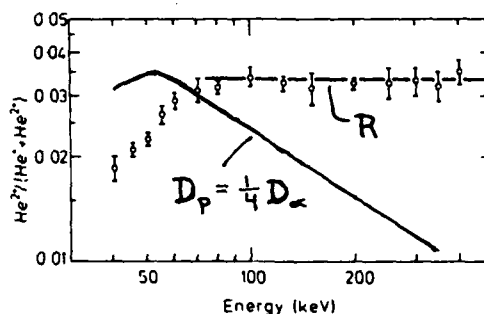
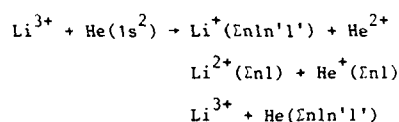
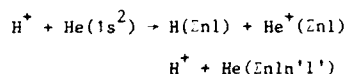


Figure 1 Ratio of double to single ionization versus energy for $H^+ + He \rightarrow H^0 + He^{i+}$. R represents final state rearrangement and D direct double ionization.

CHARGE TRANSFER IN TWO ELECTRON SYSTEMS
IN THE TIME DEPENDENT HARTREE FOCK PICTURE

W. Stich, H.J. Lüdde and R.M. Dreizler
Institut für Theoretische Physik der Universität
Frankfurt am Main, Federal Republic of Germany

Following previous work¹ on the collision system $\text{He}^{2+} + \text{He}$ we have investigated the systems $\text{H}^+ + \text{He}$ and $\text{Li}^{3+} + \text{He}$ within the framework of the TDHF picture. In particular we calculate global charge transfer cross sections for the channels



in the energy range of 5-40 keV/amu. The TDHF equations for the time development of the orbitals are solved by basis expansion techniques (144 state Hylleraas basis) with the aid of predictor-corrector methods. The effective potential at each time step is obtained by solving Poissons's equation, also in terms of basis expansion. Global cross sections are extracted with the half space projection technique outlined in Ref. 2.

In Table 1 we indicate the cross section for one electron capture in $\text{H}^+ + \text{He}(1s^2)$ in comparison with the experimental results of de Heer et al³ and Stier and Barnett⁴.

Energy[keV]	Ref. 3	Ref. 4	Theory
10	1.15	0.95	0.95
20	2.21	1.8	1.8
30	1.75	1.7	1.52
40	1.35	1.4	1.4

Table 1: Total cross section for one electron capture in $\text{H}^+ + \text{He}(1s^2)$ in $10^{-16} [\text{cm}^2]$

In Fig. 1 we show the cross section for one electron capture in $\text{Li}^{3+} + \text{He}(1s^2)$ in comparison with the results of Wirkner-Bott et.al.⁵ The present results for the two electron capture channel, for which no experimental information is available, are also indicated.

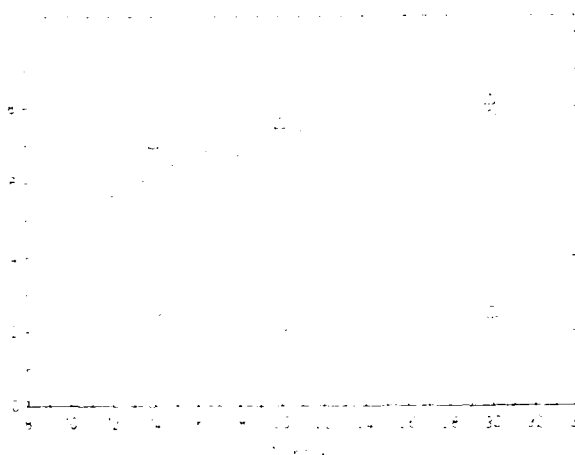


Fig. 1: Total cross sections for one and two electron capture in $\text{Li}^{3+} + \text{He}(1s^2)$ one electron capture: \diamond experimental results of Ref. 5, Δ present theoretical results
two eletron capture: \square present theoretical results.

In both systems we find very satisfactory agreement of theory and experiment at the level of the global quantities. The resolution with respect to individual excitation - and charge transfer channels remains to be performed.

References

1. W. Stich, H.J. Lüdde and R.M. Dreizler, Phys. Lett. 99A(1983), 5
2. H.J. Lüdde and R.M. Dreizler, J. Phys. B16(1983)3973
3. F.J. de Heer, J. Schutten and H. Moustafa, Physica 32(1966),1766
4. P.M. Stier and C.F. Barnett, Phys. Rev. 103(1956)896
5. I. Wirkner-Bott, W. Seim, A. Müller, P. Kester and E. Salzborn, J. Phys. B14(1981),3987.

A UNIFIED AOMO EXPANSION TREATMENT OF $p-H$, $C^{6+} + H$ AND $p-He$ COLLISIONS

M. Kimura,* and C. D. Lin*

*Joint Institute for Laboratory Astrophysics, University of Colorado and National Bureau of Standards, Boulder, Colorado 80309

†Department of Physics, Kansas State University, Manhattan, Kansas 66506

Theoretical models for the investigation of inelastic ion atom collisions have been based mostly upon the close-coupling expansion method in the impact parameter approximation. The basis functions used in the expansion are either the molecular orbitals (MO) of the collision system or the traveling atomic orbitals (AO) of the two collision centers. The traditional MO expansion, known as the perturbed stationary state (PSS) approximation, has the problem that the expansion is not Galilean invariant. Various forms of electron translational factors (ETF's) have been proposed to resolve this difficulty. From the AO expansion viewpoint, a modified AO expansion (AO+) and a triple-center AO expansion where united-atom's atomic orbitals are included in the basis set have been investigated in recent years.

Recently a different approach has been suggested.^{1,2} By recognizing that it is desirable to adopt an expansion using MO's in some inner region to account for the relaxation of the electronic orbitals and using traveling AO's in the outer region to account for the translational motion of the electron, a unified AOMO expansion was proposed. In this method, the time-dependent wave function is expanded in terms of a set of traveling AO's in the outer region which is integrated to a certain internuclear separation R_0 . At this point, the wave function is matched to an expansion using MO's without ETF's. The resulting coefficients then serve as initial conditions for the time integration (in the MO basis) in the inner region to another internuclear separation R_1 (we usually choose $R_0 = R_1$) where the wave function is matched to an expansion using traveling AO's. Integration from R_1 in the traveling AO basis to a large internuclear separation then allows the extraction of scattering amplitudes.

This model has been applied to study charge transfer in $p-He^+$ and in $He^{++} + H$ collisions. In this contribution, we report the application of this general method to three collision systems:

(1) Excitation and charge transfer to 2s and 2p states in $p-H$ collisions from 1-15 keV. This system has been studied in recent years using a large basis set in many elaborate close-coupling calculations. Our results for the partial cross sections to 2s and 2p are in general in good

agreement with these calculations. The comparison will be presented at the meeting.

(2) Partial electron capture cross sections in $C^{6+} + H$ collisions. This collision system has been studied recently in a 33-state MO expansion³ and in a 35-state AO expansion.⁴ The capture is predominantly into the $n = 4$ states for collision energies in the 0.1-1.0 keV/amu region. Although the total cross sections are in reasonably good agreement in the two calculations, the MO model predicts a relatively larger contribution to the $n = 5$ states. In our present calculation, we used 25 MO's in the inner region and 26 AO's ($n = 4$ and 5 of C and 1s of H) in the outer region, the results for the $n = 5$ states are in good agreement with the conclusion from the AO expansion. For the total cross sections, the present results also agree with the most recent experimental data from Phaneuf.⁵

(3) Excitation and charge transfer in $p-He$ collisions. This system has been the favorite of many experimental studies. *Ab initio* calculations so far are unsatisfactory, particularly for excitation or capture to the excited 2s and 2p states in the energy region from 1 keV to 25 keV. We have employed the unified AOMO matching procedure to this system. To get decent results, the molecular correlation diagram for the $p-He$ has to be reproduced accurately. We have investigated the charge transfer probabilities, the partial cross sections, the alignment parameters for excitation and charge transfer to 2s and 2p states. The results will be presented at the meeting.

This work is supported in part by the U. S. Department of Energy, Division of Chemical Sciences.

References

1. M. Kimura and C. D. Lin, Phys. Rev. A **35**, 590 (1987).
2. T. C. Winter and N. F. Lane, Phys. Rev. A (to be published).
3. T. A. Green, E. T. Shipsey and J. T. Braken, Phys. Rev. A **22**, 1304 (1980).
4. W. Fritsch and C. D. Lin, Phys. Rev. A **29**, 3039 (1984).
5. R. A. Phaneuf (private communication, 1984).

ATOMIC-ORBITAL EXPANSION REPRESENTATION OF ELECTRON TRANSFER IN TWO-ELECTRON SYSTEMS

Wolfgang Fritsch* and Chii-Dong Lin*

* Bereich Kern- und Strahlenphysik, Hahn-Meitner-Institut Berlin, D-1000 Berlin 39, West Germany
 * Department of Physics, Kansas State University, Manhattan, Kansas 66506, U.S.A.

In theoretical investigations of electron transfer in (quasi-)one-electron ion-atom collision systems, the semiclassical close-coupling method with atomic orbitals (AO) basis sets has been proven as very effective and reliable.¹ This method is particularly suited for application to distant collisions and for the extraction of partial cross sections for transfer into (nlm) projectile subshells,² and calculated results compare favourably with experimental data³ (typically over two orders of magnitude in collision energy) wherever available. With suitable modifications by united-atom orbitals (AO+ method), partial cross sections have been calculated in close collisions, too, and have been found to agree well with experiment.⁴ Another not unimportant merit of the AO(+) expansion method is its technical simplicity which allows for an easy adaption of multi-channel problems.

In this work, we investigate the application of the AO(+) expansion method to two-electron systems. We start from a set of travelling two-electron orbitals

$$\psi(r_1, r_2) = P^{S, \pm} \phi_i^{C_1}(r_1) \phi_j^{C_2}(r_2) \exp(\pm i v(r_1 \pm r_2)/2) \quad (1)$$

where r_1, r_2 are the coordinates of the two electrons, index C_i labels the atomic center with which ϕ_i moves, v is the collision velocity, the \pm signs depend on the choice of C_1, C_2 , and the operator $P^{S, \pm}$ (anti-)symmetrizes the spatial wavefunction according to spin-singlet (triplet) conditions. The Hamiltonian H ,

$$H = H_0(1) + H_0(2) + 1/r_{12} \quad (2)$$

is the sum of $H_0(i)$, the Hamiltonian of electron i with respect to the two nuclei (or atomic cores), and the electron-electron interaction $1/r_{12}$. With the electron wavefunction expanded in appropriately chosen AO(+) basis sets, with Hamiltonian (2) and with a curved-line internuclear trajectory, the time-dependent Schrödinger equation is solved within the basis space without further approximations. In this respect we differ from recent work at higher energies⁵ where the translational factor (ETF) term in (1) is approximated in the evaluation of the $1/r_{12}$ matrix. From the final occupation amplitudes of orbitals (1), partial and total cross sections are derived as usual.

In the course of this investigation, most of the numerical effort and the computing time is devoted to the evaluation of matrix elements of Hamiltonian (2). Among those the most difficult is the matrix element of $1/r_{12}$ between orbitals positioned at different centers since there the ETF term precludes the direct use of methods

from molecular structure studies. We have, however, chosen to generalize molecular-structure expressions derived in ref. 6, which are based on the Neumann expansion of $1/r_{12}$. The final expression is essentially a sum of folding integrals over functions, each of them accessible by methods known from one-electron problems.

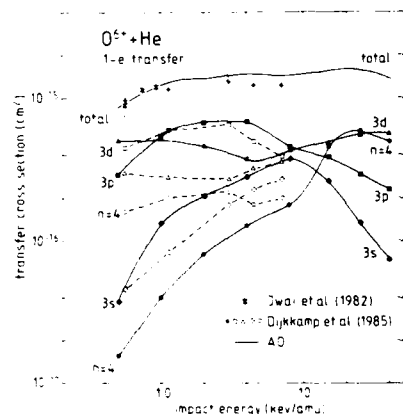


FIGURE 1:
One-electron
transfer in
 $O^{6+} + He$ collisions,
see text

Fig. 1 shows results of calculated one-electron transfer cross sections for $O^{6+} + He$ collisions. Total transfer agrees well with experiments^{7, 8}. The calculated partial transfer for $n=3$ O^{5+} orbitals is fairly close to the data⁹ with deviations of the same order as encountered for one-electron systems³. The measured population of $n=4$ orbitals at low energies is much larger than in the calculations and does not seem to be compatible with the molecular energy diagram for this system. A one-electron potential representation for He leads to results very different from those presented here. We expect that more results will be available at the time of the conference.

This work is supported in part by IIS Department of Energy, and by NATO Research Grant 120/84.

References

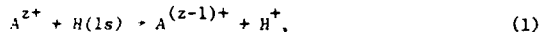
1. W. Fritsch and C.D. Lin, in *Electronic and Atomic Collisions*, eds. J. Eichler et al. (North-Holland, Amsterdam, 1984), p. 331.
2. see, e.g., W. Fritsch and C.D. Lin, *J. Phys. B* **17**, 3271 (1984); *Phys. Rev. A* **29**, 3039 (1984); W. Fritsch, *Phys. Rev. A* **30**, 3324 (1984).
3. D. Ciric, D. Nijkamp, E. Vlieg and F.J. de Heer, *J. Phys. B* **18**, L17 (1985).
4. W. Fritsch and C.D. Lin, *Phys. Rev. A* **27**, 3361 (1983).
5. R.H. Bransden, A.M. Ermolaev and R. Shingal, *J. Phys. B* **17**, 4515 (1984).
6. F.L. Mehler and K. Rüdenberg, *J. Chem Phys.* **50**, 2575 (1969).
7. T. Iwai, Y. Kaneko, M. Kimura, N. Kobayashi, S. Othani, K. Okuno, S. Tadaki, H. Tawara and S. Tsurubuchi, *Phys. Rev. A* **26**, 105 (1982).
8. D. Nijkamp et al., *J. Phys. B* **18** in print.

CONTINUOUS ENERGY STATE MODEL FOR CHARGE TRANSFER IN COLLISIONS OF FULLY STRIPPED IONS WITH HYDROGEN ATOMS

Fumihiro Koike

School of Medicine, Kitasato University, Sagami-hara, Kanagawa 228 Japan

Recently, a continuous energy state model was proposed¹ for the charge transfer process:



where A and z represents an atom and its atomic number, respectively. In the present paper, the formulation is improved and the numerical calculation has been extended to include the higher- z ions.

The probability amplitude for finding the system in the initial state, a_0 , is given by the overlap of the initial state wavefunction ψ_0 with the total wavefunction Ψ , i.e., $a_0 = \langle \psi_0 | \Psi \rangle$. If Ψ is expanded in terms of the final state wavefunctions, ψ_q , as $\Psi = \sum_q a'_q \psi_q$ and also if Ψ satisfies the semiclassical time-dependent Schrodinger equation, i.e., $H\Psi = i(\partial/\partial t)\Psi$, we can derive the following coupled equation by differentiating the present overlap integral with respect to the time t . We have

$$\dot{a}_0 = -i \sum_q \langle \psi_q | H - i\partial/\partial t | \psi_0 \rangle^* a'_q. \quad (2)$$

It can be shown² that we can solve equation (2) with respect to a_0 to the lowest order without any knowledge about a'_q if we employ the continuous energy state model for the final states. We obtain

$$a_0(t) = \exp[-i \int_{-\infty}^t E_* dt'], \quad (3)$$

where E_* is the resonance energy that may be a complex number. The final state component is given by $\Psi = a_0 \psi_0$, and this may be expanded in terms of ψ_q as $\Psi = a_0 \psi_0 = \sum_q a'_q \psi_q$. Then we have the following coupled equations for a'_q , which are solved numerically. That is

$$\dot{a}'_q = -i \langle \psi_q | H - i\partial/\partial t | \psi_0 \rangle^* a_0 - i \sum_{q'} \langle \psi_q | H - i\partial/\partial t | \psi_{q'} \rangle^* a'_{q'}. \quad (4)$$

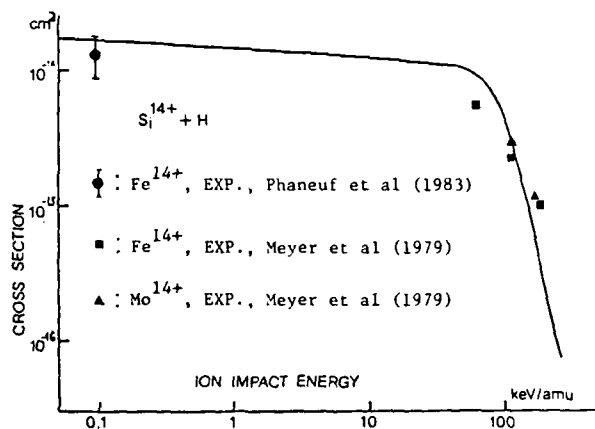


Figure 1a

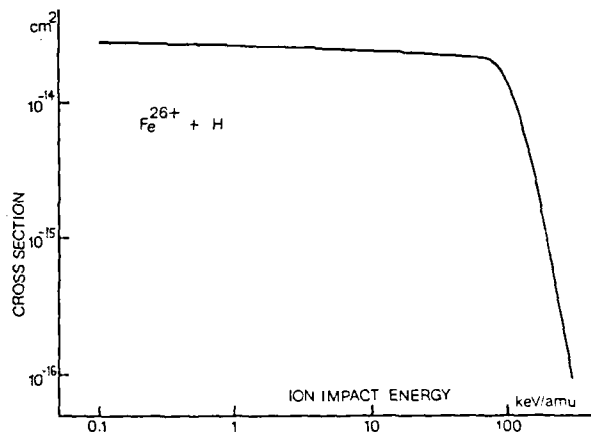


Figure 1b

In order to facilitate the large scale numerical calculations, the use of a super computer, HITAC S810/20, has been made. In figure 1a is shown the total electron capture cross section for $Si^{14+} + H$ system with the available experimental data for partially stripped ions. The agreement between the theory and experiment at $z=14$ suggests the validity of the present method for higher- z ions, because the present method is based on the high- z approximation. The result for $Fe^{26+} + H$ system is illustrated in figure 1b as an example of high- z system. In figure 2, the electron capture cross sections into the states with the specified principal quantum number are given for $Si^{14+} + H$ system with other theoretical results.

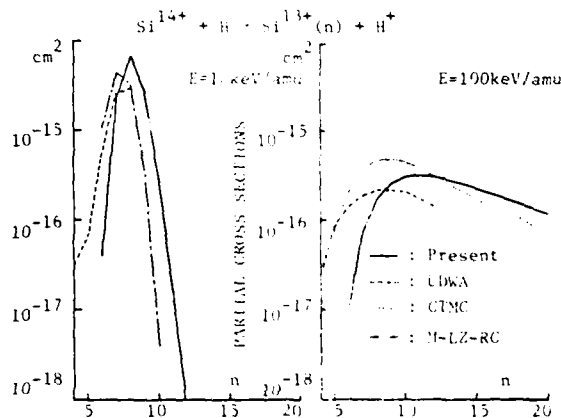


Figure 2

Reference

1. F.Koike, XIII ICPEAC Book of Abstracts, 571(1983)
2. F.Koike, XIII ICPEAC Book of Abstracts, 405(1983)

ANGULAR DISTRIBUTIONS OF IONS AFTER FAST ION-ATOM COLLISIONS

A.K. Kaminsky, M.I. Popova

Institute of Nuclear Physics, Moscow State University, Moscow 119899, USSR

We report the results of calculations of the cross sections $\frac{d\sigma}{d\Omega}$ differential in the scattering angle ϑ for elastic and inelastic collisions between two fast atoms or ions each having its own electrons. The $\frac{d\sigma}{d\Omega}$ calculation method is based on the use of the first Born approximation and of the sum rule. The validity of such an approach to the calculations of the doubly differential cross sections of the ionization in fast ion-atom collisions was demonstrated earlier^{1,2}.

Figs. 1 and 2 present some results of calculating the values of $\frac{d\sigma}{d\Omega}$ for the ionization and scattering of 300 keV hydrogen atoms in their collisions with H and C atoms. We used the analytical expressions for the elastic and inelastic form factors given in³. Similar calculations for the collisions of the simplest particles (ions and atoms of hydrogen and helium) were carried out in⁴.

The features of the angular distributions $\frac{d\sigma}{d\Omega}$ for various processes may be outlined as follows.

At small scattering angles ϑ , the ionization cross sections $\frac{d\sigma_i}{d\Omega}$ exceed both the elastic scattering cross sections $\frac{d\sigma_e}{d\Omega}$ and the cross sections $\frac{d\sigma_m}{d\Omega}$ of scattering by the screened Coulomb potential. The difference between $\frac{d\sigma_i}{d\Omega}$ and $\frac{d\sigma_m}{d\Omega}$ increases with atomic number of the target atom. Among the angular distributions, the values of $\frac{d\sigma_i}{d\Omega}$ for collision with nuclei are nearest to the Rutherford cross sections.

At the collision velocities V exceeding the atomic electron velocities in ionized sub-shell the values of $\frac{d\sigma_i}{d\Omega}$ approach the Rutherford cross sections in some range of angles ϑ . This range of ϑ increases with V . The rapid decrease of $\frac{d\sigma_i}{d\Omega}$ at large angles ϑ , as compared with the Rutherford cross sections, indicate that these approximations can not be used in this case.

Such calculations of the angular distributions give information on their behaviour at small angles ϑ and are of interest in particular, with a view of making the multiple scattering theory more accurate. The proposed method make it possible to calculate the angular distributions of fast ions to within accuracy sufficient for quite a number of applications and, at the same time, to avoid cumbersome cal-

culations.

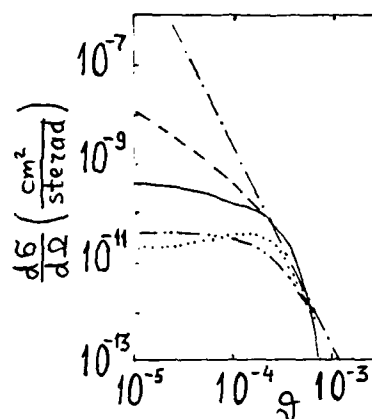


Figure 1. Values of $\frac{d\sigma}{d\Omega}$ for fast p or H after the collisions of 300 keV H with hydrogen target. Solid and dash lines - $\frac{d\sigma_i}{d\Omega}$ for ionization of H on H and p respectively. Dotted line - $\frac{d\sigma_e}{d\Omega}$ for elastic scattering of H on H. Double dot-dash - $\frac{d\sigma_m}{d\Omega}$ for scattering on screened Coulomb potential. Dash-dot - scattering of p on p.

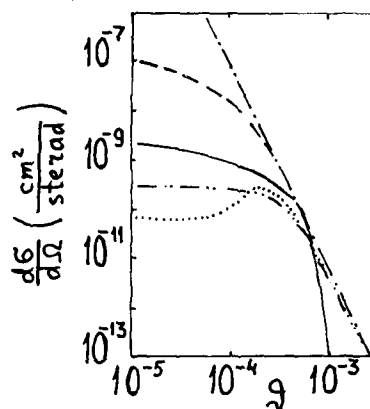


Figure 2. The same as in Fig. 1 except for carbon target.

References

1. A.K. Kaminsky et al. Nucl. Instrum. Meth. **180**, 231 (1981).
2. A.K. Kaminsky, M.I. Popova, J. Phys. B **15**, 403 (1982).
3. A.K. Kaminsky et al. Proc. Radiotechnical Institute Acad. Sci. USSR, **16**, 330 (1973).
4. Y.T. Lee, J.C.Y. Chen, Phys. Rev. A **15**, 526 (1979).

DOUBLE AND SINGLE ELECTRON CAPTURE IN 1-2 MeV/u O^{8+} -He COLLISIONS

R. Hippler*, S. Datz, P. D. Miller, and P. L. Pepmiller

Oak Ridge National Laboratory,* Oak Ridge, TN 37831 USA

We report results of an experimental study of charge changing collisions of bare nuclei with He atoms; with particular emphasis on the double-capture process. In Fig. 1, we present the results for 16- to 32-MeV O^{8+} -He collisions. Our measured single-capture cross sections agree with measurements of MacDonald and Martin¹ within the quoted accuracy ($\pm 10\%$ for the present measurements). Our measured double capture cross sections are typically more than two orders of magnitude smaller than single-capture cross sections (Fig. 1). At 1 MeV/u, the double-capture to single-capture ratio is $\sim 6 \times 10^{-3}$, it drops to 4×10^{-3} at 2 MeV/u. These numbers are consistent with a ratio of $\sim 10^{-2}$ estimated by Tawara et al.² for 15-MeV F^{9+} -He collisions. However, our measurements for double-capture cross sections are a factor of ~ 10 smaller than those reported by MacDonald and Martin¹ for the same system. The discrepancy may be due to the small ratio of double- to single-capture cross sections which makes it particularly difficult to separate true double capture from two-sequential single-capture events. This separation was achieved, in the present investigation, by performing measurements at different gas pressures and by a careful analysis of this pressure dependence.

The present double- to single-capture cross section ratios are also considerably smaller than first-order theoretical estimates. Using, for example, a classical Bohr-Lindhard model, the probability P_C for electron capture may be expressed as³

$$P_C = (v/a) (R_C/v_i)^2$$

with v and a the target electron velocity and radius, respectively, and v the projectile velocity. The distance R_C below which capture occurs is given as

$$R_C = 2 q a_0 (v_0/v_i)^2$$

with a_0 and v_0 Bohr radius and velocity, respectively, and q the projectile charge. In an independent electron model, the double- to single-capture cross section ratio is $\sim P_C/2$, amounting to 0.22 and 0.08 at 1 and 2 MeV/u, respectively. These numbers are larger than the experimental values by factors of about 36 and 20, respectively.

At the velocities under consideration here, a large fraction of electrons is expected to be captured into excited projectile states. For two-electron capture, these states can autoionize, and hence, escape detection as double-capture events.⁴ To be detected as a double-

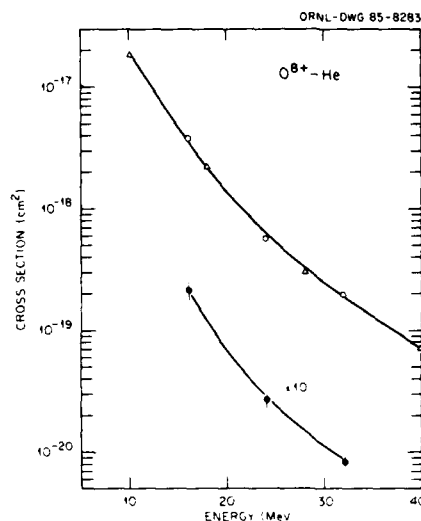


FIGURE 1. Present data for single (○) and double (●) electron capture cross section for O^{8+} -He collisions. △, data of Ref. 1 for single capture.

capture event either one or both of the two electrons must be captured into a 1s state (about 0 and 5% probability at 1 and 2 MeV/u) or the doubly excited state must be radiatively stabilized (estimated fluorescence yield $\sim 10\%$). With these considerations, the present data are qualitatively understandable. Data which will be presented on other bare nucleus-He atom collisions show similar tendencies.

References

- * Permanent address: Fakultät für Physik, Universität Bielefeld, Bielefeld, F.R. Germany.
- + Research sponsored by the U.S. Department of Energy, Division of Basic Energy Sciences under Contract No. DE-AC05OR21400 with Martin Marietta Energy Systems, Inc.
- 1. J.R. MacDonald, F.W. Martin, Phys. Rev. **A4**, 1965 (1971).
- 2. H. Tawara, P. Richard, K.A. Jamison, T.J. Gray, J. Newcomb, C. Schmiedekamp, Phys. Rev. **A19**, 1960 (1979).
- 3. H. Knudsen, H.K. Haugen, P. Hvelplund, Phys. Rev. **A23**, 597 (1981).
- 4. J. Newcomb, T.R. Dillingham, J. Hall, S.L. Varghese, P.L. Pepmiller, P. Richard, Phys. Rev. **A30**, 106 (1984).

ATOMIC CHARGE EXCHANGES IN CLOSE COLLISIONS BETWEEN Ar^{+q} IONS
AND TARGETS IN THE MeV ENERGY REGION

I. Ben Itzhak*, D.W. Mingay** and B. Rosner*

*Department of Physics, Technion, Haifa 32000, Israel

**Nuclear Development Corporation, Pretoria, South Africa

Charge state distributions of argon ions after small impact-parameter collisions with nitrogen, neon, argon, krypton and xenon gases were studied. Argon beams in the 1.5-3.0 MeV energy range with charges 3^+ and 4^+ were obtained from 5.75 MeV van de Graaff accelerator at Pelindaba and were scattered under conditions allowing only single close collisions by nitrogen, neon, argon, krypton and xenon gas targets to angles between 0.5° and 4.0° . The differentially pumped target cell in the form of a hollow cylinder 10 mm in diameter, with 0.5 mm diameter entrance and 1 mm diameter exit apertures, was mounted in the centre of a π off-set 1.1 m diameter scattering chamber.

The incoming beam was defined by a variable collimator prior to its entrance into the chamber. A given charge state was then selected by appropriately setting an electrostatic deflector, resulting in the beam being directed along the radius of the chamber into the gas cell. The selected target gas was continually fed into the gas cell through a regulator and needle valve to maintain the desired pressure, and thereby the target

thickness. The scattering angle was defined by a pair of adjustable slits. Particles scattered through the slit system continued into a second electrostatic analyser where the different emergent charge states were separated and detected by a position-sensitive detector. The defining slits, charge analyser and detector were mounted on a radial support arm for which the angular position could be externally controlled to an accuracy of $\pm 0.03^\circ$.

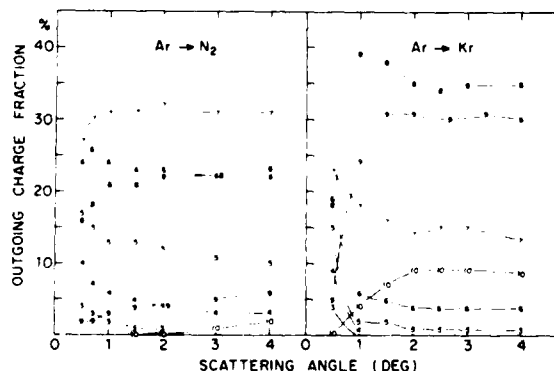


FIGURE 1

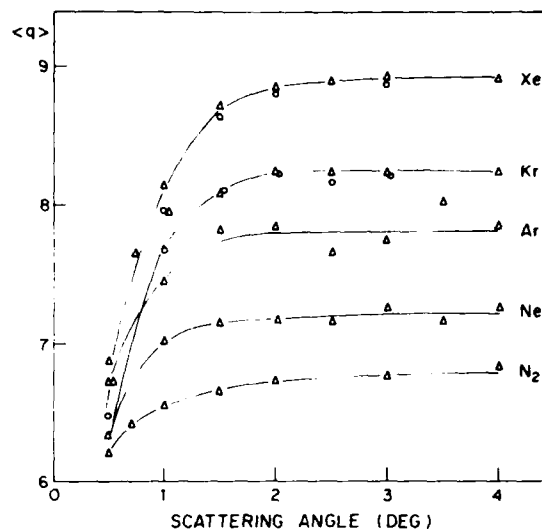


FIGURE 2

Figure 1 presents the angular distribution of the individual outgoing charge states for scattering of 3 MeV Ar^{+4} ions from light N_2 and heavy Kr gas targets under single collision conditions. It can be clearly seen that the distributions become almost independent of the scattering angle for small impact parameter collisions of the order of the K-shell radius of the united atom, where the electron clouds of the colliding partners almost overlap.⁽¹⁾

The angular distributions of the average outgoing charge $\langle q \rangle$ for all five gas targets are shown in Figure 2. The average charges depend on the target gas and have higher values for the heavier targets. They are even higher from the corresponding values obtained for the passage of argon ions in solid targets at the same bombarding energy.

Reference

1. Charge-exchange processes in close atomic collisions, I. Meron and B. Rosner, Phys. Rev. A 30, (1984), 132.

DOUBLE K- TO K- SHELL VACANCY TRANSFER IN SLOW COLLISIONS
OF BARE IONS AND ATOMSE. Justiniano, M. Schulz, R. Schuch, A. Oppenländer, H. Schmidt-Böcking*, W. Schadt*, and P. Mokler⁺Physikalisches Institut, Universität Heidelberg, 6900 Heidelberg, FRG
Institut für Kernphysik, Universität Frankfurt, 6000 Frankfurt, FRG
⁺Gesellschaft für Schwerionenforschung, 6100 Darmstadt, FRG

We have recently reported the observation of oscillating Ar K-vacancy production probabilities as a function of impact parameter in slow collisions of hydrogen-like S ions with Ar¹. These oscillations could be explained as interferences arising from the coherent sum of the 1s σ - 2p σ vacancy transfer amplitude on the incoming and outgoing parts of the collision trajectory. Comparison of those results with theoretical calculations revealed discrepancies in the predicted height of the interference extrema. These discrepancies could arise from, e.g. the contribution of charge transfer to states other than 1s σ and 2p σ or from a general limitation of the theories, namely their treating of this problem as that of an active K-electron in the presence of an average field. Experiments with bare ions are especially well suited for testing this second possibility since here two electrons can be transferred and possibly in a correlated fashion.

In the present work we report measurements of impact parameter dependent single and double K-vacancy transfer probabilities for 0.5 MeV/amu S¹⁶⁺ on Ar and 4.6 MeV/amu Kr³⁶⁺ on Mo collisions. These experiments were carried out at the MP-Linac facility at MPI-Kernphysik in Heidelberg and at the UNILAC at GSI in Darmstadt by poststripping the desired beams at high energy followed by deceleration with the single resonators to the chosen low energies. In a multi-parameter experiment K x-rays and scattered projectiles were observed in coincidence which allowed the determination of impact parameter dependent probabilities for double K-vacancy transfer, single K-vacancy transfer, and no K-vacancy transfer from the projectile to the target atom.

The results of this work will be discussed in comparison to different theoretical calculations.

This work supported by EMFT.

1. R. Schuch, H. Ingwersen, E. Justiniano, H. Schmidt-Böcking, M. Schulz and F. Ziegler, J. Phys. B: At. Mol. Phys. **17**, 2319 (1984).

ELECTRON CAPTURE CROSS SECTIONS IN FAST ION-ATOM COLLISIONS

H.-D. Betz and R. Jöppel

Sektion Physik, Universität München, 8046 Garching, W.-Germany

Electron capture by fast ions in collisions with target atoms has received appreciable attention for some 5 decades. Nevertheless, important progress could be achieved in recent years: the Eikonal (EA^-) treatment¹ allows calculation of cross sections $\sigma_c(n, \ell)$ which are much more accurate than the first Born approximation (OBK, B1) and a multiple scattering theory² (CDW) has been developed to obtain cross sections $\sigma_c(n, \ell)$ in a higher-order approximation. In the past, there have been only a few attempts to investigate experimentally the final-state (n, ℓ) population following high-velocity capture³, although theoretical predictions may substantially differ. We present such an investigation which is sensitive to the total capture cross section and to the distribution of ℓ -states.

The Munich Tandem van-de-Graaff accelerator has been used to pass 125-MeV sulphur ions with initial charge 16^+ (fully stripped) through dilute target gases of He, N_2 and Ne. An x-ray

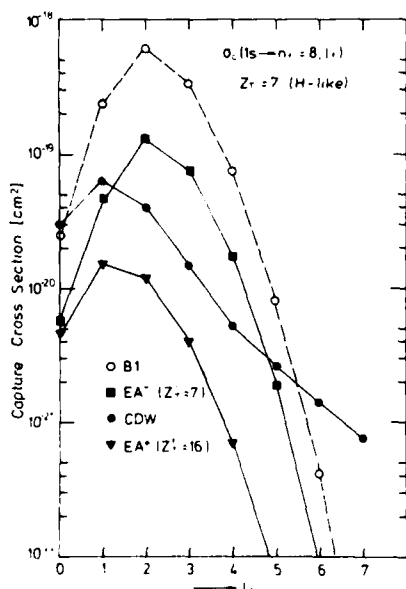


Fig.1: Calculated capture cross sections for 125-MeV sulphur (16^+) in nitrogen, as a function of final state ℓ for fixed $n=8$.

	$\sigma_c [10^{-18} \text{ cm}^2]$			$I(\text{Ly-}\alpha)/I(\text{Ly-}\beta)$		
	He	N_2	Ne	He	N_2	Ne
OBK	0.2	55	32	8.0	4.8	4.0
EA^-	.06	8.4(9.0)	4.2(5.4)	8.3	4.5(4.7)	3.3(3.9)
EA^+	.02	3.4		4.2	4.0	
CDW	.04	10.6	8.8	3.7	3.4	3.7
EXP	.06	11 ± 1.5	7.1 ± 1	3.6	3.7	4.1

Tab.1. Capture cross sections and intensity ratios of Ly- α and Ly- β radiation for 125-MeV sulphur (16^+) ions colliding with various target species. Values in parenthesis take into account capture from the L-shell of target atoms.

detector recorded K x-rays following capture into excited states. This data was then compared with x-ray intensities which follow from initial excited-state populations given by various theories for electron capture, whereby cascading has been taken into account.

Fig.1 displays the greatly differing ℓ -distributions obtained from the various models. Tab.1 lists both total cross sections and the ratio of Ly- α and Ly- β x-ray intensities obtained from experiment and theory; it turns out that this ratio is sensitive to the ℓ -distribution of the initial population. Inspection of Tab.1 reveals that the CDW approximation gives the best reproduction of the experimental data. In particular, it can be stated that both OBK and EA^- do not lead to ℓ -distributions which are realistic for all targets. We stress, though, that all theoretical models are not strictly applicable for non-hydrogenic targets.

This work was supported by the Bundesministerium für Forschung und Technologie.

References

1. J. Eichler, Phys. Rev. A23, 498 (1981).
2. L.J. Dubé, J. Phys. B17, 641 (1984).
3. R. Bruch, L.J. Dubé, E. Träbert, P.H. Heckmann, B. Raith, and K. Brand, J. Phys. B15, L 857 (1982).

THE ENERGY DEPENDENCE OF ELECTRON-CAPTURE AND-LOSS CROSS SECTIONS IN MeV/amu, HIGHLY-STRIPPED, HEAVY ION COLLISIONS

W.G. Graham^{††}, J.A. Tanis^{*}, E.M. Bernstein[‡], M. Clark^{*}, R.H. McFarland[§], T.J. Morgan^{||}, M.P. Stockli^{**}, K.H. Berkner[†], R.V. Pyle[†], A.S. Schlachter[†], J.W. Stearns[†], B.M. Johnson[†], K.W. Jones[†] and M. Meron[†]

^{††}, Physics Department, University of Ulster, Coleraine, N. Ireland; ^{*}, Physics Department, Western Michigan University, Kalamazoo, U.S.A.; [‡], Physics Department, University of Missouri, Rolla, U.S.A.; [§], Physics Department, Wesleyan University, Middletown, U.S.A.; ^{**}, Physics Department, Kansas State University, Manhattan, U.S.A.; [†], Lawrence Berkeley Laboratory, Berkeley, U.S.A.; ^{||}, Brookhaven National Laboratory, Upton, U.S.A.

Single-electron-capture and-loss cross sections for collisions of a number of ion species (S^{q+} , Ar^{q+} , V^{q+} and Ca^{q+} ($q=13$ to 23)), incident on various gas targets (H_2 , He, Ne and Ar) have been measured over a wide energy range (0.5 MeV/amu to 9 MeV/amu).

The energy dependence of the electron-capture cross sections will be compared with the general predictions of various theoretical approaches and an empirical scaling rule. For the present collisions $\frac{v}{v_0}$ varies from 4.4 to 19, where v is the projectile velocity and v_0 is the Bohr velocity. This is generally considered to be in the intermediate to high velocity regime for electron capture.

In the electron-loss collisions $\frac{v}{v_e}$ varies from 0.6 to 2.0, where v_e is the velocity of the electron most likely to be lost by the projectile. Classical theory¹ predicts the energy dependence of the electron-loss cross sections should exhibit a broad maximum in this region.

Over a wide energy range, for example that available in the present measurements for S^{13+} in He (0.45 to 6 MeV/amu), the electron-capture cross section energy dependence is found to steepen with increasing energy. However, over a more limited range of energies it was found that the electron-capture cross sections for a particular ion-target pair could be fitted to a simple power law $\sigma = \sigma_0 E^\alpha$, where E is the projectile energy in MeV/amu. The value of the exponential, α , was found to be approximately the same for different charge states of the same species in the same target gas. For example, for $Ca^{16+,17+18+}$ in He, the energy dependence was $E^{-4.2 \pm 0.2}$, for energies between 3.5 and 9 MeV/amu.

From figure 1 it appears that the energy dependence over the same energy range is dependant on the target gas, with collisions in heavier gas targets having a less pronounced energy dependence. The present data is consistent with the empirical scaling rule for electron capture² which can be applied to various gas targets.

In general terms the measurements are consistent with theoretical work on electron capture which, based on atomic hydrogen targets, suggests that the energy dependence at the present energies should be increasing towards the high energy asymptotic limit of either $E^{-3.5}$ or E^{-6} .

The electron-loss cross sections for all the present measurements exhibit a broad maximum. The velocity at which the peak value is found is between v_e and $2v_e$, which is consistent with classical theory¹. The position of the peak value appears to be dependent on the target gas, being around v_e for He, $1.5 v_e$ for Ne and $1.75 v_e$ for Ar.

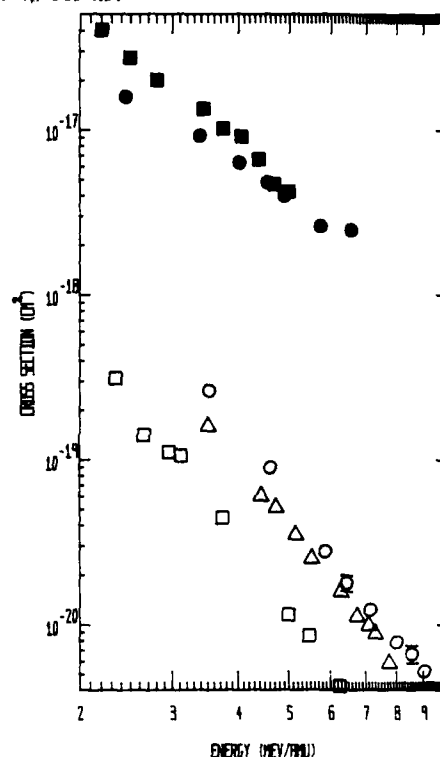


Fig. 1 The energy dependence of the present electron-capture cross sections for Li-like ions, S^{13+} in He, S^{13+} in Ar, Ar^{13+} in He, Ca^{17+} in He, V^{17+} in He.

This work was supported in part by the U.S. D.O.E., Division of Chemical Sciences and Office of Fusion Energy, by the S.E.R.C. U.K., and the Research Council, U.S.A.

Reference

1. H. Bohr and J. Lindhard, *Phys. Med. Biol.*, **10**, 1 (1965).
2. A.S. Schlachter, J.W. Stearns, W.G. Graham, E.H. Berkner, R.V. Pyle and J.A. Tanis, *Phys. Rev. A*, **17**, 111 (1978).

COMPARISON OF ELECTRON CAPTURE PROCESS IN GAS AND SOLID TARGETS FOR 35 MeV/u Kr³⁶⁺ IONS*

J.P. Rozet, A. Chetoui, P. Bouisset

Institut Curie and Université P & M Curie, 11 rue P & M Curie, 75231 Paris Cedex 05, France

and C. Stephan

Institut de Physique Nucléaire, BP n°1, 91405 Orsay, France

New results on electron capture for high velocity, fully stripped heavy ions will be reported.

A preliminary experiment has been achieved on the LISE facility at GANIL in Caen (France). Post stripping of the incident 35 MeV/u Kr³⁶⁺ ions by a 6 mg/cm² carbon foil leads to the production of fully stripped Kr³⁶⁺ ions with an efficiency of about 50%. X-ray spectra corresponding to the Lyman and Balmer transitions emitted from the excited states of hydrogen-like Kr³⁵⁺ produced by electron capture have been recorded for three solid targets (C: 20 μg/cm², Al: 5 μg/cm², V: 3 μg/cm²) and one argon gaseous target.

Most prominent features of the results are summarized in figure 1 and figure 2. One may note that :

- (i) The total Lyman X-ray emission cross-section, equivalent to the total capture cross section to excited states of projectile (for this high Z element, radiative lifetime of 2 s state is short enough to allow observation of its radiative decay within the observation region) measured in the case of gaseous argon target is in good agreement with CDW calculation (1), whereas those obtained for solid targets are significantly larger ;

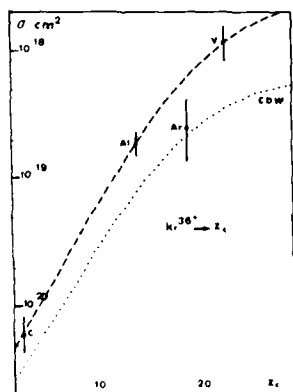


Figure 1. Total Lyman line emission cross sections: Experiment (---); CDW calculations (.....).

Reference

- (1) Dz Belkic, R. Gayet and A. Salin, Comp. Phys. Com. 32 (1984) 385.

* work performed at GANIL (Caen) France.

- ii) The measured population ratios of $n = 2$, $n = 3$ and $n = 4$ excited states (α/β and α/γ relative intensities) also differ for solid and gaseous targets. Together with the previous result they indicate an excess of population in the low lying excited p states for solid targets. This could be due to an increase of the capture cross sections in projectile's states of small principal quantum number or in states of high angular momenta (Yrast decay).

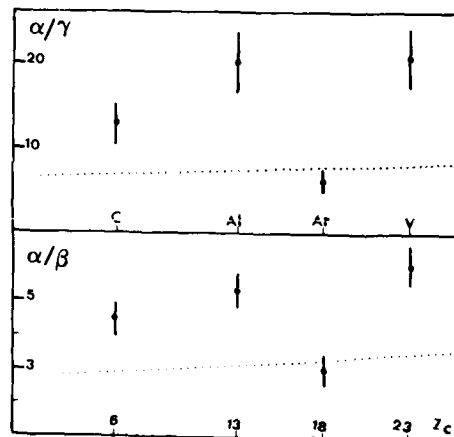


Figure 2. Lyman α /Lyman β and Lyman α /Lyman γ relative intensities (lines and dots: same as figure 1).

Note that in this experiment, a direct comparison of gaseous and solid target measurements is achieved. Indeed, a very important feature of the elementary atomic collision processes for these high velocity collisions is their very small cross-sections. As a consequence, the total probability for interaction of the ions inside our thin solid targets remains very low and doesn't exceed few percents, all processes included. In other words, the single collision condition is fulfilled.

In conclusion, the GANIL accelerator offers the opportunity to study under new conditions all possible effects related to the solid state structure of the target, or those due to the exit interface.

CONTINUUM DISTORTED WAVES

Derrick S.F. Crothers

Department of Applied Mathematics and Theoretical Physics
The Queen's University of Belfast,
Belfast BT7 1NN, Northern Ireland.

Closed analytical results are obtained¹ for the first order continuum distorted-wave non-relativistic double-scattering Thomas total cross sections for $1sZ_A$ to $n_B^2mZ_B$, $n_B^2Z_B$, n_BZ_B and Z_B charge transfer transitions, where omission of a quantum number implies summation. Specimen l and m distributions are presented. It is concluded that for the higher values of l , even at intermediate energies, the m distributions² are given essentially by $(l-|m|)! [P_l^{|m|}(\cos \pi/3)]^2 / (l+|m|)!$ in accordance with the second-order Oppenheimer-Brinkman-Kramers theory and a reflection of the double-scattering Thomas mechanism involving two successive deflections of the electron through 60° .

A continuum distorted wave (CDW)³ theory of charge transfer is developed to second order⁴. Closed analytical results are obtained for the second-order CDW (CDW2) non-relativistic double-scattering Thomas total cross sections for $1sZ_A$ to $n_B^2mZ_B$, $n_B^2Z_B$ and n_BZ_B charge transfer transitions, where the omission of a quantum number implies summation. It is proven that these cross sections agree exactly with the corresponding second-order Oppenheimer-Brinkman-Kramers (OBK2) non-relativistic double-scattering Thomas cross sections. The first-order CDW (CDW1) Thomas theory is shown to be correct fortuitously for only $1sZ_A$ to $1sZ_B$ transitions. It is shown that the CDW2-OBK2 cross section for the $1sZ_A$ to n_BZ_B transition is simply the corresponding CDW1 cross section multiplied by the Jacobi polynomial ${}_2F_1(1-n_B, 1; 2; (4Z_A Z_B / n_B) / (Z_A + Z_B / n_B)^2)$. Specimen l and n_B distributions are presented. It is concluded that existing criticisms of CDW theory are not well founded.

References

1. Crothers D.S.F., 1985, J. Phys. B.: At. Mol. Phys., 18, in press.
2. Crothers, D.S.F. and McCann J.F., 1982, Phys. Lett. A., 92, 170-4.
3. Crothers D.S.F., 1985, J. Phys. B.: At. Mol. Phys., 18, in press.
4. Crothers D.S.F. and McCann J.F., 1984, J. Phys. B.: At. Mol. Phys., 17, L177-184.

SINGLE AND DOUBLE ELECTRON CAPTURE FROM LITHIUM BY FAST ALPHA PARTICLE

S.C.Mukherjee, Mita Ghosh and G.K.Mandal

Indian Association for the Cultivation of Science, Jadavpur, Calcutta 700032, India.

Charge exchange for heavy ion-atom collision has important application in the diagnosis of fusion plasma. Electron capture by He^{2+} from Li helps to determine the alpha particle distribution in hot plasma in nuclear fusion reactor. McCullough et al.¹ have made their measurements of single and double electron capture in He^{2+} -Li collision up to 800 keV. Sasao et al.² have recently reported their measurements on double electron capture cross section of the same reaction up to 2.0 MeV. Only theoretical investigation on this system in high energy region has so far been reported by Olson³. He has calculated single and double electron capture cross sections in He^{2+} -Li system within the energy range 50 to 400 keV amu⁻¹ in the framework of classical trajectory Monte Carlo (CTMC) method. In the present paper, we propose to study single and double electron capture cross sections for He^{2+} -Li collision in the continuum distorted wave approximation. In the present independent electron model approach, we consider the electronic state to be described by Hartree-Fock function and the effective charge seen by the active electron is determined from its binding energy with a hydrogenic model. Consideration of effective charge over perfectly screening charge is more realistic and this has recently been examined by Banyard and Shirtcliffe⁴ in connection with their study of H^+ -Li collision in CDW approximation.

In Fig.(1), we compare our results for single electron capture cross section with the experimental results of McCullough et al and CTMC results of Olson. In Fig.(2), we have compared our calculated results for double electron capture with the experimental results of McCullough et al., Sasao et al. and CTMC results of Olson. In this figure, in (i), the electron-electron interaction in the final state of helium is neglected during the collision and its state is written as a product of two hydrogenic orbital in the field of He^{2+} nucleus. In (ii), the final state of helium is written as a product of two Hartree-Fock functions or equivalently the electron-electron interaction is replaced by an average Hartree-Fock potential.

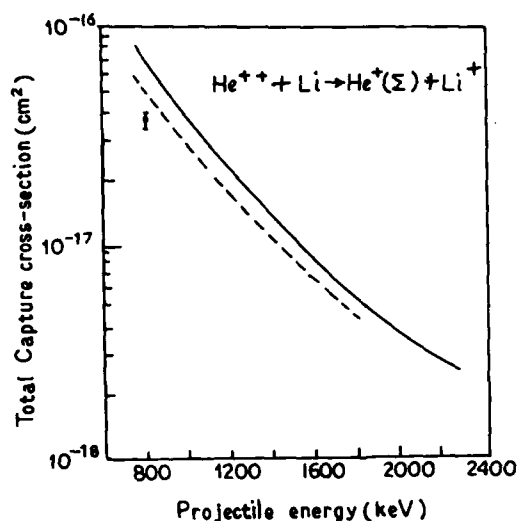


Fig.1. Total single electron capture cross section 4He^{2+} incident on a lithium atom, —, present CDW results, --- results from ref.3, \diamond Expt. results from ref.1.

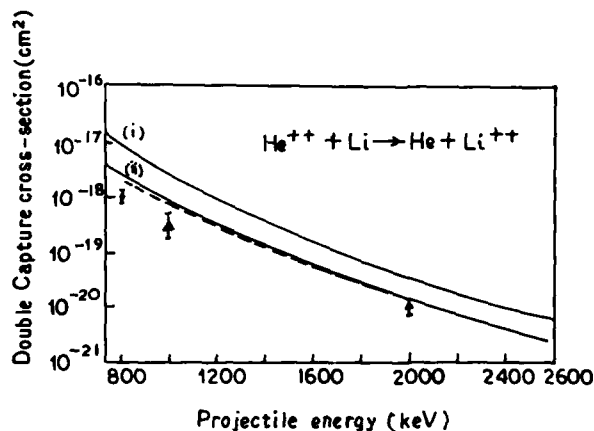


Fig.2. Double electron capture cross section for the projectile 4He^{2+} incident on lithium atom. — present CDW, results (i) and (ii). --- results from ref.3, \circ Expt. results (Ref.1), \triangle Expt. results (Ref.2)

References

- 1 K.W.McCullough, T.V.Gorfe, M.B.Shan, M.Lenon and H.B.Gilbody, J. Phys. B15 111 (1982).
- 2 M.Sasao et al., XIII ICPEAC, Abs. 569 (1983).
- 3 K.E.Olson, J. Phys. B15 L163 (1983).
- 4 K.E.Banyard and G.W.Shirtcliffe, J. Phys. B12, 3247 (1979).

CALCULATION OF CROSS SECTIONS FOR ELECTRON CAPTURE FROM MULTI-ELECTRON ATOMS BY FAST IONS

S.C.Mukherjee, G.C.Saha* and Shyamal Datta

Department of Theoretical Physics
Indian Association for the Cultivation of Science, Jadavpur, Calcutta 700032, India.

*F.C.College, Diamond Harbour, 24-Parganas, West Bengal, India.

Charge transfer cross sections from the K-shell of N and O atoms by fast protons are calculated in the framework of the continuum intermediate-state approximation¹ for the incident energy varying between 1 to 5 Mev for the $H^+ + O$ and 1 to 10 Mev for $H^+ + N$ asymmetric collisions ($Z_p(Z_t)$). We consider the active electron moving in the field of an effective nuclear charge and expand the bound-state wavefunction of complex atoms onto the basis of Slater-type orbitals. The other electrons are considered to be passive and provide only screening during the collision process. The use of this independent-particle model is justified due to the wide separation of binding energies for the inner subshell electrons².

In the Strong Potential Born Approximation³ or Impulse Approximation the calculation of cross sections for electron capture from the multi-electron atoms with realistic wave function into the final hydrogenic states with arbitrary quantum numbers is very difficult.

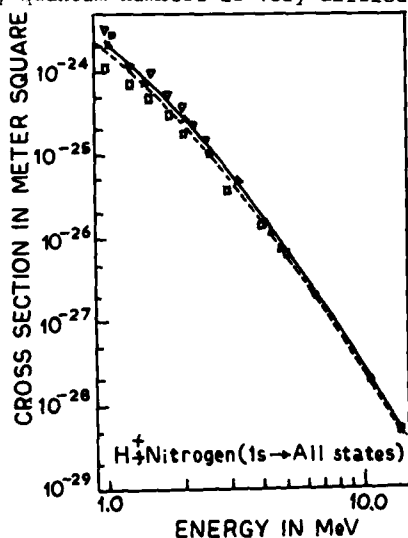


Fig.1: Capture into all states by protons from the K-shell of nitrogen atoms: Theory: —, present work; --- CDWA calculations (ref.1); Expt: atomic target: \square , (ref.8); molecular targets: \triangle (Ref.6); \bullet , (ref.4); \blacksquare , (ref.5); ∇ , (Ref.7).

Although our method introduces an error of the order of $(Z_p/v)^2$, one can have an estimation of cross section with reasonable accuracy in the high energy region. The present method has been developed for the evaluation of Coulomb integral containing the product of a Coulomb wave function with Slater type orbital in a closed form in terms of the Gaussian hypergeometric function.

The theoretical values for the total cross sections are obtained from the relation, $\sigma_{total} = \sigma_{1s} + 1.616(\sigma_{2s} + \sigma_{2p})$, as the contributions from the higher excited states are found to be negligible. Our results are in excellent agreement with the Continuum Distorted wave Approximation (CDWA) calculations¹ and the observed data⁴⁻⁸ throughout the energy range.

References :

1. Dz. Belkic, R. Gayet and A. Salin, Phys. Rep. **56**, 280 (1979).
2. C.E. Briggs, Rep. Prog. Phys. **39**, 217 (1976).
3. J. Macek and A. Alston, Phys. Rev. A **26**, 250 (1982); S. Alston, Phys. Rev. A **27**, 2342 (1983).
4. K.H. Berkner, S.N. Kaplan, G.A. Paulikas, and R.V. Pyle, Phys. Rev. A **14**, 729 (1965).
5. I.M. Welsch, K.H. Berkner, S.N. Kaplan and R.V. Pyle, Phys. Rev. **158**, 85 (1967).
6. U. Schryber, Helv. Phys. Acta **40**, 1023 (1967).
7. L.H. Toburen, M.Y. Nakai and R.A. Langley, Phys. Rev. **171**, 114 (1968).
8. G.L. Cooke, R.K. Srinivas, B. Gurnette, L. Bratton and T.K. Saylor, Phys. Rev. A **16**, 2246 (1977).

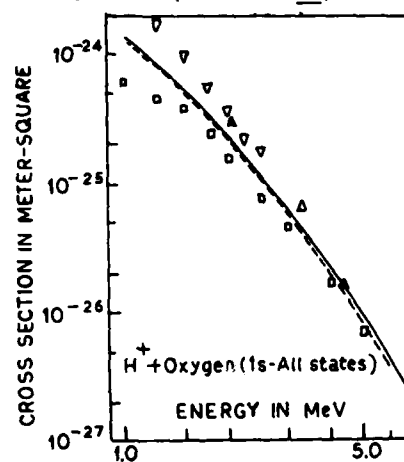


Fig.2: For Oxygen, Same as in Fig.1.

POTENTIAL SCREENING IN INNER-SHELL ELECTRON CAPTURE

J.E. Miraglia*, R.O. Barrachina⁺ and C.R. Garibotti⁺

* Instituto de Astronomía y Física del Espacio, C.C. 67, Suc. 28, 1428 Buenos Aires, Argentina
 + Centro Atómico Bariloche, 8400 S. C. de Bariloche, Argentina

We consider the electron capture process from the inner shell of an atom of large nuclear charge Z_p by an incident bare ion of charge Z_r , for which $Z_r \gg Z_p$. The traditional Impulse Approximation (IA) is intended to solve the high ion velocity v region problem, in spite of two severe assumptions which are included in this approach. First the intermediate electronic wave function is approximated by a Coulomb wave centered at the target nucleus. It may be a good ansatz for hydrogenic targets, but for inner-shell electron capture processes we are fully entitled to consider a target potential shielded at a radius R of some outer shell. Here we want to explore the possible consequences of a shielding. Second the pure coulombian electronic wave function is approximated by its on-shell version. The difference Δk between the impulse k_i of the electron on the intermediate state and that k on the final state is about $Z_p^2/2v$. It is large enough to require the use of an off-energy-shell wave function for the electron-target nucleus relative motion. A coulombian state has a branch point when $\Delta k \rightarrow 0$ and does not approach a defined on-energy limit. The exact expression of that state is quite complicated, but when Δk is small it can be approximated by a corrective factor

$$g_{\alpha}(k, k_i) = e^{-\pi a/2} \frac{\Gamma(1+ia)}{\Gamma(1-ia)} \left[\frac{k_i^2 - (k+i\epsilon)^2}{4k_i^2} \right]^{ia} ; a = -\frac{Z_r}{k} \quad (1)$$

times the on-shell wave function. Nonanalyticity means that this factor will persist even for $\Delta k \rightarrow 0$. The Strong Potential Born (SPB) approximation¹ is intended to be valid when $Z_r \gg Z_p$ and introduces the off-shell correction given by Eq. (1) for extending the IA down to the intermediate ion energy region. Neglecting orders Z_p/v the SPB cross section can be written as a projectile-independent factor

$$|M_{\alpha}(\frac{Z_r}{v})|^2 = \left| \frac{4Z_p}{\pi} \int_0^{\infty} g_{\alpha}(v, v + \frac{u^2 + Z_p^2}{2v}) \frac{u^2 du}{(u^2 + Z_p^2)^2} \right|^2 \quad (2)$$

times the peaking IA. This factor is a direct consequence of an off-shell intermediate electronic wave function, corresponding to a pure Coulomb electron-nucleus interaction whose long range nature is the responsible for the on-shell branch. However for shielded potentials these branch singularities disappear in a well defined

on-shell limit is obtained for wave function and scattering amplitude. On this basis alone, it is apparent that the coulombian off-shell correction factor is not substantiated.

Let us investigate the consequences arising in inner-shell capture calculations when the electron-target potential is cut at distances larger than certain radius R . A similar problem has been recently discussed for the capture to continuum process². For finite R , Eq. (2) is no longer valid. In this case a dependence on the cutoff procedure is likely to appear. For the cutoff Coulomb potential, the off-shell corrective factor is given, to order $1/R$, by³

$$g_{\alpha}(k, k_i) = e^{-ia \ln(2kR)} {}_1F_1(-ia; 1-ia; i(k-k_i)R) \quad (3)$$

In the usual IA approach g_{α} is taken as unity, while in the SPB correction its pure Coulomb limit $R \rightarrow \infty$ is considered. Quite obviously none of these limits is valid. In particular the SPB limit requires $R \gg 2v/Z_p^2$, a condition which evidently is not fulfilled at the intermediate energy region where this modified IA approach is supposed to be valid.

Finally we have to point out that using expression (3) in order to correct the SPB factor (2) may lead to unrealistic conclusions in view that it is related just to a large range limit of the off-shell function for the cutoff Coulomb potential. This expression is not valid for R small and the exact screened T matrix is required. In this case an off-shell correction is likely to appear, but it will surely be less dramatic than the one provided by Eq.(2) in the SPB correction of the IA approach.

References

1. J. Macek and S. Alston, Phys. Rev. A **26**, 250 (1982).
2. C.R. Garibotti and R.O. Barrachina, Phys. Rev. A **28**, 2792 (1983).
3. W.F. Ford, J. Math. Phys. **7**, 626 (1966).

CALCULATION OF DIFFERENTIAL CHARGE-TRANSFER CROSS SECTION IN THE INTERMEDIATE AND HIGH ENERGY RANGE BASED ON THE FADDEEV-MERKURIEV EQUATIONS

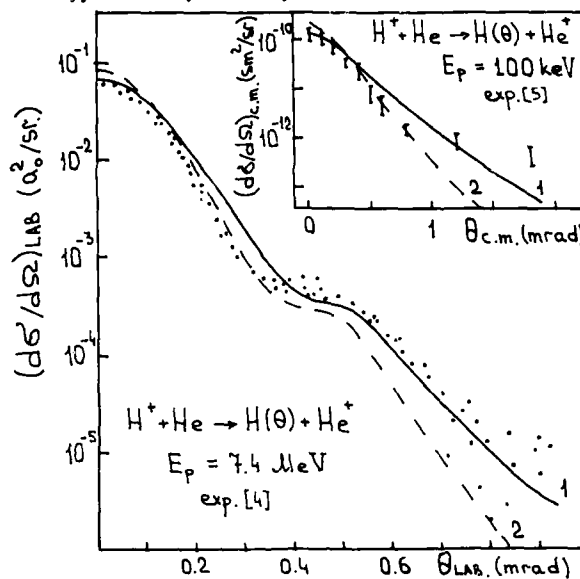
A.L. Godunov, Sh.D. Kunikeev, V.S. Senashenko

Institute of Nuclear Physics, Moscow State University, Moscow, 119899, USSR

We discuss the differential cross section of charge exchange between protons and hydrogen or helium obtained by the method¹ of theoretical description of ion-atom collisions allowing for the interaction in final state. According to this method, the amplitude of electron capture by a fast particle is calculated with the final-state wave function which is an approximate solution to the Faddeev-Merkuriev equation for the system of three charged particles when two of them form a bound state. The nonorthogonality of the initial- and final-state wave functions with respect to the variables of the bound pair having been taken into account, certain modifications arise in the transition operator². If, however, the amplitude is calculated disregarding heavy particle interaction in both the wave function and the transition operator, the resulting simplified expression will coincide with the peaking form of the impulse approximation³.

The differential cross section of electron capture by protons in helium and hydrogen calculated within the above approximations are analyzed in a wide energy range of colliding particles. The calculations have shown that inclusion of electron interaction with residual ion by the method¹ yields the Thomas peak observed in the differential cross section of fast proton charge exchange with helium⁴. Replacement of the Coulomb wave function describing the effect of residual ion field on the captured electron motion by its asymptotic expression leads to the monotonically varying differential cross section without any peculiarities in its angular dependence.

Fig. 1 illustrates the results of calculations of the differential cross section of charge exchange between protons and helium together with the available experimental data. Curve 1 presents the complete calculations, and curve 2 the calculations without the interaction between heavy particles. Comparison of the calculated and experimental data shows that the inclusion of the heavy-particle interaction can significantly improve the agreement between the calculated and experimental charge-transfer cross section for large scattering angles. Besides that the cross section calculated without heavy-particle interaction taken into account in the transition operator coincide actually with the calculations made



when the transition operator is modified by the allowance for the nonorthogonality of the initial- and final-state wave function. This is a consequence of the fact that charge transfer processes occur mainly at relatively small internuclear distances. Thus, the agreement obtained between the calculated and experimental data leads us to the conclusion that the method¹ is quite adequate for calculating the differential charge-transfer cross section in a wide energy range.

References:

1. A.L. Godunov, Sh.D. Kunikeev, V.N. Milyov, V.S. Senashenko, Proc. XIII ICPEAC, Abstr. of Paper, Berlin, 1983, p.383.
2. D.R. Bates, Proc. Roy. Soc., A247, 291 (1958).
3. L.J. Dube, J. Phys., B: At. Mol. Phys., 17, 641 (1984).
4. E. Horsdal-Pedersen et al., Phys. Rev. Lett., 50, 1910 (1983).
5. P.J. Martin et al., Phys. Rev., A23, 2878 (1981).

THEORY OF ELECTRON CAPTURE AT HIGH ENERGIES

Steven Alston

Fakultät für Physik, Universität Freiburg, D-7800 Freiburg, BRD

Differential cross sections for electron capture in proton-Helium collisions have been measured¹ recently at MeV energies. The classically introduced Thomas double-scattering mechanism, whereby the almost free electron is scattered first off the projectile at 60° to the forward direction, attaining a velocity equal to that of the projectile, and subsequently off the target nucleus elastically in order to redirect its motion to be parallel to the projectile's, is thought to play a significant role in the dynamics of the capture process at these energies, and, in fact, to dominate at asymptotically high energies. Yet the second-Born approximation to the capture amplitude which represents the lowest order quantum analogue of the Thomas mechanism reproduces the data¹ quite inadequately (except in order of magnitude).

Recently, a higher-order distorted-wave Born (DWB) theory² of capture has been derived as a symmetric extension of the asymmetric strong-potential Born (SPB) theory³. The DWB capture amplitude takes the form

$$T^{\text{DWB}} = T^{\text{BI}} + \langle \chi_f^- | V_T G_0^+ V_P | \chi_i^+ \rangle, \quad (1)$$

where T^{BI} is the first Born amplitude, V_P , V_T are the electron-projectile and electron-target nucleus potentials, and G_0^+ is the free-particle Green's operator. The SPB distorted waves are defined

$$|\chi_f^-\rangle \equiv (1 + G_T^- V_T) |\phi_f^-\rangle, \quad |\chi_i^+\rangle \equiv (1 + G_P^+ V_P) |\phi_i^+\rangle; \quad (2)$$

G_P^+ (G_T^-) is a Green's operator for the potential V_P (V_T) with the target-nucleus (projectile) propagating freely. Plus and minus signs denote out- and in-going wave boundary conditions, respectively. The initial and final asymptotic states ϕ_i , ϕ_f are products of plane-waves of relative motion and bound state wavefunctions.

Simply rewriting (1) using (2), one obtains the expression

$$T^{\text{FW}} = T^{\text{BI}} + \langle \phi_f | T_P G_0^+ T_P | \phi_i \rangle, \quad (1')$$

which is the second-order approximation to the Faddeev-Watson amplitude⁴. Here, T_P and T_T denote the transition operators $V_P + V_P G_P^+ V_P$, $V_T + V_T G_T^- V_T$, respectively. Thus, the DWB amplitude is an application of the general Faddeev-Watson scattering formalism (with the internuclear potential set equal to zero).

The amplitude (1') has a very straightforward interpretation in terms of the Thomas mechanism. When the heavy-particle motion is integrated, T_T and T_P become two-

body Coulomb transition operators. Clearly then, the full Coulomb nature of the two collisions in the mechanism is accounted for by the use of Coulomb T-operators. I have evaluated (1') approximately by neglecting the dynamic effects of the initial and final binding of the electron. This leads to an impulse approximation to the Coulomb T-matrices. Due account is taken of the off-shell effects characteristic of the Coulomb problem⁵. Figure 1 shows the present results for 1s-1s captures in 7.40 MeV proton-Helium collisions along with those of the continuum distorted-wave theory,^{5a} the SPB^{5b}, and the data¹. For the DWB and SPB results, an effective charge of 1.6875 in a hydrogenic model is used for the Helium wavefunction.

1. E. Horsdal-Pedersen, C.L. Cocke, and M. Stockli, Phys. Rev. Lett. **50**, 1910 (1983)
2. K. Taulbjerg and J.S. Briggs, J. Phys. B **14**, 3811 (1983)
3. J. Macek and S. Alston, Phys. Rev. A **26**, 250 (1982)
4. C.J. Joachain, *Quantum Collision Theory* (North Holland, Amsterdam 1975), Eq. (19.92)
- 5a. R.D. Rivarola, A. Salin, and M.P. Stockli, J. Physique Lett. **45**, L-259 (1984); b.S. Alston, Phys. Rev. **A27**, 2342 (1983)

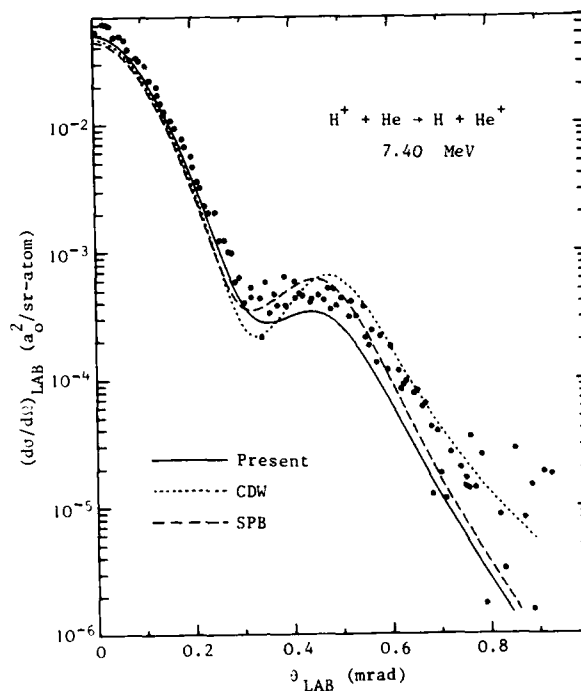


FIGURE 1 1s-1s capture from Helium by protons.

UNDERSTANDING THE EXACT SECOND-BORN CAPTURE CROSS SECTION

Steven Alston

Fakultät für Physik, Universität Freiburg, D-7800 Freiburg, BRD

The second-Born approximation¹(B2) to the electron capture amplitude is known to represent the lowest-order quantum analogue of Thomas' classically derived two-step picture of capture where a double scattering of the electron, first off the projectile and then off the target nucleus, provides the means of giving the electron a velocity vector roughly equal to that of the projectile so that it can be captured. At asymptotically high velocities, the second-order part of this amplitude yields the leading velocity dependence, namely v^{-11} , of the total cross section.

Over the last decade or so, various exact (numerical) evaluations¹ of the B2 amplitude have been made, improving on the original peaking approximation of Drisko² (linearized-propagator approximation or LPA) which concentrates on treating the Thomas mechanism contribution accurately. The exact and approximate differential cross sections differ greatly, however, at realistic but still large velocities. For example, in 10 MeV proton-Hydrogen atom collisions corresponding to $v=20$ a.u., the discrepancies range from 33% at $\theta=0^\circ$ to a factor of 5.9 at the cross section minimum (see Fig. 1) to 18% at the Thomas peak, $\theta=0.054^\circ$. The reason for the LPA being so inadequate, since errors of the order v^{-2} should be introduced, has not been fully addressed.

In momentum space, the second-order part of the B2 amplitude takes the form²

$$T_2^{B2} = \int d\mathbf{k}_i d\mathbf{k}_f \tilde{\phi}_f^*(\mathbf{k}_f) \tilde{V}_T(\mathbf{k}_i + \mathbf{J}) G_0^+ \tilde{V}_P(\mathbf{k}_f - \mathbf{K}) \tilde{\phi}_i(\mathbf{k}_i)$$

Here, a tilde denotes a Fourier transform and ϕ_i, ϕ_f are the initial and final bound states, V_P, V_T the electron-projectile and electron-target nucleus potentials, and G_0^+ the free-particle Green's function. The momenta transferred to the projectile and target nucleus are \mathbf{K}, \mathbf{J} , respectively. A close look at T_2^{B2} shows that, besides the peak in the integrand at $\mathbf{k}_i = \mathbf{k}_f = 0$ which leads to the LPA when $\tilde{V}_T(\mathbf{k}_i + \mathbf{J}) \sim \tilde{V}_T(\mathbf{J})$ and $\tilde{V}_P(\mathbf{k}_f - \mathbf{K}) \sim \tilde{V}_P(\mathbf{K})$, there are two other peaks at $\mathbf{k}_i = 0, \mathbf{k}_f = \mathbf{K}$ and $\mathbf{k}_f = 0, \mathbf{k}_i = -\mathbf{J}$ which have heights of the same order of magnitude, viz. $(Z_P Z_T)^{-1/2} v^{-6}$, away from the Thomas peak. This is seen by putting (to avoid infinities) small cut-offs on the potentials, say $k_f \geq Z_P, k_i \geq Z_T$, and looking at the magnitude of the integrand at each peak. Z_P, Z_T are the projectile and target-nuclear charges.

I have evaluated T_2^{B2} for 1s+1s captures using pea-

king approximations to obtain contributions from all three peaks, taking due care to avoid double counting.

The result is

$$T_2^{B2} = -2^5 \pi \frac{(Z_P Z_T)^{5/2}}{(JK)^2} \{ (K^2 - v^2 + Z_P^2 - 2Z_P J i - 2Z_T K i)^{-1} \\ + \frac{i Z_P K^2}{(K^2 + Z_P^2)^2} \left[\frac{1}{v} \ln(1 - i \frac{v}{Z_T}) - \frac{1}{2(v + i Z_P)} \right] \\ + \frac{i Z_T J^2}{(J^2 + Z_T^2)^2} \left[\frac{1}{v} \ln(1 - i \frac{v}{Z_P}) - \frac{1}{2(v + i Z_T)} \right] \}$$

Use of this simple analytic expression together with T_1^{B1} leads to significantly better agreement with the exact¹ cross section as Fig. 1 shows.

Physically, the present idea corresponds to allowing some freedom in the momenta transferred in the two collisions as opposed to the LPA where only the fixed values $\mathbf{K}, -\mathbf{J}$ are allowed. A fuller discussion of the evaluation and of its implications for other capture theories will be presented at the conference.

1. P.R. Simony and J.H. McGuire, J. Phys. B14, L737 (1981)

2. L.J. Dubé and J.S. Briggs, J. Phys. B14, 4595 (1981)

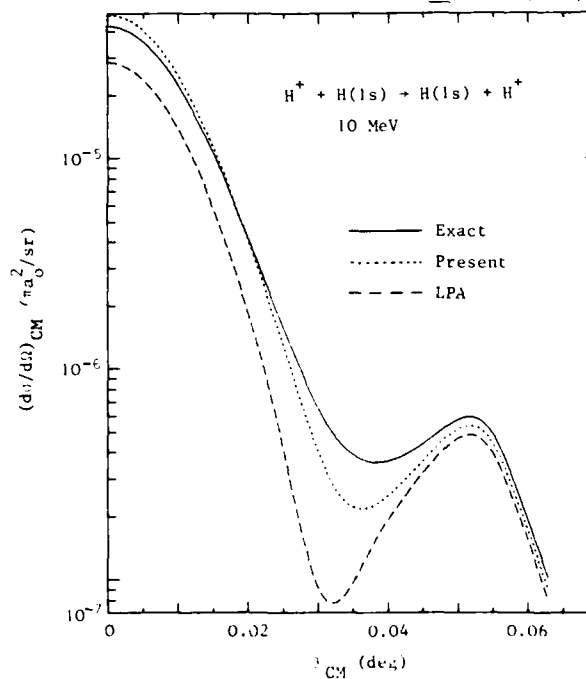


FIGURE 1 Exact and approximate B2 capture cross sections.

THE NORMALIZATION OF APPROXIMATE SCATTERING STATES

S. Alston,* J.S. Briggs,* and K. Taulbjerg*

* Fakultät für Physik, Universität Freiburg, D-7800 Freiburg, BRD

+ Institute of Physics, Aarhus University, DK-8000 Aarhus, Denmark

The theory of atomic collisions is generally concerned with constructing approximations to the exact scattering state $\psi_i^+(K_i)$, where K_i is the initial, relative momentum of the projectile and target and the plus sign denotes outgoing-wave boundary conditions. It is well known that both $\psi_i^+(K_i)$ and the asymptotic state $\phi_i(K_i)$ from which it evolves satisfy a delta-function normalization condition

$$\langle \psi_i^+(K_i') | \psi_i^+(K_i) \rangle = \langle \phi_i(K_i') | \phi_i(K_i) \rangle = \delta(K_i' - K_i)$$

corresponding to the necessity of conserving flux in the collision. A good approximate scattering state should also be comparably normalized or, if not exactly so, then the errors should be small as in the case of a rapidly convergent perturbation series.

One widely used method for obtaining an approximate scattering state $\chi_i^+(K_i)$ is the distorted-wave formalism¹ in which the initial perturbation V_i is split into a distorting potential U_i treated exactly and a residual interaction W_i . Using various operator manipulations the scalar product for $\chi_i^+(K_i)$ can be written

$$\langle \chi_i^+(K_i') | \chi_i^+(K_i) \rangle = \langle \phi_i(K_i') | \phi_i(K_i) \rangle \times (E' - E - i\delta)^{-1} \langle \chi_i^+(K_i') | (U_i^+ - U_i) | \chi_i^+(K_i) \rangle, \quad (1)$$

with E the total system energy and $\delta \rightarrow 0^+$. If the distorting potential is hermitian, $\chi_i^+(K_i)$ is obviously normalized, but for nonhermitian U_i , the situation is not so clear.

Significant strides in understanding electron capture at intermediate to high energies have been made in recent years in the form of the strong-potential Born² (SPB) and distorted-wave Born³ (DWB) theories. These theories provide an example where the distorting potential U_i is nonhermitian; in this case the residual interaction W_i assumes the explicit form $V_T G_O^+(E) V_P$. Here, V_P , V_T represent electron-projectile and electron-target nucleus potentials and $G_O^+(E)$ is the free-particle Green's operator. When the defining expression for $\chi_i^+(K_i)$ is introduced and the consequent relation³

$$W_i | \chi_i^+(K_i) \rangle = V_T | \chi_i^+(K_i) \rangle - \phi_i(K_i)$$

used, equation (1) takes the form

$$\langle \chi_i^+(K_i') | \chi_i^+(K_i) \rangle = \delta(K_i' - K_i) + (E' - E - i\delta)^{-1} \times \langle \phi_i(K_i') | V_T | \chi_i^+(K_i) \rangle - \langle \chi_i^+(K_i') | V_T | \phi_i(K_i) \rangle. \quad (2)$$

We have employed the method of continuum-state nor-

malization whereby the expression Eq. (2) is integrated over the angles of $K_i' - K_i$ and over a small interval $\Delta K_i = K_i' - K_i$ with $\Delta K_i \rightarrow 0$ at the end, to obtain a value for the normalization constant. This has been done together with the use of the off-the-energy-shell Coulomb T-matrix element⁴ and we find the resulting constant N to be

$$N = 1 + \frac{5}{4} (Z_P/Z_T)^2 \frac{2\pi\eta}{(e^{2\pi\eta} - 1)}. \quad (3)$$

The Sommerfeld parameter η equals Z_P/v , with v the incident velocity, and Z_P , Z_T are the projectile and target-nuclear charges, respectively. Clearly, N is not unity and we argue that a properly normalized distorted-wave should be defined as $N^{-1/2} \chi_i^+(K_i)$.

For large velocities, $\eta \rightarrow 0$ and $N \approx 1 + (5/4)(Z_P/Z_T)^2$ while for $v \rightarrow Z_P$, $\eta \rightarrow 1$ and $N \approx 1 + (0.01)(5/4)(Z_P/Z_T)^2$. In the SPB theory $Z_P \gg Z_T$ and one finds a large normalization constant. Since the SPB (or DWB) scattering state involves the summation of an infinite-order perturbation series, it is not surprising that a significant loss of normalization can occur. The implications of the normalization of the scattering state for direct and radiative electron capture will be discussed at the conference.

1. C.J. Joachain, Quantum Collision Theory (North Holland, Amsterdam 1975), Ch. 17
2. J. Macek and S. Alston, Phys. Rev. A **26**, 250 (1982)
3. K. Taulbjerg and J.S. Briggs, J. Phys. B **16**, 3811 (1983)
4. J. Nuttall and R.W. Stagat, Phys. Rev. A **3**, 1355 (1971)

NUMERICALLY GENERATED OFF-SHELL RADIAL WAVEFUNCTIONS

Hermann Marxer and Steven Alston

Fakultät für Physik, Universität Freiburg, D-7800 Freiburg, BRD

A recent advance in the theory of electron capture in asymmetric collisions at intermediate velocities has been the recognition of a strong-potential Born (SPB) approximation¹ as the proper first-order term in a consistent expansion of the transition operator in the weaker of the two perturbation potentials. Although the theory is independent of the explicit form of the strong potential, in practice it has proven convenient to work with a hydrogenic model, as, for example, is the case in inner-shell capture, because the supporting analytic formalism is more fully developed, thus facilitating evaluation and interpretation.

Various difficulties concerning this model exist, however. In particular, the problem of which charge, the bare nuclear one or some screened value, to use in the off-shell factor and the sensitivity of the cross section to the introduction of a realistic potential, e.g. Hartree-Slater, are two worth mentioning.

As a first step toward addressing these issues and eventually toward calculating cross sections for realistic potentials, a set of routines for generating numerical radial off-shell wavefunctions is being developed. These wavefunctions are solutions of the inhomogeneous radial Schrödinger equation

$$\left(\frac{d^2}{dr^2} - \frac{l(l+1)}{r^2} - 2V(r) + \kappa^2\right) u_l(r) = (\kappa^2 - k^2)kr j_l(kr), \quad (1)$$

where the complex $u_l(r)$ is related to the full wavefunction by the expansion

$$\psi_{k,\epsilon}^+(\underline{r}) = \frac{1}{kr} \sum_{l=0}^{\infty} i^l (2l+1) u_l(r) P_l(\hat{k} \cdot \hat{r}).$$

Equation (1) is solved by converting it into an integral equation involving the radial Green's function $G_l^+(\epsilon; r, r')$ for the potential $V(r)$; G_l^+ is constructed from the regular and irregular solutions of the homogeneous version of (1). The off-shell energy ϵ is equal to $\kappa^2/2$, j_l is a spherical Bessel function, and P_l is a Legendre polynomial.

For the case of a Yukawa potential, $-Ze^{-Zr/6}/r$ and $Z=10$ (neon), Fig. 1 shows a comparison with the regular homogeneous solutions (solid curves) of the real part of u_0 and the imaginary part of u_1 for various κ values with k fixed at 5.2 au. The imaginary part of u_0 and the real part of u_1 deviate much less from the homogeneous wavefunctions and are therefore not shown. The on-shell version of this case has been considered in a recent Letter.²

Significant variations of u_0 and u_1 versus κ are apparent and these could lead to modifications of the conclusions in Ref. 2. Results involving a Hartree-Slater potential will be presented at the conference along with a more complete discussion of the construction procedure.

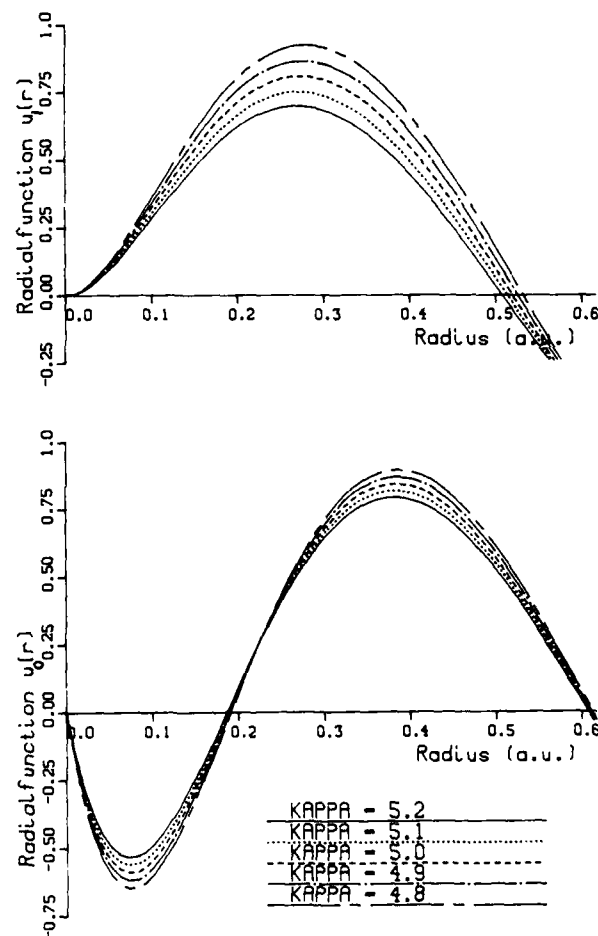


FIGURE 1 Off-shell radial wavefunctions.

References

1. J.S. Briggs, J.H. Nacek, and K. Taulbjerg, Comment At. Mol. Phys. **12**, 1 (1982)
2. L. Kocbach and K. Taulbjerg, J. Phys. B **18**, L79 (1985)

BOUNDARY CONDITIONS AND THE STRONG POTENTIAL BORN
 APPROXIMATION FOR ELECTRON CAPTURE

D. P. Dewangan* and J. Eichler†

*Physical Research Laboratory, Navrangpura, Ahmedabad, 380 009, India

†Molecular Physics Department, SRI International, Menlo Park, CA 94025 USA

It is shown¹ that the Strong Potential Born approximation² (SPB) in its rigorous form leads to an electron capture amplitude which contains a diverging contribution, a fact that seems to have escaped attention so far. The singularity is attributed to the neglect of the proper Coulomb boundary conditions.

While the SPB has originally been formulated² in the wave picture we choose here the equivalent formulation in the impact parameter picture. Let $\Phi_i(t)$ be the initial time-dependent (undistorted) wave function of the electron in the target (Z_T), and $\Phi_f(t)$ the final wave function in the projectile (Z_P) traveling with the constant velocity \vec{v} . If, furthermore, V_{Te} and V_{Pe} are the electron-target and the electron-projectile interactions, respectively, the impact parameter version of the SPB capture amplitude is given by

$$C^{SPB} = -i \int_{-\infty}^{\infty} dt \langle \Phi_f(t) | V_{Te} | \Phi_i(t) \rangle \quad (1)$$

$$+ (-i)^2 \sum_n \int_{-\infty}^{\infty} dt \langle \Phi_f(t) | V_{Te} | \Phi_n(t) \rangle \int_{-\infty}^t dt' \langle \Phi_n(t') | V_{Pe} | \Phi_i(t') \rangle$$

where the sum is over a complete set of asymptotically undistorted target-centered states Φ_n . We immediately realize that the elastic matrix element $\langle \Phi_i | V_{Pe} | \Phi_i \rangle$ behaves as $-Z_P/R$ for large internuclear separations $R(t)$; and hence the associated time integral diverges.

If we consider the wave picture¹ instead of the impact parameter picture we arrive at the same conclusion.

The singularity arises from the long-range nature of the Coulomb interactions involved in the problem. The difficulty is, therefore, avoided in a natural way if we impose the proper Coulomb boundary conditions³ on the asymptotic solutions, i.e.

$$\begin{aligned} \lim_{t \rightarrow -\infty} \Psi_i^+(t) &= \Phi_i(t) e^{-i\sigma_i(t)} \\ \lim_{t \rightarrow \infty} \Psi_f^-(t) &= \Phi_f(t) e^{i\sigma_f(t)} \end{aligned} \quad (2)$$

with $\sigma_i(t) = (Z_P/v) \ln(R - vt)$ and $\sigma_f(t) = (Z_T/v) \ln(R + vt)$. Note that the logarithmic phases are related to the residual Coulomb interaction between electron

and projectile or target and not to the internuclear interaction. If the boundary conditions for the Coulomb interaction are incorporated, a converging second-order approximation may be derived from the exact amplitude³

$$B(t) = -i \int_{-\infty}^{\infty} dt \langle \Phi_f(t) | e^{i\sigma_f(t)} \left| \frac{Z_T}{R(t)} + V_{Te} \right| \Psi_i^+(t) \rangle \quad (3)$$

by introducing a complete set of distorted target wave functions $\Phi_n(t) \exp(-i\sigma_i(t))$. The resulting "boundary-corrected" second-order Born (B2B) amplitude is given by

$$\begin{aligned} B^{B2B}(\infty) &= -i \int_{-\infty}^{\infty} dt \langle \Phi_f(t) | e^{i\sigma_f(t)} \left| \frac{Z_T}{R(t)} + V_{Te} \right| \Phi_i(t) e^{-i\sigma_i(t)} \rangle \\ &+ (-i)^2 \sum_n \int_{-\infty}^{\infty} dt \langle \Phi_f(t) | e^{i\sigma_f(t)} \left| \frac{Z_T}{R(t)} + V_{Te} \right| \Phi_n(t) e^{-i\sigma_i(t)} \rangle \\ &\quad \cdot \int_{-\infty}^t dt' \langle \Phi_n(t') | \left| \frac{Z_P}{R(t')} + V_{Pe} \right| \Phi_i(t') \rangle \end{aligned} \quad (4)$$

Note that the use of distorted intermediate target states introduces an additional perturbation term Z_P/R into B^{B2B} which is absent in C^{SPB} . As a consequence, the elastic matrix element now yields a potential of short range, and the time integral converges.

Having concluded that the singularity in the SPB amplitude² (which gets lost in subsequent approximations²) originates from the neglect in (1) of the proper boundary conditions, we show how to avoid the difficulty by satisfying the Coulomb boundary conditions for all states involved. Recently, the problem has also been treated in different ways.^{4,5}

† On leave from Bereich Kern- und Strahlenphysik, Hahn-Meitner Institut Berlin, D-1000 Berlin 39, W-Germany

1. D. P. Dewangan and J. Eichler, J. Phys. B., in press.
2. J. Macek and S. Alston, Phys. Rev. A **26**, 250 (1982), J. Macek and R. Shakeshaft, Phys. Rev. A **22**, 1441 (1980), J. Macek and K. Taulbjerg, Phys. Rev. Lett. **46**, 170 (1981).
3. Dz. Belkic, R. Gayet and A. Salin Phys. Rep. C **56**, 279 (1979).
4. J. Macek, J. Phys. B., in press.
5. J. H. McGuire, J. Phys. B., in press.

COMPARISON OF EIKONAL AND STRONG POTENTIAL BORN CROSS SECTIONS FOR HIGH VELOCITY CAPTURE AT FORWARD ANGLES

J. H. McGuire⁺ and J. Eichler⁺⁺

⁺ Department of Physics, Kansas State University, Manhattan, KS 66506 USA

⁺⁺ Molecular Physics Department, SRI International, Menlo Park, CA 94025 USA

Historically the eikonal and the strong potential Born (SPB) approximations have developed from conceptually different origins. The eikonal approximation,^{1,2} which represents a solution to the Schrodinger equation that is slowly varying in coordinate space, does not fully incorporate strong distortions that may occur in close collisions. Hence the eikonal approximation is better suited to large impact parameter collisions, rather than close collisions. On the other hand the SPB approximation^{3,4} was designed to treat the Thomas peak accurately, i.e. a close collision phenomenon at high velocities. Consequently it is not surprising that in the very high velocity limit, where the Thomas peak is dominant, the eikonal and SPB approximations give very different cross sections⁵ near the vicinity of the Thomas peak.

The purpose of this paper is to compare the eikonal and SPB approximations at forward scattering angles, well within the Thomas peak. It has been noted previously⁶ that in this forward angle limit the full peaking approximation^{3,7} is valid even for symmetric systems. This means that there is a simple analytic form for the 1s-1s SPB differential cross section, at forward angles namely in the limit as $v \rightarrow \infty$

$$\frac{d\sigma}{d\Omega}(\theta=0)_{\text{SPB}} = \frac{4}{9} \frac{d\sigma}{d\Omega}(\theta=0)_{\text{BK}} \quad (1)$$

where BK denotes the well known Brinkman-Kramers approximation.

Similarly there is a simple form for the 1s-1s eikonal approximation at forward angles, namely

$$\frac{d\sigma}{d\Omega}(\theta=0)_E = \alpha \frac{d\sigma}{d\Omega}(\theta=0)_{\text{BK}}$$

where

$$\alpha = \frac{\pi}{\sinh \pi} e^{-2\pi \tan^{-1}(-P_-/Z_T)}$$

$$\times \left[\frac{9}{16} + \left(\frac{3}{4} + \frac{1}{4} \frac{Z_T^2}{v^2} \right) n^2 + \frac{1}{4} e^{-2\pi} n^4 \right] \quad (2)$$

Z_T = target charge, $n = v^{-1}$

$v = Z_T/v$, $P_- = e n - \frac{1}{2} v$, $e = e_f - e_i$

This holds at all velocities. As v goes to infinity, α goes to 9/16.

Thus from Eqns (1) and (2), at very high velocities, the ratio, R , of eikonal to SPB differential

cross sections at zero scattering angle is 1.27.

Because many experiments are done in a regime where forward angle scattering is dominant, it is useful to compare the ratio of eikonal to SPB cross sections at forward angles and finite energies. This is shown in the figure for p+H at 2-20 MeV.

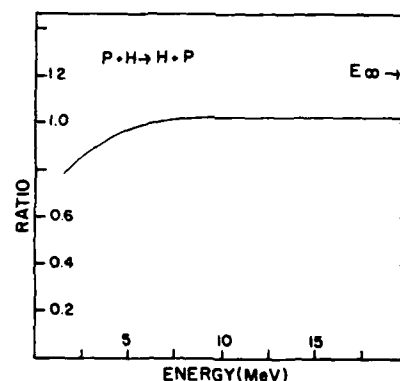


FIGURE 1 Ratio, R , of eikonal cross sections to SPB cross sections at forward angles versus projectile energy for 1s-1s electron capture in p+H.

We conclude that the forward scattering angles, corresponding to distant collisions, there is close agreement between eikonal and SPB cross sections for high velocity electron capture.

J. H. McGuire is supported by the Division of Chemical Sciences, U.S. Department of Energy. J. Eichler is on leave from the Hahn-Meitner Institut, Berlin.

References

1. J. Eichler and F. T. Chan, Phys. Rev. A **20**, 104 (1979).
2. D. P. Dewangan, J. Phys. B **8**, L119 (1975).
3. J. H. Macek and S. Alston, Phys. Rev. A **26**, 250 (1982).
4. N. C. Sil and J. H. McGuire, J. Math. Phys. (April, 1985) (in press).
5. Also see J. S. Briggs, J. H. Macek and K. Taulbjerg, Communication Atomic and Molecular Physics **12**, 1 (1982).
6. J. H. McGuire, N. C. Sil and R. E. Kletke, preprint.
7. J. S. Briggs, J. Phys. B **10**, 3075 (1977).

CHARGE TRANSFER CROSS SECTIONS IN THE EIKONAL APPROXIMATION

A.C. Sil and C. Sinha

Indian Association for the Cultivation of Science, Calcutta 700032, India.

Of late, much theoretical attention has been paid to the eikonal approximation for the study of the charge transfer processes. Recently Dewan¹ has pointed out that when the internuclear potential term is neglected in the eikonal approximation, as is usually done, the boundary conditions are not satisfied and the charge transfer amplitude becomes uncertain by an undefined phase factor. So he has investigated the ground state proton-hydrogen charge transfer problem in the eikonal approximation including the internuclear potential term. However, to simplify his calculations, he has used peaking approximation which is supposed to be valid only for very high projectile velocity. Here we propose a method to calculate the exact eikonal amplitude for the rearrangement collision process, taking account of the full interaction and without resorting to any peaking approximation. We have reduced the transition amplitude to a simple one dimensional integral which is to be evaluated numerically. As a

first application of our proposed technique, we have studied the charge transfer process : $p + H(1s) \rightarrow H(1s) + p$.

The charge transfer transition amplitude in the post form is given by

$$T_f = \iint d\vec{x} d\vec{r} e^{-i\vec{k}_f \cdot \vec{r}} \psi_{1s}^*(\vec{x}) \left(\frac{1}{R} - \frac{1}{r} \right) \psi_{1s}(\vec{r}) e^{i\vec{k}_i \cdot \vec{r}} e^{-i\eta \ln \left(\frac{x+z'}{R-z} \right)} \quad (1)$$

where \vec{x} and \vec{r} are the position vectors of the electron (e) with respect to the projectile (p) and the target proton (p) respectively. \vec{c} and \vec{r} are the position vectors of the electron and proton respectively to the center of mass of the system (H₂) and (H₂) respectively. R is the internuclear separation. ψ is the bound state wave function of the hydrogen atom and $\eta = 1/v$; v being the projectile velocity.

The direction of the incident wave vector is chosen as the z axis. z' and z are the z components of the vectors \vec{x} and \vec{r} respectively.

Using the integral representation (cf. ref.2)

$$e^{-i\eta \ln} = \frac{(-1)^{n+1}}{2i \sin(i\eta) \Gamma'(i\eta-n)} \int_{C'} (-\lambda)^{i\eta-n-1} e^{-\lambda y} d\lambda \quad (2)$$

in Eq.(1), the space integrations can be performed analytically. The result of this integration can be obtained by suitable parametric differentiations of the mother integral of the type

$$I = \int_{C_1}^{\infty} \int_{C_2} \left(\frac{du(-\lambda_1)^{-i\eta-1}(-\lambda_2)^{i\eta-1} d\lambda_1 d\lambda_2}{Au^2 + Bu + C} \right) \quad (3)$$

where A , B and C are linear functions of λ_1 and λ_2 and also depend on the incident and final momentum vectors and the bound state parameters. The contour integrations over λ_1 and λ_2 in (3) are carried out analytically, whereby we are finally left with a one dimensional integral over u . This method can be easily extended to calculate the cross section of charge transfer to any higher excited state.

Our proposed technique is also suitable for calculation of elastic and excitation cross sections in electron atom scattering in the frame work of unrestricted Glauber approximation, including the electron exchange effect.

Numerical results will be presented at this conference.

References

- 1 D.P.Dewan, Phys. Rev. A26, 1946 (1982).
- 2 I.S.Gradsteyn and I.M.Ryzhik, Tables of Integrals, Series and Products, p.933, § 8.310(2) (Academic Press, New York, 1980).

ANALYTIC EVALUATION OF SPB AMPLITUDE FOR ARBITRARY ANGULAR MOMENTUM STATES

N. C. Sil and N. C. Deb

Indian Association for the Cultivation of Science, Jadavpur, Calcutta 700032, India.

The strong potential Born (SPB) approximation has emerged in recent years as a fairly good approximation for the investigation of electron capture problems in high energy asymmetric collisions. In this approximation the weaker of the interactions - electron target nucleus and electron-projectile nucleus interactions - is taken to first order and the stronger interaction is kept to all orders via Coulomb Green's function whereas the nuclear-nuclear interaction is completely neglected.

Macek and Alston¹ first systematically derived the SPB amplitude for electron capture from the ground state to a final state ϕ_f (hydrogenic) for the asymmetric collision where the target charge Z_T is greater than the projectile charge Z_p as (in their notation)

$$T_{SPB} = -4\pi Z_p \left(d\vec{p} \tilde{\phi}_f^*(\vec{p}) \left| \vec{p} - \vec{k} \right|^{-2} \left(\frac{4\pi^2}{(2\pi)^{3/2}} N_1 \tau \frac{e^{-i\pi\tau}}{\sin(\pi\tau)} \right) \right. \\ \left. \frac{\partial}{\partial u} (u^2 + J^2)^{-1} \left\{ \frac{[(u-iv)^2 + K^2 + 2\vec{p} \cdot (\vec{J} - iu\hat{v})](p^2 + Z_p^2/n^2)}{4(u^2 + J^2)(v^2 + 2\vec{v} \cdot \vec{p})} \right\}^{-\tau} \right) \quad (1)$$

Treating the term responsible for the Thomas peak exactly, Sil and McGuire² expanded other terms in Eq. (1) in power of Z_p/v of which terms through first order were considered and reduced the amplitude into a linear combination of one dimensional integrals. We consider the zeroth order term in this expansion

$$T_{SPB}^{(0)} = \frac{Ch}{K^2} K^{2i\nu-2} \left(d\vec{p} \tilde{\phi}_f^*(\vec{p}) (TS)^{-i\nu} \right) \quad (2)$$

where C , h , ν , K , T , S are defined in Ref. (2)

Using the general expression for $\phi_f(\vec{p})$ and the integral representation (cf. Ref. 3)

$$x^{-(i\eta-n)} = \frac{(-1)^{n+1}}{2i \sin(i\eta\pi)} (i\eta-n) \int_D (-\lambda)^{i\eta-n-1} e^{-\lambda x} d\lambda \quad (3)$$

the \vec{p} -integral in Eq. (2) can be reduced to the type integral

$$I = \int_0^\infty p^R (p^2 + \lambda^2)^{-M-i\nu} \left[\frac{1}{2i \sin(i\pi\tau)} \Gamma(i\nu) \right. \\ \left. \int_D (-\lambda)^{i\nu-1} e^{-\lambda A} f(\lambda, p) d\lambda \right] dp \quad (4a)$$

where

$$f(\lambda, p) = \int e^{2i\lambda\vec{x} \cdot \vec{p}} Y_{\ell m}(\hat{p}) d\Omega \quad (4b)$$

with

$A = (u-iv)^2 + K^2$, $\vec{x} = i(\vec{J} - iu\hat{v})$, R and M are positive integers.

The θ , ϕ integrations in Eq. (4b) can be carried out in terms of spherical Bessel functions:

$$f(\lambda, p) = \frac{2\pi(i)}{\lambda^{\ell}} \lambda^{\ell} Y_{\ell m}(\hat{x}) \sum_{r=0}^{\ell} \frac{1}{(2\lambda i L p)^{r+1}} \\ \left[a_{rt} e^{-2\lambda L p} + a_{rt}^* e^{2\lambda L p} \right] \quad (5)$$

where

$$L = (\vec{L} \cdot \vec{L})^{1/2}, \quad \vec{L} = -i\vec{x} \quad \text{and} \quad a_{rt} = \frac{i^{r-\ell-1} (\ell+r)!}{r! (\ell-r)! 2^r}$$

Substituting the results for $f(\lambda, p)$ from Eq. (5) in Eq. (4a) we can perform the contour integration with the help of Eq. (3). The integral I can now be expressed in terms of the type integrals

$$G = \int_0^\infty p^J (p^2 + \lambda^2)^{-M-i\nu} (A+2Lp)^{N-i\nu} dp \quad (6)$$

where J , M and N are positive integers.

The integral G has been evaluated analytically. When $J=2k$ (even J)

$$G = \sum_{s=0}^k (-1)^s K_{Cs}(\lambda^2) s_{\lambda_1}(2L)^{N-i\nu} H(M-k+s, N) \quad (7)$$

and when $J = 2k+1$ (odd J)

$$G = \sum_{s=0}^k (-1)^s K_{Cs}(\lambda^2) s_{\lambda_2} \frac{\partial}{\partial L} \left[(2L)^{N+1-i\nu} H(M-k+s, N+1) \right] \quad (8)$$

where λ_1 and λ_2 are two different constants depending on N , M , λ and $i\nu$ and

$$H(M, N) = e^{\frac{i\pi(2\tau_1+1)/2}{(a-1)}} \frac{2^{\tau_1+\tau_2+1}}{\Gamma(1/2) \Gamma(-2\tau_1-\tau_2-1) \Gamma(-\tau_1-1/2)} \\ \frac{2^{\tau_1+1}}{\Gamma(-\tau_1-\tau_2) \Gamma(-2\tau_1-1)} \\ {}_2F_1(-2\tau_1-\tau_2-1, -\tau_1; -\tau_1-\tau_2; 2) \quad (9)$$

with

$$\tau_1 = -M-i\nu, \quad \tau_2 = N-i\nu, \quad a = A/2L\lambda \quad \text{and} \quad Z = (a+i)/(a-i).$$

Reference

1. J. Macek and S. Alston, Phys. Rev. A **26**, 250 (1982).
2. N. C. Sil and J. H. McGuire, J. Math. Phys. (in press).
3. I. S. Gradshteyn and I. M. Ryzhik, Tables of Integrals, series and products, p. 933, § 9.310 (2) (Academic Press, New York, 1980).

CONVOY ELECTRONS FROM 100 KeV H ON CARBON FOILS MEASURED IN COINCIDENCE WITH EMERGING PROTONS AND H ATOMS

P. Focke, W. Meckbach and I. Nemirovsky;* S.D. Berry and I.A. Sellin;* M.G. Menendez and M.M. Duncan**

* Centro Atomico Bariloche and Instituto Balseiro, S.C. de Bariloche, Argentina

+ University of Tennessee, Knoxville, TN 37996 and Oak Ridge National Laboratory, Oak Ridge, TN 37831

** University of Georgia, Athens, GA 30602

There continues to be a great deal of interest in pinpointing the processes responsible for the production of beam-foil convoy electrons. Much of the recent work has been devoted to attributing the origin of these electrons to either production near the exit surface or within the bulk^{1,2,3,4}.

In a previous experiment performed by Laubert, *et al.*⁵, using carbon, oxygen, and silicon projectiles (12-30 MeV) incident on carbon, aluminum, and gold foils, the shape of the convoy spectrum measured in coincidence with each emerging charge state and the yield per emergent ion were found to be substantially independent of the ion charge state. The results of this experiment argues strongly against a surface-layer origin for the convoy electrons, at least, for fast, heavy ion projectiles.

Recently, we have performed a version of the above experiment with a substantially different projectile Z and velocity. Proton beams from the Centro Atomico Bariloche Kevatron at 107 KeV were charge neutralized in a low pressure gas cell. Electrostatic plates downstream removed the proton component of the beam. The incident H atom beam traversed a $2\text{-}3\text{ }\mu\text{g}/\text{cm}^2$ carbon foil (equilibrium thickness) located at the entrance focus of a cylindrical mirror electrostatic electron energy analyzer where convoy electrons emitted within a half-angle of 2.6° were collected. The protons and hydrogen atoms emergent from the foil passed through another electric field which served to deflect the protons. A movable ceramic channel electron multiplier was placed so as to selectively collect each charge state.

Some preliminary results of this experiment were:

(1) unlike Ref. [5], the coincidence yield exhibited a strong dependence on the charge state of the emergent particle; (2) the coincidence yield per emergent H atom was found to be non-zero — this is qualitatively consistent with H atoms arising from the subsequent neutralization of protons associated with a convoy electron production event toward the end of the projectile's path through the foil.

These measurements at 100 KeV/amu are being repeated and extended to higher energies at The University of Georgia.

This work has been supported, in part, by CNEA (Argentina), NSF Divisions of International Programs and Physics, and US-DOE under contract DE-AC05-84OR21400 with Martin Marietta Energy Systems, Inc.

References

1. M. Breinig, *et al.*, Phys. Rev. **A25**, 3015 (1982).
2. H.-D. Betz, *et al.*, Phys. Rev. Lett. **50**, 34 (1983).
3. Y. Yamazaki and N. Oda, Phys. Rev. Lett. **52**, 29 (1984).
4. I.A. Sellin, *et al.*, Lecture Notes in Physics **213**, 109 (1984).
5. Roman Laubert, S. Huldt, M. Breinig, L. Liljeby, S. Elston, R.S. Thoe and I.A. Sellin, J. Phys. B **14**, 859 (1981).

CHARGE CHANGING PROCESSES IN HIGHLY CHARGED ($v \gg v_0$) ION-ATOM COLLISIONS STUDIED BY O^D -ELECTRON SPECTROSCOPY

L.H.Andersen, P.Hvelplund, H.Knudsen, and J.O.Pedersen

Institute of Physics, University of Aarhus, DK-8000 Aarhus, Denmark

In collisions between highly charged ions of medium and high velocity (V) and atoms both single electron processes (Electron Capture to the Continuum) and multiple electron processes (Transfer Ionization, and in some cases Transfer Excitation and Double Excitation) lead to creation of free electrons that are slow in the projectile frame. Essential features of these processes can therefore conveniently be studied by O^D -electron spectroscopy which is especially sensitive to such electrons (1). In order to establish in which reaction channel the electron was created it is often necessary to measure emitted electrons in coincidence with the outgoing ionic charge state.

The ECC mechanism leads to a cusp at $V_e = V$. Taking into account the spectrometer transmission function such spectra can be fitted to a multipole expansion of the double differential cross section for electron scattering in the projectile rest frame where the leading terms are:

$$\left(\frac{d^2\sigma}{d\Omega dE}\right)_{\text{proj}} = B_0^{(o)} \left(1 + (B_1^{(o)}/B_0^{(o)}) \cos \Theta' + \dots\right) \quad (1)$$

and Θ' is the projectile frame scattering angle. The basic information about the ECC process lies in the two coefficients of eq.(1). In our experimental investigation we used a He target and 1-3 MeV H^+ , 1-10 MeV He^{2+} , 12-40 MeV O^{8+} , and 20-72 MeV Au^{11+} projectiles to determine the ion velocity and charge dependency of the two coefficients.

We have performed a similar cusp-shape analysis to investigate the TI process in the collision system 20 MeV $Au^{11+} + He$ as it was found that in this case TI results in one projectile bound-state electron and one low-energy projectile continuum electron. Thus TI results in a cusp of electrons in the $q \rightarrow q-1$ coincidence channel. From the cusp-shape analysis, it was shown that for $q \sim 15$, most likely two electrons are transferred to the projectile, one of which is subsequently lost to the continuum. By considering total TI cross sections, it was found (2) that the independent-particle approximation is invalid for this process, and we suggest that the electron loss is caused by the creation and decay of a highly excited, highly correlated two-electron state. Thus, despite the high ionic charge, electron-electron correlation is believed to play a significant role in this process.

The TE process may lead to emission of projectile frame slow electrons of discrete energy. We have studied the cross section for such emission for the collision

systems C^{2+} , O^{4+} , $F^{5+}(1s^2 2s^2)$ on Ar and 20 MeV Au^{11+} on He at medium projectile velocity. At high projectile velocity double projectile excitation (DE) takes over as the dominating process leading to such emission.

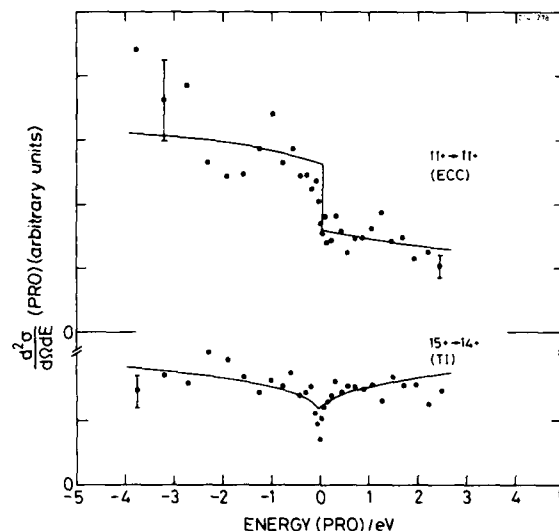


Figure 1 ECC and TI electron spectra for 20 MeV Au ($q=11,15$) on He.

References

- (1) L.H.Andersen, M.Frost, P.Hvelplund, and H.Knudsen, J. Phys.B **17**, 4701 (1984)
- (2) M.R.C.McDowell and R.K.Janev, J.Phys.B **17**, 2295 (1984)

THRESHOLD LAW FOR SIMULTANEOUS RYDBERG ELECTRON AND CONVOY ELECTRON PRODUCTION

H.-P. Hülshöfter, M. Breinig, J. Burgdörfer, S.B. Elston, P. Engar and I. A. Sellin

University of Tennessee, Knoxville, TN 37996 and Oak Ridge National Laboratory, Oak Ridge, TN 37831

The threshold behavior of the cross section for break-up of a three-body Coulomb interacting system has become of considerable interest in recent years [1]. Previous experiments involving these threshold laws have been carried out with either electron [2] or photon impact [3] to produce doubly excited states in the threshold continuum. They show agreement with the pioneering classical analysis by Wannier [4] predicting a threshold law

$$\sigma \propto E^m \quad (1)$$

$$E \rightarrow 0$$

where the Wannier exponent is given by

$$m = \frac{1}{4} \left[\left(\frac{100Z-9}{4Z-1} \right)^{1/2} - 1 \right]. \quad (2)$$

This exponent has later been confirmed by a quantum mechanical analysis using three-body Coulomb wave functions near threshold [5]. Extrapolating the Wannier continuum functions across the ionization limit Feagin and Macek [6] have calculated the positions and width of a Rydberg series of doubly excited resonances.

Our experiment tests the Wannier threshold law for a closely related but not previously explored process in which a doubly excited state is produced with the one electron in the low-energy continuum while simultaneously another electron is excited to a high Rydberg state close to one-electron ionization threshold. Since the total energy of this doubly excited state is close to the three-body break-up threshold energy, the Wannier threshold law should be reflected in the n distribution of the Rydberg electron and the velocity distribution of the continuum electron.

Fast O_9^+ ions traversing solid targets may exit in highly excited states or may be accompanied by convoy electrons moving with velocity, v_e approximately equal to ion velocity v . Those convoy electrons lie in the low-energy continuum in the rest frame of the projectile. We measure triple coincidences of a convoy electron, a Rydberg electron, and the charge state of the outgoing projectile.

The experimental setup consists of a 30° analyzer, with its focus at the foil, to detect the convoy electrons, an inhomogeneous-field stripper followed by a spherical sector analyzer to detect the Rydberg electrons and

finally an electrostatic charge state analyzer. The dimensions of the 30° -analyzer have been chosen to minimize the field strength and consequently to maximize the transmission of Rydberg electrons. The inhomogeneous-field stripper consists of two concentric spheres. The ion beam passes through it in a radial direction. Because different n -states are ionized at different positions inside the stripper, an interval of approximately 10 to 20 n -levels is detected with one applied voltage. Since the gain in kinetic energy depends on the position of ionization of the Rydberg electron [7], the n -distribution within such an interval can be measured with high resolution. By varying the voltage we scan over the Rydberg distribution.

Experimental data will be presented for the energy partition between convoy and Rydberg electrons and the Z dependence of the Wannier exponent.

Work supported in part by the National Science Foundation; and by the U.S. Department of Energy, under contract DE-AC05-84OR21400 with Martin Marietta Energy Systems, Inc.

References

- [1] See for example, XIII ICPEAC (Berlin) 1983, book of invited papers.
- [2] P. Hammond, F.H. Read and G.C. King, J. Phys. B. **17**, 2925 (1984).
- [3] Y.K. Bae, M.J. Coggiola and J.R. Peterson, XIII ICPEAC (Berlin) 1983, p. 783.
- [4] G.H. Wannier, Phys. Rev. **90**, 817 (1953).
- [5] A.P. Rau, Phys. Rev. A **4**, 207 (1971).
- [6] J.M. Feagin and J. Macek, J. Phys. B **17**, L245 (1984).
- [7] K.B. MacAdam and R.G. Rolfes, Rev. Sci. Instrum. **53**, 592 (1982).

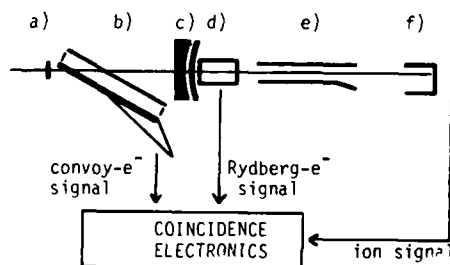


Fig. 1. A schematic diagram of the experimental setup: a) foil, b) 30° analyzer, c) inhomogeneous-field stripper, d) spherical sector analyzer, e) charge state analyzer, f) Faraday cup

STATISTICAL MULTIPOLES FOR CUSP ELECTRONS AND RYDBERG ELECTRONS

Joachim Burgdörfer

University of Tennessee, Knoxville, TN 37996 and Oak Ridge National Laboratory, Oak Ridge, TN 37831

Cross sections for electron emission in inelastic ion-atom collisions show a strong enhancement at electron velocities v_e approximately equal to the projectile velocity v_p . This gives rise to a cusp in the experimentally observed doubly-differential cross section (DDCS) $d\sigma/dv$ where $v = v_e - v_p$ denotes the electron velocity in the rest frame of the projectile. Two different processes contribute to the cusp: target ionization (i.e., electron capture to continuum (ECC)) and projectile ionization (i.e., electron loss to continuum (ELC)). In both cases, the final electronic state lies in the low-energy continuum ($v \rightarrow 0$) of the projectile.

Recent experiments^{1,2} display a large variety of anisotropies and asymmetries described by nonvanishing anisotropy coefficients β_k in the multipole expansion of its DDCS

$$\frac{d\sigma}{dv} = \frac{\sigma}{v} \sum_{k=0}^{\infty} \beta_k P_k(\cos \theta) \quad (1)$$

High-order multipoles ($k > 2$) in the electron distribution provide detailed information on the excitation function not easily accessible by other means (e.g., dipole radiation). The presence of high-order multipoles in the near-zero velocity continuum is linked to Wigner's threshold law for an attractive Coulomb field³ predicting that all partial-waves are present at threshold. Cusp anisotropies can therefore be traced to coherences between different partial waves.

We have developed a unified description of cusp anisotropies in terms of statistical multipoles $\langle U_k^k \rangle$,

$$\beta_k = (2k+1)^{1/2} \frac{\langle U_k^k \rangle}{\langle U_0^0 \rangle} \quad (2)$$

The spherical multipoles U_k^k are built up by the two generators of the dynamical $O(4)$ symmetry group of the Coulomb field, the angular momentum L and the Runge-Lenz vector A . The statistical multipoles $\langle U_k^k \rangle$ contain the orientation and alignment parameters introduced by Fano and Macek⁴ for bound-state excitation as a subset. They yield a systematic expansion of various cusp anisotropies in terms of partial-wave coherences in the threshold continuum.

The present approach permits a unified description of anisotropic electronic distribution in high Rydberg states and low-lying continuum states. The same set of multipoles $\langle U_k^k \rangle$ determines the multipolarity of the bound-state electronic distribution in high Rydberg states and the multipolarity of the emitted low-energy

electrons. Using the continuity of $\langle U_k^k \rangle$ across the ionization limit the multipole moments of Rydberg electrons may be deduced when anisotropies of cusp electrons are known, and vice versa.

As an application of this approach we present a simultaneous theoretical determination of bound-state and continuum state multipoles for direct excitation (Fig. 1) and charge transfer in the Born and the Continuum Distorted Wave approximations, respectively. Comparison will be made with recent experimental data^{2,5} for ELC ($n 5^+ + \text{He} \rightarrow n 6^+ + \text{He} + e$) and the ECC ($\text{C} 6^+ + \text{H} \rightarrow \text{C} 6^+ + e + \text{H}^+$). The dipole moment of a high Rydberg orbit formed by charge transfer will be determined for the first time.

Work supported by the National Science Foundation, the U.S. Department of Energy, under contract DE-AC05-84OR21400 with Martin Marietta Energy Systems, Inc., and the Deutsche Forschungsgemeinschaft (Sonderforschungsbereich 161).

References

1. W. Meckbach, R. Vidal, P. Focke, I. B. Nemirowski, and C. E. Gonzales-Lepera, Phys. Rev. Lett. **52**, 621 (1984).
2. S. B. Elston, S. D. Berry, M. Breinig, R. DeSerio, C. E. Gonzales Lepera, I. A. Sellin, K. O. Groeneveld, D. Hofmann, P. Koschar, I. B. Nemirowski, and L. I. Liljehy in Lecture Notes in Physics **213** (Springer-Verlag, Berlin, 1984), p. 75.
3. E. P. Wigner, Phys. Rev. **73**, 1002 (1948).
4. U. Fano and J. Macek, Rev. Mod. Phys. **43**, 553 (1973).
5. S. D. Berry, G. A. Glass, I. A. Sellin, K. O. Groeneveld, D. Hofmann, L. H. Andersen, M. Breinig, S. B. Elston, P. Engar, and M. Schauer, Phys. Rev. A (1985) in press.

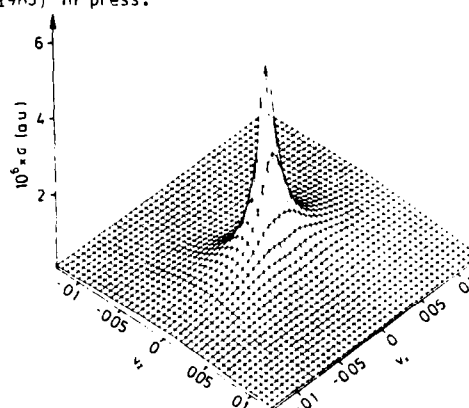


Figure 1: Electron distribution for ELC $\text{H}(2s) + \text{He} \rightarrow \text{H}^+ + \text{He} + e$ at $v_p = 10 \text{ a.u.}$

THE $v=v_p$ PEAK IN H^0+H_2O COLLISIONS*M.E. Rudd and M.A. Bolorizadeh,[†] University of Nebraska, Lincoln, NE 68588-0111

Charge transfer to the continuum¹ (CTC) is known to produce a peak in the spectrum of electrons ejected in ion-atom collisions at a velocity $v=v_p$ where v_p is the projectile velocity. A similar peak appears in collisions in which the incident ion carries one or more electrons. This peak, first noted by Wilson and Toburen,² arises from electrons, detached from the projectile, making elastic collisions with the target. The peak due to this mechanism (called electron loss to the continuum or ELC) is not as sharply peaked in the forward direction as the CTC peak, but as for elastic electron scattering, it falls off with increasing angle. ELC peaks have also been seen in H^0 -He collisions³ and in H^+ -Ar collisions.⁴

Our recent measurements of doubly differential cross sections for ejection of electrons from water vapor by H^+ and H^0 from 20-150 keV yield additional information about the $v=v_p$ peak. Fig. 1 shows the peaks in plots of the ratio of cross sections of H^0 to H^+ . For small angles the size of the peak decreases with increasing angle, but the peak becomes unexpectedly large again at large angles. Fig. 2 shows the peak height vs angle. Also shown is the absolute height to indicate that the rise of the $v=v_p$ cross section in the backward direction is real and not just relative to the proton cross section.

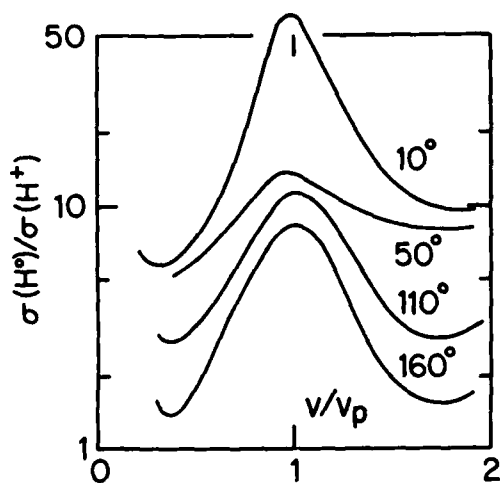


Fig. 1: Ratio of cross sections for ejection of electrons by H^0 to those for H^+ . The curves have been displaced in the vertical direction by arbitrary amounts for clarity. Beam energy, 150 keV.

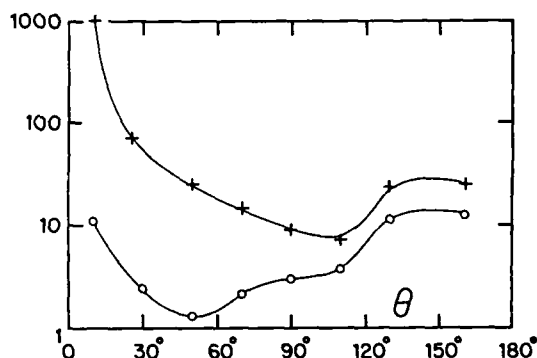


Fig. 2: Lower curve; height of the peak in the ratio of H^0 to H^+ cross sections vs angle. Upper curve; height of the peak in the curve of $v^2 [\sigma(H^0) - \sigma(H^+)]$. For this curve the units on the ordinate are $10^{-22} \text{ m}^2/\text{sr}$.

The rise in the backward direction can be partially explained as follows. In the reference frame of the H^0 projectile, the target molecule has a velocity v_p in the backward direction. During a binary collision it ejects an electron from the H^0 at an angle θ' with a velocity $2v_p \cos \theta'$. See Fig. 3. Translating to the laboratory frame, we add the vector v_p in the forward direction. The resultant can easily be shown to be a velocity v_p at an angle θ where $\theta > 90^\circ$. So, while the forward $v=v_p$ peak is due to ELC, the backward peak can be interpreted as due in part to the binary encounter peak from the projectile translated to the laboratory reference frame.

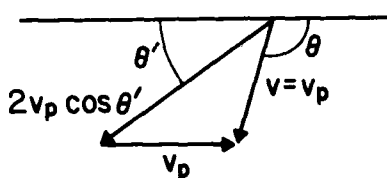


Fig. 3: Velocity vector diagram

We wish to thank J. Macek for helpful discussions.

*This paper is based on work performed under National Science Foundation Grants No. PHY82-25500 and PHY-8401328.

[†]Present address, Kerman University, Kerman, Iran.

References

1. Joseph Macek, Phys. Rev. A **1**, 235 (1970).
2. W.E. Wilson and L.H. Toburen, Phys. Rev. A **7**, 1535 (1973).
3. M.E. Rudd, J.S. Risley, J. Fryar, and R.G. Rolfs, Phys. Rev. A **21**, 506 (1980).
4. M.M. Duncan and M.G. Menendez, Phys. Rev. A **19**, 49 (1979).

ON THE PRODUCTION OF CONVOY-ELECTRONS IN ION-FOIL INTERACTION

R.Schramm*, H.-D.Betz*, P.Koschar*, M.Burkhardt*, J.Kemmler*, O.Heil*, and K.O.Groeneveld*

*Sektion Physik, Universität München, 8046 Garching, W.-Germany

*Institut für Kernphysik, August-Euler-Str. 6, 6 Frankfurt, W.-Germany

In a recent Letter¹ it has been predicted that the yield of convoy electrons obtained in fast ion-solid interaction should exhibit a dependence on the charge state of the incident ions, in marked contradiction to other assumptions^{2,3}. So far, pronounced target-thickness dependent yields have been observed especially for molecular ions (H_2^+) traversing carbon foils⁴.

The Munich Tandem van-de-Graaff accelerator was used to pass 125-MeV sulfur ions with initial charge states 10^+ to 16^+ through carbon foils with thicknesses between 2- and 200 $\mu\text{g}/\text{cm}^2$. A magnetic spectrometer served to measure convoy electrons ejected into the forward direction ($0 \pm 0.3^\circ$). Fig.1 displays an electron spectrum and shows both the cusp shaped convoy-electron peak and the binary-encounter peak which reflects the doppler-broadened Compton profile of the target electrons.

Fig.2 gives the yield of convoy electrons for various target thicknesses and incident charge states. Below $\sim 50 \mu\text{g}/\text{cm}^2$ the yield is found to depend strongly on the target thickness, whereas above $\sim 100 \mu\text{g}/\text{cm}^2$ all measured yields agree within less than 10%. It becomes obvious that the yield increases with the number of projectile electrons brought into the collisions in the target, and equilibrates in accordance with the distribution of ionic charge- and excitation states¹. We conclude as follows:

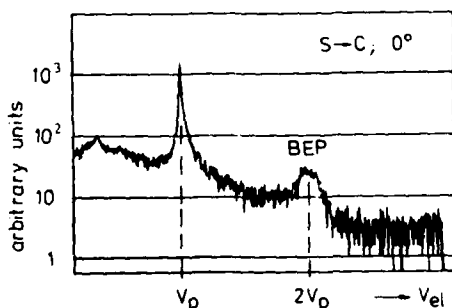


Fig.1: Yield of electrons observed in forward direction, for 125-MeV sulfur ions in $4.5 \mu\text{g}/\text{cm}^2$ carbon, as a function of electron velocity.

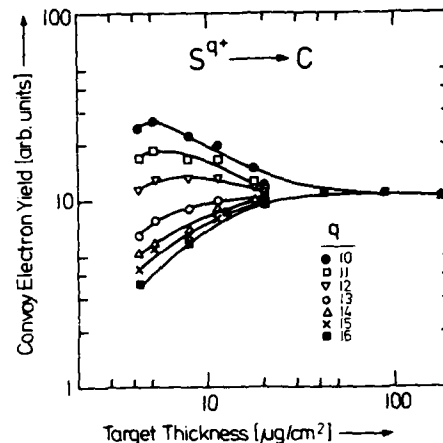


Fig.2: Yield of convoy electrons as a function of carbon target thickness; parameter is the charge of the incident 125-MeV sulfur ions.

- the major part of convoy electrons arises due to loss of projectile electrons to the continuum (ELC-process);
- the form of the target-thickness dependence of the convoy electron yield reflects the evolution of charge- and excitation states of the projectile inside the solid.

As regards the latter point, we like to emphasize that the mean free path of convoy electrons can not be directly extracted from the type of data shown in Fig.2; such attempts must be viewed with suspicion⁵. At present, we try to exploit our data to obtain realistic mean free paths taking into account charge exchange of the ions and multiple scattering of the electrons.

This work was supported by the Bundesministerium für Forschung und Technologie.

References

1. H.-D.Betz et al., PRL **50**,34(1983).
2. I.A.Sellin et al., NIM **170**,557(1980).
3. I.A.Sellin, in "Physics of Electronic and Atomic Collisions (S.Datz,ed.), p.195, North-Holland, New York (1982); see also section IV, available from the author.
4. P.Koschar et al., in "Lecture Notes in Physics" (H.Araki et al., ed.), Vol.213, p.129 Springer, Berlin (1984).
5. I.A.Sellin et al., ebd., p. 109.

DEPENDENCE OF THE ECC "CUSP" YIELD ON THE PROJECTILE Z
FROM THE STUDY OF THE SIMPLEST COLLISION SYSTEMS

D. Berényi⁺, Á. Kovér⁺, Gy. Szabó⁺, L. Gulyás⁺, K.O. Groeneveld^{*},
D. Hoffmann^{*} and M. Burkhard^{*}

⁺ Institute of Nuclear Research of the Hung. Acad. Sci., Debrecen, Hungary

^{*} Institute for Nuclear Physics of J.W. Goethe Univ. Frankfurt/M. Germany

As is well-known, in the electron spectrum from ion-atom collisions a cusp-shaped peak is observed in the forward direction centered near the velocity of the projectile. The dependence of the cusp yield on the Z of the projectile has been studied only in the case of heavy ions^{1,3/}. However, no experimental data have been published on this dependence for the simplest collision systems.

In the present study the cusp was studied in H⁺-He and He⁺⁺-He collisions at 0.4, 0.5 and 0.6 MeV/amu impact energies.

The measurements were carried out at the 2.4 MV Van de Graaff accelerator of the Institute for Nuclear Physics of the J.W. Goethe University, Frankfurt/M. by using a special double pass cylindrical mirror electron spectrometer /ESA-13/ constructed in ATOMKI, Debrecen^{2/}. Here the angular acceptance of the measured electrons is determined at the exit of the spectrometer.

The evaluation of the spectra from the point of view of Z dependence was carried out in two different ways. First the cusp intensities were determined by subtraction of the continuous "background" in the spectra, and on the basis of these values, the exponent of Z was calculated. On the other hand the basis for the determination of Z dependence was the cusp intensity between the velocity limits /1-a/ and /1+a/, where $a = \pm 0.04$ around the top of the cusp. Both methods gave 2.5 ± 0.3 for the exponent in the present study /the corresponding value obtained at heavy ions is equal to 2.3 ± 0.3 /^{3/}.

If we insert our cusp intensity values for He⁺⁺ projectile into the diagram of Sellin et al.^{3/} /after normalization at H⁺/, it fits well on straight line as can be seen in Fig. 1 /the geometrical conditions and the energy resolution are nearly the same in the two cases/, although the present datum was determined in the 0.4 - 0.6 MeV/amu impact energy interval and that of Sellin et al. was observed at 2.5 MeV/amu in case of Fig. 1.

It can be stated that the Z dependence of the cusp yield at bare projectiles seems to be the same in a broad impact energy region both for light and heavier incident ions.

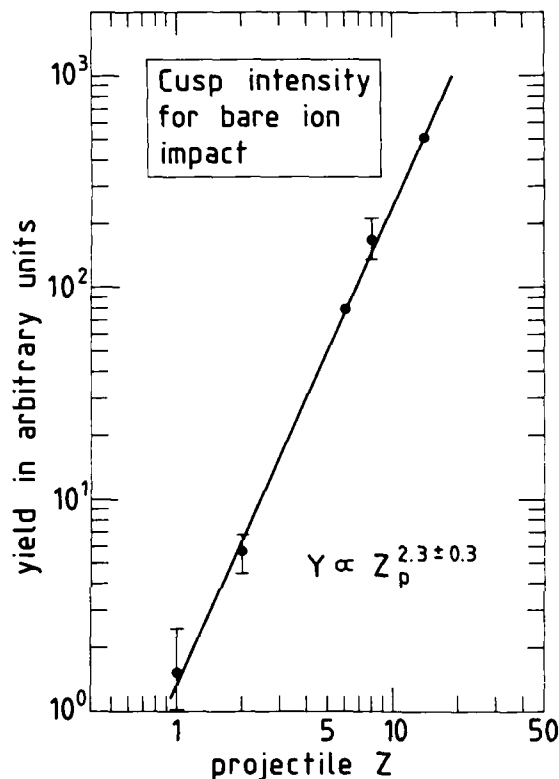


Fig.1. The present yield value for He⁺⁺ projectile /normalized by the help of our datum for H⁺/ fits well to Breinig et al.^{3/} data in the Z dependence diagram obtained at heavier incident ions /C⁶⁺, O⁸⁺, Si¹⁴⁺/.

References

- 1/ C.R. Vane, I.A. Sellin, M. Suter, G. Alton, S.B. Elston, P.M. Griffin and R.S. Thoe, Phys. Rev. Lett. **40** /1978/ 1020.
- 2/ D. Berényi, L. Gulyás, Á. Kovér, E. Szmola, Gy. Szabó, M. Burkhard and K.O. Groeneveld, Proc. Aarhus Conf., Lecture Notes in Phys. **213**. Springer Vlg., 1984. p.71.
- 3/ M. Breinig, S.B. Elston, S. Hultdt, L. Kilgeby, C.R. Vane, S.D. Berry, G.A. Glass, M. Schauer, I.A. Sellin, G.D. Alton, S. Datz, S. Overbury, R. Laubert and M. Suter, Phys. Rev. **A25** /1982/ 3015.

RADIATIVE ELECTRON CAPTURE IN PROTON-HYDROGEN COLLISION

Jorge E. Miraglia

Instituto de Astronomía y Física del Espacio, C.C.: 28, Suc.: 28, 1428 Buenos Aires, Argentina

The IS-IS proton-hydrogen radiative electron capture has been studied within the nonrelativistic semiclassical approximation. In this approach the radiation-matter matrix element is calculated in first perturbative order¹, with the use of distorted wave functions currently used in mechanical collision theory.

Several three-particle theoretical methods such as: the continuum distorted wave² (CDW), first Born, and the exact and peaking impulse approximations (EIA and PIA) have been applied.

The CDW is found to present a projectil angular distribution with two critical angles, i.e. two enhancements. These critical angles depend on the emitted photon energy. The positions of these peaks occur at projectile angle

$$\theta^{\pm} = \theta_{Th} \sqrt{\left(1 \pm \frac{2\omega}{v^2}\right) - \frac{1}{4}\left(1 \pm \frac{2\omega}{v^2}\right)^2}$$

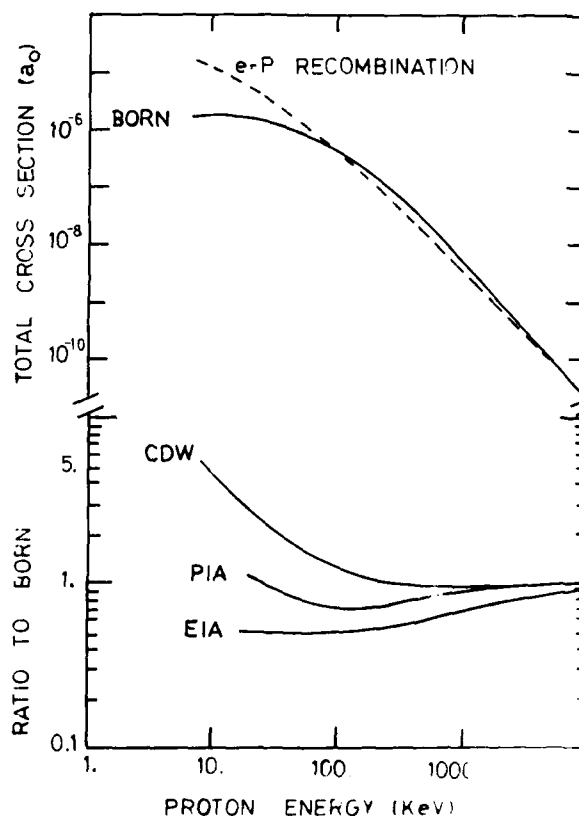
where θ_{Th} is the critical angle of Thomas³ which occurs in the mechanical electron capture, ω is the photon energy and v is the projectile velocity. At θ^{\pm} the differential cross section presents delta-type behaviours. These critical angles can be physically explained in terms of a mechanical collision with the projectile (or the target) followed (or preceded) by an interaction with the radiation field. Note when $\omega = 0$, θ^{\pm} coincide with the Thomas' one. Unlike the mechanical electron capture⁴, we found that the contribution of these critical angles to the total cross section can be neglected.

We found that the exact impulse approximation presents no critical angle.

We have also calculated total cross sections, and found that all the distorted wave methods considered tend to the first order Born approximation as the projectile velocity increases, in contrast with the strong potential Born theory⁵ (see the figure). Furthermore, the three-particle Born approximation tends, as far as the total cross section is concerned, to the binary electron-projectile radiative recombination, as proved in reference 1.

References

1. J.S. Briggs and K. Dettmann, Phys. Rev. Lett. **33**, 1123 (1974).
2. A. Gonzalez and J.E. Miraglia, Phys. Rev. A **30**, 2292 (1984).
3. K. Dettmann, Springer Tracts in Modern Physics **58**, 119 (1971).
4. R.D. Rivarola and J.E. Miraglia, J. Phys. B **15**, 2221 (1982).
5. H. Gorritz, J.S. Briggs and S. Alston, J. Phys. B **16**, L665 (1983).



AD-A163 497

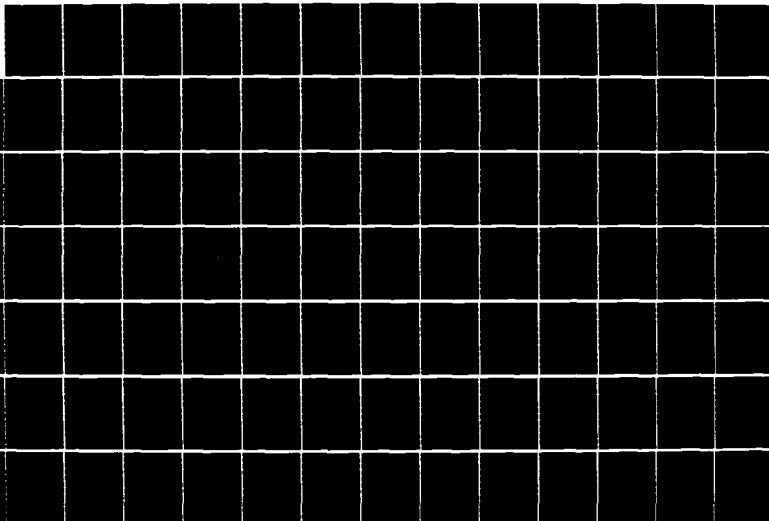
ELECTRONIC AND ATOMIC COLLISIONS ABSTRACTS OF
CONTRIBUTED PAPERS INTERNAT. (U) SRI INTERNATIONAL
MENLO PARK CA MOLECULAR PHYSICS CENTER
H J COGGIOLA ET AL. 1985

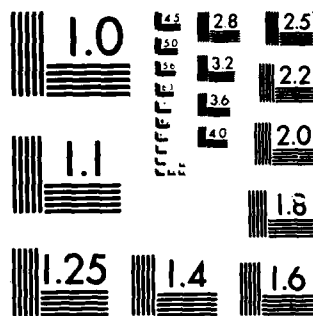
778

UNCLASSIFIED

FFG 7/4

NL





MICROCOPY RESOLUTION TEST CHART
NATIONAL BUREAU OF STANDARDS-1963-A

X-RAY DIFFERENTIAL CROSS SECTION FOR RADIATIVE ELECTRON CAPTURE

J.E. Miraglia^{††}, C.R. Garibotti^{††} and A. Gonzalez^{††}[†] Instituto de Astronomía y Fis. del Espacio, CC 67, Suc. 28, 1428 Buenos Aires, Argentina.^{††} Instituto Balseiro, 8400 S.C. de Bariloche, R.N., Argentina.
Consejo Nacional de Investigaciones Científicas y Técnicas.

X-ray cross sections for high energy Ar^{17+} and Ne^{10+} ions passing through neutral He and Ne targets have been measured by Kienle et al.¹. The structures and enhancements in the experimental photon spectrum produced in radiative electron capture (REC) are not fully explained by the K-K capture considered up to now. Here we obtain a detailed description of it, in terms of electronic transitions from K or higher target shells to projectile shells. We applied the usual theoretical treatment². Using first order Born wave functions, the five-fold differential cross section reads³:

$$\frac{d\sigma^{\text{REC}}}{d\omega d\Omega d\Omega'} = \frac{v_T v_P \omega}{2^4 \pi^4 c^3} |\tilde{\phi}_i(\mathbf{w}_T) \tilde{\phi}_f(\mathbf{w}_P)|^2 \sum_{j=1}^2 |\hat{\lambda}_j \cdot \tilde{\mathbf{w}}_P|^2$$

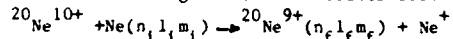
Here $\tilde{\phi}_i$ and $\tilde{\phi}_f$ are the Fourier transformations of the initial and final states; $\tilde{\mathbf{w}}_T$ and $\tilde{\mathbf{w}}_P$ depend on the initial and final momenta: $\tilde{\mathbf{w}}_T = \mathbf{k}_f - \mu \mathbf{k}_i$, $\tilde{\mathbf{w}}_P = \mathbf{k}_i - \mu \mathbf{k}_f$, and $\hat{\lambda}_j$ are the polarization vectors. The electronic initial and final states are described by Clementi-Roetti and hydrogenic wave functions respectively.

The X-ray spectrum associate with the i-f REC transition has an enhancement with a shape determined by the momentum distribution of the initial state $\tilde{\phi}_i(\mathbf{w}_T)$. The position of the peak occurs when \mathbf{w}_T is minimum and is located near $\omega_0 = v^2/2 + \epsilon_i - \epsilon_f$, since the projectile is mainly scattered in forward direction.

Our theoretical results for the photon emission cross section at 90 degrees relative to the incident beam are compared in figs. 1 and 2 with the corresponding experimental data for two different processes. In figure 1, the results for the reaction: $^{20}\text{Ne}^{10+} + \text{He}(1s) \rightarrow ^{20}\text{Ne}^{9+}(n_f l_f m_f) + \text{He}^+(1s)$

are displayed for 140 Mev incident energy. The $K \rightarrow K$ ($1s-1s$), $K \rightarrow L(1s-2s, 1s-2p_{0,\pm 1})$ transitions are

included. In fig. 2 we show results for:



at 140 Mev. The $K \rightarrow K, L, M$ and $L \rightarrow K, L, M$ transitions are considered. In both figures the solid curve represents the sum of all contributions to the cross section.

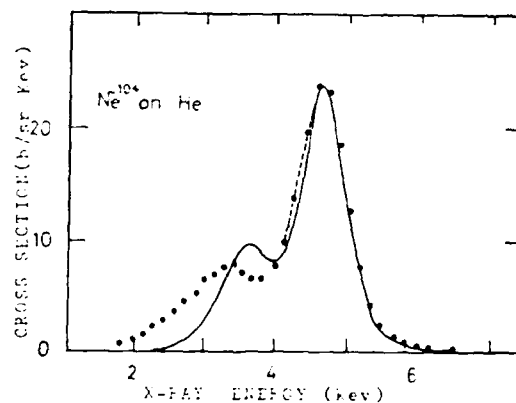


Fig. 1: Differential cross section for x-rays emitted at 90 degrees from the incident beam. Ne on He at 140 Mev incident energy. —, present theoretical results. ----, previous theoretical results¹. •, experimental results.

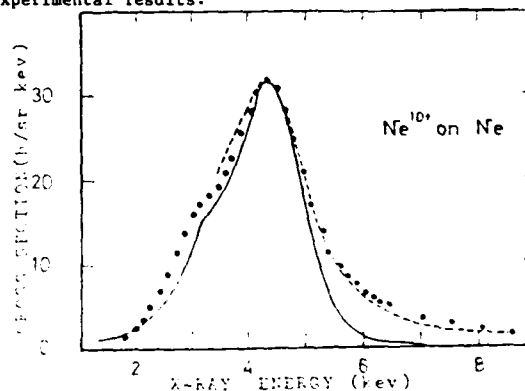


Fig. 2: As in fig. 1 for the process Ne on Ne at 140 Mev incident energy.

We conclude that the enhancements in the photon spectrum associate with REC processes, and not explained before, are due to the capture into excited projectile states or to the capture of electrons coming from higher target shells.

1. P. Kienle et al, Phys.Rev.Lett. **31**, 1099 (1973).
2. J.S. Briggs, K. Dettmann, Phys.Rev.Lett. **33**, 1123(1974)
J. Phys. B **10**, 1113 (1977)
3. A.D. González, J. Miraglia, Phys.Rev. **A30**, 2292 (1984).

RELATIVISTIC TREATMENT OF RADIATIVE ELECTRON CAPTURE

K.HINO, I.SHIMAMURA*, and T.WATANABE*

Department of Applied Physics, Tokyo University, Bunkyo-ku, Tokyo 113 Japan

*The Institute of Physical and Chemical Research, Wako-shi, Saitama 351-01 Japan

It has been clarified that the process of radiative electron capture (REC) cannot be treated by the non-relativistic quantum mechanical theory. The first reason is that non-relativistic formula for REC process except in the c.m. frame leads always to the so-called "spurious radiation"⁽¹⁾. Secondly, if the interaction of radiation field with the three charged particles; i.e. projectile nucleus (charge Z_a and mass m_a), target nucleus (Z_b and m_b), and a bound electron (Z_c and m_c), are considered in the c.m. frame by non-relativistic quantum mechanical method, another radiation term comes out. This term depends on the masses of projectile and target nuclei, that is, the nuclear contributions to the photon emission cross section become comparable to the electron contribution. The transition matrix, T_{fi} , of the 1st.- order Born approximation for REC process is written in natural units ($M=c=1$) by

$$T_{fi} = -(\pi/2\omega)^{1/2} (e \cdot \mu \nu) [Z_a/m_a - (Z_b + Z_c)/(m_b + m_c)] \psi_i(p_i) \cdot Q_f^*(-v), \quad (1)$$

where $\mu = m_a(m_b + m_c)/(m_a + m_b + m_c)$, e is the polarization vector, v the incident velocity, and the others have usual meanings. However, such projectile mass dependence (isotope effect) was not observed in the recent experiment of Ne^{9+} on ^3He target and on ^4He target.

In addition, recent experimental measurements in relativistic impact velocity region shows that the differential cross section for REC is proportional to squared sine of scattering angle in the laboratory frame. On the other hand, that in the c.m. frame is proportional to squared sine of scattering angle in the c.m. coordinate.

In this article we will present the formulation of REC process from the viewpoint of relativistic quantum field theory; particular attention will be paid for the elimination of nuclear mass dependence term from the transition matrix element. However, all features of cross section for REC will be able to be successfully explained by introducing this covariant formulation.

Here, all of the particles are considered as half-spin fermions. The grand assumption is set up as follows. Non-relativistic Weinberg equation would be extended directly to the relativistic formula except for two-body interaction term. Weinberg-like relativistic equation can be symbolically written as

$$K_{abc} = (1 - F_{abc})^{-1} S'_{F,a} G_{bc}, \quad (2)$$

where $S'_{F,a}$, G_{bc} , and K_{abc} stand for a one-body, a two-body, and a three-body propagators, respectively, and F_{abc} represents the relativistic Weinberg kernel. A three-body REC propagator, $K_{abc,\mu}$, is easily introduced, by using Schwinger's method of functional derivative about the external c-number source, J_μ ,⁽²⁾ as

$$K_{abc,\mu} = \langle 0|U|0 \rangle^{-1} i \delta \langle 0|U|0 \rangle K_{abc} / \delta J_\mu, \quad (3)$$

where $\langle 0|U|0 \rangle$ means a scattering matrix bracketted by vacuum states. The terms, M , corresponding to those in the square bracket of eq.(1) are expressed as

$$M = Z_a (r^a e) D_b(K') D_c(P-K') + Z_b D_a(K) (r^b e) D_c(P'-K) + Z_c D_a(K) D_b(K') (r^c e). \quad (4)$$

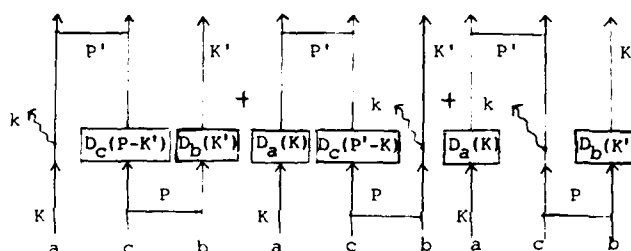


Fig.1 Feynman diagrams of the 1st.-order REC S-matrix

K : incident vector of a , K' : recoil vector of b , P and P' : barycentric vectors of $(b-c)$ and $(a-c)$, respectively, and k : emitted photon vector

$$D_k(p) = -i p \gamma^k m_k \quad (k=a, b, \text{ and } c)$$

Furthermore, the Feynman diagrams of the lowest-order S-matrix are described in Fig.1 including the meanings of some vectors and $D_a(K)$, etc. Taking the non-relativistic limit in eq.(5) by means of the approximation,

$\langle \gamma \rangle \sim -p/m$ and $\langle \gamma^4 \rangle \sim 1$, where $\langle \gamma \rangle = \langle u^+ \gamma u \rangle$, gets to the following conclusion in the c.m. frame;

$$\langle M \rangle \sim (e \cdot \mu \nu) [m_b m_c Z_a / m_a - m_a (m_c Z_b + m_b Z_c) / (m_a + m_b + m_c)]. \quad (5)$$

By the way, another interaction, M' , instead of M is defined as

$$M' = Z_a (r^a e) + Z_b (r^b e) + Z_c (r^c e), \quad (6)$$

which, in fact, leads to the same result of the isotope effect expressed in eq.(1). However, M' cannot be obtained from the covariant treatment.

References

- (1) R. Shakeshaft and L. Spruch: Phys. Rev. Lett. **38**, 175 (1977)
- (2) J. Schwinger: Proc. Nat. Acad. USA, **38**, 452 and 455 (1951)

INNER SHELL VACANCY PRODUCTION AND RADIATIVE ELECTRON CAPTURE IN ATOMIC COLLISIONS WITH HIGH ENERGY HEAVY IONS

D.H.H. Hoffmann*, R. Anholt**, P.H. Mokler*, W.A. Schönfeldt*, E. Morenzoni*

* GSI-Darmstadt, Germany ** Stanford University, Stanford, California 94305 USA

* ETH-Zürich, Switzerland

The processes of inner shell excitation have been investigated only very little for energies above 10 MeV/u, but very intensive studies to explore inner shell ionization phenomena have been performed in previous years¹ and only very recently these experiments have been extended to include relativistic energies².

At low impact energies (≤ 6 MeV/u) typical molecular effects govern the mechanisms of inner shell vacancy formation, whereas at relativistic projectile energies atomic models of inner shell ionization and excitation apply. Thus, at energies above 10 MeV/u a transition from the molecular to the one center atomic model is expected to take place.

For three different projectile species and energies - ^{36}Kr (19.1 MeV/u), ^{54}Xe (11 and 18.3 MeV/u), and ^{92}U (17.2 MeV/u) - target and projectile x-ray cross sections and radiative electron capture (REC) cross sections were measured at the GSI-UNILAC. Solid targets with atomic numbers Z ranging from $6 \leq Z \leq 92$ were used. $\text{Si}(\text{Li})$ and $\text{Ge}(\text{i})$ detector systems were applied to analyze the characteristic target and projectile x-rays. The REC x-rays were analyzed by a $\text{Ge}(\text{i})$ detector positioned at 90° with respect to the beam direction. The angular distribution of the REC photons in the laboratory frame is known to be proportional to $\sin^2\theta$ even at relativistic velocities of the projectile³. Some results of REC cross sections at 18.3 MeV/u are shown in Fig. 2 together with data³ taken at 82 MeV/u.

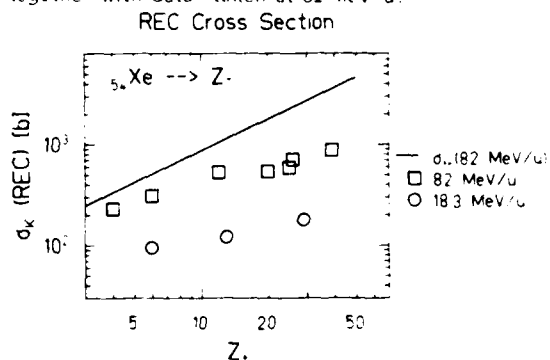


Fig. 2: REC cross sections for Xe at 18.3 and 82 MeV/u. The solid line the calculated REC cross section for a bare Xe nucleus at 82 MeV/u.

The REC process can be described as the time inverse of the photo effect and is therefore proportional to the photon cross section. Comparing the calculated cross section (solid line in fig. 2) - which is for REC

into bare ions- provides a tool to determine the average number of K-shell vacancies N_{KV} while the projectile is passing through the material according to the relation $[N_{KV}/2] \approx [\sigma_K \text{ REC}(\text{exp})/\sigma_K \text{ REC}(\text{theory})]$. (1) At 82 MeV/u this yields a number N_{KV} between 0.5 and 1.5 depending on the target material. Though the average charge state of Xe ions at 18.3 MeV/u moving through solid matter is about 48 there is still a small number of K shell vacancies available ($\leq 1\%$) while the ion is still inside the target and experiences a high collision frequency with target atoms.

First results for projectile K_α cross sections are shown in Fig. 2, in comparison with results from previous experiments¹.

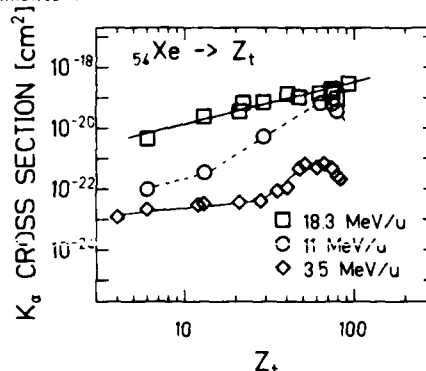


Fig. 2: Projectile K_α cross sections at 3.5, 18.3 and 197 MeV/u for Xe ions incident on solid targets.

The low energy data once more emphasize the importance of molecular effects, as can be seen from the enhanced cross section for symmetric collisions. The influence of these effects decreases with increasing impact energy, and they are already negligible in the energy range of 20 MeV/u.

¹R. Anholt, H.H. Behncke, S. Hagmann, P. Armbruster, F. Folkmann, and P.H. Mokler, Z.Phys. A289(1979)349

²R. Anholt, W.E. Meyerhof, Ch. Stoller, E. Morenzoni, S.A. Andriamonje, J.D. Molitoris, K.O. Baker, D.H.H. Hoffmann, H. Bowman, J.-S. Xu, Z.-Z. Xu, K. Frankel, D. Murphy, K. Crowe, and J.O. Rasmussen, Phys. Rev. A30(1984)2234

³R. Anholt, S.A. Andriamonje, E. Morenzoni, Ch. Stoller, J.D. Molitoris, W.E. Meyerhof, H. Bowman, J.-S. Xu, Z.-Z. Xu, J.O. Rasmussen, and D.H.H. Hoffmann, Phys. Rev. Lett. 53(1984)234

EIKONAL CALCULATIONS OF ELECTRON CAPTURE BY RELATIVISTIC PROJECTILES

J. Eichler** and R. Anholt*

*Department of Physics, Stanford University, Stanford, CA 94305

**Molecular Physics Department, SRI International, Menlo Park, CA 94025

Recently, experimental data¹ on relativistic heavy-ion-atom collisions have been analyzed² to extract electron capture cross sections for a variety of collision systems. In this work, we present a comparison with experiment that is based on a parameter-free relativistic capture theory, the eikonal approximation, which, for $Z_p < Z_T$, treats the electron-projectile (Z_p) interaction to first order and the electron-target (Z_T) interaction to all orders of perturbation theory (albeit in an approximate fashion). We have calculated eikonal cross sections for capture from relativistic $1s_{1/2}$, $2s_{1/2}$, $2p_{1/2}$, and $2p_{3/2}$ target states into relativistic $1s_{1/2}$ states of a projectile moving with a relativistic velocity.

If $Z_p, Z_T \ll 137$ one may derive an approximate closed formula for the $1s_{1/2}$ - $1s_{1/2}$ transition. This expression reduces to the corresponding OBK formula³ if the distorting final-state interaction characterizing the eikonal approach is switched off by setting the appropriate parameter equal to zero.

A comparison with the OBK approximation shows that the relativistic eikonal cross section is significantly smaller (by a factor 5-15) than the OBK cross section³, and, still much smaller than the second-Born result.⁴ This is precisely what is needed to bring theory into better agreement with experiment as displayed in Figures 1 and 2. This agreement demonstrates the importance of multiple-scattering contributions for relativistic as well as for nonrelativistic electron capture.

*This work was supported in part by the National Science Foundation grant NO PHY-83-13676. J. Eichler is on leave from the Hahn-Meitner Institute, D-1000 Berlin 39, W. Germany.

1. H. J. Crawford, Ph.D. thesis, University of California, LBL report 8807 (1979) and H. J. Crawford, L. Wilson, D. Greiner, P. J. Lindstrom, and H. Heckman, to be published.
2. R. Anholt, ms. submitted to Phys. Rev. A.
3. B. L. Moiseiwitsch and S. G. Stockman, J. Phys. B13, 2975 (1980).
4. W. J. Humphries and B. L. Moiseiwitsch, J. Phys. B17, 2655 (1984) and to be published.

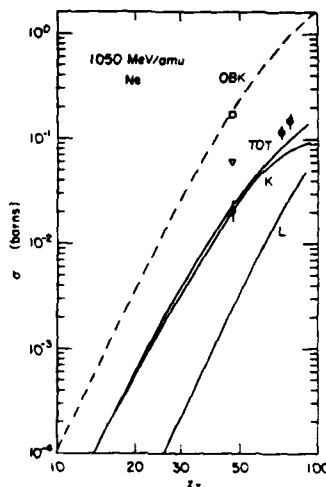


Figure 1 Projectile K electron capture cross sections (per naked atom) for 1050-MeV/amu Ne ions. The OBK results³ are shown by the dashed lines and the open square, and the eikonal calculations with shielding for target K, L, and the sum of K and L capture are shown by the solid lines. A second-Born approximation calculation is shown by the 7 point.⁴ Data (●) from Crawford et al.¹ and Anholt.²

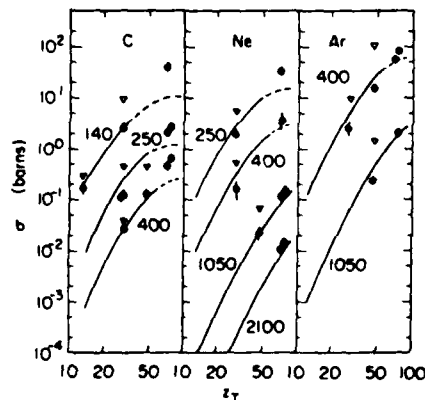


Figure 2 Calculated eikonal projectile K capture cross sections compared with measurements^{1,2} and second-Born calculations⁴ (7 points, always lying above the data points ●). The dashed part of the curves show the region where the eikonal approximation, including target K and L capture, may not be valid.

TOTAL CROSS SECTIONS FOR K - K SHELL ELECTRON CAPTURE AT RELATIVISTIC ENERGIES

A. J. Humphries and B. L. Moiseiwitsch

Department of Applied Mathematics and Theoretical Physics,
The Queen's University of Belfast,
Belfast BT7 1NN, Northern Ireland

Total cross section curves for k-shell to k-shell capture of electrons from target hydrogenic ions by incident fully stripped C^{6+} , Ne^{10+} , Ar^{18+} ions having impact energies of 140, 250, 400, 1050 MeV/amu have been calculated using relativistic forms of the Oppenheimer-Brinkman-Kramers (OBK)¹ and second Born (B2)² approximations together with exact Dirac relativistic atomic wave functions.

We have derived approximate analytical formulae for the scattering amplitudes by carrying out an expansion in powers of $1/Z_T$ and $1/Z_P$ assuming that $1/Z_T, 1/Z_P \ll 1$, where Z_T and Z_P are the atomic numbers of the target and projectile ions respectively and α is the fine structure constant, and retaining the leading terms only. This means that our capture cross sections are likely to be reliable only for small values of Z_T, Z_P . For this reason we have not extended our calculations past $Z_T = 50$.

In Figure 1 a comparison is made between our OBK and B2 approximation capture cross sections for incident C^{6+} ions and the values derived by Anholt³ from the experimental data of Crawford⁴. We see that the B2 cross section curves are smaller than the corresponding OBK curves by as much as a factor of about 3. Regrettably the experimental data are rather meagre and moreover much of the data relates to large values of Z_T for which our theory is not applicable. Even so our B2 curves lie considerably above the experimental points except for the low value of the target atomic number $Z_T = 13$ (Al) and, in some instances, for $Z_T = 29$ (Cu).

Experimental data for small values of Z_T and Z_P and at relativistic energies are needed.

References

1. B. L. Moiseiwitsch and S. G. Stockman, J. Phys. B13, 2975 (1980).
2. A. J. Humphries and B. L. Moiseiwitsch, J. Phys. B17, 2655 (1984).
- J. Phys. L, in course of publication (1985).
3. P. Anholt, private communication.
4. H. J. Crawford, Ph.D. thesis, University of California, LBL report 8807 (1979).
H. J. Crawford, L. Wilson, D. Greiner, P. J. Lindstrom and H. Heckman, to be published.

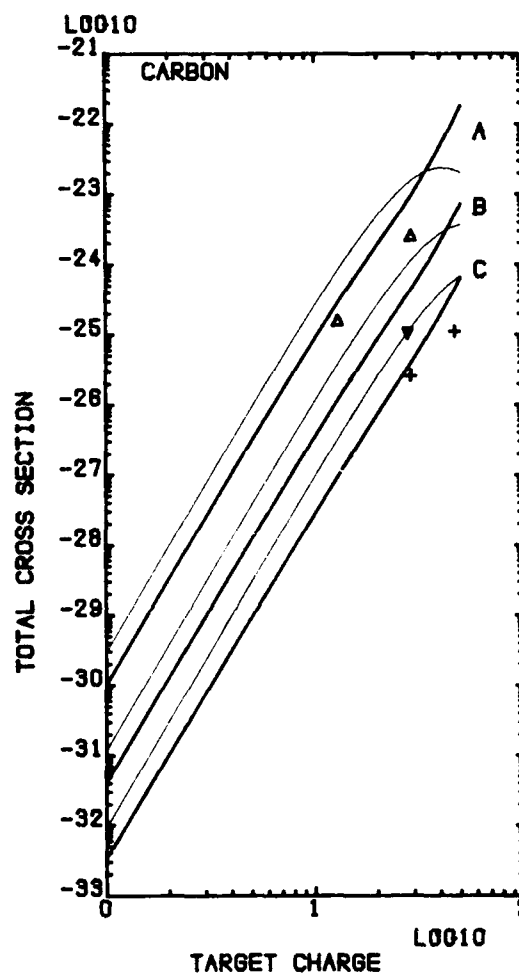


FIGURE 1 K - K shell electron capture cross sections for incident C^{6+} ions.

Curves A and data points Δ : 140 MeV impact energy;
curves B and data point \circ : 250 MeV impact energy;
curves C and data points $+$: 400 MeV impact energy.
Thin lines : OBK approximation;
thick lines : B2 approximation.

ANALYSIS OF CHARGE DISTRIBUTIONS OF RELATIVISTIC HEAVY IONS PENETRATING THROUGH SOLID TARGETS*

W.E.Meyerhof,⁺ R.Anholt,⁺ P.Thieberger,^{**} H.E.Wegner,^{**}
H.Gould,⁺⁺ J.Alonso⁺⁺ and Ch.Munger⁺⁺

⁺Department of Physics, Stanford University, Stanford, California 94305

^{**}Brookhaven National Laboratory, Upton, New York 11973

⁺⁺Lawrence Berkeley Laboratory, Berkeley, California 94720

Charge distributions of selected projectiles ranging from 85- to 960-MeV/amu Fe^{16+} , Xe^{45+} , Au^{61+} and U^{68+} penetrating through solid targets such as Be, C (Mylar), Al, Cu, Ag, Ta and Au have been determined by magnetic analysis.¹⁻² The experimental charge state distributions were analyzed theoretically by inserting into the integrated rate equations³ charge-changing cross-sections based on the following relatively simple concepts: (1) All electrons are assumed to be in their ground states at the instant of charge change. This assumption is valid for heavy ions, since the lifetimes of excited states typically are much shorter than the time between exciting, ionizing or capturing collisions. (2) Electron loss cross sections for a given shell are assumed to be proportional to the number of electrons in the shell.⁴ (3) Electron attachment cross sections for a given shell are assumed to be proportional to the number of vacancies in the shell.⁴ (4) Of the various possible multiple-charge changing cross sections, only two-electron loss is taken into account.

Optimum ionization and capture cross sections were found by a least-squares fitting procedure.^{3,5} Our overall results can be summarized as follows: Most of the optimum reduced chi-square values of the charge distribution fits lie between 0.5 and 3. The extracted K- and L- ionization cross sections generally lie within a factor 1.0 to 1.5 of those predicted by Anholt⁶ in a relativistic PWBA calculation. For electron capture from light targets, where radiative capture (REC) dominates, there is general agreement with the findings obtained from direct REC detection.⁷ For capture from heavy targets, nonradiative capture (NRC) and REC compete. Fig. 1 shows that the NRC into the projectile K and L shells (from target, K, L and M shells) is in very good agreement with new relativistic eikonal calculations by Eichler.⁸ On the other hand, the relativistic OBK calculations by Moiseiwitsch and Stockman⁹ overestimate the observed NRC. The top part of Fig. 1 shows the extracted total capture cross section into bare Au projectiles impinging on an Au target. The bottom of Fig. 1 gives the extracted total capture cross section into two-electron Au projectiles. In the other examined cases, the findings are generally similar.

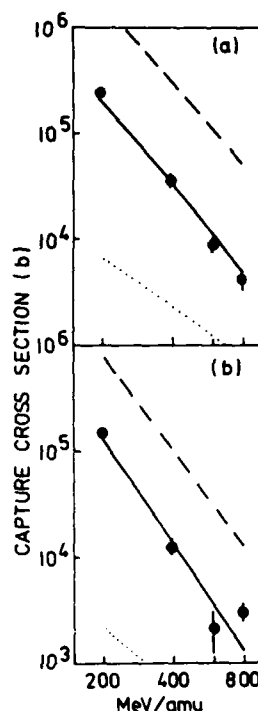


Figure 1. Capture cross sections for (a) $\text{Au}^{79+} + \text{Au}$ and (b) $\text{Au}^{77+} + \text{Au}$ as a function of bombarding energy, extracted from measured charge distributions from Au^{61+} projectiles impinging on Au targets of varying thickness. Dotted lines are REC, full lines are relativistic eikonal calculations (Ref. 8) + REC, dashed lines are relativistic OBK calculations (Ref. 9).

References

* Supported in part by the National Science Foundation under Grant No. PHY 83-13676 and by the U.S. Department of Energy under Contracts No. DE-AC-03-76SF00098 and DE-AC-02-76CH00016.

1. H.Gould et al, Phys. Rev. Lett. **52**, 180 (1984) and unpublished results.
2. H.Wegner, P.Thieberger and H.Gould, unpublished results.
3. S.Datz et al, Phys. Rev. A **2**, 430 (1970).
4. V.S.Nikolaev, Soviet Phys. Usp. **8**, 269 (1965).
5. D.W.Marquardt, J. Soc. Indust. App. Math. **11**, 431 (1963).
6. R.Anholt, Phys. Rev. A **19**, 1004 (1979).
7. R.Anholt et al, Phys. Rev. Lett. **53**, 234 (1984).
8. J.Eichler, to be published.
9. B.L.Moiseiwitsch and S.G.Stockman, J. Phys. B **13**, 2975 and 4031 (1980).

CHARGE DISTRIBUTION OF 85-200 MeV/amu Xe^{54+} , Xe^{53+} AND Xe^{52+}
IONS PENETRATING THROUGH SOLID TARGETS*

H.Gould,⁺ J.Alonso,⁺ Ch. Munger,⁺ R.Anholt,^{**}
W.E.Meyerhof,^{**} P.Thieberger,⁺⁺ and H.E.Wegner⁺⁺

⁺Lawrence Berkeley Laboratory, Berkeley, California 94720

^{**}Department of Physics, Stanford University, Stanford, Ca. 94305

⁺⁺Brookhaven National Laboratory, Upton, New York 11973

Charge changing cross sections of relativistic heavy ions can be obtained by analyzing their charge distributions after penetration through solid targets of varying thicknesses.¹ A less ambiguous method consists of preparing the ions in a given charge state and then letting them penetrate through targets thin enough so that the yields of one-electron loss and one-electron capture vary linearly with the target thickness.² In that case, the ionization and capture cross sections can be obtained directly from the linear target thickness dependence.

By stripping Xe^{45+} ions accelerated in the Lawrence Berkeley Laboratory BEVALAC by means of 2 to 10 mil Mylar foils, beams of two-electron, one-electron and bare Xe ions were prepared with energies between 85 and 200 MeV/Amu. These ions were passed through thin foils of Be, Mylar, Al, Cu, Ag and Au. The yields of the resulting charge states were determined by magnetic analysis.³ The most time consuming and critical part of the experiment was the proper focusing of the charge state beams onto the position sensitive detector of the magnetic spectrometer, to assure a uniform detection efficiency along the sensitive area of the detector.

Analysis of the results is presently under way. Preliminary inspection of the data indicates that the K ionization cross sections of Xe^{52+} and Xe^{53+} are close to those predicted by a relativistic calculation of Anholt⁴, and that the non-radiative capture cross sections into the K shell of Xe^{54+} differ from the relativistic predictions of Moiseiwitsch and Stockman⁵.

References

* Supported in part by the U. S. Department of Energy under Contracts No. DE-AC-03-76SF00098 and DE-AC-02-76CH00016 and by the National Science Foundation under Grant No. PHY 83-13676.

1. S. Datz et al, Phys. Rev. A, **2**, 430 (1970).
2. V.S.Nikolaev, Soviet Phys. Usp. **8**, 269 (1965).
3. H.Crawford, Ph.D.Thesis, University of California, Berkeley (1979).
4. H.Gould, et al, Phys. Rev. Lett. **52**, 180 (1984).
5. R.Anholt, Phys. Rev. A **19**, 1004 (1979).
6. B.L.Moiseiwitsch and S.G.Stockman, J. Phys. B. **13**, 2975 and 4031 (1980).

ULTRARELATIVISTIC ELECTRON CAPTURE IN ION-ATOM COLLISIONS

G.R.Deco and R.D.Rivarola

Instituto de Física Rosario (CONICET-UNR) Av.Pellegrini 250, 2000 Rosario, Argentina

In previous works¹⁻³ the non-relativistic Continuum Distorted Wave (NRCDW) model⁴ has been used to study K-K shell electron capture in ion-atom collisions at high energies. Comparisons were given with non-relativistic-Second Order-Born (NRB2) calculations. Recently, relativistic-Second Order-Born (RB2) approximations have been introduced^{5,6} in order to correct the high energy behaviour of the NRB2 approximation. In the present work, we develop an ultrarelativistic-Continuum Distorted Wave (URCDW) model where ultrarelativistic continuum states⁷ of the projectile and of the target have been considered into the distorted initial and final wave functions respectively. Calculations of the T-scattering amplitude are reduced to the evaluation of one-dimensional-integrals. When relativistic initial and final bound functions are approximated by Schroedinger wave functions (which will be valid for light targets and

projectiles) closed analytical expressions are obtained for T. Double scattering structures which arise in differential cross sections are studied using the URCDW model and comparisons are given with RB2 calculations. Dependence of URCDW-total cross sections on the impact energy E is analysed when $E \rightarrow \infty$.

References

1. Belkić Dz, Gayet R and Salin A, Phys.Rep. **56**, 279 (1979)
2. Rivarola R and Miraglia J, J.Phys.B, **15**, 2221 (1982)
3. Rivarola R and Salin A, J.Phys.B, **17**, 659 (1984)
4. Cheshire I, Proc.Phys.Soc., **84**, 89 (1964)
5. Moiseiwitsch B, J.Phys.B, **15**, 3103 (1982)
6. Humphries W and Moiseiwitsch B, J.Phys.B, **17**, 2655 (1984)
7. Berestetskii V, Lifshitz E and Pitaevskii L. Relativistic Quantum Theory (1971) Oxford: Pergamon

GALERKIN METHODS FOR SOLVING THE SCHRÖDINGER AND DIRAC EQUATIONS

C. Bottcher and M. R. Strayer

Oak Ridge National Laboratory,* Oak Ridge, TN 37831 USA

Over the past few years, we have attacked a wide range of problems in atomic physics through direct solution of the Schrödinger (or Dirac) equations in 2 and 3 dimensions by finite element techniques. These problems include charge exchange in simple systems and electron-impact ionization,¹ complex ion-atom collisions,² and pair production in very heavy ion collisions.³

We now propose to reach a new level of accuracy and efficiency by introducing Basis Spline and Collocation (Galerkin) techniques.⁴ The former are just localized piecewise differentiable polynomials in which the wavefunction can be expanded, e.g., in one dimension (summations understood)

$$\psi(x) = \psi^j u_j(x). \quad (1)$$

At a set of collocation points ξ_α

$$\psi(\xi_\alpha) = \psi_\alpha = B_{\alpha j} \psi^j, \quad B_{\alpha j} = u_j(\xi_\alpha). \quad (2)$$

We demand that the Schrödinger equation

$$i \frac{\partial \psi}{\partial t} = \left[-\frac{1}{2} \frac{d^2}{dx^2} + V(x) \right] \psi \quad (3)$$

be satisfied at each collocation point, leading to the equations

$$i \frac{\partial \psi_\alpha}{\partial t} = K_{\alpha\beta} \psi_\beta, \quad K_{\alpha\beta} = -\frac{1}{2} B_{\alpha j}'' B_{j\beta} + V_\alpha \delta_{\alpha\beta} \quad (4)$$

In Eq. (4), B'' is the matrix of 2nd derivatives of u_j and the raised indices refer to an inverse matrix.

The advantages of this formulation over the variational finite element method in 2 and 3 dimensions are: (a) the matrices involved are more sparse, (b) easier to encode, (c) better conditioned, and (d) estimates of numerical error can be extracted.

At the conference, we will present results on some model problems to illustrate techniques, as well as some studies of realistic problems, notably collisions of heavy ions at relativistic velocities. This involves solving the Dirac equation in 3D with all retardation and magnetic effects included.

1. C. Bottcher in "Electronic and Atomic Collisions," Eds. J. Eichler, I. V. Hertel, and N. Stolterfoht, (Elsevier Science Publishers B.V., 1984), p. 187.
2. C. Bottcher, to be published in Nuclear Instruments and Methods in Physics Research, 1985.
3. C. Bottcher and M. S. Strayer, to be published in Physical Review Letters, 1985.
4. C.A.J. Fletcher, "Computational Galerkin Methods," (Springer-Verlag, 1984).

K-SHELL IONIZATION BY RELATIVISTIC HEAVY IONS*

Ulrich Becker, Norbert Grün and Werner Scheid

Institut für Theoretische Physik der Justus-Liebig-Universität Gießen, West-Germany

In order to study the ionization of strongly bound K-shell electrons in collisions with relativistic heavy ions, we calculated K-shell ionization probabilities and cross sections in the semi-classical approximation (SCA). Ionization cross sections for relativistic collisions have also been obtained in the plane-wave-Born-approximation (PWBA) with semi-relativistic wave functions by Anholt et al.¹⁻³ and Davidovic et al.⁴

In the SCA the differential ionization probabilities from a filled shell is given for a projectile with charge number Z_P and velocity v ^{5,6}:

$$\frac{dI_b^{(f,i)}}{dE_f} = (8Z_P^2/v^2) \sum_{l,m} |Y_{lm}(\hat{r})|^2 \frac{sds}{s^2 - q^2} \quad (1)$$

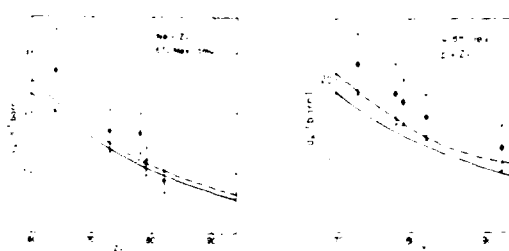
$$B_{lm}(b, q, s) = \int_0^\infty r^2 dr (1 - \exp(-iqr)) Y_{lm}(\hat{r}) \quad (2)$$

where $q = (E_f - E_i)/\hbar v$, $\beta = v/c$, $\alpha = e^2/\hbar c$.

The quantities B_{lm} are the straight-line path factors. For the initial and final electronic states we chose hydrogenic Dirac-wave functions⁶. In the case of straight-line trajectories the differential ionization cross section can be easily obtained by integrating Eq. (1) over the impact parameter b .

Fig. 1 shows the K-shell ionization cross section for collisions of 670 MeV/amu Ne with various targets as a function of the target charge. The experimental values of Anholt et al.³ are compared with our calculations (solid curve) using experimental binding energies for E_i and with calculations of Anholt³ (dashed curve) using semi-relativistic wave functions.

Fig. 2 shows calculations and measurements of K-shell ionization cross sections for 4.88 GeV protons on various targets. The experimental values are given by Anholt et al.¹. The solid curve represents our calculation and the dashed one the calculation of Anholt². The differences between both calculations are explained by the fact that we are using fully relativistic wave functions. Also we have to evaluate a multipole expansion for the interaction potential, converging slowly in the ultrarelativistic energy region.



K-shell ionization cross sections
Fig. 1: 670 MeV/amu Ne Fig. 2: 4.88 GeV/amu protons on various targets.

Fig. 3 shows interesting structures in the differential ionization probabilities to the $s_{1/2}$ -continuum ($l_f = 0$) for $\beta = 0.99$ ($\gamma = 7.1$) and various impact parameters. The minima of the curves arise due to a cancellation in the integration over s in Eq. (1).

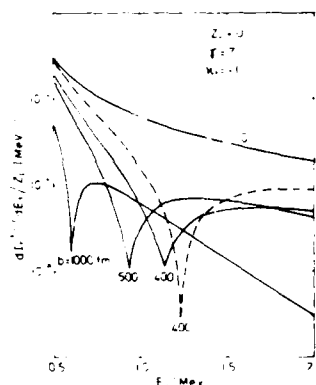


Fig. 3 K-shell ionization probabilities for the transition to the positive $s_{1/2}$ -continuum for the collisional system $Z_P + U$ at $\beta = 0.99$ ($\gamma = 7.1$) as a function of the energy of the ionized electron.

References:

- ¹ R. Anholt et al., Phys. Rev. A **14**, 2103 (1976)
- ² R. Anholt, Phys. Rev. A **19**, 1004 (1979)
- ³ R. Anholt et al., Phys. Rev. A **30**, 2234 (1984)
- ⁴ D.M. Davidovic et al., J. Phys. B **11**, 847 (1978)
- ⁵ P.A. Amundsen et al., J. Phys. B **14**, 4047 (1981)
- ⁶ S.R. Valluri et al., J. Phys. B **17**, 4359 (1984)

* Supported by BMFT and GSI (Darmstadt)

DIRECT ELECTRON-POSITRON PAIR CREATION IN RELATIVISTIC HEAVY ION COLLISIONS*

Ulrich Becker, Norbert Grün and Werner Scheid

Institut für Theoretische Physik der Justus-Liebig-Universität Giessen, West-Germany

A considerable increase of the direct pair-creation cross section is expected for relativistic heavy ion collisions because the electromagnetic fields of the projectile can contribute high momentum components to the pair creation in the Coulomb field of the target nucleus. This presumption is supported by calculations of Soff¹, who used the virtual photon method to calculate pair-creation cross sections for ^{238}U collisions with projectile energies $> 10 \text{ GeV/amu}$. In this contribution we present pair-creation probabilities and cross sections for incident energies of ions between 20 MeV/amu and 10 GeV/amu.

Using the semiclassical approximation we obtain the following differential pair-creation cross section for pair creation of mass m_e and velocity β in the Coulomb field of a target nucleus, where the projectile is on a straight-line trajectory, with the impact parameter b and the atomic numbers of the projectile and target nuclei Z_p and Z_T :

$$\frac{d^2\sigma}{d\beta d\Omega} = \frac{Z_p^2 Z_T^2}{4} \frac{1}{\beta^2} \frac{1}{\Gamma^2} \frac{1}{\sin^2(\theta/2)} \exp\left(-\frac{2\pi}{\beta} \frac{1}{\Gamma} \frac{1}{\sin(\theta/2)}\right) \exp\left(-\frac{2\pi}{\beta} \frac{1}{\Gamma} \frac{1}{\sin(\theta/2)}\right) \exp\left(-\frac{2\pi}{\beta} \frac{1}{\Gamma} \frac{1}{\sin(\theta/2)}\right)$$

where $\Gamma = \frac{1}{\sqrt{1-\beta^2}}$, $\theta = \arcsin(\beta \sin(\theta/2))$, and $\Omega = 4\pi$.

This result is identical to that of the plane wave Born approximation (PWBA). The total cross section for pair-creation is obtained by integration over the final electron and positron energies. We used hydrogenic continuum limit wave functions for the electron and positron states.

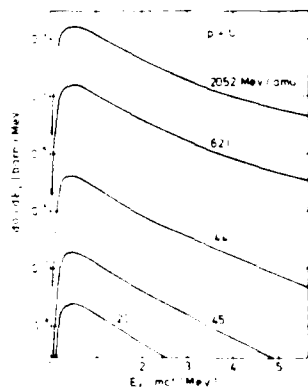
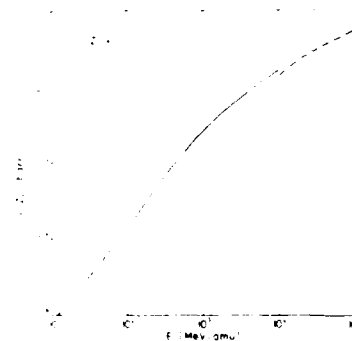


FIG. 1

The differential pair-creation cross sections for the collision of ^{238}U with a projectile of mass M_p as a function of the positron energy E_+ for projectile energies E_{lab} denoted at the curves.

Fig. 1 shows single differential pair-creation cross sections as a function of the energy of the emitted positron and integrated over all electron energies. The target is assumed to be an Uranium nucleus ($Z_T=92$), and the screening effects from atomic electrons are neglected. The decrease of the cross sections for small positron energies is due to Coulomb deflection effects of the positron by the target nucleus. For increasing projectile energies the cross sections decrease slower at high positron energies because of the increasing high momentum components in the electromagnetic fields of the projectile.

Fig. 2 shows the total pair-creation cross section for Z_p+U collisions as a function of the projectile energy. For $E=20 \text{ MeV/amu}$ the values agree with those of Anhalt et al.² using the PWBA and neglecting retardation and Coulomb deflection effects. For $E=10 \text{ GeV/amu}$ our cross section agrees with calculations of Soff¹ (dashed curve, within roughly a factor of 1.5).



The total pair-creation cross sections (solid curve) are shown as a function of the projectile energy E . The dashed curve is obtained by Soff¹.

References:

1. U. Soff, Proc. of XVIII Winter School, Bielsko-Biala, Poland, ed.: A. Balanda, Z. Stachura (1980).
2. R. Anhalt et al., Phys. Rev. A **27**, 680 (1983)

* Supported by BMFT and GSI (Darmstadt)

PRECISION X-RAY MEASUREMENTS IN ONE- AND TWO-ELECTRON ARGON RECOIL IONS

H.F. Beyer, R.D. Deslattes*, F. Folkmann**, and R.E. LaVilla*

GSI, P.O. Box 110541, D-6100 Darmstadt, Federal Republic of Germany

*National Bureau of Standards, Washington D.C., USA

**University of Aarhus, Denmark

Highly charged argon recoil ions were produced by collisions of 5.9 MeV/amu U^{66+} (average charge) ions with an argon gas target and x rays of one- and two-electron states of argon were measured with a high precision. Those excited states play an important role in other x-ray sources including fusion plasmas because the corresponding transitions serve as diagnostic indicators for density and temperature. However, the x-ray lines are usually accompanied by a satellite structure, due to excitation of doubly excited states, which may obscure the measurement. Therefore, we went through a very careful analysis of the satellites and their influence on final wavelength precision.

The transitions of interest are

$$2p_{3/2,1/2} + 1s(\text{Lyman } \alpha_{1,2}) \text{ in } \text{Ar}^{17+} \quad \text{and} \quad (i)$$

$$1s2p \ ^3P_{1,2}, \ ^1P_1 + 1s^2 \ ^1S_0 \text{ in } \text{Ar}^{16+}. \quad (ii)$$

Using high-resolution crystal spectrometers and x-ray transfer standards we were able to achieve a calibration of the wavelength scale relative to visible standards with a precision of up to 2 ppm. The high precision is partly due to the absence of Doppler-shift problems in the recoil light source. For (i) we obtained a final precision of 5 ppm as limited by model uncertainties arising from spectator-electron satellites whereas for (ii) the uncertainty of 12 ppm is dominated by the transfer standard used.

We will compare our experimental wavelengths to recent theoretical calculations. In case of the Lyman- α transitions our error bars allow a 1.5 % test of the QED corrections to the 1s binding energy whereas in the two-electron case electron-electron correlation effects and the treatment of the two-body QED contributions become important.

The figure displays the x-ray region of the helium-like transitions demonstrating the strong increase of satellites population with gas pressure along with the quenching of the long-lived 3P_2 state. In the high pressure spectrum the results (dashed curve) of our a priori model calculations for the $1s2n\bar{n} \ n \leq 9$ satellites are given for comparison.

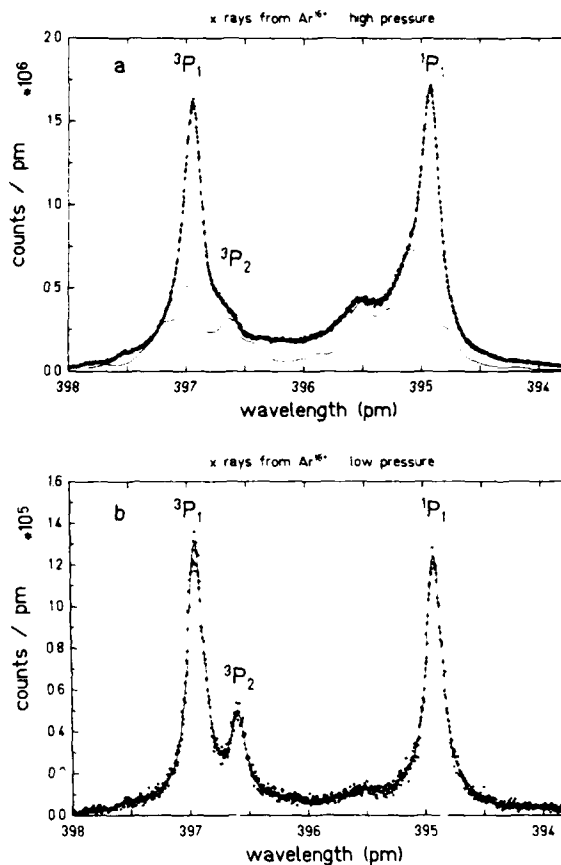


FIGURE 1 Argon x-ray spectra induced by impact of 5.9 MeV/amu uranium projectiles.

References

1. H.F. Beyer, R.D. Deslattes, F. Folkmann, and R.E. LaVilla, *J. Phys.* **B18** (1985) 207
2. R.D. Deslattes, H.F. Beyer, and F. Folkmann, *J. Phys.* **B17** (1984) L689

ACCURACY OF TRANSFER CALIBRATIONS IN HIGH RESOLUTION HIGH PRECISION X-RAY SPECTROSCOPY

Martin P. Stöckli, J. L. Shinpaugh, J. M. Sanders, and Patrick Richard

James R. Macdonald Laboratory, Kansas State University, Manhattan, Kansas 66506

Over the last few years several groups have undertaken precision measurements of x-ray lines of rare ion species (e.g. hydrogenlike, heliumlike and doubly-excited heavy ions). Because yields of such ions are rather limited the experiments used spectrometers with a high efficiency, e.g., a curved crystal spectrometer combined with a position sensitive detector.¹ Such a spectrometer can be calibrated to high precision using a more common x-ray line with an energy which is a known x-ray standard or which can be determined accurately in a separate experiment using state-of-the-art techniques and methods. Future experiments need to improve the accuracy of such transfer calibrations which could be limited by the accuracy of the x-ray standards, presently in the 0.6-10.0 ppm range.² One of the limiting factors in this accuracy is, in some cases, the unknown satellite structure in the vicinity of the calibration line. In order to obtain identical satellite structure, the calibration has to be done with the same excitation method which is or was used in the measurement of the standard. However, in general the two spectra are not identical because of unequal resolution, background and total intensity. The present work investigates the accuracy and uncertainty of such transfer calibrations by using various defined standards. 3-MeV proton induced x-ray spectra were measured with a spectrometer as described above using an Ar target (Fig. 1; total 8×10^5 counts) and a Mn target (Fig. 2; total 2×10^6 counts). These two typical calibration spectra were fitted with a least squares fitting routine based on a first order Taylor expansion.

Historically the x-ray standards refer to the location of highest intensity evaluated by the division of chords.³ Recently we developed a method to determine this location and its error with a least squares fitting routine.⁴ Since this location is not well defined, its error is rather large (see Table 1, Line A1). Nearby satellites cause a shift which depends on the resolution, which can be essentially eliminated by treating the spacing between the major satellites as a known parameter. This improves the uncertainty only slightly (Table 1, Line A2).

Today it is more common to fit the calibration lines with approximative Voigt functions⁵ and to include a reasonable number of satellites if needed for a reasonable chi square. These additional satellites, which are indicated in the figures, represent groups

of unresolved satellites. The line positions of the major satellites are much better defined compared to the location of highest intensity. However, the position uncertainties remain sizeable (Table 1, Line B1) because of the strong correlation with the unresolved additional satellites. If the line shape parameters⁵ are predetermined (e.g. in the measurement of the standard) they can be treated as known parameters which improves the position uncertainties (Table 1, Line B2). If in addition the spacings among the satellites are predetermined, the position uncertainty (which now refers rather to the line group than to an individual line) is further improved (Table 1, Line B3). If in addition the intensity ratios among the satellites are predetermined, the position uncertainties are further improved (Table 1, Line B4) and come very close to the statistical limits.

A more detailed study on the effects of different resolution, line shape and cutoffs is in progress.

This work is supported by the Department of Energy, Division of Chemical Science.

References

1. e.g. R. D. Deslattes, R. E. LaVilla, P. L. Cowan, and A. Henins, Phys. Rev. A **27**, 923 (1983).
2. e.g. E. G. Kessler, Jr., R. D. Deslattes, D. Girard, W. Schwitz, L. Jacobs, and O. Renner, Phys. Rev. A **26**, 2696 (1982).
3. J. A. Bearden, Phys. Rev. **43**, 92 (1933).
4. M. P. Stöckli, J. L. Shinpaugh, J. M. Sanders, and P. Richard, BAPS **30** (1985).
5. e.g. G. K. Wertheim, M. A. Butler, K. W. West and D. N. E. Buchanan, Rev. Sci. Instrum. **45**, 1369 (1974).

Table 1: Statistical Uncertainty of Wavelength [ppm]

Line	Ar K α 1	K α 2	Mn K α 1	K α 2
A1	12	25	8	15
A2		11		7
B1	1.1	1.9	1.1	9
B2	0.9	1.2	0.9	5
B3		0.7		0.9
B4		0.6		0.4

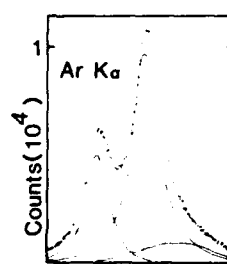


Fig.1: Wavelength

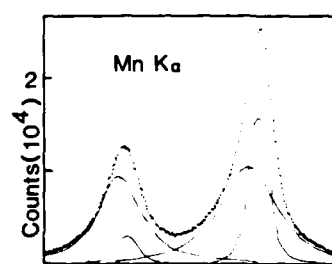


Fig.2: Wavelength

PROJECTILE DEPENDENCE OF L-MM AUGER ELECTRONS EJECTED FROM AR TARGET BY HEAVY-ION IMPACT

H.Shibata, T.Matsuo*, Y.Awaya, T.Kambara, M.Kase, H.Kumagai, and N.Tokoro#

The Institute of Physical and Chemical Research (RIKEN), Hirosawa, Wako-shi, Saitama 351-01, Japan

* Medical Research Institute, Tokyo Medical and Dental University, Bunkyo-ku, Tokyo 113, Japan

Research Laboratory for Nuclear Reactors, Tokyo Institute of Technology, Meguro-ku, Tokyo 152, Japan

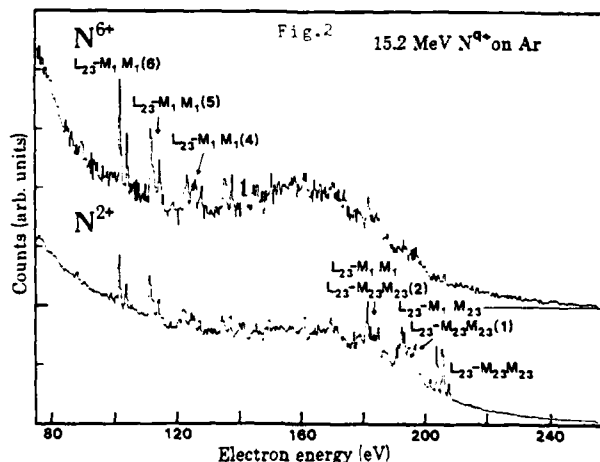
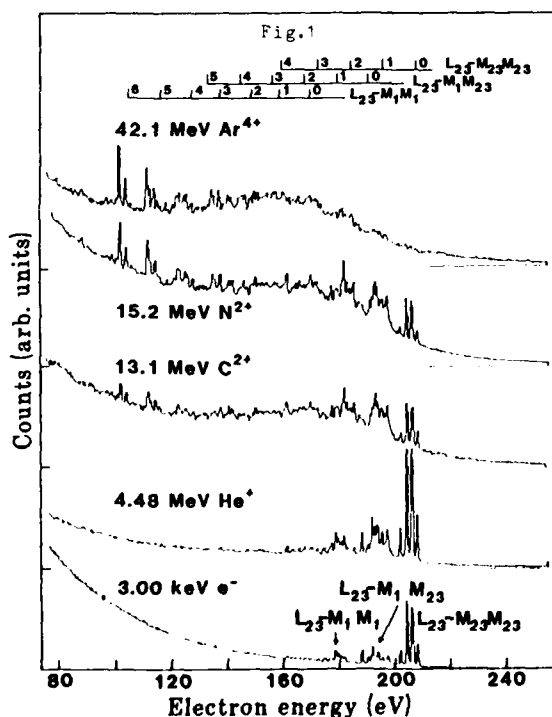
We have measured the energy distributions of ejected electrons in $\text{Ar}^{3,4+} + \text{Ar}$ collisions with a high energy-resolution spectrometer in order to study the ionization mechanism in heavy-ion atom collisions and the energy levels of highly ionized atoms. $L_{23}-M_1M_1$ Auger electrons from highly ionized target argon atoms, such as $\text{Ar}^{7+}(2s^22p^53s^2)$, $\text{Ar}^{6+}(2s^22p^53s^23p)$, and $\text{Ar}^{5+}(2s^22p^53s^23p^2)$, have been observed, which appears when 3p ionization occurs simultaneously with 2p ionization.¹⁾

In the present study, we have measured the projectile and charge state dependences of the L_{23} -MM Auger transitions of Ar. Though it is well-known that the normal L_{23} -MM Auger lines appear strongly in the electron or proton impact (see Fig.1), very few experiments have been made in the heavy-ion impact to study how the degree of the ionization increases as the atomic number of projectile increases. The spectra of the L_{23} -MM Auger electrons ejected from Ar targets by about 1 MeV/amu He, C, N, Ne, Al, and Ar ion bombardments have been measured at an ejected angle of 135° with respect to the beam direction. He^+ , C^{2+} , N^{2+} , Ne^{2+} , Al^{3+} , and Ar^{4+} ions were accelerated by the linear accelerator of ICPR (RILAC) and highly charged He^{2+} , C^{5+} , N^{6+} , Ne^{8+} , Al^{9+} , and Ar^{12+} ions were produced by passing the ions through a carbon foil stripper. The other experimental conditions and apparatus were described elsewhere.²⁾

The ejected electron spectra obtained by He^+ , C^{2+} , N^{2+} , and Ar^{4+} impacts are shown in Fig.1 together with a 3.00 keV electron impact data for the comparison. The measured energy range of electrons was from 80 to 250 eV. The lines above spectra in Fig.1 indicate L_{23} -MM Auger electron energies calculated by Larkins³⁾ using the adiabatic model. The number of each line indicates the number of 3p vacancies in the initial state of Auger transition. We have compared the spectra with the theoretical calculations and obtained the following results. In the case of He^+ impact, the normal Auger lines, $L_{23}-M_{23}M_{23}$, $L_{23}-M_1M_{23}$, and $L_{23}-M_1M_1$, appeared strongly and they are very similar to the case of electron impact. However, as the atomic number Z of the projectiles increases, the normal Auger lines weakened and the intensities of satellite lines enhanced. Namely, for Ar impact the normal Auger lines disappeared and the intensities of the Auger lines from the charge states of $7+$, $6+$ and $5+$ of Ar increased.

Fig.2 shows an example of the charge state dependence of the projectiles having the same velocity. A drastic change is seen between N^{2+} and N^{6+} ion bombardments. For N^{2+} impact the normal Auger transitions were clearly observed; on the other hand, for the case of N^{6+} the normal transitions diminished and satellite lines from the highly ionized atoms enhanced. This may be attributed to the 3p electron transfer from target to projectile, because the one-electron transfer cross section from the target to N^{6+} ion has about two orders of magnitude larger than that for the case of N^{2+} ion.⁴⁾

Further systematic measurements and analysis are in progress.



References

- 1) T.Matsuo et al., to be published
- 2) T.Matsuo et al., J.Phys.B **16**, L233 (1983)
- 3) F.P.Larkins, J.Phys.B **4**, 1 (1971)
- 4) V.S.Nikolaev et al., Sov.Phys. JETP **11**, 98 (1971)

K FLUORESCENCE YIELDS, AUGER AND X-RAY DECAY RATES FOR MULTIPLY IONIZED ATOMS.

F. Combet Farnoux

Laboratoire Spectroscopie Atomique et Ionique - Batiment 350 -
Université Paris-Sud - 91405 Orsay (France)

Fluorescence yields as well as radiative and radiationless transition energies and intensities of multiply ionized atoms are of interest in the study of ion-atom collision phenomena as well as in connection with astrophysics. Because K-shell vacancies produced in heavy-ion-atom collisions are usually accompanied by multiple inner shell ionization (in contrast to proton-atom or electron-atom collisions), reliable values of the K fluorescence yield for various defect configurations of many atoms and ions are imperatively needed. Up to now, only few approaches have been achieved and the published results concern essentially ions of neon⁽¹⁾, argon⁽²⁾ and some iso-electronic series⁽³⁾.

This work presents numerical results of Auger, X-Ray rates and K fluorescence yields (as well as the corresponding transition energies) for many defect configurations with an atomic number Z varying between 11 and 18, i.e. between Al ($1s2s^22p^63s^23p$) and Ar ($1s2s^22p^63s^23p^5$). The calculations concern many ions with a configuration obtained, either by stripping down the outer shell, or by creating vacancies L-shell without changing the structure of M subshells.

Both K Auger (T_A) and X-Ray (T_X) rates have been determined in the framework of non relativistic models (since dealing with relatively low atomic numbers) T_X in order to calculate the fluorescence yield $\omega_K = \frac{T_X}{T_X + T_A}$. Radiative and Auger decay rates of a 1s vacancy in ions whose configurations contain L-shell vacancies (for example $1s2p^63s^23p^2$ of Si) have been calculated in the same approximations as used for the stripped configurations (for examples $1s2s^22p^63s^2$ and $1s2s^22p^4$ in Si). The Herman and Skillman Hartree-Slater potential was used to generate the wavefunctions needed for computing T_A and T_X . However, two series of calculations have been performed: the first one considers that both the discrete and continuum wavefunctions are eigenfunctions of the potential of the initial state, while in the second series, the continuum wavefunction describing the ejected electron is determined with the potential of the ion in the final state (once more ionized) after filling the 1s vacancy. In both cases, I have determined an averaged fluorescence yield, the various multiplet yields and an effective fluorescence yield for a given configuration n:

$$\bar{\omega}_K(n) = \sum_{LS} C_n(LS) \omega_K(LS, n) \quad \text{where the } C_n(LS)$$

are the population probabilities of multiplet states LS in the configuration n. A statistical population is supposed.

Electronic Configurations of Silicon	Rates($10^3/a.u.$) Total Auger	Total X-Ray	Averaged ω_K
$1s 2s 2p^6 3s^2 3p^2$	14.0395	1.027	0.06816
$1s 2s 2p^5 3s^2 3p^2$	11.403	0.930	0.07541
$1s 2s 2p^4 3s^2 3p^2$	8.6786	0.8131	0.08566
$1s 2s 2p^3 3s^2 3p^2$	6.022	0.674	0.10068
$1s 2s 2p^2 3s^2 3p^2$	3.661	0.511	0.12252
$1s 2s 2p 3s^2 3p^2$	1.872	0.322	0.14691
$1s 2s^2 2p^6 3s^2 3p^2$	15.7247	0.9644	0.05778
$1s 2s^2 2p^5 3s^2 3p^2$	15.6284	0.9576	0.05773
$1s 2s^2 2p^4 3s^2 3p^2$	15.4800	0.9484	0.05773
$1s 2s^2 2p^3 3s^2 3p^2$	15.4436	0.9538	0.05817
$1s 2s^2 2p^2 3s^2 3p^2$	15.0027	0.9569	0.05996
$1s 2s^2 2p^5$	12.4292	0.85728	0.06452
$1s 2s^2 2p^4$	9.71326	0.73604	0.07043
$1s 2s^2 2p^3$	7.05235	0.5913	0.07736
$1s 2s^2 2p^2$	4.6854	0.4212	0.08248
$1s 2s^2 2p$	2.8919	0.2242	0.07197

The values given above for some silicon ions illustrate some general conclusions, although minor discrepancies are pointed out when we compare results obtained in the different approximations mentioned above: some cases deserve to be treated with more sophisticated models, introducing initial state correlations (for instance, the $1s2s^22p$ configuration should be mixed with $1s2p^3$) and intermediate coupling to describe the final state. Anyway, among these general conclusions, we will mention:

A) K fluorescence yields are found to increase with the ionization degree, but stripping of outer shells has a much smaller effect than creation of an empty inner subshell of spectator electrons.

B) While multiple 2p vacancies alter ω_K slightly as long as two 2s electrons are present, the fluorescence yield may be up to 4 times greater if one or two vacancies are simultaneously created in the 2s subshell.

A relativistic extension of the codes is in progress in order to treat ions with higher atomic number.

- 1- C.P.Bhalla, N.O.Folland and M.A.Hein
Phys.Rev.A **8**, 649 (1973)
M.H.Chen, B.Crasemann and D.L.Matthews
Phys.RevLett. **34**, 1309 (1975)
- 2- C.P.Bhalla
Phys.Rev.A **8**, 2877 (1973)
- 3- M.H.Chen, B.Crasemann, Kh.R.Karim and H.Mark
Phys.Rev.A **24**, 1852 (1981)

$K_{\beta\beta}$ - AND $K_{\alpha\beta}$ - DECAY RATES IN DOUBLY IONIZED ATOMS

G.B. Baptista and E.C. Montenegro

Departamento de Física, Pontifícia Universidade Católica
Cx.P. 38071, Z.C. 19, Rio de Janeiro, RJ, 22453, BRASIL

An alternative decaying mode for atoms bearing two internal vacancies, usually produced by heavy ion collision, is the simultaneous jumping of two external electrons to fill the vacancies resulting in the emission of only one photon. When the decaying electrons are both from the M shell or one from the L-shell and one from the M-shell jumping into two K-shell vacancies they are usually denominated $K_{\beta\beta}$ - or $K_{\alpha\beta}$ - transitions, respectively. Although the evidency of this decaying mode can be found in recent publications^(1,2,3,4), quantitative results are very rare and theoretical calculations are limited to a few cases^(5,6).

In the present work the transition rates for this two-electron one-photon decaying process for atoms bearing initially two vacancies in the K-shell were evaluated, considering that the decay process is a result of the interaction between the atom and the radiation field. Assuming that the atom can be approximated by a separable N-electron single particle Hamiltonian. The following expression for the two electron one-photon transition probability is obtained:

$$W_{fi} = \frac{2\pi}{h} W(k_f, k'_f, 1\omega; k_i, k'_i, 0\omega) \delta(E_i - E_f) \quad (1)$$

where

$$W(k_f, k'_f, 1\omega; k_i, k'_i, 0\omega)$$

$$= \left| \sum_{k_p, k_q} \frac{\langle k_f, k'_f | e^2 / r_{12} | k_p, k_q \rangle \langle k_p, k_q | 1\omega | \sum_{i=1}^2 H_i(A) | k_i, k'_i \rangle}{\epsilon_p + \epsilon_q + \hbar\omega - \epsilon_i - \epsilon'_i} + \sum_{k_p, k_q} \frac{\langle k_f, k'_f | 1\omega | \sum_{i=1}^2 H_i(A) | k_p, k_q \rangle \langle k_p, k_q | e^2 / r_{12} | k_i, k'_i \rangle}{\epsilon_p + \epsilon_q - \epsilon_i - \epsilon'_i} \right|^2 \quad (2)$$

A detailed description of the calculational procedure can be found in recent publications^(7,8).

The results shown in Figure 1 for the transition rates $W_{K_{\alpha\beta}}$ and $W_{K_{\beta\beta}}$, for Al up to Zr, were obtained using LSJM representation and screened hydrogenic wave functions. The screening for each electron state was obtained decreasing two units from tabulated values of Froese Fischer⁽⁹⁾. This procedure was followed to compensate the absence of the K-shell electrons and was followed in previous calculation of the $K_{\alpha\alpha}$ - transition rates⁽⁸⁾ giving results in good agreement with available experimental data. The two values reported for each element were obtained considering two values for the electron energy: tabulated values⁽⁹⁾ corrected for the decrease of the screening due to the internal vacancies and hydrogenic energies using screened Z values.

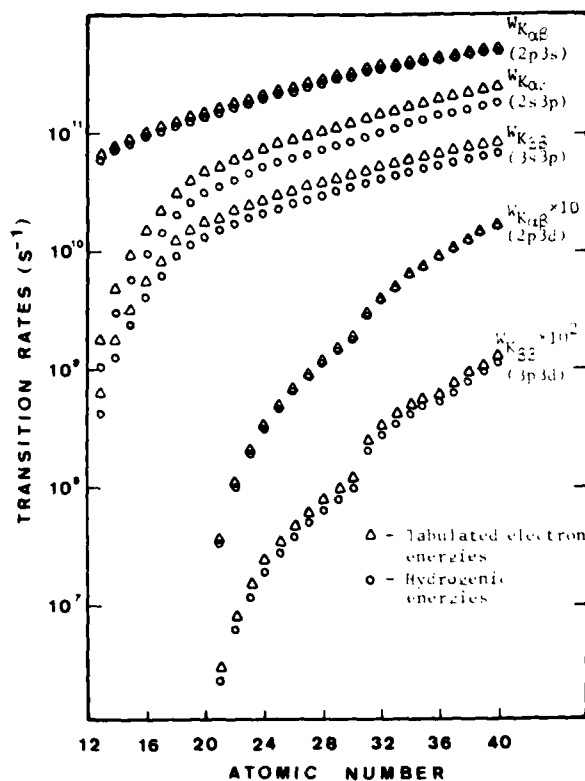


FIGURE 1 - $W_{K_{\alpha\beta}}$ - and $W_{K_{\beta\beta}}$ - transition rates

The present approach allow an insight of the decaying process and only correlation between the jumping electrons are considered. The calculation is greatly simplified and requires only single particle wave functions. Besides that the allowed decaying electron pair is chosen directly from the theory according to angular momenta selection rules for each initial state.

References

1. Ch. Stoller, W. Wölfl, C. Bonani, M. Stöckli, and M. Suter. Phys. Rev. 15A, 990 (1977).
2. W.L. Luken, J.S. Greenberg and P. Vincent. Phys. Rev. 15A 2305 (1977).
3. A.R. Kundson, K.W. Hill, P.C. Burkhalter and D.J. Nagel. Phys. Rev. Lett. 37, 679 (1976).
4. J.S. Greenberg, P. Vincent and W. Lichten. Phys. Rev. 16A, 964 (1977).
5. M. Ya. Amusia, I.S. Lee and A.N. Zinoviev. Phys. Lett. 60A, 300 (1977).
6. Hugh P. Kelly. Phys. Rev. Lett. 37, 386 (1976).
7. V.O. Kostroun and G.B. Baptista. Phys. Rev. 14A, 363 (1976).
8. G.B. Baptista. J. Phys. B: At. Mol. Phys. 17, 2177 (1984).
9. C. Froese Fischer. At. Data Nucl. Data Tables 12, 87 (1973).

IONIZATION BY NUCLEAR RESONANCE SCATTERING WITHIN THE BLAIR MODEL

James M. Feagin,* David W. Joyce,* and Ladislav Kocbach*

*California State University, Fullerton, CA 92634, USA

*University of Bergen, 5000 Bergen, Norway

The idea that inner-shell ionization could be used as an atomic clock for nuclear resonance excitation changed considerably when Blair showed¹ that the nuclear scattering amplitude could be included in a simple way into semiclassical calculations of the ionization probability. Blair's work has prompted a wealth of theoretical and experimental investigations on a variety of systems.²

Blair's "broken-line-trajectory" model follows³ from a short-wavelength or peaking approximation applied to a distorted-wave calculation of electron ionization. The distortion is generated by nuclear resonance scattering. Recently, Rosenberg⁴ considered corrections to the peaking approximation as an expansion that arises from the use of a more accurate asymptotic representation of the scattering wave function. In particular, he estimated explicitly for $l = 0$ electrons corrections that account for the presence of a long-range proton-nucleus Coulomb interaction.

In this report we consider a correction that should account for the small flux of nuclear projectiles (and ejectiles) that initially follow a trajectory nearby the broken-line trajectory and are deflected by electron scattering onto the broken-line. Although Rosenberg's expansion includes such corrections in the $l = 0$ terms, our method appears to sum the series at once.

The distorted-wave approximation leads to a pair of (diffraction-like) integrals of the form

$$I_{\pm L}(\hat{k}_i, \hat{k}_f) = \int d^3R g_{\pm L}(\vec{R}) f(\vec{R} \cdot \hat{k}_i) \frac{e^{ik_i R}}{R} e^{-ik_f \cdot \vec{R}} \quad (1)$$

which are amplitudes for electron ionization with nuclear scattering. Here \hat{k}_i and \hat{k}_f are nuclear projectile and ejectile wave vectors, $f(\vec{R} \cdot \hat{k}_i)$ is the nuclear scattering amplitude along a trajectory \vec{R} , and $g_{\pm L}(\vec{R}) = \sum_{\vec{k}} \langle \vec{k} | \psi_{\pm L}(\vec{R}) \rangle$ is an atomic form factor. Also, we ignore here the Coulomb phase of the wavefunction that Rosenberg carried through explicitly and thus concentrate on diffraction corrections that result from trajectories nearby the broken-line trajectory.

In the peaking approximation, $g_{\pm L}(\vec{R}) f(\vec{R} \cdot \hat{k}_i)$ is replaced in (1) by $g_{\pm L}(\vec{R} \hat{k}_i) f(\hat{k}_i \cdot \hat{k}_i)$ and the integral over $d\vec{k}$ is performed, leading directly to a semiclassical electron ionization amplitude and one leg

of the broken-line model. Corrections can be generated as an expansion of $g_{\pm L}(\vec{R}) f(\vec{R} \cdot \hat{k}_i)$ about $\vec{R} = \hat{k}_i$ which, as Rosenberg shows, includes gradients of the form $\nabla_R g_{\pm L}(\vec{R})$ and $\nabla_R f(\vec{R} \cdot \hat{k}_i)$.

In generalizing the peaking approximation, we find it more appropriate, however, to perform first the radial integral in (1). For example, taking $l = 0$ and $g_{\pm 0} = N e^{-F/a}$, where N is a constant and $a = a_0/ZK$ is the K -shell radius, one finds that

$$I_{\pm 0} = -2\pi a^2 N \int \frac{(k_i a + i) f(\cos \theta) d\cos \theta}{[(k_i a + i)^2 - k_f^2 a^2 \sin^2 \theta]^{3/2}} \quad (2)$$

Here for simplicity we have taken the scattering angle $\theta = 90^\circ$ such that $\hat{k}_i \cdot \hat{k}_f = 0$ and $\cos \theta = \vec{R} \cdot \hat{k}_i$. Eq. (2) already sums for $l = 0$ the $\nabla_R f(\vec{R} \cdot \hat{k}_i)$ terms in the series, for if $f(\cos \theta)$ is replaced by $f(0) = f(\hat{k}_i \cdot \hat{k}_i)$, then (2) integrates to the $l = 0$ peaking approximation:

$$I_{\pm 0}^{\text{peak}} = \frac{4\pi a^2 N f(\hat{k}_i \cdot \hat{k}_i)}{(1 - ik_i a)^2 + k_f^2 a^2} \quad (3)$$

Possible corrections to (3) become evident when one considers an example of experimental interest. Chemin et al.⁵ observed 90° scattering of protons by ^{88}Sr at $E_p = 6.06$ MeV, and for K -shell ionization at this energy, one has that $k_i a = 832$ while $k_f a = 829$. Although these numbers could appear to justify a short-wavelength approximation, one finds that the integrand in (2) peaks at $\theta = 90^\circ$ with a FWHM of over 8° . The integral (2) thus accounts for nuclear scattering away from the broken-line trajectory which also contributes by electron scattering to the Blair amplitude.

We shall present our evaluation of (2) and compare our results with the data of Chemin et al.

References

1. J. S. Blair, P. Dyer, F. A. Snover, and T. A. Trainor, Phys. Rev. Lett. **41**, 1712 (1978).
2. W. E. Meyerhof, Invited talk, XIII ICPEAC, Berlin, **31** (1983).
3. J. M. Feagin and L. Kocbach, J. Phys. B **14**, 4349 (1981).
4. I. Rosenberg, Phys. Rev. A **28**, 3238 (1983).
5. J.-F. Chemin, W. E. Meyerhof, R. Anholt, J. D. Molitoris, and Ch. Stoller, Phys. Rev. A **26**, 1239 (1982).

LARGE-ANGLE SCATTERING AND NUCLEAR-RESONANCE EFFECT IN ELECTRON CAPTURE IN $H^+ + C$ AND $H^+ + N$ COLLISIONS*J.N. Scheurer,** O.K. Baker,[†] D. Spooner,[†] and W.E. Meyerhof[†]

** NATO Fellowship holder, Centre d'Etudes Nucleaires, University of Bordeaux 1 and INPNPP

[†]Department of Physics, Stanford University, Stanford, California 94305 USA

We are investigating the total probability $P(E, \theta)$ for electron capture at scattering angles of 30° and 150° in order to study large angle scattering and predicted nuclear resonance effects in charge transfer reactions in ion-atom collisions.¹ So far, we have investigated proton scattering on carbon (CH_4) and nitrogen (N_2) using a magnetic separation method for the scattered H^+ and H^0 particles. The data for $H^+ + C$ at $E_{lab} = 350$ -1000 keV is shown in Figure 1. At 30° , this data is consistent in absolute magnitude with the calculations of Amundsen and Jakubassa-Amundsen.¹ The data also agrees with previous experimental values of Horsdal-Pederson et al.² below 600 keV. (The disagreement between our values at $E_{lab} = 1000$ keV is currently being investigated.) The data at $\theta_{lab} = 150^\circ$ deviates considerably from calculations as can be seen.

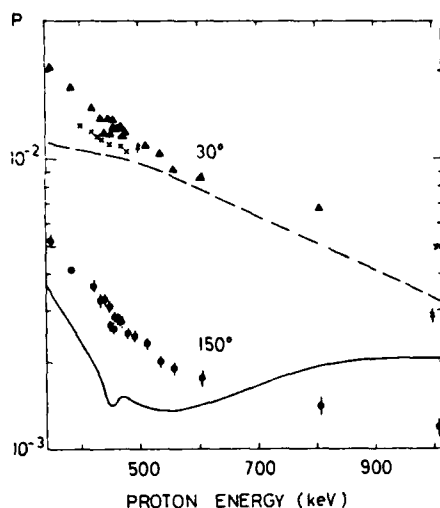


Figure 1. Electron capture probabilities for $p + CH_4$ collisions as a function of proton energy. Experimental values at $\theta_{lab} = 30^\circ$ from Ref. 2 (x), at $\theta_{lab} = 30^\circ$ (Δ) and 150° (\bullet) from present work. Theoretical values at $\theta = 30^\circ$ (-----) and at $\theta = 150^\circ$ (—) from Ref. 1.

Figure 2 gives $P(E, 150^\circ)$ in the resonance regions for $H^+ + C$ ($E_{lab} = 460$ keV) and $H^+ + N$ ($E_{lab} = 1058$ keV) as well as the nuclear cross section ratio. Within the statistical and systematic errors, the predicted modulation of $P(E, \theta)$ cannot be definitely ascertained for the $H^+ + C$ resonance, but for the $H^+ + N$ resonance, our experimental results are in qualitative agreement with the theoretical predictions.¹

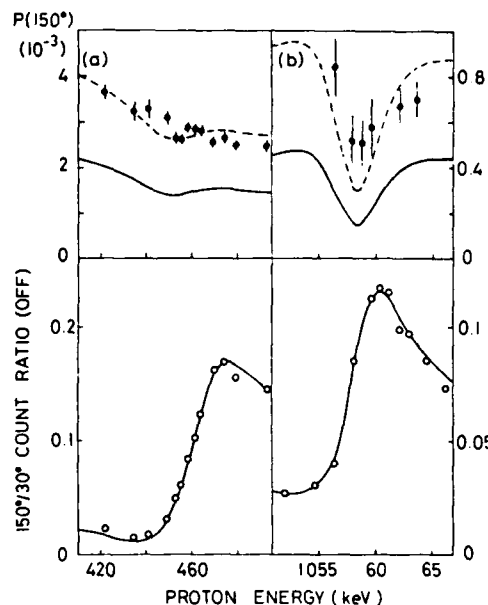


Figure 2 (a) Electron capture probabilities at $\theta_{lab} = 150^\circ$, for $p + CH_4$ collisions in the neighborhood of the 462-keV resonance. (b) Electron capture probabilities at $\theta_{lab} = 150^\circ$ for $p + N_2$ collisions in the neighborhood of the 1058-keV resonance. The $150^\circ/30^\circ$ counting ratios, proportional to the nuclear cross section ratios, are shown in the bottom parts of the figure. The solid curves are from Ref. 1. The dashed curves are scaled to fit the experimental magnitudes.

References:

* Supported in part by NSF (Grant PHY 83-13676).

1. P.A. Amundsen and D.H. Jakubassa-Amundsen, Phys. Rev. Lett. **53**, 222 (1984) and private communications.
2. E. Horsdal-Pedersen, P. Loftager, and J.L. Rasmussen, J. Phys. B. **15**, 2461 and 4423 (1982).

NUCLEAR-REACTION TIME DELAY STUDIES OF $U + U$ DEEP INELASTIC COLLISIONS AT 7.5 MeV/a.m.u.*

J. D. Molitoris, Ch. Stoller, R. Anholt, D. W. Spooner, W. E. Meyerhof
Department of Physics, Stanford University, Stanford, CA 94305

R. J. McDonald, L. G. Sobotka[†], G. J. Wozniak, L. G. Moretto
Nuclear Science Division, Lawrence Berkeley Laboratory,
University of California, Berkeley, CA 94720

E. Morenzoni, M. Nessi, W. Wölfl
Laboratorium für Kernphysik, Eidg. Technische Hochschule, CH-8093 Zürich

Several years ago, Anholt¹ proposed that the theory of atomic inner-shell ionization could be applied to the determination of nuclear reaction times in suitable deep inelastic reactions. If the K -shell ionization probability P_K is measured as a function of the total kinetic energy loss of the reaction $-Q$, the average nuclear time delay associated with a certain Q value can be deduced.

Recently, Ch. Stoller *et al.*² inferred a nuclear delay time of approximately 10^{-21} s at $-Q \approx 100$ MeV in the deep inelastic reaction $U + U$ at a bombarding energy of 7.5 MeV/a.m.u. This experiment relied on the unambiguous detection of two unfissioned U -like reaction products in coincidence. However, the detection of coincidences up to apparent $-Q$ values of ~ 250 MeV suggested that the fission-rejection criteria may not have been stringent enough. We therefore repeated this experiment with a different detection method in order to improve fission event rejection and to extend the measurement to larger $-Q$ values. Incorrect fission event rejection not only falsifies the $-Q$ value, but also the corresponding value of P_K . The reason for this is that any fissioning U -like nucleus will do so in a time ($\sim 10^{-21}$ sec) much shorter than the lifetime of a K vacancy ($\sim 10^{-18}$ to 10^{-17} s). Hence, no U -like x-ray will be emitted, and P_K is effectively reduced. Indeed, the entire P_K dependence on $-Q$ can be fortuitously decreasing if the fission rejection decreases as $-Q$ increases.

Our experimental set up is shown in Fig. 1. The 7.5 MeV/a.m.u. U -beam from the Lawrence Berkeley Laboratory SuperHILAC was directed on to 600 – 750 $\mu\text{g}/\text{cm}^2$ ^{238}U targets. Particles emerging from the collision were detected by an ionization chamber on one side of the beam and by two parallel plate avalanche counters (PPACs) on the other side. The main element here is the LBL large-solid-angle ionization chamber³ which can determine $\Delta E_1 - \Delta E_2 - E_{\text{rest}}$, Θ (in plane) and Φ (out of plane) for the detected particle. In this chamber, unfissioned U nuclei were unambiguously selected, and from the energy and angle alone, we determine $-Q$, independent of the behavior of the partner product. For the P_K determination we used two large area PPAC's to see if the reaction partner has fissioned or not. The front (transmission) PPAC allowed time-of-flight measurements with

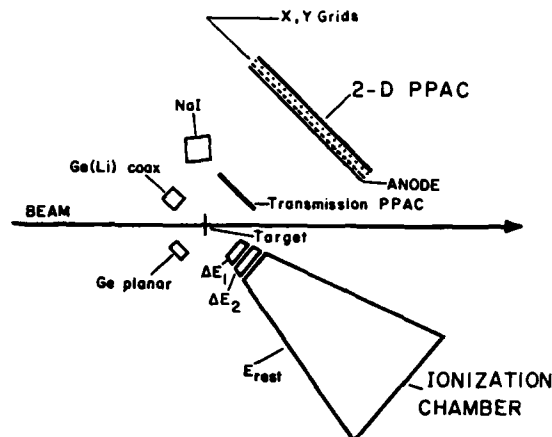


Fig. 1. Experimental set up.

the rear 2 dimensional position sensitive (stop) PPAC. The rear PPAC also provided a ΔE measurement. One can now require either that one partner has fissioned and determine $P_K^{(f)}$, or that both partners are intact and determine $P_K^{(u)}$. If the nuclear time delays associated with fission at a certain $-Q$ are equal to those encountered with no fission in the exit channel, we expect to find $P_K^{(u)} = 2P_K^{(f)}$. This consistency requirement provides a valuable check of the method. The U K x-rays were detected by an 8-mm thick intrinsic Ge planar detector directly opposite the PPAC arm of the experiment.

We will present preliminary results and compare them with the findings of Stoller *et al.*²

References

* Supported in part by the National Science Foundation (Grant PHY-83-13676).

[†] Presently at Washington University, St. Louis, MO.

1. R. Anholt, Phys. Lett. **88B**, 262 (1979).
2. Ch. Stoller *et al.*, Phys. Rev. Lett. **53**, 14 (1984).
3. L. G. Sobotka, (unpublished).

INTERMOLECULAR ENERGY TRANSFER INVOLVING ELECTRONICALLY EXCITED MOLECULES: $\text{He}(1S) + \text{H}_2(\text{B } ^1\Sigma_u^+)$ Randall M. Grimes[†], William A. Lester, Jr.[‡] and Michel Dupuis^{*}

Materials and Molecular Research Division, Lawrence Berkeley Laboratory, Berkeley, CA 94720

[‡]Also: Department of Chemistry, University of California, Berkeley, CA 94720^{*}Present address: IBM Research Laboratory, Kingston, NY 12401

Improvements in experimental techniques of preparation and detection of electronically excited molecules have increased interest in their collision phenomena. In an early experimental study, cross sections for rovibrational and electronic energy transfer were measured for $\text{HD}(\text{B } ^1\Sigma_u^+, v=3, j=2)$, excited by an argon lamp, in the presence of He, Ne, and $\text{HD}(\text{X } ^1\Sigma_g^+)$.¹ The He-HD system is small enough to allow an accurate quantum mechanical treatment of both the electronic and nuclear motion. Progress made toward understanding the collision processes of the closely related $\text{He} + \text{H}_2(\text{B } ^1\Sigma_u^+)$ system will be reported.

The potential energy surface (pes) was determined using self-consistent field plus configuration interaction methods. In addition to interaction energies calculated using this procedure, energies calculated using a similar method by Römelt, et. al.² and Nicolaides, et. al.³ have been used to construct the pes employed in this study. The long range interactions are described by a multipole expansion.

The pes has several noteworthy features. An attractive interaction, with a minimum of ~ 0.03 eV, is found at a He to H_2 center-of-mass separation of ~ 4.0 a.u., H_2 bond length (r) at the equilibrium separation (r_e) of 2.4 a.u., and angle θ ($\vec{R} \cdot \vec{r}$) of 90° . An avoided crossing with the $\text{He} + \text{H}_2(\text{B } ^1\Sigma_u^+)$ pes causes a bump centered at $R \approx 4.0$ a.u., $r \approx 2.4$ a.u., and $\theta \approx 0^\circ$. These features combine to make the pes highly anisotropic (see figure 1) and thus will strongly affect rovibrational energy exchange. Another avoided crossing, this one with the ground state ($\text{He} + \text{H}_2(\text{X } ^1\Sigma_g^+)$) pes, leads to a very deep

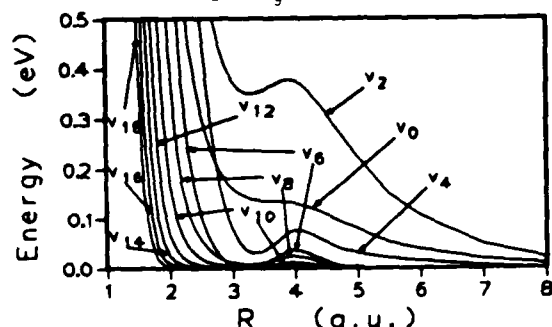
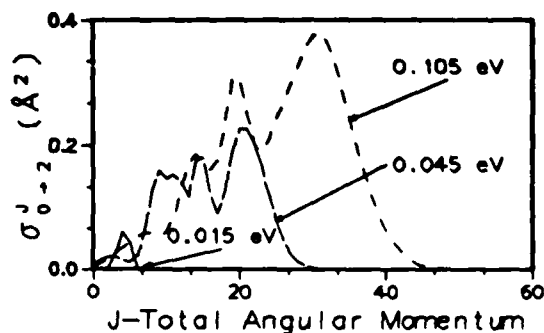


Figure 1: Legendre Coefficients for Rigid-Rotator PES

(~ 1.5 eV) well centered at $R \approx 1.5$ a.u., $r \approx 4.0$ a.u., $\theta \approx 45^\circ$.³ This avoided crossing provides an explanation of the fluorescence quenching observed in the experimental study.³ Overall, the pes for electronically excited He- H_2 is much more complex than those generally encountered in ground state studies.

As a first step in the dynamics studies, cross sections for rotational excitation have been calculated in the rigid rotator model using the space-fixed coupled-channel formalism and an analytical fit to the *ab initio* pes. Standard methods are used to solve the coupled equations for c.m. energies of 0.015-0.165 eV. In this range at least three closed rotational levels must be included to converge total inelastic cross sections to three significant figures. Partial cross sections show a high degree of structure compared to previously studied systems (see figure 2). This structure appears to be mainly due to the change in anisotropy with R . The magnitudes of total cross sections for $\Delta j = \pm 2$ transitions are comparable to those for ion-molecule systems.

Computations of cross sections for rovibrational energy transfer are in progress and will be described.

Figure 2: Partial cross sections versus Energy for the $0 \rightarrow 2$ Rotational Transition

References

1. E. H. Fink, D. L. Axins, and J. B. Mann, *Chem. Phys.* **56**, 900 (1972).
2. J. Römelt, S. D. Peyerimhoff, and K. L. Bunker, *Chem. Phys.* **34**, 493 (1978).
3. S. C. Farantos, G. Theodorakopoulos, and J. H. Nicolaides, *Chem. Phys. Lett.* **101**, 763 (1983).

*This work was supported by the Director, Office of Basic Energy Sciences, Chemical Sciences Division, of the U.S. Department of Energy under Contract No. DE-AC03-76SF0009.

EFFICIENCY OF (R,T) ENERGY TRANSFERS
IN He, Ar COLLISIONS WITH N₂ AND O₂

F. A. Gianturco, A. Palma and M. Venanzi

Department of Chemistry, University of Rome,
Città Universitaria, 00100 Roma, AD, Italy.

When only rotational energy transfers are considered the final cross sections, integral and differential, that are obtained depend mainly on the anisotropic part of the corresponding potential energy surface (PES) and therefore their measurements constitute a primary source of information on the orientational features of that PES. The recent availability of such data^{1,2} has therefore spurred a renewed interest, for some of the simpler atom-diatomic neutral cases, in establishing a specific link between the energy distribution among the numerous rotational final channels and the various features of the interaction itself.

In the present study we have directed our attention to the case of weakly interacting Van der Waals (VdW) molecules, i.e. to the analysis of specific aspects of the potential surfaces between a Nitrogen molecule or an Oxygen molecule and two of the rare gases, He and Ar. The primary motivation for this study came from the existence, for the above systems, of rather accurate multiproperty analysis of their full interaction^{3,4}.

Calculations were therefore carried out, both within the approximate coupling scheme of the Infinite Order Sudden Approximation (IOSA) and with a rigorous inclusion of all the necessary open and closed channels (CC equations). The examined range of collision energies went from the region in which experiments are available for He-N₂, He-O₂ and Ar-N₂ systems to values of E_{coll} for which the impulse approximation was still deemed to be valid for $j \rightarrow j'$ transitions as large as 30.

Figure 1 shows the IOS results for He-N₂ and Ar-N₂ as function of j_{fin} , while Fig. 2 indicates that the angles for which rotational rainbows appear move to smaller values for He-N₂ when the Ar-N₂ reduced mass is used in the calculations ('scaled' curve). This is an indicator of the He-N₂ PES being more anisotropic than Ar-N₂. Further differences of behaviour will be discussed at the Conference.

References

1. M. Faubel, K. M. Kohl and J. P. Toennies, *Faraday Discuss.* **73**, 205 (1982).

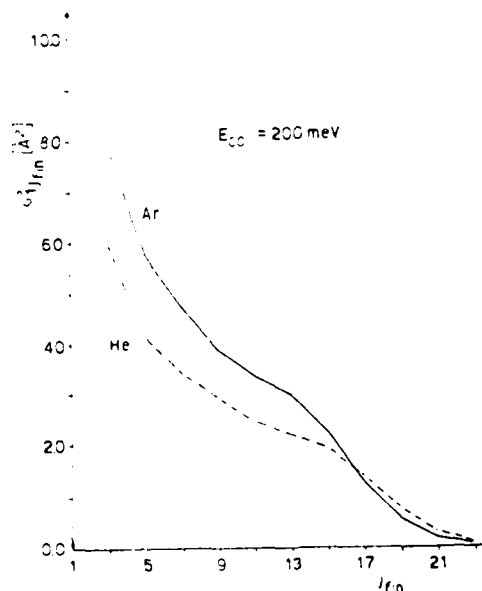


FIGURE 1

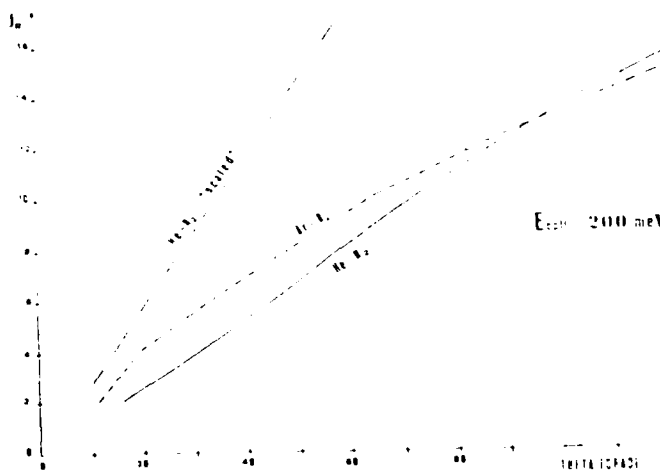


FIGURE 2

2. M. Faubel, K.M. Kohl, J.P. Toennies and F.A. Gianturco, *J. Chem. Phys.* **78**, 5629 (1983).
3. F.A. Gianturco and A. Palma, in *Intramolecular Dynamics* (Reidel, Amsterdam, 1982).
4. R. Candori, F. Pirani, F. Vecchiocattivi, F.A. Gianturco and M. Venanzi, *J. Chem. Phys.* (in press).

THEORETICAL STUDIES OF THE BOUND STATES AND SCATTERING OF H_2-H_2 AND $HD-H_2$.
A GENERAL COMPARISON OF THE $HD-H_2$ AND $HD-He$ SCATTERING SYSTEMS.

Joachim Schaefer

Max-Planck-Institut für Physik und Astrophysik, Institut für Astrophysik, 8046 Garching, FRG

Improved interaction potentials of H_2-H_2 and $HD-H_2$ (D_2) have been determined based in the previously tested ab initio potential of H_2-H_2 (M80). Experimental results of the second virial coefficient of H_2 have been used for evaluating a significant correction in the attractive potential range. As a consequence of this, the dimer binding energies became significantly larger. The relative anisotropy of the potential has been conserved in the fit procedure for maintaining the correct rotationally inelastic features previously tested.⁽¹⁾

The source of the main shortcoming of the previous 10-term $HD-H_2$ interaction potential showing up in too large $j = 1$ transition cross sections⁽²⁾ could be removed simply by determining all anisotropic terms of this potential involved in the dynamics in a converged representation. Results of extensive close coupled scattering calculations and the determination of various

kinds of cross sections obtained from the new $HD-H_2$ potential contribute the main part of this paper.

Several effective cross sections of the $HD-He$ system will also be shown for a general comparison of the $HD-H_2$ and $HD-He$ system.

References:

- 1) L. Monchick and J. Schaefer, *J.Chem.Phys.* 73, 6153 (1980);
R.O. Watts and J. Schaefer, *Mol.Phys.* 47, 933 (1982);
U. Buck et.al., *J.Chem.Phys.* 78, 4439 (1983);
W.E. Köhler and J. Schaefer, *J.Chem.Phys.* 78, 4862, 6602 (1983)
- 2) U. Buck et.al., *J.Chem.Phys.* 74 535 (1981); *ibid*, 78, 4430 (1983)

VIBRATIONAL-ROTATIONAL DE-EXCITATION OF SiO
IN COLLISION WITH RIGID-ROTOR H₂

Ronald J. Bieniek

Department of Physics, University of Missouri-Rolla, Rolla, Missouri 65401 USA

State-to-state cross sections for vibrational-rotational de-excitation of SiO through collisions with structureless H₂ have been reported.¹ These are required to understand the mechanism of the astrophysical SiO masers that arise in the outer atmosphere of certain late-type stars.^{2,3} In the calculation of cross sections, the SiO was treated as a vib-rotor within the context of the adiabatic, distorted-wave, infinite-order sudden (ADWIOS) approximation.^{4,5} An He-SiO potential was used as the electronic hypersurface.⁶ This included long-range interaction of the polarizability of He with the permanent dipole and quadrupole moments of SiO.

However, by treating the H₂ as structureless (i.e., as a "low-mass" He atom), the possible long-range effects of the quadrupole moment of H₂ were neglected. Because of the large dipole moment of SiO, the quadrupole-dipole interaction can dominate at long-range. The quadrupole-dipole term has now been included in a new ADWIOS calculation of SiO + H₂ collisions in which the H₂ is treated as a rigid-rotor. The collisional energy is that characteristic of a temperature of $T \approx 2500$ K. Although the sudden approximation is not accurate for the investigation of rotational excitation of H₂ at this energy, it can indicate the importance of the quadrupole-dipole

interaction in state-to-state SiO cross sections if the contributions from all H₂ states are summed. This issue is astrophysically interesting, for changes of less than an order of magnitude in collisional cross sections may significantly affect our understanding of circumstellar SiO masers.

Support for this research from the Research Corporation and the University of Missouri is gratefully acknowledged.

References

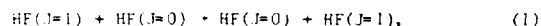
1. R. J. Bieniek and S. Green, *Astrophys. J. Lett.* **265**, L29 (1983); **270**, L101 (1983).
2. L. R. Western and W. D. Watson, *Astrophys. J.* **275**, 195 (1983).
3. S. H. Langer and W. D. Watson, *Astrophys. J.* **284**, 751 (1984).
4. L. Eno and G. G. Balint-Kurti, *J. Chem. Phys.* **71**, 1447 (1979).
5. R. J. Bieniek, *J. Chem. Phys.* **73**, 851 (1980).
6. R. J. Bieniek and S. Green, *Chem. Phys. Lett.* **84**, 380 (1981).

ROTATIONAL AND VIBRATIONAL ENERGY TRANSFER IN LOW-VELOCITY MOLECULAR COLLISIONS

Kazuo Takayanagi, Takashi Wada and Atsushi Ichimura

Institute of Space and Astronautical Science, Komaba 4-6-1, Meguro-ku, Tokyo 153 Japan

The dipole-dipole interaction plays a dominant role in the collisional rotational transitions of molecules in polar gases. The relevant cross sections are usually much larger than the geometrical cross sections of the colliding molecules.¹ Recently, Vohralik and Miller² have measured the resonant rotational energy transfer cross section for HF



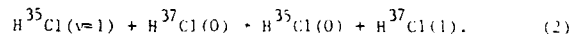
J being the rotational quantum number. They obtained a cross section of approximately 300 \AA^2 at the mean collision energy of 0.15 eV. We have applied the Perturbed Rotational State approach to (1) in the very-low-velocity collisions, while the close-coupling method was used for somewhat higher velocities.³ For all these calculations the straight classical trajectories have been assumed, so that these methods are called IP-PRS and IP-CC, respectively. Outline of these approaches has been given in ref.1, where rotational excitations have been studied. We assume the simple dipole-dipole interaction. Then, the energy transfer probability P per collision is a function of the reduced (dimensionless) impact parameter $p = b(D^2/B)^{1/3}$ and the reduced velocity $v = \pi v / (DB)^{2/3}$, where b and v are the impact parameter and the collision velocity, and B and D are the rotational constant and the dipole moment of the molecule, respectively. Thus, our result can be applied not only to HF, but also to any other pair of identical linear polar molecules.

In Fig. 1, the calculated $2 \cdot pP$ as a function of p is shown for $v = 0.3$ (the curve $v = 1$). It is emphasized that $p = 1$ corresponds to $b = 9.36 \text{ \AA}$ for HF. Unless the reduced velocity v is higher than unity, the main contribution to the cross section comes from distant collisions (far outside the size of molecules) so that the use of the straight line trajectory and the neglect of all the interactions other than the dipole-dipole force are justified. The integrated cross section is a rapidly decreasing function of v . The calculated cross section at 0.15 eV is somewhat larger than 400 \AA^2 . The experimental cross section² was obtained by detecting molecules scattered into a small solid angle in the forward direction. Taking account of ambiguities involved in the analysis of the experimental data, the theoretical value is not inconsistent with the experimental finding.

Similar calculations are being made for collision of dissimilar molecules. The product of dipole moments

D_1 and D_2 of the two molecules replaces D^2 in the theory. When the ratio ξ of the rotational constants B_1 and B_2 deviates from unity considerably, the transfer cross section becomes smaller. Fig. 1 also shows results for $\xi = 0.9$ and 0.5.

Horwitz and Leone⁴ have measured the rate of near-resonant vibrational energy transfers such as



The first-order perturbation theory gives cross section much less than the experimental values. The short-range forces may be important. We suggest that the distortion of the molecular rotation during collision may be also helpful to increase the vibrational energy transfer in low-velocity encounters. We are preparing for detailed calculations and hope to report some results at the conference.

References

1. T.Wada, J. Phys. Soc. Japan **53**, 3362 (1984) and references therein.
2. P.F.Vohralik and R.E.Miller, Resonant rotational energy transfer in HF (preprint).
3. K.Takayanagi and T.Wada, to be published.
4. A.B.Horwitz and S.R.Leone, J. Chem. Phys. **69**, 5319 (1978); **70**, 4916 (1979).

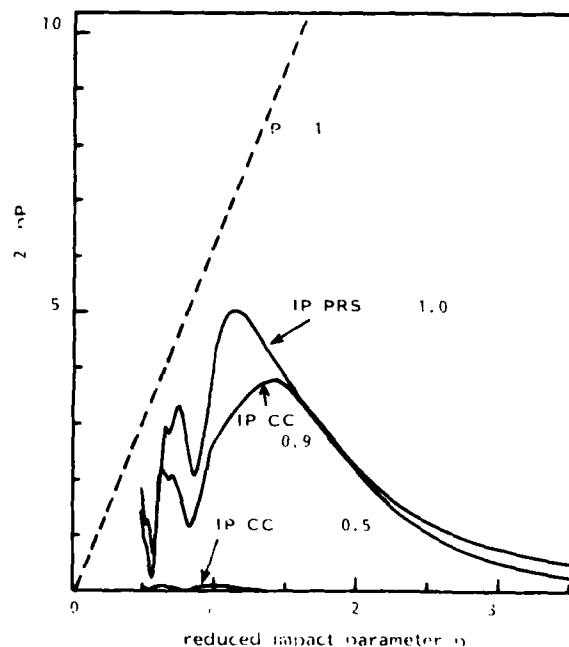


Fig. 1. IP-PRS, $p = b(D_1 D_2 / B_1 B_2)^{1/3}$
 $v = \pi v / (B_1 B_2 D_1 D_2)^{2/3} = 0.3$

ANISOTROPIC POTENTIALS FOR $\text{NO}(^2\Pi)$ -RARE GASES FROM HIGH-RESOLUTION TOTAL DIFFERENTIAL SCATTERING CROSS SECTIONS

L.Beneventi, P.Casavecchia, and G.G.Volpi

Dipartimento di Chimica, Università di Perugia, 06100 Perugia, ITALY

The anisotropy of the $\text{NO}(^2\Pi)$ -rare gas (R) interaction is investigated by measuring total (elastic + inelastic) differential cross sections (DCSs) at different collision energies in high-resolution scattering experiments. Information on the anisotropy of the potential energy surfaces (PESs) is obtained from the quenching of the rainbow and diffraction oscillations in the total DCS. Diffraction oscillations are resolved for the first time in an atom-molecule system not containing He or H_2 (and isotopes).

The experiments are performed on a newly-built high resolution crossed beam apparatus by crossing two well collimated supersonic beams of pure NO and rare gas and detecting the in-plane scattering by a rotatable UHV mass spectrometer.¹ The beam velocity distributions are measured by a computer controlled TOF system.

The most prominent features observed in the total DCS are a well resolved rainbow structure for NO-Ar, Kr¹ and Xe and diffraction pattern oscillations for He-NO, while for Ne-NO both types of oscillations are seen. In Fig. 1 we report the angular distribution $I(\theta)$ for Ne-NO obtained with both beams at room temperature.

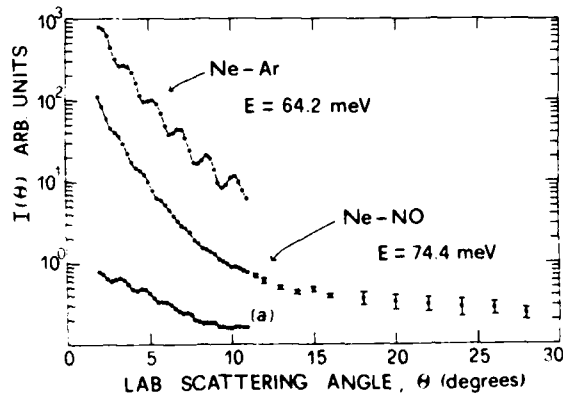


Fig. 1 - Total angular distribution for Ne-NO. The small angle $I(\theta)$ for Ne-Ar is also shown for comparison. Curve (a) represents the small angle data for Ne-NO plotted as $I(\theta) \sin \theta$ versus θ . The solid lines connect the data points.

The circles are the average of four angular scans. The error bars, representing ± 1 standard deviation, are smaller than the experimental points at angles $< 10^\circ$. The high-frequency oscillations superimposed on the fall-off of the main rainbow are resolved. They can be more clearly localized by plotting the data as $I(\theta) \sin \theta$ versus θ (see curve (a) in Fig. 1). An experiment with a liquid nitrogen cooled Ne beam is now being carried

out to observe a much more sizeable portion of the rainbow and resolve even better the diffraction pattern.

The two possible quantum oscillations observable in the DCS appear considerably damped in atom-molecule systems when compared with those observed for the corresponding isotropic rare gas-rare gas systems. The amount of this damping can be evaluated accurately, knowing the damping due to experimental averaging. It has been shown that the damping of the rainbow and diffraction oscillations in the total DCS is directly related to the potential well depth and minimum position anisotropy, respectively.² In Fig. 1 we report also the small angle $I(\theta)$ for Ne-Ar measured under the same experimental arrangement as for Ne-NO. A dramatic quenching of the diffraction structure can be seen in the Ne-NO case. The high quality of the data for Ne-Ar (see for example Ref. 3 for comparison) witnesses the high-resolution characteristics of the present experiment.

The NO-R collision can be described¹ in terms of elastic scattering occurring separately on each of the two identical adiabatic PES correlating with the two molecular states of NO, $^2\Pi_{1/2}$ and $^2\Pi_{3/2}$. Data analysis proceeds by using anisotropic flexible potential forms and calculating the total DCS within the infinite-order-sudden (IOS) approximation⁴ which is expected to work well for these systems under the present experimental conditions. Alternative coupling schemes, more rigorous than the IOS prescription, are also being considered.

Anisotropic PES for NO-Ar and NO-Kr derived from the best-fit of total DCSs were found¹ to be in agreement with the results of another experimental investigation with state selected NO.⁵ NO-Ar was found to exhibit a larger ($\sim 20\%$) anisotropy than the related O_2 -Ar and N_2 -Ar systems.¹ The results for He-NO will be compared with those recently obtained for the related He- N_2 , O_2 systems.⁶ The variation of the anisotropy along the NO-R series will be examined.

References

1. P.Casavecchia, A.Laganà, and G.G.Volpi, *Chem.Phys. Lett.* **112**, 445 (1984)
2. P.T.Pack, *Chem.Phys.Lett.* **55**, 197 (1978)
3. C.Y.Ng, Y.T.Lee, and J.A.Barker, *J.Chem.Phys.* **61**, 1096 (1974)
4. G.A.Parker and R.T.Pack, *J.Chem.Phys.* **68**, 1585 (1978)
5. H.H.W.Thuis, J.Reuss, J.J.H. Van den Biesen, and C.J.N. Van den Meijdenberg, *Chem.Phys.* **52**, 211 (1980)
6. M.Faebel, K.H.Kohl, J.P.Toennies, K.T.Tang, and Y.Y. Yung, *Faraday Disc.Chem.Soc.* **73**, 205 (1982); M.Faebel, K.H.Kohl, J.P.Toennies, and F.A.Gianturco, *J.Chem.Phys.* **78**, 5629 (1983)

ENERGY TRANSFER IN COLLISIONS OF NH_3 AND $(\text{NH}_3)_2$ WITH HELIUM

U. Buck, H. Meyer, R. Schinke

Max-Planck-Institut für Strömungsforschung, D3400 Göttingen, Federal Republic of Germany

In a crossed molecular beam experiment differential energy loss spectra have been measured for NH_3 -He and $(\text{NH}_3)_2$ -He by time-of-flight analysis of the scattered particles. The ammonia beam is produced by expanding an 8 % mixture of NH_3 in He. By detecting NH_3 -monomers and dimers at different laboratory angular ranges we are able to distinguish between these two species by their different kinematic behaviour in the scattering process. Therefore, the measured spectra are independent from the fragmentation during the ionization process and the cluster distribution in the beam. Two typical spectra are shown in Fig. 1.

For the monomer scattering a most probable energy transfer of about 25 % of the collision energy is observed in the backward direction. It is completely attributed to rotational excitation. From these data, a complete rigid rotor potential energy surface for NH_3 -He is determined by combining large basis set SCF calculations with damped dispersion coefficients and fitting two parameters of the damping function by comparison of experimental and calculated cross sections.¹ The dynamical calculations are performed in the coupled states approximation. The results of such a calculation

are shown in the upper part of Fig. 1 by the solid line.

The time-of-flight (TOF) spectra for dimer scattering show a much larger energy transfer at a collision energy of 108 meV. A most probable energy transfer of about 55-60 % of the collision energy is observed at large center-of-mass scattering angles. To investigate the origin of the observed energy transfer a classical trajectory calculation has been performed.² In this calculation the ammonia dimer is treated as a rotating-vibrating diatom (NH_3 is assumed to be structureless). To construct the $(\text{NH}_3)_2$ -He potential surface spherically averaged pair potentials are added. The classical calculation predicts a maximum rotational-vibrational energy transfer of about 35 %. This calculation, shown as solid line in the lower part of Fig. 1, is not able to reproduce the measured data. The lack of larger energy transfer is very probably due to the additional excitation of internal degrees of freedom (torsion) of a single ammonia molecule in the dimer, which is not included in the model calculations.

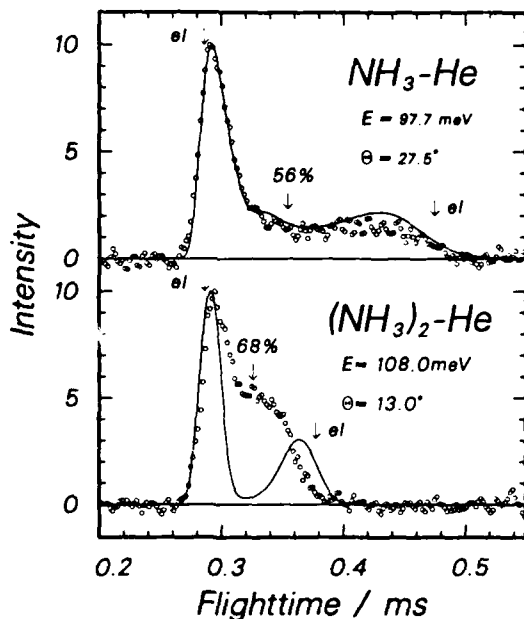


FIGURE 1 Time-of-flight spectra for the ammonia monomer and dimer scattering. The positions of elastically scattered particles are indicated by arrows. Also marked are the flighttimes corresponding to the maximum possible energy transfer of each spectrum.

References

1. U. Buck, H. Meyer, R. Schinke, and G.H.F. Diercksen, J.Chem.Phys., to be submitted.
2. Z. Bacic, U. Buck, H. Meyer, and R. Schinke, Chem. Phys.Lett., to be submitted.

ROTATIONAL AND VIBRATIONAL EXCITATION IN COLLISIONS OF Na^+ IONS WITH N_2 , CO , O_2 , AND CO_2 MOLECULES

S. Kita, T. Hasegawa, A. Kohlhasse,* and H. Inouye*

Research Institute for Scientific Measurements, Tohoku University, Katahira-Nichome, Sendai 980, Japan

Differential scattering of Na^+ ions in collisions with N_2 , CO , O_2 , and CO_2 molecules was studied with a crossed-beam technique using supersonic molecular beams. The experiments were performed at laboratory collision energies of $50 \text{ eV} \leq E_{\text{lab}} \leq 350 \text{ eV}$, and at scattering angles of $\theta \leq 70^\circ$. The energy of the scattered particles was analyzed by a time-of-flight technique. Figs. 1 and 2 show typical energy loss spectra of Na^+ ions after collisions with N_2 , CO , O_2 , and CO_2 at $E_{\text{lab}} = 200 \text{ eV}$ and $\theta = 20^\circ$. As seen in the figures, the spectra for Na^+-N_2 and Na^+-O_2 contain two peaks, while the spectrum for Na^+-CO contains three peaks. The spectrum for Na^+-CO_2 is also composed of three peaks. The arrows N, C, and O in the figures indicate the locations determined by the spectator mechanism. The measurements of the angular and energy dependences show that the energy losses in the spectra are due to rotational and vibrational excitation of the molecules. The contribution of electronic excitation can be neglected under these experimental conditions.

In the diatomic cases of N_2 , CO , and O_2 , the differential cross sections for rotational excitation were calculated with the hard-shell model and the uniform semiclassical sudden approximation.^{1,2} The calculations show structures similar to those found in the experiment, two peaks for N_2 and O_2 , and three peaks for CO . The peaks at $\Delta E/E = 0$ in the calculation are Jacobian peaks, while the others are rotational rainbow peaks. The calculated rainbow positions agree well with the locations of peak (2) for N_2 and O_2 , and of peaks (2) and (3) for CO . Therefore one can attribute the measured peaks (2) and (3) to the rotational rainbow effect. The rotational rainbows are caused by rotational excitation around the

molecular orientations $\gamma = 53^\circ$ and 130° . Where γ , defined at the turning point in the collision, is the angle between the molecular axis and the vector from the approaching ion to the center-of-mass of the molecule. The experimental peak (1) is located in the vicinity of $\Delta E/E = 0$, but the peak location depends on the scattering angle and the collision energy. Classical trajectory calculations were performed to understand these experiments. The result of the calculations is that peak (1) arises from vibrational excitation around the molecular orientation of $\gamma = 93^\circ$.

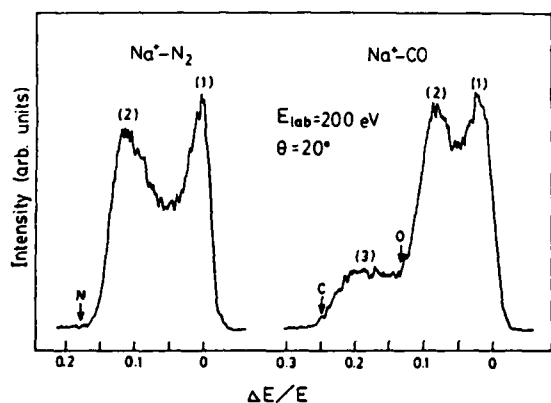
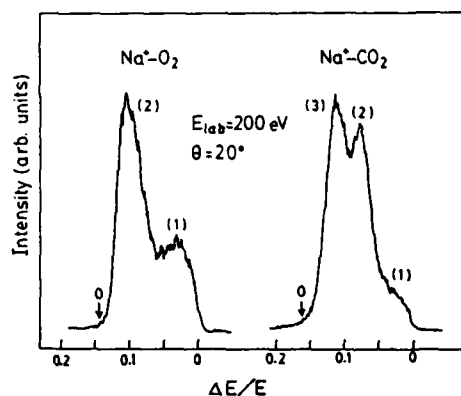
Also in the Na^+-CO_2 case differential cross sections for rotational excitation were calculated. The computed classical rainbow position was too far on the high energy loss side. A classical trajectory calculation has not yet been performed. However, if one imagines the interaction of the Na^+ ion with only the CO component of the molecule, the main peaks (2) and (3) for Na^+-CO_2 can be well related to the peaks (1) and (2) for Na^+-CO , respectively.

* JSPS fellow.

* Present address: Department of Chemistry, Bunri University Tokushima, Yamashiro-cho, Tokushima 770

References

1. H. J. Korsch and R. Schinke, J. Chem. Phys. **73**, 1222 (1980).
2. H. J. Korsch and R. Schinke, J. Chem. Phys. **75**, 3850 (1981).


 Fig. 1. Energy loss spectra for Na^+-N_2 and Na^+-CO .

 Fig. 2. Energy loss spectra for Na^+-O_2 and Na^+-CO_2 .

KEV-ENERGY DIFFERENTIAL SCATTERING: CROSS SECTIONS, INTERACTION POTENTIALS AND DIFFRACTION

J. H. Newman, D. A. Schafer, K. A. Smith, and R. F. Stebbings

Space Physics and Astronomy Department, Rice University, Houston, TX 77251 USA

Interaction Potentials

Measurement of accurate differential cross sections (DCS's) for keV-energy atomic and molecular collisions permits determination of the interaction potentials between the colliding particles by direct inversion of the DCS data using techniques described by Smith¹ and others.² Interaction potentials have been computed from DCS's measured for the scattering of 0.5 to 5 keV H, He, and O atoms from He, H₂, N₂, and O₂ for laboratory-frame scattering angles between 0.1° and 5°.

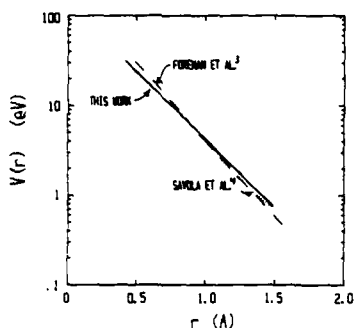


Fig. 1. Interaction potentials for He-He collisions. Present results are from differential cross section measurements, others are from total cross section data.

Fig. 1 shows the interaction potential produced by inversion of the DCS data for He - He scattering, along with potentials derived from total cross section measurements.

Diffraction Effects

A characteristic of small-angle differential scattering cross sections plotted in reduced coordinates ($\tau = E\theta$, $\rho = \theta \sin^2 \theta d\sigma/d\Omega$) is that ρ for one projectile energy agrees with that for other energies where the data overlap in τ . This behavior is consistent with classical scattering from a single potential curve.¹ Yet, in the present data, there are distinct regions where the reduced-coordinate cross sections for projectiles of different energies do not agree with one another. This disagreement is particularly pronounced for He - N₂ DCS shown in Fig. 2. In the region of disagreement, the structure is sharper at lower projectile energies and broader at higher energies, consistent with a recent discussion of diffraction effects by Russek.⁵ There are several oscillations in the DCS data for 500 eV H-atom collisions with N₂ (Fig. 3), but much of this structure disappears at higher energies.

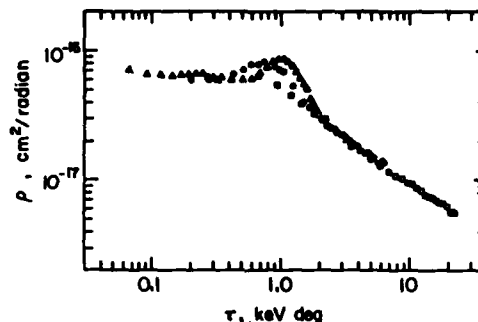


Fig. 2. Reduced cross sections: He + N₂. Δ : E 500 eV, \circ : E = 1500 eV, \square : E = 5000 eV.

Kalinin, Leonas and Rodinov⁶ observed a similar anomalous behavior in the reduced cross sections for keV-energy He collisions with N₂, which they attributed to a vibrational "rainbow" in scattering from molecules. The present observation of structure in the DCS for atomic hydrogen scattering by helium (Fig. 3) suggests, however, that an alternate explanation may be required.

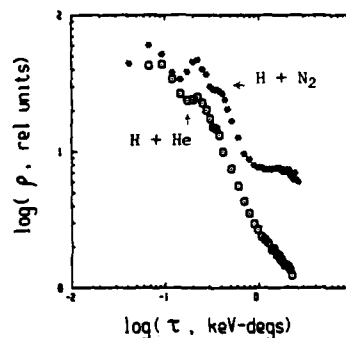


Fig. 3. 500-eV H scattering by He and N₂.

This work was supported by National Science Foundation under grant ATM 8023219 and by National Aeronautics and Space Administration under grant NSG 7386.

References

1. F. T. Smith, R. P. Marchi, and K. G. Dedrick, *Phys. Rev.*, **150**, 79 (1966).
2. See U. Buck, *Rev. Mod. Phys.*, **46**, 369 (1974).
3. P. B. Foreman and P. K. Rol, *J. Chem. Phys.*, **61**, 1658 (1974).
4. W. J. Savola, Jr., F. J. Erickson, and E. Polack, *Phys. Rev. A*, **7**, 932 (1973).
5. A. Russek, *Phys. Rev. A*, **20**, 113 (1979).
6. A. P. Kalinin, V. B. Leonas, and I. D. Rodinov, *Sov. Phys. Doklady*, **28**, 39, 1983.

BREAKDOWN OF ENERGY-LOSS SCALING IN $\text{Ne} + \text{D}_2$ COLLISIONS

Ralph Snyder and Arnold Russek

Department of Physics, University of Connecticut, Storrs, CT 06268, USA

In many atom-molecule collisions the most probable energy loss, f , is a function only of the reduced scattering angle, $t = E\theta$, with no other dependence on the projectile energy, E . The qualitative prediction of this scaling property was first made by Sigmund¹, and it has been verified experimentally in several collision systems^{2,3}. In our earlier work⁴ we made quantitative calculations of the specific functional dependence of f upon t for $\text{He} + \text{D}_2$ collisions, using ab initio SCF potential surfaces and the impulse approximation. In this paper we present the results of more elaborate calculations of $f(t)$ which do not invoke the impulse approximation and which show the manner in which energy-loss scaling breaks down.

As described in the earlier work of Refs. 3 and 4 we use classical mechanics to calculate the energy loss and the scattering angle in a sampling of both impact positions and molecular orientation angles, and we can assemble from those values the doubly differential and the singly differential cross sections and the most-probable- f versus t curves. Unlike that earlier work however, we now discard the impulse approximation (which leads to scaling) and instead numerically integrate the equations of motion for each impact configuration at each projectile energy, E . In this paper we discuss $\text{Ne} + \text{D}_2$ collisions, for which a semi-empirical energy surface derived from low t data was available⁴.

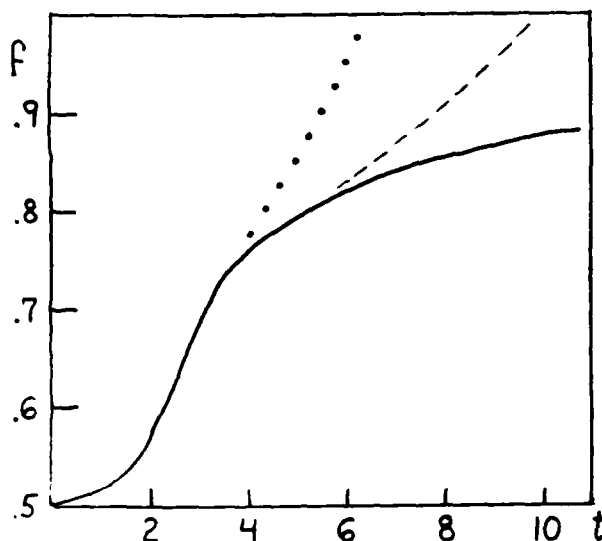
The figure shows our results for most-probable- f versus t at projectile energies of 1 and 2 keV. At low t these results match the scaled results of the impulse calculations. The salient manifestation of scaling breakdown is that there is now a maximum attainable value of t at each projectile energy (approximately 7.0 and 12.5 keV-degrees for $E = 1$ and 2 keV respectively). The appearance of that maximum t is important and can be qualitatively explained in that very large scattering angles can only occur in collisions in which the projectile has a close encounter with one of the target atoms. Such a collision resembles a two-body atom-atom collision for which kinematics determines an energy-independent maximum scattering angle $\theta = \sin^{-1} 2/20$. This suggests a breakdown of the scaling near reduced scattering angle $t = E\theta = 5.7$ keV-degrees for $E = 1$ keV

and near $t = 11.4$ keV-degrees for $E = 2$ keV. These values are approximately, but of course not precisely, in agreement with those of the figure: the actual adiabatic molecular-scattering energy surface remains three-body in nature, and this two-body argument is only an instructive, zero-order approximation. In fact, we believe that the comparison between the simple, two-body kinematical result and the full atom-molecule results (theoretical and experimental) may become a fruitful new tool for analyzing such collisions. The difference between them may provide another sensitive probe of three-body contributions to the energy surfaces, diagnostically similar to the 'breakaway' region where the energy loss first departs significantly from pure elasticity.

This work was supported by the National Science Foundation.

References

- 1) P. Sigmund, J. Phys. B, 11, L145 (1978).
- 2) N. Andersen, M. Vedder, A. Russek, and E. Pollack, Phys. Rev. A 21, 782 (1980).
- 3) J. Jakacky, E. Pollack, R. Snyder, and A. Russek, Phys. Rev. A 31, to be published, (1985).
- 4) R. Snyder and A. Russek, Phys. Rev. A 26, 1931 (1982).



Most probable f vs. reduced scattering angle, t . Solid line, scaled results of impulse approximation. Dotted line, present results for $E = 1$ keV. Dashed line, present results for $E = 2$ keV.

ENERGY LOSS SCALING FOR SMALL ANGLE ROTATIONALLY INELASTIC SCATTERING

F. E. Budenholzer, M. H. Chang, and S. C. Hu

Department of Chemistry, Pu Jen Catholic University, Taipei, Taiwan ROC

We consider small angle, rotationally inelastic collisions between an atom or atomic ion and an initially non-rotating diatomic molecule at collision energies from a few eV to several hundred eV. In this region we have used classical perturbation scattering theory (CPST) to calculate translational-rotation energy transfer.^{1,2} We found that for scattering at a particular reduced deflection angle $\tau = \theta/\theta_0$, where θ is the initial relative translational energy and θ_0 the center of mass scattering angle, the energy transferred into rotation scales with the collision energy,

$$E\Delta E_{\text{rot}} = f(\tau). \quad (1)$$

$f(\tau)$ is a complicated function dependent on the atom (ion)-diatomic potential and the collision masses. Formulas and prescriptions for calculation can be found in ref. 3.

Several researchers commented on the seemingly unusual nature of this scaling relationship. We have therefore verified it using full classical trajectories. A model $\text{Li}^+ - \text{Cl}^-$ potential surface was constructed and classical trajectories were run over this surface. 600 trajectories were run at a translation energy of 1.1 eV and 600 at an energy of 4.8 eV. The initial vibrational and rotational energies were set to zero. All other parameters were selected randomly in the usual way. If the scaling relationship of eq 1 were true, we would expect $E\Delta E_{\text{rot}}$ to be the same for various combinations of E and θ whose product is a particular value of τ . This was indeed found to be the case.

Though at first this result may seem somewhat surprising, it is in fact a logical extension of earlier theoretical work. Smith³ has shown that under the conditions considered here the reduced deflection angle $\tau = \theta/\theta_0$ is only a function of the impact parameter b . Thus one set of impact parameters gives scattering at reduced angle τ irrespective of the collision energy E . To the extent that CPST is valid, the collision may be described by calculating the impulse delivered to the molecule as the projectile moves along a straight line trajectory. The impact parameter is the distance of closest approach on this trajectory; it is also the moment arm of the torque acting on the molecule. Thus the degree of rotational excitation at a given value of b , and equivalently for a given value of τ , will be proportional to the impulse delivered. For higher energies (faster velocities) the impulse will be smaller and the consequent rotational energy transfer will also be smaller, while at lower energies a larger impulse

will be delivered leading to a larger ΔE_{rot} . This is the meaning of the scaling relationship of eq 1. A similar scaling relationship has been used to describe ion-molecule, vibrationally, rotationally inelastic scattering in the keV range.^{4,5}

A short report of this work has already been published in ref 1. This research was supported by the National Science Council of the Republic of China.

References

1. Frank E. Budenholzer, Ming-Hsiung Chang and Ping-Piao Lu, J. Phys. Chem. **89**, 199 (1985).
2. F. E. Budenholzer and C. C. Lee, Chem. Phys. **73**, 323 (1982).
3. F. T. Smith, P. P. Marchi, and K. T. Dedrick, Phys. Rev. **150**, 79 (1966).
4. P. Sigmund, J. Phys. B, **14**, L321 (1981).
5. M. Anderson, M. Vedder, A. Russek, and E. Pollak, Phys. Rev. A, **21**, 782 (1980).

A STUDY OF LOW KEV ENERGY $\text{Li}^+ + \text{D}_2$ COLLISIONS*

V. Heckman, S.J. Martin, J. Jakacky, Jr., and E. Pollack

Department of Physics, University of Connecticut, Storrs, CT 06268

We have recently completed a study of $\text{He}^0 + \text{D}_2$ collisions at low keV energies.¹ Emphasis was placed on the quasi-elastic channel since it yields information on the ground state potential energy surface. In our current investigation we find significant differences in the collisional behavior of $\text{Li}^+ + \text{D}_2$ when compared to the iso-electronic $\text{He}^0 + \text{D}_2$ case.

The experimental arrangement¹ is basically the same as that used in our $\text{He}^0 + \text{D}_2$ study. The apparatus was modified by replacing the glow discharge source with a α -eucryptite $^7\text{Li}^+$ ion emitter, resulting in a narrower energy spread in the beam. Energy analysis of the scattered Li^+ is made with an electrostatic energy analyzer² having a resolution of 0.5 eV per 1000 eV. In our Li^+ studies, the scattering angle is computed from the measured energy loss in the elastic channel using He target gas. D_2 gas is then leaked into the scattering cell and the energy loss of the scattered Li^+ is measured at the known angle.

Electronically elastic scattering is found to be the dominant direct collision process in $\text{Li}^+ + \text{D}_2$ in the 4.5 keV deg range studied. Weak electronically inelastic channels are seen at excitation energies ~ 12.5 eV. This behavior is in sharp contrast with the $\text{He}^0 + \text{D}_2$ case where electronically inelastic processes dominate the collision for ~ 2.0 keV deg. The measured energy loss (ΔE) of the scattered Li^+ beam is plotted as a function of $E\theta^2$ at 3.0 keV in Fig. 1. The $\text{Li}^+ + \text{D}_2$ collision at this energy is seen to be elastic for $E\theta^2 < 0.5$ keV deg². The vibro-rotational excitation (ΔE) is the difference between the measured ΔE and the

energy loss (T) for a purely elastic collision. The quantity $f=1/2(1+Q/T)$ when plotted vs $E\theta$ is particularly significant.^{1,3,4} To date we have determined the f vs $E\theta$ behavior in $\text{Li}^+ + \text{D}_2$ at an energy of 3.0 keV. The results of our measurements are shown in Fig. 2.

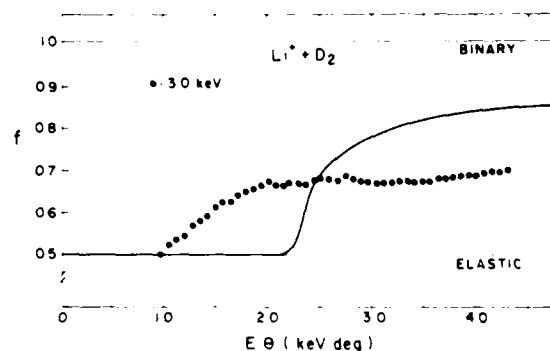


FIG. 2. f vs $E\theta$ for $\text{Li}^+ + \text{D}_2$. The solid curve represents the results for $\text{He}^0 + \text{D}_2$ at energies of 1.0, 1.5, and 2.0 keV.

The solid curve represents the results for $\text{He}^0 + \text{D}_2$ at energies of 1.0, 1.5, and 2.0 keV. The $\text{Li}^+ + \text{D}_2$ collisions are seen to break away from the elastic limit at ~ 1.0 keV deg, in contrast to the ~ 2.25 keV deg found for $\text{He}^0 + \text{D}_2$. The f values then rise slowly to a plateau at about 0.68 which lies below the corresponding values for $\text{He}^0 + \text{D}_2$. Another finding of particular interest is that at small angles the scattered Li^+ spectra from D_2 and the purely elastic spectra of $\text{Li}^+ + \text{He}$ are almost identical showing that there is little if any vibro-rotational excitation. Additional results will be presented.

References

*Supported by the National Science Foundation and the University of Connecticut Research Foundation.

1. J. Jakacky, Jr., E. Pollack, B. Sander, and A. Pussek, Phys. Rev. A, (to be published).
2. S.M. Fernandez, E.L. Eriksen, A.L. Bray, and E. Pollack, Phys. Rev. A 12, 1252 (1975).
3. N. Andersen, M. Keller, A. Pussek, and E. Pollack, Phys. Rev. A 11, 751 (1970).
4. P. Sigmund, N. Phys. B 14, 1321 (1967).

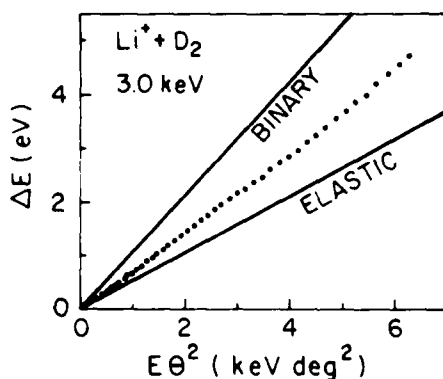


FIG. 1. Measured energy loss for the quasi-elastic channel.

ION ENERGY-LOSS SPECTROSCOPY IN THE COLLISIONS OF $\text{Ar}^+(^2P_{1/2})$ WITH H_2

Tomohisa Nakamura, Nobuo Kobayashi and Yozaburo Kaneko

Department of Physics, Tokyo Metropolitan University, Setagaya-ku, Tokyo 158, Japan

By means of ion energy-loss spectroscopy¹⁾, excitation and de-excitation processes in collisions of $\text{Ar}^+(^2P_{1/2})$ with H_2 molecules were studied in the energy range from 200 to 1000 eV.

Argon ions are produced by the electron impact at 10 kV. The ions extracted from the source contain $^2P_{1/2}$ and $^2P_{3/2}$ states with the statistical ratio, 2:1²⁾. This ion beam is mass- and energy-selected, then is injected into the collision chamber. After passing through the collision chamber, ions are energy-analyzed.

A typical energy-loss spectrum for 1000 eV Ar^+ incident on H_2 is shown in Fig. 1. The observation angle was 1° and the acceptance angle of the analyzer was 1.5° . In this spectrum, I fine structure transitions between different states of $\text{Ar}^+(^2P_{1/2})$, II vibrational excitations of H_2 molecules were observed. In addition to that, III coupled transitions of fine structure transitions and vibrational excitations were found. These processes (I, II and III) are represented as follows,

- I. $\text{Ar}^+(^2P_{1/2}) + \text{H}_2(v=0) \rightarrow \text{Ar}^+(^2P_{1/2}) + \text{H}_2(v=0)$
 II. $\text{Ar}^+(^2P_{1/2}) + \text{H}_2(v=0) \rightarrow \text{Ar}^+(^2P_{1/2}) + \text{H}_2(v=v')$
 III. $\text{Ar}^+(^2P_{1/2}) + \text{H}_2(v=0) \rightarrow \text{Ar}^+(^2P_{1/2}) + \text{H}_2(v=v')$
 $J, J' = 3/2 \text{ or } 1/2, J \neq J'$
 $v = 1 \text{ or } 2$

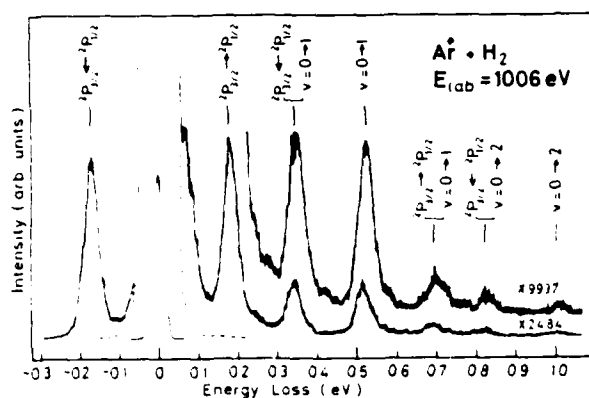


Fig. 1. A typical energy-loss spectrum.

The angular distributions of the primary ion beam and the scattering ions were measured. The angular profile of the scattered ions was found to be almost the same as that of primary beam above 300 eV. Therefore, the integral cross sections for each transitions can be

determined from the peak height ratio of the inelastic peak to the primary beam above 300 eV. The measured cross sections are shown in Fig. 2. Below 250 eV, however, the profile of the scattered ions was a little broader than that of the primary beam. Therefore the cross sections below 250 eV must be considered as partial cross sections for scattering within the acceptance angle of the analyzer, $\pm 0.5^\circ$ and they are supposed to be fairly smaller than the true values.

The de-excitation cross section $3/2 \rightarrow 1/2$ is twice the excitation cross section $3/2 \leftarrow 1/2$ in accordance with detailed balance. The cross sections of other transitions decrease with the increase of the energy-loss.

It was found that the cross sections $3/2 \leftarrow 1/2$ ($1/2 \rightarrow 3/2$) and $1/2 \rightarrow 3/2$ ($v=0 \rightarrow 1$) are almost independent on the ion energy above 300 eV, on the contrary, the cross sections of other transitions increase with the increase of ion energy.

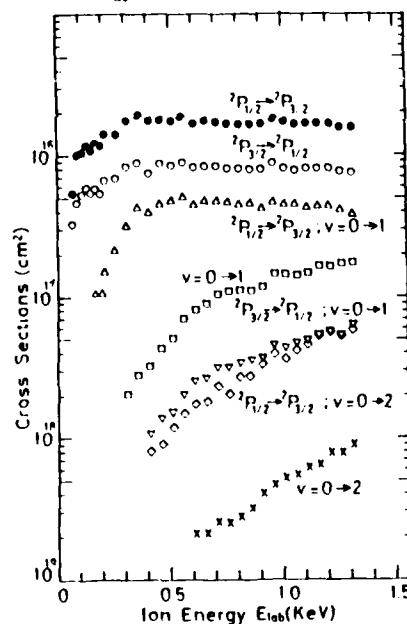


Fig. 2. Measured cross sections for excitations and de-excitations.

Reference

1. N. Kobayashi, Y. Itoh and Y. Kaneko: J. Phys. Soc. Jpn. **50**, 1707 (1981).
2. Y. Itoh, N. Kobayashi and Y. Kaneko: J. Phys. Soc. Jpn. **50**, 364 (1981).

ION ENERGY-LOSS SPECTROSCOPY FOR VIBRATIONAL TRANSITIONS OF N_2^+ IN THE COLLISIONS WITH Ne, Ar AND Kr

Tomohisa Nakamura, Nobuo Kobayashi and Yozaburo Kaneko

Department of Physics, Tokyo Metropolitan University, Setagaya-ku, Tokyo 158, Japan

The vibrational excitations and de-excitations of N_2^+ in collisions with Ar and Ne were studied by means of high resolution ion energy-loss spectroscopy¹⁾.

The N_2^+ ions are produced by electron impact ionization of N_2 gas at 150eV. They are mass- and energy selected, and injected into the collision chamber. The scattered ions are, then, energy analyzed. It takes more than 20nsec for N_2^+ ions from the ion source to the collision chamber. The excited states, whose life time is shorter than 26nsec, should almost decay to the ground state before entering the collision chamber.

Typical energy-loss spectra of scattered N_2^+ ions from Ne, Ar and Kr are shown in Fig. 1. The collision energy was 812eV and the observation angle was 0°. The intensity of the primary beam and the target gas pressure were fixed. In the case of Ar and Kr target, the energy-loss and energy-gain peaks were observed at about $\Delta E = \pm 245$ meV. With the experimental results of Josky et al.²⁾ by using of photofragment spectroscopy and the calculation of Taylor³⁾, these transitions were identified as the vibrational excitation and re-excitation in the ground state of $N_2^+(X^1\Sigma^+)$:

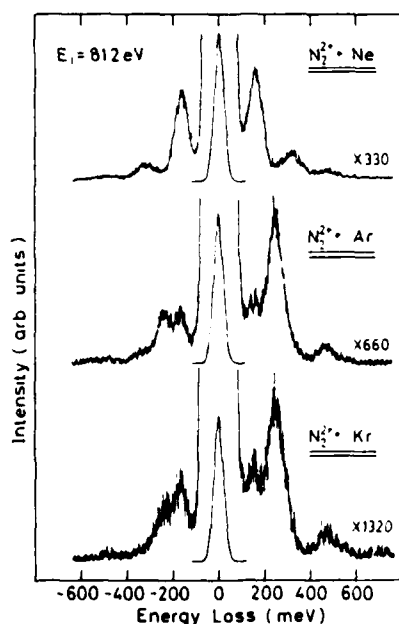
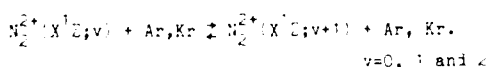
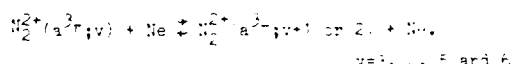


Fig. 1
Typical energy-loss spectra.

In addition to that, the energy-loss and energy-gain peaks were observed at about $\Delta E = \pm 160$ meV. These transitions were observed more clearly in the case of Ne target. In this case, the energy-loss and energy-gain peaks were observed at about $\Delta E = \pm 160$ meV and ± 320 meV. These ΔE 's suggest that the peaks correspond to the transitions of one and two vibrational quanta. Taylor has indicated theoretically that the energy defects of $v=3-4$, $4-5$ and $5-6$ of $N_2^+(a^3\Sigma^-)$ are 167.8, 163.3 and 158.8meV, respectively, and those of $v=3-5$ and $4-6$ are 331.1 and 322.1meV, respectively. Therefore the observed peaks were identified as



From the results, it was concluded that the present N_2^+ ion beam involves $N_2^+(a^3\Sigma^-)$ state and this state must be metastable with a life time longer than 20nsec.

It should be noted that these collision-induced transitions of vibrational states seem to be strongly dependent on the target species. With Ar and Kr target, transitions in $X^1\Sigma^+$ state were dominant while Ne target only those of $a^3\Sigma^-$ state were observed. The reason of such a remarkable distinction is not known at present.

Reference

1. N. Kobayashi, Y. Itoh and Y. Kaneko: J. Phys. Soc. Jpn. **45**, 1677 (1978).
2. P. C. Josky, R. Miller and J. Heint: Phys. Rev. A **12**, 200 (1975).
3. R. L. Taylor: Mol. Phys. **12**, 177 (1968).

COLLISIONAL QUENCHING AND ENERGY TRANSFER OF NS $B^2\Pi$

Jay B. Jeffries, David R. Crosley, and Gregory P. Smith
Chemical Physics Laboratory, SRI International, Menlo Park, CA 94025

Measurements have been made of rate constants for collisional quenching and energy transfer in the $B^2\Pi$ state of the NS radical, for a variety of collision partners. NS was chosen for the study because it is an open-shell radical species containing two heavy atoms, and in the ground state possesses a large dipole moment (1.8D).

The NS was produced in a low pressure flow system at room temperature, by adding a trace of SCl_2 downstream from a microwave discharge of N_2 in He. All quencher gases were added further downstream and the experiments were performed at room temperature. Frequency-doubled, Raman-shifted radiation from a pulsed (10 ns) tunable dye laser was used to excite the radicals to individual J levels within $v'=0-12$ of the B-state¹. For these collisional studies, the fluorescence was spectrally resolved with a 0.35 m spectrometer and temporally resolved with a 100 MHz transient digitizer. Pressures of added gas were measured with a Baratron.

Overall decay rates have been measured by the time dependence of the emission for several collision partners (He, N_2 , O_2 , SF_6 , N_2O , H_2 , NH_3 , CH_4 , CO_2 , H_2). Except for NH_3 , the quenching cross sections σ_Q are small, $<10^{-22}$. This is much less than those for OH (which also has a large dipole moment) with many of the same collision partners^{2,3}. For OH, a reasonable correlation of σ_Q could be obtained using a simple picture involving multipole interactions between OH and the collision partner^{3,4}. Such interactions should be comparable for NS, but the quenching appears to proceed by a different mechanism.

The fluorescence decay rate from the $B^2\Pi$ state as a function of pressure of added nitrogen is shown in Figure 1 for $v'=0$ (squares), $v'=1$ (diamonds), and $v'=6$ (triangles). The total collisional decay rate constant is given by the slopes of the lines. It is composed of both quenching from $B^2\Pi$ and vibrational relaxation within the $B^2\Pi$ manifold. The intercept is the radiative decay rate ($1.5 s^{-1}$) plus a small ($\sim 0.2 \mu s^{-1}$) collisional loss contribution from the carrier flow tube pressure of 1 torr.

The total decay rate constant k_d is larger in $v'=1$ than in $v'=0$ for all gases studied. However, k_d for $v'=6$ is smaller than that in $v'=1$ for N_2 , SF_6 , N_2O and CO_2 , but larger for H_2 , O_2 and He. This unusual collision-partner-specific vibrational level dependence

of the σ_Q cannot be simply explained on the basis of known perturbations in $B^2\Pi$, and may provide detailed information on the dynamics and state-mixing responsible for electronic quenching.

Fluorescence scans show that for the partners N_2 , O_2 , N_2O and SF_6 , vibrational transfer ($v'=1 \rightarrow 0$) constitutes about 20-25% of the total $v'=1$ decay, and that $\sigma_Q(v'=1) \approx 2\sigma_Q(v'=0)$.

This study was supported by the Basic Energy Sciences Division of the Department of Energy.

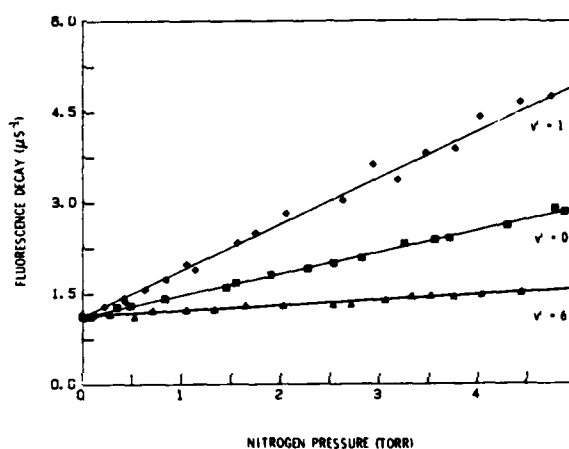


Figure 1. NS ($B^2\Pi$) decay rates in nitrogen, for $v'=0$, 1 and 6.

1. J. B. Jeffries, G. P. Smith and D. R. Crosley, *Bull. Amer. Phys. Soc.* **28**, 1320 (1983).
2. R. A. Copeland and D. R. Crosley, *Chem. Phys. Lett.* **107**, 295 (1984).
3. R. A. Copeland, M. J. Dyer and D. R. Crosley, *J. Chem. Phys.*, in press, 1985.
4. P. W. Fairchild, G. P. Smith and D. R. Crosley, *J. Chem. Phys.* **79**, 1795 (1983).

QUENCHING OF $\text{NH}(\text{A}^3\text{--}_1)$ AT 1400K

Nancy L. Gariand, Jay B. Jeffries, Richard A. Copeland, Gregory P. Smith and David R. Crosley

Chemical Physics Laboratory, SRI International, Menlo Park, California 94025

The role of attractive forces in the collisional quenching of electronically excited states of open-shell radicals is a question of recent interest. For OH, experimental quenching cross sections σ_0 for a variety of partners have been compared with theoretical calculations involving multipole interactions,^{1,2} indicating that attractive forces^{3,4} are important here. On the other hand, results for NS (having a dipole moment similar to that of OH) do not show such a correlation.⁵ Further evidence could be found in the temperature dependence of σ_0 , which for attractive forces would be expected to decrease with increasing T. This is the case for OH,¹ but direct measurements exist for no other open-shell diatomics. We report here measurements of σ_0 for NH at high T, in an attempt to address these questions.

The measurements are made using a laser pyrolysis/laser fluorescence technique.^{1,6} A slowly flowing mixture of SF_6 (ir absorber), CF_4 (bath gas), NH_3 (radical precursor) and quencher is irradiated by a pulsed CO_2 laser. This rapidly heats it to selected temperatures up to 1400K, as measured by excitation scans furnishing rotational distributions in the NH ground state. A few F-atoms are formed by thermal dissociation of the SF_6 ; these react with the NH_3 to form NH. A pulsed (10ns), frequency-doubled tunable dye laser excites fluorescence in the NH. Transient digitizer measurements of the real-time decay rate as a function of added quencher gas furnish σ_0 . The intercept yields the radiative rate, in good agreement with flow tube laser-induced fluorescence measurements.⁷

The pressure of SF_6 and CF_4 is typically 13 torr. We found these gases to be poor quenchers of excited NH, ensuring rotational thermalization in $\text{A}^3\text{--}_1$ as was the case for excited OH.⁶ Thus the measured σ_0 is that for a rotational distribution peaking near $N'=5$. This is important because room temperature measurements show that σ_0 depends on N' for OH,² and there is some evidence⁸ that this is true for NH as well.

The results for NH_3 and CO quenchers at $T=1400\pm 50\text{K}$ are given in the table. The values are large, of the order of gas kinetic, which suggests immediately that attractive forces are involved in the quenching of this diatomic hydride. The ratio of the σ_0 's for these two gases is about 3.5, similar to the ratio for NH_3 ⁹ and CO^1 in OH, which has multipole moments like those of

NH. The values themselves are also similar, and are listed for comparison in the table.

Recently,⁸ σ_0 for NH has been measured at room temperature, using the decay of emission following pulsed uv laser photolysis of NH_3 which forms the radical directly in the $\text{A}^3\text{--}_1$ state. The results of Ref. 8 are also included in the table. A comparison would indicate that for NH_3 , σ_0 decreases with temperature, in accordance with expectations for attractive collisions, but for CO the opposite is the case. Note however, that the room temperature values represent quenching from a very hot rotational distribution ($N'_{\text{max}}=8-12$) formed in the photolysis. In OH, σ_0 decreased more rapidly with increasing N' for CO than for NH_3 as a collision partner². If this were true for NH as well, it would account for at least some of the discrepancy.

Measurements with further colliders are in progress, as well as measurements in a room temperature discharge flow system.

This research was supported by the Basic Energy Sciences Division of the Department of Energy.

References

1. P. W. Fairchild, G. P. Smith and D. R. Crosley, *J. Chem. Phys.* **79**, 1795 (1983).
2. R. A. Copeland, M. J. Dyer and D. R. Crosley, *J. Chem. Phys.*, in press, 1985.
3. H. M. Lin, M. Seaver, K. Y. Tang, A.E.W. Knight and C. S. Parmenter, *J. Chem. Phys.* **70**, 5442 (1979).
4. D. L. Holtermann, E.K.C. Lee and R. Nanes, *J. Chem. Phys.* **77**, 5327 (1982).
5. J. B. Jeffries, D. R. Crosley and G. P. Smith, XIV ICPEAC, Stanford, California, July 1985.
6. G. P. Smith, P. W. Fairchild, J. B. Jeffries and D. R. Crosley, *J. Phys. Chem.*, in press, 1985.
7. P. W. Fairchild, G. P. Smith, D. R. Crosley and J. B. Jeffries, *Chem. Phys. Lett.* **107**, 181 (1984).
8. A. Hofzumahaus and F. Stuhl, *J. Chem. Phys.*, in press, 1985.
9. J. B. Jeffries, G. P. Smith and D. R. Crosley, *J. Chem. Phys.*, to be published.

$\text{NH}(\text{A}^3\text{--}_1)$	T	$\sigma_0(\text{NH}_3)$	$\sigma_0(\text{CO})$	Ratio
This Work	1400 K	30-42	8-22	3.8
Ref. 8, high N'	300	44	5.4	6.9
$\text{OH}(\text{A}^2\text{--}_1)$				
Ref. 1, $N'=5$	300	83	24	3.5
Ref. 1	1400	-	20	2.4
Ref. 9	1400	44	-	-

COLLISIONAL QUENCHING OF $A^2\Sigma^+$ OH BETWEEN 230 AND 310K

Richard A. Copeland and David R. Crosley
Molecular Physics Department, SRI International, Menlo Park, California 94025

Measurements have been made of the temperature dependence of the velocity averaged cross section σ_Q for collisional quenching of the $v'=0$ level of the $A^2\Sigma^+$ electronically excited state of the OH radical. For all quenchers examined (CO_2 , H_2 , N_2 and O_2), we observed that σ_Q increases as the temperature is decreased. This result is in accord with a picture of the collisional encounter involving attractive forces, and has implications for the use of laser-induced fluorescence as a monitor of OH in practical systems such as flames and the atmosphere.

The cross sections are extracted from the collider gas concentration dependence of the time decay of laser-induced fluorescence of the OH. Excitation is via a frequency-doubled, tunable, pulsed dye laser. The OH is produced in a discharge flow cell in a background gas pressure of 8 to 10 Torr Ar; quencher gas is added in amounts up to about 200 mTorr. The fluorescence is detected with an unfiltered photomultiplier and captured with a 100 MHz transient digitizer connected to a laboratory computer.

The cell is cooled by packing it in dry ice surrounded by styrofoam insulation. The rotational temperature of the OH in the observation region is measured by computer-controlled excitation scans across 25 selected rotational lines of the (0,0) band of the A-X transition. Temperatures as low as 230K have been obtained. The translational and rotational temperatures should be nearly equal under the cell conditions.

The background pressure of Ar is necessary to thermalize the OH in the ground state, and provide rotational relaxation in the upper electronic state. Previous measurements¹⁻³ have shown that σ_Q depends on rotational quantum number in the excited state. Here, the presence of the Ar bath ensures that we measure quenching from a thermal distribution of rotational levels.

The results for four collider gases are shown in the accompanying table. Quoted error bars are at the 2 σ level. In each case σ_Q increases significantly as the temperature is lowered.

A model incorporating attractive forces between the excited OH and the collision partner exhibits a similar qualitative temperature variation. In this picture^{3,4}, a collision complex is formed due to multipole interactions (OH has a large dipole moment)

and then dissociates into either the ground or excited state. σ_Q would then be composed of a cross section for complex formation (which can be calculated from known multipole moments of OH and the collision partner) and a probability for $\Sigma-\Pi$ state mixing during the lifetime of the complex. Previous comparisons at room temperature³ and 1100K⁴ of experimental and calculated σ_Q showed reasonable correlation for many gases. However, quenching by N_2 had a much smaller σ_Q than expected from such calculations.

For the four gases studied here, σ_Q is expected to increase ~10% in going from 300 to 230 K, according to the multipole model calculation. In each case, the increase is actually larger, and particularly so in the case of the N_2 . Here, effects of the relatively poor $\Sigma-\Pi$ mixing may be enhanced by the increased collision duration which occurs at lower temperatures. Interestingly, N_2 also shows a larger decrease in σ_Q , compared with other colliders, in going from room temperature to 1100K⁴.

Research supported by the National Aeronautics and Space Administration.

1. I. S. McDermid and J. B. Laudenslager, J. Chem. Phys. **76**, 1824 (1982).
2. R. A. Copeland and D. R. Crosley, Chem. Phys. Lett. **107**, 295 (1984).
3. R. A. Copeland, M. J. Dyer and D. R. Crosley, J. Chem. Phys., in press, 1985.
4. P. W. Fairchild, G. P. Smith and D. R. Crosley, J. Chem. Phys. **79**, 1795 (1983).

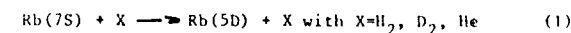
CO_2		H_2	
T, K	σ_Q, A^2	T, K	σ_Q, A^2
230 \pm 5	69.5 \pm 2.0	238 \pm 5	12.7 \pm 0.5
259 \pm 8	63.7 \pm 3.7	278 \pm 7	10.9 \pm 0.4
278 \pm 8	61.4 \pm 1.9	304 \pm 6	9.2 \pm 0.5
296 \pm 9	57.4 \pm 1.6		
N_2		O_2	
T, K	σ_Q, A^2	T, K	σ_Q, A^2
232 \pm 5	7.0 \pm 0.6	266 \pm 5	20.2 \pm 0.8
250 \pm 4	5.5 \pm 0.5	268 \pm 5	21.1 \pm 1.6
311 \pm 10	4.0 \pm 0.7	299 \pm 8	18.7 \pm 1.0

QUASI-RESONANT COLLISIONAL ELECTRONIC TO ROTATIONAL
 ENERGY TRANSFER AT THERMAL ENERGIES

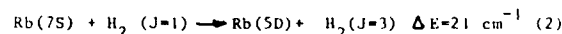
 J. Cuvellier, L. Petitjean, J.M. Mestdagh, D. Paillard
 and P. de Pujo

 Service de Physique des Atomes et des Surfaces, CEN/SACLAY
 91191 Gif-sur-Yvette Cedex, France

We have studied the electronic energy transfer induced by atomic or molecular collisions at thermal energies, for a lowly excited atomic state ($\text{Rb}(7s)$), searching for the occurrence of a quasi-resonant electronic to rotational energy transfer. We have considered the particular inelastic transfer



which can lead, for H_2 , to the quasi-resonant process



Three perturbers have been studied in order to compare situation where quasi-resonances can occur ($\text{Rb}-\text{H}_2$ collisions) with situations where quasi-resonances do not exist ($\text{Rb}-\text{D}_2$ and $\text{Rb}-\text{He}$ collisions), the $\text{Rb}(7S - 5D)$ splitting being 608 cm^{-1} .

We have measured the cross section of process (1) as a function of the collision energy by using a cross beam experiment¹. This experiment allows the measurement of absolute cross sections and also the determination of the molecular rotational distribution. This work constitutes the first detailed study of quasi resonant energy transfer for intermediate excited states, when Hertel and his group² have reported studies of electronic to vibrational and rotational energy transfer involving large energy defect. Measured cross sections are presented in figure 1. The energy dependence of the cross sections is almost identical for the three perturbers for collision energy larger than 0.16 eV. However, H_2 exhibits for the low energy range ($E_{\text{coll}} < 0.12 \text{ eV}$) a quite different behaviour than those reported for D_2 and He. We have checked that the cross sections remain only weakly dependent upon the rotational temperature in the considered range.

The cross section for $\text{Rb}(7S \rightarrow 5D)-\text{He}$ collisions has been calculated within the frame of a Landau-Zener approach using potential energy curve calculated by Pascale³. A fair agreement is found with experimental data (fig.1). For D_2 we have recently proposed a model describing the experimental data where the intermultiplet transition is due to Landau-Zener coupling between slightly modified "Rb-He" like potential curves⁴. This result shows that D_2 act like a structure-less particle.

For H_2 the different behavior with collision energy has been attributed to the occurrence of process (2). We have compared in figure 2 the experimental data, di-

vided by the corresponding $J=1$ rotational population ($n(J=1) \approx 0.7$), to the predictions of the impulse approximation (IA). This approach has been shown particularly reliable to describe Rydberg states-molecule collisions⁵. One can notice that the IA gives the good energy dependence of the cross section in the energy range 0.02-0.12 eV. For higher energies H_2 acts like a structure-less particle as D_2 and He. This clearly supports our description of the $\text{Rb}(7S \rightarrow 5D)-\text{H}_2$ collision: this collision is dominated at low energy by the quasi-resonant process (2). This study constitutes the first experimental evidence of the occurrence of efficient quasi resonant energy transfer for low atomic state whose cross section can reach values as much as 200 \AA^2 .

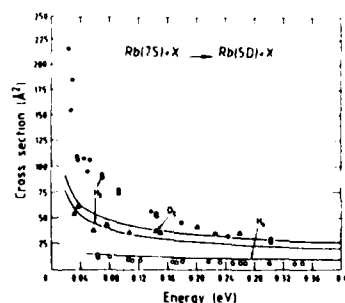


Fig.1 - Cross-sections for the $\text{Rb}(7S - 5D)$ collisional transition. Solid lines result from Landau-Zener calculation.

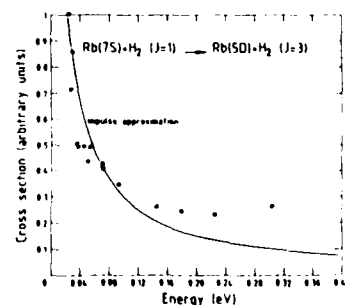


Fig.2 - Comparison between the impulse approximation and the experimental data divided by the corresponding $J=1$ rotational population.

1. J.M. Mestdagh, J. Berlande, J. Cuvellier, D. de Pujo, A. Binet, J. Phys. B **15**, 439 (1982).
2. L.V. Hertel in "Dynamics of the Excited state", edited by K.P. Lawley John Wiley and Sons Ltd (1982).
3. J. Pascale, Phys. Rev. A **23**, 632 (1983).
4. J. Cuvellier, L. Petitjean, J.M. Mestdagh, D. Paillard and P. de Pujo (submitted to Phys. Rev.A).
5. L. Petitjean, F. Gounand and P.R. Fournier, Phys. Rev. A **30**, 71 (1984); *ibid* **30**, 736 (1984).

PSEUDOPOTENTIAL MOLECULAR-STRUCTURE CALCULATIONS
OF ALKALI-H₂ SYSTEMS

F. Rossi and J. Pascale

Service de Physique des Atomes et des Surfaces -CEN/SACLAY
91191 Gif-sur-Yvette Cedex, France

In order to obtain the ground-state and numerous excited states of alkali-H₂ systems we have extended the ϵ -dependent pseudopotential approach previously developed for alkali-He interactions /1/. In our approach, we have fixed the H-H distance to 1.4 a.u. corresponding to the ground state of H₂ in its first vibrational level.

The pseudopotential interaction for e⁻-H₂ consists of long-range and short-range terms. The long-range interaction is relatively well-known /2/ and contains an anisotropic part limited to terms in $P_2(\cos\theta)$, where θ is the angle between the direction H-H and the vector position of e⁻ relative to the center of mass of H₂. Then the short-range interaction is defined by generalizing the isotropic λ -dependent pseudopotential for e⁻-He /1/ and by introducing an anisotropic part :

$$V_{sr} = \sum_{l=0}^{\infty} \sum_{m=-l}^l V_l^{(s)}(r) |l m\rangle \langle l m| + \sum_{l=0}^{\infty} \sum_{m=-l}^l V_l^{(a)}(r) \{P_l, |l m\rangle \langle l m|\}$$

where $\{ \}$ denotes an anticommutator; P_2 is an operator defined as $P_2 |l m\rangle = P_2(\cos\theta) |l m\rangle$. As in ref. /1/ Gaussian-type forms of the potentials $V_l^{(s)}(r)$ were fitted to available experimental data for e⁻-H₂ elastic scattering /3/. For lack of experimental data concerning the anisotropic short-range part of the alkali core-H₂ interaction we have determined this interaction by a stationary perturbative method; it uses a simple LCAO wave function for H₂ and pseudo-potentials for the interactions between the alkali core and an electron (proton). Three-body terms were also included in the calculations in order to have the correct behavior of the alkali-H₂ interaction at large distances.

The electronic energies were determined by standard variational calculations using a large basis set of Slater-type orbitals centered on the alkali core. The C_{∞v} and C_{2v} symmetries were considered, but the same method can be used for the C_{1h} symmetry.

Our calculations agree well with recent "ab initio" data as illustrated in Figs. 1-2 for Na-H₂/4/.

References

1. J. Pascale, Phys. Rev. **28**, 632 (1983).
2. K. Takayanagi and S. Geltman, Phys. Rev. A **138**, 1003 (1965).
3. F. Linder and H. Schmidt, Z. Naturforsch **26a**, 1603 (1971).

4. P. Botschwina et al., J. Chem. Phys. **75**, 5438 (1981).

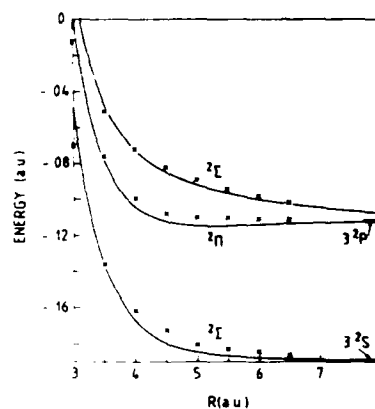


Fig. 1 - Potential curves for Na-H₂ in C_{∞v} symmetry. —, present results; X, ab initio calculations (RHF-SCF) of Botschwina et al. /4/ correlated asymptotically to the experimental levels.

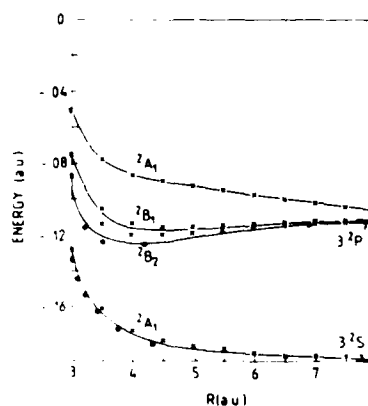


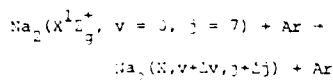
Fig. 2 - Potential curves for Na-H₂ in C_{2v} symmetry. As in Fig. 1. The full circles are the best ab initio calculations (PNO-CEPA) of Botschwina et al. /4/.

ENERGY DEPENDENCE OF ANGLE RESOLVED VIBROTATIONALLY INELASTIC COLLISIONS

W.P. Moskowitz, B. Stewart,* J.L. Kinsey,* and D.E. Pritchard

Dept. of Physics and Research Lab. of Electronics, M.I.T., Cambridge, MA 02139 USA
 *Dept. of Chemistry, M.I.T., Cambridge, MA 02139 USA

We have measured the energy dependence of angle resolved cross sections for the vibrationally inelastic process



using crossed beams and our ADDS Doppler technique¹ to determine the scattering angle. The rotational rainbow in the angular distribution, observed in previous vibrationally inelastic studies² is retained. The dependence of its angular position on j and collision energy is well represented by a simplistic classical hard ellipse model. Suppression of low angle scattering is observed for small rotational inelasticities, as predicted.³

References

1. J.A. Serri, J.L. Kinsey, and D.E. Pritchard, J. Chem. Phys. **75**, 663 (1981).
2. J.A. Serri, C.H. Becker, M.B. Elbel, J.L. Kinsey, W.P. Moskowitz, and D.E. Pritchard, J. Chem. Phys. **74**, 5116 (1981).
3. J.A. Serri, R.M. Bilotta, and D.E. Pritchard, J. Chem. Phys., **77**, 2940 (1982).

INDUCING RESONANT V-R TRANSFER BY HIGH ROTATION AND LOW VELOCITY

Thomas Scott, Peter Magill, Neil Smith, Brian Stewart* and David Pritchard

Dept. of Physics and Research Laboratory of Electronics, M.I.T., Cambridge, MA 02139 USA
*Dept. of Chemistry and Research Laboratory of Electronics, M.I.T., Cambridge, MA 02139 USA

We have uncovered striking quasi-resonant V-R energy transfer in the vibrationally inelastic process

$$Li_2^+ + H_2(v, j_1) \rightarrow X + Li_2^+(v+Lv, j_2) + X$$

where $X = Li, He, Ar, Xe$, both in level-specific rate constants measured by a conventional LIF technique, and in velocity dependent cross sections determined by our Doppler VSDS technique. The central feature of this behavior is a dramatic peaking in the j_2 distribution as j_1 increases. The position of the peak is given by $j_{2,max} = j_1 + 4v$, irrespective of the sign or magnitude of Lv , and corresponding to about 70% conversion of vibrational to rotational energy; for this reason we have termed the process quasi-resonant V-R transfer.

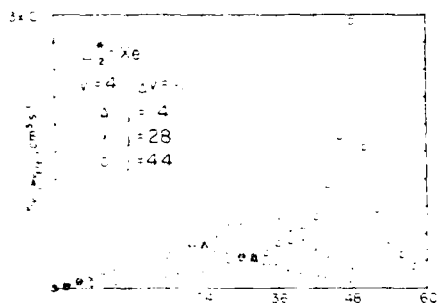


FIGURE 1. Rate constants $k_{v,j_1 \rightarrow v+Lv, j_2}$ vs. j_2 for Li_2^+-Xe with $v_1 = 4$ and $Lv = -1$ for $j_1 = 14, 28$, and 44 .¹

Noteworthy features of the rate constant data include:

- In the case of He, Ar , and Xe , the shape of the quasi-resonant distribution is identical within experimental error.
- An increase in j_1 not only induces the resonant transfer, but also increases the rate constants. In addition, despite the fact that the rotationally summed vibrationally inelastic rate constants increase with j_1 , so does the narrowness of the j_2 distribution.

Our velocity dependent cross section data indicate that²:

- The total vibrationally inelastic cross section is very large at low v_{rel} , especially for low velocity, where it is $\sim 10^{-16}$ cm². This indicates moderate to fast rate collisions in the vibrationally inelastic collision process.

- For $Lv < 0$, the cross section decreases as $1/v_{rel}$ for all j_1 .

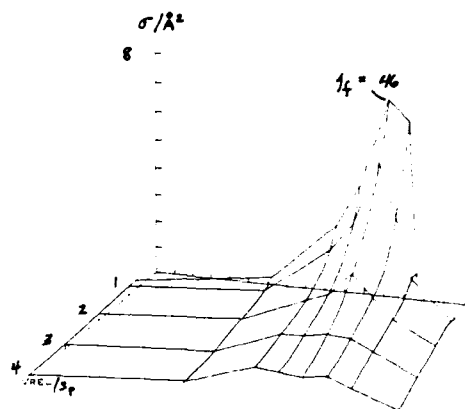


FIGURE 2. Velocity dependence of cross section vs. j_1 for $v_1 = 9, j_1 = 42; Lv = -1$.

- As can be seen in the above figure, the width of the quasi-resonant peak decreases as v_{rel} decreases; this increase in specificity is even more pronounced in Li_2^+-He collisions.

Classical trajectory calculations performed recently in our laboratory have shown a strong correlation between j_2 and Lv , which in turn gives rise to behavior like that seen in our experiments.

1. K.L. Saenger, N. Smith, S.L. Dexheimer, C. Engelke, and D.E. Pritchard, *J. Chem. Phys.* **79**, 4376 (1983).
2. T. Scott, Ph.D. Thesis, M.I.T. (1985).

DISSOCIATIVE ELECTRON CAPTURE OF H_2^+

I. Alvarez, C. Cisneros, J. de Urquijo, A. Morales and H. Martínez

Instituto de Física, UNAM, 04515, México, D.F.

In this paper we present angular distributions of H^- formed by dissociative electron capture of H_2^+ from Mg and Ar for incident H_2^+ energies of 1, 2, 3, 4 and 5 keV and for scattering angles from -4° to 4° . Absolute values for the angular distributions were obtained with the apparatus previously described¹.

The measured distributions are discussed in terms of a theory for fragment angular distributions produced by molecular dissociation. From very general assumptions, a scaling law was derived,¹

$$\frac{1}{E_i} \frac{d\sigma_-}{d\Omega_L} = f(E_i \theta^2) \quad (1)$$

where $d\sigma_-/d\Omega_L$ is the differential cross section for finding a negative ion at laboratory angle and E_i is the incident ion energy.

Using the fact that the dissociation energies are small compared with the incident molecular ion beam velocities, the relationship between the differential solid angle in center of mass-frame and laboratory frame is derived as:

$$d\Omega_{cm} = \frac{E_i}{E_d} d\Omega_L / (1 - \frac{E_i \theta^2}{E_d})^{1/2} \quad (2)$$

A peak in the angular distribution for a fragment can be interpreted as due to a singularity in the Jacobian of the transformation². Using (2) the dissociation energy can be determined from the location of the peak

$$E_d = E_i \theta_{peak}^2 \quad (3)$$

Figure 1 shows the experimental results plotted according to (1) for Mg and Ar, respectively. In the case of Mg as a target we have observed three maxima corresponding to E_d values of 4.0, 7.2 and 12.1 eV, whereas in the case of Ar a richer structure was observed with maxima at E_d values of 2.8, 5.2, 7.1, 10.2 and 12.3 eV. Previous data obtained for dissociation of D_2^+ on Cs show a very sharp peak at $E_d \approx 7.2$ eV, which corresponds to the same center of mass energy of the sharp peak observed by Peterson and Bae² in their energy distribution measurements of D^- arising from $D_2^+ + Cs$.

The dissociation energies of about 4 eV for Mg and 7.2 eV for Cs, are very close to those obtained by de Bruijn et al.³ in their studies of dissociative charge exchange of H_2^+ with the same targets. An interpretation based on transitions from different electronic states may be very similar to that given by de Bruijn.

Research supported in part by CONACyT, Grant PCCBBEU 0102238.

References

1. C. Cisneros, I. Alvarez, C.F. Barnett, J.A. Ray and A. Russek, Phys. Rev. A **14**, 88 (1976)
2. J.R. Peterson and Y.K. Bae, Phys. Rev. A **30**, 2807 (1984)
3. D.P. Bruijn, J. Neuteboom, V. Sidis and C. Los, Chem. Phys. **85**, 215 (1984)

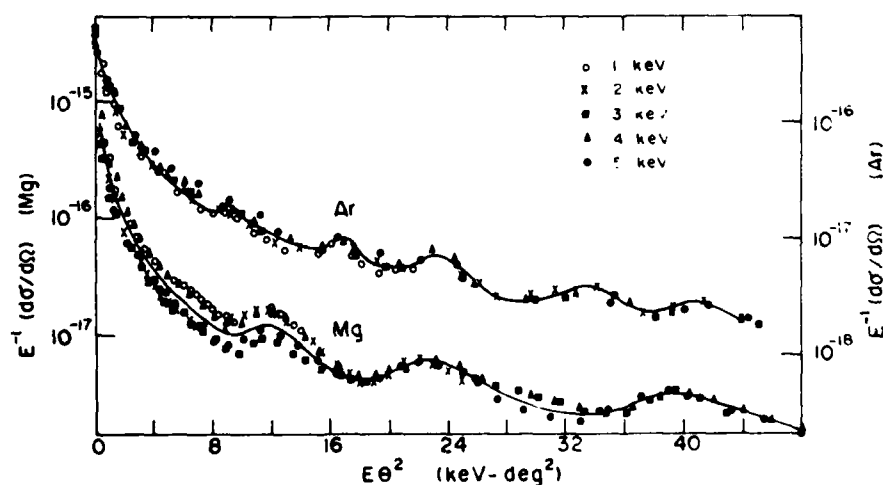


FIGURE 1. Experimental results in Mg and Ar plotted in terms of the reduced variables $E_i^{-1} \frac{d\sigma}{d\Omega}$ and $E_i \theta^2$ according to eqn. (1).

NEGATIVE ION FORMATION IN POLAR DISSOCIATION OF H_3^+ , HD_2^+ AND D_3^+ C. Cisneros,^{*} I. Alvarez,^{*} J. de Urquijo,^{*} H. Martínez^{*}
and T.J. Morgan^{*}^{*} Instituto de Física, UNAM México D.F. 04515
Wesleyan University, Middletown Ct. 06547

Most of the theoretical development and all the experiments involving threshold phenomena have been carried out for cases where the final products are two electrons and positive ion.

A heavy-particle analog to the threshold ionization process $e^- + He \rightarrow He^- + 2e^-$ is the reaction system^{1,2} $H^+ + H_2 \rightarrow (H_3)^+ \rightarrow H^+ + H^- + H^+$. One problem in studying the threshold region from reactions such as $H^+ + H_2$ is that the collision dynamics may restrict the available $(H_3)^+$ state and the three-body break-up of interest not to take place with a sufficiently large cross section so as to be observed.

An alternative method for obtaining near-threshold dynamics of massive three particle systems¹ is to start with the three particle ion H_3^+ , HD_2^+ or D_3^+ in this case, and collisionally excite it to levels which decay to the ionic states $H^+ + H^- + H^+$, $H^+ + D^- + D^+$, $D^+ + H^- + D^+$ or $D^+ + D^- + D^+$, respectively.

We present here the first absolute measurements of both total and differential cross sections for polar dissociation of the triatomic ions H_3^+ , HD_2^+ and D_3^+ in the energy range 0.33 to 1.61 keV/amu using a He target³. Since electron promotion is much more likely to occur than charge transfer at these energies, the detected H^- or D^- is interpreted to originate from polar dissociation.

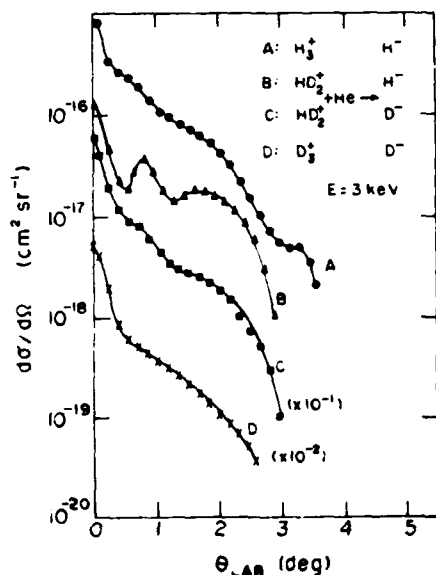


FIGURE 1 Absolute differential cross sections

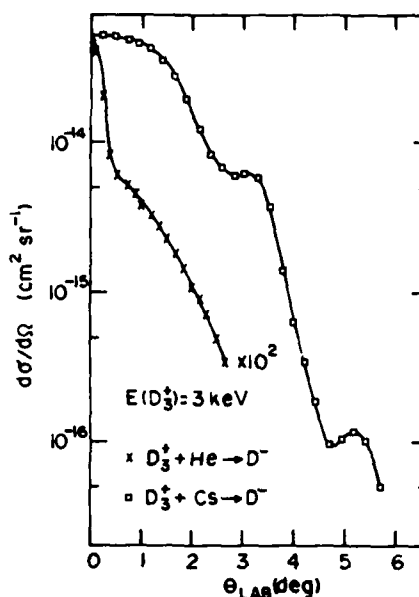


FIGURE 2

Figure 1 shows absolute differential cross sections measured for H^- and D^- from H_3^+ , HD_2^+ and D_3^+ . Figure 2 shows a comparison between D^- arising from D_3^+ dissociation in He and Cs. As it can be observed, there is a striking difference due most probably to the fact that in the first case most of the ions formed in the collision result from the three body polar dissociation, whereas in the second case the ions are formed mainly by electron capture⁴.

Center of mass energy distributions for the negative ions obtained by translational spectroscopy are also reported and show that the negative ions are formed with very small center of mass energy.

Further measurements of the center of mass velocity of the three particles and their angular correlations would provide a good test for the generalized description of the three-particle Coulomb interaction.

Research partially supported by CONACYT, grant PCCBBEL 0102238

References

1. D.L. Montgomery and D.H. Jaacks, Phys. Rev. Lett. 51, 1982 (1983)
2. J.M. Feagin, J. Phys. B, 17, 2433 (1984)
3. I. Alvarez, C. Cisneros, J. de Urquijo and T.J. Morgan, Phys. Rev. Lett. 53, 740 (1984)
4. C. Cisneros, I. Alvarez, C.F. Barnett, J.A. Ray and A. Russek, Phys. Rev. A 19, 631 (1979)

EXCITATION AND DISSOCIATION MECHANISMS
IN 3.22 KEV H_2^+ - NE COLLISIONS *

O. Yenen and D. H. Jaecks

Behlen Laboratory of Physics, The University of Nebraska,
Lincoln, NE 68588-0111 USA

The quasidiatomic generalization of Lichten-Barat MO correlation rules to atom-molecule systems is further tested by the polarization analysis of L_{α} radiation in coincidence with H^+ scattered to specific laboratory angles for 3.22 keV H_2^+ on Ne. The least squares fit of the data to a general dipole intensity pattern, shown in Fig.1, is radically different than that obtained by using a He target¹ where the polarization pattern was perfectly aligned in the beam direction. For the Ne target, at $\vartheta=3.2^\circ$, the H_2^+ internuclear axis is nearly perpendicular to the beam and the electron wavefunction has the alignment of $2p_0$.

The ground state of H_2^+ being nearly spherical and its excited wavefunctions atomic in character, one can attempt to construct a quasidiatomic correlation diagram by conserving the number of radial nodes to describe the approximate nodal character and behavior of the electronic wavefunction during the diabatic collision (Fig.2). During the collision, due to the high asymmetry of H_2 -Ne system, some amplitude from $3dq\sigma$ is drained

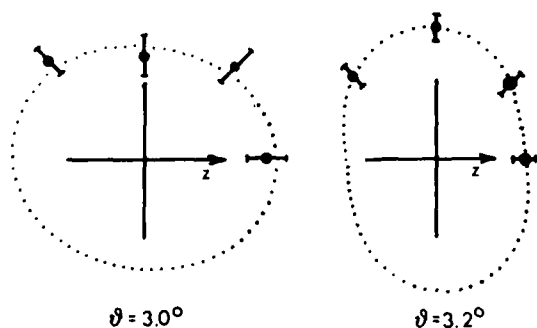


fig. 1

off to $3sq\sigma$, $3pq\sigma$, $3pq\pi$, and $4sq\sigma$.⁴ Since $3pq\sigma$ is the only quasidiatomic orbital ending on H_2 , $2s\sigma$ of H_2 can be very efficiently populated and subsequently dissociate into $H(2s, 2p_0) + H^+$. The remaining amplitude will be promoted to $3d\pi$ by rotational coupling and will end on either $2p\sigma$ or $2p\pi$ depending upon H_2^+ orientation. Our interpretation is consistent with the earlier measurement of the 2s and 2p production ratio by D.H.Jaecks and E.Tynan.³

References

1. D.H.Jaecks, O.Yenen, M.Natarajan, and D. Mueller, Phys.Rev.Lett.50, 825(1983).
2. Chiling Wang and J.Macek, Contribution to this conference.
3. D.H.Jaecks and E.Tynan, in Proceedings of 4th ICPEAC, p.315(1965)

* This work is supported by NSF

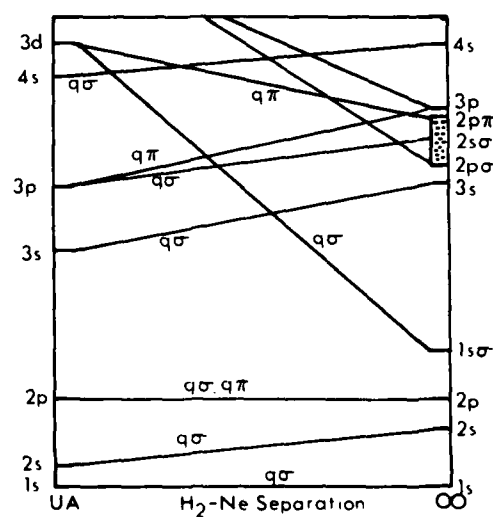


fig. 2

FORMATION OF He_2^0 AND He_2^{2+} MOLECULES BY CHARGE EXCHANGE COLLISIONS
OF He_2^+ IONS IN THE SUB-MeV REGION

O. Haber, I. Ben-Itzhak, I. Gertner, A. Mann and B. Rosner

Department of Physics, Technion, Haifa 32000, Israel

Six dissociation and two charge-exchange channels populated by single collisions of He_2^+ molecular ions have been studied at 00 and 800 keV. In Figure 1 we present

area of the detector due to the repulsive interaction between them. To take advantage of this spatially

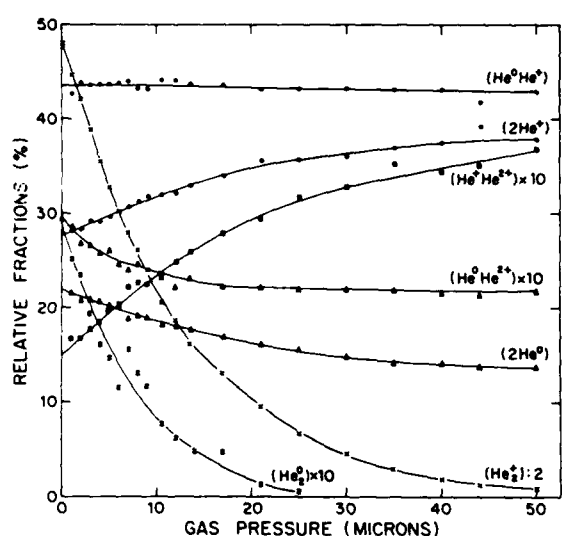


FIGURE 1

the relative fractions of the observed dissociation channels as functions of the Ar target gas pressure for $E_{\text{He}^+} = 400$ keV. At low pressures each fraction has a value corresponding to the relative probability for that channel under a single collision condition. At higher pressures each fraction tends to a constant value which depends on the loss and capture cross-sections of atomic helium at half the beam energy. The fraction of the undissociated incoming He_2^+ beam is also shown in the figure.

The separation of the counts in the full energy peak into the (2He^0) and (He_2^0) channels, as well as the separation between the (2He^+) and (He_2^{2+}) was done by the grid method. The method is based on the different probability for the passage of a single undissociated molecule through a grid as compared with the probability that both fragments of a dissociated molecule will do the same. The relative fraction of the (He_2^0) and (He_2^{2+}) channels are smaller by more than an order of magnitude compared with the relative fraction of the (2He^0) and (2He^+) channels. However, it is possible to amplify the relative intensity of the generally weak molecular channels. This can be done because all undissociated molecules are expected to reach the center of the detector, whereas pairs of the two-fragments channel cover a large

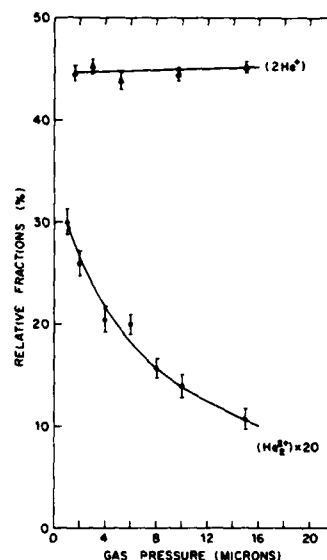


FIGURE 2

different behaviour, a variable circular iris aperture was placed in front of the detectors. The aperture could be varied from a maximum diameter corresponding to the full size of the detector to a minimum value of 1 mm.

In Figure 2 the separation of the (He_2^{2+}) and (2He^+) channels by the grid method as a function of the Ar gas pressure obtained with the smallest setting of the iris aperture is clearly seen.

The table summarizes the experimental results.

Charge exchange channels	Relative fractions	
	400 keV	800 keV
He^0	0.27 ± 0.005	0.010 ± 0.002
He_2^{2+}	0.002 ± 0.002	0.015 ± 0.002
Dissociation channels		
2He^0	$0.217 \pm .005$	0.068 ± 0.009
$\text{He}^0 \text{He}^+$	0.438 ± 0.006	0.330 ± 0.013
2He^+	0.274 ± 0.005	0.445 ± 0.010
$\text{He}^0 \text{He}_2^{2+}$	0.028 ± 0.002	0.072 ± 0.004
$\text{He}^+ \text{He}_2^{2+}$	0.014 ± 0.003	0.059 ± 0.004
2He_2^{2+}	0.001 ± 0.001	0.002 ± 0.001

COLLISION - INDUCED LUMINESCENCE STUDIES ON CF_4 BY He^+ , Ne^+ AND Ar^+ IMPACT

J. Sasaki*, I. Kuen and F. Howorka

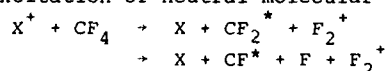
Institut für Experimentalphysik der Universität Innsbruck, 6020 Innsbruck, Austria

*) Permanent address: Department of Electrical Engineering, Faculty of Science and Technology, Keio University, Yokohama, Japan

Excitation processes in the collisions of He^+ , Ne^+ and Ar^+ with CF_4 have been observed in the energy range 1 - 1800 eV laboratory frame and the wavelength region 2000 - 8000 Å. Absolute cross sections dependent on energy are measured.

The following processes lead to the emission of light:

a) Excitation of neutral molecular fragments



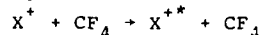
Emission bands of CF_2 between 2400 and 3300 Å (the transitions levels are unknown) and CF between 2200 and 2600 Å ($\text{A}^2\Pi \rightarrow \text{X}^2\Pi$ / 1,2/ are observed.

In collisions of Ar^+ with CF_4 both band systems are not excited.

b) Excitation of atomic and ionic carbon and fluorine lines



c) Projectile excitation



This process is observed for Ne^+ and Ar^+ , but not for He^+ .

d) Neutralized projectile excitation

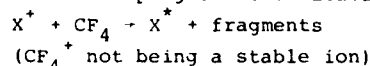


Fig. 1 shows spectra of He^+ , Ne^+ and Ar^+ - CF_4 at a laboratory energy of 1800 eV. Atomic and ionic lines are superimposed on the CF_2 and CF bands.

The energy dependence of the cross sections shows a somewhat similar behavior for all processes: a threshold near the endoergicity is observed, then the cross section rises to a broad peak around 800 eV.

Acknowledgements:

The Fonds zur Förderung der wissenschaftlichen Forschung supported the study in the past.

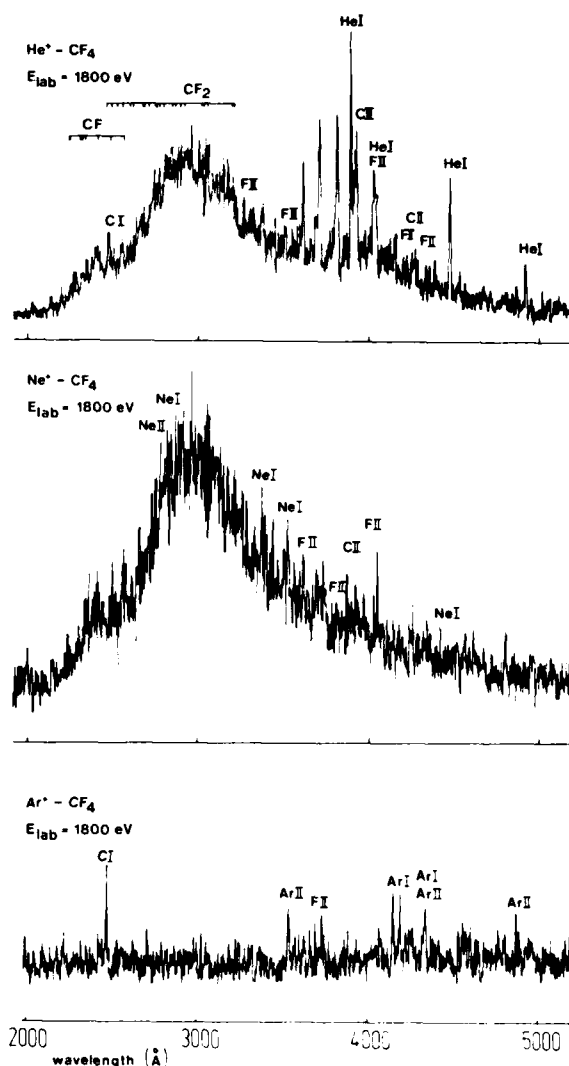


Fig. 1: Spectrum of He^+ , Ne^+ and Ar^+ - CF_4 at a laboratory energy of 1800 eV

References:

1. Pearse R.W.B and Gaydon A.G., The Identification of molecular spectra; Third ed., Chapman and Hall Ltd, London (1963)
2. Huber K.P. and Herzberg G, Molecular Structure; IV Constants of Diatomic Molecules. Van Nostrand Reinhold Co., New York (1979)

DISSOCIATIVE IONISATION OF HYDROGEN BY FAST PROTONS

B G Lindsay, F R Simpson and C J Latimer

Department of Pure and Applied Physics, The Queen's University of Belfast,
Belfast, United Kingdom

Studies of the dissociative ionisation of hydrogen by electrons¹ and photons² show that, in addition to normal repulsive states, autoionising states can make an important contribution to the production of energetic H^+ ions. However, in the case of collisions between H^+ and H_2 , where dissociative ionisation can proceed either with or without electron capture, such states have not been observed³. Energetic fragment protons were only found to have energies between 7 and 9 eV and were all accounted for by Frank-Condon transitions to the two states, $2p\sigma_u$ and the repulsive $H^+ + H^+$.

We have investigated the energy distribution of fragment protons produced in the dissociative ionisation of hydrogen by 2-25 keV protons. The proton beam was crossed by a hydrogen gas jet and the secondary ions produced at a prescribed angle were energy analysed (using a parallel plate energy analyser) and mass analysed (by time of flight).

The energy spectra of the H^+ ions (figure 1) consist of two broad composite features at around 6 and 9 eV. A computer fit of the theoretical H^+ energy distributions, obtained using the reflection approximation and the potential energy curves of hydrogen⁴ shows that the observed energetic protons must arise from at least four repulsive states. The lower energy group consists of protons arising from excitation to both the $2p\sigma_u$ and $2s\sigma_g$ states of H_2^+ while the higher energy group comes from the $2p\sigma_u$ and the $H^+ + H^+$ states. At 5 keV protons are produced mainly through the $2p\sigma_u$ and $2s\sigma_g$ states in approximately equal amounts while at 25 keV all four states contribute significantly. It should be noted that the computer fits are very poor in the region 2.5 - 5.0 eV where protons from autoionising states should appear if produced. Thus although clear evidence for the excitation of these states is not apparent it seems likely that they too must also be added to the list of states which make significant contribution to the dissociative ionisation process in $H^+ + H_2$ collisions.

References

1. A Crowe and J W McConkey, *Phys Rev Lett* **31** 192 (1973).
2. S Strathdee and R Browning, *J Phys B* **12** 1789 (1979).
3. V V Afrosimov, G A Leiko, Yu A Mamaev and M N Panov, *Sov Phys JETP* **29** 648 (1969).
4. R M Wood, A K Edwards and M F Stener, *Phys Rev A* **15** 1433 (1977).

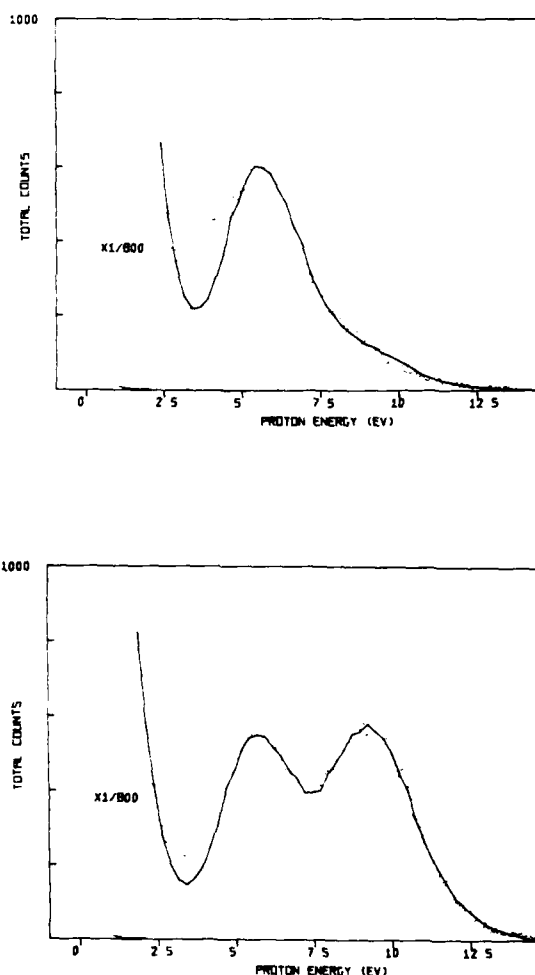


Figure 1 : Energy spectrum of protons produced at 90° in 5 keV (upper) and 25 keV (lower) $H^+ + H_2$ collisions. The solid curves are a theoretical fit to the data.

ELECTRONIC EXCITATION TRANSFER, COLLISIONAL DISSOCIATION AND
PHOTODISSOCIATION IN SODIUM VAPOUR.

H. Hulsman* and P. Willems*

* Department of Physics, University of Antwerp, U.I.A.

+ Dienst experimentele Natuurkunde, University of Antwerp, RUCA

Electronic excitation of diatomic alkali molecules by means of laser light may lead to atomic resonance radiation ($D_{1,2}$ -lines). An experiment is presented in which various processes, contributing to this phenomenon are separated and studied.

In the present experiment Na_2 molecules are irradiated by light from an Ar^+ -laser at 4765\AA , which can excite molecules from some specific vibration-rotation (v, J)-levels of the ground state to the excited B-state¹⁾. The laser is single-mode and its frequency is tuned to the transition from (v, J) = (0, 28) in $X^1\Sigma_g^+$ to (6, 17) in $B^1\Pi_u$. Diatomic sodium molecules occur as a small fraction in sodium vapour. In the experiment the vapour is mixed with a large fraction of noble gas.

Under these circumstances atomic radiation may be caused by the following processes:

- 1° transfer of electronic excitation. When the molecule during its excited lifetime ($\approx 7 \times 10^{-9}$ s) collides with a Na atom, this may result in a transfer of electronic excitation:
 $\text{Na}_2(B^1\Pi_u, v', J') + \text{Na}(3s) \rightarrow \text{Na}_2(X^1\Sigma_g^+, v'', J'') + \text{Na}(3p)$
- 2° collisional dissociation. When the excited molecule collides, this may also cause dissociation:
 $\text{Na}_2(B^1\Pi_u, v', J') + X \rightarrow \text{Na}(3s) + \text{Na}(3p) + X$
 Here the collision partner is arbitrary, but the energy balance of the reaction is such, that a large quantity of collisional energy is needed.
- 3° photo dissociation
 $\text{Na}_2 + h\nu \rightarrow \text{Na}(3s) + \text{Na}(3p)$
 For the given laser frequency this is energetically possible for groundstate molecules in vibrational levels with $v \geq 17$.
- 4° different types of two-photon excitation. These are only important at laser intensities higher than those used in our experiment.

The relative importance of the processes 1°, 2° and 3° depends on the density and temperature of the gas: As the density is lower, the number of collisions is smaller and the importance of 1° and 2° decreases. In the limit of zero pressure (or in molecular beams) only photodissociation occurs, but at high densities the combined effect of 1° and 2° is dominant. When the temperature is lowered, the contributions of 2° and 3° are expected to diminish drastically; at low tempera-

tures there are few collisions with enough kinetic energy to induce dissociation (2°) and there are also few molecules with enough vibrational energy to allow photodissociation (3°). Electronic excitation transfer (1°), however, is expected to be only weakly dependent on temperature.

The processes have been studied for various alkali systems (e.g. refs. 2-4, see also ref. 3). Photodissociation is studied preferably in a molecular beam set-up. The other processes are mostly studied in a vapour cell.

These cell measurements are handicapped by conflicting requirements: the density should be low to minimize radiation trapping, while it should be high for the photodissociation to be negligible compared to the collisional processes. Further the accessible range of temperatures is limited: At a given density the vapour cannot be cooled below its saturation temperature, while heating reduces the Na_2 fraction. These restrictions complicate the analysis and make it difficult to distinguish the various contributions. Therefore we conducted such experiments in a free jet expansion, which has the following advantages:

- the very strong known density evolution in the jet allows the observation of the transition from a collisional region (where 1° and 2° are dominant) to a free molecular region (where only 3° occurs). During this transition the Na_2 fraction remains constant.
- for each position in the expansion the excitation mechanism of the Na_2 molecules⁵⁾ makes it possible to separate the contributions of (1°+2°) and 3° via their different dependence on the laser intensity.
- the strong known temperature evolution in the jet and the possibility to vary the "stagnation"-pressures of the noble gas and of the Sodium allows us to distinguish the contributions of 1° and 2°.
- the effect of radiation trapping is minimized in a free jet.

At the conference the method will be explained in more detail and the first results will be shown.

References

1. P. Kusch and M.M. Bessel, J.Chem.Phys. 68(1978)2591.
2. E.W. Rothe, W. Krause and R. Dören, J.Chem.Phys. 72(1980)5145.
3. S.M. Papernov, G.V. Shlyapnikov and M.L. Yanson, Sov. Phys. Dokl. 23(1978)58.
4. M.L. Yanson and J.P. Klavins, Chem.Phys.Letters 86, (1982)453.
5. P.Willems, H.Hulsman and F.Aerts, Chem.Phys. 71(1982)27.

TOTAL AND PARTIAL DIFFERENTIAL CROSS SECTIONS FOR THE PROCESSES:
 $K, Cs + O_2(v=0) \rightarrow K^+, Cs^+ + O_2^-(v')$

M.R. Spalburg, M.G.M. Vervaat, A.W. Kleyn and J. Los

FOM-Institute for Atomic and Molecular Physics, Amsterdam, The Netherlands

Ion-pair forming collisions between atoms and molecules can give a considerable insight into the vibronic excitation. We present total differential cross sections measured without any selection of the final vibrational state of the molecular ion and partial differential cross sections which show only alkali ions from collisions which leave the molecular ion in a vibrational state $v' > 3$. The division between $O_2^-(v' \leq 3)$ and $O_2^-(v' > 3)$ is possible because this molecular ion autoionizes rapidly after the collision for $v' > 3$. The partial differential cross sections are accumulated by measuring the scattered alkali ion in (delayed) coincidence with the electrons emitted when the molecular ion autoionizes.

In figure 1 an example of experimental total and partial differential cross sections is shown. Both cross sections feature an (ionic) rainbow around the reduced scattering angle ≈ 160 eV°. The shoulder present on the left side of the ionic rainbow is due to the vibrational motion of the molecular ion during the collision. It is remarkable that the shoulder is much less intense in the partial differential cross section. In addition the position of the ionic rainbow is shifted to smaller scattering angles in the partial differential cross section.

In figure 2 an example of theoretical total and partial differential cross sections is shown. The cross sections are calculated using the semi-classical Vibronic Impact Parameter model [1]. The model is extended to allow to calculate differential cross sections. The extension is based on the evolution of the (eikonal) phases of the vibronic waves [2]. Clearly this model is capable to reproduce the vibronic effects.

The absence of the shoulder in the partial cross sections is attributed to the following facts:

- 1) The influence of the vibrational motion of the molecular ion on the cross section arises from interference between ionic vibronic waves. These waves are created in a coherent fashion at the beginning of the collision. At the end of the collision the waves mix and interfere. The mixing prefers transitions with $\Delta v' = -1$ [2].

- 2) The ionic vibronic state $v'=4$ dominates the partial differential cross section. The higher states are, due to several reasons, much less populated than the state with $v'=4$.

Consequently, as there are no states significantly populated above $v'=4$, the partial differential cross section lacks interference effects related to the vibrational motion of the molecular ion. The shift in the position of the ionic rainbow is due to the fact that the coulomb forces are switched on later in the collision for higher vibrational states than for the lower ones.

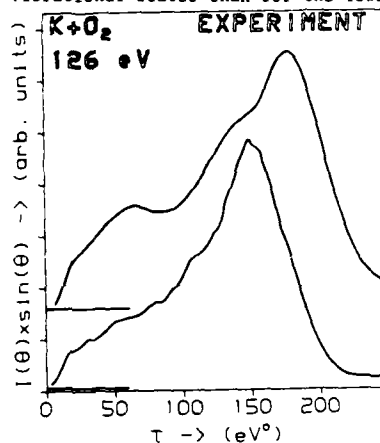


Fig. 1.

Total (top) and partial (bottom) experimental differential cross sections for ion-pair formation in $K+O_2$ collisions. The curves are scaled and shifted in vertical direction for the sake of clarity.

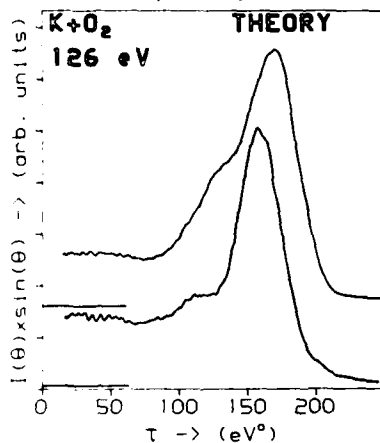


Fig. 2.

Total (top) and partial (bottom) theoretical differential cross sections for ion-pair formation in $K+O_2$ collisions. The cross sections are convoluted to remove the rapid oscillations due to angular scattering interference.

REFERENCES

- /1/ U.C. Klomp, M.R. Spalburg and J. Los, Chem.Phys. **83** (1984) 33.
- /2/ M.R. Spalburg, V. Sidis and J. Los, Chem.Phys.Lett. **96** (1983) 14.

BALMER α EMISSION IN COLLISIONS OF H, H^+ , H_2^+ AND H_3^+ WITH N_2 , O_2 AND H_2O

F Yousif, J Geddes and H B Gilbody

Department of Pure and Applied Physics, The Queen's University of Belfast,
Belfast, United Kingdom

Beams of neutral isotopes of hydrogen at megawatt power levels are being developed for supplementary heating of plasmas in Tokamak devices. Optical measurements of the Doppler shifted and unshifted H_α radiation emitted through collisions with the background gas provide a means of determining the spacial and energy profile of the beam. Recently cross sections¹ have been measured for H_α emission in collision of hydrogen atoms and ions with H_2 molecules.

In the present investigation we are studying H_α formation at energies within the range 3-100 keV for the processes



where $m = 1, 2$ or 3 , $X = N_2, O_2$ or H_2O and \square represents all bound and continuum states.

The experimental arrangement is similar to that used previously¹ in our laboratory. The selected fast hydrogen ion or atom beam passes through a target gas cell and the H_α radiation from different positions along the beam is monitored. The H_α photon detector comprises a lens, interference filter and cooled photomultiplier.

With the H_α detector viewing the beam at a position sufficiently far downstream from the target, all the short lived 3p and 3d states have decayed to a negligibly small level and the cross sections for the formation of the long lived 3s state (reaction 1) can be determined. Here a 50 Å band pass filter centred at 6550 Å is used.

Cross sections for total H_α emission (reaction 2) are determined using a 3 Å bandpass filter centred at 6564 Å. When the detector is positioned at 90° with respect to the beam axis and views the beam within the target cell at a point where H_α emission from decay of the 3p and 3d states has equilibrated the recorded signal also includes a contribution from (a) decay of the long lived 3s state, (b) molecular band radiation

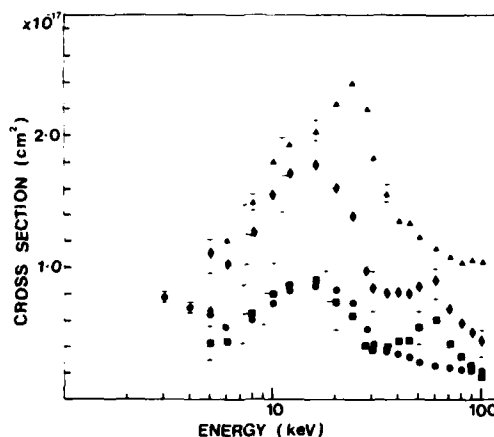


Figure 1 : Balmer α emission cross sections for collisions of $H(1s)$ with H_2O . \circ , $\sigma(3s)$ reaction (1) : Δ , $\sigma(H\alpha)$ reaction (2) : \square , $\sigma(3d) + 0.12 \sigma(3p) = \sigma(H\alpha) - \sigma(3s)$.

from excited states of the target and (c) in the case of H_2O, H_α radiation from dissociative excitation of the target. A knowledge of the target geometry, lifetimes and velocities allows the contribution of the 3s state to be deduced. Tilt tuning of the 3 Å filter to reject H_α radiation allows assessment of contributions arising from molecular band emission. In the case of H_2O the H_α emission arising from reaction (3) was studied in a separate experiment. With the detector set to view the target at 54.7°, the Doppler shifted radiation from the fast projectile was blocked and only target H_α emission recorded.

Cross sections for reactions (1) - (3) in $H - H_2O$ collisions are shown in figure 1.

Cross sections have been normalised to earlier measurements¹ for the $H^+ - H_2$ system.

Our results for H and H^+ in collision with N_2 and O_2 are compared with those reported by other workers.

Reference

1. Williams I D, Geddes J and Gilbody H B. 1982, J Phys B : At Mol Phys **15**, 1377-89.

DOUBLE ELECTRON CAPTURE IN $\text{Ar}^{2+} + \text{D}_2^*$ S.J. Martin, V. Heckman, J. Stevens^{**}, and E. Pollack

Department of Physics, University of Connecticut, Storrs, CT 06268

^{**}Department of Chemistry and Physical Sciences, Quinnipiac College, Hamden, CT 06517

Our laboratory has been studying the Argon- D_2 collision system. To date we have reported on Ar^0 and Ar^+ collisions^{1,2} with D_2 . We now present results on double electron capture in $\text{Ar}^{2+} + \text{D}_2$.

Time-of-flight techniques are used to study the Ar^0 resulting from the double electron capture collisions. The experimental arrangement employs a flight path length of 64 cm. and has been previously described.³ Since there is a change in charge state in $\text{Ar}^{2+} + \text{D}_2 \rightarrow \text{Ar}^0$ collisions there is no direct reference channel from which kinetic energy losses (or gains) of the Ar^0 may be determined. Spectra from the $\text{Ar}^{2+} + \text{Ar} \rightarrow \text{Ar}^0$ collision provide the necessary reference.

Figure 1 shows typical energy spectra of the Ar^0 from $\text{Ar}^{2+} + \text{D}_2$ and $\text{Ar}^{2+} + \text{Ar}$ collisions at an energy of 1.0 keV and small θ . The spectra correspond to $Q=0$ processes in $\text{Ar}^{2+} + \text{Ar}$ and $Q \sim 0$ in $\text{Ar}^{2+} + \text{D}_2$. Although there have been no direct studies of the Ar^0 states following double electron capture from Ar, the oscillatory structure in the cross sections for the direct and double electron capture channels⁴ was found to be characteristic of resonant charge exchange and attributed to it. The dominance of the resonant processes at small scattering angles is now confirmed by our present studies.

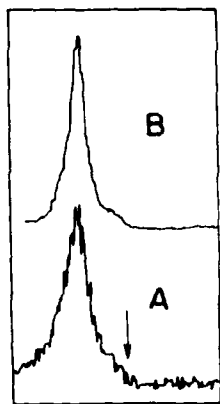


FIG 1 Energy spectra of the Ar^0 resulting from double electron capture at 1.0 keV, $\theta=0$. (A) $\text{Ar}^{2+} + \text{D}_2 \rightarrow \text{Ar}^0$. (B) $\text{Ar}^{2+} + \text{Ar} \rightarrow \text{Ar}^0$. The arrow is drawn at the $Q=12\text{eV}$ position which would correspond to final ground state Ar^0 with the two D^+ ions having threshold energies.

In the double electron capture from D_2 the $Q \sim 0$ processes found at small θ are consistent with capture to electronically excited Ar^0 states. Over the $1 < \theta < 2$ keV deg. range studied, double electron capture was seen to occur to channels with Q near 0. Capture to the ground state of Ar^0 with the two D^+ ions leaving at threshold energies would correspond to an exothermic process with $Q \sim 12\text{eV}$.

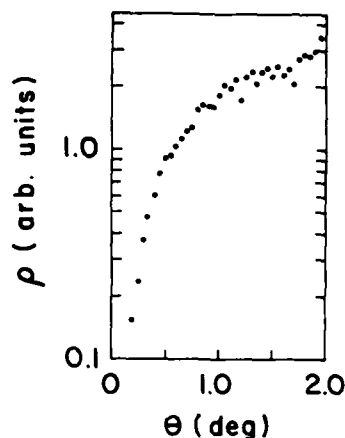


FIG 2 The reduced cross section, for double electron capture, as a function of scattering angle in 2.0 keV $\text{Ar}^{2+} + \text{D}_2$ collisions.

We have measured the cross section for the double electron capture processes. Figure 2 shows our preliminary results at 2.0 keV. At small angles the cross section for double electron capture is found to be weak compared to the direct channel.

The present study continues to show the importance of accidental energy resonant processes in ion-molecule collisions. Several different channels can result in Q values near zero. Our work to date however suggests that the dominant two electron capture channel is $\text{Ar}^{2+} + \text{D}_2 \rightarrow \text{Ar}^0 + 2\text{D}^+$ with the two D^+ ions having kinetic energies near threshold.

References

*Supported by the National Science Foundation and the University of Connecticut Research Foundation.

1. S.J. Martin, V. Heckman, J. Jakacky, Jr., and E. Pollack, Bull. Am. Phys. Soc. 29, 814 (1984).
2. S.J. Martin, V. Heckman, J. Stevens, J. Jakacky, Jr., and E. Pollack, submitted to Bull. Am. Phys. Soc.
3. W.L. Hodge, Jr., A.L. Goldberger, M. Vedder, and E. Pollack, Phys. Rev. A 16, 2360 (1977).
4. J. Stevens, R.S. Peterson, and E. Pollack, Phys. Rev. A 27, 2396 (1983).

ELECTRON CAPTURE IN $\text{Li}^+ + \text{H}_2$ AND $\text{Ar}^+ + \text{H}_2$ COLLISIONS IN THE keV ENERGY REGION AND STUDY OF ORIENTATION EFFECT OF THE TARGET MOLECULE*

M. Kimura,[†] S. Chapman^{*} and N. F. Lane[†]
 Joint Institute for Laboratory Astrophysics
 University of Colorado and National Bureau of Standards
 Boulder, Colorado 80309 USA

We have performed semiclassical close-coupling calculations by using molecular orbital expansion methods with the inclusion of electron translation factors to investigate electron capture mechanisms in $\text{Li}^+ + \text{H}_2$ and $\text{Ar}^+ + \text{H}_2$ collisions. To compensate for the complexity of the polyatomic system which is difficult to deal with accurately, we have employed the diatoms-in-molecules (DIM) method¹ to obtain "reasonably accurate" adiabatic potentials as well as eigenfunctions. Since the keV energy region is of interest, the adiabatic (sudden) approximation is appropriate for internal motion and accordingly, the relative nuclear coordinate of the target molecules was frozen at its equilibrium value. These two systems, $\text{Li}^+ + \text{H}_2$ and $\text{Ar}^+ + \text{H}_2$, are of particular interest from a theoretical point of view, because the $(\text{LiH}_2)^+$ system has near Σ symmetry (relative to the ion-molecule axis) in initial and final ground states, while the $(\text{ArH}_2)^+$ system has open p-orbitals in the Ar^+ ion which give rise to Π symmetry in the initial state. Hence, we can expect that mechanisms governing electron capture in these two systems are quite different.

In Fig. 1, adiabatic potential curves as functions of internuclear distance R between Ar^+ and H_2 and

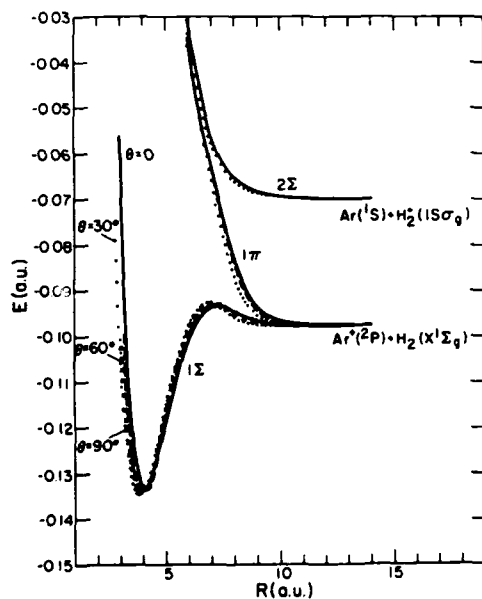


Fig. 1.

orientation θ (angle between the molecular axis and the internuclear coordinate) of the target H_2 molecule are shown. As we have noted, the initial state, $\text{Ar}^+ + \text{H}_2(X^1\Sigma_g; v)$, consists of both Σ and Π symmetries whereas only Σ symmetry is present in the final state, corresponding to $\text{Ar} + \text{H}_2^+(1s\sigma_g, v')$. Because of the involvement of p-orbitals in $\text{Ar}^+ + \text{H}_2$ collisions, orientation effects of the target molecule are expected to be strong. Indeed, our calculation reveals the strong dependence of the probability on orientation at all energies studied. On the other hand, since both colliding partners in the $\text{Li}^+ + \text{H}_2$ system have approximately spherically symmetric electronic charge distributions, the effect of orientation of the target molecule might be expected to be weak and this is what was found.

Total electron capture cross sections for $\text{Ar}^+ + \text{H}_2$ collisions are plotted in Fig. 2 along with some experimental measurements.²⁻⁴ Due to the near resonant character of the $\text{Ar}^+ + \text{H}_2$ collision, the cross section does not drop as the collision energy decreases. This finding is also quite different from that seen in non-resonant $\text{Li}^+ + \text{H}_2$ collisions.

*MK and NFL were supported by the U. S. Dept. of Energy, Basic Energy Sciences.
[†]Also Rice University, Houston, TX.
[†]1984-85 JILA Visiting Fellow. Permanent address: Dept. of Chemistry, Barnard College, Columbia Univ., New York, NY 10027.

References

1. S. Chapman and R. K. Preston, J. Chem. Phys. **60**, 650 (1974).
2. C. J. Latimer, J. Phys. B **10**, 515 (1977).
3. A. F. Hedrick, T. F. Moran, K. J. McCann and M. R. Flannery, J. Chem. Phys. **66**, 24 (1977).
4. R. C. Amme and J. F. McIlwain, J. Chem. Phys. **45**, 1224 (1966).

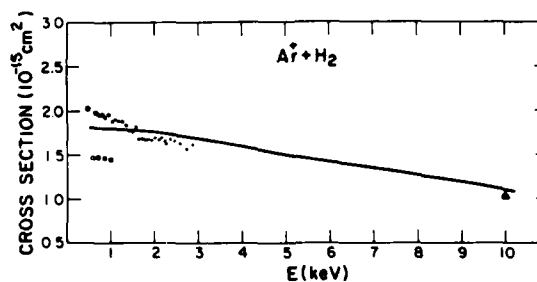


Fig. 2.

CHARGE TRANSFER IN ION-MOLECULE COLLISIONS AT THE keV ENERGY REGION: STUDY OF $H^+ + H_2$ COLLISIONS*

M. Kimura

Joint Institute for Laboratory Astrophysics, University of Colorado and
National Bureau of Standards, Boulder, Colorado 80309 USA

In contrast to theoretical study of charge transfer in ion-atom collisions in the low to intermediate energy range, theoretical investigations of ion-molecule collisions in this energy region are very scarce. This may be partly attributed to the following reasons: (i) it is quite a complex problem to obtain even "reasonably accurate" adiabatic potentials and eigenfunctions as functions of internuclear coordinates and molecular orientations for the polyatomic system; (ii) for the polyatomic system, the number of internal degrees of freedom that need a proper dynamical treatment increases dramatically. To partially compensate for these difficulties, we have adopted the diatoms-in-molecules (DIM) method¹ to obtain "reasonably accurate" adiabatic potentials as well as eigenfunctions. Also, since the keV energy region is of interest, we have employed the adiabatic (sudden) approximation to freeze vibrational and rotational motions of the target molecule. Accordingly, we have fixed the internuclear distance of the H_2 molecule at its equilibrium distance.

Two-state [$H^+ + H_2(X^1\Sigma_g)$ and $H + H_2^+(1s\sigma_g)$] semi-classical close coupling calculations have been performed to investigate $H^+ + H_2$ collision dynamics by using the molecular orbital expansion method with the inclusion of plane wave electron translation factor effect. Adiabatic potential curves are displayed in Fig. 1 for several values of θ and with $\phi = 0^\circ$. The figure indicates that the colliding particles can approach more closely for $\theta = 90^\circ$ than for $\theta = 0^\circ$.

The influence of orientation of the target molecule on the charge-transfer probability has been examined, and the charge transfer cross section is found to be very sensitive to the molecular orientation at energies below 0.5 keV or above 10 keV. Between these energies, however, the orientation effect was small. Calculated total cross sections are plotted in Fig. 2 along with experimental measurements.²⁻⁵ Overall agreement between theory and experiment is satisfactory.

*Work supported by the U. S. Department of Energy, Office of Basic Energy Sciences.

References

1. J. C. Tully, J. Chem. Phys. **58**, 1396 (1973); *ibid.*, **59**, 5122 (1973).
2. J. F. Williams and D. N. Dunbar, Phys. Rev. **149**, 62 (1966).
3. O. Holtricher, Z. Phys. **187**, 41 (1965).
4. Yu. S. Gordeev and M. N. Panov, Sov. Phys. **9**, 656 (1964).
5. F. J. de Heer, J. Schutten and H. Moustafa, Physica **32**, 176R (1966).

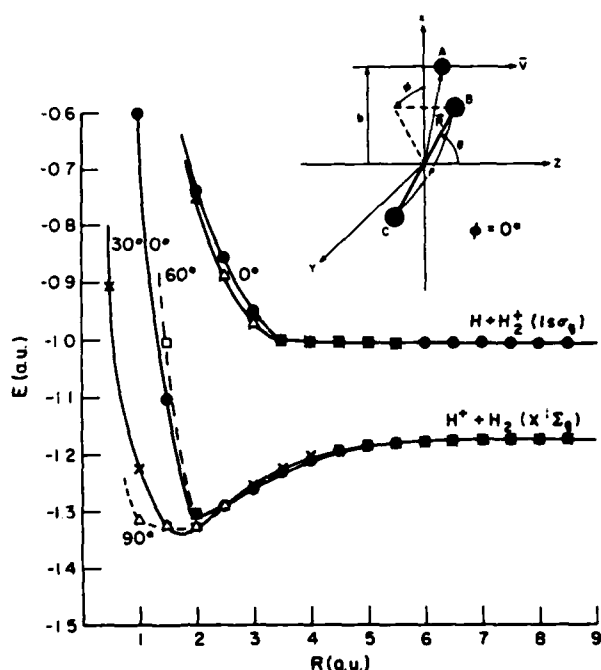


Fig. 1. Adiabatic potential curves as functions of R and θ .

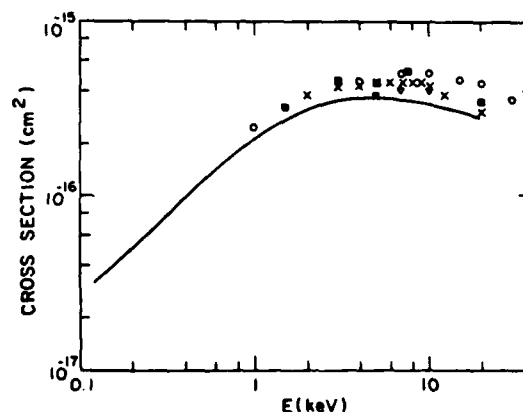


Fig. 2. Charge transfer cross section on the process $H^+ + H_2(X^1\Sigma_g) \rightarrow H(1s) + H_2^+(1s\sigma_g)$.

ABSOLUTE CHARGE TRANSFER CROSS SECTIONS OF 50 eV - 4 keV H^+ , H_2^+ , H_3^+ , N^+ , and N_2^+ in Cs

M. J. Coggiola, Y. K. Bae, and J. R. Peterson

Chemical Physics Laboratory, SRI International, Menlo Park, California 94025 USA

We have recently measured the total attenuation cross sections for H^+ , H_2^+ , H_3^+ and their deuterium analogs, and for N^+ and N_2^+ incident on a Cs target. The experimental conditions were arranged such that single electron capture was the dominant attenuation mechanism. The energy range investigated for the hydrogen ions was 50 eV to 4 keV, while that for the nitrogen ions was 350 eV to 4 keV.

The desired positive ion beam was extracted from a Colutron ion source, focussed and accelerated to the final beam energy and mass-analyzed by magnetic deflection. The collimated projectile beam is directed through the Cs target cell and onto a suppressed Faraday cup. The collector has a $\pm 8^\circ$ acceptance angle to reduce the effects of angular scattering on the beam attenuation. The alkali target cell can be moved rapidly into and out of the projectile beam path, giving measurements of the attenuated and incident beam intensity, respectively. Fixed defining apertures before and after the movable target cell collimate the projectile beam. The Cs target thickness was determined experimentally by measuring the total attenuation of a He^+ projectile beam and then using the accurately measured absolute σ_{+0} cross sections for $He^+ + Cs$.¹

Our results for $H^+ + Cs$ are in excellent agreement with the data of Meyer² between 100 eV and 4 keV. The present results extend the energy range down to 50 eV/amu, where σ_{+0} is found to decrease with energy as expected for an asymmetric charge transfer process. The σ_{+0} results for H_2^+/D_2^+ and H_3^+/D_3^+ in Cs are shown in Figure 1. Good agreement is again found with the previously reported results of Meyer et al.³ An interesting feature of the data in Figure 1 is the nearly flat energy dependence of σ_{+0} down to the lowest energies measured. Although the D_2^+ cross section is apparently falling below 40 eV/amu, its magnitude is still 75% of the maximum value. At the same time, the D_3^+ cross section shows no sign of a low energy falloff down as low as 17 eV/amu. The increased range of velocities over which the cross section is relatively constant is apparently attributable to the large number of final states in the molecules that can undergo near-resonant reactions.

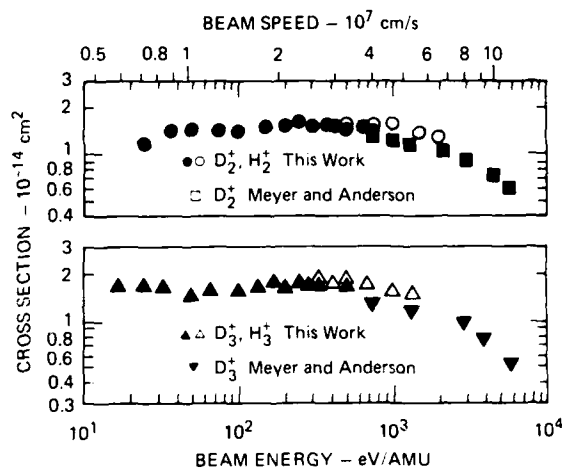


Figure 1 Total attenuation cross sections for H_2^+/D_2^+ and H_3^+/D_3^+ in Cs vapor.

This work was supported by the U.S. Department of Energy, Division of Magnetic Fusion Energy, under contract DE-AT03-80ER53091.

Reference

1. J. R. Peterson and D. C. Lorents, Phys. Rev. **182**, 152 (1969).
2. F. W. Meyer, J. Phys. B. Atom. Molec. Phys. **13**, 3823 (1980).
3. F. W. Meyer, C. J. Anderson, and L. W. Anderson, Phys. Rev. **A15**, 455 (1977).

METASTABLE EXCITED OH^- AND NH_2^- IONS FROM H_2O^+ AND NH_3^+ BEAMS IN Rb

Y. K. Bae and J. R. Peterson

Molecular Physics Department, SRI International, Menlo Park, CA 94025 USA

We apparently have discovered the existence of a metastable ($\tau > 1 \mu\text{s}$) excited state of OH^- produced by passing a H_2O^+ beam of several keV kinetic energy through Rb vapor. We conjecture that this ion is a quintet state based on the lowest bound quartet Rydberg state of OH, in analogy with He_2^- .^{1,2} Rapid autodetachment would thus be forbidden by its spin configuration as in the cases of other known metastable negative ions, such as He^- , He_2^- , Be^- and Ar^- .³ Unlike these other metastable negative ions, however, OH^- also has a stable state below the ground state of OH.

Negative ions were formed from a momentum-analyzed H_2O^+ parent beam transiting Rb vapor, presumably by near-resonant dissociative electron-capture production of the quartet Rydberg OH, followed by a second electron capture collision with Rb. This mechanism is also only conjectured, in analogy to the production of other metastable negative ions.³ After traversing the vapor target the +, 0, and - charged-beam components were separated by an electrostatic quadrupole deflector Q1 which can be used as a low resolution energy analyzer. See Figure 1. After passing two defining apertures, the energy-selected negative ion component entered a second quadrupole Q2 where it was deflected to a Faraday cup. The voltage of two quadrupoles were coordinated to deflect the same energy negative ions. Fast neutrals formed from either collisional- or autodetachment along the field-free drift path between Q1 and Q2 pass through Q2 undeflected to the neutral detector. CEM

Figure 2 shows the energy scans of negative ions produced from a parent H_2O^+ beam and the neutrals produced from them between Q1 and Q2. Although the O^- ion currents were much more intense than the OH^- ions, the O^- ions produced far fewer neutrals than did OH^- . When we increased the background pressure, the intensity of neutrals from OH^- was essentially constant, indicative of autodetachment, while the neutrals from O^- increased linearly from zero with the pressure, as expected from collisional detachment. Apparent decay rates measured at several delay times between 3 and 6 μsec after formation decreased monotonically from 4×10^4 to 2×10^4 /s. These rates assume a unit counting efficiency for the neutrals, and thus represent only lower limits.

Similarly, metastable autodetaching states of NH_2^- ions produced from NH_3^+ ions in Rb were also observed, but decay rates have not yet been measured.

Both of these ions are isoelectronic with F^- , so we will perform similar experiments with it. Mindful of our negative findings of other reported metastable ions,⁴ these results should be considered as tentative pending further study, even though the preliminary results for OH^- are fairly convincing.

Supported by NSF Grant PHY 84-10980 and AFOSR Contract F49620-82-K-0030.

References

1. Y. K. Bae, M. J. Coggiola, and J. R. Peterson, Phys. Rev. Lett. **52**, 747 (1984).
2. H. H. Michels, Phys. Rev. Lett. **52**, 1413 (1984).
3. Y. K. Bae, J. R. Peterson, A. S. Schlachter, and J. W. Stearns, Phys. Rev. Lett. **54**, 789 (1985).
4. Y. K. Bae, M. J. Coggiola, and J. R. Peterson, Phys. Rev. A **29**, 2888 (1984).

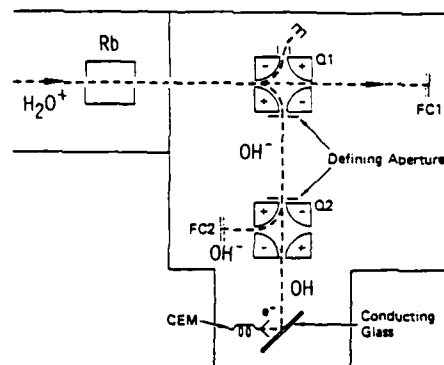


Figure 1 Schematic of experimental arrangement.

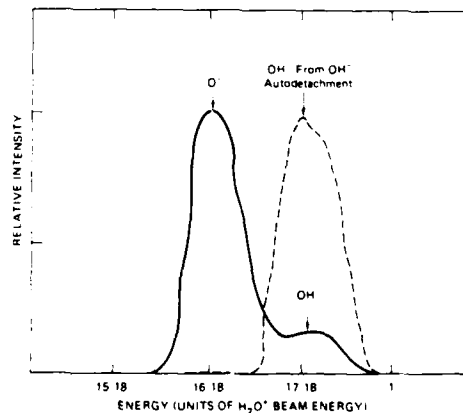


Figure 2 Energy scans of negative ions (solid curve), and neutrals (dashed) produced from them between Q1-Q2.

ENERGY AND CHARGE TRANSFER IN O_2^+ ON O_2 COLLISIONS — EFFECTS OF A "VIBRATIONAL RAINBOW"

K. B. McAfee, Jr., R. S. Hozack

AT&T Bell Laboratories, Murray Hill, New Jersey 07974

ABSTRACT

The efficient conversion of up to eight vibrational quanta into translational energy is found to occur during $O_2^+ - O_2$ collisions. The high efficiency and low deflection angle which are observed in the experiment reported are explained by the occurrence of multiple crossings of the $O_2^+ - O_2$ system interaction potentials, specifically the attractive and repulsive symmetry potentials. The energy and charge transfer model evolved from the experimental data proposes that energy transfer in symmetric molecule — ion collisions takes place at very large intermolecular separations. It differs in an important way from previous concepts which suggest that impulsive momentum transfer at relatively short distances is necessary to the exchange of vibrational energy. To explain the data, a distortion of the electron cloud surrounding the colliding systems is conceived to produce charge-transfer oscillations whose frequencies at the crossing points are multiples of molecular vibration frequencies. Such resonances are similar to the more familiar rainbows often observed in molecular collisions.

The experimental data are obtained by colliding a 130 eV O_2^+ beam at right angles to a narrow beam of target O_2 molecules which are produced in a free jet. The energy of the O_2 neutral beam molecules is determined after charge exchange has occurred using a hemispherical analyzer. From an analysis of the deflection angle and the energy of these ions it is possible to determine the center-of-mass angle change and the number of vibrational quanta which are transferred from the projectile ion to the neutral which is in its ground vibrational state. For collisions which are exothermic the laboratory scattering angle shown in Figure 1 is negative and vice versa. Only the predicted positions of the band heads is shown in the figure, however, we find that it is possible for light molecules to resolve band systems which differ by one quantum up to Δv equal to about 8. The important result shown in Figure 1 is that energy transfer occurs efficiently up to, at least, $\Delta v = 8$ and for center-of-mass angles of a few tenths of a

degree. As proposed above this implies that vibrational energy transfer can take place easily at large impact parameters and that impulsive transfer at small impact parameters such as described by Bates, and Reid^[2] for hydrogen is not required in larger systems.

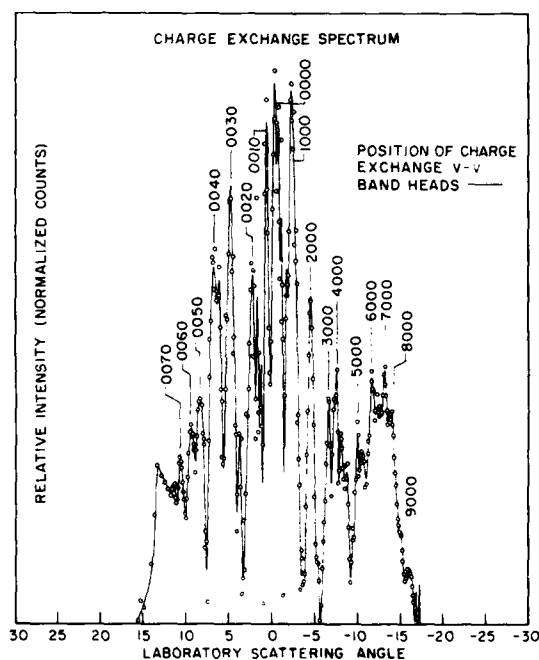


Figure 1: The relative intensity of low-energy scattered ions is plotted against the laboratory deflection angle for $O_2^+ - O_2$ collisions at 130 eV projectile energy. The numbers shown adjacent to the peaks show the position of the band head according to the convention $O_2^+(v_1) + O_2(v_2) \rightarrow O_2(v_3) + O_2^+(v_4)$. Individual transitions are labeled (v_1, v_2, v_3, v_4) .

1. K. B. McAfee, Jr., C. R. Szmanda, R. S. Hozack, R. E. Johnson, *J. Chem. Phys.* 77, 2399 (1982).
2. D. R. Bates and R. H. G. Reid, *Proc. Roy. Soc. London Ser. A* 310, 1 (1968).

METASTABLE EXCITED OH^- AND NH_2^- IONS FROM H_2O^+ AND NH_3^+ BEAMS IN Rb

Y. K. Bae and J. R. Peterson

Molecular Physics Department, SRI International, Menlo Park, CA 94025 USA

We apparently have discovered the existence of a metastable ($\tau > 1\text{ ns}$) excited state of OH^- produced by passing a H_2O^+ beam of several keV kinetic energy through Rb vapor. We conjecture that this ion is a quintet state based on the lowest bound quartet Rydberg state of OH, in analogy with He_2^- .^{1,2} Rapid autodetachment would thus be forbidden by its spin configuration as in the cases of other known metastable negative ions, such as He^- , He_2^- , Be^- and Ar^- .³ Unlike these other metastable negative ions, however, OH^- also has a stable state below the ground state of OH.

Negative ions were formed from a momentum-analyzed H_2O^+ parent beam transiting Rb vapor, presumably by near-resonant dissociative electron-capture production of the quartet Rydberg OH, followed by a second electron capture collision with Rb. This mechanism is also only conjectured, in analogy to the production of other metastable negative ions.³ After traversing the vapor target the +, 0, and - charged-beam components were separated by an electrostatic quadrupole deflector Q1 which can be used as a low resolution energy analyzer. See Figure 1. After passing two defining apertures, the energy-selected negative ion component entered a second quadrupole Q2 where it was deflected to a Faraday cup. The voltage of two quadrupoles were coordinated to deflect the same energy negative ions. Fast neutrals formed from either collisional- or autodetachment along the field-free drift path between Q1 and Q2 pass through Q2 undeflected to the neutral detector. CEM

Figure 2 shows the energy scans of negative ions produced from a parent H_2O^+ beam and the neutrals produced from them between Q1 and Q2. Although the O^- ion currents were much more intense than the OH^- ions, the O^- ions produced far fewer neutrals than did OH^- . When we increased the background pressure, the intensity of neutrals from OH^- was essentially constant, indicative of autodetachment, while the neutrals from O^- increased linearly from zero with the pressure, as expected from collisional detachment. Apparent decay rates measured at several delay times between 3 and 6 μsec after formation decreased monotonically from 4×10^4 to 2×10^4 /s. These rates assume a unit counting efficiency for the neutrals, and thus represent only lower limits.

Similarly, metastable autodetaching states of NH_2^- ions produced from NH_3^+ ions in Rb were also observed, but decay rates have not yet been measured.

Both of these ions are isoelectronic with F^- , so we will perform similar experiments with it. Mindful of our negative findings of other reported metastable ions,⁴ these results should be considered as tentative pending further study, even though the preliminary results for OH^- are fairly convincing.

Supported by NSF Grant PHY 84-10980 and AFOSR Contract F49620-82-K-0030.

References

1. Y. K. Bae, M. J. Coggiola, and J. R. Peterson, Phys. Rev. Lett. 52, 747 (1984).
2. H. H. Michels, Phys. Rev. Lett. 52, 1413 (1984).
3. Y. K. Bae, J. R. Peterson, A. S. Schlachter, and J. W. Stearns, Phys. Rev. Lett. 54, 789 (1985).
4. Y. K. Bae, M. J. Coggiola, and J. R. Peterson, Phys. Rev. A 29, 2888 (1984).

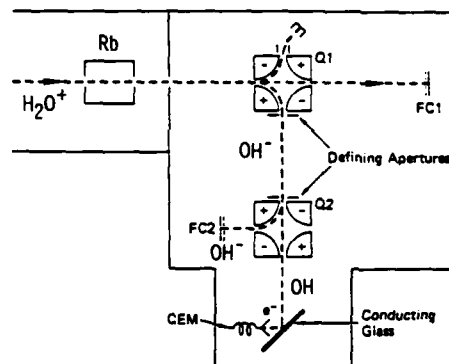


Figure 1 Schematic of experimental arrangement.

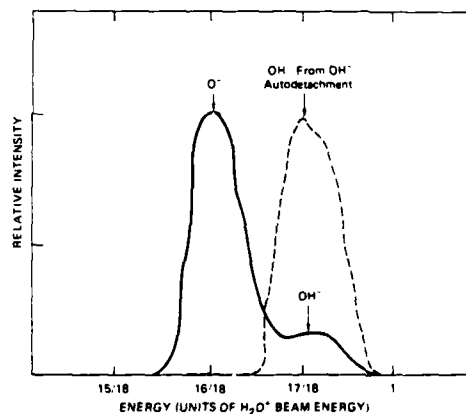


Figure 2 Energy scans of negative ions (solid curve), and neutrals (dashed) produced from them between Q1-Q2.

ENERGY AND CHARGE TRANSFER IN O_2^+ ON O_2 COLLISIONS — EFFECTS OF A "VIBRATIONAL RAINBOW"

K. B. McAfee, Jr., R. S. Hozack

AT&T Bell Laboratories, Murray Hill, New Jersey 07974

ABSTRACT

The efficient conversion of up to eight vibrational quanta into translational energy is found to occur during $O_2^+ - O_2$ collisions. The high efficiency and low deflection angle which are observed in the experiment reported are explained by the occurrence of multiple crossings of the $O_2^+ - O_2$ system interaction potentials, specifically the attractive and repulsive symmetry potentials. The energy and charge transfer model evolved from the experimental data proposes that energy transfer in symmetric molecule — ion collisions takes place at very large intermolecular separations. It differs in an important way from previous concepts which suggest that impulsive momentum transfer at relatively short distances is necessary to the exchange of vibrational energy. To explain the data, a distortion of the electron cloud surrounding the colliding systems is conceived to produce charge-transfer oscillations whose frequencies at the crossing points are multiples of molecular vibration frequencies. Such resonances are similar to the more familiar rainbows often observed in molecular collisions.

The experimental data are obtained by colliding a 130 eV O_2^+ beam at right angles to a narrow beam of target O_2 molecules which are produced in a free jet. The energy of the O_2 neutral beam molecules is determined after charge exchange has occurred using a hemispherical analyzer. From an analysis of the deflection angle and the energy of these ions it is possible to determine the center-of-mass angle change and the number of vibrational quanta which are transferred from the projectile ion to the neutral which is in its ground vibrational state. For collisions which are exothermic the laboratory scattering angle shown in Figure 1 is negative and vice versa. Only the predicted positions of the band heads is shown in the figure, however, we find that it is possible for light molecules to resolve band systems which differ by one quantum up to Δv equal to about 8. The important result shown in Figure 1 is that energy transfer occurs efficiently up to, at least, $\Delta v = 8$ and for center-of-mass angles of a few tenths of a

degree. As proposed above this implies that vibrational energy transfer can take place easily at large impact parameters and that impulsive transfer at small impact parameters such as described by Bates, and Reid^[2] for hydrogen is not required in larger systems.

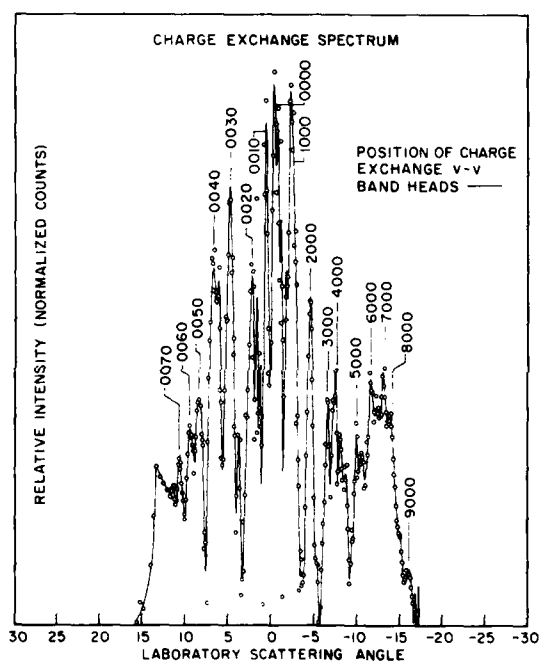


Figure 1: The relative intensity of low-energy scattered ions is plotted against the laboratory deflection angle for $O_2^+ - O_2$ collisions at 130 eV projectile energy. The numbers shown adjacent to the peaks show the position of the band head according to the convention $O_2^+(v_1) + O_2(v_2) \rightarrow O_2(v_3) + O_2^+(v_4)$. Individual transitions are labeled (v_1, v_2, v_3, v_4) .

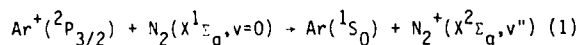
1. K. B. McAfee, Jr., C. R. Szmanda, R. S. Hozack, R. E. Johnson, J. Chem. Phys. 77, 2399 (1982).
2. U. R. Bates and R. H. G. Reid, Proc. Roy. Soc. London Ser. A310, 1 (1968).

OBSERVATION OF COLLISION-ENERGY, PRODUCT-STATE, AND ANGULAR-SCATTERING SPECIFICITY
IN THE CHARGE-TRANSFER REACTION OF $\text{Ar}^+(\text{}^2\text{P}_{3/2})$ WITH $\text{N}_2(\text{}^1\text{E}_g, v=0)$

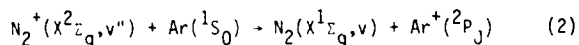
Alan L. Rockwood, Stephen L. Howard, Du Wen-Hu, Paolo Tosi, Werner Lindinger, and Jean H. Futrell

Department of Chemistry, University of Utah, Salt Lake City, Utah 84112

The charge transfer reaction



and its inverse

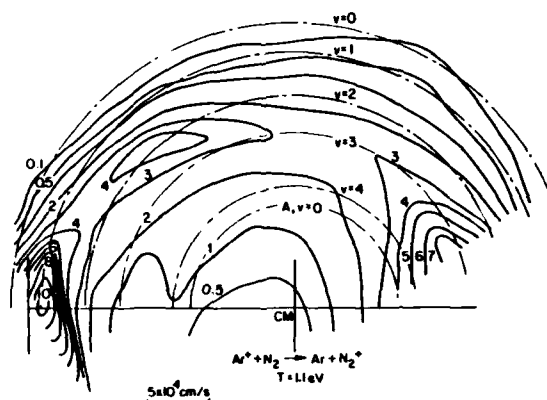


have been extensively investigated by modern techniques capable of probing state-to-state specificity in these reactions. It has been established that reaction (1) gives the $v=0$ product exclusively at 80°K , but that at all temperatures above 140°K the formation of vibrationally-excited levels of the ground electronic state of N_2^+ dominate the reaction kinetics. This has been definitely shown in a laser-induced fluorescence study of the reaction products at a collision energy less than 0.3 eV^2 , which indicates that the product ions consist of a distribution of rotational states for the $v=0$ and $v=1$ states of the product ion with the vibrationally-excited component constituting $87 \pm 10\%$ of the total; the rotational state distribution for $\text{N}_2^+(v=1)$ was analyzed in detail, showing $\bar{N}=12-13$ compared with $\bar{N}=7$ for the N_2 reactant at room temperature. Further, the very strong vibrational state dependence of the reverse reaction (2) has been demonstrated in the elegant study by Govers *et al.*³ using electronically and vibrationally state-selected ions.

A recent paper from our laboratory demonstrated the formation of primarily $\text{N}_2^+(\text{}^2\text{E}_g, v=1)$ in reaction (1) at collision energies of 1.73 and 4 electron volts⁴. The angular scattering observed in that study showed that the mechanism was direct and that very little momentum was transferred in the electron transfer mechanism. A curve-crossing model was suggested to explain these results. This model has been elaborated in great detail in the work of Govers, *et al.*³ who demonstrate that a semi-quantitative rationalization of their results for reaction (2) is possible using the Bauer-Fischer-Gilmore curve-crossing model. Their calculations identify the outer crossing region as the critical one for determining the overall probability of charge transfer (inner crossings are traversed adiabatically in their model), and they infer that a single crossing, the $(v'', v''-1)$ vibronic crossing, very likely governs reaction probability. Our previously-reported beam study of reaction (1) is completely consistent with the microscopic reversibility predictions of their elaboration of the BFG model and with the

observed distribution of products reported by Leone, *et al.*,² at low energy.

That the reaction dynamics of the system is somewhat more complex than deduced from the results referenced above is revealed by the Newton diagram for reaction (1) at a collision energy of 1.1 eV. Principal



conclusions are as follows: (1) Extensive large-angle scattering the N_2^+ product is observed in addition to the forward-scattering N_2^+ product reported previously. (2) Extensive translational to internal energy conversion takes place with the formation of $v=2,3$, and probably 4 levels of the ground electronic state in addition to the $v=1$ vibrational level detected previously. (3) A high degree of quantum-state specificity correlated with angular-scattering specificity is observed in the distribution of product ions.

References

1. D.L. Smith and N.G. Adams, Phys. Rev. A 23 (1982) 2327.
2. L. Huwel, D.R. Guyer, G. Lin, and S.R. Leone, J. Chem. Phys., 81 (8) 1984).
3. T.R. Govers, P.M. Guyon, T. Baer, K. Cole, H. Fröhlich, and M. Lavollée, Chem. Phys. 87 (1984) 373.
4. B. Friedrich, W. Trafton, A.L. Rockwood, S.L. Howard, and J.H. Futrell, J. Chem. Phys. 80 (1984) 2537.

STUDIES OF CHARGE TRANSFER PROCESSES IN A FLOW TUBE

R.G. Keesee, B.L. Upschulte, R.J. Shul, R. Passarella, R.E. Leuchtner, and A.W. Castleman, Jr.

Department of Chemistry, The Pennsylvania State University, University Park, PA 16802

A recently completed selected ion flow tube (SIFT) apparatus was utilized to measure the room temperature bimolecular charge transfer rates between Ar^+ , Ar_2^+ , and a variety of neutral species including O_2 , CO_2 , SO_2 , H_2O , H_2S , NH_3 , and SF_6 . A few of the charge transfer reactions have been studied previously, and the accepted rate coefficients in the literature were compared to our measurements. Our rate coefficients are well within the typical uncertainty of $\pm 30\%$ for all of these reactions except the $\text{Ar}^+ + \text{CO}_2 \rightarrow \text{CO}_2^+ + \text{Ar}$ reaction, in which case there appears to be some discrepancy in the literature, possibly due to the two spin-orbit states of Ar^+ . (The only Ar_2^+ charge transfer reaction studied previously is with H_2O . Our rate constant of $1.98 \times 10^{-9} \text{ cm}^3/\text{sec}$ is in excellent agreement with the literature value of $2.00 \times 10^{-9} \text{ cm}^3/\text{sec}$.¹ The remaining Ar_2^+ reactions have not previously been measured, and will be reported. The charge transfer reactions which were found to proceed at or near the collisional limit correlate nicely with the dipole moment of the reactant neutral species. Those reactions which were found to proceed at fractions of the collisional rate do not appear to correlate with any molecular or ionic parameter. All of the measured rate constants are relatively fast (one tenth of collisional rate) except the $\text{Ar}^+ + \text{O}_2 \rightarrow \text{O}_2^+ + \text{Ar}$ reaction. According to the suggestions of previous researchers in the field, these reactions should show excellent energy resonance between the recombination energy of the reactant ion and a vibrational level of the product ion state; furthermore, the product ion state should be linked to the ground neutral state of the molecule via a favorable Franck-Condon factor. These suggestions were tested by comparing the recombination energy of the reactant ion to the photoelectron spectra of the reactant neutral species. This criterion for fast charge transfer reactions was not obeyed; for example, the $\text{Ar}_2^+ + \text{NH}_3 \rightarrow \text{NH}_3^+ + 2\text{Ar}$ was measured to react at approximately half the collisional rate, yet the recombination energy of Ar_2^+ (14.4 eV) is about 0.5 eV from the closest vibrational level of (NH_3^+) with a favorable Franck-Condon factor. The ratios of rate constants for the $\text{Ar}^+/\text{Ar}_2^+$ reactions with a particular neutral species were calculated. These were compared to the ratios of the rate constants to the collisional rate for both the monomer and dimer ions or argon. In no case did both the monomer and dimer ions react at fractions of the collisional limit; at least one of the ions reacted at the collisional rate. Comparisons with the photo-

electron spectra showed a very interesting result. In every case tested, the ion, Ar^+ or Ar_2^+ , whichever was closer to energy resonance and favorable Franck-Condon factor, reacted faster than the ion which was further from energy resonance.

Mass spectrometric and optical studies of CS_2 in a flowing Ar plasma were initiated to determine the excitation source of $\text{CS}_2^+(A^2-)$. A plasma was established in a flow tube by glow discharge. The pressure was dominated by the carrier gas, Ar, and ranged from 0.8-1.5 torr. The reactant gas, CS_2 , was added downstream and allowed to react with the plasma. A quadrupole mass spectrometer was used to detect the ionic species of interest and a photodiode array detector to monitor the fluorescence. The spectra were displayed on an optical multichannel analyzer with the use of a fiber optic probe and monochromator.

The visible light emission was identified as the A^2-X^2- electronic transition of the CS_2^+ ion. Strong spectral features occur throughout the 4600Å-5300Å region and were used to determine relative vibrational populations of the A^2- first excited electronic state of CS_2^+ . The plasma consisted of five species capable of populating the A^2- state of CS_2^+ : Ar^+ , Ar^+ , Ar^{++} , Ar_2^+ and electrons. Fluorescence was completely suppressed when only electrons or neutrals were allowed to react with CS_2 , thus eliminating both as possible re-excitation sources. The concentration of ionic species of Ar and the fluorescence were monitored as a function of probe voltage, pressure, and flow velocity under conditions where all three were varied independently of one another. The fluorescence intensity did not increase as the concentration of Ar_2^+ increased; therefore, Ar_2^+ was discounted as the source. This identifies Ar^+ or Ar^{++} as the excitation source in a bimolecular charge-transfer reaction; $\text{Ar}^+ + \text{CS}_2 \rightarrow \text{CS}_2^+ + \text{Ar}$ or $\text{Ar}^{++} + \text{CS}_2 \rightarrow \text{CS}_2^+ + \text{Ar}^+$. Such studies determine the energy states of the reaction products which account for the excess energy often observed in a charge-transfer reaction. The findings and the implications will be discussed.

Reference

1. Faraday Discuss. Chem. Soc., 53, 192-200 (1972).

Support of the Department of the Army under Grant No. DAAG29-84-K-0087 is gratefully acknowledged.

THE ELECTRONIC STRUCTURE OF FREE LIQUID SURFACES. ELECTRON SPECTROSCOPY UNDER $\text{He}(2^3\text{S})$ VERSUS HeI -PHOTON IMPACT.

Wolfgang Keller, Harald Morgner, and Werner Müller

Fakultät für Physik, Hermann Herder-Str. 3, D-7800 Freiburg

The excitation energy of metastable $\text{He}(2^3\text{S})$ as well as the HeI -photon energy suffice to release electrons from other matter, let it be atoms, molecules or condensed matter. Indeed, HeI -photoelectron spectroscopy has been applied in all three cases in order to study the respective electronic structure. Electron spectroscopy under $\text{He}(2^3\text{S})$ impact has been studied as well, but the main emphasis was to a lesser extent the investigation of the target but rather the understanding of how the excitation energy is transferred from $\text{He}(2^3\text{S})$ to the target. It is only within the last few years that metastable atoms were used as investigative tool to study condensed matter in the solid state [1,2,3].

In this contribution we report on the first measurements which apply metastable impact electron spectroscopy (MIES) to liquid surfaces. In the same machine under exactly the same conditions we have taken data from MIES and from ultraviolet photoelectron spectroscopy (UPS) for several organic liquids and for liquid mercury.

We find remarkable differences between both modes of ionization. For the non-metallic liquids they must be attributed to the well known fact that metastable rare gas atoms release their energy only to the outermost layer whereas photons penetrate several layers deep. Making use of this knowledge in the interpretation of our data we are able to derive interesting information on the surface structure of the liquids. For liquid formamide (H_2NCOH) we find clear evidence that the surface is composed of molecules which lie flat on the surface.

For this interpretation we have made use of the relative strength of different electronic bands as populated in MIES versus UPS. However, independent of the relative band intensities we can try to evaluate from our data the apparent band width of a given band as found in MIES and UPS. A preliminary evaluation indicates that the widths are systematically smaller in MIES compared to UPS. It seems justified to identify the MIES result with the surface density of states and the UPS data with the volume density of states. We have carried out model calculations which show that a comparison of these two quantities allows rather direct conclusions on the amount of disorder within the liquid. This type of information can be obtained only

by a comparative study of both ionization methods under otherwise identical conditions but not by either method alone.

References

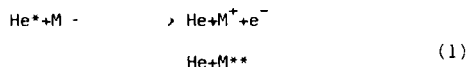
1. Kubota H., Munakata I., Hirooka I., Kuchitsu K., and Harada Y., Chem.Phys.Lett. 74 (1980) 409
2. Sesselmann W., Conrad H., Fritl G., Kuppers J., Woratschek, and Haberland H., Phys.Rev.Lett. 50 (1983) 446
3. Bozso F., Arias J.M., Hanrahan C.P., Yates J.I., Metiu H., and Martin R.M., Surf.Sci. 138 (1984) 488

EXCITATION TRANSFER INTO BOUND AND CONTINUUM ELECTRONIC STATES. $\text{He}(2^3\text{S}, 2^1\text{S}) + \text{HALOGEN CONTAINING MOLECULES}$

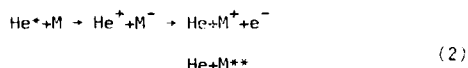
Kai Beckmann, Oskar Leisn and Harald Morgner

Fakultät für Physik, Hermann Herder-Str. 3, D-7800 Freiburg

Excitation transfer from metastable helium $\text{He}^*(2^3\text{S}, 2^1\text{S})$ to molecules with positive electron affinity can proceed either in a direct process



or via an ion pair intermediate

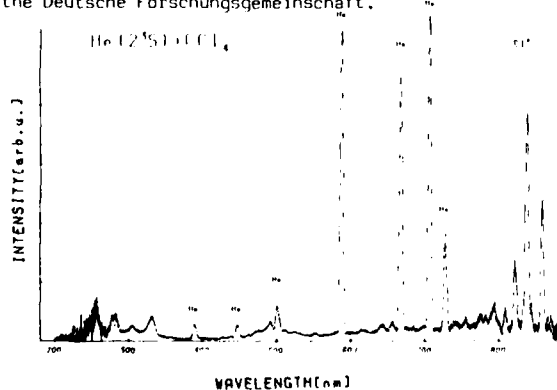


Whereas (1) can be viewed as a one electron process which is accompanied by the emission of a second spectator electron /1/ the second step of process (2) requires a strong interaction between the two electrons which are removed from the negative ion M^- . Therefore it is of interest to compare the details of both processes. The first step in this approach must consist in the identification of both reaction pathways for a given molecule M. Combination of electron spectroscopy and optical spectroscopy helps in this respect /2,3,4/.

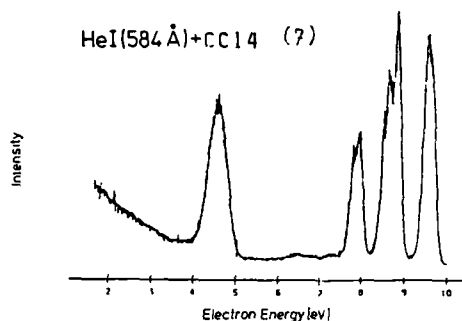
We present both types of spectra taken simultaneously in a molecular beam machine for a large number of halogen containing molecules: Cl_2 , Br_2 , I_2 , IBr , HI , $\text{CF}_{4-n}\text{Cl}_n$ ($n=1,4$), ortho-, meta-, para-dichlorobenzene and trichlorobenzene.

The data of the diatomic molecules allow to identify both processes (1) and (2). The data for the polyatomic molecules cannot as convincingly be interpreted in these terms. In particular the reaction of He^* with CF_3Cl still exhibits puzzling features in spite of detailed experimental material /5,6/. A detailed discussion will be presented at the conference.

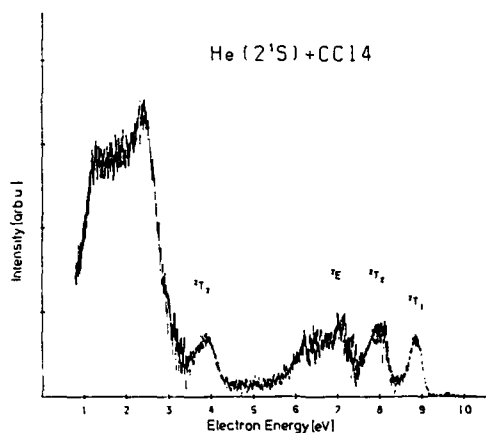
We gratefully acknowledge financial support from the Deutsche Forschungsgemeinschaft.



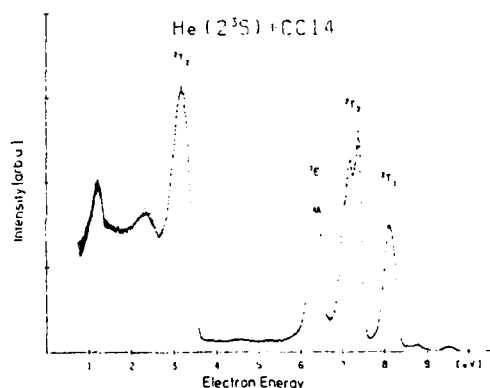
HeI(584 Å) + CCl4 (?)



He(2^1S) + CCl4



He(2^3S) + CCl4



References

1. Morgner, H., J. Phys. B 18 (1985) 251
2. Benz A., Leisn O., Morgner H., Seiberle H., and Stegmaier J., Z. Physik A 320 (1985) 11
3. Leisn O., Morgner H., Duller W., Seiberle H., and Stegmaier J., Hol. Phys. 5 (1985) in press
4. Leisn O., Morgner H., Duller W., Seiberle H., and Stegmaier J., Hol. Phys. 1985, accepted for publ.
5. Kischlat W., and Morgner H., J. Electr. Spec. Rel. Phen. 1985, in press.
6. Baus J., Benz A., and Morgner H., J. Phys. B (1985) acc. for publ.
7. Kimura K. et al., Handb. of Hel. Phys. Vol. 1, Plenum NY (1981)

TRANSITION STATE SPECTROSCOPY WITH ELECTRONS: THE REACTION OF $\text{He}(2^3\text{S}, 2^1\text{S})$ WITH HALOGEN MOLECULES

Arnulf Benz and Harald Morgner

Fakultät für Physik, Hermann Herder-Str. 3, D-7800 Freiburg

It is well known that the chemical behaviour of excited rare gas atoms is very similar to the alkali atoms which follow in the periodic system. For the heavier noble gas atoms this is familiar from the pumping mechanism of rare gas halide lasers:

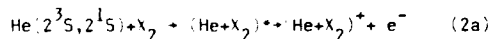


where A denotes a rare gas and X a halogen atom.

If one starts reaction (1) with $\text{A}^* = \text{He}(1s2s)$ then the complex $(\text{AX}_2)^*$ has an excitation energy which is so high that autoionization of the complex is possible. Since autoionization can be a very fast process with lifetimes of 10^{-16} sec it can compete successfully with the chemical reaction (1). This is a disadvantage if one wishes to produce AX^* reaction products. However, it turns into an advantage if one intends to investigate the complex state $(\text{AX}_2)^*$ itself, because electron emission occurs effectively in spite of the short lifetime of the complex. A second favourable feature rests in the fact that neither of the reactants He^* nor X_2 can emit electrons as long as they are separate. Emission of electrons is enabled only as a consequence of the close contact between the excited He^* atom and the target molecule. Therefore the electrons carry information on the structure of the complex $(\text{AX}_2)^*$ but not on the separated collision partners.

Recently some work has been published on the optical spectroscopy of transition states of chemical reactions of alkali atoms. Spectra were taken in emission /1/ and in absorption /2/. These measurements are very difficult because the lifetime of a transition state is usually by orders of magnitude smaller than the average time which elapses until a photon is emitted or absorbed. Consequently the signal is rather low and careful tests have been used to control the background.

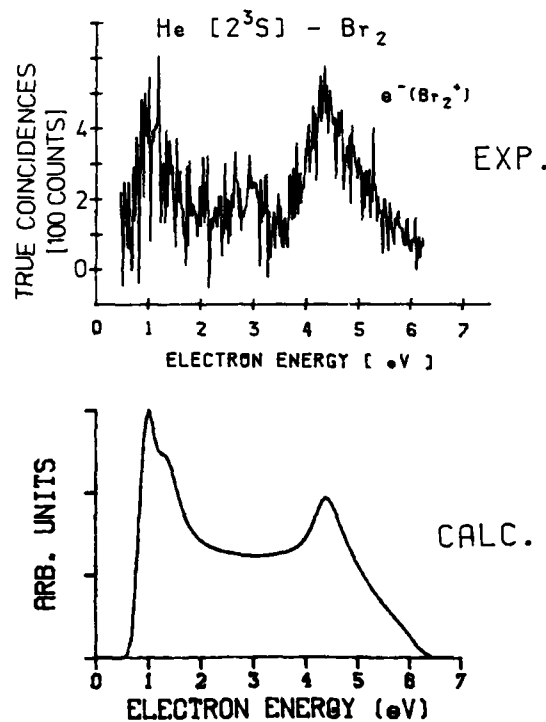
We have studied the reactions ($\text{X} = \text{Cl}, \text{Br}, \text{I}$):



Both reaction pathways can clearly be identified in the electron energy spectra [cf. /3/ for Cl_2]. By means of trajectory calculations we have determined the potential surface of the transition state $(\text{He}^* + \text{X}_2)^*$ of reaction path (2b). The used computer code is similar to the one used earlier in /3/. For Cl_2 we have repeated the calculations of ref. /3/ and achieved a significantly

better fit to the measured electron energy spectrum. Experiments and calculations for Br_2 and I_2 are presented for the first time. We find that the measured electron energy spectra impose already a constraint on the possible $\text{He}^* + \text{X}_2^*$ potential surfaces. However, spectra of those electrons which are coincident with either X_2^* or X^* give much more detailed information on the potential surface. An instructive example is shown in the figure for the molecule Br_2 .

Financial support from the Deutsche Forschungsgemeinschaft is gratefully acknowledged.



Reference

1. Polanyi, J.C., and Wolf, R.J., J.Chem.Phys. **75** (1981) 5951
2. Maguire, T.C., Brooks, P.R., and Curl, R.F. Jr., Phys.Rev.Lett. **50** (1983) 1918
3. Kischlat, W., and Morgner, H., Z.Physik **A312** (1983) 305

PENNING IONIZATION OPTICAL SPECTROSCOPY OF HCl

Andrew J. Yench,† Abul K. Khan, and Sam Brown

Department of Chemistry, State University of New York at Albany, Albany, New York 12222 USA

We have studied the collisional energy transfer process of Penning ionization (PI) of gaseous HCl employing $\text{He}^*(2^3\text{S})$ and $\text{Ne}^*(3p_{2,0})$ metastables by observing the $\text{HCl}^+(\text{A } 2\Sigma^+ - \text{X } 2\Pi_i)$ emission on a flowing afterglow apparatus. This emission is of particular interest because it has been cited,^{1,2} in the $\text{He}^*(2^3\text{S})$ -HCl system in flowing afterglow studies, as an example of a nonvertical Penning process, based on the differences found in the vibrational distributions in the $\text{HCl}^+(\text{A})$ state as determined by photoelectron spectroscopy and PI optical spectroscopy. We have re-examined the flowing afterglow from the $\text{He}^*(2^3\text{S})$ -HCl system over the helium bath gas pressure range of 0.1-3.0 Torr and found no changes in the $\text{HCl}^+(\text{A} - \text{X})$ emission, in agreement with the previous studies,^{1,2} indicating that collisional quenching of the $\text{HCl}^+(\text{A})$ state by helium gas does not occur over this pressure range. We have extended our flowing afterglow study to include the $\text{Ne}^*(3p_{2,0})$ -HCl system, and we have similarly found no spectral changes to occur over the neon bath gas pressure range of 0.1-3.0 Torr. However, the $\text{HCl}^+(\text{A})$ state vibrational distribution found in this case is quite different from that obtained in the $\text{He}^*(2^3\text{S})$ -HCl system, as can be seen from a comparison of the flowing afterglow emission spectra given in Fig. 1 (a. for $\text{He}^*(2^3\text{S})$ -HCl and d. for $\text{Ne}^*(3p_{2,0})$ -HCl). Furthermore, the $\text{HCl}^+(\text{A})$ state vibrational distribution obtained in the $\text{Ne}^*(3p_{2,0})$ -HCl system was found to be very similar to the Franck-Condon (FC) factors for direct photoionization of HCl. A comparison of these FC factors with numerous vibrational distributions of the $\text{HCl}^+(\text{A})$ state obtained by a variety of means will be given at the conference.

Recently, de Vries et al.³ and Snyder et al.⁴ examined the $\text{HCl}^+(\text{A} \rightarrow \text{X})$ vibrational distributions resulting from $\text{He}^*(2^1\text{S})$ -HCl and $\text{Ne}^*(3p_{2,0})$ -HCl, respectively, under single-collision beam conditions. Their spectra are reproduced in Fig. 1 (b. and c., respectively). The agreement in the vibrational distributions of their spectra with the $\text{Ne}^*(3p_{2,0})$ -HCl flowing afterglow results (Fig. 1d.) is quite apparent. Thus, it would appear that the non-FC vibrational distribution obtained in the $\text{He}^*(2^3\text{S})$ -HCl afterglow study is an inherent feature of the helium flowing afterglow system.

Based on a thorough evaluation of the operation of our helium flowing afterglow system, as it pertains to PI of HCl, we conclude the following:

1. $\text{HCl}^+(\text{A})$ emission results from the combined effects of two energetic species; they being $\text{He}^*(2^3\text{S})$ plus an other species.

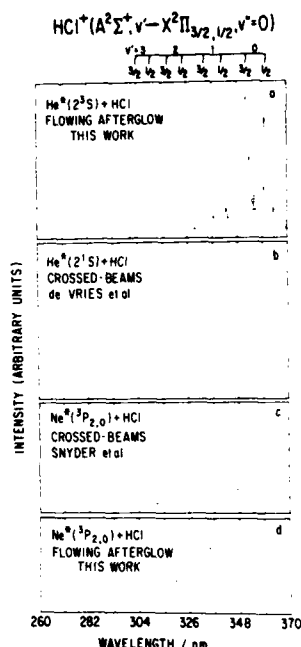


Fig. 1 PI optical emission spectra obtained for the given interacting systems. Spectra a. and d.: this work; spectrum b.: Ref. 3; and spectrum c.: Ref. 4.

2. The 'other' species is produced within the afterglow.
3. The 'other' species produces $\text{HCl}^+(\text{A})$ exclusively or at least preferentially in $v' = 0$.
4. This 'other' species is probably the same "reactive intermediate" postulated by Haugh⁵ to explain his observed $\text{HCl}^+(\text{A})$ state vibrational distribution (non-FC-like) in fast He^+ -HCl collisions.
5. The cross section for the reaction of the 'other' species with HCl to produce $\text{HCl}^+(\text{A}, v'=0)$ must be very large.
6. The identity of the 'other' species is probably thermal He^+ ions.

Thus, it may firmly be concluded that PI of HCl by $\text{He}^*(2^3\text{S})$, $\text{He}^*(2^1\text{S})$, and $\text{Ne}^*(3p_{2,0})$ metastables proceeds by a vertical transition from an essentially unperturbed HCl molecule (i.e. PI in these cases is a FC process).

†Also Department of Physics

References

1. W.C. Richardson et al. *Chem. Phys. Let.* 12, 349 (1971)
2. W.C. Richardson and D.W. Setser, *J. Chem. Phys.* 58, 1809 (1973)
3. M.S. de Vries et al., *J. Chem. Phys.* 80, 1366 (1984)
4. H.L. Snyder et al., *Chem. Phys. Let.* 94, 90 (1983)
5. M.J. Haugh, *J. Chem. Phys.* 56, 4001 (1972)

ROLE OF HELIUM AND NEON IN GLOW DISCHARGES
WITH NITROGEN AS A TRACE COMPONENT:
THE FIRST NEGATIVE $N_2^+(B+X)$ AND
SECOND POSITIVE $N_2(C+B)$ EMISSION
SYSTEMS OF NITROGEN

M. J. Weiss, and H. Mooney

Litton, Guidance and Control Systems, Woodland Hills, California 91367 USA

Emission from glow discharges in N_2 -He-Ne mixtures were spectroscopically determined under a variety of conditions: content of N_2 , total gas pressure, discharge currents and neon-helium ratio.

The emission from mixtures containing N_2 as a controlled impurity component was examined between 3000 and 5000 Å at N_2 concentrations from 0.8% to 30% and at total pressures from 1.5 to 10 Torr. The effect of helium and neon on N_2 emission was checked individually by operating glow discharges in N_2 -Ne mixtures.

The dependence of the emission on discharge location was also investigated by monitoring the N_2 emission in the First Negative ($B+X$) and Second Positive ($C+B$) Systems in the region between the anode and cathode.

Discharge currents were varied from 0.5 to 9 ma to determine whether there were any gross effects of the current on the individual nitrogen emission system components. In all cases studied, the components of the N_2 Second Positive ($C+B$) system were present.

As the partial pressure of N_2 is reduced from 10% to 0.8%, the presence of the First Negative system becomes increasingly prominent. Figures 1 and 2 show the emission for a 10% and 0.8% mixture of N_2 in He-Ne, respectively. Note the prominence of the 0-0 component of the $N_2^+(B+X)$ band at 3914.4 Å. The ratio of the N_2^+0-0 component ($B+X$) to the N_2 0-2 ($C+B$) of N_2 increases by more than a factor of 50 when the partial pressure of N_2 is reduced from 10% to 0.8%.

When pure neon is substituted for the helium-neon mixture in N_2 , the emission systems consist primarily of the $N_2(C+B)$ system with the $N_2^+(B+X)$ suppressed considerably.

The result of the discharge current studies show that for all cases studied, low discharge currents favor the $N_2^+(B+X)$ emission while high emission currents favor $N_2(C+B)$ emission.

The appearance of N_2^+ emission is probably due to the presence of excited helium species, such as the $He\ 2^1S$ and $He\ 2^3S$ since electron-molecule ionization in glow discharges of nitrogen and neon do not show much ion emission compared to helium-neon mixtures containing $\leq 1\%$ nitrogen.

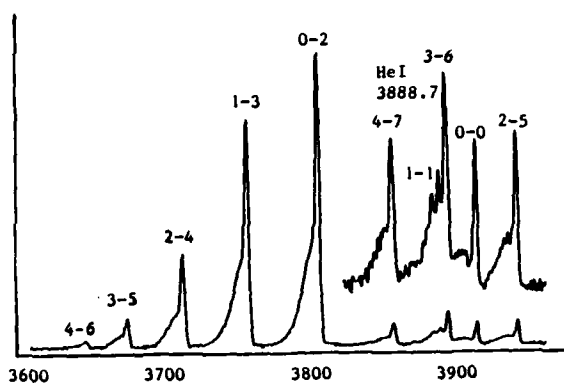


Figure 1. Emission spectrum of a glow discharge in He-Ne containing 10% N_2 . Note the small contribution of the 0-0 and 1-1 components of the $B+X$ system in N_2^+ .

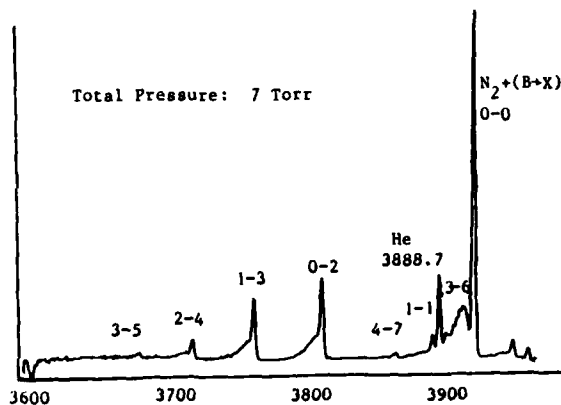


Figure 2. Emission spectrum of a glow discharge in He-Ne containing 0.8% N_2 . Note the much larger contribution of the 1-1 and 0-0 components of the $B+X$ system.

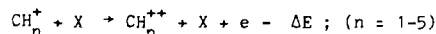
IONIZATION OF CH_n^+ IONS BY ELECTRON-LOSS COLLISION SPECTROSCOPY

D. Mathur, C. Badrinathan, U.T. Raheja and F.A. Rajgara

Tata Institute of Fundamental Research, Bombay 400 005, India

Introduction

There remains a paucity of data concerning double ionization of molecules and molecular radicals. We report the measurement of double ionization energies of CH_n^+ ions by means of single electron loss collisions of the type



where CH_4 , Kr, H_2 and laboratory air were used as target X and the collision energy was 3 keV. The energy defect, ΔE , is a measure of the difference between the single and double ionization energies of CH_n^+ .

Experimental

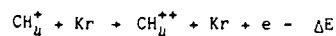
Singly charged CH_n^+ ions were produced in a low-voltage arc, extracted at 3 keV energy and focussed by an einzel lens on to the entrance plane of a Wien filter (crossed electric and magnetic fields). The mass selected ions passed through a double-differentially-pumped collision chamber containing gas at $\sim 10^{-4}$ torr pressure. Ions in the post-collision region (10^{-7} torr pressure) were passed through a parallel plate energy analyser and were detected by a channeltron operating in the particle counting mode.

The apparatus was interfaced on-line to a micro processor-controlled multichannel analyser.

If the incident CH_n^+ ions were transmitted through the energy analyser at a parallel plate voltage V, the corresponding CH_n^{++} ions of the same kinetic energy would be transmitted at $(0.5 V - \Delta V)$, where ΔV is related to the ΔE by a factor determined by the analyser geometry. By measuring the voltage displacement of the onset of CH_n^{++} from 0.5 V the minimum energy defect $\Delta E(\text{min.})$, hence the energy threshold for ionizing CH_n^+ , is determined.

Results

A typical inelastic spectrum produced by scanning the analyser voltage is shown in Fig.1 for the collision



$\Delta E(\text{min.})$ is measured to be 26.26 ± 0.25 eV, where energy calibration is accomplished by measuring the threshold for He^{++} formation in the collision

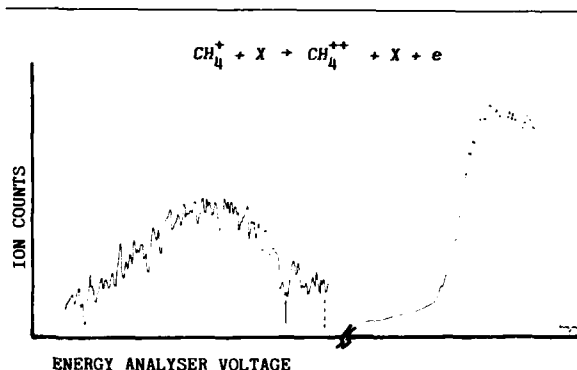
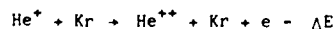


FIG.1: Typical electron stripping spectrum. The peak on the right is the elastic CH_4^+ peak; Solid vertical line indicates onset for CH_4^{++} production.

$\Delta E(\text{min.})$ for CH_4^+ is found to be independent of the nature of target gas used; this suggests that negligible amounts of kinetic energy and internal energy are transferred from the fast incident ion to the target. Moreover, the rapidity of the collision process makes intramolecular energy transfer very unlikely.

Table 1 gives the preliminary values for ionization energies of molecular species which appear to possess doubly-charged ions whose lifetimes have a lower limit of about 3.5×10^{-6} s, which is the transit time for 3 keV ions to traverse the distance between the collision region and the detector.

Table 1

Species	$\Delta E(\text{min.})^a$ (eV)
CH_5^+	21.0
CH_4^+	26.26
CH_3^+	20.8
CH_2^+	b
CH^+	23.67
C^+	24.76

a ± 0.25 eV

b No signal corresponding to CH_2^{++} could be detected.

SINGLE AND DOUBLE ELECTRON DETACHMENT FROM
 Cl^- BY MOLECULAR OXYGEN AND NITROGEN

B. Hird and F. Rahman

Physics Department, University of Ottawa, Ottawa K1N 6N5, Canada.

The cross sections for the production of a fast neutral or a positive ion in a single negative ion-molecule collision, have been measured from 20 keV to 100 keV. There is a significantly higher relative probability of double detachment from O_2 and N_2 than from monatomic targets, and the double detachment cross section σ_{-+} is respectively nearly half, and nearly a third of the single detachment cross section at our highest energies. Also there is a different energy dependence of the single detachment cross sections σ_{-0} for O_2 and for N_2 .

Experimental conditions were such that the probability of two successive collisions with different molecules was small and could be allowed for by correction factors.

When the target is diatomic there is an added possibility that the double detachment may be sequential, with the detachment occurring at the first atom

encountered, and the ionization of the fast neutral at the second atom, in the same molecule. Assuming that the σ_{-0} cross section is roughly πR^2 , where R is the detachment radius, then a simple geometric argument gives a probability of about one third that the second atom, at a binding radius of 1.2 Å, will be within an impact parameter distance R of the second atom. This assumes that the σ_{0+} ionization cross section is roughly the same as the atomic detachment cross section σ_{-0} .

The considerable difference between the energy dependence of the O_2 and the N_2 σ_{-0} cross sections suggests that the electron transfer process may contribute significantly for the oxygen target, forming slow O^- or O_2^- recoil ions, whereas this process is impossible in N_2 because of the absence of stable nitrogen negative ions.

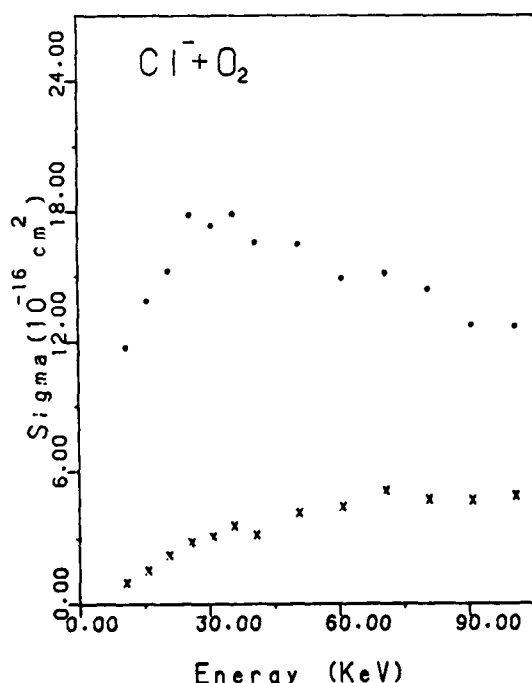


FIG. 1. Molecular cross sections for the detachment of one electron (circles), and for the detachment of two electrons (crosses) in a single $\text{Cl}^- - \text{N}_2$ collision.

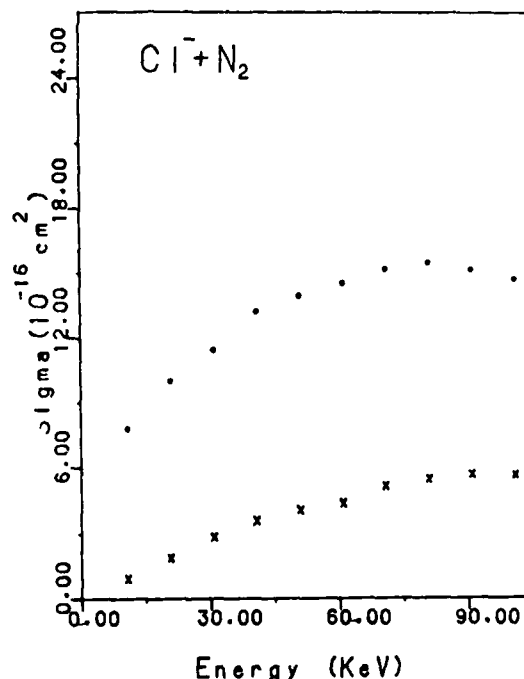


FIG. 2. Same as FIG. 1 but for $\text{Cl}^- + \text{O}_2$ collisions.

THE STATE SPECIFIC REACTION OF ELECTRONICALLY EXCITED SODIUM ATOMS WITH OXYGEN MOLECULES

H. Schmidt, P. S. Weiss, J. M. Mestdagh, M. H. Covinsky and Y. T. Lee

Materials and Molecular Research Division, Lawrence Berkeley Laboratory and
Department of Chemistry, University of California, Berkeley, California 94720 USA

The reaction: $\text{Na}(3^2\text{S}) + \text{O}_2(\text{X}^3\Sigma^-_g) \rightarrow \text{NaO}(\text{X}^2\Pi^+) + \text{O}(^3\text{P})$ is endothermic, with $\Delta H = 57.9$ kcal/mole, but the electronic energy of the Na atoms in the 4D or 5S states, or with the additional translational energy of 9.5 kcal/mole for Na atoms in the 3P states is more than enough to overcome this endothermicity. The purpose of this experiment was to study the effect of electronic energy and symmetry on chemical reactivity.

The reaction of electronically excited sodium atoms with molecular oxygen has been studied in a modified universal crossed molecular beams machine. Briefly, a seeded supersonic sodium atomic beam was crossed at 90° to a seeded or neat supersonic O_2 beam in a vacuum chamber under single collision conditions. The laser beams used for the excitation of sodium atoms crossed the atomic beam in this interaction region from the third perpendicular direction. Scattered product was detected with a mass spectrometer which could rotate in the plane defined by the atomic and molecular beams.

The measurements of laboratory angular distributions of product were carried out for each of the three optically pumped Na levels, as well as for the ground state at three collision energies: 7, 16, and 18 kcal/mole. At the lower collision energy (7 kcal/mole) no reaction was observed for any of the Na levels. At the upper two collision energies (16 and 18 kcal/mole) reaction to $\text{NaO} + \text{O}$ was observed only when the sodium atoms were optically pumped to the $\text{Na}(4^2\text{D})$ state. The measured laboratory angular distribution at a collision energy of 18 kcal/mole is shown in Figure 1. This distribution was taken with the mass spectrometer tuned to mass to charge ratio of 23 (Na^+) because most of the product NaO fragments to Na^+ in the electron bombardment ionizer.

There are four very striking features of these measurements. First, the reaction only proceeded from the $\text{Na}(4^2\text{D})$ state, even though the $\text{Na}(5^2\text{S})$ state (only 1350 cm^{-1} lower) and the $\text{Na}(3^2\text{P})$ state (if collision energy was included) were energetically allowed to react.

Secondly, the NaO product angular distributions were strongly backwards peaked relative to the incoming sodium atoms in the center of mass frame of reference. This implies that a collinear or near collinear approach geometry was favored, and that the reaction proceeded directly with no collision complex formation.

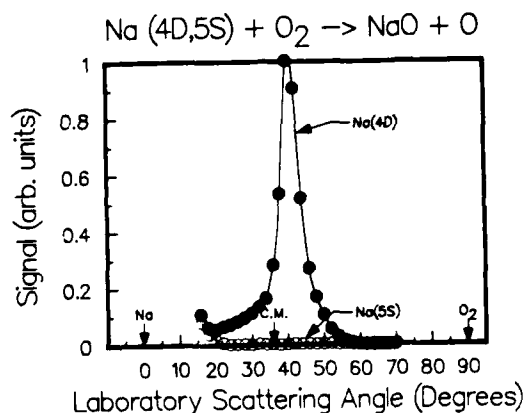


Fig. 1. Laboratory angular distributions of NaO at a collision energy of 18 kcal/mole. The upward trend at low laboratory angle is elastic scattering of Na as the detector is moved closer to the Na beam.

Thirdly, the very small angular range over which the reactively scattered NaO was detected shows that the products were very highly internally excited (>2 eV). While our detector is not state selective, we were able to determine the product translational energy, and thus by using thermochemical information and invoking conservation of energy, we found that the total product internal energy corresponds to the formation of $\text{NaO}(\text{A}^2\Sigma^+) + \text{O}(^1\text{D})$.

Lastly, the lack of reaction at low collision energy shows that there must be an entrance channel barrier of at least 7 kcal/mole, but less than 16 kcal/mole.

ACKNOWLEDGMENT

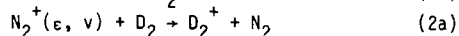
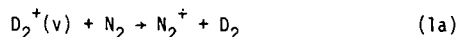
This work was supported by the Director, Office of Energy Research, Office of Basic Energy Sciences, Chemical Sciences Division of the U.S. Department of Energy under Contract No. DE-AC03-76SF00098. The laser used in this research was a loan from the San Francisco Laser Center supported by the National Science Foundation under Grant No. CHE79-16250 awarded to the University of California at Berkeley in collaboration with Stanford University.

A STATE SELECTED STUDY OF ION-MOLECULE REACTIONS IN THE $(D_2 - N_2)^+$ SYSTEM

Kenichiro Tanaka, Tatsuhisa Kato, and Inosuke Koyano

Institute for Molecular Science, Myodaiji, Okazaki 444, Japan

In order to elucidate the reaction mechanism of ion-molecule reactions, we have applied our TESICO technique¹ to the internal state selection of the primary ions in the reactions



The threshold electron spectrum of D_2 shows well resolved peaks which correspond to the production of vibrational states $v=0-7$ of the D_2^+ ion, while that of N_2 shows similarly well resolved peaks corresponding to the production of $v=0-4$ of $N_2^+(X^2\Sigma_g^+)$ and $v=0-8$ of $N_2^+(A^2\Pi_u)$.² This enables us to study the reactions of these states individually by means of TESICO.

The results for reaction (1) obtained at 2.5 eV of collision energy are summarized in Figure 1, where the relative cross sections are plotted as a function of the vibrational quantum number of D_2^+ . As can be seen from the figure, the cross section of reaction (1a) shows an interesting variation as the vibrational quantum number changes. The cross section varies regularly with the vibrational quantum number, increasing at odd quantum numbers and decreasing at even quantum numbers. In contrast, the cross section of reaction (1b) is found to be almost independent of the vibrational quantum number. These trends are essentially the same for all collision energies studied (2.5, 6.0, and 9.0 eV).

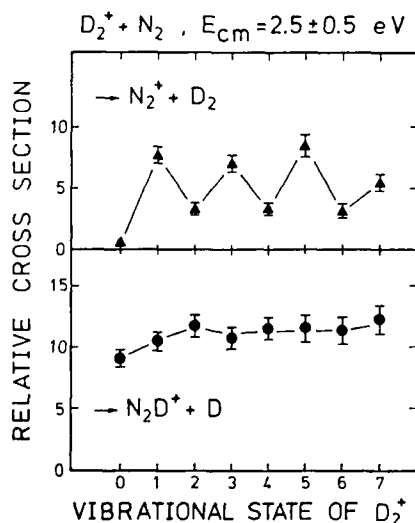


Fig. 1 : Dependence of reaction cross sections on the vibrational state of D_2^+

Results for reaction (2) obtained at 1.3 eV of collision energy are shown in Figure 2. Here, the relative reaction cross sections have been determined for vibrational states $v=0-3$ of $N_2^+(X^2\Sigma_g^+)$ and $v=0-3$ of $N_2^+(A^2\Pi_u)$. It is seen that, while the cross sections for $N_2^+ + D_2$, $E_{cm}=1.3\pm 0.4$ eV

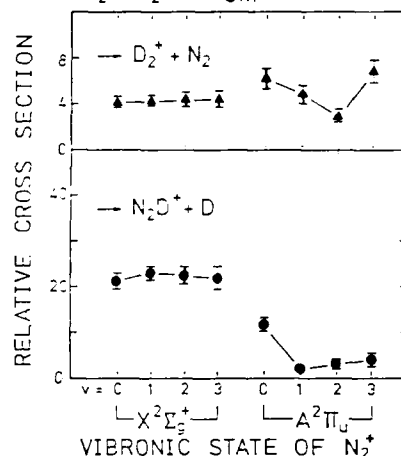


Fig. 2 : Dependence of reaction cross sections on the vibrational and vibronic states of N_2^+

both reactions (2a) and (2b) are almost independent of the vibrational state in the $X^2\Sigma_g^+$ electronic state, they exhibit interesting dependence on the vibrational state in the $A^2\Pi_u$ electronic state. Moreover, the effect of the electronic excitation to the $A^2\Pi_u$ state on the magnitude of the cross sections are found to be quite different between the two channels (2a) and (2b). This latter point is more conspicuous at lower collision energies.

The distinct vibrational state dependence of the cross sections for reaction channels (1a) and (1b) would strongly suggest that the chemical reaction (1b) proceeds adiabatically on a potential energy surface correlating with $D_2^+ + N_2$ at infinite intermolecular separation (i.e., without hopping to the $D_2 + N_2^+$ surface). On the other hand, the similarity in the vibrational state dependence between reaction channels (2a) and (2b) with $N_2^+(X^2\Sigma_g^+)$ would indicate that the chemical reaction (2b) with this state proceeds via a nonadiabatic transition to the surface correlating with $D_2^+ + N_2$ at infinite intermolecular distance.

References

1. I. Koyano and K. Tanaka, J. Chem. Phys. **72**, 4858 (1980)
2. T. Kato, K. Tanaka, and I. Koyano, J. Chem. Phys. **77**, 334 (1982)

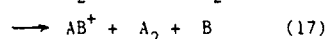
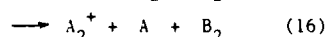
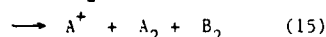
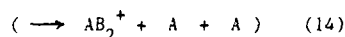
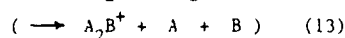
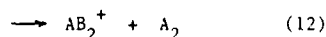
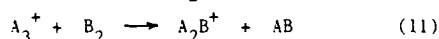
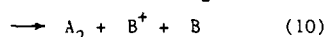
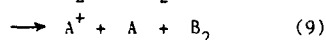
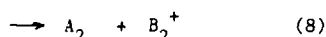
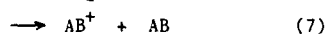
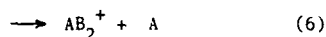
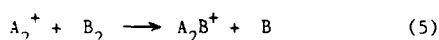
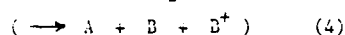
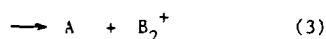
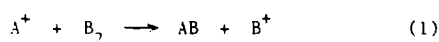
ION-MOLECULE REACTIONS IN COLLISION SYSTEMS OF H^+ , H_2^+ , H_3^+ AND THEIR ISOTOPIC IONS
WITH HYDROGEN AND DEUTERIUM MOLECULES FROM 0.1 TO 1000 eV.

Kazuhiko Okuno and Yozaburo Kaneko

Department of Physics, Tokyo Metropolitan University, Setagaya-ku, Tokyo 158, Japan

An octo-pole ion-beam guide (OPIG) technique has been used to study on ion-molecule reactions in collisions of H^+ , H_2^+ , H_3^+ and their isotopic ions with hydrogen and deuterium molecules in the energy range from 0.1 to 1000 eV. The OPIG is united with a collision cell placed in the middle of tandem mass spectrometer as shown in Fig.1. An r-f field supplied to the OPIG stores and guides product ions formed in the collision cell to the entrance of the second mass spectrometer.

The types of reaction channels taking place in the collision systems studied were identified by using various combinations of isotopic species as follows.



Here A and B are H or D.

The integral cross sections of these reactions were determined as a function of the collision energies from 0.1 to 1000 eV in the center-of-mass system and

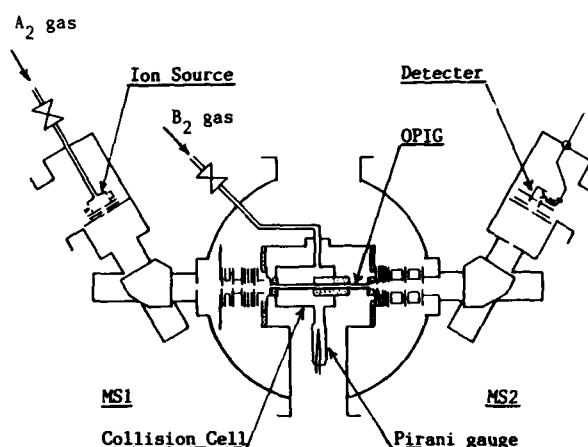


Fig.1 A schematic diagram of the apparatus used.

kinetic energies of product ions were analyzed from the mass positions of product peaks in the mass spectra observed.

The obtained cross sections except for that of symmetric charge transfer process (8) are very strongly dependent on the collision energy. Their energy dependences can be classified according to whether $\Delta E \geq 0$ or $\Delta E < 0$ where ΔE is the exothermicity of reaction. The reactions of (1), (5), (6), (7), (11) and (12), which are the former case, are predominant at low energy region and their cross sections decrease rapidly above several electron volts. On the other hand, the cross sections of reactions which are endothermic raise up rapidly from each threshold, have a maximum around 10 eV and decrease with the increase of collision energy. The cross section of reaction (3) raises up again above 200 eV very sharply. It seems that there are two different charge transfer mechanisms in the $H^+ + H_2$ collision system.

The cross sections will be presented and the collision dynamics will be discussed.

THE PRODUCTION OF H_3^+ IONS WITH LOW INTERNAL ENERGY

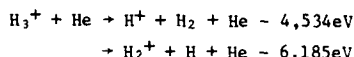
A. Sen and J.B.A. Mitchell

Department of Physics and Centre for Chemical Physics
The University of Western Ontario, London, Ontario, Canada. N6A 3K7

The dissociative recombination of H_3^+ is a process of great importance to astrophysics and to negative ion source production. A number of recombination studies have been performed¹⁻⁶ which agreed quite well with each other. The most recent measurement⁷ however indicates that ground state H_3^+ ($v = 0$) ions have a very low recombination rate coefficient. This supports theoretical studies^{8,9} which had also predicted a small rate coefficient because of a non-favourable crossing of the dissociating neutral state with the potential energy surface of the ion. Some of the earlier studies certainly involved excited H_3^+ ions but for the studies of Peart & Dolder and Biondi, the ions were believed to be vibrationally cold. Clearly there remains considerable uncertainty regarding this important reaction.

An r.f. storage ion source⁽¹⁰⁾ has been built in our laboratory for production⁽¹¹⁾ of vibrationally de-excited ions. The studies of the vibrational states of these ions emanating from it have been performed by examining the threshold for collisional dissociation with He atoms in a low energy cross beam (ion-atom) apparatus. Our results on H_2^+ indicate that these ions are basically formed in the lowest two vibrational levels under appropriate source conditions.⁽¹¹⁾

H_3^+ ions are formed in the source mainly through the reaction $H_2^+ + H_2 \rightarrow H_3^+ + H$. These ions have been examined by looking at the threshold level for the reactions



where the H^+ and H_2^+ fragments have been measured. Fig.1 shows the results of our measurement where the relative cross sections for the two channels have been plotted against ion kinetic energy. It can be seen that the H_3^+ ions have less than 0.5eV of internal energy.

Later, measurements of the dissociative recombination of H_3^+ will be performed using this ion source in conjunction with the Merged Electron Ion Beam Experiment, (MEIBE) at UWO.

Reference

1. Leu, M.T., Biondi, M.A. & Johnson, R. Phys. Rev. A8, 413, 1973.
2. Peart, B. and Dolder, K.T., J. Phys. B7, 1948.
3. Auerbach, D., Cacuk, R., Caudano, R., Gailv, T.D., Keyser, C.J., McGowan, J. Wm., Mitchell, J.B.A. and Wilk, S.F.J. J. Phys. B10, 3797, 1977.
4. Mathur, D., Hasted, J.B. and Khan, S.U. J. Phys. B12, 2043, 1979.

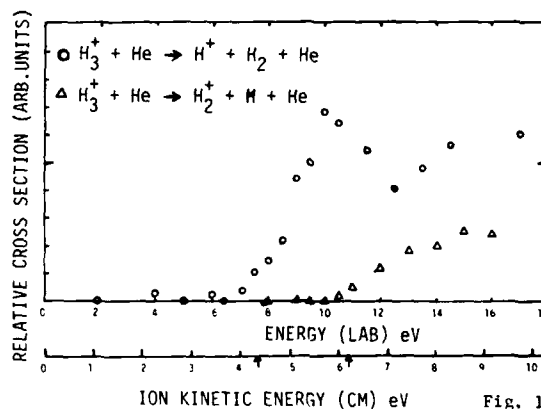


Fig. 1

5. MacDonald, J.A., Biondi, M.A. and Johnson, R. Planet Space Sci. 32, 651, 1984.
6. Mitchell, J.B.A., Ng, C.T., Forand, L., Janssen, R. and McGowan, J. Wm. J. Phys. B17, L909, 1984.
7. Adams, N.G., Smith, D. and Alge, E. J. Chem. Phys. 81, 1778, 1984.
8. Michels, H.H. and Hobbs, R.H. App. J. Lett. 286, L27, 1984.
9. Kulander, K.C. and Guest, M.F. J. Phys. B16, L101, 1979.
10. Teloy, E. and Gerlich, D. Chem. Phys. 4, 417, 1974.
11. Sen, A., McGowan, J. Wm. and Mitchell, J.B.A. (This Conference).

THE SELF-CONSISTENT TIME-DEPENDENT, HARTREE-FOCK METHOD OF MOLECULE-ION COLLISIONS: THEORY AND APPLICATION

Detlev H. Tiszauer

Dept. of Applied Science, University of California, Davis, California

A film of the time development of the electron density during a colinear reactive collision of H^+ on H_2 at a scattering energy of 3eV is presented. This time dependent density was produced by the numerical integration of a fully self-consistent set of Time Dependent Hartree Fock (TDHF) equations for the electrons and classical equations for the nuclei.

(1) The inherent approximations in this method are discussed in comparison to the full quantum solution of the colinear H^+ on H_2 collision, and a comparison is made to an Eikonal self-consistent time dependent scheme. (2)

Finally, some of the computational problems of the coupled TDHF method as applied to low energy reactive molecular collisions are discussed, along with the potentials of this method for treating more complex molecular collision systems.

Reference

- (1) D. Tiszauer and K.C. Kulander, Phys. Rev. A, 29, 2909 (1984).
- (2) David A. Micha, J. Chem. Phys., 78, 7138 (1983).

ANALYSIS OF DISTORTED-WAVE AND COUPLED-CHANNEL-WAVE TRANSITION AMPLITUDES

S.H. Suck Salk

Department of Physics and Graduate Center for Cloud Physics Research
University of Missouri-Rolla, Rolla, Missouri 65401

Recently perturbation methods have become highly promising for studying rearrangement collisions (reactive scattering) involving atom-diatom-molecule systems. The single-step (single-channel) DWBA⁽¹⁾ has shown a good predictive power for relative (not absolute) angular distributions⁽²⁾ and relative cross-sections⁽³⁾. A coupled-channel-wave perturbation method⁽⁴⁾ has demonstrated a remarkable success even in the prediction of absolute cross-sections close to the quality of the exact close-coupling calculations⁽⁵⁾ up to a moderately high collision energy.

Studies have often centered on computational analysis. A comparative study of making distinctions between perturbation methods has not yet appeared. In anticipation of greater use for the perturbation methods based on both the distorted-wave and coupled-channel-wave representations, in the present study we will place emphasis on the analytic analysis of the distorted-wave and coupled-channel-wave transition amplitudes beyond and including the first Born approximations, DWBA and CCBA and make a comparative study of the two perturbation methods. In addition, a formal description of reactive resonance scattering will be presented. Some of the important observations obtained from the present study are summarized below.

For the absolute magnitude predictions of angular distributions and cross-sections, not only the conventional DWBA but variants such as the 'perturbed molecular DWBA' method should not be used for rearrangement collisions in which the contribution of intermediate inelastic channels is not negligible. Any claim that the perturbed molecular DWBA method accurately predicts absolute cross-sections is not soundly based, since this method cannot guarantee that it correctly accounts for the effects of coupling to the intermediate inelastic channels which correspond to the higher order Born terms.

The first Born term or CCBA transition amplitude in the coupled-channel-wave representation will yield accurate absolute cross-sections for rearrangement collisions in which coupling to intermediate arrangement channels is weak. Indeed, a recent

study^(4b) of H_3 reactive system based on a method^(4a) qualitatively similar to our CCBA method⁽⁶⁾ indicates the correctness of this claim.

The second Born term in the distorted-wave transition amplitude is shown to contain the effects of coupling to both the intermediate arrangement channels and inelastic channels. Thus it is possible that consideration of only the first and second Born terms in the distorted-wave representation is sufficient for reliable cross-sections in the reactions which involve either weak or strong coupling to intermediate arrangement channels, although they are less complete compared to the first two terms that appear in the coupled-channel-wave representation. Since the distorted wave calculations are much simpler, such consideration is highly desirable. However the coupled-channel-wave transition amplitude which includes up to the second Born term is expected to yield accurate results close to the quality of the exact close-coupling calculations in many elementary direct reaction processes.

Comparative studies of the distorted-wave and coupled-channel-wave perturbation methods will be of great value for detailed understanding of microphysical direct reaction mechanisms. For example, the difference between the CCBA and DWBA results will reveal the knowledge of the effects of coupling to inelastic channels before and after the reaction. Finally it is hoped that our present analytic study of the transition amplitudes in the two different waves representation will not only improve the discriminatory understanding of the two important perturbation methods but serve as a guide for their effective treatments.

REFERENCES

1. S.H. Suck Salk, Phys. Rev. A15, 1893 (1977).
2. S.H. Suck Salk, and R.W. Emmons, Phys. Rev. A24, 129 (1981).
3. S.H. Suck Salk, and C.K. Lutrus, J. Chem. Phys. submitted.
4. a) L.M. Hubbard, S.H. Shi, and W.H. Miller, J. Chem. Phys. 78, 2381 (1983);
b) G.C. Schatz, L.M. Hubbard, P.S. Dardi, and W.H. Miller, *ibid*, 81, 231 (1984).
5. G.C. Schatz, and A. Kuppermann, J. Chem. Phys. 65, 4668 (1976); *ibid*, 65, 4642 (1976).
6. S.H. Suck Salk, Phys. Rev. A27, 187 (1983).

A SEMICLASSICAL THEORY IN PHASE SPACE FOR MOLECULAR PROCESSES:
SCATTERING MATRIX AS A SPECIAL CASE OF DYNAMICAL CHARACTERISTIC FUNCTION

Kazuo Takatsuka and Hiroki Nakamura

Division of Theoretical Studies, Institute for Molecular Science, Okazaki 444, Japan

I. Introduction

Our primary aim in this study is to present a new phase-space semiclassical theory to describe chemically reactive scattering and intramolecular dynamics. One of the difficulties inherent to dealing with wave functions and propagators for chemical reactions is associated with their rapid oscillations. In case of a multidimensional problem, it is extremely difficult to extract the scattering (S-) matrix directly from such an oscillating wave function. Here we consider a time-dependent phase space function which gives directly the S-matrix at $t(\text{time}) = \infty$. This function, called a dynamical characteristic function (DCF), is regarded as a simple generalization of the S-matrix. The DCF extends also the concepts of phase space distribution function and of phase space path integrals,¹ being defined on twin phase spaces, with each of which a Hamiltonian is associated.

II. Theory

For two given wave functions $\phi_1(q, t) = \langle q | \exp[-iH_1 t/\hbar] | \phi_1(0) \rangle$ and $\phi_2(q, t) = \langle q | \exp[-iH_2 t/\hbar] | \phi_2(0) \rangle$,

where the Hamiltonians H_1 and H_2 may have different potential functions V_1 and V_2 , respectively, a DCF is defined as^{1,2}

$$a_{12}(\eta, \xi; \eta_0(t), \xi_0(t); t) = \int dq \phi_1(q + \eta_0(t), t) \phi_2^*(q + \eta, t) \exp[iq(\xi - \xi_0(t))/\hbar]. \quad (1)$$

The set of the independent variables (η, ξ) and the time-dependent variables $(\eta_0(t), \xi_0(t))$, the explicit functional forms of which will be determined later, constitutes two phase spaces. The DCF thus defined has a very interesting characteristic; if it happens that $\eta_0(t) = \eta$ and $\xi_0(t) = \xi$, then a_{12} equals the overlap integral between $\phi_1(q, t)$ and $\phi_2(q, t)$.

Here it should be noted that the S-matrix itself is also an overlap integral, viz.,

$$S_{i \rightarrow f} = \lim_{t \rightarrow \infty} \langle e^{-iH_f t/\hbar} | e^{-iH_i t/\hbar} | \phi_i \rangle, \quad (2)$$

where $H_f (= H_2)$ is the Hamiltonian for an exit channel and $H_i (= H_1)$ is the full scattering Hamiltonian. In Eq.(2), the origin of time is taken practically at the remote past. Thus the S-matrix, more rigorously the S-matrix in a wave packet representation, can be regarded as a special case of DCF.

Suppose that $\eta_0(t)$ and $\xi_0(t)$ satisfy classical equations of motion on the potential V_1 ,

$$\dot{\eta}_0(t) = \xi_0(t)/m, \quad \dot{\xi}_0(t) = -V_1'(\eta_0(t)), \quad (3)$$

where m is the mass.

Then we can show² that the semiclassical approximation to the equation of motion for the DCF is

$$\frac{D}{Dt} a_{12}(\eta, \xi; \eta_0(t), \xi_0(t); t) = \frac{i}{\hbar} [L_1(\eta, \xi) - L_2(\eta_0(t), \xi_0(t))] \times a_{12}(\eta, \xi; \eta_0(t), \xi_0(t); t) \quad (4)$$

where D/Dt indicates the classical Liouville operator, which in turn leads to classical equations of motion on the potential V_2 ,

$$\dot{\eta} = \xi/m, \quad \dot{\xi} = -V_2'(\eta). \quad (5)$$

$L_1(q, p)$ in Eq.(4) means the Lagrangian

$$L_1(q, p) = p^2/2m - V_1(q). \quad (6)$$

Equation (4) can be integrated exactly to give

$$a_{12}(\eta(t), \xi(t); \eta_0(t), \xi_0(t); t) = \exp\left[\frac{i}{\hbar} [S_1(\eta_0(t), \eta_0(0)) - S_2(\eta(t), \eta(0))]\right] \times a_{12}(\eta(0), \xi(0); \eta_0(0), \xi_0(0); 0) \quad (7)$$

where S_i 's ($i=1,2$) are the action integrals taken along the classical trajectories defined above. Thus the DCF is propagated as a path integral in the twin phase

spaces.

If a DCF is constructed from the rapidly oscillating wave functions of the form

$$\phi_i(q, t) = R_i \exp\left[\frac{i}{\hbar} S_i\right], \quad (8)$$

where S_i is an action integral and R_i is a slowly varying function of q , then the error due to the semiclassical approximation can be shown to be very small.² In fact, the magnitude of the error terms is expected to be smaller than that of the DCF itself by one order of \hbar .

The S-matrix of Eq.(2) can be expressed in terms of the semiclassical DCF thus constructed from the oscillatory wave functions. The time evolution of this DCF is actually made by running the two kinds of classical trajectories $(\eta_0(t), \xi_0(t))$ [Eq.(3)] and $(\eta(t), \xi(t))$ [Eq.(5)] which coincide with each other at $t=\infty$. The propagation of the wave functions is not necessary.

References

1. K. Takatsuka and H. Nakamura, J. Chem. Phys. **82**, March (1985).
2. K. Takatsuka and H. Nakamura, to be published.

COMPARISON BETWEEN APPROXIMATE (PERTURBATION) AND EXACT (CLOSE-COUPLED) THREE-DIMENSIONAL
QUANTAL CALCULATIONS, ORIENTATION OF TRANSFERRED ANGULAR MOMENTUM PROJECTION.

C. K. Lutrus, C. R. Klein, and S. H. Suck Salk

University of Missouri-Rolla, Missouri 65401 USA

Direct comparison between the single-step DWBA¹ and exact close-coupling calculations² is made by examining reactive scattering angular distribution of $H + H_2 \rightarrow H_2 + H$. We find that despite the fact of coupling strongly affects the absolute magnitude of cross sections,

- (1) the structures of the angular distributions remain agreeable with exact close-coupling results;
- (2) the difference between the DWBA predicted state-to-state integrated (total) cross section and the exact close-coupling results increases with collision energy;
- (3) the peak position of reaction probability and the range of impact parameters are two of the most important factors in shaping the angular distribution.

Comparison using the DWBA are made on the orientation of the transferred angular momentum projection for the direct reactions of $H + H_2 \rightarrow H_2 + H$ and $H + D_2 \rightarrow HD + D$. From the knowledge of favored transferred angular momentum and its projection, we find that the dominant geometric configuration is well understood. It is found that the cross sections exhibit dominance of the largest transferred angular momentum and of the projection quantum number of the transferred angular momentum $m = 0$. Details of, and differences between, the two reactions will be examined.

Reference

1. S. H. Suck Salk, Phys. Rev. A 15, 1893 (1977)
2. G. C. Schatz and A. Kuppermann, J. Chem. Phys. 65, 4668 (1976)

COUPLING SCHEMES AND DECOUPLING APPROXIMATIONS FOR INELASTIC AND REACTIVE COLLISIONS

V. Aquilanti, S. Cavalli and G. Grossi
Dipartimento di Chimica dell'Università, 06100 Perugia, Italy

The mapping of three-body interactions onto hyperspheres¹ allows to treat in a unified manner both inelastic and reactive collisions, and to develop a consistent framework for the interpretation of molecular beams experiments of increasing sophistication. Recent results along these lines include the elucidation of a number of relatively simple problems of restricted dimensionality (such as the collinear A + BC chemical reaction)² and model potentials (such as the physical pendulum and the Hénon-Heiles potential) of interest for the description of intramolecular mode transitions.³ These techniques are now being extended to treat problems of increasing complexity.

I. COUPLING SCHEMES

The usefulness of developing alternative coupling schemes in the treatment of atom-atom collisions has been demonstrated, in a number of previous investigations:⁴ they allow a physically motivated description of experimental effects and a framework for efficient decoupling approximations.

Their extension to atom-molecule interaction is made possible by the introduction of a discretization procedure, which is based upon the theory of representation for the higher rotation groups.⁵ The technique allows the close-coupling expansion over complete and orthonormal sets which have very convenient convergence properties, superior to the usual ones especially when the interactions are strong.

II. THE ROLE OF ROTATIONS IN MOLECULAR COLLISIONS

An analysis of alternative coupling schemes for atom-molecule collisions is presented, with particular reference being made to recent experimental results from our⁶ and other laboratories. The regions of validity of the various diabatic representations are assessed, an adiabatic approximation is introduced and the role of ridges in the potential for nonadiabatic effects is individuated: the analogy with similar effects in other contexts is stressed. In particular, the usefulness of the discrete angular representations⁵ is demonstrated.

III. DECOUPLING APPROXIMATIONS FOR ELEMENTARY CHEMICAL REACTIONS

The theory of elementary chemical reactions can be effectively formulated as a three-body collision problem in hyperspherical coordinates.¹ Although the problem restricted to collisions on a line is relatively easy to

be solved, and its investigation has provided interesting results on kinematic, resonance and interference effects² its extension to the full three-dimensional case is nontrivial.

Progress along this line include:

- i) a systematic characterization of properties of alternative coordinates;
- ii) the development of the coupling approximations by individuation of approximately conserved quantum numbers (see Ref. 7 for an example restricted to Coulomb three-body interactions);
- iii) the implementation of discrete angular representations⁵ in this context;
- iv) the assessment of relative merits of approximations of classical or semiclassical type.

REFERENCES

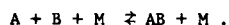
1. V. Aquilanti, G. Grossi and A. Laganà, *J. Chem. Phys.* **76**, 1587 (1982); *Chem. Phys. Letters* **93**, 174 (1982); G. Grossi, *J. Chem. Phys.* **81**, 3355 (1984).
2. V. Aquilanti, S. Cavalli and A. Laganà, *Chem. Phys. Letters* **93**, 179 (1982); V. Aquilanti, S. Cavalli, G. Grossi and A. Laganà, *J. Mol. Structure* **93**, 319 (1983); *ibid.* **107**, 95 (1984); *Hyperfine Interact.* **16**, 739 (1984).
3. V. Aquilanti, S. Cavalli and G. Grossi, in "Chaotic Behaviour in Quantum Systems", G. Casati ed., Plenum Press, N. Y. (1984); *Chem. Phys. Letters* **110**, 43 (1984); in "Fundamental Processes in Atomic Collision Physics", H. Kleinpoppen ed., Plenum Press, N. Y. (1985).
4. V. Aquilanti and G. Grossi, *J. Chem. Phys.* **73**, 1165 (1980); V. Aquilanti, P. Casavecchia, G. Grossi and A. Laganà, *J. Chem. Phys.* **73**, 1173 (1980); V. Aquilanti, G. Grossi and A. Laganà, *Nuovo Cim.* **63B**, 7 (1981); V. Aquilanti, G. Grossi and F. Pirani, in *Electronic and Atomic Collisions*, J. Eichler et al. eds., Elsevier (1984).
5. V. Aquilanti and G. Grossi, *Lettere al Nuovo Cim.*, in press.
6. P. Casavecchia, A. Laganà and G. G. Volpi, *Chem. Phys. Letters* **112**, 445 (1984).
7. V. Aquilanti, G. Grossi, A. Laganà, E. Pelikan and H. Klar, *Lettere al Nuovo Cim.* **41**, 541 (1984).

ASSOCIATION/DISSOCIATION IN DENSE GASES

M. R. Flannery

School of Physics, Georgia Institute of Technology, Atlanta, Georgia 30332, USA

A comprehensive theory¹ is developed for the time-dependent relaxation of some initial non-equilibrium distribution of (dissociated or molecular) subsystems AB towards eventual equilibrium with a gas M via the association/dissociation processes,



Various sets of Master Equations for the evolution of the two particle distribution function of subsystem (A-B) are derived in terms of the internal energy E , internal angular momentum L and internal separation R of AB via streaming and collisions with the heat bath M .

Expressions are obtained for the overall macroscopic rates $R^{A,D}(t)$ at time t of association (A) and of dissociation (D) in terms of collision kernels and of the net probability $p_i^{A,D}$ of collisional association (A) or dissociation (D) of molecules $AB(v_i)$ in bound vibrational levels v_i .

The theory naturally leads to derivation of a new Variational Principle which states that the probabilities $p_i^{A,D}$ are such that the macroscopic rates $R^{A,D}(t)$ at any time t are extrema. If the overall direction is association, then $R^A(t)$ is minimum and $R^D(t)$ is maximum and the time evolution towards equilibrium is hindered. This Principle permits an alternative procedure to direct solution of the Master Equations - a set of coupled integro-differential equations - by the direct search for extrema in the rates $R^{A,D}(t)$. These extrema are then the required rates for the process. Accurate trial solutions, based on weak-collision approximations, have in general been derived and these converge very rapidly onto the exact numerical results.

This Variational Principle is shown to be the full generalization of the so-called "bottleneck" method which seeks a minimum (located at the bottleneck) to the one-way equilibrium rate, useful in the absence of any knowledge of the above probabilities $p_i^{A,D}$.

This research is supported by AFOSR Grant No.

AFOSR-84-0233.

References

1. M. R. Flannery, Phys. Rev. (to be published).

THRESHOLD FRAGMENTATION OF THE THREE-BODY SYSTEMS:
THE CLASSICAL THEORY

N. Simonović and P. Grujić

Institute of Physics, P.O. Box 57, 11000 Belgrade, Yugoslavia

The theory previously developed to describe the near-threshold behaviour of the double-escape functions for the system with an ion, electrons and positrons in the final channel,^{1,2} has been generalized to the class of the inverse power law potentials, with arbitrary masses of the outgoing particles. This allows the dissociation cross section behaviour just above the breakup threshold to be estimated as function of the total energy. We consider the onedimensional final-state configuration of the process



where the lhs denotes an intermediate excited complex of three atoms, which may correspond to a number of initial channels. We apply the generalized Wannier classical theory to deduce the exponent in the threshold law

$$\sigma \sim E^{\kappa}, \quad E \ll E_{th} \quad (2)$$

where E_{th} is the threshold energy of the dissociation of the initial system, with the final-state interaction at large interatomic separations V . We shall

$$V = \sum_{i,j} C_{ij}^k R_{ij}^{-k}, \quad i,j = 1,2,3 \quad (3)$$

restrict ourselves to the plane case, with the total angular momentum $L=0$. Writing (see Fig.1) $\vec{a} \parallel \vec{R}$, $\vec{b} \perp \vec{R}$

$$\vec{R}_{12} = \vec{R} + \vec{a} + \vec{b}, \quad \vec{R}_{13} = \vec{R} + \vec{b} + \vec{a}, \quad \vec{R}_{23} = \vec{R} \quad (4)$$

one obtains from the Newton equations for the small relative deviations

$$\frac{\Delta}{R} = C_1 R^{\gamma-a\mu} + C_2 R^{\mu+a\mu} \quad (C_1 \text{ -arbitrary constants}) \quad (5)$$

$$\frac{\delta}{R} = C_3 R^{\mu-a\mu} + C_4 R^{\gamma+a\mu} \quad (6)$$

$$\gamma = \frac{k-2}{4}, \quad a = \frac{k+2}{4}, \quad \mu = \sqrt{1+4\lambda'}, \quad \nu = \sqrt{1+4\lambda''} \quad (7)$$

$$\lambda' = \frac{k(k+1)[m_1 m_2 + m_2 m_3 (1-\beta)] [C_{12} + C_{23} (1-\beta') / |1-\beta|^{k+2}]}{2(1+\frac{k}{2})^2 [m_1 m_2 + m_2 m_3 (1-\beta')] [C_{12} + C_{23} (1-\beta) / |1-\beta|^{k+2}]} \quad (8)$$

$$\lambda'' = - \frac{\lambda' (\beta' - \beta'')}{k+1} \quad (9)$$

The correlation parameters β are obtained in the standard way.² We make use of the scaling laws,

which in our case read

$$E \sim \theta^{-k} E, \quad \vec{R}_{ij}(t) \sim \theta \vec{R}_{ij}(\theta^{\frac{k}{2}+1} t) \quad (10)$$

with θ a real parameter. If we confine ourselves to the analytically tractable case: $B=C$ (symmetric conf.), we have: $\beta = -1$, $\beta' = \beta'' = 1$ and ν in the equation (7) appears imaginary for $k < 19$: $\nu = i\zeta$. Then the dissociation cross section behaves for $E \rightarrow 0$ as

$$\sigma \sim E^{\kappa}, \quad \kappa = (\gamma + a\mu)/k \quad (11)$$

We quote some of the results for the typical cases.

The Coulomb interaction: $k=1$

$$(i) m_1 \gg m_2 = m_3, \quad C_{12} = C_{13} = -Z \text{ au.}, \quad C_{23} = 1 \text{ au.}$$

$$\kappa (Z=1) = 1.127 \quad (\text{Wannier case})$$

$$(ii) H^+ + H \rightarrow 2H^+ + e^- : \quad \kappa = 69.74$$

These results have been obtained previously by Klar,³ by his WKB theory.

van der Waals interaction: $k=6$

$$(i) m_1 \gg m_2 = m_3 : \quad \kappa = 1 \quad (\text{Wigner case})$$

$$(ii) A \approx B : \quad \kappa = 1.526$$

Cases with $k=2,3$ shall be considered too

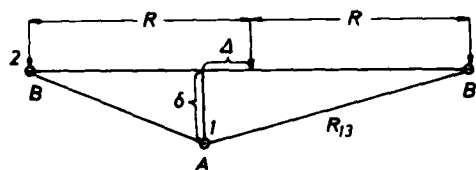


FIGURE 1. The final-state configuration.

This work has been supported by RZN of Serbia.

References

- ¹I. Vinkalns and M. Gaillitis, Latv. Acad. Sci. Rep. No 4 (Zinatne, Riga, 1967)
- ²P. Grujić, J. Phys. B15, 1913 (1982).
- ³H. Klar, Z. Phys. A, 307, 75 (1982)

SYMMETRY PROPERTIES OF 3-FERMION SYSTEMS WITH TWO IDENTICAL PARTICLES

Shen Hengyi, Birte Christensen-Dalsgaard and John Avery

Kemisk Laboratorium IV, H.C. Ørsted Institute
DK-2100 Copenhagen Ø, Denmark

In this paper, the hyperspherical coordinate method is used to study three-Fermion systems in which two particles are identical and the third different, extending earlier studies by Burden.¹ In H^- , the third particle is much heavier than the two identical particles, whereas in H_2^+ the opposite is true. However, from the standpoint of the intrinsic symmetry group of the Hamiltonian, H^- and H_2^+ are the same. We can therefore construct a correlation diagram representing a smooth transition from H^- to charge-reversed H_2^+ , with the mass-ratio as a variable parameter. The symmetry labels are preserved in this transition, although the energies depend strongly on the mass-ratio. Application of the hyperspherical coordinate method to this problem is of special interest, since it avoids both the independent-particle approximation and the Born-Oppenheimer approximation. As Herrick and Kellmann² have pointed out, correlation of the electronic wave function in an atom produces a molecule-like "structure". Thus the excited states of (for example) helium have features which are similar to the vibrational states of a linear triatomic molecule. Conversely, when a molecule has sufficient vibrational energy, the nuclear wave functions become delocalized and, as Longuet-Higgins has pointed out,³ the molecular point group is no longer appropriate for the analysis of the spectrum. The purpose of the present paper is to study which features of the eigenfunctions remain constant and which change in a transition from atom to molecule with the mass-ratio as a smoothly-varying parameter.

In the present work we use the coordinates

$$\vec{r}_+ \equiv \frac{1}{\sqrt{2}}(\vec{r}_1 + \vec{r}_2) \quad \text{and} \quad \vec{r}_- \equiv \frac{1}{\sqrt{2}}(\vec{r}_1 - \vec{r}_2)$$

as shown in the figure. After separation of the center of mass motion, we obtain the Hamiltonian

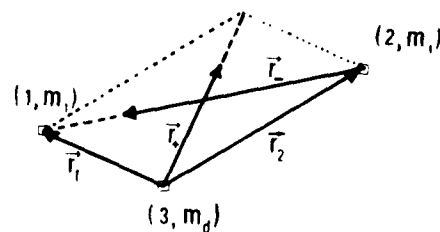
$$H = -\frac{1}{2}\left(\frac{1}{u} + \frac{1}{m_d}\right)\nabla_+^2 - \frac{1}{2}\left(\frac{1}{u} - \frac{1}{m_d}\right)\nabla_-^2 + V$$

where $u \equiv m_1 m_d / (m_1 + m_d)$, m_1 is the mass of the identical particles, and m_d is the mass of the different particle. This Hamiltonian clearly exhibits the limits H^- and H_2^+ . For H_2^+ , $u/m_d \gg 1$, so that the kinetic energy of relative motion of the two identical particles becomes small. In making a gradual transition from $u/m_d \gg 1$ to $u/m_d \approx 10^{-3}$, we gradually increase the importance of the relative motion of the two identical particles, which causes the approximate validity of the molecular point group to fail.

To make the actual calculations, we use hyperspherical coordinates with a hyperradius defined by $P^2 \equiv |\vec{r}_+|^2 + |\vec{r}_-|^2 = |\vec{r}_1|^2 + |\vec{r}_2|^2$. We use the adiabatic approximation, in which the Schrödinger equation is solved at fixed values of P to yield an effective potential for the radial motion.⁴

1. F.R. Burden, J. Phys. **11**, 1129 (1976)
2. M.E. Kellmann and F.R. Herrick, J. Phys. **81**, 1735 (1978)
3. H. Longuet-Higgins, J. Chem. Phys. **6**, 445 (1963)
4. J.H. Macek, J. Phys. **81**, 1001 (1965)

This work is supported by the Danish National Science Foundation (P. C.-D.) and by the Ministry of Education of the People's Republic of China (J.A.).



THREE PARTICLE BOUND STATES

Joseph Macek

Behlen Laboratory of Physics, University of Nebraska, Lincoln, NE
68588-0111 USA

Efimov¹ showed that three bosons, all interacting through short range forces of a strength such that two alone form a zero energy bound state, exhibit an energy spectra with an infinite number of bound states. This was demonstrated by separating the three particle Schrodinger equation for zero range potentials in hyperspherical coordinates (R, Ω) and showing that the hyper-radial equation incorporated an effective potential β/R^2 with $\beta = -5$. Since an infinite number of bound states exist when $\beta = -4.25$ it follows that there is an infinite number of three particle states bound in the effective hyper-radial potential. When non-zero range potentials of range b are present,

the effective hyper-radial potential $-5/R^2$ holds only asymptotically.

Extension of this result to obtain an effective potential valid, at least approximately, for all hyper-radii is accomplished by employing the hyperspherical adiabatic approximation². In this approximation the three particle wave function Ψ has the form,

$$\Psi(R, \Omega) = \phi(R; \Omega) F(R)$$

where $\phi(R; \Omega)$ is an adiabatic hyperspherical function. It is not necessary to obtain $\phi(R; \Omega)$ exactly, rather an upper bound to the effective potential is obtained by using a variational function for $\phi(R; \Omega)$. One then obtains an effective potential $\beta(R)/R^2$ for any type of potential at any R .

To test the reliability of this approximation with relatively simple trial functions,

$\beta(R)$ for three particles interacting through square well potentials was calculated for large R . The preliminary result of these calculations is $\beta(R) = -4.75 + O(1/R)$. Since $\beta = -4.75$ gives a more attractive potential than the critical value of $\beta = -4.25$, the approximate potential $\beta(R)/R^2$ supports an infinite number of bound states.

Support for this research by the National Science foundation under grant number PHY81-07147 is gratefully acknowledged.

References

1. V.N. Efimov, *Yad. Fiz.* **10**, 107 (1969).
[English Translation: *Soviet J. of Nuc. Phys.* **12**, 589 (1971).]
2. J. Macek, *J. Phys. B* **1**, 831 (1968).

"PSEUDO - MODEL" FOR Ba^+ ION : APPLICATION TO Ba^+X^+ MOLECULAR POTENTIALS WITH $X = \{H, Li, Na, K, Rb, Ba^+\}$

A. VALANCE*, A. BERNIER* AND H. BERGERON*

* LURE, Université de Paris-Sud, Bât. 209 C, 91405 ORSAY Cédex FRANCE

* Service de Physique des Atomes et des Surfaces, CEA, CEN, SACLAY FRANCE

Barium vapor is extensively studied both in laser experiments and in collision experiments.

Firstly, we determine a potential model for Ba^+ ion describing the active electron interaction with the Ba^{++} ion core.

Secondly, we calculate the adiabatic potential energies of $(BaH)^{++}$, $(BaLi)^{++}$, $(BaNa)^{++}$, $(BaK)^{++}$, $(BaRb)^{++}$ and Ba_2^{3+} molecular ions.

In the model determination of Ba^+ , the difficulty lies in the fact that the 5d excited state is located between the 6s ground state and the 6p excited state (see Table 1).

The main purpose of this abstract is to obtain the simplest description of Ba^+ while retaining a reasonable degree of accuracy.

Usually in this situation we have to choose between an "l" dependent pseudo-potential and a model-potential including core states. We propose, here, a "PSEUDO-MODEL POTENTIAL" which involves the association of an "l" independent pseudo-potential and a model-potential with reduced number of core states.

The $Ba^{++}-e$ interaction is represented by :

i) An Hellmann type potential

$$V = Z/r + A \exp(-2Kr)/r$$

with 2 adjustable parameters : A and K

ii) 3 hydrogenlike core-states (1s, 2s, 2p)

iii) 2 hydrogenlike pseudo-valence states (3p, 3d) reproducing exactly the ground and the first excited states (see Table 2).

iiii) A linear combination ($|3p\rangle + |4p\rangle$) of hydrogenlike pseudo-valence states to reproduce better than 2% the experimental 6p energy state. The results are reported in Table 2.

The "pseudo-model potential" parameters (A, K) and the exponential coefficient " $c_{n,l}$ " wave functions are obtained by a variational procedure so as to yield the observed values E_{6s} , E_{5d} and E_{6p} for the 6s, 5d and 6p states of the Ba^+ . To obtain the good experimental 6p energy, we need a linear combination ($1/\sqrt{2}(|3p\rangle + |4p\rangle)$) pseudo-states, when the separated contributions of these states are -0.3595 and -0.1711 a.u.

Finally the calculated Σ potential curves for the double ionized ion $(BaH)^{++}$ are plotted on figure.

For the ground Σ state $H(1s)Ba^{++}$ we predict a well depth of (1.46 eV at 5 a.u.).

We note the slow decreasing behaviour (1/R) for the $H^+Ba^+(n,l)$ type states.

We note also, for immediate R values, two well-depths of 0.1 eV at $R \approx 9.2$ a.u. and 0.25 eV at $R \approx 15$ a.u. for the Σ states correlated, for $R \rightarrow \infty$, to $H^+Ba^+(6s)$ and $H^+Ba^+(6p)$ states respectively.

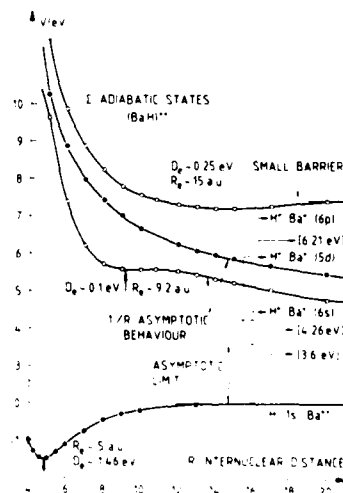
This work was partially supported by the Service de Physique des Atomes et Surfaces du C.E.N. SACLAY GIF sur YVETTE FRANCE.

Table 1 : Ba^+ spectroscopic energies (eV.)

State	6s	5d	6p	7s	6d	4f	8s
Energy (eV)	-10	-9.34	-7.39	-4.75	-4.3	-4.01	-2.8

Table 2 : $(Ba^{++}-e)$ interaction : $V = -2/r - 1.26 \exp(-0.3r)$

Experimental states	Pseudo-model states	Energies (a.u.)	
		Calculated	Experim.
4s	1s	-4.9519	Core State ?
5s	2s	-1.0289	Core State ?
5p	2p	-1.016	Core State ?
6s	3s	-0.3676	-0.3676
5d	3d	-0.3432	-0.3432
6p	$3p+4p$	-0.265	-0.2701
7s	4s	-0.1755	-0.1746
6d	4d	-0.1626	-0.1577
4f	4f	-0.1505	-0.1471
8s	5s	-0.1025	-0.1032
7p	5p	-0.1002	?
7d	5d	-0.0959	-0.0949



* Present address : Laboratoire de Physique Quantique Université Paul Sabatier, 118 rue de Narbonne, 31062 TOULOUSE Cédex

FINE-STRUCTURE EXCITATION IN ION-ION COLLISIONS

R. S. Walling*† and J. C. Weisheit*

*Physics Department, Lawrence Livermore National Laboratory, Livermore, CA 94550 USA

†Department of Applied Science, University of California at Davis, Livermore, CA 94550 USA

Proton impact collisions can be an important mechanism for inducing transitions among closely spaced energy levels in a plasma ion. This process was investigated by Seaton¹ for the case of a quadrupole transition in Fe^{+13} . Within the semi-classical approximation, Seaton calculated the excitation probability using a modification of first order perturbation theory.

We have used standard formulae for Coulomb excitation² to generalize the method of Seaton to provide a numerically fast calculation of ion-induced transitions in an arbitrary target ion. The transitions can correspond to dipole, quadrupole, or higher order multipolarity. The projectile ion can be multiply charged, but is assumed to be structureless. In this poster, we discuss how cross sections and thermal rate coefficients depend on certain important parameters, including the ionic charges of the target and projectile ions, the closeness of the level spacing, the ionic line strength for the analogous radiative transition, and the multipolarity of the transition.

For examples we chose target ions from the hydrogen-like, helium-like, and neon-like isoelectronic sequences. These ions allow us to examine the relative importance of ion-ion versus electron-ion collisional mixing of excited levels. The accuracy of the method is assessed by comparing our estimates of cross sections and rate coefficients with more elaborate calculations. Figure 1 displays thermal rate coefficients $\langle\sigma v\rangle$ we computed for the excitation of the $2p_{1/2} - 2s_{1/2}$ transition in Ar^{+17} , as induced by protons (1), He^{+2} ions (2), and Ar^{+18} ions (18) in a plasma of temperature T ; crosses represent the close coupling results of Zygelman and Dalgarno³, for the case of proton impact. The excitation energy is $\Delta E = 0.161$ eV.

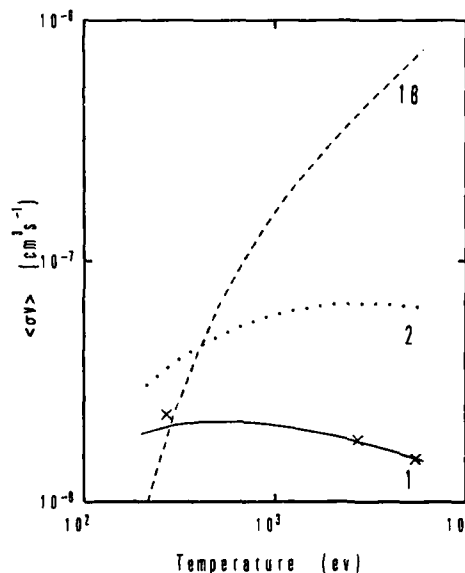


Fig. 1 $\text{Ar}^{+17}(2p_{1/2} + 2s_{1/2})$ excitation rate coefficient.

This work was performed under the auspices of the U. S. Department of Energy by the Lawrence Livermore National Laboratory under contract number W-7405-ENG-48.

References

1. M. J. Seaton, Mon. Not. R. Astron. Soc. **127**, 191 (1964).
2. L. C. Biedenharn and P. J. Brussard, Coulomb Excitation (Clarendon Press, Oxford, 1965), Ch. 2.
3. B. Zygelman and A. Dalgarno, private communication, 1985.

AB INITIO STUDIES OF SLOW $\text{Li}^+ - \text{Li}^+$ AND $\text{Na}^+ - \text{Na}^+$ COLLISIONSI.L. Cooper,* A.S. Dickinson,[†] and S.K. Sur[†]

* Department of Physical Chemistry, The University, Newcastle upon Tyne, NE1 7RU, U.K.

[†] School of Physics, The University, Newcastle upon Tyne, NE1 7RU, U.K.

Current interest in collisions between heavy, homonuclear ions originates from their importance in heavy-ion fusion studies.¹ The design of the storage rings for intense ion beams of GeV energies critically depends on the cross sections for charge-transfer collisions between the constituent ions of the beam. Singly ionised alkali atoms with their closed outer shells are the obvious choices. Whereas Cs^+ has attracted the most interest because of its ease of production, a series of measurements for Rb^+ , K^+ , Na^+ , and Li^+ also have been available² for some time, providing the scope for a systematic evolution of the theory from simple to increasingly complex systems. However, relatively few theoretical studies³ have been undertaken so far on these systems.

Slow collisions between atomic systems can be studied using the method of perturbed stationary states according to which electronic transitions are associated with the close approach of the potential energy curves of the quasi-molecule formed by the colliding species.

We have undertaken ab initio studies of some of the above identical alkali-ion systems. Potential curves for Li_2^{++} and Na_2^{++} have been obtained by configuration interaction (CI) calculations using the MROCI package.⁴ The molecular orbitals used as input to the CI calculations are obtained from self-consistent-field Hartree-Fock calculations with the GAMESS package.⁵

For Li_2^{++} , the CI excitation energies of the lowest four $1^1\Sigma_g^+$ and four $1^1\Pi_g$ states studied are within 0.5% of the spectroscopic values, while for Na_2^{++} , the difference is slightly less than 3%.

The potential curves for Li_2^{++} at small R shown in figure 1 are conveniently plotted relative to the ground $1^1\Sigma_g^+$ state. The basic excitation mechanism is the promotion of the $2p\sigma_g$ MO, as for the isoelectronic system He-He .⁶ This leads to a degeneracy of the $2^1\Sigma_g^+$ and $2^1\Pi_g$ molecular states at the ionic state $\text{Li}^{++}(1s^2 2p^2) [^3P^o \rightarrow ^1D^o]/[^3S]$. Here rotational coupling may cause the excitation of the $2p$ electrons. At intermediate internuclear distances, the pseudo-crossing between the $1^1\Sigma_g^+$ and $2^1\Sigma_g^+$ states at $R \approx 2.27 a_0$ arises from a crossing between the diabatic $2s\sigma_g$ and $2p\sigma_g$ MO's.

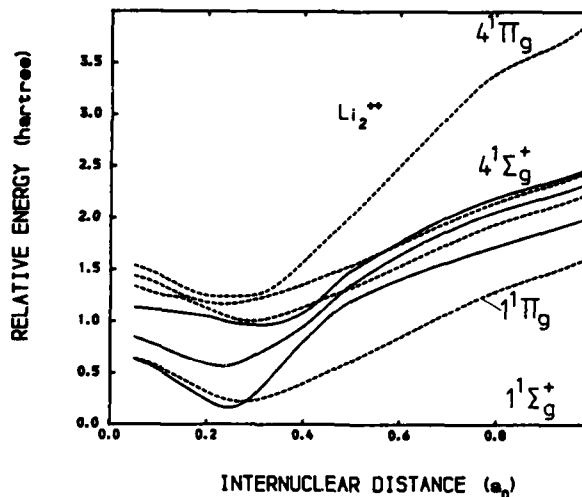


Figure 1.
Potential Curves for $\text{Li}_2^{++} - 1^1\Sigma_g^+$ states, ... $1^1\Pi_g$ states

For Na_2^{++} , the molecular states at large and small values of R qualitatively show behaviour similar to those of Li_2^{++} . The basic excitation mechanism, however proceeds through a promotion of the $4f\sigma_g$ MO, as for the iso-electronic system Ne-Ne .⁷

Further clarification of the excitation and charge-transfer processes can be obtained from a knowledge of the various radial and rotational couplings. Calculations for these are now in progress and will be reported at the symposium.

This work is supported by a grant from the Science and Engineering Research Council.

References

1. K. Seldner, *Ann. Phys. (New York)*, **11**, 11 (1961).
2. G. Beatty, *Phys. Rev. Lett.*, **11**, 11 (1961).
3. A.Y. Ermakov, *Sov. Phys. Usp.*, **11**, 11 (1961).
4. A.J. Cohen, *Adv. Phys.*, **11**, 11 (1961).
5. M.J. Frisch, *J. Chem. Phys.*, **11**, 11 (1961).
6. G. Beatty, *Phys. Rev. Lett.*, **11**, 11 (1961).
7. G. Beatty, *Phys. Rev. Lett.*, **11**, 11 (1961).

CHARGE TRANSFER AND IONISATION IN COLLISIONS OF PROTONS WITH Al^+ , Ga^+ , In^+ AND Tl^+ IONS

K F Dunn, M F Watts, G C Angel and H B Gilbody

Department of Pure and Applied Physics, The Queen's University of Belfast,
Belfast, United Kingdom

In previous work in this laboratory (see review¹) we have studied charge transfer and ionisation in collisions between positive ions at keV energies by the use of an intersecting beam technique.

In the present work, we have measured cross sections $\sigma(\text{X}^{2+})$ for X^{2+} production from the combined processes of charge transfer (with cross section σ_c)



and ionisation (with cross section σ_i)

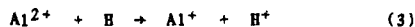


for the target ions Al^+ , Ga^+ , In^+ and Tl^+ .

An understanding of reactions of this type is relevant to particle loss and plasma cooling in Tokamak devices through collisions with impurities. A knowledge of such cross sections is also required for plasma diagnostics using heavy ion beam probes. The present study with ions of the Group III B elements has been designed to explore the extent to which measured cross sections relate to other relevant data and to simple scaling relations.

Measurements have been carried out at c.m. energies within the range 60–580 keV. In each case, the target ions were produced from a thermionic source thereby ensuring that only ground state species were present.

At the lower impact energies, charge transfer process (1) is expected to provide the main contribution to our measured values of $\sigma(\text{X}^{2+})$. Comparison is made with theoretical values² for H^+-Tl^+ and, in the case of H^+-Al^+ collisions with cross sections³ for the inverse charge transfer process



assuming that initial and product excited states are not greatly different. Direct measurements of σ_c are also being carried out by counting the X^{2+} products in coincidence with the H atoms formed from (1) in the same events.

At the higher energies, where ionisation provides the main contribution, our measured cross sections for Al^+ , Ga^+ and Tl^+ are compared with previously measured cross sections^{4,5,6} for ionisation by equivalent

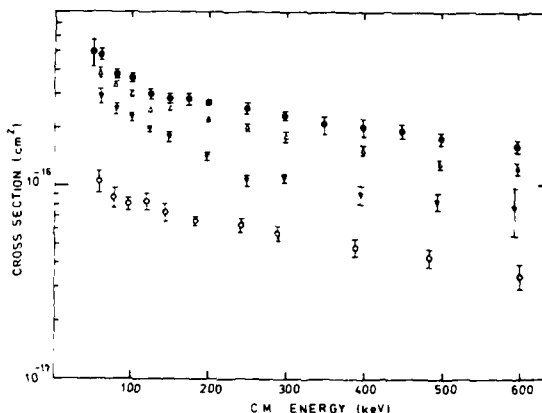


Figure 1 : Cross section $\sigma(\text{X}^{2+})$ for X^{2+} formation in $\text{H}^+ + \text{X}^+$ collisions.

● Tl Δ In ▽ Ga ○ Al

electrons. A simple classical scaling relation⁷ has previously been successfully applied to ionisation of light ions by H^+ impact. A modification of this relationship to take account of inner shell contributions yields a universal scaling law of the form

$$\sigma_i = R^2 Z_p^2 \sum_{i=1}^N n_i / u_i^2$$

where R is the Rydberg constant, Z_p is the projectile charge, u_i is the ionisation energy of the electrons in the i th subshell and n_i is the number of such electrons. This simple expression is shown to give reasonable agreement, to within a factor of 2 with our experimental values of $\sigma(\text{X}^{2+})$.

References

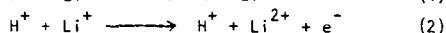
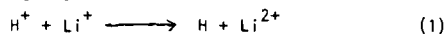
1. H B Gilbody, *Physics of Electronic and Atomic Collisions* (S Datz, Editor). N Holland, 223 (1982).
2. R A Mapleton, M F Schneeburger and C A Steele. USAF report AF-CRL-TR-75-0053 (1975).
3. M A Lennon, PhD thesis, Queen's University of Belfast (1983).
4. R G Montague and M F A Harrison, *J Phys B* **16** 3045 (1983).
5. W T Rodgers, G Stefani, R Carnillon, G H Dunn, A Z Msezane and R J W Henry, *Phys Rev* **A25** 737 (1982).
6. T F Devine, R K Feeney, W E Sayle and J W Hooper, *Phys Rev* **A13** 54 (1976).
7. P A Neill, G C Angel, K F Dunn and H B Gilbody, *J Phys B* **16** 2185 (1983).

IONIZATION AND CHARGE TRANSFER TOTAL CROSS SECTIONS FOR $H^+ + Li^+$ COLLISIONS

C.O. Reinhold and C.A. Falcón

Instituto de Astronomía y Física del Espacio, C.C.:67, Suc.:28, 1428 Buenos Aires, Argentina

Classical Trajectory Monte Carlo (CTMC) calculations have been performed to determine total cross sections for the reactions:



The calculations were carried out between 82 and 350 KeV. (CM) where experimental results¹ for charge exchange and Li^{2+} production are available. The collision dynamics is solved by numerical integration of Hamilton's classical equations of a three-particle system composed of a proton, a Li^{2+} core and one active electron. The cross sections for the processes (1) and (2) are obtained by statistical methods after having analysed the reaction products of a large number of trajectories with randomly chosen initial conditions. In addition, the independent electron model is assumed to hold. The CTMC method, originally proposed by Abrines and Percival², is well adapted to calculate charge exchange and ionization processes for colliding systems where the three particles, explicitly considered, are subject to Coulomb interactions between them. The case of more general systems have been treated in almost all the calculations up to now replacing the real interactions by Coulomb interactions with appropriate effective charges^{3,4,5}. The use of general potentials present no problem for the integration of Hamilton's equations. However, in this case, the variables proposed by Abrines and Percival² to generate the initial electronic conditions using the microcanonical ensemble are not uniformly distributed. McDowell and co-workers⁶ have used model potential interactions to study electron capture and ionization in collisions of He^+ with H and He^+ targets and their inverse capture reactions. In the conference we shall outline an alternative method that we have developed for the generation of the initial electronic conditions in the case of non-coulomb interactions. In this method, five uniformly distributed variables are obtained that enable to determine the initial electronic state. The method is valid for general potentials and is of easier numerical implementation than the method of Abrines and Percival in the sense that Kepler's equation for the electronic orbit need not to be integrated. We have used this method to calculate the total cross sections for reactions (1) and (2). The electron single capture cross section is plotted in figure 1a. In figure 1b it is shown the total cross section for Li^{2+} production obtained by addition of single capture and single ionization cross sections. In the same figures we also show standard CTMC

calculations by Olson as reproduced in the article of Sewell et al.¹. The agreement of our theoretical results is most encouraging.

References

1. E.C. Sewell, G.C. Angel, K.F. Dunn and H.B. Gilbody 1980, J. Phys. B **13** 2269.
2. R. Abrines and I.C. Percival 1966, Proc. Roy. Soc. **88** 861.
3. R.E. Olson and A. Salop 1977, Phys. Rev. A **16** 531.
4. R.E. Olson 1978, Phys. Rev. A **6** 2464.
5. R.E. Olson 1982, J. Phys. B **15** 1163.
6. M.R.C. McDowell, G. Peach and S.L. Willis, Electronic and Atomic Collisions, XIII ICPEAC Abstracts of Contributed Papers 512, Berlin 1983.

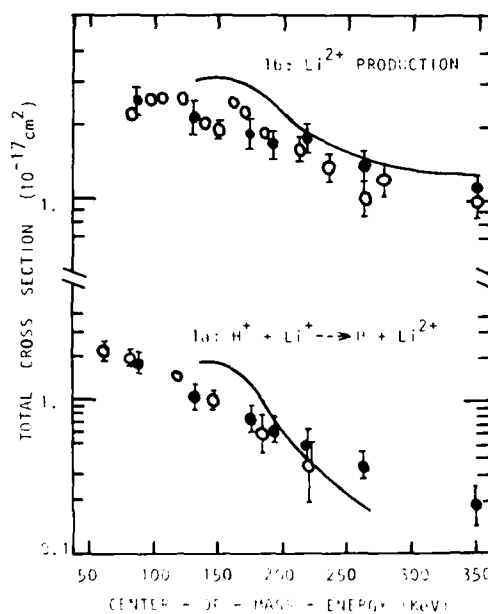


FIG.1: ♦ : Present Theoretical results
 ○ : Experimental results by Sewell et al.¹
 — : Classical calculations by Olson (as reported by Sewell et al.).

ELECTRON TRANSFER IN COLLISIONS BETWEEN PROTONS AND Li^{++} IONS

Thomas G. Winter

Department of Physics, Pennsylvania State University
Wilkes-Barre Campus, Lehman, Pennsylvania 18627

With the exception of He^+ , very little theoretical work^{1,2} and no experimental work appears to have been done on electron transfer in collisions between protons and hydrogenic ions (He^+ , Li^{++} , ...) at intermediate energies. Such processes are the simplest examples of non-resonant electron transfer.

As has already been shown for the case of He^+ ions,³⁻⁵ continuum intermediate states are very important to bridge the gap(s) between the tightly bound initial state and one or more relatively weakly bound states centered on the proton. These continuum states are mostly "centered on" He^+ , Li^{++} , They would be expected to become more and more important, the more non-resonant the collision. At the same time, the cross section for electron transfer would be expected to become very small as the nuclear charge of the hydrogenic ion is increased. At keV proton energies, the initial and final states would be expected to be strongly coupled to the intermediate states, as is the case for He^+ .³⁻⁵ A coupled-state approach using a pseudostate basis such as a (systematic) Sturmian basis^{6,7,3} is therefore appropriate, as applied by the author to He^+ targets³; other pseudostate methods have also been applied by others.^{4,5}

To explore trends in collisions of this type, the next more highly charged hydrogenic ion, Li^{++} , is being considered here. A preliminary result has been obtained for the electron transfer probability at one

impact parameter and energy--a proton energy of 17.5 keV relative to Li^{++} (corresponding to a relative velocity of 0.837 a.u.). The result is orders of magnitude below that for He^+ ions at the same energy and impact parameter. (Of course, the energy- and impact-parameter dependence are expected to be different for the two cases.) In spite of this very large reduction on changing the ion, the results still appear to be stable: For example, no state tested beyond the 26 basis states finally included (most of which are centered on the Li nucleus) contributes more than 2% to the total capture probability; the Sturmian basis is not very much larger than that used by the author for He^+ ions.³ A more complete study is now being carried out: convergence with respect to the size of the basis is being studied at several energies and impact parameters, and cross sections obtained by integrating the probabilities over impact parameter will be reported at several energies.

References

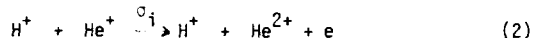
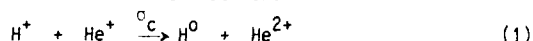
1. B. H. Bransden and C. J. Noble, J. Phys. B 15, 451 (1982).
2. A. L. Ford, J. F. Reading, and R. L. Becker, J. Phys. B 15, 3257 (1984).
3. T. G. Winter, Phys. Rev. A 25, 697 (1982).
4. W. Fritsch and C. D. Lin, J. Phys. B 15, 1253 (1982).
5. B. H. Bransden, C. J. Noble, and J. Chandler, J. Phys. B 16, 4191 (1983).
6. D. F. Gallaher and L. Wilets, Phys. Rev. 169, 139 (1968).
7. R. Shakeshaft, Phys. Rev. A 14, 1626 (1976).

CROSS SECTIONS FOR ELECTRON CAPTURE AND IONIZATION IN $H^+ + He^+$ COLLISIONS*

K.Rinn, F.Melchert, K.Rink and E.Salzborn

Institut für Kernphysik, Universität Giessen, D-6300 Giessen, West Germany

A crossed-beams experiment has been set up for the measurement of cross sections for electron capture, σ_c , and ionization, σ_i , in ion-ion collisions. First results were obtained for the reactions



in the center of mass energy range $8 \text{ keV} \leq E_{cm} \leq 100 \text{ keV}$.

Two well collimated and momentum analyzed beams (H^+ : 10-150 keV, He^+ : 5-15 keV) are arranged to intersect in an ultra high vacuum chamber. The collision products formed in both beams are separated by electrostatic analyzers from the parent ion beams and detected by single particle detectors. The overlap of the two beams is measured by a scanning slit which is moved perpendicularly across the interaction region.

Although the experimental approach, in principle, appears to be straightforward, inherent difficulties result from the low ion densities obtainable in the two intersecting ion beams. Since the residual gas density, even at pressures of $1 \cdot 10^{-10}$ mbar, exceeds the ion beam densities by orders of magnitude a low signal rate (\sim Hz) has to be detected in the presence of a large background rate (\sim kHz) of reaction products originating from ion collisions with residual gas particles.

A coincidence technique was employed to separate signal from background events in measuring the cross section σ_c for electron capture. The cross section σ_i for ionization is obtained from the difference $\sigma_i = \sigma_{2+} - \sigma_c$ with σ_{2+} being the cross section for the total He^{2+} ion production (sum of reactions (1) and (2)). In measuring σ_{2+} a beam pulsing technique was employed to discriminate signal from background events.

Careful tests were performed to ensure the proper function of the apparatus. Difficult but very important is a unity transmission probability through the analyzers even for particles scattered in the reaction observed. The analyzers were designed carefully to reach maximum angular acceptance. Small variations of the analyzer voltages did not change the reaction rate measured, indicating the detection of all products. Cross sections for every single center of mass energy were determined with different energy combinations of the beams in the laboratory frame. No dependence on the laboratory energies was observed.

Fig. 1 shows a coincidence spectrum of the collision products H^0 and He^{2+} of the electron capture reaction (1).

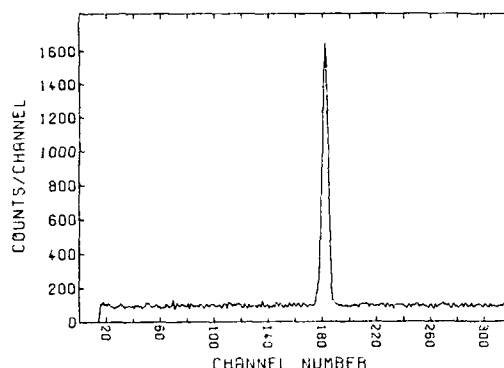


Fig. 1: $H^0 + He^{2+}$ coincidence spectrum of 66 keV H^+ ions colliding with 10 keV He^+ ions. Rate of true coincidences: 15 s^{-1} .

Fig. 2 shows a spectrum measured for the total He^{2+} production with pulsed beams.

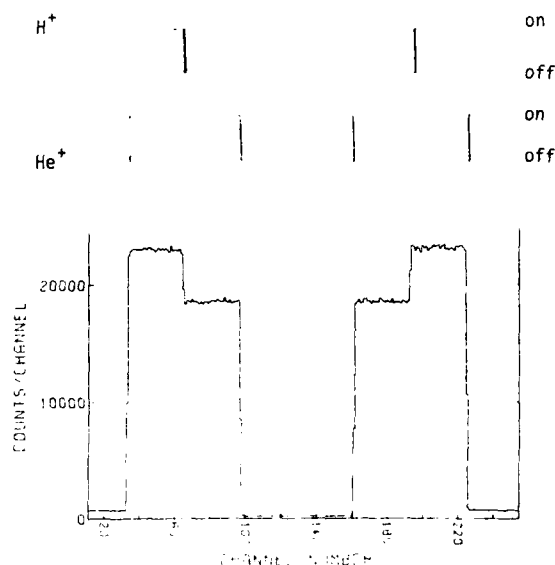


Fig. 2: Total He^{2+} production employing pulsed beams.

* Work supported by BMFT

THEORETICAL STUDIES OF MUTUAL NEUTRALIZATION IN $P + H^-$ COLLISIONS
USING MODEL POTENTIALS.

A.M.Ermolaev

Department of Physics, University of Durham, South Road, Durham DH1 3LE, England.

Earlier impact-parameter close-coupling calculations of charge transfer in collisions between positive ions and atoms at intermediate energies ⁽¹⁾ have been extended to study the mutual neutralization reaction



in the energy region 0.4-50.0 keV lab. In the one-active electron approximation for (1), the total wavefunction $\Psi(r,t)$ is expanded in terms of a two-centred AO (pseudo) state basis with PWETFs, and interaction between the active electron and the H^- core is described by a fast falling-off potential U_{eff} supporting a bound state with the experimental binding energy of the ion. Cross sections $\sigma(n\ell m)$ for capture into $H(n\ell m)$, $n \leq 3$, have been obtained using expansions with up to 19 states centred on the projectile and up to four target states ($1s, 2s, 2p$). This model suggested ⁽²⁾ as an AO alternative to the MO model introduced by Sidis et al. ⁽³⁾ gave a dipole polarizability of $175 a_0^3$.

Fig.1 and 2 present total neutralization cross sections σ_{tot} computed using expansions of different length and several model potentials of Yukawa and exponential types. The polarization term has been dropped from U_{eff} because of relatively high impact velocities in question. At the maximum ($E \approx 0.6$ keV lab), σ_{tot} is affected by a particular choice of the expansion as well as that of U_{eff} whereas for higher E , the cross sections tend to a limit which is virtually independent of the choice of U_{eff} . A marked difference (by a factor of two) between the present σ_{tot} and data in ⁽³⁾ at $E \approx 3$ keV lab is probably due to the lack of proper PWETFs in the expansions ⁽³⁾.

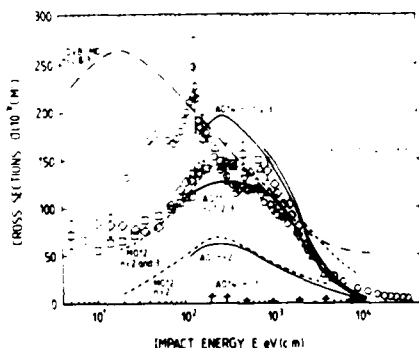


Fig.1. Cross sections for reaction (1). Theoretical data: DVB - Dalgarno (1970); MO - Sidis (1983); AO(N) - present (in order N) using a Yukawa potential. Experimental data: ∇, Δ, \circ - Rundel (1969), Gaily (1970), Moseley (1970), Peart (1976); \square, \diamond - Szucs (1984).

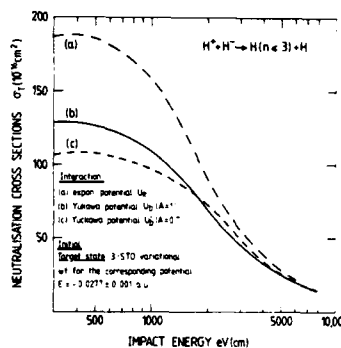


Fig.2. Theoretical total cross sections for reaction (1) computed using several model potentials U_{eff} . AO expansions with ten bound projectile-centred states ($n \leq 3$) and a single target state $|1s\rangle$.

For a non-singular exponential potential $U_{eff}(r) = A \exp(-\gamma r)$, the exact solution of the one-particle Schrödinger equation is expressible in terms of a Bessel function and this model is particularly convenient for ascertaining the relative importance of various features of the AO method as well as for discussing some numerical problems. It appears from the results obtained by now that an adequate representation of the low-energy continuum in the AO basis is, perhaps, more important, in a certain sense, than further refinements, particularly at large r , of the model ground state $|1s\rangle$. Simple STO sets (that is without the Hulthen-type orbitals used often in accurate variational calculations of the negative hydrogen ion) seem to be sufficient to produce good estimates of cross sections for reaction (1). These conclusions may also lead to some practical implications for a two-active electron theory for (1) and for the correlation account in this reaction.

References.

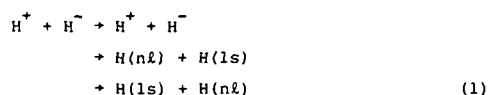
1. A.M.Ermolaev, J. of Phys. B, **17**, 1069 (1984), A.M.Ermolaev and B.H.Brandsden, *ibid.*, **17**, 1083 (1984).
2. A.M.Ermolaev, J. of Phys. B, to be published.
3. V.Sidis, C.Kubach, and D.Fussen, Phys.Rev. **A27**, 2431 (1983).

MUTUAL NEUTRALIZATION IN $H^+ + H^-$ COLLISIONS

R. Shingal and B.H. Bransden

Department of Physics, University of Durham, South Road, Durham DH1 3LE, U.K.

The understanding of neutralization and double charge exchange in collisions of protons with negative hydrogen ions is still an outstanding problem. In two recent papers^{1,2} we have considered a two electron model for the reaction



The total and partial charge exchange cross-sections were calculated using a multi-state impact parameter model³. Two centred travelling atomic orbitals were used to expand the wave function of the system. In this expansion, apart from the exact $n = 1-3$ hydrogenic states, we also considered several pseudo-states.

However, in these calculations we used a simple Chandrasekhar⁴ wave function to represent H^- . We also considered a variant of this function in which one of the exponent was determined using the experimental ionization energy of H^- . Further, in the appropriate time dependent phase factors, the eigenenergy of H^- was replaced by the experimental energy.

In the present work we have removed these uncertainties in the earlier results. We have constructed an improved CI wave function for H^- . This wave function is used to calculate the total and partial neutralization for reaction 1. The computations are in progress and the results will be reported at the time of the Conference.

References

1. R. Shingal, B.H. Bransden and D.R. Flower, J. Phys. B (1985) (in press).
2. R. Shingal, B.H. Bransden and D.R. Flower, 2nd ECAMP, Amsterdam (1985).
3. B.H. Bransden, 'Atomic Collision Theory', 2nd Edn. (Benjamin Cummings, N.Y.) (1983).
4. S. Chandrasekhar, Astrophys. J. 100, 176 (1944).

CHARGE EXCHANGE BETWEEN He^{++} AND H^- AT LOW ENERGIES

M. Terao*, C. Harel* and A. Salin*

*Laboratoire de Physique Atomique et Moléculaire, Université Catholique de Louvain-la-Neuve, Chemin du Cyclotron, 2 1348 Louvain-la-Neuve, Belgique

*Laboratoire des Collisions Atomiques, Université de Bordeaux I, rue Lamartine, 40 - 33400 Talence, France

By contrast with the $\text{H}^+ - \text{H}^-$ system which has been studied extensively both theoretically and experimentally, very few is known on the collision of He^{++} and H^- ions. As can be verified from a schematic correlation diagram, the latter system is very similar to a collision between a multicharged ion and an atom because of the very small binding energy of H^- :

- single electron capture may be expected to occur into a highly excited state.
- double electron capture may lead to the formation of autoionizing states.

We present here a theoretical study of charge exchange in $\text{He}^{2+} - \text{H}^-$ collisions. An experimental study has been done simultaneously in Louvain (see contribution of M. Terao, M. Cherkani and S. Szücs).

At low barycentric energies where the experiments have been done (1-2000 eV), the molecular description seems to be the most appropriate. The wave function of the system was expanded on a basis built with screened OEDM orbitals - a method which has already been successfully tested on various reactions¹. The screened OEDM orbitals are defined from the essential requirement that the basis correctly describes the H^- ion. It is well known that because of the small nuclear charge, the electronic correlations in H^- are very strong and the screening of the proton by one of the electrons is important in the s-wave. The simplest wave function for H^{-2} is of the form

$$\Psi(r_1, r_2) = \frac{N}{\sqrt{2}} \left[\phi_{1s}^Z(r_1) \phi_{1s}^{Z'}(r_2) + \phi_{1s}^{Z'}(r_1) \phi_{1s}^Z(r_2) \right] \\ \left[\alpha(1)\beta(2) - \beta(1)\alpha(2) \right]$$

where ϕ_{1s}^Z is the 1s hydrogenic wave function with nuclear charge $Z = 1.039$ and $Z' = 0.283$.

For the molecular description of $\text{He}^{++} - \text{H}^-$, we used the OEDM orbitals that correlate with the atomic orbitals of H^- in presence of the electric field of He^{++} , i.e. with the $(2p\sigma)$ and $(8k\sigma)'$ orbitals (actually we use a diabatic orbital crossing the $(7j\sigma)'$ and $(6i\sigma)'$ orbitals). For a good description of H^- , angular correlations must be taken into account². This was achieved by including the $(2p_0^{Z''}) (2p_0^{Z''})$, $(2p_+^{Z''}) (2p_-^{Z''})$ and $(2p_+^{Z''}) (2p_+^{Z''})$ configurations. A variational calculation gives $Z'' = 1.95$ and a binding energy for H^- of 0.5233 a.u.. The molecular configurations are shown in table 1.

Table 1 - Definition of the configuration describing the initial channel

Atomic orbitals	Molecular orbitals	Configurations	
1s ($Z = 1.039$)	$2p\sigma(Z_A=2, Z_B=1.039)$	$(2p\sigma)(6i\sigma)'$	radial correlation
1s ($Z' = 0.283$)	$(6i\sigma)'(Z_A=2, Z_B=0.283)$		
$2p_0(Z'' = 1.95)$	$(3p\sigma)''$	$(3p\sigma)''^2$	angular correlation
	$(4f\sigma)''(Z_A=2, Z_B=1.95)$	$(4f\sigma)''^2$	
$2p_{\pm}(Z'' = 1.95)$	$(3d\pi_{\pm})''$	$(3d\pi_{\pm})''$	

The asymptotic energy curve of the ionic channel crosses those of the exchange channels $\text{He}^+(n=3,4,5) + \text{H}(1s)$ at respectively 10, 20 and 35 a_0 . On each of these exchange channels, we selected the Σ state and the Π state in which the OEDM orbitals are the most strongly coupled with the entrance channel, i.e. $(2p\sigma)(5g\sigma, \pi)'$, $(2p\sigma)(4f\sigma, \pi)'$ and $(2p\sigma)(3d\sigma, \pi)'$ configurations.

The potential curves and the couplings were obtained by configuration interaction and the coupled equations integrated by means of standard programs. Rectilinear trajectories have been used so far. Coulomb effects - most important below 10 eV - are being considered. The problem of electronic momentum transfer was solved by use of the Errea's "common translation factor"⁴.

The final results will be presented at the conference, but it is already established that the cross section of single transfer is very large (about $5 \cdot 10^{-14} \text{ cm}^2$) and that the dominant contributions are in the $n=5$ and $n=4$ channels. There are no published theoretical results available for comparison. Preliminary data on a calculation by Ermolaev (private communication) differ from our values.

References

1. C. Harel and A. Salin, J. Phys. B., **16**, 55 (1983); S. Bliman, D. Hitz, B. Jacquot, C. Harel and A. Salin, J. Phys. B., **16**, 2849 (1983); L.F. Errea, L. Méndez, A. Riera, M. Yáñez, J. Hanssen, C. Harel and A. Salin, Journal de Physique, in press (1985)
2. S. Chandrasekhar, Ap. J., **100**, 176 (1944)
3. F. Borondo, A. Macías and A. Riera, Chem. Phys., **81**, 303 (1983)
4. L.F. Errea, L. Méndez and A. Riera, J. Phys. B., **15**, 101 (1982)

ONE ELECTRON TRANSFER IN $\text{He}^{++} - \text{H}^-$ COLLISIONS INTO EXCITED STATES OF He^+

M. Terao, M. Cherkani, S. Szücs and F. Brouillard

Université Catholique de Louvain, Institut de Physique, Chemin du cyclotron, 2
B1348 Louvain-la-Neuve - BELGIUM

The cross section for the electron transfer reaction $\text{He}^{++} + \text{H}^- \rightarrow \text{He}^+ + \text{H}$ was measured in the CM energy range between 1 and 2200 eV, with merged beams and coincident product detection (1). The initial kinetic energies of He^{++} and H^- are respectively 20 keV and 10 keV. The two beams are merged over a distance of about 7.5 cm. The precise length of interaction is determined by the voltage V applied on the collision cell. The H atoms are detected some 130 cm ahead by channelplates with a large solid angle (25×25 [millirad] 2). The He^+ ions are momentum analysed in a magnetic field and counted by an EMI electron multiplier about 180 cm ahead. The multichannel analysis of the time lags between pulses from both detectors yields the electron transfer rate above a uniform background due to the uncorrelated signals from reactions with the residual gas.

The results are shown in Fig. 1. Most of them were obtained with isotopic $^3\text{He}^{++}$ instead of $^4\text{He}^{++}$ in order to avoid contamination by H_2^+ . As a check of consistency, some measurements were performed with the H^- slower or faster than the He^{++} ions, and thus with very different kinematics.

It is well known that the reaction energies of monoenergetic ion beams can be determined by high precision time-of-flight technics (2). In this sense, merged beams are particularly sensitive to the reaction exothermicity, due to the amplification of the CM energy in the laboratory system.

Table 1 shows the time lags versus the observation voltage V around the critical value of -2000 volts ** , where the sign of the relative velocity is reversed.

Calculations were performed by assuming that
i) the ions move on unscreened Coulomb trajectories;
ii) the transitions occur at the curve crossings;
iii) the deflection is given by the half of Rutherford angle.

The observed shift around 0 eV reveals that transitions to the He^+ ($n=6$) state occur.

Theoretical cross sections for this reaction are presented at this conference by M. Terao, Ch. Parel and A. Salin.

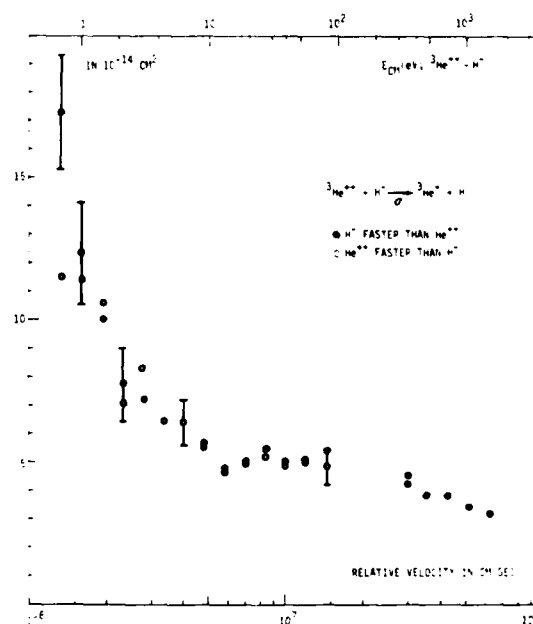


Fig. 1

Table 1. Shift of the time lags between V and V' (n sec)

V	V'	calculated for			observed
		n=5	n=6	n=7	
- 1900	- 2100	44	35	30	34
- 1800	- 2200	61.5	52.5	47.5	51.5
- 1700	- 2300	77	70.5	66	69.5
- 1600	- 2400	94.5	89.0	86	88.0

** If the observation potential is V volts, the collision energy is given by :

$$E(\text{eV}) = u \left[\sqrt{(20.000 - q_1 V) / m_1} - \sqrt{(10.000 - q_2 V) / m_2} \right]^2$$

where (q_1, m_1) , (q_2, m_2) are the charges and masses of the He^{++} and H^- respectively.

References

- (1) S. Szücs, M. Karemera, M. Terao and F. Brouillard, J. Phys. B, **17**, 1613 (1984).
- (2) R. Rundel, K.L. Aithen and M.F.A. Harrison, J. Phys. B, **2**, 954, (1969).

ORIENTATION EFFECTS IN THERMAL COLLISIONS BETWEEN
RYDBERG ATOMS IN CIRCULAR STATES AND GROUND STATE HELIUM

E. de PRUNELE

Service de Physique des Atomes et des Surfaces, CEN/SACLAY
91191 Gif-sur-Yvette Cedex, France

INTRODUCTION

A state to state collision between a Rydberg Atom A and a ground state neutral atom B, with relative momentum q , can be written as :

$$A(i) + B, (q) \rightarrow A(i') + B, (q') \quad (1)$$

The initial state $|i\rangle$ of A is assumed to be an eigenstate of the atomic angular momentum relative to some axis z, i.e :

$$L_z |i\rangle = m |i\rangle \quad (2)$$

The present work studies the influence of the angle α between \vec{q} and the axis z on the magnitude of the cross sections for process (1), within the framework of the impulse approximation [1, 2]. This approximation was found [2] to be most valid when the eccentricity $[1 - (\ell+1)/n^2]^{1/2}$ of the state $|i\rangle$ is small. The "circular" Rydberg states, which are highly anisotropic, are therefore particularly suitable for a study of the orientation effects according to the impulse approximation.

RESULTS

A general formulation of the problem allows computation of the cross sections for process (1), for arbitrary values of the angle α , (beam experiments), as well as a direct computation of the angle averaged cross sections (cell experiments). Numerical applications are made for the collisions between Na in a circular state with He :

$$Na(n=20, \ell=19, m=19) + He \rightarrow Na(n=20, \ell', m') + He \quad (3)$$

The relative velocity between Na and He is taken to be the thermal averaged velocity for 296°K as in Ref.[1].

The processes (3) are found to be highly sensitive to the orientation. A selection rule concerning the parity of $\ell'-m'$ is found for the case $\alpha=0$, but it becomes weaker and disappears as α increases. For fixed values of ℓ' the cross sections are found to be most important when $|m'| = \ell'$. The influence of an external electric field is also discussed. More detailed results will be presented at the conference.

In view of the present results, the study of these orientation effects using a beam experiment would be a crucial test for the validity of the impulse approximation for the thermal processes (3).

m'	$\alpha = 0$	$\alpha = \pi/2$	$\langle \sigma \rangle$
2	.239 E + 2	.326 E+1	.505 E+1
1	.714 E - 2	.303	.457
0	.144 E + 2	.188 E+1	.291 E+1
-1	.874 E - 2	.286	.434
-2	.239 E + 2	.293 E+1	.455 E+1

Table I

Cross sections $S(\alpha)$ for processes (3) with $\ell'=2$.

$\langle \sigma \rangle$ corresponds to the average over α ($\int_0^\pi S(\alpha) \sin^2 \alpha d\alpha / \int_0^\pi \sin^2 \alpha d\alpha$)

REFERENCES

1. T. Yoshisawa and M. Matsuzawa, J. Phys. B17, L485 (1984).
2. E. de Prunel , Phys. Rev.A 27, 1831 (1983).

IMPACT IONIZATION OF STATE-SELECTED Na RYDBERG ATOMS BY ION BOMBARDMENT

K. MacAdam,* N.L.S. Martin,* D.B. Smith,* and R.G. Rolfes**

*Department of Physics and Astronomy, University of Kentucky, Lexington, KY 40506

**Department of Physics, Presbyterian College, Clinton, SC 29325

The cross section for electron removal from laser-excited Na(41s) and Na(40d) atoms by impact of singly charged ions has been measured for projectile velocities between 1.3 and 4.4 times the Bohr orbital velocity in the target atoms. The cross section is insensitive to the projectile species because the internal structure of the projectile ion is unimportant on the scale of energies and distances that is significant for the Rydberg collision process and because no significant deflection occurs. Ar⁺ at energies down to 1 keV and Ne⁺ up to 6 keV were used to cover the velocity range. The experiments measure the sum of ionization and charge-transfer cross sections (dominated by ionization at these velocities) and were carried out as follows. In a crossed-beam geometry a Na atomic beam was excited by two tunable pulsed lasers to the desired initial states. The few thousand state-selected Rydberg atoms excited by each pulse were exposed to ion bombardment for $\Delta t = 3 \mu s$. A 1- μs 60-V/cm electric-field pulse was then applied, and Na⁺ ions, which had negligible initial recoil velocities, were swept by this pulse into an electron multiplier. Na⁺ produced in the target by blackbody or multiphoton ionization or other processes constituted a background to be subtracted by comparing signals obtained with the projectile beam gated on and off. Following the sweeping and detection of free target ions, field ionization of the remaining Rydberg atoms was induced to measure the target population.

Figure 1 shows a transient-digitizer recording of a typical electron-multiplier signal. The ratio of the area of the first or "ion" peak and the second or "parent" peak, divided by ion-beam current density and target exposure time, yields the electron-removal cross section, which in this example equals approx. $3.8 \times 10^{-10} \text{ cm}^2$ or $1.7 \pi a_0^2$. The intense ion bombardment of the 40d target causes substantial l mixing,^{1,2} which may be seen by its effect on the field-ionization peak shape. Thus electron removal from "40d" proceeds from a broad distribution of l states, but because of the much smaller l -change cross section from s states the 40s target remains relatively pure.³

Absolute cross sections, velocity dependences, and comparison of s -state and l -mixed targets will be presented. This work was supported in part by the National Science Foundation.

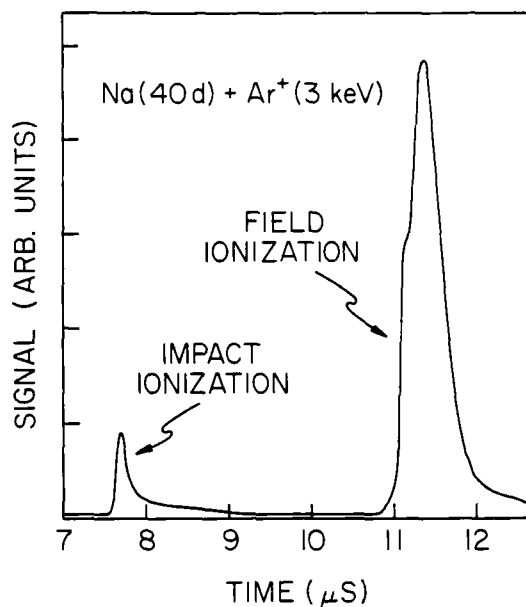


Figure 1. Transient digitizer recording of electron multiplier signal.

References

1. K.B. MacAdam, R.G. Rolfes, and D.A. Crosby, Phys. Rev. 24, 1286 (1981).
2. K.B. MacAdam, D.B. Smith, and R.G. Rolfes, J. Phys. B 18, 441 (1985).
3. K.B. MacAdam and R.G. Rolfes, contributed paper, 16th Annual Meeting APS-DEAP (May 1985).

INFORMATION-THEORETICAL ANALYSIS OF CHARGE TRANSFER
 FROM RYDBERG ATOMS

A. Blomberg and T. Åberg

 Helsinki University of Technology, Laboratory of Physics,
 SF-02150 Espoo, Finland

Recently Rolfes and MacAdam¹ have obtained distributions of final n states populated in charge transfer collisions of Na^+ ions with Na atoms in Rydberg states (initial $n_i \approx 30$). No satisfactory quantum-mechanical theory of these distributions exists. For $l_i \geq 2$ classical trajectory Monte Carlo calculations² have been performed showing some agreement with experiment.¹ Due to the large number of final l -states presumably involved it is of interest to examine whether a purely statistical description is sufficient to explain the n -distributions for both $l_i=0$ and $l_i=2$. This we have done using information theory which has proved to be an efficient tool for separating random behavior from specific processes in the case of transfer ionization.³

In Ref. 1 the distributions were given with respect to the Stark quantum number n_s which in the following is not distinguished from n because of the assumption of large l -mixing inherent in any statistical description. In our analysis the a priori distribution is taken to be $P_0(n) \sim n^{-3}$ as given by the density of states in a Rydberg series. To take into account the resonant enhancement effect and the relation between the initial and final state RMS velocity of the transferred electron,¹ constraints on the average final state binding energy and RMS velocity are introduced. The energy is taken to be $\epsilon \sim n^{-2}$, and the velocity $v \sim n^{-1}$. Then, according to the maximum entropy principle,⁴ the least biased probability distribution is given by

$$P(n) = n^{-3} \exp[\lambda_0 + \lambda_1 n^{-1} + \lambda_2 n^{-2}] = \quad (1)$$

$$= n^{-3} \exp[\lambda'_0 + \lambda_2 (\frac{1}{n} - \frac{1}{n_0})^2]$$

where λ_0 , λ_1 and λ_2 are Lagrange parameters, determined by the constraints, and $\lambda'_0 = \lambda_0 - \lambda_1^2/\lambda_2$ and $n_0 = -(\lambda_2/\lambda_1)$. As a preliminary test of Eq. (1) we have plotted the "surprisals"⁵ $\ln |P_{\text{exp}}(n)/P_0(n)|$ as functions of $(\frac{1}{n} - \frac{1}{n_0})^2$, where the experimental distributions $P_{\text{exp}}(n)$ were taken from Ref. (1). In this representation straight lines with, negative slopes λ_2 should be obtained with a suitable choice of n_0 if $P_{\text{exp}}(n)$ is of the form (1).

The results of our analysis show reasonable agreement for both initial ns and nd states indicating that

the final-state distributions are not influenced by l_i . They seem to be completely determined by the average change in internal orbital energy and velocity. In terms of velocity the distribution (1) takes the simple form

$$P(v) = v \exp[\lambda'_0 + \lambda_2 (v - v_0)^2] \quad (2)$$

This suggests the possibility of a derivation based on considering the motion of the electron in the transient electric field of the projectile as a stochastic process.

References

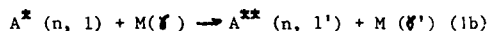
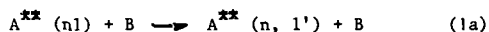
1. R.G. Rolfes and K.B. MacAdam, J. Phys. B **15**, 4591 (1982).
2. R.L. Becker and A.D. MacKellar, J. Phys. B **17**, 3923 (1984).
3. T. Åberg, A. Blomberg and O. Goscinski, Phys. Rev. Letters **52**, 1207 (1984).
4. E.T. Jaynes in The Maximum Entropy Formalism, edited by R.D. Levine and M. Tribus (The MIT Press, Cambridge 1979), p. 15.
5. R.D. Levine and J.L. Kinsey in Atom-Molecular Collision Theory, edited by R.B. Bernstein (Plenum, New York, 1979), p. 693.

SIMPLE ANALYTICAL FORMULAS FOR COLLISIONAL l-MIXING, n-CHANGING
AND IONIZATION OF RYDBERG ATOMS WITH NEUTRAL PARTICLES AT THERMAL ENERGY

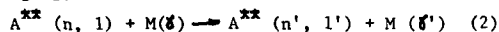
L. Petitjean and F. Gounand

Service de Physique des Atomes et des Surfaces, CEN/SACLAY
91191 Gif-sur-Yvette Cedex, France

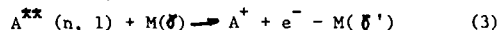
In general the experimental data about inelastic collisions of Rydberg states give the total depopulation cross sections which include many exit channels through different processes such as l-mixing,



n-changing,



and ionization,



where B represents an atomic target and δ specifies the quantum state of molecule M. We have derived simple analytical formulas that can be used to estimate the cross section for reaction (1)-(3) to about a factor of 2. Such formulas appear very useful since they provide an easy way to calculate the quenching cross section of Rydberg state by neutral particle. Moreover they allow one to display in a transparent way the influence of the relevant physical parameters (for example, the energy defect of processes (1) and (2)).

The impulse approximation¹ is known to describe reasonably well the processes (1)-(3). Within this approach, the evaluation of the atomic transition form factor $F_{n1, n'1'}(K)$

$$F_{n1, n'1'} = \frac{1}{(2l+1)} \sum_{m, m'} | \langle n'1'm' | e^{i \vec{K} \cdot \vec{r}} | n1m \rangle |^2 \quad (4)$$

is a key step in the derivation of the cross section. \vec{K} represents the momentum transfer and \vec{r} is the coordinate of the Rydberg electron. The Binary Encounter Theory have been shown to offer a very powerful means for the rapid evaluation of the atomic form factor. $F_{n1, n'}(K)$ (averaged over $1'$)².

Since the cross section appears to be much more sensitive to the energy defect of the reaction than to the initial orbital momentum value l , it seems reasonable to approximate $F_{n1, n'}(K)$ by its l -averaged value, i.e.,

$$F_{n1, n'}(K) \approx \frac{1}{n} \sum_{l=0}^{n-1} F_{n1, n'}(K) = \frac{23}{3\pi K} \frac{n}{n^3} \frac{1}{(n^2 p_0^2 + 1)^2} \quad (5)$$

with $p_0 = (E_{n1} - E_{n'}) - K^2/2 / K$

We have recently reported detailed comparisons between the BET form factor and the above equations³. The

overall agreement is good. This is quite interesting since the simple expression of the form factor (Eq.(5)) provides analytical expressions of the cross section for process (1)-(3).³

Let us as example consider the process 1a, whose cross section is given by

$$n1 \rightarrow n(Q_{\min}) = \frac{2\pi L^2}{n^3 v^2} \left[\frac{2}{\pi} \arctan\left(\frac{1}{y}\right) - \frac{2y}{3\pi(1+y^2)^2} \right] \quad (6)$$

with $y = nQ_{\min}/2$ ($Q_{\min} = \frac{|\Delta E|}{V}$, ΔE : energy defect, V : relative velocity of the colliding partners). L is the e^- -B scattering length. The agreement between this formula and BET calculation is especially good in the range of validity of the IA (fig.1). The influence of the energy defect is investigated in Table I. One can see that the experimental data are nearly constant when $nQ_{\min} < 0.1$ and decrease strongly when nQ_{\min} varies from 0.2 to 4.9, as predicted by relation (6).

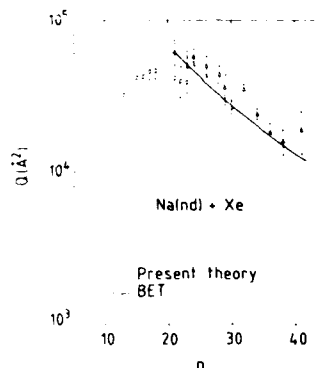


Figure 1 - The l-mixing cross sections for Na(nd)+Xe. ¹: Kachru et al., Phys. Rev.A 27, 795 (1983), ²: Chapelet et al., J. Phys. B15, 3455 (1982).

E_{n1}	ΔE	nQ_{\min}	Present theory	Present theory
11	0.00	0.00	1.00	1.00
12	0.00	0.00	1.00	1.00
13	0.00	0.00	1.00	1.00
14	0.00	0.00	1.00	1.00
15	0.00	0.00	1.00	1.00

Table I - Na^{**}-He l-mixing cross sections.

References

1. M. Matsuzawa in "Rydberg states of Atoms and Molecules" edited by R.F. Stebbings and F.B. Dunning, (Cambridge University, NY 1983).
2. F. Gounand and L. Petitjean, Phys. Rev.A 30, 61 (1984).
3. L. Petitjean and F. Gounand, Phys. Rev.A 30, 2946 (1984).

THE POSSIBLE INFLUENCE OF CORE EFFECTS IN RYDBERG
 ATOM-NEUTRAL COLLISIONS AT THERMAL ENERGIES

F. Gounand and L. Petitjean

 Service de Physique des Atomes et des Surfaces, CEN/Saclay
 91191 Gif-sur-Yvette Cedex, France

The Rydberg atom-neutral system (P) provides a good example of a simple three-body collision system, because the outer Rydberg electron is located on the average at large distances from the A^+ core. One expects collisional processes to be governed by either the e^-P or the A^+P interaction. It has been shown¹ in the last few years that cross-sections calculated within the frame of the impulse approach (IA) with only taking into account the e^-P interaction provides reasonable agreement with the available data². But it still remains some controversy about the possible influence of the A^+P interaction on the collisional cross-sections.

We report here on the evaluation of the core contribution by using the same IA approach, the validity of which will not be addressed here. The cross-section for the $A(nl) + P \rightarrow A(n'l') + P$ process is found to be:

$$(1) \sigma_{nl \rightarrow n'l'}^{A^+P} = \frac{2\pi}{\alpha^2 \mu^2 v^2} \int_{Q_{\min}}^{Q_{\max}} F_{nl \rightarrow n'l'}(K) |f_{A^+}|^2 K dK$$

where F is the atomic squared form factor, f_{A^+} the amplitude for A^+P elastic scattering and $Q_{\min}(\max)$ are the minimum (maximum) value of the momentum transfer K . μ is the reduced mass of the two colliding atoms, v being their average relative velocity. Finally $\alpha \approx (m_{A^+})^{-1}$. Eq.(1) has the same form than σ^{e^-P} except for the mass-factor $(\alpha \mu)^{-2}$ and for the range of integration. If, as usual, we adopt a diffusion length approximation for f_{A^+} the key parameter remains F , for which simple methods of calculation have been recently developed^{3,4}. Eq.1 allows a systematic discussion of possible core effects. In particular it is easy to show that such effects are expected to be noticeable, in particular, for light ion core and strong A^+P interaction. This is also demonstrated in Fig.1 where some calculations are reported together with available data. Finally it appears⁴ that the situation for which strong core effects are expected (Li^2-Ne or H^2-He pairs) have not yet been explored, calling for further experimental works. Other points will be discussed at the conference.

References

1. M. Matsusawa, J. Phys. B12, 3743 (1979).
2. F. Gounand and J. Berlande in Rydberg states of Atoms and Molecular Chap.7, edited by R.F. Stebbings and F. B. Dunning, Cambridge University Press, N.Y. 1983.
3. L. Petitjean and F. Gounand, Phys. Rev. A30, 2946 (1984).
4. L. Petitjean and F. Gounand, submitted to Phys. Rev.A.
5. M. Chapelet, J. Boulmer, J.C. Gauthier and J.F. Delpech J. Phys. B15, 3455 (1982).
6. M. Hugon, B. Sayer, P.R. Fournier and F. Gounand, J. Phys. B15, 2391 (1982).

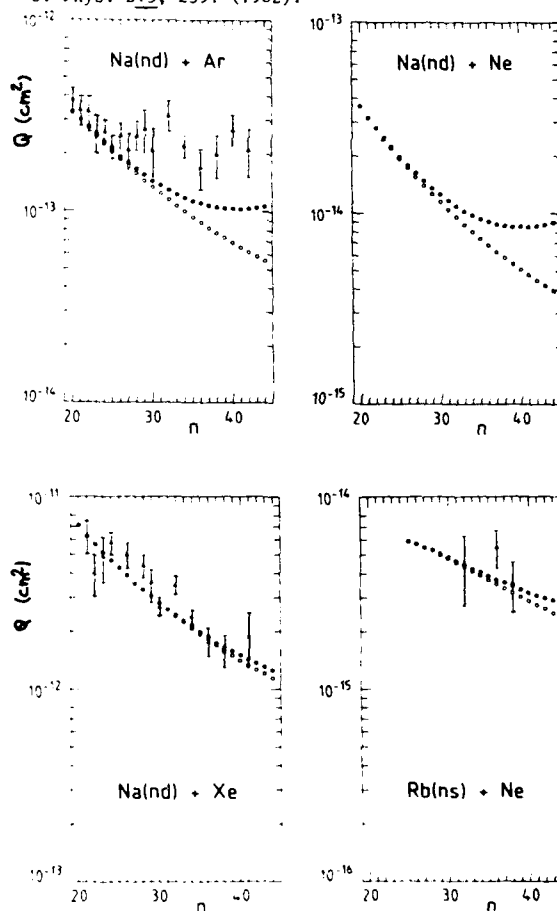


Figure 1

Depopulation cross-sections for Na(nd) and Rb(ns)-P collisions. Open circles give the contribution of the (e^-P) interaction only. Black circles are the sum of both (A^+P) and (e^-P) contribution. Experimental data, when available^{5,6} are also reported. Calculations are performed for a cell temperature of 293 K.

AD-A163 497 ELECTRONIC AND ATOMIC COLLISIONS ABSTRACTS OF
CONTRIBUTED PAPERS INTERNAT. (U) SRI INTERNATIONAL
MENLO PARK CA MOLECULAR PHYSICS CENTER
UNCLASSIFIED M J COGGIOLA ET AL. 1985 FFG 7/

**ELECTRONIC AND ATOMIC COLLISIONS ABSTRACTS OF
CONTRIBUTED PAPERS INTERNAT. (U) SRI INTERNATIONAL
MENLO PARK CA MOLECULAR PHYSICS CENTER
M J COGGIOLA ET AL. 1985 FFG 7/**

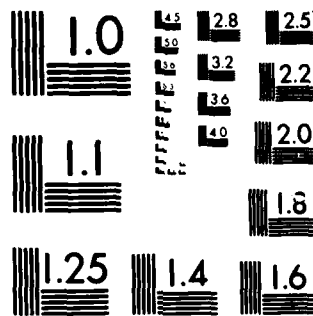
2/8

UNCLASSIFIED

FFG 7/4

NL

END



MICROCOPY RESOLUTION TEST CHART
NATIONAL BUREAU OF STANDARDS 1963-A

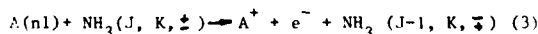
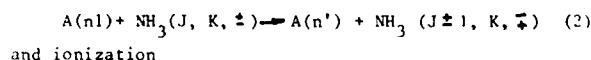
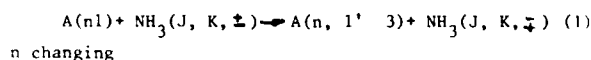
COLLISIONS OF RUBIDIUM RYDBERG ATOMS WITH AMMONIA

L. Petitjean, F. Gounand and F.R. Fournier

Service de Physique des Atomes et des Surfaces, CEN/SACLAY
91191 Gif-sur-Yvette Cedex, France

Following a previous study on rubidium Rydberg states-CO collisional system¹, well-described by using the impulse-approach (IA), we have measured the total depopulation cross section of Rb(ns) and Rb(nd) Rydberg states by collisions with NH₃ molecules². This system offers the opportunity to study a particular transition and to exhibit experimentally the importance of the energy defect for a dipole induced transition. Experimental data for Rb(nd) states are reported in figure 1.

The depopulation of Rydberg states by NH₃ occurs through three distinct dipole induced mechanism: l-mixing:



J denotes the total angular momentum, K represents the angular momentum along some direction and +(-) stands for a symmetric (antisymmetric) level.

Cross section expressions for the relevant processes have been derived by Petitjean and Gounand³ within the frame of the IA. The sum of the n-changing and ionization cross section is plotted (dashed line) in figure 2 and remains approximately constant for $n \geq 30$. The total depopulation including the three distinct processes presents as a function of n a maximum near the 47d level. This is clearly due to l-mixing reaction induced by NH₃ inversion.

When one compares Fig.1 and 2, one can notice that the IA gives the correct relative behavior of the cross section with n, despite it over estimates by one order of magnitude the cross sections. Then, it seems reasonable to attribute the experimental maximum of the cross section for the d levels to l-mixing transitions. These results show that the use of the impulse approach becomes questionable when the molecular perturber present, a large dipole moment. These results also prove that for high Rydberg states the efficiency of a dipole induced reaction decreases by one order of magnitude when the energy defect varies from $\sim 0.01 \text{ cm}^{-1}$ to 0.5 cm^{-1} .

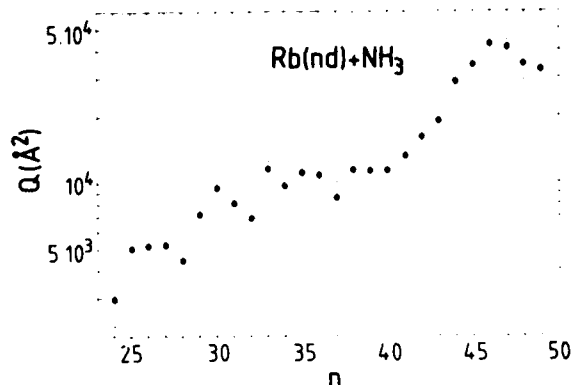


Figure 1 - Quenching cross sections for the Rb(nd) levels by NH₃ versus n.

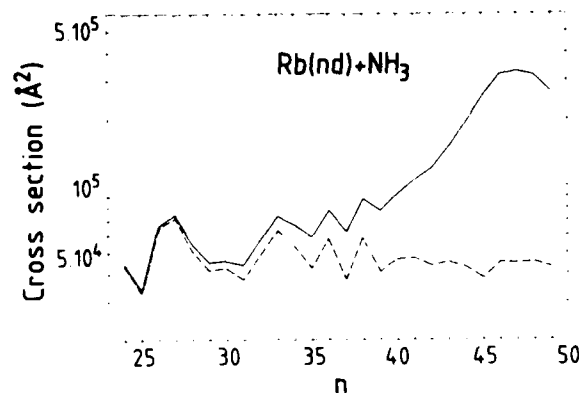


Figure 2 - Rb(nd)-NH₃ collisional cross-sections in the impulse approximation. The collisional ionization appears as a dotted line. The dashed line represents the sum of n-changing and ionization processes. The total depopulation (including l-mixing, n-changing and ionization) is shown as a solid line.

References

1. L. Petitjean, F. Gounand and P.R. Fournier, Phys. Rev. A, **30**, 71 (1984).
2. L. Petitjean, F. Gounand and P.R. Fournier, submitted to Phys. Rev. A.
3. L. Petitjean and F. Gounand, Phys. Rev. A, **30**, 2946 (1984).

THEORETICAL SEMICLASSICAL STUDY OF STATE-CHANGING COLLISIONS BETWEEN RYDBERG ATOMS AND ROTATING MOLECULES*

M. Kimura[†] and N. F. Lane[†]Joint Institute for Laboratory Astrophysics
University of Colorado and National Bureau of Standards
Boulder, Colorado 80309 USA

A full three-dimensional classical trajectory Monte-Carlo method has been applied in a study of excitation and ionization of Rydberg atoms in collisions with polar molecules.¹ Although this classical calculation reproduces certain observed trends, the quantitative agreement with measurements was not satisfactory. This is not unexpected, since a complete classical representation was utilized to describe the Rydberg atom as well as the rotating molecule. In the present work, we have carried out semiclassical close-coupling calculations in a study of J-changing in collisions between Rydberg atoms and rotating molecules,

$$RA(n\ell m) + M(JM) \rightarrow RA(n'\ell'm') + M(J'M')$$

Approximations in the calculation are:

(a) Semiclassical impact parameter method with straight line trajectories for C.M. of projectile relative to target.

(b) Quantum treatment of internal dynamics -- rotation of molecule and motion of Rydberg electron.

(c) Electron-molecule interaction is approximated by a cut-off dipole interaction with the form $-[D \cdot \hat{R}_m / R_m^3] \chi(R_m)$ where R_m is the electron distance relative to the molecule, D is the molecular dipole moment and $\chi(R)$ smoothly forces the potential to zero at certain R_m .

(d) "Perturbed Rotor State" is used as the molecular rotational basis.

(e) Optical potential methods are used to represent "bands" of Rydberg states not in "near resonance."

In this formalism, the dominant coupling causing rotational transitions is "nonadiabatic coupling" between perturbed rotor states. These perturbed rotor states have a constant energy gap and may introduce the Demkov coupling effect analogous to that found in ion-atom or atom-atom systems. And correspondingly, the nonadiabatic coupling matrix elements have a large peak at the point where two potential curves depart.

Detailed results of the calculation will be presented at the meeting.

*This work is supported by the U. S. Department of Energy, Office of Basic Sciences.

[†]Also Rice University, Houston, TX.

References

1. (a) S. C. Preston, Ph.D. Thesis, Rice University (1984). (b) S. C. Preston and N. F. Lane, XIII ICPEAC Abstracts, p. 664 (1983). (c) S. C. Preston and N. F. Lane, Phys. Rev. A (in preparation).

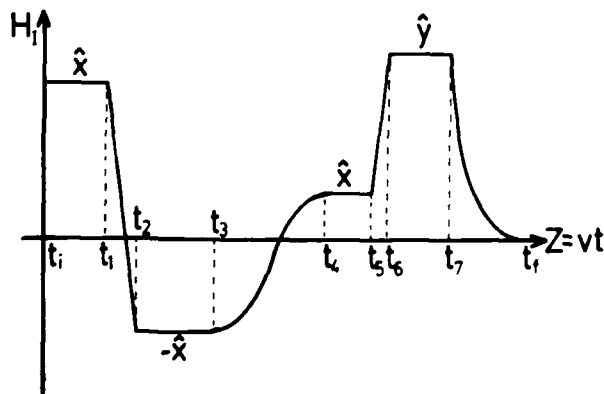
ANGULAR MOMENTUM SHIFTS OF HIGH RYDBERG STATES BY TIME-DEPENDENT EXTERNAL FIELDS

Y. Hahn, K. LaGattuta and I. Nasser

Department of Physics, University of Connecticut, Storrs, CT 06268 USA

High Rydberg states (HRS) created by multiphoton excitation or by low energy electron capture are sensitive to small external perturbations. In particular, such HRS ions can undergo serious changes in their structure (n, l, m shifts) between the time of their creation and their detection. Various l -changing¹⁻⁴ and m -changing⁵ collisions, with or without the presence of weak external electric or magnetic fields may occur. Of special interest here is the dielectronic recombination (DR) process, in which an incoming electron is captured by an ionic target to a HRS, while one of the inner-shell target electrons is excited. The cross section for this process has been measured⁶ recently in a coincidence experiment. Both the photon emitted by the inner-shell excited electron and the HRS recombined atoms are detected. The HRS is detected by field-strip-ping. As the HRS atomic beam traverses the space between the interaction region and the detector, it passes through several distinct regions in which electric fields have been introduced for the purpose of analysis. A recent theoretical study⁷ suggests that these fields may induce changes⁸ in the quantum numbers of the states that are being measured.

We have formulated a time-dependent, nonperturbative theory to examine the effect of time-varying fields on HRS. Since the perturbations are often very strong as compared to level spacings between the states involved (e.g. for different l or m of the same n), the theory has to be nonperturbative. In the limits of both adiabatic and sudden changes in the perturbation, our general theory gives the correct limiting behavior. Consider a perturbation H_I of the form given in Fig.1.

Figure 1. A model $H_I(t)$ vs $t=Z/v$.

where H_I measures the interaction of a HRS electron with an external electric field. For this system, we can write the transition operator in the interaction representation, as

$$U(t_f, t_i) = U(t_f, t_7) U(t_7, t_6) \cdots U(t_i, t_1), \quad (1)$$

where

$$U(t_b, t_a) = T \left\{ \exp \left[-i \int_{t_a}^{t_b} H_I(t') dt' \right] \right\} \quad (2)$$

and

$$H_I(t') = e^{iH_0 t'} H_x e^{-iH_0 t'}$$

For this example, it can be shown, using spherical coordinates for the Coulomb function Ψ , describing the HRS that

$$U(t_i, t_1) |\Psi_i(t_i)\rangle = |\Psi^{\text{st}}(t_i)\rangle = \text{Stark representation,} \quad (3)$$

$F \rightarrow \text{large}$

while

$$U(t_6, t_5) = R = \text{rotation operator for } \phi=90^\circ \text{ around the z-axis.} \quad (4)$$

In general, we will consider the rate at which H_I changes, and the influence of the rate of this change on the final state probability. A detailed numerical calculation will be presented for H_I that simulates the actual physical situation⁶. The results should aid in interpreting the recent DR experiment, and may also facilitate understanding of other situations involving HRS.

This work was supported in part by a DOE grant.

References

1. R. G. Rolfe et al, J. Phys. **B16**, L533 (1982).
2. T. F. Gallagher et al, Phys. Rev. **A17**, 904 (1978).
3. D. R. Mariani et al, Phys. Rev. Lett. **50**, 1261 (1983).
4. P. Pillet et al, Phys. Rev. Lett. **50**, 1042 (1983) and Phys. Rev. **A30**, 280 (1984).
5. R. G. Hulet and D. Kleppner, Phys. Rev. Lett. **51**, 1430 (1983).
6. D. S. Belic et al, Phys. Rev. Lett. **50**, 339 (1983) and G. Dunn, ICAP July 1984, Seattle, invited talk.
7. K. LaGattuta et al, Phys. Rev. Lett. (1985).
8. D. Richards, J. Phys. **B17**, 1221 (1984).

EFFECTS OF ULTRA-LOW-ENERGY RESONANCES IN ELASTIC SCATTERING OF ELECTRONS BY ALKALI METAL ATOMS ON COLLISION OF HIGH-RYDBERG ATOMS WITH ALKALI METAL ATOMS

Michio Matsuzawa* ** and Naoto Koyama*

Department of Physics, University of Toronto, Toronto, Ontario Canada*
Department of Engineering Physics* and Institute for Laser Sciences**,
The University of Electro-Communications, Chofu-shi, Tokyo 182 Japan

Using the free-electron model (FEM) based on the impulse approximation (IA), one of us (MM)¹ theoretically pointed out that an ultra-low-energy resonance in e-molecule scattering causes an oscillating behavior in the n-dependence of pressure shift and width of high-Rydberg series perturbed by that molecule. Using this approach, Kaulakys² and Rabin and Rebentrost³ attempted to explain observed oscillating structures of pressure shift and width of high-Rydberg $K^{**}(n^2S, n^2D)$ and $Rb^{**}(n^2S, n^2D)$ series perturbed by their ground-state atoms⁴ for $15 \leq n \leq 30$ in terms of the ultra-low-energy resonance in e-alkali metal atom (M) scattering theoretically predicted by Sinfailam and Nesbet.⁵

However, two experiments^{6,7} recently performed on the pressure shift and width of alkali-metal high-Rydberg series perturbed by different alkali-metal atoms do not seem to support the above-mentioned interpretation because the oscillating structures do not depend on the kind of perturber but on the Rydberg series itself. This could come from the fact that one of the conditions for IA, i.e., $\tau_r/\tau_n \ll 1$ is not well satisfied for this range of n where τ_r is the life time of the resonance and τ_n is the period of electronic motion.

In order to detect the narrow ultra-low-energy resonance in the e-M scatterings, we propose to use the high-Rydberg alkali-metal atom with the highest allowed angular momentum $A^{**}(n, l=n-1)$. The total cross section of the A^{**} -M system $\sigma_{nl}^t(V)$ is expressed as follows⁸

$$V\sigma_{nl}^t(V) = \int_0^\infty v \sigma_e(q) |g_{nl}(q)|^2 q^2 dq \quad (1)$$

where we have employed the Breit-Wigner type resonance formula with some modification as the total cross section σ_e for e-M scattering. Here V is the relative velocity between A^{**} and M, g_{nl} is the radial wave function of the Rydberg electron in the (n, l) state in the momentum representation, and q and v are the momentum and velocity of the relative motion of e to M, respectively. Expression (1) may be considered to be a good approximation for high n such as $n=70$. Fig.1 shows the calculated cross sections for $E_r=2.4$ meV and $\Gamma=0.58$ meV (Ref.5). One sees that $\sigma_{n, n-1}^t(V)$ has a single peak at $n=75$ which coincides with the value of n_r estimated from $E_r=2.4$ meV. The number of the peaks in $\sigma_{nl}^t(V)$ for each l state corresponds to those of $|g_{nl}|^2$ and are smeared out as l decreases. The validity condition

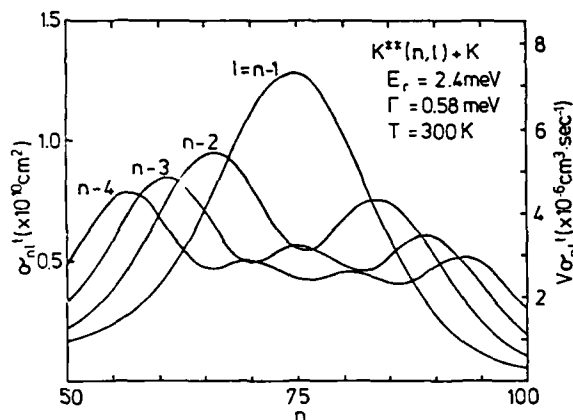


FIGURE 1 Total cross sections σ_{nl}^t and rate constant $V\sigma_{nl}^t$ (right-hand scale) against the principal quantum number n.

$\tau_r/\tau_n \ll 1$ is well satisfied around $n=75$. Therefore we conclude that this can be used to detect the ultra-low-energy resonance in e-M scattering.

References

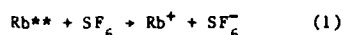
1. M. Matsuzawa, J. Phys. B **8** L382 (1975), ibid **10** 1543 (1977)
2. B.P. Kaulakys, J. Phys. B **15** L719 (1982)
3. Y. Rabin and F. Rebentrost, Opt. Comm. **40** 257 (1982)
4. B.P. Stoicheff, D.C. Thompson and E. Weinberger, Spectral Line Shapes ed. B. Wende (Walter de Gruyter, Berlin, 1981) 826 references therein
5. A.-L. Sinfailam and R.K. Nesbet, Phys. Rev. A **7** 1987 (1973)
6. B.P. Stoicheff, D.C. Thompson and G.-X. Xu, 8th ICAP, Göteborg B 91 (1982)
7. H. Heinke, J. Lawrenz, K. Niemax and K.-H. Weber, Z. Phys. A **312** 329 (1983)
8. M. Matsuzawa, J. Phys. B **12** 3743 (1979)

COLLISIONS OF Rb(ns,nd) ATOMS WITH SF₆[†]

B. G. Zollars, F. Lu, C. W. Walter, L. N. Goeller L. G. Gray, K. A. Smith
F. B. Dunning and R. F. Stebbings

Departments of Space Physics and Astronomy, and Physics,
Rice University, Houston, Texas 77251 USA

Ionization of highly-excited Rb atoms in collisions with SF₆ proceeds via electron transfer reactions of the type



One motivation for the study of such reactions is to test the validity of the so-called "essentially-free" electron model. This model assumes that the separation between the Rydberg electron and its associated ionic core is so large that both do not simultaneously interact with a target particle. The collision is then analyzed by considering only the Rydberg electron-target interaction. The model predicts that the rate constant for reaction (1) will equal that for attachment, by the same target, of free electrons having the same velocity distribution as the Rydberg electron. To further test this prediction we have measured rate constants for collisional ionization in Rb(ns,nd) - SF₆ collisions for values of principal quantum number *n* in the range 38 to 84. Measurements at high *n* are particularly valuable because the Rydberg electron-core separation is large and because interactions between the product ions should be minimal.

The present experimental technique is similar to that described elsewhere.¹ Rb atoms contained in a collimated thermal-energy beam are excited, in the presence of target gas and in zero electric field, to a selected ns or nd state by two-photon excitation using the modulated output of a single-mode CW dye laser. After allowing collisions to occur for a selected time *t* the total number *N(t)* of excited atoms remaining is determined by selective field ionization (SFI). Measurements of the time dependence of *N(t)* at different target gas densities permits the rate constant for collisional destruction to be determined. Our earlier measurements¹ showed that, for the present range of *n*, destruction proceeds primarily through collisional ionization. It is thus reasonable to equate the measured rate constants for collisional depletion of the total Rydberg population with those for collisional ionization.

Preliminary data are presented in Fig. 1

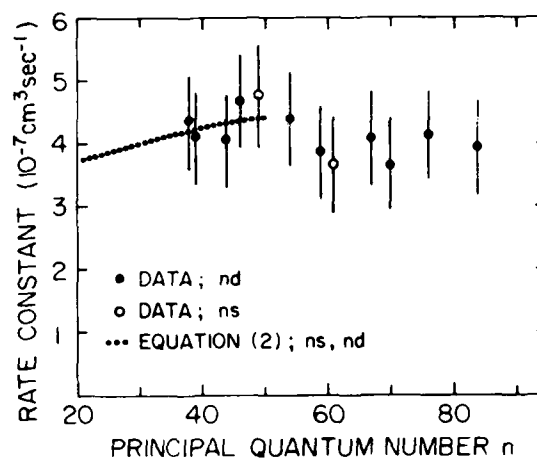


Fig. 1. Rate constants for collisional ionization in Rb(ns,nd) - SF₆ collisions.

together with rate constants derived using the expression

$$k = \int_0^{\infty} v \sigma_e(v) f(v) dv \quad (2)$$

where *f(v)* is the Rydberg electron velocity distribution and $\sigma_e(v)$ a theoretical free electron attachment cross section derived by Klots.²

The agreement between the Rydberg atom and free electron data is good, showing that studies with Rydberg atoms can produce information on very-low-energy electron collisions. The measured rate constants are relatively independent of *n*, indicating that at low electron velocities $\sigma_e(v)$ is approximately inversely proportional to *v*. The present measurements will be extended to low *n* to look for effects due to interactions between the product Rb⁺ and SF₆⁻ ions.

References

1. B. G. Zollars, K. A. Smith and F. B. Dunning, *J. Chem. Phys.* **81** 3154 (1984).
2. C. E. Klots, *Chem. Phys. Letts.* **38** 61 (1976).

[†]Research supported by the NSF under grant #PHY 84-05945 and the Robert A. Welch Foundation.

STATE-CHANGING IN Rb(ns,nd)-Xe COLLISIONS: PRODUCT STATE DISTRIBUTIONS[†]

G. B. McMillian, L. N. Goeller, K. A. Smith, F. B. Dunning and R. F. Stebbings

Departments of Space Physics and Astronomy, and Physics,
Rice University, Houston, Texas 77251 USA

The distribution of product states resulting from state-changing in Rb(ns,nd)-Xe collisions has been investigated. Rubidium atoms contained in a thermal-energy collimated beam are excited, in the presence of target gas and in zero electric field, to a selected ns or nd state. After allowing collisions to occur for a specified time, the product state distribution is determined by selective field ionization (SFI). Typical SFI profiles observed for Rb($55^2D_{5/2}$), both with and without target gas present, are shown in fig. 1. The feature labelled P_0 results from adiabatic ionization of parent atoms, while P_1 results from diabatic ionization of $|m_l| > 3$ collision products. The product-state distribution is inferred by comparing observed P_1 profiles with those calculated¹ for different assumed final-state distributions.

The P_1 profiles obtained for very low (high) target gas densities that correspond to single (multiple) collision conditions are shown in figs.

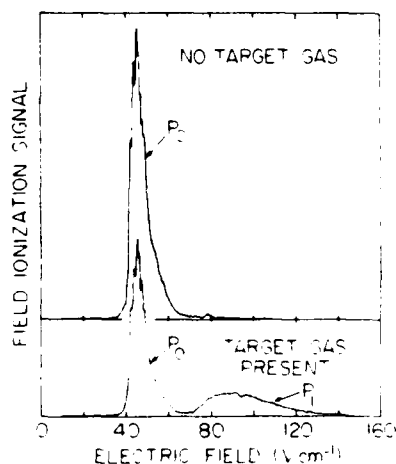


Fig. 1. SFI profiles obtained with and without target gas present.

2a(b). Figure 2 also includes P_1 profiles calculated assuming that: i) collisions populate states in the adjacent $n=54$ manifold of higher- l states with the populations in individual $|m_l|$ states being linearly weighted toward low $|m_l|$ (Fig. 2c), ii) collisions populate each state in the $n=54$ manifold with equal probability (Fig. 2d), iii) collisions populate states in several adjacent n -manifolds with

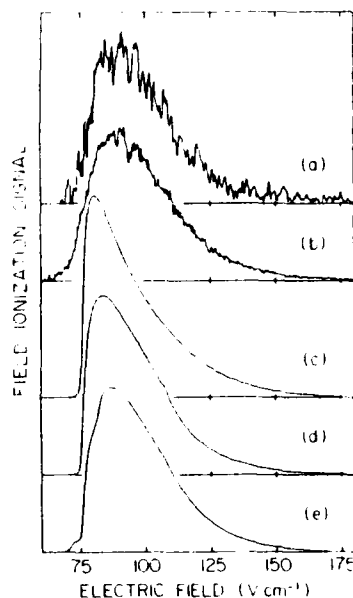


Fig. 2. Observed and calculated P_1 profiles.

an n -state distribution equal to that calculated by Gounand² (3% $n=52$, 26% $n=53$, 65% $n=54$, 6% $n=55$) and with individual states within each manifold populated with equal probability (Fig. 2e).

The agreement between the present results and the predictions of Gounand demonstrates that state-changing results primarily from transitions to the n -manifold lying closest in energy to the parent state, but that transitions to other neighboring manifolds are also possible. The data indicate that collisions populate states within each manifold with essentially equal probability and provide no evidence of a propensity rule on the changes in $|m_l|$ that can occur. Indeed, similar P_1 profiles are observed under both single-collision conditions and conditions where further collisional state-changing of the product is expected. Data for other s and d states lead to similar conclusions.

References

1. F. G. Kellert, T. H. Jeys, G. B. McMillian, K. A. Smith, F. B. Dunning and R. F. Stebbings, *Phys. Rev. A*, **23**, 1127 (1981).
2. F. Gounand - private communication.

[†]Research supported by NSF under grant #84-05945 and the Robert A. Welch Foundation.

STATE SELECTIVE LASER DETECTION OF RYDBERG ATOMS

V. Lange, U. Eichmann, G.A. Ruff and W. Sandner

Fakultät für Physik, Universität Freiburg, Hermann-Herder-Str. 3, 7800 Freiburg, West Germany

Atomic Rydberg states have for long times been predominantly studied using highly selective laser excitation techniques, whereas recently they also gain increasing attention as final products of particle collision processes, e.g. in dielectric recombination or electron capture experiments. This raises the need for an accurate and efficient method to detect and analyze atoms in unknown high Rydberg states. We demonstrate that laser excitation into autoionization states is not only a highly efficient detection method, but can also be extremely state selective.

For the method to work the Rydberg species (atom, ion, molecule etc.) under consideration must have a strong core transition, which can be driven by tunable lasers. Detuning the laser from the center of such a core transition exhibits characteristic variations in the absorption cross section^{1,2}. In particular, the cross section vanishes periodically in energy. It can be shown that the energy spacing between the points of zero cross section is, to first approximation, merely a function of n^* , the effective quantum number of the initial Rydberg state, which can thus be measured. Taking into account the effects of higher order corrections (arising from long range polarization potentials of the core) we were able to directly measure the effective quantum number n^* of the Barium $6s42d(^1D_2)$ state to a relative accuracy of few parts in 10^{-4} . It is important to point out that this n^* determination is insensitive to channel mixing effects in multi electron Rydberg systems, and requires no explicit knowledge of the ionization potential of the system. Therefore, it may in turn be utilized to determine the ionization potential of complicated systems, a method which is currently investigated in our laboratory.

For the quantitative analysis of ensembles of atoms in different Rydberg states n , as they frequently occur in collision experiments, we have developed the following scheme of a "Rydberg Filter". It is based on two observations:

- a) Cross section zeroes in the "sidebands" of the core transition occur at different energies for different Rydberg states n (more specifically: for different n^*).
- b) The cross section between the zeroes can always be saturated (100% excitation to autoionizing states²).

Hence we can find laser frequencies for a "Selection Laser" at which all but one particular Rydberg state n_0

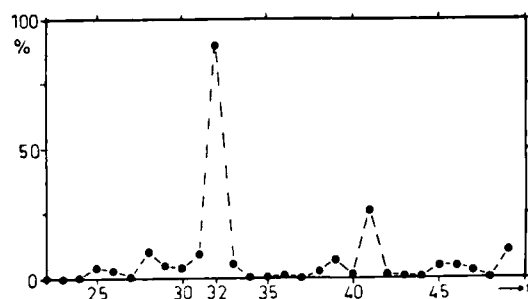


Fig. 1: Transmission curve of the Rydberg Filter.

are excited to an autoionization state and are thus destroyed. The number of remaining neutral Rydberg atoms in state n_0 may subsequently be determined from the autoionization electron signal of a "Probe Laser", tuned to the center of the core transition and thus exciting all remaining Rydberg atoms.

A first demonstration of the Rydberg Filter is given on fig. 1. Shown is the "transmission curve" of the filter, i.e. the fraction of Barium Rydberg atoms in various nd -states after firing of the selection laser, which was tuned to select $6s32d$ states. Initial Rydberg population was 100% in each state. In contrast to electric field ionization the selectivity of the Rydberg filter in this range is sufficient to clearly distinguish between single n states. Most of the deviations from the ideal transmission curve $T(n) = 1/n_{32}$ result from the finite bandwidth of the laser, 0.33 cm^{-1} . An exception is the large fraction of Rydberg atoms in the $n=41$ state, which originates from an accidental coincidence of zero absorption points for $n=32$ and $n=41$. Such unwanted coincidences are expected to occur periodically in n for $n \approx n_0$, however, their influence on the filter selectivity can be eliminated if electric field ionization is used for a coarse preselection of the n range under investigation.

References

1. N.H. Tran, R. Kachru and T.F. Gallagher, Phys. Rev. A 26 (1982) 3016
2. S.A. Bhatti and W.E. Cooke, Phys. Rev. A 28 (1983) 756

DELAYED EMISSION OF 2p-1s AND 3p-1s X-RAYS FROM 40 MeV Ne IONS IONIZED IN A THIN CARBON FOIL

J. Pálkás, R. J. Maurer, and R. L. Watson

Cyclotron Institute, Texas A&M University, College Station, Texas 77843 USA

A significant fraction of a beam of MeV/amu projectiles incident on a thin foil emerges with electrons in high Rydberg states, and these electrons may subsequently cascade down to low-lying np states. In ions having zero or one-electron cores, this process ultimately results in the emission of delayed np-1s radiation at large distances from the foil¹. These delayed x-rays provide important information about the population mechanism of the Rydberg states, which - as recent studies^{2,3} have shown - are not yet fully understood.

In the present study, the K x-ray spectra of Ne projectiles excited by passing a beam of 40 MeV Ne²⁺ ions through a 50 $\mu\text{g}/\text{cm}^2$ carbon foil were measured at various distances behind the foil using a Johansson-type curved crystal spectrometer equipped with a rubidium acid phthalate crystal. The He-like 1s2p(¹P)-1s(²S), H-like 2p(²P)-1s(²S), and H-like 3p-1s(²S) transitions are dipole-allowed with lifetimes of less than 0.6 ps, but even at 1 cm (i.e. 0.5 ns) behind the foil, considerable intensity is still detected for these short lifetime transitions indicating that electrons are cascading from very high n levels.

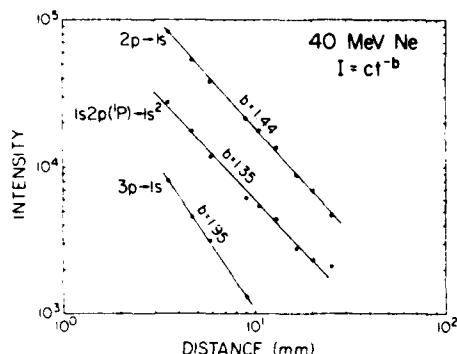


FIG. 1. Measured decay curves for the indicated lines of 40 MeV Ne projectiles. The solid lines are the $I=ct^{-b}$ functions fitted to the experimental data.

Fig. 1. shows the intensities of the delayed He-like 1s2p(¹P)-1s(²S), H-like 2p-1s, and H-like 3p-1s transitions as a function of the distance behind the foil. The decay curves of the 2p-1s transitions are well represented by the $I=ct^{-b}$ power law⁴, where b is equal to 1.35 for 1s2p(¹P)-1s(²S)

and 1.44 for 2p(²P)-1s(²S). These results, when compared with the theoretical decay curves⁴, support the assumption that the different l-states in a given n-manifold are populated uniformly.

The measured decay curve for the H-like 3p-1s line gives a larger slope ($b = 1.95$) than those for the 2p-1s transitions. Electrons cascading down from Rydberg states feed the 2p and 3p states through different channels, and the 3p-1s/2p-1s intensity ratio must also reflect the initial l-distribution of the Rydberg states. The measured 3p-1s/2p-1s intensity ratio as a function of distance behind the foil, when compared with theoretical calculations⁴, shows that both the absolute value of the 3p-1s/2p-1s ratio and its dependence on the distance behind the foil give good agreement with the assumption that the l-states are uniformly populated.

Previous measurements performed with 16 MeV O and 127 MeV S projectiles indicate that in oxygen mainly low angular momentum states are populated, while in sulfur, high l-states are populated preferentially. This apparent change in the l-distribution from O to S will be discussed.

In addition to the decay curves, important structural differences in the prompt and delayed x-ray spectra (e.g. the nonstatistical ratio of the intensity of the He-like (1s2p)³P₁ - (1s²)¹S and (1s2p)¹P - (1s²)¹S lines, and the absence of 1s21p-1s²21, 2121-1s21, and 2pn1-1sn1 satellite lines in the delayed spectra) will be discussed.

References

1. W. J. Braithwaite, D. L. Matthews, and C. F. Moore, Phys. Rev. A **11** 465 (1975)
2. H. -D. Betz, D. Rosenthaler, and J. Rothermel, Phys. Rev. Lett. **50** 34 (1984)
3. E. P. Kanter, D. Schneider, and Z. Vagner, Phys. Rev. A **28** 1193 (1983)
4. H. D. Betz, J. Rothermel, and F. Bell, Nucl. Inst. and Meth. **170**, 243 (1980).
5. J. Rothermel, H. -D. Betz, F. Bell, and V. Zacek, Nucl. Inst. Meth. **194** 341 (1982)

Acknowledgements This research was supported by the Division of Chemical Sciences of the Department of Energy, the Robert A. Welch Foundation and the Texas A&M Center for Energy and Mineral Resources.

Observation of "Stark Beats" in Gas Excited 100 MeV Ne^{6+} Ion BeamsD. Schneider, W. Zeitz, G. Schiwietz, N. Stolterfoht
and U. Wille

Hahn-Meitner-Institut für Kernforschung

1 Berlin 39, Glienicker Str. 100

100 MeV Ne^{6+} ions are excited into high Rydberg states following the impact on a He-gas target. The effect of a transverse electric field on the Rydberg states is investigated by measuring the integral field ionization yield in an additional constant electric field¹. Strong oscillations are observed in the yield as function of the field strength. The experimental arrangement is similar to that described in Ref. 2. A tightly collimated 100 MeV Ne^{6+} beam traverses a gas cell and a well-defined transverse electric field which is located downstream from the target. Exiting from the field the beam passes through a 45° parallel plate electrostatic electron spectrometer where Rydberg states are partially field ionized by the spectrometer field. A tandem spectrometer as described in detail in Ref. 3 was used in order to reduce the background. Fig. 1 shows a spectrum from 100 MeV Ne^{6+} incident on a He gas target. The spectrum shows a decrease in the total yield with increasing field strength and a superimposed oscillatory structure. The differential yield curves are plotted in the inset. An attempt is made to qualitatively interpret the results on the basis of a model which has been outlined recently² for foil excited ion beams.

In the case of beam foil excitation it was found² that the high Rydberg states may include coherently excited superpositions of Stark levels. These levels have been inferred from the observation of an oscillatory structure superimposed on the electron yield curves as they result from the field ionization of the high n states. An approximate value for the threshold field is given by $n^4 \cdot F_c / Z^3 = 1/16$ a.u.; this is the assumed threshold field for ionization of one-electron atoms or ions by a static electric field. From the relationship for the thresh-

old field it follows for a core charge 6^+ that principal quantum numbers for the field ionized Rydberg states are in the range between $100 < n < 150$. The lower limit corresponds to the spectrometer field required to analyze beam-velocity electrons

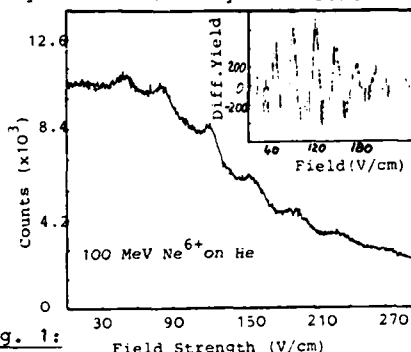


Fig. 1: Total and differential electron yield from field ionized fast Rydberg atoms as function of field strength (transverse field after target).

The main observable period in the spectrum is about 30 V/cm. This period cannot be reproduced with predictions based on the model given in Ref. 2 for the case of foil excited ions. This disagreement suggests a modification of the model. A time differential measurement could in general show oscillations if the orbital frequency is comparable with the interaction time. A possible picture is that the "beats" are due to field induced oscillation of the population of continuum and Rydberg states.

- ¹) E.P. Kanter, D. Schneider, Z. Vager, D.S. Gemmell, B.J. Zabransky, Gu Yuan-Zhung, P. Arcuni, P.M. Koon, D.R. Mariani, and W. Van de Water, Phys. Rev. A29, 583 (1983)
- ²) Z. Vager, B.J. Zabransky, D. Schneider, E.P. Kanter, Gu Yuan-Zhuang and D.S. Gemmell, Phys. Rev. Lett. 48, 592 (1982)
- ³) A. Iton, D. Schneider, T. Schneider, T.J.M. Zouros, G. Nolte, G. Schiwietz, W. Zeitz, N. Stolterfoht, Phys. Rev. A31, 538 (1985)

OPTICAL COLLISION SPECTRA FOR Na-Ar BY THE QUANTUM COUPLED-CHANNELS METHOD

F. Rebentrost

Max-Planck-Institut für Quantenoptik, D-8046 Garching b. München, West Germany

The absorption of nonresonant photons outside the impact region of a spectral transition occurs during collisions with the perturber gas. This correlation between the atomic excitation and the collision dynamics e.g. results in a breakdown of the factorization approximation known from the theory of collisional redistribution of light. Particularly interesting is the aspect of a spectroscopic investigation of the collision dynamics by the information contained in the intensity and polarization of the fluorescence after a far-wing excitation of collision pairs¹⁻³. In the limit of zero-perturber pressure the observables are directly related to the frequency-dependent optical collision cross sections.

Recently we have made much progress in developing the quantum methods to calculate optical collision spectra. This allows to perform such calculations for a large range of detunings and collision energies. As an example, Fig. 1 shows the thermal-averaged relative fluorescence intensity from the two D-lines following far-wing excitation of Na-Ar collision pairs. With respect to earlier results for a single collision energy⁴, the improvement is mainly in the red wing, that depends most sensitive on the energy requirement of the collision. Excellent agreement with experimental data reported by Havey et al.³ is found. From the analysis of

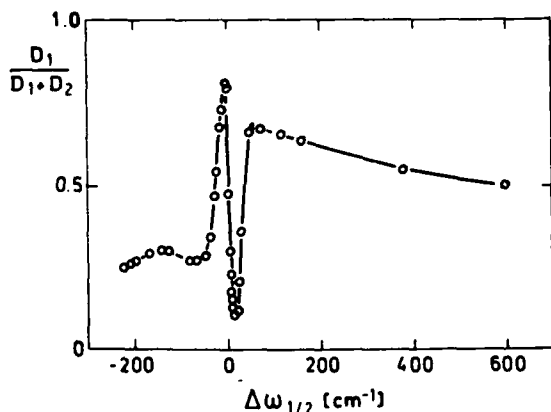


FIGURE 1 Calculated relative D_1 excitation probability (at $T = 400$ K) versus detuning from the Na- D_1 line.

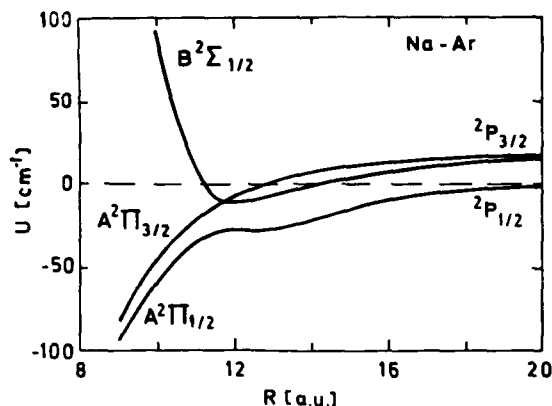


FIGURE 2 Long-range behaviour of the excited Na-Ar potentials after Dören et al.⁶.

the calculation a clear and quantitative picture is derived on the role of the various couplings that determine the final outcome of the collision during the dissociation of the collision pair. For example the behavior of the D_1 excitation probability at large detunings in the blue wing reflects the energy dependence of a nonadiabatic transition involving the $B^2\Sigma_{1/2}$ and $A^2\Pi_{1/2}$ states (Fig. 2).

A detailed discussion of fluorescence depolarization under single-collision conditions following from this calculation has been given recently⁵.

References

1. P. Thomann, K. Burnett and J. Cooper, Phys.Rev.Lett. 45, 1325 (1980).
2. V. Kroop and W. Behmenburg, Z.Phys. A294, 299 (1980); W. Behmenburg and V. Kroop, J.Phys.B 14, 427 (1981).
3. M.D. Havey, G.E. Copeland and W.J. Wang, Phys.Rev. Lett. 50, 1767 (1983).
4. K.C. Kulander and F. Rebentrost, Phys.Rev.Lett. 51, 1262 (1983); J.Chem.Phys. 80, 1767 (1984).
5. W. Behmenburg, V. Kroop and F. Rebentrost, J.Phys B in print (1985).
6. R. Dören, E. Hasselbrink and G.E. Moritz, Z.Phys. A 307, 1 (1982).

FAR INFRARED ABSORPTION IN H_2 , AND IN MIXTURES OF H_2 WITH He, N_2 , CH_4 , Ar,
INDUCED BY BINARY COLLISIONS*

Lothar Frommhold, Aleksandra Borysow, Massimo Moraldi,**
Physics Department, University of Texas at Austin, TX 78712,
Wilfried Meyer,
Fachbereich Chemie, Universität Kaiserslautern, F.R.G.,
and George Birnbaum,
National Bureau of Standards, Gaithersburg, MD 20899.

Hydrogen (H_2) and helium (He) are non-polar and do not have an infrared dipole spectrum unless some perturbation induces one. In H_2 -X collisions, where X may be He or another H_2 , transient dipoles occur which give rise to collision-induced infrared absorption in the far infrared. Translational and rotational spectra are observed which are known for some time. We present here the first ab initio computations of the induced dipole components obtained with highly correlated wavefunctions,¹ for both systems, H_2 - H_2 and H_2 -He. The most important induced dipole components arise from polarization of the collisional partner in the quadrupole field of the H_2 molecule, and for H_2 -He collisions an isotropic dipole component due to electron exchange. Weak dispersion dipoles are also evident, as well as anisotropic overlap and hexadecapole-induced components. Based on these calculations, and on accurate semi-empirical interaction potentials, we compute the far infrared translation/rotation absorption spectra of these systems at the temperatures from 77 to 300 K for which accurate measurements of such spectra exist. For H_2 - H_2 , the comparison of the ab initio line shape computations with the measurements shows agreement from 0 to $1,500\text{ cm}^{-1}$ at the $\pm 5\%$ level, on an absolute intensity scale, no adjustable parameters are used. For H_2 -He, the agreement with the measurements is nearly as good.^{1,2} The successful computation of these spectra from the fundamental theory is significant for the modeling of the atmospheres of the outer planets, which is possible with precision even at the low temperatures of the outermost planets for which no laboratory measurements exist.¹⁻³

The binary spectra of other systems, such as H_2 - N_2 and H_2 - CH_4 , can at present not be modeled with comparable rigor because the interaction potentials are not so well known, and no ab initio dipole calculations exist; no laboratory spectra were obtained for the H_2 - N_2 system in the far infrared. These systems are of interest for the interpretation of the Voyager IRIS spectra of Titan. We present quantum calculations of our best estimates of these spectra. The computations are based on pure quadrupole, octopole and hexadecapole induction.⁴ Interesting theoretical dimer features are obtained which

may help to understand unexplained features of the Voyager Titan spectra near the $S_0(0)$ line center of hydrogen. These features have attracted special attention recently. Dimer structures in H_2 - N_2 are similar, but different from the structures of the hydrogen dimer ($(H_2)_2$) seen in Jupiter and Saturn's atmosphere.⁵ The hydrogen dimer features involve the $1=2$ and $1=3$ scattering resonances of the free pair.

Other systems of interest for Titan's atmosphere are, of course, N_2 - H_2 and H_2 -Ar which we will also consider.⁴ For the first time, collision-induced rotational spectra are obtained for these systems with the help of a quantal formalism which accounts for the anisotropy of the interaction potential.⁶ All previous work was done with isotropic potentials and the role of the anisotropy was not well understood. Especially for nitrogen the anisotropy is considerable, and the systematic investigation of the role of the anisotropy for collisional induction has just been tackled.

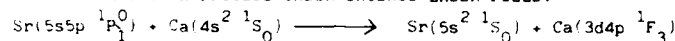
*The support of the National Science Foundation, grant AST-8310786 is gratefully acknowledged.

**On leave from the Physics Department, University of Florence, Italy.

References

1. W. Meyer, L. Frommhold, G. Birnbaum, in preparation.
2. G. Birnbaum, S.-L. Chu, A. Dalgarno, L. Frommhold, E.L. Wright, Phys. Rev. **A20**, 595 (1984).
3. J. Borysow, L. Trafton, L. Frommhold, G. Birnbaum, Astrophys. J., submitted.
4. A. Borysow, L. Frommhold, in preparation.
5. L. Frommhold, K. Samakia, G. Birnbaum, Astrophys. J., **261**, L79 (1984).
6. M. Moraldi, L. Frommhold, W. Meyer, in preparation.

TRANSITION PROCESS UNDER INTENSE LASER FIELD:



Hideki Yagisawa

Division of General Education, Takachiho University
2-19-1 Omiya, Suginamiku, Tokyo

A large amount of studies concerning laser induced collision energy transfer (LICET) have been made both experimentally¹ and theoretically². The cross section of this LICET process increases linearly with the field intensity when it is weak as is understood by the perturbation theory. It, however, decreases with large intensity beyond a certain value. Here we report the relations of total cross section with the field intensity and relative velocity for strontium and calcium atomic system.

The system is simplified to have three states:

$$|f_1\rangle = |A_2\rangle|B_1\rangle, |f_2\rangle = |A_1\rangle|B_2\rangle \text{ and } |f_3\rangle = |A_1\rangle|B_3\rangle$$

where A_1 and B_3 are atomic states shown in Fig.1. The coupled equations are

$$i\hbar \frac{d}{dt} c_k = \sum_j U_{jk} \exp(i\omega_{jk}t) c_j$$

with c_j the coefficient of the state $|f_j\rangle$, U_{12} = dipole-quadrupole interaction, U_{23} = dipole-field interaction, $\omega_{jk} = 0$ and ω_{jk} the energy difference divided by Planck's constant.

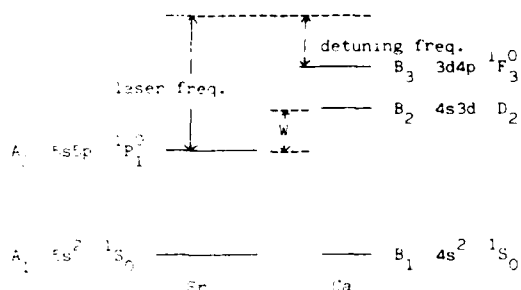


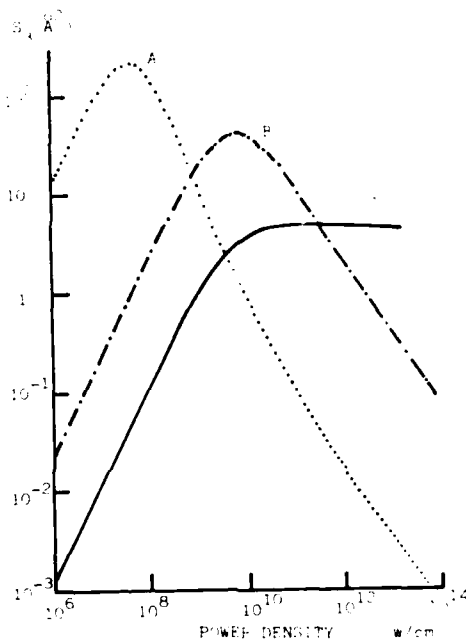
FIGURE 1 Energy diagram of the system

By the method proposed previously³ the cross section S_3 of the transition from $|f_1\rangle$ to $|f_3\rangle$ is obtained as

$$S_3 = 0.314(2Wv^2g)^{1/10} v\omega_{23}^{-1.5} \ln(Q),$$

$$Q = 3.14gv^{-1} L_0^{-3} \text{sqrt}(1+Q), \quad L_0 = (2Wv^2g)^{1/10} U_{23}^{-1/2}$$

and Q is a effective frequency (dimensionless) and is too complicated to be explained here. In the expression above v is the relative velocity, L_0 is a impact parameter to make Q zero and g is the constant part of dipole-quadrupole interaction U_{23} .

FIGURE 2 Several examples of S_3 , A: $v=10^3$ cm/sec, B: $v=10^5$ cm/sec and C: $v=10^7$ cm/sec.

At large limit of U_{23} the cross section S_3 roughly changes as

$$S_3 \propto U_{23}^{-1.5} v^{6/5}.$$

A few examples are shown in Fig.2. In these cases we did not consider the detuning frequency effect which is controversial in that theoretical works differ from experiments. Our method produces same result with other theoretical works.

References

1. S.E.Harris et al, Atomic Physics 7, D.Kleppner and F.M.Pipkin, eds. (1981), Plenum (Proceeding of VII-th International Conference of Atomic Physics), pp. 407-428, and references therein.
2. L.I.Gudzenko and S.I.Yakovlenko, Sov.Phys. JETP **35**, 877(1972).
3. H.Yagisawa et al, Phys. Rev. A **29**, 2479(1984).

LASER ASSISTED CHARGE TRANSFER REACTIONS IN SLOW ION-ATOM COLLISIONS:
COUPLED DRESSED QUASIMOLECULAR-STATES APPROACHES*

T. S. Ho,[†] C. Laughlin[‡] and Shih-I Chu[§]

[†]Department of Chemistry, University of Kansas, Lawrence, Kansas 66045

[‡]Mathematics Department, University of Nottingham, Nottingham, England

[§]Joint Institute for Laboratory Astrophysics, University of Colorado and
National Bureau of Standards, Boulder, Colorado 80309 USA

Semiclassical coupled dressed-quasimolecular-states (DQMS) approaches will be presented for the non-perturbative treatment of charge transfer reactions at low collision velocities and high laser intensities. The DQMS are first obtained via the Floquet theory.¹ The laser assisted collision process can then be treated as the electronic transitions among the DQMS driven by the nuclear motion only. The expansion of the total electronic wave function in a truncated DQMS basis results in a set of coupled adiabatic equations. The adiabatic DQMS and their associated quasienergies (depending parametrically upon the internuclear separation R) exhibit regions of avoided crossings, where the electronic transition probabilities are large due to strong radial couplings induced by the nuclear movement. By further transforming the adiabatic DQMS into an appropriate diabatic DQMS representation, defined via the vanishing of the aforementioned radial couplings,² we obtain a new set of coupled diabatic equations which offer computational advantage.³ The method will be illustrated by a case study of the laser assisted charge exchange process $\text{He}^{++} + \text{H}(1s) + h\nu \rightarrow \text{He}^+(n=2) + \text{H}^+$, in a two-state approximation, for the velocity range from 1.5×10^5 to 2×10^7 cm/s and for the laser intensity in the range of 0.4 to 4.0 TW/cm².

Also to be presented is a further extension of the coupled DQMS approach, incorporating the implementation of the generalized Van Vleck (GVV) perturbation theory.⁴ The GVV technique allows block partitioning of the infinite dimensional Floquet Hamiltonian to a finite-dimensional model DQMS space, thereby reducing greatly the number of coupled channels for more complex systems. Furthermore, the GVV-Floquet basis minimizes the part of the radial coupling matrix that is provoked

mainly by the resonant laser field, yielding a new set of coupled equations (neither adiabatic nor diabatic) which provides additional advantages for multi-channel calculations. The coupled GVV-DQMS approach has been recently applied successfully to a detailed study of the laser-assisted process: $\text{Li}^{+3} + \text{H}(1s) + h\nu \rightarrow \text{Li}^{+2}(n=3) + \text{H}^+$, using the two-, five-, and 15-DQMS basis. It is found that while the five-state results agree well with the 15-state calculations even up to very high intensities ($I \leq 100$ TW/cm²), the two-state model is much less satisfactory at high intensity and lower wavelength regimes, indicating the importance of including sufficient channels in the treatment of complex charge-exchange reactions in the presence of laser fields. Our coupled DQMS studies further reveal new dynamical features for the first time such as the nonlinear dependence of the charge-exchange cross sections upon laser intensity and impact velocity, etc. Detailed results will be presented.

*Supported by DOE and ACS-PRF.

[†]JILA Visiting Fellow (1985). Permanent address: Dept. of Chemistry, Univ. of Kansas, Lawrence, Kansas 66045.

References

1. For a recent review, see S. I. Chu, Adv. At. Mol. Phys. **21**, xxxx (1985).
2. F. T. Smith, Phys. Rev. **179**, 111 (1969); T. G. Heil and A. Dalgarno, J. Phys. B **12**, L557 (1979).
3. T. S. Ho, S. I. Chu and C. Laughlin, J. Chem. Phys. **81**, 788 (1984).
4. B. Kirtman, J. Chem. Phys. **49**, 3890 (1968); P. R. Certain and J. O. Hirschfelder, J. Chem. Phys. **52**, 5977 (1970).
5. T. S. Ho, C. Laughlin and S. I. Chu, Phys. Rev. A (submitted).

SATELLITE SPECTRA IN LASER ASSISTED CHARGE TRANSFER COLLISIONS

Y. P. Hsu and R. E. Olson

Department of Physics, University of Missouri-Rolla, Rolla, MO 65401 USA

A six-state coupled-channel calculation using the molecular-state expansion method has been performed on the laser-assisted charge transfer reaction $H^+ + Na + H(n=2) + Na^+$. We have used a collision velocity of 0.002 a.u. and a laser power density of 1 GW/cm^2 in the calculations. The computational method has been described in detail in a previous paper.¹

The potential energy curves of the Born-Oppenheimer molecular states of NaH^+ are shown in Fig. 1. For the laser frequency range of interest, the main charge transfer contribution comes from $1\bar{2}-2\bar{2}$ transitions, with a secondary contribution coming from $1\bar{2}-5\bar{2}$ transitions. At low collision velocity, the transitions will mainly take place around the stationary points where the photon energy matches the difference potential between initial and final states. The difference potentials between $1\bar{2}$ and $2\bar{2}$ and between the $1\bar{2}$ and $5\bar{2}$ states are shown in Fig. 2. Note that the ϵ_{21} curve has an extremum at $R_s = 13.82 \text{ a.u.}$, the satellite point, with a magnitude of $\epsilon_{21}(R_s) - \omega_s = 0.0473 \text{ a.u.}$ For a laser frequency of $\omega_1 > \omega_s$, there exists two stationary points, R_{ca} and R_{cb} , while for $\omega_2 < \omega_s$, there exists no stationary point. A greatly enhanced cross section is realized for $\omega \gtrsim \omega_s$, due to the coherence effect of

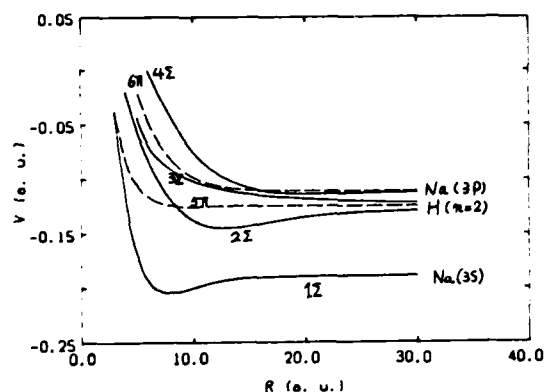


Figure 1

The computed charge transfer cross section to the $2\bar{2}$ state is represented by triangles in Fig. 3, where it is plotted against applied laser frequency. The dashed line in the same figure represents a Sando-Womhoudt type approximation² while the dot-dashed line represents a Uniform Stationary Phase Approximation.³ These two approximations are based on an expansion of the phase integral around the stationary

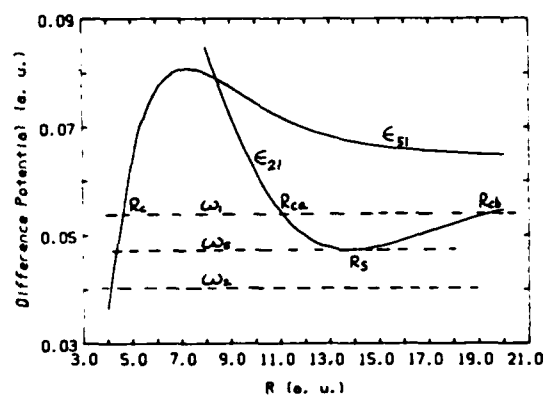


Figure 2

points and enjoy some success in explaining the satellite spectra in molecular emission. They produce unsatisfactory results here. A new expansion about the satellite point, the results of which are represented by the solid line in Fig. 3, fit the data well. The details of the calculations will be presented at the conference.

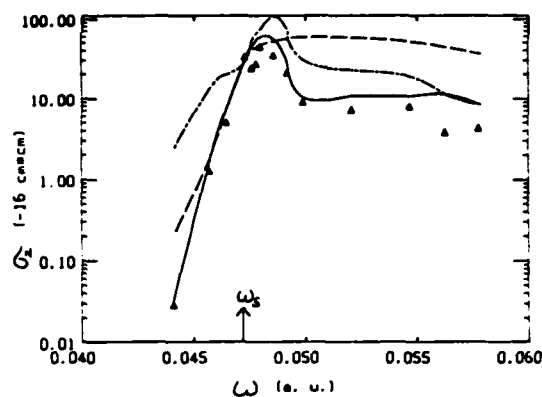


Figure 3

Work supported by the Office of Fusion Energy, U.S. Department of Energy.

References

1. Y. P. Hsu, M. Kimura and R. E. Olson, Phys. Rev. A31, 576 (1985).
2. K. M. Sando and J. C. Womhoudt, Phys. Rev. A7, 1889 (1973).
3. See R. J. Bienie and T. J. Streeter, Phys. Rev. A28, 3328 (1983) and related references.

NON-LINEARITY AND PHOTON CORRELATION IN LASER-ASSISTED CHARGE TRANSFER IN HELIUM

S. Ganguly, K. Rai Dastidar and T. K. Rai Dastidar,
Indian Association for the Cultivation of Science, Calcutta 700032, INDIA

recently¹ we demonstrated theoretically the effect of a single-mode laser field on He⁺-He charge transfer collision. In the present work we include the following two effects not considered earlier :

(i) Photon correlation effect due to a finite bandwidth of the laser, which is supposed to be "on" during the entire collision process, and

(ii) Non-linearity effect due to multiple-photon emission/absorption by the colliding system.

Within the impact parameter formalism, the coupled equations for a two-state quasi-molecular diabatic representation^{1,2} are set up in the form

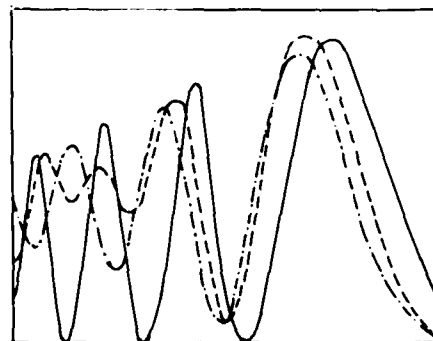
$$\frac{d}{dt} A_i^r(t) = -\sqrt{\frac{2\pi}{c}} D_{ij}^{-1} \left[A_i^{r-1} \int_{\omega_0-\delta/2}^{\omega_0+\delta/2} \frac{\sqrt{I(\omega)}}{\omega} e^{-i\omega t} dt' \right. \\ \left. + A_i^{r+1} \int_{\omega_0-\delta/2}^{\omega_0+\delta/2} \frac{\sqrt{I(\omega)}}{\omega} e^{i\omega t} dt' \right] \times \text{phase factor}$$

Here A_i^r is the occupation coefficient of the i -th state with r photons absorbed from the field, $D_{ij} = \langle \vec{r} | [\vec{r}, H_{el}] | j \rangle$, and $I(\omega)$ is the frequency distribution of the intensity centered around ω_0 with a bandwidth δ . t_0 marks the instant at which the boundary conditions on A are known. Linear polarization along \vec{e} is assumed. Note that the rotating-wave approximation used earlier¹ has been dispensed with.

Putting $\sqrt{I(\omega)} \sim E(\omega)$ and taking the frequency denominator out of the ω -integral, we find that the latter gives, as an inverse Fourier transform, the electric field with the first-order photon correlation built in as determined by the frequency distribution $I(\omega)$. Assuming a Gaussian lineshape, we solved the equations for values of r upto 1,2,... till 'saturation' i.e. the full non-linear photon emission/absorption effect showed up in the charge transfer probability, which is obtained by summing over all r .

Representative results showing the onset of saturation on the charge transfer probability

are shown in the figure. The effect of increasing the bandwidth (upto 50 Å) is found to be marginal and undetectable in the scale of the figure. We wish to present detailed results of the laser field effect upon the charge transfer cross-section at the conference.



Impact parameter times charge transfer probability plotted vs impact parameter. Laboratory ion energy = 300 eV. Full-line curve, field-free results; broken line, single-photon emission/absorption; chain line, nonlinear (saturation) emission/absorption at a wavelength of 5000 Å and intensity 1×10^{14} W/cm², with \vec{e} chosen parallel to the particle trajectory.

References

1. S. Ganguly, K. Rai Dastidar and T. K. Rai Dastidar, Phys. Rev. A (to be published)
2. T. K. Rai Dastidar and K. Rai Dastidar, Chem. Phys. Letts. **85**, 229 (1982)

COMPARISON OF Na^+ ION PRODUCTION IN 100-2000 eV $[\text{He}^+/\text{Ar}^+] + \text{Na}(3s, 3p)$
COLLISIONS USING CROSSED LASER, ION AND ATOM BEAMS

C. R. Hummer, A. Berlin and W. W. Smith

Department of Physics, University of Connecticut, Storrs, Connecticut 06268

We have constructed a crossed beam apparatus, shown schematically in Figure 1, for studying ion-atom collisions with laser-excited atoms. The apparatus incorporates time-of-flight mass analysis to identify the product ion species and uses a commercial single-mode ring dye laser to provide strong steady-state excitation of the Na atoms at 589 nm on the $F=2$ to $F=3$ hyperfine transition. To date we have obtained data using He^+ and Ar^+ projectiles on a beam of Na atoms.

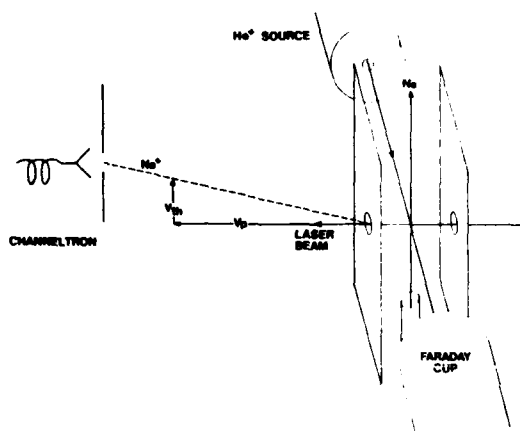


FIGURE 1 Schematic of triple crossed-beam apparatus for studying ion-beam collisions with a laser-excited atomic beam under single-collision conditions. A low-energy 100eV - 1000eV ion beam intersects the polarized laser beam and perpendicular atomic beam, between a pair of parallel electrodes. A 30-volt pulse is used to collect the accumulated slow target ions.

Preliminary data for 250 and 500 eV $\text{He}^+ + \text{Na}$ suggest that laser excitation to the 3p state with circularly-polarized light perpendicular to the incoming ion beam reduces the Na^+ ion production signal relative to the 3s state signal with the laser off. This effect is particularly clear at 250 eV and is less pronounced at 500 eV. We are presently continuing these measurements at lower energies and making a systematic study of $\text{Ar}^+ + \text{Na}(3p)$ collisions as well.

The laser was locked to the peak of the fluorescence from the sodium beam by using a slow feedback loop. An error signal is fed back to the laser, to center the frequency of the laser to the peak of the fluorescence. This technique was used by Prof. Hertel's group at Berlin in a similar study of $\text{Na}^+ + \text{Na}$ collisions.¹

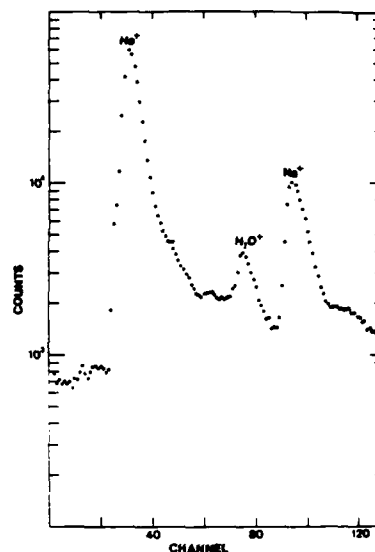


FIGURE 2 Time-of-flight spectrum of the ions produced in the present experiment (with laser off). The spectrum shows a large helium peak caused by resonant charge transfer and a peak from water. Both of these gases are present in the chamber as a background gas. It is also seen that a peak due to sodium is well resolved.

On the basis of level-matching considerations and prior energy loss studies², it seems reasonable to assume that the primary production mechanism for slow Na^+ ions is $\text{He}^+ + \text{Na} \rightarrow \text{He}(1snl) + \text{Na}^+$ quasi-resonant charge transfer rather than direct ionization at the energies we are using. The present experiment does not determine the state of the helium atom after the charge exchange collision. It is expected, however, that a large portion of these atoms are in the 2^3S or higher states as shown by Reynaud et al. We are in the process of performing further experiments to pin down the collision mechanism in more detail. Preliminary indications show variations in the slow ion signals depend on the laser polarization. These alignment/orientation effects on the charge-transfer process are being studied systematically.

References

1. C. Reynaud, et al., Phys. Rev. Lett. 43, 579 (1979).
2. A. Bähring et al., Z. fr Phys. A 312, 293 (1983). This work was supported by the National Science Foundation and the Univ. of Connecticut Research Foundation.

CHARGED PARTICLE SCATTERING IN STRONG STOCHASTIC RADIATION FIELDS

R. Daniele⁺, G. Ferrante⁺, F. Morales^o and F. Trombetta⁺⁺ Istituto di Fisica della Facoltà di Scienze, via Archirafi 36, 90123 Palermo, Italy.^o Istituto di Fisica della Facoltà di Ingegneria, Parco d'Orleans, 90128 Palermo, Italy.

In this work we consider the theory of charged particle scattering by a static potential in the presence of strong Markovian stochastic radiation fields. Two models of such are considered: (a) the phase diffusion model (PDM), in which the field undergoes only phase fluctuations, it corresponding to an intensity-stabilized single mode laser; and (b) the chaotic field model (CH), in which the field undergoes both amplitude and phase fluctuations, it corresponding to a pulsed multimode laser with a large number of uncorrelated modes.

The scope of this work is two-fold: (i) to learn how are changed the cross sections in comparison with those obtained within the ideal, single mode model of a radiation field; and (ii) to investigate the role of the field statistical properties in highly nonlinear domains of particle-field interaction. The consideration of the statistical properties of strong radiation fields adds a new dimension of the field-assisted collisions, as in several cases the field is treated exactly, at all orders. Investigations on this aspect of field-assisted collisions are only at their beginning¹⁻⁵. Specifically we report on

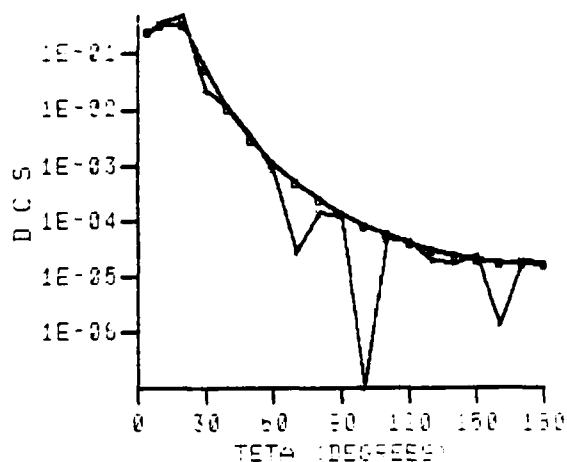


FIGURE 1 Differential cross sections ($\pi a_0^2 \text{ ster.}^{-1}$) vs the scattering angle. Single mode field (lower curve), chaotic field with bandwidth $\Delta\omega = 0$ (upper curve). $n = 1$ photon exchanged.

field-assisted electron scattering by a screened coulomb potential, treated in the first order of the scattering potential. Figs 1 and 2 anticipate some of the results which will be presented at the Conference. The incident particle beam energy is taken $\epsilon_i = 100$ eV, the laser photon energy $\hbar\omega = 1.17$ eV, the field intensity $I = 10^{13}$ W/cm²; the field bandwidth is chosen such that the ratio $\Delta\omega/\omega \approx 0$ and 10^{-3} .

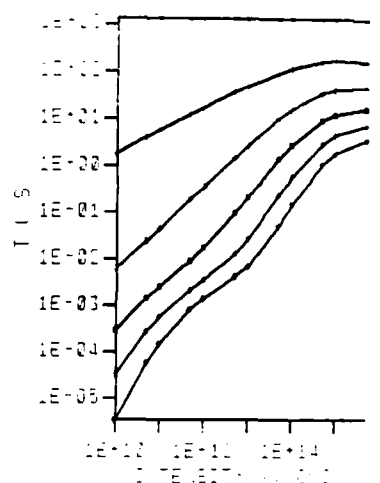


FIGURE 2 Total cross sections (πa_0^2) vs the laser intensity. Chaotic field case for n photon exchanged.

References

1. P. Zoller, J. Phys. B: At. Mol. Phys. **13**, L249, 1980.
2. R. Daniele and G. Ferrante, J. Phys. B: At. Mol. Phys. **14**, L635, 1981.
3. R. Daniele, F.H.M. Faisal and G. Ferrante, J. Phys. B: At. Mol. Phys. **16**, 3831, 1983.
4. F. Trombetta, C.J. Joachain and G. Ferrante, in: Collisions and Half-Collisions with Lasers, eds C. Guidotti and N.K.H. Rahman (London: Harwood), 1984.
5. F. Trombetta, G. Ferrante, K. Wodkiewicz and P. Zoller, "Field Correlation Effects in Laser Assisted Electron Scattering. The Phase Diffusion Model", J. Phys. B: At. Mol. Phys. (in press).

ELECTRON ATOM SCATTERING IN THE FIELD
OF A SYMMETRIC MODE LOCKED LASER*

Marvin H. Mittleman

Physics Department, The City College of New York
New York, NY 10031

When an electron scatters from an atom near the forward direction the cross section is essentially determined by the long range potential. For spherically symmetric atoms this is the polarization potential $\sim r^{-2}$. If the experiment takes place in a laser field then the atom is polarized by the laser and this induces an oscillating dipole and a permanent quadrupole potential in the electron-atom interaction. The forward scattering is then greatly enhanced. If the laser is nearly resonant with an allowed transition in the atom the effect occurs even when the laser is weak.¹ (A few W/cm² is enough to saturate a typical transition.) If the laser is not resonant it has to be more intense for the effect to occur.²

Little has been done in this context with lasers which are not "ideal" (i.e., single mode and constant amplitude) but one could deal with chaotic lasers by well established techniques.³ Perhaps a more interesting case is that of mode-locked lasers in which the beating among the modes results in a laser intensity which can have sharp temporal spikes and thereby affect the atom more intensely. Asymmetric-mode-locked-laser of the form

$$E = (E_0 + \sum_{n=1}^N E_n \cos(n\omega t)) \cos(\omega t + \theta) \quad (1)$$

is a special case in which the two-state rotating-wave-approximation wavefunctions can be obtained analytically for small detunings.⁴ For the simplest case, $N=1$, the time averaged probability of finding the excited P state is

$$P_{ex} = \frac{1}{2} \left(1 - \frac{\Delta\omega^2 J_0^2(\frac{\Lambda_1}{n})}{\Delta\omega^2 J_0^2(\frac{\Lambda_1}{n}) + \Omega^2} \right) \quad (2)$$

where the quantities are defined as follows: $\Delta\omega$ is the detuning of the central mode of (1) from resonance and we assume

$$|\Delta\omega| \ll n. \quad (3)$$

$\Lambda_i = d \cdot E_i$ ($i=0,1,\dots,N$) and d is the dipole moment connecting the two states. v is the integer closest to $(-\Lambda_0/n)$ and we have also assumed that

$$\Omega = (\Lambda_0 + vn) \ll n. \quad (4)$$

Examination of (2) shows a resonance-like behavior of P_{ex} as a function of the (central) laser frequency, or more interestingly, as a function of laser intensity via Ω .

Forward elastic scattering of the electron acts as a probe of the P component of the atom so the cross section will be a rapidly varying function of laser frequency and amplitude. If fluorescence is neglected, if the final atomic state is not observed, and if the fine structure of the energy distribution of the electron (on the scale of n) is also not observed, then the cross section is proportional to P_{ex} and exhibits the resonance structure found there.

References

1. J.I. Gersten and M.H. Mittleman, Phys. Rev. A 13 123 (1976)
2. F.W. Byron Jr. and G.J. Joachain, J. Phys. B 17 L295 (1984)
3. R. Daniele, F.H.M. Faisal and G. Ferrante, J. Phys. B 16 3831 (1983)
4. M.H. Mittleman, Phys. Rev. A _____

*This research was supported by a contract with the U.S. Office of Naval Research.

DIRECT RADIATIVE RECOMBINATION IN A HYDROGENIC NON-MAXWELLIAN LASER-PLASMA

M. Lamoureux⁺, C. Möller⁺, R. Yin⁺⁺, J. P. Matte⁺⁺⁺ and J. Delettrez^{****}⁺ LSAI, Bât. 350, Université Paris-Sud, 91405, Orsay, France.⁺⁺ Department of Physics, University of Pittsburgh, Pittsburgh, PA 15260, USA.⁺⁺⁺ Institut National de la Recherche Scientifique-Energie, Université du Québec, CP 1020, Varennes, Québec, J0L 2P0, Canada.^{****} Laboratory for Laser Energetics, University of Rochester, 250 East River Road, Rochester, NY 14623, USA.

Direct Radiative Recombination emission is evaluated in a hydrogenic Be plasma which exhibits a strongly non-Maxwellian character due to the inverse bremsstrahlung heating by a Nd laser. The non-Maxwellian electron distribution functions have been obtained from a Fokker-Planck simulation by Matte et al.¹, and the resulting DRR emissivity coefficients are shown in the figure for three positions along the laser direction with electron densities lower than the critical density $n_c = 10^{21}$ e/cc (i. e. where the laser penetrates and the Maxwellian equilibrium is perturbed). The predicted spectra are obviously strongly non-Maxwellian, though not to the point as when electron-electron collisions are neglected². The fact that the slope is not constant invalidates the traditional temperature diagnostic $d \ln J_\omega(M_\omega) / d(M_\omega) = -1/kT_e$. The deduced temperature would be overestimated by an order of magnitude right at the 1s threshold, and is exact within 50 % for photon energies larger than 2 keV above that threshold. We also evaluate the polarization of the DRR emission caused by the anisotropy of the electron distribution; the degree of polarization appears to be significant only at large photon energies.

References

1. J. P. Matte, T. W. Johnston, J. Delettrez and L. L. McCrory, Phys. Rev. Letters, **53** 1461 (1984)
2. M. Lamoureux, C. Möller and P. Jaeglé, Phys. Rev. A **30**, 429 (1984)

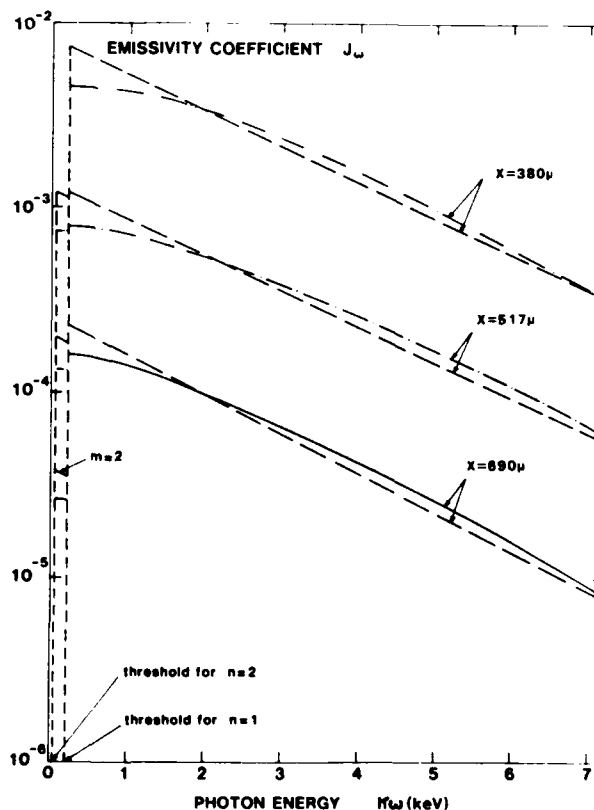
Acknowledgment

We are grateful to Drs R.H. Pratt and P. Jaeglé for having made it possible for R. Yin to visit LSAI at Orsay in the fall 1984.

Figure: Radiative recombination emissivity coefficients $J_\omega(M_\omega)$ in $J m^{-3}$ (per steradian and polarization mode) as a function of photon energy M_ω for three positions along the laser direction¹.

(—) : $X = 690\mu$, $N_e = 0.16 N_c$, $T_e = 2.07$ keV;
 (- -) : $X = 517\mu$, $N_e = 0.40 N_c$, $T_e = 2.27$ keV;
 (- . -) : $X = 380\mu$, $N_e = 0.97 N_c$, $T_e = 2.24$ keV.

The dashed lines correspond to the Maxwellian results for the same N_e , T_e values.



RADIATIVE ELECTRON-ATOM COLLISIONS IN A STRONG LASER FIELD

F.H.M. Faisal

Fakultät für Physik, Universität Bielefeld, Fed. Rep. Germany

This paper is concerned with a number of problems in the theory of electron-atom collision in a strong radiation field (a laser field). Higher energy "off-shell" excitations of atoms by the simultaneous electron-photon collisions are considered for the H and the He atoms. Comparison of the results support the view that atoms with the higher dipole polarizabilities are to be preferred for the higher "off-shell" signals. In the presence of a laser field the distribution of the states of the target atoms is generally driven far away from the thermal equilibrium. The problem of the initial distribution for the electron scattering is examined from the point of view of the steady-state beam experiments. An explicit distribution in the presence of the losses due to the field induced ionization and the transit of the beam atoms is analyzed, the result compared with special cases, and the significance of a conjecture of Hertel et al. is pointed out. Some of the most dominant phenomena to occur during the radiative electron scattering at low energies ($E_i \lesssim \hbar\omega$) are discussed using a simple model referring to the e-H scattering. They include such effects as the "reflection" of the bound negative-ion state (H^-) in the scattering channel, the resonant-excitation of H with "subthreshold" electrons, and the possibility of photon amplification by resonant radiative scattering.

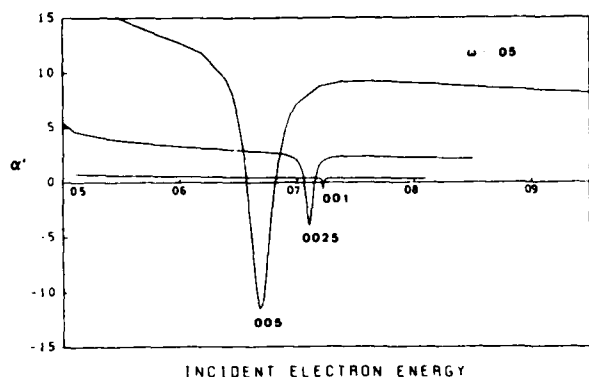


FIGURE 2 The photon-absorption coefficient $\gamma'(E_i)$ vs. the incident electron energy E_i for the radiative scattering of electrons with H atoms at $\omega = 0.05$ a.u. and three different field strengths $F_0 = 0.001, 0.0025$, and 0.005 a.u. Note that the negative absorption or the gain occurs resonantly. The scales are in a.u.

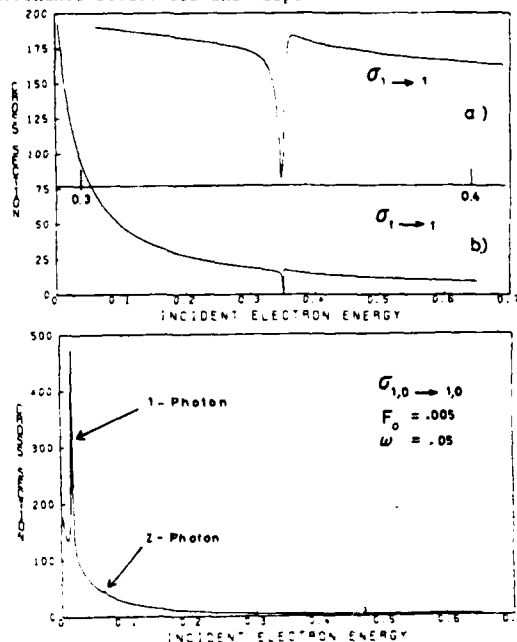
Electron-Hydrogen Scattering in a Laser Field
Resonance Structures and Cusps

FIGURE 1 Low-energy phenomena in radiative e-H scattering. Upper diagram: $\sigma_{1 \rightarrow 1}$ is model 1s-1s cross section at zero field. Inset is magnification of the 1s resonance at 9.558 eV (width ≈ 0.04 eV). Lower diagram: $\sigma_{1,0 \rightarrow 1,0}$ is 1s \rightarrow 1s cross section in presence of the field (with no net exchange of photons). $F_0 = 0.005$ a.u. ($I \sim 0.85 \times 10^{12}$ W/cm², $\omega = 1.35$ eV). Sharp structure at ~ 0.6 eV is one-photon resonance with H^- state (at ~ 0.75 eV). Small peak at ~ 1.95 eV is two-photon resonance with the H^- state. The scales are in a.u.

SIMULTANEOUS ELECTRON PHOTON EXCITATION OF HYDROGEN ATOM

R.S.Pundir* and K.C. Mathur

Department of Physics, University of Roorkee, Roorkee 247 667, INDIA

The 1s-2s excitation of hydrogen atom by simultaneous electron and laser photon impact is investigated in the framework of the time dependent perturbation theory. The laser-atom interaction is treated in the dipole plus quadrupole approximation.

The scattering amplitude for the joint excitation of H atom, in which only one photon is absorbed from the laser beam is given by¹ (a.u. are used)

$$F_{fi} = -4^{\frac{1}{2}} Q_0(z) d_1^{\frac{1}{2}} \sum_m (-m_g - 1)^{-1} f(0, m, m, H^{(0)}; g) + \sum_n (n_f + 1)^{-1} f(H^{(0)}; n, n, 0, g) \quad (1)$$

with $d_1^{\frac{1}{2}} = (q^{-2} \pm p^{-2})$, $\vec{q} = \vec{p}' - \vec{p}$

$$2(z) = J_0(z) \exp(i z \cos \theta_q), z = E_0 q \sin \theta_q^{-1},$$

$$m_g = m - g \text{ and } \theta = \exp(i \vec{q} \cdot \vec{r}_1)$$

F and G are the direct and exchange amplitudes m and n are the intermediate states with atomic frequencies ω_m and ω_n respectively. \vec{r}_1 is the position vector of the atomic electron θ_q and θ are the polar angles of \vec{q} , \vec{p} and \vec{p}' are the momenta of the incident and scattered electron. E_0 is the amplitude of the electric field of the laser and ω is the laser frequency. $H^{(0)}$ is the laser-atom interaction in the dipole plus quadrupole approximation². The laser is assumed to be circularly polarised.

To perform the sum over intermediate states in equation (1), we take 2p, 3p, 3d, 4p and 4d states explicitly and account for the remaining states through closure. We also perform a calculation using exact 2p state and 3p, 3d, 4p and 4d pseudostates³. The total cross section σ is given by

$$\sigma = \frac{d\sigma}{d\Omega} d\Omega \text{ where } \frac{d\sigma}{d\Omega} = \frac{p'}{p} \left[F + G^2 + \frac{3}{4} F - G^2 \right] \quad (2)$$

The wavelength variation of σ for the 1s-2s excitation of hydrogen atom at an incident electron energy of 100eV and at a laser intensity of $10^{14} \text{ W cm}^{-2}$ is shown in Fig.1. Curves P_1 and P_2 represent σ with closure and without closure respectively. Curve P_3 gives the results using pseudostates. From the figure we see that there is a considerable difference between P_1 and P_2 in the off resonance region (975-1005Å²) which shows that in this region the closure contribution is

significant. Near the resonance regions closure contribution becomes insignificant. We also notice that there are significant enhancements in σ in the region close to 970-975Å², 1023-1028Å² and 1210-1220Å². The increase in σ in these regions occurs because of (4p;4d), (3p;3d) and 2p resonant states respectively. The curve P_3 shows a gradual variation in σ from 965Å² to 1030Å². In the region away from resonances P_3 is in reasonable agreement with P_1 . In region 1210-1220Å², all curves P_1 , P_2 and P_3 give identical results showing that the dominant contribution comes from the 2p state which is taken exactly in all three calculations.

* Present address: Defence Electronics Applications Laboratory, Dehradun 248001, India

References

1. K.C.Mathur, IEEE J. Quant. Elect. QE-17, 2233(1981)
2. R.S.Pundir and K.C.Mathur, Phys. Lett. 95A, 149 (1983).
3. W.C. Fon, K.A. Berrington, P.G.Burke, A.E.Kingston, J. Phys. B14, 1041 (1981).

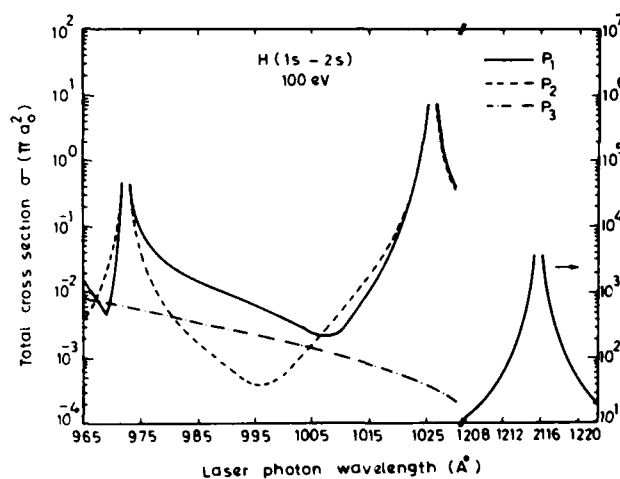


Fig. 1

THE INFRARED SPECTROSCOPY OF WEAKLY BOUND HYDROGEN CLUSTER IONS

L. I. Yeh, Mitchio Okumura, and Y. T. Lee

Materials and Molecular Research Division, Lawrence Berkeley Laboratory and
Department of Chemistry, University of California, Berkeley, California 94720 USA

We are studying the vibrational predissociation spectra of hydrogen cluster ions. Although very little spectroscopy has been done on cluster ions, cluster chemistry is important since clusters are a first approximation to the liquid phase. Because of their relatively few electrons, hydrogen cluster ions, in particular, are valuable as a test of *ab initio* theory. Yamaguchi, Gaw, and Schaefer have predicted *ab initio* structures and frequencies of H_5^+ , H_7^+ , and H_9^+ .¹

We have seen an absorption peak corresponding to an H-H stretching motion in the cluster ions H_n^+ ($n = 5, 7, 9, 11, 13, 15$). The agreement with theory is within 40 cm^{-1} after a term primarily due to anharmonicity is subtracted. It is unclear whether we are exciting a rotational band of the H-H stretch alone or the fundamental with a combination band.

The ions are created by supersonically expanding a beam of pure hydrogen followed by electron bombardment ionization. A sector magnet selects the desired ion mass which is directed into a radio frequency octupole trap. Here, tunable infrared light from a Nd:YAG pumped optical parametric oscillator interacts with the trapped ions. The fragment ions from dissociation then pass through a quadrupole and are detected. By computer scanning the OPO, and monitoring the fragment ion mass, we are able to see the absorption spectra.

Figure 1 shows the absorption spectra from H_9^+ dissociating to H_7^+ , H_5^+ , and H_3^+ . Several features are noteworthy. The three peaks are quite broad and may contain structure underneath. A small depletion peak is evident in the $H_9^+ \rightarrow H_7^+ + H_2$ spectrum. Its location corresponds to the H_7^+ absorption peak. It will be interesting to study the power dependence of the lower energy side of the $H_9^+ \rightarrow H_3^+ + 3H_2$ peak. It is not unrealistic that a multiphoton process could be responsible for the signal here. Another observation we have made is that the peak of the band shifts to higher energies with increasing cluster size. In H_5^+ , the peak is $\sim 250\text{ cm}^{-1}$ lower than that of free H_2 , whereas in H_{15}^+ , the peak is only $\sim 107\text{ cm}^{-1}$ lower.

There may be structure under our broad peaks. In order to see this, we will be repeating the experiments with a couple of modifications. Our current linewidth

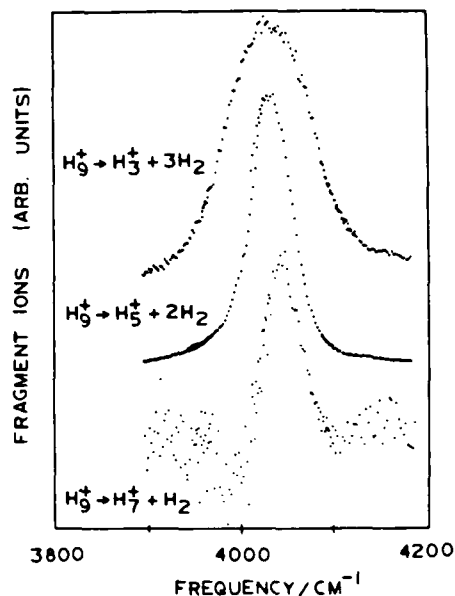


Fig. 1. Photodissociation spectra of H_9^+ detected by monitoring fragment ion signal for all three channels.

is $10\text{--}20\text{ cm}^{-1}$, whereas the rotational spacing in H_5^+ is approximately 7 cm^{-1} . One necessary change, then, is going to a narrower linewidth laser. We plan on using a difference frequency laser and an F-Center, which have linewidths of 0.2 cm^{-1} and less than 0.1 cm^{-1} respectively. Another improvement will be changing to a cooler ion source. The current one produces ions rotationally and vibrationally hot. We will be using a corona discharge source for the higher resolution experiments.

Reference

1. Y. Yamaguchi, J. Gaw, and H. Schaefer III, J. Chem. Phys. **79**, 4074 (1983).

Acknowledgment

This work was supported by the Director, Office of Energy Research, Office of Basic Energy Sciences, Chemical Sciences Division of the U.S. Department of Energy under Contract No. DE-AC03-76SF00094. LY acknowledges a National Science Foundation Fellowship.

PHOTOFRAGMENTATION OF MASS RESOLVED CLUSTERS OF Si_n^+

L.A. Bloomfield, R.R. Freeman, and W.L. Brown
AT&T Bell Labs, Murray Hill, NJ 07974

We have constructed an apparatus that produces, isolates and photofragments ionic clusters on a mass resolved basis. This apparatus has been used to determine the structure of small clusters of Si_n^+ and Ge_n^+ for n from 2 to 12. In addition, the structure of larger clusters (n up to 30) can be inferred from our data. A model of cluster formation based upon microcrystal fragments is found to be consistent with our data, especially when considerations of kinetics as well as stability are included.

The apparatus is shown in Fig. 1. The design makes use of a pulsed source of clusters, pulsed ionization and fragmentation lasers, and time-of-flight (TOF) techniques to isolate a given cluster size. The apparatus is cycled at 10 Hz, and the complete mass scan for each shot is accumulated by a 200 MHz transient digitizer. A pulsed mass isolator is installed half way down the TOF region, and operates as a fast valve, allowing only clusters with the mass of interest to proceed to the only fragmentation region where they are exposed to the beam of an intense photofragmentation laser. After irradiation, the resulting charged photofragments are reaccelerated and dispersed in the second half of the TOF region. The upper portion of Fig. 2 displays the fragmentation spectra obtained when Si_{12}^+ is isolated and photofragmented by a saturation fluence of 266 nm light.

The transient digitizer is programmed to record the fragmentation spectra for each cluster for each shot of the laser, and the signal in each fragmentation channel is subsequently analyzed as a function of laser intensity. A relative cross section for direct photofragmentation can be extracted for those channels that demonstrate a low intensity linear dependence of signal upon light intensity. A complete "family tree" for the breakup of any Si_n^+ at any intensity can be constructed by analyzing all of the data starting with Si_n^+ and working up to Si_n^+ .

The relative cross sections for photofragmentation at 532 nm of $\text{Si}_n^+ \rightarrow \text{Si}_m^+$ for $n=2$ to 12, and all $m < n$ are shown in Fig. 3. These values for a given n are found to be largely insensitive to

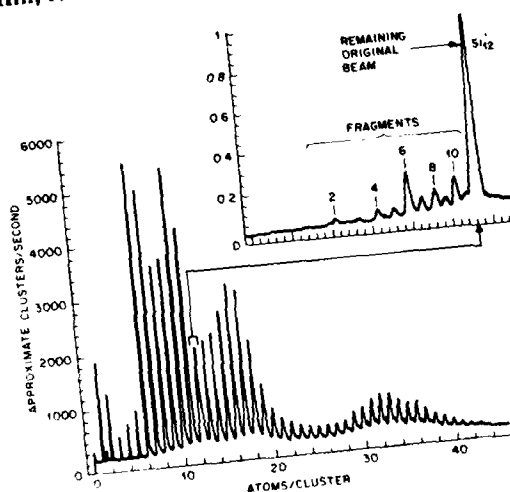


Fig. 2 Cluster production of Si_n^+ showing fragmentation of Si_{12}^+

Analysis of this photofragmentation data suggests that Si_n^+ clusters for $n=10$ and greater are micro-crystals, although for $n > 10$ there is now reason to believe that these clusters are not "grown", but are formed by stacking additions of $n=10$ and $n=6$ fragments.² Experiments on Ge, Sn, C and Pb are in progress to help unravel the mechanism of cluster formation in these network systems. Photofragmentation plays a crucial role in establishing the stable or "preferred" geometry of these clusters.

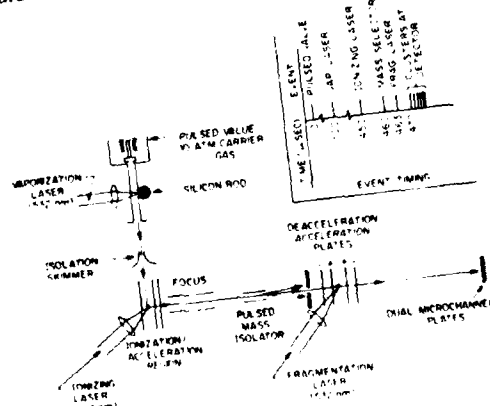


Fig. 1 Laser-based apparatus for cluster photofragmentation

the wavelength of the photofragmenting laser. Notice that the charge remains on the larger fragment, and that $n=6$ is a particularly prominent photofragment. We have also made total fragmentation cross section measurements for each cluster size. $n=6$ has the lowest cross section (absolute value $\sim 7(2) \cdot 10^{-18} \text{ cm}^2$) with other relative minima at $n=4$ and 10.

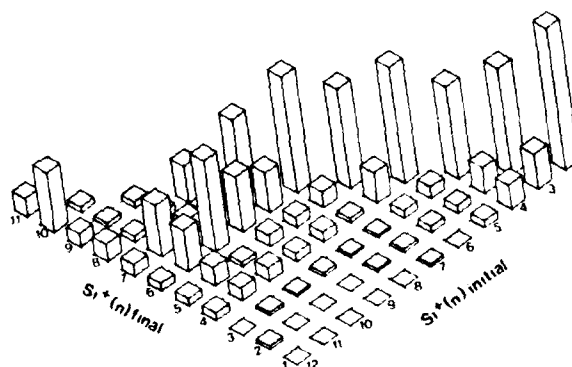


Fig. 3 Relative photofragmentation crosssections for Si_n^+

REFERENCES

- 1) J.B. Hopkins et. al, J. Chem. Phys. 78, 1627 (1983)
- 2) J.C. Phillips, unpublished

PHOTOFRAGMENTATION OF CLUSTER IONS OF CESIUM

Rolf Möller and Hanspeter Helm

Molecular Physics Department, SRI International, Menlo Park, CA 94025

In a fast beam (1-5 keV) we have studied photodissociation of cluster ions of cesium which we formed by field ionization¹ on a microscopic (40 μm) droplet of molten cesium. A Wien filter and two stages of energy analysis of the charged photofragments allows us to separate individual products from a single parent and also to photodissociate energy selected photofragments, uniquely defining the fragmentation pattern and the c.m. energy release in the dissociation event. Fig. 1 shows the wavelength dependence for photodissociation of Cs_n^+ into Cs_m^+ obtained by illuminating the entire parent beam with 50 mW CW laser beams. The parentage of a given feature in Fig. 1 can be unambiguously identified by operating the Wien filter in the parent beam line. The dominant contributions in Fig. 1 arise from product/parent mass ratios $m/n = 1/5, 1/4, 1/3, 2/5, 3/7, 1/2$, and $2/4$. The fragmentation patterns show a pronounced wavelength dependence.

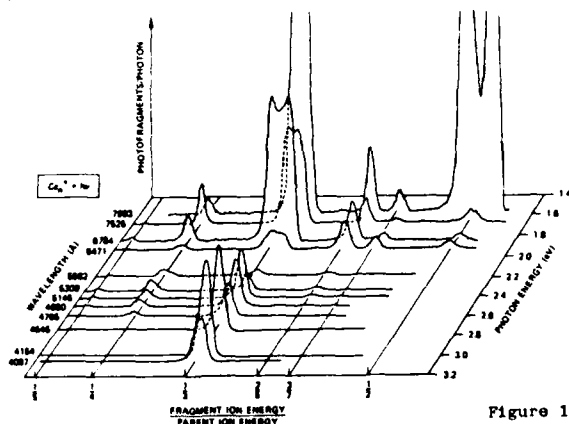


Figure 1

Photodissociation of the trimer ion to Cs^+ in the region between 8000 and 6700 Å produces c. m. energy releases which increase linearly with photon energy; kinetic arguments imply preferential dissociation into three ground state products in this wavelength range. From the measured energy release a bond energy of the trimer ion of $\sim 1.3\text{eV}$ can be estimated. By contrast the dissociation of the trimer between 4000 and 5000 Å reveals little kinetic energy release ($< 40\text{ meV}$). In this wavelength range dissociation preferentially populates the channels $\text{Cs}^+ + \text{Cs}_2$, and $\text{Cs}_2^+ + \text{Cs}$, the excess energy appearing as internal excitation. The photofragmentation tree of Cs_3^+ in Fig. 2 shows the three

possible branches with relative cross sections being represented by the length of each branch. The absolute cross section for photodestruction of Cs_3^+ at 4880 Å was determined to be $\sim 2\text{Å}^2$. The full circles in Fig. 2 represent photodissociation measurements using the fixed frequency lines of ion lasers. The data points are connected as a guide to the eye. The ir-portion of the branch $\text{Cs}^+ + 2\text{Cs}$ was scanned continuously by a dye laser. The wavelength dependence for photodissociation in the infrared is similar in appearance to that observed for photodissociation of the dimer ion² but extends over a broader energy range and is blue shifted.

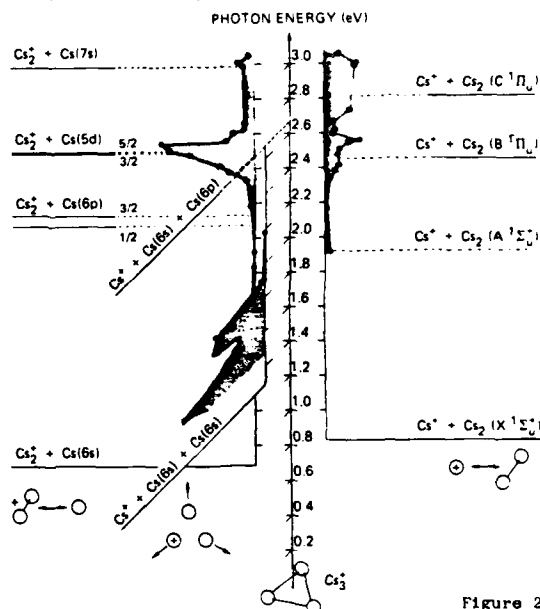


Figure 2

Our experiments demonstrate that photofragmentation of mass-selected cluster ions provides a unique means to trace the evolution of electronic structure as a function of cluster size. Theoretical efforts to predict this evolution would greatly aid in this interpretation.

Research supported by NSF under grant PHY 8411517.

1. H. Helm and R. Möller Rev. Sci. Instr. 54, 837 (1983).
2. H. Helm, P. C. Cosby, and D. L. Huestis, J. Chem. Phys. 78, 6451 (1983), H. Helm and R. Möller, Phys. Rev. A 27, 840 (1983).

FRAGMENTATION OF MICROCLUSTERS BY ELECTRON IMPACT IONIZATION

U. Buck, H. Meyer, and M. Tolle

Max-Planck-Institut für Strömungsforschung, D3400 Göttingen, Federal Republic of Germany

We have recently developed a method, which allows to derive information on the distribution of neutral clusters of atoms and molecules formed in supersonic expansions.^{1,2} In a crossed molecular beam experiment the clusters are scattered from a He-atom and the scattered intensity is detected by electron impact ionization and a mass spectrometer. The measured angular and velocity distribution is proportional to the cluster density, the differential scattering cross section, and the product of fragmentation probability and total ionization cross section. If the experimental resolution is high enough, the different clusters can be separated from each other by their different kinematical behaviour. In particular, the measurements allow the direct determination of the fragmentation probabilities $f_{n,k}$, which give the fraction of the cluster X_n detected at the mass k with $\sum_k f_{n,k} = 1$.

First results on Ar_n -clusters showed appreciable fragmentation for the dimer and the trimer.¹ The new revised fragmentation probabilities, where the slight influence of collision induced dissociation of the He are given in Tab. 1. The extension of the measurements to larger clusters reveals that 95 % of the clusters up to $n = 6$ are fragmented and appear mainly on the dimer mass Ar_2^+ . Similar measurements have been performed for ammonia clusters $(NH_3)_n$, which are hydrogen bonded with a bond strength of more than a factor of 10 larger than for Ar_n . The clusters are predominately detected on their protonated $(NH_3)_nH^+$ masses with the loss of one NH_3 radical.^{3,4} In addition, they show appreciable fragmentation as indicated in Tab. 1. In contrast to Ar , a complete dominance of the dimer ion is not found.

The measurements have been extended to the molecular van der Waals clusters $(CO_2)_n$. The CO_2 beam is produced by expanding a mixture of 5 % CO_2 in Ne through a nozzle of $d = 100 \mu m$ diameter at a stagnation pressure of 4 bar. A typical time-of-flight spectrum is shown in Fig. 1. The expected positions of elastically scattered monomers and dimers are marked by arrows. Since the heavy molecules are scattered from a light atom, there are always two contributions at one laboratory angle. The measurement is performed at the monomer mass. Therefore, the result immediately shows the heavy fragmentation of the dimer and the relatively large dimer content in the beam. The fragmentation probabilities derived from these measurements are also given in

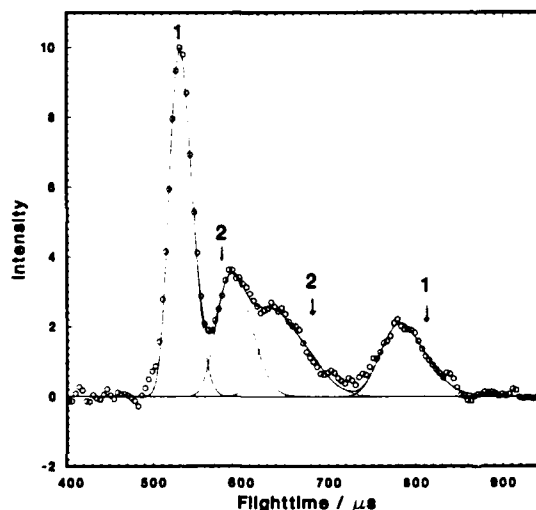


FIGURE 1 Measured time-of-flight spectra of $(CO_2)_n+He$ collisions at $\theta = 10^\circ$ lab angle detected on the monomer mass.

atom impact on the Ar_2 dimer was taken into account, Tab. 1. By contrast to the other two investigated systems, the fragmentation into the monomer is largest and for f_{11} , a measurable though small intensity is observed in contrast to Ar_1 , where no signal could be detected. The method gives the first quantitative results on the fragmentation of molecular clusters by electron impact ionization.

Table 1: Fragmentation probabilities for different clusters at electron energies of $E = 100$ eV.

	f_{21}	f_{22}	f_{31}	f_{32}	f_{33}
Ar	0.40	0.60	0.30	0.70	0.00
NH_3	0.50	0.50	0.34	0.56	0.10
CO_2	0.82	0.18	0.75	0.22	0.03

References

1. U. Buck and H. Meyer, Phys.Rev.Lett. 52, 109 (1984)
2. U. Buck and H. Meyer, Ber.Bunsenges.Phys.Chem. 88, 254 (1984)
3. J.H. Futrell, K. Stephan and T.D. Märk, J.Chem.Phys. 76, 5893 (1982)
4. H. Shinohara and N. Nishi, Chem.Phys.Lett. 87, 561 (1982)

PHOTOIONIZATION OF VAN DER WAALS-CLUSTERS
INVESTIGATED BY A PHOTOION-PHOTOELECTRON-COINCIDENCE TECHNIQUE

A. Ding, L. Cordis, K. Kretzschmar, and J. Hesslich
Hahn-Meitner-Institut für Kernforschung Berlin, Bereich Strahlenchemie
D-1000 Berlin 39, F.R.G.

Experiments with atomic and molecular clusters have aroused great interest in the last years as they not only represent an intermediate state between the gas phase and the liquid or solid state but also may be used as a model for frozen intermediate states formed in binary collisions. By inserting an exact amount of energy it is possible to investigate the decay of this intermediate complex as a function of excess energy. This leads to information about the stability of the complex and the dynamics of its fragmentative behaviour.

We have investigated the photoionization of van der Waals-clusters using monochromatized radiation from the Berlin Synchrotron facility BESSY. In order to determine the amount of energy present in the cluster ion a new coincidence technique on the line of the previously used TEPICO and PEPICO methods has been developed¹⁾. Monochromatic photons from a synchrotron source produce ion-electron pairs. The electron pulse is used to start a time-of-flight multi-channel analyzer which stores each ion impinging on the detector in a channel proportional to the arrival time. Due to the particular design of the extracting electrodes only electrons below a certain energy (typically 0.1 eV), determined by the magnitude of the extraction field, are efficiently collected.

The method has been applied to the investigation of the van der Waals-clusters (Ar_n , Kr_n , $(\text{N}_2\text{O})_n$, $(\text{CO}_2)_n$). Fig. 1 shows time-of-flight mass spectra of $(\text{N}_2\text{O})_n$ -clusters as a function of photon energy. The spectra show a significant difference to conventional photoionization yields. Most sizes appear only in a very limited wavelength interval. Photons of low energy will produce only the most stable cluster ions, while photons of higher energy produce ion-electron pairs with hot electrons which are rejected by the present detection system. It is apparent from Fig. 1 and from additional experimental results not shown here²⁾ that $(\text{N}_2\text{O})_7$ has the lowest ionization energy (12.16 eV) and can therefore be regarded as the most stable of the $(\text{N}_2\text{O})_n^+$ cluster ions. It appears furthermore that additional energy regenerates a symmetrically broadened mass distribution which leads us to the tentative conclusion that the binding force in the cluster is lowered equally by addition or removal of N_2O molecules. A prominent feature of the size distribution is the fact that all larger cluster peaks are split indicating that fragmentation is significant even at low photon energies.

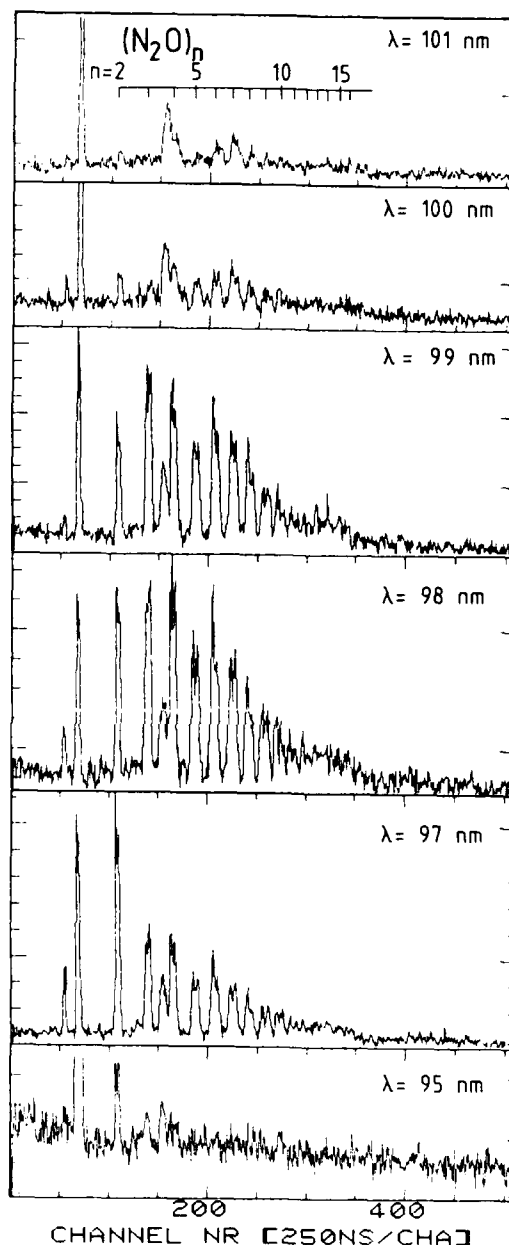


Fig. 1. Photoion-photoelectron-coincidence, time-of-flight spectra of N_2O clusters taken with different photon energies.

References

- 1) Kretzschmar, K. and Cordis, L., *Zeitschrift für Naturforschung*, **39a** (1984), p. 43, and references cited therein; K. Tanaka, T. Kato, H. M. Gouyon, and L. Hovav, *J. Chem. Phys.*, **77**, 4441 (1982) and **79**, 4332 (1983).
- 2) L. Cordis, J. Hesslich, K. Kretzschmar, and A. Ding, to be published.

UNIMOLECULAR AND COLLISION INDUCED FRAGMENTATIONS OF SMALL $(\text{N}_2\text{O})_n^+$ -CLUSTER IONS

W. Kamke, B. Kamke, H.U. Kiefl and I.V. Hertel

Institut für Molekülphysik, Freie Universität Berlin, D-1000 Berlin 33, West Germany

$(\text{N}_2\text{O})_n$ -clusters, $n=1\dots 6$, formed in a supersonic jet have been ionized by synchrotron radiation from the electron storage ring BESSY at Berlin (wavelength region $\lambda=(55\dots 116)\text{nm}$). The ions were accelerated, passed a field free drift region and were mass- and energy selected by a quadrupole mass filter and a 90° electrostatic deflector. Ions of mass m may undergo a fragmentation process $m^+ \rightarrow m_1^+ + \Delta m$ somewhere on their way to the detector. Having acquired an energy $e \cdot U(t)$ they will lose a fraction $\Delta m/m$ of that energy when they fragment (see 1). All fragmentation processes occurring within the field free flight region (time of flight $(1.4\dots 6.3)\mu\text{s}$) give rise to a peak in the observed ion current when the ionization potential is scanned. Fig.1 shows energy loss scans at three different background pressures. Such studies show that only the removal of a single neutral N_2O from the cluster can occur by unimolecular decay. The removal of more than 1 molecule is collision induced.

By varying the time at which the ions enter the drift region we determined the trimer lifetime for the metastable process $(\text{N}_2\text{O})_3^+ \rightarrow (\text{N}_2\text{O})_2^+ + \text{N}_2\text{O}$ to be $(1.83 \pm 0.15)\mu\text{s}$.

Photoionization efficiency (PIE-) curves were measured for the "prompt" ions formed in the excitation region and for the metastable ions dissociating in the drift region. Whereas the threshold shape changes significantly with clustersize, the onsets of the curves are all similar indicating similar binding energies. Comparison of the prompt and metastable PIE-curves and the basically rectangular shape of the thresholds lead us to conclude that the cluster ions are formed initially with a rather well defined energy content independent of the incident photon energy. Any excess energy breaks the weak cluster bond.

Whereas our prompt dimer spectrum at $p_0=0.95$ bar (fig.2b) agrees with others published (2), the spectrum shows more pronounced structures and a different threshold shape when the amount of clusters with $n=3$ in the jet is reduced ($p_0=0.2$ bar fig.2a). Fig. 2c shows that autoionization (similar to the monomer (3)) is clearly observable in the delayed predissociation channel in contrast to the prompt channel.

More experimental results will be presented and discussed at the conference.

This work was supported by the Bundesministerium für Forschung und Technologie.

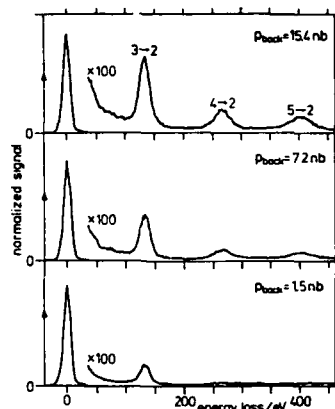


Fig. 1 Energy loss scans for $(\text{N}_2\text{O})_2^+$ at three different background pressures.

$n \rightarrow (n-m)$ means $(\text{N}_2\text{O})_n^+ \rightarrow (\text{N}_2\text{O})_{n-m}^+ + (\text{N}_2\text{O})_m$

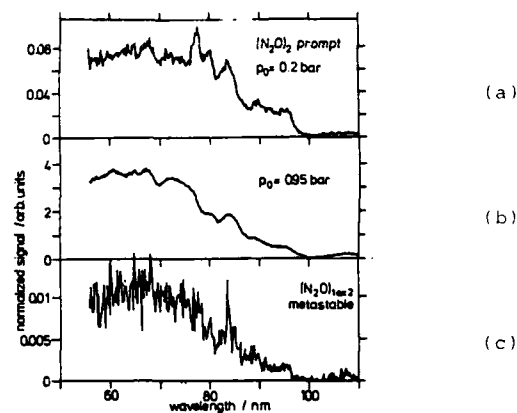


Fig. 2 PIE curve for prompt dimers at stagnation pressures

(a) $p_0=0.2$ bar, (b) $p_0=0.95$ bar,

(c) PIE curve for dimers fragmenting into two monomers within $(1.4\dots 6.3)\mu\text{s}$

References

1. I.V.Hertel, Ch.Ottinger, Z.Naturforschg. **22a**, 1141 (1967)
2. S.H.Linn, C.J.Ng, J.Chem.Phys. **75**, 4921 (1981)
3. J.Berkowitz, J.H.D.Eland, J.Chem.Phys. **67**, 2740 (1977)

METASTABLE AND SPONTANEOUS FRAGMENTATION OF BENZONITRILE IONS (AND -CLUSTER IONS)

W. Kamke, B. Kamke, H.U. Kiefl and I.V. Hertel

Institut für Molekülphysik, Freie Universität Berlin, D-1000 Berlin 33, West Germany

A supersonic molecular beam was ionized by light from the electron storage ring BESSY at Berlin ($\lambda=50\dots140\text{nm}$). The ions are accelerated, pass a field free flight region and are mass- and energy analyzed by a quadrupole and a 90° electrostatic deflector.

After ionization the ion (mass m) may fragment on its way to the analyzer and the fragment ion's energy will be reduced by $\Delta m/m \cdot eU$ (Δm =mass of the neutral fragment) with respect to the parent ion's energy $e \cdot U$ (see 1). All ions which fragment in the field free region give rise to the same energy loss for a given $\Delta m/m$. Thus by measuring this energy loss it is possible to detect metastable fragmentation

ment C_6H_4^+ formed by metastable ($1.7\dots5.3\mu\text{s}$) decay of $\text{C}_6\text{H}_5\text{CN}^+$ for both seeding gases. The onset at $\sim 89\text{nm}$ for He is shifted by approx 4nm to the blue when Ar is used.

Presently measurements are performed to clarify whether the differences in the PIE-curves for different seeding gases and stagnation pressures are due to cluster formations in the beam only or directly to the cooling of the beam. The dependence of the metastable signals on background pressure is studied and also the extraction voltage is varied in order to measure the $\text{C}_6\text{H}_5\text{CN}^+$ -lifetime for distinct fragmentation channels.

All these measurements will be presented and discussed at the conference.

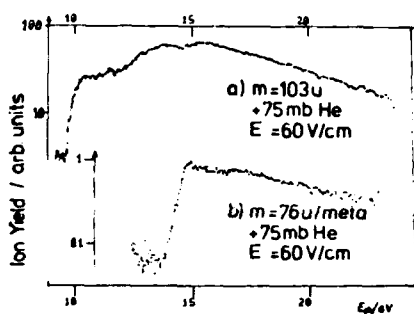


Fig. 1 PIE curve for (a) $\text{C}_6\text{H}_5\text{CN}$ and (b) C_6H_4 formed by fragmentation of $\text{C}_6\text{H}_5\text{CN}$ between $1.7\mu\text{s}$ and $5.3\mu\text{s}$. Seeding gas: Helium

channels. Comparison of figs. 1a and 2a shows that the $\text{C}_6\text{H}_5\text{CN}$ photoionization efficiency (PIE) curve exhibits significant structures in the range around 105nm when Argon is used as seeding gas instead of Helium. The structures strongly depend on the stagnation pressure. PIE-curves of Benzonitrile dimers and of the heterogeneous cluster $\text{C}_6\text{H}_5\text{CNAr}$ (fig. 2c) suggest that these structures (close to the Ar-resonance line at $\sim 107\text{nm}$) are remnants of autoionization lines in the heterogeneous cluster fragmenting to a large extent spontaneously into an Ar-atom and a Benzonitrile ion. Figs. 1b and 2b show PIE-spectra for the frag-

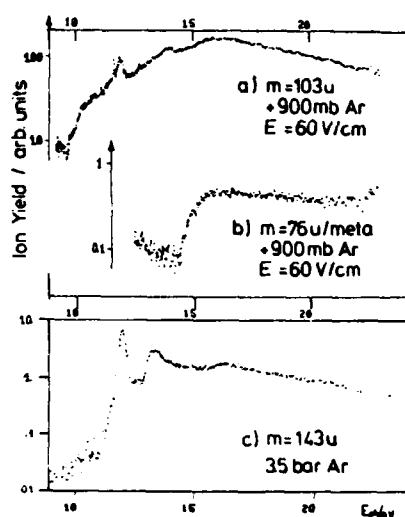


Fig. 2 PIE-curves for (a) $\text{C}_6\text{H}_5\text{CN}$ and (b) C_6H_4 (see fig. 1) and (c) $\text{C}_6\text{H}_5\text{CNAr}$. Seeding gas: Argon

This work was supported by the Bundesministerium für Forschung und Technologie.

References

1. I.V. Hertel, Ch. Ottinger, Z. Naturforsch. 22a, 1141 (1967)

PHOTOIONIZATION AND PHOTODISSOCIATION OF HYDROGEN BONDED ALKYLAMINE CLUSTERS

P.G.F. Bisling, E. Rühl, B. Brutschy, and H. Baumgärtel

Inst. Physik. Chemie, Freie Universität Berlin, Takustr. 3, D-1000 Berlin 33

Among the intermolecular processes, proton transfer represents probably the most important class of reactions in chemistry. A large number of gas phase ion-molecule equilibrium studies on proton transfer is available yielding relative data on gas phase proton affinity (PA) values (Ref. 1) from the enthalpy change $\Delta H = PA(A) - PA(B)$ of the reaction (1)



Nevertheless, there are only few measurements of absolute PA values obtained through direct determinations of the appearance energy of BH^+ . Some of these recent measurements (Ref. 2) use the formation of hydroxen containing dimers as an excellent precursor for dissociation into BH^+ . However, even internally-consistent gas phase PA values are now considered to be rather unreliable, because absolute PA data in the scale above the PA value of ammonia did not yet exist. The present experiment is designed to measure appearance energies of aliphatic amine clusters by the photoionization mass spectrometry to help clarify the above problems.

The molecular beam apparatus is essentially the same as used for R2PI laser spectroscopy of fluoro-benzene clusters (Ref 3). In this experiment synchrotron radiation provided by the Berlin electron storage ring BESSY is dispersed by a 1 m normal incidence monochromator and focused onto a skimmed supersonic nozzle beam (Figure 1).

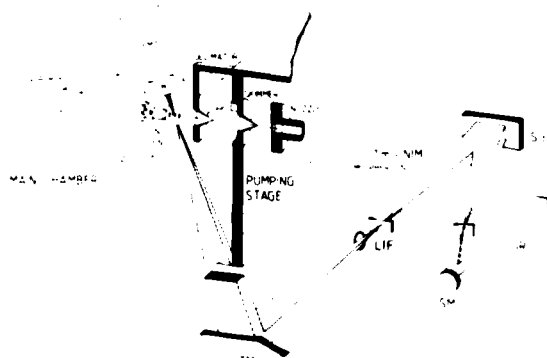


FIGURE 1 Experimental arrangement. SR: synchrotron radiation, SM: spherical mirror, SG: spherical grating, LIF: lithium fluoride filter, TM: toroidal mirror, W: window coated with sodium salicylate.

The cluster and fragment ions are created by scanning the photon energy and analysed in a quadrupole mass spectrometer. The ion yield is normalized to the photon count rate.

In principle threshold measurements for the dissociative ionization of the amine clusters M ($n = 1, 2, 3$) give absolute PA values of the monomer and oligomers via the set of reactions (2), (3), and (4)

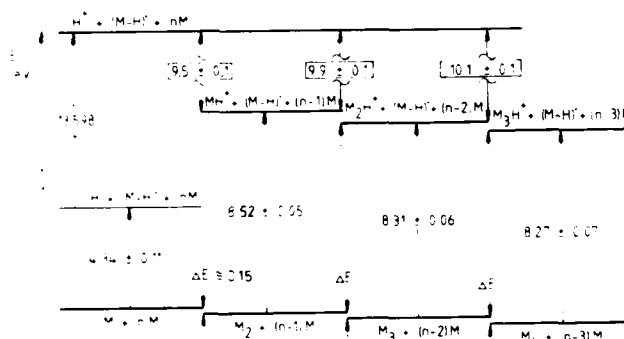
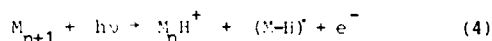
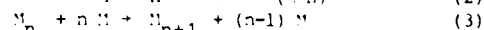
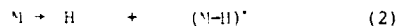


FIGURE 2 Energetics of the protonated methyl amine cluster system.

The cycles shown in Figure 2 allow the absolute PA values to be calculated. These values (M = methyl amine, dimethyl amine, and ethyl amine) are listed in Table I and compared with calibrated relative values (Ref. 1). The absolute data have uncertainties of about 0.1 eV resulting from difficulties in adiabatic threshold determinations and from literature values of both the neutral cluster and the $N-H$ binding energies.

TABLE I PA values of some alkylamines and their clusters in eV (1 eV = 96.48 kJ/mol).

M	Ref. 1 PA (M)	this work		
		PA (M)	PA (M)	PA (M)
CH_3NH	9.29	9.50	9.9	10.1
C_2H_5NH	9.41	9.58	10.1	10.5
$(CH_3)_2NH$	9.57	9.64	10.0	---

Further results of aliphatic amine clusters and on their dissociation bonding energies $D(M_n^+ - M)$ have been obtained and will be presented at the conference.

References

1. S.G. Lias, J.F. Liebmann, and R.D. Levin, J. Phys. Chem. Ref. Data **13**, 695 (1984)
2. S.T. Ceyer, P.W. Tiedemann, B.H. Mahan, and Y.T. Lee, J. Chem. Phys. **70**, 14 (1979)
3. K. Rademann, B. Brutschy, and H. Baumgärtel, Chem. Phys. **80**, 129 (1983)

ONE- AND TWO-COLOR RESONANCE ENHANCED MULTIPHOTON IONIZATION OF VAN DER WAALS MOLECULES:
STUDIES OF SPECTROSCOPIC SHIFTS AS A FUNCTION OF DEGREE OF AGGREGATION

A.W. Castleman, Jr., P.D. Dao, S. Morgan and R.G. Keesee

Department of Chemistry, The Pennsylvania State University, University Park, PA 16802

Cluster research is a rapidly growing field which offers promise of bridging the gap between the gaseous and the condensed state. In particular, an investigation of the shifts in the spectral absorption features as a function of the degree of aggregation enables the basic mechanisms of nucleation and solvation to be probed at the molecular level. Recent advances in the field of molecular beam research, coupled with pulsed lasers and time-of-flight mass spectrometry, enabled the details of these various processes to be studied.

In the present work both single and two-color multiphoton ionization is utilized, enabling control of the excess energy introduced into a cluster. This is accomplished using a Q-switched ND:YAG laser to simultaneously pump two tunable dye lasers whose output is frequency doubled in KDP crystals.

Clusters of the desired molecules are formed via adiabatic cooling from a pulsed nozzle system, with detection of the products of resonance enhanced MPI being made in a time-of-flight mass spectrometer located beyond the ionization region. The combination of ionization and mass selection has the advantage of direct mass determination of the probed van der Waals molecule. A general concern is that, because of the weak bonding in complexes, dissociative ionization may possibly complicate the spectroscopic assignments. However, the results to be presented show that fragmentation can be greatly suppressed through the use of two-color resonance enhanced photoionization whereby the ionization process is accomplished with the use of little excess energy in contrast to one-color experiments.

In the present study, van der Waals molecules of the type $A \cdot M_n$ (A-phenyl acetylene (PA), paraxylene (PX); $M=R$ (rare gas atom), N_2 , O_2 , N_2O , NH_3 , H_2O , CCl_4 , and CH_4), were investigated using both one- and two-color resonance enhanced MPI techniques. Studies of the perturbed $L_b(^1B_2)$ states reveal a wide range of red spectral shifts as well as small blue shifts with respect to the pure aromatic molecule, depending on the nature of the clustering partner. In cases where $M=Ne$, Ar , Kr and Xe , the shift is red; the magnitude of the shift increases with the polarizability of the rare gas atom where the shift in frequency of the band origin is linear with polarizability of the clustering atom.

The vibrational excitation of different vdW modes were also measured for $M=R$. $PA \cdot Ar^+$ was found to have three vdW modes at 43, 30 and 16 cm^{-1} ; three modes are also identified in the $PX \cdot Ar^+$ spectrum at 54.9,

41.8 and 19.5 cm^{-1} . Studies of the spectroscopic shifts show that the magnitude of the shift for $(PA \cdot Ar_2)$ and $(PX \cdot Ar_2)$ is approximately twice the shift for the single argon containing species. Investigations of higher order PA complexes with Ar reveal violations of the spectral shift additivity rule for a large range of n ($3 \leq n \leq 15$). In the limit of large n the main spectral shift converges to a 50 cm^{-1} red shift. The observed spectral shifts for $PX \cdot Ar_n$ ($2 \leq n \leq 7$) remain smaller than the red shift of $PX \cdot Ar_2$. We speculate that the additivity rule is valid up to the point where all equivalent adsorption sites on the aromatic ring are occupied by rare gas atoms. Red shifts were also seen for clusters with N_2 , O_2 , N_2O , CCl_4 , NH_3 , and CH_4 while blue shifts were observed in the case of CO_2 and H_2O . The spectroscopic studies reveal the expected van der Waals modes of each cluster shifted to the blue of the band origin. Comparing the spectra of successively larger clusters, and studying variations in intensity with pressure in the stagnation chamber, enables an identification of cluster fragmentation to be readily made.

The appearance potentials of $(PX \cdot Ar_n)^+$ ions were determined through studies in which the energy of one photon was fixed at the L_b resonance and the wavelength of the other was scanned. The observed appearance potentials are found to vary with the square-root of the electric field present in the region of ionization in accordance with expectations and the findings of others. Extrapolation to zero field enables a determination of the ionization potentials of paraxylene and its clusters with rare gas atoms. In an electric field (150 V/cm), the appearance potentials (AP) of $PX \cdot Ar_n^+$ are red shifted by 115 ± 5 , 181 ± 5 , 383 ± 10 , 509 ± 20 , 578 ± 20 , $710 \pm 30 \text{ cm}^{-1}$, for $n = 1-6$, respectively. This corresponds to an average shift from $AP(PX^+)$ by approximately 120 cm^{-1} per Ar atom, with major deviations from this trend for the dimer and pentamer.

Studies of appearance potentials (AP) and stagnation pressure dependencies reveal evidence for the existence of a minor chemical isomer of $PX \cdot Ar_2$ in the expansion. Although higher spectral resolution is needed to confirm this assignment.

Support of the Department of the Army, Grant No. DAMD-29-82-K-0160 and the Department of Energy, Grant No. DE-AC02-82-ER60070, is gratefully acknowledged.

NEGATIVE ION FORMATION BY IMPACT OF RYDBERG ATOMS ON VAN DER WAALS CLUSTERS

Koichiro Mitsuke, Tamotsu Kondow and Kozo Kuchitsu

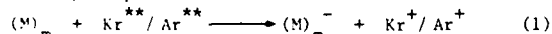
Department of Chemistry, Faculty of Science, The University of Tokyo, Bunkyo-ku, Tokyo 113, Japan

This report describes the ionization of van der Waals clusters, $(\text{CO}_2)_m$ and $(\text{CH}_3\text{CN})_m$, in collision with high-Rydberg atoms of Kr and Ar, Kr^{**} and Ar^{**} . This method is found to be useful for gentle production of negative cluster ions and provide information on the vertical electron affinity (EA) of the clusters and the relaxation involved in the ionization.

Neutral clusters were produced by condensation in a nozzle beam expansion. The skimmed cluster beam was allowed to collide with Kr^{**} or Ar^{**} prepared by electron impact in a triple-grid collision chamber. Negative ions thus formed were observed by conventional mass spectrometry.

Cluster ions, $(M)_n^-$, were detected as shown in Fig. 1, where the ion intensities are plotted as a function of the size of the cluster ions, n . Each intensity distribution has a threshold size, n_L , and a broad maximum. The n_L values for $(\text{CO}_2)_n^-$ and $(\text{CH}_3\text{CN})_n^-$ are found to be 7 and 10, respectively. The intensity distribution for $(\text{CO}_2)_n^-$ has a region of significant depletion between $n=11$ and 13. Furthermore, outstanding peaks are observed at $n=14, 16, 19, 21$ and 32 for $(\text{CO}_2)_n^-$, and at $n=13, 16, 23, 26$ and 29 for $(\text{CH}_3\text{CN})_n^-$ (magic numbers).

The results are interpreted in terms of the following evaporative electron transfer:



where $q=m-n$ gives the number of evaporation. The existence of the threshold size implies that the vertical EA increases with the size of the neutral clusters, m , and changes its sign at $m=n_L+q$, since the electron captured by a cluster is stabilized by the surrounding molecules through charge-dipole and charge-induced dipole interactions.

In the case of $(\text{CO}_2)_m$, the excess energy, E_{ex} , which should be released in process (2) is estimated to be about 3.5 eV, since the captured electron in the cluster is subsequently trapped on CO_2 forming a monomeric CO_2^- ion with a bent geometry. At $m=13$, the temperature increase (ΔT) due to E_{ex} reaches 900 K, which is much higher than the boiling point¹ of $(\text{CO}_2)_{13}$, 110 K; therefore, a number of CO_2 molecules are evaporated from $(\text{CO}_2)_m^-$ [process (2)] until the cluster is cooled down below the boiling point. Since E_{ex} and

ΔT do not depend strongly on m , q is expected to be a slowly varying function of m . Process (2) is stopped when a distinctly stable ion is formed. Evidently, the remarkable depletion in the distribution shows that q molecules are evaporated from $(\text{CO}_2)_m^-$ with $m \leq 14$, whereas the clusters with $15 \leq m \leq 18$ are largely dissociated forming the stable ion, $(\text{CO}_2)_{14}^-$ or $(\text{CO}_2)_{16}^-$. Accordingly, the maximum number of q is estimated to be 4. Thus the magic numbers demonstrated in Fig. 1 are closely related to the stability of the cluster ions or their sublimation energy.

In the case of $(\text{CH}_3\text{CN})_m$, E_{ex} is estimated to be about 1 eV, as a sum of the EA of the monomer unit and the solvation energy of the monomer anion in the cluster: charge-dipole interaction energy. In this case, ΔT is at most 200 K and is probably below the boiling point of $(\text{CH}_3\text{CN})_m^-$ expected by the well-depth ϵ of the Lennard-Jones potential of CH_3CN .² Therefore, no significant evaporation takes place. Accordingly, the magic numbers observed for $(\text{CH}_3\text{CN})_n^-$ are associated with the stability of the parent neutral clusters; a portion of the constituent molecules are vaporized in a supersonic beam due to the heat released by the condensation until the cluster size reaches its optimum value³.

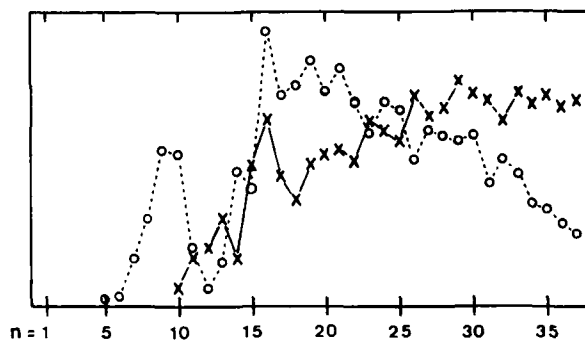


Figure 1 Ion intensities of $(M)_n^-$ versus the size of the cluster ions, n .

○ : $(\text{CO}_2)_n^-$, x : $(\text{CH}_3\text{CN})_n^-$

References

1. R.D. Etters, K. Flurchick, R.P. Pan and V. Chandrasekharan, J. Chem. Phys. **75**, 929 (1981).
2. J. Farges, M.F. de Feraudy, B. Raoult and G. Trochet, Surface Science **106**, 95 (1981).
3. J.M. Soler and N. García, Phys. Rev. A **27**, 3307 (1983).

PHOTOELECTRON SPECTROSCOPY USING A CCD MULTICHANNEL DETECTOR

Andrea Haworth, David G Wilden and John Comer

Physics Department, The University, Manchester M13 9PL, UK

A photoelectron spectrometer has been constructed in which the efficiency is enhanced by using a position sensitive detector. This detector is of the type developed by Hicks et al¹ and uses microchannel plates at the exit plane of the electron analyser together with a charge coupled imaging device. A vacuum ultraviolet photon beam is generated by that Daresbury Synchrotron radiation source and the wavelength selected beam is crossed with a gas beam from a narrow tube. The electron analyser can be rotated about the photon beam in order to collect photoelectrons at specific angles to the direction of polarization of the photon beam.

One clear advantage of synchrotron radiation sources over line sources for photoelectron spectroscopy is the possibility of examining the excitation of ion states as a function of photon wavelength in order to obtain information about autoionization processes. This is illustrated in the figure which is one of the spectra obtained on the present instrument. It shows the photoelectron yield obtained as a function of both incident wavelength and collected electron energy. Each line at fixed wavelength represents a photoelectron

spectrum for that wavelength and the peaks correspond to vibrational levels of the N_2^+ , $X^2\Sigma$ state. Following any one of these peaks diagonally across the surface, i.e. constant difference between photon and electron energy, gives an excitation function for a specific vibrational level of the ion. An example of an effect which is immediately apparent from such a curve is the difference between the branching ratios for the two arrowed autoionizing states. Such a spectrum gives the most comprehensive information about the excitation and decay processes involved. It has the advantage that autoionization, direct ionization and backgrounds are measured on the same spectrum and this greatly improves normalization. It can therefore be used subsequently to make accurate allowance for backgrounds and direct ionization. Taking such a spectrum with 10^4 data points and reasonable signal to noise ratio in about four hours is made possible by the use of the multi-detector. Similar data will also be presented for CO and O_2 .

Reference

1. Hicks P J, Daviel S, Wallbank B and Comer J.
J Phys E:Sci Instrum 13, 713-5 (1980).

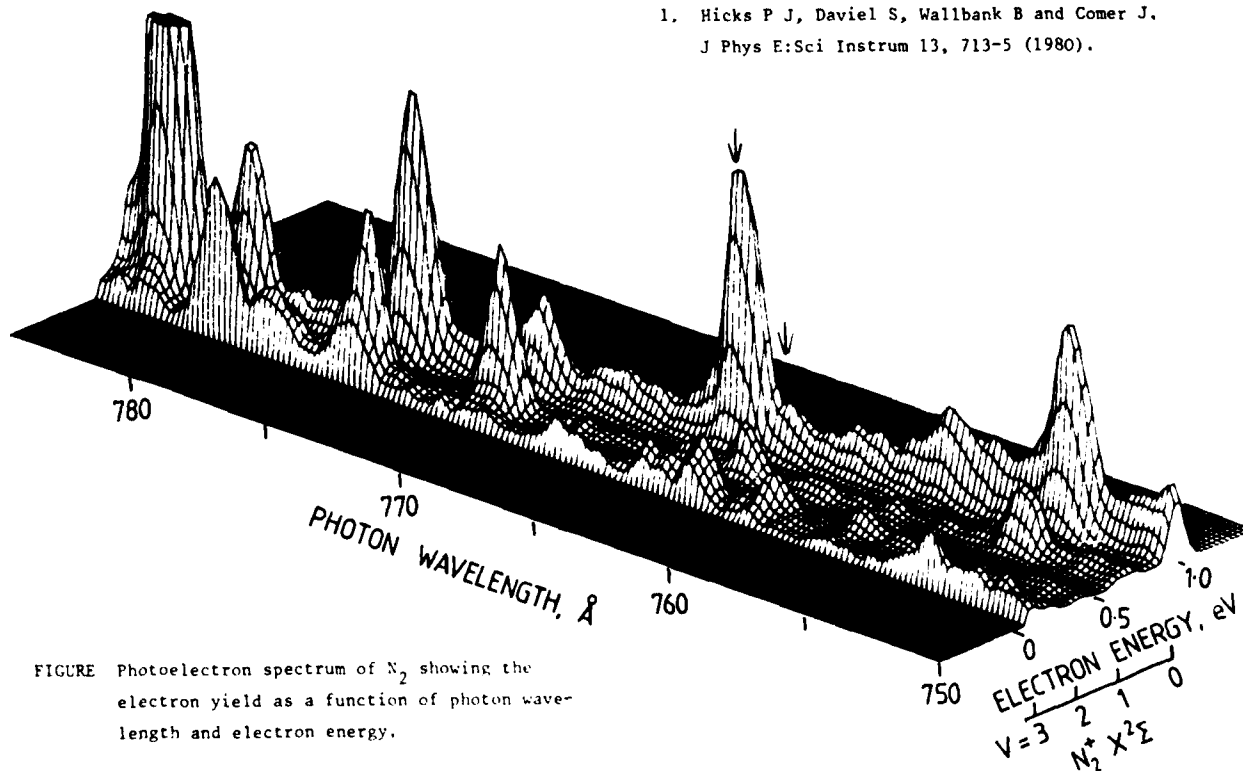


FIGURE Photoelectron spectrum of N_2 showing the electron yield as a function of photon wavelength and electron energy.

MONOCHROMATIC ELECTRON SOURCE FOR POLARIZED ELECTRON-ATOM SCATTERING*

C. S. Feigerle, D. T. Pierce, A. Seiler, and R. J. Celotta

National Bureau of Standards, Radiation Physics Division, Gaithersburg, Maryland 20899 USA

Many electron scattering experiments benefit from the additional resolution obtainable when an electron monochromator is used to narrow the energy spread of an electron beam emitted from a thermionic cathode. Unfortunately, the maximum electron beam current available from a monochromator, as indicated by the solid line in Fig. 1, decreases dramatically with increasing energy resolution. The apparatus described here is capable of producing currents of monochromatic electrons¹ in excess of that possible with conventional monochromators and has the additional advantage of providing a spin polarized electron beam if desired.

This monochromatic electron gun is an extension of the widely used source² of polarized electrons based on photoemission from negative electron affinity GaAs. It consists of a GaAs crystal which has been cleaned in ultra-high vacuum and coated with cesium and oxygen. The surface treatment has the effect of reducing the work function to the point where the conduction band lies above the vacuum level by an energy difference defined as the (negative) electron affinity. Electrons which are photoexcited and relax down to the conduction band minimum have positive energies with respect to the vacuum level when they leave the photocathode which equal the value of the electron affinity (~ 0.3 eV). Since they may lose up to this same amount of energy on exiting and still escape the solid, the final beam could have an energy spread which equals the electron affinity. The electrons reach thermal equilibrium while in the conduction band and consequently there is also a contribution to the energy distribution which depends on the crystal temperature.

We were able to obtain low energy spread, high current electron beams by modifying the composition of the surface layer and cooling the photocathode. The surface layer was adjusted so as to maintain a smaller but still negative electron affinity. Energy distribution measurements were made using 210 nm radiation and a hemispherical energy analyzer which sampled the high current electron beam. At 300 K a current of 7 μ A was produced with an energy spread of 97 meV (FWHM). On cooling to 77 K, a 1 μ A current was obtained and the energy width was reduced to 31 meV.

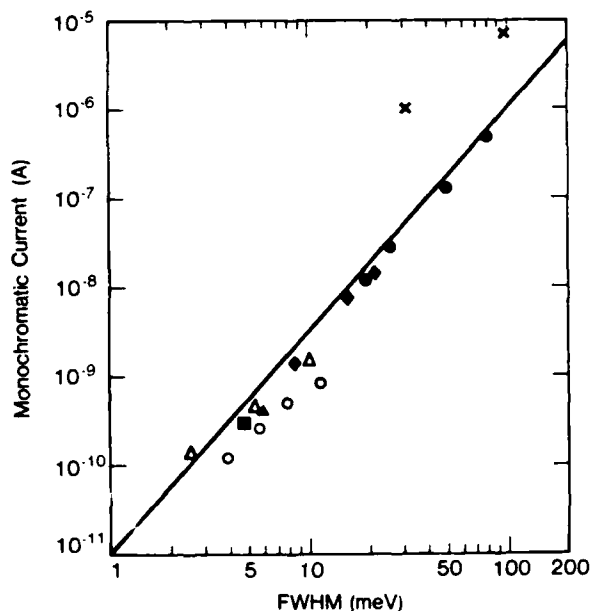


FIGURE 1. Cathode current and energy distribution width obtained by photoemission from NEA GaAs (X) as compared to the best reported performance of spherical (solid symbols) and cylindrical (open symbols) deflector monochromators. References for each point are given in Ref. 1. The solid line represents the current being proportional to the 5/2 power of the distribution width.

Figure 1 compares the performance of this electron source to the best reported performance of electron monochromators. A measured increase in current at the same resolution of a factor of 10-20 has been realized. Additionally, since circularly polarized light was used, the electrons produced had an optically controllable spin polarization.²

References

1. C. S. Feigerle, D. T. Pierce, A. Seiler, and R. J. Celotta, *Appl. Phys. Lett.* **44**, 866 (1984).
2. D. T. Pierce, R. J. Celotta, G.-C. Wang, W. N. Inertl, A. Galejs, C. E. Kuyatt, S. R. Mielczarek, *Rev. Sci. Instrum.* **51**, 478 (1980).

* Supported in part by the Office of Naval Research.

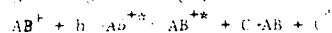
CHARGE EXCHANGE DETECTION OF LASER-INDUCED
TRANSITIONS IN MOLECULAR IONS

C. H. Kuo, I. W. Milkman, T. C. Steimle, and J. T. Moseley

Chemical Physics Institute and Department of Physics
University of Oregon, Eugene, Oregon 97403

A selected ion flow tube (SIFT) apparatus has been used to improve on our previously demonstrated use of charge exchange as a means to detect laser induced transitions. This charge exchange technique can be used both as a sensitive method to study molecular ion spectroscopy, or as a means to investigate charge exchange, and by extension other reactive processes, of state-selected excited ions. The use of a SIFT allows the injection of mass selected ions in such a way as to drastically reduce the concentrations of species that cause background signals, with a resulting increase in sensitivity. In addition, the ions in the flow tube are relaxed to near thermal rotational, vibrational, and translational temperature.

Absorption spectra are recorded by monitoring the ion counts of a charge exchanger using a quadrupole mass filter, as a function of the dye laser frequency. When the laser is tuned to a resonance in the ion of interest, excited state ions are produced which can undergo charge exchange, i.e.:



By choosing a suitable charge exchanger C such that the reaction is exothermic for the A state but endothermic for the X state, it is possible to eliminate essentially all of the background signal. For example, our typical spectra have a background of less than 25 counts/second and a signal of about 200 counts/second with the laser tuned to a strong resonance. Being at the shot noise limit with such good signal-to-noise allows us to simply use a rate meter with a time constant of 2 seconds to record spectra, such as shown in Fig. 1, in only about 2 minutes. No data averaging is required. Fig. 1 shows a sample spectral line from the $N_2^+ A-X(4,0)$ band, obtained with Doppler-limited resolution using a single mode laser. The upper signal in the figure is laser induced fluorescence (LIF) of N_2^+ taken for wavelength calibration purposes. The charge exchanger used was Ar.

Using this method, we have obtained the first Doppler-limited spectra of the $CO^+ A-X(1,0)$ band, and we are in the process of obtaining improved molecular constants for this band. The charge exchanger used was again Ar, which is exothermic for the $CO^+ A$ state but endothermic for the X state.

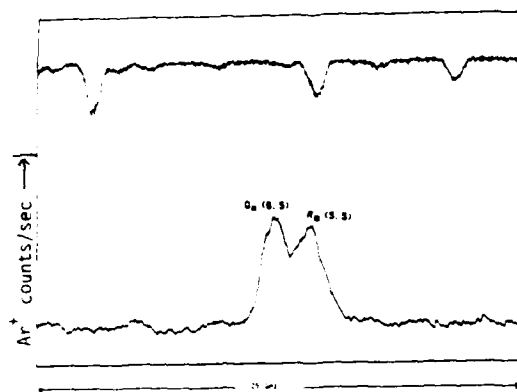


Figure 1 $N_2^+ A-X(4,0)$ Absorption Spectrum Recorded by Laser Induced Charge Exchange Spectroscopy

In addition to the CO^+ data, a Doppler-limited spectrum of the $N_2^+ A-X(5,0)$ Meinel band has been obtained. We measured approximately 35 transitions in all of the branches, and, with the aid of LIF calibration spectra, have fitted the results to an effective hamiltonian developed by Brown and co-workers. These are the first experimentally determined molecular constants for this band. The sensitivity of this technique is indicated by the fact that the $N_2^+(5,0)$ band has a small Franck-Condon factor and has never been seen in emission, or with LIF.

We plan to use this technique to explore the spectroscopy of less well-known species and to obtain some sub-Doppler measurements, as well as to investigate the charge exchange reactions of excited states. Anticipated future investigations include:

- Use of the Lamb dip technique to observe the hyperfine structure of the $N_2^+ A$ state.
- Use of microwave-optical double resonance to observe the ground state lambda-doubling splitting in NH^+ .
- Measurement of the charge exchange cross sections for the A states of N^+ and CO^+ as a function of rotational and vibrational level.

References

- J.C. Hansen, C.B. Fao, J.L. Crickman, and J.T. Moseley, *J. Chem. Phys.*, **79**, 1111 (1983).
- J.M. Brown, M. Kaise, J.M.L. Kerr, and D.J. Milton, *Molec. Phys.*, **35**, 553 (1973).

A DETECTION SYSTEM TO STUDY THE STEREOCHEMISTRY OF MOLECULAR-IONS*

A. Faibis, W. Koenig, E. P. Kanter, Z. Vager, and B. J. Zabransky

Physics Division, Argonne National Laboratory, Argonne, IL 60439

In the last decade a rather large number of experiments studying the collision induced dissociation of fast (MeV) molecular ions were reported. Foil-induced dissociation (Coulomb explosion) has allowed the study of a) the interaction of correlated clusters with the target, and b) parameters characterising the structure of the molecular projectile prior to dissociation.

Recent work at the Weizmann Institute in Rehovot¹ showed that a complete measurement of the final momenta for all the fragments can be used to generate the spatial part of the phase-space distribution describing the molecular ion. This opens the possibility of determining the molecular potential energy surface for small (3-4 atoms) molecular-ions. Also, by selective excitation one could study the above-mentioned phase-space distribution for different excitation regimes of the molecular ion.

The experimental requirement is to detect in coincidence all of the break-up fragments and to determine for each one of them the three momentum components in the center of mass of the molecular ion. To this end we designed, built and tested a Multi-Particle Position And Time Sensitive (MUPPATS) detector.² The MUPPATS is a large-area (30 cm in diameter), Breskin-like gas detector³ with a wide dynamical range. It is capable to detect 0.1- to 3-MeV ions from protons to neon ions, with no change in the operating conditions.

The main elements of the detector are three electrode planes made of thin, parallel tungsten wires, with wire spacing 0.3-1 mm. The planes are 2 mm apart and rotated by 60°, one with respect to another. The detector volume is filled with isobutane at 2-3 Torr pressure. As charged particles pass through the anode-cathode gap, the electron avalanche formed along their trajectory is amplified and collected by an anode wire. Simultaneously, electrical signals of opposite sign are induced in the neighbouring cathode wires. In this way, for each detected particle one obtains three in-plane coordinates. The lapse of time between the arrival of two fragments originating in the break-up of the same molecular-ion is also accurately determined. It measures the component of the particle separation which is perpendicular to the detector plane.

To avoid the extremely expensive single-wire read-out for all of the 900 wires we chose to connect the cathode wires through delay lines. After being amplified and discriminated the output of the delay line is fed into a FASTBUS pipelined TDC. This module, belongs to the new generation of standardized electronics developed for high-energy physics. It provides rapid and intelligent handling of multiple stops allowing the processing of multiparticle events.

The MUPPATS detector has been now mounted and is undergoing preliminary tests with particle beams from the 5 MV Dynamitron accelerator at ANL. Preliminary results with H_2^+ , H_3^+ and probably H_2O^+ should be available by the time of the Conference.

*Work supported by the U. S. DOE, Office of Basic Science under Contract W-31-109-ENG-38.

References

1. A. Faibis. Ph.D.-Thesis. Weizmann Institute of Science (1983).
2. W. Koenig, A. Faibis, E. P. Kanter, Z. Vager and B. J. Zabransky, NIM, to be published.
3. A. Breskin, Nucl. Instrum. Meth. 196 (1982) 11.

X-RAY PHOTOELECTRON SPECTROSCOPY OF ATOMS AND MOLECULES:
A WINDOWLESS X-RAY TUBE FOR HIGH TEMPERATURE MEASUREMENTS

M. S. Banna and B. H. McQuaide

Vanderbilt University, Department of Chemistry, Nashville, Tennessee 37235

One of the main difficulties encountered in high temperature gas phase XPS is the failure of the thin window used to transmit the x-rays into the ionization region. Without a window, the x-rays will be quickly attenuated due to condensation of the sample onto the anode surface. For temperatures below 600°C Al foil can often be used, while carbon or beryllium films are suitable at higher temperatures. In some cases, however, the vapor reacts with the window material or simply condenses on the surface due to the difficulty of keeping the window hotter than the remainder of the oven. Add to this the fragility of carbon films and the toxicity and cost of beryllium foil. Thus it is highly desirable to eliminate windows altogether.

We have constructed an x-ray tube with a slowly rotating (~ 60 rpm) anode, which makes possible the continuous scraping of the anode surface. In this manner a sufficient x-ray flux can be maintained without using a window. This arrangement paves the way for the study of numerous more species in the gas phase at high temperatures. Sample spectra illustrating the performance of the x-ray tube will be presented.

MULTICHARGED ION-ATOM MERGED-BEAMS APPARATUS

C. C. Havener, H. F. Krause, and K. A. Phaneuf

Physics Division, Oak Ridge National Laboratory*
Oak Ridge, Tennessee 37831 USA

An ion-atom merged-beams apparatus has been developed to measure total electron-capture cross sections for collisions of multicharged ions with neutral atoms in the energy range from 1-500 eV/amu. The objective is to extend existing measurements for these collisions to considerably lower energies, where theoretical models and methods remain essentially untested. In some multiply-ionized systems, an orbiting mechanism may be expected to produce very large electron-capture cross sections with a $1/v$ velocity dependence at low collision energies.

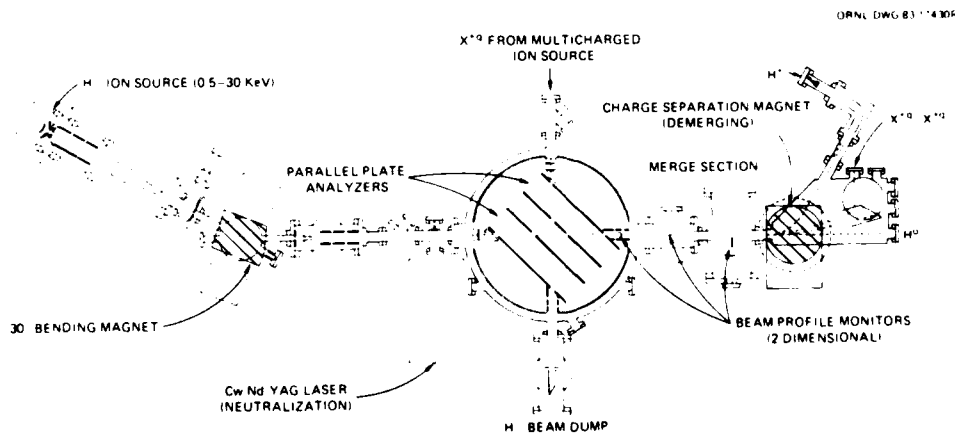
The current arrangement of this experiment is shown in the figure. A 2-5 keV/amu, highly-collimated beam of H^+ or D^+ from a duoplasmatron ion source passes through the optical cavity of a 1.06- μ m Nd:YAG laser, where 1-2 kW of cw circulating intracavity power is maintained. Photodetachment of roughly 1% of the negative ions produces a highly-collimated flux of ground-state neutral H^0 or D^0 atoms of up to 2×10^{11} per second. The undetached H^- or D^- beam is electrostatically separated from the neutrals, and collected in a differentially-pumped beam dump. For initial tests, the apparatus has been operated on-line using the ORNL-PIC multicharged ion source, which generates a highly-collimated 1 μ A beam of N^{3+} at 36 keV. This beam has been successfully merged with a 3 keV/amu D^0 beam in the 75-cm ultrahigh vacuum merge path. A two-dimensional real-time scan of the spatial overlap of the beams at one position near the center of the merge-path is generated by a commercial rotating-wire beam profile monitor. The ions are magnetically demerged, separating the H^+ or D^+ from the N^{3+} , N^{2+} , and the neutral H^0 beams. The H^+ and D^+ productions are further electrostatically analyzed at 90° from the plane of magnetic dispersion and focused onto a channel electron multiplier where they are counted. Signals in the $H^+(D^+)$ detector resulting from beam-beam interactions have been measured above background due to

beam-gas interactions by using a standard beam-modulation scheme to chop both the multicharged ion and neutral beams, and to gate dual counters to record both signal-plus-background and background events. Current operating parameters for the experiment are summarized in Table 1. The signal-to-background ratio is sufficient to permit the necessary diagnostic measurements to be made on the signal in several minutes. Developments to allow additional measurements of the spatial overlap of the beams at different points along the merge path are under way. This will be required for definitive absolute cross-section measurements. Since such electron-capture collisions are predominantly exoergic, we hope also to be able to obtain some information above the electronic states of the product protons or deuterons. With minor modifications, the present apparatus can also be applied to the study of electron capture in collisions of $H^+ + H$ at low energies.

Table 1. Typical operating parameters

D^- beam: $E = 6.00$ keV; $I(D^-) = 2$ μ A; $I(D^0) = 15$ nA
N^{3+} beam: $E = 36.0$ keV; $I(N^{3+}) = 1$ μ A
Center-of-mass energy: 16.5 eV/amu
Merge path = 75 cm
Merge path pressure = 1.5×10^{-10} torr (base), 7×10^{-10} torr (w/beams)
H^+ background count rate = 3×10^3 s $^{-1}$
Noise from N^{3+} beam = 50 s $^{-1}$
Beam-beam signal = 80 s $^{-1}$
Time for s.d. of 10% on signal = 4 minutes
2-dim beam-overlap factor = 0.25 cm 2

*Research sponsored by the Division of Chemical Sciences, U.S. Department of Energy under Contract No. DE-AC05-84OR21400 with Martin Marietta Energy Systems, Inc.



ION-ATOM MERGED-BEAMS EXPERIMENT

REALIZATION OF A TRUNCATED SPHERICAL ANALYZER FOR PARALLEL MEASUREMENT OF ANGULAR DISTRIBUTIONS

D. Tremblay, D. Roy, and D. Dubé

Département de Physique et Centre de Recherche sur
les Atomes et Molécules (CRAM) Université Laval,
Québec, G1K 7P4, Canada

We present here the current state of the realization of a new electrostatic electron spectrometer based on a modified design of the electrostatic spherical mirror proposed by Sar-EI¹. In the latter proposal, both the source and the detector lie inside the inner one of two concentric spheres and on a common diameter which represents a symmetry axis of the analyzer. The electrons leaving the source in a direction normal to the axis enter the gap between the two spheres and are deflected by the electrostatic field. Those with pass energy reach a first focus inside the gap but, because of the symmetry about the axis, all the emission (or scattering) angles are thus separated. After the first focus, electrons are focussed back inside the inner sphere at the opposite point of the source where Sar-EI suggested that the detector should be placed.

In a previous work², we proposed to perform electron detection at the first focus inside the gap. The addition of a retarding lens moves the effective source (see Fig. 1) and the focus locii. We computed the performances of the modified analyzer and showed that good energy resolution together with parallel detection of angular distributions were possible.

The analyzer under realization is designed for electron-gas applications although photo-emission and surface studies could be possible. The monochromatic projectile electron beam is produced by a classic 127.3° cylindrical deflector outside the spheres and carried to the collision zone by electrostatic lenses. Inside the analyzer gap, electric field distortions caused by lenses are prevented by correcting plates. These plates divide the analyzer into two parts. In the first one, 19 continuous-dynode electron multipliers achieve the discrete multi-detection in a scattering angle range of 150°. In the second part, an extended Faraday cup measures the total cross section. Data acquisition is performed by independent 32 bit counters controlled by a TI 9900 microprocessor.

The spheres were made of aluminum in a lathe with tolerances of about 0.05 mm for the larger one over a 260 mm diameter and half these values for the smaller one. In order to allow easy access to the

inside, the large sphere was cut into two halves, which accounts for the reduced precision.

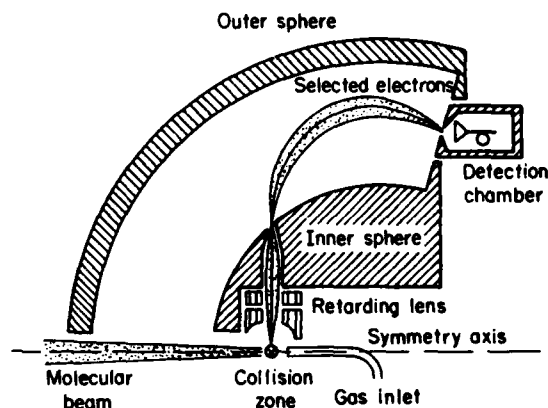


Fig. 1 Schematic view of the analyzer: The projectile electron beam is coming out of the plane. The analyzer is symmetrical about the axis shown and thus parallel detection is possible.

References

1. H.Z. Sar-EI, Nucl. Instr. Meth. **42**, 71 (1966).
2. D. Tremblay and D. Roy, Nucl. Instr. Meth. **220**, 270 (1984).

SIMPLE, LOW COST, DATA ACQUISITION SYSTEM FOR EELS

G. G. B. de Souza, F. C. Pontes, H. Gamal

Instituto de Química da Universidade Federal do Rio de Janeiro
Cidade Universitária - 21.910 - Rio de Janeiro - RJ - Brasil

A simple and inexpensive data acquisition system has been developed and interfaced to an intermediate energy, low resolution, electron-energy loss spectrometer, which has been described earlier¹.

The system is based on an Apple II micro-computer with 64 kbytes of RAM, a 2-80 card and a 5 1/4" disk-drive.

The data acquisition interface contains a programmable timer and pulse counter, input and output parallel ports and two serial-data links. The input/output ports are used for reading the pressure inside a high vacuum chamber by means of a digital ionization gauge (Varian 845) and to control the output voltage of a programmable power supply (Bertan 205-A-01R). The timer-counter was designed around an Intel 8253 integrated circuit and uses the Apple clock as time base. It allows for the counting of up to $2^{**}32$ pulses per channel and for dwell times in the range of 1 to $2^{**}16$ msec.

A versatile software has been developed offering the following capabilities:

A) Setting of various experimental parameters, such as the number of scannings, power supply voltages, range of allowed pressures, etc.

B) Normalization and presentation of the spectrum, during acquisition time. Each scan can be stopped and the spectrum expanded and integrated between two chosen points. The operations are eased by the use of a potentiometer which controls a cursor on the screen. The acquisition can be restarted from the current point or from the beginning, with or without parameter modifications.

C) Automatic data saving after a chosen number of scans and reading of another data file; arithmetic operations with the two sets of data.

The serial data links are software controlled. One of them turns the microcomputer in a TTY-like terminal of a Burroughs 6700 computer, where data can be saved in magnetic ta-

pes, hard disks or plotted out by a high quality color plotter. The other link is used for transferring data from or to the memory of a multichannel analyzer (Tracor-Northern 1705).

The programs have been written in FORTRAN although some critical parts have been written in 2-80 or 6502 assembly language.

When compared to the previously described system¹ the present one has demonstrated a comparable performance and a definite advantage as far as simplicity and cost are involved.

Financial support from the Conselho Nacional de Desenvolvimento Científico e Tecnológico (CNPq) and Financiadora de Estudos e Projetos (FINEP) is gratefully acknowledged.

REFERENCES:

- 1) G.G.B. de Souza, A.C. de A. e Souza, R. de B. Faria, in *Electronic and Atomic Collisions*, J. Eichler, W. Fritsch, editors. North-Holland, Amsterdam, Oxford, New York and Tokyo, 1983 (page 707).

DETECTION OF LOW-LYING METASTABLE MOLECULES BY PHOSPHORESCENCE OR FLUORESCENCE

Hiroshi Kume, Tamotsu Kondow, and Kozo Kuchitsu

Department of Chemistry, Faculty of Science, The University of Tokyo, Bunkyo-ku, Tokyo 113, Japan

The $A^3\Sigma_u^+$ and the $a^1\Pi_g$ states of N_2 molecules were detected selectively by observing the phosphorescence from biacetyl and the fluorescence from anthracene respectively adsorbed on a copper substrate with detection efficiency of about 10^{-3} . This technique was also applied to detection of other low-lying metastable states, such as the lowest triplet states of aromatic molecules, where a detection efficiency of 2×10^{-3} was attained by using biacetyl as a phosphor.

A nozzle beam of metastable molecules was produced by electron impact (energy spread: 0.8 eV) and was allowed to collide on a phosphor surface. A spectrum of the resulting emission was observed when the metastable molecules excited by a continuous electron beam were impinged on the phosphor surface. The time dependence of the emission (TDE) was also measured by use of the metastable beam excited by pulsed-electron bombardment. The phosphor was deposited continuously on a cold copper substrate (77 K) during the measurement.

Phosphorescence of biacetyl was observed when metastable N_2 molecules were allowed to collide on biacetyl surface. The shape of TDE was found to be independent of the electron impact energy and determined by the velocity distribution of the N_2 beam and the lifetime of the phosphorescence; the lifetime was estimated to be 1 ms. An excitation function estimated from the integrated TDE is shown in fig. 1. The threshold energy (6.2 ± 0.8 eV) corresponds to the excitation energy of the $A^3\Sigma_u^+$ state. This threshold energy and the peak position at 12 eV agree with those in the excitation function of $N_2(A^3\Sigma_u^+)$ measured using Auger electron emission from Cs metal.¹ However, our measurement gives significantly higher intensity in the low-energy region (6–9 eV). The detection efficiency for $N_2(A^3\Sigma_u^+)$ was measured to be about 10^{-3} , which is comparable with the secondary electron yield of a typical Cu-Be-O surface by $N_2(A^3\Sigma_u^+)$.²

By using anthracene instead of biacetyl, $N_2(a^1\Pi_g)$ was detected selectively by observing its fluorescence. The excitation function estimated from the integrated intensity of TDE agrees well with that measured by electron energy loss spectroscopy.³ The fluorescence spectrum accords with that for an anthracene single crystal. This agreement implies that anthracene molecules on the surface are well-oriented. The detection efficiency was about 10^{-3} .

The present technique was further extended to detection of benzene in the lowest triplet state (T_1).

Biacetyl was used in this case, and the phosphorescence spectrum and the corresponding TDE were measured. It was found that benzene in T_1 was actually detected with an efficiency of about 2×10^{-3} . This metastable detector was found to be stable and reliable for more than 10 h at a pressure of 10^{-5} torr.

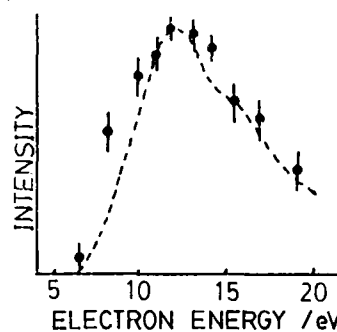


Fig. 1: Excitation function for $N_2(A^3\Sigma_u^+)$. Broken line shows the excitation function measured by Auger electron emission from a Cs surface.¹

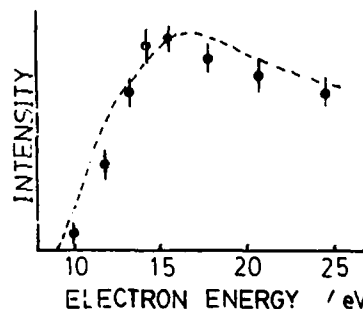


Fig. 2: Excitation function for $N_2(a^1\Pi_g)$. Broken line shows the excitation cross section for $N_2(a^1\Pi_g)$ formation by electron impact.³

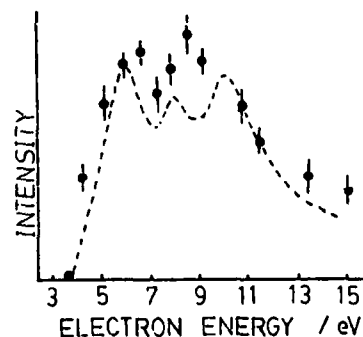


Fig. 3: Excitation function for benzene(T_1). Broken line shows the excitation function measured by Auger electron emission from a sodium surface.⁴

References

1. J.C. Hemminger, B.G. Wicke, and W. Klemperer, *J. Chem. Phys.*, **65**, 2798(1976).
2. W.L. Borst, *Rev. Sci. Instr.*, **42**, 1543(1978).
3. D.C. Cartwright, S. Trajmar, A. Chutjian, and W. Williams, *Phys. Rev. A*, **16**, 1041(1977).
4. K.C. Smyth, J.A. Schiavone, and R.S. Freund, *J. Chem. Phys.*, **61**, 4747(1974).

MEASUREMENTS OF LASER EXCITED ATOM POPULATION IN Na VAPOR AND FAST Na BEAMS*

D. P. Wang, S. Y. Tang and R. H. Neynaber

University of California, San Diego, La Jolla, CA 92093, USA and
La Jolla Institute, La Jolla, CA 92038, USA

A beam-gas technique involving ion-pair production in alkali-halogen collisions has been used to measure the fraction, f^* , of laser excited Na atoms, Na^* , in Na vapor and fast (keV) Na beams. The method as applied to a beam will be described first. The beam consists of Na^* in the $3^2P_{3/2} F=3$ state and of Na in the $3^2S_{1/2} F=1, 2$ ground state (GS). The Na^* is produced from $F=2$ GS Na by a Coherent 599-21 single frequency CW dye laser pumped by a Coherent Innova-5 Ar ion laser. The bandwidth of the laser is approximately 1 MHz. The laser is aligned so that the light beam is coincident with the atomic beam, which is generated by charge-transferring Na^+ (from a surface ionization source of fused silica glass) in Na vapor. The method consists of passing the atomic beam through a vapor of I_2 in a cell and measuring, with the laser on and off, the Na^+ current resulting from the ion-pair production reaction $\text{Na} + \text{I}_2 \rightarrow \text{Na}^+ + \text{I}_2^-$. The technique works because the crossing radii are quite different for GS Na and Na^* and allow only the former to react. For an optimum laser power of 100 mW/cm^2 , measurements of f^* were made for a laboratory energy, E , of the Na atoms from 1000 to 5500 eV and ranged in value from about 3% at the lowest E to 6.8% at the highest. The technique should work for much lower E but with more difficulty because of smaller beam intensities and increased elastic scattering.

The theoretical maximum f^* , f_{max}^* , for our accelerated beam can be calculated from the statistical weights of the GS hyperfine levels, i.e., $f_{\text{max}}^* = (5/8)/2 = 5/16 = 31\%$. This calculation assumes that the Doppler width (full width at half maximum, i.e., FWHM) falls within the 10 MHz natural linewidth of Na-D₂ line. This is the case since accelerating the beam drastically reduces the velocity spread due to the source. For example, at $E = 5000 \text{ eV}$, the calculated Doppler width due to the 1300 K source is only 3.9 MHz. Actual Doppler widths are determined by fitting a calculated lineshape to the measured curve (ion-pair production versus laser frequency). The calculated lineshape is obtained from

a Voigt formula modified for power broadening. As an example, at $E = 5000 \text{ eV}$, the measured linewidth is 45 MHz, and the derived Doppler width and power broadened natural linewidth are each about 30 MHz. A rough value of f^* , which is more realistic than f_{max}^* , can be obtained by assuming that all of the atoms with Doppler frequencies within the power broadened natural linewidth are excited whereas those outside are not. Thus, $f^* \approx (30/45) \times (5/16) = 0.21$. Contributions to the Doppler width from angular divergence are negligible compared to the velocity spread associated with the source.

Two obvious facts emerge from the previous discussion: a) the calculated f^* of 21% is considerably larger than the measured value of 6.5% and b) the actual Doppler width of 30 MHz is much greater than the 3.9 MHz calculated for the accelerated beam. The first fact can be explained by optical pumping, which arises from wing absorption of the power broadened natural linewidth. The second could be the result of a large velocity spread of Na^+ from the source due to resistivity and a variable work function of the fused silica glass.

The method of measuring f^* for a partially excited vapor of Na confined to a cell will now be described. The vapor is typically at a pressure of 0.1 mTorr and is excited by the same single frequency CW laser described previously. Coincident with the laser is a Cl beam at, typically, $E = 4000 \text{ eV}$. This beam is generated by electron detachment of Cl^- in O_2 . The Cl^- , in turn, is formed from CCl_4 in an electron impact source. As before, ion-pair formation is used to determine f^* ; Cl^- is detected from $\text{Na} + \text{Cl}^- \rightarrow \text{Na}^+ + \text{Cl}^-$. The measured linewidth for the function of Cl^- intensity versus laser frequency is about 3.9 GHz. The Na^* is in the $3^2P_{3/2}$ state, but the hyperfine distribution cannot be specified. If n_0 is the constant density of GS Na atoms in the cell and $n^*(x)$ the variable density of Na^* along the axis x of the cell of length L , then f^* is defined as $f^* = (n_0 L)^{-1} \int_0^L n^*(x) dx$. A typical $f^* = 0.02$ for a laser power of 1000 mW/cm^2 .

The Na^* generated in both beams and vapors has recently been used to investigate the reaction $\text{Na}^* + \text{Na} \rightarrow \text{Na}^+ + \text{Na}^-$.

* Supported by NSF CPE83-10965 and the Air Force Office of Scientific Research (AFSC), under Contract No. F49620-84-C-0058.

PRODUCTION OF H_2^+ IONS IN LOW VIBRATIONAL STATES
USING A RADIO FREQUENCY STORAGE ION SOURCE

A. Sen, J. Wm. McGowan and J.B.A. Mitchell

Department of Physics, The University of Western Ontario,
London, Ontario, Canada. N6A 3K7

A storage ion source⁽¹⁾ based on the principle of confinement of charged particles by inhomogeneous oscillatory electric field has been built for production of H_2^+ ions in the lowest two vibrational levels. The source consists of a stack of plates each having a U-shaped hole in it (see Fig. 1) and alternate plates are connected to a suitable radio frequency source.

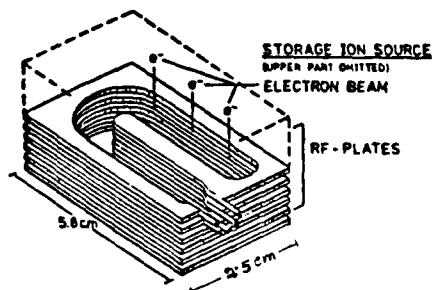
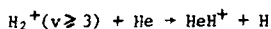


Fig. 1 Plates of storage ion source and the U-shaped holes.

Electrons from a filament are accelerated into the source through one limb of the U-cavity and ions are formed by electron impact on gas molecules. The inhomogeneous r.f. field produces an effective potential well with steep wall, in which ions are stored for some time before being extracted through an exit hole in the other limb of the U-cavity. During the storage, the ions suffer many collisions with the neutral gas which is the key to vibrational de-excitation.

From the photoionization of H_2 with rare gas mixtures,⁽²⁾ the following reactions are known to have definite threshold for ion vibrational energy.



By using a mixture of Ne or He with H_2 in appropriate proportion⁽³⁾ in the ion source and operating the source at high pressure (about 0.1 torr) higher vibrational levels of H_2^+ ions have been effectively quenched leaving the lowest two vibrational levels. State selected H_2^+ ion beam of 10^{-8} A or more has been obtained.

A new low energy cross beam (ion-atom) apparatus has been built for the determination of the quality of these ions by threshold measurement of collisional dissociation of H_2^+ with He. Ions from the storage ion source are extracted, focused by an einzel lens and are mass selected by a Wien Filter before being decelerated to the required energy by a deceleration lens⁽⁴⁾. Then the H_2^+ ions cross a modulated jet of He at right angles. The

primary and secondary ions are accelerated, focused by an electrostatic quadrupole doublet and analyzed by a magnetic mass spectrometer. The secondary ions are detected on a channeltron.

The results of the threshold measurement for the process, $H_2^+(v) + He \rightarrow H^+ + H + He$, is shown in Fig. 2 where the relative cross section of H^+ production has been plotted against the ion kinetic energy. With H_2+Ne (1:5 ratio) mixture in the ion source at a pressure 80 mtorr, only $v = 0$ and 1 levels are seen to be populated. For comparison, the source was tried with pure H_2 at 10 mtorr and the data clearly indicates that higher vibrational levels up to $v = 10$ are present. By taking a mixture of $H_2 + He$ (1:10 ratio) at 100 mtorr, vibrational levels above $v = 3$ are effectively quenched.

Reference

1. E. Teloy and D. Gerlich. Chem. Phys. 4, 417 (1974).
2. W.A. Chupka and M.E. Russell. J. Chem. Phys. 48, 1527 (1968).
3. Z. Herman and V. Pacak. Int. J. of Mass Spec. and Ion Phys. 24, 355 (1977).
4. Z. Herman, J.D. Kerstetter, T.L. Rose and R. Wolfgang. Rev. Sci. Instrum. 40, 538 (1969).

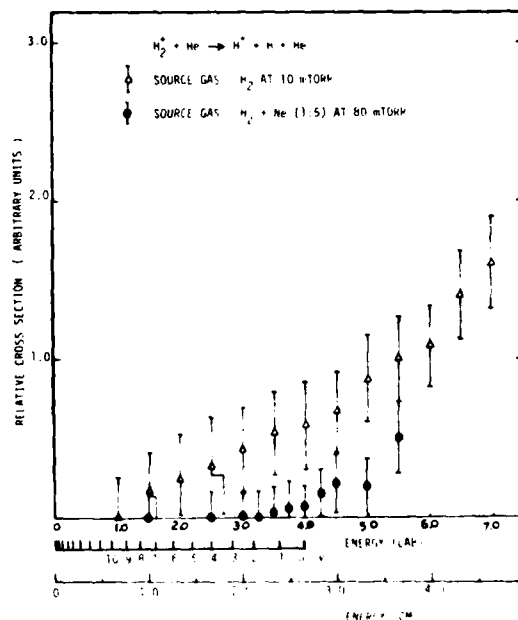


Fig. 2 Relative cross section of collisional dissociation of H_2^+ on He as a function of ion kinetic energy for different source conditions as indicated. Thresholds for different vibrational levels of H_2 are also shown.

CHARACTERISTICS OF A LASER-GENERATED PLASMA
AS SOURCE OF SOFT X-RAYS (200 eV - 1 keV)

H.C. Gerritsen, H. van Brug, F. Bijkerk and M.J. van der Wiel

FOM-Institute for Atomic and Molecular Physics,
Kruislaan 407, 1098 SJ Amsterdam, The Netherlands

The plasma generated by a pulsed laser beam focused on a metal target has attractive properties as a source of soft X-rays. We report a study of the characteristics of such plasmas from various target materials, including emission spectra from 200 eV - 1 keV, source size and photon flux. The plasmas were generated using a 20 J, 15 ns YAG-glass laser; frequency doubling was used in order to optically isolate the laser from the reflecting plasma. Focussing with an $f = 120$ mm lens produces a power density at the target of 10^{13} W cm $^{-2}$. The target is rotated after each laser shot (rep. rate 2/minute).

X-rays within an opening angle of $2 \cdot 10^{-5}$ rad are accepted by a toroidal mirror to give a stigmatic image of the source. A scan of a narrow slit across this image allows a determination of the source size, which we found to be approx. $85 \mu\text{m}$. This value is to a large extent independent of the target material and the X-ray wavelength. The image serves as the object for an X-ray polychromator¹ covering the spectral range from 1.2 - 6.5 nm. The polychromator employs a holographic grating to disperse wavelengths in the range indicated across a position-sensitive X-ray detector. This detector consists of a Au electrode, from which photoemitted electrons are guided by a 1 kgauss magnetic field to a channelplate/phosphor combination, with optical read-out. The overall photon energy resolution is 6 eV FWHM, which is limited but sufficient for the (surface) EXAFS studies planned with this instrument.

The emission by the plasmas consists of a smooth bremsstrahlungs background, on which atomic lines are superposed in certain spectral regions (see figure 1). We have recorded spectra for Mg, Al, Ti, Fe, Ni, Cu, Mo, Ag, Ta, Pb and Bi. The features in the Mg and Al spectra are easily identified as arising from He-like ($1s^2$) configurations, which capture an electron and - after cascade - produce the lower lines of the MgX and AlXI spectra. Similarly, in Ti, Fe, Ni and Cu, Ne-like ions are responsible for the line-emission. In both cases, plasma temperatures of at least 200-300 eV are required. The heavy elements Ta, Pb and Bi show no atomic lines in the range under investigation, reason for which these are the preferred choice for absorption studies. Nevertheless, spectra from one of the lighter elements can conveniently be used for rapid energy calibration.

The total flux of X-rays from Bi, integrated over

the range shown in fig. 1, amounts to approx. 10^9 photons per laser shot. The output is remarkably reproducible, in the order of $\pm 1\%$ from one shot to the next. The dependence on laser pulse power is approximately linear. The X-ray flux quoted above suffices to perform transmission EXAFS measurements on gases and thin foils in single laser shots (fig. 2). Strobe measurements on transient phenomena are presently being considered.

Reference

1. H.C. Gerritsen, H. van Brug, M. Beerlage and M.J. van der Wiel, Nucl. Instr. and Methods, to be published.

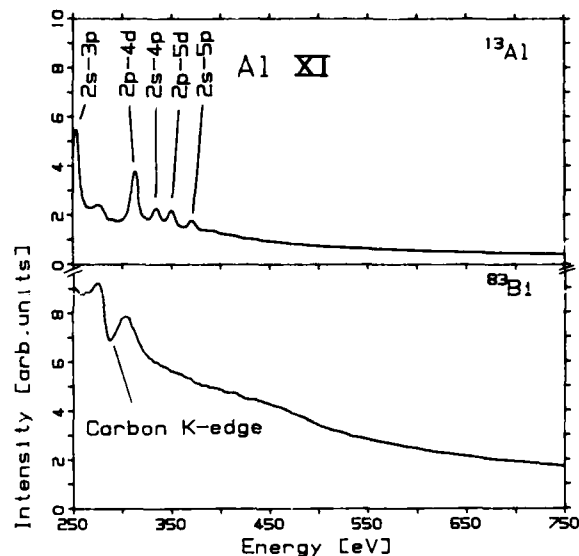


FIG. 1. Emission spectra of Al and Bi targets, uncorrected for polychromator transmission. Integrated yield for Bi approx. 10^9 photons per laser shot.

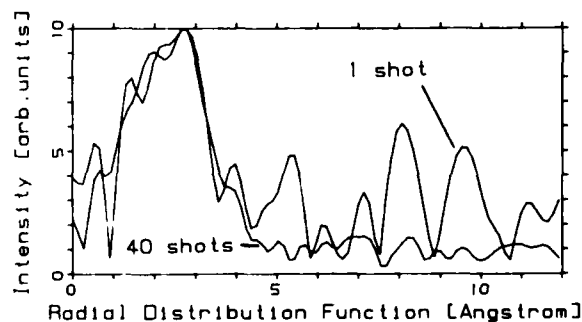


FIG. 2. Radial distribution function of distances in Ti foil (150 nm thick), derived from EXAFS spectrum taken in one laser shot, resp. forty shots.

DIAGNOSIS OF SPIN POLARIZATION IN AN OPTICALLY PUMPED SODIUM BEAM*

J. J. McClelland and M. H. Kelley

Radiation Physics Division
National Bureau of Standards
Gaithersburg, MD 20899

The recent development of an apparatus for measuring spin-polarized electron scattering from spin-polarized atoms¹ has provided the impetus for an investigation, both experimental and theoretical, of the degree of ground-state atomic spin-polarization achievable with laser optical pumping in sodium. From the simplest description of the optical pumping process one expects that, using a circularly polarized pump laser tuned to the $3S_{1/2}$ $F=2 \rightarrow 3P_{3/2}$ $F=3$ transition, an atomic polarization of $5/8$ can be achieved.² This corresponds to all the $3S_{1/2}$ $F=2$ population being concentrated in $M_F=+2$, and the $3S_{1/2}$ $F=1$ population being uniformly distributed. In fact, the net polarization can be less, as a result of either residual population of levels with $M_F < 2$ in $F=2$, or a transfer during the optical pumping process of population from $F=2$ to $F=1$.

We have investigated these two potential sources of incomplete atomic polarization by observing the intensity and polarization of the fluorescence arising from a second, probe laser intersecting the atom beam 3 cm downstream from the pump. Residual population in $F=2$, $M_F < 2$ is diagnosed by monitoring the polarization of the fluorescence when the probe laser is circularly polarized and tuned to the $3S_{1/2}$ $F=2 \rightarrow 3P_{3/2}$ $F=3$ transition. Transfer of population to $F=1$ is detected by tuning the probe to the $3S_{1/2}$ $F=1 \rightarrow 3P_{1/2}$ $F=1$ transition and monitoring any change in the fluorescence when the pump laser is turned on.

The theoretical investigation consists of a calculation of the time dependences of the atomic state populations in the optical pumping process using a numerical solution to the equations governing the time evolution of the density matrix.³ This approach has the advantage that the power-broadened transition probabilities can be correctly treated in the transient period (before optical pumping is complete) where coherence phenomena such as Rabi oscillations may have important effects. The time dependences are integrated over a transit time distribution, which arises from the velocity spread in the atomic beam, and the resulting average increase in $F=1$ population is compared with experiment. The comparison is favorable when account is taken of the small but finite residual doppler width in the atom beam.

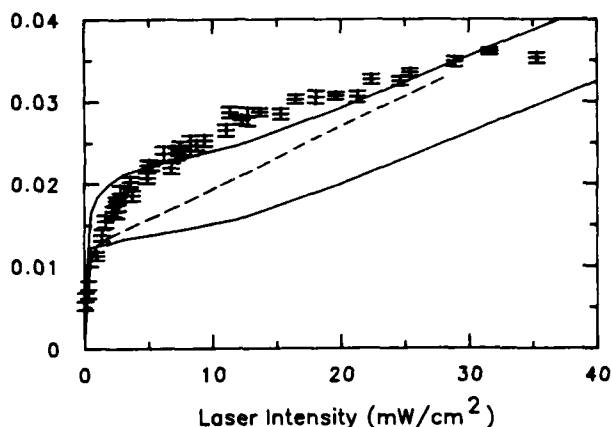


Fig. 1. Fractional increase in $3S_{1/2}$ $F=1$ population as a function of pump laser intensity. Lower solid curve: Calculation with no transverse doppler width. Dashed curve: Calculation with 0.5% "wrong" polarization. Upper solid curve: Calculation with 10 MHz FWHM transverse doppler width.

Both experimental and theoretical results show that an atomic spin polarization of 0.609 ± 0.018 can be achieved reliably and reproducibly, given the following experimental conditions: a residual magnetic field less than 10 mG, a degree of circular polarization in the pump laser better than 0.9998, frequency stability of the pump laser better than 2 MHz, laser intensities in the range 6-12 mW/cm², and an interaction length of 1 cm.

*Work supported in part by the Department of Energy, Office of Basic Energy Sciences, Division of Chemical Science.

¹M. H. Kelley, W. T. Rogers, R. J. Celotta and S. R. Mielczarek, Phys. Rev. Lett. **51**, 2141 (1983).

²I. V. Hertel and W. Stoll, Adv. in Atomic and Molecular Collisions **13**, 113 (1974).

³J. J. McClelland and M. H. Kelley, Phys. Rev. A, (submitted).

ELECTRON LENSES WITH CONTROLLED MAGNIFICATION

D W O Heddle, N Papadovassilakis and Carol Trager

Physics Department, Royal Holloway & Bedford New College,
Egham, Surrey TW20 0EX, U.K.

We have examined the behaviour of a class of electrostatic lens systems which exhibit controllable magnification over a wide range of voltage ratio. The lens systems can be considered as two lenses a distance d apart placed centrally between two conjugate points a distance $2d$ apart. For the photon optical analogue of thin lenses in air it is easy to show that the focal lengths must satisfy

$$f_1/d = (1-3f_2/d)/(3-8f_2/d) \quad (1)$$

and that the transverse magnification can be expressed in terms of one focal length by

$$M = -(3-d/f_2) = -1/(3-d/f_1) \quad (2)$$

The lenses we have studied consist of two 3-element cylinder lenses with the central element in common thus forming a 5-element lens. The use of such a lens as an afocal or telescopic lens was described several years ago¹ and it has been used in a number of laboratories both in electron guns and as the output lens of electron monochromators.

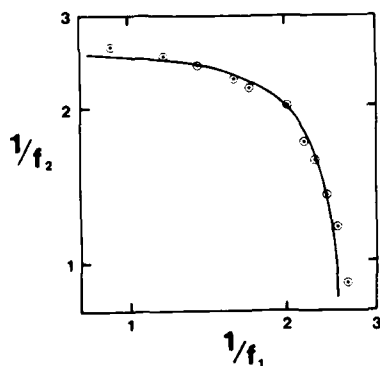


FIGURE 1 The focal length relation of equation 1. The points are for a 5-element lens.

It has the probably unique property of a magnification which can be expressed in terms of the overall voltage ratio as $M = -(V_5/V_1)^{-1/2}$ and which does not depend on details of the lens dimensions or the position of the conjugate points. Figure 1 shows that the behaviour of this lens is reasonably well described by equation 1 for the special case of $V_3/V_1 = 1$ which approximates the "thin lenses in air" condition.

For other overall voltage ratios it is convenient to express our results as lines of constant parameter on axes which show the potentials of the second and fourth electrodes (the "focusing" electrodes of the 3-element lenses) in terms of the potential of the first electrode.

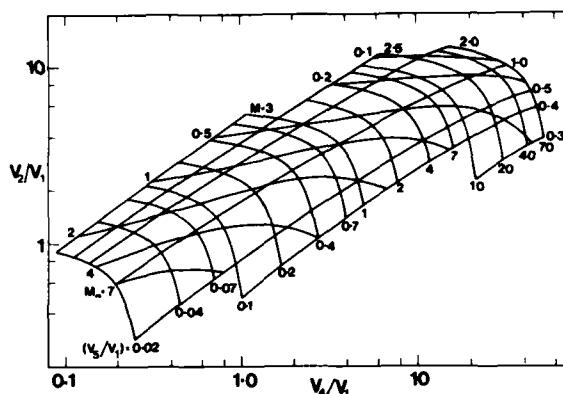


FIGURE 2 Lines of constant M , M_α and voltage ratio for the 5-element lens having $2d = 9D$

Figure 2 shows such lines of constant magnification M , angular magnification, M_α and overall voltage ratio, V_5/V_1 , for a lens having $2d$, the separation of the conjugate points, equal to 9 times the lens diameter. These three parameters are naturally linked by the Law of Helmholtz and Lagrange, but it is clear that a wide range of either magnification may be obtained at a given value of V_5/V_1 .

The data of fig.2 were all obtained with the potential of the central electrode, V_3 , constrained to be such that $(V_3/V_1) = (V_5/V_1)^{1/2}$. In principle it should be possible to adjust a further lens parameter if V_3 is not so constrained and we shall show measurements of the spherical aberration coefficients of these and similar lenses.

We have made further measurements on a similar, but shorter, lens ($2d = 6D$) and find that the range of magnifications is smaller, but it may be the case that the aberration behaviour is better.

¹D.W.O.Heddle J.Phys.E.Sci.Instrum.4, 981 (1971)

SECOND ORDER REDUCTION OF DOPPLER BROADENING OF PROJECTILE ELECTRON SPECTRA
IN A POSITION SENSITIVE 30° PARALLEL PLATE ANALYSER

Joseph K. Swenson

University of North Carolina, Chapel Hill, NC 27514
and Triangle Universities Nuclear Laboratory, Durham, NC 27706

In order to study correlated and uncorrelated electron transfer (e.g. RTE and NTE as has been done by Clark et al.¹) through observation of the Auger decay channel, an electron spectrometer must be capable of resolving Auger lines which arise from different ionic charge states and electronic configurations. These objectives can be attained by means of a position sensitive microchannel plate detector which can be remotely positioned in the focal plane of a parallel plate electron spectrometer.²

Through re-analysis of the focal properties of a parallel plate analyser (PPA), taking into account the angular dependence of the electron energy due to the kinematics of a moving source, second order focusing of projectile electrons can be achieved.³ For a given source velocity and observation angle, kinematically shifted electrons are focused, as a function of electron energy, along a curve which is displaced from the normal focal line. This curve can generally be approximated by a straight line as can be seen in fig. 1. This enables one to make use of a position sensitive electron detector, in an appropriately designed analyser.²

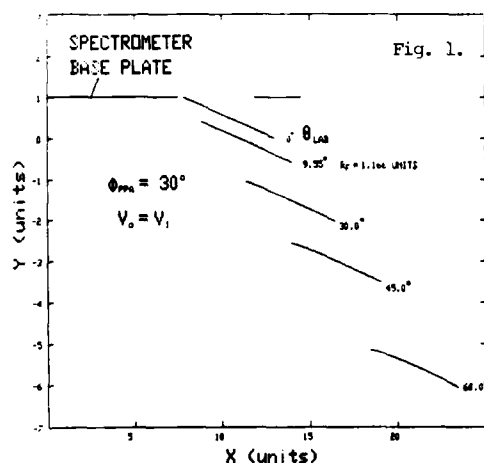


Fig. 1 shows the computed focal curves, which have a lab energy width $\Delta E/E = 100\%$, in a 30° PPA for observation angles θ from 0° to 60° where the center of mass electron velocity equals the ion velocity at the center of each curve. At 0° the focal curve coincides with the normal focal plane derived for a stationary source. Second order focusing occurs at the center of $\theta = 9.55^\circ$ curve. As the θ increases, the curve moves further from the analyser and becomes more curved.

Fig. 2.

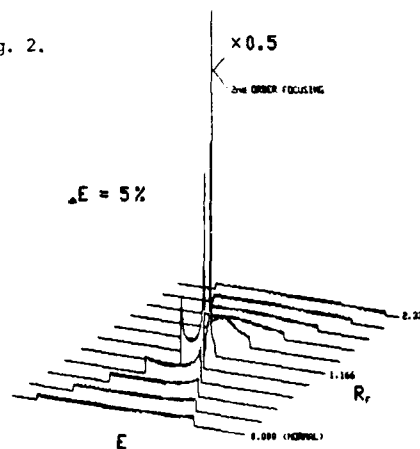


Figure 2 shows the computed point source line shape on the detector line, which is tangent to the focal curve in fig. 1, where $\theta = 9.55^\circ$, and the angular acceptance of the PPA is $\Delta\theta = \pm 3^\circ$. Each successive plot shows the line shape at the center of the detector. As the detector is moved from its normal location (for a stationary source, $R_f = 0$) to the location where second order focusing occurs ($R_f = 1.166$ in units of plate separation) a net reduction in base width of 14 and an increase in intensity of 117 results.

For the above case ($\Delta\theta = \pm 3^\circ$), the base width of the second order refocused peak about 60% greater than that which results for a stationary source. For electrons moving at or greater than twice the ion velocity, the base width of the second order focused line shape is 10% - 20% greater than that for a stationary source. This is a significant improvement in performance as compared to when only first order refocusing⁴ is achieved. Therefore one can almost entirely eliminate kinematic line broadening and thus acquire high resolution projectile electron spectra with high efficiency, using this technique.

This work is supported by the Chemical Sciences Division, U.S. D.O.E.

References

1. M. Clark, D. Brandt, J. K. Swenson, S. M. Shiffrith, Phys. Rev. Letters, **54**, 544 (1985).
2. J. K. Swenson, Proceedings of the 8th Conference on the Application of Accelerators in Research and Industry (Nucl. Instrum. and Meth. May 1985).
3. J. K. Swenson, (to be published).
4. P. Bachmann, A. Eberlein, and R. Bruch, J. Phys. E: Sci. Instrum. **15**, 207 (1982).

CHARACTERISTICS OF A GaAs POLARIZED ELECTRON SOURCE

F.C. Tang,* M. Eminyan,* M.S. Lubell,* J. Slevin,† and A. Vasilakis*

*Department of Physics, City College of CUNY, New York, NY 10031, USA

†Universite Paris 7, 75221 Paris, France

‡Department of Physics, University of Stirling, Stirling FK94LA, Scotland

In conjunction with an experiment treating the spin dependence in electron-hydrogen scattering we have been working with a GaAs photoemission polarized electron source. Like most other sources, our source utilizes a $\langle 100 \rangle$ crystal 0.325 mm thick that is cleaved outside the vacuum system to a dimension of 0.5 cm x 1.0 cm and is etched chemically just prior to insertion into its ultra-high vacuum chamber. Following the Bonn method, our etch consists of a 10 minute bath in a solution of 98% H_2SO_4 , 30% H_2O_2 and distilled water in a ratio of 8:1:1. Upon removal from the bath, we place our p-type Zn doped crystal in a sapphire mount and rapidly insert it in the vacuum system. Typically, the etched crystal is under vacuum at $<5 \times 10^{-6}$ Torr in less than 30 minutes.

Once we have ensured the vacuum integrity of the electron source we begin a 250°C bakeout and maintain it for several days during which we continuously outgas all high-temperature components such as filaments and Cs dispensers. With the use of an ion pump and a room-temperature Ti sublimator we achieve base pressures of $1-2 \times 10^{-10}$ Torr after the bakeout has been completed. Prior to activation with Cs and O_2 we heat the GaAs to ~600°C for several minutes by direct passage of current through the wafer itself. Then we apply Cs and O_2 layers using a Cs dispenser (SAES Getters) and research grade O_2 (99.99% purity) controlled by LN_2 line-cooling and a Granville/Phillips variable leak valve. The "yo-yo" method, in which alternate layers of Cs and O_2 are applied sequentially, appears to provide longer lifetimes.

Initially we use a "white" light lamp for illumination of the crystal, as shown in Fig. 1. As the photocurrent increases we replace the lamp first with a HeNe laser for ease of monitoring and finally with a GaAlAs IR laser for polarized electron emission. During the course of our work we have observed quantum yields ranging from 1% to 6%, which is consistent with measurements made by many other groups.

The major purpose of our report is to call attention to three observations we made which have not been reported by other groups. First, with low level cesiation employed during operation, lifetime (e -folding $>> 270$ h) and stability appear to be enhanced by having O_2 rather than Cs as the final layer applied during activation. Second, with this activation technique and operation procedure, we obtained satisfactory

performance when the source chamber pressure was

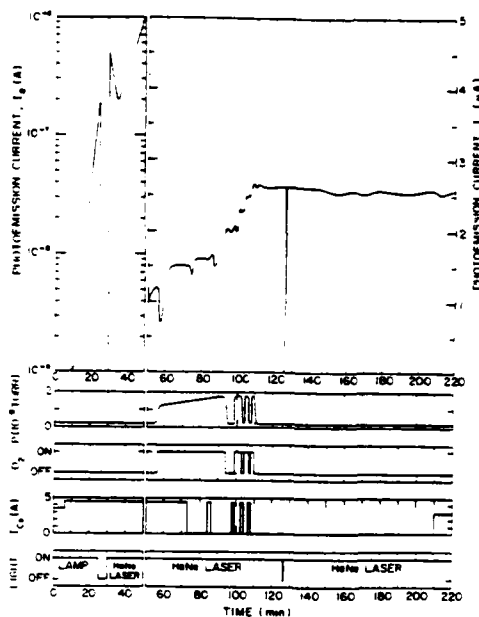


FIGURE 1 Typical Crystal Activation.

allowed to rise to 5×10^{-7} Torr from its base pressure of 2×10^{-10} Torr through a regulated reduction of pumping speed. Finally, and most significantly, we obtained satisfactory photoemission even when the base pressure in our system started at 3×10^{-9} Torr after pumpdown from atmosphere. This behavior is illustrated in Fig. 2.

Research supported by U.S. NSF, U.K. SERC, and NATO.

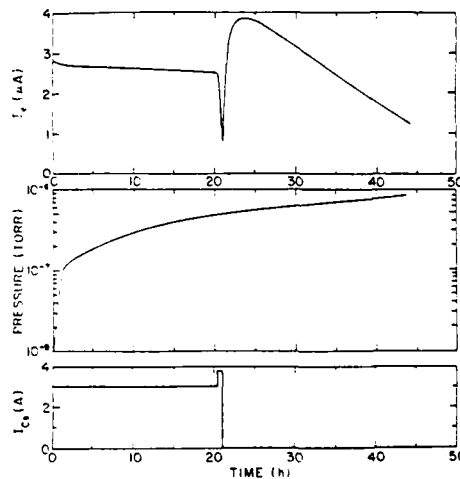


FIGURE 2 High Pressure Photoemission Behavior.

ANTI-COMPTON X-RAY SPECTROMETER

J.F. Chemin, J.N. Scheurer, S. Andriamonje

Institut National de Physique Nucleaire et de Physique des Particules - Universite de Bordeaux I
 Centre d'Etudes Nucleaires de Bordeaux-Gradignan - Le Haut-Vigneau 33170 GRADIGNAN FRANCE

Several applications require a dispersive analysis of the X-rays energies in presence of gamma rays. The analysis of trace elements in radioactive samples is one example. Recently a large attention has been paid to the study of prompt X-rays emitted in nuclear reactions^{1,2}. In this situation several γ rays can be emitted simultaneously with the X-rays. The resulting effect of the γ rays on the X-ray spectrum is the production of a continuous background which severely limits the sensitivity of the X-ray detection. This background is mainly produced by the Compton interaction of the γ -rays with the electrons in the active volume of the detector. We have developed an anti-compton X-rays spectrometer based on the following principles.

A Compton interaction in the detector volume produces a free electron and a photon at an angle θ with respect to the primary photon. The electrons stopped in the detector volume have a continuous distribution energy. In X-ray analysis the relevant X-ray energies are ranging between a few keV to a hundred keV. The kinematic of the Compton effect indicates that electron energies in this range are related to small scattering angle θ of the photon. More energetic Compton electrons may also induce a background in this range if they are not fully stopped within the active volume of the detector. This well known edge effect is enhanced in the case of γ -ray interaction.

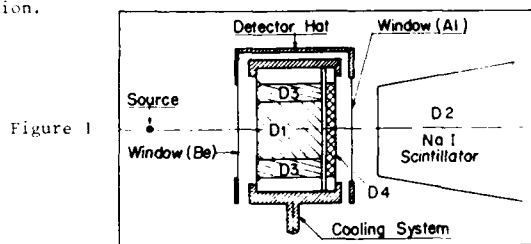


Figure 1

The schematic diagram of the spectrometer is shown in Fig. 1. Four independent detectors participate to the anti-compton effect. D_1 , a 200 mm^2 , 5 mm thick Si(Li) detector; D_2 , a $5'' \times 5''$ NaI scintillator, whose the front-side is located 4 cm from the backside of D_1 ; D_3 , a Si(Li) annular diode surrounding D_1 , which acts as an active guard ring detector responding³ to the escaping electrons from D_1 ; and D_4 , a thin surface barrier detector located 2 mm from the rear side of D_1 , which responds to the electrons escaping from the back side of D_1 . A coincident signal, given by a fast coincidence circuit, between D_1 and D_2 or D_3 or D_4 means a spurious event in

the X-ray energy range of the spectrum, due to a γ -ray Compton interaction or an incomplete charge collection in D_1 . Such a signal is prevented to proceed through the linear gate of the ADC working in the anti-coincidence mode.

The performances of the spectrometer have been measured with radioactive γ -ray sources ^{109}Cd , ^{22}Na , ^{60}Co . The spectra in Fig. 2 show the result obtained with a

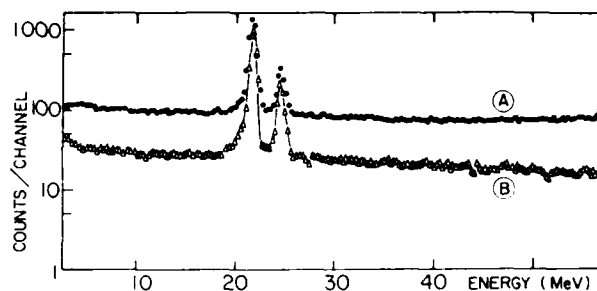


Figure 2

^{22}Na source mounted at 1 cm from the Be window. A ^{109}Cd source deposited on a thin backing was placed at 1 mm. An aluminium absorber, 100 μm thick, was fixed against the Be window. The counting rate in the D_1 detector was equal to $700 \text{ counts s}^{-1}$. The spectrum A was recorded in the direct mode. The spectrum B was taken for the same time than the spectrum A in the anti-coincidence mode.

The comparison between the spectra shows directly the effect of the system on the background reduction. The flat background induced by the γ -ray source is reduced by a factor of 3 almost independent of the energy. On the contrary the net intensities of the K_{α} and K_{β} lines of Ag emitted by the ^{109}Cd source are only reduced by 5%. This last number is a direct measurement of the specific dead time brought by the anti-coincidence system.

In this experimental situation the anti-compton system brought a net improvement of the signal to background ratio equal to 300%. A more detailed analysis of the performances will be given in a forthcoming publication. The main part of the remaining background is due to multiple Compton scattering taking place in the material around the detector. In principle increasing the volume of D_2 will reduce it, but unfortunately will also increase considerably the dead time of the detector in situation where a large γ -ray multiplicity is expected.

References

1. J.F. Chemin and al - Nucl. Phys. A 331 (1979) 407
2. W.E. Meyerhof and J.F. Chemin - Advances in Atomic Physics, Vol. 20 (1984)
3. D.A. Landis, F.S. Goulding, B.R. Jarrett-NIM101(1972)127

PRODUCTION OF A FAST BEAM OF HYDROGEN ATOMS IN THE 3s STATE

W. Claeys, A. Cornet, V. Lorent and D. Fussen

Université Catholique de Louvain, Institut de Physique, Chemin du cyclotron, 2
B 1348 Louvain-la-Neuve, BELGIUM

In an earlier work (1) we have described a method to produce a fast intense beam of H(3p) atoms by laser excitation of metastable hydrogen. The very short lifetime of the 3p state (5.4 nsec) limits severely the domain of applicability of the method. The 3s state has a 30 times larger lifetime (160 nsec) and is therefore a better candidate for experimental work. Direct 2s-3s optical transitions are not allowed, but if the atoms are placed in an electric field, dipole transitions between Stark states are allowed.

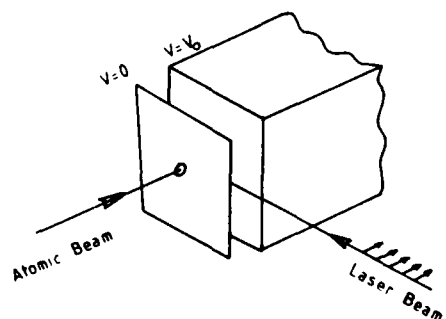


Fig. 1

We produce H(3s) atoms in a two step process. First H(2s) atoms are entered adiabatically in an electric field region where they are crossed by an intense frequency adjustable laser light (see figure 1). Laser excitation will induce transitions between Stark states. For a given field strength, all n=3 Stark states can be selectively populated by tuning the laser frequency; in particular, transitions to the Stark state which correlates at zero field to the 3s state can be selected. Afterwards, the excited atoms leave the electric field region and evolve adiabatically towards non perturbed atomic states.

The initial metastable hydrogen beam is obtained by charge exchange of protons on a gaseous Cs target. The excitation light is produced in a singlemode ring dye laser. In order, for such an hydrogen beam, to be of practical use in the field of collision physics, one has to assess the fraction of excited atoms in the neutral beam. This is obtained in determining the excitation efficiency absolutely by measuring the relative change in metastable content of the beam due to laser excitation. This is done at a location distant enough from the laser atom interaction point for all n=3 atoms to have decayed radiatively. Lyman α light is detected from the induced emission of 2s atoms passed in a strong electric field. In the absence of laser excitation, N_1 the Lyman α count

rate is proportional to the 2s beam intensity $N(2s)$:

$$N_1 = k N(2s)$$

With the laser on, the excitation leading to the formation of 3s atoms, depopulates the metastable beam

$$N_2 = k N(2s)(1-\beta) \quad \text{where } \beta \text{ is the } (2s-3s) \text{ excitation efficiency.}$$

We have computed the n=2 and 3 energy levels and Stark states as a function of the static field strengths and derived the dipole moments; our experimental observed values are in good agreement. These were obtained from 2s depopulation measurements.

Figure 2 shows the 3s hydrogen beam fraction after laser excitation for different field strengths at the laser-atom interaction point. The results were obtained with a 3 keV beam and a laser power of 400 mW, the electric field is obtained between two plates 2mm apart. The absolute accuracy is estimated 0.02. For low values of field strengths ($F < 300$ V/cm) the Stark separation between the n=3 levels is not sufficient for our spectral resolution (~ 1 MHz) to allow absolute efficiency measurements. To extend the range of our measurements, we have placed a second Lyman α detector 15cm beyond the laser-atom interaction point and observed spontaneous decay light from the 3s atoms. This detector has shown that only one n=3 Stark state contributes to the formation of H(3s) atoms.

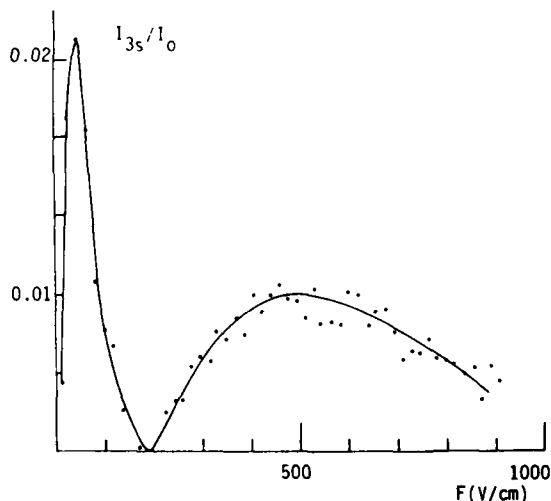


Fig. 2

Reference (1)

A. Cornet et al., J. Phys. B: At. Mol. Phys. **17**, 2643

ELECTRONIC, IONIC AND ATOMIC DENSITIES AND TEMPERATURES
IN H^- MULTIPOLE SOURCES

M. P. S. Nightingale, A. J. T. Holmes and T. S. Green

UKAEA, Culham Laboratory, Abingdon, Oxon. OX14 3DB, England

Spectroscopic, probe and beam measurements have been used to investigate the underlying physics of H^- production in volume multipole sources for possible fusion applications. Measured electronic, ionic and atomic populations and energies will be reported and discussed in terms of the dominant collision processes.

DIFFERENTIAL CROSS-SECTION FOR SINGLE AND DOUBLE CAPTURE IN Ne^{7+} -He COLLISIONS

P. Roncin*, H. Laurent*, J. Pommier*, D. Hitz**, S. Dousson**
and M. Barat*

**CENG, Agrippa-CEA-CNRS, 85X, F 38041 GRENOBLE Cedex
*LCAM, Bât. 351, Université Paris-Sud, F 91405 ORSAY Cedex
*IPN, Bât. 100, Université Paris-Sud, F 91405 ORSAY Cedex

A parallel plate electrostatic analyzer, associated with a two-dimensional position sensitive detector has been built allowing a simultaneous determination of the energy gain and of the scattering angle θ . This device was used to study, by "translational spectroscopy" the various electron-capture processes as a function of the collision energy. Experiments were performed using an ECR ion source available at the AGRIPPA facilities in Grenoble.

As an example, we present here results obtained for electron capture in Ne^{7+} -He collisions. Figure 1 shows that the spectra are dominated (peak I) by one electron capture into the He^{6+} ($n=4$) + He^+ channel as already been observed by several authors^{2,3}. However two weaker peaks show up that were attributed³ to two electron capture into autoionizing states (DCA) :

peak II $\text{Ne}^{5+}(n=3, n'=4) + \text{He}^{++}$

peak III $\text{Ne}^{5+}(n=4, n'=4) + \text{He}^{++}$

It is readily seen that the angular behaviour is very different for the 3 processes. Fig. 2 shows the relative probability at a collision energy of $E=10.5$ keV. In

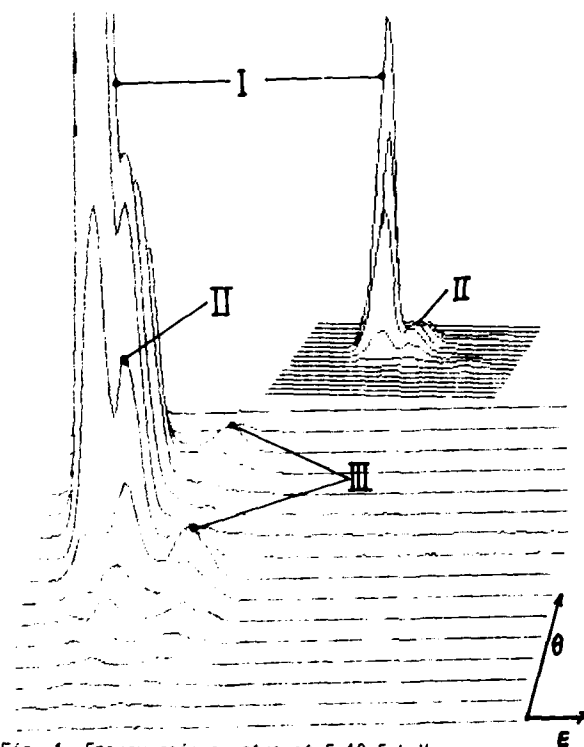


Fig. 1. Energy gain spectra at $E=10.5$ keV.

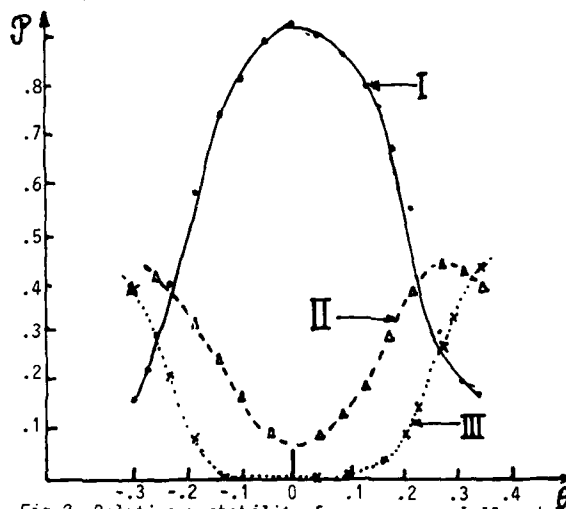


Fig.2. Relative probability for processes I,II and III

particular, it is seen that the DAC processes are characterized by a much larger scattering angle. Data obtained at $E=7.5$ keV is similar and perfectly scale in the $\tau=E\theta$ reduced coordinates.

A scheme of the potential curves is shown in the insert of fig. 2. The present angular behaviour strongly suggests that double capture processes occur via a two step mechanism (one electron is captured at the A crossing the second electron at the B or B' crossing). This is at variance with a mechanism involving a simultaneous capture (via electron correlation) at the C or C' crossing. Actually the large scattering angle is associated with the path along the repulsive AC and AC' curve on the way in. Furthermore one see that inner the crossing (C or C'), larger the scattering angle.

References

1. P. Roncin, H. Laurent and M. Barat, Submitted to J. Phys. E (1985)
2. H. Tawara *et al.*, Phys. Rev. **29**, 1529 (1984)
3. C. Schmeissner, C.L. Cocke, R. Mann and W. Meyerhof, Phys. Rev. **30** 1661 (1984)

FORMATION OF LOW LYING AUTOIONIZATION STATES IN Li^- , C and C^- PROJECTILE IONS STUDIED BY ZERO-DEGREE ELECTRON SPECTROSCOPY

R. Bruch,* D. Schneider,+ and N. Stolterfoht,++

*Department of Physics, University of Nevada Reno, Reno, NV. 89557 USA

+Department of Physics, University of Toledo, Toledo, OH 43606 USA

++Hahn-Meitner-Institut für Kernforschung Berlin, D-100 Berlin 39, West Germany

Low lying resonances and bound states in H^- , He^- , Li^- , Be^- , B^- and C^- may be formed by electron capture and excitation in ion-atom and ion-foil collision processes. Such negative ions are of fundamental importance in fusion research and reflect strong electron-electron correlation effects, which require accurate many-body theoretical calculations.¹

This contribution is concerned with high resolution electron spectroscopy of low energy electrons (<2 eV) following the decay of low-lying autoionizing states formed in gas (He , CH_4 , Ne , Ar) or C-foil collisions with Li^- and C^- ions (100-500 keV). In this study the zero-degree Auger spectroscopy method² has been used for the following reasons: (i) High energy resolution of the order of 10^{-3} is maintained due to drastic reduction of kinematic line broadening effects. (ii) Transformation from the laboratory to the source particle frame allows to accurately measure and identify autoionization transitions with energies even below one eV. Electrons ejected from the interaction region are analyzed by a tandem-type electrostatic electron spectrometer.² Fig. 1 and 2 display characteristic electron spectra from foil and gas excited Li and C ions. The inserted spectra indicate discrete peaks in the vicinity of the high energy cusp tails after background subtraction and transformation into the center of mass system. In the Li spectrum three sharp lines occur below 1 eV which most likely stem from autoionizing transitions involving Li^- ($1s^2 2s 2p$) $1,3P^0$ and ($1s^2 2p^2$) $1D$ and $1S$ initial states. We also note that the structures between one and two eV may arise from doubly excited states in Li^- such as $1s^2 n'n''$ with n and $n' > 3$. Principally also high Rydberg states associated with doubly excited levels in Li^+ ($n'n''$), Li ($1s n'n''$) and triply excited Li ($n'n''n'''$) states may contribute to the observed spectrum.³

A similar tentative interpretation is assumed for the carbon autoionization structures. A very intense line centered at 0.25 eV may result from C $1s^2 2s^2$ $n'n''(n,n'+2)$ or C^- $1s^2 2s^2 2p n'n''(n,n'+2)$ initial configurations.

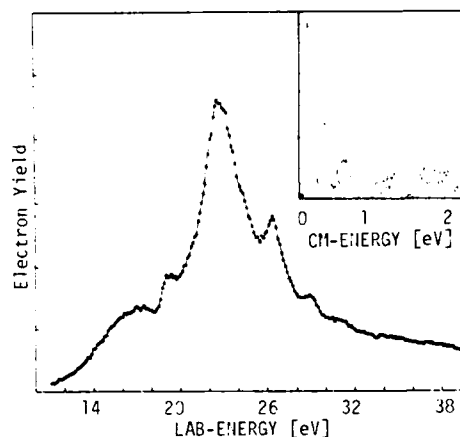


Fig. 1 Lithium autoionization spectrum for 300 keV Li^+ incident on a $5 \mu\text{g}/\text{cm}^2$ carbon foil.

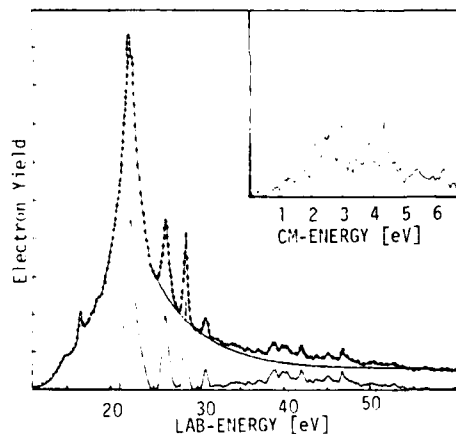


Fig. 2 Carbon autoionization spectrum for 400 keV C^+ on Ne .

References

1. D. R. Beck and C. A. Nicolaides, Int. J. Quantum Chem. S18, 467 (1984)
2. A. Itoh et al., Phys. Rev. A31, 684 (1985)
3. M. Rødbro, R. Bruch and P. Bisgaard, J. Phys. B12, 2413 (1979)

IONIZATION-EXCITATION AND DOUBLE EXCITATION OF HELIUM BY H^+ , C^{4+} , C^{3+} AND C^+ AT HIGH VELOCITIES

R. Bruch*, E. Träbert*, S. Fülling*, P. H. Heckmann* and B. Raith*

*Institut für Experimentalphysik III, Ruhr Universität Bochum, 4630 Bochum, West Germany

*Department of Physics, University of Nevada, Reno, Reno, NV. 89557, USA

At sufficiently high velocities the dominant mechanism for multiple excitation and ionization of atoms by highly charged ions is closely related to the photoionization process.¹ On the other hand at intermediate velocities multiple ionization-excitation may be described in terms of the independent electron approximation.² Due to electron-electron correlation during the collision this independent electron model may break down for specific collision systems. Therefore we have investigated ionization-excitation and double excitation of helium by 1 to 6 MeV H^+ , C^+ , C^{3+} and C^{4+} impact on He. The basic experimental arrangement is similar to that used in our previous work on electron capture.³ High resolution EUV spectra from the recoiling target ions are analyzed at right angles with an intensity calibrated 2.2 m grazing incidence monochromator. A detailed spectroscopic line identification reveals new information on multiple processes such as ionization-excitation and double excitation of the target. A typical spectrum showing the HeII ($np + 1s$) series for 1 MeV H^+ on He is plotted in Fig. 1. It is interesting to note that mainly the first three $np(n \leq 4)$ states in HeII are formed by H^+ impact. In comparison the $C^{4+} + He$ data clearly indicate that also higher Rydberg levels up to $n = 12$ are efficiently populated. Some relative cross sections for 2-5 MeV $C^{4+} + He$ are given in Fig. 2. We have also investigated the production of doubly excited (n, n') states. In particular due to strong collision induced electric fields the formation of exotic new He^{**} levels has been observed for the first time.⁴ Moreover we have studied the role of projectile ionization-excitation. A striking result is that for $C^+ + He$ the observed EUV spectrum is completely dominated by transitions associated with $C^{2+}(1s^2; n^2)$ states.

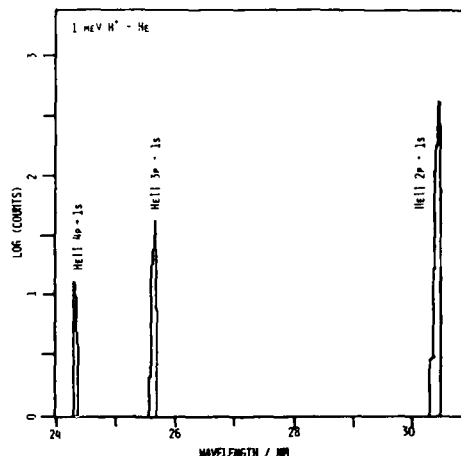


Fig. 1. EUV spectrum corresponding to $He^+ np + 1s$ ($n \leq 4$) transitions observed with a 2.2 m grazing incidence spectrometer.

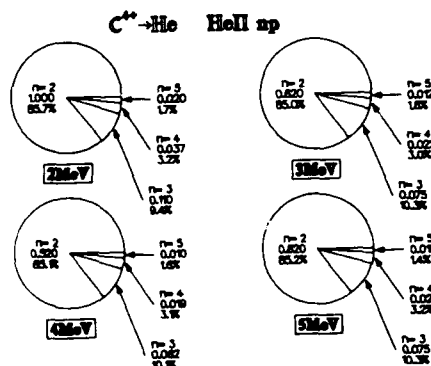


Fig. 2. Relative cross sections for ionization-excitation of helium by 2-5 MeV $C^{4+} + He$ impact.

References

1. J. H. McGuire, J. Phys. B1779 (1984).
2. R. Bruch, L. Kochbach, E. Träbert, P. H. Heckmann, and B. Raith, Nucl. Instr. Meth. (1985) in press.
3. L. J. Dube, U. Will, R. Bruch, E. Träbert and P. H. Heckmann, Nucl. Instr. Meth. (1985) in press.
4. R. Bruch, P. L. Altick, E. Träbert and P. H. Heckmann, J. Phys. B17, L655 (1984).

AN EFFECTIVE OPERATOR FOR DIELECTRONIC RECOMBINATION

Peter Winkler

Department of Physics, University of Nevada, Reno, Nevada 89557 USA

Viewing the dielectronic recombination as an inverse photoionization process of an atom or molecule in a Rydberg state, a unified many-body theory of radiative and dielectronic recombination has been proposed which includes a treatment of the competing autoionization decay channel on the same footing.

Propagator methods have become quite a standard tool in the study of photoelectron spectra.^{2,3} Their use in connection with electron scattering resonances has been proposed and discussed in a previous publication.⁴ Autoionizing states may be interpreted as resonances in the scattering cross section of electrons off positive ions. The cross section for the elementary recombination process is proportional to the square of the T matrix element connecting the initial state (ion + free electron) with the final state (Rydberg atom or molecule). The following representation of the T matrix element is useful:³

$$T_{pk} = i/d^3 r f_p^*(r) r f_k(r) + i/d^3 r d^3 r' d^2 r_1 f_p^*(r) \left[\frac{\delta \hat{\Sigma}(r, r')}{\delta u(1)} r_1 \right] f_k(r')$$

with the first term on the right describing radiative and the second dielectronic recombination. The term in square bracket is the effective dipole operator containing the response of the decaying system. A particular diagrammatic representation of this term is given in Fig. (b). The functions f_m are the self consistent solutions of Dyson's non-relativistic amplitude equation

$$\{E_m(e) - [L_2^{-2} + U]\} f_m(r) - i/d^3 r' \hat{\Sigma}(r, r'; e) f_m(r') = 0$$

with U being an appropriately chosen one-electron potential and $\hat{\Sigma}$ the self-energy operator. A particular diagrammatic representation of the self-energy is depicted in Fig. (a). The diagram of Fig. (b) is obtained by replacing the last interaction matrix element by an elementary dipole matrix element. All essential many-body effects are contained in the matrix \hat{h}_p . The simplest decaying intermediate states are of the 2 particle 1 hole type. It is well known from other approaches (e.g. hyperspherical coordinates) that such states are best described by the introduction of collective coordinates. The corresponding tool in propagator theory is the summation of certain diagrams in infinite order. It is shown that several such summations are required in the present case in order to assure the correct convergence of various resonance series.

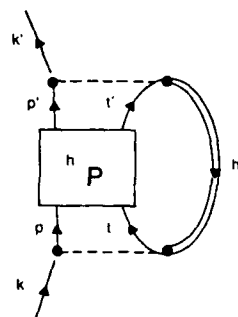


Fig. (a)

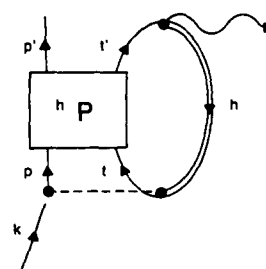


Fig. (b)

References

1. P. Winkler, to appear in Int. Jour. Quant. Chem.
2. L. S. Cederbaum and W. Domcke, Adv. Chem. Phys. **36**, 205 (1977).
3. B. Schneider, Phys. Rev. **A7**, 557 (1973); and 2222 (1973) (E).
4. P. Winkler, Z. f. Physik **A291**, 199 (1979); Phys. Rev. **A23**, 1787 (1981).

Na^+ ION PRODUCTION IN A MICROWAVE DISCHARGE

M.J. Hogan and P.P. Ong

Physics Department, National University of Singapore, Kent Ridge, Singapore 0511

In recent years microwave discharges have often been used as sources for gaseous ions. Such sources have a number of attractive features¹ of which an important one is simplicity of construction. We describe here the use of a microwave discharge for the production of non-gaseous ions, specifically Na^+ .

The ion source which was used is shown in Figure 1. It consists of a quartz tube closed at one end with a molybdenum disk. The ions produced exit through a cluster of seven 0.67 mm diameter holes in the disk. The quartz tube is surrounded by a foreshortened $1/4$ wave coaxial microwave cavity² operating at 2.45 GHz.

Na^+ ions were produced by all three substances studied; i.e. sodium iodide in argon, sodium in argon and pure sodium vapor. The ions were sampled through a 0.8 mm diameter exit orifice at the far end of a drift tube. The relative and absolute numbers of the sampled ions were measured with a quadrupole mass spectrometer. By pumping through a bypass valve the drift tube pressure was kept low enough to ensure that the ions had a very low possibility of collision before being detected.

Temperature was a critical parameter in the production of Na^+ ions since the vapor pressure of sodium increases very rapidly with temperature. Elevated temperatures were achieved by reducing the cooling air flow on the quartz tube and/or increasing the microwave power.

In the cases of NaI in Ar and Na in Ar, the rate of production of Na^+ ions was strongly dependent on the argon pressure with larger numbers at lower pressures. The amount of Na^+ ions also increased relative to the total ion production as the pressure decreased.

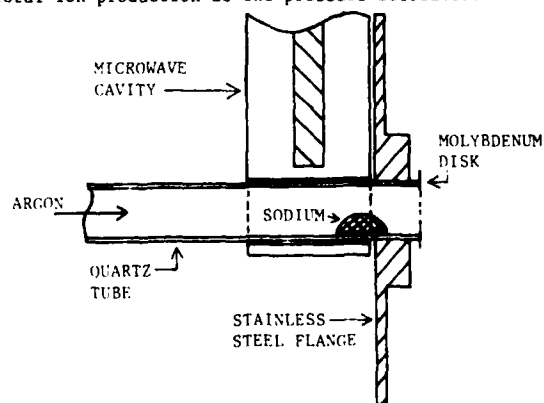


FIGURE 1 Microwave Ion Source

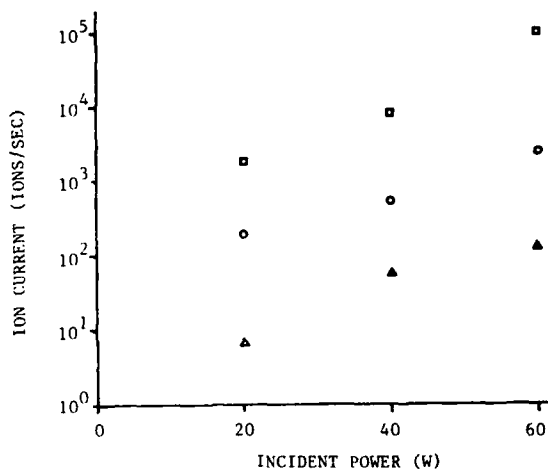


FIGURE 2 Na^+ ion current for Na in Ar
(□ = 0.016 mbar, ○ = 0.041 mbar, △ = 0.065 mbar)

Higher levels of incident power also greatly increased the rate of Na^+ ion production. Figure 2 shows a logarithmic plot of the number of sampled Na^+ ions as a function of incident power for three different argon pressures in the case of Na in Ar. For the point at 0.016 mbar and 60 W, a total current measuring approximately $5 \mu\text{A}$ was recorded by an electrometer to be flowing into the drift tube. Similar graphs were obtained for NaI in Ar, but with somewhat lower ion number counts both in absolute and relative terms.

After a Na in Ar discharge had been running for some time at 60 W, it was possible to cut off the argon supply and still maintain a discharge in the sodium vapor alone. The sampled rate was in excess of 2×10^5 ions/sec and a mass spectrum showed the ions produced to be more than 95% Na^+ ions. However, such a discharge was only stable for long periods of time when the sodium had been newly placed into the quartz tube. After the source had been running for many hours, a pure sodium discharge could not be maintained presumably due to depletion of the sodium in the tube. More details of the operating conditions will be presented.

References

1. P.P. Ong, M.J. Hogan, and K.L. Tan, Proceedings of the First Asia-Pacific Physics Conference, Singapore, 1983, edited by A. Arima et al (Institute of Physics, Singapore, 1984)
2. F.C. Fehsenfeld, K.M. Evenson, and H.P. Broida, Rev. Sci. Instr. **36**, 294 (1965)

VELOCITY DISTRIBUTIONS OF Ne^+ AND Ar^+ IN THEIR PARENT GASES

P. P. Ong and M. J. Hogan

Physics Department, National University of Singapore, Kent Ridge, Singapore 0511

Although knowledge of velocity distributions of ions drifting in gases under the influence of an electric field is necessary for unfolding cross sections from data on ion-neutral reaction rates, there has been to date few such measurements made. We report here the velocity distributions of Ne^+ and Ar^+ ions drifting in their respective parent gases. Data was obtained for neon from 60 to 220 Td and for argon from 80 to 320 Td.

A drift tube mass spectrometer was used for this work.¹ Ions were produced in a microwave discharge and then passed into a drift tube where a uniform electric field and collisions with the buffer gas caused them to attain a non-Maxwellian velocity distribution. The ions were sampled through a small exit orifice which led to a specially designed ion optics system containing a retarding potential grid. Ions surviving the applied retarding potential were analyzed by a quadrupole mass spectrometer of wide acceptance angle and detected by single particle counting technique. The output was recorded on a multichannel analyzer which was triggered by a pulse that coincided with the start of a ramp voltage applied to the grid. The resulting data was smoothed by Fourier analysis and differentiated numerically to yield the velocity distribution.

The ions detected were those which had a predominant z-direction component; the angle which their path made with the central axis being no more than 14° . The distribution curve measured was consequently that of the z-component of velocity of ions moving nearly parallel to the electric field. Under this experimental condition the measured distributions can be interpreted as the speed distributions of ions moving exactly and nearly parallel to the direction of the electric field with an error of less than 3%.

Figure 1 shows representative results. Presented are a Ne^+ in Ne curve at a relatively low ratio of electric field to neutral number density (E/N) and an Ar^+ in Ar curve at a relatively high ratio. Features common to all curves are peaks that are shorter and broader than the corresponding Maxwellian speed distribution with the same rms velocity, together with enhanced high velocity tails. As E/N is increased for a given gas, the experimental peak is shifted by ever larger amounts to the low velocity side of the Maxwellian peak. The curves also become increasingly asymmetric.

The measured rms velocity was found to be always greater than the rms velocity calculated from Wannier's equation.² This is expected³ since the ions moving in the

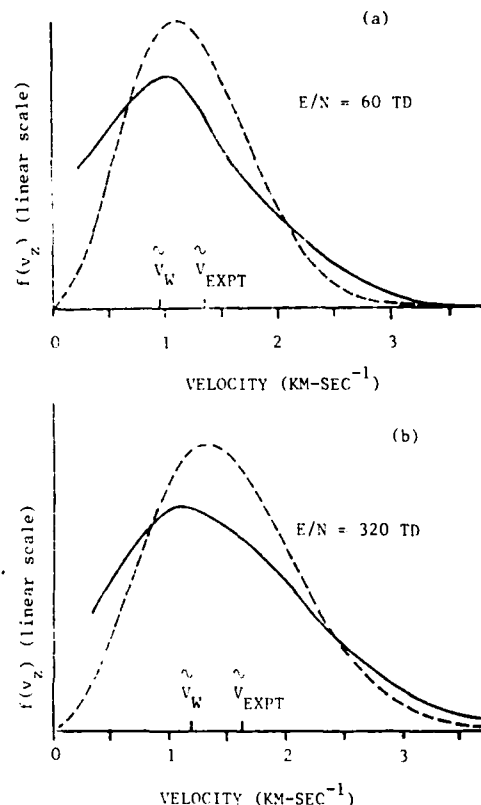


FIGURE 1 Velocity distributions of (a) Ne^+ in Ne and (b) Ar^+ in Ar. Solid line is experimental curve and broken line the equivalent Maxwellian. \tilde{v}_{EXPT} and \tilde{v}_W are the rms experimental and Wannier velocities respectively.

near z-direction contain the majority of the high velocity ions whereas the Wannier expression is for the entire ion population.

These results provide values with which theoretical calculations can be compared if the corresponding velocity distributions are calculated.

REFERENCES

1. N. J. Hogan, P. P. Ong, and K. L. Tan, *Sing. J. Phys.* **1**, 37 (1984)
2. G. H. Wannier, *Bell Syst. Tech. J.* **32**, 170 (1953)
3. N. J. Hogan and P. P. Ong, *Int. J. Mass Spectrom. Ion Processes* (1985) in press

LATTICE SOLUTION OF THE TWO- AND THREE-PARTICLE SCHRÖDINGER EQUATION

Michael V. Ivanov

Institute of Precambrian Geology and Geochronology USSR Academy of Sciences, Leningrad 199164 USSR

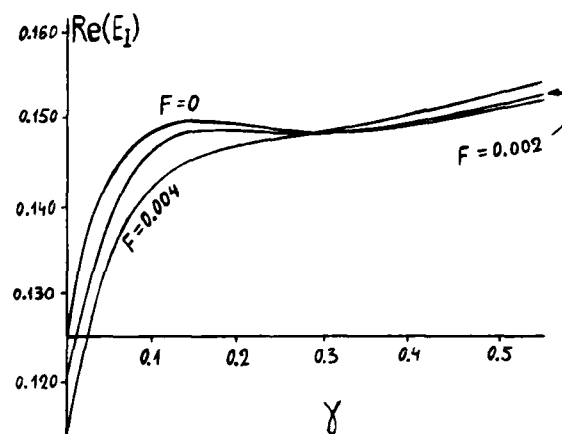
The variables in the Schrödinger equation for majority of the non-relativistic quantum systems are not separable. In this case for the numerical calculations the decomposition of the wave function Ψ into basis functions is usually used. The choice of the basis has the essential influence to the precision and must fulfil all over again for every new problem. Such choice is connected generally with the rather complicated analytical calculations and not always is successful. For the two- and threeparticle systems as the alternative to the wave function decomposition the lattice methods and, in particular, the finite-difference-method may be proposed.

The accuracy of the calculations with the finite-difference-method is less depended on the such arbitrary acts as the choice of basis and this accuracy can be sufficiently increased by means of the standard ways of the computing mathematics: the use of high orders of the approximation of derivatives, Richardson's extrapolation, the non-uniform lattices. Besides, the volume of the analytical calculations decreases considerably.

The systematic development of these considerations permitted to make the computer program for the calculation of the energy eigenvalues of the stationary and quazistationary eigenstates of systems, which are described with two- or three-dimensional Schrödinger equation.

The most part of the problems solved by now applies to the hydrogen atom in cylindrical-symmetric external fields (the equation in cylinder coordinates). For a hydrogen atom in magnetic field B when $0 \leq \gamma \leq 10^4$ ($B = \gamma B_0$, $B_0 = 2.35 \cdot 10^9$ Gs) the relative error of the ionisation energy computation for the ground and lower excited states is about 10^{-5} for the maximal lattice 30×30 (3 min. on the 0.7 Megaflop computer). This accuracy is little less than accuracy in the best calculations.¹ The calculations were made also for a hydrogen atom in a magnetic field when the electron-proton interaction potential is $-e^2 \exp(-\delta r)/r$ and for a hydrogen atom in the electric F and magnetic fields ($F \parallel B$). The escape of electrons for $F \neq 0$ was taken into account with complex boundary condition of diverging wave. The results

for $\gamma = 0$ and $0 \leq F \leq 0.25$ a.u. are in a good agreement with the results.² Some results of these calculations are shown in the figure.



Re $(E_I)(\gamma)$ for the 2s state of H atom when $F = 0$ and the corresponding dependences for $F \neq 0$. (F in a.u., $E_I = \gamma/2 - E$).

Nowdays for the three-particle systems the calculation of the He atom ground state energy for the screened (that is multiplied by $\exp(-\delta r)$) interparticle interactions potential for $0 \leq \delta \leq 2.1$ has been made. The length of vectors r_1 and r_2 and the angle between them θ were taken as coordinates. For $\delta = 0$ the error (ΔE) of the solution of the equation for $\Psi = r_1 r_2 \Psi$ is $5 \cdot 10^{-4}$ a.u. for the maximal lattice $10 \times 10 \times 10$.

REFERENCES

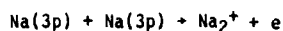
- ¹ W. Rösner, G. Wunner, H. Herold, H. Ruder, J. Phys. B **17**, 29 (1984).
- ² M. Hehenberger, H. V. McIntosh, E. Brändas, Phys. Rev. A **10**, 1494 (1974).

DIRECT MEASUREMENT OF THE VELOCITY DEPENDENCE OF
ASSOCIATIVE IONIZATION CROSS SECTION IN Na(3p) + Na(3p) COLLISIONS

M-X Wang, M.S. DeVries, J. Keller, J. Weiner

Department of Chemistry, University of Maryland, College Park, Maryland 20742, USA

The velocity dependence of associative ionization cross section for collisions between Na(3p) atoms is determined in a crossed-beam experiment using a Doppler shift velocity selection technique.



Previously reported AI cross sections exhibit a rather small value (about 10^{-16} cm^2) and the disparity between those results suggest that the AI probability may strongly correlate with collision velocity.¹⁻³ The present study has directly measured this correlation in the collision energy range 0.08 eV - 0.29 eV. We achieve highly resolved velocity selection through laser excitation of narrow velocity groups in the Doppler profile of two crossed Na beams. The inherent advantages of this technique, which was developed by Pritchard et al. for cell experiments,⁴ are significantly enhanced in the present crossed-beam experiment due to a much wider range of high-resolution velocity selection. Since both collision partners are optically excited and hence, velocity selected, the collision velocity resolution is also greatly improved.

Two collimated atomic-beam sources (angular divergence less than 35 milliradian) are oriented at 90° with a cw ring dye laser bisecting the angle between the sodium beams. The cw laser (bandwidth = 1 MHz) is tuned to $3s \ ^2S_{1/2}(F=2) \rightarrow 3p \ ^2P_{3/2}(F=3)$ transition. A UV laser ($\lambda=351 \text{ nm}$), collinear with and counterpropagating to the dye laser, probes the excited atomic state population by selective photoionization out of the 3p level. The atomic density in the interaction region is $5.2 \times 10^{10} \text{ cm}^{-3}$, and the velocity distribution fits a Mach 6 free jet expansion.⁵ We detect the ion signal Na_2^+ , Na^+ using a particle multiplier, coupled with TOF mass analysis. By measuring the ratio of Na_2^+ to Na^+ signal as a function of dye laser frequency, we obtain the AI cross section as a function of collision velocity.

Figure 1 shows the AI cross section dependence on collision energy. A calculated cross section using the semi-classical treatment of Miller⁶ fits the measured curve in the energy range 0.19 eV - 0.29 eV. The calculation indicates that the $X^1\Sigma_g^+$ state of $\text{Na}(2p + 2p)^7$ is a dominant contributor to AI in the fitted energy region; but since it cannot account for the low energy part (below 0.19 eV), at least another potential surface of $\text{Na}(2p + 2p)$ must be involved. An attractive potential of $\text{Na}(2p + 2p)$ crossing the ground state of Na_2^+ at collision energy = 0.08 eV could be a possible candidate.

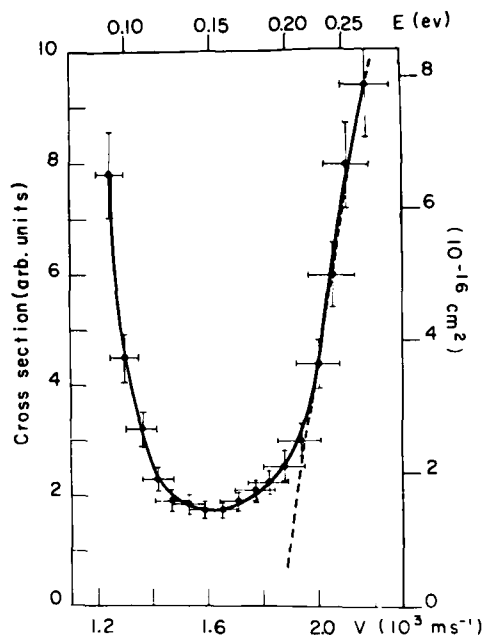


Figure 1: AI cross section vs. collision velocity (lower abscissa) and energy (upper abscissa). Dashed line is fit using Miller's theory (following $X^1\Sigma_g^+$ state of $\text{Na}(2p+2p)^7$). Right ordinate is the estimated absolute cross section.

References

1. J. Huennekens and A. Gallagher, Phys. Rev. A **28**, 1276(1983).
2. R. Bonanno, J. Boulmer and J. Weiner, Phys. Rev. A **28**, 604(1983).
3. V.S. Kushawaha and J.J. Leventhal, Phys. Rev. A **25**, 346(1982).
4. W.D. Phillips and D.E. Pritchard, Phys. Rev. Lett. **33**, 1254(1974).
5. R. Campargue, Ph.D. thesis (Documentation Frangine, Paris, 1970).
6. W.H. Miller, J. Chem. Phys. **52**, 3503(1970).
7. R. Montagnani, P. Riani, O. Salvetti, Chem. Phys. Lett. **102**, 571(1983).

TWO-PHOTON IONIZATION OF Ca ATOM WITH TAKING INTO ACCOUNT THE ELECTRON CORRELATIONS

M.I.Haysak,* V.I.Lengyel,* D.M.Petrina,* I.M.Shuba,* O.I.Zatsarinny*

*Institute for Nuclear Research, Ukrainian Academy of Sciences, USSR
*Uzhgorod State University, Uzhgorod, USSR

The analysis of the experimental data on barium and strontium atoms ionization shows^{1,2} that this process has a resonance character and that it is quite probable that the autoionizing states (AIS) of atoms play an essential role here. The role of AIS in multiphoton processes has not been studied yet. It is quite clear that the existence of the AIS can result in an additional resonance structure of ionization cross-section.

The differential cross-section of the two-photon ionization of an atom by linearly polarized field of non-resonant frequency ω has a form³

$$\frac{d^2\sigma}{dE d\Omega} = 2\pi(2\pi\alpha\omega)^2 |K_{fi}|^2,$$

where α is the fine-structure constant, K_{fi} is the composite matrix element of second order. With the taking into account AIS the f state in the matrix element K_{fi} has a form^{4,5}

$$\langle f | = \langle f |_{HF} + \sum_j \frac{\langle f | \hat{V}_{ij} | \phi_j \rangle \langle \phi_j |}{E - \epsilon_j - 2i\Gamma_j} + \sum_j \frac{\Gamma_j \langle \phi_j |}{E - \epsilon_j - 2i\Gamma_j}$$

where Γ_j is a resonance width.

We have carried out the calculation of a one-photon and two-photon ionization of Ca atom with the use of diagonalization method modification of Balashov et.al.⁵ The Ca atom and AIS wave functions were obtained by configuration interaction method in the ionic frozen-core (of Ca double ion) approximation with taking into account the core polarization.

The results of the calculation of one-photon ionization, we have carried out, are in a good agreement with those, obtained in the work⁶

In fig.1 the total cross-section of two-photon ionization of Ca atom as a function of energy is shown. The energy region corresponding to the double and tripple frequencies of ruby and neodyme lasers is choosen. As it is seen from fig.1, AIS $3d5s^1S$ ($E=7.1$ eV) results in an unessential increase of the cross-section, while AIS $3d5d^1D$ ($E=7.15$ eV) results in an increase by an order.

In table 1 we have shown the polarizability of some levels of Ca atom for the frequ-

ences which are multiple to the ground frequencies of the ruby and neodyme lasers (in a. u.). For the calculation of polarizabilities both discrete and continuous spectrum was taken into account. As it is seen from table1 the dynamic polarizability for small ω reaches quite large values, which results in an energy shift equal $10-100$ cm⁻¹ at the external field value 10^6 v/cm. The experiments on measuring the cross-sections and shifts will be eagerly awaited.

References

1. N.B.Delone, I.I.Bondar, V.V.Suran, B.A.Zon, Opt.Comm., **40**, 263 (1982).
2. D.Feldmann, A.J.Krantwald and K.H.Welge, J.Phys.B,**15**, 529 (1982).
3. H.B.Bebb, Phys.Rev., **149**, 25 (1966).
4. M.I.Haysak, V.I.Lengyel, D.M.Petrina, I.M.Shuba, O.I.Zatsarinny, Nonlinear processes in two-electron atoms, Moscow (1984), p.115-136.
5. V.V.Balashov, S.I.Grishanova, V.S.Senashenko, Opt.Spectr., **28**, 859 (1970).
6. P.Scott, A.E.Kingston, A.Hibbert, J.Phys.B, **16**, 3945 (1983).

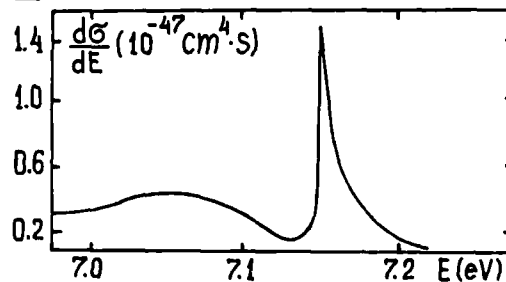


Fig.1

ω	$4s^2 \ ^1S$	$3d5d \ ^1S$	$4s5s \ ^1S$	$4s4p \ ^1P$
0	163	5.54+7	4395	47
1.17	191	-1.41+3	-3017	8.93+3
2.34	418	-439	87	-178
3.51	-351	-174	-256	329
3.56	-312	-169	-241	415

Table 1

APPLICATION OF INDEPENDENT UNITED ATOM MODEL TO INELASTIC SCATTERING OF ELECTRONS BY HYDROGEN MOLECULE

N.S.Rao

Physical Research Laboratory, Theoretical Physics Area, Navrangpura, Ahmedabad 380 009, INDIA

An independent united atom model¹ (IUAM) is applied to study inelastic scattering of the electrons by hydrogen molecule at intermediate and high incident energy regions. The collision cross sections are calculated at $E \leq 400$ eV. No other data are available for the comparison of present results. Basically IUAM¹ is found to be better approximation than the earlier independent atom model² (IAM) to study the molecular problems.

Independent united atom model¹ (IUAM), recently proposed by Khare and Jhanwar is applied in this present paper to study $e - H_2$ inelastic scattering. Earlier to this, IAM² has been employed recently to study scattering of electrons³ and positrons by hydrogen molecule. In view of some discrepancies in the formulation of IAM, Khare and Jhanwar¹ proposed this IUAM to study molecular problems. This new method is more general and reliable than the IAM. The advantages of IUAM are i) this model is valid for elastic as well as inelastic scattering process, ii) especially for inelastic scattering the collision cross sections are more reliable than the IAM³ results. Motivated to the importance of the collision cross sections⁴, I have applied IUAM in the present paper to study inelastic scattering of electrons by hydrogen molecule. In order to conform the present cross sections, I have converted the GES (Glauber eikonal series)⁵ results for the present purpose to compare my results. The present results are expected to be better than the earlier IAM results³.

In the present paper the direct scattering amplitude for inelastic scattering of electrons by helium atom are derived analytically through Born and Glauber approximations^{6,7}. Using the IUAM and the present direct scattering amplitude the differential scattering cross sections (DCS) are studied at $E \leq 400$ eV. The scattering amplitude in IUAM can be written as

$$I(H_2) = 0.5 \times I(He) \left[1 + J_0(2qr) \right]$$

Where $I(He)$ is the scattering amplitude for

the helium atom, the square bracket term in the above equation is called as diffraction term, q is momentum transfer to the target during the collision process and $2r$ being the equilibrium internuclear distance. In the present work $I(He)$ is derived to study $I(H_2)$ problem through the above equation.

By comparing the IAM results³ and present results, I conclude that the IAM^{2,3} is not good for the study of inelastic scattering of electrons, positrons by molecules. The present collision cross sections will be presented at the time of conference.

The author N. S. R is thankful to the Physical Research Laboratory, Ahmedabad, India for the award of a Post-Doctoral Fellowship. I am also grateful to Prof. H.S. Desai (M. S. Uni) Baroda, for his nice guidance through the present work.

References

1. S. P. Khare and B. L. Jhanwar, XIII th I.C.P.E.A.C. abstracts, 225 (1983)
2. H. S. W. Massey et al " Electronic and the Ionic Collision Phenomena " Oxford (1969)
3. K. N. Joshipura and H. S. Desai Ind. J. of Pure and Apply. Phys. 22, 236 (1984).
4. M. Massey, " Atomic and Molecular Physics " London, (1979).
5. S. N. Singh and A. N. Tripathi. Phys. Rev. A 21, 105. (1980).
6. A. C. Yates. Phys. Rev. A 19, 1550 (1979).
7. A. C. Yates. Chem. Phys. Lett 25, 480 (1974).

ELECTRON - ION (He^+) SCATTERING AT INTERMEDIATE AND HIGH INCIDENT ELECTRON ENERGY REGIONS ($E \geq 1000$ eV)

N. S. Rao

Physical Research Laboratory, Theoretical Physics Area, Navrangpura, Ahmedabad 380 009, INDIA.

In the present work, I study elastic scattering of electrons by helium positive ion (He^+) using Born approximation. The collision cross sections are calculated at incident energy $E \leq 1000$ eV. No other data are available for the comparison of present results. The present results are expected to be reasonable and the present method is computationally simpler than the earlier approximations used to study the electron - ion scattering problems.

Generally, the electron - ion scattering processes have important applications in astrophysics and plasma physics, theoretical investigations of these collision processes are of practical interest. Apart from this considerable theoretical interest is attached to the study of electron impact with a one - electron ion such as He^+ as this should reveal the influence of long range Coulomb interaction on the effectiveness of the different approximations. In recent past few theoretical models are applied to study electron - ion problems¹, out of these models Close Coupling (CC) model was found to be more accurate than the other models². But this CC model is computationally more tedious and requires a good amount of computer time. Especially, at intermediate and high incident energies all models will generate identical results³, and one can use plane wave approximation⁴ instead of other complicated approximations^{1,2}. In view of this and motivated to the importance of the present study³ I study $\bar{e}-\text{He}^+$ elastic scattering at $E \leq 1000$ eV through the Born approximation⁴. The advantages of the present Born approximations are mentioned earlier⁵.

Throughout the work atomic units are used. The basic scattering amplitudes in the Born approximation are given earlier^{1,4}. Here I will consider He^+ as hydrogen atom like with the nuclear charge $Z = 2$, the initial and final state target wavefunctions of He^+ are assumed to be similar to the H - atom wavefunctions, assuming the plane waves for both incident and scattered electrons, I have obtained the second Born amplitude⁴ in the closed form for $\bar{e} - \text{He}^+$ elastic scattering. The total collision cross sections (TCS) are calculated through the Optical theorem⁵ at $E \leq 1000$ eV. These results are shown in table - 1.

Table - 1. TCS in units of a_0^2 for $\bar{e} - \text{He}^+$ elastic scattering at incident energy $E \leq 1000$ eV.

Incident energy E eV	Present results
100	3.497
200	2.042
300	1.476
400	1.168
500	0.973
600	0.835
700	0.736
800	0.658
900	0.596
1000	0.545

From the Table-1 it is noted that the He^+ TCS results are nearer to the TCS results of He scattering⁵ at $E \leq 300$ eV and very much smaller than these results⁵ at $E \geq 400$ eV. The DCS results for He^+ will be presented at the time of conference. Comments on this work are open for discussions.

The author N.S.R is thankful to Prof. V. B. Sheorey, for introducing me to the field of electron - Ion scattering problems. I am also thankful to P.R.L for the award of P.D.F.

References

1. M.C. Chidichimo et al J.Phys.B **15** 3333 (1982)
2. S. Dham Oh et al Phy. Rev. A **17** 873 (1978)
3. N. F. Mott and H. S. W Massey " The theory of atomic Collisions " (Oxford) (1965)
4. A.C. Yates Phys. Rev. A **19**, 1550 (1979)
5. N.S.Rao and H.S.Desai Ind. J. of. Pure and Apply. Phys. **21** 159 (1983).

GAPHYOR : AN ATOMIC AND MOLECULAR DATA CENTRE AT ORSAY

Konstantinos KATSONIS, Jean-Loup DELCROIX, William ASSAL and Claudette L'PRINCE.

Centre de Données GAPHYOR, Laboratoire de Physique des Plasmas,
CNRS and Université Paris-Sud, 91405 Orsay CEDEX, FRANCE.

An atomic and molecular data centre has been established at the Orsay campus of the Paris-Sud University, France. Activities at this centre named GAPHYOR (Gaz PHYsique ORsay) were initially oriented towards collection and handling of bibliographic data. These data are collected from the published papers, books, or reports by a team of fifteen scientists collaborating with this project. The arrangement of the data allows the user to obtain more information than the one provided by standard bibliographic patterns. The identification and sorting of data is based on a simple code for writing molecules and collision processes or chemical reactions instead of using keywords. Molecules including up to eight atoms of no more than four different elements can be coded, by indicating the chemical formula, the constituting elements, and the excitation and ionization stage. The sorting of the data file is based on the Mendeleev families order and on "second-level" descriptors arranged in five standard "first-level" categories :

- a) Properties of atoms and molecules.
- b) Photon collisions.
- c) Electron collisions.
- d) "Heavy particles" (i.e. atoms, molecules and their ions) collisions.
- e) macroscopic properties.

A handy interactive system called SYGAL (SYstem Gaphyor Language) developed for the user's convenience allows on-line retrievals worldwide through the existing data transmission networks in "natural" physicochemical language without using the internal code of GAPHYOR.

Activities at ORSAY were recently enlarged to include collection, evaluation and dissemination of numerical data pertinent to atomic processes encountered in common (e.g. astrophysical, thermonuclear, arc and laser) plasmas. In the development of numerical data files emphasis is given to unique sets of "recommended" data. Especially for applications (e.g. modelling, diagnostics etc.) these are more convenient than files including all the available values. Moreover, the anticipated use of each file determines not only the output form to be selected (computer readable files, printed tables, graphs) but also its internal structure. The general lines followed in implementing "recommended" data files are described elsewhere¹.

The computer system used for the storage (and possibly the exchange) and retrieval of numerical data is

closely related to AMDIS and EXFOR systems, previously developed in Nagoya and Vienna correspondingly. Special effort is paid to establish a system compatible with the aforementioned ones allowing straightforward exchange of data. In so doing the periodicals, processes, quantum states, units etc, dictionaries used in the system follow standards currently used in the field.

Another characteristic of the system is its close connection with the existing wider bibliographic data base. In fact, the bibliographic part and the retrieval of the data sets are based on the GAPHYOR software².

International collaboration in data assessment and exchange is also part of the GAPHYOR data centre activities. In this context a proposal has been made to CODATA for standardisation and unification of atomic and molecular data currently used in various applications. The choice of evaluated data is initially oriented towards two well-known data sets obtained :

1. as a result of the IAEA Coordinated Research Programme on "Atomic collision data for diagnostics of magnetic fusion plasmas" run essentially from 1981 to 1984³. The bulk of these data was recommended for fusion applications by the IFRC subcommittee for atomic and molecular data for fusion.
2. during the recent workshop on "atomic data for fusion and astrophysics" held in March 1985 at the Daresbury Laboratory, UK⁴. This set of data consists essentially of recommended data for electron impact excitation of atoms and ions.

Work in data evaluation is also carried out on charge exchange collisions parametrisation in collaboration with the University of Belgrade, Yugoslavia (Dr R. Janev). Also, promotion of astrophysical applications of atomic data was recently developed through collaboration with the Meudon Astrophysical Laboratory.

References

1. K. Katsonis, *Comp. Phys. Commun.* **33**, 115 (1984).
2. J.L. Delcroix, in "Gaseous Electronics" vol.2, ed.M.L. Hirsh (Academic Press, 1983), also Report DG/18 (Plasma Physics Laboratory, Orsay 1982).
3. K. Katsonis and A. Lorenz eds, Reports INDC(NDS)-136, -150, -160 (IAEA, Vienna 1982, 1983, 1984).
4. K.M. Aggarwal, K.A. Berrington, W. Eissner, *Proceeding of Workshop on Atomic Data for Fusion and Astrophysics*, Daresbury Laboratory Report, in press.

DATABASE ON ELECTRON IMPACT IONIZATION

M.A. Lennon, K.L. Bell, H.B. Gilbody, J.G. Hughes,
A.E. Kingston and F.J. Smith

School of Physics and Mathematical Sciences
The Queens University of Belfast
N. Ireland

The database on electron impact ionisation of light atoms and ions developed at Queens University, Belfast and reported earlier¹ has been extended to include recommended cross sections and rates for electron impact ionization of all ions from Fluorine to Nickel. Recommended cross sections are based on an assessment of all available data to date and used to evaluate recommended Maxwellian rate coefficients over a wide range of temperatures. The database is implemented on a Vax 11/780 computer and allows rapid retrieval of the data in both graphical and tabular form.

The work which is supported by Culham Laboratory (Euratom/UKAEA Association) will be reported in full in a UKAEA report to be published shortly. Requests for data or for on-line access to the database may be made in writing to Dr. M.A. Lennon, Department of Computer Science, Queens University of Belfast.

Reference

1. Atomic and Molecular Data for Fusion, Part 1. Recommended Cross Sections and Rates for Electron Ionisation of Light Atoms and Ions. K.L. Bell, H.B. Gilbody, J.G. Hughes, A.E. Kingston and F.J. Smith. UKAEA Report, CLM-216.

X-Ray Incoherent Scattering Factors for N_2 as
Determined by High Energy Electron Impact Spectroscopy*

S. N. Ketkar and R. A. Bonham

Department of Chemistry, Indiana University
Bloomington, Indiana 47405

Electron impact spectra for N_2 have been obtained in the angular range 0.3° to 2.0° using 25 keV electrons. Intensities were measured with a resolution of ~ 1 eV in a preset time mode, in the energy loss range 0 to 80 volts and 400 to 480 volts. In the range 80 to 200 volts and 480 to 800 volts intensities were measured at 8 points in a preset count mode with a counting statistics of $\sim 3\%$. The measured intensities were converted into, $\frac{df(K,E)}{dE}$, the generalized oscillator strength (GOS) distribution at each scattering angle and the energy moments of the GOS distribution $S(n,K) = \int E^n \frac{df}{dE} dE$ for $n = 0, -1, -2, -3$ were obtained. In order to obtain the moments, a matched Coulomb tail for a hydrogenic atom was used to simulate intensities not measured experimentally (i.e. for energy loss > 200 V for the valence shell and for energy loss > 800 V for the K-shell).

Use was made of the Bethe sum rule, $S(0,K) = N$, where N is the number of target electrons, to place the GOS on an absolute scale. The energy moments $S(n,K)$ for $n = -1, -2, -3$ agree, in the optical limit, with previously reported values.¹ The $S(-1,K)$ moment is used to determine the x-ray incoherent scattering factor. Our experimentally determined x-ray incoherent scattering factors are compared with the results of a Hartree-Fock calculation² and a recent CI calculation.³

Experiments are in progress to measure the absolute, small angle, elastic cross section for 25 keV electrons scattering from helium.

*Work supported by NSF Grant No. CHE 83-09934

1. G. D. Zeiss, W. J. Meeth, J. C. F. MacDonald and D. J. Dawson, Can. J. Phys. 55, 2080 (1977).
2. J. Epstein and R. F. Stewart, J. Chem. Phys. 66, 4057 (1977).
3. M. Breitenstein, H. Meyer and A. Schweig, Z. Naturforsch., A 39a, 120* (1984).

Energy and Angular Distributions of Secondary Electrons
Produced by the Electron Impact Ionization of Helium and Molecular Nitrogen*

R. R. Goruganthu, W. G. Wilson and R. A. Bonham

Chemistry Department, Indiana University, Bloomington, IN 47405

The energy and angular distributions of secondary electrons produced in the electron impact ionization of helium and molecular nitrogen have been made experimentally using a pulsed electron beam time-of-flight spectrometer. The measurements are made at ejection angles between 30 and 150 degrees. The primary electron energies are 200 and 500 eV in the case of helium and 200, 500, 1000 and 2000 eV in the case of N_2 . In these experiments the photon emission from the excited neutral or ionic species is also detected along with the scattered electrons. Because the angular distribution of fluorescent photons is expected to be isotropic

the total photon yields were used to place measurements at different ejection angles on the same relative scale. The relative measurements are then made absolute by normalizing the elastic intensity at one angle to available absolute cross sections for the same angle. We also observed the autoionization lines in N_2 below 2.5 eV. The agreement in the peak positions between our data and the literature values served as a check on our energy scale. The angular distributions of the autoionization lines in helium were also investigated.

*Work supported by NSF Grant No. CHE 8309934

RESONANCES IN THE INTERACTION OF ELECTRONS WITH SODIUM ATOMS

I.I.Cherlenyak*, V.I.Lendyel*, F.F.Papp**, N.I.Romanjuk**, E.P.Sabad**, O.B.Shpenik**
and O.I.Zatsarinny*

*Uzhgorod State University, Uzhgorod 294000 USSR

**Institute for Nuclear Researches of Ukrainian SSR Academy of Sciences,
Uzhgorod 294000 USSR

In experiments on studying of the energy dependences of differential cross-sections of $e+Na$ and $e+K$ -scattering the structure in the vicinity of the first excited state has been revealed¹. The close coupling calculations show the existence of resonances in energy region in question. It was pointed out² that only 1S autodetachment state (ADS) of Na^- ion can be formed which can manifest itself in a form of resonance in optical excitation functions (EF) of Na atoms.

In present paper we analyse in details the possibility of formation of ADS of Na^- ion using the configuration interaction method and study resonances and threshold features on optical excitation functions of Na atom. The configuration interaction method has been employed and numerical Hartree-Fock functions were

Feature	Energy (eV)	Classification
1	2.10	$^1P^o3p10s$
2	2.99	$^1D3p^2$
	3.19	$^1S4s^2$
3	3.55	$^1P^o4s7p$
	3.56	1D3d6s
	3.57	1D3d8s
	3.58	1D3d10s
	3.68	1D3d4d
	3.72	$^1P4p^2$
4	3.75	1P4p9p
	4.0	$^1S5s^2$
	4.09	1P5s5p
5	4.21	$^1D4d^2$
	4.25	1D4d7s
	4.26	1D4d11s
	4.27	1D4d12s
6	4.34	1P5p10s
7	4.43	$^1S6s^2$

used as a basic ones with taking into account the core polarisation. While solving the eigenvalue problem we have included into hamiltonian a single-electron polarisation of both electrons as well as dielectronic polarisation potential. The resulting ADS spectrum is given

in table.

Electron beam in the experiment was about 10^{-8} Å, while electron energy spread did not exceed 0.04 eV. The accuracy of calibration of the energy scale was ± 0.02 eV.

We have analysed the optical EF of the lowest members of principal, sharp and diffusion series in a near-threshold energy region. We have presented on figure 1 the EF of the first two members of the principal and the se-

cond member of diffusion series. On absciss axis the electron energy is shown while on the ordinate axis the cross-section for the excitation in relative units is given.

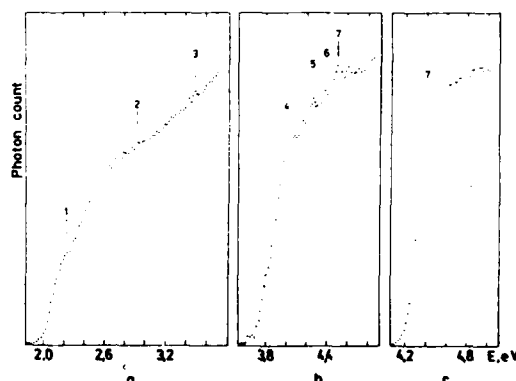


Fig.1 a/ EF of $\lambda 5889/95\text{\AA}$,

b/ EF of $\lambda 3302/03\text{\AA}$, c/ EF of $\lambda 5688\text{\AA}$ lines

Resonance line EF reveals an almost linear increase of cross-section near threshold interrupted at 2.2 eV, after that the curve slope changes and the series of shoulders and irregularities are observed in 3.0-3.3 eV and 3.5-3.8 eV energy region, correspondingly. EF of the second member of principal series demonstrates a sharper increase near the threshold and reveals better expressed features in 4.1-4.5 eV energy region. From figure one can see that the position of features on curves coincides in general with the calculated energies of ADS.

Optical EFs demonstrate that the rate of growth of cross-section near threshold increases as the principal quantum number increases. For some curves the threshold - first maximum interval does not exceed the electron beam energy spread. This behaviour of EF confirms the resonance character of spectral lines excitation.

1. M.Eyb, H.Hofman, J.Phys.B. 1975, 8, No7, 1005
2. A.Pung, J.Matese, Phys.Rev.A. 1972, 5, No1, 22

RESONANCES IN THE DIFFERENTIAL CROSS-SECTIONS FOR $e + \text{Li}$ - SCATTERING

I.I. Cherlenyak*, S.M. Kazakov†, O.V. Kristoforov†, V.I. Lengyel*, E.A. Masalovich*, and E.P. Sabad**

*Uzhgorod State University, Uzhgorod, USSR

†Chuvash State University, Cheboksari, USSR

**Uzhgorod Department of Institute for Nuclear Researches, Ukrainian Academy of Sciences, Uzhgorod, USSR

The study of scattering of slow electrons on Li atoms was carried out in a number of works¹⁻⁵. The calculations³ of 1P and 1D phase-shifts of the elastic scattering has revealed two closed-channel resonances under first 2p-excitation threshold ($E=1.85$ eV) and one 3P shape-resonance at the incident electron energy 0.1 eV. However, there is no information about resonances in cross-sections above the 2p-level though the calculations⁴ have revealed the existence of the $^1S(E=3.15$ eV) and $^3S(E=3.35$ eV) autodetachment states (ADS) of Li^- ion under the 3s-threshold, and four ADS under the 3p-threshold. It should be noted that no data concerning the widths of these ADS have been published yet.

Therefore it is of certain interest the study of the influence of ADS on $e + \text{Li}$ - scattering cross-sections and the calculations of the widths of ADS as well at energies above 2p-threshold. In this work we report the results of experimental study and theoretical calculations of differential cross-sections at 90° angle in energy region 2.25 - 4.25 eV. In experiment the electronic beam crossed the cell filled with the vapour of Li and electrons scattered at right angles were detected by the energy analyser. Differential pumping of electronic gun and the energy analyser was used. The energy spread of electrons did not exceed 0.3 eV. The calculations were carried out by use of modified Feshbach⁶ method proposed by Balashov. This method makes it possible to take into account quite accurately the interelectron correlations at short distances. For the positions and widths of ADS we have obtained the following values: $^1S(E=3.09$ eV, $\Gamma=0.08$ eV), $^3P(E=3.28$ eV, $\Gamma=0.12$ eV), $^3S(E=3.35$ eV, $\Gamma=0.07$ eV). Energy dependence of the differential cross-sections for elastic scattering (a) and excitation of the 2p-state (b) is shown in Fig.1 (—○—○— experiment, — — — theoretical calculation, — — — — the theoretical cross-section averaged over Gaussian distribution with spread equal to 0.3 eV).

As it is seen from Fig.1 the agreement of the theoretical calculation with the experiment is quite satisfactory. The additional maxima in the measured cross-section at energy 3.7 eV can be, probably, explained by influence of $^1D(E=3.74$ eV) and $^1S(E=3.75$ eV) ADS which were not taken into account in the present calculations.

References

1. B. Jadusliver, A. Tino, and B. Bederson, Phys. Rev. A **24**, 1249 (1981).
2. D. Leep and A. Gallagher, Phys. Rev. A **10**, 1082 (1974).
3. P.G. Burke and J.A. Taylor, J. Phys. B **2**, 859 (1969).
4. A.C. Fung and J.J. Matese, Phys. Rev. A **5**, 22 (1972).
5. C.D. Lin, J. Phys. B **16**, 723 (1983).
6. M.I. Haysak, V.I. Lengyel, V.T. Navrotsky and E.P. Sabad, Ukrainian Phys. J. (USSR), **27**, 1617 (1982).

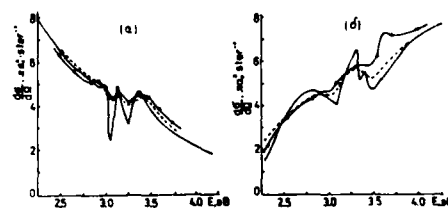


Fig.1

THE RESONANT STATES OF He^- ON THE METAL SURFACE

O.S. Erkovich, V.V. Komarov, A.M. Popov, A.E. Romanovsky, S.G. Serebryakov

Institute of Nuclear Physics, Moscow State University, Moscow 119899, USSR

In the present paper, the energies of the He^- ion resonant states are analyzed. The energies of the resonant states are calculated in the cases where (1) He^- ion is placed in vacuum and (2) He^- ion is placed near a metal surface.

The Hamiltonian for the He^- ion can be presented as

$$H = \sum_i \left(T_i - \frac{2}{|\vec{r}_i - \vec{R}|} \right) + \sum_{i,j} |\vec{r}_i - \vec{r}_j|^{-1} + \sum_i V_c(\vec{r}_i),$$

where T_i is the kinetic energy operator, $\frac{-2}{|\vec{r}_i - \vec{R}|}$ is the operator of the potential energy of the i -th electron in the field of the α -particle; $|\vec{r}_i - \vec{r}_j|^{-1}$ is the operator of the Coulomb interaction between the i -th and j -th electrons; $V_c(\vec{r}_i)$ is 0 in the first case; in the second case this operator describes the interaction between the i -th electron and the metallic surface. The potential $V_c(\vec{r}_i)$ was chosen to be of the form developed in [1] (the "image" potential). The energy of the He^- ion resonance states was calculated by the proposed in [2].

The total energy of the resonance level in the metallic surface field can be calculated in terms of the perturbation theory [1,3].

The energies of the $(1s^2 2s)^2S$, $(1s^2 2p)^2S$, $(1s^2 2s 2p)^2P$, $(1s^2 2s 2p)^4P$ states were also calculated. The total energy of the resonant state can be presented by the expression

$$E = E_r + \frac{C}{4(Z - R_c)},$$

where E_r is the energy of an isolated-ion resonance state, Z is the distance between the α -particle and the metal surface; R_c is a constant which describes the given metal [3]; C is a constant which may be inferred from the results of numerical calculations.

The method was applied to the interaction of a He^- ion with copper. The calculation has yielded the following results: $E_r = 2.181$; 2.183 ; 2.191 ; 2.224 au and $C = 0.8307$; 1.8373 ; 1.2121 ; 1.341 au, for the $(1s^2 2s)^2S$, $(1s^2 2p)^2S$, $(1s^2 2s 2p)^2P$, $(1s^2 2s 2p)^4P$ states respectively.

Reference

1. A.D. Lang, W. Kohn, Phys. Rev. B, **1**, p. 1557-1568 (1970).

2. O.S. Erkovich, V.V. Komarov, A.M. Popov, Izvestia AN SSSR, (Russian) **48**, 968-971 (1984).
3. N.D. Lang, W. Kohn, Phys. Rev. B, **3**, No. 4, p. 1215-1223 (1972).

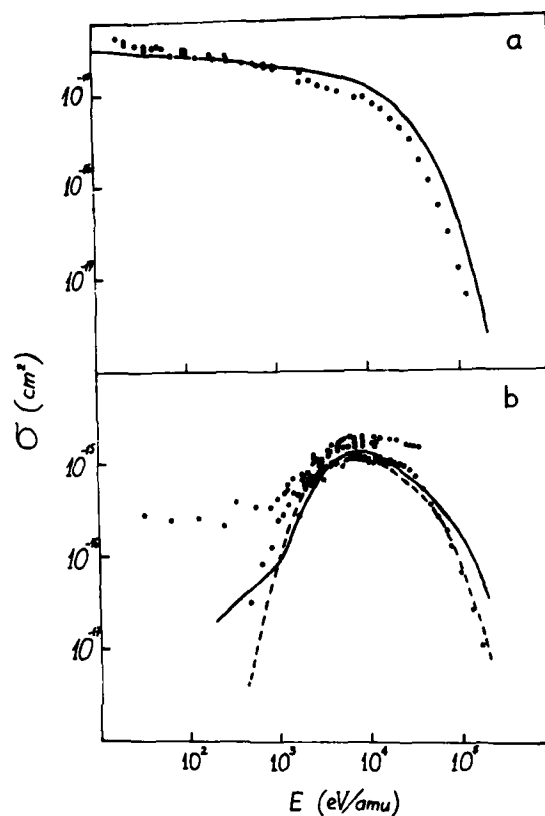
CHARGE-TRANSFER IN ION-ATOM COLLISIONS AS THE THREE-BODY PROBLEM

A.R. Ashurov, G.V. Avakov, L.D. Blokhintsev, A.M. Mukhamedzhanov

Institute of Nuclear Physics, Moscow State University, Moscow 119899, USSR

The electron-transfer process in ion-atom collisions is considered as the three-body problem. The proposed approach is based on the three-particle Sloan version¹ of Faddeev equations which was previously used for the limited class of charge-transfer reactions². Our approach makes use of the approximate formula for the summation over quantum numbers l and m of the bound electron in the intermediate and final states. The set of the algebraic equations for the charge-transfer scattering amplitudes $M_n(\rho)$ is obtained where ρ is the impact parameter and n denotes the main quantum number of the transferred electron in the final state. The amplitudes $M_n(\rho)$ satisfy the two-particle unitarity conditions. The ionization channel is not considered. The total cross sections of the electron pick-up by fully stripped ions with $Z = 1-6$ from atomic hydrogen are calculated. The Brinkman-Kramers amplitude is chosen as the effective potential in the Sloan equations for the $H^+ + H(1s)$ collisions. In the case of heavier ions the Coulomb interaction between the one-electron ion and the proton is effectively taken into account by using the Coulomb wave function of proton-ion scattering in place of the plane wave.

The calculated charge-transfer cross sections are shown by solid lines in Fig. 1 for the reactions $H^+ + H(1s) \rightarrow H + H^+$ (a) and $He^{++} + H(1s) \rightarrow He^+ + H^+$ (b). Dots correspond to the experimental data of various groups. At high energies the theoretical cross sections exceed the experimental ones which may be due to neglecting the ionization channel contribution. The dashed line in Fig. 1b corresponds to the unitarized distorted wave approximation (UDWA)³.



References

1. L.H. Sloan, Phys.Rev., **165**, 1587 (1968).
2. J. Chaudhuri, A.S. Ghosh, N.C. Sil, Phys.Rev., **A7**, 1544 (1973).
3. H. Ryufuku, T. Watanabe, Phys.Rev., **A18**, 2005 (1978).

ELECTRON IMPACT EXCITATION OF CUPRUM ATOMS
FROM METASTABLE STATES

I.S.Aleksakhin*, I.P.Zapesochny*, T.A.Snegurskaya*, I.I.Shafranyosh*

* Uzhgorod State University, Uzhgorod, 294000 USSR

+ Institute for Nuclear Researches of Ukrainian SSR Academy of Sciences, Uzhgorod, 294000 USSR

Results of excitation process studies for cuprum atomic spectral lines arising from metastable states are presented. Experiments were performed by crossed electron and atomic beams method¹. Metastable atomic Cu beam was formed with help of a device, consisting of effusion cuprum atom source, a converter of atoms from ground into metastable state, a system of collimating slits and a separating condenser. Metastable atoms concentration in the beam was measured by the spectral line self-absorption magnitude and made up $(1 \pm 3) \cdot 10^9 \text{ cm}^{-3}$. An electron beam was formed by a five-electrode system.

Electron current density in the beam was about $(1 \pm 3) \cdot 10^{-3} \text{ A/cm}^2$ at energy spread less than 1 eV (for 90% of electrons). The emission was registered in synchronic detection mode.

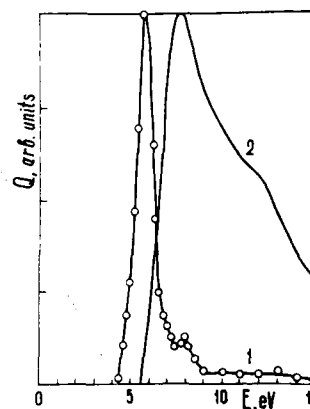
We have measured in our experiments the excitation functions of $4s^2 2D_{5/2} - 4p^2 F_{7/2}$ (296.1 nm) and $4s^2 2D_{5/2} - 4p^2 P_{3/2}$ (510.6 nm) spectral lines (EFSL), arising from the metastable $4s^2 2D_{5/2,3/2}$ states.

In order to analyse the results we have compared EFSL arising from metastable states with EFSL arising from the ground state of the same spectral line (see figure).

One can see from the figure that EFSL arising from metastable states expose a resonance appearing near the excitation threshold.

The resonance width is here comparable with the energy spread of electron beam. Nevertheless near-threshold features are not displayed on EFSL arising from

the ground state. One can suppose from these experimental data that excitation of lines arising from metastable



Excitation functions of $4s^2 2D_{5/2} - 4p^2 F_{7/2}$ (296.1 nm) spectral line arising from metastable (curve 1) and ground (curve 2) states, respectively.

ble states most probably takes place through some intermediate state. We have assumed that negative ion excited state can play the role of such an intermediate state.

Reference

1. И.И.Шафраньш, И.С.Алексахин, И.П.Запесочный, Письма в ЖТ 10, 271 /1974/

OBSERVATION OF RADIATIVE TRANSITIONS BETWEEN AUTOIONIZING STATES
OF LITHIUM ATOMS EXCITED BY ELECTRON BEAM

I.S.Aleksakhin*, C.G.Bogachev*, I.P.Zapsochnyi*, E.N.Postoi*, S.Yu. Ugrin*

* Uzhgorod State University, Uzhgorod 294000 USSR

* Institute for Nuclear Researches of Ukrainian SSR Academy of Sciences, Uzhgorod 294000 USSR

In hollow cathode experiments for lithium atom¹, as well as in beam-foil experiments² in the 180-300 nm region there appeared lines attributed by the authors to the transitions between quartet autoionizing states. However we can get an unambiguous identification of such lines only from experiments on interaction of monoenergetic electrons with atoms. For this special purpose we have studied spectra in 120-360 nm region excited by collisions of lithium atoms with electron beam of regulated energy.

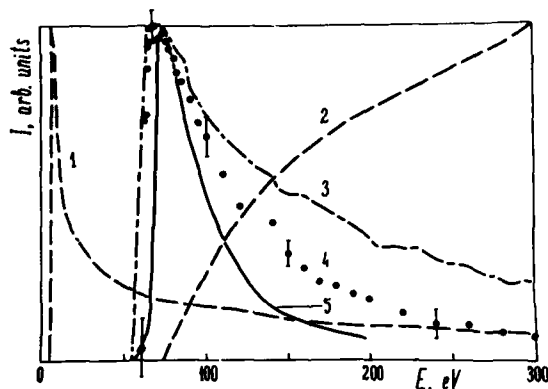
The apparatus with intersecting electron and atomic beams for carrying out the experiment was described in details earlier³. A diffraction grating replica coated by an aluminium film and MgF_2 film was applied in vacuum monochromator based on optical Seya-Namioka scheme. A solar-blind photomultiplier with a MgF_2 window served to detect the radiation.

Due to the careful measurement and analysis of spectra excited at different electron energy values we were able to receive the following results. Except the lines of principal series $LiI\ 2s - np\ (n=3+11)$ and $LiII$ lines a series of less intensive lines is presented in spectra which cannot be identified with the help of well-known spectroscopic tables. Nevertheless one can give sufficiently definite identification for six of them, namely: 193.1, 198.5, 204.0, 217.3, 233.7 and 293.4 nm.

Energy excitation values for the first five lines defined in our experiment make up 63 ± 1.0 eV, whereas for 293.4 nm line it is 61.5 ± 0.5 eV. As far as it is much higher than ionization potential of the atom, but is less than excitation thresholds of $LiII$ lines, apparently, we must conclude that the initial levels of given lines may belong only to the system of autoionizing states of Li atom⁴. Since energy interval values corresponding to these lines do not exceed 6 eV the lower levels of these lines are also autoionizing (the energy of the lowest among the known autoionizing states $1s2s^2\ ^2S_{1/2}$ is 65.35 eV). Therefore, we come to a conclusion that the observed lines are the result of combinations in the system of autoionizing states of Li atom. One can note that the wavelengths of series of these lines coincide with those of several lines observed in Ref. 1 and 2.

We have succeeded in measuring the effective excitation cross-section for the most intensive line of this kind (293.4 nm). Its maximum value obtained was $3 \times 10^{-19} \pm 0.3\ cm^2$. The 293.4 nm line excitation function

is presented in the figure (curve 4). One can see that

Excitation function of Li atom spectral lines:

- 1 - $LiI\ 247.5\ nm\ (2s^2S - 6p^2P^o)$,
- 2 - $LiII\ 165.3\ nm\ (2p^3P^o - 3s^3S)$,
- 3 - $LiI^{**}\ 20.75\ nm\ (2p^2P - 1s2p^2\ ^2P)$ (Ref. 4),
- 4 - $LiI^{**}\ 293.4\ nm$ (our experiment),
- 5 - $LiI^{**}\ 57.41\ eV$ (electron spectrum line, corresponding to the $1s2s2p^4P^o$) (Ref. 6).

its form differs greatly from typical excitation function form of ordinary lines of LiI (curve 1) and of $LiII$ (curve 2). On the other hand the curve we have obtained in general behaves analogically to the excitation functions of quartet⁶ (curve 5) and doublet optically forbidden^{5,6} (curve 3) autoionizing states. This fact as well as the mentioned above coincidence of line wavelengths confirm our statement.

References

1. G.Herzberg, H.R.Moore, Can. J. Phys. **37**, 1293 (1959)
2. S.Mannervik, H.Cederquist, Phys. Scr. **27**, 175 (1983)
3. И.С.Алексахин, Г.Г.Богачев, И.П.Запесочный, С.К.Угрин, ЖЭТФ **81**, 2187 /1981/
4. И.С.Алексахин, А.А.Боровик, Письма в ЖТФ **3**, 1183 /1977/
5. Ю.В.Меняк, В.С.Вукстич, И.П.Запесочный, в сб. "Автоионизационные явления в атомах", М.: МГУ, 1981, с. 159
6. V.Pejcev, K.J.Ross, D.Rassi, J. Phys. B: Atom. Molec. Phys. **10**, L579 (1977)

INFLUENCE OF COLLISION REDUCTION OF NATURAL LIFE-TIMES OF RESONANCE
LEVELS ON COUNT RATE EFFECT OF PROPORTIONAL COUNTERS

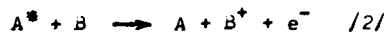
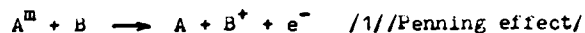
T.Z. Kowalski, K.W. Ostrowski, J. Zajac

Institute of Physics and Nuclear Techniques, University of Mining and
Metallurgy, 30-059 Kraków, Al. Mickiewicza 30, Poland

When an electron, in the electron avalanche in proportional counter moves through the mixtures of gases and vapours, its energy is essentially lost by elastic and inelastic collisions with the atoms, and/or molecules of the mixtures. The interaction of electron with medium gives atoms or molecules excited or ionized.

So the avalanche contains: ions, excited atoms and molecules, electrons, neutral atoms and molecules. The ions can be excited or not, mostly single charged. Excited atoms are in several levels.

For the mixtures at very low pressure one can neglect the atomic collisions due to the thermal agitation, so the radiatively deexcitation is limited only by the natural life-time of the excited state. In the gas under sufficient pressure the excited atoms take part in the binary and ternary collisions leading to reduction of their natural life-time. For theory of the growth of electron avalanche in proportional counter, the excitation of main gas to resonance levels, or to metastable levels, is very important. The struck of excited atoms with the molecules, or atoms of quench gas can produce additional electrons when the energies of the excited states are higher than the ionization potential of the admixture,



/nonmetastable Penning effect/,

A^m , A^* - atom of main gas excited to metastable or resonance level, B - atom or molecule of quench gas.

These processes /1/ and /2/ are quick events, occurring in time period less than 10^{-5} second, and can be immediately included in electron avalanche multiplication.

The mean life-time of resonance state $t_r \sim 10^{-9}$ s, and that of metastable state is $t_n \sim 10^{-5}$ s. During the mean life-time the excited atoms may collide with other atoms "n" times

$$n = v_{mp} \cdot t_o \cdot \lambda^{-1} \quad /3/$$

v_{mp} - the most probably velocity of atoms,

t_o - mean life-time /resonance or metastable states,

λ - mean free path of atoms.

Assuming that every collision between an excited atom of main gas, and an atom of admixture gas leads to deexcitation, the life-time of both resonance and metastable states in mixture can be calculated.

If the product $c \cdot n / c$ - concentration of admixture/ is smaller than 1, this value may be treated as the probability of collision of the excited atom with the atom of admixture. If the product $c \cdot n$ is higher than 1, it means that during the life-time t_o each excited atom should collide with an atom of admixture. This leads to the decrease of mean life-time of the excited states in relation $t_1 = t_o / c \cdot n$.

The calculation of the reduced life-time t_1 for metastable levels is a simple procedure. the value of t_m is near 10^{-5} s. The calculation of t_1 for resonance levels is more complicated. Though the radiative life-time of the resonance levels is of a few nanoseconds it is strongly reabsorbed and reemitted /radiation retention/, leading to an increase in the duration of these excited states, that may last a few μ s. The value of $t_r = 2 \cdot 10^{-8}$ s was taken for the calculation of t_1 for resonance levels. The obtainable reduced life-time for both metastable and resonance states is comparable to the rise time of the pulse generated in counter. The increase of concentration of admixture up to 1.5% leads to the decrease of the mean life-time of metastable levels only. For the concentration $c = 1.5\%$, for $t_r = 2 \cdot 10^{-8}$ s, the product $c \cdot n$ is equal one, so the higher concentrations cause the decrease of average life-time of both resonance and metastable levels. This leads to the shortening of the pulse rise time which, in its turn, decreases the count rate effect.

The influence of concentration of quench vapour on count rate effect has been investigated. A very rapid decrease of pulse height shift was found for the concentration of admixture $c \sim 1.5\%$. The obtained results are in very good agreement with the explanation.

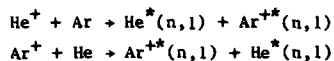
ONE ELECTRON CAPTURE INTO EXCITED STATES AND EXCITATION OF TARGETS BETWEEN
 He^+ OR Ar^+ IONS AND He OR Ar ATOMS COLLISIONS IN THE ENERGY RANGE
 OF 70-150 KeV

Pan Guang Yan, Lei Ziming, and Liu Jia Rui

Institute of Physics, Chinese Academy of Sciences
 P.O. Box 603, Beijing, China

An experimental study of capture of an electron into excited states and excitation of target atoms between He^+ or Ar^+ and He or Ar collisions has been done by means of optical methods, in the energy range of 70-150 KeV.

The main processes studied are:



From the measured emission cross sections, the excitation cross sections for capture into singlet and triplet He I levels with principal quantum numbers n from 3 to 5 has been estimated. The excitation cross sections of the target atoms has been estimated also. The comparison of the results of our experiment and other experiments shows satisfactory agreement.

Reference

1. F. T. de Heer, Experimental Studies of Excitation in Collisions Between Atomic and Tonic Systems, *Advances in Atomic and Molecular Physics*, Vol. 2. (1966). Edited by D. R. Bates et al.
2. L. Wolterbeek Muller and F. J. de Heer, Electron Capture into Excited States by Helium Ions Incident on Noble Gases. *Physica* 48, 345-396, 1970.
3. Pan Guang Yan et al., Electron Capture into Excited States in Collisions Between Multiply Charged Ions and Atoms. *Phys. Scripta* 73, 120, 1983.

ELECTRON BEAM ATTENUATION AND ABSORPTION THROUGH MATTER USING
MONTE CARLO CALCULATIONS

A. Antolak* and W. Williamson, Jr.†

* Theoretical Division 8341, Sandia National Laboratories, Livermore, CA 94550 USA

† Dept. of Physics and Astronomy, The University of Toledo, Toledo, OH 43606 USA

Monte Carlo calculations have been performed with the electron-photon transport code SANDYL to predict electron scattering and the associated electron energy distributions.¹ Several domain configurations with various materials, incident electron energies and angles of incidence were studied and the results compared with available experimental data. In general we find about ten percent variation between the theoretical predictions and experiments at the higher incident electron energies but somewhat greater disagreement as the energy is decreased. Based upon these comparisons several possible improvements of the theoretical data base for the code are suggested.

Reference

1. H. M. Colbert, "SANDYL: A Computer Program for Calculating Combined Photon-Electron Transport in Complex Systems", SAND 74-0012, Sandia National Laboratories, Livermore, CA.

THE DISSOCIATION OF IONS AND ION CLUSTERS BY MULTIPLE COLLISIONS*
WITH A NEUTRAL BUFFER GAS

F. L. Eisele

Electromagnetics Laboratory, CTRL, Georgia Institute of Technology, Atlanta, GA 30332 USA

The collisionally induced dissociation of several ions of atmospheric interest have been studied as a function of their average collision energy. The ions studied are derived from a variety of sources including flames, x-ray ionization of air and those ions which occur naturally in air (produced by background radioactive decay and cosmic rays). An attempt to better understand and identify the ions sampled from the latter source is the primary impetus for the present study. Ions which occur naturally at very low concentrations in the atmosphere near ground level have recently been sampled and mass identified.^{1,2} Mass identification of the parent ion does not however necessarily mean that the ion (even if of relatively low mass) can be chemically identified. Thus a second means of identification such as fragmentation of the ions followed by mass analysis would be quite helpful. Collisionally induced dissociation provides a means of preferentially dissociating ions (but not

producing additional ionization of neutral species) while not significantly reducing the number of ions available to be analyzed. Collisional dissociation has now become part of our method for identifying atmospheric ions and its energy dependence is being studied both to improve our present measurements and because it is of considerable interest in its own right.

The ions of interest are initially carried into the dissociation chamber by a buffer gas (typically N_2 or Ar) which expands after passing through a 180 μ diameter aperture. This aperture separates the ion formation region in which the pressure is about 1 atmosphere and the dissociation region which is typically operated at 10^{-1} Torr. Once in the dissociation chamber the ions are accelerated through the buffer gas by a uniform electro-static field, and are allowed to make several collisions with the buffer gas before exiting this region. The ions leave the dissociation region by passing through a fine stainless steel screen (which allows the electric field to be

abruptly terminated) just before exiting through an aperture into a 2-stage differentially pumped vacuum system. A quadrupole mass filter and an electron multiplier are housed in the high vacuum portion of this vacuum system making possible the mass analysis (ions and fragments are single charged) of the parent ion and ion fragments. A further description of the analysis (vacuum) portion of this apparatus and a discussion of ion breakup and clustering in and around the vacuum entrance aperture has been published previously.^{1,2}

Figure 1 shows the removal of H_2O clusters from the $NH_4^+ \cdot (H_2O)_n$ ion at low field strengths, while Figure 2 shows the fragmentation of a far more stable ion NO_3^- into NO_2^- . These results are still quite preliminary and the E/N values (E/N is the electric field strength divided by the gas number density and is given in Td where $1Td = 10^{-17} V cm^2$) contain considerable uncertainty because of pressure variations near the exit aperture. Modifications to the system will be completed shortly and improved E/N values

should be available at that time.

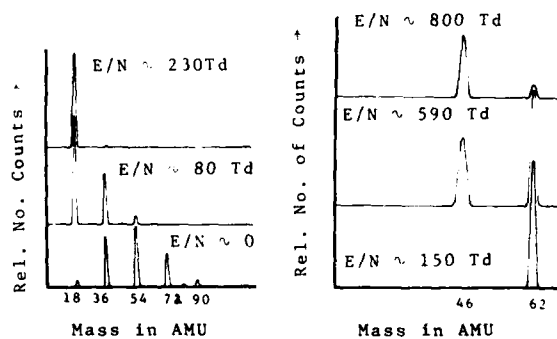


Figure 1. $NH_4^+ \cdot (H_2O)_n$
in N_2

Figure 2. NO_3^- in N_2

References

1. F. L. Eisele, Int. J. Mass Spect. Ion Proc., **54**, 119 (1983).
2. M. D. Perkins and F. L. Eisele, J. Geophys. Res. **89**, 9649 (1984).

*Supported by the National Science Foundation under Grant No. ATM-84-14-198

LARGE ORDER PERTURBATION THEORY FOR $Z_1 e Z_2$

R.J.Damburg,* R.Kh.Propin,* and V.V.Martyschchenko +

* Institute of Physics, Latvian SSR Academy of Sciences, 229021 Riga, Salaspils, USSR

+ Institute of Electronics and Computer Sciences, Latvian SSR Academy of Sciences, Riga, USSR

1. The Coulomb angular spheroidal equation (c.a.s.e.) is considered

$$\frac{d}{dz} \left[(1-z^2) \frac{dY}{dz} \right] + \left[-A - p^2(1-z^2) + 2pxz - \frac{m^2}{1-z^2} \right] Y = 0 \quad (1)$$

where X is constant, m is positive integer or zero. The asymptotic solutions of Eq.(1) are obtained for $p \rightarrow \infty$. It is convenient to introduce, instead of eigenvalue A , the value

$$\beta = \frac{2p(x-m-1) - A}{4p} \quad (2)$$

By using perturbation expansion, one obtains

$$\beta_{pt} = \sum_{k=0}^{\infty} \frac{\beta_k}{(4p)^k}, \quad \beta_0 = n_1 \quad (3)$$

where n_1 is positive integer or zero.

It appeared that there are four kinds of solutions of Eq.(1) depending on value of X :

1) X is not integer 2) X is integer,
 $n_1 + m + 1 - X \leq 0$ 3) X is integer,

$$n_1 + m + 1 - X > 0, \quad n_1 + 1 - X \leq 0$$

4) X is integer, $n_2 = n_1 - X \geq 0$.

The most interesting result was got in the case 3. For this case perturbation series (3) is converging if $p > p_0$, where $4p_0$ is a radius of convergence which depends on n_1 , m and X . However, β_{pt} does not represent the correct value β . For example, for $n_1=1, m=2, X=2$ the correct value β is given by

$$\beta_{as} = \frac{1}{2} + \frac{1}{4p} + \frac{1}{2} \sqrt{1 - \frac{2}{p} + \frac{1}{4p^2}} + \frac{(4p)^6}{6} e^{-4p} \left[1 - \frac{26}{4p} + \frac{222}{(4p)^2} + \dots \right] \quad (4)$$

At the same time β_{pt} does not include exponentially small terms.

Thus, from the fact that β_{pt} can be calculated exactly, one cannot deduce that

β_{as} does not possess the intrinsic error which is characteristic for the asymptotic expansions.

2. By applying the results obtained for c.a.s.e. to the $Z_1 e Z_2$, it is possible to examine the perturbation series for electronic terms which are valid when the distance between Z_1 and Z_2

is large

$$E(n_1, n_2, m) = \sum_{k=0}^{\infty} \frac{E_k}{R^k} \quad (5)$$

We obtained the asymptotic formulae in K for the coefficients E_k for arbitrary Z_1, Z_2, n_1, n_2, m . It appeared that in contrast to the case of H_2^+ for some cases the series (5) are sign changing when $K \rightarrow \infty$. The cumbersome expressions for E_k will be presented at the conference.

Reference

1. R.J.Damburg, R.Kh.Propin, S.Graffi, V.Grecci, E.M.Harrell II, J.Cizek, J.Paldus and H.J.Silverstone, Phys. Rev. Lett. 52, 1112, 1984

ON THE PROTON IMPACT EXCITATION OF ZINC, CADMIUM AND MERCURY ATOMS

M.Ju.Ciple,* V.L.Ovchinnikov,* O.B.Shpenik*

* Uzhgorod State University, Uzhgorod 294000 USSR

* Institute for Nuclear Researches of Ukrainian SSR Academy of Sciences, Uzhgorod 294000 USSR

Emission spectra (2200–8000 Å), excited in low energy proton collisions with Zn, Cd and Hg has been studied. Absolute cross-sections and excitation functions of the majority of emissions were measured. Experimental conditions: LAB-energy range 10 to 1500 eV; target atoms vapor pressure was about 10^{-4} to $6 \cdot 10^{-3}$ Torr; proton beam density was about $5 \cdot 10^{-5}$ A/cm² and energy inhomogeneity ~ 3 eV. Emission spectra were assembled by scanning the diffractational monochromator through the wavelength region of interest with no worse than 5 Å resolution. The effective excitation cross-sections absolute values Q_i were defined by comparison of spectral line intensities excited in the investigated processes and reference lines of Zn, Cd and Hg atoms excited by electron impact in similar conditions. Q_i definition accuracy was about 50%, excitation functions measurement error was about 4%.

Principal results are the following:

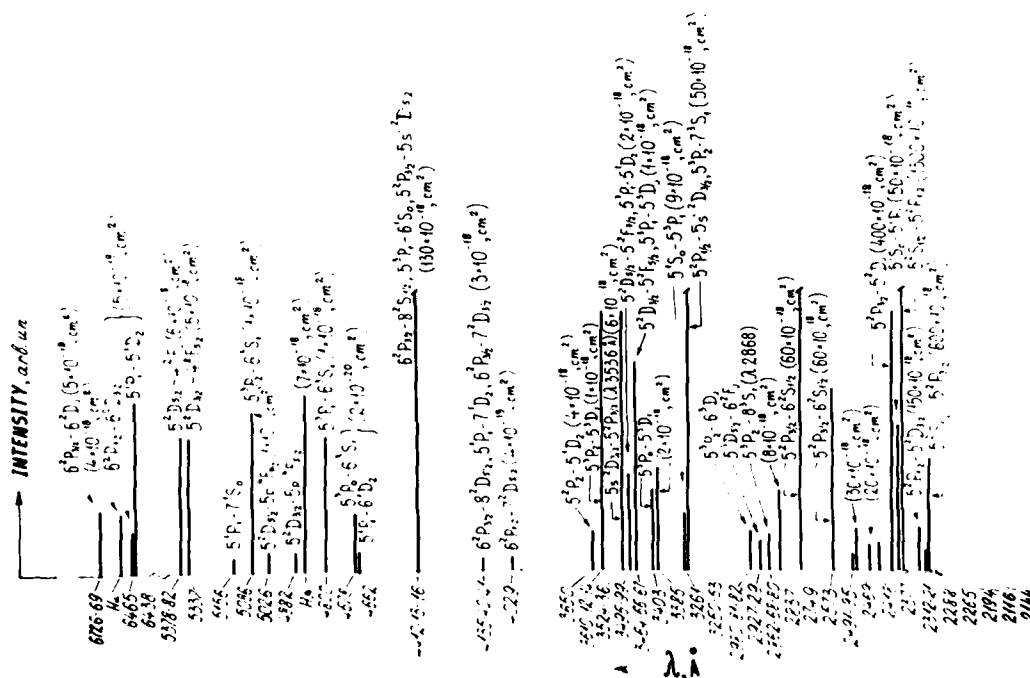
1. Absolute emission cross-sections were found to vary in the range of 10^{-19} to 10^{-15} cm².
2. The atomic and ionic states excitation efficiency in one-electron or two-electron processes accordingly is similar. Moreover, some lines originate from upper states (n > 7) both atomic and ionic were

observed in spectra. In the figure the example of the emission spectrum of 1000 eV (LAB) H⁺ + Cd collisions is given. Absolute excitation cross-sections values for the most intensive spectral lines (their values given in brackets) were measured at the same energy.

3. In studied spectra the intensive atomic lines originate from triplet states are present, although forbidden due to the Vigner rule. We suppose these emissions to be the result of relativistic effect, first of all of spin-orbital interaction. Since the relativistic correction for inner electrons have the order of $(Z/137)^2$, producing the changes in self-agreed field, where the outer electrons are moving, the efficiency growth of triplet states excitation in Zn + Cd and Hg transitions, as we observed in our experiment, serves as an indirect confirmation of our hypothesis.

Reference

1. See, for example, Hans A. Bethe and Edwin E. Salpeter Quantum mechanics of one- and two-electron atoms, edited by Göttinger, Heidelberg (Springer-Verlag, Berlin, 1957).



ON OSCILLATIONS OF TOTAL CROSS-SECTION FOR EXCITING THE 2312 Å LINE IN $\text{Ar}^+ + \text{Cd}$ SYSTEM

Yu.A.KSAVERY

Uzhgorod department of the Institute for nuclear researches, Uzhgorod

M.-T.I.Soskida et al.¹ have reported at IX-th ICPEAC about discovery the pronounced oscillation structure on excitation function $\sigma(E)$ of the 2312 Å line (as a function of centre of mass energy E) at slow Argon ion - Cadmium atom collisions. The 2312 Å line is correspond to $5d^2 \nu_{5/2} - 5p^2 \nu_{3/2}$ transition in the Ca^+ ion. Having been carry out a phenomenological analysis of the observable structure on this line in $v \approx 500$ eV energy range one may persuaded that the oscillations of radiation intensivity has a complicated nature. - Actually they are being observable at some smooth σ^{sm} curve's background, and they are consist of at least of two harmonic oscillations of simple cosine-like type with different periods as well as with uniformity of local extrema positions in the colliding argon ions inverted velocity $1/v$ scale. A comparatively good reproduction of the data one may obtain by the formal functional dependence of the following type

$$\sigma = \sigma^{\text{sm}} + \Delta\sigma^{\text{osc}}.$$

Here σ^{sm} is Landau-Zener cross-section and the oscillating part

$$\Delta\sigma^{\text{osc}} = 2.9 \times [\cos \pi(6.1 \times 10^4 \text{ m/sec} \times v^{-1} + 2.2) + \cos \pi(3.9 \times 10^4 \text{ m/sec} \times v^{-1} + 0.4)].$$

- at any rate all main peculiarities of the experimentally observable dependence is contain in this function in the whole energy range. Because of the ground oscillations amplitudes are even the resulting oscillation must become deeply modulated, at all 100%. This is the reason for which one is being observe existence of a high peak on data at $E = 17.7$ eV energy where the maximum of beating has taken place.

It is one of the some possible varieties for the model of four semimolecular terms with additional interaction at large internuclear separations in the framework of which one can reach a simple and natural exploration for the effect of deep modulation of the oscillations

on energy dependence of total cross-section in exciting the 2312 Å line at slow Argon ion - Cadmium atom collisions. - It is the simplest analogy of the well-known Rosenthal-Bobashev model^{2,3}. The essence of the new proposed model is that there are three excited semimolecular ion $(\text{ArCd})^+$ terms which are situated close together each to other and which has an intersection at large internuclear separations. At small internuclear separations these terms are being coherently populated via semicrossings with the main term when the particles have had growing together. When the particles are being fly away then the interaction of excited terms at large internuclear separations have lead to appearance of additional Landau-Stueckelberg oscillations which are still remain on total cross-section under the certain conditions too. The frequencies of these oscillations are - for the first approximation - proportional to the areas of reserved loops which are being formed on term's scheme on the interval from small internuclear separations up to great one, and which are in fact approximately equal to $6.1 \times 10^4 \text{ m/sec}$ and $3.9 \times 10^4 \text{ m/sec}$ within the $1/\sqrt{\pi}$ -factor accuracy for the $\text{Ar}^+ + \text{Cu}$ system. It has been follow from the correlation diagram for $\text{Ar}^+ + \text{Cu}$ system that it is natural to choose $5s5p^1 P_1^0$ -state of Cadmium atom and $5d^2 \nu_{3/2}$, $5d^2 \nu_{5/2}$ -states of Cadmium ion as an excited terms in the model mentioned above. Apparently it is the semimolecular interference of at least of three inelastic channels of reaction resulting the excitation of these levels because of which the deeply modulated oscillations on the excitation function of the 2312 Å spectral line in $\text{Ar}^+ + \text{Cu}$ system are being to appear.

REFERENCES

- 1 M.-T.I.Soskida et al. IX ICPEAC, Abstracts of Papers, vol.I, Seattle, 179 (1975).
- 2 H.Rosenthal. VI ICPEAC, Abstracts of Papers, Cambridge, 302 (1969).
- 3 S.V.Bobashev. Sov. Phys. JETP Letters 1, 260 (1970).

IMPACT-PARAMETER DEPENDENCE OF δ -ELECTRON EMISSION IN FAST ION-ATOM COLLISIONS*

C. Kelbch, J. Ullrich, V. Dangendorf, S. Kelbch,
W. Schadt, K. Bethge, H. Schmidt-Böcking

Institut für Kernphysik der Universität Frankfurt
D-6000 Frankfurt/Main / FRG

In basic perturbation theories, the matrix element for an ionization process in fast ion-atom collisions is mainly given by $\langle \psi_f V(R) \psi_i \rangle$ where ψ_i is the initial state of the electron and ψ_f is the final continuum state, $V(R)$ represents the perturbation potential for a given trajectory $R(t)$, i.e. the measurement of triple differential δ -electron probabilities

$$\frac{d^3 P(b, E_e, \theta_e)}{db dE_e d\theta_e}$$

for a fixed projectile trajectory enables a direct comparison with calculated matrix elements (b is the impact parameter, E_e the electron energy, θ_e the electron emission angle).

Measuring subsheath ionization probabilities or doubly differential cross sections for electron ejection, the experimental value reflects generally only an integral over many matrix elements.

Only a few data have been published concerning impact-parameter dependent δ -electron spectroscopy [1,2,3]. The published data sets were measured in the range of very heavy collision systems, where the δ -electron energies exceed the classical binary encounter energy limits [3] or in the range of light, nearly symmetric systems (e.g. F on Ne [1] or S on Ar [2]) where quasi-molecular effects may play a major role.

These data [1,2] show a surprising rise at small impact parameters in the δ -electron emission probability with increasing b . This rise, which is in disagreement with theoretical calculations, (done in the SCA-approach [4] is at present not understood at all. Stimulated by these results, we have started a systematic study of δ -electron emission probabilities from very asymmetric to symmetric ion-atom collision systems.

The experiments were performed at the 2.5 MV and the 7 MV Van-de-Graaff accelerator of the Institut für Kernphysik der Universität Frankfurt. The ion beam was collimated down to $0.2 \times 0.2 \text{ mm}^2$ and passed through a target gas jet, placed in the focus point of a hemispherical electrostatic electron analyzer. The scattered particles were detected by a position sensitive parallel-plate avalanche detector which consists of concentric rings to determine 16 scattering angles between 0.1° and 1° simultaneously.

The energy-analyzed electrons were detected in coincidence with the scattered particles. The probability for the ejection of a δ -electron with energy E_e for a

certain impact parameter b is then derived from

$$\frac{d^3 P(b, E_e, \theta_e)}{db dE_e d\theta_e} = \frac{d^3 N_c(b, E_e, \theta_e)}{dN_{\text{Tot}}(b) db dE_e d\theta_e}$$

where $d^3 N_c$ is the number of true coincidences per electron energy interval dE_e and electron detection solid angle $d\theta_e$, and $dN_{\text{Tot}}(b)$ is the total number of particles detected at scattering angle $\theta = \theta(b)$.

We have measured the impact-parameter dependence of the δ -electrons in the systems:

- | | |
|---------------|------------------------------|
| 1, 2.2 MeV He | Ne, Ar; 1000fm < b < 12000fm |
| 4 MeV O | Ne, Ar; 4000fm < b < 12000fm |
| 5, 10 MeV Ne | Ne; 2000fm < b < 11000fm |

in the energy-range $150\text{eV} < E_e < 1000\text{eV}$.

We also observed a rise of the emission probabilities for small impact parameters. Theoretical calculations from Trautmann et al. [5] are in significant disagreement with the measured data.

REFERENCES

- /1/ A. Skutlartz, S. Hagmann; Phys. Rev. A 28 (1983) 3268
- /2/ C.L. Cocke, H. Schmidt-Böcking, R. Schuch; J. Phys. 315 (1982) 651
- /3/ F. Güttner et al.; Z. Phys. A 304 (1982) 207
- /4/ D. Trautmann, F. Rösel; Nucl. Instr. Meth. 169 (1980) 259
- /5/ D. Trautmann, F. Rösel; private communication

* partially supported by BMFT

EVIDENCE FOR INDEPENDENT PARTICLE BEHAVIOR IN FAST RYDBERG HYDROGEN ATOM COLLISIONS WITH NEUTRAL ATOMS AND MOLECULES

M. King*, L. Wang, and T.J. Morgan

Physics Department, Wesleyan University, Middletown, Connecticut 06457 USA

We have performed a series of experiments in order to confirm unambiguously that in fast collisions between high Rydberg atoms and neutral perturbers both the Rydberg electron and the ionic core scatter quasifreely. Previous measurements by Koch¹ using 3.3-6.2 keV/amu high Rydberg deuterium atoms in collision with N₂ hinted this is true, and served as motivation. We have carried out absolute measurements of the total destruction cross section (sum of ionization, excitation, and deexcitation) for 2.5-40 keV/amu high Rydberg (20 ≤ n ≤ 30) hydrogen and deuterium atoms in collision with Ar, N₂, and CO₂.

The model for these collisions treats the Rydberg electron e_R^- and core ionic proton as independent scatterers. This view is based on two important characteristics of the collision: (1) the effective interaction between the charge components of the Rydberg atom and the neutral perturber is short ranged compared to the e_R^- -p separation and (2) the translational velocity of e_R^- is large compared to its orbital velocity. In this case the Rydberg destruction cross section σ_D should equal the sum of the free electron and free proton

cross sections, i.e., $\sigma_D = \sigma_e + \sigma_p$.

A fast beam of hydrogen Rydberg atoms H(n) is prepared by electron detachment of H⁻ in H₂. H(n) then passes through a static gas target with the absolute pressure measured by a capacitance manometer. After the target, the population in a band of high Rydberg states is measured using static electric field ionization. The experiment relies on a determination of the intensity of H(n) after the target as a function of absolute target pressure. Background contributions due to collisional production of H⁺ are reduced by application of a constant electric field just prior to the field ionization region and by voltage labeling the field ionized H⁺ signal. Background contributions due to neutrals in the beam other than H(n) are subtracted by electric field modulation techniques. In this way a well defined band of n states can be isolated and detected.

The attenuation of H(n) is exponential and the slope of the transmitted H(n) signal versus target thickness yields the collisional destruction cross section. Least square fits to the data were performed up to target thickness of 3×10^{14} cm⁻² corresponding to about 70% attenuation. Operating pressure in the detector region was 1.5×10^{-7} torr.

The results for Ar are shown in Fig. 1. They are compared with free electron and free proton data.² As

the energy of the Rydberg beam is decreased the dominant collisional mechanism changes from e_R^- scattering to core scattering with the cross over at about 11 keV. This occurs because the H⁺ electron capture cross section rises to a maximum at low keV energies while the e_R^- scattering cross section decreases due to the Ramsauer-Townsend effect. It is clear that $\sigma_D = \sigma_e + \sigma_p$ over the entire energy range and that H(n) scatters with a large cross section even in the presence of a deep Ramsauer-Townsend minimum in the free electron scattering. Additional data will be presented at the conference to support the independent particle behavior of Rydberg atoms in fast collisions.

Work supported by the NSF and DOE, Office of Fusion Energy.

References

*Permanent address: Lawrence Livermore National Laboratory, Livermore, California 94550 USA

1. P.M. Koch, Phys. Rev. Lett. **43**, 432 (1979).
2. Average values of several experiments.

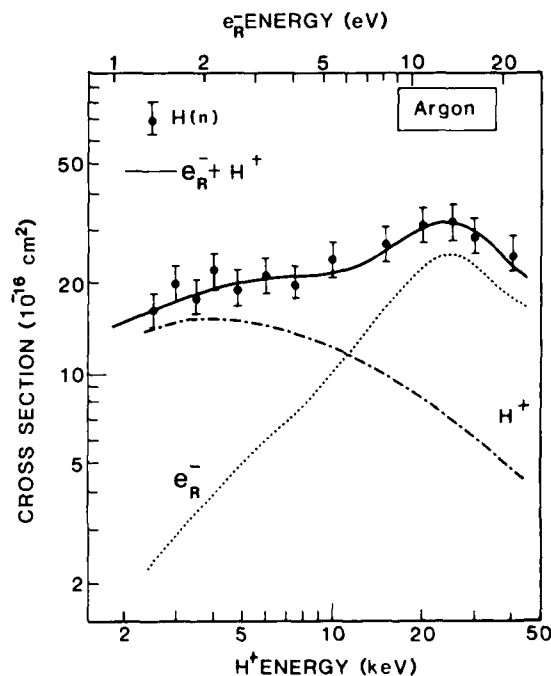


FIGURE 1. Cross section versus energy for H(n) + Ar collisions.

IONIZATION CROSS-SECTION OF YTTERBIUM ATOMS BY ELECTRON IMPACT

M.M.Ali,* P.N.Volovich,* V.L.Ovchinnikov,* L.L.Shimon*

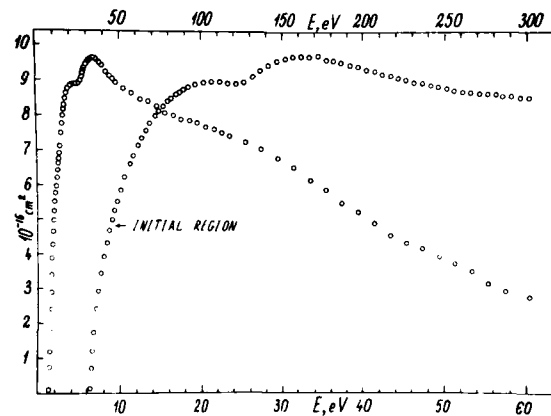
* Uzhgorod State University, Uzhgorod 294000 USSR

+ Institute for Nuclear Researches of Ukrainian SSR Academy of Sciences, Uzhgorod 294000 USSR

Total ionization cross-section of atoms 5 to 300eV impact energy range is measured for the first time.

Measurements were performed in crossed electron and atomic beams. Atomic beam was modulated by a vibrational interrupter while measuring the ionization function. The variable component of ion current was deposited by selective amplifier and synchronous detector. Atomic beam density was measured due to the shifting of quartz resonator frequency, resulting from the ytterbium sputtering on its surface. Experimental conditions were the following: atomic density in collisional regions $(1,5 - 1,5) \cdot 10^{10} \text{ cm}^{-3}$; electron current magnitude $(4 - 10) \cdot 10^{-7} \text{ A}$; electron energy spread did not exceed 1eV; ion current magnitude $(1 - 3) \cdot 10^{-11} \text{ A}$; residual gas pressure $5 \cdot 10^{-7} \text{ Torr}$. The error cross-section definition was about 30%; the error in ionization function measuring was about 4%. Effective cross-section increases rapidly from the ionization threshold (6,25eV) with the growth of electron energy (the initial zone of the function is given in a stretched scale of the figure). There are some maxima emphasized on the curve at 22eV and 33eV energies. They exist, probably, due to single

ionization from 6s and 4f Yb atomic shells. Through the entire energy range the measured cross-section value is close to the one obtained by Mann formula¹ for



calculation of single atomic ionization cross-section in slow electron collisions.

Reference

1. J.B.Mann, J.Chem.Phys. 46, 1646 (1967)

K-EMISSION INVESTIGATION BY ELECTRON BOMBARDMENT OF FREE POTASSIUM ATOMS

ZAPESOCHNY I.P., VUKSTICH V.S., SOLOMON A.M.

Uzhgorod department, Institut of Nuclear Research, Uzhgorod, Ukrainian SSR

The study of K-shell ionization processes by electron impact via detection of accompanied X-ray emission is difficult because of influence number of factors: 1) the ionization cross-section for deep inner shells of atoms are relatively small ($\sim 10^{-21} \text{ cm}^2$); 2) the fluorescence yield for light and middle atoms is small in comparison with an Auger electron ejection; 3) the intensive bremsstrahlung reduct to the small values of the signal to noise ratio; 4) the efficiency of the dispersive spectral apparatus in the X-ray region is small also.

Besides in the case of free metall atoms its concentration in the beam is a few order smaller then in the case when one utilize for the same purpose films on substrate.

Recently a number of investigation for K- and L-shells ionization are carried out by utilization of electron bombardment of thin films and gaseous targets in the near threshold energy region^{1,2,3} or in the case of relatively high energies⁴.

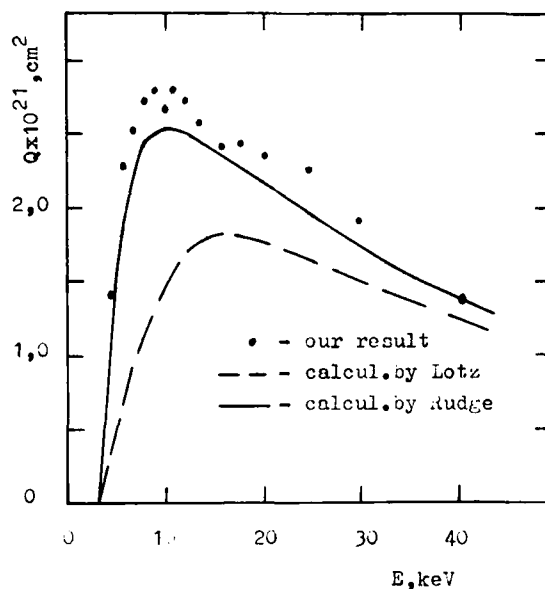
In spite of all difficulties the investigation of this problem for free metall atoms is actual. For fulfilment of systematic K-shell ionization investigations for metall atoms in the wide range of the threshold energies the apparatus with intersected electron and atom beams was constructed. The accompanied to K-shell ionization X-ray emission was registered by an Si(Li) semiconductor detector in the direction perpendicular to intersecting beams plane. The main parameters of the apparatus are: the concentration of atoms in beam was $\sim 10^{11} \text{ cm}^{-3}$; the incident electron energies varied from 500 eV to 50 keV; the electron current was 1 nA; the pressure was $5 \cdot 10^{-7} \text{ Torr}$. The energy separation of the detector was 260 eV for the line 5,9 keV, the quanta detection region was 2-30 keV.

It was forsee the modulation of the atomic beam to take into account in spectra the substrate from bremsstrahlung and fluorescence effects from the chamber surface be in the field of view of detector. The modulation permits us extract the influence of slow variation

in time of the experimental parameters in case of the long exposition duration.

On the base of the constructed apparatus we at the first investigate the excitation of K-series for potassium atoms in the energy range up to 11 threshold energy values. The obtained dependence of efficiency of K-emission excitation as function of incident electron energy has a maximum at 3,5 - 4 threshold energy values.

On the figure our results are in comparison with semiempirical calculations carried out by Lotz⁵ and Rudge - Schwartz⁶ formulae.



1. M. Shimizu, T. Nakagawa, K. Motoki and A. Ikuno. *Phys. Rev. A*, **2**, 70, 1961.
2. M. Asara, R. J. Harrison and P. J. Lee. *Physica*, **22**, 551, 1975.
3. Carroll Quarles and J. R. Samson. *Phys. Rev. A*, **20**, 147, 1962.
4. A. Schlenker et al. *Physica Scripta*, **11**, 155, 1975.
5. A. Lotz. *Phys. Rev. A*, **22**, 105, 1975.
6. A. Rudge, J. D. Schwartz. *Proc. Phys. Soc.*, **52**, 263, 1969.

ELECTRON-ELECTRON COINCIDENCE SPECTROSCOPY FOR THE STUDY OF RELATIVE TRIPLE DIFFERENTIAL CROSS SECTIONS FOR AUTOIONISING TRANSITIONS IN METALS

A.A. BOROVIK, V.V. VAKULA

INSTITUTE FOR NUCLEAR RESEARCHES OF UKRAINIAN SSR ACADEMY OF SCIENCES, UZHGOROD 294000 USSR

The investigation of angular correlations between scattered and ejected electrons associated with the autoionisation processes is the powerful method for studying the energy structure of atom in ionization continua. Such experiments, first, lead to the determination of the triple differential cross section and enable comparison to be made with theoretical models for these processes. Second, it should be made the accurate spectroscopic identification of the lines in electron spectra.

For these purposes in our laboratory has been constructed apparatus mainly consisted of (e,2e) spectrometer and electronic coincidence circuit (see figure).

The scattered and ejected electrons are analysed with respect to their energy and scattering angle by two identical 127° electrostatic cylindrical condensers A_1, A_2 . The source of metal vapour atoms is an heating oven with the aperture 0,4 mm in diameter. In order to obtain the gas beam the tube of 6 mm in length and 0,4 mm in diameter was used. The (e,2e) spectrometer parameters are the following:

- the incident beam energy - $5 + 1500$ eV and the beam current - $1 + 100 \mu A$,
- energy and angular resolutions of both electron analysers is 0,2 eV and 2° respectively;
- the rotation of analysers can be provide over an angular range from 15° to 140° with respect to the incident beam;
- the vapour target density in the scattering centre equals about 10^{11} cm^{-3} ;

The spectrometer is mounted in stain-less steel chamber which is pumped down to $1 \cdot 10^{-7}$ Torr by an 500 liter/sec turbomolecular pump.

The signal-processing electronics are shown schematically in figure. The charge pulses from each of the detectors D are processed by the preamplifier-amplifier-discriminator system to give fast logic pulses. Pulses from

the "scattered"-electron analyser start a time-to-amplitude converter TAC while pulses from the "ejected"-electron analyser is delayed by a length of coaxial cable and stop the TAC. The arrival of a pair of electrons with a given time correlation then corresponds to a particular pulse height out of the TAC.

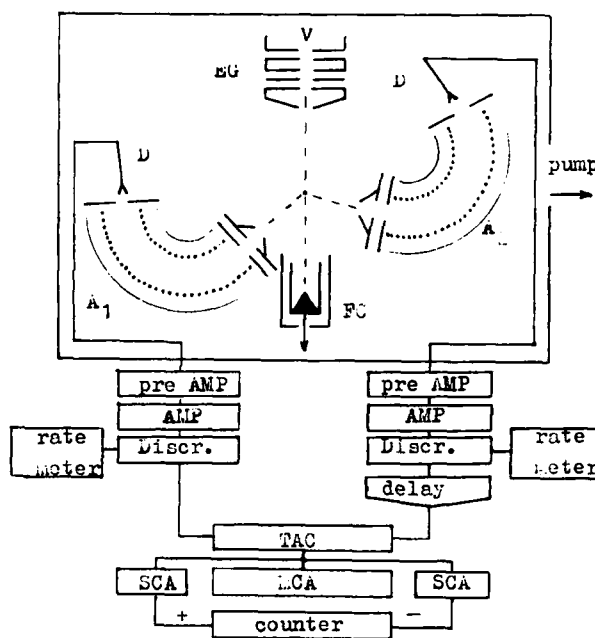
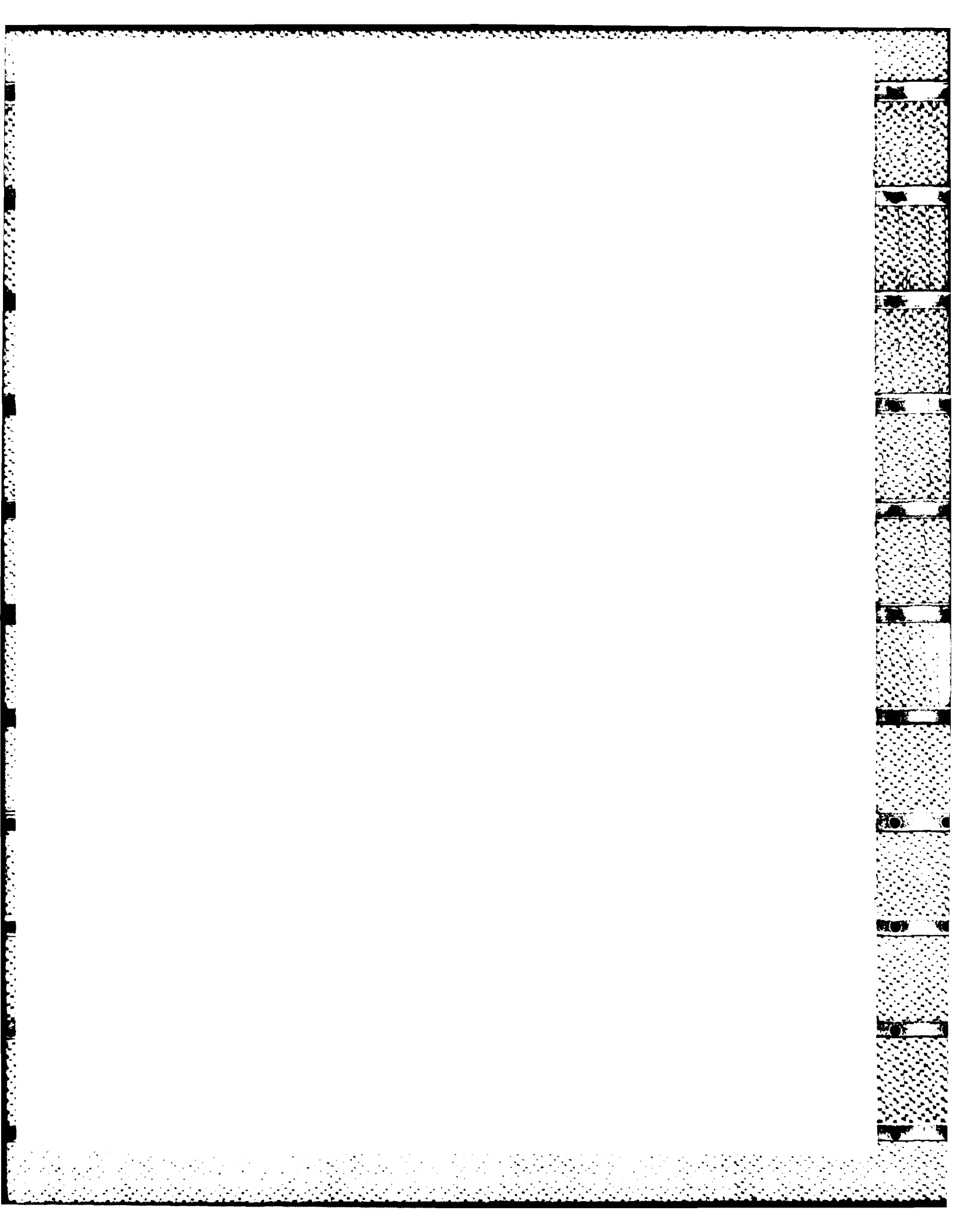


Fig.1. Schematic diagram of (e,2e) spectrometer and coincidence electronics.

A multi-channel analyser LCA performs a pulse-height analysis on the TAC output. In order to isolate the true coincidences, two single-channel analysers SCA with variable widths of windows and up-down counter are set up.

With the apparatus explained above, the preliminary measurements of energy loss- and ejected electron spectra of lithium vapour have been made.



Author Index

- Abdel-Raouf, M.A.* 317, 318, 335, 336, 337
Åberg, T. 456, 623
Achenbach, Ch. 301
Aggarwal, K.M. 287, 305
Ajello, J.M. 248
Alajajian, S.H. 283
Aleksakhin, I.S. 696, 697
Ali, M.M. 707
Alijah, A. 27
Allen, J.S. 385
Alonso, J. 537, 538
Alston, S. 516, 517, 518, 519
Altman, J.C. 139
Alton, G.D. 415
Alvarez, I. 572, 573
Andersen, L.H. 474, 525
Andersen, N.O. 121, 359
Andersen, T. 51
Anderson, L.W. 385
Andriamonje, S. 432, 673
Angel, G.C. 6, 34, 613
Anholt, R. 430, 432, 446, 534, 535, 537, 538, 550
Antar, A.A. 429
Anthony, J. 398
Antolak, A. 700
Antoni, T. 249
Aquilanti, V. 350, 605
Arai, S. 55, 277
Arikawa, T. 674
Armour, E.A.G. 330, 331
Arseneau, D.J. 344, 345, 346
Ashurov, A.R. 695
Assal, W. 688
Astner, G. 470
Aumayr, F. 487, 488
Avakov, G.V. 695
Avaldi, L. 157, 176, 177
Avery, J. 608
Awaya, Y. 451, 452, 545
Backe, H. 433
Badrinathan, C. 167, 594
Bae, Y.K. 48, 49, 584, 585
Bähring, A. 437
Bai, Y.Y. 73
Baker, D.J. 331
Baker, O.K. 432, 549
Balanda, A. 433
Baliyan, K.S. 170
Baluja, K.L. 24, 242
Barnford, D.J. 66
Bandarage, G. 412
Banna, M.S. 38, 661
Baptista, G.B. 547
Bárány, A. 468, 469, 470, 474
Barat, M. 677
Barbier, L. 371
Barbieri, R.S. 105, 224
Bardsley, J.N. 74
Barrachina, R.O. 514
Barros, H.G.P.L. de 201
Bartschat, K. 23, 193, 194
Barzen, K. 351
Basu, A. 94
Basu, D. 102
Basu, M. 152
Basuchoudhury, K. 280, 342
Baum, G. 182
Baumgärtel, H. 654
Bawagan, A.O. 261
Be, S.H. 407, 448
Bechler, A. 28
Becker, K. 111, 282, 383
Becker, R. 301
Becker, R.L. 454
Becker, U. 12, 13
Becker, U. 541, 542
Beckmann, K. 590
Bederson, B. 200
Begemann, M. 433
Beijers, J.P.M. 206
Beland, M. 596
Belić, D. 299, 307
Bell, K.L. 360, 689
Ben Arfo, M. 239
Ben Itzhak, I. 506, 575
Bender, Ch. 353
Beneventi, L. 556
Benoit-Cattin, P. 464, 465
Benz, A. 591
Berényi, D. 530
Berger, O. 191
Bergeron, H. 610
Berinde, A. 399, 400, 401
Berk, A. 141
Berkner, K.H. 393, 395, 396, 509
Berlin, A. 641
Bernier, A. 610
Bernstein, E.M. 393, 394, 395, 396, 509
Berrington, K.A. 109, 305
Berry, R.S. 71
Berry, S.D. 449, 524
Bethge, K. 433, 705
Betz, H.-D. 508, 529
Beyer, H.F. 543
Beyer, H.-J. 117, 118
Beyer, W. 353
Bhatia, A.K. 103, 141
Bhattacharya, G. 382
Bhattacharya, N. 333
Bhattacharya, S.K. 17, 20
Bhattacharyya, S. 280, 342, 343
Bhattacharyya, S.S. 90
Bielschowsky, C.E. 201, 207
Bieniek, R.J. 554
Bijkerk, F. 668
Bilau, R. 427
Birnbaum, G. 636
Bischel, W.K. 66, 81
Bisling, P.G.F. 654
Bizau, J.M. 7, 8
Bjerre, N. 29, 56
Blankenship, D.M. 386, 489
Blokhintsev, L.D. 695
Blomberg, A. 456, 623
Bloomfield, L.A. 648
Blum, K. 194, 196
Boesten, L. 237
Bogachev, G.G. 697
Bokemeyer, H. 433
Bolorizadeh, M.A. 528
Bonani, G. 458
Bonanno, R.E. 69
Bonham, R.A. 690, 691
Bordenave-Montesquieu, A. 464, 465
Borgmann, H. 190
Borovik, A.A. 709
Borsella, E. 87
Borysow, A. 636
Botelho, L.F.C. 218
Botero, J. 334
Bottcher, C. 150, 308, 540
Bottrell, G.J. 480
Bouisset, P. 492, 510
Brandsen, B.H. 494, 618
Bregel, T. 368
Breinig, M. 449, 526
Breitenstein, M. 232
Brendlé, B. 459, 460
Brenn, R. 426
Briggs, J.S. 147, 384, 461, 518
Brion, C.E. 37, 256, 261, 262
Broad, J.T. 27, 79, 169
Brooks, D.L. 324
Brouillard, F. 299, 620
Brower, M.C. 493
Brown, C.J. 320
Brown, S. 592
Brown, W.L. 648
Bruch, R. 678, 679
Brug, H. van 668
Brunger, M.J. 113, 183, 202
Brutschy, B. 654
Bryant, H.C. 50
Buck, U. 557, 650
Buckman, S.J. 106, 202
Budenholzer, F.E. 561
Bühler, B. 84
Burgdörfer, J. 526, 527
Burgi, P.J.M. van der 156
Burke, P.G. 39, 109, 193, 217, 242
Burkhard, M. 530
Burkhardt, M. 529
Burns, D.J. 114
Burrow, P.D. 238
Bußer, W. 368, 376
Butterfield, K.B. 50
Cai, J.-L. 200
Callaway, J. 124, 285
Cambi, R. 268
Camilloni, R. 157, 177
Câmpeanu, R.I. 99, 304
Caneve, L. 87
Carré, B. 7
Cartwright, D.C. 110, 199, 249

- Casaubon, I.* 496
Casavecchia, P. 556
Castleman, A.W., Jr. 588, 655
Cavalli, S. 605
Cederquist, H. 470, 474
Celotta, R.J. 185, 658
Chakrabarti, M.K. 90
Champion, R.L. 420
Chandra, N. 47
Chang, M.H. 561
Chang, T.N. 19
Chantrenne, S. 298, 299
Chapman, S. 582
Chatterjee, L. 280, 342, 343
Chaudhry, A.A. 166
Chemin, J.F. 673
Cheng, X. 341
Cheret, M. 371
Cherkani, M. 620
Cherlenyak, I.I. 692, 693
Chetoui, A. 463, 492, 510
Chhaya, V.M. 255
Cho, U.-I. 122
Chornay, D.J. 245
Christensen-Dalsgaard, B. 148, 608
Chu, S.-I. 17, 75, 638
Chung, K.T. 143
Church, D.A. 449
Chutjian, A. 283, 289
Ciorte, C. 399, 400, 401
Ciple, M.Ju. 703
Cipolla, S.J. 425
Cisneros, C. 572, 573
Claeys, W. 675
Clapis, P. 428
Clark, C.W. 69
Clark, D.A. 50
Clark, M. 396, 398, 509
Clark, M.W. 393, 394, 395
Cocke, C.L. 446, 453, 472, 473, 475
Coffman, D. 100
Coggiola, M.J. 49, 584
Cohen, J.S. 365, 373
Cohen, S. 50
Cohen, S.A. 348
Coleman, P.G. 324
Collin, J.E. 263
Collins, L.A. 43, 204, 241
Comella, M. 74
Comer, J. 226, 258, 259, 657
Compton, R.N. 415
Comtet, G. 50
Cook, J.P.D. 173
Cooper, I.L. 612
Copeland, R.A. 566, 567
Coptan, M.A. 245
Cordis, L. 651
Cornet, A. 675
Covinsky, M.H. 597
Cowan, T. 433
Cremer, C. 84
Crosley, D.R. 565, 566, 567
Crothers, D.S.F. 154, 511
Crowe, A. 115, 116, 159, 160
Csanak, G. 110, 199, 246
Cubaynes, D. 7, 8
Cubrić, D. 260
Currell, F. 226
Cuvellier, J. 568
Cvejanović, D. 260
Cvejanović, S. 158, 172, 257, 260
Dababneh, M.S. 230, 328
Dahler, J.S. 358, 379
Dalgarno, A. 483, 484
Damburg, R.J. 702
Danared, H. 468, 470
Dangendorf, V. 705
Daniele, R. 642
Danjo, A. 108
Danzmann, K. 447
Dao, P.D. 655
Dark, C.A. 339
Dasgupta, A. 103
Dastidar, K.R. 89, 640
Dastidar, T.K.R. 89, 640
Dateo, C.E. 61
Datta, K.K. 90
Datta, S. 513
Datz, S. 306, 505
Davidson, S.A. 356
Davis, B.F. 143
De, B.N. 114
Deb, N.C. 523
Debus, S. 442
Deco, G.R. 539
Defrance, P. 298, 299
Dehmer, J.L. 70, 85
Dehmer, P.M. 70, 85
Delaunay, M. 477
Delcroix, J.-L. 688
Delettrez, J. 644
Delos, J.B. 390, 419
Delwiche, J. 31, 33, 263
DePaola, B.D. 307
Desai, H.S. 98, 129, 220, 240
DeSerio, R. 449
Deslattes, R.D. 543
DeVries, M.S. 684
Dewangan, D.P. 95, 198, 520
Dexter, J.L. 72
Diana, L.M. 324
Dickinson, A.S. 612
Dillon, M.A. 267
Ding, A. 651
Diserens, M.J. 300
Dittner, P.F. 306
Djerad, M. 371
Djurić, N. 307
Donahue, J.B. 50
Dourneuf, M.I. 210
Dousson, S. 464, 465, 477, 677
Doverspike, L.D. 420
Drachman, R.J. 323
Drake, G.W.F. 383
Dreizler, R.M. 498, 500
Drentje, A.G. 466
Dressler, K. 312
Du, M.L. 419
Du, W.-H. 587
Dubé, D. 663
DuBois, R.D. 408, 490
Dubreuil, D. 367
Duguet, A. 176
Dujardin, G. 30
Dulieu, O. 155
Duncan, A.J. 166
Duncan, M.M. 422, 423, 524
Dunn, G.H. 307
Dunn, K.F. 613
Dunning, F.B. 362, 630, 631
Dupuis, M. 61, 551
Dutta, S. 102
Eck, J. van 156, 206, 445
Ederer, D. 7
Ehrhard, H. 153, 234
Eichler, J. 66, 462, 520, 521, 535
Eichmann, U. 15, 632
Eisele, F.L. 701
Eland, J.H. 31
Elford, M.T. 485
Elliott, D.S. 405
El-Sheikh, A. 117
Elston, S.B. 449, 526
Eminyan, M. 180, 672
Emmichoven, P.A.Z. van 206
Engar, P. 526
Engelking, P.C. 88
Enulescu, Al. 399, 400, 401
Erkovich, O.S. 694
Ermolaev, A.M. 617
Errea, L.F. 478
Estep, L. 140
Faibis, A. 457, 660
Fainelli, E. 157
Faisal, F.H.M. 645
Falcón, C. 496, 614
Fantoni, R. 87, 268
Farnoux, F.C. 546
Fassett, J.D. 69
Faust, M. 440
Faustov, R.N. 347
Feagin, J.M. 147, 392, 548
Fehrer, M. 477
Feigerle, C.S. 658
Feldmann, D. 67
Feldt, A.N. 219
Ferch, J. 233
Ferrante, G. 642
Ferrett, T.A. 10, 11
Fiegel, R.P. 119
Fineman, M.A. 229
Fink, M. 100
Flaig, H.-J. 165
Flannery, M.R. 197, 606
Fleming, D.G. 344, 345, 346
Florescu, V. 65
Flower, D.R. 494
Fluerasu, D. 399, 400, 401
Focke, P. 524
Folger, H. 433
Folkman, F. 543
Forand, J.I. 111, 282
Ford, A.L. 455
Fornari, L.S. 324
Forrest, L.F. 162

- Fournier, F.R. 626
 Freeman, R.R. 648
 Freitas, L.C.G. 109, 218
 Freund, R.S. 161
 Friedrich, B. 482
 Fritsch, W. 411, 502
 Froelich, P. 80
 Fromme, D. 325
 Frommhold, L. 636
 Frost, L. 256
 Fujita, Y. 227, 228, 254
 Fukuroda, A. 674
 Fülling, S. 679
 Fumagalli, P. 458
 Furlan, M. 263
 Furst, J.E. 113, 119, 221
 Furtado, F. 388
 Fussen, D. 675
 Futrell, J.H. 587
 Gallagher, A. 355, 356
 Gallagher, J.W. 121
 Gallagher, T.F. 16, 72
 Gamal, H. 664
 Gangopadhyay, P. 78
 Ganguly, S. 89, 640
 Ganz, J. 368
 Gargaud, M. 479
 Garibotti, C.R. 514, 532
 Garland, N.L. 566
 Garner, D.M. 344, 345, 346
 Gay, T.J. 386, 489
 Gayet, R. 459, 460
 Gealy, M.W. 361, 443
 Geddes, J. 580
 Geesmann, H. 189
 Geller, R. 477
 Gérard, P. 7, 8
 Gerber, G. 54, 84
 Gerritsen, H.C. 668
 Gertner, I. 575
 Ghosh, A.S. 102, 152, 329
 Ghosh, M. 512
 Gianturco, F.A. 212, 552
 Giardini-Guidoni, A. 87, 268
 Gibson, T.L. 219, 235
 Gien, T.T. 92, 120
 Giese, J.P. 472, 473
 Gilbody, H.B. 405, 476, 580, 613, 689
 Gillen, K.T. 366
 Giusti-Suzor, A. 41
 Gleizes, A. 464, 465
 Godunov, A.L. 413, 515
 Goeke, J. 188, 190
 Goeller, L.N. 630, 631
 Goffe, T.V. 406
 Gohil, P. 393
 Goldberg, I.B. 133, 134, 135, 136
 Golden, D.E. 119, 221
 Golub, J. 352
 Golubkov, G.V. 63, 213, 357
 Gomez, R.D. 322
 Gonzalez, A. 532
 Goruganthu, R.R. 691
 Goscinski, O. 456
 Gould, H. 537, 538
 Gounand, F. 624, 625, 626
 Gräf, D. 175
 Graham, W.G. 393, 394, 395, 396, 509
 Gram, P.A.M. 50
 Granitza, B. 233
 Grant, I.P. 132
 Gray, L.G. 362, 630
 Green, T.S. 676
 Greenberg, J.S. 433
 Greene, C.H. 334
 Grein, H. 433
 Griffin, D.C. 308
 Grimes, R.M. 551
 Grisogono, A.M. 265
 Groeneveld, K.O. 529, 530
 Grosser, J. 387, 441, 442
 Grossi, G. 605
 Grover, P.S. 329
 Grujić, P. 607
 Grün, N. 541, 542
 Gruppe, A. 433
 Guerra, M. 238
 Gulyás, L. 530
 Gupta, G.P. 123
 Haber, O. 575
 Haberland, H. 53, 68, 353
 Hagmann, S. 446, 453
 Hahn, U. 186
 Hahn, Y. 391, 628
 Hammond, P. 142, 158, 260
 Hanne, G.F. 188, 189, 190, 209
 Hara, S. 46, 244
 Harbich, W. 440
 Harel, C. 619
 Harmin, D.A. 25, 26
 Harrison, I. 271
 Harrison, M.F.A. 300
 Harth, K. 368
 Harvey, C.J. 50
 Hasegawa, T. 558
 Hasenburg, K. 194
 Hasse, R. 387
 Hatano, Y. 55, 277
 Hausamann, D. 353
 Havener, C.C. 444, 491, 662
 Haworth, A. 657
 Hayaishi, T. 14
 Hayes, T.R. 161
 Haysak, M.I. 685
 Haywood, S.E. 419
 Hazi, A.U. 278
 He, M. 354
 Heckenkamp, Ch. 2, 3, 4, 5
 Heckman, V. 562, 581
 Heckmann, P.H. 679
 Heddle, D.W.O. 670
 Heer, C.V. 338
 Heideman, H.G.M. 156, 206, 378, 445
 Heil, O. 529
 Heil, T.G. 480, 481
 Heimann, P.A. 10, 11
 Heinzmann, U. 2, 3, 4, 5
 Hellner, L. 30
 Helm, H. 29, 56, 86, 284, 649
 Hengyi, S. 608
 Henriët, A. 372
 Henry, R.J.W. 288, 289, 290, 291, 294, 295, 302
 Herman, Z. 482
 Hertel, I.V. 121, 377, 437, 652, 653
 Hertzner, A. 364
 Hesslich, J. 651
 Heuvell, H.B. van L. van den 72
 Heuzé, J. 367
 Hickman, A.P. 81, 309
 Hicks, L. 425
 Hink, W. 175
 Hino, K. 533
 Hintermayer, R. 435
 Hinze, J. 27
 Hippler, R. 166, 440, 505
 Hirayama, T. 303
 Hird, B. 595
 Hironaka, K. 55, 277
 Hitchcock, A.P. 269, 270
 Hitz, D. 464, 465, 677
 Ho, T.S. 75, 638
 Ho, Y.K. 288
 Hobbs, R.H. 253
 Hoffmann, D. 530
 Hoffmann, D.H.H. 397, 534
 Hoffmann, H.J. 426
 Hoffmann, R. 431
 Hogan, M.J. 681, 682
 Höhne, J. 68
 Holle, A. 1
 Holmes, A.J.T. 676
 Hölscher, C. 190
 Holtkamp, G. 107
 Hölzel, R. 12, 13
 Holzscheiter, H.M. 449
 Hood, D.M. 126
 Hopkins, J.L. 422, 423
 Höppler, R. 508
 Horsley, J.A. 269
 Hoshihara, K. 227, 228, 254
 Hotop, H. 368, 376
 Howald, A.M. 491
 Howard, S.L. 587
 Howorka, F. 576
 Hozack, R.S. 586
 Hsieh, Y.-F. 230, 322, 328, 332
 Hsu, Y.P. 639
 Hu, S.C. 561
 Huang, K.-N. 195
 Huber, B.A. 168, 471
 Hubin-Franskin, M.J. 31, 33, 263
 Hudson, D. 363
 Huestis, D.L. 49
 Hughes, J.G. 689
 Hult, S. 470
 Hülskötter, H.-P. 526
 Hulsman, H. 578
 Humberston, J.W. 320
 Hummer, C.R. 114, 641
 Humphrey, I. 112
 Humphries, W.J. 536
 Hunter, J.E. III 71
 Huo, W. 235
 Huq, M.S. 420

- Hus, H.* 313
Hutcheon, R.J. 314
Hvelplund, P. 469, 470, 474, 525
Hyder, G.M.A. 328
Ibraheim, K.S. 118
Ichimori, T. 251, 403
Ichimura, A. 555
Iga, I. 105, 224
Iguchi, K. 340
Iida, Y. 37
Ikezaki, Y. 303, 417
Imschweiler, J. 57
Inouye, H. 558
Ishihara, T. 497
Itikawa, Y. 14, 292
Ito, K. 55
Itoh, A. 406, 467
Itoh, Y. 14
Ivanov, G.K. 63, 213, 357
Ivanov, M.V. 683
Jacob, B. 498
Jaduszliwer, B. 200
Jaacks, D.H. 574
Jain, A. 214, 215, 236
Jakacky, J., Jr. 562
James, G.K. 37, 162
Janev, J. 84
Janssen, R. 313
Jeffries, J.B. 565, 566
Jerjian, K.A. 294
Jerram, P.A. 374, 375
Jetzke, S. 169
Jitschin, W. 438, 439
Joachain, C.J. 388
Johnson, A. 470
Johnson, A.L. 269
Johnson, B.M. 394, 509
Johnson, C.T. 296
Jones, D.M. 379
Jones, K.W. 394, 509
Jones, T.J. 172
Jordan, K.D. 238
Joshiyura, K.N. 240
Jost, K. 107
Joswig, H. 59
Joyce, D.W. 548
Juengerman, E.M. 339
Jung, K. 153, 234
Jungen, Ch. 83
Junker, B.R. 141
Jureta, J. 257, 260
Jusinski, L.E. 66
Justiniano, E. 431, 507
Kachru, R. 29
Kambara, T. 407, 448, 451, 452, 545
Kaminsky, A.K. 504
Kamke, B. 652, 653
Kamke, W. 652, 653
Kaneko, Y. 563, 564, 599
Kang, I.-J. 122
Kano, S.S. 227, 228, 254
Kanter, E.P. 457, 660
Kapoor, M. 179
Karashima, S. 450
Karimkhodzhaev, A. 347
Kase, M. 407, 448, 451, 452, 545
Katano, M. 417
Katiyar, A.K. 293
Kato, T. 598
Katsonis, K. 688
Kaupila, W.E. 230, 322, 328, 332
Kaussen, F. 189
Kawazumi, H. 279
Kazakov, S.M. 144, 163, 693
Keese, R.G. 588, 655
Keiffer, R.S. 362
Kelbch, C. 705
Kelbch, S. 446, 453, 705
Keller, J. 684
Keller, J.C. 7
Keller, J.S. 71
Keller, W. 589
Kelley, M.H. 185, 669
Kelly, J.F. 356
Kemmler, J. 529
Kempler, V. 436
Kenefick, R.A. 449
Kerkhoff, H.G. 12, 13
Kessel, Q.C. 428, 429
Kessler, J. 107, 186, 188, 189, 190, 191
KeBler, G. 435
Ketkar, S.N. 690
Khadkikar, S.B. 198
Khakoo, M.A. 111, 247
Khan, A.K. 592
Khan, P. 102
Khare, A. 315
Khare, S.P. 93
Khristoforov, O.V. 144, 163
Khurana, I. 380
Kiefl, H.U. 652, 653
Kikuchi, K. 674
Kim, L. 138
Kim, Y.S. 19
Kimura, M. 501, 582, 583, 627
King, G.C. 142, 158, 172, 260, 271
King, M. 706
King, S.J. 116
Kingston, A.E. 109, 296, 297, 689
Kinsey, J.L. 570
Kirby, K. 481
Kita, S. 558
Klein, C.R. 604
Kleinpoppen, H. 117, 118, 166, 438, 440
Kleyn, A.W. 579
Klüver, M. 433
Knoth, G. 153
Knudsen, H. 470, 474, 525
Knudson, S.K. 390
Kobayashi, K. 497
Kobayashi, N. 563, 564
Kobayashi, S. 303
Kochach, L. 548
Koenig, W. 457, 660
Koenraad, P.M. 414
Kohlhase, A. 558
Kohn, I. 407, 448
Koike, F. 421, 503
Koizumi, H. 55
Koizumi, T. 14
Komarov, V.V. 694
Kondow, T. 656, 665
Konrad, J. 431
Koschar, P. 529
Kouchi, N. 277
Kövé, Á. 530
Kowalski, T.Z. 698
Koyama, N. 629
Koyano, I. 598
Kraus, B. 165
Krause, H.F. 662
Kresin, V.Z. 61
Kretschmar, K. 651
Kristoforov, O.V. 693
Krüger, W. 442
Ksavery, Yu.A. 704
Kuchitsu, K. 656, 665
Kuen, I. 576
Kuiper, A.G. 418
Kulander, K.C. 62
Kumagai, H. 407, 448, 451, 452, 545
Kumar, M. 231, 327
Kume, H. 665
Kunikeev, Sh. D. 515
Kuo, C.H. 659
Kuppermann, A. 126
Kurepa, M. 162
Kuroki, K. 251
Kvale, T.J. 415
Kwan, C.K. 230, 322, 328, 332
Lablanquie, P. 31, 32
LaGattuta, K.J. 310, 628
Lahmam-Bennani, A. 176
Lais, U. 426
Lakits, G. 487
Lamanna, U.T. 212, 222
Lambropoulos, P. 78
Lamoureux, M. 644
Lane, N.F. 365, 582, 627
Lange, V. 15, 632
Langer, B. 12, 13
Lapicki, G. 402
Larciprete, R. 87
Larsen, M. 358
Larsen, P. 485
Latimer, C.J. 577
Laucagne, J.J. 367
Laughlin, C. 638
Laurent, H. 677
LaVilla, R.E. 543
Le Sech, C. 155, 372
Leach, S. 30
Lee, J. 302
Lee, L.C. 58, 229
Lee, M.-T. 105, 218, 224
Lee, Y.T. 597, 647
Lefebvre-Brion, H. 41
LeGouët, J.L. 7
Leisin, O. 590
Leiter, K. 266
Lembo, L. 447
Lengyel, V.I. 685, 692, 693
Lennon, M.A. 689
Leprince, C. 688

- Lester, W.A., Jr. 61, 551
 Leuchtner, R.E. 588
 Leung, K.T. 261
 Leyh, B. 42
 Lie, G.C. 82
 Ligtenberg, R.C.G. 276
 Liljehy, L. 470
 Lima, M.A.P. 235
 Lin, C.C. 385
 Lin, C.-D. 411, 501, 502
 Lindinger, W. 587
 Lindle, D.W. 10, 11
 Lindsay, B.G. 577
 Lineberger, W.C. 51, 52
 Liou, H.T. 88, 275
 Liu, B. 60
 Liu, J.W. 245
 Liu, Y. 341, 450
 Liu, Z. 341
 Ljepojevic, N.N. 314
 Llorente, J.M.G. 478
 Lohmann, B. 106, 196
 Lopes, M.C.A. 224
 Lorent, V. 675
 Lorents, D.C. 86, 284
 Lorentz, S.R. 119
 Los, J. 579
 Lu, F. 630
 Lu, K.T. 77
 Lubell, M.S. 180, 672
 Lucas, C.A. 207, 252
 Lucatorto, T.B. 69
 Lüdde, H.J. 498, 500
 Ludescher, H.P. 353
 Ludewig, C. 53
 Ludwig, N. 187
 Lutrus, C.K. 604
 Lutz, H.O. 427, 438, 439, 440
 Luzzatti, E. 350
 Lykke, K.R. 51
 Ma, Q. 341
 MacAdam, K. 622
 MacArthur, D.W. 50
 Macek, J. 424, 609
 MacGillivray, W.R. 208
 Machado, L.E. 205
 Macias, A. 149
 Mack, M. 466
 Madison, D.H. 127, 194
 Magill, P. 571
 Mahgerefteh, M. 221
 Majumdar, P.S. 152
 Malegat, L. 210, 239
 Malutzki, R. 9, 38
 Mandal, C.R. 512
 Mandal, P. 151
 Mann, A. 575
 Mann, R. 446, 475
 Mansky, E.J. 197
 Manson, S.T. 20, 21, 22, 408, 410
 Maor, D. 457, 495
 Marian, T. 65
 Marich, Z. 347
 Märk, T.D. 266
 Martin, N.L.S. 622
 Martin, R.L. 365
 Martin, S.J. 562, 581
 Martinez, H. 572, 573
 Martyschenko, V.V. 702
 Marxer, H. 519
 Masalovich, E.A. 693
 Masnou-Seeuws, F. 83, 372
 Mason, N.J. 145
 Massaro, P.A. 96, 97
 Masuoka, T. 35, 36
 Mathur, D. 167, 594
 Mathur, K.C. 123, 179, 646
 Matsuda, T. 108
 Matsuo, T. 545
 Matsuzawa, M. 629
 Matte, J.P. 644
 Mauldin, C.R. 422, 423
 Maurer, R.J. 633
 Mawhorter, R.J. 232
 McAfee, K.B., Jr. 586
 McCarroll, R. 479
 McCarthy, I.E. 131, 173
 McClelland, J.J. 185, 669
 McConkey, J.W. 111, 246, 250, 282
 McCullough, R.W. 476
 McCurdy, C.W. 44, 128
 McDonald, R.J. 550
 McEachran, R.P. 192, 326
 McFarland, R.H. 393, 394, 395, 396, 509
 McGowan, J.Wm. 667
 McGuire, J.H. 499, 521
 McKoy, V. 235
 McLaughlin, B.M. 297, 360
 McLaughlin, D. 391
 McMillian, G.B. 631
 McPherson, A. 276
 McQuaide, B.H. 661
 McWhirter, R.W.P. 314
 Meckbach, W. 524
 Mehlhorn, W. 174, 435
 Meijer, H.A.J. 378
 Melchert, F. 616
 Méndez, L. 478
 Menendez, M.G. 422, 423, 524
 Menezes, G.D. 205
 Meron, M. 394, 509
 Merts, A.L. 204
 Merz, H. 186
 Merzbacher, E. 392
 Mestdagh, J.M. 568, 597
 Meulen, H.P. v. d. 378
 Meyer, E. 377
 Meyer, F.W. 491
 Meyer, H. 232, 557, 650
 Meyer, W. 636
 Meyerhof, W.E. 430, 432, 447, 537, 538, 549, 550
 Michels, H.H. 253, 281
 Miers, R.E. 385
 Milkman, I.W. 659
 Miller, J.H. 410
 Miller, P.D. 306, 505
 Miller, T.M. 52, 119
 Millie, P. 31, 33
 Mingay, D.W. 506
 Miraglia, J.E. 381, 514, 531, 532
 Mitani, S. 35
 Mitchell, J.B.A. 313, 600, 667
 Mitroy, J.D. 131, 173
 Mitsuoka, K. 656
 Mittleman, M.H. 643
 Mizogawa, T. 452
 Modelli, A. 238
 Moede, M. 182
 Mohanty, J.P. 416
 Moiseiwitsch, B.L. 536
 Mokler, P.H. 397, 431, 507, 534
 Molitoris, J.D. 432, 550
 Möller, C. 644
 Möller, R. 54, 649
 Möller, T. 596
 Molter, K. 57
 Monchicourt, P. 367
 Montenegro, E.C. 547
 Mooney, H. 593
 Moore, J.H. 245
 Moorhead, P.S.K. 159, 160
 Moorman, L. 445
 Moraldi, M. 636
 Morales, A. 572
 Morales, F. 642
 Morenson, E. 430, 432, 458, 534, 550
 Moretto, L.G. 550
 Morgan, L.A. 217
 Morgan, S. 655
 Morgan, T.J. 393, 394, 395, 396, 509, 573, 706
 Morgenstern, R. 378, 414
 Morgner, H. 364, 589, 590, 591
 Morikawa, Y. 303
 Morin, P. 31, 32, 33
 Morita, M. 55, 277
 Morrison, M.A. 219
 Moseley, J.T. 88, 275, 659
 Moskowitz, W. 570
 Mossberg, T.W. 352
 Mott, C. 216
 Msezane, A.Z. 21, 289, 290, 291, 302
 Mueller, D. 307, 438
 Mukhamedzhanov, A.M. 695
 Mukherjee, S.C. 512, 513
 Mukoyama, T. 411
 Müller, A. 301, 307, 393, 395, 396, 446
 Muller, H.G. 64
 Müller, R. 234
 Müller, W. 589
 Müller-Fiedler, R. 261
 Mullins, O.C. 16
 Munger, Ch. 537, 538
 Murakami, J. 14
 Murray, K.K. 52
 Nagata, T. 14
 Nagy, L. 304
 Nahar, S.N. 321
 Nakajima, K. 279
 Nakamura, H. 316, 603
 Nakamura, T. 563, 564
 Nakanishi, K. 340
 Nasser, I. 628

- Naß, P.* 187
Nee, J.B. 58
Neher, K. 436
Neill, P.A. 115, 116
Neitzke, H.-P. 387
Nemirovsky, I. 524
Nenner, I. 31, 32, 33
Nessi, M. 550
Neumann, H. 361
Neumark, D.M. 51
Newbury, D.C. 269
Newby, C.W. 494
Newell, W.R. 145
Newman, J.H. 486, 559
Neynaber, R.H. 369, 370, 666
Nickel, J.C. 164, 216, 246
Nickich, V. 209
Niehaus, A. 418, 466
Nielsen, S.E. 358, 359
Nienhuis, G. 156, 378, 445
Niessen, W. von 265
Nightingale, M.P.S. 676
Nishimura, F. 251
Nishimura, H. 108
Noble, C.J. 39, 217, 242, 494
Nogueira, J.C. 105, 224
Noid, D.W. 390
Noll, T. 57
Norcross, D.W. 214, 215
Norrington, P.H. 132
O, C.S. 449
O'Callaghan, M. 355
Oda, K. 303
Oda, N. 251, 277, 403
Ogawa, T. 279
O'Halloran, M.A. 59
Ohsaki, A. 340
Okumura, M. 647
Okuno, K. 599
Olson, R.E. 639
Onda, K. 225
O'Neil, S.V. 215
Ong, P.P. 681, 682
Ono, H. 417
Ono, T. 303
Ono, Y. 88, 275
Oppenländer, A. 431, 507
Opradolce, L. 496
Orel, A.E. 62
Orient, O.J. 272, 273, 274
Ormsby, P.S. 443
Oschwald, M. 68
Osimitsch, S. 438
Ostrowski, K.W. 698
Otto, G. 67
Ovchinnikov, V.I. 703, 707
Oza, D.H. 285, 286
Padhy, B. 125
Padial, N.T. 43, 215, 223
Pagan, C.B. 205
Paikeday, J.M. 101
Paillard, D. 568
Paisner, J.A. 81
Paixão, F.J. da 121
Pálinkás, J. 633
Palma, A. 212, 552
Pantano, L. 212
Papadovassilakis, N. 670
Papp, F.F. 692
Parcell, L.A. 326
Park, G.T. 122
Park, J.T. 386, 489
Pascale, J. 569
Passarella, R. 588
Passarge, T. 435
Patel, J. 383
Peacher, J.L. 382, 386, 489
Pedersen, J.O.K. 474, 525
Peek, J.M. 137
Pegg, D.J. 415
Peitzmann, F.J. 107
Pejcev, V. 162
Pendleton, P.K. 324
Pepmiller, P.L. 306, 505
Perdrix, M. 373
Perera, N.W.P.H. 114
Pesnelle, A. 373
Peterson, J.R. 48, 49, 584, 585
Petitjean, L. 568, 624, 625, 626
Petrina, D.M. 685
Petring, D. 67
Pfeiffer, H. 387
Phaneuf, R.A. 491, 662
Piancastelli, M.N. 10, 11
Picqué, J.L. 7
Pierce, D.T. 658
Pindzola, M.S. 301, 308
Pipkin, F.M. 493
Pirani, F. 350
Piticu, I. 399, 400, 401
Pitzer, R.M. 44
Plessner, I. 457
Pollack, E. 562, 581
Pommier, J. 677
Pontes, F.C. 664
Popov, Yu. V. 177
Popova, A.M. 694
Popova, M.I. 504
Postoi, E.N. 697
Porvliege, R.M. 388
Pradel, P. 367
Prakash, S. 93
Pratt, R.H. 28, 135, 136, 138
Pratt, S.T. 70, 85
Preston, S. 483
Pritchard, D.E. 570, 571
Propin, R.Kh. 702
Prunele, E. de 621
Puerta, J. 168, 471
Pujo, P. de 568
Pundir, R.S. 646
Pyle, R.V. 509
Quadrelli, P. 312
Quarles, C. 139, 140
Raah, M. 368
Rachafi, S. 298, 299
Raheja, U.T. 594
Rahman, F. 595
Rai, D.K. 125, 130, 416
Raith, B. 679
Raith, W. 182, 233, 325
Rajgara, F.A. 594
Rao, N.S. 98, 129, 178, 220, 243, 686, 687
Raoult, M. 40, 45
Raseev, G. 41, 42, 45
Ratliff, J.M. 362
Rauch, W. 446
Read, F.H. 158, 172, 260
Reading, J.F. 455
Rebentrost, F. 635
Redd, E. 386, 489
Reddish, T. 226
Reed, K.J. 302, 428
Reeves, T.M. 392
Reichert, E. 187
Reid, I.D. 344, 345, 346
Reihl, H. 438
Reinhold, C.O. 381, 614
Rensfelt, K.-G. 470
Rescigno, T.N. 128
Reymann, K. 165
Richard, P. 446, 544
Riera, A. 149, 478
Riley, J.L. 113, 183, 184, 202
Rink, K. 616
Rinn, K. 616
Risley, J.S. 276, 434, 444
Rivarola, R.D. 539
Roberty, H.M.B. 207
Rockwood, A.L. 587
Rolfes, R.G. 622
Romanjuk, N.I. 692
Romanovsky, A.E. 694
Ron, A. 135, 136
Roncin, P. 677
Roser, R. 428
Rosi, M. 268
Rosmus, P. 215
Rosner, B. 506, 575
Ross, K.J. 162
Rossi, F. 569
Rossi, M.J. 86, 284
Roszman, L.J. 311
Roth, K. 364
Rottke, H. 1
Rouze, N. 276, 434, 444
Roy, A.C. 171, 211
Roy, D. 33, 263, 663
Roy, K. 151
Roy, P. 33
Rozet, J.P. 463, 492, 510
Rubin, K. 180
Rudd, M.E. 406, 528
Ruf, M.-W. 368, 376
Ruff, G.A. 632
Rühl, E. 654
Rui, L.J. 699
Runge, S. 373
Russek, A. 174, 560
Rustgi, O.P. 34
Ruzic, D.N. 348
Sabad, E.P. 692, 693
Sadilek, M. 482
Saha, B.C. 219

- Saha, G.C.* 513
Saha, S. 90
Sakaguchi, K. 433
Sakimoto, K. 292
Salin, A. 619
Salk, S.H.S. 602, 604
Salop, A. 462
Salzborn, E. 301, 616
Samson, J.A.R. 6, 34
Sanders, J.M. 544
Sandner, W. 15, 632
Sasaki, J. 576
Sasaki, T. 14
Sato, H. 244
Sato, Y. 14
Saxena, S. 123, 179
Saxon, R.P. 60, 66
Schadt, W. 431, 507, 705
Schaefer, J. 553
Schäfer, D.A. 486, 559
Schäfers, F. 2, 3, 4, 5
Schartner, K.-H. 165
Scheibner, K.F. 365
Scheid, W. 541, 542
Scheurer, J.N. 549, 673
Schindler, H.-G. 53
Schinke, R. 557
Schiwietz, G. 409, 634
Schlachter, A.S. 393, 395, 396, 446, 509
Schlemmer, P. 153
Schmidt, H. 377, 437, 597
Schmidt, V. 9, 38
Schmidt-Böcking, H. 431, 446, 453, 507, 705
Schmoranz, H. 57, 351
Schneider, B.I. 43, 91, 241
Schneider, D. 467, 634, 678
Schneider, Th. 467
Schöller, O. 384, 461
Scholten, R. 202
Schönfeldt, W.A. 397, 534
Schönhense, G. 3, 4
Schramm, R. 529
Schröder, W. 182
Schuch, R. 431, 453, 507
Schulz, M. 507
Schwalm, D. 433
Schweig, A. 232
Schwepe, J. 433
Scott, D. 420
Scott, N.S. 23, 193
Scott, T. 571
Seay, B.E. 324
Seely, D.G. 386, 489
Seiler, A. 658
Sellin, I.A. 449, 524, 526
Semke, J. 186
Sen, A. 600, 667
Senashenko, V.S. 413, 515
Senba, M. 344, 345, 346
Serebrjakov, S.G. 694
Shafer, Y. 6
Shafranyosh, I.I. 696
Shafroth, S.M. 398
Shah, M.B. 405
Shakeshaft, R. 78
Sharma, S.C. 324, 339
Shemansky, D.E. 248
Shen, G.F. 200
Sheorey, V.B. 94
Shergin, A.P. 427
Shibata, H. 14, 407, 448, 451, 452, 545
Shima, K. 452
Shimamura, I. 211, 533
Shimon, L.L. 707
Shingal, R. 494, 618
Shinpaugh, J.L. 544
Shinsaka, K. 55
Shirley, D.A. 10, 11
Short, R.T. 449
Shoufu, P. 389
Shpenik, O.B. 692, 703
Shuha, I.M. 685
Shul, R.J. 588
Sil, N.C. 151, 522, 523
Silim, H.A. 117
Sillmen, U. 182
Simonović, N. 607
Simpson, F.R. 577
Sinapius, G. 325
Singh, B. 104
Singh, C.S. 130, 416
Sinha, C. 522
Sinha, K.V. 329
Slevin, J. 142, 180, 672
Smith, A.C.H. 300, 374, 375
Smith, A.D. 245
Smith, D.B. 622
Smith, F.J. 689
Smith, G.P. 565, 566
Smith, K.A. 486, 559, 630, 631
Smith, N. 571
Smith, S.J. 332
Smith, V.H., Jr. 231, 245
Smith, W.W. 50, 641
Snegurskaya, T.A. 696
Snyder, J.J. 69
Snyder, R. 560
Sobotka, L.G. 550
Sodhi, R.N.S. 262
Sohn, M. 209
Sokolov, J. 457
Solomon, A.M. 708
Sonntag, B. 14
Souza, A.C.A. e 264
Souza, G.G.B. de 32, 207, 252, 264, 664
Spalburg, M.R. 579
Spence, D. 267
Spiess, G. 367
Spooner, D. 549, 550
Srivastava, B.B. 104
Srivastava, M.K. 170
Srivastava, R. 293, 327, 380
Srivastava, S.K. 272, 273, 274
Standage, M.C. 208
Stapelfeldt, J. 596
Starace, A.F. 76
Staudenmayer, B. 436
Stauffer, A.D. 192, 326
Stearns, J.W. 393, 395, 396, 509
Stebbing, R.F. 486, 559, 630, 631
Stefani, G. 157, 176
Stefani, J. 177
Stefanski, K. 73
Steimle, T.C. 659
Stein, J. 135, 136
Stein, T.S. 230, 322, 328, 332
Stelbovics, A.T. 131
Stephan, C. 463, 492, 510
Stettner, U. 409
Stevens, J. 581
Stewart, B. 570, 571
Stewart, J.E. 50
Stich, W. 500
Stiebing, K.E. 433
Stockli, M.P. 393, 509, 544
Stöhr, J. 269, 270
Stoller, Ch. 446, 447, 550
Stolterfoht, N. 409, 467, 634, 678
Stötzel, R. 427
Straten, P. van der 414
Strayer, M.R. 540
Stubbs, R.J. 258, 259
Sundaram, B. 74
Sur, S.K. 612
Suto, M. 58
Suzuki, H. 227, 228, 254, 303, 417
Swenson, J.K. 398, 671
Szabó, G. 530
Sze, K.H. 262
Szostak, D. 12, 13
Szücs, S. 620
Takagi, H. 316
Takatsuka, K. 603
Takayanagi, K. 555
Takayanagi, T. 227, 228, 254, 303, 417
Takuma, H. 227, 228, 254
Tambe, B.R. 22
Tanaka, H. 237
Tanaka, K. 598
Tang, F.C. 180, 672
Tang, S.Y. 369, 370, 666
Tang, X. 78
Tanis, J.A. 393, 394, 395, 396, 509
Tarantelli, F. 268
Taulbjerg, K. 518
Taute, E. 196
Tawara, H. 407, 448
Tayal, S.S. 295
Taylor, H.S. 73
Taylor, K.T. 24
Temkin, A. 141, 225
Tennyson, J. 39, 242
Terao, M. 619, 620
Teubner, P.J.O. 113, 183, 184, 202
Thareja, R.K. 315
Theodosiou, C.E. 18
Thieberger, P. 537, 538
Thomas, B. 449
Thompson, D.G. 236
Thompson, J.S. 415
Thorson, W.R. 412
Thumm, U. 461
Timmer, C. 307
Tinschert, K. 301

- Tiribelli, R. 268
 Tiszauer, D.H. 601
 Tiwary, S.N. 203
 Toburen, L.H. 404
 Toepfer, A. 498
 Tokoro, N. 403, 545
 Tolle, M. 650
 Tonuma, T. 407, 448
 Toshima, N. 497
 Tosi, P. 587
 Tossell, J.A. 245
 Touati, A. 492
 Träbert, E. 679
 Trager, C. 670
 Trajmar, S. 164, 246, 247, 249
 Trautmann, N. 433
 Tremblay, D. 663
 Tripathi, A.N. 231, 327, 380
 Tripathi, D.N. 333
 Tripathy, D.N. 349
 Trombetta, F. 642
 Tronc, M. 210, 239
 Tsuboi, T. 366
 Tung, M. 82
 Tunnell, L.N. 472, 473
 Turner, R.E. 345
 Tüshaus, M. 188
 Ugrin, S.Y. 697
 Ullrich, J. 446, 705
 Upschulte, B.L. 588
 Urquijo, J. de 572, 573
 Vager, Z. 457, 660
 Vakula, V.V. 709
 Valance, A. 610
 Valiron, P. 479
 Van Zyl, B. 361, 443
 Vancura, J. 482
 Varga, P. 477
 Varghese, S.L. 473
 Varracchio, E.F. 222, 319
 Vasilakis, A. 180, 672
 Venanzi, M. 552
 Vernhet, D. 492
 Vervaat, M.G.M. 579
 Vincent, P. 433
 Völkel, M. 15
 Volonté, S. 314
 Volovich, P.N. 707
 Volpi, G.G. 350, 556
 Vukstich, V.S. 708
 Wada, T. 555
 Wadehra, J.M. 281, 321
 Waggoner, W.T. 472
 Waibel, H. 376
 Wakiya, K. 227, 228, 254, 303, 417
 Walling, R.S. 611
 Walter, C.W. 630
 Walters, G.K. 362
 Wan, Y.J. 322
 Wang, C. 424
 Wang, D.P. 369, 370, 666
 Wang, G. 354
 Wang, L. 706
 Wang, M-X 684
 Wang, R.-G. 267
 Wang, W.C. 229
 Wang, Z. 354
 Warczak, A. 397
 Ward, M.H. 339
 Warner, C.D. 142
 Watanabe, T. 340, 341, 450, 533
 Watel, G. 373
 Watson, D.K. 146
 Watson, R.L. 633
 Watts, M.F. 613
 Weatherford, C.A. 225
 Webb, C.J. 208
 Wegner, H.E. 537, 538
 Wehlitz, R. 12, 13
 Weigold, E. 173, 256, 265
 Weiner, J. 684
 Weisheit, J.C. 611
 Weiss, A.W. 311
 Weiss, M.J. 593
 Weiss, P.S. 597
 Weissert, T.P. 147
 Welge, K.H. 1, 67
 Wellenstein, H. 100
 Wendin, G. 7
 Werner, U. 439
 West, J.B. 14
 Westerveld, W.B. 250, 276, 434, 444
 Wetzel, R.C. 161
 Wiel, M.J. van der 64, 668
 Wiesemann, K. 168, 471
 Wijngaarden, A. van 383
 Wilden, D.G. 657
 Wilkie, F.G. 476
 Wille, U. 634
 Willems, P. 578
 Williams, I.D. 289
 Williams, J.F. 112, 181
 Williamson, W., Jr. 700
 Wilson, M. 162
 Wilson, W.G. 691
 Winkler, P. 680
 Winkoun, D. 30
 Winter, H. 477, 487, 488
 Winter, T.G. 615
 Witte, R. 377, 437
 Wohrer, K. 463, 492
 Wolcke, A. 188, 190
 Wöflü, W. 458, 550
 Wollenweber, P. 351
 Worsnop, D.R. 53
 Wozniak, G.J. 550
 Wright, L.A. 253
 Wuilleumier, F. 7, 8
 Xu, E.Y. 16
 Yagi, S. 227, 228, 254
 Yagisawa, H. 637
 Yagishita, A. 14, 55
 Yan, P.G. 699
 Yeh, L.L. 647
 Yench, A.J. 592
 Yenen, O. 574
 Yin, R. 644
 Yodh, A.G. 352
 York, T.A. 258, 259
 Yoshida, T. 55
 Yoshimi, Y. 55
 Yoshino, M. 14
 Yousif, F. 580
 Yu, C-H 44
 Yuan, J.-M. 82
 Zabransky, B.J. 457, 660
 Zajac, J. 698
 Zaffman, D. 495
 Zannoli, G. 479
 Zapesochny, I.P. 696, 697, 708
 Zare, R.N. 59
 Zatsarinny, O.I. 685, 692
 Zeippen, C.J. 8
 Zeitz, W. 634
 Zetner, P.W. 250
 Zhu, Y. 16
 Ziming, L. 699
 Zimmerer, G. 596
 Zimmermann, G. 364
 Zollars, B.G. 630
 Zoller, P. 76
 Zoran, V. 399, 400, 401
 Zouros, T.J.M. 409
 Zuolin, C. 389
 Zygelman, B. 484

END

FILMED

3-86

DTIC